

WCAP-14253

AP600
LOW-PRESSURE INTEGRAL SYSTEMS TEST
AT OREGON STATE UNIVERSITY
FINAL DATA REPORT

MAY 1995

WESTINGHOUSE ELECTRIC CORPORATION
Nuclear Technology Division
P. O. Box 355
Pittsburgh, Pennsylvania 15230-355

© 1995 Westinghouse Electric Corporation
All Rights Reserved

9509190267 950915
PDR ADOCK 05200003
A PDR

COPYRIGHT NOTICE

The reports transmitted herewith each bear a Westinghouse copyright notice. The NRC is permitted to make the number of copies of the information contained in these reports which are necessary for its internal use in connection with generic and plant-specific reviews and approvals as well as the issuance, denial, amendment, transfer, renewal, modification, suspension, revocation, or violation of a license, permit, order, or regulation subject to the requirements of 10 CFR 2.790 regarding restrictions on public disclosure to the extent such information has been identified as proprietary by Westinghouse, copyright protection notwithstanding. With respect to the non-proprietary versions of these reports, the NRC is permitted to make the number of copies beyond those necessary for its internal use which are necessary in order to have one copy available for public viewing in the appropriate docket files in the public document room in Washington, D.C. and in local public document rooms as may be required by NRC regulations if the number of copies submitted is insufficient for this purpose. Copies made by the NRC must include the copyright notice in all instances and the proprietary notice if the original was identified as proprietary.

TABLE OF CONTENTS

<u>Section</u>	<u>Title</u>	<u>Page</u>
SUMMARY		1
ACKNOWLEDGMENTS		2
1.0	INTRODUCTION	1-1
1.1	Background	1.1-1
1.2	Pre-Operational Test Objectives	1.2-1
1.2.1	Cold Pre-Operational Tests	1.2-1
1.2.2	Hot Pre-Operational Tests	1.2-1
1.3	Matrix Test Objectives	1.3-1
2.0	TEST FACILITY DESCRIPTION	2-1
2.1	Overall Facility Description	2.1-1
2.1.1	Reactor Coolant System	2.1-1
2.1.2	Steam Generator System	2.1-1
2.1.3	Passive Core Cooling System	2.1-2
2.1.4	Automatic Depressurization System	2.1-3
2.1.5	Lower Containment Sump	2.1-3
2.1.6	Normal Residual Heat Removal System and Chemical and Volume Control System	2.1-4
2.1.7	Break and ADS Measurement System	2.1-4
2.1.8	Orifices and Nozzles	2.1-6
2.2	Facility Scaling	2.2-1
2.2.1	Methodology	2.2-1
2.2.2	Facility Scaling Parameters	2.2-2
2.2.3	Mass/Energy Balances	2.2-3
2.3	Facility Component Description	2.3-1
2.3.1	Reactor Vessel	2.3-1
2.3.2	Rod Bundle	2.3-2
2.3.3	Reactor Internals	2.3-4
2.3.4	Hot-Leg Piping	2.3-5
2.3.5	Cold-Leg Piping	2.3-6
2.3.6	Pressurizer Surge Line	2.3-7
2.3.7	Pressurizer	2.3-8
2.3.8	Steam Generators	2.3-9
2.3.9	Reactor Coolant Pumps	2.3-11
2.3.10	Accumulators	2.3-11
2.3.11	Core Makeup Tanks	2.3-12
2.3.12	In-Containment Refueling Water Storage Tank	2.3-14

TABLE OF CONTENTS (Continued)

<u>Section</u>	<u>Title</u>	<u>Page</u>
	2.3.13 Safety Injection Lines	2.3-15
	2.3.14 Containment Sumps	2.3-15
	2.3.15 Automatic Depressurization System, Stages 1-3	2.3-16
	2.3.16 Automatic Depressurization System, Stage 4	2.3-17
	2.3.17 Nonsafety Injection Systems	2.3-18
	2.3.18 Passive Residual Heat Removal	2.3-19
	2.3.19 Break Simulators	2.3-20
	2.3.20 Break and ADS Measurement System (BAMS)	2.3-21
	2.3.21 Test Support Systems	2.3-22
2.4	Instrumentation	2.4-1
	2.4.1 General Information on Instrumentation	2.4-1
	2.4.2 Calibration Methods and Standards	2.4-6
	2.4.3 Phenomena Affecting Readings	2.4-11
2.5	Data Acquisition System	2.5-1
	2.5.1 System Hardware	2.5-1
	2.5.2 DAS Architecture	2.5-1
	2.5.3 Software	2.5-1
	2.5.4 LabVIEW Description	2.5-2
	2.5.5 Sequence-of-Events Log	2.5-2
2.6	Test Facility Control System	2.6-1
	2.6.1 Operator Panel	2.6-1
	2.6.2 Test Signal or Safety Signal (S Signal)	2.6-2
	2.6.3 CVS Pump and Discharge Valve Control	2.6-3
	2.6.4 RNS Pump Control	2.6-4
	2.6.5 IRWST Valve Control	2.6-5
	2.6.6 Main Feed Pump and Discharge Valve Control	2.6-5
	2.6.7 Pressurizer Pressure Control	2.6-5
	2.6.8 RCP Gland Seal Cooling System Control	2.6-6
	2.6.9 CMT Valve Control	2.6-6
	2.6.10 CMT Steam Trap Isolation Valves	2.6-6
	2.6.11 RCP Control	2.6-7
	2.6.12 Reactor Heater Control	2.6-7
	2.6.13 Passive Heat Removal	2.6-8
	2.6.14 Condensate Return Pump Control	2.6-9
	2.6.15 Reactor Heater Sheath High-Temperature Trip	2.6-9
	2.6.16 Automatic Depressurization System Control	2.6-9
	2.6.17 Steam Generator-1 Level Control	2.6-10
	2.6.18 Steam Generator-1 Main Steam Valve	2.6-11
	2.6.19 Steam Generator-2 Control	2.6-11

TABLE OF CONTENTS (Continued)

<u>Section</u>	<u>Title</u>	<u>Page</u>
	2.6.20 Steam Generator-2 Main Steam Valve	2.6-12
	2.6.21 Main Steam Control Valve Control	2.6-12
	2.6.22 Large-Break BAMS Control	2.6-12
2.7	Pre-Test Operation	2.7-1
2.8	Drawings	2.8-1
3.0	DATA REDUCTION	3-1
3.1	Introduction	3-1
3.2	Test Validation	3.2-1
3.3	Pre-Operational Tests	3.3-1
3.4	Matrix Tests	3.4-1
3.5	Instrumentation Error Analysis	3.5-1
	3.5.1 General	3.5-1
	3.5.2 Definitions	3.5-3
	3.5.3 Results	3.5-3
3.6	Zero-Time Shift File Correction	3.6-1
	3.6.1 Test Data Collection Tiring	3.6-1
	3.6.2 Time Correction Method	3.6-1
4.0	PRE-OPERATIONAL TEST RESULTS	4-1
4.1	Cold Volume Determinations	4.1-1
	4.1.1 Accumulator Volume Test	4.1-1
	4.1.2 CMT Volume Test	4.1-4
	4.1.3 Pressurizer Volume Test	4.1-8
	4.1.4 IRWST Volume Test	4.1-9
	4.1.5 Primary and Secondary Sump Tank Volume Test	4.1-10
	4.1.6 SG-1 and SG-2 Secondary-Side Volume Test	4.1-12
	4.1.7 ADS and BAMS Moisture Separators Volume Test	4.1-14
	4.1.8 Reactor Vessel Volume Test	4.1-15
4.2	Pressure Drop Determination	4.2-1
	4.2.1 Background Information	4.2-1
	4.2.2 Test Procedure, Instrumentation, and Results	4.2-4
	4.2.3 RCP Flow Test	4.2-7
	4.2.4 CMT Injection Flow Test	4.2-9
	4.2.5 Accumulator Injection Flow Test	4.2-15
	4.2.6 IRWST Injection Flow Test	4.2-18
	4.2.7 Primary Sump Tank Injection Flow Test	4.2-24
	4.2.8 Cold-Leg Balance Line Injection Flow Test	4.2-26
	4.2.9 ADS 1-3 Flow Test	4.2-28

TABLE OF CONTENTS (Continued)

<u>Section</u>	<u>Title</u>	<u>Page</u>
	4.2.10 Normal Residual Heat Removal Flow Balance	4.2-32
4.3	HS01 Ambient Heat Losses	4.3-1
	4.3.1 Ambient Heat Loss Data at 100°F (Test Procedure Step 4.1.3)	4.3-2
	4.3.2 CMT Cooldown	4.3-2
	4.3.3 IRWST Cooldown	4.3-2
	4.3.4 Conclusion	4.3-2
5.0	MATRIX TESTS RESULTS	5-1
5.1	Cold-Leg Breaks with a Single Failure	5-2
	5.1.1 Reference 2-In. Cold-Leg Break (Matrix Test SB01)	5.1.1-1
	5.1.2 Test Repeatability (Matrix Test SB18 Comparison with Matrix Test SB01)	5.1.2-1
	5.1.3 Effect of Backpressure (Matrix Text SB19 Comparison with Matrix Test SB01)	5.1.3-1
	5.1.4 Effect of a Larger Break Size (Matrix Test SB21 Comparison with Matrix Test SB01)	5.1.4-1
	5.1.5 Effect of a Smaller Break Size (Matrix Test SB23 Comparison with Matrix Test SB01)	5.1.5-1
	5.1.6 Effect of an Intermediate Break Size (Matrix Test SB05 Comparison with Matrix Test SB01))	5.1.6-1
5.2	Cold-Leg Breaks with Operation of Nonsafety Systems	5.2-1
	5.2.1 Reference 2-In. Cold-Leg Break (Matrix Test SB04)	5.2.1-1
	5.2.2 Effect of a Smaller Break Size (Matrix Test SB24 Comparison with Matrix Test SB04)	5.2.2-1
5.3	Core Makeup Tank/Cold-Leg Balance Line Breaks	5.3-1
	5.3.1 Reference Double-Ended Guillotine Line Break (Matrix Test SB10)	5.3.1-1
	5.3.2 Effect of a Smaller Break Size (Matrix Test SB09 Comparison with Matrix Test SB10)	5.3.2-1
5.4	Direct Vessel Injection Line Breaks	5.4-1
	5.4.1 Reference Double-Ended Guillotine Line Break (Matrix Test SB12)	5.4.1-1
	5.4.2 Effect of a Smaller Break Size (Matrix Test SB13 Comparison with Matrix Test SB12)	5.4.2-1
	5.4.3 Effect of Additional Failures (Matrix Test SB28 Comparison with Matrix Test SB12)	5.4.3-1
5.5	Automatic Depressurization System Impact	5.5-1
	5.5.1 Inadvertent ADS Actuation (Matrix Test SB14)	5.5.1-1
	5.5.2 Multiple ADS Failures (Matrix Test SB26)	5.5.2-1
5.6	Inadvertent S Signal (Matrix Test SB31)	5.6-1
	5.6.1 System Configuration and Initial Conditions	5.6-1

TABLE OF CONTENTS (Continued)

<u>Section</u>	<u>Title</u>	<u>Page</u>
	5.6.2 Inoperable Instruments	5.6-2
	5.6.3 Sequence of Events	5.6-2
	5.6.4 Test Results and Evaluation	5.6-3
	5.6.5 Mass Balance	5.6-4
	5.6.6 Conclusions	5.6-5
5.7	Hot-Leg Break (Matrix Test SB15)	5.7-1
	5.7.1 System Configuration and Initial Conditions	5.7-1
	5.7.2 Inoperable Instruments	5.7-2
	5.7.3 Sequence of Events	5.7-3
	5.7.4 Test Results and Evaluation	5.7-5
	5.7.5 Component Responses	5.7-8
	5.7.6 Mass Balance	5.7-16
	5.7.7 Conclusions	5.7-16
6.0	MATRIX TEST GROUP COMPARISONS	6-1
6.1	Effect of 2-In. Break Location (Matrix Tests SB13 and SB15 Comparison with Matrix Test SB01)	6.1-1
6.2	Effects of Nonsafety Systems (Matrix Test SB04 Comparison with Matrix Test SB01)	6.2-1
7.0	OTHER TEST OBSERVATIONS	7-1
7.1	Condensation Events	7.1-1
7.2	CMT Temperature Measurement	7.2-1
	7.2.1 Matrix Test SB13 (U0113) Observation and Evaluation	7.2-1
	7.2.2 Matrix Test SB12 (U0112) Observation and Evaluation	7.2-4
	7.2.3 Matrix Test SB01 (U0001) Observation and Evaluation	7.2-5
	7.2.4 Matrix Test SB10 (U0110) Observation and Evaluation	7.2-6
	7.2.5 Summary	7.2-6
8.0	REFERENCES	8-1

TABLE OF CONTENTS (Continued)

<u>Section</u>	<u>Title</u>	<u>Page</u>
APPENDICES		
A	DATA REDUCTION METHODS AND VALIDATION PROCESS	A-1
B	DATA ACCEPTANCE RESULTS	B-1
C	INSTRUMENTATION DATA BASE	C-1
D	DATA ERROR ANALYSIS	D-1
E	MASS BALANCE	E-1
F	DECAY HEAT COMPARISONS	F-1
G	PIPING AND INSTRUMENTATION DRAWINGS	G-1
H	KEY FACILITY DRAWINGS	H-1
I	DATA FILES	I-1

LIST OF TABLES

<u>Table</u>	<u>Title</u>	<u>Page</u>
1.3-1	OSU Matrix Test Summary	1.3-2
2.2-1	Summary of System Scaling Results for the 1/4-Length Scale Model Primary Loop	2.2-4
2.3-1	Rod Bundle Characteristics	2.3-25
2.3-2	Insulation Applications	2.3-26
2.6-1	Programmable Controller Summary	2.6-16
2.6-2	Process Control System Components	2.6-19
3.2-1	Overall Acceptance Criteria	3.2-3
3.2-2	Critical Instrument List	3.2-4
3.6-1	Data Files - Correction of Zero Time	3.6-4
4.1-1	ACC-1 Volume Raw Test	4.1-17
4.1-2	ACC-1 Volume Test Results Versus Design	4.1-18
4.1-3	ACC-2 Volume Raw Test	4.1-19
4.1-4	ACC-2 Volume Test Results Versus Design	4.1-20
4.1-5	CMT-1 Volume Test Data	4.1-21
4.1-6	CMT-1 Volume Test Data	4.1-22
4.1-7	Comparison of Test Results with Design Values	4.1-23
4.1-8	Pressurizer Volume Test Raw Data	4.1-24
4.1-9	Summary of Test Results	4.1-25
4.1-10	IRWST Volume Data	4.1-26
4.1-11	Summary of IRWST Volume	4.1-27
4.1-12	Primary Sump Volume Data	4.1-28
4.1-13	Secondary Sump Volume Data	4.1-29
4.1-14	SG-1 Secondary-Side Volume Data	4.1-30
4.1-15	SG-2 Secondary-Side Volume Data	4.1-31
4.1-16	Summary of SG Secondary-Side Volume	4.1-32
4.1-17	ADS 1-3 Separator Volume Data	4.1-33
4.1-18	ADS 4-1 Separator Volume Data	4.1-33
4.1-19	ADS 4-2 Separator Volume Data	4.1-34
4.1-20	Break Separator Volume Data	4.1-35
4.1-21	Reactor Vessel Volume Data	4.1-36
4.1-22	Reactor Vessel Volume Summary	4.1-38
4.2-1	Summary of Reactor Vessel and Primary Loop Instrumentation Used in Flow Tests	4.2-34
4.2-2	Reactor Vessel Test Data Summary - First Flow Test Series	4.2-38
4.2-3	Reactor Vessel Test Data Summary - Third Flow Test Series	4.2-40
4.2-4	Comparison of OSU-F-01 and OSU-F-02 Data for Reactor Vessel	4.2-43

LIST OF TABLES (Continued)

<u>Table</u>	<u>Title</u>	<u>Page</u>
4.2-5	RCP Total Developed Head Summary	4.2-44
4.2-6	Summary of Line Resistance for Reactor Vessel and Primary Loops	4.2-45
4.2-7	CMT-1 and CMT-2 Injection Test Raw Data	4.2-52
4.2-8	ACC-1 and ACC-2 Injection Test Raw Data	4.2-53
4.2-9	IRWST-1 and IRWST-2 Injection Test Raw Data	4.2-55
4.2-10	Primary Sump Tank Injection Flow Test - Test Data Summary	4.2-56
4.2-11	CMT to Cold-Leg Balance Line Injection Flow Test - Test Data Summary	4.2-57
4.2-12	ADS 1-3 Flow Test - Test Raw Data Summary	4.2-58
4.2-13	Comparison of Calculated and Measured Pressure Drop for ADS 1-3 Lines	4.2-59
4.2-14	Line Resistance FL/D+K From Point 0 to Point 3	4.2-60
4.2-15	RNS Injection Data	4.2-61
4.2-16	Comparison of Test Results for Injection Lines	4.2-62
4.3-1	Raw Data File Identification and Description	4.3-3
4.3-2	Failed Instrumentation	4.3-4
4.3-3	Instrumentation Outside Test Boundary But Affected By CMT Cooldown	4.3-5
4.3-4	Instrumentation Outside Test Boundary But Affected By IRWST Cooldown	4.3-6
5.1.1-1	Matrix Test SB01 Initial Conditions	5.1.1-30
5.1.1-2	Matrix Test SB01 Inoperable Instruments/Invalid Data Channels	5.1.1-32
5.1.1-3	Matrix Test SB01 Sequence of Events	5.1.1-35
5.1.2-1	Matrix Test SB18 Initial Conditions	5.1.2-12
5.1.2-2	Matrix Test SB18 Inoperable Instruments/Invalid Data Channels	5.1.2-14
5.1.2-3	Matrix Test SB18 Sequence of Events	5.1.2-16
5.1.2-4	Data Recorded in SB18 Test Log	5.1.2-25
5.1.3-1	Matrix Test SB19 Initial Conditions	5.1.3-14
5.1.3-2	Matrix Test SB19 Inoperable Instruments/Invalid Data Channels	5.1.3-16
5.1.3-3	Matrix Test SB19 Sequence of Events	5.1.3-18
5.1.4-1	Matrix Test SB21 Initial Conditions	5.1.4-16
5.1.4-2	Matrix Test SB21 Inoperable Instruments/Invalid Data Channels	5.1.4-18
5.1.4-3	Matrix Test SB21 Sequence of Events	5.1.4-21
5.1.5-1	Matrix Test SB23 Initial Conditions	5.1.5-7
5.1.5-2	Matrix Test SB23 Inoperable Instruments/Invalid Data Channels	5.1.5-9
5.1.5-3	Matrix Test SB23 Sequence of Events	5.1.5-12
5.1.6-1	Matrix Test SB05 Initial Conditions	5.1.6-9
5.1.6-2	Matrix Test SB05 Inoperable Instruments/Invalid Data Channels	5.1.6-11
5.1.6-3	Matrix Test SB05 Sequence of Events	5.1.6-13
5.2.1-1	Matrix Test SB04 Initial Conditions	5.2.1-22
5.2.1-2	Matrix Test SB04 Inoperable Instruments/Invalid Data Channels	5.2.1-24

LIST OF TABLES (Continued)

<u>Table</u>	<u>Title</u>	<u>Page</u>
5.2.1-3	Matrix Test SB04 Sequence of Events	5.2.1-27
5.2.2-1	Matrix Test SB24 Initial Conditions	5.2.2-9
5.2.2-2	Matrix Test SB24 Inoperable Instruments/Invalid Data Channels	5.2.2-11
5.2.2-3	Matrix Test SB24 Sequence of Events	5.2.2-13
5.3.1-1	Matrix Test SB10 Initial Conditions	5.3.1-35
5.3.1-2	Matrix Test SB10 Inoperable Instruments/Invalid Data Channels	5.3.1-37
5.3.1-3	Matrix Test SB10 Sequence of Events	5.3.1-40
5.4.1-1	Matrix Test SB12 Initial Conditions	5.4.1-34
5.4.1-2	Matrix Test SB12 Inoperable Instruments/Invalid Data Channels	5.4.1-36
5.4.1-3	Matrix Test SB12 Sequence of Events	5.4.1-39
5.4.1-4	Temporary Test Thermocouples	5.4.1-47
5.4.2-1	Matrix Test SB13 Initial Conditions	5.4.2-24
5.4.2-2	Matrix Test SB13 Inoperable Instruments/Invalid Data Channels	5.4.2-26
5.4.2-3	Matrix Test SB13 Sequence of Events	5.4.2-29
5.4.3-1	Matrix Test SB28 Initial Conditions	5.4.3-16
5.4.3-2	Matrix Test SB28 Inoperable Instruments/Invalid Data Channels	5.4.3-18
5.4.3-3	Matrix Test SB28 Sequence of Events	5.4.3-20
5.4.3-4	Temporary Test Thermocouples	5.4.3-28
5.5.1-1	Matrix Test SB14 Initial Conditions	5.5.1-34
5.5.1-2	Matrix Test SB14 Inoperable Instruments/Invalid Data Channels	5.5.1-36
5.5.1-3	Matrix Test SB14 Sequence of Events	5.5.1-39
5.5.2-1	Matrix Test SB26 Initial Conditions	5.5.2-18
5.5.2-2	Matrix Test SB26 Inoperable Instruments/Invalid Data Channels	5.5.2-20
5.5.2-3	Matrix Test SB26 Sequence of Events	5.5.2-22
5.6-1	Matrix Test SB31 Initial Conditions	5.6-6
5.6.2	Matrix Test SB31 Inoperable Instruments/Invalid Data Channels	5.6-8
5.6.3	Matrix Test SB31 Sequence of Events	5.6-10
5.7-1	Matrix Test SB15 Initial Conditions	5.7-17
5.7.2	Matrix Test SB15 Inoperable Instruments/Invalid Data Channels	5.7-19
5.7.3	Matrix Test SB15 Sequence of Events	5.7-22
6.2.1-1	Sequence of Events for Effects of Nonsafety Systems on 2-in. Breaks	6.2-3
7.2-1	Matrix Test SB13 CMT-2 Fluid Temperature Condition Changes Summary	7.2-7
7.2-2	Matrix Test SB13 CMT-1 Fluid Temperature Condition Changes Summary	7.2-7
7.2-3	CMT Superheating Parameters Summary	7.2-8

LIST OF FIGURES

<u>Figure</u>	<u>Title</u>	<u>Page</u>
2.1-1	Reactor Vessel	2.1-8
2.1-2	IRWST and Reactor Vessel	2.1-9
2.1-3	Primary Sump Tank and Break Separator	2.1-10
2.1-4	Upper Level (Reactor Vessel Cover in Foreground)	2.1-11
2.1-5	Isometric Drawing of OSU Test Facility	2.1-12
2.1-6	Simplified Flow Diagram of the OSU Test Facility	2.1-13
2.2-1	General Scaling Methodology	2.2-5
2.3-1	RCP Performance Head Versus Flow	2.3-27
2.3-2	Flow Schematic for the ADS	2.3-28
2.3-3	CVS Pump Head Versus Flow	2.3-29
2.3-4	RNS Pump Head Versus Flow	2.3-30
2.3-5	Electrical One-Line Diagram	2.3-31
2.5-1	DAS Hardware	2.5-4
2.5-2	DAS Architecture	2.5-5
2.6-1	Photograph of Operator Panel	2.6-20
2.6-2	Drawing of Operator Panel	2.6-21
3.2-1	Data Documentation Steps	3.2-9
3.2-2	Steps in OSU Data Processing	3.2-10
4.1-1	Schematic of Accumulator Volume Test Setup	4.1-39
4.1-2	Schematic of CMT Test Setup	4.1-40
4.1-3	CMT-1 Volume versus Height from Bottom	4.1-41
4.1-4	CMT-2 Volume versus Height from Bottom	4.1-42
4.1-5	Schematic of Pressurizer Test Setup	4.1-43
4.1-6	IRWST Test Setup	4.1-44
4.1-7	Schematic of Containment Sump Test Setup	4.1-45
4.1-8	Schematic of SG Secondary-Side Volume Test Setup	4.1-46
4.1-9	Schematic of ADS and BAMS Separator Test Setup	4.1-47
4.1-10	Schematic of ADS and BAMS Separator Test Setup	4.1-48
4.2-1	CMT-1 Injection Test Flow Path	4.2-64
4.2-2	CMT-2 Injection Test Flow Path	4.2-65
4.2-3	CMT-1 Injection Line Pressure Drop Versus Flow Square	4.2-66
4.2-4	CMT-1 Injection Line Pressure Drop Versus Flow Square	4.2-66
4.2-5	CMT-1 Injection Line Pressure Drop Versus Flow Square	4.2-67
4.2-6	CMT-2 Injection Line Pressure Drop Versus Flow Square	4.2-67
4.2-7	CMT-2 Injection Line Pressure Drop Versus Flow Square	4.2-68
4.2-8	CMT-2 Injection Line Pressure Drop Versus Flow Square	4.2-68
4.2-9	CMT-1 Total Line Pressure Versus Flow Rate Square	4.2-69
4.2-10	CMT-2 Total Line Pressure Versus Flow Rate Square	4.2-69
4.2-11	ACC-1 Injection Test Flow Path	4.2-70

LIST OF FIGURES (Continued)

<u>Figure</u>	<u>Title</u>	<u>Page</u>
4.2-12	ACC-2 Injection Test Flow Path	4.2-71
4.2-13	ACC-1 Injection Line Pressure Drop Versus Flow Square	4.2-72
4.2-14	ACC-1 Injection Line Pressure Drop Versus Flow Square	4.2-72
4.2-15	ACC-1 Injection Line Pressure Drop Versus Flow Square	4.2-73
4.2-16	ACC-2 Injection Line Pressure Drop Versus Flow Square	4.2-73
4.2-17	ACC-2 Injection Line Pressure Drop Versus Flow Square	4.2-74
4.2-18	ACC-2 Injection Line Pressure Drop Versus Flow Square	4.2-74
4.2-19	ACC-1 Injection Line Pressure Drop Versus Flow Square	4.2-75
4.2-20	ACC-2 Injection Line Pressure Drop Versus Flow Square	4.2-75
4.2-21	IRWST Injection Test Flow Path	4.2-76
4.2-22	IRWST-1 Injection Line Pressure Drop Versus Flow Rate	4.2-77
4.2-23	IRWST-1 Injection Line Pressure Drop Versus Flow Rate	4.2-77
4.2-24	IRWST-1 Injection Line Pressure Drop Versus Flow Rate	4.2-78
4.2-25	IRWST-2 Injection Line Pressure Drop Versus Flow Rate	4.2-78
4.2-26	IRWST-2 Injection Line Pressure Drop Versus Flow Rate	4.2-79
4.2-27	IRWST-2 Injection Line Pressure Drop Versus Flow Rate	4.2-79
4.2-28	Primary Sump Tank Injection Test Flow Path	4.2-80
4.2-29	Primary Sump Tank Injection Pressure Drop Versus Flow Rate	4.2-81
4.2-30	Primary Sump Tank Injection Pressure Drop Versus Flow Rate	4.2-81
4.2-31	CMT-1 to CL-3 Balance Line Injection Test Flow Path	4.2-82
4.2-32	CMT-2 to CL-1 Balance Line Injection Test Flow Path	4.2-83
4.2-33	CMT-1 to CL-3 Balance Line Injection Pressure Drop Versus Flow Rate	4.2-84
4.2-34	CMT-1 to CL-3 Balance Line Injection Pressure Drop Versus Flow Rate	4.2-84
4.2-35	ADS 1-3 Injection Test Flow Path	4.2-85
4.2-36	ADS 1-3 Test Level Comparisons	4.2-86
4.2-37	Pressure Drop Via ADS-1	4.2-87
4.2-38	Pressure Drop Via ADS-2	4.2-87
4.2-39	Pressure Drop Via ADS-3	4.2-88
4.2-40	Pressure Drop Via ADS-1	4.2-88
4.2-41	Predicted Pressure Drop Versus Flow Rate Square	4.2-89
4.2-42	Pressure Drop Via ADS-1	4.2-89
4.2-43	Pressure Drop Via ADS-2	4.2-90
4.2-44	Pressure Drop Via ADS-3	4.2-90
4.2-45	RNS Injection Test Flow Path	4.2-91
5.1.1-1	Primary Loop and Break Piping Layout	5.1.1-45
5.1.1-2	Primary Loop and Break Pipe Arrangement	5.1.1-46

LIST OF FIGURES (Continued)

<u>Figure</u>	<u>Title</u>	<u>Page</u>
5.1.2-1	Primary Loop and Break Piping Layout	5.1.2-26
5.1.2-2	Primary Loop and Break Pipe Arrangement	5.1.2-27
5.1.3-1	Primary Loop and Break Piping Layout	5.1.3-26
5.1.3-2	Primary Loop and Break Pipe Arrangement	5.1.3-27
5.1.4-1	Primary Loop and Break Piping Layout	5.1.4-30
5.1.4-2	Primary Loop and Break Pipe Arrangement	5.1.4-31
5.1.5-1a	Primary Loop and Break Pipe Arrangement	5.1.5-20
5.1.5-1b	Primary Loop and Break Pipe Arrangement	5.1.5-21
5.1.6-1a	Primary Loop and Break Pipe Arrangement	5.1.6-20
5.1.6-1b	Primary Loop and Break Pipe Arrangement	5.1.6-21
5.2.1-1a	Primary Loop and Break Pipe Arrangement	5.1.5-33
5.2.1-1b	Primary Loop and Break Pipe Arrangement	5.1.5-34
5.2.2-1a	Primary Loop and Break Pipe Arrangement	5.2.2-16
5.2.2-1b	Primary Loop and Break Pipe Arrangement	5.2.2-17
5.3.1-1	ADS-4 to Separator Pipe Arrangement for Matrix Test SB10	5.3.1-48
5.3.1-2	CMT-1 Balance Line DEG Break Pipe Arrangement	5.3.1-49
5.4.1-1	Primary Loop and Break Pipe Arrangement	5.4.1-48
5.4.1-2	ADS 1-3 and Break Separator Liquid Flows	5.4.1-49
5.4.2-1	Primary Loop and Break Pipe Arrangement	5.4.2-37
5.4.3-1	Primary Loop and Break Pipe Arrangement	5.4.3-29
5.7-1a	Primary Loop and Break Pipe Arrangement (Sh. 1 of 2)	5.7-31
5.7-1b	Primary Loop and Break Pipe Arrangement, Side View (Sh. 2 of 2)	5.7-32

ACRONYMS

ACC	accumulator
ADS	automatic depressurization system
APEX	Advanced Plant Experiment test facility at OSU
ASME	American Society of Mechanical Engineers
BAMS	break and ADS measurement system
CCT	condensate collection tank
CD ROM	compact disk read-only memory
CMT	core makeup tank
CRP	condensate return pump
CVS	chemical and volume control system
DAS	data acquisition system
DEG	double-ended guillotine
DP	differential pressure
DVI	direct vessel injection
FMM	magnetic flow meter
GSM	general scaling methodology
H2TS	hierarchical two-tiered scaling analysis
HPS	heated phase switch
HX	heat exchanger
IRWST	in-containment refueling water storage tank
LAN	local area network
LBLOCA	large-break loss-of-coolant accident
LCS	lower containment sump
LDP	level
LOCA	loss-of-coolant accident
LRGMS	large main steam
MSS	main steam system
NSS	nonsafety systems
OSHA	Occupational Safety and Health Administration
OSU	Oregon State University
PC	personal computer
PCS	passive containment cooling system
PIRT	phenomena identification ranking table
PPIRT	plausible phenomena identification ranking table
PQP	project quality plan
PRHR	passive residual heat removal
PT	pressure transducer
PWR	pressurized water reactor
PXS	passive core cooling system
PZR	pressurizer
RCP	reactor coolant pump
RCS	reactor cooling system
RNS	normal residual heat removal system
RV	reactor vessel
SASM	severe accident scaling methodology
SBLOCA	small-break loss-of-coolant accident
SCR	silicon-controlled rectifier
SG	steam generator
SGS	steam generator system
VI	virtual instrumentation

SUMMARY

Westinghouse Electric Corporation and the Nuclear Engineering Department of Oregon State University (OSU) have designed and constructed a 1/4-scale model of the AP600 plant that includes the reactor coolant system (RCS), steam generators (SGs), passive core cooling system (PXS), automatic depressurization system (ADS), and nonsafety injection systems—such as partial normal residual heat removal system (RNS) and partial chemical and volume control system (CVS)—in the Radiation Center at OSU in Corvallis, Oregon. This facility was used to perform tests of the AP600 passive safety systems in a reduced size and at lower temperatures and pressures for validation of the safety analysis codes. The test facility, fabricated completely from austenitic stainless steel, was designed for normal operation at 450°F and 400 psig, and was scaled using the hierarchical, two-tiered scaling analysis (H2TS) method developed by the U.S. Nuclear Regulatory Commission (NRC).⁽¹⁾ Simulated piping breaks were tested in the hot leg, cold leg, pressure balance line between the cold leg and the core makeup tank (CMT), and the direct vessel injection (DVI) line. Decay heat that scales to 3 percent of the full power (about 2 minutes after shutdown) was supplied by electrically heated rods in the reactor vessel. Simulated accidents were programmed by the control system to proceed automatically. About 850 data channels were recorded by the data acquisition system (DAS) for each test and downloaded to compact disks for subsequent data reduction and plotting.

Data from the test facility were transmitted to the Westinghouse Energy Center for reduction and review. To the extent that instrument indications provided an understanding of the system response to a transient, the system response was defined. Final analysis of system behavior will be part of AP600 *Low-Pressure Integral Systems Test at Oregon State University, Test Analysis Report, WCAP-14292*.⁽²⁾ Conclusions from the test program are discussed with each test in Section 5 of this report.

ACKNOWLEDGMENTS

The authors express their appreciation for the extensive discussions and inputs obtained from the key designer of the test facility, Mr. L. K. Lau, and the developer of the scaling analyses, Dr. J. N. Reyes. The Westinghouse engineers, Mike Carter, Jerry Schlaman, Ralph Ferrell, and team leader Carl Dumsday, who performed these tests, and their very patient families deserve special recognition. Each of them lived "on-the-road" during the final phases of construction, facility check-out, pre-operational test, and formal test program. With the cooperation of the Oregon State University (OSU) test facility operators, the facility was in check-out or testing 24 hours a day, 7 days a week for 11 months.

Sue Fanto, Tim Andreychek, Larry Hochreiter, and Mike Roidt provided invaluable consultation in developing an understanding of the facility performance characteristics and served as final reviewers of the report.

The word-processing team members, led by Denise Kephart, deserve special thanks not only for their skill but for their cooperation, long hours, and enthusiasm.

1.0 INTRODUCTION

The low-pressure integral systems test facility at Oregon State University (OSU) is a scale model of the AP600 reactor used to evaluate the thermal-hydraulic characteristics of the AP600 during various accident conditions. Westinghouse performed a matrix of tests at OSU, as part of an integrated test plan (described in *AP600 Test and Analysis Plan for Design Certification*, WCAP-14141⁽³⁾), to provide data to verify the capability of the analytical methods used to predict the response of the AP600 integrated passive safety systems. Experiments were designed to simulate small-break loss-of-coolant accidents (SBLOCAs), the greatest challenge to the passive safety systems. The purpose of this report is to provide final verification of test results by comparing instrument indications to plausible phenomena expected or demonstrated by the test facility and to document the data results of each test used for validation of the safety codes applied to the AP600 plant.

Requirements for the test program are detailed in, *Long-Term Cooling Test Specification*, WCAP-13234.⁽⁴⁾ The test program consisted of a series of pre-operational tests performed to characterize the plant in both cold and hot conditions, followed by a series of tests performed to supply test data during the facility's response to a break in the primary system. The pre-operational tests confirmed system volumes, line resistances, and heat losses through the pressure boundary. In addition, a complete check-out was performed on the facility's instrumentation, associated instrument channels, and the data acquisition system. This check-out included testing of all control interlocks, trips, and alarms. In the matrix tests, breaks were simulated in the primary cold leg, direct vessel injection (DVI) line, and core makeup tank-1 (CMT-1) balance line. Additional tests were performed to evaluate break size, containment backpressure, nonsafety systems, and break location. The reference loss-of-coolant accident (LOCA), a 2-in. break in a cold leg, was performed twice to show test repeatability. An inadvertent automatic depressurization system (ADS) actuation and an inadvertent safety systems actuation (S) signal leading to ADS actuation were also evaluated.

Testing was performed at OSU from June through September, 1994, with a combined test staff of OSU and Westinghouse Electric Corporation engineers. Tests were run according to specific procedures developed by the Westinghouse Safety and Licensing Group and the Test Engineering Group at the Energy Center in Pittsburgh, Pennsylvania, in consultation with the Onsite Test Group. Test results were recorded in the data acquisition system (DAS) and were subject to several reviews. The initial review took place at the OSU test facility to determine if the test met the acceptance criteria or had to be repeated. The Day-of-Test Report was issued by the Onsite Test Group to the Test Engineering Group at the Energy Center documenting the initial data review and delineating the acceptability of the test. Additional reviews of the data were conducted at the Energy Center, in an expedited fashion, to make the data available to the Nuclear Regulatory Commission (NRC) so that it could evaluate the test results. The data were released in the preliminary form of Quick Look Reports for each test.

1.1 Background

The low-pressure, 1/4-height integral systems tests were conducted at the Corvallis campus of OSU. Scaling studies indicated that a scaled, low-pressure test facility could be constructed to capture the thermal-hydraulic phenomena of interest for the lower pressure characteristics of the AP600.

The OSU test facility is a new facility that was constructed specifically to investigate the AP600 passive system characteristics. The facility design accurately models the detail of the AP600 geometry, including the primary system, pipe routings, and layout for the passive safety systems. The primary system consists of one hot leg (HL) and two cold legs (CLs) with two active pumps and steam generator (SG) for each of the two loops. There are two CMTs, each connected to a cold leg of one primary loop. The pressurizer is connected to the other primary loop, as in the AP600 plant design. Gas-driven accumulators are connected to the DVI lines. The discharge lines from a CMT and one of the two in-containment refueling water storage tank (IRWST) and reactor sump lines are connected to each DVI line. The two independent lines of each stage of ADS 1, 2, and 3 are modeled by one line containing an orifice. The two-phase flow from the ADS 1-3 is separated in a swirl-vane separator, and the liquid and vapor flows are measured to obtain the total flow rate. The separated flow streams are then recombined and discharged into the IRWST through a sparger. Thus, the mass and energy flows from the ADS into the IRWST are preserved.

The time period for simulation included not only IRWST injections, but also IRWST draining and sump injection in order to simulate the long-term cooling mode of the AP600. The time scale for the OSU test facility is approximately one-half; that is, the sequence of events occurred approximately twice as fast as it would in the AP600.

To model the long-term cooling aspects of the transients, the two-phase flow from the break was separated in a swirl-vane separator, and the liquid and vapor portions of the total flow were measured. The liquid fraction of the flow was discharged to the reactor sump, as in the AP600 plant. The vapor was discharged to the atmosphere, and the equivalent liquid flow was capable of being added to the IRWST and sump to simulate the condensate return from the passive containment. A similar approach was also used for the two ADS-4 valves on the hot legs. The two-phase flow was separated in a swirl-vane separator, the two stream flows were measured, the liquid phase was discharged into the reactor sump while the vapor phase was discharged to the atmosphere, and the liquid equivalent was capable of being added to the IRWST and sump. The IRWST, reactor sump, and separators could be pressurized to simulate the containment pressurization following a postulated LOCA.

A multi-tube passive residual heat removal heat exchanger (PRHR HX) was located in the IRWST. The HX used the same C-tube design as the AP600 and two tubes were instrumented with thermocouples and flow meters to obtain wall heat fluxes during the tests. Data from fluid thermocouples, wall thermocouples, and level transmitters were used to determine HX performance. The IRWST had vertical rods containing fluid thermocouples located at various radial and axial

locations to determine the degree of mixing in the tank and assess the temperature of the liquid in the IRWST as it was delivered to the reactor vessel.

The reactor vessel for the OSU tests included a 3-ft. heated core simulator consisting of 48 1-in. diameter heater rods. The heater rods had a top-skewed power shape. There were wall thermocouples swaged inside some of the heater rods to measure the heater rod temperature and five fluid thermocouple rods in the heater rod bundle to measure the axial and radial coolant temperature distribution. The scaled flow area in the core and the flow area in the vessel upper plenum were preserved. There were simulated reactor internals in the upper plenum to preserve the flow area and the scaled coolant volume. The reactor vessel included an annular downcomer, into which the four cold legs and the two DVI lines were connected. The two hot legs penetrated the reactor annulus and connected with the loops. The AP600 reactor vessel neutron reflector was simulated using a ceramic liner to reduce the metal heat release to the coolant.

The OSU test facility had approximately 600 kW of electrical power available. This corresponds to about 3 percent decay heat.

The OSU experiments examined the passive safety system response for the SBLOCA and the large-break loss-of-coolant accident (LBLOCA) transitions into long-term cooling. A range of SBLOCAs was simulated at different locations on the primary system—such as the cold-leg, hot-leg, CMT-1 balance line, and DVI line. The break orientation, at either the top or bottom of the cold leg, was also examined. Selected tests continued into the long-term cooling, post-accident mode during which the passive safety injection was from the reactor sump and the IRWST. A larger-break, post-accident, long-term cooling situation was also simulated.

1.2 Pre-Operational Test Objectives

Pre-operational tests were performed to provide an understanding of facility control and operating characteristics, to confirm design features essential to scaling, and to ensure that the instruments and DAS were performing as expected. Formal tests were conducted while the plant was in cold conditions to measure system pressure drops and volume of the components. Pressure drops in the test facility were adjusted to their desired scale AP600 values by using orifice plates, when required. Pre-operational testing was performed in the hot condition to characterize system heat losses. Results of the pre-operational tests are presented in Section 4.

1.2.1 Cold Pre-Operational Tests

Volume determination tests were performed in January and February, 1994 for the accumulators, CMTs, pressurizer, IRWST, sumps, SG secondary sides, and reactor vessel to compare the actual volumes with the calculated volumes. Volume determination was made by filling the vessels with water and then measuring the weight of the water in the vessel. The weights were determined by draining the water into a container and then placing the container on a precision scale, or by using calibrated load cells under the larger tanks.

Flow test/line resistance determination tests were performed in February and September, 1994. The objective of the first set of tests was to measure line resistance for the accumulator lines, IRWST lines, and sump injection lines for a given flow rate. The pressure drop in CMT injection and ADS 1-3 lines was measured over a range of flows. Resistance of the normal residual heat removal system (RNS) injection lines was measured to ensure that they were within 10 percent of each other. The reactor coolant pump head was measured for full flow and pump coastdown conditions. Flow tests were repeated in September to obtain additional information on the pressure drop around the primary circuit and PRHR HX.

1.2.2 Hot Pre-Operational Tests

Three separate and formal hot functional tests were performed. The objectives of the tests were to ensure proper operation of the equipment prior to the formal matrix test program and to provide data necessary to document temperature characteristics of the system. The first hot functional test (OSU-HS01) measured the steady-state heat loss, natural-circulation flow, and forced-flow characteristics. These data were used to verify the AP600 thermal-hydraulic computer codes (the test results are reported in Subsection 4.3). The objective of the second test (OSU-HS-02) was to verify the measuring capability of the break and ADS measurement system (BAMS) and the control of the ADS. The third hot functional test (OSU-HS03), inadvertent ADS-1 Actuation, was a rehearsal for the formal matrix test program. (Data from OSU-HS02 and HS03 are not used in AP600 safety analysis computer code validation and are not included in this report.)

OSU-HS01 was performed to determine surface heat losses from the system at 100°, 200°, 300°, and 400°F; characterize PRHR under natural circulation and forced cooling; characterize the primary cooling system state at 100 kW, 300 kW, 500 kW, and 600 kW; and characterize the CMT natural convection characteristics.

1.3 Matrix Test Objectives

The objective of the Matrix Test Program was to obtain test data for a series of AP600 simulated transients, varying the test parameters on a one-at-a-time basis, and to overlap the test program at SPES-2, a full-height, full-pressure test facility. Tests at OSU were specifically designed to evaluate the passive safety system response to a range of SBLOCAs, during the transition into long-term cooling. The reference LOCA, Matrix Test SB01, is a 2-in. cold-leg break with a simulated failure of one of the two ADS-4 valves in one ADS-4 line. The effect of break location was determined by also testing a break in the DVI line (Matrix Test SB12), a break in the CMT-1 balance line (Matrix Test SB10), and a break in hot leg-2 (Matrix Test SB15). The impact of a larger break size was evaluated comparing the results of SB01 with SB21, a 4-in. cold-leg break test case. Matrix Tests SB05 and SB23 were performed to demonstrate the impact of smaller break sizes.

The reference 2-in. cold-leg LOCA, Matrix Test SB01, was duplicated in Matrix Test SB18, the last matrix test performed to demonstrate test facility repeatability over a period of time. Matrix Test SB19 repeated SB01 with the objective of showing the effect of high containment backpressure.

Possible interactions of the nonsafety systems with the passive safety systems were addressed by performing Matrix Test SB04, a repeat of Matrix Test SB01, with the nonsafety systems running. The impact of a smaller break size was evaluated in Matrix Test SB24.

Additional tests were performed to evaluate the effects of a CMT/cold leg balance line breaker of a smaller size (Matrix Test SB09) and a DVI break of a smaller size (Matrix Test SB13). A DVI double-ended break with additional failures was evaluated in Matrix Test SB28.

Several tests were performed to show the effect of transients not involving breaks. Matrix Test SB14 tested the impact of an inadvertent ADS actuation, Matrix Test SB26 evaluated multiple ADS failures, and Matrix Test SB31 tested an inadvertent S signal scenario.

A summary of the matrix tests used in the AP600 thermal-hydraulic code validation is provided in Table 1.3-1. The pertinent facility conditions for each test are also noted. There were additional matrix tests performed and omitted from this report because of their similarity to other tests. Those test results, issued in preliminary Quick Look Reports, will be re-issued in final Quick Look Reports.

**TABLE 1.3-1
OSU MATRIX TEST SUMMARY**

Test No.	Break Size and Location	PRHR HX	CVS Pump	RNS Pump	ADS 4-1 (HL-1)	ADS 4-2 (HL-2)	Comments
SB01	2-in. CL-3 bottom of cold leg (CMT side)	On	Off	Off	50 percent flow area in AP600	100 percent flow area in AP600	Failure of one of two lines in ADS 4-1; reference cold-leg break case
SB04	2-in. CL-3 bottom of cold leg (CMT side)	On	On	On	50 percent flow area in AP600	100 percent flow area in AP600	Same as SB01 except safety and nonsafety system interaction
SB05	1-in. CL-3 bottom of cold leg (CMT side)	On	Off	Off	50 percent flow area in AP600	100 percent flow area in AP600	Same as SB01 except break size change
SB09	2-in. CL-3 to CMT-1 balance line	On	Off	Off	50 percent flow area in AP600	100 percent flow Area in AP600	Same as SB01 except different break location; asymmetric behavior of CMTs
SB10	DEG CL-3 to CMT-1 balance line	On	Off	Off	50 percent flow area in AP600	100 percent flow area in AP600	Limiting break on balance line; asymmetric behavior of CMTs; failure of one of two lines in ADS 4-1
SB12	DEG DVI-1 line break	On	Off	Off	100 percent flow area in AP600	100 percent flow area in AP600	Limiting break on DVI line; Failure of one of two lines of ADS-1 and ADS-3
SB13	2-in. DVI-1 line break	On	Off	Off	50 percent flow area in AP600	100 percent flow area in AP600	Same as SB01 except different break location
SB14	Inadvertent ADS (no break)	On	Off	Off	50 percent flow area in AP600	100 percent flow area in AP600	No-break case with one failure of two lines in ADS 4-1
SB15	2-in. HL-2 bottom of pipe	On	Off	Off	50 percent flow area in AP600	100 percent flow area in AP600	Same as SB01 except break location

**TABLE 1.3-1 (Continued)
OSU MATRIX TEST SUMMARY**

Test No.	Break Size and Location	PRHR HX	CVS Pump	RNS Pump	ADS 4-1 (HL-1)	ADS 4-2 (HL-2)	Comments
SB18	2-in. CL-3 bottom of cold leg (CMT side)	On	Off	Off	50 percent flow area in AP600	100 percent flow area in AP600	Repeat test of SB01; confirm behavior of system and instrumentation
SB19	2-in. CL-3 bottom of cold leg (CMT side)	On	Off	Off	50 percent flow area in AP600	100 percent flow area in AP600	Same as SB01 except containment backpressure simulated
SB21	4-in. top of and 4-in. bottom of CL-3 (CMT side)	On	Off	Off	50 percent flow area in AP600	100 percent flow area in AP600	Same as SB01 except larger break size; largest break size simulated in matrix tests
SB23	1/2-in. CL-3 bottom of cold leg (CMT side)	On	Off	Off	50 percent flow area in AP600	100 percent flow area in AP600	Same as SB01 except smaller break size
SB24	1/2-in. CL-3 bottom of cold leg (CMT side)	On	On	On	50 percent flow area in AP600	100 percent flow area in AP600	Safety and nonsafety system interaction; single failure
SB26	Inadvertent ADS with multiple failures (no break)	Off	Off	Off	N/A isolate this line	N/A isolate this line	No-break PRA case with ADS-1 isolated and failure of one of two lines of ADS 4-1; PRHR HX isolated
SB28	DEG DVI-1 line break	Off	Off	Off	N/A isolate this line	N/A isolate this line	Limiting break on DVI line with ADS 4-1, ADS 4-2, accumulator-1, and PRHX HX isolated.
SB31	Spurious S signal (no break)	On	Off	Off	50 percent flow area in AP600	100 percent flow area in AP600	Failure of one of two lines in ADS 4-1

Note:

DEG -- double-ended guillotine

PRA -- probabilistic risk assessment

2.0 TEST FACILITY DESCRIPTION

The Oregon State University (OSU) test facility is designed for operation at 400 psig and 450°F, in accordance with the requirements of the American Society of Mechanical Engineers (ASME) Pressure Vessel Codes, Section VIII, Pressure Piping B31 (ANSI/ASME B31.1)⁽⁵⁾; Occupational Health and Safety Administration (OSHA) Standards; and Oregon State Fire Protection Codes. In this section, the overall test facility and each component are described.

2.1 Overall Facility Description

The OSU test facility is a scaled model of the AP600 reactor coolant system (RCS), steam generator system (SGS), passive core cooling system (PXS), automatic depressurization system (ADS), lower containment sump (LCS), chemical and volume control system (CVS), and normal residual heat removal system (RNS). In addition, the facility is capable of simulating the AP600 passive containment cooling system (PCS) condensate return process. Figures 2.1-1 through 2.1-4 are photographs of the completed facility. Figure 2.1-5 is an isometric drawing of the test facility, and Figure 2.1-6 is a simplified flow diagram of the test facility. Appendix G contains detailed piping and instrumentation diagrams (P&IDs) for the test facility and its systems. The facility accurately reflects the AP600 geometry, including the piping routings. All components and piping are fabricated from austenitic stainless steel. Flanged, gasketed connectors are used throughout the test facility. The relative locations of all tanks and vessels—such as the in-containment refueling water storage tank (IRWST), core makeup tanks (CMTs), and accumulators—are properly modeled both horizontally and vertically. The facility uses a unique break and ADS measurement system (BAMS) to measure two-phase break and ADS flow.

2.1.1 Reactor Coolant System

The RCS is composed of a reactor vessel, which has electrically heated rods to simulate the decay heat in the reactor core, and two primary loops. Each primary loop consists of two cold-leg pipes and one hot-leg pipe connecting a steam generator (SG) to the reactor vessel. A reactor coolant pump (RCP) on each cold leg takes suction from the SG channel head (downstream of the SG U-tubes) and discharges it into the downcomer region of the reactor vessel. A pressurizer with an electric heater is connected to one of the two hot legs through surge-line piping. The surge line is formed to a spiral geometry to accommodate piping expansion loads at the pressurizer during thermal transients. The top of the pressurizer is connected to the ADS 1-3 line. An ADS-4 line is connected to each hot leg.

The reactor vessel also contains two direct vessel injection (DVI) nozzles that connect to the DVI lines of the passive core cooling system (PXS). A flow venturi is incorporated in each DVI nozzle to limit the loss of inventory from the reactor vessel in the event of a double-ended DVI line break. Each hot leg provides a connection to one of the two ADS-4 lines. Detailed descriptions of RCS components are discussed in Subsection 2.3.

2.1.2 Steam Generator System

This test models the primary side of the SGS with two SGs, one per primary loop. A simulated feedwater line is used for each SG to maintain proper SG secondary water level. The steam produced in each SG is measured and exhausted to the atmosphere through a common diffuser and stack.

Proper AP600 SGS operations during loss-of-coolant accident (LOCA) transients are simulated. In the AP600, a drop in primary water level produces a safety systems actuation (S) signal, which shuts the

feedwater supply and maintains SG secondary-side pressure at its proper value. The test control logic simulates the response of the AP600 by providing an S signal at a fixed time following a break. Consequently, the proper initial conditions for the transient behavior of the facility are provided. A detailed description of the SGS is provided in Subsection 2.3.

2.1.3 Passive Core Cooling System

The PXS consists of two CMTs, two accumulators, one IRWST, and one passive residual heat removal heat exchanger (PRHR HX). The test facility simulates the AP600 IRWST with a cylindrical tank with properly scaled water volume and height. The IRWST is located above the reactor core; two injection lines connect to the two DVI lines—one per DVI line. Each IRWST injection line also communicates with the sump tank with interconnecting piping and isolation valves. Two additional conditions are simulated in the test model: venting of the IRWST to the containment and water overflowing the IRWST to the sump.

Two CMTs and two accumulators are used in the PXS. One CMT and one accumulator are connected to one DVI line; the other CMT and accumulator are connected to the second DVI line. Both DVI lines enter the downcomer of the reactor vessel at the DVI nozzles. The PRHR HX is located inside the IRWST, using IRWST water as the cold reservoir. The inlet of the PRHR HX is connected to the pressurizer side hot leg, via a tee at the ADS-4 line, and the outlet is connected to the SG channel head at the cold-leg side. Since the inlet is hot and the outlet is cold, water is circulated through this system by natural convection. The water volume and elevation of each CMT are properly scaled and modeled. They are elevated above the reactor vessel and the DVI lines. A line connecting the top of each CMT to its cold leg provides pressure balance between the RCS and the CMT. Therefore, the CMT injects cooling water by its own elevation head. The accumulators are also modeled with proper volume and height. However, they are pre-pressurized and, therefore, inject when RCS pressure is below the preselected accumulator pressure.

The PXS and the ADS provide adequate reactor core cooling for the complete range of LOCAs. In the event of a LOCA, the CMTs inject ambient water to the reactor vessel when the injection isolation valve opens. The accumulators also inject water when RCS pressure drops below the pre-set accumulator pressure. As the CMT water level drops, the ADS-1 through ADS-4 isolation valves open sequentially to depressurize the RCS. The opening of the ADS-4 valves reduces the RCS pressure to equal containment pressure; hence, the IRWST injects by its own elevation head. Finally, the sump injects water to the reactor vessel when enough elevation head is established.

Accurate, direct measurement of the two-phase flows vented from the system (simulated breaks, ADS flows) are difficult and expensive. A unique system, the BAMS, was specifically designed to measure these two-phase flows. The BAMS is based on separating the two-phase flows into individual single-phase flow streams that can be accurately measured with conventional instrumentation.

2.1.4 Automatic Depressurization System

The AP600 uses four stages of valves to depressurize the RCS. The first three stages of the ADS are provided through connections to the pressurizer. The three stages are arranged in parallel with each stage containing two lines and each line containing an isolation valve and control valve. The fourth stage of ADS contains four separate lines. Two lines have a common connection to HL-1, and two lines have a common connection to HL-2. Similar to ADS 1-3, each line contains an isolation valve and control valve.

The OSU test facility uses only one line of valves to model the ADS 1-3 stages of AP600. This is done using removable flow nozzles to match the scaled flow characteristics of either one or two lines of valves. The first-, second-, and third-stage lines of the ADS split into parallel lines from one connection off the pressurizer. Each line includes a pneumatically operated, full port ball valve and a flow nozzle. The ball valve simulates the isolation valve in the AP600, and the flow nozzle simulates the flow control valve in the AP600. Two sets of flow nozzles are used to simulate single- or double-line operation, allowing proper flow area scaling.

The discharge lines from the ADS 1-3 valves are joined into one line that is connected to the ADS 1-3 separator. These valves are opened by the test logic controller. Once the ADS valves are opened by the test logic controller, RCS pressure drops and the flow flashes into two-phase flow. This two-phase flow is separated using a swirl-vane separator, and the liquid and vapor flows are measured to obtain the ADS total flow for mass and energy balance analysis. The separated flow streams are then recombined and discharged into the IRWST through a sparger. Thus, the mass flow and energy flow from ADS 1-3 into the IRWST are preserved.

The OSU test facility uses one ADS-4 line connected to the top of each hot leg. Each line contains a pneumatically operated, full port ball valve acting as the ADS-4 isolation valve and a flow nozzle simulating the flow area in the AP600. Two sets of flow nozzles are used in the test: one simulates 100-percent flow area, and the other simulates 50-percent flow area. For those tests which require a complete failure of the ADS-4 lines on one hot leg, the ADS-4 line is closed. In the AP600 plant, when the ADS-4 isolation valves open, the flow is directed inside the containment. In the test, the ADS-4 discharge flows to the ADS-4 separators, where the steam and liquid flows are separated. The steam flow is measured and exhausted to the atmosphere. The liquid flow is measured and directed to the primary sump tank. This two-phase flow measuring scheme is part of the BAMS, which is discussed in more detail in Subsection 2.1.7.

2.1.5 Lower Containment Sump

The LCS in the AP600 consists of two volumes—normally flooded and normally nonflooded. The normally flooded volume consists of those compartments which collect liquid break flow and ADS flow. For example, the compartments that house the reactor vessel or the SGs are normally flooded. The normally nonflooded volume includes those compartments which do not collect any liquid flow.

The only communication path between the normally flooded volume and normally nonflooded volume is at the top of these compartments, which is called the *curb*. In the test, a cylindrical tank (primary sump tank) is used to model the normally flooded volume. The normally nonflooded volume is modeled with another cylindrical tank, identified as the secondary sump tank. These two tanks are connected with a line at a level simulating the curb level in the AP600.

The primary sump tank is designed to properly scaled water volume and height. It includes sump injection lines that inject water into the DVI lines. These injection lines also communicate with the IRWST injection lines at the properly scaled elevation and locations. The overflow from the IRWST is also collected in this tank, simulating the overflow path in the AP600.

The secondary sump is also designed to properly scaled water volume and height. It is connected to the primary sump tank by a short length of 6-in. Sch. 40 pipe. This pipe is very short in order to minimize flow resistance, since the flooded and nonflooded AP600 containment volumes are only separated by the curb. The pipe also has a flange joint with a weir in between. The height of this weir models the curb level in the AP600. Detailed descriptions of LCS components are included in Subsection 2.3.

2.1.6 Normal Residual Heat Removal System and Chemical and Volume Control System

In the AP600, the RNS is used to provide nonsafety cooling water injection to the reactor core. In this case, the RNS pump takes suction from the IRWST and discharges it into the DVI lines. The delivered flow rate is a function of RCS pressure. This process and its time-dependent flow are modeled in the test. During testing, the RNS pump takes suction from the IRWST at the properly scaled location and elevation, and it discharges the flow to both DVI lines at properly scaled locations. These two lines are balanced so that equal flow can be delivered to each DVI line. The pressure-dependent flow in the AP600 is also modeled and automatically controlled by the proportional, integral, derivative (PID) controller. Subsection 2.3.17 provides more details of the RNS components.

The makeup line in the AP600 CVS is modeled in the test. This line contains a pump taking suction from the feed storage tank and discharging to the SG-2 (pressurizer side) channel head at the cold-leg side. The makeup flow is scaled from the AP600 makeup flow rate as a function of RCS pressure and is controlled automatically by the process controller.

2.1.7 Break and ADS Measurement System

The mass and energy of the test facility, both on individual components and the overall system, must be maintained in order to properly scale the long-term cooling phenomenon in the AP600. To do this, the flow rate at various locations and equipment must be known. For those locations where single-phase flow exists, the flow rate measurement is relatively simple and reliable. However, there are some locations and equipment in the test facility with two-phase flows. Since direct measurement of two-phase flow is not practical and is extremely expensive, an indirect method is used—the BAMS.

The BAMS is uniquely designed for the test facility to indirectly measure two-phase flow and energy. This system uses separators to separate the two-phase flow into single-phase liquid and single-phase steam flows for direct flow rate and temperature measurements. This system also measures all break flows; that is, LOCA operations and inadvertent ADS operations. The BAMS consists of steam-liquid separators and the interconnecting pipes and valves to the various break sources, the primary sump tank, the ADS 1-3 lines, and the main steam header.

2.1.7.1 ADS 1-3 Separator and Pipe Route

One separator is dedicated as the ADS 1-3 moisture separator; it has one inlet and two outlets. Two-phase flow (steam and water) from the ADS 1-3 lines enters the ADS 1-3 separator, where the steam is separated from the mixture. The steam flows out of one outlet while the liquid drains down the other. These two lines recombine at some distance downstream and discharge into the IRWST via the sparger located inside the IRWST. To prevent the steam from blowing through the liquid drain, a liquid loop seal is incorporated to the liquid drain line of the separator. Also, the steam and liquid lines are carefully sized so that at full flow, the pressure drop from the steam outlet to the recombined common point is smaller than that from the liquid drain outlet to the same recombined point. This ensures that the steam outlet pressure is less than the liquid drain line outlet pressure; hence, steam can only exit the dedicated steam line, where it is measured by a vortex flow meter and fluid thermocouples.

The ADS 1-3 separator, the steam line, the liquid line, and the recombined line are all insulated to minimize heat loss to the atmosphere. Furthermore, both the separator tank and the steam line are heat-traced to maintain a temperature of approximately 200°F to minimize nonprototypical steam condensation. Consequently, prototypical quality is preserved. The liquid loop seal is prefilled with hot water at approximately 180°F prior to actual testing. All these features ensure negligible energy flow to the atmosphere and proper energy transfer directly to the IRWST, as in the AP600.

2.1.7.2 ADS-4 Separators and Pipe Route

Two ADS-4 separators are used—one for each ADS-4 line. The separator connecting to the ADS-4 line from hot leg-1 (HL-1 on the CMT side) is the ADS 4-1 separator. The separator connecting to the ADS-4 line from HL-2 (pressurizer side) is the ADS 4-2 separator. The ADS 4-2 separator is sized to perform two functions—it serves to separate two-phase ADS-4 flow and separate break flow for certain cases. The ADS 4-1 separator is designed to separate two-phase ADS-4 flow only, and it can handle 150 percent of normal ADS-4 flow.

Each ADS-4 separator separates the two-phase mixture into single-phase steam and single-phase liquid for flow rate, pressure, and temperature measurements. The steam exits the top outlet nozzle while the liquid drains at the bottom outlet. A loop seal is used in the liquid drain line to prevent steam blowdown through the liquid line. The steam line connects to a common steam header, and the liquid

line connects to the primary sump tank. These connections simulate the ADS-4 operation process in the AP600, where the steam flow rises to the containment wall and liquid drains to the sump.

The ADS-4 separators, the liquid lines, and steam lines are all insulated to minimize condensation and heat loss. Also, the steam lines and separators are all heat-traced to maintain a temperature of approximately 200°F, and the liquid line loop seal is prefilled with hot water of approximately 180°F prior to actual testing.

2.1.7.3 Break Separator and Pipe Route

The following break simulations are tested:

- Small break at bottom of DVI line
- Double-ended break at DVI line
- Small break at bottom of cold-leg/CMT balance line
- Double-ended break at cold-leg/CMT balance line
- Small break at bottom of cold leg
- Small break at top of cold leg
- Small break at bottom of hot leg

The break separator is designed to receive two-phase break flow from the break source and separate steam and liquid for single-phase flow pressure and temperature measurement. The separator and steam lines are heat-traced, and the loop seal is prefilled with hot water to minimize heat loss and nonprototypical condensation.

In the event of a double-ended CMT-1 balance line break simulation, the break separator receives break flow from the cold-leg side of the break. The ADS 4-2 separator receives break flow from the CMT side of the break, and the ADS 4-1 separator receives all ADS-4 flow.

When a double-ended DVI line break is simulated, the break separator receives the flow from the reactor vessel side of the break. The sump receives the break flow from the DVI line.

2.1.8 Orifices and Nozzles

Orifices or flow nozzles are used in critical lines to scale the line resistances in the OSU test facility to the AP600. The bases for these devices are discussed in this section.

2.1.8.1 ADS 1-3 Flow Nozzles

Proper scaling of the flow through the ADS 1-3 lines requires that the quality of the flow be considered in sizing the nozzles. Since the mass flow through the nozzle depends on the flow quality, two venturi-type flow nozzles are used. Sharp-edged orifice plates are not suitable for this application

because their discharge coefficients vary with the Reynolds number, leading to wide ranges in mass flow as the quality changes. The flow nozzles were sized as follows:

- One set of flow nozzles for single-line simulation with small-break LOCA (SBLOCA)
- One set of flow nozzles for double-line simulation with SBLOCA
- One set of the nozzles for single-line simulation with large-break LOCA (LBLOCA)
- One set of flow nozzles for double-line simulation with LBLOCA

2.1.8.2 ADS-4 Flow Nozzles

Two types of flow nozzles are used in the test. The first type simulates a 50-percent flow area of one AP600 ADS-4 stage, and the second type simulates a 100-percent flow area of one AP600 ADS-4 stage. Fluid similarity is the scaling basis.

The scaling analysis requires that each line be properly scaled to have proper fluid similarity. For all scaling criteria, the pressure drop scaling ratio is an important criterion. The pressure drop ratio is $[\dots]^{a,b}$. Any line that does not meet this requirement must be fitted with an orifice plate to bring the pressure drop ratio to $[\dots]^{a,b}$.

2.1.8.3 Direct Vessel Injection Venturi

The DVI venturi scaling criteria are the same as break hole (venturi) scaling criteria. This is because the DVI venturi is used to restrict the break flow out of the reactor vessel. The geometry of the DVI venturi is the same as the AP600, and the throat diameter and the L/D ratio are properly scaled.

Figure 2.1-1 through Figure 2.1-4 are not included in this nonproprietary version.

Figure 2.1-5 Isometric Drawing of OSU Test Facility

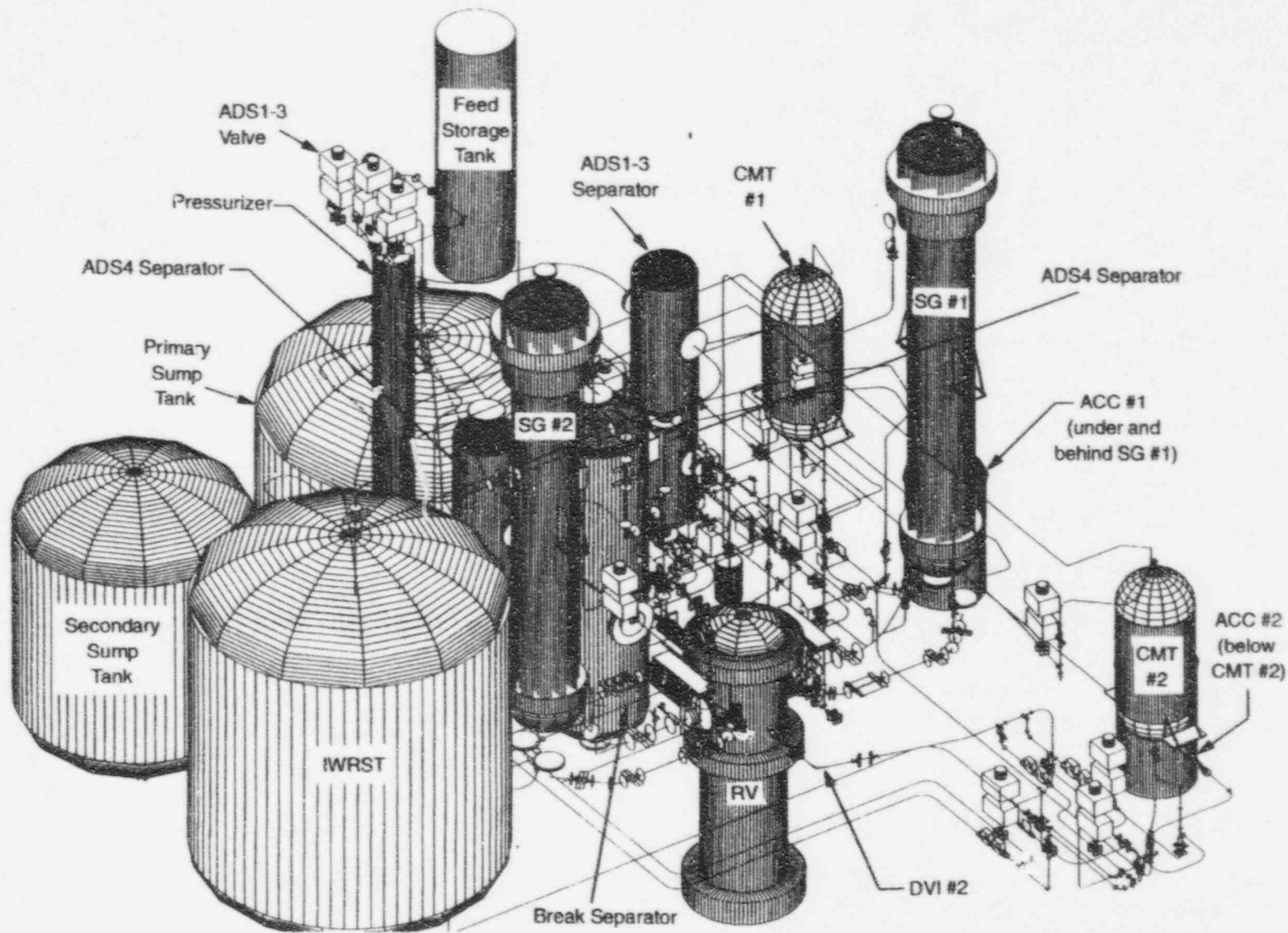


Figure 2.1-6 is not included in this nonproprietary document.



2.2 Facility Scaling

The design basis of the OSU test facility is the scaling analysis of the AP600, presented in *AP600 Low-Pressure Integral Systems Test at Oregon State University, Facility Scaling Report, WCAP-14270*.⁽⁶⁾ The scaling analysis guides the design of the test facility so that the thermal-hydraulic performance of the test facility properly simulates the phenomena important to the passive safety features of the AP600. The test facility is designed with reduced dimensions and lower temperatures and pressures than the actual reactor. The scaling methodology and the overall results are provided in this section.

2.2.1 Methodology

To ensure that the scaling objectives were met in an organized and traceable manner, a general scaling methodology (GSM) for the OSU test facility was developed. The model development methodology can be found in *Facility Scaling Report*.⁽⁶⁾ A flow diagram describing the GSM is presented in Figure 2.2-1.

The first step is to specify the experimental objectives. The experimental objectives define the types of tests to be performed in order to respond to specific licensing and design needs. The experimental objectives determine the general modes of operation to be simulated in the test facility.

The second step is to develop plausible phenomena identification ranking tables (PPIRTs). The nature of scaling prohibits exact similitude between the AP600 and the test facility operating conditions. As a result, the design and operation of the test facility are based on simulating the processes most important to passive safety system performance and long-term cooling. The function of the PPIRTs is to identify the key thermal-hydraulic phenomena to be scaled in the context of LOCA transients. Many of the phenomena of importance to AP600 LOCA behavior were already identified by existing phenomena identification ranking tables (PIRTs). However, some of the AP600 modes of operation were not verified. Therefore, additional thermal-hydraulic phenomena of importance were identified and included in the PPIRTs. Hence, PPIRTs were used rather than PIRTs.

The third step is to perform a scaling analysis for each of the modes of operation specified by the experimental objectives and further defined by the PPIRTs. The hierarchical, two-tiered scaling analysis (H2TS) developed by the U.S. NRC⁽¹⁾ was selected for the scaling analysis of this facility. Detailed discussion of the application of this method for the OSU test facility is also provided in *Facility Scaling Report*.⁽⁶⁾

The fourth step is to use the scaling analysis results to develop a set of characteristic time ratios (dimensionless π groups) and similarity criteria for each mode of operation. Because it is impossible to identically satisfy all of the similarity criteria simultaneously, the set included only those criteria which had to be satisfied in order to scale the most important phenomena identified by the PPIRT.

Step five is an evaluation of the scaling criteria to determine if the scale model geometry, initial conditions, or operating conditions would introduce significant scaling distortions. Distortions are also evaluated relative to other modes of operation.

2.2.2 Facility Scaling Parameters

The height scaling ratio was set at 1:4, and the diameter scaling ratio at 1:6.93. These ratios were based on the objective of minimizing power requirements while maximizing height and maintaining sufficient system volume to properly model loop pressure drop and three-dimensional flow in the downcomer, core, and plenum regions.

The important factors that were considered in determining the height scaling ratio were:

- Minimum diameter ratio was satisfied so that skin friction pressure drop requirements could be met easily with commercially available pipe and drawn tubing.
- Diameter choice was consistent with two-phase scaling and flow regime transitions.
- Fluid volume requirements were reasonable (e.g., IRWST volume ~3000 gal).
- Power requirements were reasonable (~600 kW).
- Time scale made long-term cooling test duration reasonable ($\tau_r = 0.5$).
- L/D ratio indicated that multi-dimensional flow effects would scale well under fluid property similitude ($L/D = 1.73$).
- Elevation was sufficient such that differential pressure measurements between hot and cold legs were well within instrument capability.
- Construction and material costs were economical.

The scaling ratio for the piping was selected to ensure that the frictional losses due to piping roughness did not bias the buoyancy effects that determine natural convection rates. Analysis of the buoyancy-friction balance equation resulted in a minimum diameter ratio of [\dots]^{a,b(3)}. Therefore, a minimum diameter ratio of [\dots]^{a,b} was selected because it was greater than the minimum and could be obtained with commercial pipe sizes. Also, thermal effects of this size piping (that is, heat losses and heat storage effects) could be modeled.

Once the length and diameter scaling ratios were determined, the dimensions of the test facility could be geometrically scaled. Table 2.2-1 summarizes the scaling ratios for the test facility.

2.2.3 Mass/Energy Balances

Since accurate measurements of the components of a two-phase flow mixture are difficult and the equipment to do these measurements is very expensive, two-phase flow was separated into its single phases and the individual single-phase flows were measured with conventional instrumentation. Therefore, all two-phase streams vented from the RCS are measured using conventional vapor-liquid separation devices. Where required to simulate AP600 systems, the resultant single-phase flows are recombined before being returned to the system. In other cases, the steam is vented and hot water from an auxiliary storage tank is injected to match the mass of the steam that would have condensed had the steam been released into the AP600 containment. It should be noted that the heat transport processes in the containment are not modeled in this test facility; however, the condensate return process is modeled.

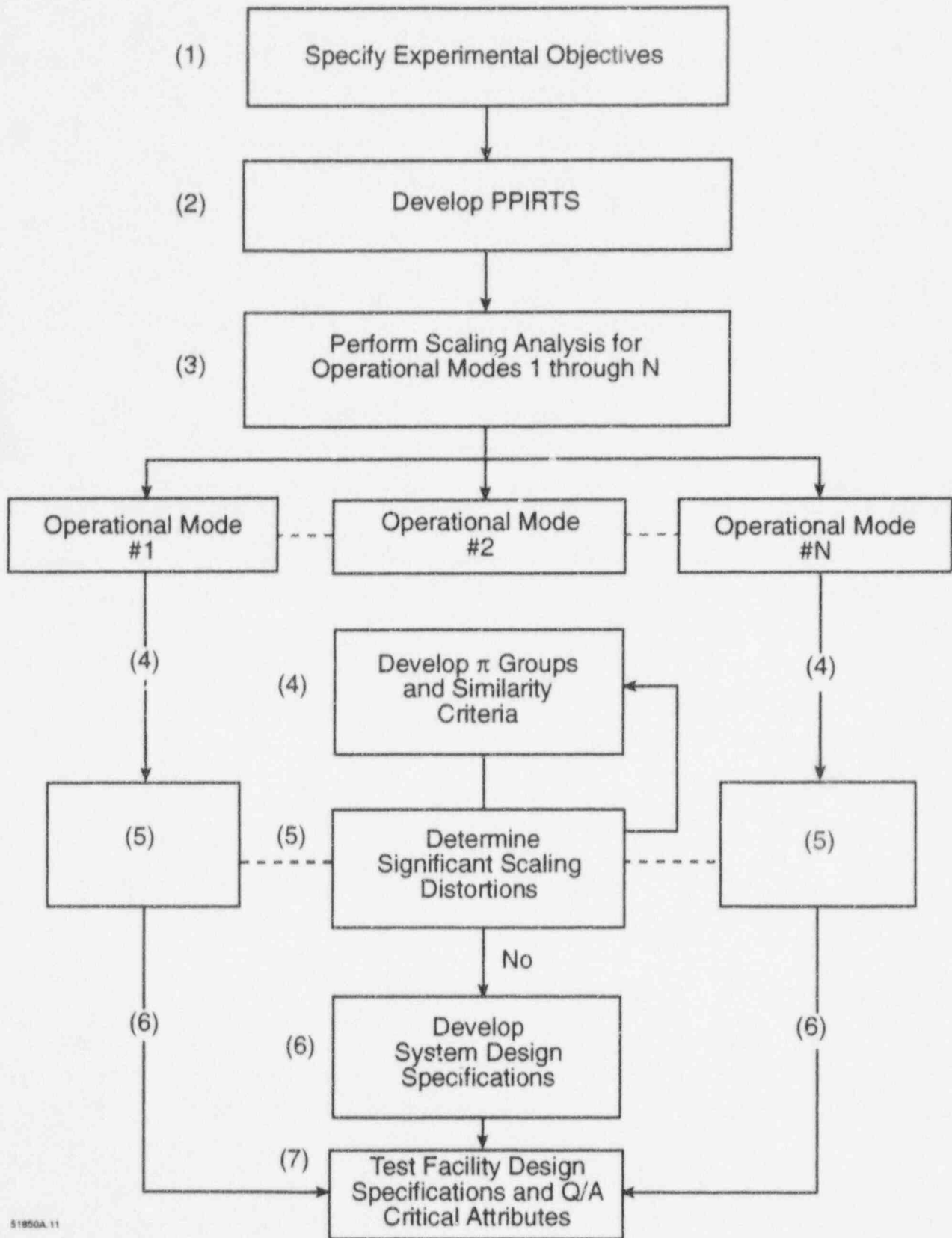
This approach permits accurate measurement of the two-phase flows released from the RCS with simple, relatively inexpensive components. Thermal-hydraulic similitude is maintained either by recombining the single-phase streams or by makeup of hot water for vented steam that would have been condensed.

TABLE 2.2-1
SUMMARY OF SYSTEM SCALING RESULTS FOR THE
1/4-LENGTH SCALE MODEL PRIMARY LOOP

Geometry					
	Length scaling ratio	1:4			
	System diameter scaling ratio	1:6.93			
	Area scaling ratio	1:48			
	Volume scaling ratio	1:192			
Flow					
	Velocity scaling ratio	1:2			
	Mass flow rate scaling ratio	1:96			
Residence Time					
	Time scaling ratio	1:2			
Power					
	Power scaling ratio	1:96			
	Power density scaling ratio	2:1			
Model Power Requirements					
		Percent of total power			
		5%	4%	3%*	2%
	AP600 decay power (MW)	97.00	77.60	58.20	38.80
	Model power (kW)	1009.58	807.66	605.75	403.83

Note:

*Nominal power used to simulate the decay heat in the model was 600 kW.



51850A.11

Figure 2.2-1 General Scaling Methodology

2.3 Facility Component Description

The system components are described in this section.

2.3.1 Reactor Vessel

The reactor vessel is a right-circular cylinder with a flanged hemispherical upper head and a flanged flat bottom. It models the following regions:

- Lower plenum
- Core
- Upper plenum
- Upper head

The lower plenum region is the region below the lower core plate of the reactor core. The net water volume in the AP600 lower region is modeled in the test. Since the reactor vessel inner diameter (I.D.) is determined by the proper scaling of upper-plenum volume, core region volume, and special downcomer region scaling criteria, the lower-plenum region cross-sectional area is slightly distorted on the scaling basis.

2.3.1.1 Vessel Design/Dimensions

All components of the reactor vessel are fabricated of Type 304 stainless steel. The reactor vessel, designed to Section VIII of the ASME Pressure Vessel Code,⁽⁵⁾ consists of a [] diameter, right-circular cylinder made by rolling and welding [] thick stainless steel plate, with a flanged hemispherical top and a flanged flat-plate bottom. Both the bottom and top flanges are []

[] flanges, which are machined to fit the outside diameter (O.D.) of the shell and are seal-welded. To facilitate assembly, the reactor vessel is fabricated in two sections, a [] lower section. These two sections are joined by welded [] slip-on flanges, machined to fit the O.D. of the shell. The vessel is fitted with four cold-leg flanged nozzles (300 lb), two hot-leg flanged nozzles (300 lb), and DVI flanged nozzles (300 lb). The bottom flange carries an endplate through which the heater tubes penetrate for connection to the electric power source. The bottom flange is fitted with a 1/2-in. thick Teflon™ insert to minimize the effect of the heat capacity of this flange. A 1/8-in. thick stainless steel plate retains the Teflon™ insert in this flange.

2.3.1.2 Reactor Vessel Instrumentation

Thirty-three Type K thermocouples (1/4 in. diameter, Type 304 stainless steel sheath) are installed in the reactor vessel to measure both wall and fluid temperature. Twenty-one differential pressure transmitters are connected to the various fluid volumes (upper plenum, lower plenum, downcomer,

etc.) to measure liquid levels, and eleven differential pressure transmitters measure pressure gradients. Specific instrument identifications and locations are shown in Appendix G, the P&IDs.

2.3.2 Rod Bundle

The rod bundle furnishes heat to the primary coolant in the reactor vessel to simulate the decay heat released by the AP600 following a plant trip or plant shutdown. The power scaling ratio for the rod bundle is 1:96.1, and the power density scaling ratio is 2:1. Since the maximum electrical power available at the test facility is 700 kW, the rod bundle at this power and with the power scaling factor of 1:96.1 simulates the AP600 decay heat at []^a of full core power. The AP600 decay power at 3.7 percent occurs about 70 seconds after the reactor is shut down; therefore, the heat input from the core during this short period is not fully modeled.

During the tests, most of the reactor transients were performed with the heater power at 600 kW, which is equivalent to a decay heat power of about 3 percent of full power. The rod bundle heaters were programmed to follow the calculated decay heat power starting at 600 kW.

The heater rod bundle controller was programmed to follow one of the two possible decay heat power input algorithms defined below, depending on the test configuration:

- For $0 \leq \text{time} < 140$ seconds

$$\text{Power (kW)} = 600 \text{ kW}$$

For time > 140 seconds

$$\text{Power (kW)} = \frac{600}{[1 + (0.01021 (\text{Time} - 140))]^{0.2848}}$$

- For $0 \leq \text{time} < 300$ seconds

$$\text{Power (kW)} = 600 \text{ kW}$$

For time > 300 seconds

$$\text{Power (kW)} = \frac{600}{[1 + (0.01021 (\text{Time} - 300))]^{0.2848}}$$

2.3.2.1 Rod Bundle/Heater Description

The rod bundle consists of 48 Type 304 stainless steel clad heaters, each with a maximum power of 15 kW. Overall rod bundle characteristics are shown in Table 2.3-1. The 1-in. diameter heater rods are 60-in. in overall length, with a 36-in. heated length and a wall thickness of 0.061-in. Power is skewed to provide higher heat fluxes at the top of the core by means of the resistance heater coil winding density. The power produced in each 6-in. incremental length of each heater rod (beginning at the bottom; that is the end closest to the electrical and thermocouple leads) is shown in the following:

Section	Heated Length (in.)	Power (W)	Heater Wire Size AWG No.	Heater Length (in.)
1	6	623	31	55-1/2
2	6	1758	28	39-1/4
3	6	2697	27	32-1/2
4	6	3373	26	32-1/2
5	6	3644	26	30-1/2
6	6	2905	26	37-3/4
Total	36	15,000		

A section of the heater with a reduced diameter of 0.5-in. passes through the lower flange and is sealed by a Swagelok fitting.

The following materials are used in the heated section with their available pertinent physical properties:

Electrical Insulation	Thermal Conductivity (Btu/°F in.-ft. ²)	Specific Heat (Btu/lb-°F)
80% boron nitride 20% magnesium oxide	95	0.306
Resistance wire 80% Ni 20% Cr (ASTM B-344)	---	---
Conductor 10 Ga nickel (ASTM B-160/E-39)	---	---

2.3.2.2 Rod Bundle Instrumentation

Type K thermocouples are installed in two groups of the heater rods; one group of heater rods does not have thermocouples. These groups and the location of the thermocouples are shown in the following:

Heater Group	No. of Heaters	Location of Thermocouples (Inches from Lower End of Heated Zone)
H-A	32	None
H-B	10	15, 21, 27, 33
H-C	6	3, 9, 21, 27

The leads for these thermocouples exit the rod at the lower end, together with the electrical power leads, through the Swagelok pressure seal. These thermocouples are provided as overtemperature protectors and are also recorded by the DAS.

Core coolant temperatures are measured by five thermocouple rods, each carrying at least three type K thermocouples.

2.3.3 Reactor Internals

The reactor internals have several functions related to core support and fluid flow. Specifically, the following components of the reactor internals provide these functions:

- Core barrel -- Separates core flow from downcomer
- Lower core plate -- Supports the fuel rods and distributes the flow
- Upper core plate -- Retains fuel rods in the axial position and provides support for the upper internals
- Upper support plate -- Supports upper head components
- Upper internals -- Provide guide tubes for the insertion of the in-core instrumentation and control rods
- Downcomer -- Provides a flow path for cold-leg fluid from the cold-leg nozzles to the core inlet plenum

2.3.3.1 Reactor Internals Design/Description

Core Barrel

The core barrel is composed of two sections of []° Sch. 30, type 304 stainless steel pipe []° flanged together at the center. The top section is []° and the bottom section is []° long. The top barrel plate is a ring []° O.D., welded to the top of the core barrel. This ring is sealed to the I.D. of the reactor vessel by two radial O-rings installed on O.D.s, thus permitting vertical expansion while limiting leakage. This plate includes 10 1/4-in. tapped holes that can be blocked with screws to adjust the leakage flow for the downcomer volume to the upper plenum.

During cold testing, it was found that all of these holes were needed to obtain the desired []° bypass flow. The loss coefficients (K) measured for one tapped hole were []^{ab} (upward flow) and []^{ab} (downward flow).

The bottom of the lower core barrel is welded to the lower core support plate. The lower core support plate, which is [] thick, is drilled with [] and [] diameter holes for the heater rods. This plate is supported from the reactor vessel on four pads, 90 degrees apart, on Belleville washers retained by a plunger that passes through the lower core support plate and the support pads.

The core barrel is sized to maintain the total core volume scaling ratio at 1:192 and the length ratio of 1:4.

Reflectors

The reflectors are simulated by cast ceramic inside a cylindrical shell that fits inside the barrel. A stainless steel liner is welded to the shell to provide the stepped cruciform flow volume for the simulated core. The reflectors are fabricated in two sections, separated horizontally at the simulated core midplane to facilitate assembly. The reflector sections are secured by four tie rods that pass through the two reflector sections and connect the upper reflector plate with the lower core support plate.

Grid Ring

A gridded support for the heater rods consists of 0.109-in. thick by 0.19-in. high bars welded to form an egg crate. Four bolts are used to attach the grid ring to the core barrel at the joint between the upper and lower core barrel.

Upper Internals

The upper internals are simulated by 41 guide tubes, each consisting of a rod [] in diameter with a 1-in. long threaded lower end. The threaded section screws into the upper core support plate. The guide tube top consists of a []

2.3.4 Hot-Leg Piping

Hot-leg piping provides a flow path from the outlet nozzle of the reactor vessel to the inlet to the SG. It also provides connections to the pressurizer surge line and to the fourth stage of the ADS and the PRHR.

Each primary loop has an identical hot leg made of [] Sch. 40 stainless steel pipe with an I.D. of [] The piping is a horizontal, straight run with an upward bend, [] between the reactor vessel and the SG. The vertical rise of the hot leg (centerline of the horizontal run to the centerline of the SG nozzle) is [] A flanged spoolpiece is provided at the reactor vessel nozzle.

Each hot leg is provided with the following instrumentation:

- One differential pressure transmitter
 - 0 to 25 in. of water
- One heat flux meter
 - 0 to 10 Btu/hr.-ft.²
- One heated thermocouple (fluid phase)
 - 70° to 550°F
- Two differential pressure transmitters (liquid level)
 - 0 to 20 in. of water
 - 0 to 25 in. of water
- One pressure transducer
 - 0 to 600 psig
- Two thermocouples
 - One 40° to 450°F
 - One 40° to 550°F

2.3.5 Cold-Leg Piping

The cold leg provides the coolant flow conduit from the outlet coolant nozzles of the SG to the inlet coolant nozzles of the reactor vessel. It also provides a connection for the line to the CMT.

Each of the two reactor coolant loops has two cold legs, each made of 3-1/2 in. Sch. 40 stainless steel pipe. The cold legs, which are entirely horizontal, are fitted with 300-lb, 45-degree flanged elbows at each end and a horizontal spoolpiece with 300-lb flanges. One end of each cold leg is connected to the discharge flange of the RCP, and the other end is connected to the coolant inlet flange of the reactor vessel.

The following instrumentation is provided for each of the four cold legs:

- Two differential pressure transmitters
 - 0 to 25 in. of water
- One magnetic flow meter (with transmitter; removed after the first matrix test due to repeated mechanical failure)
 - 0 to 250 gpm

- One heat flux meter
 - 0 to 10 Btu/hr.-ft.²
- One heated thermocouple (liquid phase)
 - 70° to 550°F
- One differential pressure transmitter (liquid level)
 - 0 to 25 in. of water
- One thermocouple (fluid temperature)
 - 70° to 450°F
- One thermocouple (metal temperature)
 - 70° to 550°F

2.3.6 Pressurizer Surge Line

The pressurizer surge line provides the flow path between the RCS and the pressurizer to transmit the pressures from the pressurizer to the flow system and to transfer fluid during volume changes. The pressurizer surge line consists of 3.5-in. Sch. 40, type 304 stainless steel piping that connects HL-2 with the bottom of the pressurizer. The line is provided with two sets of 300-lb flanges to facilitate assembly. The piping is arranged with six 90-degree bends to form a full 360-degree loop with a vertical line leading to the bottom of the pressurizer.

The pressurizer surge line is fitted with the following instrumentation:

- Six differential pressure transmitters (liquid level)
 - Three 0 to 20 in. of water
 - One 0 to 5 in. of water
 - One 0 to 10 in. of water
 - One 0 to 40 in. of water
- One differential pressure transmitter
 - 0 to 1 in. of water
- One heat flux meter
 - 0 to 100 Btu/hr.-ft.²
- Three heated thermocouples (fluid)
 - Two 0 to 100°F
 - One 70 to 500°F

- Two pressure transmitters
 - One 0 to 500 psig
 - One 0 to 400 psig

- Two thermocouples (fluid)
 - 70 to 450°F

- One thermocouple meter
 - 70 to 450°F

2.3.7 Pressurizer

The pressurizer provides the pressure control for the RCS. Pressurizer pressure is maintained at the required level by modulating the power input to the pressurizer heater. The control pressure is transmitted to HL-2 through the pressurizer surge line. The pressurizer also must provide degassing for the primary coolant.

The pressurizer consists of a shell of []^a type 304 stainless steel pipe with []^a Sch. 40 welded pipe caps at each end and an overall length of []^a

The 3-1/2 in. pressurizer surge line is butt-welded to the bottom weld cap. Four electrically heated 1-in. diameter rods, with an active length of []^c are installed through the bottom weld cap and are sealed by Swagelok fittings. Each heater rod is rated at []^c at full power. A []^a Sch. 80 line with a 90-degree elbow is provided on the top weld cap near the outer diameter for connection to the ADS.

A 1-in. diameter vent line is connected through a blind 300-lb flange with a high-pressure seal located at the center of the top weld cap. The vent line is controlled by a 3/4-in. electrically operated valve with a manually operated globe shut-off valve.

The following instrumentation is installed in the pressurizer:

- One heat flux meter
 - 0 to 100 Btu/hr.-ft.²

- One electric power meter/transmitter
 - 0 to 15 kW

- One differential pressure transmitter (liquid)
 - 0 to 120 in. of water

- One pressure transmitter
 - 300 to 400 psig
- One pressure transmitter
 - 0 to 500 psig
- Two thermocouples (fluid)
 - 70° to 450°F
- Three thermocouples (wall)
 - 70° to 450°F
- Four heater thermocouples
 - 70° to 450°F

2.3.8 Steam Generators

The SGs transfer heat from the primary coolant and generate steam from the secondary coolant. The SGs of the test model must meet the following additional functional requirements:

- Each of the test model SGs must be capable of removing 360 kW of thermal energy from the primary fluid while single-phase natural circulation conditions exist on the primary side. This represents a combined energy removal rate for both SGs equivalent to 3.8 percent of scaled decay power, which is the maximum rated power of the core heaters. The actual maximum heat rejection by the SGs is slightly less than the core heater input because of system heat losses.
- To properly model the initial conditions of SBLOCA scenarios, the test model SGs must be capable of removing the core energy deposited in the primary fluid while operating with secondary-side pressures that are very close to primary-side pressures. This requires that the tube surface area be sufficiently large to permit heat transfer with small temperature differences between the primary and secondary sides.

Each SG is fabricated of Type 304 stainless steel and is installed with its axis vertically oriented. The shell is []° in length, and the total length including axial nozzles is []° A hemispherical head, []° I.D. and 3/8-in. minimum thickness, is attached at the bottom by a flange. A conical section at the top enlarges the I.D. to []° to facilitate vapor separation. Steam is discharged from a []° diameter, flanged nozzle located axially at the center of the top semi-elliptical head, []° in O.D., []° minimum thickness. An air-operated ball valve is installed in the steam discharge line. This valve is controlled by a logic controller to maintain the appropriate pressure in the steam side during the test transients.

The tube bundle consists of []° U-tubes, []° average length, 11/16-in. O.D., 0.040-in. wall welded into a 2-in. thick flange at both the front and back faces. A shroud of []° thick Type 304 stainless steel plate surrounds the tubes and is welded to []° support rods that attach it to the tube sheet. The tube sheet is captured between the flanges of the lower head and is sealed by gaskets on both faces. Moisture is separated by a chevron-type device manufactured by Dyna-Therm™. This separator is located in the expanded diameter, upper section of the SG.

Feedwater is supplied to the shell side of the SG through a []° diameter line connected to an []° diameter spray ring made of []° Sch. 80 pipe supported inside the vessel by brackets. The hot leg is connected to the SG by a []° nozzle connected to the lower head and supplies hot coolant to the tubes. Primary coolant is discharged from the tube-side header through two []° diameter nozzles. Upon an S signal, the motor-operated feedwater isolation globe valve is closed.

The following instrumentation measures the important characteristics on the primary (tube) side of each SG:

- Two differential pressure transmitters
 - 0 to 3 in. of water
- Seven differential pressure transmitters (liquid level)
 - One 0 to 30 in. of water
 - Two 0 to 115 in. of water
 - Two 0 to 110 in. of water
 - Two 0 to 20 in. of water
- Five thermocouples (wall)
 - 40° to 450°F
- Six thermocouples (fluid)
 - 40° to 450°F
- One pressure transmitter
 - 0 to 500 psig
- One heat flux meter
 - 0 to 100 Btu/hr.-ft.²

The following instrumentation is provided to measure the secondary-side conditions during steady-state or transient operations:

- Two differential pressure transmitters (liquid level)
 - One 0 to 33 in. of water
 - One 0 to 135 in. of water

- Four thermocouples (fluid)
 - 40° to 450°F

- Two heat flux meters
 - 0 to 100 Btu/hr.-ft.²

2.3.9 Reactor Coolant Pumps

The RCPs provide the mechanical energy to circulate the primary coolant at its required flow rate through the RCS. Extended coastdown of the pump is not required.

There are four RCPs installed in the OSU test facility, one close-coupled to each of the cold primary coolant outlet nozzles from the lower head of each SG. These pumps are mounted vertically with the motor in the downward direction. The pump (which is a model QPHT5-4™ manufactured by the Queen Pump Co., Portland, Oregon) is a centrifugal pump with an internal fluid volume of 0.306 ft.³ and is driven by a 5-hp motor. The pump impeller and volute are modeled to simulate the AP600 pump components. During the tests, the coastdown of this pump was so rapid that the flow became immeasurably low as soon as the power was interrupted. The pump head-versus-flow correlation is shown in Figure 2.3-1.

The following instrumentation is provided for each of the pump seal cooling systems:

- One flow meter (visual)
 - 0 to 5 gpm

- One thermocouple (fluid)
 - 40° to 450°F

Flow meters and pressure devices that monitor and record pump performance are included with the cold-leg piping instrumentation.

2.3.10 Accumulators

The accumulators provide automatic, passive injection of water into the RCS following a loss of primary coolant.

One accumulator tank is connected to each of the DVI lines. The two accumulator tanks are identical, except that the coolant discharge line for the second tank is about []° further below the bottom of the tank than the discharge line for the first tank. The tanks are designed to the ASME Pressure Vessel Code, Section VIII, Division 1.⁽⁵⁾

Each tank consists of a []° type 304 stainless steel pipe. The top head is a welded []° stainless steel pipe cap, and the bottom is a []° thick plate that is welded to the barrel. Each tank is supported from the floor by a stand comprised of 61.3-in. long, 20-in. diameter carbon steel pipe, welded to 1/2-in. thick carbon steel base, 26-in. O.D. by 18-in. I.D. The base ring is anchored to the floor, and the upper end of the support is welded to the bottom plate of the tank. The centrally located discharge line, 1-1/4 in. Sch. 160, is fitted with a 90-degree elbow and exits horizontally through a cut-out in the tank support.

The vent/nitrogen inlet line enters the bottom of the tank through a Swagelok seal. The 1/2 in., 0.045 in. wall line is supported by a 6-in. long guide tube welded to the inside of the tank, with its center 9 in. from the barrel-top head weld. The height of this line can be adjusted by loosening the Swagelok, moving the tube to its new location, and resealing the Swagelok. Teflon™ ferrules are used for this Swagelok seal to facilitate this adjustable length. However, during the test program, the height of this line remained fixed at 36.8 in. from the inside surface of the bottom flange.

Each of the accumulators is equipped with the following instrumentation:

- One differential pressure transmitter (liquid level)
 - 0 to 55 in. of water
- One magnetic flow meter with transmitter
 - 0 to 40 gpm
- One heat flux meter
 - 0 to 100 Btu/hr.-ft.²
- One pressure indicator
 - 0 to 500 psig
- One pressure meter
 - 0 to 400 psig
- Three thermocouples
 - 40° to 450°F

2.3.11 Core Makeup Tanks

The CMT provides a volume of water maintained at cold-leg pressure by a balance line so that the water flows by gravity into the cold leg of the RCS on a loss of coolant. Each CMT is a cylindrical vessel oriented vertically and designed for operation at 400°F and 400 psi, according to the ASME Pressure Vessel Code, Section VIII.⁽⁵⁾ The vessel consists of a []°

]°

The cold-leg pressure balance line, which is made of []^a pipe, enters the CMT through the steam distributor. The steam distributor consists of a []^a long with a welded plug at the bottom. The stub is drilled with []^a diameter through-holes from a distance []^a above the end plug for a length of []^a. The steam distributor is retained between the faces of a []^a 300-lb flange joint with O-ring seals installed at the top of the CMT.

A vent line consisting of []^a is welded to the top head. A []^a O.D. nipple is welded to the center of the bottom head for connection to the DVI piping.

Each CMT has the following instrumentation:

- Four differential pressure transmitters (liquid level)
 - One 0 to 12 in. of water
 - One 0 to 40 in. of water
 - One 0 to 20 in. of water
 - One 0 to 65 in. of water
- Three heat flux meters
 - 0 to 100 Btu/hr.-ft.²
- One pressure transmitter
 - 0 to 500 psig
- 26 thermocouples (fluid)
 - 40° to 450°F
- Three thermocouples (heat flux meter)
 - 40° to 450°F
- 28 thermocouples (wall)
 - 40° to 450°F

In addition to the instrumentation on the CMTs, the following sensors are located on the cold-leg pressure balance line:

- One differential pressure transmitter
 - 0 to 30 in. of water
- One magnetic flow meter (with transmitter)
 - 0 to 15 gpm

- One heat flux meter
 - 0 to 100 Btu/hr.-ft.²
- Three heated thermocouples (fluid phase)
 - Two 0° to 100°F
 - One 0° to 500°F
- One differential pressure transmitter (liquid level)
 - 0 to 95 in. of water
- Two thermocouples (fluid)
 - 40° to 450°F
- One thermocouple (heat flux meter)
 - 40° to 450°F
- One visual temperature indicator
 - 40° to 450°F

2.3.12 In-Containment Refueling Water Storage Tank

In the AP600, the IRWST supplies water to fill the refueling cavity during refueling and stores water during normal plant operation. The IRWST also supplies water for emergency core cooling during a LOCA after the RCS has been depressurized and the water from the CMTs and accumulators has been exhausted. It also serves as the heat sink for PRHR during a normal shutdown. In the test model, the injection during loss-of-coolant events and the PRHR operation are modeled and investigated.

The IRWST is fabricated entirely of Type 304 stainless steel and is designed to meet the ASME Section VIII, Division 1 code⁽⁵⁾ requirements of []° The vertically oriented tank consists of a cylindrical section, []° It is made of []° thick plate, rolled and welded, with a 2:1 elliptical top head, []° thick. The bottom head is a []° The top and bottom differ because these components were available at the time the tank was fabricated. The bottom head is filled with ceramic covered with a []° to simulate the flat bottom of the AP600 IRWST.

A 30-in., 150-lb blind flange is welded to the top head to provide a manway for access to the tank internals. Steam vented from the ADS is condensed in the IRWST through a sparger. This component is discussed with the ADS in Subsection 2.1.4.

Two discharge lines are provided from the bottom head to the IRWST. The line to DVI-1 is []° and the line to the DVI-2 is []° Two 1-1/2 in., 150-lb flanges are

welded to the bottom head to mount two tubes that house thermocouples for internal fluid temperature measurements.

The PRHR HX is mounted inside the IRWST, and the inlet/outlet piping connections are made through welded 3-in., 150-lb flanges. Details of the PRHR HX are described in Subsection 2.3.18.

The following instrumentation measures the significant parameters of the IRWST during the transients being investigated:

- Three heat flux meters
 - 0 to 100 Btu/hr.-ft.
- Four load cells
 - 0 to 11,000 lbm
- One differential pressure transmitter (level)
 - 0 to 150 in. of water
- One pressure transmitter
 - 0 to 100 psig
- 19 thermocouples (fluid)
 - 40° to 450°F

2.3.13 Safety Injection Lines

The safety injection lines provide flow conduits for the water that is injected directly into the reactor vessel from the CMTs, accumulators, and IRWST.

The instrumentation for the safety injection lines is summarized in the following:

Instrumentation	CMT	ACC	IRWST	DVI
Differential pressure transmitter	1	1	2	
Magnetic flow meter	1	1	2	2
Magnetic flow meter transmitter	1	1	2	2
Thermocouple (fluid)	3	2	4	---

2.3.14 Containment Sumps

The LCS recirculates water from the containment sump through the reactor vessel to provide passive cooling for removal of decay heat. Recirculation starts when the water level in the LCS has reached

the elevation of the DVI. At this level, the recirculation line is filled and a density driving force exists as boiling in the core reduces the density of the liquid in the core compared to the cooler water in the sump. Steam is released to the containment through the ADS-4 valves on the hot legs and is condensed in the containment, eventually returning to the sump.

The model containment sumps simulate the volume in which water can collect from the leakage during hypothetical LOCAs. For most break locations, the AP600 reactor sump would fill and recirculation through the LCS would be initiated as soon as the water level reached the DVI line. However, some breaks could occur in compartments that are hydraulically isolated from the reactor sump, and those compartments must flood above a given elevation before the reactor sump begins to fill. This flow behavior is modeled by a primary sump tank that represented the reactor sump and a secondary sump tank that simulated the isolated compartments.

2.3.15 Automatic Depressurization System, Stages 1-3

The ADS consists of four stages. Stages 1 through 3 are described in this section. The function of the ADS is to reduce the pressure in the RCS by venting steam in a controlled manner to permit injection of cooling water from the CMTs, accumulators, and IRWST.

ADS 1-3, shown schematically in Figure 2.3-2, is connected to the top of the pressurizer through a []° Sch. 80 pipe. Separate branch lines are provided for each of the valves, and flanged nozzles are installed in each branch to permit adjustment of the flow resistance in each branch. A []° relief valve is tied into this line before the line is reduced for each of the ADS valves. The ADS-1 valve, which opens at the highest pressure, is a []° valve joined by []° Sch. 80 piping to the []° ADS-2 line from the []° ADS-3 line. The combined line from the ADS-1 and 3 valves is expanded to []° tubing with a []° wall thickness by a welded reducer. The []° line carrying the ADS-2 valve is connected to the []° tubing. The ADS valves are pneumatically operated ball valves; each valve is programmed to open at descending pressures.

Two-phase flows vented through the three valves are piped to a vapor-liquid separator. The liquid and steam mass flow rates are individually measured and then recombined and flow to the ADS 1-3 sparger through a []° pipe. Flow from the ADS enters the IRWST through a []° 300-lb flanged connection and is dispersed at about midlevel in the tank by a sparger. The sparger consists of a []° inlet line, which is expanded to []° Sch. 40 at the hub. []° sparger arms are connected to the hub in a cruciform arrangement. Each sparger arm has an active length of about []° which is drilled with []° holes []° in diameter.

The following instrumentation is installed in the ADS 1-3:

- Three flow meters (differential pressure)
 - Two 0 to 60 in. of water
 - One 0 to 325 in. of water

- Two magnetic flow meters
 - 0 to 60 gpm
- One heat flux meter
 - 0 to 100 Btu/hr.-ft.²)
- Three heated thermocouples (fluid)
 - Two 0° to 100°F
 - One 0° to 500°F
- One differential pressure transmitter (liquid level)
 - 0 to 140 in. of water
- Two pressure transmitters
 - 0 to 500 psig
- Three thermocouples
 - 40° to 450°F
- One thermocouple (heat flux meter)
 - 40° to 450°F

2.3.16 Automatic Depressurization System, Stage 4

The function of ADS-4 is to reduce RCS pressure near containment pressure. RCS pressure must be near the containment pressure in order for the IRWST water to be injected.

Two ADS-4 vent lines are provided, each connected to one of the hot legs. Each line, which models two lines in the AP600, consists of []^c which is connected to the hot leg through a flanged tee. The []^c pneumatically operated ball valve programmed to open after the ADS 1-3 valves open. After passing through a flanged flow nozzle used to adjust the line resistance, the two-phase flow enters a separator. The liquid from the separator flows to the primary sump; the steam flow is measured and then exhausted to the atmosphere.

The following instrumentation is provided for each ADS-4 line and separator:

- One vortex flow meter
 - 0 to 2000 scfm
- One differential pressure transmitter (liquid level)
 - 0 to 90 in. of water

- One pressure transmitter
 - 0 to 100 psig

- Two pressure transmitters
 - 0 to 500 psig

- Three thermocouples
 - 40° to 450°F

- One thermocouple (heat flux meter)
 - 40° to 450°F

2.3.17 Nonsafety Injection Systems

Two nonsafety injection systems, the CVS and the RNS, simulate the systems' operation during transient tests. Descriptions of these systems are provided in this section.

In the test facility, the CVS provides injection of additional feedwater into the SG channel head. In the AP600, this system is used to adjust the RCS water chemistry and maintain the system liquid volume. In the test facility, the RNS injects demineralized water into the CMT/DVI line, simulating properties of the AP600 RNS.

The CVS pump inlet is connected to the SG main feed header by 3/4-in. pipe. The pump, model 3333, type CB5-45, manufactured by Gould, is a multistage centrifugal pump with a 5-hp motor. Figure 2.3-3 shows the head-flow correlation for this pump. It discharges through a 3/4-in. pipe and check valve to an expanded section of 1-in. x 0.87-in. I.D. tubing with a motor-operated ball valve to the channel head of SG-2. A 1-in. diameter branch line with a manually operated ball valve is connected to the feed line of SG-1.

The RNS pump (Grundfos Pumps Corp., Clovis, CA, series C, model CR4-100N) receives flow from the main feed line through a 2-in. pipe.

Flow from the pump discharge is piped through 1-in. pipe and 1-1/4 in. diameter (1-in. I.D.) tubing with a 1-in. check valve and a 1-in. pneumatically operated ball valve. The pump performance curve is illustrated in Figure 2.3-4. A 2-in. diameter line is also connected to the discharge line from the pump to the IRWST injection line. This line is equipped with a 2-in. manually operated ball valve.

The following instrumentation is provided for these systems:

Instrument	CVS	RNS
Magnetic flow meter	0 to 8 gpm	0 to 60 gpm
Visual pressure indication	0 to 600 psig	0 to 300 psig
Pressure transmitter	0 to 500 psig	0 to 250 psig
Temperature	40° to 450°F	40° to 450°F

2.3.18 Passive Residual Heat Removal

The PRHR HX removes decay heat from the core absolutely passively during an emergency shutdown in which heat cannot be rejected through the SGs or RNS.

The AP600 has two 100-percent capacity PRHR HXs, each capable of removing 2 percent of the core power using natural circulation. The C-type tube HXs are located in the IRWST and can operate at full system pressure.

A single PRHR HX is installed in the OSU test facility. This loop consists of piping from the reactor vessel to the C-tube HX mounted inside the IRWST. Heat is transferred from the C-tubes to the water in the IRWST by conduction and natural convection. Flow from HL-2 enters the C-tube HX through a 1-1/2 in. Sch. 80 line with a normally open ball valve and a magnetic flow meter. The cooled liquid flows from the bottom header of the C-tube HX through 1-1/2-in. tubing (1.26-in. I.D.) with a normally closed pneumatically operated ball valve and magnetic flow meter to the channel head of SG-2. A drain line with a normally closed needle valve is connected to the condenser drain header.

The following instrumentation is provided for the PRHR:

- Two magnetic flow meters (with transmitter)
 - 0 to 15 gpm
- Two heat flux meters
 - 0 to 100 Btu/hr.-ft.²
- Three heated thermocouples (fluid)
 - Two 0° to 100°F
 - One 0° to 500°F
- Two differential pressure transmitters (liquid level)
 - One 0 to 10 in. of water
 - One 0 to 70 in. of water

- Nine thermocouples (fluid)
 - 40° to 450°F
- Two thermocouples (heat flux meter)
 - 40° to 450°F
- One visual temperature indicator
 - []°
- Eight thermocouples (wall)
 - []°

2.3.19 Break Simulators

The break simulators provide controlled leakages that simulate failures of RCS piping in the AP600. Each break simulation for the hot leg and cold leg consists of a flanged spoolpiece installed in the line in which the break is to be simulated. A line with a pneumatically actuated ball valve is connected to the spoolpiece and conducts the leakage flow to the BAMS, which is described in Subsection 2.3.20.

There are four break simulation locations in the test facility—one at the hot leg, one at the cold leg, one at the DVI line, and one at the CMT-1 balance line. All break locations are capable of simulating a single-ended break of a desired size. In addition, the DVI line break and the CMT-1 balance line break can also simulate double-ended guillotine (DEG) piping failures. The flow out of each of these breaks is typically two phase.

The break separator is equipped with four inlets and two outlets. Only one of these four inlets is used at a time, and their elevations are important. There are three inlets located below the curb/overflow level—one at cold-leg elevation for cold-leg break simulation, one at hot-leg elevation for hot-leg break simulation, and one at DVI elevation for DVI break simulation. For example, the cold-leg break inlet must be at the same elevation as the cold-leg break location. If it is located at a higher elevation, it will create backpressure at the break source (that is, break hole at the cold leg) and subsequently will change the thermal-hydraulic characteristics of the break flow. Similarly, the hot-leg break inlet is located at the hot-leg break hole elevation, and the DVI break inlet is located at the DVI break elevation.

The fourth inlet of the break separator is located at a level between the curb/overflow level and the lowest break above the curb/overflow level. This inlet is used for the CMT-1 balance line break. This arrangement allows one inlet for several break locations above the curb/overflow level without introducing improper backpressure on the break source. The break separator also has a loop seal at the liquid drain line to prevent steam from blowing out of the liquid drain line and ensure valid liquid flow measurements.

Instrumentation for the break system is included in the discussion of the BAMS.

The steam outlet line is directed to the common header, as described previously. The separator, the loop seal lines, and the steam line are preheated and insulated to minimize heat loss to the atmosphere and to prevent steam condensation. Heating the loop seal lines also ensures that the temperature of the condensate is close to the temperature at which it would collect in the AP600 containment sump.

2.3.20 Break and ADS Measurement System (BAMS)

The BAMS accurately measures the steam and liquid flows from the four ADS stages and each break simulator being tested. The approach used to accurately measure these two-phase flows is to separate each two-phase flow stream into its liquid and vapor components and then to measure the flow rate and temperature of each single-phase flow stream. For the ADS-4 and break separator, the vapor streams are vented to the atmosphere and the liquid phases are collected in the primary sump, which simulates the containment sump in the AP600. The capability exists to pump heated water from the condensate tank into the primary sump tank at a mass flow rate equivalent to the rate of vented steam. This water simulates the flow of condensate from the steam vented into the containment that would be condensed and would drain into the containment sump. The steam and liquid flows from the ADS 1-3 separator are recombined and flow into the IRWST through the sparger.

The BAMS consists of four separators and the associated piping and instrumentation to measure the single-phase flows and to conduct streams to the appropriate location. The following provides the data for the separators, which are made of type 304 stainless steel by Wright-Austin Company, Detroit, Michigan:

SEPARATOR DATA						
Tank	Model No.	Length (in.)	Diameter (in.)	Inlet	Vapor Outlet Diameter	Liquid Outlet Diameter
ADS 1-3	8-in. type RR	56	20	4 in.	4 in.	4 in.
ADS 4 (two tanks)	5-in. type 14R	62	20	3-1/2 in. Sch. 40	5-in. Sch. 40	3-1/2 in. Sch. 40
Break	14-in. type 14RR	146	32	4-in. Sch. 40	10-in. Sch. 40	4-in. Sch. 40

Instrumentation provided for the BAMS fluid measurements are as follows:

- Three magnetic flow meters (liquid)
 - Two 0 to 45 gpm
 - One 0 to 60 gpm

- Five vortex flow meters (steam)
 - One 0 to 7060 scfm
 - One 0 to 12,500 scfm
 - One 0 to 22 scfm
 - One 0 to 6000 scfm
 - One 0 to 11,000 scfm

- Three pressure transmitters
 - 0 to 60 psig

- 10 thermocouples (fluid)
 - 40° to 450°F

- 14 thermocouples (trace heater)
 - 40° to 450°F

2.3.21 Test Support Systems

Several systems that are not AP600 models are required to operate the test facility. These systems are as follows:

- Demineralized water system
- Fill-and-drain system
- RCP seal cooling system
- Electrical system
- Trace heaters
- Insulation

2.3.21.1 Demineralized Water System

City water is passed through two filters, connected in parallel, each with a differential pressure transmitter to indicate plugging. The combined flow from the filters is split into two streams, each passing through a separate and isolatable bank of demineralizers. After passing through another set of filters, the demineralized water flows to the feed storage tank. Feed lines that bypass the demineralizers are also provided to fill the RCP seal cooling system and the direct condensate tank. All lines are 1-in. stainless steel tubing with manually operated ball valves.

2.3.21.2 Fill-and-Drain System

Demineralized water from the feed storage tank is pumped by a single feedwater pump to the SGs. The feedwater line consists of a 2-in. Sch. 80 pipe from the feedwater tank and 1-in. tubing, with a 0.87-in. I.D. from the feedwater pump to the SGs.

Fill lines to the primary and secondary sumps are connected to the main feed header upstream of the feedwater pump. The RNS pump suction also is connected to the main feed header.

2.3.21.3 RCP Seal Cooling System

Heat is removed from the seals of the four RCPs by the closed-circuit RCP seal cooling system. Water is circulated by a centrifugal pump, through a jacket surrounding each pump seal. Heat is rejected from the coolant by a fan-driven, water-to-air HX. An expansion tank with a liquid level switch is mounted on the building roof. Thermocouples measure the temperature at each seal, and the flow to each seal is monitored by a visual flow indicator.

2.3.21.4 Electrical System

The electrical system for the OSU test facility is shown in Figure 2.3-5. Three-phase, 480-V electric power is supplied to the facility from a 1000-kVA, 4160-V transformer located outside the building. Power is divided into five circuits, two 600-A circuits and three 200-A circuits. The 600-A circuits supply the rod bundle heaters, and the 200-A circuits power the pressurizer heaters, trace heaters, and motors. Current transformers connected to the 600-A circuits and the 200-A circuits to the pressurizer supply input to the power meters for each bank of reactor heaters and the pressurizer heaters. Redundant current transformers and power meters are provided for the reactor heaters to verify the important data and to provide instrumentation backup.

Eight rod bundle heaters are connected in parallel, and three sets of heaters form a delta connection of 24 heaters connected to one of the SCR power controllers. A circuit breaker is installed in the circuit to provide a safety trip. An identical electrical system is provided for the other 24 rod bundle heaters.

The four 3-1/4 kW pressurizer heaters are connected to the 200-A line, which is also equipped with a circuit breaker for emergency trip. Power to the heaters, which are wired in a delta arrangement, is controlled by an SCR.

A 200-A line supplies power to the trace heaters. Power to the motor control panel is furnished by the 100-A line.

2.3.21.5 Trace Heaters

The BAMS separators and piping (up to and including the flow meters) are heated to about 220°F to prevent condensation of the steam content, which would affect the steam/water mass ratios and the accuracy of the energy balances being measured. These trace heaters (rated at 20 kW/ft. and 277 V), which are arranged in 14 separate zones, each with on-off control, are Raychem Chemelex Heat Tracing Systems, Model 20XTV2-CT™.

For the tests, heater density was based on raising the BAMS tanks to 220°F from an initial temperature of 180°F in 4 hours, including heating water in the tanks. Piping heaters were based on preheating the piping in the BAMS to the same temperature.

2.3.21.6 Insulation

Thermal insulation is installed on all tanks and piping, except the CMTs and accumulators. Four types of insulation are used:

- 2-in. Fiberglass, Manville Micro-lok™, $k_{eff} = 0.31$ Btu-in./hr.-ft.²-°F at 200°F
- 1-in. Fiberglass, Manville Micro-lok™, $k_{eff} = 0.31$ Btu-in./hr.-ft.²-°F at 200°F
- 1-1/2 in. Polyisocyanurate Foam, Dow Plastics, $k_{eff} = 0.141$ Btu-in./hr.-ft.²-°F at 75°F
- Removable Blankets, Ceramic Fiber, Lewco Specialty Products, $k_{eff} = 0.55$ Btu-in./hr. ft²-°F at 600°F

Table 2.3-2 is a matrix listing the insulation types for the major components and piping systems.

TABLE 2.3-1
ROD BUNDLE CHARACTERISTICS

Characteristic	Metric	English
Number of heater rods	48.	48
Maximum power per rod	15. kW	51,200. Btu/hr.
Rod diameter	2.54 cm	1.00 in.
Heated length	91.4 cm	36. in.
Heated surface area	730.3 cm ²	113. in. ²
Rod cross-sectional area	5.07 cm ²	0.785 in. ²
Heated volume	46. cm ³	28.3 in. ³
Total heated surface area	35,000. cm ²	5420. in. ²
Total heated cross-sectional area	243. cm ³	37.7 in. ²
Total heated volume	22,300. cm ³	1360. in. ³
Heater rod pitch	4.01 cm	1.58 in.
Pitch/diameter ratio	1.58	1.58
Subchannel flow area	11.0 cm ²	1.71 in. ²
Hydraulic diameter	5.52 cm	2.18 in.
Average rod heat flux	11.5 W/cm ²	
Radial power peaking factor	1.31	
Axial power peaking factor	1.47	
Hot channel factor	1.93	

**TABLE 2.3-2
INSULATION APPLICATIONS**

	Insulation		
	2-in. Fiberglass	1-in. Fiberglass	1-1/2 in. Urethane
RCS	X		
Pressurizer	X		
ADS 1-2		X	
ADS - common line	X		
SGs	X		
Condensate return tank	X		
Steam line		X	
Condensate piping		X	
IRWST			X
Primary sump			X
Primary sump piping			X
Secondary sump			X
DVI system piping		X	
ADS separators and piping			X
Drain collection tank			X
Break separator tank and piping to primary sump			X

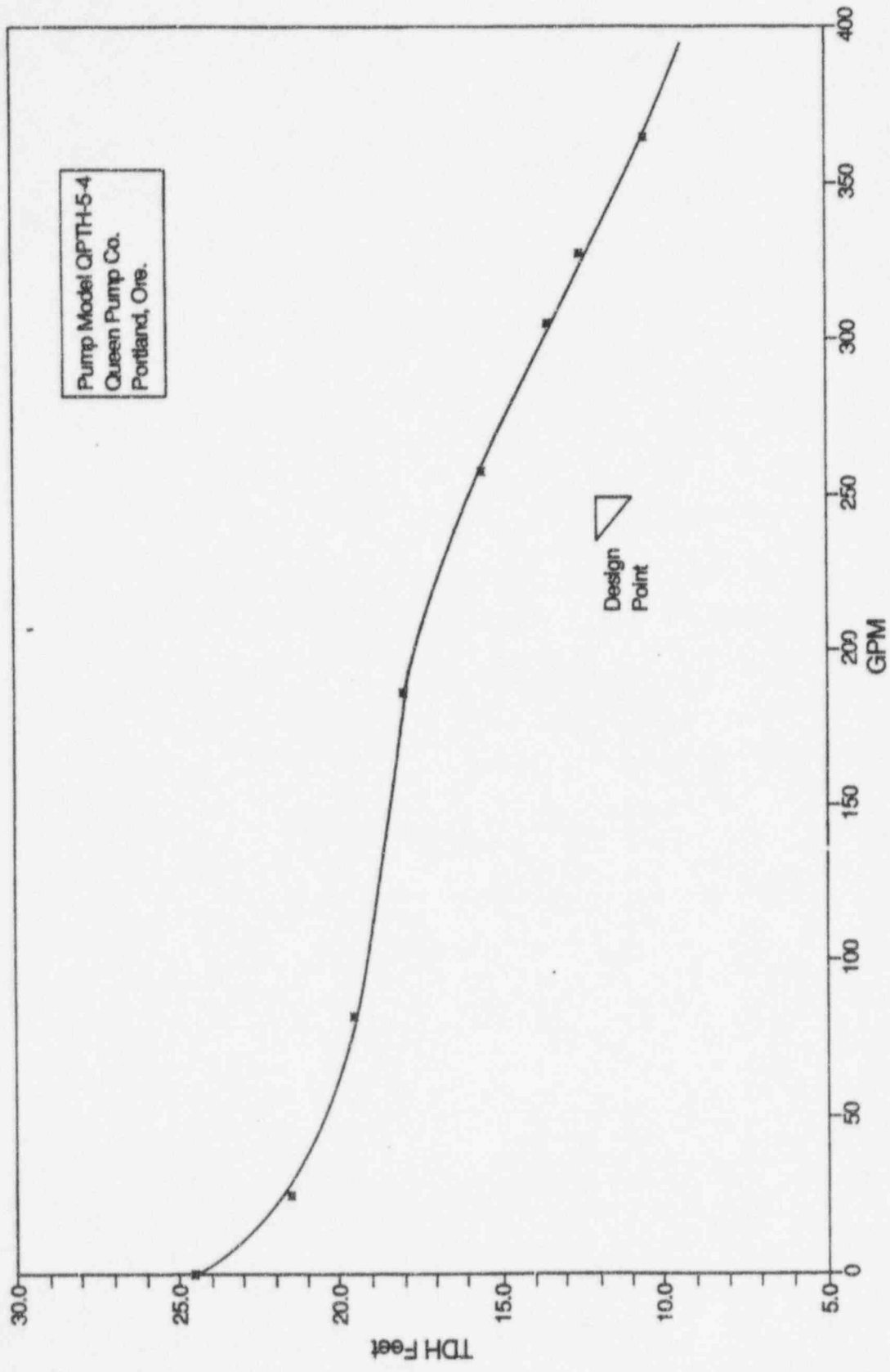


Figure 2.3-1 RCP Performance Head Versus Flow

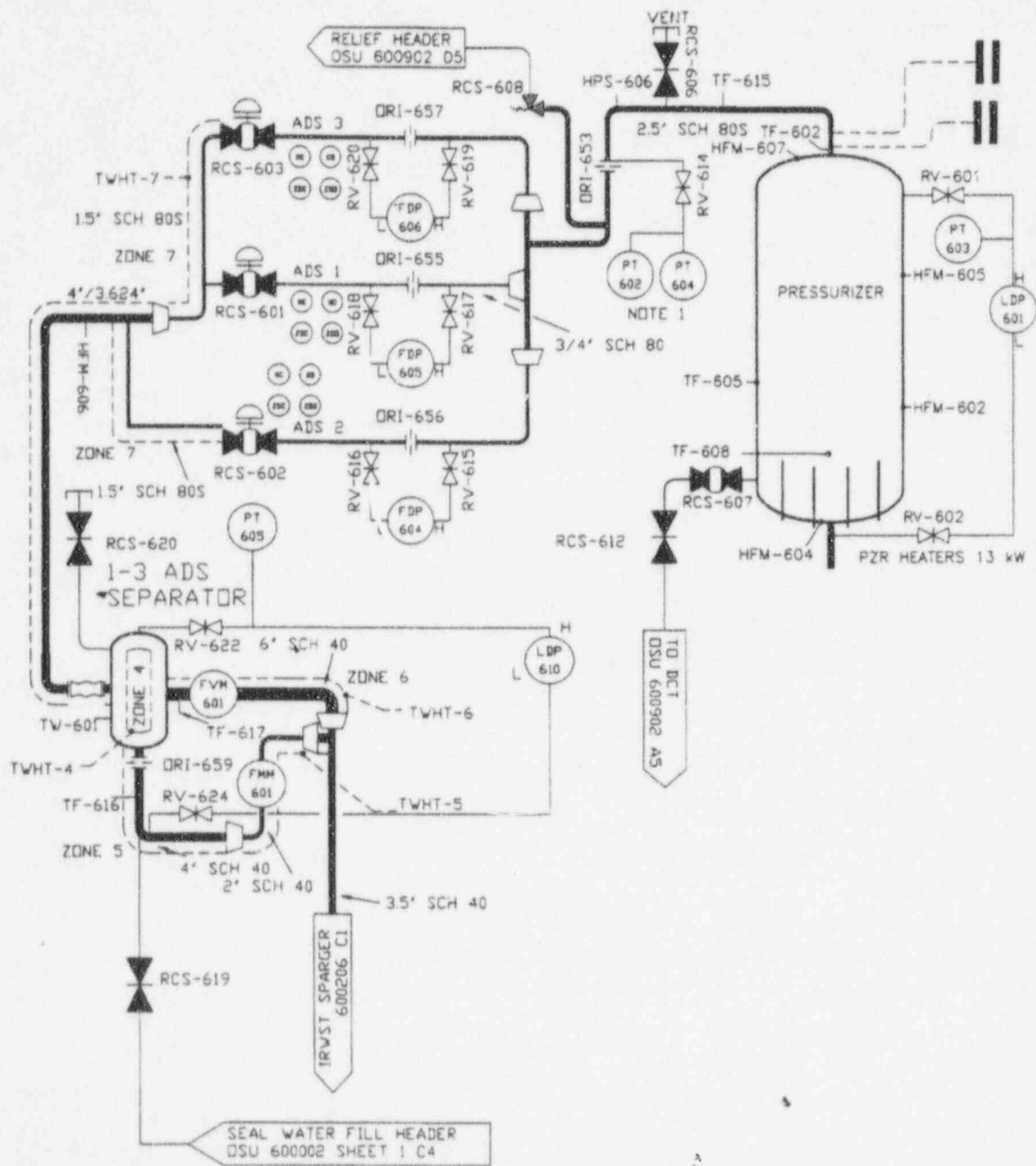


Figure 2.3-2 Flow Schematic for the ADS

Figure 3.18.3-1: CVS Pump Head vs. Flow

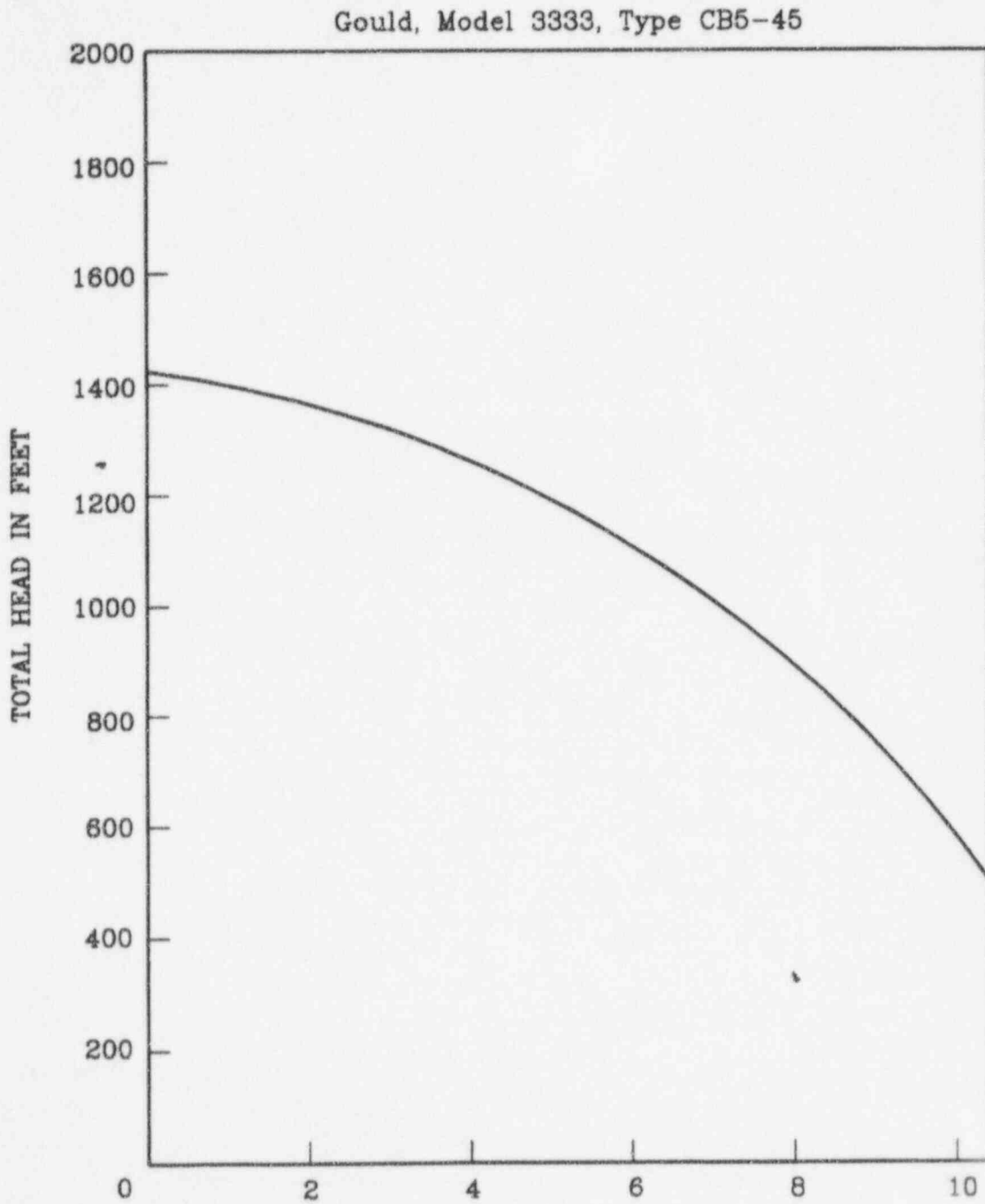


Figure 2.3-3 CVS Pump Head Versus Flow

Figure 3.18.3-2: RNS Pump Head vs. Flow

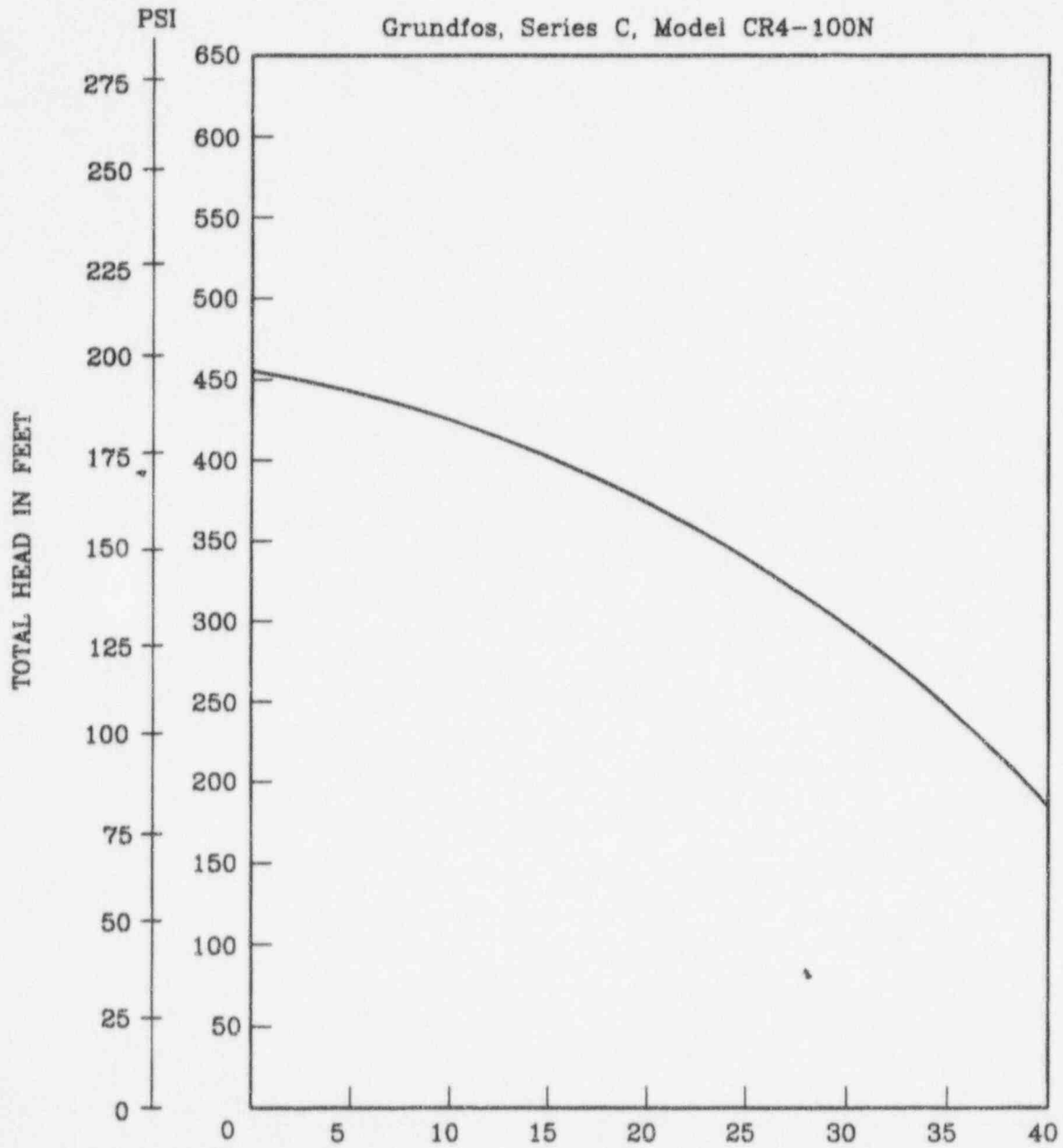


Figure 2.3-4 RNS Pump Head Versus Flow

Figure 2.3-5 is not included in this nonproprietary document.

2.4 Instrumentation

This section provides general information about instrumentation used at the OSU test facility and specific instrumentation anomalies that occurred during testing.

All instruments referenced in this section can be found in the OSU test facility piping and instrumentation drawings (P&IDs), Appendix G, and in the OSU AP600 Instrumentation Data Base, Appendix C. The first two drawings of the P&IDs are a legend (OSU 600LEG, Sh. 1 and 2), which provide information about instrument numbering. In general, all instrument identifications contain a two- or three-letter prefix, followed by a three-digit number. The letters represent the type of instrument; the number provides the system number and sequential number of that instrument in that system. For example, PT-107 is a pressure transmitter (PT), located in the pressure vessel (100 series), and has the sequential number 7.

2.4.1 General Information on Instrumentation

This subsection contains general information about the OSU test facility instrumentation. The instrument channel designator for each instrument is provided in parentheses at the beginning of the subsection describing the instrument.

2.4.1.1 Differential Pressure Transmitters (FDP, LDP, DP)

Differential pressure transmitters measure three different parameters and have a prefix representing their application. The transmitters measure flow (FDP), level (LDP), or differential pressure (DP). Rosemount™ Model 3051 transmitters measure small differential pressures of 0 to 150 in. H₂O, and Rosemount™ Model 1151 transmitters measure differential pressures greater than 150 in. H₂O.

The only application of FDPs is to measure the differential pressure across the flow orifices in the ADS-1, ADS-2, and ADS-3 lines (FDP-604, FDP-605, and FDP-606). Differential pressure transmitters measure levels in all facility tanks, the RCS hot-leg and cold-leg pipes, SG tubes, and PRHR HX tubes.

The high- and low-pressure sides of all differential transmitters are plumbed to a component via two 3/8-in. O.D. stainless steel tubing sense lines. The transmitters are mounted on one of several instrumentation racks at the ground elevation of the facility, at a lower elevation than both of the sense line taps at the component. The sense lines are filled and vented via vent plugs at the transmitter and high-point vent tees with caps located on the sense lines above the sense line connection to the component. The instrument can be isolated by closing root valves on the sense lines close to the sense line taps at the component, or by closing isolation or block valves at the manifold of the transmitter at the instrument rack. An equalizing valve is provided for each transmitter to equalize the high- and low-pressure sides of the transmitter.

The bench calibration of all differential pressure transmitters is the same. The 4- to 20-mA signal output of the transmitters is input to the DAS. However, the field setup is different for LDPs than for DPs and FDPs, because LDPs are designed to measure levels and not differential pressures due to flow head loss.

For the performance of the tests, the LDPs were aligned in the field to output a minimum signal, 4 mA, when the measured level in the component was at or below the lower sense line tap or variable leg tap. Maximum output from the transmitter, 20 mA, occurred when the level reached the upper sense line tap or reference leg tap. In this way, the DAS could directly interpret the output of the transmitter as level indication. The configuration file included in every test data file provides the range of each LDP, corresponding to the distance between the level taps. It should be noted that the field adjustment of LDPs did not affect the bench calibration of the transmitter because the adjustment was made in the digital space of the transmitter electronics.

The LDPs were calibrated at ambient temperature. The transmitters did not mechanically or electronically temperature-compensate their output to correct for measuring levels of fluid at elevated temperatures. Therefore, level data recorded by the facility's DAS were uncompensated.

2.4.1.2 Pressure Transmitters (PT)

The pressure transmitters (PTs) are Rosemount™ Model 1151 transmitters, identical to the differential pressure transmitters, except the low-pressure side of the transmitter senses atmospheric pressure. The transmitters are plumbed to the component by a 3/8-in. O.D. sense line.

2.4.1.3 Magnetic Flow Meters (FMM)

Foxboro™ magnetic flow meters (FMMs) measure liquid flow. The FMMs consist of a ceramic-lined flanged flow tube connected to a remotely-mounted transmitter. The transmitter energizes the flux-producing coils of the flow tube, which then produces voltage across a pair of electrodes proportional to the liquid flow rate in the tube. This flow tube voltage is measured by the transmitter and converted to a 4- to 20-mA signal measured by the DAS.

The FMMs are not designed to accurately measure steam or two-phase flow. The data from the transmitters are invalid when either of these are measured.

2.4.1.4 Heated Phase Switches (HPS)

Heated phase switches (HPSs) manufactured by Reotherm™ measure fluid phase. There are 12 switches: one each on the cold and hot legs, CMT balance lines, PRHR HX inlet, and ADS 1-3 header. In addition, two switches are installed in the pressurizer surge line. The design of the HPS is an adaptation of a flow meter design used to measure flow rate.

An HPS consists of two elements, a transducer and electronics unit. The transducer is a single probe containing two sensors inserted 1 in. into a pipe. One of the sensors is at equilibrium with the fluid; the other is located near a heater so that its temperature is slightly above that of the unheated sensor. The temperature of the sensor located near the heater is a function of fluid state. The signals from the two temperature sensors are sent to remote electronics mounted inside a cabinet.

The HPS electronics process the two input temperature signals and output three signals to the DAS identified as HPS-XXX-Y, where XXX is the unique instrument channel number assigned to the HPS and Y is 1, 2, or 3. The instrument channel identified as 2 is the delta temperature between the heated and unheated temperature sensors, the channel identified as 3 is the fluid temperature measured by the unheated temperature sensor, and the channel identified as 1 indicates the phase of the fluid.

During testing, the 1 instrument channel output of the HPS was a 0- to 10-volt signal that was converted by the DAS to a 0 to 100 percent indication. A low voltage, or small percentage, was designed to indicate a gas phase; a high voltage, or large percentage, was designed to indicate a liquid phase. When the HPS was functionally checked after installation, it operated properly, providing more than 9 volts with water in the system and providing -2 volts with the system drained and air in the system. Test results from the 3 instrument channel during matrix testing when steam and two-phase fluid were present were not conclusive. Further analysis is required to determine the accuracy and usefulness of the 1 data. The fluid temperature measurement of the 3 channel is considered accurate.

2.4.1.5 Heat Flux Meters (HFM, TFM)

The RdF heat flux meters measure heat flux through pipe or tank walls. The small, wafer-thin instruments are glued to a pipe or tank surface. Three thermocouples are imbedded in to each HFM. Two thermocouples measure temperature on either side of the HFM. The thermocouple signals are measured by the DAS, and their temperature difference is converted to a heat flux using coefficients provided by the vendor. The third thermocouple measures the temperature of the surface.

During testing, the heat flux calculation of the DAS was designated as a HFM data channel. The wall temperature measurement of the heat flux meter was designated as a TFM data channel. An energy balance was not performed, so the output of the HFM was not evaluated.

2.4.1.6 Vortex Flow Meters (FVM)

Fourteen Foxboro™ vortex flow meters (FVMs) measure steam flow in the test facility. The FVMs consist of a flanged flow tube connected to remote electronics. The FVMs measure steam flow from the ADS 1-3, ADS 4-1, ADS 4-2, and break separators. In addition, they measure steam flow from the primary sump, the IRWST, and in the BAMS header.

As steam flows through the flow tube, a vortex-shedding element causes vortices to form and shed at a rate proportional to the flow velocity of the steam. The vortices create an alternating differential

pressure that is sensed by a detector and converted to a voltage output to remote electronics. Remote electronics convert the voltage input signal to a 4- to 20-mA signal measured by the DAS.

2.4.1.7 Load Cell Transmitters (LCT)

The mass of water in the IRWST, primary sump, and secondary sump is measured by load cells mounted under the four supports of each tank. The load cells contain strain gages that are stressed by applied shear forces from the weight of the tank and its contents. The strain gage produces a millivolt output proportional to the mass of the water in the tank. The input signal from the four load cells of the tank is processed by a transmitter mounted in close proximity to the load cells. The 4- to 20-mA output of the transmitter is measured by the DAS.

After the transmitter was calibrated, it measured only the weight of water in the tank. The transmitter also provided local indication of weight in the tank for use by test personnel.

2.4.1.8 Thermocouples (TF, TW, TH, TR)

Thermocouples are assigned one of four instrument designations, depending on the thermocouple's application. A TF thermocouple inserted through the wall of a pipe or tank or mounted on a thermocouple rod measures fluid temperature. TW thermocouples are mounted on the inside or outside walls of a tank or pipe. TR thermocouples, unique to the reactor vessel, are mounted on vertical thermocouple rods installed in the reactor vessel. TH thermocouples are mounted on the heaters for the reactor vessel and the pressurizer.

Thermocouple type and thermocouple diameter are specified in the OSU AP600 Instrumentation Data Base, Appendix C. The database also specifies the insertion depth of through-wall fluid thermocouples (TF). Inside wall thermocouples are mounted in a groove cut into the wall of the component and silver-soldered to keep them in place.

The reactor vessel contains TH thermocouples to measure temperatures of selected heaters. Selected heater thermocouples are used as inputs to the safety shutdown of the reactor heaters to detect abnormally high temperatures. Appendix G, Dwg. OSU 600007 and 600008 provide information on the location of the heater thermocouples. The drawings provide the orientation of the heater thermocouples in the core, as well as the mounting elevation of the thermocouples. The elevation of the thermocouples specified on the drawings is referenced to the bottom of the reactor vessel. Heater thermocouples are also mounted in heaters of the pressurizer. Appendix G, Dwg. OSU 600203 provides the location of the three pressurizer heater thermocouples.

Thermocouples mounted in hollow rods (TR thermocouples) are unique to the reactor vessel. Five thermocouple rods are installed in the reactor vessel to provide radial and axial fluid temperature distributions in the heated section of the reactor vessel. Each rod contains thermocouples mounted along its entire length. Thermocouples protrude from the hollow rod and are sealed from the outside

with silver solder. Wires for the thermocouples are routed inside the rod, through the bottom of the rod, and then through a seal at the bottom of the reactor vessel. The orientation of the five thermocouple rods in the core is provided in Appendix G, Dwgs. OSU 600007 and 600008. As the drawings indicate, one of the four thermocouple rods is at the center of the core and the other four thermocouples are located in the third of four concentric rings.

The CMTs are instrumented with numerous fluid and wall thermocouples, as indicated on Appendix G, Dwgs. OSU 600501 and 600502. Each CMT contains two short and one long thermocouple rods, or rakes, instrumented with thermocouples along its entire length. In addition, inside and outside wall thermocouples, fluid thermocouples installed 1 in. from the inside wall, and tank centerline thermocouples are installed at the same elevation to measure the temperature of the fluid and walls at that elevation.

Note: Appendix G, Dwgs. OSU 600501 and 600502 incorrectly identify the orientation of the long thermocouple rake in CMT-1 and CMT-2 as 135°az . The actual orientation is 315°az .

The IRWST also contains two thermocouple rods, or rakes, as shown in Dwg. OSU 600701. The thermocouple rod located on the 45°az is mounted 3 in. from the PRHR HX tube bundle to measure the effects of HX operation. The thermocouple rake mounted at 270°az measures temperature distribution from sparger operation.

One long and one short tube of each SG are instrumented with shell-side (secondary side) wall thermocouples and tube-side (primary or RCS-side) fluid thermocouples as shown in Dwg. OSU 600301. Originally, each tube had two wall thermocouples mounted on the hot-leg side and two wall thermocouples mounted on the cold-leg side. Several thermocouples were damaged during installation. The thermocouples were inaccessible, so they were not repaired. Thus, the drawing indicates the loss of these thermocouples.

2.4.1.9 Signal Conditioners (SC)

It is necessary to provide selected signals to DAS and control panel instrumentation at the same time. For instrumentation loops containing transmitters, two dropping resistors in series are used in the instrument loop to provide the signal to both locations. To split a thermocouple signal between the DAS and the control panel, a signal conditioner is needed. Sixteen signal conditioners provide control panel indication and control input for hot and cold leg, pressurizer vapor space, SG steam, primary and secondary sump, and IRWST temperatures. In addition, six signal conditioners split selected heater temperatures. The heater temperatures are used for control panel indication and as input to logic to trip all heaters when an abnormally high temperature is detected.

In Appendix C, the Instrumentation Data Base indicates that the signal conditioners are designated by the prefix SC. However, the P&IDs (Appendix G) contain no instruments with an SC prefix. Inputs to the signal conditioners are either fluid thermocouples or heater thermocouples. If the input to the

SC is a fluid thermocouple (TF), the SC has the same number as the thermocouple. For example, SC-101 is the signal conditioner for CL-3 temperature. The thermocouple monitoring this temperature is TF-103. If the input to the SC is a heater thermocouple (TH), the SC number contains the entire number of the thermocouple. For example, SC-TH-101-3 is the signal conditioner for heater thermocouple TH-101-3.

Data from the 22 thermocouples that are inputs to the signal conditioners are not listed in the test data files by their thermocouple designator (TF or TH), but by their signal conditioner designator (SC). Using the previous example, temperature data from CL-3 thermocouple TF-103 are identified as SC-103 data.

2.4.1.10 Programmable Logic Controller (PLC)

The Omron PLCTM contains the control logic of the test facility written in a ladder logic format. The PLC is the interface between the control panel instrumentation and the equipment to provide proper control and safe operation of the equipment. All inputs to the PLC are digital, except heater temperature signals used to trip the reactor heaters. The PLC provides digital control such as opening and closing air-operated valves, starting and stopping pumps, providing inputs to control panel alarms, and commanding the automatic operation of equipment during a matrix test. It does not provide analog functions such as reactor heater (power) control or SG steam flow control via a motor-operated valve. Digital events in the facility are recorded by an additional software program that monitors the input and output of the PLC.

2.4.1.11 Control Panel Instrumentation

The control panel instrumentation provides manual and automatic control of the equipment in the facility and operator indication of facility parameters, but does not provide input to the DAS. Subsection 2.6 discusses the details of control panel instrumentation and how it was used to operate the test facility.

2.4.2 Calibration Methods and Standards

The general process used for calibration of the OSU test instruments is described below:

- The instrument was identified by manufacturer and model number.
- Accuracy, input values, and output values, considered critical characteristics of the instrument were identified.
- The instruments were receipt-inspected to verify that the correct model numbers were received and no damage had occurred during shipping.

- Critical characteristics were verified by calibrating the instrument before the beginning of matrix testing and by performing post-test calibration after completion of matrix testing.

The instruments installed in the field served a number of purposes and, therefore, had different calibration requirements. The instrument types were divided into the following three functional groups based on their function and calibration requirements.

Functional Groups:

- Group I -- Instruments used for data acquisition which were calibrated onsite. These instruments had an input to the DAS.
- Group II -- Instruments used for local indication (such as pressure indicators), local monitoring (such as pressure switches), and indicators and controllers located on the control panel. These instruments did not provide an input to the DAS.
- Group III
 - Instruments which had no onsite calibration and had vendor-supplied calibration data sheets (e.g. heat flux meters, flow meters, or flow tubes for magnetic flow meters).
 - Valves, solenoids, limit switches, etc., not normally included in the definition of an instrument.
 - Thermocouples which were functionally checked initially (not calibrated), could not be re-spanned or re-ranged, and required no further calibration.

Calibration Periodicity Categories:

- Category I -- Calibration frequency of 12 months due to importance in testing and data reduction. All category I instruments either had an input to the DAS or were a functional part of the instrument loop.
- Category II -- Calibration frequency of 18 months. Although these instruments did not have a direct input to the DAS, they were important for the control and safety of the equipment.
- Category III -- Required no further calibration beyond functional test or vendor calibration.

Calibration Periodicity Table			
Prefix	Category	Description	Frequency (months)
DP	I	Differential pressure transmitter - headloss	12
FDP	I	Differential pressure transmitter - flow	12
FMM	I	Flow meter magnetic	12
FVM	I	Flow meter vortex	12
HFM	III	Heat flux meter	N/A
HPS	III	Heated phase switch	N/A
LCT	I	Load cell transmitter	12
LDP	I	Differential pressure transmitter - level	12
PT	I	Pressure transmitter	12
SC	I	Signal conditioner - temperature	12
TF	III	Fluid thermocouple	N/A
TFM	III	HFM thermocouple	N/A
TH	III	Heater rod thermocouple	N/A
TR	III	Core Instrument rod thermocouple	N/A
TW	III	Wall thermocouple	N/A

The calibration methods used for specific instrument types are described below.

2.4.2.1 Thermocouples

A thermocouple calibrator (Tegam Model 840) and a dry-well tester were used to check the calibration of the standard rod-type thermocouples. These thermocouples were inserted into the 1/4-in., 1/2-in., or 3/8-in. inserts of the dry-well tester.

The thermocouple probe supplied with the calibrator was connected to the terminals labelled *thermometer input*. This measured the reference temperature of the dry well. Type J, K, or T thermocouples were calibrated with this setup. Most of the thermocouples used at OSU were type K.

The thermocouple being tested was checked for temperature at room temperature, 245°F, and 450°F. Between every setpoint, 10 minutes were allowed for the tester to reach the setpoint and stabilize.

Non-standard thermocouples, which could not be placed in the dry-well tester, were checked using a heat gun set at 250°F. These thermocouples were not checked at 450°F.

2.4.2.2 Pressure Transmitter

The pressure transmitters are one-piece capacitance-based absolute-gage pressure sensors and transmitters. Pressure is converted to capacitance by the transducer. The transmitter electronics and a digital converter convert the output signal to a range of 4 to 20mA. The milliampere signal is then transmitted to an indicator or the DAS.

A digital multimeter (HART Communicator Interface, Rosemount Model 268) and a pressure gauge (Transman Model 1090) were used to check the calibration of the pressure transmitters. The pressure transmitter output range was established from 4 to 20mA and, if the measured outputs were satisfactory, a linearity check of the digital to analogue converter was performed. The linearity check of the digital to analogue converter confirmed that output requests of 0, 25, 50, 75, and 100 percent corresponded to amplifier outputs of 4, 8, 12, 16, and 20mA, respectively.

The pressure transmitters were initially bench-calibrated from 0 psig to about 600 psig. Once installed, the transmitter output was a combination of system pressure and pressure of the water column. Field calibration of the pressure sensors was performed to offset the effects of the height of the sensing line water column.

The pressure transmitter loop check and DAS calibration were accomplished by applying power to the transmitter and recording the DAS voltage reading at 4, 12, and 20mA applied-current signals. From these voltages, the slope and Y intercept values for the instrument, required for the DAS, were calibrated.

2.4.2.3 Differential Pressure Transmitters

The differential pressure transmitters were bench-calibrated in a manner similar to the pressure transmitters described previously. In addition, the differential pressure transmitters were bench-calibrated to a span greater than the physical tap-to-tap height differential of the plant. Therefore, the full tank level was bench-set for 4mA output, and the empty tank level was less than 20mA. A field calibration procedure was carried out to set the output range of the transmitters to correspond to the actual tank level by using the transmitter output, in engineering units, at the tank empty level (4mA) and tank full level (20mA). This set the output range of the transmitter to a value within the bench calibration range and was consistent with the level being measured.

2.4.2.4 Load Cells

The load cells were vendor-calibrated and required no further calibration. A loop calibrator (Transmation Model 1090 or equivalent) was used to calibrate the load cells. Using the loop calibrator, power was applied to the control panel and field instrumentation. The loop calibrator was connected to the loop at the transmitter and the DAS voltage reading was recorded at 4, 12, and 20mA applied-current signals. From these voltages, the slope and Y intercept for the instrument, required for the DAS, were calculated. The slope and Y intercept are stored in the DAS system. The engineering units of the signal are calculated from this slope and Y intercept.

2.4.2.5 Magnetic Flow Meters

The magnetic flow meter transmitters use a pulsed-DC technique to energize the flux-producing coils of the flow tube. As liquid passes through the magnetic field in the flow tube, low-level voltage pulses develop across a pair of electrodes. The voltage level is directly proportional to the average velocity of the liquid.

The flow tube and its electronics were not part of the calibration. Using a digital multimeter, the magnetic flow meter transmitter amplifier was calibrated for a 4 to 20mA output range. Transmitter loop check and DAS calibration were carried out by applying power to the transmitter and recording the DAS voltage readings at 4, 12, and 20mA applied-current signals. From these voltages, the slope and Y intercept values for the instruments, required for the DAS, were calculated.

2.4.2.6 Turbine Flow Meters

A frequency calibrator (Transmation Model 1070) and a digital multimeter were used to check the calibration of the turbine flow meters. The transmitter amplifier was calibrated for a 4 to 20mA output range. The frequency (or pulse) input to the amplifier was polarity-sensitive. Negative pulses were applied to the transmitter to check the amplifier polarity. Transmitter loop check and DAS calibration of the turbine flow meters were accomplished by applying power to the transmitter and recording the DAS voltage readings at 4, 12, and 20mA applied-current signals. From these voltages, the slope and Y intercept values for the instrument, required for the DAS, were calibrated. Negative pulses were applied to the transmitter to check polarity.

2.4.2.7 Vortex Flow Meters

Fluid passing through the flow meter body passes a specially shaped vortex shedder which causes vortices to alternately form and shed from the sides of the shedder at a rate proportional to the flow rate of the fluid. These shedding vortices create an alternating differential pressure which is sensed by a detector located above the shedder. A pulsed voltage is generated by the detector and the voltage conditioned by the amplifier to produce a 4 to 20mA output signal.

A frequency calibrator (Transmation Model 1070) and a digital multimeter were used to check the calibration of the vortex flow meters. The transmitter amplifier was calibrated for an output range of 4 to 20mA corresponding to a frequency calibrator range of 0 to 100 percent. The transmitter loop check and DAS calibration were accomplished by applying power to the transmitter and recording the DAS voltage readings at 4, 12, and 20mA applied-current signals. From these voltages, the slope and Y intercept values for the instrument, required for the DAS, were calibrated.

2.4.2.8 Noncalibrated Instrumentation (Heat Flux Meters and Heated Phase Switches)

The heat flux meters measure heat passing over the surface of the sensor attached to the vessels or pipes of interest. These devices were calibrated by the manufacturer and did not require any further calibration.

2.4.3 Phenomena Affecting Readings

This subsection examines the effects of different phenomena on instrument measurements. The discussion is intended to assist in the review of data from the matrix tests.

2.4.3.1 Flow and Temperature Effects on Level Differential Pressure (LDP) Transmitters

The LDPs measure fluid level between the upper reference leg tap and the lower variable leg tap of a component. The LDP tubing is connected to the component to be measured so that any pressure (such as steam pressure) will act equally on the reference leg and the variable leg and, thus, have no effect on the indicated level data.

The difference between the constant reference leg level and measured fluid column level creates a differential pressure that is measured by an LDP and electronically converted to a level signal. An accurate level signal is dependent on static conditions, i.e., no flow in the fluid column measured.

Flow in a component creates a dynamic differential pressure due to pressure loss between the component LDP taps as fluid flows through the component. When this dynamic component of differential pressure is superimposed on the static differential pressure, the resulting transmitter signal produce invalid data. If the flow direction in the component is from the LDP variable tap (low-pressure side) towards the reference tap (high-pressure side), the dynamic and static differential pressures will be additive, creating indicated level data greater than actual level. Conversely, if flow is in the opposite direction, the indicated level data are lower than actual level.

The LDPs installed at the OSU test facility were bench calibrated at ambient temperature and had no electronic temperature compensation. The temperature in the fluid column to be measured was, in many cases, elevated above ambient conditions. When the temperature of the fluid column was elevated with respect to the temperature of the tubing between the component and the LDP, the

resulting transmitter signal provided indicated level data lower than actual due to the expansion of fluid with increasing temperature.

For some of the data plots in this report, a program was developed that compensates selected level data for temperature. The temperature-compensated level data on those figures have the LDP designator preceded by a C. For example, CLDP-127 is the temperature-compensated data for level channel LDP-127. None of the raw level data transmitted with this report have been temperature compensated.

2.4.3.2 Effect of Two-Phase or Steam Flow on Magnetic Flow Meters (FMM)

The FMMs are in-line flow instruments that measure liquid flow. As long as the flow stream is liquid solid in the forward direction, the FMMs provide accurate and valid data. During the performance of the matrix tests, the LOCA caused the flow stream through some of the FMMs to become two-phase fluid and, in some cases, all steam. Also, in some instances, reverse flow occurred.

The effects of two-phase fluid, steam, or gas flow on FMM data were varied and unique to the meter. Some meters indicated erroneously high flow, some zero flow, and some negative flow. As an example, the CMT/cold-leg balance line flow meters indicated oscillating flow as the CMT transitioned from recirculation mode to draindown, and two-phase fluid or steam appeared in the balance line. Balance line flow data after the transition occurred are considered invalid. In another example, the accumulator injection flow meter indicated negative flow as the accumulator emptied and the meter was placed in a gas environment. Again, the data are considered invalid after the accumulator was empty of water.

For liquid-solid reverse flow, an FMM provides negative flow data. In this case, the negative data provide an accurate indication of flow reversal, but the absolute negative value of the data would be inaccurate and should be considered invalid. As an example, negative flow data were recorded in the IRWST-1 injection line when the primary sump valves opened late in a matrix test. Although the negative flow indication is valid, the actual value of the data is not.

2.4.3.3 Effect of Backflow on Vortex Flow Meters (FVM)

The FVMs are in-line flow instruments designed to measure forward steam flow. FVMs measure flow of any gas going through them and in either direction. During reverse flow, the FVMs provide indication of positive flow, but the data are considered invalid.

An example of FVM positive flow indication during reverse flow occurred when the break valve opened during a matrix test. When the break valve first opened, the steam flow from the break pressurized the BAMS steam header. The header pressurization caused a backflow of steam into the ADS-4 separators until the pressures were equalized. The backflow of steam into the ADS-4 separators resulted in positive flow data. Therefore, all ADS-4 separator steam flow data prior to the ADS-4 valves opening are considered invalid.

2.4.3.4 Effect of Two-Phase Liquid or Steam on Differential Pressure Transmitters (DP) Installed in a Vertical Orientation

The DPs are bench calibrated to a range suited for the particular application. However, if the DP is installed in a vertical orientation, its data have a zero offset when a liquid level exists below the elevation of the upper sense line's tap.

In DP installations where both taps are at the same elevation, as when measuring flow differential pressure in a horizontal pipe, the static pressure from the weight of fluid above the taps is sensed by both legs of the transmitter and therefore does not affect the differential pressure measurement of the transmitter. This is true if the fluid is liquid, steam, or a two-phase mixture. However, the two sense lines of a vertically-mounted transmitter experience unequal static pressures when the liquid level of the component drops below the elevation of the upper sense line's tap. When this occurs, one side of the transmitter senses static pressure equal to the column of water in the upper sense line; the other side of the transmitter senses static pressure equal to the water column in the lower sense line, plus the static pressure from the water level in the component above the elevation of the lower tap. The maximum offset results when the liquid level in the component decreases to an elevation below the lower tap.

As an example during testing, DP-130 measured the differential pressure across the core bypass holes located in the upper core barrel flange of the reactor vessel. When the liquid level was above the upper tap of DP-130, both sides of the transmitter sensed the same static pressure due to the weight of water above it. Thus, the differential pressure experienced by the transmitter was due to a flow head loss only. With a decreasing level in the reactor vessel, both sides of the transmitter sensed the same decrease in pressure due to the decreasing water column above it until the liquid level dropped below the level of the upper tap. After this, the side of the transmitter measuring the upper sense line pressure did not see any additional decrease in static pressure; it sensed only the water column in the upper sense line. Thus, the desired pressure indication of the transmitter was offset by an amount equal to the difference between the elevation of the upper tap and the water level in the component. The maximum offset was -22 in. H₂O, which was equal to the distance between taps for the upper and lower sense lines. In most matrix tests, the level in the reactor quickly drained below the lower tap of DP-130. When no flow existed through the bypass holes, the data from DP-130 indicated a differential pressure of -22 in. H₂O.

2.4.3.5 Effect of Reactor Coolant System Draindown on Steam Generator U-Tube LDPs

A phenomenon occurred with respect to the SG U-tube level instruments during the performance of matrix tests due to the unique LDP tubing installation. The reference and variable legs for the U-tube LDPs penetrated the SG at the tube-sheet elevation. The variable leg was routed to the bottom of the respective tube, and the reference leg traversed the axial length of the tube bundle, internal to the SG, and was connected to the top of the respective tube (Appendix H, Dwgs. 20175-D1 and 20175-D2).

The routing of the LDP tubing inside the SG exposed the tubing to the secondary-side temperature environment of the SG. Therefore, after break valve opening during a matrix test, when the fluid in the SG U-tubes transitioned from recirculation to draindown, uncovering the reference leg tap, the fluid in the LDP reference leg began to vaporize. The decreasing level in the reference leg provided a false high indication for U-tube level. When the U-tubes were completely drained, the level data erroneously indicated that the U-tubes were partially filled. As the reference leg continued to vaporize, decreasing the reference leg level, the level data incorrectly indicated the U-tubes refilling. When the reference leg was completely voided, the differential pressure between the reference and variable legs was equal indicating full U-tubes. The U-tube temperature data confirmed that the U-tubes remained drained because the temperatures superheated and remained superheated after the U-tubes drained.

It is important to understand that the level data can be interpreted to determine the time that the U-tubes began to drain and when the U-tubes were completely drained for analysis purposes.

2.5 Data Acquisition System

The DAS receives data from the test instrumentation, records it, and prepares it for review. This section describes the DAS, including architecture, hardware, and processing software.

2.5.1 System Hardware

The DAS consists of about 750 data channels that are monitored during test operations. Figure 2.5-1 illustrates system hardware. The channels are distributed among three separate Fluke Helios Data Acquisition Units® racks. Each rack is serially connected directly to a separate 486DX PC system. Each system PC is tied to the others by an Ethernet connection. The system software used for the local area network (LAN) is Microsoft Workgroup® for Windows. Rack 1 Helios contains about 300 channels and acquires data from the rapid-responding inputs such as pressure or flow instruments. The remaining channels, primarily thermocouples, are split between rack 2 and rack 3.

2.5.2 DAS Architecture

Figure 2.5-2 is a schematic of the DAS architecture. The system is initialized by the user from the user's PC with the time and the system configuration data base. On triggering, either by input from the user or by signal input at the start of a test, the Helios begins acquiring data. Data are sent from the Helios to the PCs for all channels with instrument inputs and are stored by the PCs. Predefined channels are processed and displayed from incoming data. Burst data are acquired at a higher rate for all channels and stored in the Helios until the end of the test. Data files are recorded on a writable CD-ROM.

2.5.3 Software

DAS software is divided into five main functions: initialization, data acquisition, burst data acquisition, display channel monitoring, and data storage. Before DAS execution can begin, the system configuration file must be extracted from the system data base, formatted, and transferred to the DAS PCs. The system configuration files are distributed in three main files sorted by rack and row, where each row is an analog-to-digital (A/D) converter card. As a convenience, each row is also separated into a file that correlates with burst data acquisition. From the configuration file, a set of channels is chosen to be displayed. A file is created containing parameters for the display channels to be monitored during test operations.

The initialization function prompts the user for input data, sends the channel configuration to the Helios equipment, and then waits for an acknowledgment of the channel definitions. Other configuration data sent to the Helios include burst rate, system time, and other setup parameters. This function also sets up the PCs to display channel information and burst delay time.

The data acquisition function is designed to retrieve channel data and write it to a system disk, continuously, every 8 to 10 seconds from the start to the end of the test. The start of acquisition is triggered either by a transient signal or operator input. Operator action is required to stop acquisition.

Burst data acquisition acquires data at a faster rate, but for a shorter length of time, than continuous acquisition. The burst rate is user-defined and can be from once per second to once every 10 seconds. The start of burst is input by the test operator and can begin immediately with the start of continuous acquisition or can be delayed minutes or hours. The burst data system can store up to 1900 scans for each channel. This means that at a burst rate of once per second, burst data can be acquired for about one-half hour. Burst data are stored on the Helios until the end of the test. Then the operator initiates the transfer of data from the Helios to the system PC, where the data are stored in an ASCII file.

The display channel monitor function selects channel values from the continuous data stream for predefined channels. These channel values are converted from voltages into engineering units and displayed on the PC monitor. From the predefined channels, the test operator can choose up to four to be dynamically charted on the monitor. The channel display indicates an alarm condition if the channel value falls outside the alarm value limit.

The data storage function accumulates all configuration files, continuous data files, display data files, and burst data files and transfers them to a single system via the LAN. PSCRIBE™ software is used to write the data files onto a CD-ROM for post-test processing, as described in Section 3.0.

2.5.4 LabVIEW Description

The software is written using LabVIEW for Windows, which uses a graphic programming language to create programs in block diagram form. LabVIEW is a general-purpose programming system, but it also includes libraries of functions and development tools designed specifically for data acquisition and instrument control. LabVIEW subprograms are called virtual instruments (VIs) because their appearance and operation imitate actual instruments. VIs accept parameters from higher level VIs and have an interactive user interface and a source code equivalent. Figure 2.5-3 illustrates the AP600 DAS hierarchical VI.

The interactive user interface of a VI is called the *front panel* because it simulates the panel of a physical instrument. The front panel can contain knobs, pushbuttons, graphs, and other controls and indicators. Data are input using a mouse and keyboard. Results are viewed on the computer screen.

2.5.5 Sequence-of-Events Log

The DAS acquires information during any given test without reference to an event initiated by the facility control system, such as a valve opening or pump trip. The sequence of and timing of these events are recorded on a separate PC using a software program named Intouch® made commercially available by Wonderware. A Wonderware data base was constructed using the programmable logic

controller (PLC) data base as a model. Signals from the facility instrumentation that affected the PLC program were included in the data base. While the software is running, it automatically logs every signal input to the PLC.

The logging format used in the following test sections is an ASCII file generated by the software:

MM/DD/YY: HH:MM:SS:MSC PRI Tagname Value

As an example, consider air-operated valves in the facility. All of these valves have limit switches at each end of the stroke so that the PLC has a positive indication of the valve in a fully open or fully closed position. Both switch signals are logged as an individual point as they go through a transition. A typical message for a single stroke of CMT-1 pressure balance line valve RCS-503 would be listed as follows:

```
07/08/94 11:04:38.539 1 RCS503_Open Not Closed  
07/08/94 11:04:38.846 1 RCS503_Closed Closed
```

Four groups of messages are placed in the log file, including Valve Position Log, Pump Status Log, Console Log, and Alarm Log.

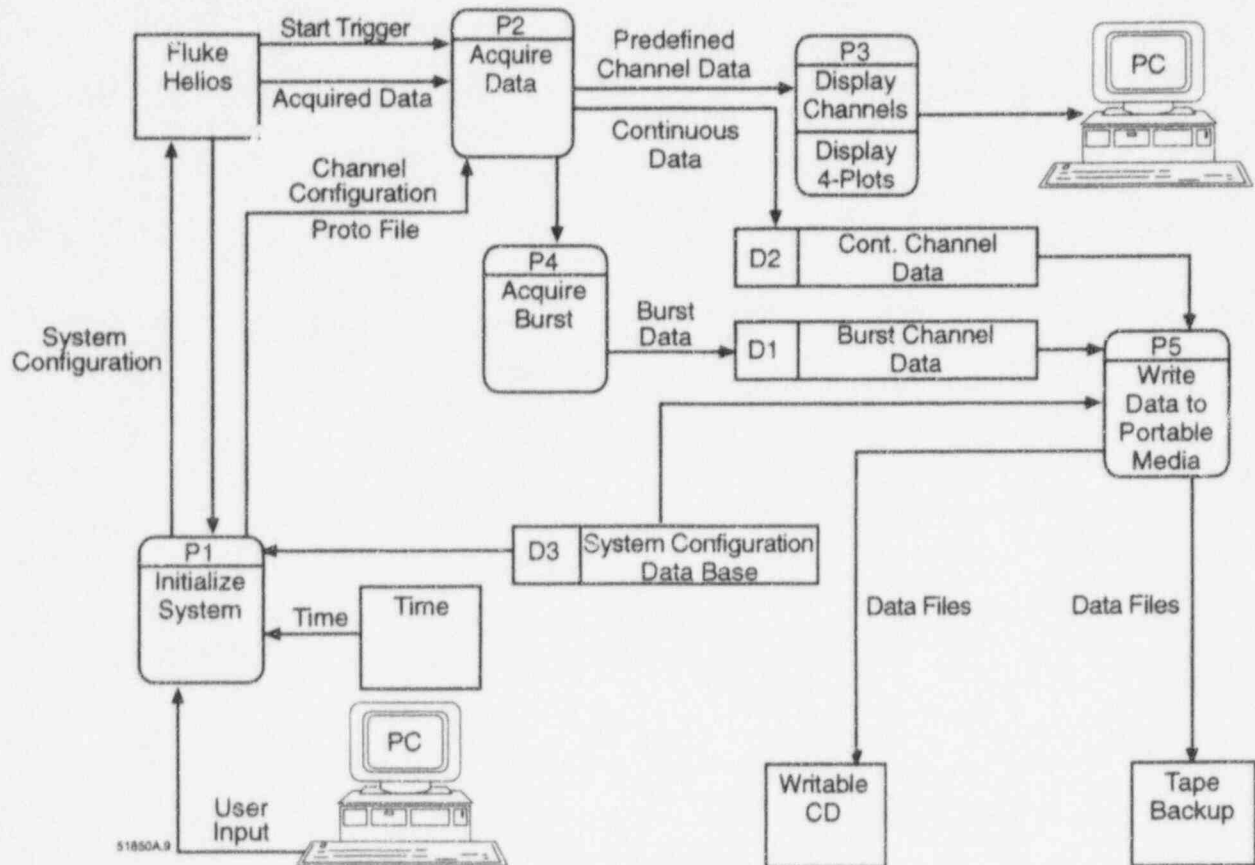


Figure 2.5-1 DAS Hardware

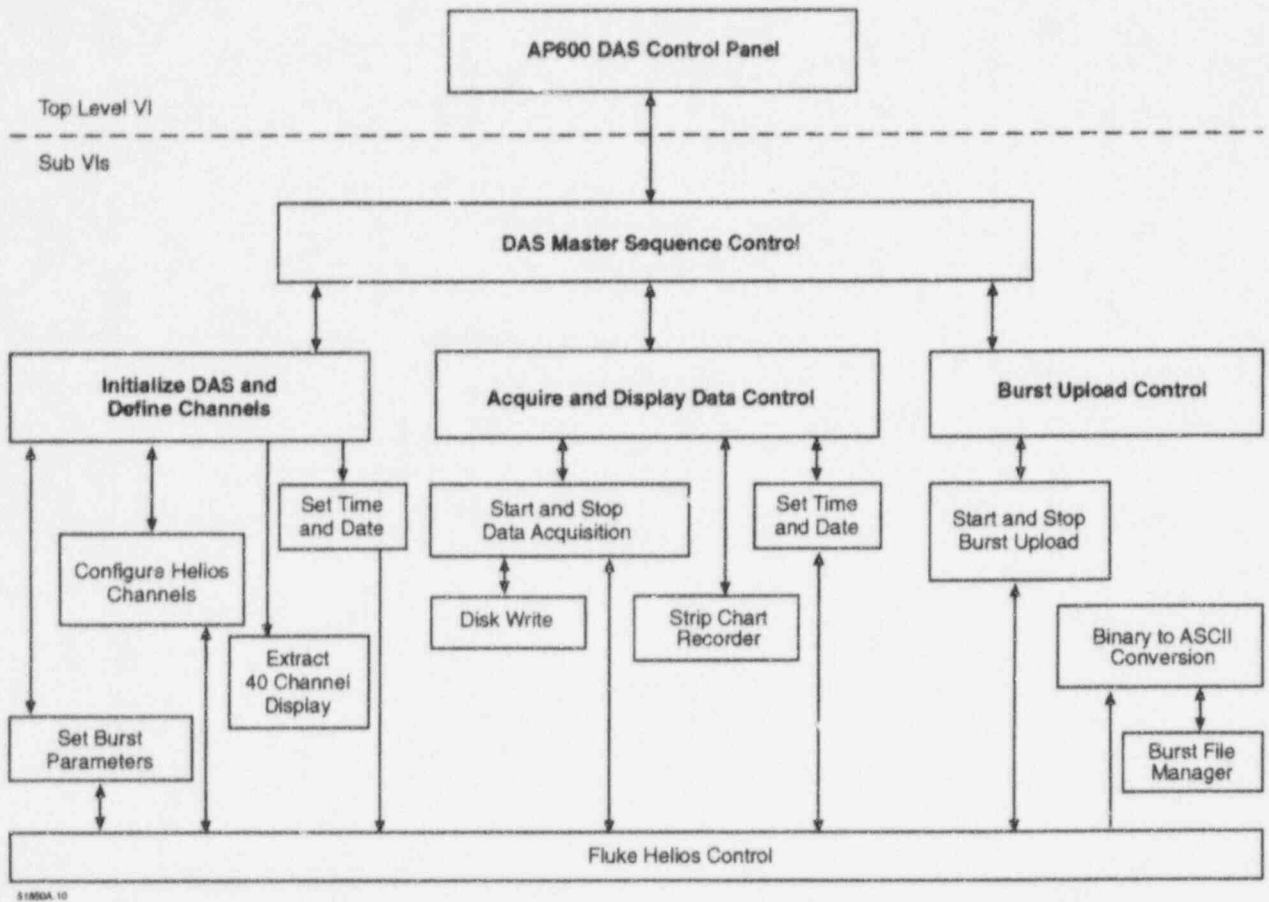


Figure 2.5-2 DAS Architecture

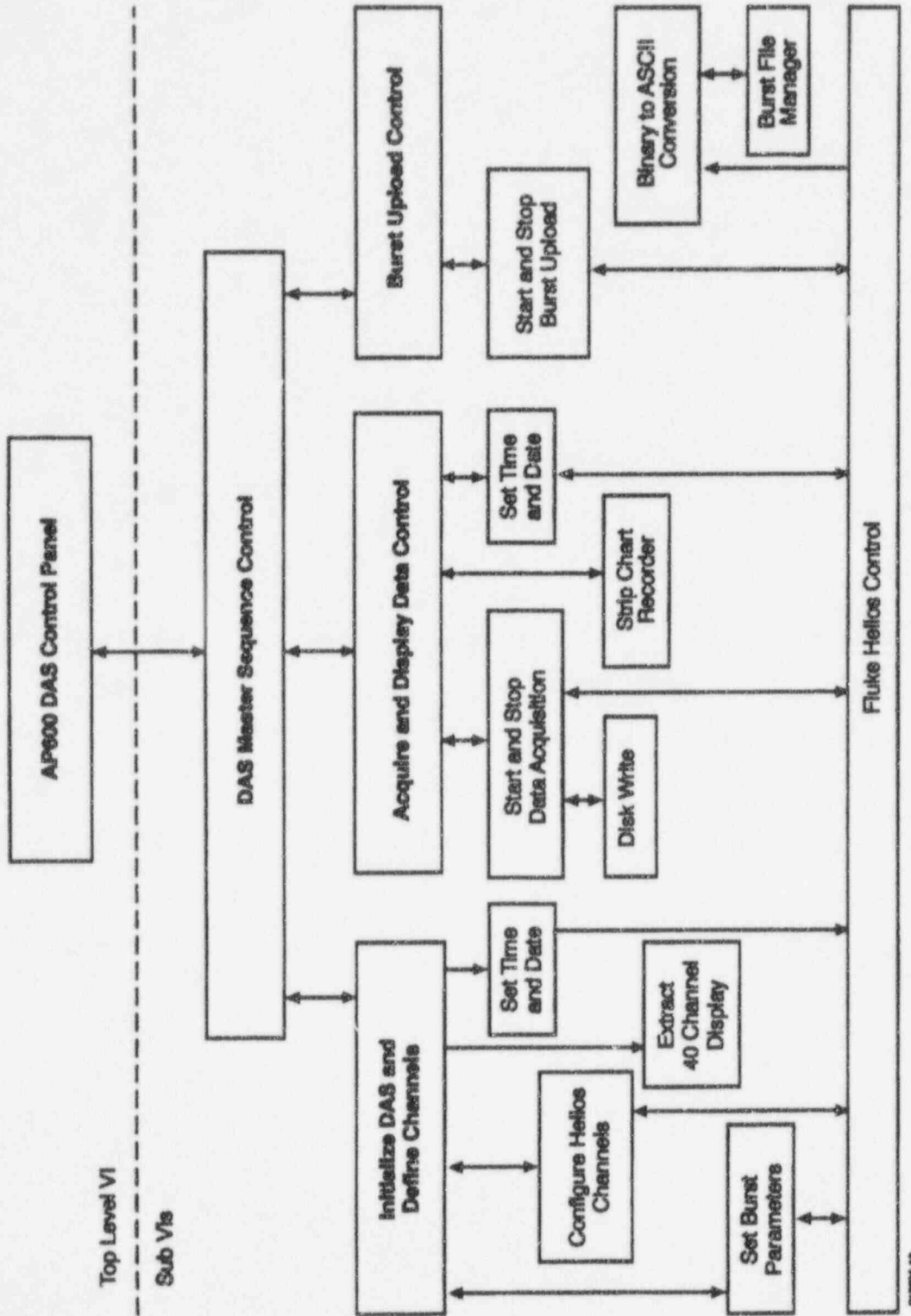


Figure 2.5-3 DAS Software Hierarchy

2.6 Test Facility Control System

This section describes the manual and automatic functions of the test facility control system. The test facility control system operates in either manual or automatic mode. Control panel and local switches allow operator manual control of the equipment for the following:

- To open and close valves
- To start and stop pumps
- To control the power of heaters

The automatic control mode provides signals for the following:

- To automatically operate the facility at steady-state
- To initiate a simulated break and transmit automatic control signals to simulate AP600 control logic during a LOCA
- To control the reactor heaters to simulate decay heat production of an AP600 nuclear core
- To operate the BAMS
- To provide automatic control of the nonsafety systems (CVS and RNS pumps)
- To provide automatic equipment operation to mitigate out-of-specification conditions in order to prevent equipment damage and injury to personnel
- To provide control of heat tracing
- To provide alarms

2.6.1 Operator Panel

Figure 2.6-1 is a photograph of the operator panel in the test facility control room. It shows the programmable controllers and the process control system components listed in Tables 2.6-1 and 2.6-2, respectively. Figure 2.6-2 shows the arrangement of these components on the operator panel. The major components of the operator panel, the manufacturer, model number, function, and operation are as follows:

- Temperature scanner, Omega™ CN34025-DC, indicates the temperatures of trace heaters.
- Temperature scanner, Omega™ CN101K-1000F, provides an alarm if RCP cooling water exceeds the adjustable setpoint.

- Power meters, Power Measurements™ 3710 ACM, indicate the power to each bank of rod bundle heaters.
- Bar-graph indicators, Universal™ VB-120-2-4, indicate the percent range for level parameters. The bar-graph indicators have programmable setpoints that when reached, operate a bistable to provide input to the PLC for appropriate action.
- Panel switches and lights, Square D™, provide CLOSE/AUTO/OPEN control for air-operated valves, pump/fan power, and STOP/RUN indicator lights.
- Alarms, Panalarm™ Series 90, provide an alarm annunciator and horn.
- Process indicators, Newport™ Model 82, indicate pressure, temperatures, levels, and flows. The process indicators have programmable setpoints that when reached, operate a bistable to provide an input to the PLC for appropriate action.
- Process controllers, Fischer/Porter™ 53HC3300C, process field variables.

2.6.2 Test Signal or Safety Signal (S signal)

The PLC is programmed to automatically operate equipment in a timed sequence when the TEST pushbutton on the control panel is pressed to initiate a matrix test. Equipment operation is described in detail in the following sections. However, the following is the sequence of operation with time zero referenced as the time when the break valve open signal is generated. The actions listed after the S signal were initiated by the S signal.

Equipment Operated	Time
DAS triggered to start collecting data	-120 seconds
Break valve signal to open; start of test	0 second
S signal generated	0.5 second
SG pressure control reset to 335 psig	0.5 second
Reactor control shift to kW mode	0.5 second
Main feed pump trips	3.6 seconds
Pressurizer heater trips	6.1 seconds
CMT valve control (open)	6.1 seconds
RCP control (trip)	8.6 seconds

Equipment Operated	Time
PRHR HX outlet isolation valve (open)	6.1 seconds
SG feedwater valve (close)	3.6 seconds

2.6.3 CVS Pump and Discharge Valve Control

The CVS pump operates automatically when its control panel switch is placed in the AUTO position. In automatic control, the pump starts when the pressurizer level is below its low-low level setpoint of 30 in. H₂O and stops when pressurizer level increases to 45 in. H₂O. The CVS pump operated in automatic during matrix testing of the interactions of the nonsafety systems with the passive systems.

To scale the AP600 CVS flow rate to the CSU test facility, the CVS pump curve is simulated by automatically throttling the CVS pump discharge valve, RCS-808, thereby controlling flow from the pump. A Fischer/Porter™ process controller uses pressurizer pressure (PT-604) as an input to the following flow function:

$$\text{Flow} = -0.003827954 \times \text{pressurizer pressure} + 5.32547 \text{ gpm}$$

In automatic control, the function provides the setpoint to the discharge valve's proportional, integral, derivative (PID) software controller. The setpoint is compared with CVS pump flow measured by flow meter FMM-801.

Note: The original CVS pump flow meter was a turbine meter (FTM-801). This meter was replaced by a magnetic flow meter (FMM-801) by the time the first matrix test was performed.

To prevent exceeding the design pressure drop across the CVS pump discharge valve, pump speed is controlled by the same controller that controls the discharge valve. The input function for the pump speed is the same as the input to the CVS discharge valve control and pressurizer pressure (PT-604). The speed function is:

$$\text{Speed} = 3.7312 \times \text{pressurizer pressure} + 2000.0 \text{ rpm}$$

When the pressurizer is at atmospheric pressure, the speed of the pump is at its minimum, 2000 rpm. The lower pump speed allows the discharge valve to throttle at a position that precludes cavitation across the valve. As pressurizer pressure increases, the speed of the pump increases.

Pump protection is provided by a low-suction pressure trip of 12 in. H₂O. The low-suction pressure trip is disabled for 3 seconds after the pump starts to allow for the initial suction pressure spike during pump start. The pump also trips on a low supply voltage of less than 480 vac.

To protect the RCS against overpressurization, the CVS pump trips when pressurizer pressure exceeds its high-high pressure setpoint of 385 psig and is reset at 380 psig decreasing.

To restart the CVS pump after an automatic trip, the operator must place the control panel switch in the OFF position and then return it to the AUTO or RUN position.

2.6.4 RNS Pump Control

The RNS pump operates automatically when its control panel switch is in the AUTO position. In automatic control, the pump starts if an S signal is present and pressurizer pressure is below its high-pressure reset point of 225 psig and stops when pressurizer pressure increases to 230 psig. The pump operated in automatic during matrix testing of the interactions of the nonsafety systems with the passive systems. In addition, the RNS pump has a local controller located near the pump that can be used by the operator for fill operations or maintenance activities. Consequently, there is safety interlock so that the RNS pump can only be started from the local panel when the local pushbutton is in the STOP position and the RNS pump switch on the control panel is in the LOCAL position.

To scale the AP600 RNS flow rate to the OSU test facility, the RNS pump curve is simulated by automatically throttling the discharge valve of the RNS pump (RCS-811) thereby controlling the flow from the pump. A Fischer/Porter™ process controller uses pressurizer pressure (PT-604) as input to the following flow function:

$$\text{Flow} = 20.05 - (0.03051 \times \text{pressurizer pressure})^{1.864} \text{ gpm}$$

The function provides the setpoint to the discharge valve's PID software controller. The setpoint is compared to RNS pump flow measured by flow meter FMM-805.

Note: The original RNS pump flow meter was a turbine meter (FTM-804). The meter was replaced by a magnetic flow meter (FMM-805) by the time the first matrix test was performed.

Pump protection is provided by a low-suction pressure trip of 12 in. H₂O. The low-suction pressure trip is disabled for 3 seconds after the pump starts to allow for the initial suction pressure spike during pump start. The pump also trips on a low supply voltage of less than 480 vac.

To protect the pump from operating at shutoff head conditions, the RNS pump trips when pressurizer pressure exceeds its high-pressure setpoint of 230 psig increasing, with a reset point of 225 psig decreasing.

To restart the RNS pump after any one of the automatic trips, the operator must place the control panel switch in the OFF position and then return it to the AUTO or RUN position.

2.6.5 IRWST Valve Control

The IRWST-1 discharge isolation valve, RCS-711, and IRWST-2 discharge isolation valve, RCS-712, are normally closed valves provided with manual and automatic control. The valves are opened in manual control by placing their respective control panel switch in the OPEN position. When their control switches are placed in the AUTO position, the valves open when reactor vessel upper-head pressure (PT-107) decreases to less than 30 psig.

The IRWST isolation valves in the AP600 design are normally open valves. The OSU test facility control logic maintains the valves closed in automatic control until reactor coolant pressure is sufficiently low to prevent back leakage through the check valves in series with the isolation valves. Conversely, the setpoint to open the valves is sufficiently high so that IRWST injection is delayed for a period of time after the valves open, so the closed valves never prevent IRWST injection flow.

2.6.6 Main Feed Pump and Discharge Valve Control

The main feed pump operates automatically when its control panel switch is placed in the AUTO position. In automatic control, the pump starts and runs continuously. The pump is automatically tripped 3.1 seconds after an S signal is generated. At the beginning of each matrix test, the pump was in the AUTO position.

Pump protection is provided by a low-suction pressure trip of 12 in. H₂O. The low-suction pressure trip is disabled for 3 seconds after the pump starts to allow for the initial suction pressure spike during pump start. The pump is also tripped on a low supply voltage of less than 480 vac. The main feed pump also trips if either SG wide-range level exceeds 117 in. H₂O and is reset at 116 in. H₂O.

To restart the main feed pump after any one of the automatic trips, the operator must place the control panel switch in the OFF position and then return it to the AUTO or RUN position.

A low-pressure alarm informs the operator if feed pump discharge pressure (PT-001) decreases to less than 200 psig. The alarm alerts the operator to take action to protect the pump against run-out conditions.

2.6.7 Pressurizer Pressure Control

The pressurizer controller controls power to the pressurizer heaters through an SCR heater controller. In automatic control, the pressurizer controller maintains pressurizer pressure within a band of 365 to 375 psig by controlling power to the pressurizer heaters.

In manual control, the operator adjusts the pressure setpoint on the pressurizer controller, and the controller controls the heater power to maintain the setpoint.

The pressurizer heaters are disabled on high-high pressurizer pressure of 385 psig, low-low pressurizer level of 30 in. H₂O, SCR cabinet high temperature, or 5.6 seconds after an S signal is generated. The heaters are enabled when none of these signals is present.

2.6.8 RCP Gland Seal Cooling System Control

In the AUTO mode, seals for the RCPs are cooled by a separate water cooling system that consists of a pump and a fan to cool the HX located on the roof of the OSU test facility. The cooling fan and pump, if in the AUTO position, are turned on as soon as one-out-of-four RCPs starts.

When all RCPs are turned off, the cooling pump and fan are turned off after a 15-second delay. This is important because during a matrix test, the RCPs are not operating and the heat loss through the seal cooling system is minimized by turning the seal cooling system off.

The cooling fan and pump can be turned on in the manual mode by placing individual switches on the control panel in the RUN position.

2.6.9 CMT Valve Control

The CMT discharge isolation valves, RCS-535 and RCS-536, are normally closed valves provided with manual and automatic control. The valves are opened in manual control by placing their respective control panel switch in the OPEN position. When their control switches are placed in the AUTO position, the valves open 5.6 seconds after the S signal is generated.

The CMT cold-leg balance line isolation valves, RCS-529 and RCS-530, are normally open valves. The valves are closed in manual control by placing their respective control panel switch in the CLOSED position.

2.6.10 CMT Steam Trap Isolation Valves

The CMT steam trap valves, RCS-503 and RCS-504 are normally closed valves provided with manual and automatic control. The valves are opened in manual control by placing their respective control panel switch in the OPEN position. When their control switches are placed in the AUTO position, the valves remain closed.

2.6.11 RCP Control

The RCPs (RCP-1, RCP-2, RCP-3, and RCP-4) operate automatically when their control panel switches are placed in the AUTO position. In automatic control, the pumps start when pressurizer level is above the low-low level reset point of 45 in. H₂O and stop when pressurizer level decreases to 30 in. H₂O. The pumps were run in automatic control at the beginning of each matrix test and were automatically tripped 8.1 seconds after an S signal was generated.

The pump trips on the following:

- Low supply voltage of less than 480 vac
- Gland seal water temperature (TS-001) greater than the high setpoint of 150°F
- RCP gland seal water flow low

The pumps can be run in the JOG position, a manual mode of operation. The pumps run as long as the control switch is held in the JOG position. When the switch is released, it spring-returns to the OFF position.

To restart the RCP pumps after the occurrence of pressurizer low-low level, seal water temperature high, or low voltage, the operator must place the control panel switch in the OFF position and then return it to the AUTO or JOG position.

An alarm is sent to the control panel to alert the operator if the RCP seal water temperature exceeds the high-temperature setpoint (150°F) or RCP cooling water flow is low.

2.6.12 Reactor Heater Control

There are two groups of heater rods in the reactor vessel. Each group is controlled by a separate SCR controller. During steady-state operation of the test facility, the heater controller maintains the average reactor hot-leg temperature at a setpoint selected by the operator. When an S signal is received and a test starts, the control signal to the heater banks simulates decay power expected in the AP600 plant scaled to the OSU test facility. This control is done by a Fischer/Porter™ process controller.

The standard algorithm for decay power was used for all the matrix tests, except Matrix Test SB21.

The algorithm was:

For $0 < \text{time} \leq 140$ seconds; power (KW-101 or KW-102) = 300 kW

For time > 140 seconds; power (KW-101 or KW-102) = $300/[\quad]^c$

The Matrix Test SB21 decay power algorithm was:

For $0 < \text{time} < 300$ seconds; power (KW-101 or KW-102) = 300 kW

For time > 300 seconds; power (KW-101 or KW-102) = $300/[B \cdot \text{time} + C]$

where:

$$B = 0.01021$$

$$C = 0.2848$$

Safety interlocks similar to a pressurizer heater are programmed in the PLC. Reactor heaters are tripped when the following occur:

- High sheath temperature is detected
- RCP cooling water flow is low with an S signal
- RCP gland seal temperature is high (150°F) without an S signal
- Emergency button is pressed
- KEY switch is not operated
- Power to at least one heater bank (KW1 or KW2) is more than 396 kW
- Average of the hot-leg temperature (TF-140 and TF-141) is more than 440°F
- Pressurizer pressure is greater than 385 psig
- SCR cabinet high temperature occurs
- Total power (KW1 + KW2) > 756 KW

Once the reactor heaters are tripped because of a safety condition of high sheath temperature, high gland seal temperature, low RCP cooling flow, or high SCR cabinet temperature, the heater power cannot be applied unless the condition for the safety violation has cleared and the KEY switch is in the OFF position. The power can be applied by placing the KEY switch first in the OFF and then in the ON position.

A control panel alarm alerts the operator if the average temperature of HL-1 and HL-2 is higher than the high-high setpoint of 440°F. At this temperature, the heaters are disabled.

2.6.13 Passive Heat Removal

The PRHR HX outlet isolation valve, RCS-804, is a normally closed valve provided with manual and automatic control. The valve is opened in manual control by placing the respective control panel switch in the OPEN position. When the control switch is placed in the AUTO position, the valve

opens when the ADS-1 valve opens because of CMT low level or 5.6 seconds after an S signal is generated.

2.6.14 Condensate Return Pump Control

The condensate return pump (CRP) is capable of transferring water from the condensate return tank (CRT) to the primary sump or to the IRWST when the CRT level (BGI-14, LDP-903) is more than the low setpoint of 10 in. The water in the CRT is maintained at a specified temperature (180°F) during testing, and an alarm is sent to the operator if this temperature exceeds the high setpoint.

The automatic function of this control was not used during the matrix test program due to the small RCS inventory that left the facility and the rather coarse controls of the condensate return system.

2.6.15 Reactor Heater Sheath High-Temperature Trip

Reactor heater rod sheaths are monitored for any increase in temperature above a 625°F setpoint by analog boards in the PLC. The reactor heaters are disabled if any of the following exceeds the 625°F setpoint.

- Sheath temperature of two-out-of-four rods selected (TH101-4, TH319-4, TH103-3, TH104-4)
- Sheath temperature of the heater rod TH507-4
- Sheath temperature of the heater rod TH501-4
- Or if temperature of the SCR cabinet greater than 120°F

Heater sheath temperatures of the same heater rods, as described in the preceding paragraph, are annunciator at the IND-103 panel indicator. If any one of the heater rod temperatures exceeds 600°F, the operator is alerted by an alarm.

2.6.16 Automatic Depressurization System Control

2.6.16.1 ADS-1, ADS-2, and ADS-3

The ADS-1, ADS-2, and ADS-3 valves are designed to open in sequence after CMT-1 (LDP-507) or CMT-2 (LDP-502) level is below the low setpoint of 41 in. and the ADS-1, ADS-2, and ADS-3 switches are in the AUTO position. The opening sequence timing of ADS valves is given in the following.

The ADS logic is similar to AP600 logic. The ADS-1 valve, RCS-601, is opened after a delay of 15 seconds, when either CMT-1 or CMT-2 level is less than or equal to the low setpoint of 41 in. and the ADS-1 switch on the control panel is in the AUTO position.

The ADS-1 valve, when in the AUTO position, is also actuated when reactor vessel upper-head pressure (PT-107, IND-107) is more than the high-high setpoint of 400 psig. The valve recloses when RCS pressure decreases below 360 psig. In this mode, the ADS-1 valve acts like a power-operated relief valve.

The ADS-2 valve, RCS-602, is opened after a delay of 62 seconds when either CMT-1 (LDP-507) or CMT-2 (LDP-502) level is less than or equal to the low setpoint of 41 in. and the ADS-2 switch on the control panel is in the AUTO position.

The ADS-3 valve, RCS-603, is opened after a delay of 122 seconds, when either CMT-1 or CMT-2 level is less than or equal to the low setpoint of 41 in. and the ADS-3 switch on the control panel is in the AUTO position.

If any one of the ADS-1, ADS-2, or ADS-3 switches is in the OPEN position, it opens that specific ADS valve.

2.6.16.2 ADS 4-1 and ADS 4-2

If the ADS 4-1 switch is in the AUTO position, valves RCS-615 and RCS-625 are opened, after a delay of 180 seconds when either CMT-1 (LDP-507) or CMT-2 (LDP-502) level is less than or equal to the low setpoint of 41 in. and when either CMT-1 (LDP-507) or CMT-2 (LDP-502) level is less than or equal to the low-low setpoint of 17.14 in.

Similarly, if the ADS 4-2 switch is in the AUTO position, valves RCS-616 and RCS-626 are opened, after a delay of 180 seconds from the time when either CMT-1 (LDP-507) or CMT-2 (LDP-502) level goes below the low setpoint of 41 in. and when either CMT-1 (LDP-507) or CMT-2 (LDP-502) level is less than or equal to the low-low setpoint of 17.14 in.

If any one of the ADS 4-1 or ADS 4-2 switches is in the OPEN position, it opens the associated ADS valves.

2.6.17 Steam Generator-1 Level Control

The SG-1 controller maintains level in the SG above the U-tubes but low enough so that the generator moisture separator does not flood. The controller takes input from the narrow-range SG-1 level (LDP-303) and determines if the SG feedwater regulator valve, MF-11, should open or close to match the current steam demand. Since the steam-out controller maintains a relatively constant steam flow by regulating the main steam valve, MS-008, the controller's main purpose is to make up for small variations and transients as well as allowing a method for filling the generators manually, if desired.

When the S signal is received, the controller drives the output to 0 percent, thereby shutting the feedwater regulator valve.

The water level in SG-1 is temperature-compensated by the correction factor:

$$(TCF) = T_{SG-1} \times (0.00049) + 0.94025$$

where:

$$T_{SG-1} = \text{SG-1 temperature TF-301}$$

The temperature-corrected water level is used in the PID level control loop and as an input to an alarm. A control panel alarm alerts the operator if the compensated SG-1 level (LDP-301) is less than the low setpoint of 99 in. or above the high setpoint of 115 in. H₂O.

A control panel alarm alerts the operator if SG-1 steam outlet pressure (PT-301) has exceeded the high setpoint of 310 psig.

The SG-1 controller display monitor shows the steam flow (FVM-001) and feed flow (FMM-001) mismatch.

2.6.18 Steam Generator-1 Main Steam Valve

The SG-1 main steam valve, MS-001, is a normally open valve provided with manual and automatic control. The valve is closed in manual control by placing the respective control panel switch in the CLOSED position. When the control switch is placed in the AUTO position, the valve remains open.

2.6.19 Steam Generator-2 Control

The SG-2 controller maintains level in the SG above the U-tubes but low enough so that the generator moisture separator does not flood. The controller takes input from narrow-range SG-2 level (LDP-304) and determines if the SG feedwater regulator valve, MF-012, should open or close to match the current steam demand. Since the steam-out controller maintains a relatively constant steam flow by regulating the main steam valve, MS-008, the controller's main purpose is to make up for small variations and transients and to allow a method for filling the generators manually, if desired.

When the S signal is received, the controller drives the output to 0 percent, thereby shutting the feedwater regulator valve.

The water level in SG-2 is temperature-compensated by the correction factor:

$$(TCF) = T_{SG-2} \times (0.00049) + 0.94025$$

where

$$T_{SG-2} = \text{SG-2 temperature, TF-310}$$

The temperature-corrected water level is used in the PID level control loop and as an input to an alarm. A control panel alarm alerts the operator if the compensated SG-2 level (LDP-302) is less than the low setpoint of 99 in. or above the high setpoint of 115 in. H₂O.

A control panel alarm alerts the operator if the SG-2 steam outlet pressure (PT-302) has exceeded the high setpoint of 310 psig.

The SG-2 controller display monitor shows the steam flow (FVM-002) and feed flow (FMM-002) mismatch.

2.6.20 Steam Generator-2 Main Steam Valve

The SG-2 main steam valve, MS-002, is a normally open valve provided with manual and automatic control. The valve is closed in manual control by placing the respective control panel switch in the CLOSED position. When the control switch is placed in the AUTO position, the valve remains open.

2.6.21 Main Steam Control Valve Control

The main steam control valve controller has two functions when it is in the AUTO position. First, it takes input from both SG pressures (PT-301, PT-302), averages them, and maintains the position of the main steam control valve, MS-008, so that the average pressure is 285 psig during nonmatrix-test operation. When an S signal is detected, the average pressure maintained by MS-008 is 335 psig. Second, break separator pressure (PT-902) from the BAMS controller via the microlink, is processed. If break separator pressure exceeds the high-high setpoint of 40 psig, the PLC provides a signal to open the containment pressure control valve, CSS-902.

2.6.22 Large-Break BAMS Control

The BAMS was designed to measure two-phase flow indirectly. The system uses separators to separate the two-phase flow into single-phase liquid and single-phase steam flows for direct flow rate and temperature measurements.

The BAMS controller provides several process functions as described in the following:

2.6.22.1 Break Separator Steam Isolation Valve

The break separator 8-in. steam line isolation valve, CSS-906, is a normally open valve provided with manual and automatic control. The valve is closed in manual control by placing the respective control panel switch in the CLOSED position. When the control switch is placed in the AUTO position, the valve closes when break separator steam flow (FVM-905 and FVM-906) decreases below 5000 cfm after the initial steam flow spike from the LOCA.

To set CSS-906 for automatic operation prior to a test, the following actions have to occur:

1. The valve is opened by selecting the OPEN position, and then the control switch is placed in the AUTO position.
2. When the break valve opens, the steam flow has to go above the low flow setpoint of 5000 cfm to reset the logic.
3. When the steam flow decreases to 5000 cfm, the BAMS controller sends a signal to the PLC and the PLC closes the valve.

After the initial burst of steam, the PLC controller uses an edge-triggered function to maintain the valve in the open position at the beginning of the test, when the total break separator steam flow (FVM-905 + FVM-906) is below 5000 cfm. The PLC is triggered to close the valve if the steam flow decreases below the setpoint of 5000 cfm.

2.6.22.2 Containment Pressure Isolation Valve

The containment 10-in. pressure isolation valve, CSS-902, is a normally closed valve provided with manual and automatic control. The valve is opened in manual control by placing the respective control panel switch in the OPEN position. When the control switch is placed in the AUTO position, the valve closes when break separator steam flow (FVM-901 and FVM-902) decreases below 6000 cfm after the initial steam flow spike from the LOCA.

To set CSS-902 for automatic operation prior to a test, the following actions have to occur:

1. The valve is opened by selecting the OPEN position, and then the control switch is placed in the AUTO position.

2. When the break valve opens, the steam flow has to go above the low flow setpoint of 6000 cfm to reset the logic.
3. When the steam flow decreases to 6000 cfm, the BAMS controller sends a signal to the PLC and the PLC closes the valve.

After the initial burst of steam, the PLC uses an edge-triggered function to maintain the valve in the open position at the beginning of the test, even though the total break separator steam flow (FVM-901 + FVM-902) is below 6000 cfm. The PLC then triggers to close the valve if the steam flow decreases below the setpoint of 6000 cfm.

2.6.22.3 Containment Pressure Control Valve

The containment pressure isolation valve, CSS-901, simulates backpressure in a post-LOCA condition by controlling the position of the valve. During the tests, the backpressure was a function of time and was different for each of the three breaks (2-in., 4-in., or DVI break). The BAMS controller simulated containment pressure during the breaks. The automatic containment backpressure control function was only used in Matrix Test SB19.

For 2-in. and 4-in. breaks, the following equations were implemented:

$$\begin{aligned} \text{For } 0 \leq t \leq 555 \text{ sec.}; P &= 2.753 \times 10^{-2} \times t \\ \text{For } 555 < t \leq 1056 \text{ sec.}; P &= 20.359 - 9.152 \times 10^{-3} \times t \\ \text{For } 1056 < t \leq 1556 \text{ sec.}; P &= 10.695 \\ \text{For } 1556 < t \leq 4667 \text{ sec.}; P &= 16.042 - 3.437 \times 10^{-3} \times t \\ \text{For } t > 4667; P &= 0 \text{ psig} \end{aligned}$$

where

$$\begin{aligned} P &= \text{PT-902 (psig)} \\ t &= \text{time (sec.)} \end{aligned}$$

For DVI break, the following equations are implemented:

$$\begin{aligned} \text{For } 0 \leq t \leq 77 \text{ sec.}; P &= 0.2265 \times t \\ \text{For } 77 < t \leq 228 \text{ sec.}; P &= 19.48 - 0.2265 \times t \\ \text{For } 228 < t \leq 530 \text{ sec.}; P &= 12.29 + 0.004934 \times t \\ \text{For } 530 < t \leq 1306 \text{ sec.}; P &= 19.79 - 0.009226 \times t \\ \text{For } 1306 < t \leq 3741 \text{ sec.}; P &= 11.88 - 0.003176 \times t \\ \text{For } t > 3741; P &= 0 \text{ psig} \end{aligned}$$

where

$P = \text{PT-902 (psig)}$

$t = \text{time (sec.)}$

2.6.22.4 Condensate Return Pump IRWST Control Valve

The condensate return pump IRWST control valve, CSS-928, simulates post-LOCA condensate makeup flow to the IRWST. The condensate return pump primary sump control valve, CSS-927, simulates post-LOCA condensate makeup flow to the primary sump. The condensate makeup flow was a function of time and the following functions were applied:

- The fraction of condensate that went to the primary sump changed over time, and the fraction that was made up to the IRWST was equal to $1 - \text{primary sump fraction}$. Equations showing the primary sump fraction:

$0 \leq t \leq 25 \text{ sec.}; \text{ fraction} = 1$

$255 \leq t \leq 600 \text{ sec.}; \text{ fraction} = 1.32 \times \text{time}^{-0.167}$

$600 \leq t \leq 2911 \text{ sec.}; \text{ fraction} = 0.5668 - 0.0001947 \times \text{time}$

$t > 2911 \text{ sec.}; \text{ fraction} = 0$

- This fraction was multiplied by the total steam flow (FVM-901 + FVM-902) that was exiting the building. In the calculation process, all units were in lbm/sec.
- Condensate flow proportioning was independent of the type of break that was initiated and therefore was always the same function of time.

2.6.22.5 ADS 4-1 Separator Steam Isolation Valve

The ADS 4-1 separator steam isolation valve, CSS-905, is a normally open valve provided with manual and automatic control. When in the AUTO position, the valve opens coincident with the TEST pushbutton being pressed to initiate a test.

**TABLE 2.6-1
PROGRAMMABLE CONTROLLER SUMMARY**

Controller	Inputs	Outputs	Trip Signals	Alarms
Reactor heaters	SCR-1 power (KW-101) SCR-2 power (KW-102) HL-2 temperature (TF-140) HL-1 temperature (TF-141) Emergency pushbutton signal (PLC) External trip PZR pressure high-high trip S signal (test start)	Current output to SCR-1 Current output to SCR -2 Reactor water temperature high (panel alarm)	SCR-1 high output power SCR-2 high output power Total output power high Avg. hot-leg temp high Emergency pushbutton External trip: 2/4 rod sheath temp. high TH-507-4/TH-501-4 temp. high KEY switch in OFF SCR cabinet temp. high PZR pressure high-high RCP cooling water low flow without S signal Gland seal water temp. high without S signal	Reactor water temp. high
SG-1	SG-1 wide-range level (LDP-301) SG-1 steam temperature (TF-301) SG-1 narrow-range level (LDP-303) SG-1 feed flow (FMM-001) S signal (PLC) SG-1 steam flow (FVM-001)	Control signal to valve motor (MF-011) SG-1 level high/low (PLC) Input to feed pump trip logic (PLC)	S signal (PLC) SG-1 level high-high (LDP-301)	SG-1 level high/low
SG-2	SG-2 wide-range level (LDP-302) SG-2 temperature (TF-310) SG-2 narrow-range level (LDP-304) SG-2 feed flow (FMM-002) S signal (PLC) SG-2 steam flow (FVM-002)	Control signal to valve motor (MF-012) SG-2 level high/low (PLC) Input to feed pump trip logic (PLC)	S signal (PLC) SG-2 level high-high (LDP-302)	SG-2 level high/low

TABLE 2.6-1 (Continued)
PROGRAMMABLE CONTROLLER SUMMARY

Controller	Inputs	Outputs	Trip Signals	Alarms
BAMS	Condensate flow to sump (FMM-903) Condensate flow to IRWST (FMM-904) Break steam flow (6-in line) (FVM-905) Break steam flow (8-in line) (FVM-906) Break separator pressure (PT-902) Steam flow main (6-in line) (FVM-901) Steam flow main (10-in line) (FVM-902) S signal (PLC)	Control signal to valve motor (CSS-927) Control signal to valve motor (CSS-928) Indication total break steam flow (IND-905) Control signal to valve motor (CSS-901) Shut signal for air-operated valve (CSS-906) Shut signal for air-operated valve (CSS-902) BAMS header pressure high-high (P-P, SOC) (PT-902)	Low steam flow shut signal (CSS-906) Low steam flow shut signal (CSS-902)	Break separator pressure high-high (processed through steam out controller)
PZR Heater	PZR level (LDP-601) PZR temperature (TF-608) Narrow-range PZR pressure (PT-602) Wide-range PZR pressure (PT-604) External trip	PZR level bar graph (BGI-6, LDP-601) Current output to SCR control PZR pressure high to RCS (PLC, PT-604) PZR pressure high/low (panel alarm) (PLC) PZR pressure high-high (logic) (RXC) PZR pressure (analog) (P-P, CVS, and RNS)	PZR pressure high-high (PT-604) PZR level low-low (LDP-601) PZR temp. high (IND-608, TF-608) External trip: SCR cabinet temp. high (PLC, TSH-001) S signal (PLC) Emergency pushbutton KEY switch	PZR pressure high/low PZR pressure level high/low
CVS and RNS pumps	CVS discharge flow (FMM-801) ⁽¹⁾ RNS discharge flow (FMM-805) ⁽¹⁾ CVS pump start signal (PLC) RNS pump start signal (PLC) PZR pressure (PZRC)	Control signal to valve motor (RCS-808) Control signal to valve motor (RCS-811) Speed signal to CVS pump speed controller (in the field)	PZR pressure (PT-604) 385 psig increasing, trip CVS pump 230 psig increasing trip RNS pump	None

TABLE 2.6-1 (Continued)
PROGRAMMABLE CONTROLLER SUMMARY

Controller	Inputs	Outputs	Trip Signals	Alarms
Steam out	SG-1 pressure (PT-301) SG-1 steam flow (FVM-001), Total steam flow (FVM-003) SG-2 pressure (PT-302) SG-2 steam flow (FVM-002) S signal (PLC) Break separator pressure flow (BAMS controller, PT-902)	Control signal to valve control motor (MS-008) SG-1 steam flow (SG1 controller) SG-2 steam flow (SG2 controller)	Break separator pressure high-high trip for CSS-902 to open	None

Note:

(1) Prior to the matrix tests, FTM-801 was changed to FMM-801, and FMM-804 was changed to FMM-805.

**TABLE 2.6-2
PROCESS CONTROL SYSTEM COMPONENTS**

Component	Mfr./Model No.	Number	Function
Temperature scanner	Omega™ CN34025-DC	2	Indicates temperatures of trace heaters; off-on control at adjustable setpoint
Temperature scanner	Omega™ CN101K-1000F	1	Provides alarm if RCP seal cooling water exceeds adjustable setpoint
Power meters	Power Measurements™, 3710 ACM	2	Indicate power to each bank of rod bundle heaters
Bar-graph indicators ⁽¹⁾	Universal™ VB-120-2-4	14	Indicate percent of range for the following parameters: ADS 1-3 separator level ADS 4-1 separator level ADS 4-2 separator level Break separator level CRP level Feed storage tank level CMT-1 level CMT-2 level IRWST level ACC-1 level ACC-2 level Primary sump level Secondary sump level Pressurizer level
Panel switches and lights	Square D™	33	Provides CLOSE/AUTO/OPEN control for air-operated valves, pump/fan power with STOP/RUN indicator lights.
Alarms	Panalarm™ Series 90	1	Alarm annunciator with 14 individual lights and a horn.
Process indicators ⁽²⁾	Newport™ Model 82	31	Indicates value of process parameters: pressure, temperature, and flow.

Note:

- (1) The bar-graph indicators had setpoints programmed in for the appropriate process function alarms, contacts, and bistables.
(2) The process indicators had setpoints programmed in for the appropriate process function alarms, contacts, and bistables.

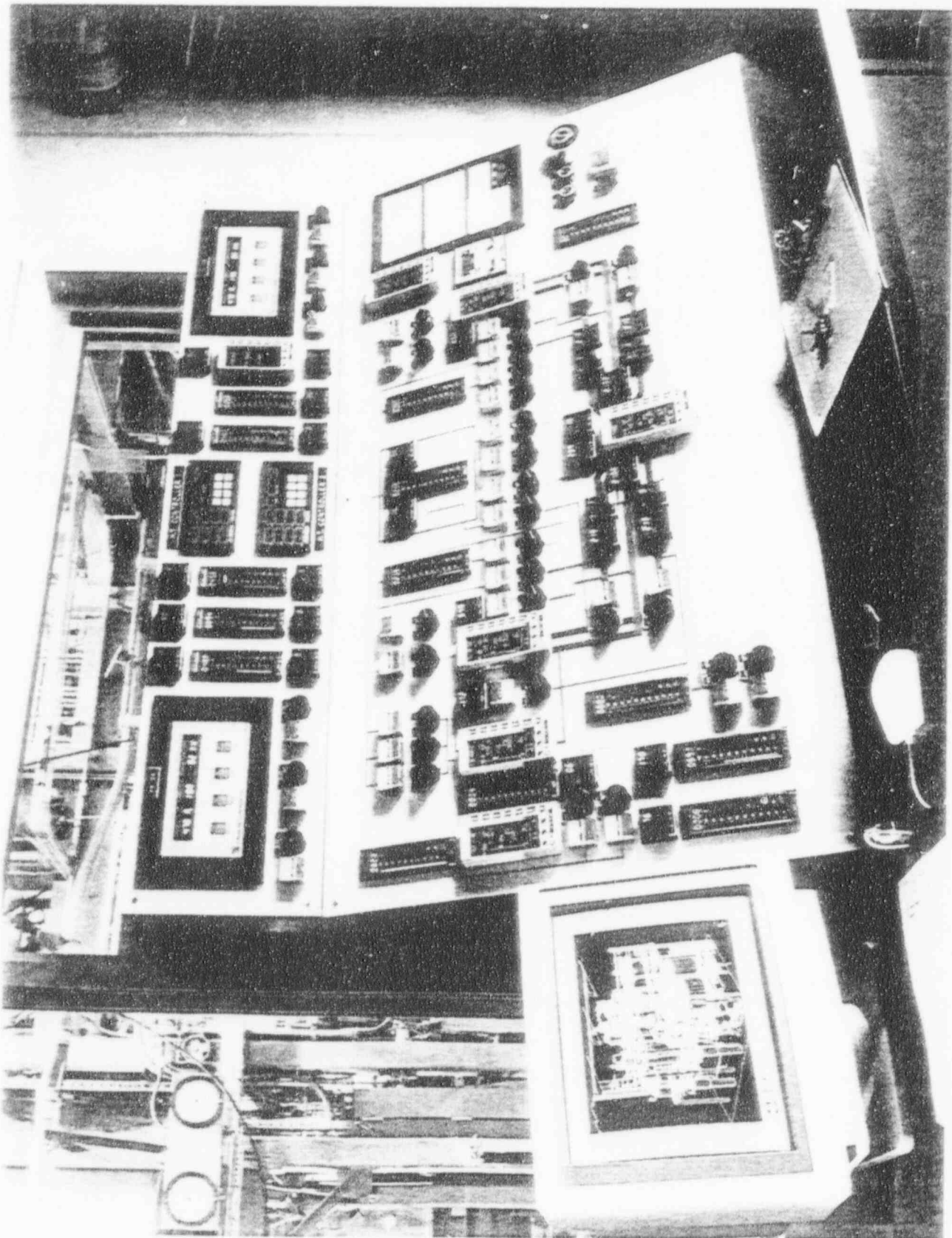


Figure 2.6-1 Photograph of Operator Panel

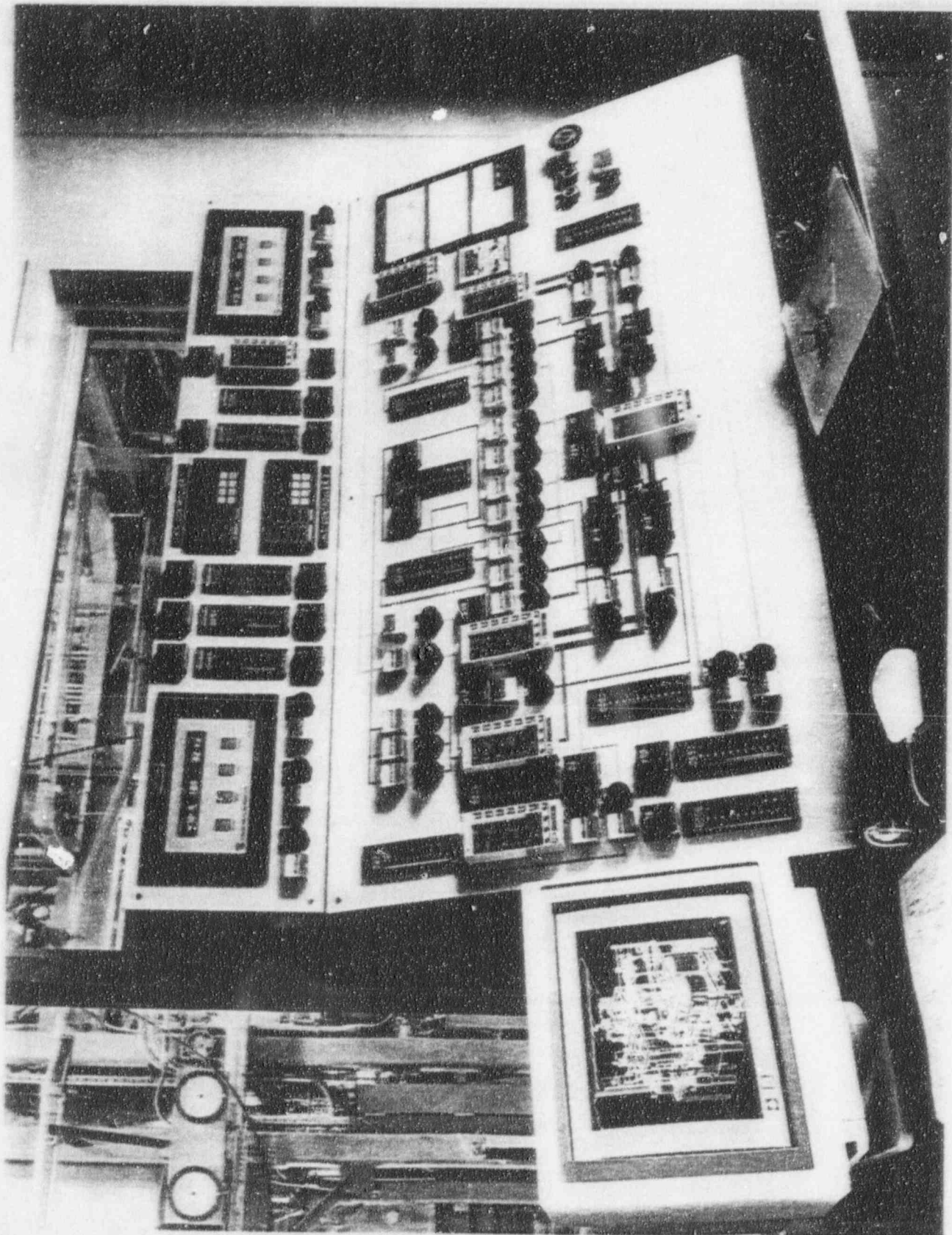


Figure 2.6-1 Photograph of Operator Panel

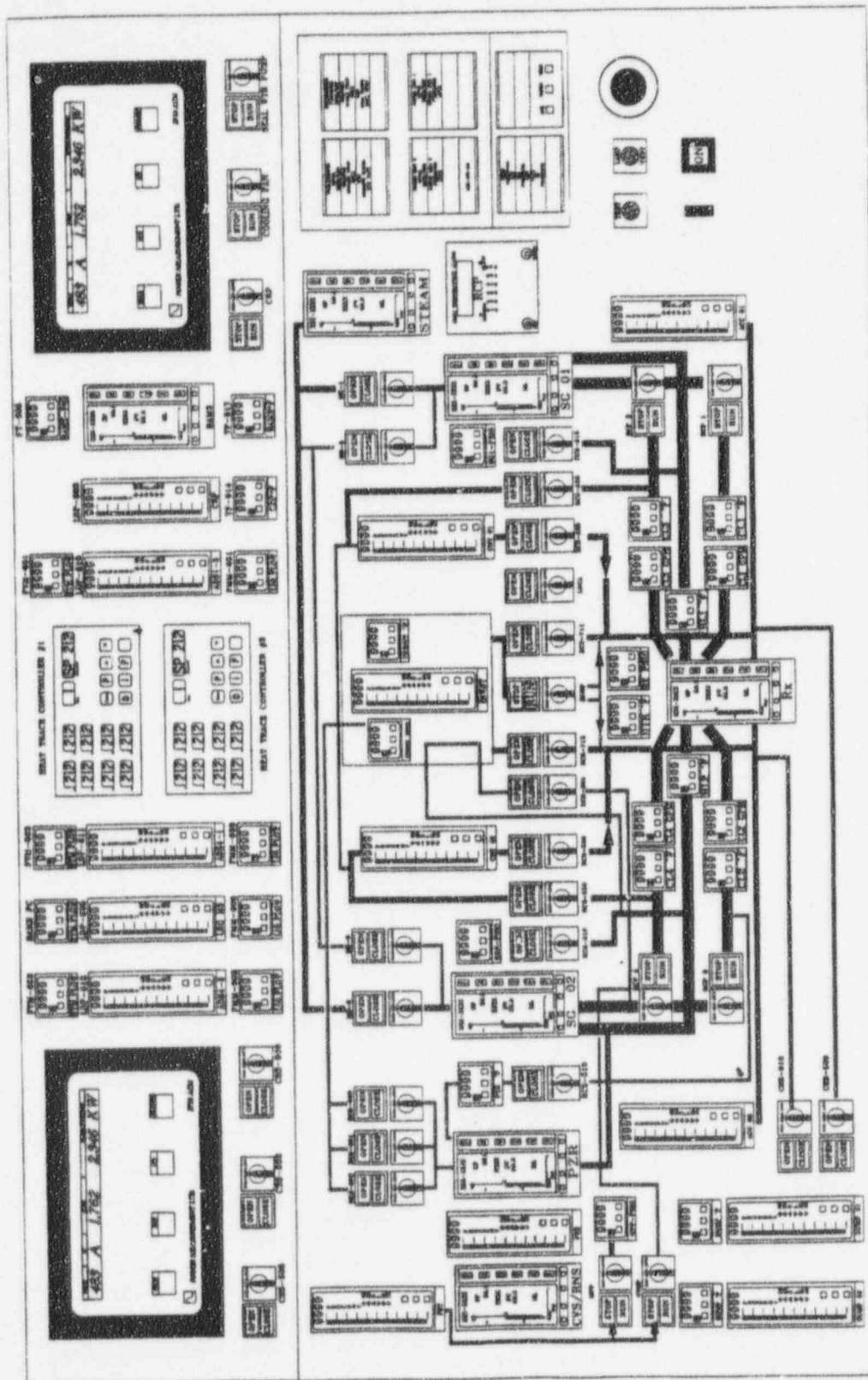


Figure 2.6-2 Drawing of Operator Panel

2.7 Pre-Test Operation

Prior to every test, a series of operations is performed to ensure that every test is performed with the facility in a defined and documented condition. A fill-and-vent procedure was performed using an approved operating procedure. Then, a valve line-up (filling the accumulators, IRWST, and loop seals to the overflow levels) was completed using an approved operating procedure.

The initial accumulator levels were established by filling the accumulator until flow was observed from an overflow standpipe. The standpipe was inserted and its elevation set during cold pre-operational facility testing, which ensured that the accumulators were set at the same level for each test. The accumulators were also pressurized to their initial pressure with nitrogen. Local pressure indicators PI-401 and PI-402 indicated the proper pressure for accumulator-1 (ACC-1) and accumulator-2 (ACC-2), respectively.

The initial level for the IRWST was also established by filling the tank with water until water was observed flowing in its overflow line. The filling was then stopped, and the tank was allowed to drain to the level of the fill tap of the tank. Similar to the accumulators, the fill standpipe level was set during cold pre-operational testing, ensuring that the level was the same for all tests.

During these initial system preparations, a check of the DAS was made for the proper response of level and differential pressure transmitters. During heatup, the remaining channels of the DAS were checked for proper response to changing system parameters.

The facility was brought to normal operating temperature (420°F) and normal operating pressure (370 psig) using the reactor heaters in manual mode. The secondary side was brought to normal operating pressure (285 psig) during heatup. The secondary pressure was controlled in automatic by the secondary steam pressure controller. Prior to test initiation, the reactor controller was placed in automatic control to maintain the average temperature of the hot legs (420°F). The reactor and steam controllers interacted as they automatically controlled RCS temperature and secondary steam pressure.

When all prerequisites were met, and the facility was at the required temperature and pressure, a final valve line-up was performed from the control panel. The final preparations were conducted using the "Initial Conditions" section of the test procedure. As part of these initial conditions, the pressures and levels of the SGs, pressure and level of the pressurizer, and hot-leg temperatures were established within tolerances specified by the procedure. When these parameters met the initial conditions, the control board indication was recorded, and the TEST pushbutton was pressed.

Per design, 2 minutes elapsed between pressing the TEST pushbutton and generating the signal to open the break valves. Pressing the TEST pushbutton also initiated a signal for the DAS to begin recording data. The three racks of the DAS began recording data 12 to 14 seconds after the TEST

pushbutton was pressed. The delay, due to the DAS communication time, was typical and did not affect test results. All DAS channels acquired steady-state data for almost 2 minutes before the break valves opened.

One minute after pressing the TEST pushbutton, the operator opened CMT-1 balance line isolation valves RCS-529 and RCS-530. These valves are normally open in the AP600 plant; however, in an attempt to establish the required initial test conditions at the top of the CMTs (less than 80°F), these valves remained closed until 1 minute before break initiation.

Control board data for initial conditions of the SGs, pressurizer, and hot legs were recorded in the procedure. Indications for SG and pressurizer levels were density-compensated by local controllers on the control panel. The same data were monitored and recorded by the DAS after the TEST pushbutton was pressed. However, during the time when initial conditions were being established, the DAS initialized and was awaiting a trigger to start. The DAS did not start acquiring data until after the TEST pushbutton was pressed. Thus, it was necessary to use control board indications to establish initial conditions.

2.8 Drawings

Physical characteristics of the test facility are documented in sketches that were prepared for several purposes, including the following:

- Westinghouse-prepared sketches defined hardware and instrumentation design requirements.
- Vendor drawings (TIC, Wright-Austin 6, Harris Thermal Transfer Products)TM provided component fabrication details.
- Westinghouse-prepared sketches prepared at OSU documented the as-installed features of the facility piping.

P&IDs prepared by OSU documented the interconnection of components and instrumentation are included in Appendix G. The major systems and component drawings are included in *Facility Description Report*, WCAP-14124.⁽⁷⁾ A review of the test data indicated an inconsistency between the drawings and the facility condition. P&ID 600203 shows an orifice at the bottom of the ADS 1-3 separator. This orifice (ORI-659) was not in place for either the flow or matrix tests.

3.0 DATA REDUCTION

3.1 Introduction

The following sections describe the data reduction and validation processes used for the low-pressure integral systems tests performed at Oregon State University (OSU). The data were transmitted in ASCII format on recordable compact disks (CD-R) from the OSU test site to Westinghouse. As part of the data reduction and validation process, the OSU data files were run through several manipulations at Westinghouse to create usable data files and plots. Various data plotting methods were used to review, validate, and present the data.

3.2 Test Validation

The OSU test facility data were reviewed and validated using a three-step process. The first step was performed at the OSU test facility immediately following the test and was documented in the Day-of-Test Report. The Day-of-Test Report and the CD-Rs were sent to Westinghouse within 1 or 2 days of the test. All of the data from one test fit onto one CD-R. The Day-of-Test Report evaluated the test from a very basic standpoint, including operability of key instruments and deviations from specified initial conditions (that is, Did the test meet the minimum acceptance criteria?). The Day-of-Test Report also documented any facility modifications or onsite test observations. Specifically, the Day-of-Test Report assessed whether the test needed to be rerun because of some significant problem observed during the performance of the test. See Appendix A for a sample of the Day-of-Test Report format.

The overall test acceptance criteria are shown in Table 3.2-1. Although not an explicit part of the pre-test acceptance criteria, an overall facility mass balance objective of 10 percent was established. The critical instruments were the minimum set of instruments identified by the safety analysis personnel to perform a transient, component-by-component mass and energy balance. Critical instruments are listed in Table 3.2-2.

The second step in the data validation process was performed primarily by the test engineering personnel at the Energy Center in Pittsburgh, Pennsylvania. This step was performed after receiving the Day-of-Test Report and processing the CD-R. This data validation was documented in the Quick Look Report (QLR). The Quick Look Report provided a preliminary validation of all test data (that is, Did the data meet all acceptance criteria?). A standard outline was issued to and accepted by the Nuclear Regulatory Commission (NRC) prior to writing the Quick Look Reports. The key purpose of the Quick Look Report was to issue to the NRC some "pedigree" of the data, without specifically evaluating the data for code validation purposes (reviewed but not yet validated data) shortly after the test was performed.

The Quick Look Report examined the test in more detail than the Day-of-Test Report, including items such as calculation of an overall facility mass balance; deviations from specified initial conditions (heater rod bundle power decay); and identification of any out-of-range, suspicious, or failed instruments. As part of the Quick Look Report process, different types of instruments were reviewed to verify response of other instruments.

The safety analysis personnel reviewed and signed the Quick Look Reports prior to issuance. This ensured that there was an understanding of how the test performed and determined if any unusual facility responses occurred. Preliminary data files on digital audio tape (DAT) were transmitted to the NRC with the Quick Look Report. A Quick Look Report was issued for each accepted test. Several tests were judged unacceptable and were rerun until an acceptable run was accomplished. Then a Quick Look Report was issued.

The final step included a detailed review of the transient progression, facility and component performance, and cross-test comparisons. This report provides the final assessment as to whether the respective data are acceptable for code validation purposes.

Figure 3.2-1 illustrates how the data validation process progressed from the OSU test site to the Energy Center. This figure shows the building-block approach followed in reviewing, evaluating, validating, and documenting the data. Each step in the process was based on the previous step, utilizing information and knowledge from the previous step, but was generally performed by a different set of personnel. As the process progressed from left to right, the steps evolved from problem identification to problem resolution. This three-step process allowed various personnel from different disciplines to review the data prior to final publication. These steps were followed in order to provide a high level of data quality assurance.

**TABLE 3.2-1
OVERALL ACCEPTANCE CRITERIA**

- Test initial conditions shall be achieved in a specified tolerance.
- Setpoints shall be achieved in an acceptable tolerance band.
- Sufficient instrumentation shall be operational before the test (exceptions shall be approved by the Westinghouse test engineer).
- Critical instruments not operating shall be identified to the Westinghouse test engineer before the tests. These instruments must be operational before and during the test, or exceptions should be approved.
- A zero check of LDPs, DPs, and FDPs shall be in acceptable tolerances.

The zero check was eliminated from the acceptance criteria for Category III tests. The earlier pre-test and post-test checks of zero shift showed acceptable variation in the readings of these instruments. Performing these checks required that each instrument be manually isolated and then returned to service. Based on the consistency of the readings from earlier tests and the large number of manual operations, it was decided that the risk of an instrument remaining isolated after the check was greater than an instrument having a zero shift.

**TABLE 3.2-2
CRITICAL INSTRUMENT LIST**

Channel ID	Description
Vessel	
PT-107	Pressure at top of vessel head
DP-130	Pressure difference between top of vessel head and top of downcomer
LDP-127	Level measurement from bottom of vessel to bottom of upper head
LDP-140	Level measurement from top of downcomer to bottom of vessel
TF-105 or TF-107	Fluid temperature measurement in CL-1
TF-106 or TF-108	Fluid temperature measurement in CL-2
TF-101 or TF-103	Fluid temperature measurement in CL-3
TF-102 or TF-104	Fluid temperature measurement in CL-4
TF-120	Fluid temperature at bottom of vessel upper head
TF-141 or TF-143	Fluid temperature measurement in HL-1
TF-140 or TF-142	Fluid temperature measurement in HL-2
Total of four heater rod thermocouples	Temperature near surface of heater rod
Pressurizer	
PT-603	Pressurizer pressure
LDP-601	Pressurizer liquid level
TF-605 or TF-608	Pressurizer liquid space fluid temperature measurement

**TABLE 3.2-2 (Continued)
CRITICAL INSTRUMENT LIST**

Channel ID	Description
SG-1 Primary Side	
PT-201	Primary-side pressure at top of long U-tubes
LDP-215	Pressure difference along hot side of SG-1 long U-tube
LDP-219	Pressure difference along cold side of SG-1 long U-tube
FMM-201	CL-1 mass flow rate; magnetic flow meter
FMM-203	CL-3 mass flow rate; magnetic flow meter
SG-1 Secondary Side	
PT-301	SG-1 secondary-side pressure, main steam line
FMM-001	Feed flow to SG-1; magnetic flow meter
FVM-001	SG-1 steam flow; vortex flow meter
LDP-301	SG-1 secondary-side level
SG-2 Primary Side	
PT-204	Primary-side pressure at top of long U-tubes
LDP-218	Pressure difference along hot side of SG-2 long U-tube
LDP-222	Pressure difference along cold side of SG-2 long U-tube
FMM-202	CL-2 mass flow rate; magnetic flow meter
FMM-204	CL-4 mass flow rate; magnetic flow meter
SG-2 Secondary Side	
PT-302	SG-2 secondary-side pressure, main steam line
FMM-002	Feed flow to SG-2; magnetic flow meter
FVM-002	SG-2 steam flow
LDP-302	SG-2 secondary-side level

TABLE 3.2-2 (Continued)
CRITICAL INSTRUMENT LIST

Channel ID	Description
ACC-1	
PT-401	Tank pressure
LDP-401	Level transducer
FMM-401	Flow measurement magnetic flow meter
TF-401	Liquid temperature at accumulator discharge
ACC-2	
PT-402	Tank pressure
LDP-402	Level transducer
FMM-402	Flow measurement; magnetic flow meter
TF-402	Liquid temperature at accumulator discharge
CMT-1	
PT-501	Tank pressure
LDP-507	Tank level measurement
FMM-501	CMT discharge line flow rate measurement
TF-501 and TF-529	CMT fluid temperatures from long rake
CMT-2	
PT-502	Tank pressure
LDP-502	Tank level measurement
FMM-504	CMT discharge line flow rate measurement
TF-504 and TF-532	CMT fluid temperatures from long rake

**TABLE 3.2-2 (Continued)
CRITICAL INSTRUMENT LIST**

Channel ID	Description
IRWST/PRHR HX	
FMM-802	Flow rate into PRHR HX; magnetic flow meter
LDP-802	Level measurement in PRHR HX
FMM-804	Flow rate of PRHR HX; magnetic flow meter
LDP-701	Level measurement in IRWST
FMM-701	Flow measurement, IRWST to DVI line-1; magnetic flow meter
FMM-702	Flow measurement, IRWST to DVI line-2; magnetic flow meter
TF-701 and TF-709	Fluid temperature measurements in IRWST adjacent to PRHR HX
ADS-1, ADS-2, ADS-3, and ADS-4 Actuation	
FDP-605	ADS-1 actuation line flow; differential pressure cell
FDP-604	ADS-2 actuation line flow; differential pressure cell
FDP-606	ADS-3 actuation line flow; differential pressure cell
PT-605	Pressure measurement on ADS-1, ADS-2 and ADS-3 separator
FVM-601	Steam flow from ADS-1, ADS-2 and ADS-3 separator; vortex flow meter
FMM-601	Liquid flow from ADS-1, ADS-2 and ADS-3 separator; magnetic flow meter
PT-611	Pressure in the ADS-4 separator for the loop 1
FMM-603	Flow rate from the ADS-4 separator for the loop 1; magnetic flow meter
FVM-603	Flow rate from loop 1 ADS-4 separator; vortex flow meter
PT-612	Pressure in the ADS-4 separator for the loop 2
FMM-602	Flow rate from the ADS-4 separator for the loop 2; magnetic flow meter
FVM-602	Flow rate from the ADS-4 separator for the loop 2; vortex flow meter

**TABLE 3.2-2 (Continued)
CRITICAL INSTRUMENT LIST**

Channel ID	Description
Sump, Power, and Other Instruments	
PT-901	Pressure in primary sump vessel
LDP-901	Level measurement in primary sump vessel
LDP-902	Level measurement in secondary sump vessel
PT-905	Pressure of break flow separator
LDP-905	Levels measurement for break flow separator
FMM-905	Flow measurement from break flow separator to primary sump; magnetic flow meter
FVM-901	Flow measurement in BAMS, vortex flow meter
FVM-902	Flow measurement in BAMS, vortex flow meter
FVM-903	Flow measurement in BAMS, vortex flow meter
FVM-905	Flow measurement from break flow separator, vortex flow meter
FVM-906	Flow measurement from break flow separator, vortex meter
TF-916	Fluid temperature measurement in BAMS exhaust line
TF-917	Fluid temperature measurement in BAMS exhaust line
KW-601	Watt meter for power to the pressurizer
KW-101, KW-102, KW-103, and KW-104	Watt meters for power to core simulation

STEP 3		
		Perform evaluation of parametric effects, i.e., break sizes
		Provide and review cross-plots of data between tests
		Perform data uncertainty analysis
		Perform transient and component evaluation
STEP 2		
	Perform simple benchmark evaluation on rod bundle	Perform system-wide transient evaluation
	Perform overall mass balance	Confirm overall mass balance
	Provide minimum facility design information	Provide adequate facility design information
STEP 1	STEP 2	STEP 3
Identify if test met minimum acceptance criteria	Identify if test met ALL acceptance criteria	Identify all tests performed, valid and invalid, and reason for validity
Provide unqualified data files for all tests	Provide unqualified data files for acceptable tests only	Provide qualified data files with zero time shift (valid data only)
Provide key data plots	Review key multichannel plots, e.g., HL-1 versus HL-2	Provide key multichannel plots, e.g., HL-1 versus HL-2
Identify anomalous data	Identify/resolve anomalous data	Identify/resolve anomalous data
Provide test observations	Provide test observations	Provide and discuss test observations; resolve problems
Provide sequence of events	Compare actual and specified sequence of events	Resolve differences in actual and specified sequence of events
Identify procedure deviations	Identify procedure deviations; briefly describe procedure	Resolve procedure deviations; describe test procedure
Identify facility configuration/modifications	Identify facility configuration/modifications	Identify facility configuration/modifications
Check key initial conditions	Check all initial conditions (ICs)	Resolve deviations in ICs
Identify inoperable instruments	Identify inoperable and erratic instruments	Compare inoperable instrument lists between tests
Check critical instruments	Check all instruments	Verify all instruments
Day-of-Test Report at OSU test site	Quick Look Report at Westinghouse Energy Center	Final Data Report at Westinghouse Energy Center

Figure 3.2-1 Data Documentation Steps

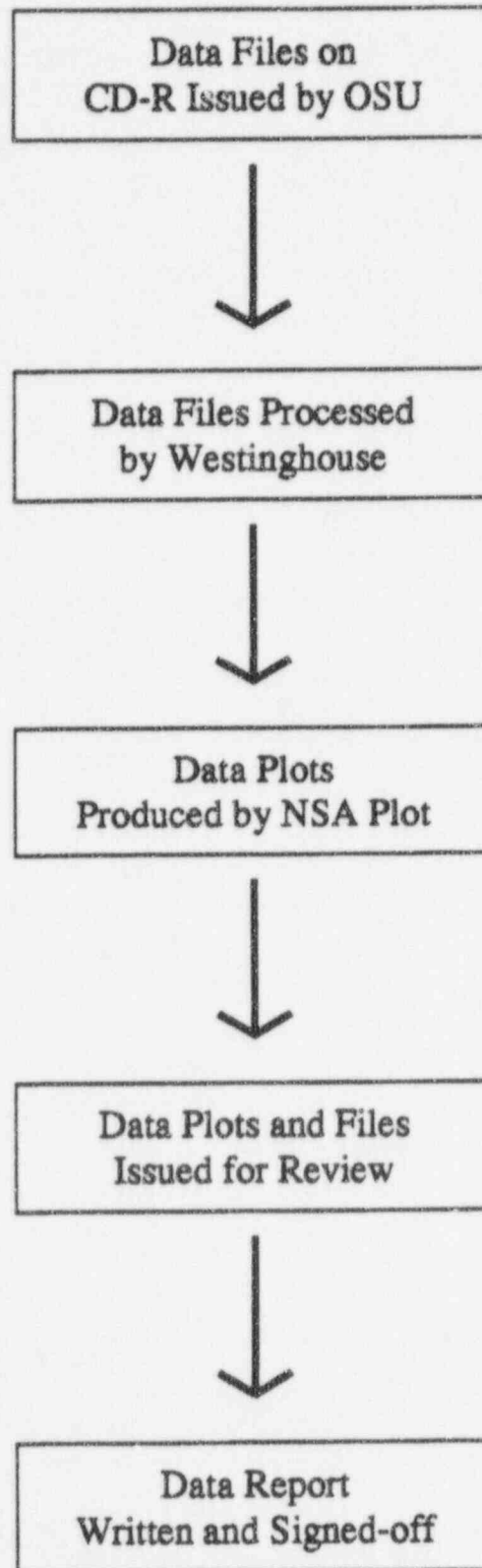


Figure 3.2-2 Steps in OSU Data Processing

3.3 Pre-Operational Tests

The pre-operational tests were segregated into cold and hot tests. The purpose of the cold pre-operational tests was to determine facility characteristics such as tank volumes and component flow resistances using cold water. The tank volumes and flow resistances were calculated directly by OSU test site personnel. The cold pre-operational test data were provided by OSU in hard-copy form only. The report issued from OSU was reviewed at Westinghouse and, subsequently, transformed into a Quick Look Report format. This Quick Look Report was issued to the NRC. See Subsections 4.1 and 4.2 for a description of results from the cold pre-operational tests.

The purpose of the hot pre-operational tests was to determine facility characteristics such as the facility heat losses and verify operation of the facility under hot operating conditions. The hot pre-operational test data were provided on CD-R. The hot pre-operational test data were generally processed and reviewed in the manner described in Subsection 3.4. The data files for the final hot pre-operational test (HS01) are provided with this report. The data files for the other two pre-operational tests (HS02 and HS03) are not transmitted in this report, since they were not needed for code validation purposes. See Subsection 4.3 for the description of results from the hot pre-operational tests.

3.4 Matrix Tests

All data for the matrix tests were provided by OSU on CD-Rs in 12 files. These 12 files contained the data for the three data acquisition system (DAS) racks with each rack segregated into two parts, burst scan and continuous scan data files. The LTCT number (run and matrix number) was incorporated into the filenames. The data provided by OSU were in English engineering units with both a clock time in HH:MM:SS and a zero test start time. Zero time was defined as the time of break valve opening. The DAS was started about 2 minutes in advance of the test initiation; therefore, the data files included about 120 seconds of negative test time. In addition to the 12 data files, a configuration file for each of the three DAS racks was provided on the CD-R. The configuration file contained the calibration information for the instruments.

A series of data reduction steps was developed and implemented to process the data. The overall data reduction process is illustrated in Figure 3.2-2. The process followed for the Quick Look Reports was slightly different than that followed for this report because of some issues discovered during testing and data review. The key differences included resetting the data to the correct test initiation time (zero time), merging the burst scan and continuous scan files, correcting the zero settings for some pressure transmitters, and correcting the calibration files for several instruments. These steps are briefly described in the following three paragraphs.

The zero time assigned by the DAS at OSU was off generally by about 10 seconds; therefore, the data files were adjusted for the correct zero time. Several channels were reviewed for each instrumentation rack to ascertain the precise time that the break was initiated. The respective time correction was then added to each time stamp in each of the files. See Appendix A for more details on this data reduction step.

The burst scan and continuous scan files were merged to form a hybrid data file. This hybrid file provided the most practical form for the data. The burst scan data were copied into the continuous scan data file for the overlapping time period, generally between the first 30 to 60 minutes of the test. Thus, the hybrid file contained data with a scan rate of []^{a,b,c} for the first 30 to 60 minutes and a []^{a,b,c} scan rate for all data thereafter. An evaluation was performed on the differences between the burst scan and continuous scan data. It was found that the data were very similar, except for the spikes in the burst scan data, which were recorded due to the faster scan rate. For the Quick Look Report, only the continuous scan data files were reviewed and provided to the NRC (on DAT).

After most of the tests were completed, it was discovered at the site that several of the pressure transmitter zero settings were incorrectly set, and the calibration files for nine instruments were incorrect. These were corrected in the processing of the data for this report.

The DAS at the OSU test facility assigned a noninteger character to those data fields that exceeded the typical instrument ranges. These noninteger characters could not be handled in the Westinghouse

plotting package (called *NSAPlot*); therefore, they were replaced with integer values. The noninteger characters were generally attributed to those occasional times when the instrument was out of range. This would not prohibit the data from being validated.

After these corrections were made to the data files, the data were plotted by *NSAPlot*, which is capable of plotting the data in a variety of ways. A set of single- and multiple-channel plots was produced and issued for internal Westinghouse review. The multiple-channel plots generally included data from the different loops (for example, from the four cold legs or the two hot legs) or a family of instruments from a key component like the core makeup tank (CMT). The plots also contained 20-character instrument descriptions and locations. The processed data file was made available for use to safety analysts at Westinghouse. However, the data (both hard-copy plots and electronic files) for the blind test (Matrix Test SB09) were controlled to make them unavailable to safety analysis personnel.

After the plots of all data channels were distributed for internal Westinghouse review, two sets of calculations were produced to help validate the data. The first set calculated the average initial conditions for channels important to establishing facility steady-state conditions prior to test initiation, such as pressurizer pressure and hot-leg temperature. Comparisons of this report to specified initial conditions and allowable tolerances were performed and reported in the Quick Look Report and Section 5 as a table in the review of each matrix test. Any deviations outside the allowable tolerance were generally quite small and acceptable.

The deviations from the established tolerances were accepted due to the tighter-than-needed tolerances imposed in the test procedure. The restrictive test tolerances were established to achieve tests conditions that were, as much as possible, repeatable from test to test.

In addition to the calculation of the initial test conditions, the actual and specified heater rod power decay curves were also generated and plotted on the same graph. These curves were reviewed and are included in Appendix F of the Quick Look Report for both power supplies (KW-101 and KW-102). The redundant power supply measurements (KW-103 and KW-104) were also plotted against the specified power decay curves.

The actual sequence of events for each test was tabulated, reviewed, and compared to the expected sequence of events in the Quick Look Report. This sequence of events included pump trip times, automatic depressurization system (ADS) actuation times, CMT low-low level times, etc. This sequence of events review provided a quantitative assessment on the test performance. An expanded sequence of events is included in this report in Section 5. A table and bar chart are included for the review of each test.

As part of the Quick Look Report data review process, an overall facility mass balance was performed. This mass balance consisted of calculating the water masses in each of the major components prior to the test, calculating the water masses in each of the same components after the test, and calculating the

percent difference between the two time periods. The percent difference included only the in-containment refueling water storage tank (IRWST) water injected into the system, since this water contributed directly to the cooling of the heater rod bundle. Using the water remaining in the IRWST would have distorted the calculations of the percent difference. This facility mass balance provided a quantitative measure of confidence in the response of the component differential pressure transmitters and catch tanks and overall facility performance during the test. If the overall mass balance had been significantly affected (that is, greater than 10 percent), the test would have been repeated. The overall mass balance results are reported in Appendix E. The results of a transient mass and energy balance will be reported in the *AP600 Low-Pressure Integral Systems Test at Oregon State University Test Analysis Report*, WCAP-14292.⁽²⁾

As the last step in the Quick Look Report data review process, the fluid levels in the heater rod bundle, upper plenum, upper head, and hot legs were reviewed. These fluid levels were then evaluated with respect to the actuation and termination of the safety systems (such as accumulators, CMTs, and IRWST) to determine if the respective differential pressure transmitter response was reasonable. For example, Was there any impact of the accumulator injection on the fluid level in the heater rod bundle? This evaluation, however, did not include the effect of the density difference as the heater rod bundle cooled down. A similar evaluation of the fluid levels in the heater rod bundle is contained in this report including density compensation for differential pressure transmitter.

For this report, several additional steps were performed to validate the data, including a detailed review of the transient progression; a review of the performance of each of the major components; a detailed comparison of the different tests to ascertain effects of break size, break location, containment backpressure, and nonsafety system operation; and performance of an instrument error analysis. For this report, wherever appropriate, the saturation temperature corresponding to the component pressure (or system pressure) was plotted on temperature graphs to help understand the response of the respective thermocouples.



3.5 Instrumentation Error Analysis

The instrumentation error associated with the data from the OSU test series was derived from the equipment manufacturer's specifications, and these specifications were used to compute the error estimate for the data path. Component calibrations were performed to verify that the actual equipment performance was consistent with the manufacturer's specifications.

The data path for the OSU instruments consists of three parts: sensor, signal conditioner, and data acquisition system (DAS). In the case of a thermocouple, a signal conditioner is used only when its value is also displayed on the control panel. In most cases, thermocouple signals are fed directly into the DAS.

The errors due to the transmission wires between the elements and power supply variations were not included in this analysis; these errors are typically very small (± 0.001 percent) in comparison to the element errors and are considered negligible.

3.5.1 General

This section provides an estimate of the instrumentation error associated with the OSU test facility.

Test temperatures were generally measured using type-K thermocouples. Type-K thermocouple installation is discussed in Subsection 2.4.1 by individual component. Installation of the remaining instrumentation, such as pressure transmitters and flow meters is also discussed in Subsection 2.4.1 by type of instrument. These instruments were installed consistently throughout the facility.

In general, the error associated with the measurement's sensor or transducer and the signal conditioning and DAS equipment was considered in determining the total error for any given data channel. Because the transducer or sensor is normally dominant, total error and sensor error are typically very similar.

System and/or component calibration data were used, when available, to calculate an estimate of the overall error for each data channel; multiple sources of error were combined by summing the variances for each component of error.

Individual sources of error were combined in accordance with:

$$E = \left[\sum_{i=1}^N (E_i)^2 \right]^{1/2}$$

where:

- E = estimate of data channel error or total probable error
 E_i = value of i^{th} source of error component maximum error
 N = number of sources of error

All significant bias error is assumed to be accounted for using the appropriate corrections obtained from equipment calibrations. Where appropriate, when calibration data were not available (such as the case in which calibration was performed only to verify compliance with the manufacturer's specifications), the manufacturer-specified error was used. In these cases, the manufacturer-specified error was considered to be the maximum error and assumed to be uniformly distributed over the error interval. Since the variance of a uniformly distributed random variable over the interval $-\alpha < x < \alpha$ is $\frac{\alpha^2}{3}$, standard deviation of the maximum error was calculated from the maximum instrument errors by:

$$E = \left[\sum_{i=1}^N \frac{(E_i)^2}{3} \right]^{1/2}$$

where:

- E = standard deviation of maximum error
 E_i = maximum error of component i
 N = number of individual sources of error

For the OSU test facility, the calculated errors for individual channels are tabulated in Appendix D, Tables D-1 through D-9.

LIST OF TABLES		
Table No.	Header	Page No.
D-1	Errors for DPs	D-3, D-4
D-2	Errors for LDPs	D-5, D-6, D-7
D-3	Errors for PTs	D-8
D-4	Errors for FMMs	D-9
D-5	Errors for FVMs	D-10
D-6	Errors for Thermocouples	D-11, D-12, D-13, D-14, D-15, D-16, D-17, D-18, D-19, D-20
D-7	Errors for HFMs, HPs, and LC	D-21, D-22, D-23, D-24
D-8	Errors for FDPs	D-25
D-9	kW Errors	D-26

The standard deviation of the maximum error is not tabulated although it can be calculated from the calculated errors in Tables D-1 through D-9.

3.5.2 Definitions

The error analysis used standard statistical terms and methods to calculate the instrument errors. Some of these terms and their definitions are:

- Error -- Manufacturer's specified maximum deviation from mean value of the measured parameter.
- Total probable error -- Calculated error; defined as the square root of the sum of the squares of all errors. This is the expected most-probable error for a particular type of instrument and its channel.

3.5.3 Results

The probable error for each of the OSU test facility instruments is provided in Appendix D, Tables D-1 through D-9 along with the individual component errors.

These instruments were also calibrated upon completion of the matrix testing and, in some cases, the measured error was found to be larger than the reported probable error. This would be expected because, according to statistics, there is always a chance that a measurement will fall outside the total probable error. Therefore, the calculated probable errors are reported consistently for use in evaluating measurement uncertainty.

Based on the reported probable error, the OSU test facility instrumentation satisfied the accuracy requirements specified in the test specifications (± 2 percent).

3.6 Zero-Time Shift File Correction

The test data files from the test facility DAS contained event times referenced to the opening of the break valve. Test evaluation and analysis required that a correction be made to the test files to compensate for a zero-time shift of the data. The correction was performed using data from the uncorrected test data files sent from OSU. This section describes the method used to correct the zero-time shift of the data and to document the results of the correction. Time corrections for each test are included in Table 3.6-1.

3.6.1 Test Data Collection Timing

Test data were collected at the test facility by three computers, referred to as racks. Each computer, or rack, communicated with and acquired data from separate portions of the DAS, data acquisition system which interfaced directly with facility instrumentation. A matrix test was initiated 120 seconds after pressing the TEST pushbutton on the control panel. When the TEST pushbutton was pressed, the microprocessor-based timer of the facility's programmable logic controller (PLC) was started. When the timer timed out 120 seconds, the PLC generated an open signal for the break valve, which started the transient and the test. Pressing the TEST pushbutton also generated a control signal that was immediately sent to each of the three computers. This control signal, processed separately by each computer, commanded the three separate subsystems of the DAS to begin acquiring data. The signal process time of the computer and data acquisition subsystems created a time delay between the actuation of the TEST pushbutton and the start of data acquisition. DAS testing demonstrated the time delay was not the same for the three racks and was not a constant between tests.

The data acquisition design assumed that the first time stamp of every test data file occurred 120 seconds before the break valve opened. Thus, when the data was reduced, an assignment of time = 0 was given to the data obtained 120 seconds after the first time stamp, presuming data acquisition started immediately when the TEST pushbutton was pressed and the break valve opened 120 seconds later. However, due to the time delay between pressing the TEST pushbutton and the time of the first time stamp, the break valve did not open 120 seconds after the first time stamp in the test data file. A zero-time shift error was introduced because a time = 0 in the file corresponded to a real time later than the opening of the break valve. The magnitude of the test data file's zero-time shift was equal to the delay between pressing the TEST pushbutton and the start of data acquisition by the corresponding rack. The validated test data files received from the test site contained this error in the files' time references. Although the errors in the time references were known before the final data validation was performed at the OSU test facility, a decision was made to correct the files' zero-time shifts at the Energy Center.

3.6.2 Time Correction Method

A method was developed to correct the zero-time shift of each OSU test data file and is described in this section. When the correction factor for a given file was determined, the time was added to each

time entry in the file. Once the corrections were completed, time = 0 in the file corresponded to the time an open signal was sent to the break valve, and a zero-time shift of the data was eliminated.

Within 10 seconds after the break valve opened, the control logic created a trip of the main feed pumps, reactor coolant pumps (RCPs), pressurizer heaters, and the reactor heaters. In addition, the passive residual heat removal heat exchanger (PRHR HX) outlet valve opened and the main steam controller was reset, thereby closing the main steam control valve. In each instance, the operation of the equipment affected system parameters that were monitored by test instrumentation and recorded by the DAS. In addition to being programmed to open the break valve 120 seconds after the test pushbutton was pressed, the PLC was programmed to open the PRHR HX outlet valve, trip the pumps, and trip the heaters after a specified time delay. The operation of the equipment was monitored by a software program that recorded the inputs and outputs to the PLC. There were no time shifts in the data recorded for the PLC.

Using the Wonderware software program (Subsection 2.5.5), which monitored the inputs and outputs of the PLC, a difference in time between the open signal of the break valve and the operation of the other equipment was determined, using the open signal of the break valve as time = 0. The uncorrected test data files from the test facility were then reviewed to determine the time a specific system parameter was affected by the equipment operation. The time recorded from the test data files was referenced to the incorrect zero-time reference. A comparison was made between the correct time from the PLC and the incorrect time from the test data files. The difference between these times provided the time added to the test data files to correct the time shift.

The correction process applied to Matrix Test SB01 is provided as an example. The correction data for Matrix Test SB01, which has the filename U0001, is in Table 3.6-1. The first column is labeled Design Time Delta T (sec.). This is the time the equipment operated in the test, using the actual time an open signal was sent to the break valve as time = 0. The Parameter column is a description of the equipment operation that creates a change in the system. The two columns, Instrument Channel and Instrument Channel Description, are the channel number and description of the channel that monitors the change in system parameter affected by the equipment operation. The two columns are Time Stamp of Change (sec.). Review of the data plot and actual data from the instrument channel provided the time the parameter changed in value as a result of the equipment operation. The time stamp was obtained from the test data file that was referenced to the incorrect time = 0 of the test data file. The Earliest column is the last time stamp before the system parameter changed, and the Latest column is the first time stamp when a change in the system parameter was noted. The last column is Time Added to File to Correct Zero Time (sec.). The entry in this column is the average of the Earliest and Latest data entries added to the design time from column 1.

When the table was completed, a time correction was selected for each rack. The time selected was the largest entry in the Time Added to File to Correct Zero Time (sec.) taken to the nearest data scan. The data scan rate varied for each test, but was either once per second, once per 2 seconds, or once

per 4 seconds. When a time correction was selected, it was entered in the data sheet for the appropriate rack.

The selected zero-time correction was added to each of the OSU test data files originally validated at the test facility. The new corrected files had a time = 0, which corresponded to the actual time of the open signal to the break valve. The first time stamp of each data file varied between []^{a,b,c} for the largest time correction of []^{a,b,c} for the smallest time correction of []^{a,b,c}

Table 3.6-1 on pages 3.6-4 through 3.6-20 is not included in this nonproprietary document.

4.0 Pre-operational Test Results

Pre-operational tests were performed to assure that the facility was performing and recording data in a manner consistent with the expectations for the matrix tests. Several of these tests were performed to characterize the physical attributes of the facility including component volume measurements, pressure drop determinations, and a series of hot functional tests.

4.1 Cold Volume Determinations

This section reports the following volume tests:

- OSU-V-01 Accumulator Volume Test, performed on 1/11/94 (Subsection 4.1.1)
- OSU-V-02 Core Makeup Tank (CMT) Volume Test, performed on 1/14/94 and 1/16/94 (Subsection 4.1.2)
- OSU-V-03 Pressurizer Volume Test, performed 1/18/94 through 1/20/94 (Subsection 4.1.3)
- OSU-V-04 In-Containment Refueling Water Storage Tank (IRWST) Volume Test, performed on 1/30/94 (Subsection 4.1.4)
- OSU-V-05 Primary Sump Tank and Secondary Sump Tank Volume Test, performed on 2/4/94 and 2/5/94 (Subsection 4.1.5)
- OSU-V-06 Steam Generator-1 (SG-1) and SG-2 Secondary-Side Volume Test, performed from 1/20/94 through 1/27/94 (Subsection 4.1.6)
- OSU-V-07 Automatic Depressurization System (ADS) and Break and ADS Measurement System (BAMS) Moisture Separators Volume Test, performed on 2/6/94 (Subsection 4.1.7)
- OSU-V-08 Reactor Vessel Volume Test, performed on 2/5/94 (Subsection 4.1.8)

The objectives of these tests were to measure the volumes of the major components of the test facility and to compare these volumes with the designed volumes. All tests were performed in accordance with an approved procedure. Specific objectives and test results for each test are discussed in detail in each subsection.

4.1.1 Accumulator Volume Test

The objectives of this test were to determine:

- Total volume and gas volume of accumulator-1 (ACC-1) and ACC-2

Note: Only the cylindrical shell contained water. The 2:1 elliptic upper head and part of the upper cylindrical shell contained gas.

- Average cross-sectional area of the cylindrical section of ACC-1 and ACC-2 without the standpipe installed
- Insertion depth of the standpipe for each accumulator to verify that the water volume contained inside each accumulator was within the acceptable range [8.75 to 8.95 ft.³]

Note: Design water volume was [8.85 ft.³] for each accumulator.

- Average cross-sectional area of the cylindrical section of each accumulator with the standpipe installed

4.1.1.1 Test Procedures

Figure 4.1-1 provides a schematic of the test setup. A general description of the procedures is provided here.

Each accumulator was filled with water through its accumulator fill isolation valve using a temporary line connected to the normal residual heat removal system (RNS) pump. When the accumulator was about 50 percent full, the accumulator direct vessel injection (DVI) isolation valve was opened to remove any trapped air in the accumulator injection line and then closed. The accumulators were filled until a steady stream of water issued from a temporary vent valve installed at the accumulator pressure relief valve (temporarily removed) connection. Water temperature in the accumulator was measured. Accumulator volume was determined using a precision scale to weigh the water drained from the accumulator. The draining and weighing process was performed in steps. The measured water weight was converted to a water volume using the measured temperature to obtain the water density. Also, a temporary tygon level indicator was installed along the tank to provide a visual indication of the tank water level. The tygon level indicator measured the accumulator volume without the standpipe installed.

The standpipe ensured the same water volume and level in the accumulator each time it was filled. The standpipe was inserted to a predetermined depth, and the accumulator was filled completely again. The accumulator was then drained via the standpipe, and the water drained out of the standpipe was weighed again using the precision scale. The water weight was converted to a water volume that represented the water volume drained out of the accumulator. The remaining water volume in the accumulator was calculated using the previously measured overall water volume and compared with the acceptance criteria. This process was repeated, as necessary, to get the proper standpipe insertion height and water volume.

As an initial condition of the test, the calibration of the precision scale was checked against a certified weight. At the end of the test, the scale was checked again using the same certified weight to verify the calibration of the scale remained valid during the test.

4.1.1.2 Inoperable Instruments

During testing, LDP-401 and LDP-402 measured false water levels for ACC-1 and ACC-2, respectively. Both level sensors recorded some level of water even when the accumulators were completely drained, and they consistently recorded a higher water level as the accumulators drained. The problem stemmed from the physical configuration of the upper-pressure tap on each accumulator. The upper-pressure tap was installed with a vertical rise before it turned horizontally and was used as the reference leg. During calibration of the sensors, the accumulator was filled completely with water, and reference and variable legs were filled and vented. The pressure drop across the level differential pressure sensor (i.e., reference-leg pressure minus variable-leg pressure) was 0, and the transmitter was calibrated as full. The accumulator was then drained quickly and completely. The pressure drop across the sensor was the maximum, and the transmitter was calibrated as null. This calibration would be correct if the reference leg stayed full, and if both the reference and variable legs were free of air at all times. Since the upper tap was installed with a vertical rise at the accumulator, part or all of the water in the vertical rise drained out in time and left a partial vacuum behind. This partial vacuum reduced the reference-leg pressure and, consequently, gave a lower pressure drop across the sensor, translating to a higher level. Thus, the level measurements from LDP-401 and LDP-402 were not used in this test.

The level measurement error mentioned previously should be minimal in actual matrix testing, since the upper heads of the accumulators were pressurized with nitrogen gas, preventing drainage of the water in the vertical stub of the reference leg.

The precision scale measurement and the temporary tygon level readings were accurate and were used to calculate the tank volume and set the standpipe insertion depth.

4.1.1.3 Test Results and Evaluation

Table 4.1-1 lists raw test data measured for ACC-1, and Table 4.1-3 lists data measured for ACC-2. Table 4.1-2 provides the calculated results using raw test data and compares the data with the design values for ACC-1. Table 4.1-4 provides the data-versus-design values for ACC-2. The design values were obtained from Table 7-6 of *AP600 Low-Pressure Integral Systems Test At Oregon State University, Facility Scaling Report, WCAP-14270*.⁽⁶⁾

Once the standpipes were installed inside the accumulators, they remained at the same position throughout the entire test program. Thus, the water volume in each accumulator was the same from test to test. Any level variation measured by LDP-401 and LDP-402 was due to the instrumentation error described in Subsection 4.1.1.2.

The total volume of each accumulator was in agreement with the design volume. The water volume per inch of height in the cylindrical shell portion was in agreement with the design value.

The water volume in each accumulator with the standpipe installed was within the specified acceptable range; however, ACC-2 contained slightly more water than ACC-1. Water volume with the standpipe installed was []^{a,b,c} for ACC-1. Water volume with the standpipe installed was []^{a,b,c} for ACC-2. These water volumes should be the same from test to test since they were controlled by the standpipes.

The average water volume per inch of cylindrical shell height was []^{a,b,c} for both accumulators. Each accumulator had a flat bottom, and all water was contained inside the cylindrical shell.

4.1.2 CMT Volume Test

The objectives of the test were to determine:

- Upper- and lower-head volume for CMT-1
- First- through fourth-stage ADS volumes in CMT-1
- Upper- and lower-head volume for CMT-2
- First- through fourth-stage ADS volumes in CMT-2

4.1.2.1 Test Procedures

Figure 4.1-2 provides a schematic of the test setup. A general description of the procedures is provided here.

Each CMT was filled with water by the RNS pump through a temporary fill/drain valve installed at the outlet flange at the bottom of the tank. Each CMT was filled until a steady stream of water issued from its vent valve located at the top of the tank. Water temperature in the tank was measured and recorded. The required CMT volumes were determined by weighing the water drained from the tank, then converting the water weight to a water volume using the measured temperature to obtain the water density. This draining and weighing process was performed in steps. The measured volumes were compared with the design volumes. A temporary tygon level indicator was installed along the tank to provide a visual indication of the tank water level. As an initial condition to the test, the calibration of the precision scale was checked against a certified weight. At the end of the test, the scale was checked again using the same certified weight to verify the calibration of the scale remained valid during the test.

4.1.2.2 Inoperable Instruments

Each CMT was measured with four level differential pressures, one temporary tygon hose level scale, one precision weight scale, and one thermocouple for water temperature measurements. The precision scale provided extremely accurate weight measurement because it was calibrated against a known certified weight. The tygon hose level scale measurement was within ± 0.125 in. One of the four

level differential pressure sensors measured the wide-range overall level; the other three measured narrow-range upper-head, bottom-head, and middle cylindrical-shell levels. Piping and instrumentation diagrams (P&IDs) Dwg. OSU 600501 and Dwg. OSU 600502 (Appendix G) show the arrangement of these level differential pressures. Instrumentation anomalies were experienced in this test and are discussed in the following text.

CMT-1 Inoperable Instruments

CMT-1 levels were measured by a tygon hose with a scale and by four level differential pressure sensors (LDP-501, LDP-503, LDP-505, and LDP-507). LDP-501 measured the bottom-head level; LDP-503 measured the middle cylindrical-shell level; LDP-505 measured the upper-head level; and LDP-507 measured the overall CMT-1 level.

The tygon hose and differential pressure sensors LDP-501 and LDP-507 recorded a higher-than-expected level (Table 4.1-5). For example, the tygon hose level instrument recorded []^{a,b,c} of water; LDP-501 recorded []^{a,b,c} of water; and LDP-507 recorded []^{a,b,c} of water when the water level was about []^{a,b,c}. All of these instruments measured about []^{a,b,c} higher than the actual levels every time a data point was obtained. The reference zero level was at the bottom of the tank. The actual cause of this shift in level measurements is not known. It is possible an air bubble was trapped at the bottom instrument line at the bottom of the tank. Then, as water filled the tank, the air bubble compressed raising the tygon hose scale readings and causing false level readings. This effect was common to the tygon hose level and level differential pressure sensors LDP-501 and LDP-507 since they shared the same bottom tap. The magnitude of actual level shift was difficult to determine since the degree of compression in the air bubble was not known.

LDP-505 also experienced some anomalies. The physical span of this instrument was about []^{a,b,c} and it measured []^{a,b,c}—an increase of []^{a,b,c}. The most likely cause for this anomaly was similar to that of the accumulator level differential pressures, i.e., the vertical upper tap introduced measurement error (see Subsection 4.1.1.2 for a detailed discussion).

LDP-503 was designed to measure the middle-shell level. It covered a span of about []^{a,b,c} with respect to the bottom of the CMT) and functioned well. For example, LDP-503 measured []^{a,b,c} of water in the middle shell versus the design water level of []^{a,b,c} (Table 4.1-5). The bottom tap of LDP-503 was located at about []^{a,b,c} above the bottom of the tank; therefore, when it measured 0 in., the water level was at []^{a,b,c}. Thus, []^{a,b,c} measured by LDP-503 corresponded to []^{a,b,c}. As another example, LDP-501 measured []^{a,b,c} percent volume. This corresponded to a level of []^{a,b,c} with respect to the bottom of the tank. The design level for []^{a,b,c} percent volume was []^{a,b,c}. Thus, the measurement was in excellent agreement with the design. The main reason for this agreement was that both top and bottom taps of LDP-503 were horizontal taps and free of air bubbles; therefore, none of the previously mentioned anomalies occurred.

CMT-2 Inoperable Instruments

CMT-2 levels were also measured by a tygon hose with a scale and by four level differential pressure sensors (LDP-502, LDP-504, LDP-506, and LDP-508). LDP-504 measured the bottom-head level; LDP-506 measured the middle cylindrical-shell level; LDP-508 measured the upper-head level; and LDP-502 measured the overall CMT-2 level.

The tygon hose and differential pressure sensors LDP-504 and LDP-502 shared the same bottom tap located at the bottom of CMT-2, and the upper tap of LDP-502 was vertical, similar to CMT-1. The tygon hose level and LDP-504 measurements agreed with the design levels very well, indicating that these lines were free of air bubbles and that the measurements were acceptable (Table 4.1-6).

Differential pressure sensors LDP-502 and LDP-508 recorded slightly higher-than-expected levels (less than []^{a,b,c} higher in CMT-1). This was most likely due to the vertical tap geometry at the top. For a detailed discussion of vertical-tap-induced error, see Subsection 4.1.1.2.

LDP-506 was designed to measure the middle cylindrical-shell level (similar to CMT-1). LDP-506 covered a span of about []^{a,b,c}—from []^{a,b,c} with respect to the bottom of the CMT. It functioned well, with the exception of one data-point measurement. Step 4.4.8H in Table 4.1-6 shows that LDP-506 measured []^{a,b,c}. This data point is believed to be a misprint for the following two reasons:

- All other measurements were in good agreement with design values
- The measurement was beyond the physical span of the instrument

Again, the main reason for this agreement was that both top and bottom taps of LDP-506 were horizontal taps and free of air bubbles. Therefore, no unacceptable discrepancies occurred.

4.1.2.3 Test Results and Evaluation

Tables 4.1-5 and 4.1-6 list raw test data for CMT-1 and CMT-2 respectively. The following columns were added to compare with raw data:

- Design water level
- Conversion of temporary tygon hose level measurements to levels with reference to the bottom of the CMTs
- Water-specific volume derived from the ASME steam table for each measured water temperature

Raw data for level differential pressure sensors, precision scale measurements, and water temperature measurements were listed as measured.

CMT-1 Test Results and Evaluation

Table 4.1-7 summarizes the test results and compares them with design values. Total tank volume measurements for CMT-1 were in agreement with design values. Test procedures clearly identified when the tanks were full or empty, and precision scale and thermocouple measurements were extremely accurate.

Lower-head volume for CMT-1 was also in agreement with the design value, implying that the lower-head height should be in good agreement with the design lower-head height. Table 4.1-5, however, shows the measured lower-head height as []^{a,b,c} higher than the design value. This discrepancy was due to instrument anomaly, as described previously. Because the measured lower-head volume was in agreement with the design value, it was concluded that the CMT-1 bottom-head height should be the same as the design height.

Cylindrical-shell height ([]^{a,b,c}) was comparable to design-shell height ([]^{a,b,c}). The zero shift due to the air bubble had little effect on this measurement, because the shell height was the difference between level measurements of the upper- and lower-head weld joints. The zero shift cancelled out.

CMT total volume, lower-head volume, lower-head height, shell volume, and shell height were in agreement with design values. Thus, there was no reason why the upper head did not agree with the design value. Therefore, the design tank height can be used as the real height. Figures 4.1-3 and 4.1-4 plotted the measured volume as a function of tank level.

Because of the error introduced by the vertical upper tap of LDP-507, this vertical upper tap was moved to the inlet nozzle of the CMT, and was placed horizontally after volume testing was complete and before matrix testing began.

CMT-2 Test Results and Evaluation

CMT-2 measured total volume was in agreement with design volume. The upper- and lower-head volumes were slightly lower than expected; however, they were within []^{a,b,c} percent of the design values.

Level measurements taken by the tygon hose and bottom-head level differential pressure sensors were more accurate than those in CMT-1. The discrepancy was small. The overall level differential pressure sensor still read higher level than expected, as discussed previously. Figures 4.1-3 and 4.1-4 plotted the measured volume as a function of tank level.

Because of the error introduced by the vertical upper tap of LDP-502, this vertical upper tap was moved to the inlet nozzle of the CMT and was placed horizontally after volume testing was complete and before matrix testing began.

4.1.3 Pressurizer Volume Test

The objectives of the test were to determine:

- Volume of the pressurizer upper and lower elliptic heads
- Pressurizer cylindrical volume above the pressurizer heaters
- Pressurizer cylindrical volume containing pressurizer heaters

4.1.3.1 Test Procedures

Figure 4.1-5 provides a schematic of the test setup. A general description of the procedures is provided here.

The pressurizer was filled with water through the pressurizer drain valve until a steady stream of water issued from a thermocouple connection at the top of the tank. (The thermocouple was removed for the test.) The fill line was disconnected from the water supply source and re-routed to a plastic container into which water in the pressurizer would be drained. Tank water temperature was measured and recorded. Pressurizer volume was determined by weighing the water drained from the pressurizer with a precision scale, then converting the water weight to a volume using the measured temperature to obtain the water density. This draining and weighing process was performed in several steps. A temporary tygon level indicator was installed along the tank to provide a visual indication of the tank water level. LDP-601 was also used to measure tank water level.

As an initial condition of the test, the calibration of the precision scale was checked against a certified weight. At the end of the test, the scale was checked again using the same certified weight to verify the calibration of the scale remained valid during the test.

4.1.3.2 Test Results and Evaluation

Table 4.1-8 lists raw test data used to calculate volume in the pressurizer. Tygon hose level measurements were used to calculate water volume of the pressurizer and were in agreement with the design level. Level measurements made by LDP-601 were also in reasonable agreement with the design level. Calculated volumes at selected elevations are listed in Table 4.1-9. Design volume for the pressurizer was []^{a,b,c}. Measured pressurizer volume of []^{a,b,c} was within []^{a,b,c} percent of the design volume.

The calculated volume per inch of height in the cylindrical shell portion was []^{a,b,c}

4.1.4 IRWST Volume Test

The objectives of the test were to determine:

- IRWST total volume
- IRWST overflow (to primary sump tank) water volume was between []^{a,b,c}
- IRWST normal water volume was between []^{a,b,c}

Note: The design net normal water volume was []^{a,b,c} (Table 7-10), *AP600 Low-Pressure Integral Systems Test at Oregon State University, Facility Scaling Report, WCAP-14270*⁽⁶⁾

- IRWST minimum gas volume
- IRWST normal gas volume

4.1.4.1 Test Procedures

Figure 4.1-6 provides a schematic of the test setup. A general description of the procedures is provided here.

The IRWST filled with water through the IRWST manway at the top of the tank until the water level reached the top of the IRWST manway flange. Water temperature in the tank was measured using a thermocouple. Tank volume was determined by measuring the weight of water using calibrated load cells on the feet of the tank, converting the measured water weight to a water volume using the measured temperature to obtain the water density. Water in the IRWST was drained then, and the remaining water in the IRWST was measured. This draining process was repeated several times. A temporary tygon level indicator was installed along the tank to provide a visual indication of the tank water level. LDP-701 was also used to measure the water level in the tank.

4.1.4.2 Test Results and Evaluation

Table 4.1-10 lists raw test data used to calculate volume in the IRWST. The test data showed that LDP-701 measured a maximum level of []^{a,b,c} which was in agreement with the design distance ([]^{a,b,c}). The data also showed that the incremental level changes recorded by LDP-701 were very close to those measured by the tygon hose level scale.

Measured data were converted into volumes and listed in Table 4.1-11. Measured net normal water volume in the tank (i.e., water volume from the bottom of the tank to the top of the fill overflow pipe)

was []^{a,b,c} percent above the design volume ([]^{a,b,c}). This measured volume was within an acceptable range (between []^{a,b,c}).

4.1.5 Primary and Secondary Sump Tank Volume Test

The objectives of the test were to determine:

- Primary sump curb elevation (so that overflow from the primary to the secondary sump occurred between []^{a,b,c}).
- Primary and secondary sump total volumes
- Primary sump gas volumes

4.1.5.1 Test Procedures

Figure 4.1-7 provides a schematic of the test setup. A general description of the procedures is provided here.

Primary Sump Tank Volume Test

A blank flange was installed at the primary/secondary sump cross-connect line. The primary sump tank was filled through the manway using water from a temporary source. The water was isolated when the level reached the top of the primary sump manway flange. Total tank volume was determined by measuring the weight of water using calibrated load cells on the feet of the tank, then converting the measured water weight to a water volume using the measured temperature to obtain the water density.

Water in the tank was drained in several steps. The remaining water weight, level, and temperature were measured for volume calculation.

The required overflow volume/mass of the primary sump (i.e., volume from the bottom of the primary sump to the overflow level) were calculated based on the design volume of the tank first, then measured in the test. As water drained from the primary sump, the level corresponding to the design overflow volume/mass was marked on the primary sump overflow flange. Following the initial tank draindown, an overflow weir was placed at the level marked on the flange to set the overflow level.

The draining process continued until the tank emptied. The tank was refilled (with the weir installed) until the level did not change, indicating that it was at the overflow level. Tank volume/mass were verified against the required overflow volume.

A temporary tygon level indicator was installed along the tank to provide a visual indication of the tank water level, and LDP-901 was used to measure the water level.

Secondary Sump Tank Volume Test

A blank flange was installed at the primary/secondary sump cross-connect line. The secondary sump tank was filled through the manway using water from a temporary source. The water was isolated when the level reached the top of the secondary sump manway flange then drained via the bottom drain line. The volume of water remaining in the tank was determined by measuring the weight of the water using calibrated load cells on the feet of the tank, then converting the water weight to a water volume using the measured temperature to obtain the water density. This draining process was performed in several steps.

A temporary tygon level indicator was installed along the tank to provide a visual indication of the tank water level. LDP-902 was also used to measure the tank water level.

4.1.5.2 Test Results and Evaluation

Tables 4.1-12 and 4.1-13 list raw data for the primary and secondary sump tanks, respectively. Two columns of information were added in each table—one includes the corresponding design level values and the other includes the reduced tygon hose level, with respect to the bottom tap of LDP-901 for the primary sump tank and LDP-902 for the secondary sump tank. Design levels were obtained from Dwg. 787-PS01 and 787-SS01 in *AP600 Low Pressure Integral Systems Test at Oregon State University, Facility Description Report, WCAP-14124.*⁽⁷⁾

Primary sump tank levels measured by the temporary tygon hose scale were in agreement with design values. LDP-901 measurements were off from []^{a,b,c}. It was discovered that LDP-901 was calibrated to have a span from []^{a,b,c} of water, and the physical span was about []^{a,b,c}. Although the exact cause of this discrepancy was not known, the error was within the 2 percent required instrument accuracy.

Secondary sump tank levels measured by both the tygon hose level scale and LDP-902 were in agreement with design values. For example, LDP-902 recorded a maximum span of []^{a,b,c} versus the design span of []^{a,b,c}. The centerline of the overflow pipe was designed to be at the upper-head weld joint. The corresponding height with respect to the bottom tap was []^{a,b,c}. LDP-902 measured []^{a,b,c} and the tygon hose measured []^{a,b,c}.

Table 8-9 in *AP600 Low-Pressure Integral Systems Test at Oregon State University, Facility Scaling Report, WCAP-14270,*⁽⁶⁾ provides the following design water volumes:

- Primary sump water volume at simulated flood-up level []^{a,b,c}
- Secondary sump water volume at curb (overflow) level []^{a,b,c}

In addition, the document specifies the primary sump tank curb (overflow) level to be []^{a,b,c} above the simulated flood-up level, resulting in a volume of []^{a,b,c} at the overflow level.

The following volumes were calculated using raw test data:

- Overflow from the primary to the secondary sump occurred at []^{a,b,c} within the specified acceptance criteria of []^{a,b,c} and was the same as the design value. The corresponding level was at the middle of the upper-head weld. This level was transferred to a weir that would provide the same water volume from test to test.
- Total primary sump volume was []^{a,b,c}
- Primary sump gas volume was []^{a,b,c}
- Total secondary sump volume was []^{a,b,c}
- Curb overflow level at the secondary sump tank was controlled by the weir set in the primary sump tank volume test. The corresponding level at the secondary sump tank was at the middle of the upper-head cylinder weld, and the corresponding volume was []^{a,b,c} within []^{a,b,c} percent of design volume.

In addition, the average cross-sectional area of the cylindrical portion of the primary sump tank was calculated to be []^{a,b,c} versus the design cross-sectional area of []^{a,b,c} of height). Similarly, the average cross-sectional area of the cylindrical portion of the secondary sump tank was []^{a,b,c} of height versus the design value of []^{a,b,c} of height.

4.1.6 SG-1 and SG-2 Secondary-Side Volume Test

The objectives of the test were to determine:

- SG-1 upper-shell volume (volume above the cylindrical section of the vessel)
- Volume of the SG-1 cylindrical section
- Total volume of SG-1
- SG-2 upper-shell volume (volume above the cylindrical section of the vessel)
- Volume of the SG-2 cylindrical section
- Total volume of SG-2

4.1.6.1 Test Procedures

Figure 4.1-8 provides a schematic of the test setup. A general description of the procedures is provided here.

The secondary side of each SG was filled with water through its top steam outlet flange until water reached the top of the steam outlet flange. Water temperature in each SG was measured. SG volumes were determined using a precision scale to weigh the water drained from the SG, then converting the measured water weight to a water volume using the measured temperature to obtain the water density. The container used to receive the water drained from the SG was weighed and emptied because the water volume in the SG was much larger than the volume of the container. This process was repeated several times to obtain the desired test data.

A temporary tygon level indicator was installed along the SG to provide a visual indication of the water level. LDP-301 and LDP-302 were also used to measure water level in SG-1 and SG-2, respectively.

As an initial condition of the test, the calibration of the precision scale was checked against a certified weight. At the end of the test, the scale was checked again using the same certified weight to verify the calibration of the scale remained valid during the test.

4.1.6.2 Test Results and Evaluation

Tables 4.1-14 and 4.1-15 list raw data for SG-1 and SG-2, respectively. Two columns of information were added in each table—one included the corresponding design levels and the other includes the reduced temporary tygon hose level with respect to the drain line at the bottom of each SG. Design levels were obtained from Harris Thermal Transfer Products Dwg. 20175-D1 and 20175-D2 (Appendix H). The bottom taps of LDP-301 and LDP-302 for SG-1 and SG-2 were also located at the same elevation as the drain lines. Thus, both the level differential pressure sensors and the tygon hose shared the same reference zero.

Levels obtained by both the tygon hose level scale and the level differential pressure sensors were in agreement with design values. The measured maximum range of the level differential pressure sensors were []^{a,b,c} for SG-1 and []^{a,b,c} for SG-2, which compared well with the design distance of []^{a,b,c}. The tygon hoses recorded []^{a,b,c} for the level of the top of the steam outlet flange for both SGs, indicating agreement with the design value ([146.60 in.]).

The measured total volume of the secondary side of the SGs ([]^{a,b,c} for SG-1 and []^{a,b,c} for SG-2) differed by []^{a,b,c} percent. In the cylindrical sections, the difference in volume was less than 1 percent ([]^{a,b,c} for SG-1 and []^{a,b,c} for SG-2). The main discrepancy between the two SGs was that the volume in the upper-head region above the cylindrical shell ([]^{a,b,c} for SG-1 and []^{a,b,c} for SG-2) differed by []^{a,b,c} percent due to manufacturing differences in the upper-shell volume; however, this upper-head region was the vapor region, and precision control of vapor volume was not required in the test program. Table 4.1-16 summarizes these results.

4.1.7 ADS and BAMS Moisture Separators Volume Test

The objectives of the test were to determine:

- Volume of the ADS 1-3 separator ([]^{a,b,c} separator)
- Volume of the break separator ([]^{a,b,c} separator)
- Volume of the ADS 4-1 separator ([]^{a,b,c} separator)
- Volume of the ADS 4-2 separator ([]^{a,b,c} separator)

4.1.7.1 Test Procedures

Figure 4.1-9 provides a schematic of the test setup. A general description of the procedures is provided here.

Each separator was filled with water through a temporary fill/drain valve. For the ADS 1-3 separator, this fill line was installed at the separator flow-meter flange located at the bottom of the separator. All other separators used a fill line connected to the top flange. The ADS 1-3 separator was filled until a steady stream of water issued from a temporary vent valve installed at the top of the separator. The remaining separators were filled until the water level reached the top of the separator outlet flange. Due to the unavailability of the DAS at the time of testing, direct water temperature measurement was not recorded. Instead, the water temperature was assumed to be a constant 56°F. This was consistent with the temperature of the water in the primary and secondary sump tank volume test. Separator volume was determined using a precision scale to weigh the water that was drained from the separator, then converting the measured water weight to a water volume using the water density at 56°F. The draining and weighing process was performed in several steps. A temporary tygon level indicator was installed along each separator to provide a visual indication of the water level.

As an initial condition of the test, the calibration of the precision scale was checked against a certified weight. At the end of the test, the scale was checked again using the same certified weight to verify the calibration of the scale remained valid during the test.

4.1.7.2 Test Results and Evaluation

The following tables list raw test data:

- Table 4.1-17 ADS 1-3 Separator Volume Data
- Table 4.1-18 ADS 4-1 Separator Volume Data
- Table 4.1-19 ADS 4-2 Separator Volume Data
- Table 4.1-20 Break Separator Volume Data

The total water volume measured and listed in these tables includes the volume of the separator vessel itself and the water volume of the interconnecting pipes; however, the volume of the interconnecting pipes was negligible compared with the volume of the separator.

There were no specific requirements on the water volume in the separators. Measured total volume of the moisture separators was included for information only. Sizing of the separators was based on expected steam flow. Each separator met minimum relative locations of the internal separating element above the liquid surface and a specified pressure drop across the element.

Volume for the ADS 1-3 separator ([]^{ab,c} separator) was measured as []^{ab,c} volume for the large-break separator ([]^{ab,c} separator) was measured as []^{ab,c} volume for the ADS 4-1 separator ([]^{ab,c} separator) was measured as []^{ab,c} and volume for the ADS 4-2 separator ([]^{ab,c} separator) was measured as []^{ab,c}. ADS 4-1 and ADS 4-2 separators were designed to be the same physically, except that the separating elements, which occupied negligible volume, were different. The identical (measured) volumes of these two separators indirectly proved that the volume test results were acceptable.

4.1.8 Reactor Vessel Volume Test

The objectives of the test were to determine:

- Upper-head volume
- Upper-plenum volume
- Volume between the upper support plate and the top of the upper core plate
- Volume between the upper core plate and the top of the heater rods
- Volume in the top core region from the top of the heater rods to the rod bundle midpoint
- Volume of the lower core from the rod bundle midpoint to the top of the lower core plate
- Volume of the lower plenum below the core region
- Total reactor-vessel volume

4.1.8.1 Test Procedures

Figure 4.1-10 provides a schematic of the test setup. A general description of the procedures is provided here.

The RNS pump filled the reactor vessel with water through a temporary fill valve installed on the DVI-1 flange next to the reactor vessel. Blank flanges were installed at the DVI-2 flange and at the cold-leg and hot-leg flanges. The vessel was filled until a steady stream of water issued from its vent valve located at the upper head. Water temperature at the bottom of the reactor vessel was measured. This temperature was the same at all locations inside the reactor vessel.

After the reactor vessel was completely filled and the calibrations of the level differential pressure sensors were verified, the isolation valve at the drain line was opened to drain the water to a plastic

container. Draining stopped at a designated level, and the drained water was weighed using a precision scale. Water weight was converted to water volume using the measured temperature to obtain the water density. On completion of weighing process, the container was emptied and ready to collect a new batch of water. This draining and weighing process was performed several times to obtain individual volume information at the desired level. Therefore, the total weight of water in the vessel was the sum of the individual measurements.

Since the drain line was located 2 in. above the bottom of the reactor vessel, some water remained inside the reactor vessel at the end of the draining process. Therefore, the total vessel volume calculation should include the water volume that remained inside the vessel following draindown. A temporary tygon level indicator was installed along the vessel to provide a visual indication of the water level.

As an initial condition of the test, the calibration of the precision scale was checked against a certified weight. At the end of the test, the scale was checked again using the same certified weight to verify the calibration of the scale remained valid during the test.

4.1.8.2 Test Results and Evaluation

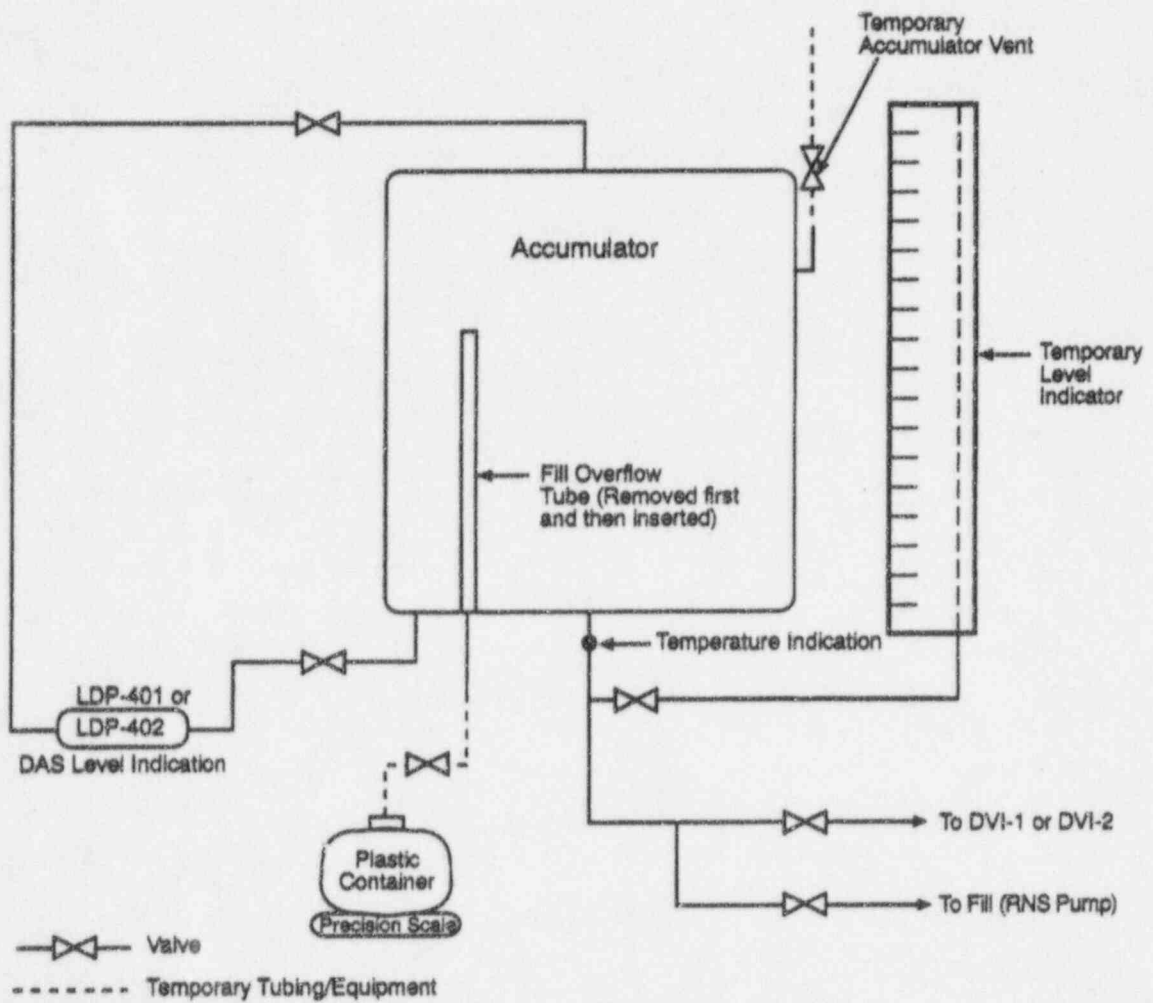
Table 4.1-21 lists raw test data. Two columns of information were added in the table—one includes the corresponding design values and the other includes the reduced tygon hose level, with respect to the bottom tap of LDP-127 (the centerline of the drain line).

Level measurements made by the level differential pressure sensors and the temporary tygon hose level scale were both in good agreement with design values. Full span measurements of LDP-127 and LDP-115 were larger than the physical distance between the upper and lower taps because they shared the common vertical upper tap. This vertical upper tap had a vertical riser that increased the calibrated span of the sensors. Data indicate that this vertical rise was about 5 in. As water drained out of the reactor vessel, the levels measured by the two level sensors agreed with the design values. The anomalies associated with the vertical tap, described in Subsection 4.2.1.1, did not occur in this test.

Mass measurements made by the precision scale were accurate. The temperature was measured and recorded by a thermocouple and was also accurate. Both mass and temperature measurements were independent of level measurements and, therefore, were not affected by level measurement deviations. Thus, volumes calculated using the measured weight and temperature represented the exact volume of the reactor vessel. Table 4.1-22 lists these volumes.

The water volume per inch of height varies from elevation to elevation. This value is calculated using the information obtained in this test.

Table 4.1 on pages 4.1-17 through 4.1-38 is not included in this nonproprietary document.



Note: LDP-401 and DVI-1 are for accumulator 1
 LDP-402 and DVI-2 are for accumulator 2

81620A.3

Figure 4.1-1 Schematic of Accumulator Volume Test Setup

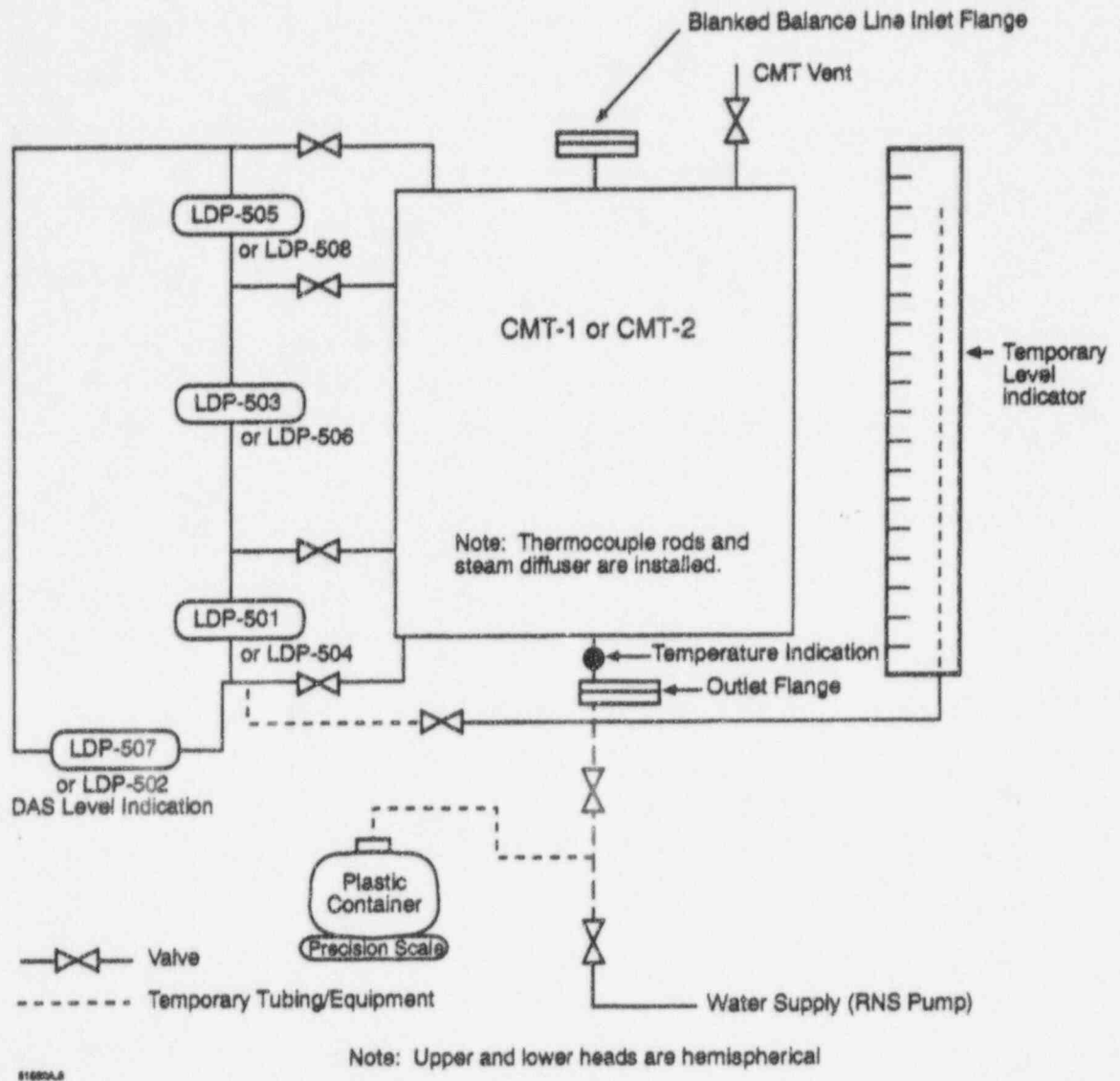


Figure 4.1-2 Schematic of CMT Test Setup

CMT-1 VOLUME VERSUS HEIGHT FROM BOTTOM

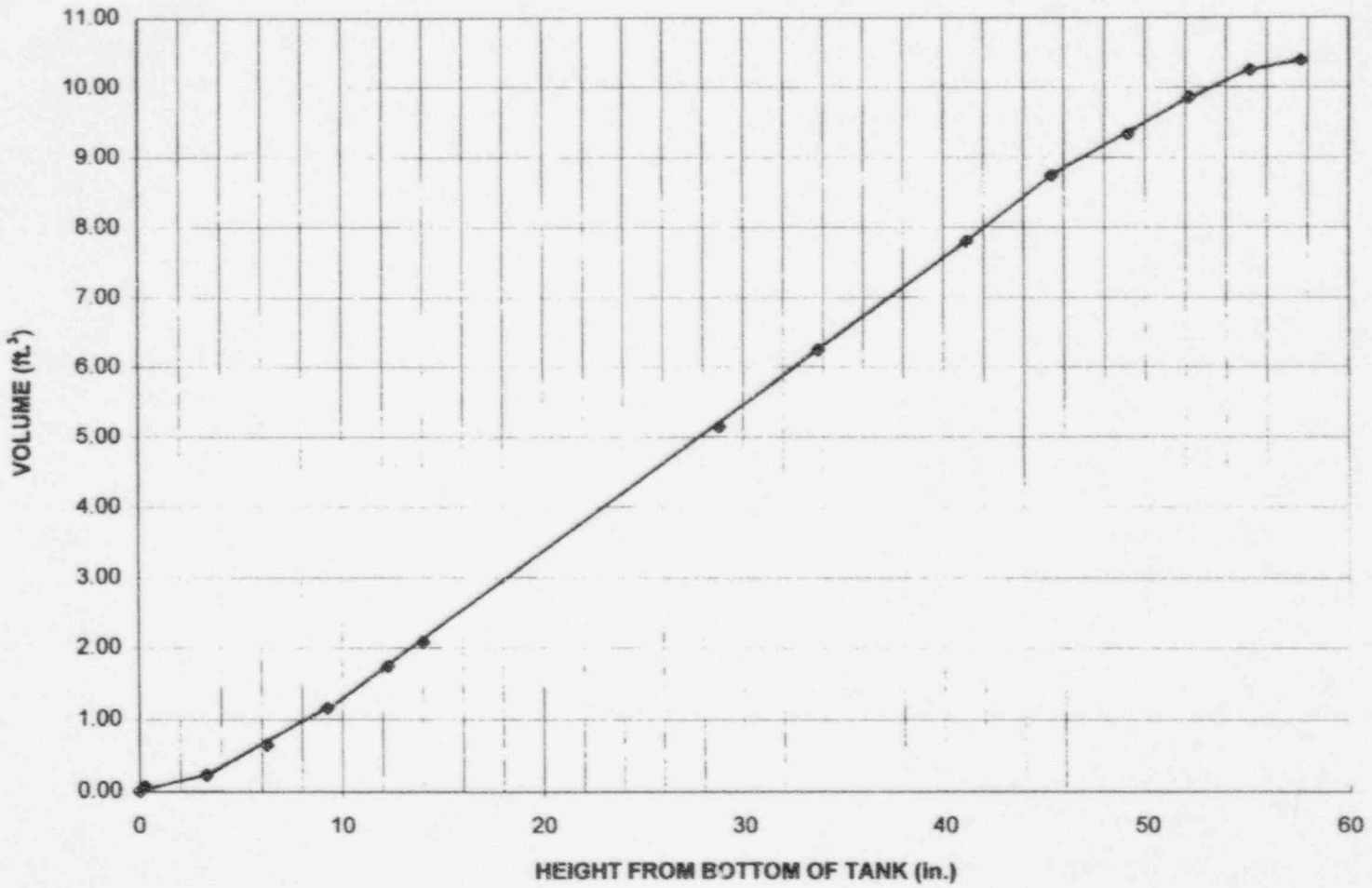


Figure 4.1-3 CMT-1 Volume versus Height from Bottom

CMT-1 VOLUME VERSUS HEIGHT FROM BOTTOM

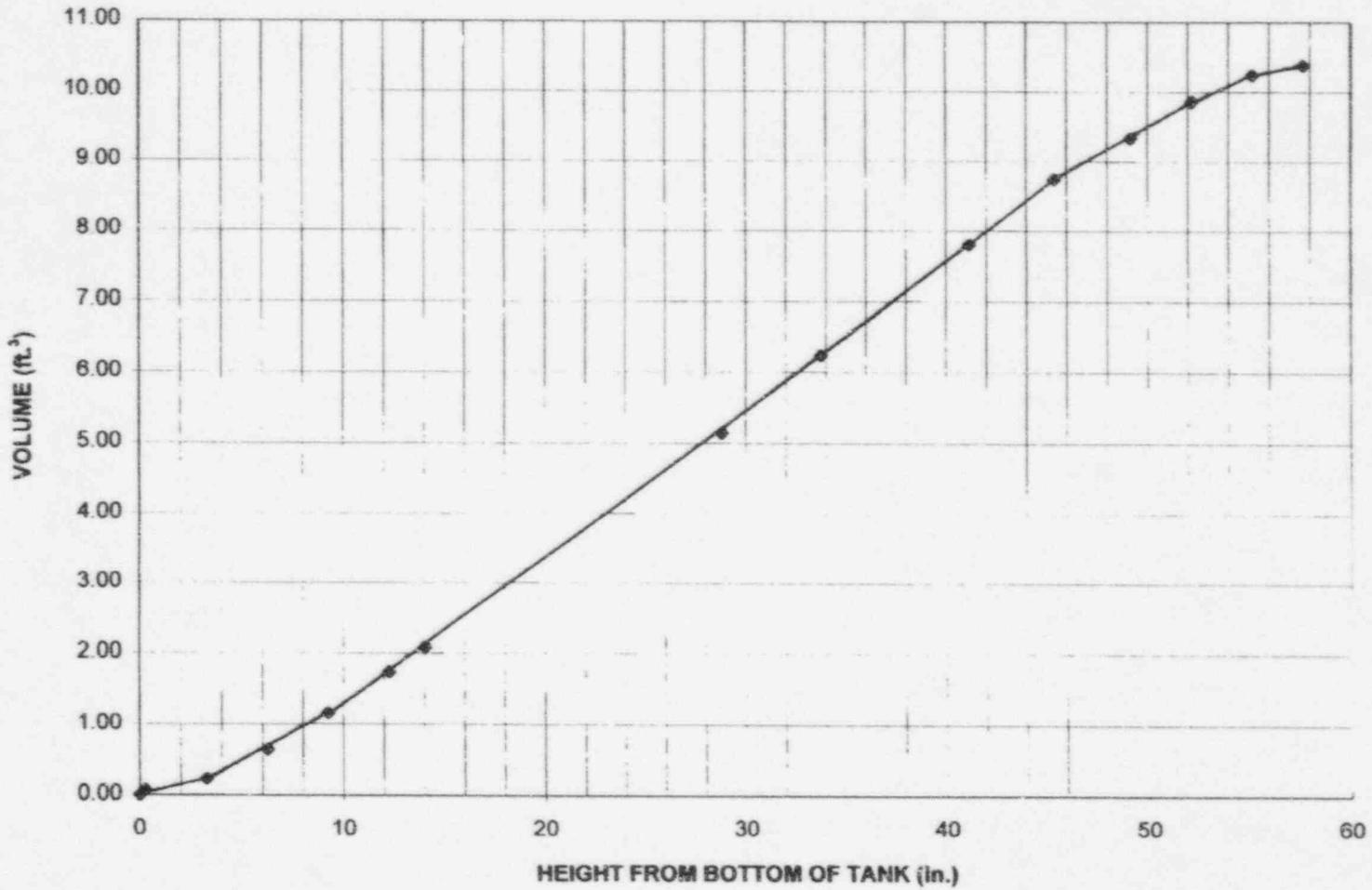


Figure 4.1-4 CMT-2 Volume versus Height from Bottom

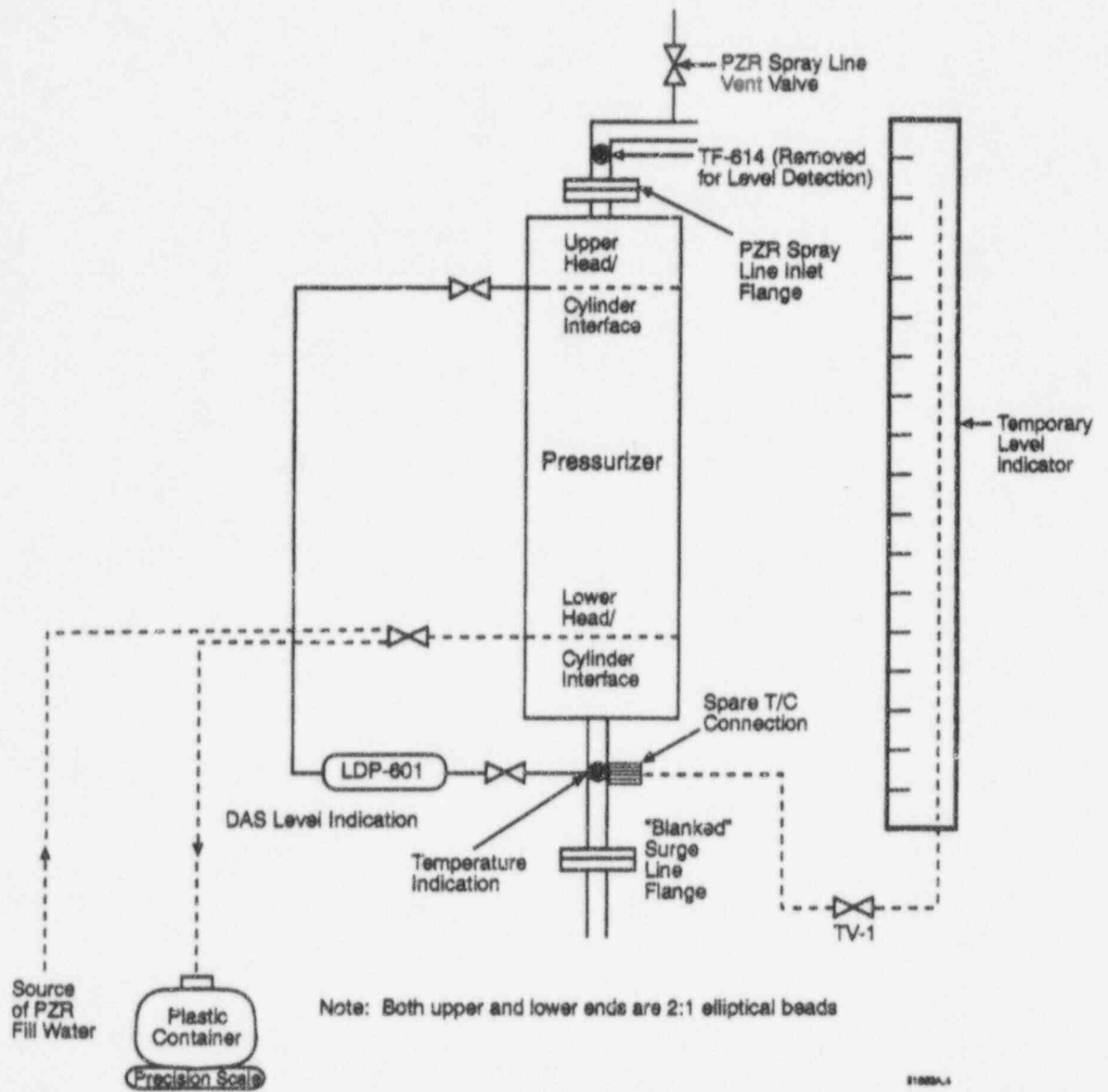


Figure 4.1-5 Schematic of Pressurizer Test Setup

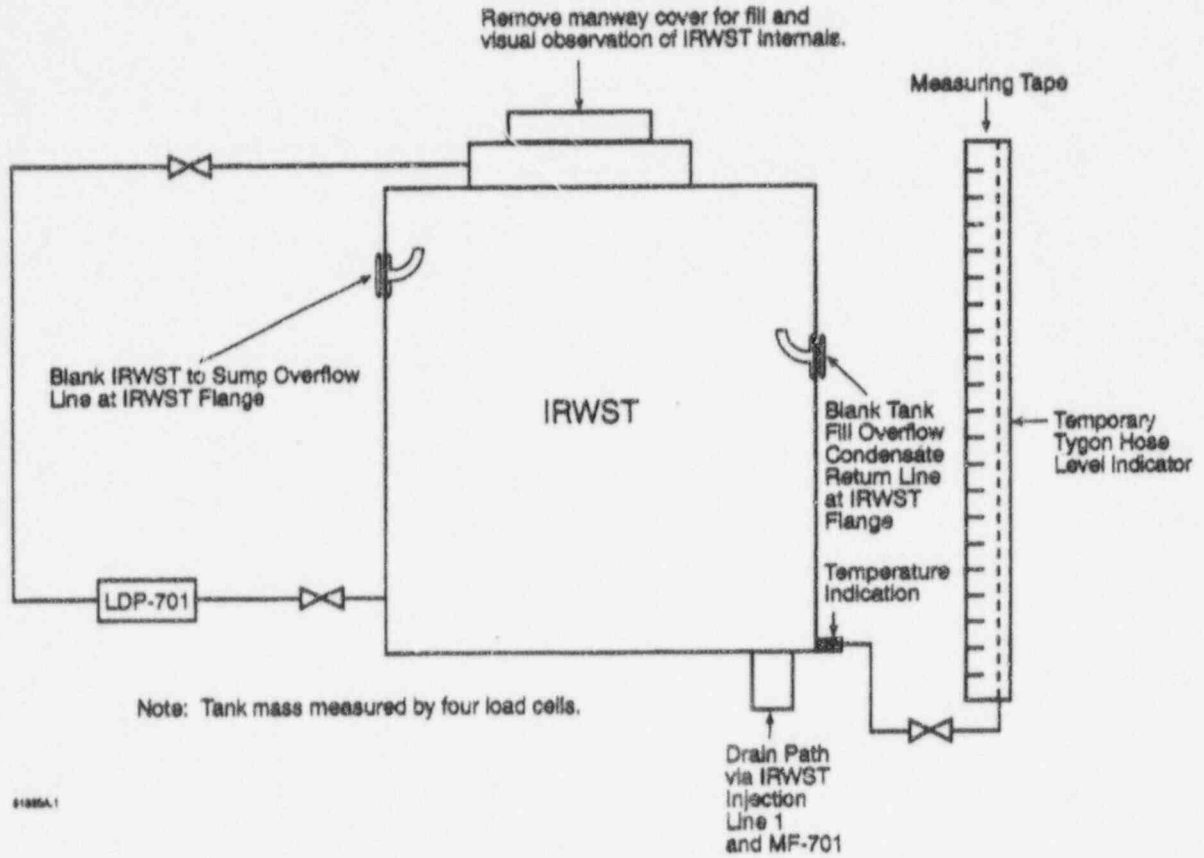


Figure 4.1-6 IRWST Test Setup

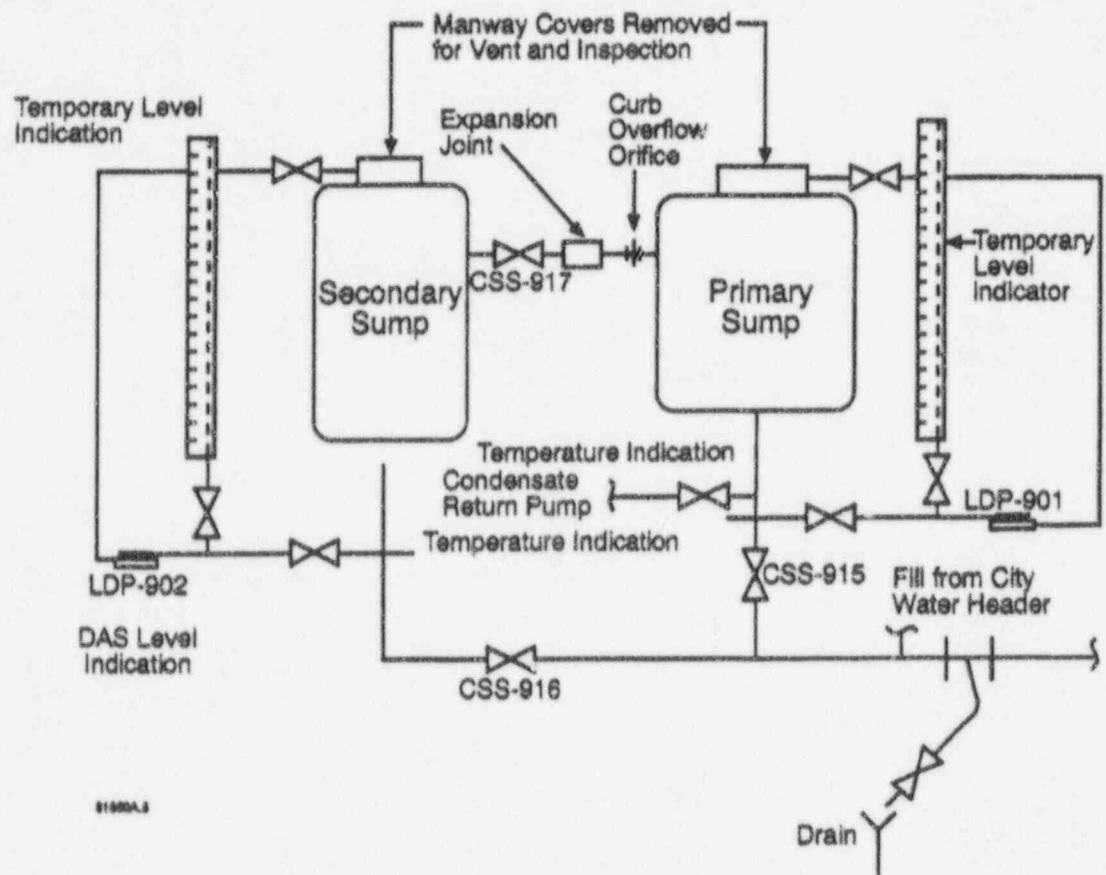


Figure 4.1-7 Schematic of Containment Sump Test Setup

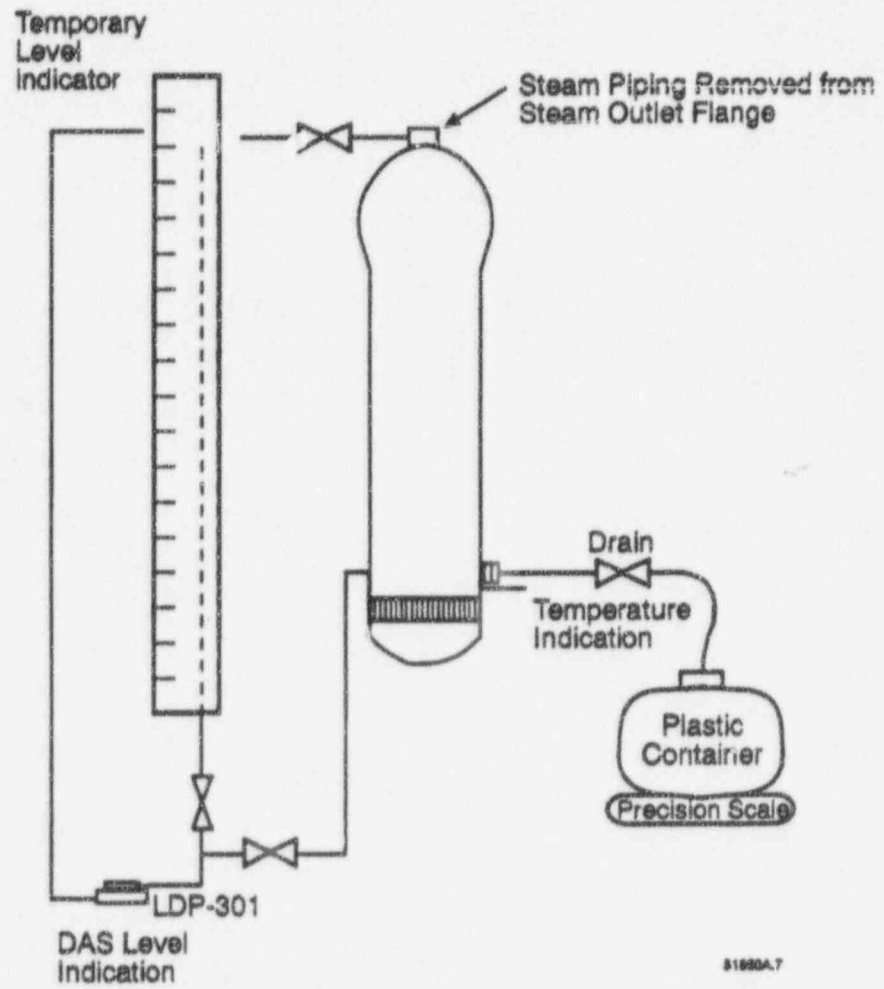


Figure 4.1-8 Schematic of SG Secondary-Side Volume Test Setup

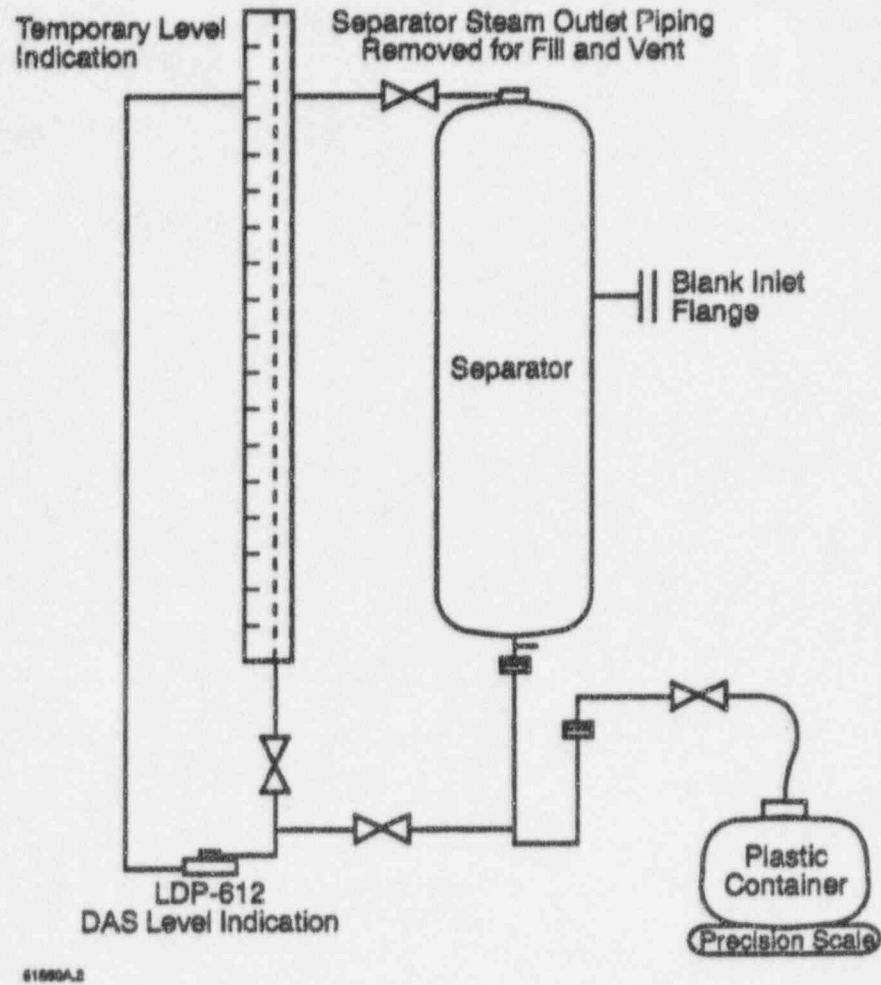


Figure 4.1-9 Schematic of ADS and BAMS Separator Test Setup

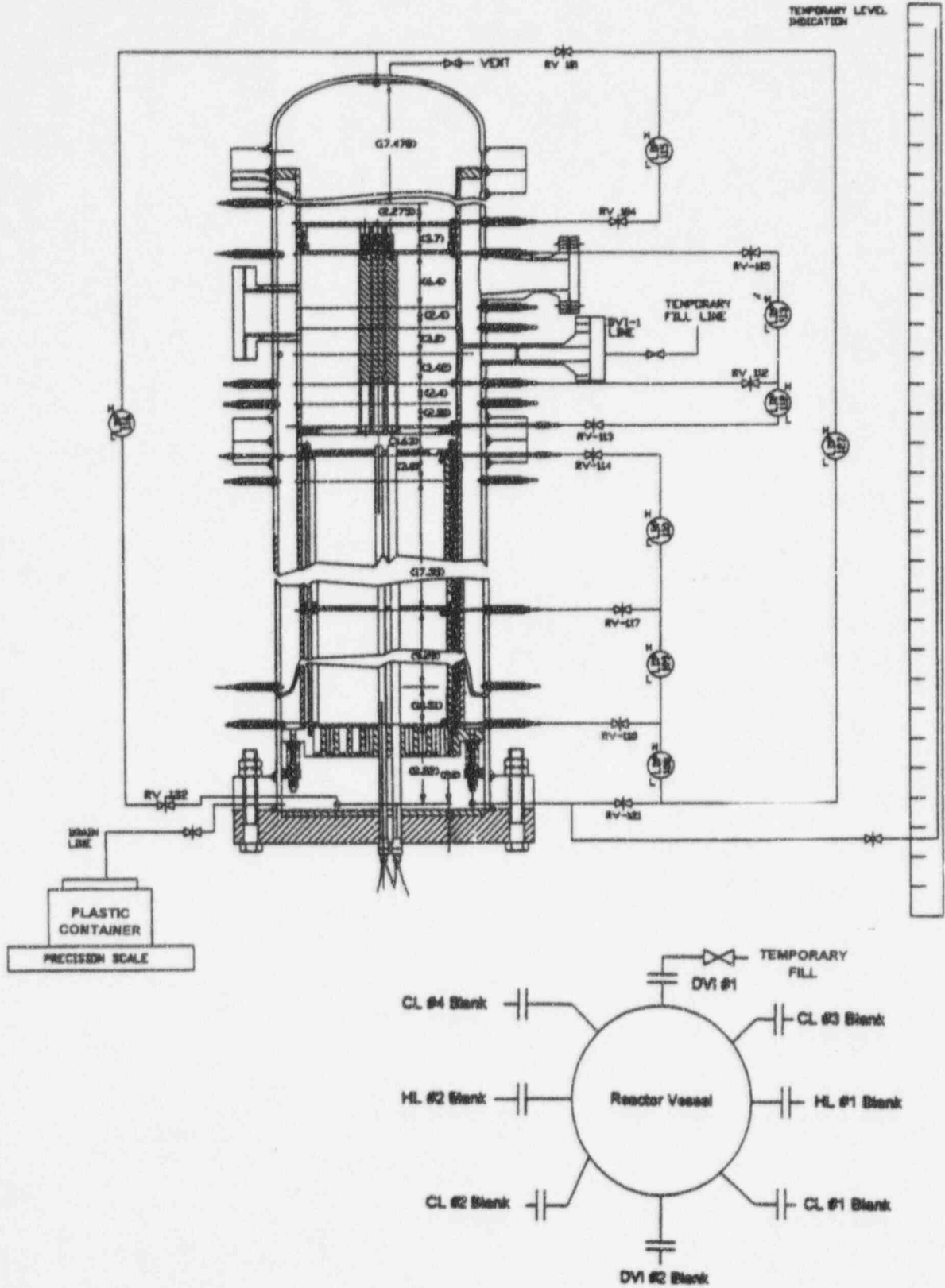


Figure 4.1-10 Schematic of ADS and BAMS Separator Test Setup

4.2 Pressure Drop Determination

4.2.1 Background Information

The design of the test facility started in early 1992. The design work was performed concurrently with the scaling analysis for the test facility. Although the scaling analysis was revised several times, the basic principles and the design criteria related to hardware design did not change. For additional details, see *AP600 Low-Pressure Integral Systems Test at Oregon State University, Facility Scaling Report*, WCAP-14270.⁽⁶⁾ According to the scaling analysis, the following parameters related to hardware design must be properly scaled:

- AP600 physical geometry including layout and elevation head modeling
- Each AP600 injection line in size, length, area, volume, and physical geometry
- Pressure drop across each line
- Each tank volume and height
- Critical thermal hydraulic phenomena

Since the AP600 design was still evolving in 1992, the test facility design was constantly updated to reflect the revised AP600 design. Each injection line in AP600 went through the following design process:

- (a) The AP600 line geometries were exactly modeled, including length, elevations, bend, number of elbows, and valves.
- (b) Line losses were calculated for AP600 conditions, and the results were verified to be within an acceptable range. This step ensured that proper line geometry was modeled and proper calculation methodology was used.
- (c) Line characteristics for the test facility were scaled, including consideration of the operating pressure, temperatures, fluid density, flow rate, flow velocity, line length, line height, line inside diameter, flow area, and flow volume.
- (d) Instrumentation for each line was selected.
- (e) Pressure drop calculations were performed using the same methodology as in (b), and the results were compared with AP600 pressure drops in (b). The ratio of the two pressure drops should equal the required scale ratio. An orifice plate was used to provide the proper pressure drop ratio where required.

Note: A properly scaled line inside diameter was never a standard pipe or tubing size. Therefore, the next closest standard-size pipe or tubing was used. This would change the line flow area, volume, velocity, and pressure drop ratio. A non-ideal line would

result in scaling distortion. Therefore, (c) and (d) were iterated several times to obtain the optimal line size that provided proper pressure drop scale ratio with minimum volume distortion.

The scaling analysis required that frictional loss should NOT be the major pressure drop in the line. Therefore, tubing was selected whenever possible.

- (f) The wall thickness of the selected line was sized using industry standards. The ASME code was used for piping and vessels; ANSI B3.11 was used for tubing.
- (g) Finally, each line was translated into isometric drawings for fabrication.

Each AP600 line was modeled for this test facility using the previous process, and each line was flow tested to verify proper pressure drop and line resistance. The first flow test was completed on May 9, 1994, and pressure drop data were obtained for the following lines:

- CMT-1 injection line (from bottom of CMT-1 to DVI-1 flange and from DVI-1 flange to reactor vessel downcomer at DVI-1)
- CMT-2 injection line (from bottom of CMT-2 to DVI-2 flange and from DVI-2 flange to reactor vessel downcomer at DVI-2)
- ACC-1 injection line (from bottom of ACC-1 to DVI-1 flange and from DVI-1 flange to reactor vessel downcomer at DVI-1)
- ACC-2 injection line (from bottom of ACC-2 to DVI-2 flange and from DVI-2 flange to reactor vessel downcomer at DVI-2)
- CMT-1 to CL-3 balance line (from top of CMT-1 to top of CL-3)
- CMT-2 to CL-1 balance line (from top of CMT-2 to top of CL-1)
- ADS 1-3 lines and the line from ADS 1-3 separator through the sparger inside IRWST
- IRWST-1 injection line (from bottom of IRWST-1 to DVI-1 flange and from DVI-1 flange to reactor vessel downcomer at DVI-1)
- IRWST-2 injection line (from bottom of IRWST-2 to DVI-2 flange and from DVI-2 flange to reactor vessel downcomer at DVI-2)
- Primary sump-1 injection line (from bottom of primary sump tank to DVI-1 flange and from DVI-1 flange to reactor vessel downcomer at DVI-1)

- Primary sump-2 injection line (from bottom of primary sump tank to DVI-2 flange and from DVI-2 flange to reactor vessel downcomer at DVI-2). In addition, total developed head as a function of flow rate for RCPs

Soon after the first series of flow tests was performed, the AP600 design was revised to add a venturi nozzle at the DVI-1 flange next to the reactor vessel. Another identical venturi nozzle was added at the DVI-2 flange next to the reactor vessel. This change increased the pressure drop from each DVI flange to the reactor vessel downcomer. Therefore, the line sizing and pressure drop calculations were re-evaluated. The evaluation concluded that the line size was still adequate. However, the orifice plates originally installed at the DVI lines between the CMT/accumulator tee and the reactor vessel downcomer (ORI-253 for DVI-1 and ORI-254 for DVI-2) had to be removed to compensate for the pressure drop increase introduced by the DVI venturi nozzles. Another series of flow tests was performed on May 20, 1994, to measure pressure drop deviations due to the installation of DVI venturi nozzles and the removal of orifice plates ORI-253 and ORI-254.

A third series of flow tests was performed on September 27, 1994, after the completion of the matrix tests. This series of flow tests measured pressure drops and line resistances on other lines not covered in the first two series of flow tests. In addition, some of the pressure drop measurements related to the reactor vessel obtained in the first series of flow tests were found to be questionable. These measurements were repeated in the third series of flow tests.

The objectives of the flow tests were as follows:

- To provide flow and pressure drop data for RCP operation
- To determine RCP coastdown data
- To verify that CMT-1 and CMT-2 injection line pressure drops were between 63.6 and 81.6 in. H₂O when injection flow was 8.3 ± 0.3 gpm
- To verify that the ACC-1 and ACC-2 line pressure drops were between 277 and 346 in. H₂O when flow was 22.7 ± 0.3 gpm
- To verify that the CMT-1 and CMT-2 cold-leg balance line pressure drops were between 4.0 and 5.4 in. H₂O when flow was 4.6 ± 0.3 gpm
- To determine pressure drop versus flow information for the RNS injection line and verify that the two RNS injection line pressure drops were balanced to within ± 10 percent
- To determine pressure drop versus flow for the ADS 1-3 lines

- To verify IRWST-1 and IRWST-2 pressure drops were between 63.6 and 81.6 in. H₂O when injection flow was 8.3 ± 0.3 gpm
- To verify primary sump-1 and primary sump-2 pressure drops were between 63.6 and 81.6 in. H₂O when injection flow was 8.3 ± 0.3 gpm
- To determine the pressure drop for each of the four primary loops and across individual line sections or components
- To determine the pressure drop for the PRHR HX loop from hot-leg entrance to SG channel head

4.2.2 Test Procedure, Instrumentation, and Results

This section provides a brief description of the facility initial filling procedures followed by a description of the test procedures for each line. The instrumentation used for each line and the corresponding test results are also discussed in detail.

There were no specific temperature or pressure requirements associated with the cold pre-operational flow tests.

4.2.2.1 Facility Initial Filling for the First Two Series of Flow Tests

Dwg. OSU 600002 and Dwg. OSU 600206 (Appendix G) provide visual representation of facility filling routes. The RNS pump was used to fill the entire primary sump tank and part of the IRWST, taking suction from the feed storage tank. The discharge line of the RNS pump was connected to the IRWST-1 injection line, which in turn directed the water to fill the primary sump tank and the IRWST tank. The filling of the primary sump tank was achieved via the bypass line of the sump-1, through the primary sump tank isolation valve (CSS-909). The piping arrangement was also used to partially fill the IRWST. This piping arrangement is shown in Dwg. OSU 600206 (Appendix G).

The primary sump tank was filled to the simulated overflow level, i.e., the simulated AP600 curb level. The IRWST was partially filled to the corresponding level simultaneously. The RNS pump was secured once this level was obtained and CSS-909 was isolated.

The primary sump tank had a large water volume because it was designed to accommodate water from all components, including IRWST and reactor vessel. Therefore, it was used as the water source during the initial system fill process. All other lines connected to the RNS pump discharge line were isolated during the initial filling process.

Once the primary sump tank and partial IRWST were filled with water, the RNS pump suction line was then rerouted to take suction from the bottom of the primary sump tank and discharged to two parallel lines leading to the DVI injection lines. Because check valves upstream of the DVI lines

(CMT and accumulator injection line check valves), the water was discharged into the reactor vessel and its interconnecting components such as the pressurizer and the SGs. The CMTs were filled via the cold leg balance lines. All vent valves on these components were initially open and closed once water issued from the valves. The two RNS discharge lines were isolated once the primary loop, the reactor vessel, the pressurizer, the PRHR HX, the SGs and the CMTs were filled and vented.

Still taking suction from the bottom of the primary sump tank, the RNS now discharged to fill the accumulators via a common fill and drain line. This common fill and drain line enabled filling and draining of the accumulators and the CMTs. The vent valves at the accumulators and CMTs were initially open and were closed when water issued from them.

After the facility was filled, the RNS pump continued to operate to keep the plant pressurized at shutoff head and the RCPs were jogged for a few seconds and the selected vent valves were open and closed to remove any trapped air in the system. The RCS was then refilled again and the RNS pump stopped.

The system was now completely filled, water solid, free of air, and ready for flow testing.

4.2.2.2 Facility Initial Filling for the Third Series of Flow Tests

The filling sequence of the test facility for the third series of flow tests was essentially the same as for regular matrix tests. See Subsection 2.7 for fill and vent procedures.

4.2.2.3 Methodology of Pressure Drop Data Analysis

Line losses were calculated from differential pressure data measured by differential pressure cells manufactured by Rosemount Co. Subsection 2.4 provides a detailed description of the differential pressure cells which measure the pressure difference between any two taps installed in the facility. For these tests, the taps were usually located in piping or within the reactor vessel. The method of converting the measured data to line losses is based on Bernoulli's equation with line loss. The equations are defined below.

Vertical Line with Different Temperatures

When the flowing fluid temperature is different from fluid temperature in the DP cell instrument lines, temperature compensation is necessary. The following equation can be used.

$$DP_{\text{loss}} = (P_H - P_L) + \text{RHO}_F * (V_1^2 - V_2^2)/(2g) + (\text{RHO}_F - \text{RHO}_R) * (h_1 - h_2) \quad (1)$$

where:

- DP_{loss} = pressure loss in line between two static taps, psf
 $(P_H - P_L)$ = measured pressure difference from high-pressure side of instrument sensing line to low-pressure side of line, psf
 RHO_F = weight density of flowing fluid, lb/ft.³
 V_1 = flow velocity at high-pressure side of differential pressure cell, ft./sec.
 V_2 = flow velocity at low-pressure side of differential pressure cell, ft./sec.
 g = gravitational acceleration, ft./sec.²
 h_1 = vertical distance of high-pressure side pressure tap with respect to arbitrary datum, ft.
 h_2 = vertical distance of low-pressure side pressure tap with respect to arbitrary datum, ft.
 RHO_R = Weight density of fluid in sensing lines, lb/ft.³

When the pipe diameters at the taps are the same, $V_1 = V_2$, and the second term disappears.

Vertical Line with Same Temperatures

When the flowing fluid in the vertical line has the same temperature as the differential pressure cell sensing line temperature, the following equation can be used:

$$DP_{loss} = (P_H - P_L) + RHO_F * (V_1^2 - V_2^2)/(2g) \quad (2)$$

Horizontal Line with Different Temperature

When the flowing fluid temperature is different from the differential pressure cell tap line temperature, Equation 1 can be modified to the same equation as Equation 2.

Horizontal Line with Same Temperature

When the flowing fluid temperature is the same as the differential pressure cell tap line temperature, Equation 2 can also be used to calculate pressure loss in the line from point 1 (high-pressure side) to point 2 (low-pressure side)

Note: The assumed high-pressure side is referred to as the high side of the differential pressure cell, and the low-pressure side is referred to as the low side of the differential pressure cell. Each differential pressure cell (or LDP cell) was assigned with predetermined high and low sides clearly marked in the piping and instrumentation diagrams (P&IDs) in Appendix G. The flow direction was assumed to be from the high-pressure side to the low-pressure side and the differential pressure cell was calibrated accordingly. When the pressure drop measurement turned out to be negative, the actual flow direction was just the opposite of the presumed flow direction, or the pressure at the low side was actually

higher than the high side of the differential pressure cell. In either event, the magnitude of the measurements was still valid.

4.2.3 RCP Flow Test

4.2.3.1 Procedures

Dwg. OSU 600203, Dwg. OSU 600301 (Appendix G), and Dwg. LKL911218 (Appendix H) provide details of the test loop setup and instrumentation locations. The facility was filled and vented prior to actual RCP flow testing as described previously. On completion of initial filling and venting, all four RCPs were run to assess pressure drops and flows. All four reactor coolant pumps were then tripped and restarted several times to assess coastdown time. This procedure was performed for the first series of flow tests.

The RCP total developed head as a function of flow was also measured and recorded in the first series of flow tests.

The third series of flow test was performed after the initial facility fill and vent. Test data were recorded at ambient temperature, 100°, 200°, 300°, and 400°F. At each temperature, the reactor coolant pumps were first started with the PRHR HX line isolated by closing the outlet isolation valve. Pressure drops and temperature around the reactor vessel and within the reactor vessel were measured and recorded. Then the PRHR HX line was open and the pressure drops and temperature around the PRHR HX line were measured and recorded.

Pressure drops around the reactor vessel and within the reactor vessel were measured and recorded during the first and last series of flow tests. Note that the first series of flow test was conducted at ambient temperature and the third series of flow tests was conducted at various flow temperatures, including ambient temperature. The following instrumentation and their designated functions were used in the tests. See Dwg. LKL911218 (Appendix H) for physical locations of these instruments.

4.2.3.2 Instrumentation

Flow rate measurements:

- FMM-201 Magnetic flow meter located at CL-1
- FMM-202 Magnetic flow meter located at CL-2
- FMM-203 Magnetic flow meter located at CL-3
- FMM-204 Magnetic flow meter located at CL-4

Temperature and pressure drop measurements:

Table 4.2-1 provides a detailed description of instrumentation within the reactor vessel and other interconnecting major components.

4.2.3.3 Results

Total Developed Head of RCP

The total developed head for each RCPs was measured directly by differential pressure cells across each pump. The total developed head for each pump was measured in both the first and the third series of flow tests. Table 4.2-5 summarizes the test results. DP-203 was used to measure pressure drop across RCP-1, DP-202 for RCP-2, DP-205 for RCP-3, and DP-206 for RCP-4.

Each pump was single speed centrifugal pump. The test results show that the total developed head and flows are almost the same for all four pumps at the same temperature. Comparison of test results between the first and third series of tests shows that the test results are repeatable. This is shown in the table by the ratio of pressure drop to flow rate square (psi/gpm^2).

The results of the third series of flow tests also reveals that the total developed head for each RCPs decreases as the fluid temperature increases.

Performance curves for the pumps supplied by Queen Pump Company of Portland Oregon indicate that the pump was rated at 250 gpm at 144 in. H_2O of total developed head at ambient temperature. All four pumps were operating at near runout flow during testing with flows of approximately 330 gpm and 167 in. H_2O of total developed head. However, no cavitation or net positive suction head problems were observed.

RCPs Coastdown Time

Coastdown times for the RCPs could not be evaluated using the DAS due to relatively long sampling rate. Testing indicated that RCPs coastdown time was about 1 to 3 seconds. But the fastest data sampling rate available in the DAS was about 8 seconds. Therefore, no coastdown data were obtained in these tests. Data obtained during matrix testing indicated coastdown time was about 2 seconds.

Reactor Vessel Pressure Drops

Table 4.2-1 summarizes the locations of pressure and pressure drop measurements in and around the reactor vessel. Table 4.2-2 summarizes the test data obtained during the first series of flow tests. Table 4.2-3 summarizes the test data obtained during the third series of flow tests.

The third series of flow tests repeated all pressure drop measurements in the first series of flow tests and more. Table 4.2-1 provides a comparison of the instrumentation used in these two series of flow tests. Table 4.2-4 provides a comparison of the test data of these two series of flow tests at same temperature. Data from the third series of flow tests did not agree with data from the first series of

flow tests. It is believed that the data from the first series of flow test were not accurate. In fact, this was one reason the third series of flow tests was performed. The test data from the third series of flow tests appear to be more realistic. This conclusion is based on the following observations:

- The total developed head for each RCP recorded in the last series of flow test is in good agreement with that recorded in the first series of flow tests (Table 4.2-5).
- The DAS had been verified by the time the third series of tests was performed.
- The test results from the last series of flow test compared well with steady state matrix test results.
- Some data from the first series of tests agree well with the last series of flow tests and some do not. For example, the pressure drop across the upper support plate (LDP-114) in the first series of flow test agrees well with the last series of flow test, 27.6 in. H₂O versus 27.2 in. H₂O. However, the pressure drop from the bottom of the upper grid inside the core to the top of the upper core plate (LDP-111) in the first series of flow tests is totally different from the last series of flow test, 7.89 in. H₂O versus 2.33 in. H₂O. The exact cause of the discrepancy is not known. It is suspected that the configuration file for the first series of flow tests was not verified properly. In fact the configuration file was being verified when the first series of flow test was conducted. Also, an improper configuration file explains why some data agree well and some do not. The electronic signals generated from the transducers appear to be correct; the problem with the first series of flow tests seems to have been caused by the data recording system.

Using the test results from the last series of flow tests, the line pressure loss and line resistance within and around the reactor vessel were calculated and summarized in Table 4.2-6. Equations 1 and 2 were used to calculate the line loss.

Primary Loop Pressure Drops

Similar to the pressure drops across the reactor vessel, the pressure loss in hot legs, cold legs and other components associated with the reactor vessel in the last series of flow tests were used to estimate the line resistance. The results are also summarized in Table 4.2-6.

4.2.4 CMT Injection Flow Test

Hydraulic characteristics of the CMT-1 and CMT-2 injection lines from the bottom of each CMT to the DVI tees and to the reactor vessel downcomer via the DVI-1 and DVI-2 injection nozzles are discussed in this section. The CMT injection flow test was performed twice in the first series of flow tests only, first with the original orifice plates and then with the DVI venturi nozzles.

4.2.4.1 Procedures

Figures 4.2-1 and 4.2-2 provide schematics of the test arrangement for each CMT. A flow path was set up using the RNS pump and a temporary tygon hose. The hose was connected to the service connection downstream of the RNS pump discharge to pump water from the bottom of the primary sump tank to the top of the CMT, down to the DVI tee and into the reactor vessel downcomer via the DVI nozzle. Flow was then directed to the pressurizer and ADS valves. Finally, flow was directed to the IRWST via the ADS 1-3 sparger located inside the IRWST.

The temporary tygon hose was connected from the pump discharge service connection to the top of the CMT. The ADS-1 valve was opened, and the pump started. The desired flow rate was obtained by throttling RCS-806 (the isolation valve at the service connection downstream of the RNS pump discharge). The desired pressure drops were measured and recorded.

The test was performed the first time with the original configuration, i.e., with orifice plates ORI-253 and ORI-254 and without DVI venturi nozzles. The test was performed the second time with the new venturi nozzles installed in each DVI line at the DVI nozzles next to the reactor vessel. Due to the increased head loss in each injection line from the venturi nozzles, it was necessary to remove orifice plates ORI-253 and ORI-254 located between the DVI tees and the DVI nozzles next to the reactor vessel.

The water temperature for this test was at ambient conditions.

4.2.4.2 Instrumentation

Figures 4.2-1 and 4.2-2 provide schematics of the test arrangement and locations of instrumentation.

Two differential pressure indications were taken. For CMT-1, DP-501 provided the pressure drop from the bottom of CMT-1 to the DVI-1 flange next to the reactor vessel and DP-128 provided the exit loss into the vessel, from the DVI-1 flange to the reactor vessel downcomer. FMM-501 measured the flow rate through the DVI-1. Note that the pressure drop measured by DP-501 included the pressure drop across either orifice plate ORI-253 or the DVI venturi nozzle, but not both. Figure 4.2-1 shows this pressure drop measurement.

For CMT-2, DP-502 provided the pressure drop from the bottom of CMT-2 to the DVI-2 flange next to the reactor vessel and DP-129 provided the exit loss into the reactor vessel from the DVI-2 flange to the reactor vessel downcomer. FMM-504 measured the flow rate through DVI-2. Similar to CMT-1, DP-502 included the pressure drop across either orifice plate ORI-254 or the DVI venturi nozzle, but not both. Figure 4.2-2 shows this pressure drop measurement.

4.2.4.3 Results

Each CMT injection flow path consists of two line sections. The first line section is normally referred to as the true CMT injection section, and runs from the bottom of the CMT to the DVI tee junction where the accumulator and the IRWST injection lines meet. The second line section is referred to as the DVI line which begins at the DVI tee junction and ends at the reactor vessel downcomer. This DVI line is common to the CMT, accumulator, and IRWST injection lines, and it contains either the DVI venturi nozzle or the orifice plate (ORI-253 or ORI-254). All matrix tests used the DVI venturi nozzle; orifice plates ORI-253 and ORI-254 were removed.

The test data are summarized in Table 4.2-7. Data were plotted in Figures 4.2-3 through 4.2-10 as the pressure drop rate versus the square of the flow rate and fitted with linear regression methodology. The plots show excellent linear results, indicating that Darcy's equation can be used to predict pressure drops through the line.

Line Resistance

The plots show that the pressure drop is directly proportional to the square of the flow rate. This is in agreement with Darcy's equation. The slope of each curve was used to calculate the overall line resistance ($fL/D+K$) using Darcy's equation as follows:

$$h_L = (fL/D+K) * V^2 / (2g) \quad (3)$$

This equation can be re-arranged as follows:

$$h_L = (12) * (fL/D+K) * Q^2 / (2 * g * A^2 * 448.86^2) \quad (4)$$

where:

- h_L = pressure drop through the line, in. H_2O
- $fL/D+K$ = line total resistance, dimensionless
- g = gravitational acceleration = 32.2 ft./sec.²
- A = flow area, ft.²
- Q = volumetric flow rate, gpm
- f = friction factor, dimensionless
- D = diameter, ft.
- L = length, ft.
- K = form loss coefficient, dimensionless

Equation 5 was represented by each curve plotted in the figures. Therefore, the slope of each plot was used to calculate the total line resistance as follows:

$$\text{Slope} = 12 * (fL/D+K) / (2 * g * A^2 * 448.86^2)$$

or

$$fL/D+K = \text{slope} * (2 * g * A^2 * 448.86^2) / 12 \quad (5)$$

Equation 5 was used to calculate total line resistance. For example, Figure 4.2-3 shows a slope of 1.0733, using Equation 6:

$$fL/D+K = (1.0733)(2)(32.2)(0.006842)^2 (448.86^2) / 12$$

$$fL/D+K = 54.32$$

The flow area for the CMT injection line is 0.006842 ft.² (inside diameter = 1.12 in.)

The line resistance for each line section was calculated and is summarized in Table 4.2-16.

Pressure Drop Comparison

Table 4.2-16 compares the measured pressure drop with the design (predicted) pressure drop and the specified acceptable pressure drop range (defined as the acceptance criteria). The design (predicted) pressure drop was obtained mathematically using Darcy's equation and the same flow path configuration as the test article.

The following observations were made for both CMT-1 and CMT-2 injection lines:

1. All measured pressure drops were in agreement with Darcy's equation.
2. Both CMT-1 and CMT-2 pressure drop measurements were within the acceptable range. This applied to all tests with either the orifice plates or the DVI venturi nozzles installed.
3. The measured pressure drop was in agreement with the design (predicted) value, implying that the analytic model was valid. The measured total pressure drop for the entire CMT-1 injection flow path was 72.9 in. H₂O versus the design value of 67.7 in H₂O at the specified flow rate of 8.24 gpm. For the CMT-2 injection flow path, the measured pressure drop was 71.7 in. H₂O versus the design value of 67.4 in. H₂O at the same flow rate as CMT-1. Therefore, the measured and design pressure drops were within 7.7 percent of each other.

Note: This observation only applied to the tests with orifice plates ORI-253 and ORI-254 and without DVI venturi nozzles installed. No design (predicted) pressure drop information was available for the tests with the DVI venturi nozzles installed. Design calculations were not required since the pressure drops were within the acceptable range.

4. The measured pressure drops in both CMT lines for the case with orifice plates ORI-253 and ORI-254 but without DVI venturi nozzles installed were very close: 72.8 in. H₂O in CMT-1 and 71.7 in. H₂O in CMT-2 — within 1.6 percent of each other.

For the case with the DVI venturi nozzles installed and the orifice plates removed, the pressure drop was 77.8 in. H₂O for CMT-1 and 74.1 in. H₂O for CMT-2 — within 4.9 percent of each other.

In either case, the conclusion was that CMT-1 and CMT-2 flow lines were well balanced.

Calculation of Form Loss Coefficient K for DVI Venturi Nozzle

The second series of flow tests measured pressure drops with the DVI venturi nozzles installed and orifice plates ORI-253 and ORI-254 removed. The tests were run for CMT-1, CMT-2, ACC-1 and ACC-2 only. Since the DVI venturi nozzles were installed immediately upstream of the DVI flange (nozzles), they were also part of IRWST-1, IRWST-2, primary sump-1 and primary sump-2. It is desirable to estimate the loss coefficient for the venturi nozzle alone. With the known K for the venturi nozzle, the total line resistance for IRWST-1, IRWST-2, primary sump-1 and primary sump-2 can be obtained from test data.

The loss coefficient (K) for each of the DVI venturi nozzles was calculated using the following process:

1. Line resistances from the bottom of each CMT to the DVI flange (nozzle) for both CMT-1 and CMT-2 lines without orifice plates ORI-253 and ORI-254 and DVI venturi nozzles were calculated using the results from the first series of flow tests (Table 4.2-16).

The measured pressure drops agreed with the design (predicted) values for the first series of flow tests, i.e., with orifice plates ORI-253 and ORI-254 and without DVI venturi nozzles. The analytic model was acceptable, and included ORI-253 for CMT-1 and ORI-254 for CMT-2. These orifice plates were sharp-edged and well-defined mathematically; therefore, the analytic loss coefficient (K) for the orifice plate was subtracted from the measured line resistance for the line section from the bottom of the CMT to the DVI flange (nozzle), measured by DP-501 or DP-502. Consequently, the line resistances for the CMT lines from the bottom of the CMTs to the DVI flanges, without orifice plates ORI-253 and ORI-254 or DVI venturi nozzles installed were calculated.

2. The loss coefficient (K) for each of the DVI venturi nozzles was calculated using test results from the second series of flow tests.

Test results for the second series of flow tests were acceptable since they met the acceptance criteria. Line resistances from the bottom of each CMT to the DVI flange (nozzle), measured

by DP-501 and DP-502, were subtracted from the product of step 1, resulting in the K value for the venturi nozzle.

- Steps 1 and 2 were performed for CMT-1 and CMT-2. The results were used to obtain an average K for the DVI venturi nozzle.

CMT-1 DVI Venturi Nozzle Loss Coefficient Estimation

Bottom of CMT-1 to DVI-1 flange (fL/D+K) = 53.6
(With orifice plate ORI-253 only)

Design K for orifice plate ORI-253 = 1.27
(From analytic model)

Thus, fL/D+K for the line from bottom of CMT-1 to DVI-1 flange = 52.4
(Without orifice plate ORI-253 or DVI venturi nozzle)

Bottom of CMT-1 to DVI-1 flange (fL/D+K) = 58.0
(DVI venturi nozzle only)

Therefore, DVI-1 venturi nozzle K = $58.0 - 52.4 = 5.6$ (For CMT-1 line)

CMT-2 DVI Venturi Nozzle Loss Coefficient Estimation

Bottom of CMT-2 to DVI-2 flange (fL/D+K) = 52.5
(With orifice plate ORI-254 only)

Design K for orifice plate ORI-254 = 2.02
(From analytic model)

Thus, fL/D+K for the line from bottom of CMT-2 to DVI-2 flange = 50.5
(Without orifice plate ORI-254 or DVI venturi nozzle)

Bottom of CMT-2 to DVI-2 flange (fL/D+K) = 55.2
(With DVI venturi nozzle only)

Therefore, DVI-2 venturi nozzle K = $55.2 - 50.5 = 4.72$ (For CMT-2 line)

K for Each DVI Venturi Nozzle

The K value is the same for both DVI venturi nozzles because they were identical; therefore:

$$K_{\text{venturi}} = (5.62+4.72)/2 = 5.17$$

Table 4.2-7 lists raw data for the second series of flow tests after the DVI venturi nozzles were installed and the orifice plates were removed. Flow was fully recovered when it exited into the reactor vessel downcomer. Test results show that the pressure drop was negligible (0 or negative psig).

These results demonstrated that the instrumentation was functioning properly and that the major pressure drops were in the lines containing the venturi nozzles.

4.2.5 Accumulator Injection Flow Test

Hydraulic measurements of the ACC-1 and ACC-2 injection lines from the bottom of each accumulator to the DVI tees and to the reactor vessel downcomer via the DVI-1 and DVI-2 injection nozzles are discussed in this section. The accumulator injection flow test was performed twice in the first series of flow tests only, first with the original orifice plates and then with the DVI venturi nozzles.

4.2.5.1 Procedures

Figures 4.2-11 and 4.2-12 provide schematics of the test arrangement for each accumulator injection line.

In the accumulator injection flow test, a flow path was set up using the RNS pump and a temporary tygon hose connecting to the service connection downstream of the RNS pump discharge. Water was pumped from the bottom of the primary sump tank to the top of the accumulator, down to the bottom of the accumulator and the DVI tee to the reactor vessel downcomer via the DVI nozzle. Flow was then directed up to the pressurizer and ADS valves. Finally, flow was directed to the IRWST via the ADS 1-3 sparger located inside the IRWST.

The temporary tygon hose was connected from the pump discharge service connection to the top of the accumulator. ADS-1 was opened, and the pump started. The desired flow rate was obtained by throttling RCS-806 (the isolation valve at the service connection downstream of the RNS pump discharge). The desired pressure drops were measured and recorded.

The test was performed the first time with the original configuration, i.e., with orifice plates ORI-253 and ORI-254 and without DVI venturi nozzles. The test was performed the second time with the new venturi nozzles installed in each DVI line at the DVI nozzles next to the reactor vessel. Due to the increased head loss in each injection line from the venturi nozzles, it was necessary to remove orifice

plates ORI-253 and ORI-254. In addition, the orifice plate in the ACC-1 injection line (ORI-451) was increased from 0.616 in. throat diameter to 0.66 in. throat diameter in order to adjust the line resistance so that it was within the acceptable criteria range.

The water temperature for this test was at ambient conditions.

4.2.5.2 Instrumentation

Figures 4.2-11 and 4.2-12 provide schematics of the test arrangement and locations of instrumentation.

Two differential pressure indications were taken. For ACC-1, DP-401 provided the pressure drop from the bottom of the ACC-1 to DVI-1 nozzle next to the reactor vessel. DP-128 provided the entrance loss into the vessel from DVI-1 nozzle to the reactor vessel downcomer. FMM-401 measured the flow rate through the ACC-1 injection line. The pressure drop measured by DP-401 included the pressure drop across either orifice plate ORI-253 or the DVI venturi nozzle, but not both.

For ACC-2, DP-402 provided the pressure drop from the bottom of ACC-2 to the DVI-2 nozzle next to the reactor vessel. DP-129 provided the entrance loss into the vessel from the DVI-2 nozzle to the reactor vessel downcomer. Similar to ACC-1, DP-402 included the pressure drops across either orifice plate ORI-254 or the DVI venturi nozzle, but not both. FMM-402 measured the flow rate through the ACC-2 injection line.

4.2.5.3 Results

Each accumulator injection flow path consists of two line sections. The first line section runs from the bottom of the accumulator to a tee junction upstream of the DVI tee. A very short line section connects the two tee junctions. For all practical purposes, these two tee junctions are the same. The second line section is the DVI injection line described in the CMT test result section. This DVI line is common to the CMT, accumulator, and IRWST injection lines and contains either the DVI venturi nozzle or the orifice plate (ORI-253 or ORI-254).

Test data are summarized in Table 4.2-8. Data were plotted in Figures 4.2-13 through 4.2-18 as the pressure drop versus the square of the flow rate and fitted with linear regression methodology. The plots show excellent linear results, indicating that Darcy's equation can be used to predict pressure drops through the line.

Line Resistance

Line resistances ($fL/D+K$) for the accumulator injection lines were calculated using same methodology as the CMT injection flow test. Each injection line has an inside diameter of 1.12 in. (flow area = 0.006842 ft²).

Pressure Drop Comparison

Table 4.2-16 compares the measured pressure drop with the design (predicted) pressure drop and the specified acceptable pressure drop range (acceptance criteria). The following observations were made for both the ACC-1 and ACC-2 injection lines:

1. All measured pressure drops were in agreement with Darcy's equation.
2. Both ACC-1 and ACC-2 pressure drop measurements were within the acceptable range. This applied to all tests with either orifice plates or DVI venturi nozzles installed.
3. The measured pressure drop was in agreement with the design (predicted) value implying that the analytic model is valid. The measured total pressure drop for the entire ACC-1 injection flow path was 337 in. water versus the design value of 302 in. H₂O at the specified flow rate of 22.7 gpm — within 11.25 percent of each other.

The measured pressure drop for the ACC-2 injection flow path was 324 in. H₂O versus the design value of 305 in. H₂O at the flow rate of 22.7 gpm - within 6.3 percent of each other.

Note: This observation only applied to the tests with orifice plates ORI-253 and ORI-254 and without DVI venturi nozzles installed. No design (predicted) pressure drop information was available for the tests with the DVI venturi nozzles installed. Design calculations were not required since the pressure drops were within the acceptable range.

4. The measured pressure drops in both accumulator injection lines with orifice plates ORI-253 and ORI-254 but without DVI venturi nozzles installed were very close: 337 in. H₂O in ACC-1 and 324 in. H₂O in ACC-2 — within 4.1 percent of each other.

For the case with the DVI venturi nozzles installed and the orifice plates removed, the pressure drop was 318 in. H₂O for ACC-1 and 345 in. H₂O for ACC-2 — within 8.6 percent of each other.

In either case, the conclusion was that ACC-1 and ACC-2 flow lines were well balanced.

Comparison of DVI Flange (Nozzle) with Reactor Vessel Downcomer Loss Coefficients

The exit loss coefficients from the DVI flange (nozzle) to the reactor vessel downcomer for both DVI-1 and DVI-2 were calculated using the test data in Table 4.2-16 from ACC-1 and ACC-2 flow tests. This line did not include orifice plates ORI-253 and ORI-254, or DVI venturi nozzles. This line was common to CMT-1, CMT-2, ACC-1, ACC-2, IRWST-1, and IRWST-2 injection lines; therefore, each test should measure the same K.

Since both DVI-1 and DVI-2 nozzle and exit geometries were identical, the different K_{exit} suggests that the flow patterns between DVI-1 and DVI-2 at the downcomer were not the same. Theoretically, the K value for sudden expansion is equal to 1. Since a channel guide prevented upward flow, the exit condition was somewhat less than a sudden expansion.

The CMT injection flow test results section provides the average K_{exit} for each DVI line.

4.2.6 IRWST Injection Flow Test

Hydraulic measurements of the IRWST-1 and IRWST-2 injection lines were made from the bottom of the IRWST to the DVI tees and to the reactor vessel downcomer via the DVI-1 and DVI-2 nozzles. The test was performed in the first series of flow tests only with only orifice plates ORI-253 and ORI-254 installed. Flow testing with DVI venturi nozzles installed was not performed. Since all matrix tests were performed with the DVI venturi nozzles and without orifice plates ORI-253 and ORI-254 installed, the line resistance obtained from the IRWST flow test was adjusted to account for the addition of the DVI venturi nozzles and the removal of the orifice plates. A calculation methodology is provided in the following test results section.

4.2.6.1 Procedures

Figure 4.2-21 provides a schematic of the test arrangement for each IRWST injection line.

Initially, the primary sump tank was drained to a level below the bottom of the IRWST, and the primary sump injection bypass lines were isolated by closing isolation valves CSS-909 and CSS-910. The IRWST injection lines were isolated (by closing RCS-711 and RCS-712), and the IRWST was filled to the level of the IRWST/primary sump overflow. The reactor vessel and the primary loops were drained to a level slightly above the DVI line penetrations to the reactor vessel. This arrangement assured that the primary sump tank could not provide injection flow into the reactor vessel because the IRWST gravity head was significantly higher and, therefore, blocked the primary sump tank injection lines. Since the DVI lines were filled prior to the start of flow testing, continuous IRWST injection flow at the beginning of the draining process was assured.

RCS-711 and RCS-712 were opened to gravity-drain the water from the bottom of the IRWST to the reactor vessel through the DVI-1 and DVI-2 lines, respectively, simulating the AP600 IRWST draining process. The draining flow rate and the desired pressure drops were measured and recorded.

4.2.6.2 Instrumentation

Figure 4.2-21 provides a schematic of the test arrangement and locations of the instrumentation.

The IRWST-1 injection line consists of two line sections: one from the bottom of the IRWST to the DVI-1 flange (nozzle) next to the reactor vessel, the other from the DVI-1 flange to the reactor vessel

downcomer. DP-701 provided the pressure drop from the bottom of the IRWST to the DVI-1 flange. (Orifice plate ORI-253 was installed in this line section.) DP-128 provided the entrance loss into the vessel from the DVI-1 flange to the reactor vessel downcomer. FMM-701 measured the flow rate through the entire IRWST-1 injection line.

Similarly, the IRWST-2 injection line consisted of two line sections: one from the bottom of the IRWST to the DVI-2 flange (nozzle) next to the reactor vessel, the other from the DVI-2 flange to the reactor vessel downcomer. DP-702 provided the pressure drop from the bottom of the IRWST to DVI-2 flange. (ORI-254 was installed in this line section.) DP-129 provided the entrance loss into the vessel from the DVI-2 flange to the reactor vessel downcomer. FMM-702 measured the flow rate through the entire IRWST-2 injection line.

The water temperature for this test was at ambient conditions.

4.2.6.3 Results

Each IRWST injection flow path consists of two line sections. The first line section runs from the bottom of the IRWST to the DVI tee junction. The second line section is the DVI injection line described in the CMT test result section. This DVI line is common to the CMT, accumulator, and IRWST injection lines, and contains either the DVI venturi nozzle or orifice plates ORI-253 or ORI-254.

The test data are summarized in Table 4.2-9. Data were plotted in Figure 4.2-22 through 4.2-27 as the pressure drop versus the square of the flow rate and fitted with linear regression methodology. The plots show very good linearity, indicating that Darcy's equation can be used to predict pressure drops through the line.

Line Resistance

The same methodology used in the CMT injection flow test results section can be used to calculate the line resistance for the IRWST injection lines; however, the IRWST injection line inside diameter varied from section to section. Thus, IRWST injection line resistance can not be calculated directly from the test results. Since pressure drop is more important from the scaling point of view, line resistances will not be calculated. However, the inside diameters of various sections can be found from the IRWST isometric drawings (Appendix H, Dwg. LKL 920200 and Dwg. LKL920201), and the line resistance can be calculated using Equation 3.

Pressure Drop Comparison (without DVI Venturi Nozzles)

Table 4.2-16 provides a comparison between the measured pressure drop, the design (predicted) pressure drop, and the specified acceptable pressure drop range (acceptance criteria). The following observations were made for both IRWST-1 and IRWST-2 injection lines:

1. All measured pressure drops were in agreement with Darcy's equation.
2. Both IRWST-1 and IRWST-2 pressure drop measurements were within the acceptable range. This applies to the tests with only the orifice plates installed as well as those with DVI venturi installed.
3. The measured pressure drop was in agreement with the design (predicted) value, implying that the analytic model is valid. The measured total pressure drop for the entire IRWST-1 injection flow path was 21 in. H₂O versus the design value of 17.8 in. H₂O at the specified flow rate of 5.64 gpm — within 18.1 percent of each other.

For the IRWST-2 injection flow path, the measured pressure drop was 19.6 in. H₂O versus the design value of 17.8 in. H₂O at the flow rate of 5.64 gpm. — within 10.4 percent of each other.

Note: The acceptance criteria range for both IRWST-1 and IRWST-2 is 13.4 to 26.8 in. H₂O for cases with and without DVI venturi nozzles installed. This observation applies only to tests with orifice plates ORI-253 and ORI-254 and without DVI venturi nozzles installed. No design (predicted) pressure drop information was available for tests with DVI venturi nozzles installed. The acceptance criteria, however, is the same.

4. The measured pressure drops in both IRWST injection lines for the case with orifice plates ORI-253 and ORI-254 but without DVI venturi nozzles installed were very close: 21 in. H₂O for IRWST-1 and 19.6 in. H₂O for IRWST-2 — within 7.3 percent of each other.

Comparison of Loss Coefficients from DVI Flange (Nozzle) to Reactor Vessel Downcomer

The exit loss coefficients from the DVI flange (nozzle) to the reactor vessel downcomer for both the DVI-1 and DVI-2 lines were calculated using test data from IRWST-1 and IRWST-2 flow tests (Table 4.2-16). This line did not include orifice plates ORI-253 and ORI-254, or DVI venturi nozzles, but was common to CMT-1, CMT-2, ACC-1, ACC-2, IRWST-1, and IRWST-2 injection lines. Each test should measure the same K.

Since the DVI line, flange, and exit geometries were identical for the tests of CMT, accumulator, and IRWST injections, the exit loss coefficient (K) calculated from these three tests should be comparable. The exit loss coefficient from the DVI flange to the reactor downcomer for these three tests in the first series of flow tests are compared below:

Source	K (dimensionless) DVI-1	K (dimensionless) DVI-2
CMT Flow Test	0.704	0.911
Accumulator Flow Test	0.754	0.86
IRWST Flow Test	0.607	0.87
Average	0.688	0.880

The average of the DVI-1 exit coefficients is about 20 percent lower than the average of the DVI-2 coefficients. This difference could be caused by either misalignment of the welded flange on the reactor vessel (which would cause a different trajectory for flow entering the downcomer and, therefore, different flow patterns) or protrusion of the flange gasket into the flow area (which would increase pressure loss).

Since the coefficients for DVI-1 are lower and exhibit greater scatter, it is likely that the difference was caused by some variable factor, such as gasket protrusion. This difference probably had a very small effect on the balance of flows through the DVIs because the line pressure losses were much larger than the entrance losses.

Pressure Drop Comparison (with DVI Venturi Nozzles)

IRWST injection lines with DVI venturi nozzles were not tested; therefore, pressure drop measurements are not available. The following methodology was used to estimate the pressure drop through the IRWST injection lines with the DVI venturi nozzles installed.

1. The pressure drop through orifice plates ORI-253 and ORI-254 was calculated using the analytic K values and the IRWST injection flow rate. This step is valid because the analytic K values for orifice plates ORI-253 and ORI-254 were judged to be acceptable (as discussed in the CMT injection flow test results section.)
2. The pressure drop from the bottom of IRWST to the DVI-1 or DVI-2 flange at the IRWST injection flow rate was calculated. This step includes pressure drops across orifice plates ORI-253 and ORI-254.
3. The pressure drop for the orifice plates was subtracted from the corresponding pressure drops obtained in step 2, resulting in the pressure drop through the IRWST lines without the orifice plates or DVI venturi nozzles.

4. The pressure drop through the venturi nozzles at the IRWST injection flow rate was calculated using the $K_{venturi}$ calculated in the CMT injection flow test results section.
5. The results of steps 3 and 4 were added to arrive at the pressure drop from the bottom of the IRWST to the DVI flanges. Since the pressure drop downstream of the DVI flanges (with the venturi nozzles installed cases) was negligible, the sum of steps 3 and 4 is the total IRWST injection flow path pressure drop. CMT and accumulator injection flow tests both showed that the pressure drop from the DVI flanges to the reactor vessel downcomer was negligible for those cases with DVI venturi nozzles installed (Tables 4.2-7 and 4.2-8).

The following calculations were performed using the previous steps:

$$Q = 19.65 * d_1^2 * C * h_L^{0.5} \quad (6)$$

Crane 410

where:

$$\begin{aligned} Q &= \text{rate of flow, gpm} \\ h_L &= \text{head loss, ft.} \\ d_1 &= \text{throat dia, in.} \\ C &= \text{flow coefficient} = (1 - \beta^2) / (\beta^4 * K)^{0.5} \\ \beta &= d_1 / d_2 \\ d_2 &= \text{upstream pipe diameter, in.} \end{aligned} \quad (7)$$

For ORI-253:

$$\begin{aligned} K &= 1.27 \\ d_1 &= 0.899 \text{ in.} \\ Q &= 5.54 \text{ gpm} \\ d_2 &= 1.12 \text{ in.} \end{aligned}$$

Using Equations 4 and 5:

$$h_L (\text{ORI-253}) = 0.18 \text{ ft.} = 2.16 \text{ in. H}_2\text{O}$$

For ORI-254:

$$\begin{aligned} K &= 2.023 \\ d_1 &= 1 \text{ in.} \\ Q &= 5.54 \text{ gpm} \\ d_2 &= 1.12 \text{ in.} \end{aligned}$$

Using Equations 7 and 8:

$$h_L(\text{ORI-254}) = 0.5 \text{ ft.} = 6.0 \text{ in. H}_2\text{O}$$

The measured pressure drops from the bottom of the IRWST to the DVI-1 and DVI-2 flanges were measured by DP-701 and DP-702. These values may be calculated from data listed in Table 4.2-16

For IRWST-1: DP-701 = 20.7 in. H₂O (includes ORI-253)

For IRWST-2: DP-702 = 19.1 in. H₂O (includes ORI-254)

Therefore, the pressure drop through the lines without orifice plates ORI-253 and ORI-254 are:

IRWST-1 to DVI-1 flange pressure drop = 18.5 in. H₂O

IRWST-2 to DVI-2 flange pressure drop = 13.1 in. H₂O

The pressure drop through the DVI venturi nozzles can then be estimated as follows:

For DVI-1 venturi nozzle:

$$K = 5.17$$

$$d_1 = 0.642 \text{ in.}$$

$$Q = 5.54 \text{ gpm}$$

$$d_2 = 1.12 \text{ in.}$$

Using Equations 4 and 5:

$$h_L(\text{DVI venturi nozzle}) = 0.39 \text{ ft.} = 4.68 \text{ in. H}_2\text{O}$$

Finally, the pressure drop from the bottom of the IRWST to the DVI flanges can be calculated as follows. The DVI-1 and DVI-2 venturi nozzles were identical.

IRWST-1 bottom to DVI-1 flange pressure drop = 23.2 in. H₂O (includes DVI-1 venturi nozzle)

IRWST-2 bottom to DVI-1 flange pressure drop = 17.7 in. H₂O (includes DVI-1 venturi nozzle)

These pressure drops also represent the pressure drops through the entire IRWST-1 and IRWST-2 injection lines, from the bottom of the IRWST to the reactor vessel downcomer.

The acceptance criteria for the IRWST injection lines is between 13.4 in. and 26.8 in. H₂O. Therefore, the as-built IRWST-1 and IRWST-2 injection lines were acceptable.

4.2.7 Primary Sump Tank Injection Flow Test

Hydraulic measurements were made for the primary sump-1 and primary sump-2 in this section. These lines originate at the bottom of the primary sump tank and run to the DVI tees and the reactor vessel downcomer via the DVI-1 and DVI-2 nozzles. These measurements were performed in the first series of flow test only with only orifice plates ORI-253 and ORI-254 installed. The flow test with DVI venturi nozzles was not performed. Since all matrix tests were performed with the DVI venturi nozzles and without orifice plates ORI-253 and ORI-254 installed, the line resistance obtained from the flow test was adjusted to account for the addition of the DVI venturi nozzles and the removal of the orifice plates. The same calculation methodology used in the IRWST injection flow test section was used here to estimate pressure drops with the venturi nozzles installed.

4.2.7.1 Procedures

Figure 4.2-28 provides a schematic of the test arrangement for each primary sump tank injection line.

Initially, both primary sump tank and the IRWST were drained. A blank flange was installed in the IRWST-1 injection line between the IRWST and the tee to the primary sump tank injection line. Another blank flange was installed in a similar manner for the IRWST-2 injection line. These two blank flanges prevented the IRWST from injecting. Isolation valves downstream of the primary sump tank injection lines (RCS-711 and RCS-712) were initially closed to allow filling and venting of the primary sump tank. Primary sump tank isolation valves were also closed (CSS-909 and CSS-910). The reactor vessel and the primary loops were drained to a level slightly above the DVI line penetrations to the reactor vessel. Since the DVI lines were filled prior to the start of the test, continuous primary sump tank injection flow at the beginning of the draining process was assured.

The primary sump tank was then filled to the simulated curb level where it would overflow to the secondary sump tank. RCS-711 and RCS-712 were opened to gravity-drain the water from the bottom of the primary sump tank to the reactor vessel through DVI-1 and DVI-2 nozzles, respectively. This draining process simulated the AP600 primary sump tank draining process. The draining flow rate and the desired pressure drops were measured and recorded. This test was performed with the primary sump tank injection isolation valves (CSS-909 and CSS-910) closed.

4.2.7.2 Instrumentation

Figure 4.2-28 provides a schematic of the test arrangement and locations of the instrumentation.

A few modifications to the existing instrumentation were made. For the line from the DVI-1 flange (nozzle) to the downcomer of the reactor vessel, the high side of DP-128 was connected to a thermocouple penetration at the bottom of the primary sump tank, allowing DP-128 to measure total pressure drop from the bottom of the primary sump tank to the reactor vessel downcomer, including the exit loss. This modification provided the total pressure drop from bottom of the primary tank to

the downcomer of the reactor vessel. For the line from the DVI-2 flange (nozzle) to the downcomer of the reactor vessel, the high side of DP-129 was connected to a thermocouple penetration at the bottom of the primary sump tank, allowing DP-129 to measure the total pressure drop from the bottom of the primary sump tank to the reactor vessel, including the exit loss. FMM-901 and FMM-902 measured the flow rate through DVI-1 and DVI-2, respectively. The primary sump tank level was also measured by LDP-901.

4.2.7.3 Results

Raw test data are summarized in Table 4.2-10. Data were in Figures 4.2-29 and 4.2-30 plotted as the pressure drop versus the square of the flow rate and fitted by linear regression methodology. The plots show very good linearity, indicating that Darcy's equation can be used to predict pressure drops through the line.

Line Resistance

The total line resistance for each primary sump tank injection can not be calculated directly from the test results because of the varying inside diameters from section to section. Since the pressure drop is more important from the scaling point of view, line resistance was not calculated; however, the inside diameters of various sections can be found in Appendix H, Dwg. LKL 920200 and Dwg. LKL920201. The line resistance can be calculated using Darcy's equation.

Pressure Drop Comparison (without DVI Venturi Nozzles but with ORI-253 and ORI-254)

Table 4 2-16 compares the measured pressure drop with the design (predicted) pressure drop and the specified acceptable pressure drop range (acceptance criteria). The following observations were made for both the IRWST-1 and IRWST-2 injection lines:

1. The measured pressure drops exceeded the acceptance criteria for the primary sump injection lines. Primary sump-1 measured 3.58 in. H₂O and primary sump-2 measured 5.37 in. H₂O. These pressure drops were compared with the acceptable range between 1.44 and 2.88 in. H₂O at an injection flow rate of 1.16 ± 0.3 gpm. However, numerous data points were obtained as the sump gravity-drained to the reactor vessel. These data provide a good characterization of the line, and no adjustments to the lines were necessary as long as the computer code models the same line resistance.
2. The two injection lines were not quite balanced. IRWST-1 dropped 3.58 in. H₂O; IRWST-2 dropped 5.37 in. H₂O — 50 percent more pressure than IRWST-1.

Pressure Drop Comparison (with DVI Venturi Nozzles but without Orifice Plates ORI-253 and ORI-254)

Direct measurement of pressure drops in the primary sump tank injection lines were not made. However, these pressure drops can be estimated using the same methodology as in the IRWST injection flow test section. The following results were obtained using the primary sump tank injection flow rate of 1.16 gpm.

- Pressure drop through ORI-253 at 1.16 gpm = 0.095 in. H₂O
- Pressure drop through ORI-254 at 1.16 gpm = 0.265 in. H₂O
- Measured IRWST-1 pressure drop at 1.16 gpm = 3.58 in. H₂O (including ORI-253)
- Measured IRWST-2 pressure drop at 1.16 gpm = 5.37 in. H₂O (including ORI-254)
- Calculated IRWST-1 pressure drop at 1.16 gpm = 3.485 in. H₂O (without ORI-253)
- Calculated IRWST-2 pressure drop at 1.16 gpm = 5.105 in. H₂O (without ORI-254)
- Calculated pressure drop through DVI venturi nozzle at 1.16 gpm = 0.205 in. H₂O
- Calculated pressure drop through IRWST-1 with DVI venturi nozzle at 1.16 gpm = 3.69 in. H₂O
- Calculated pressure drop through IRWST-2 with DVI venturi nozzle at 1.16 gpm = 5.31 in. H₂O

Pressure drops through the injection lines with venturi nozzles were estimated to be 3.69 in. H₂O for primary sump-1 and 5.31 in. H₂O for primary sump-2. Both exceeded the maximum allowable pressure drop of 2.88 in. H₂O at the flow rate of 1.16 gpm.

4.2.8 Cold-Leg Balance Line Injection Flow Test

Hydraulic measurements of the cold-leg balance lines from the top of CMT-1 to CL-3 and from the top of CMT-2 to CL-1 were made in this section. These two lines are independent of the DVI lines. Therefore, the test data are applicable with or without DVI orifice plates ORI-253 or ORI-254 or the DVI venturi nozzles installed. These tests were only performed for the first series of flow tests.

4.2.8.1 Procedures

Figures 4.2-31 and 4.2-32 provide schematics of the test arrangement for each cold-leg balance line.

In the cold-leg balance line injection flow test, a flow path was set up using the RNS pump to pump water from the bottom of the primary sump tank to the DVI line, down to the DVI tee, and into the reactor vessel downcomer via the DVI nozzle. Flow was then directed to the cold leg and to the cold-leg balance line. Flow exited the cold-leg balance line and flowed to the top of the CMT. Since the CMT discharge was isolated, flow exited the top of the CMT via a temporary line leading to the top of the primary sump tank. The manway cover at the top of the primary sump tank was removed to receive the flow.

The test was initiated by opening the temporary valve to the sump (TV-1 for CMT-1 and TV-2 for CMT-2), opening the cold-leg balance line isolation valve, and starting the pump. The desired flow rate was obtained by throttling the RNS pump discharge to the DVI isolation valve (RCS-801 for CMT-1 and RCS-802 for CMT-2). The injection flow rate and desired pressure drops were measured and recorded.

This test was run with orifice plates ORI-253 and ORI-254 installed. No DVI venturi flow nozzles were used. Test data are applicable to either case.

4.2.8.2 Instrumentation

Figures 4.2-31 and 4.2-32 provide schematics of the test arrangement and locations of the instrumentation.

Two differential pressure indications were taken. For CMT-1, LDP-509 was calibrated as a differential pressure cell to provide the pressure drop from the balance line near CL-3 to the top of CMT-1. The sense lines of LDP-509 were temporarily reversed for this test. The high side of LDP-509 was tubed to the balance line near CL-3; the low side of LCP-509 was connected to the inside of CMT-1. FMM-503 measured the flow rate through the CL-1 balance line.

For CMT-2, LDP-510 was calibrated as a differential pressure cell to provide the pressure drop from CL-1 to the top of CMT-2. The sense lines of LDP-510 were temporarily reversed for this test. The high side of LDP-510 was tubed to the balance line near CL-1; the low side of LDP-510 was connected to the inside of CMT-2. FMM-502 measured the flow rate through the CL-2 balance line.

The low sides of LDP-509 and LDP-510 were located inside the CMTs for this test, implying that the measured pressure drops included entrance losses from the top of the CMTs. These measurements also included the pressure drop through the steam distributors (steam diffusers) at the top of the CMTs.

The special sensing line arrangement for LDP-509 and LDP-510 was unique to this test and did not apply to matrix tests.

4.2.8.3 Results

Raw test data are summarized in Table 4.2-11. Data were plotted in Figures 4.2-33 and 4.2-34 as pressure drop versus square of flow rate and fitted by linear regression methodology. The plots show very good linearity, indicating that Darcy's equation can be used to predict pressure drops through the line.

Line Resistance

Line resistances ($fL/D+K$) for the CMT to cold-leg balance lines were calculated using the same methodology as in the CMT injection flow test section. Each balance line had an inside diameter 1.12 in. (flow area = 0.006842 ft²). The line resistances (including the CMT steam diffusers) are summarized in Table 4.2-16.

Pressure Drop Comparison

Table 4.2-16 compares the measured pressure drop with the design (predicted) pressure drop and the specified acceptance criteria. The measured pressure drop includes the pressure drop through the CMT steam diffusers but the designed (predicted) pressure drop does not. This discrepancy stems from the fact that the steam diffusers were added to the test facility later in the facility construction phase after the balance lines were already built. The addition of the diffusers was due to the relatively late design changes made to AP600. Acceptance criteria remain unchanged with the addition of the steam diffusers.

The following observations were made for both the CMT-1 and CMT-2 cold-leg balance lines:

1. The measured pressure drops in each line were in agreement with Darcy's equation.
2. The measured pressure drop was in agreement with the design (predicted) value in the CMT-1 balance line. They would agree even better if the pressure drop through the CMT diffuser was included in the design value. The measured total pressure drop for the entire CMT-1 balance line was 5.29 in. H₂O versus the design value of 4.46 in. H₂O at the specified flow rate of 4.58 gpm. The acceptance criteria was between 4.0 and 5.4 in. H₂O at the same flow rate. Therefore, the CMT-1 balance line met the acceptance criteria.

For CMT-2 to the CL-1 balance line, the measured pressure drop was 4.24 in. H₂O. No design value was available. However, the measured pressure drop met the acceptance criteria.

3. The resistances of these two lines were not quite balanced with each other. The CMT-1 balance line measured a pressure drop of 5.29 in. H₂O while CMT-2 balance line measured 4.235 in. H₂O — a 24.9 percent difference. The orifice plates in these lines could have been adjusted to improve the balance of the lines; however, this was not done. The lines were accepted because the results met the acceptance criteria.

4.2.9 ADS 1-3 Flow Test

This test measured the pressure drop through the ADS 1-3 lines using the RNS pump to inject water from the primary sump tank and the IRWST into DVI-1 and DVI-2, through the pressurizer, and back to the IRWST via the ADS valves. The orifice plates simulating the flow area of the ADS 1-3 valves

were not installed in this test. A spacer was installed between the pressurizer outlet and the ADS 1-3 branches (Figure 4.2-35).

A discrepancy was discovered between Dwg. OSU 600203 (Appendix G) and the physical ADS 1-3 separator liquid line configuration. Specifically, the drawing shows orifice plate ORI-659 at the bottom of the ADS 1-3 separator. In reality, this orifice plate was never installed.

4.2.9.1 Procedures

Figures 4.2-35 and 4.2-36 provide schematics of the test arrangement.

The primary sump tank and the IRWST were filled to the IRWST sump tank overflow level, and the sump recirculation bypass valves (CSS-909 and CSS-910) were closed. This arrangement ensured proper IRWST level and, consequently, proper backpressure on the sparger. The RNS pump was used as the motive force. Initially, the procedures called for the RNS pump to take suction from the bottom of the primary sump tank and discharge into two parallel lines leading to DVI-1 and DVI-2. The field test engineer discovered that the total flow of the two DVI lines was not much different from the flow of only one DVI line. Therefore, the procedure was changed to discharge RNS flow into DVI-1 only. (RCS-801 was throttled to obtain various flow rates; RCS-802 remained closed.) Flow was directed from DVI-1 to the reactor vessel and the pressurizer, then back to the IRWST via the ADS valves. Only one ADS valve was opened at a time. Since the IRWST was initially filled to the overflow level, any additional flow into the IRWST would flow back to the primary sump tank and creating a closed-loop operation.

ADS orifices ORI-655, ORI-656 and ORI-657) were not installed in the lines for this test in an attempt to characterize the ADS 1-3 lines. The RNS pump was started and one of the ADS valves was opened. Throttling RCS-801 provided the desired flow rate. Test data were recorded once the desired flow rate was obtained.

4.2.9.2 Instrumentation

Figures 4.2-35 and 4.2-36 provide a schematic of the test arrangement and locations of the instrumentation.

The following instrumentation was used in the test:

- PT-604 Pressure upstream of ADS branch lines (Figure 4.2-35)
- PT-603 Pressure at the top of the pressurizer
- PT-605 Pressure at the top of the ADS 1-3 separator (steam side but before the steam separating element)

- FMM-205 Magnetic flow meter at DVI-1
- FMM-206 Magnetic flow meter at DVI-2
- FMM-601 Magnetic flow meter at ADS 1-3 separator liquid line
- FDP-605 Pressure drop across the flanges at the normal ORI-655 location (representing ADS-1) (Note: ORI-655 was not installed in this test)
- FDP-604 Pressure drop across the flanges at the normal ORI-656 location (representing ADS-2)
- FDP-606 Pressure drop across the flanges at the normal ORI-657 location (representing ADS-3)
- LDP-701 IRWST water level measurement

In addition to this instrumentation, a measurement tape was installed at the top of the reference leg for LDP-701 (IRWST level) with "zero" resting at the top of the reference leg. A temporary tygon hose was routed from root valve RCS-624 and upward. RCS-624 was the isolation valve of the bottom static pressure tap of LDP-601 (ADS 1-3 separator level). This temporary level indication gave the separator level with its zero datum point at the top of the IRWST level reference leg. LDP-701 and the tygon hose level indications were recorded as water was pumped through the test flow path. The relative distances between the tygon hose, RCS-624, LDP-701, and the ADS 1-3 separator inlet and outlet are shown in Figure 4.2-36.

4.2.9.3 Results

Raw test data are summarized in Table 4.2-12. The nature of the piping and separator arrangement makes the test data rather difficult to understand. During the course of testing, the field engineer opened RCS-620, located at the top of the separator, and came to the conclusion that, because there was no water issuing from the vent line, the lines leading to the separator were not full. The Quick Look Report (LTCT-T2R-002) reported this conclusion also. However, as the test data were analyzed more carefully, there was evidence that the ADS separator inlet lines were completely filled with water and that pressure in the separator forced the water through the liquid drain line. This evidence is discussed below.

Comparison of Analytic Results with Measured Results

An analytic model (Appendix A) was set up to calculate the pressure drop from the pressurizer to the inlet of the separator using the measured flow rates for both the ADS-1 and ADS-2 lines. The ADS-3 line was identical to the ADS-2 line. Table 4.2-13 summarizes the results of the calculation.

The test recorded pressure at the pressurizer (PT-603) and in the separator (PT-605). Since the test was conducted with only one ADS line open at a time, the difference between PT-603 and PT-605 represented the pressure drop through the line from the pressurizer to the separator inlet. The measured pressure drops were compared with the predicted pressure drops in Table 4.2-13. The measured pressure drops agree with the predicted pressure drops, indicating that the lines were full.

Figures 4.2-37, 4.2-38, and 4.2-39 show the pressure drop versus the flow rate square for all three ADS lines using raw test data. A pressure offset exists when there is no flow. This pressure offset is consistent from ADS-1 to ADS-3, and was most likely due to the initial zero shift of the pressure cells. The plots also show that ADS-1 test results agree with the Darcy's equation but ADS-2 and ADS-3 do not. Therefore, only ADS-1 results were analyzed in more detail.

The pressure offset for the ADS-1 test was corrected, and the results are summarized in Table 4.2-15 and plotted in Figure 4.2-40. The adjusted pressure drops for the ADS-1 test agree with the predicted values. The analytic pressure drop is plotted as a function of the flow rate square in Figure 4.2-41. The derived equations in these two plots are virtually the same. Therefore, the adjusted ADS-1 test results are valid.

The ADS-2 and ADS-3 test results were not acceptable because of scattered data. Therefore, the pressure drop through the ADS-2 and ADS-3 parallel lines may be calculated. The following steps were used:

1. Pressure drop through ADS-1 line was estimated.

Note: The ADS-1 overall line consists of three sections. The first section begins at the pressurizer and ends at the tee junction of the ADS 1-3 parallel lines. The second line section is the ADS-1 itself (parallel to ADS-2 and ADS-3). The third line section begins downstream of the ADS 1-3 parallel lines and ends at the separator inlet. The first and third lines are common to all three ADS parallel lines.

2. The calculated pressure drop for the ADS-1 parallel line was subtracted from the measured overall line pressure drop. The ADS-1 parallel line is relatively short and simple, and the analytic result should be valid.
3. Pressure drops for the ADS-2 or ADS-3 lines were calculated and added to the result of step 1 to arrive at the pressure drop through the ADS-2 or ADS-3 lines.

Pressure Drop through Loop Seal Line

The pressure drop from the bottom of the ADS 1-3 separator to the IRWST free surface consists of two sections: from the separator to the tygon hose connection (RCS-624) and from the tygon hose

connection to the free surface of the IRWST. The reason for this breakdown is that the level measurements by the tygon hose and LDP-701 are very accurate and should be utilized fully.

$$DP_{\text{loss}} \text{ (from point 0 to point 2)} = \text{RHO} \cdot (h_1 - h_3) \quad (8)$$

$$P_0 = \text{RHO} \cdot (h_1 - h_0) - \text{RHO} \cdot V_0^2 / (2 \cdot g) \quad (9)$$

$$P_4 = \text{RHO} \cdot (h_1 - h_4) + DP_{\text{loss}} \text{ (point 4 to point 0)} \quad (10)$$

Point 0 = Tygon hose connection level

Point 1 = Tygon hose measured water level

Point 2 = downstream of sparger where velocity is negligible

Point 3 = IRWST water level measured by LDP-701

Point 4 = Water level in ADS 1-3 separator

Figure 4.2-36 provides the physical locations of assigned node points. Raw test data are summarized in Table 4.2-14. The line loss derived from the raw data is also included in the table.

Equation 8 was used to estimate the pressure loss from the tygon hose connection to the sparger using the tygon hose and LDP-701 measurements. Figures 4.2-42, 4.2-43, and 4.2-44 are correlations of the pressure drop as a function of the flow rate for ADS-1, ADS-2, and ADS-3, respectively. The plots show that the data for ADS-1 and ADS-3 agree with Darcy's equation. The ADS-2 data are scattered at low flow. However, all three plots show similar slopes and pressure drop offsets at no-flow conditions. This was to be expected because the liquid line is common to ADS-1, ADS-2, and ADS-3. Figures 4.2-42 (ADS-1) or 4.2-44 (ADS-3) should be used to characterize the line.

Equation 10 can be used to estimate the pressure loss from the ADS 1-3 separator to the tygon hose connection. However, there are two unknowns in the equation: water level inside the separator and pressure loss through the line. Since the test did not measure the water level in the separator, there is not enough information to characterize this short line section. However, since this line is a straight line with an entrance loss, the line loss should be negligible. These losses can be accurately calculated using Darcy's equation. Since there are insufficient test data, no conclusion can be drawn for this line.

4.2.10 Normal Residual Heat Removal Flow Balance

This test was performed to assure balance flow at the two parallel lines at the discharge of the RNS pump. It was essential to have relatively equal flow delivered to both DVI-1 and DVI-2.

4.2.10.1 Procedures

Figure 4.2-45 provides a schematic of the test arrangement.

RNS flow balance was performed using the RNS pump to inject water from the IRWST and primary sump to the DVI-1 and DVI-2, through the pressurizer and ADS-1 valve, then back to the IRWST. The ADS-1 isolation valve (RCS-601) was used to throttle the flow rate to a pre-determined value of about 30 gpm. Total flow and flow to DVI-2 were measured. Flow to DVI-1 was calculated. DVI-1 and DVI-2 flow rates were compared. If they were not reasonably equal, orifice plate ORI-853 in the line leading to DVI-1 was adjusted, and the process was repeated until balanced flows were achieved.

4.2.10.2 Instrumentation

Figure 4.2-45 provides a schematic of the test arrangement and locations of the instrumentation.

FMM-805 measured total flow injected. FMM-803 measured RNS flow to DVI-2 only.

4.2.10.3 Results

Because of changes in orifice locations in these lines, the original test data are no longer valid. About 5 minutes of RNS injection data (Table 4.2-15) was taken from Matrix Test SB04 and was used to evaluate RNS flow balance. Average RNS injection flow in DVI-2 (FMM-803) was 9.96 gpm. Average total injection flow (FMM-805) was 20.12 gpm. Flow in DVI-1 was calculated by subtracting the average of FMM-803 from the average of FMM-805. The calculated flow imbalance between DVI-1 and DVI-2 was less than 2 percent, within the ± 10 percent required.

TABLE 4.2-1
SUMMARY OF REACTOR VESSEL AND PRIMARY LOOP INSTRUMENTATION
USED IN FLOW TESTS

ID	Description	Flow Test Series	
		(First)	(Third)
LDP-102	Top of downcomer at 180 degrees to HL-2	Yes ⁽¹⁾	No
DP-111	Bottom of upper grid in core to top of upper core plate	Yes	Yes
DP-114	Bottom of upper support plate to top of upper support plate	Yes	Yes
DP-121	CL-1 nozzle to downcomer at 22.5 degrees	Yes	Yes
DP-122	CL-2 nozzle to downcomer at 292.5 degrees	Yes	Yes
DP-123	CL-3 nozzle to downcomer at 112.5 degrees	Yes	Yes
DP-124	CL-4 nozzle to downcomer at 202.5 degrees	Yes	Yes
DP-125	About 4.91 in. above upper core plate to bottom of HL-1 flange	Yes	Yes
DP-126	About 4.91 in. above upper core plate to bottom of HL-2 flange	Yes	Yes
DP-128	Bottom of DVI-1 flange next to reactor vessel to downcomer at top of core elevation and 270 degrees	No	Yes
DP-129	Bottom of DVI-2 flange next to reactor vessel to downcomer at top of core elevation and 270 degrees	No	Yes
DP-130	Top of upper head to top of downcomer (bypass hole DP)	Yes	Yes
DP-201	Bottom of RCP-1 discharge flange to bottom of CL-1 nozzle	Yes	Yes
DP-202	Bottom of RCP-2 suction flange to bottom of RCP-2 discharge flange	Yes	Yes
DP-203	Bottom of RCP-1 suction flange to bottom of RCP-1 discharge flange	Yes	Yes
DP-204	Bottom of RCP-2 discharge flange to bottom of CL-2 nozzle	Yes	Yes
DP-205	Bottom of RCP-3 suction flange to bottom of RCP-3 discharge flange	Yes	Yes
DP-206	Bottom of RCP-4 suction flange to bottom of RCP-4 discharge flange	Yes	Yes
DP-207	Bottom of RCP-3 discharge flange to bottom of CL-3 nozzle	Yes	Yes
DP-208	Bottom of RCP-4 discharge flange to bottom of CL-4 nozzle	Yes	Yes
DP-209	Bottom of HL-1 flange to inlet of SG-1	Yes	Yes
DP-210	Bottom of HL-2 flange to inlet of SG-2	Yes	Yes
DP-211	SG-1 U-tube entrance loss (about 6.4 in. below tube sheet to short-tube entrance)	Yes ⁽¹⁾	No

TABLE 4.2-1 (Continued)
SUMMARY OF REACTOR VESSEL AND PRIMARY LOOP INSTRUMENTATION
USED IN FLOW TESTS

ID	Description	Flow Test Series	
		(First)	(Third)
DP-211	SG-1 U-tube inlet to U-tube outlet pressure drop (both taps at 6.4 in. below tube sheet)	No	Yes
DP-212	SG-2 U-tube entrance loss (about 6.4 in. below tube sheet to short-tube entrance)	Yes ⁽¹⁾	No
DP-212	SG-2 U-tube inlet to U-tube outlet pressure drop (both taps at 6.4 in. below tube sheet)	No	Yes
DP-213	SG-1 U-tube entrance to exit (special hookup - both taps at 6.4 in. below tube sheet)	Yes ⁽¹⁾	No
DP-213	SG-1 long tube exit loss - from tube sheet to 6.4 in. below tube sheet	No	Yes
DP-214	SG-2 U-tube entrance to exit (special hookup - both taps at 6.4 in. below tube sheet)	Yes ⁽¹⁾	No
DP-214	SG-2 long tube exit loss - from tube sheet to 6.4 in. below tube sheet	No	Yes ⁽¹⁾
DP-220	Special hookup from CL-4 nozzle to HL-2 nozzle - overall reactor vessel pressure drop		
DP-221	Special hookup from bottom of CL-1 nozzle to bottom of downcomer at 0 degrees	No	Yes ⁽¹⁾
DP-801	Special hookup from bottom of HL-2 to PRHR HX inlet	No	Yes ⁽¹⁾
DP-802	Special hookup from PRHR HX inlet to outlet	No	Yes ⁽¹⁾
DP-803	Special hookup from PRHR HX outlet to SG-2 hot-leg channel head	No	Yes ⁽¹⁾
LDP-105 ⁽²⁾	Downcomer pressure drop from DVI level to top of core level	No	Yes
LDP-107 ⁽²⁾	Bottom of lower plenum at 247.5 degrees to downcomer at 270 degrees and lower core plate level	No	Yes
LDP-108 ⁽²⁾	Bottom of lower plenum at 0 degree to inside core and just above lower core plate at 0 degree	No	Yes
LDP-109 ⁽²⁾	Differential pressure inside core from top of lower core plate to bottom of middle grid plate	No	Yes
LDP-110 ⁽²⁾	Differential pressure inside core from bottom of middle grid plate to bottom of top grid plate	No	Yes
LDP-112 ⁽²⁾	Differential pressure inside upper plenum from top of upper core plate to about 10 in below center line of hot legs	No	Yes

TABLE 4.2-1 (Continued)
SUMMARY OF REACTOR VESSEL AND PRIMARY LOOP INSTRUMENTATION
USED IN FLOW TESTS

ID	Description	Flow Test Series	
		(First)	(Third)
LDP-116 ⁽²⁾	Downcomer overall differential pressure from bottom of lower plenum at 247.5 degrees to top of downcomer at 270 degrees	No	Yes
LDP-118 ⁽²⁾	Downcomer differential pressure from lower core plate level at 270 degrees to top of core level at 270 degrees	No	Yes
LDP-209 ⁽²⁾	SG-1 inlet DP from inlet to 6.4 in. below tube sheet	No	Yes
LDP-210 ⁽²⁾	RCP-2 suction flange to SG-2 cold-leg side tube sheet (tap at 6.4 in. below tube sheet)	No	Yes
LDP-211 ⁽²⁾	RCP-3 suction flange to SG-1 cold-leg side tube sheet (tap at 6.4 in. below tube sheet)	No	Yes
LDP-212 ⁽²⁾	RCP-4 suction flange to SG-2 cold-leg side tube sheet (tap at 6.4 in. below tube sheet)	No	Yes
LDP-213 ⁽²⁾	RCP-1 suction flange to SG-1 cold-leg side tube sheet (tap at 6.4 in. below tube sheet)	No	Yes
LDP-214 ⁽²⁾	SG-2 inlet differential pressure from inlet to 6.4 in. below tube sheet	No	Yes
TF-107	Temperature at bottom of CL-1 nozzle	No	Yes
TF-108	Temperature at bottom of CL-2 nozzle	No	Yes
TF-142	Temperature at bottom of HL-2 flange next to reactor vessel	No	Yes
TF-143	Temperature at bottom of HL-1 flange next to reactor vessel	No	Yes
TF-201	Temperature at bottom of RCP-1 suction flange	No	Yes
TF-202	Temperature at bottom of RCP-2 suction flange	No	Yes
TF-203	Temperature at bottom of RCP-3 suction flange	No	Yes
TF-204	Temperature at bottom of RCP-4 suction flange	No	Yes
PT-101	Pressure at bottom of CL-1 nozzle	No	Yes
PT-102	Pressure at bottom of CL-2 nozzle	No	Yes
PT-103	Pressure at bottom of CL-3 nozzle	No	Yes
PT-104	Pressure at bottom of CL-4 nozzle	No	Yes
PT-107	Pressure at top of reactor vessel upper head	No	Yes
PT-108	Pressure at bottom of reactor vessel	No	Yes

TABLE 4.2-1 (Continued)
SUMMARY OF REACTOR VESSEL AND PRIMARY LOOP INSTRUMENTATION
USED IN FLOW TESTS

ID	Description	Flow Test Series	
		(First)	(Third)
PT-109	Pressure at bottom of DVI-1 flange (nozzle)	No	Yes
PT-110	Pressure at bottom of DVI-2 flange (nozzle)	No	Yes
PT-111	Pressure at top of reactor vessel downcomer, just below bypass holes	No	Yes
PT-112	Pressure at bottom of reactor vessel downcomer, just above lower plenum	No	Yes
PT-113	Pressure below mid-core spacer grid	No	Yes
PT-201	Pressure at top of SG-1 long tube	No	Yes
PT-202	Pressure at HL-2 before inclined line leading to SG-2	No	Yes
PT-204	Pressure at top of SG-2 long tube	No	Yes
PT-602	Pressure at steam outlet of pressurizer (narrow range)	No	Yes
PT-604	Pressure at steam outlet of pressurizer (wide range)	No	Yes

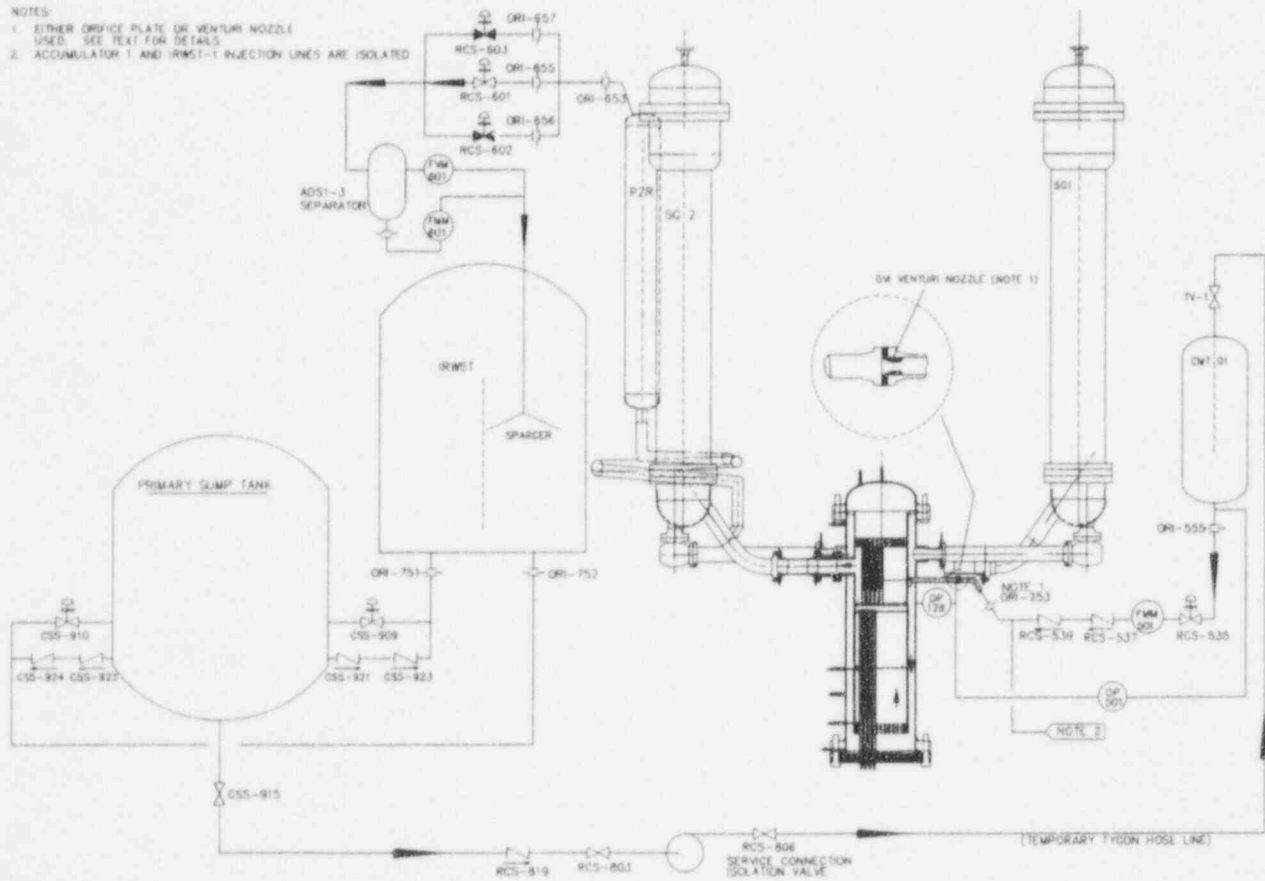
Note:

- (1) Special hookup for the test
- (2) All LDPs were calibrated and used as differential pressure transmitters

Table 4.2 on pages 4.2-38 through 4.2-63 is not included in this nonproprietary document.

NOTES

1. EITHER ORIFICE PLATE OR VENTURI NOZZLE USED. SEE TEXT FOR DETAILS.
2. ACCUMULATOR 1 AND IRWST-1 INJECTION LINES ARE ISOLATED.



C:\ADMIN\05J-01
LAYER: CMT1FLOWTEST

Figure 4.2-1 CMT-1 Injection Test Flow Path

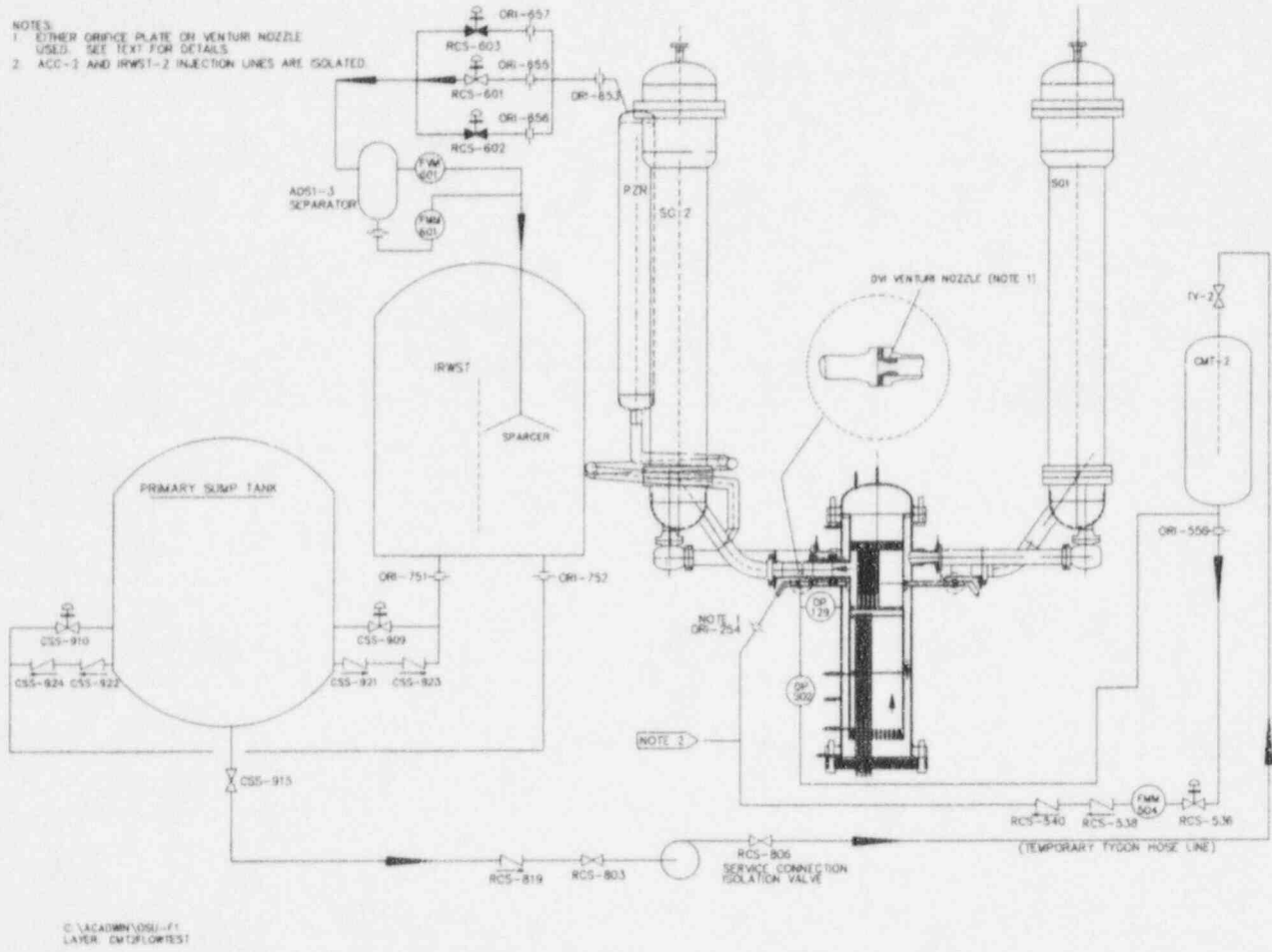


Figure 4.2-2 CMT-2 Injection Test Flow Path

Figures 4.2-3 through 4.2-10 are not included in this nonproprietary document.

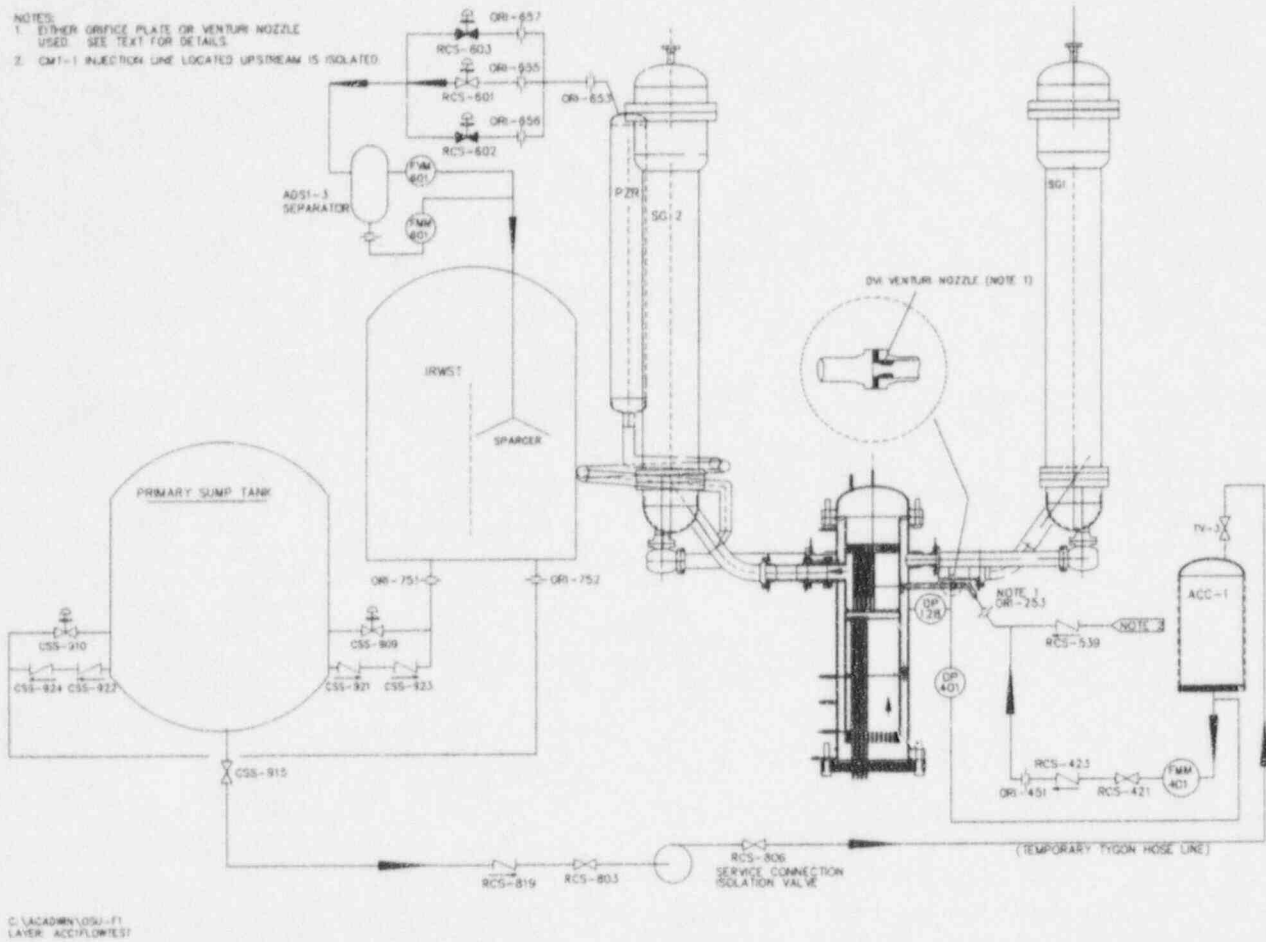
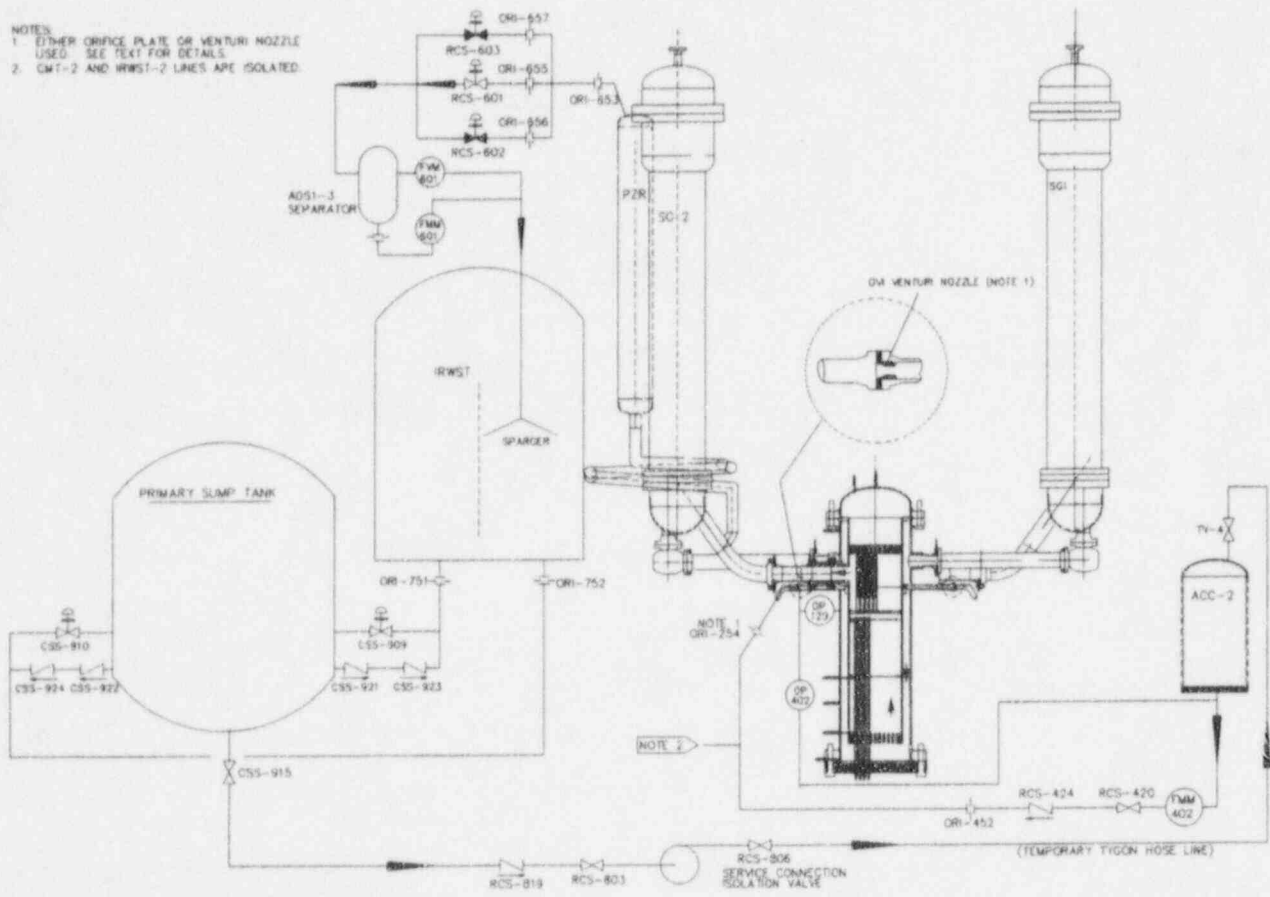


Figure 4.2-11 ACC-1 Injection Test Flow Path

NOTES

1. EITHER ORIFICE PLATE OR VENTURI NOZZLE USED. SEE TEXT FOR DETAILS.
2. CMT-2 AND RWST-2 LINES ARE ISOLATED.



C. VACADREY/ORI-FE
LAYER ACCFLOWEST

Figure 4.2-12 ACC-2 Injection Test Flow Path

Figures 4.2-13 through 4.2-20 are no included in this nonproprietary document.

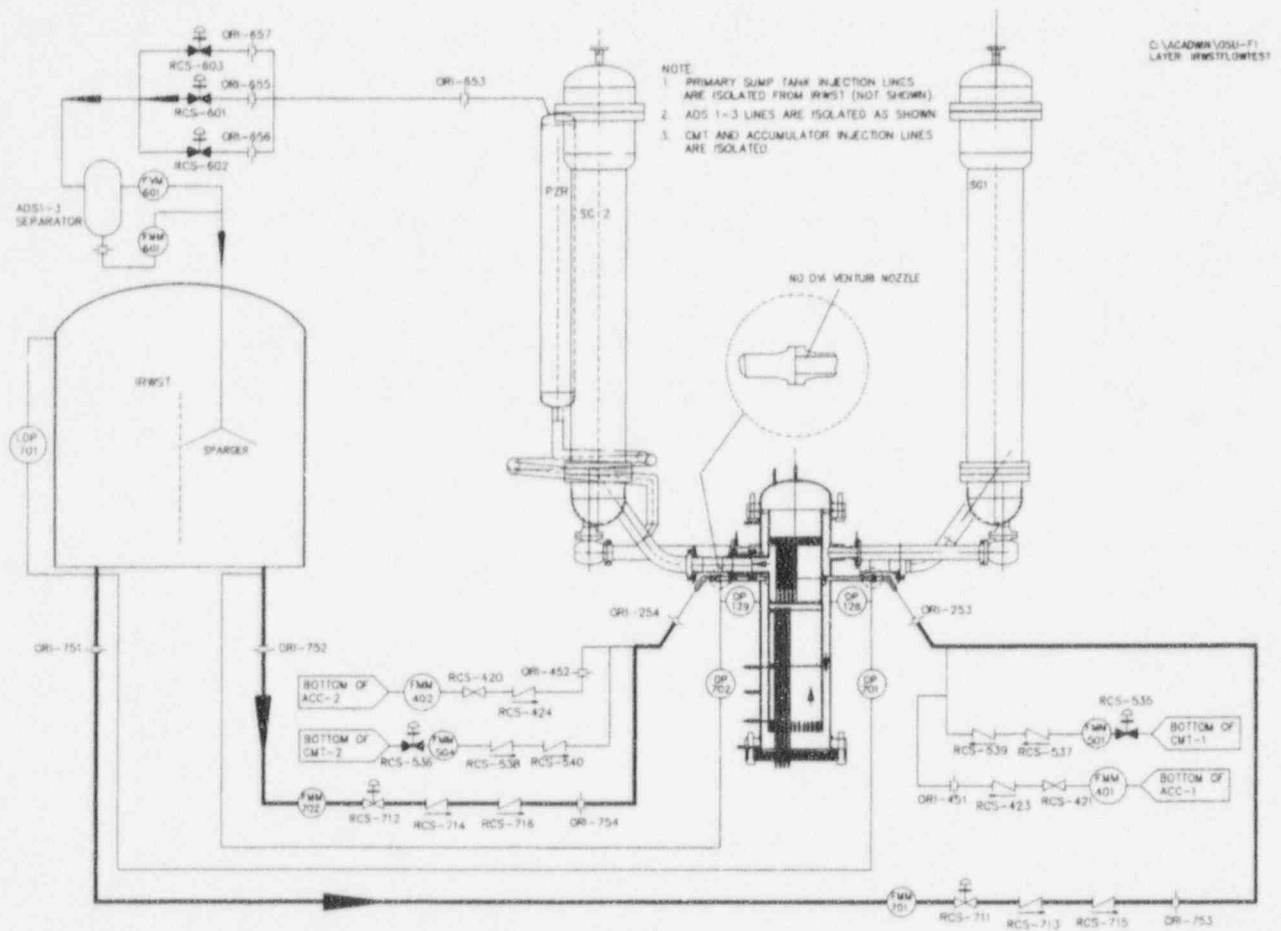


Figure 4.2-21 IRWST Injection Test Flow Path

Figures 4.2-22 through 4.2-27 are not included in this nonproprietary document.

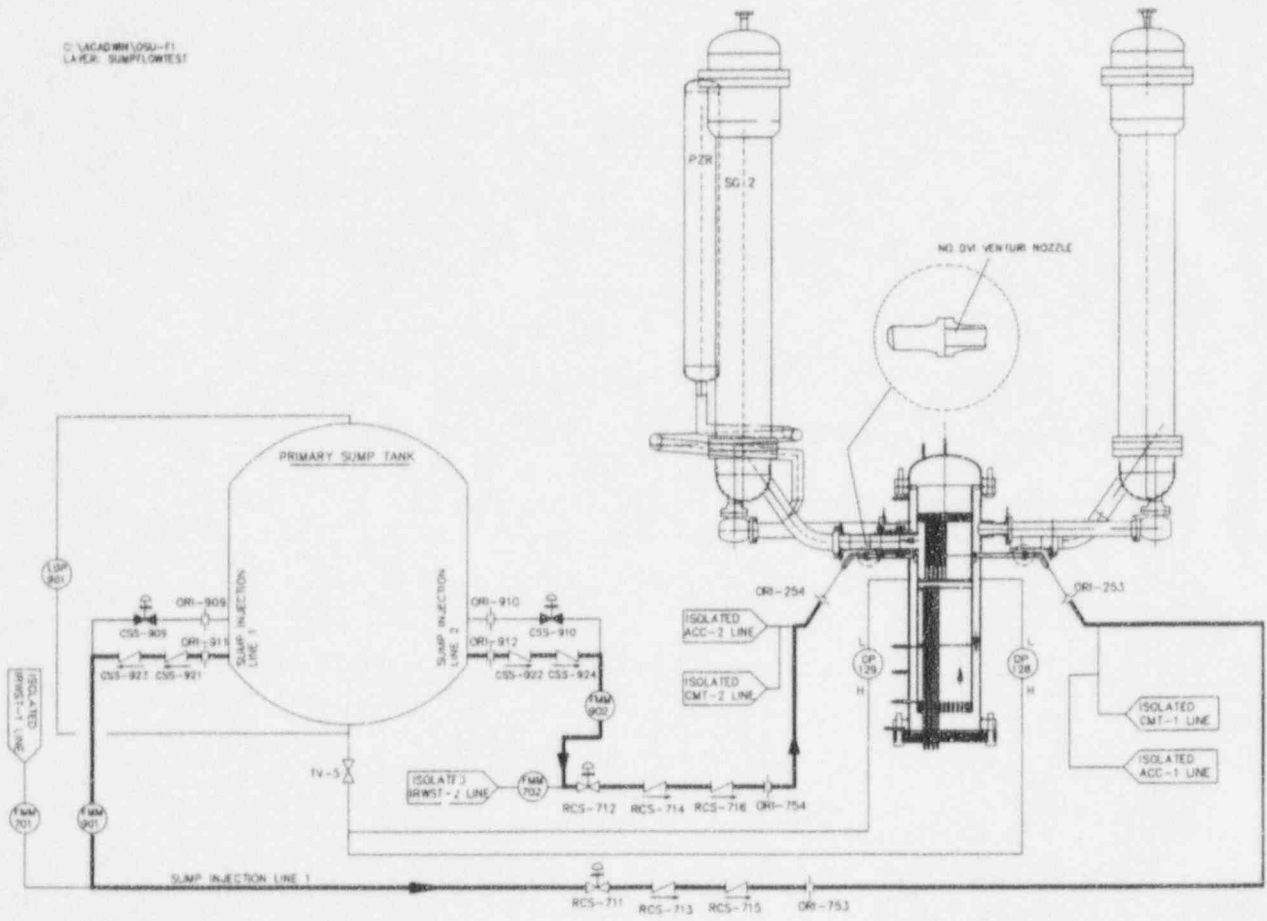


Figure 4.2-28 Primary Sump Tank Injection Test Flow Path

Figures 4.2-29 and 4.2-30 are not included in this nonproprietary document.

NOTES:

1. LDP-509 was calibrated as differential pressure cell. Its sense lines were temporarily reversed. The high side of LDP-509 was luted to RV-515 at the cold leg side entrance and the low side was connected to the inside of CMT-1 via root valve RV-507.

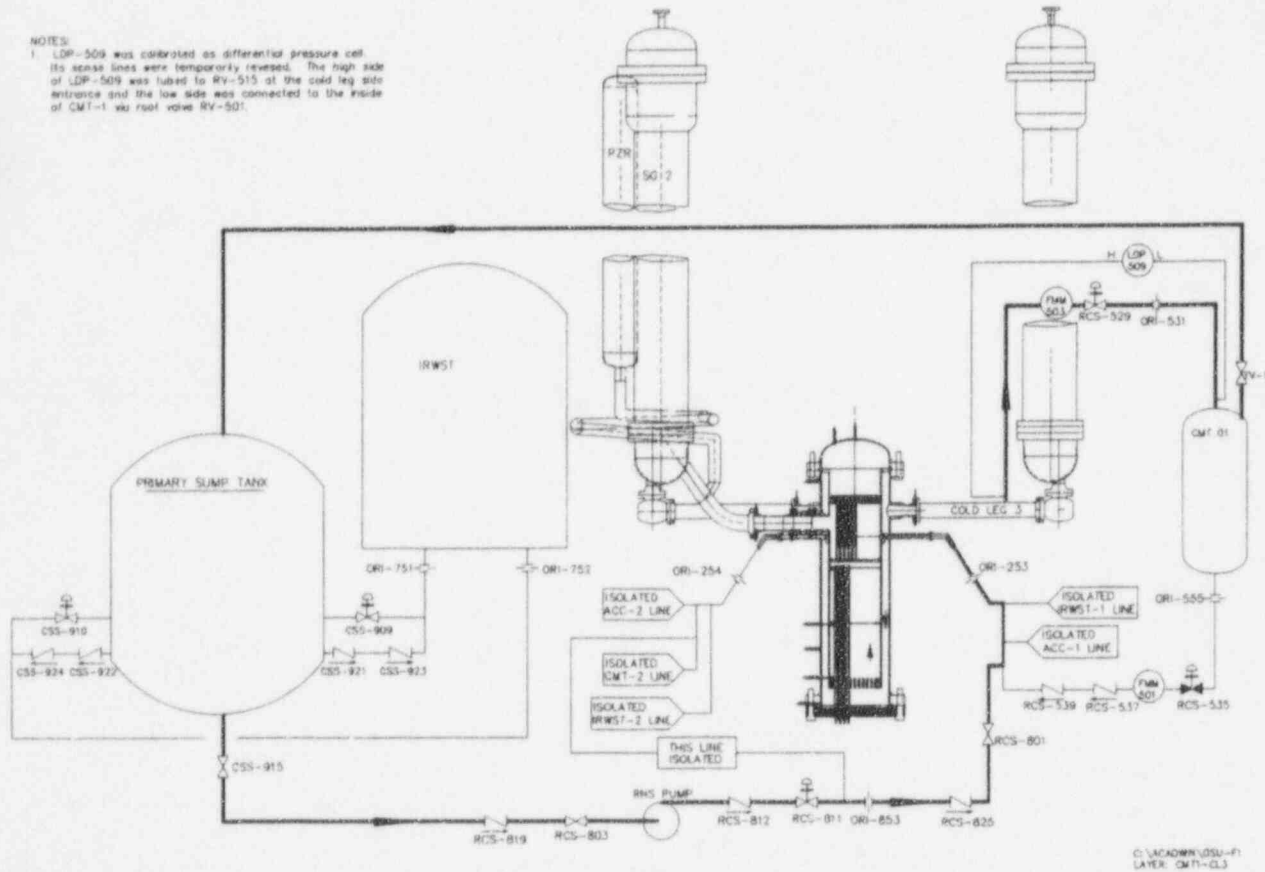


Figure 4.2-31 CMT-1 to CL-3 Balance Line Injection Test Flow Path

NOTES:

1. LDP-510 was calibrated as differential pressure cell. Its sense lines were temporarily reversed. The high side of LDP-510 was tube to RV-515 at the cold leg side entrance and the low side was connected to the inside of CMT-2 via root valve RV-502.

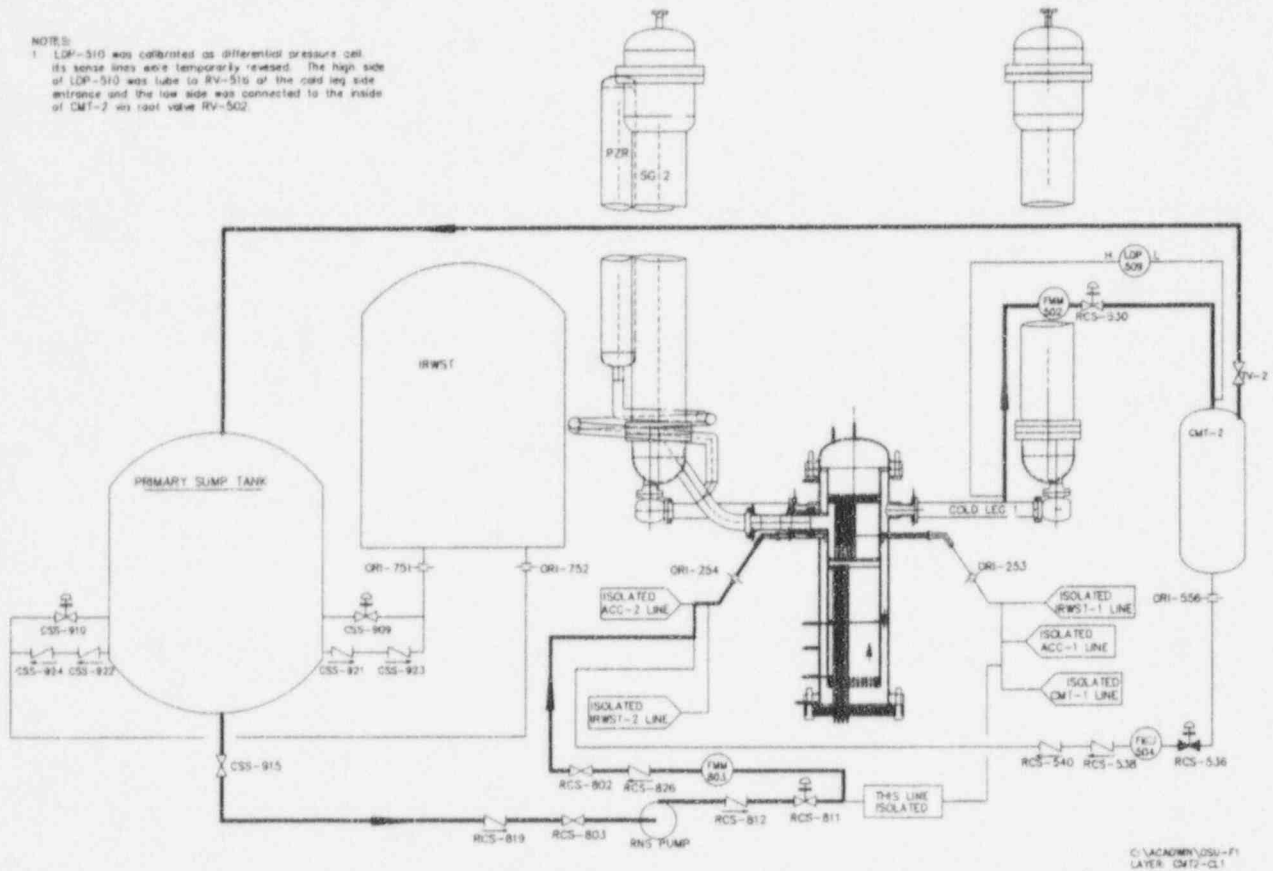


Figure 4.2-32 CMT-2 to CL-1 Balance Line Injection Test Flow Path

Figures 4.2-33 and 4.2-34 are not included in this nonproprietary document.

- NOTES
1. ORFICES WERE REMOVED FOR TEST
 2. ORF-653 WAS A SPACER PLATE
 3. ADS 1-3 SEPARATOR STEAM LINE WAS BLANKED OFF
 4. FOR DETAILS OF TYGON HOSE LEVEL LEVEL COMPARISON SEE ADS 1-3 TEST LEVEL COMPARISON (FOLLOWING)
 5. NO ORIFICE PLATE WAS INSTALLED AT THE BOTTOM OF THE ADS 1-3 SEPARATOR (SEE TEXT)

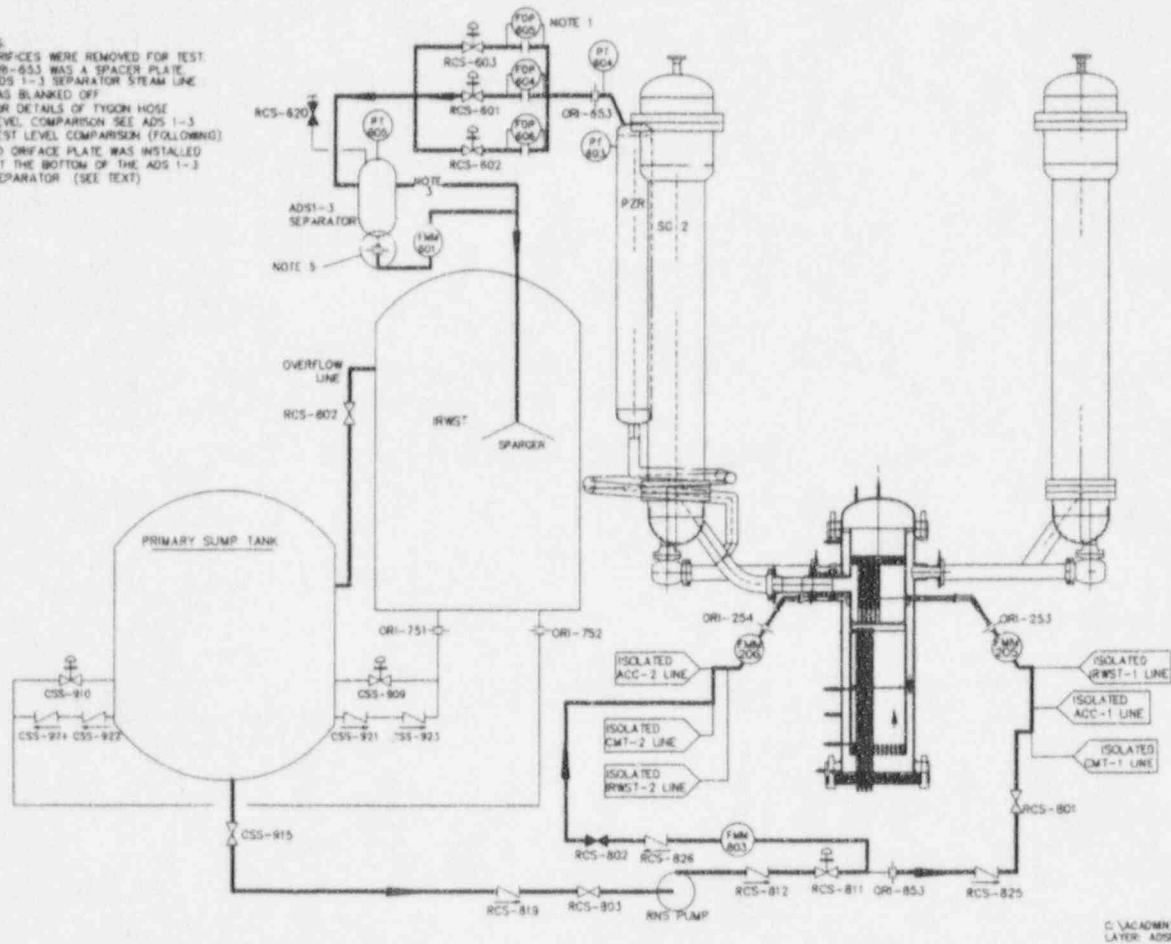


Figure 4.2-35 ADS 1-3 Injection Test Flow Path

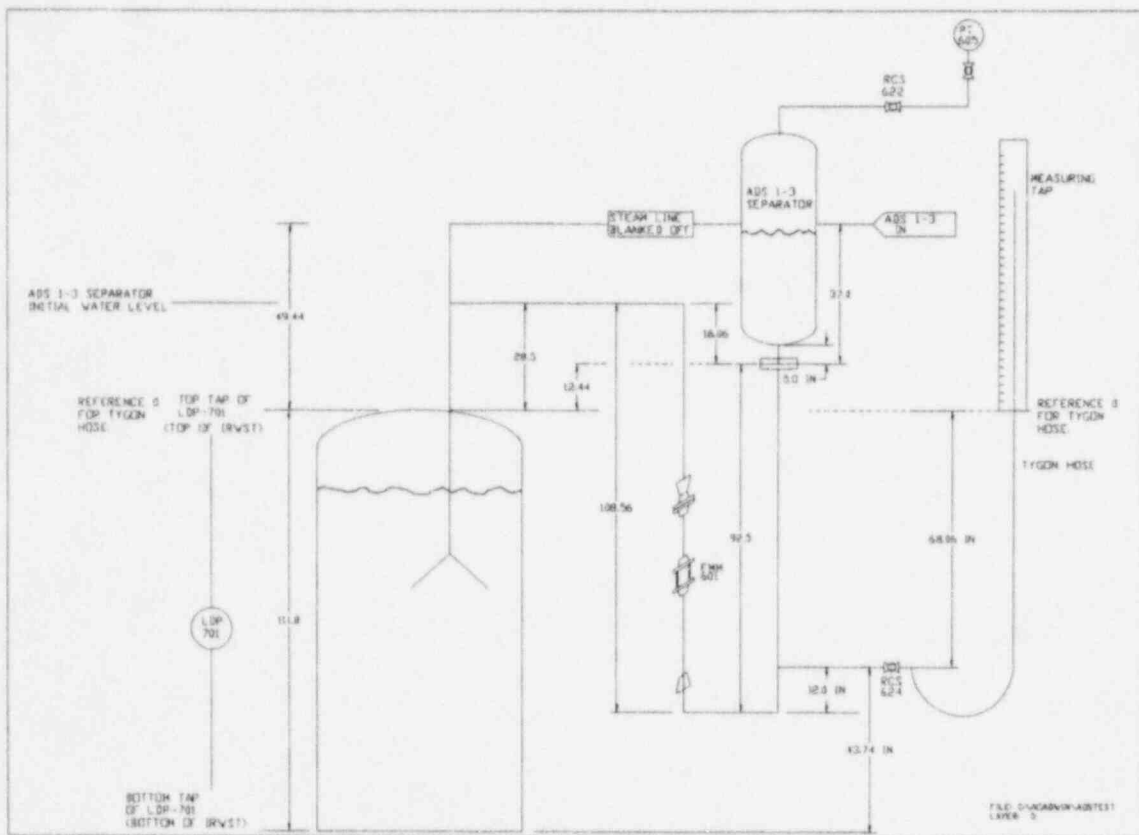


Figure 4.2-36 ADS 1-3 Test Level Comparisons

Figures 4.2-37 and 4.2-38 are not included in this nonproprietary document.

Figures 4.2-39 through 4.2-44 are not included in this nonproprietary document.

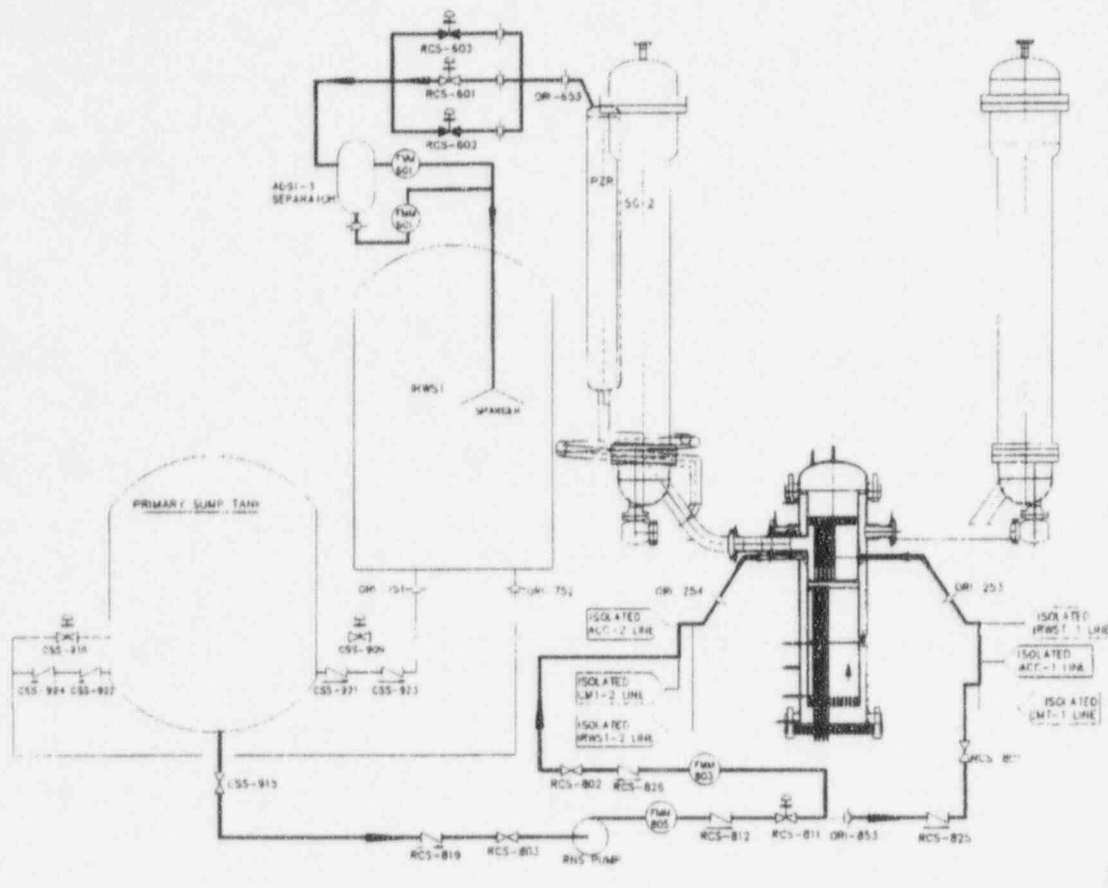


Figure 4.2-45 RNS Injection Test Flow Path

4.3 HS01 Ambient Heat Losses

The hot functional test, OSU-HS-01, was performed on May 22 through 24, 1994. The objective of the test, to obtain data under a variety of conditions to determine OSU facility characteristics, was achieved through a series of steps summarized in the following six categories:

- Ambient heat losses of the facility at 100°, 200°, 300°, and 400°F. The pressurizer heater maintained facility pressure at []^{a,b,c} and the (SGs) were isolated to prevent loss due to steam flow.
- Steady-state characteristics of the facility at power levels of 100 kW, 300 kW, 500 kW, and 600 kW (or 100 percent power). The passive residual heat removal heat exchanger (PRHR HX) was isolated. SG pressure and level controls were set at automatic.
- Performance of the PRHR HX and characteristics of facility operation during forced convection (RCPs running) at power levels of 300 kW, 500 kW, and 600 kW.
- Performance of SGs and characteristics of facility operation during natural circulation (RCPs tripped) at power levels of 300 kW, 500 kW, and 600 kW.
- Performance of CMTs and characteristics of the facility operation during natural circulation (RCPs tripped) at 500 kW. The PRHR HX was isolated. SG pressure and level controls were set at automatic.

This results in a total of 18 distinct facility configurations and conditions for which 16 data files were created from the DAS at OSU. The raw data file identification, the corresponding procedure step number, the step description, and the date and time of the recording appear in Table 4.3-1.

For the purposes of data validation, three of these test data files were closely reviewed. They were the first data file (U0000) with the facility at full pressure and 100°F; the last data file (U1636) with the facility at 600 kW power, RCPs tripped, and the PRHR HX in service; and one data file from the middle of the test (U1451) with the facility at 600 kW power, RCPs running, and the PRHR HX not in service. This review approach yielded acceptable results since the entire test was performed continuously without interruption. Therefore, if a channel did not fail at the start of the test (U0000) but failed somewhere in the middle or towards the end, it would show up as failed in the review of the last step/data file (U1636). As an extra safeguard^d, one of the steps/data files performed during the middle of test (U1451) was reviewed to determine if any channels acted as an exception. The review confirmed the accuracy of all data recorded throughout the test, except for the failed instruments noted in Table 4.3-2.

There are, however, instances where data recorded are accurate but irrelevant for the purpose of determining facility characteristics. These are instances when steady-state conditions were

unachievable or when portions of the facility were being used for component cooldown in between and during steps. The details of these circumstances are discussed in the following subsections.

4.3.1 Ambient Heat Loss Data at 100°F (Test Procedure Step 4.1.3)

The recorded data in file U0000 are unsuitable for ambient heat loss calculations at 100°F. It was virtually impossible to maintain stable conditions at the low steam and feedwater rates necessary to maintain 100°F. All possible combinations of AUTO/MANUAL between reactor, feedwater, and steam controllers were attempted with no success. The recorded data are accurate, but since the acceptance criteria (i.e., steady-state conditions at 100°F) were not met, the data should not be used for ambient heat loss calculations.

4.3.2 CMT Cooldown

On completion of step 4.4.3 (CMT Natural Convection Performance Test), test engineers initiated a cooldown of the CMTs that continued through the first []^{a,b,c} of step 4.5.1. Using the RNS pump, the test engineers injected cool water into the CMTs and discharged the warmer water to other areas of the system. This action is acceptable, since the CMTs and the equipment used to cool them down are outside the test boundary for step 4.5.1. Since data recorded by the DAS include all instrument channels, the effects of the CMT cooldown on a representative sampling of instruments outside the test boundary are presented in Table 4.3-3.

4.3.3 IRWST Cooldown

On completion of a step involving forced or natural circulation flow through the PRHR HX, test engineers initiated a cooldown of the IRWST that continued through the next step of the procedure. The test engineers injected cool water into the IRWST and discharged the warmer water via the primary sump overflow. This action is acceptable, since the IRWST and the equipment used to cool it down are outside the test boundary for that particular step. Since data recorded by the DAS include all instrument channels, the effects of the IRWST cooldown on a representative sampling of instruments outside the test boundary are presented in Table 4.3-4. This applies to step/data file 4.4.1/U1441.

4.3.4 Conclusion

The purpose of the hot functional test was to obtain data under a variety of steady-state conditions to determine OSU facility characteristics. A thorough review of three data files, one at the beginning, one at the end, and one in the middle of the test, proved the data in those files to be accurate and complete. Therefore, it is deduced that all of the data in the other 13 data files for this test are also accurate and may be used by the test analysts for determination of OSU facility characteristics.

TABLE 4.3-1
RAW DATA FILE IDENTIFICATION AND DESCRIPTION

Data File ID	Procedure Step No.	Step Description	Date	Recording Time Span
U0000	4.1.3	Ambient heat loss determination at 100°F	5/22/94	19:49 to 20:23
U1415	4.1.5	Ambient heat loss determination at 200°F	5/22/94	21:06 to 21:38
		Ambient heat loss determination at 300°F	5/22/94	23:17 to 23:52
		Ambient heat loss determination at 400°F	5/23/94	01:20 to 01:55
U1424	4.2.4	100 kW power level testing	5/23/94	04:04 to 04:39
U1431	4.3.1	300 kW power level testing	5/23/94	05:52 to 06:42
U1432	4.3.2	PRHR forced flow at 300 kW	5/23/94	07:19 to 08:06
U1441	4.4.1	500 kW power level testing	5/23/94	09:03 to 09:49
U1442	4.4.2	PRHR forced flow at 500 kW	5/23/94	10:14 to 10:47
U1443	4.4.3	CMT natural convection performance at 500 kW without PRHR HX in service	5/23/94	13:43 to 14:25
U1451	4.5.1	600 kW power level testing	5/23/94	16:46 to 17:22
U1452	4.5.2	PRHR forced flow at 600 kW	5/23/94	18:48 to 19:35
U1610	4.6.10	300 kW primary system natural convection without PRHR HX in service	5/23/94	21:25 to 21:49
U1616	4.6.16	300 kW primary system natural convection with PRHR HX in service	5/23/94	22:10 to 22:27
U1623	4.6.23	500 kW primary system natural convection without PRHR HX in service	5/23/94	22:44 to 23:18
U1626	4.6.26	500 kW primary system natural convection with PRHR HX in service	5/23/94	23:33 to 23:48
U1633	4.6.33	600 kW primary system natural convection without PRHR HX in service	5/24/94	00:05 to 00:39
U1636	4.6.36	600 kW primary system natural convection with PRHR HX in service	5/24/95	00:55 to 01:07

**TABLE 4.3-2
FAILED INSTRUMENTATION**

Instrument No.	Description
DP-212	SG-2 long tube exit loss
HFM-112	Heat losses from CL-3 flange at reactor
HFM-205	Heat losses from CL-3 flange at reactor
HFM-505	Heat loss CMT-1 top
HFM-510	Heat loss CMT-2/CL-1 balance line
HFM-603	Heat loss pressurizer surge line
HPS-509-1	CMT-1 cold-leg balance line heat transfer coefficient
HPS-509-2	CMT-1 cold-leg balance line heater dT above fluid temperature
HPS-509-3	CMT-1 cold-leg balance line fluid temperature
SC-TH-102-4	TH-102-4/group 1 heater rod signal conditioner
TF-150	Upper reactor vessel layer H-H at 186.2 degrees
TFM-112	Thermocouple, type T, for HFM-112
TFM-205	Thermocouple, type T, for HFM-205
TFM-505	Thermocouple CMT-1, type T, for HFM-505
TFM-510	Thermocouple CMT-2/cold-leg balance line, type T, for HFM-510
TFM-603	Thermocouple pressurizer surge line, type T, for HFM-603

TABLE 4.3-3
INSTRUMENTATION OUTSIDE TEST BOUNDARY BUT AFFECTED BY CMT COOLDOWN

Instrument No.	Description
FMM-803	RNS to DVI-2 flow
FMM-805	RNS discharge flow
LDP-401	ACC-1 level
LDP-402	ACC-2 level
LDP-502	CMT-2 wide-range level
LDP-505	CMT-1 wide-range level (top)
LDP-507	CMT-1 wide-range level
PT-501	CMT-1 pressure
PT-502	CMT-2 pressure
PT-802	RNS discharge pressure
TF-549	CMT-1 discharge line
TF-550	CMT-2 discharge line

TABLE 4.3-4
INSTRUMENTATION OUTSIDE OF TEST BOUNDARY BUT AFFECTED BY IRWST
COOLDOWN

Instrument No.	Description
FMM-701	IRWST-1 inject flow
FMM-703	IRWST overflow
FMM-803	RNS to DVI-2 flow
FMM-805	RNS discharge flow
LCT-701	IRWST load cell
LCT-901	Primary sump load cell
LDP-502	CMT-2 wide-range level
LDP-505	CMT-1 narrow-range level (top)
LDP-507	CMT-1 wide-range level
LDP-701	IRWST level
LDP-901	Primary sump level
LDP-902	Secondary sump level
PT-802	RNS pump discharge pressure

5.0 MATRIX TESTS RESULTS

This section contains the results of the formal matrix test program. The objective of the test program, as defined in Section 1, was to evaluate the passive safety system response to a range of small-break loss-of-coolant accidents (SBLOCAs) during transition to long-term cooling. The reference transient is a 2-in. cold-leg break with failure in the automatic depressurization system (ADS) in one valve in one ADS-4 line. This test was duplicated and repeated with variations in break size, backpressure, and operation of nonsafety systems. Other SBLOCAs were performed to evaluate the effect of moving the break location to the hot leg, core makeup tank (CMT) balance line, and direct vessel injection (DVI) line. Some tests did not involve LOCAs, but evaluated the inadvertent actuation of the ADS and an inadvertent S signal.

The matrix test report is organized by reference tests and comparison tests. The reference tests include: the cold-leg break with a single failure (Matrix Tests SB01 and SB18), a 2-in cold-leg break with nonsafety systems in operation (Matrix Test SB04), a double-ended guillotine (DEG) break of the CMT/cold-leg balance line (Matrix Test SB10), a DEG break of the DVI line (Matrix Test SB12), inadvertent actuation of the ADS (Matrix Test SB14), an inadvertent S signal (Matrix Test SB31), and a 2-in. break in the hot leg (Matrix Test SB15). Comparison tests are similar to reference tests with emphasis on system modifications and component responses in relation to the reference test. For example, the effect of a larger size break on a cold-leg LOCA response is measured in Matrix Test SB21, a double top and bottom 4-in. break, and is compared with the results of a 2-in. break evaluated in Matrix Test SB01. Four other cold-leg break comparisons are made in Subsection 5.1. There were no comparison tests for the inadvertent S signal or the hot-leg break.

Each test is organized in a similar format. The system configuration and initial conditions are reviewed, the inoperable instruments are identified, and the sequence of events is listed. The test results and evaluation are reviewed on both a system and a component level. The test period is divided into the initial depressurization phase, which occurs from simulated break initiation to ADS-1 actuation; the ADS phase, which is the period from ADS-1 actuation to the start of IRWST injection; and the IRWST injection phase, which occurs from the start of IRWST injection to the end of the test. Facility responses are documented by data plots, referenced as figures in the text.

The discussion of each test performance is based primarily on instrument indications. When the components are losing inventory and coolant is flashing to steam, a steam percent is calculated based on compensated levels. These numbers should be considered preliminary. The computer program used to calculate the compensated levels is being developed as part of the AP600 Low-Pressure Integral Systems Test at Oregon State University. The program has been through initial configuration, and final validation will be completed as part of the *AP600 Low-Pressure Integral Systems Test at Oregon State University, Test Analysis Report, WCAP-14292*,⁽²⁾ which will review the steam percent estimations from this report as part of the mass and energy balance calculation and update these values as required.

5.1 Cold-Leg Breaks with a Single Failure

There were six tests performed to evaluate the cold-leg small-break loss-of-coolant accident (SBLOCA) without operation of the nonsafety systems and a failure in one of the two automatic depressurization (ADS) valves in one ADS-4 line. Reference test SB01 simulated a 2-in break in the bottom of the cold leg. This test was the first matrix test performed; it was repeated at the end of the test program to ensure that the plant characteristics did not change. Another 2-in.-break was repeated to determine the impact of a higher containment backpressure on the passive injection system (Matrix Test SB19). Three additional cold-leg break tests were performed to simulate smaller (0.5 in. and 1.0 in.) and larger break sizes (double 4.0 in.).

5.1.1 Reference 2-In. Cold-Leg Break (Matrix Test SB01)

This section provides the test results for Matrix Test SB01 (OSU Test U0001). Matrix Test SB01 simulated a 2-in. cold-leg (CL) break loss-of-coolant accident (LOCA) with long-term cooling and without operation of nonsafety systems. The break was located at the bottom of CL-3 with a simulated failure of one of the automatic depressurization system-4 (ADS-4) lines. CL-3 is on the core makeup tank (CMT) side of the facility (Figures 5.1.1-1 and 5.1.1-2).

Subsection 5.1.1.1 provides details related to the test procedure, system configuration, and initial conditions. A description of inoperable instruments is provided in Subsection 5.1.1.2, and Subsection 5.1.1.3 references the sequence of events. Subsection 5.1.1.4 describes the test results and evaluation. Component responses are given in Subsection 5.1.1.5, and a summary of mass balance results is provided in Subsection 5.1.1.6. The conclusions as they apply to Matrix Test SB01 are given in Subsection 5.1.1.7. The facility responses to the break are documented by the data plots, referenced as figures in the text, at the end of this section. A data plot with the suffix x indicates extended time.

Matrix Test SB01 was performed on June 1, 1994. The performance of this test was successful because the reactor vessel heater rod cooling was maintained.

5.1.1.1 System Configuration and Initial Conditions

The test was conducted per an approved written procedure. All actions were automatic after the test started with no operator response required.

A flow nozzle simulating one line of flow was installed in the ADS 4-1 line—hot leg-1 (HL-1) to the ADS 4-1 separator—to provide the single failure simulation, and a flow nozzle simulating two lines of flow was installed in the ADS 4-2 line—HL-2 to the ADS 4-2 separator. Additionally, flow nozzles simulating two lines of flow each were installed in the ADS 1-3 inlet lines.

The reactor heater control decay algorithm maintained maximum reactor heater power output for 140 seconds, and then power began to decay to simulate the total post-trip energy input of the AP600 nuclear fuel (Appendix F). This test was performed with reactor heater rod HTR-C2-317 removed and replaced with a dummy rod. Refer to Subsection 2.7 for pre-test operations.

Table 5.1.1-1 shows initial facility conditions for Matrix Test SB01. There were three initial condition parameters out of specification, none of which should invalidate this test.

- HL-2 temperature, indicated by SC-140, was []^{a,b,c} or less than 0.1 percent above the required temperature band. This was within the accuracy requirements of the instrumentation system.

- CMT-2 temperature, indicated by TF-532, was []^{a,b,c} or []^{a,b,c} above the required temperature of less than []^{a,b,c}. TF-532 is located on the CMT-2 long thermocouple rod, about 0.5 in. down from the inside top of the CMT.

The next three thermocouples down on the long thermocouple rod, their dimensions from the inside top of the CMT, and their average temperature for about []^{a,b,c} prior to break valve opening are listed in the following:

<u>Thermocouple</u>	<u>Dimension</u>	<u>Average Temperature</u>
TF-548	[] ^{a,b,c}	[] ^{a,b,c}
TF-530	[] ^{a,b,c}	[] ^{a,b,c}
TF-526	[] ^{a,b,c}	[] ^{a,b,c}

Less than []^{a,b,c} percent of the CMT volume was at a temperature greater than []^{a,b,c}. Test analysis using the CMT recorded temperature data, taking into account the temperature variations at the top of the CMT, should still be possible.

- Accumulator-1 (ACC-1) pressure, indicated by PT-401, was []^{a,b,c} or []^{a,b,c} below the required pressure band. The accumulator was pressurized to the required pressure, as indicated on local pressure indicator PI-401, prior to test actuation. The loss of pressure between tank pressurization and test actuation was possibly due to the nitrogen gas cooling in the accumulator. Test analysis starting with the recorded lower accumulator overpressure should still be possible.

The test ran for about 10.5 hours.

5.1.1.2 Inoperable Instruments

Table 5.1.1-2 is a list of instruments considered inoperable or invalid during all or portions of this test. Some of the instruments listed are on the Critical Instrument List (Subsection 3.2, Table 3.2-2) and, therefore, are addressed here.

FDP-604, FDP-605, and FDP-606 measured the differential pressure (in. H₂O) across the ADS 1-3 flow nozzles. The transmitters over-ranged momentarily when their respective ADS valve opened. Total flow through the ADS 1-3 valve complex can be determined by measuring ADS 1-3 separator liquid and steam flows from FMM-601 and FVM-601.

FMM-201, FMM-202, FMM-203, and FMM-204 measured flow (gpm) in each of the four cold legs. The data from these meters were invalid after []^{a,b,c} due to possible steam in the cold legs. The meters could not measure steam flow.

FMM-402 measured ACC-2 injection flow into direct vessel injection-2 (DVI-2). FMM-402 data are approximately double DVI-2 flow data, as indicated by FMM-206, when accumulator injection was providing the only flow to DVI-2. FMM-206 was confirmed to be accurate by comparison to FMM-504, which measured CMT-2 injection flow, and FMM-702, which measured IRWST-2 injection flow, when each flow was the only injection flow in progress. ACC-2 injection flow rates can be ascertained by a comparison of the other injection flows through the DVI-2 nozzle. CMT-2 level data channel LDP-402 can also be used as a backup to this measurement.

CMT-1 and CMT-2 injection flow meters FMM-501 and FMM-504 and passive residual heat removal (PRHR) inlet and outlet flow meters FMM-802 and FMM-804 provided accurate data when sensing liquid, but became inaccurate when sensing two-phase or steam flow.

FMM-701 measured in-containment refueling water storage tank-1 (IRWST-1) injection flow when the primary sump valves were opened. The flow meter indicated a negative flow as water flowed from the primary sump to the IRWST. The meter was not designed to measure reverse flow, so this measurement was invalid. However, total IRWST flow was measured by FMM-702.

FMM-905 measured break separator loop seal flow to the primary sump. As the transient proceeded, the primary sump and break separator levels exceeded the elevation of the break at the bottom of CL-3. When this occurred, break flow initially stopped and then reversed. Flow reversal through the break occurred at about []^{a,b,c} rendering subsequent data invalid.

Steam generator (SG) tube level data (LDP-215, LDP-218, LDP-219, and LDP-222) were biased by vaporization of the water in the transmitter reference leg after the SG tubes started draining. However, the data provide accurate indication of the time when the tubes are empty.

LDP-401 and LDP-402 measured ACC-1 and ACC-2 levels, respectively. Due to air trapped in the sense lines for the transmitters, the data from these transmitters were invalid. However, the initial level of the tank was established by a standpipe, so it was constant from test to test. The drain rate can be calculated using the ACC-1 and ACC-2 flow meters (FMM-401 and FMM-402, respectively). Alternately, a pressure correction may be applied directly to the level indications of LDP-401 and LDP-402.

PT-201 measured reactor coolant system (RCS) pressure at the top of the SG-1 long tube. On August 15, 1994, it was discovered that the transmitter had an incorrect zero compensation, which resulted in a negative error and negative data at low pressures. The transmitter zero was corrected at that time. PT-201 data obtained during Matrix Test SB01 had the zero correction performed, and the corrected data appear as PT_201. Negative data and corrected negative data can be used to determine

trends, but are considered inaccurate. PT_201 was not considered reliable for values less than 1.1 psig, but a sufficient amount of other pressure data are available.

TF-501 and TF-504 measured CMT fluid temperature from the long thermocouple rod location near the bottom of each CMT. The thermocouples appear to have measured ambient conditions throughout the test, which would indicate a short somewhere in the thermocouple wiring. With these thermocouples inoperable, the required long thermocouple rod thermocouple availability of "seven out of ten and no more than one in succession failed" was met.

Data provided by ADS-4 separator instrumentation prior to the ADS 4-1 and ADS 4-2 valves opening at 978 seconds were invalid due to the closed position of the ADS-4 valves and the ADS-4 separator loop seal valves. The instruments affected are: FMM-602, FMM-603, FVM-602, FVM-603, LDP-611, and LDP-612. Test analysis will not be affected, since ADS-4 flow did not begin until the valves opened.

Considering these critical instrument failures, sufficient instrumentation was available to allow the performance of mass balances as demonstrated in Subsection 5.1.1.6 and Appendix E. An energy balance will be performed and reported in the *AP600 Low-Pressure Integral Systems Test at Oregon State University Test Analysis Report, WCAP-14292*.⁽²⁾

5.1.1.3 Sequence of Events

Table 5.1.1-3 contains the sequence of events for Matrix Test SB01. The first pages of the table provide the event times of selected events in the test. The subsequent pages of the table use bar charts of the data to provide a visual representation of the sequence of events. Both the numeric table and the bar chart sort the events in chronological order.

The first pages of Table 5.1.1-3 indicate the source of the actual time data. A D in the Data Source column indicates the recorded time was obtained from a software program that monitored digital events in the facility. These events included pump starts and stops, valve limit switch actuations, and alarms. The term *valve opening* means the valve has actuated and the closed limit switch is being opened (valve coming off the seat). An A in the Data Source column indicates the time data were obtained by reviewing test data obtained from the data acquisition system (DAS). Although the test data from the DAS were in digital format, the DAS monitored analog events such as pressure, flow, and temperature from the data.

Because Matrix Test SB01 is the first test described in this report, the following is a general discussion of the events and responses from test initiation through the end of the test. The test sequence was initiated by actuating the TEST pushbutton, which triggered the DAS to begin acquiring data. Approximately the first 2 minutes of data were used to establish the initial conditions for the test. Two minutes after TEST pushbutton actuation, a signal was sent to open the break valve located at the bottom of CL-3. In the first []^{a,b,c} following the signal to the break valve, the SG

pressure setpoint was raised, the reactor shifted to power (kW) control mode with a programmed power demand, the main feedwater pump tripped and feedwater was isolated, the passive residual heat removal heat exchanger (PRHR HX) outlet valve and CMT discharge valves opened, and the reactor coolant pumps (RCPs) tripped. Forced flow was initiated through the PRHR HX and the CMTs until the RCPs stopped, at which time the flow changed to natural circulation flow.

As the RCS depressurized and lost inventory through the break, pressurizer level decreased rapidly and steam formation began in the reactor vessel upper head. At about []^{a,b,c} the CMTs began to drain. The pressurizer and pressurizer surge line became completely empty of liquid, and at the same time, steam formed in the SG tubes and pushed the remaining water out of the bottom of the tubes. Shortly thereafter, the SG channel heads began to empty. When CMT level decreased to the low level setpoint, the ADS valve sequence initiated.

The ADS-1 valve opened, causing an increase in the rate of RCS depressurization. The ADS-2 and ADS-3 valves then sequenced open, further increasing the rate of depressurization. When RCS pressure decreased to below that of the accumulators, the accumulators began to inject into the DVI lines, which stopped CMT injection by closing the CMT discharge line check valves.

The reactor pressure low-low setpoint was reached, sending an automatic opening signal to the IRWST injection valves. IRWST injection did not start at this time because RCS pressure was still too high to be overcome by the IRWST static head.

The accumulators emptied and depressurized, and CMT injection recommenced. When the CMT low-low level was reached, an automatic opening signal was sent to the ADS 4-1 and ADS 4-2 valves. These additional vent paths for the RCS helped decrease RCS pressure low enough to initiate IRWST injection.

The IRWST injection continued, and about []^{a,b,c} later, the pressurizer surge line and then the pressurizer began to reflood. The pressurizer subcooled and, with the ADS 1-3 sparger still submerged in the IRWST, the pressurizer and ADS 1-3 separator went to a negative pressure, further increasing the fluid level in the pressurizer. About this same time, the CMT levels started to increase. After about []^{a,b,c} the ADS 1-3 sparger became uncovered, breaking the negative pressure and allowing the pressurizer to drain. A fluid level was maintained in the surge line for the remainder of the test.

Primary sump injection started several hours later with flow through the injection line check valves. The primary sump injection valves opened automatically when the IRWST reached its low-low level setpoint. The RCS remained on natural circulation flow with inventory leaving through ADS 4-1 and ADS 4-2 to the primary sump and returning from the sump through the DVI lines. The driving force was the heat input to the reactor.

5.1.1.4 Test Results and Evaluation

The LOCA event simulated in the OSU test facility resulted in interactions between the systems and components in the facility. For this reason, it is convenient to subdivide the event into different phases, each characterized by the systems' behavior and thermal-hydraulic phenomena occurring within the systems. The different event phases selected for the purpose of detailed evaluation of the LOCA event are as follows:

- Initial Depressurization Phase: simulated break initiation to ADS-1 actuation
- ADS Phase: ADS-1 actuation to start of IRWST injection
- IRWST Injection Phase: start of IRWST injection to end of test

Initial Depressurization Phase

The test began with the actuation of the TEST pushbutton. After a 120-second delay, break valve TS-205, located at the bottom of CL-3, received an open signal (time zero). After an additional 0.5 second, an S signal was generated by the programmable logic controller (PLC), which time-sequences signals to initiate various events such as resetting controllers, stopping pumps, and repositioning valves.

The SG steam pressure controller reset to control pressure at []^{a,b,c} to minimize heat removal by the SGs. The value of []^{a,b,c} was high enough that the valve would not re-open, yet low enough not to challenge the SG safety valves. Simultaneously, the reactor controller transferred from the temperature (hot-leg average temperature in °F) control mode to the power (kW) control mode, with demand programmed for 600-kW total power. The main feedwater pump tripped, and the SG feedwater control valves closed at 4 seconds, isolating feedwater to the SG.

At []^{a,b,c} with the RCPs still running, the PRHR HX outlet valve opened, allowing forced flow through the PRHR HX to begin and, therefore, cooled fluid to enter the system at the SG-2 outlet channel head from the HX. At []^{a,b,c} the RCPs tripped and the flow through the PRHR HX shifted from forced to natural circulation flow.

Also at []^{a,b,c} the two CMT injection valves opened, allowing forced flow from CL-1 and CL-3 through the CMTs and into the reactor vessel downcomer area through the two DVI nozzles. This also was cool ambient temperature fluid replacing inventory lost through the break. When the RCPs tripped, flow through the CMTs shifted from forced to natural circulation flow.

At about []^{a,b,c} steam percent, as calculated from LDP-127 data, indicated that the reactor vessel began to lose inventory and flash to steam (Figure 5.1.1-3). Steam percent, as calculated from LDP-115 data, indicated that the fluid in the reactor vessel upper head began to flash to steam at []^{a,b,c} and was essentially all steam at about []^{a,b,c} (Figure 5.1.1-4). The upper

plenum area of the reactor vessel steam percent, as calculated from LDP-139 data, began to show steam collection at approximately []^{a,b,c}

Using data from the level channels and the calibrated range of the instruments, a core steam percent for each channel was calculated. The equation used to calculate steam percent was:

$$\text{Steam percent} = \left(1 - \frac{\text{compensated level}}{\text{instrument range}} \right) 100$$

The break flow caused a rapid decrease in pressurizer level (Figure 5.1.1-5) and emptied the pressurizer at approximately []^{a,b,c}. At about []^{a,b,c} the pressurizer surge line completely emptied, as indicated by LDP-602. CMT levels began to decrease, making the transition from recirculation to draindown, as indicated by LDP-509 and LDP-510, at about []^{a,b,c} respectively (Figure 5.1.1-6). After transition to draindown, the CMTs provided makeup to the RCS to compensate for the loss of inventory through the break.

After 140 seconds at 600 kW, reactor power began to follow the decay heat decay curve. (The OSU test facility power is held at a maximum of 600 kW for 140 seconds to simulate the total heat input of the AP600 nuclear reactor following a reactor trip.)

At about []^{a,b,c} a condensation/depressurization event took place in CMT-1. Data indicate a rapid refill of the CMT-1 balance line with an increase of about []^{a,b,c} in tank level (tank full) once the balance line filled (Figure 5.1.1-77). An indication of the event was an []^{a,b,c} spike decrease in CMT-1 pressure, which resulted in about a []^{a,b,c} decrease in reactor upper head and CL-3 pressures (Figure 5.1.1-78). The CMT-1 inlet line and upper tank temperatures provided additional confirmation that a condensation/depressurization event occurred (Figures 5.1.1-79 and 5.1.1-80). Condensation/depressurization events are described more thoroughly in Subsection 7.1.

The U-tubes of both SGs were completely empty by approximately []^{a,b,c} (Figures 5.1.1-7 and 5.1.1-8). The SG U-tube level instruments should be considered inoperable once the U-tubes start to empty because their reference legs were routed internal through the SGs and, therefore, steamed dry during the test. Loss of the reference legs gave a false full-level indication. The SG cold-leg channel heads were all empty by about []^{a,b,c} which was prior to ADS-1 actuation, and the hot-leg channel heads emptied at about []^{a,b,c} or shortly after ADS-1 actuation (Figures 5.1.1-9 and 5.1.1-10). Although it was ranged improperly and considered inoperable, LDP-209 would still have responded to trends.

The HL-1 level began to decrease at about []^{a,b,c} and HL-2 level at about []^{a,b,c} as indicated by hot-leg elbow level instruments LDP-207 and LDP-208, respectively (Figure 5.1.1-11). Although they were ranged improperly and considered inoperable, LDP-207 and LDP-208 would still have responded to trends. The horizontal sections of the hot legs started to drain at about []^{a,b,c}

]^{a,b,c} as indicated by LDP-205 and LDP-206, respectively. The draining of the hot legs was confirmed by LDP-139 (Figure 5.1.1-12), which indicated a level of about []^{a,b,c} at this time. LDP-139 measures level inside the core barrel between the bottom of the upper core support plate and the bottom of the upper support plate ([]^{a,b,c} above the bottom of the reactor vessel), and spans the hot legs.

The hot-leg temperatures during this time remained at saturation temperature (Figures 5.1.1-13 and 5.1.1-14). Even though they were partially or completely empty, the hot legs remained at saturation temperature and never superheated due to a small flow of saturated steam from the reactor heater bundle to the SGs.

The fluid level inside the reactor core barrel reached its minimum collapsed level of []^{a,b,c} (the indicated level at the top of the heated section of the heater rods is []^{a,b,c}) during this test at []^{a,b,c} as indicated by LDP-127 (Figure 5.1.1-15). At this level, heater rod cooling was still maintained.

At []^{a,b,c} CMT-1 reached its low level setpoint, thereby activating the ADS valve timing sequence portion of the PLC, and the ADS-1 valve opened at []^{a,b,c}

ADS Phase

The opening of the ADS-1 valve resulted in two-phase flow through the pressurizer surge line and pressurizer to the ADS 1-3 separator and then to the IRWST through a sparger. This flow caused the differential pressure instruments used to measure surge line and pressurizer level to initially produce an indication of the pressurizer and surge line reflooding, which may have been influenced by line losses (Figure 5.1.1-5). With the accumulators at their maximum injection rate, the surge line and pressurizer began to reflood at about []^{a,b,c} and the pressurizer attained its maximum level at []^{a,b,c}. The pressurizer and surge line then drained back down and were completely empty at []^{a,b,c}. This additional flow path, in conjunction with the break, caused RCS pressure to decrease at a more rapid rate.

The opening of the ADS-1 valve, followed by the ADS-2 valve approximately []^{a,b,c} later, caused an increase in the rate of RCS depressurization (Figure 5.1.1-45). When the RCS depressurized to approximately []^{a,b,c} at about []^{a,b,c} accumulator injection began. This reduced CMT-1 injection flow to 0 over the following []^{a,b,c} and CMT-2 injection flow to less than []^{a,b,c} over the following []^{a,b,c} (Figure 5.1.1-16) by closing off the CMT discharge line check valves until the accumulators were almost empty and depressurized. ACC-2 injection flow instrument FMM-402 appeared to have indications double the actual flow when compared to DVI-2 flow instrument FMM-206 and was considered inoperable. The ADS-3 valve opened at approximately []^{a,b,c} but with RCS pressure having decreased to about []^{a,b,c} by this time, the valve opening had little effect on the rate of depressurization.

When RCS pressure decreased to []^{a,b,c} at approximately []^{a,b,c} the two IRWST injection valves automatically opened (by a signal from the PLC), but IRWST injection could not occur until RCS pressure decreased to near atmospheric, since the IRWST is a static system that depends on gravity flow and operates at break and ADS measurement system (BAMS) header pressure. CMT-2 injection flow started to increase at []^{a,b,c} and CMT-1 injection flow started to increase at []^{a,b,c}. The accumulators completed injection at []^{a,b,c} for ACC-1 and []^{a,b,c} for ACC-2, at which time CMT injection resumed. At the end of accumulator injection, some of the nitrogen gas was injected into the DVI lines, momentarily cooling the injection lines. The nitrogen caused a momentary decrease in DVI-1 flow of about []^{a,b,c} and a decrease in ACC-1 outlet temperature of about []^{a,b,c} at []^{a,b,c} (Figures 5.1.1-17 and 5.1.1-18). On the ACC-2 side, there was no indicated change in DVI-2 flow, although the ACC-2 outlet temperature decreased []^{a,b,c} at []^{a,b,c}.

At approximately []^{a,b,c} a sharp "bang" was heard, apparently emanating from the upper portion of the reactor vessel. This has been determined to be a steam condensation and resulting depressurization event in the reactor vessel upper downcomer area and has been further investigated (see Subsection 7.1). The sharp increase of DP-114 to []^{a,b,c} at []^{a,b,c} DP-130 to []^{a,b,c} at []^{a,b,c} and the over-ranging of LDP-116 and LDP-140 at []^{a,b,c} were major indications of the steam condensation event (Figures 5.1.1-19 and 5.1.1-15). Test data reveal that the collapse of the superheated steam bubble in the upper portion of the reactor vessel downcomer annulus resulted in the downcomer fluid accelerating upward and impacting the bottom of the core barrel flange where the core bypass holes are located. The impact of the downcomer liquid on the solid surface of the core barrel flange produced the "bang" heard during the test. The low pressure created in the upper downcomer annulus by the collapse of the steam bubble also resulted in a rapid increase in steam flow from the core barrel, through the upper head, and into the downcomer. DP-114 and DP-130 were both calibrated to indicate either positive or negative differential pressure, depending on the direction of flow. DP-130 was calibrated as if the system were full; therefore, when the fluid level is below the lower tap, the instrument is in error by the distance between its high- and low-pressure taps, i.e., []^{a,b,c} must be added to the indicated value to obtain the correct differential pressure.

From []^{a,b,c} both DVI nozzle temperatures increased from essentially ambient conditions to as high as []^{a,b,c} and then returned to ambient conditions (Figure 5.1.1-20). The temperature increase was caused by two factors. First, there was rapid heating of the remaining water to be injected from the CMTs when they were at low levels. Second, the reactor vessel downcomer level was at the DVI nozzle level during this period, possibly partially uncovering the nozzles. The temperature transient was terminated when IRWST injection began refilling the reactor vessel at about []^{a,b,c} and temperatures returned to ambient when the CMTs were empty, terminating the hot liquid injection. This temperature transient does not appear to have affected any other facility parameters.

At []^{a,b,c} the ADS 4-1 and ADS 4-2 valves opened automatically on a signal from the PLC when CMT-1 level reached its low-low level setpoint. ADS-4 actuation started a decline in RCS inventory that would not be overcome until IRWST injection began (Figure 5.1.1-15). CMT-1 and CMT-2 were completely empty at []^{a,b,c} respectively (Figure 5.1.1-6).

Pressurizer heater thermocouples TH-601, TH-602, and TH-603 (Figure 5.1.1-21) indicated that the pressurizer was slightly subcooled at about []^{a,b,c} remained subcooled until primary sump injection began at about []^{a,b,c} and then increased to saturation temperature. System heatup can be attributed to the warmer recycled injection water provided from the sump and lower liquid levels maintained in the RCS (Figures 5.1.1-22 and 5.1.1-23). The pressurizer remained at saturation temperature until about []^{a,b,c} when the temperature began to rise into the superheated range (Figure 5.1.1-24). The PLC did not lower the pressurizer heater demand to []^{a,b,c} as required by the logic, and the heaters stayed at 1.5 kW until about []^{a,b,c} when they increased to about 3 kW and remained there until the end of the test. In subsequent tests, the heaters were de-energized by procedure, and later in the test program, the logic was changed to drop out the heater silicon-controlled rectifier (SCR) contactor.

The IRWST appeared to overflow into the primary sump during the period of []^{a,b,c} as indicated by FMM-703 (Figure 5.1.1-25). However, there was no indicated level change on LDP-701 (Figure 5.1.1-26) prior to or during this period. This early indication of overflow from the IRWST to the sump is believed to have been caused by the differential pressure between the IRWST and primary sump, which forced liquid from the overflow loop seal into the sump. The pressure in the two tanks was caused by a backpressure in the BAMS header as steam was released from the break separator following the break. A possible explanation is that the differential pressure was a result of the tank free volumes and vent pipe size (i.e., the sumps were empty and the IRWST was filled to []^{a,b,c} the IRWST has a []^{a,b,c} vent and the sump has a []^{a,b,c} vent, resulting in a faster pressure increase in the IRWST). From []^{a,b,c} an overflow and level increase occurred due to the loss-of-coolant inventory through ADS 1-3, as indicated by FMM-703 and LDP-701.

At about []^{a,b,c} RCS pressure had decreased to about []^{a,b,c} which was sufficiently low that the IRWST static head was greater than RCS pressure, and IRWST injection began. IRWST injection proceeded at a continually diminishing rate as the differential head between the IRWST and the RCS decreased.

IRWST Injection Phase

The pressurizer and pressurizer surge line emptied for the second time at approximately []^{a,b,c} respectively (Figure 5.1.1-5). The surge line then began to reflood almost immediately at []^{a,b,c} and the pressurizer at about []^{a,b,c}. This time, reflooding was confirmed by HL-2, pressurizer surge line, and pressurizer subcooled temperatures (Figures 5.1.1-14 and 5.1.1-27). In addition, the surge line completely filled first, followed by the

level rise in the pressurizer. The reflood was caused by RCS levels increasing above the reactor vessel nozzles because IRWST injection exceeded the inventory losses (Figures 5.1.1-15, 5.1.1-17, and 5.1.1-28). The maximum pressurizer level attained was about []^{a,b,c} at []^{a,b,c} but immediately began to decrease and was empty at []^{a,b,c}. The pressurizer remained empty for the remainder of the test. The surge line stayed full until []^{a,b,c} when the level decreased to about []^{a,b,c} and remained there until []^{a,b,c}. The level again decreased to about []^{a,b,c} at []^{a,b,c} and oscillated between about []^{a,b,c} for the remainder of the test.

During the time that the pressurizer had a liquid level, ADS 1-3 separator pressure (PT-605) and ADS 1-3 sparger pressure (PT-606; Figure 5.1.1-29) both went negative by as much as []^{a,b,c}. They were negative from []^{a,b,c}. The negative pressure was broken when the level in the IRWST decreased below the sparger nozzles. This negative pressure would explain much of the pressurizer level in that it would draw the level higher and hold it there. A vacuum breaker was installed on the sparger line inside the IRWST shortly after this test to prevent a recurrence of this problem. A vacuum breaker is included in the AP600 design.

Both CMT balance lines began to refill at about []^{a,b,c} when reactor vessel level, as indicated by LDP-140, was sufficiently high at []^{a,b,c} to cover and refill the cold legs (Figures 5.1.1-30 and 5.1.1-31). At about []^{a,b,c} when the CMT-2 balance line had completely refilled, CMT-2 began to rapidly refill and reached the []^{a,b,c} level (about two-thirds full) in about []^{a,b,c}. The refill of subcooled fluid caused a condensation/depressurization event to occur in CMT-2. This was reflected in reactor vessel pressure and levels and the CMT balance line level taking a sharp dip and then recovering. CMT-2 refilling also caused its internal temperatures to quickly decrease from the superheated region to subcooled at less than []^{a,b,c} and to remain subcooled until the CMT began to drain again (Figure 5.1.1-32). When the CMT-1 balance line had refilled completely at approximately []^{a,b,c} CMT-1 refilled to the []^{a,b,c} level (or about two-thirds full) in less than []^{a,b,c}. Again, the rapid refill with subcooled fluid caused another condensation/depressurization event to occur, this time in CMT-1. The CMT-1 internal temperatures responded to the subcooled fluid almost identically to those of CMT-2 (Figure 5.1.1-33). The CMTs reached a level and temperature equilibrium in which steam condensation and a resultant level increase were no longer occurring. During this period of time, there was no injection flow from the CMTs because the higher static head of the IRWST held the CMT discharge line check valves closed.

When the CMT balance lines began to refill, CMT internal pressures began to decrease with respect to the reactor vessel upper head pressure. The cause of the pressure decrease is believed to be that once the cold legs filled with subcooled fluid, displacing what had been a blanket of superheated steam, the superheated steam in the CMTs began to slowly condense and the balance lines filled over a period of about []^{a,b,c}. Once the balance lines filled and sprayed into the CMTs through the inlet diffusers, the subcooled fluid collapsed the superheated steam bubble in the CMTs, creating more of a

decrease in pressure. The subsequent in-rush of fluid from the RCS was reflected in the decrease in reactor vessel levels and pressure.

CMT-1 and CMT-2 remained at essentially constant levels for several []^{a,b,c} and then began slow draindowns at about []^{a,b,c} respectively. The draindown for both CMTs was slow and did not occur until IRWST relative level was []^{a,b,c} below that of the CMTs (Figure 5.1.1-34). Data indicate that the CMTs drained for a while, and then the differential head between the IRWST and the CMTs again closed the CMT discharge check valves, terminating draining until the time that the differential shifted the other way and draining recommenced. Both CMTs were completely empty at about []^{a,b,c} which coincides closely with the primary sump injection valve opening at []^{a,b,c}. A possible correlation is that when the primary sump valve opened, the IRWST had just reached its minimum level of about []^{a,b,c} which is about []^{a,b,c} below the instrumented level for the CMTs, and that there was still a slight negative pressure remaining in the CMTs. Also, when the primary sump injection valves opened, there was a short time period in which the IRWST and primary sump levels equalized, causing a decrease in RCS fluid levels and resulting in a rather fast drop in CMT levels from about []^{a,b,c}

LDP-905 revealed that break separator level (Figure 5.1.1-35) began to increase at the same rate as the primary sump at about []^{a,b,c}. This occurred when sump level reached the height of the break separator loop seal. As a result of this level increase, break separator level reached the height of the break in CL-3, causing break flow to reverse and flow from the break separator into the RCS through the break at about []^{a,b,c} (Figure 5.1.1-36). The break flow then remained essentially 0 or slightly negative throughout the rest of the test.

Primary sump injection began through the check valves around the sump injection valves at approximately []^{a,b,c} (Figure 5.1.1-37) when primary sump and IRWST levels were essentially equal (Figure 5.1.1-35). At []^{a,b,c} the primary sump injection valves automatically opened when the IRWST reached its low-low level setpoint of []^{a,b,c}

When sump injection began, the reactor downcomer temperatures rapidly increased to match the sump fluid temperature (Figures 5.1.1-23 and 5.1.1-38). When the primary sump injection valves opened, the DVI flows decreased and the sump and IRWST levels equalized (Figure 5.1.1-39). During the reduced DVI flow period, there was an upward spike in reactor downcomer temperatures. The downcomer thermocouples located above the DVI nozzle elevation increased to saturation at this time and remained at saturation for the rest of the test because the reactor vessel collapsed level was at the DVI nozzles (Figure 5.1.1-22).

PRHR HX outlet temperature, indicated by TF-804 (Figure 5.1.1-40), remained subcooled in the range of []^{a,b,c} during most of the test, but after sump injection, began to rise and was just reaching saturation temperature at the end of the test. The inlet temperature, indicated by TF-803, was subcooled between []^{a,b,c}. After reaching saturation at about 12,000 seconds, it remained at saturation temperature for the rest of the test.

In the early stages of the transient, the PRHR HX instrumented long- and short-tube temperatures generally remained below []^{a,b,c} with the short tube predominantly hotter and maintaining a wider delta temperature between the tube inlet and outlet. This would indicate that most of the flow was through the short tubes. This difference between long- and short-tube performance was evident until about []^{a,b,c} when the short-tube temperatures rapidly dropped to align themselves with the long-tube temperatures (Figure 5.1.1-41). The drop in temperature did not coincide with any other event and was an indication of a flow cessation through the PRHR HX, with the indicated delta temperature across the HX being the result of the temperature gradient in IRWST fluid. Flow cessation is observed from CL-2 and CL-4 data, which show that temperatures at the bottom of the reactor flange for both loops began to increase at about this same time, followed saturation from about []^{a,b,c} went into the superheated region at about []^{a,b,c} and then became subcooled when the cold legs started to refill at about []^{a,b,c} (Figures 5.1.1-42 and 5.1.1-43).

The PRHR HX inlet temperature became subcooled coincident with the ADS-4 valves opening at []^{a,b,c} and over the next []^{a,b,c} dropped to and paralleled the outlet temperature. Again, this is an indication that there was no flow through the HX during this time frame (Figure 5.1.1-40). At []^{a,b,c} the PRHR HX inlet temperature instantly jumped from []^{a,b,c} to saturation temperature. This happened about []^{a,b,c} after pressure, level, and flow oscillations began in the facility and was possibly caused by the inlet line "burping" and once again allowing the line to fill with saturated steam. Following the "burp," all of the PRHR temperatures began to slowly approach saturation.

When primary sump injection started through the check valves around the sump injection valves, IRWST injection was approximately []^{a,b,c} per side (Figure 5.1.1-37). The flow then split, with approximately []^{a,b,c} per side from the IRWST and []^{a,b,c} per side from the primary sump. When the primary sump injection valves opened, the IRWST-2 side flow increased to approximately []^{a,b,c} the IRWST-1 side flow indication went negative, the primary sump-1 side flow increased to approximately []^{a,b,c} and the primary sump-2 side decreased to approximately []^{a,b,c}. This flow split is discussed more thoroughly in the IRWST Response portion of this section. Overflow from the primary sump to the secondary sump started at about []^{a,b,c} (Figure 5.1.1-35).

Starting at about []^{a,b,c} there was a series of pressure, level, and flow oscillations that occurred throughout the components of the facility lasting until about []^{a,b,c}. Since they occur in other tests, these oscillations are addressed in the *Test Analysis Report*.⁽²⁾

In the long-term cooling mode of operation, system inventory was lost through the ADS 4-1 and ADS 4-2 valves to the primary sump. System inventory was made up through primary sump and IRWST injection through the DVI lines and some small flow from the primary sump through the break separator and into the break. The driving force for this flow was the decay heat simulation in the reactor heater rods. The hotter fluid produced in the reactor flowed out through the hot legs and

ADS-4 to the primary sump, and the cooler fluid in the sump returned from the bottom of the sump to the reactor vessel downcomer via the sump injection lines.

The test continued for an additional 4 hours in the sump recirculation mode. The final total core power at the end of the test was []^{a,b,c} (Appendix F).

5.1.1.5 Component Responses

Reactor

The reactor and its associated connections to the other systems in the facility are depicted in Dwg. OSU 600203, and its heater locations are depicted in Dwg. OSU 600007. The reactor instrumentation is shown in Dwg. OSU 600101, Sh. 1 and 2. These drawings are in Appendix G.

When the TEST pushbutton was pressed, the reactor controller was in auto-local, controlling hot-leg average temperature at 420°F (the reactor controller automatically controls that temperature by varying the demand signal to the heaters). At time zero, the PLC sent a signal to open the break valve and then 0.5 second later signaled the reactor controller to shift control to auto-remote with total power demand initially at 600 kW (the setpoint is generated by an algorithm programmed into the controller, and the controller automatically controls the demand to the heaters to control the setpoint kW). The power algorithm programs full power (600 kW) for the first 140 seconds and then lets power decay at an exponential rate that simulates the decay heat input of the AP600 nuclear reactor following a trip from full power (Appendix F).

The DVI flow into the reactor vessel began immediately when the CMT discharge isolation valves opened at 6 seconds (Figure 5.1.1-17). This flow continued at a rate averaging about []^{a,b,c} per side until about []^{a,b,c} when RCS pressure decreased sufficiently for accumulator injection to start and DVI flow increased to []^{a,b,c} per side. When accumulator injection ended, the DVI flow again dropped to about []^{a,b,c} per side while the remainder of the CMT fluid was injected.

Steam percent, as calculated from LDP-127 data (Figure 5.1.1-3), showed that the reactor vessel began to lose inventory, i.e., water began to flash to steam, at approximately []^{a,b,c}. Steam percent, as calculated from LDP-115 data (Figure 5.1.1-4), showed that the fluid in the reactor vessel upper head began to drain and flash to steam at about []^{a,b,c} and was essentially all steam at about []^{a,b,c}. Steam percent in the upper plenum area of the reactor vessel, as calculated from LDP-139, began to show steam collection at approximately []^{a,b,c}.

The initial increase in reactor vessel downcomer level indication on LDP-116 and LDP-140 was because the RCPs tripped at []^{a,b,c} and the instruments were no longer affected by the dynamic flow differential pressure and indicated a true full-range level (Figure 5.1.1-15). LDP-116 and LDP-140 showed that the level in the reactor vessel downcomer began to decrease at

[]^{a,b,c} The reference leg taps for these level differential pressure transmitters are located at []^{a,b,c} respectively, and approximately []^{a,b,c} below the core barrel support flange. This means that the level in the downcomer started decreasing some time prior to indication. The two level differential pressure transmitters share a common lower tap located at []^{a,b,c}

Fluid levels in both the reactor vessel downcomer and inside the core barrel continued to decrease due to inventory loss through the break, with LDP-116 and LDP-140 showing a level of []^{a,b,c} at []^{a,b,c} and LDP-127, which measured collapsed level inside the core barrel, showing a minimum level of []^{a,b,c} at []^{a,b,c}. The level in the downcomer was near the top of the cold legs and remained there until ADS-1 actuation. The level in the core barrel completely uncovered the hot-leg nozzles, but maintained cooling in the heated section of the heater rods. A verification that the heater rods remained cooled is that none of the upper heater rod thermocouples showed a significant increase in temperature as would be expected if they had not been sufficiently cooled (Figure 5.1.1-44).

After reaching the minimum, the reactor core barrel level increased slowly as injection flow became slightly greater than the break flow due to the decreasing RCS pressure (Figure 5.1.1-15). The level in the core barrel increased to []^{a,b,c} at []^{a,b,c} which was still about []^{a,b,c} below the hot-leg nozzles. The ADS-1 valve opened at []^{a,b,c} causing an increased rate of RCS depressurization (Figure 5.1.1-45) and an additional flow path out of the RCS. This, in turn, caused the following to occur: the level in the reactor vessel downcomer dropped rapidly to []^{a,b,c} at []^{a,b,c} and then began another slow recovery, and the level in the core barrel rose rapidly to []^{a,b,c} at []^{a,b,c} and then began another slow increase. These rapid level changes are attributed to the decreased pressure in the hot-leg area after the ADS-1 valve opened, causing an increased flow out of the reactor vessel to the pressurizer and also increased steam percent and, therefore, swell in the core barrel.

From []^{a,b,c} there was reverse flow from the upper head, through the core bypass holes, and into the upper downcomer region (Figure 5.1.1-19). This flow then rapidly returned to 0, which again was an effect of the ADS-1 valve opening. The upper head area then essentially became stagnated until about []^{a,b,c}. During this stagnant period, upper head and upper downcomer thermocouples indicated that superheating occurred in those areas (Figures 5.1.1-46 and 5.1.1-47). The superheating could have been the result of both the reduction in pressure and radiant heating from the hotter vessel wall metal.

At []^{a,b,c} test personnel heard a loud "bang" in the upper portion of the reactor vessel. The test personnel were located on the grating at the top of the reactor vessel and, therefore, were able to pinpoint the location of the noise. Later investigation determined that the "bang" was the result of a condensation/depressurization event in the upper downcomer area, causing the downcomer water level to rise very rapidly and hit the core barrel flange, resulting in the noise. The sharp increase of DP-114 to []^{a,b,c} at []^{a,b,c} DP-130 to []^{a,b,c} at []^{a,b,c} and the over-ranging of LDP-116 and LDP-140 at []^{a,b,c} are major indications of the steam

condensation event (Figures 5.1.1-19 and 5.1.1-15). This and other similar events have been investigated (see Subsection 7.1). The conclusion is that the forces resulting from these condensation/depressurization events were not sufficient to cause any facility damage.

At []^{a,b,c} after accumulator injection had been completed and only CMT injection was available to replace lost RCS inventory, the core barrel level again began to slowly decrease. At []^{a,b,c} ADS-4 actuated, providing two additional depressurization paths and decreasing RCS pressure to near atmospheric. The decreasing reactor core barrel level continued until about []^{a,b,c} when the CMTs were essentially empty and IRWST flow began to increase RCS makeup to a rate slightly greater than the losses, thereby causing a slow increase in reactor vessel levels. Minimum indicated levels reached during this period were approximately []^{a,b,c} in the core barrel and []^{a,b,c} in the downcomer (Figures 5.1.1-12, 5.1.1-15, and 5.1.1-17).

As RCS pressure decreased, IRWST injection rate increased to about []^{a,b,c} per side (Figure 5.1.1-48), which in turn raised reactor vessel levels to the highest they would attain during this test. The downcomer level instruments over-ranged at about []^{a,b,c}. At this same time, core barrel level equaled downcomer level, and the two levels remained together at []^{a,b,c} for about the next []^{a,b,c} and then increased slightly and returned to about []^{a,b,c} at about []^{a,b,c} (Figures 5.1.1-15 and 5.1.1-22).

While the reactor vessel levels increased, the upper head differential pressures again indicated steam flowing from the core barrel, through the head, and into the downcomer region. Flow stopped at about the same time that the downcomer level instruments, LDP-116 and LDP-140, over-ranged. The flow started again when reactor vessel levels dropped back down to about []^{a,b,c} at []^{a,b,c} and continued throughout the remainder of the test (Figures 5.1.1-22 and 5.1.1-49). Based on reactor vessel level effects on the flow through the core bypass holes, it can be observed that whenever the cold legs are partially to fully uncovered, there is flow; whenever the downcomer level covers the cold legs, the flow is stopped and the steam in the upper head becomes stagnant.

Reactor performance for the remainder of the test remained essentially unchanged until the primary sump injection valves opened at []^{a,b,c} when the reactor vessel levels dropped to about []^{a,b,c} and remained there until test termination.

Core Makeup Tanks

Thermal-hydraulic responses of the two CMTs were very similar throughout the performance of Matrix Test SB01. Although their responses with respect to time were different, data representing CMT-1's response are presented in this subsection, with CMT-2 times in parentheses. Where the difference in actual response is noteworthy, CMT-2 data are also addressed.

The CMTs were filled and vented with ambient temperature water prior to the initiation of facility startup and heatup for the performance of the test. The CMT balance line isolation valves were in the

AUTO and OPEN positions, and the CMT discharge isolation valves were in the AUTO and CLOSED positions. This alignment prevented flow through the CMTs, thus allowing them to remain at ambient temperature while being pressurized with the RCS during the facility startup. The CMT piping is shown in Dwg. OSU 600206, and CMT instrumentation is shown in Dwg. OSU 600501 and Dwg. OSU 600502. These drawings can be found in Appendix G.

RCP-forced flow through the CMTs to the DVI nozzles began immediately when the CMT discharge valves opened at []^{a,b,c} (Figure 5.1.1-16). Then, []^{a,b,c} later, they continued to inject due to natural circulation flow from the cold legs through the CMTs and into the DVI nozzles when the RCPs were tripped by the PLC signal. The natural circulation continued until the CMTs began to drain at []^{a,b,c} ([]^{a,b,c}) as determined by a decreasing balance line level. At []^{a,b,c} ([]^{a,b,c}), CMT wide-range level began to decrease (Figure 5.1.1-6). From that point on, all CMT injection was due to gravity and the manometer effect of colder, more dense water at a higher relative level in the CMTs, since the RCS and the CMTs were affected by the same overpressure from the steam in the facility.

At about []^{a,b,c} a condensation/depressurization event took place in CMT-1. The data indicate a rapid refill of the CMT-1 balance line with an increase of about []^{a,b,c} in tank level once the balance line filled (Figure 5.1.1-77). Other indications of the event were an []^{a,b,c} spike decrease in CMT-1 pressure, which resulted in about a []^{a,b,c} decrease in reactor upper head and CL-3 pressures (Figure 5.1.1-78). The CMT-1 inlet line and upper tank temperatures provided additional confirmation that a condensation/depressurization event occurred (Figures 5.1.1-79 and 5.1.1-80). This refill of CMT-1 probably caused some delay in the ADS 1-3 valve opening sequence. Condensation/depressurization events are described more thoroughly in Subsection 7.1.

At []^{a,b,c} ([]^{a,b,c}), RCS pressure was sufficiently low, about []^{a,b,c} that accumulator injection began. The ADS-1 valve opened at []^{a,b,c} and caused a rapid decrease in RCS pressure. RCS depressurization, coupled with the pressurized nitrogen gas-assisted accumulator injection, resulted in backpressure against the CMT discharge check valves, caused CMT-1 injection flow to decrease, then drop to essentially 0 at about []^{a,b,c} and remain there until ACC-1 injection was completed at []^{a,b,c}. During this same time frame, CMT-2 injection flow also decreased, then dropped to about []^{a,b,c} and remained at that rate until ACC-2 injection was completed at []^{a,b,c} (Figure 5.1.1-16).

At the same time that the CMT injection flows were tapering off with the CMTs at about the []^{a,b,c} level (or two-thirds full), with RCS pressure and, therefore, saturation temperature decreasing fairly rapidly, the steam space at the top of the CMTs became superheated primarily due to the pressure decrease and radiant heating from the hot CMT wall metal (Figures 5.1.1-50 and 5.1.1-51). The CMT steam space remained superheated, but at a slowly diminishing level of superheat until the CMT reflooded at []^{a,b,c} ([]^{a,b,c}), when subcooled fluid entered the CMT and cooled it (Figures 5.1.1-32 and 5.1.1-33). CMT temperature response is discussed more thoroughly in Subsection 7.2.

When accumulator injection was complete for each side, CMT injection was restored at a rate of []^{a,b,c} per side. Injection continued at a slowly diminishing rate down to about []^{a,b,c} when the CMTs emptied at []^{a,b,c} ([]^{a,b,c} Figure 5.1.1-16). As the levels came down, the fluid was displaced by superheated steam, caused by the decreasing pressure and hot CMT wall metal.

The balance line levels oscillated around zero during the period when the accumulators were injecting, but then began to indicate a level of []^{a,b,c} and stayed constant until they started to refill at about []^{a,b,c}. This same level indication would be repeated again later in the test after the second draining of the CMTs and continue for the duration of the test. The effects of a level differential pressure transmitter acting as a flow differential pressure transmitter probably was not the cause, since the amount of steam flow required to initiate that effect would be sufficient to cool the CMTs, resulting in condensation of the steam and a rising fluid level. Also, based on reactor vessel downcomer and cold-leg levels (Figures 5.1.1-15 and 5.1.1-52) and cold-leg temperature indications in the superheated region (Figures 5.1.1-53 and 5.1.1-54), the cold legs were not liquid solid and therefore could not support a column of fluid in the balance lines. A logical explanation for the continuous balance line level indication is that the level transmitter reference legs were not completely filled, causing an erroneous level indication.

Both CMT balance lines began to refill at about []^{a,b,c} when reactor vessel level, indicated by LDP-140, was sufficiently high at []^{a,b,c} to cover and refill the cold legs (Figures 5.1.1-30 and 5.1.1-31). At about []^{a,b,c} when the CMT-2 balance line had refilled completely, CMT-2 began to rapidly refill and in about []^{a,b,c} was at the []^{a,b,c} level, or about two-thirds full. The refill with subcooled fluid caused a condensation/depressurization event to occur in CMT-2. This was reflected in the reactor vessel pressure and levels and CMT balance line level taking a sharp dip and then recovering. CMT-2's refilling also caused its internal temperatures to decrease quickly from the superheated to subcooled region at less than []^{a,b,c} and to remain subcooled until the CMT drained again (Figure 5.1.1-32). When the CMT-1 balance line refilled completely at approximately []^{a,b,c} CMT-1 refilled to the []^{a,b,c} level, or about two-thirds full in less than []^{a,b,c}. Again, the rapid refill with subcooled fluid caused another condensation/depressurization event to occur, this time in CMT-1. The CMT-1 internal temperatures responded to the subcooled fluid almost identically to those of CMT-2 (Figure 5.1.1-33). The CMTs appear to have reached a level and temperature equilibrium where steam condensation and a resultant level increase were no longer taking place. Another possibility for the CMTs not refilling completely is that some of the nitrogen from the accumulators may have collected in the CMTs. During this time, there was no injection flow from the CMTs due to the higher static head of the IRWST holding the CMT discharge line check valves closed.

When the CMT balance lines began to refill, CMT internal pressures began to decrease with respect to the reactor vessel upper head pressure. It is possible that pressure decreased because once the cold legs filled with subcooled fluid, displacing what had been a blanket of superheated steam, the superheated steam in the CMTs began to slowly condense in the balance lines, thus filling them over a

period of about []^{a,b,c} Once the balance lines filled and overflowed into the CMTs, the subcooled fluid sprayed through the inlet diffuser and collapsed the superheated steam bubble in the CMTs, causing more depressurization and the subsequent in-rush of fluid from the RCS that was reflected in the decrease in reactor vessel levels and pressure.

Both CMTs remained at essentially constant levels for several thousand seconds, and then they began slow draindowns at about []^{a,b,c} respectively. The draindown for both CMTs was slow and did not occur until IRWST relative level was []^{a,b,c} below that of the CMTs (Figure 5.1.1-34). Data indicate that the CMTs drained for some time, and then the differential head between the IRWST and the CMTs closed the CMT discharge check valves, terminating the draining until such time as the differential shifted the other way and draining recommenced. Both CMTs were completely empty at about []^{a,b,c} which coincides closely with the primary sump injection valve opening at []^{a,b,c} A possible correlation for the coincidence is that when the primary sump valve opened, the IRWST had just reached its minimum of about []^{a,b,c} which is about []^{a,b,c} below the instrumented level for the CMTs, and that there was still a slight negative pressure remaining in the CMTs. Also, when the primary sump injection valves opened, there was a short time period in which the IRWST and primary sump levels equalized, causing a decrease in RCS fluid levels and resulting in a rather rapid drop in CMT levels from about []^{a,b,c}

Accumulators

Prior to test initiation, the accumulators were filled with ambient temperature fluid to an internal standpipe level, which ensures that they are filled to the same level for each test. They were then pressurized to []^{a,b,c} with nitrogen and placed in service by the accumulator discharge valves being opened once the RCS was at normal operating temperature and pressure. The accumulators represent a pure passive system that injects fluid through the DVI nozzles to reflood the reactor vessel once RCS pressure has dropped below accumulator pressure. The piping is shown in Dwg. OSU 600206 (Appendix G).

ACC-2 injection started at []^{a,b,c} and ACC-1 at []^{a,b,c} (Figure 5.1.1-16). Since RCS pressure and, therefore, CMT overpressure were less than accumulator pressure, the accumulators' injection virtually shut off CMT injection by creating a backpressure against the CMT discharge check valves. The accumulators injected at approximately []^{a,b,c} per tank, resulting in about a []^{a,b,c} increase in the reactor vessel levels. Injection continued at that rate until []^{a,b,c} for ACC-1 and []^{a,b,c} for ACC-2. The completion of accumulator injection and subsequent resumption of CMT injection resulted in a reactor vessel core barrel level decrease of about []^{a,b,c} and a virtual stabilization of downcomer levels.

Later in the OSU test program, it was discovered that when the accumulators were pressurized, the indicated level on the DAS increased several inches. The problem was the bourdon tube local pressure instruments, PI-401 and PI-402, were tubed to the bottom of the accumulator level differential pressure instrument reference leg tubing. As pressure increased during the final preparations for the

test, the reference legs were compressed into the pressure indicators, resulting in the indicated level increase. By re-routing the pressure indicator tubing to the top of the level differential pressure instrument reference legs, accumulator pressurization no longer had an effect on indicated level. The true starting level for the accumulators should be []^{a,b,c} for ACC-1 and []^{a,b,c} for ACC-2. For this test, the starting levels on the DAS were []^{a,b,c} for ACC-1 (LDP-401) and []^{a,b,c} for ACC-2 (LDP-402). However, due to the accumulators being filled to their standpipe levels, the correct critical levels were obtained.

Pressurizer

The pressurizer level at test initiation was []^{a,b,c} (uncompensated), and the pressure was []^{a,b,c} with pressure control in automatic. The PLC was programmed to adjust the pressurizer heater demand to 0 at 5.6 seconds. When the break valve opened, the initial depressurization caused heater output to go to maximum, and at 5.6 seconds, heater power decreased to about []^{a,b,c} as opposed to 0 kW per design (Figure 5.1.1-24). At []^{a,b,c} heater output increased to about []^{a,b,c} and remained there for the duration of the test. It can be postulated that the heater SCR control circuitry was not properly tuned. In subsequent tests, the heater breaker was manually opened several seconds after the S signal. Later in the test program, PLC logic was changed to open the heater contractor for positive de-energization at 5.6 seconds. The pressurizer connections to the other components in the facility are shown in Dwg. OSU 600203 (Appendix G).

When the break valve opened, pressurizer level immediately started to decrease, and the pressurizer was empty at []^{a,b,c} (Figure 5.1.1-5). The pressurizer surge line was empty at []^{a,b,c}. It is believed that the steam environment and the fairly low heater power were sufficient to maintain the pressurizer heater sheath temperatures at saturation temperature when the pressurizer was empty (Figure 5.1.1-21).

The pressurizer and surge line remained empty until the ADS-1 valve opened at []^{a,b,c} at which time test data indicate that they began to reflood at the same time. The ADS-2 valve opened at []^{a,b,c} causing flow rate through the surge line and pressurizer to increase even more (Figure 5.1.1-55). When the ADS-3 valve opened at []^{a,b,c} it had little or no effect on the rate of depressurization. The data indicate two-phase flow through the surge line and pressurizer to the IRWST. This created significant pressure drops through each component that may have influenced the level instruments (Figure 5.1.1-5).

At about []^{a,b,c} HL-2 elbow level and calculated steam percent data indicate that it was full (Figures 5.1.1-56 and 5.1.1-57). The surge line data indicate that within several seconds, it also had filled and that the pressurizer had started to reflood at about []^{a,b,c} (Figures 5.1.1-58 and 5.1.1-59).

During the period of accumulator injection between []^{a,b,c} makeup to the RCS was approximately double the losses through ADS 1-3 and the break (Figures 5.1.1-60, 5.1.1-61, and

5.1.1-62). The increasing inventory raised system fluid levels and when the hot legs filled caused reactor and pressurizer pressures to diverge. The reactor pressure was greater (Figure 5.1.1-63). This pressure differential was the force that pushed low steam percent fluid into the surge line and pressurizer.

ADS 1-3 separator steam flow went to 0 at []^{a,b,c} which was a good indication of low steam percent fluid entering the separator (Figure 5.1.1-61). ACC-1 and ACC-2 were essentially empty at []^{a,b,c} and []^{a,b,c} respectively (Figure 5.1.1-64), leaving only CMT injection in progress. RCS inventory began to decrease again.

ADS 1-3 separator level went above normal at []^{a,b,c} (Figure 5.1.1-65), and its loop seal flow began to increase (Figure 5.1.1-61), confirming that low steam percent fluid was being pushed through ADS 1-3. Another good indication of low steam percent fluid being lost through ADS 1-3 was that ADS 1-3 flow differential pressure instruments (Figure 5.1.1-55) oscillated around zero while the separator level increased.

The pressurizer attained its maximum fluid level/minimum steam percent at []^{a,b,c} and almost immediately the level started to decrease rapidly (Figures 5.1.1-58 and 5.1.1-59). This decrease rate is believed to be the result of two occurrences. First, the pressurizer was gravity-draining to the RCS to make up for a decreasing inventory in the RCS. Second, the constantly decreasing pressurizer pressure and the heaters still being powered at []^{a,b,c} was causing the percent steam to increase, thereby pushing more fluid into the ADS 1-3 separator and on to the IRWST.

At []^{a,b,c} the ADS 1-3 separator reached its maximum level and maximum loop seal flow of []^{a,b,c} (Figures 5.1.1-65 and 5.1.1-61). By []^{a,b,c} it returned to normal level, and flow was significantly lower. The rate of pressurizer level decrease/steam percent increase decreased at about that same time, since the method of inventory movement out was by gravity to the RCS. What appears to be noise on the pressurizer level data during this period is believed to be caused by the flashing of liquid to steam to keep the pressurizer at saturation pressure.

When the ADS-4 valves opened, the ADS 1-3 separator liquid flow decreased to 0 at []^{a,b,c}. The pressurizer level continued to decrease by gravity until it was empty at []^{a,b,c}. The reactor and pressurizer pressures converged to be essentially equal at []^{a,b,c} and then started to diverge when the surge line again began to refill.

At []^{a,b,c} with RCS levels approaching their maximum, the surge line began to refill. When it was full at []^{a,b,c} the pressurizer began to reflood. Coincident with the pressurizer reflooding, the ADS 1-3 separator and ADS 1-3 sparger pressures went negative by as much as []^{a,b,c} further enhancing the level rise in the pressurizer (Figure 5.1.1-29). The negative pressure was caused by the level in the pressurizer, the ADS 1-3 sparger nozzles being submerged, and condensation due to cooling of the components in between. The pressurizer reflood this time can be confirmed by HL-2, pressurizer, and surge line temperatures being subcooled

(Figures 5.1.1-14 and 5.1.1-27). In addition, the surge line completely filled first, followed by a level rise in the pressurizer. The negative pressure problem was corrected for subsequent tests by installation of a vacuum breaker on the sparger line inside the IRWST.

The pressurizer filled to a maximum of []^{a,b,c} at []^{a,b,c} and immediately began a rapid decrease to empty at []^{a,b,c} (Figure 5.1.1-5). The rapid decrease in level was coincident with IRWST level dropping below the sparger nozzles and breaking the vacuum. The rapid decrease in pressurizer level also caused an increase in reactor vessel levels until they regained equilibrium with the rest of the system (Figure 5.1.1-22). For the remainder of the test, the pressurizer remained empty. Surge line level started to decrease at []^{a,b,c} to about []^{a,b,c} where it remained until []^{a,b,c}. The level again decreased to about []^{a,b,c} at []^{a,b,c} and then oscillated between []^{a,b,c} for the remainder of the test.

Passive Residual Heat Removal Heat Exchanger

The PRHR HX was filled and vented with the rest of the system and then isolated by closing its outlet valve prior to the facility startup and heatup. Prior to test initiation, the outlet valve was placed in auto so that it would open as programmed by the PLC after the S signal. This maintained the fluid temperature in the HX equal to the IRWST temperature of []^{a,b,c} at test initiation. The PRHR HX inlet is piped from the ADS 4-2 line, which is attached to HL-2, and the outlet ties into the SG-2 outlet channel head, which is connected to CL-2 and CL-4 (Dwg. OSU 600203 and OSU 600206). The thermocouple arrangement is shown in Dwg. OSU 600701. These drawings can be found in Appendix G.

Two minutes after the TEST pushbutton was pressed, the break valve opened (time zero). At 6 seconds, the PRHR HX outlet valve received its signal from the PLC to open. The RCPs were still running, so the initial flow through the PRHR HX was forced flow. Flow became solely natural circulation flow []^{a,b,c} later, when the RCPs were stopped by an automatic signal from the PLC. The inlet flow rose from 0 to about []^{a,b,c} and the outlet flow rose from 0 to about []^{a,b,c} at []^{a,b,c} (Figure 5.1.1-66). At the same time, the temperature difference between the inlet and outlet of the HX began to increase and was []^{a,b,c} at []^{a,b,c} (Figure 5.1.1-40). The difference between inlet and outlet flows could be attributed to the density difference of the fluid and inlet flow, FMM-802, response to two-phase flow.

In the early stages of the transient, the HX instrumented long- and short-tube fluid temperatures generally remained below []^{a,b,c} with the short tube predominantly hotter and maintaining a wider delta temperature. This difference between long- and short-tube performance is evident until about []^{a,b,c} when the short-tube temperatures rapidly dropped and aligned with the long-tube temperatures (Figure 5.1.1-41). The drop in temperature did not coincide with any other event and is believed to be a flow stoppage through the PRHR HX; the indicated delta temperature was the result of the temperature gradient in the IRWST fluid. Stoppage of flow is confirmed by CL-2 and CL-4 data which show that the temperatures at the bottom of the reactor flange for both loops began

to increase around this same time, followed saturation temperature for about []^{a,b,c} went into the superheated region for about []^{a,b,c} and then became subcooled when the cold legs started refilling at about []^{a,b,c} (Figures 5.1.1-42 and 5.1.1-43).

The PRHR HX inlet temperature became subcooled coincident with the ADS-4 valves opening at []^{a,b,c} and over the next []^{a,b,c} dropped to and followed the outlet temperature. This was again an indication that there was no flow through the HX during this time frame (Figures 5.1.1-40). At []^{a,b,c} the PRHR HX inlet temperature instantly jumped from []^{a,b,c} to saturation temperature. This happened about []^{a,b,c} after pressure, level, and flow oscillations began in the facility and is believed to be caused by the inlet line "burping," allowing the line to fill with saturated steam. Following this occurrence, all of the PRHR temperatures began to slowly approach saturation.

The PRHR HX remained full until []^{a,b,c} and then began to decrease to about []^{a,b,c} indicated level at []^{a,b,c} which was the lowest level that would be encountered during this test. A level of []^{a,b,c} was maintained during most of the test (Figure 5.1.1-67). The PRHR HX wide-range level data indicate that the HX was partially filled between about []^{a,b,c} (Figure 5.1.1-68). An explanation for this occurrence is that during the long period without flow through the HX and with the RCS loops full, the cooldown of the HX and associated piping caused it to go into a negative pressure, thereby drawing fluid up into it. There was insufficient instrumentation installed on the HX to verify this. The effects of condensation events in the CMTs were reflected in the level changes at about []^{a,b,c}

When RCS levels began to decrease at about []^{a,b,c} the PRHR HX level also began to decrease and was back to its minimum indicated level of about []^{a,b,c} by []^{a,b,c}. The level oscillations from about []^{a,b,c} until the PRHR HX reached its minimum are believed to be a result of the overall facility oscillations as described in the *Test Analysis Report*.⁽²⁾ Review of the data does not reveal that flow was ever re-established through the HX during the remainder of the test.

Steam Generators

The SG primary sides were filled and vented with the RCS. The secondary sides were also filled prior to facility startup and heatup. Prior to test initiation, the SG levels were established at []^{a,b,c} on the narrow-range instruments with the feedwater pump and feedwater control valves in AUTO. The steam pressure controller was also placed in AUTO to control secondary-side pressure at []^{a,b,c}. Coincident with the S signal being generated at 0.5 second, the steam pressure controller's setpoint was reset to []^{a,b,c} which was high enough so that the control valve would remain closed yet low enough that it would not challenge the SG safety valves. At 4 seconds, the PLC signaled the feedwater pump to trip and the feedwater control valves to close, essentially bottling up the SGs to minimize any cooldown of the RCS. The SGs are shown in Dwg. OSU 600002 and OSU 600203, and SG instrumentation is shown in Dwg. OSU 600301. (These drawings can be found in Appendix G.)

The SGs initially absorbed some heat from the RCS, and their secondary pressure increased to a maximum of []^{a,b,c} at []^{a,b,c} (Figure 5.1.1-45). The pressure then stayed fairly constant until []^{a,b,c} when secondary pressure and primary pressure were essentially equal. Secondary pressure then followed primary pressure until about []^{a,b,c} at which time the SGs started transferring heat to the RCS. Following this time, the SG secondary-side pressure decay was dictated only by SG heat losses to the RCS and to ambient conditions. At the end of the test, they were at about []^{a,b,c}.

On the primary side, the SG-2 tubes began to drain at about []^{a,b,c} and SG-1 tubes began to drain at about []^{a,b,c} (Figures 5.1.1-8 and 5.1.1-7). Between []^{a,b,c} the SG-1 U-tubes were completely empty; between []^{a,b,c} the SG-2 U-tubes were completely empty. The delay in SG-2 could be caused by the effects of PRHR HX flow entering the outlet channel head, reducing the steam expansion rate in the U-tubes. The SG level data then indicate that the tubes began to refill after about 1 minute and return to their original level. It is possible that this apparent refill indication is the result of the vaporization of level instrument reference legs, which are routed internal to the SG tube bundle. This phenomenon is treated separately in Section 2.4.

Cold Legs and Hot Legs

Due to the totally different responses between the cold legs and the hot legs, they are addressed separately here. The loop components, piping, and instrumentation are depicted in Dwg. OSU 600203 (Appendix G).

The cold legs began to drain at about []^{a,b,c} when the level in the reactor vessel downcomer dropped below the tops of their nozzles (Figure 5.1.1-15). When the nozzles started to uncover, the nozzle thermocouple temperatures located at the top of the nozzle flanges quickly rose into the superheated region (Figures 5.1.1-42, 5.1.1-43, 5.1.1-53, and 5.1.1-54). At []^{a,b,c} a condensation/depressurization event took place which rapidly refilled and then partially redrained the cold legs. This can be seen on the cold-leg temperature plots as a sharp drop into the subcooled region with a quick return to superheat.

The temperature data from the CL-3 reactor vessel nozzle flange bottom thermocouple show that temperature oscillated between subcooled and superheated conditions following the ADS-1 valve opening at []^{a,b,c}. Then, at about []^{a,b,c} data indicate superheat, remaining in the superheat region until []^{a,b,c} when the RCS regained enough inventory from IRWST injection to start refilling the cold legs. It is possible that the break location, at the bottom of CL-3, placed it at a slightly lower pressure than the other cold legs and allowed the small amount of liquid in the bottom of the pipe to flash to steam, resulting in this phenomenon. During the period of about []^{a,b,c} which coincides with CL-3 being empty, there was no indicated flow through the break (Figure 5.1.1-28).

Temperature plots indicate that the other three cold-leg reactor vessel nozzle flange bottom thermocouples did not superheat until between []^{a,b,c} indicating that they were not totally empty until then. All four cold-leg bottom thermocouples became subcooled at the same time, indicating that the legs were refilling. The four cold legs were completely filled with liquid between about []^{a,b,c} when the data show that their top thermocouples became subcooled and stayed filled until approximately the time that primary sump injection began and all the cold-leg thermocouple temperatures went to saturation temperature. The temperatures remained at saturation for the duration of the test, and the legs were possibly filled with a two-phase mixture.

It is believed that the method by which cold legs become superheated is that a saturated two-phase mixture moves from the heater bundle area of the reactor through the hot legs and into the SGs, where it is superheated. The superheated steam then flows back to the reactor vessel downcomer through the cold legs. During the period that the cold legs were superheated, there was a negative differential pressure across the reactor vessel upper support plate and across the core barrel flange bypass holes. This means that the reactor vessel downcomer/cold legs were at a lower pressure than the core barrel/hot legs, which created the differential required to cause steam to flow through the SG U-tubes and become superheated (Figure 5.1.1-19).

The hot legs followed the saturation curve throughout the test, except for a few instances that will be discussed here (Figures 5.1.1-13, 5.1.1-14, and 5.1.1-15). The HL-2 thermocouple, located in the elbow at the SG, data show that the elbow became at least partially empty between []^{a,b,c} and the steam volume was superheated by the massive heat source of the SG. Both hot-leg reactor vessel nozzle flange temperatures indicated subcooling between about []^{a,b,c} coincident with the period that reactor vessel full range level (LDP-127) showed that the hot legs were submerged (Figure 5.1.1-15). The reactor vessel level decreased at about []^{a,b,c} resulting in at least partial uncovering of the hot legs and the subsequent return to saturation temperatures.

Temperatures remained at saturation until about []^{a,b,c} when reactor vessel levels again increased and refilled the hot legs with subcooled liquid. The hot legs remained subcooled until about []^{a,b,c} when the reactor vessel level again decreased. The hot legs partially voided and thus allowed saturated steam to enter from the reactor upper plenum area. Hot-leg temperatures stayed at saturation for the remainder of the test.

It is believed that the hot legs, even though partially or completely empty during the test, remained at saturation temperature and never superheated due to a small flow of saturated steam from the reactor core to the SGs, which kept the piping at saturation temperature. This steam could take several paths on the HL-2 side: it could flow to the PRHR HX; it could flow to the pressurizer through the surge line; it could flow to the SG, where it would be superheated by the secondary side; or it could flow to the ADS 4-2 system once ADS-4 actuation had taken place. On the HL-1 side of the facility, it could only flow to the ADS 4-1 system or to the SG.

In-Containment Refueling Water Storage Tank

Prior to test initiation, the IRWST was emptied, load cell transmitter LCT-701 zeroed, and the tank filled to the overflow with ambient temperature water. It was then drained to the level of the fill nozzle, which was the level set during pre-operational testing. The initial tank conditions were [] of liquid, []^{a,b,c} liquid level, and []^{a,b,c} liquid temperature. The IRWST injection valves were closed and in AUTO. Dwg. OSU 600206 shows how the IRWST is connected in the facility. Dwg. OSU 600701 depicts relative locations of the instrumentation. These drawings can be found in Appendix G.

The break valve opened at 0 second, and the resultant break flow into the break separator caused a spike pressure increase in the break separator to []^{a,b,c} and a subsequent backpressure spike in the IRWST of []^{a,b,c}. It did not result in a pressure spike in the primary sump, thereby creating a differential pressure between the IRWST and the primary sump that lasted until about []^{a,b,c}. This differential pressure could have been a result of the tank free volumes and size of the vent pipes connecting to the BAMS header. That is, the IRWST was full of liquid to the fill nozzle, and the sumps were empty; the IRWST has a []^{a,b,c} vent, and the two sumps share one []^{a,b,c} vent piped to the BAMS header. The differential pressure caused a small overflow indication (FMM-703) from the IRWST to the primary sump for approximately []^{a,b,c}. This was not a real overflow but, rather, fluid from the IRWST overflow loop seal being pushed into the sump (Figure 5.1.1-69). This can be confirmed by the fact that there was no change in IRWST level during this period (Figure 5.1.1-26).

The IRWST thermocouples located at or above the initial fluid level almost immediately following the opening of the break valve began to indicate an increasing temperature (Figures 5.1.1-70, 5.1.1-71, 5.1.1-72 and Dwg. OSU 600701, Appendix G). The increase is due to a small backflow of steam from the BAMS header into the IRWST vapor space.

The ADS 1-3 separator, associated automatic valves, and piping were discussed extensively in the Pressurizer Response description in this section; therefore, only those aspects that directly affect IRWST response will be discussed here.

The piping from the ADS 1-3 valves, including the separator and where the separator steam and liquid out piping join, is heat-traced and therefore elevated in temperature prior to test start. The ADS-1 valve opened at []^{a,b,c} initiating two-phase flow from the RCS through the pressurizer, ADS 1-3 separator, and the ADS 1-3 sparger into the fluid volume of the IRWST. There was an immediate rise in sparger tip temperature, indicated by TF-719, followed by a rapid rise in long-rod temperature TF-706 located on the long rod about []^{a,b,c} below the sparger nozzles, and a slower rise in TF-705, also located on the long rod but an additional []^{a,b,c} down, when the ADS-2 valve opened at []^{a,b,c} (Figures 5.1.1-70 and 5.1.1-72). The initial effects on TF-706 and TF-705 were due to their close proximity to the sparger nozzles.

When the ADS 1-3 valves opened and added inventory to the IRWST prior to IRWST injection, the level increased to tank overflow (Figure 5.1.1-26), causing overflow to the primary sump from about []^{a,b,c} (Figure 5.1.1-25). The cessation of overflow came within []^{a,b,c} of the beginning of IRWST injection to the DVI nozzles.

ADS 1-3 flow rate to the IRWST peaked at about []^{a,b,c} (Figure 5.1.1-61), which is coincident with the peak temperature seen at TF-719, located at the tip of the sparger nozzle (Figure 5.1.1-70). The nozzle temperature then decreased from about []^{a,b,c} over the next []^{a,b,c} coincident with the ADS 1-3 separator flow decrease from its peak to 0 at []^{a,b,c}. For the remainder of this test, there was no discernable flow from ADS 1-3 into the IRWST, and temperatures remained essentially constant until IRWST injection began to drop the fluid level in the tank.

Reactor vessel pressure (Figure 5.1.1-45) decreased to []^{a,b,c} its low-low pressure setpoint, at []^{a,b,c} and sent a signal to the PLC to automatically open the IRWST injection valves. Injection from the IRWST did not begin at this time, since RCS pressure was significantly higher than the IRWST static head. When the ADS 4-1 and ADS 4-2 valves opened at []^{a,b,c} providing two additional depressurization paths for the RCS, RCS pressure dropped to just below []^{a,b,c} allowing IRWST injection to start on the no. 2 side at []^{a,b,c} and on the no. 1 side at []^{a,b,c} (Figure 5.1.1-37). IRWST injection increased slowly to its maximum for this test of []^{a,b,c} per side at about []^{a,b,c} and then the rate slowly decreased over time as the tank static head decreased.

As IRWST injection continued and the tank level decreased, the long-rod thermocouple temperatures rose very slowly. At the time of switchover to primary sump injection/recirculation mode, none were above []^{a,b,c}. When they uncovered, their temperatures rose but still maintained a gradient with the warmest at the top and the coolest at the bottom. This is believed to be the result of no mixing, since there was no discernable ADS 1-3 flow into the tank after about []^{a,b,c}, and there would also be a temperature gradient in the tank wall with the warmest at the top due to the rather slow gravity draindown.

At the time primary sump injection started through the check valves, the IRWST injection flow rate was approximately []^{a,b,c} per side. The flow then split at approximately []^{a,b,c} per side from the IRWST and []^{a,b,c} per side from the primary sump. When the primary sump injection valves opened, the IRWST-2 side flow increased to approximately []^{a,b,c}, the IRWST-1 side flow indication went negative, the primary sump-1 flow increased to approximately []^{a,b,c} and primary sump-2 flow decreased to approximately []^{a,b,c}. These are true indications of what was happening. A portion of the primary sump-1 flow was diverted to the IRWST, and only about []^{a,b,c} flowed to the DVI nozzle. On the no. 2 side, the total flow to the DVI nozzle was the sum of the IRWST and primary sump injection flows on that side (Figure 5.1.1-37). The IRWST and primary sump flows remained essentially constant for the remainder of the test. This flow pattern is

most probably due to larger diameter piping from the IRWST to the primary sump connection on the DVI manifold on the no. 1 side ([]^{a,b,c} I.D. versus []^{a,b,c} I.D.).

Around []^{a,b,c} all of the IRWST temperatures increased, and some of the upper thermocouples reached saturation. This increase is believed to be due to the hotter primary sump fluid that was being injected into it through its no. 1 side injection line.

Break and ADS Measurement System

For the test initial conditions, the BAMS steam header was lined up so that the break separator steam flow would be directed through its 6-in. vent line and all BAMS header steam would be released through the 6-in. line containing valve CSS-901 and steam flow vortex meter FVM-901. The valves in the header were all positioned with their controls in manual. The primary sump []^{a,b,c} vent line was not installed for this test. The break separator, the ADS 4-1 and ADS 4-2 separators, and the ADS 1-3 separator loop seal liquid line were all heat-traced with their temperature controls set to maintain []^{a,b,c}. The loop seal liquid lines for the break separator and the ADS 4-1 and ADS 4-2 separators were not heat-traced. All of the steam piping and the ADS 1-3 separator were heat-traced with their temperature controls set to maintain []^{a,b,c}. The loop seals for all four separators were filled with []^{a,b,c} fluid from the condensate return system just prior to test initiation. The BAMS is shown in Dwg. OSU 600901 (Appendix G).

Almost instantly when the break valve opened, break separator pressure started to increase with a peak pressure of about []^{a,b,c} at []^{a,b,c}. All of the other components in the BAMS exhibited delayed and similar, but smaller peaks, as the result of backpressures created from the header with the exception of the primary sump (Figure 5.1.1-73). This is believed to be due to the relative sizes of components vent piping with the primary sump having the smallest vent pipe at []^{a,b,c}. Even with the RCS at steady-state conditions between []^{a,b,c} the BAMS component pressures all agreed within about 1 psig, which can be considered well within allowable instrument errors (Figures 5.1.1-74 and 5.1.1-74x).

When the break valve opened, data indicate that the break separator level dropped to a low of []^{a,b,c} at [] and then recovered right back to normal level at []^{a,b,c} (Figure 5.1.1.26). The reference leg for break separator level instrument LDP-905 is installed on the side of the tank and near the top, and the variable leg is connected to the vertical section of the loop seal leaving the separator. This type of installation, combined with the fact that the level transient was completed within []^{a,b,c} makes it very likely that the data reflect the dynamic effects of flow rather than a real level transient. All of the ADS separators experience this same type of initial response when their associated depressurization valves open.

The break separator and BAMS header steam flows are shown on Figure 5.1.1-75 and the break separator loop seal flow on Figure 5.1.1-28. It can be seen that both steam and liquid flow began immediately following the break valve opening with steam flow out of the system essentially stopped

at []^{a,b,c}. The loop seal liquid flow peaked at []^{a,b,c} at []^{a,b,c} and continued at a decreasing rate until it went to 0 at []^{a,b,c} when the ADS 4-1 and ADS 4-2 valves opened and the cold legs began to approach saturation temperature and were emptying. The data indicates that loop seal flow resumed at []^{a,b,c} which is coincident with the cold legs refilling, and continued at []^{a,b,c} until it went negative at about the same time the primary sump began to inject through its check valves. It remained negative or 0 for the duration of the test. The reason for the flow reversal is that the sump level became higher than the break level. It is also believed that the reason that the break flow went to 0 for about []^{a,b,c} is that the cold legs were filled with steam.

ADS 4-1 and ADS 4-2 opened at []^{a,b,c} and resulted in less than []^{a,b,c} of steam flow each for a period of less than []^{a,b,c} (Figure 5.1.1-76). The liquid flow from the separators had initial peaks of about []^{a,b,c} for ADS 4-1 and ADS 4-2, respectively (Figure 5.1.1-28). The liquid flow continued throughout the remainder of the test ranging from about []^{a,b,c} per side.

The ADS 1-3 separator does not tie directly into the BAMS and was extensively covered in the IRWST Response and Pressurizer Response portions of this section, so it is not covered further here.

During this test, the BAMS controller calculated the total steam loss from the facility to be []^{a,b,c}. Of that amount, []^{a,b,c} would have to be made up to the IRWST and []^{a,b,c} to the primary sump. The equivalent amount of liquid from the condensate return system at []^{a,b,c} would have been []^{a,b,c}. This was not made up since the system controls were not fine enough. These amounts were recorded in the test log.

5.1.1.6 Mass Balance

The mass balance results for Matrix Test SB01 test data were calculated based on water inventory before and after the test and are provided in Appendix E. The mass at the end of the test was within []^{a,b,c} of the mass at the beginning of test.

5.1.1.7 Conclusions

The test was performed with minimal problems and is considered acceptable. Although not all of the facility initial conditions met the specified acceptance criteria, the deviations did not impact the quality of the data. The instrumentation problems encountered were not critical to the performance of the facility mass and energy balances.

Facility response to the test was as anticipated for the conditions that were established. The data clearly demonstrate that cooling of the reactor heater rods was maintained throughout the duration of the test.

TABLE 5.1.1-1
MATRIX TEST SB01 INITIAL CONDITIONS

Parameter	Instrument No.	Specified Initial Condition	Actual Initial Condition	Comments
Pressurizer pressure ⁽¹⁾	PT-604	370 ± 2 psig	<input type="checkbox"/> ^{a,b,c}	
HL-1 temperature ⁽¹⁾	SC-141	420 ± 2°F		
HL-2 temperature ⁽¹⁾	SC-140	420 ± 2°F		[^{a,b,c}] above required temperature
SG-1 pressure ⁽¹⁾	PT-301	285 ± 5 psig		
SG-2 pressure ⁽¹⁾	PT-302	285 ± 5 psig		
Pressurizer level ⁽¹⁾	LDP-601	65 ± 5 in.		Uncompensated level (corrected for specific volume change)
SG-1 narrow-range level ⁽¹⁾	LDP-303	26 ± 3 in.		Uncompensated level (corrected for specific volume change)
SG-2 narrow-range level ⁽¹⁾	LDP-304	26 ± 3 in.		Uncompensated level (corrected for specific volume change)
IRWST temperature ⁽²⁾	TF-709	< 80°F		
CMT-1 temperature ⁽²⁾	TF-529	< 80°F		
CMT-2 temperature ⁽²⁾	TF-532	< 80°F		[^{a,b,c}] above required temperature
ACC-1 temperature ⁽²⁾	TF-403	< 80°F		
ACC-2 temperature ⁽²⁾	TF-404	< 80°F		
IRWST level ⁽²⁾	LDP-701	Level established by fill line elevation		
ACC-1 level ^(2,3)	LDP-401	Level established by standpipe at 37 in.		
ACC-2 level ^(2,3)	LDP-402	Level established by standpipe at 37 in.		
ACC-1 pressure ⁽²⁾	PT-401	232 ± 2 psig		[^{a,b,c}] below required level
ACC-2 pressure ⁽²⁾	PT-402	232 ± 2 psig	<input type="checkbox"/>	

TABLE 5.1.1-1 (Continued)
MATRIX TEST SB01 INITIAL CONDITIONS

Parameter	Instrument No.	Specified Initial Condition	Actual Initial Condition	Comments
CMT-1 level ⁽²⁾	LDP-507	Full	[] (a,b,c)	
CMT-2 level ⁽²⁾	LDP-502	Full	[]	

Note:

- (1) The test procedure for Matrix Test SB01 did not require recording the control board indications prior to this test, but the specified conditions were verified on the control board prior to test actuation. The initial conditions from DAS, averaged over 2 minutes prior to the break valve opening, are recorded here.
- (2) Data were not recorded in the procedure, but the test engineer verified that specified conditions were achieved while establishing initial conditions. The value of the parameter was determined post-test by calculating the average DAS indication for a time of about 2 minutes before the break valve opened.
- (3) The bourdon pressure tube local indicator (PI-401 or PI-402) was tubed to the lower portion of the reference leg for differential pressure transmitter (LDP-401 or LDP-402). As pressure in the accumulator increased, the air inside the bourdon tube was compressed, thereby lowering the reference leg liquid level. This resulted in a false indication of measured level.

**TABLE 5.1.1-2
MATRIX TEST SB01 INOPERABLE INSTRUMENTS/INVALID DATA CHANNELS**

Instrument No.	Instrument Type	Description of Problem
FDP-604* FDP-605* FDP-606*	Differential pressure transmitter flow	Over-ranged momentarily when associated ADS valve opened
FMM-201* FMM-202* FMM-203* FMM-204*	Magnetic flow meter	Data invalid after 16 seconds due to possible steam in cold leg
FMM-402*	Magnetic flow meter	Inoperable - reads twice DVI flow during accumulator injection
FMM-501*	Magnetic flow meter	Data invalid between [] ^{a,b,c} and after [] ^{a,b,c} when CMT is empty
FMM-502	Magnetic flow meter	Data invalid after [] ^{a,b,c} due to possible steam in balance line
FMM-503	Magnetic flow meter	Data invalid after 104 seconds due to possible steam in balance line
FMM-504*	Magnetic flow meter	Data invalid between [] ^{a,b,c} and after [] ^{a,b,c} when CMT is empty
FMM-701*	Magnetic flow meter	Negative values after primary sump valves open at [] ^{a,b,c} are invalid (Subsection 5.1.1.2)
FMM-802*	Magnetic flow meter	Data invalid after steam forms in PRHR HX inlet line, which appears to be at about [] ^{a,b,c}
FMM-804*	Magnetic flow meter	Data valid until PRHR HX initially drained at [] ^{a,b,c} after this time, the possibility of steam in the outlet line invalidates the data
FMM-905*	Magnetic flow meter	Negative values after break separator level exceeds the break elevation at about [] ^{a,b,c} are invalid
HFM-112	Heat flux meter	Out of service at test start
HFM-505	Heat flux meter	Data appear erratic
HFM-703	Heat flux meter	Inoperable throughout test
HPS-509-1 through 3	Heated phase switch	Inoperable throughout test

TABLE 5.1.1-2 (Continued)
MATRIX TEST SB01 INOPERABLE INSTRUMENTS/INVALID DATA CHANNELS

Instrument No.	Instrument Type	Description of Problem
LDP-201 LDP-202 LDP-203 LDP-204 LDP-205 LDP-206	Differential pressure transmitter – level	Data invalid due to effect of vertical portion of sense line attached to top of pipe; data can show level trends, when pipe is empty or starts to drain, but absolute level indication cannot be used
LDP-207 LDF-208 LDP-209	Differential pressure transmitter – level	Inoperable – ranged improperly; data can show level trends, but absolute level indication cannot be used
LDP-215* LDP-216 LDP-217 LDP-218* LDP-219* LDP-220 LDP-221 LDP-222*	Differential pressure transmitter – level	Inoperable – when tube voids, reference leg steams off (Subsection 2.4)
LDP-401* LDP-402*	Differential pressure transmitter – level	Data invalid (Subsection 5.1.1.2)
LDP-509 LDP-510	Differential pressure transmitter – level	Reference leg appears to not have been completely filled
LDP-801	Differential pressure transmitter – level	Inoperable – level never changed during test
PT_101	Pressure transmitter	Data less than 6.1 psig invalid
PT_102	Pressure transmitter	Data less than 6.2 psig invalid
PT_103	Pressure transmitter	Data less than 6.2 psig invalid
PT_104	Pressure transmitter	Data less than 6.4 psig invalid
PT_108	Pressure transmitter	Data less than 8.4 psig invalid
PT_109	Pressure transmitter	Data less than 6.3 psig invalid
PT_111	Pressure transmitter	Data less than 6.0 psig invalid
PT_112	Pressure transmitter	Data less than 8.8 psig invalid
PT_113	Pressure transmitter	Data less than 6.4 psig invalid
PT_201*	Pressure transmitter	Data less than 1.1 psig invalid
PT_202	Pressure transmitter	Data less than 5.9 psig invalid
PT-205	Pressure transmitter	Data less than 6.1 psig invalid
TF-169	Thermocouple fluid temperature	Data invalid due to leaking O-ring in core barrel

TABLE 5.1.1-2 (Continued)
MATRIX TEST SB01 INOPERABLE INSTRUMENTS/INVALID DATA CHANNELS

Instrument No.	Instrument Type	Description of Problem
TF-501*	Thermocouple fluid temperature	Inoperable – indicates ambient throughout test
TF-504*	Thermocouple fluid temperature	Inoperable – indicates ambient throughout test
TF-536	Thermocouple fluid temperature	Inoperable – indicates ambient throughout test
TF-542	Thermocouple fluid temperature	Inoperable – leads swapped
TF-619	Thermocouple fluid temperature	Inoperable – indicates ambient throughout test
TFM-703	Thermocouple for HFM-703	Inoperable – indicates ambient throughout test
TH-317-1 through 4	Thermocouple heater rod	Inoperable – heater rod C2-317 removed prior to test
TW-210	Thermocouple wall temperature	Data appear erratic
TW-503 TW-526 TW-530 TW-542	Thermocouple wall temperature	Inoperable throughout test
TW-534 TW-552	Thermocouple wall temperature	Inoperable – indicates ambient temperature throughout test

Note:

* Instruments marked with an asterisk are critical instruments. See Subsection 5.1.1.2 for discussion.

**TABLE 5.1.1-3
MATRIX TEST SB01 SEQUENCE OF EVENTS**

Event ⁽¹⁾	Description in Bar Chart ⁽²⁾	Data Source ⁽³⁾	Time after Break (sec.)
TEST Pushbutton Depressed	TEST PB Pressed	D	a,b,c
Break Valve Open Signal	Break Vlv Open Sig	D	
Break Valve Starts to Open	Break Vlv Open	D	
Feed Pump Trips	Feed Pump Trips	D	
CMT-1 Outlet Valve Starts to Open	CMT-1 Inj Vlv Open	D	
CMT-2 Outlet Valve Starts to Open	CMT-2 Inj Vlv Open	D	
PRHR HX Outlet Valve Starts to Open	PRHR HX Vlv Open	D	
Reactor Coolant Pumps Trip	RCPs Trip	D	
CMT-1 Recirculation Flow Stops (LDP-509)	CMT-1 Recirc Flow Stops	A	
CMT-2 Recirculation Flow Stops (LDP-510)	CMT-2 Recirc Flow Stops	A	
Pressurizer Empty (LDP-601)	Pressurizer Empty	A	
Pressurizer Surge Line Empty (LDP-602)	Surge Line Empty	A	
SG-1 Hot-Leg Short Tube Empty (LDP-217)	SG-1 HL Shrt Tube Empty	A	
SG-1 Hot-Leg L Tube Empty (LDP-215)	SG-1 HL Lng Tube Empty	A	
CL-1 Channel Head Empty (LDP-211)	CL-1 Chan Head Empty	A	
CL-3 Channel Head Empty (LDP-213)	CL-3 Chan Head Empty	A	
SG-1 Cold-Leg Short Tube Empty (LDP-221)	SG-1 CL Shrt Tube Empty	A	
SG-1 Cold-Leg Long Tube Empty (LDP-219)	SG-1 CL Lng Tube Empty	A	
SG-2 Cold-Leg Short Tube Empty (LDP-220)	SG-2 CL Shrt Tube Empty	A	
SG-2 Cold-Leg Long Tube Empty (LDP-222)	SG-2 CL Lng Tube Empty	A	
SG-1 Hot-Leg Short Tube Empty (LDP-216)	SG-2 CL Shrt Tube Empty	A	
Time of Minimum Reactor Level Observed During Test (LDP-127)	Time of Min Rx Level	A	
SG-2 Hot-Leg Long Tube Empty (LDP-218)	SG-2 HL Lng Tube Empty	A	
HL-1 Pipe Starts to Drain (LDP-205)	HL-1 Pipe Starts to Drain	A	
CL-4 Channel Head Empty (LDP-212)	CL-4 Chan Head Empty	A	
CL-2 Channel Head Empty (LDP-210)	CL-2 Chan Head Empty	A	

TABLE 5.1.1-3 (Continued)
MATRIX TEST SB01 SEQUENCE OF EVENTS

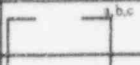
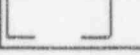
Event ⁽¹⁾	Description in Bar Chart ⁽²⁾	Data Source ⁽³⁾	Time After Break (sec.)
CMT-1 Low Level Signal	CMT-1 Level Lo	D	
ACC-2 Injection Starts (FMM-402)	ACC-2 Inj Starts	A	
ACC-1 Injection Starts (FMM-401)	ACC-1 Inj Starts	A	
ADS-1 Valve Starts to Open	ADS-1 Vlv Open	D	
CMT-2 Low Level Signal	CMT-2 Level Lo	D	
SG-2 Hot-Leg Elbow Starts Draining (LDP-208)	HL-2 Elbow Starts to Drain	A	
SG-2 Hot-Leg Channel Head Empty (LDP-214)	HL-2 Chan Head Empty	A	
HL-2 Pipe Starts to Drain (LDP-206)	HL-2 Pipe Starts to Drain	A	
HL-2 Pipe Empty (LDP-206)	HL-2 Pipe Empty	A	
ADS-2 Valve Starts to Open	ADS-2 Vlv Open	D	
HL-1 Pipe Empty (LDP-205)	HL-1 Pipe Empty	A	
ADS-3 Valve Starts to Open	ADS-3 Vlv Open	D	
Reactor Pressure Low	Reactor Pressure Lo	D	
IRWST-2 Injection Valve Starts to Open	IRWST-2 Inj Vlv Open	D	
SG-2 Hot-Leg Elbow Minimum (LDP-208)	HL-2 Elbow Level Min	A	
IRWST-1 Injection Valve Starts to Open	IRWST-1 Inj Vlv Open	D	
Pressurizer Refloods (LDP-601)	Pressurizer Refloods	A	
ACC-1 Empty (LDP-401)	ACC-1 Empty	A	
ACC-2 Empty (LDP-402)	ACC-2 Empty	A	
CMT-1 Level Low-Low	CMT-1 Level Lo-Lo	D	
ADS 4-1 Valve Starts to Open	ADS 4-1 Vlv Open	D	
ADS 4-2 Valve Starts to Open	ADS 4-2 Vlv Open	D	
CMT-2 Level Low-Low	CMT-2 Level Lo-Lo	D	
CMT-2 Empty (LDP-502)	CMT-2 Empty	A	
IRWST-2 Injection Starts (FMM-702)	IRWST-2 Inj Starts	A	
IRWST-1 Injection Starts (FMM-701)	IRWST-1 Inj Starts	A	
CMT-1 Empty (LDP-507)	CMT-1 Empty	A	
CMT-2 Starts to Reflood (LDP-502)	CMT-2 Refloods	A	

TABLE 5.1.1-3 (Continued)
MATRIX TEST SB01 SEQUENCE OF EVENTS

Event ⁽¹⁾	Description in Bar Chart ⁽²⁾	Data Source ⁽³⁾	Time After Break (sec.)
CMT-1 Starts to Reflood (LDP-507)	CMT-1 Refloods	A	 a,b,c
Primary Sump Starts to Overflow to Secondary Sump (LDP-901)	Pri Sump Overflows	A	
Primary Sump-2 Injection Starts (FMM-902)	Pri Sump-2 Inj Starts	A	
Primary Sump-1 Injection Starts (FMM-901)	Pri Sump-1 Inj Starts	A	
Primary Sump-1 Injection Valve Starts to Open	Pri Sump-1 Inj Vlv Open	D	
Primary Sump-2 Injection Valve Starts to Open	Pri Sump-2 Inj Vlv Open	D	
SG-1 Hot-Leg Channel Head Empty (LDP-209)	HL-1 Chan Head Empty	A	
SG-1 Hot-Leg Elbow Starts Draining (LDP-207)	HL-1 Elbow Starts to Drain	A	
SG-1 Hot-Leg Elbow Minimum (LDP-207)	HL-1 Elbow Level Min	A	

Note:

- (1) Data from the instrument channel in parenthesis were used to determine level, flow, or pressure conditions.
- (2) The attached bar chart provides a graphic representation of the timing of events.
- (3) D = time data obtained from a software program that monitored the input and output of the facility's PLC.
A = time data obtained by reviewing data from the instrument channel listed in the Event Description column.
- (4) O.O.S. = out of service

The bar charts for Table 5.1.1-3 on pages 5.1.1-38 through 5.1.1-44 are not included in this nonproprietary document.

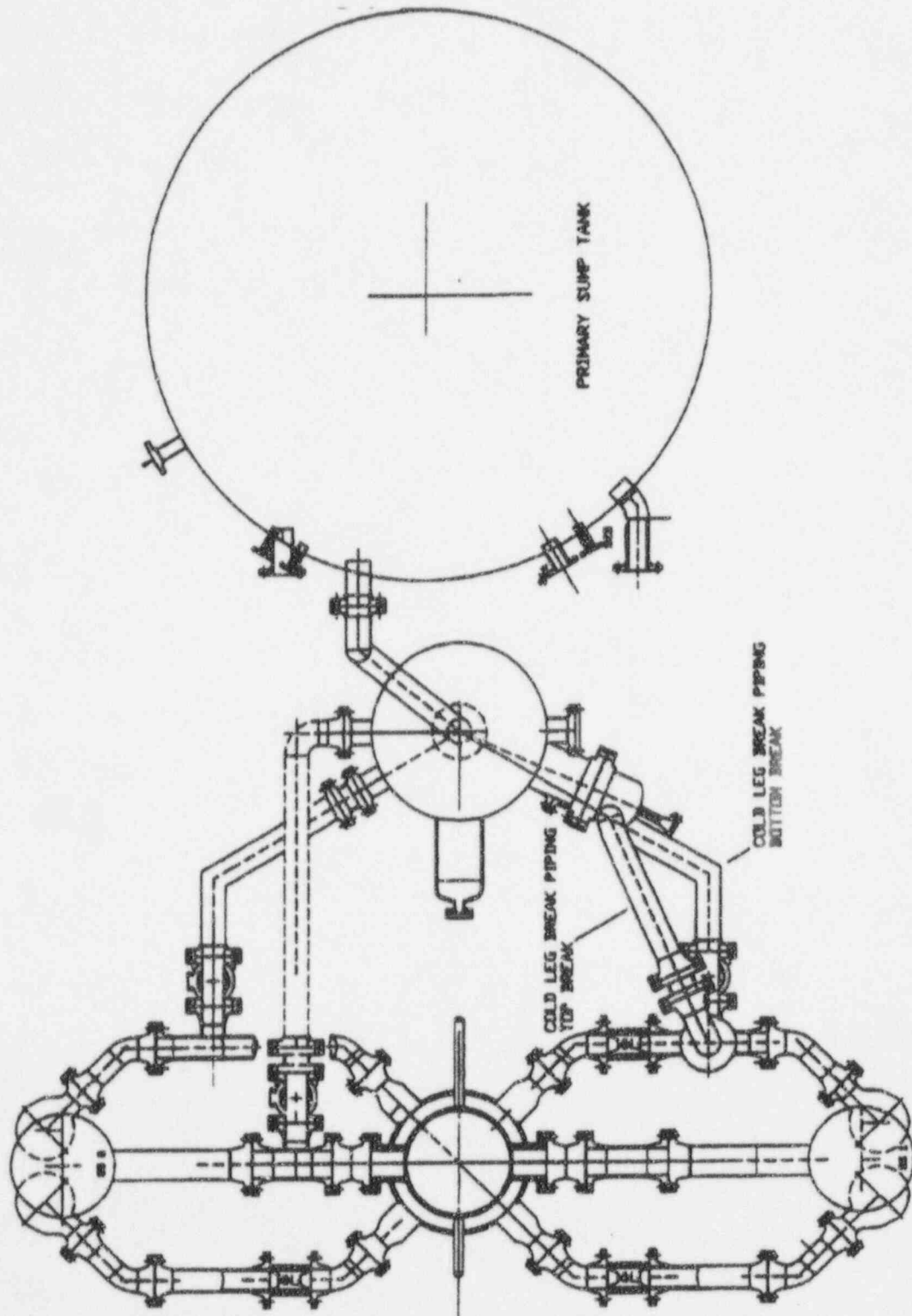


Figure 5.1.1-1 Primary Loop and Break Piping Layout

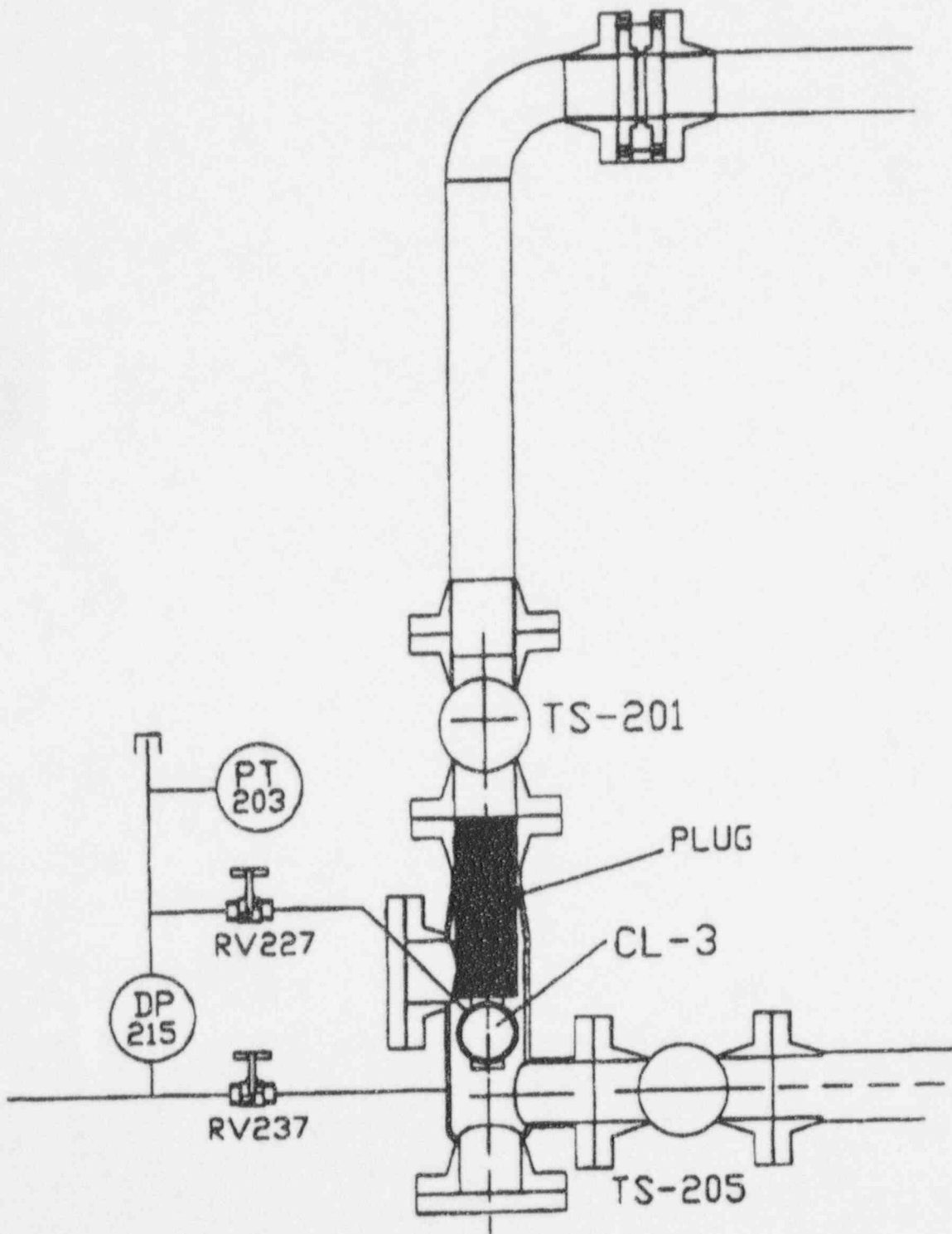


Figure 5.1.1-2 Primary Loop and Break Pipe Arrangement

Figures 5.1.1-3 through 5.1.1-80 are not included in this nonproprietary document.

5.1.2 Test Repeatability (Matrix Test SB18 Comparison with Matrix Test SB01)

This section identifies and describes the response of the facility based on a comparison between Matrix Test SB18 (OSU Test U0018) and Matrix Test SB01 (OSU Test U0001). The simulated break for Matrix Test SB18 was located at the bottom of CL-3 with a simulated failure of one of the ADS-4 lines. CL-3 is on the CMT side of the facility (Figures 5.1.2-1 and 5.1.2-2). Matrix Test SB18, the final Westinghouse-performed matrix test, duplicated Matrix Test SB01, the first test performed. The purpose of performing Matrix Test SB18 was to confirm the ability of the facility to replicate its response to a small-break loss-of-coolant accident (SBLOCA) with the same configuration from the beginning to the end of the test program.

Matrix Test SB18 was performed on September 15, 1994. This test was considered successful because the reactor heater bundle cooling was maintained throughout the test. The transient was initiated when break valve TS-205 opened and continued through ADS actuation; CMT, accumulator, and IRWST injection; and primary sump recirculation injection.

Subsection 5.1.2.1 provides details related to the systems' configuration and initial conditions. A description of inoperable instruments is provided in Subsection 5.1.2.2, and Subsection 5.1.2.3 references the sequence of events. A discussion of the test results and evaluation can be found in Subsection 5.1.2.4, and Subsection 5.1.6.5 is a comparison of component responses. A summary of the mass balance results is provided in Subsection 5.1.2.6. Conclusions, as they apply to test Matrix Test SB18, are in Subsection 5.1.2.7.

The facility responses to the break are documented by the data plots, referenced as figures in the text, at the end of this section. The numbering and content of the data plots for Matrix Test SB18 are identical to the data plots provided in Subsection 5.1.1 for Matrix Test SB01. For example, the data plot for instrument channel LDP-601 for Matrix Test SB01 is shown in Figure 5.1.1-5; the data plot for the same channel for Matrix Test SB18 is shown in Figure 5.1.2-5. Not all of the figures in the data plot package at the end of the section are referenced. Only those figures required to explain a different response from that of Matrix Test SB01 are referred to in the text. The additional figures are provided for the benefit of readers who wish to compare additional Matrix Test SB18 parameters to similar parameters for Matrix Test SB01. A data plot with the suffix x indicates extended time.

5.1.2.1 System Configuration and Initial Conditions

Matrix Test SB18 was performed per an approved written procedure, met all but two of the specified initial conditions, and all actions were automatic with no operator responses required. The two conditions that weren't met are discussed below. The test was performed without the operation of nonsafety-related systems. The normal residual heat removal system (RNS) and chemical and volume control system (CVS) pumps did not operate during the test.

A flow nozzle simulating one line of flow was installed in the ADS 4-1 line—HL-1 to ADS 4-1 separator—to provide the single failure simulation, and a flow nozzle simulating two lines of flow was installed in the ADS 4-2 line—HL-2 to the ADS 4-2 separator. Additionally, flow nozzles simulating two lines of flow each were installed in the ADS 1-3 inlet lines.

The reactor heater control decay algorithm maintained the maximum reactor heater power output for []^{a,b,c} and then power began to decay to simulate the total decay energy input of the AP600 nuclear fuel (Appendix F). This test was performed with reactor heater rod HTR-C2-317 electrically disconnected to simulate the heater conditions during the performance of Matrix Test SB01.

The differences in facility configuration for the two tests were:

- After the performance of Matrix Test SB01, a vacuum breaker was installed on the ADS 1-3 sparger line inside the IRWST to eliminate negative pressures in the pressurizer and ADS 1-3 separator.
- FMM-201, FMM-202, FMM-203, and FMM-204, which measured cold-leg flow, were removed from the system and replaced with pipe spools because of continuous failures. RCP differential pressure instrument data (DP-202, DP-203, DP-205, and DP-206) could be used to monitor pump degradation.
- Component and piping insulation had deteriorated significantly because of the amount of maintenance (such as gasket replacement) that was required during the test program.
- Pressurizer heater logic was changed so that the PLC initiated a signal to open the pressurizer heater SCR contactor at []^{a,b,c} after S signal actuation, thereby ensuring de-energization of the heaters.
- CMT balance line isolation valves RCS-529 and RCS-530 were in the AUTO and OPEN positions, as part of the initial conditions for Matrix Test SB01, but were closed and opened by the operator 1 minute after the TEST pushbutton was pressed in Matrix Test SB18 to prevent heatup at the top of the CMTs prior to break valve opening.

The facility fill and vent, startup, and heatup were performed per the same approved operating procedures used for Matrix Test SB01. A zero check was performed for all differential pressure instruments as was done for the reference test. Initial conditions for the test were established and recorded in the procedure. Refer to Subsection 2.7 for pre-test operations. The test ran for about 6 hours.

Table 5.1.2-1 shows the initial conditions recorded from the operator's panel and the average of the same parameters for about 2 minutes prior to the break valve opening from the DAS.

There were two initial condition parameters out of specification, neither of which should invalidate this test.

- ACC-1 pressure, indicated by PT-401, was []^{a,b,c} or []^{a,b,c} percent below the required pressure band. The accumulator was pressurized to the required pressure, as indicated on local pressure indicator PI-401, prior to test actuation. The loss of pressure between tank pressurization and test actuation was possibly due to nitrogen gas cooling in the accumulator. Test analysis starting with the recorded lower accumulator overpressure should still be possible.
- ACC-2 pressure, indicated by PT-402, was []^{a,b,c} or []^{a,b,c} percent below the required pressure band. The accumulator was pressurized to the required pressure, as indicated on local pressure indicator PI-402, prior to test actuation. The loss of pressure between tank pressurization and test actuation was possibly due to nitrogen gas cooling in the accumulator. Test analysis starting with the recorded lower accumulator overpressure should still be possible.

5.1.2.2 Inoperable Instruments

Table 5.1.2-2 is a list of instruments considered inoperable or invalid during all or portions of this test. Some of the instruments listed are on the Critical Instrument List (Subsection 3.2, Table 3.2-2) and, therefore, are addressed here:

FMM-201, FMM-202, FMM-203, and FMM-204 measured flow (gpm) in each of the four cold legs. A decision was made to continue testing without the availability of these instruments. Replacement flow meters repeatedly failed; their continued use was precluded due to cracking of the ceramic liners from thermal stratification in the loop piping. The necessary boundary conditions for loop flow could be determined from cold-leg differential pressure transmitters DP-202, DP-203, DP-205, and DP-206.

CMT-1 and CMT-2 injection flow meters FMM-501 and FMM-504 and PRHR inlet and outlet flow meters FMM-802 and FMM-804 provided accurate data when sensing liquid, but became inaccurate when sensing two-phase or steam flow.

FMM-905 measured break separator loop seal flow to the primary sump. As the transient proceeded, the primary sump and break separator levels exceeded the elevation of the break at the bottom of CL-3. When this occurred, break flow initially stopped and then reversed. Flow reversal through the break occurred at about []^{a,b,c} rendering subsequent data invalid.

SG tube level data (LDP-215, LDP-218, LDP-219, and LDP-222) were biased by vaporization of the water in the transmitter reference leg after the SG tubes started draining. However, the data provide accurate indication of the time when the tubes are empty.

TF-103 and TF-104 measured CL-3 and CL-4 bottom-of-pipe fluid temperatures entering the reactor vessel. Both thermocouples were removed to accommodate installation of thermal stratification measurement instrumentation. It was permissible for both thermocouples to be inoperable because TF-101 and TF-102, which measured the CL-3 reactor flange top and CL-4 reactor flange top, were operable during the performance of Matrix Test SB18.

TF-501 and TF-504 measured CMT fluid temperature from the long thermocouple rod location near the bottom of each CMT. The thermocouples appear to have measured ambient conditions throughout the test, which would indicate a short somewhere in the thermocouple wiring. With these thermocouples inoperable, the required long thermocouple rod thermocouple availability of "seven out of ten and no more than one in succession failed" was met.

Data provided by ADS-4 separator instrumentation prior to the ADS 4-1 and ADS 4-2 valves opening at [] were invalid due to the closed position of the ADS-4 valves and the ADS-4 separator loop seal valves. The instruments affected are: FMM-602, FMM-603, FVM-602, FVM-603, LDP-611, and LDP-612. Test analysis will not be affected, since ADS-4 flow did not begin until the valves opened.

Considering these critical instrument failures, sufficient instrumentation was available to allow the performance of mass balances as demonstrated in Subsection 5.1.2.6 and Appendix E. An energy balance will be performed and reported in the *AP600 Low-Pressure Integral Systems Test at Oregon State University Test Analysis Report, WCAP-14292*.⁽²⁾

5.1.2.3 Sequence of Events

Table 5.1.2-3 contains the sequence of events for Matrix Tests SB18 and SB01. The first pages of the table provide selected event times from both tests and the difference between event times. The subsequent pages of the table provide a visual representation of the time comparison using bar charts. On both the numeric table and the bar charts, the events are sorted in the chronological order in which they occurred in Matrix Test SB18.

The table defines the source of the actual time values. A D in the Data Source column indicates the recorded time was obtained from a software program that monitored digital events in the facility. These events included pump starts and stops, valve limit switch actuations, and alarms. The term *valve opening* means the valve has actuated and the closed limit switch is being opened (valve coming off the seat). An A in the Data Source column indicates the time data were obtained by reviewing test data recorded by the DAS. Although the test data from the DAS were in digital format, the DAS monitored analog events such as pressure, flow, and temperature.

5.1.2.4 Test Results and Evaluation

This section compares the results of Matrix Test SB18 with the results of reference test SB01. In doing so, the overall system response to the LOCA event in Matrix Test SB18 is evaluated. The section is divided into three different phases, each characterized by the systems' behavior and thermal-hydraulic phenomena occurring in the systems. The phases are as follows:

- Initial Depressurization Phase: simulated break initiation to ADS-1 actuation
- ADS Phase: ADS-1 actuation to start of IRWST injection
- IRWST Injection Phase: start of IRWST injection to end of test

Initial Depressurization Phase

As with Matrix Test SB01, this test began with the actuation of the TEST pushbutton. Break valve TS-205 received an open signal from the PLC []^{a,b,c} later (time zero). After an additional 0.5 second, an S signal was generated by the PLC, which time-sequences signals to initiate various events such as resetting controllers, stopping pumps, and repositioning valves.

The initial depressurization phase for Matrix Test SB18 began similarly to Matrix Test SB01. PLC timing for various event initiations was within 1 second of the same event for Matrix Test SB01. At about []^{a,b,c} steam percent, as calculated from LDP-127 data, indicated that the reactor vessel began to lose inventory, i.e., steam formation began (Figure 5.1.2-3), which was the same as in Matrix Test SB01.

CMT transition from recirculation to draindown occurred within []^{a,b,c} of the transition in Matrix Test SB01, as indicated by decreasing levels on LDP-509 and LDP-510 (Figure 5.1.2-6). In Matrix Test SB18, CMT-1 transitioned []^{a,b,c} earlier and CMT-2 transitioned []^{a,b,c} later than the same events in Matrix Test SB01.

The pressurizer and pressurizer surge line emptied within seconds for the two tests (Figure 5.1.2-5). The core decay heat simulation of reactor heater power followed the programmed algorithm just as it did in Matrix Test SB01 (Appendix F).

In Matrix Test SB18, it took slightly longer for the SG-2 U-tubes to completely empty, but the SG-1 U-tubes and SG-1 and SG-2 channel heads and hot legs drained slightly faster than in reference test SB01 (Figures 5.1.2-7 through 5.1.2-11).

There was essentially no difference in the PRHR HX response during this phase of the test (Figures 5.1.2-41, 5.1.2-66, and 5.1.2-67).

In Matrix Test SB18, the fluid level inside the reactor vessel core barrel reached its minimum collapsed level of []^{a,b,c} at about []^{a,b,c} as indicated by LDP-127 (Figure 5.1.2-15).

The minimum level occurred about []^{a,b,c} later and about 1 in. higher than in Matrix Test SB01. Matrix Test SB18 also had a low core barrel level of []^{a,b,c} during the depressurization phase prior to the ADS-1 valve opening. Heater rod cooling was maintained (Figure 5.1.2-44). Also in Matrix Test SB18, during a condensation/depressurization event that occurred at about []^{a,b,c} the indicated core barrel level transitioned from []^{a,b,c} and back to []^{a,b,c} over a []^{a,b,c} period. Heater rod cooling was maintained.

The initial RCS depressurization was similar for the two tests from break valve opening until []^{a,b,c} when the ADS-1 valve opened in Matrix Test SB18 and caused pressure to decrease at a greater rate than for Matrix Test SB01. In Matrix Test SB01, the ADS-1 valve did not open until []^{a,b,c}. The period of quasi-equilibrium pressure between the RCS and the secondary side of the SGs was about the same for Matrix Test SB18 and Matrix Test SB01, about []^{a,b,c} (Figure 5.1.2-45). In the first few seconds after the break valve opened, the SGs were isolated on both the feedwater and steam sides in order to minimize RCS heat losses. The only cooling available to the SGs was heat losses to the ambient. With RCS pressure decreasing due to the break and SG pressure increasing due to heat absorption from the RCS, the pressures converged at about []^{a,b,c}. At about []^{a,b,c} when inventory losses through the break caused RCS pressure to drop below the pressure on the SG secondary side, the SGs became a heat source for the RCS.

ADS Phase

CMT-1 reached its low level setpoint at []^{a,b,c} thus triggering the ADS-1 valve opening at about []^{a,b,c} in Matrix Test SB18. This can be compared with the CMT-1 low level setpoint being reached at []^{a,b,c} and the ADS-1 valve opening at []^{a,b,c} for Matrix Test SB01 (Figure 5.1.2-6). The RCS pressure response following the ADS-1 valve opening was the same for both tests. Facility response to the opening of the ADS-2, ADS-3, and ADS-4 valves was quite similar to that of Matrix Test SB01.

CMT injection flow data appear to be consistent for the two tests (Figure 5.1.2-16). In Matrix Test SB18, the CMT-2 low level setpoint was not reached until about []^{a,b,c} after the CMT-1 low level setpoint was reached. In Matrix Test SB01, the two CMTs attained their low level setpoints within []^{a,b,c} of each other. A possible explanation for the delay for CMT-2 in Matrix Test SB18 is the timing of initiation of accumulator injection, which began for both accumulators about []^{a,b,c} after the ADS-1 valve opened. Accumulator injection created a backpressure in the DVI header that partially or completely shut off CMT injection by closing the CMT injection line check valves.

In Matrix Test SB18, accumulator injection began about []^{a,b,c} earlier than in Matrix Test SB01 (Figure 5.1.2-16). The earlier accumulator injection in Matrix Test SB18 can be directly attributed to the ADS-1 valve opening earlier. The accumulator flow profiles and interaction with the CMTs were consistent for both tests (Figure 5.1.2-16).

Early in Matrix Test SB18, a condensation/depressurization event occurred at about []^{a,b,c} as compared with []^{a,b,c} in Matrix Test SB01. DP-114 and DP-130, which measured reactor vessel upper head differential pressure, exhibited large negative spikes, indicative of instantaneous high steam flow from the reactor vessel upper plenum through the upper head and into the downcomer area (Figure 5.1.2-19). At the same time, LDP-127 showed a sharp spike decrease in collapsed level indication, and LDP-116 and LDP-140 indicated sharp spike increases (Figure 5.1.2-15). The parameters of RCS pressure, reactor vessel levels, and DVI rates were almost identical at the time of the event in both tests (Figures 5.1.2-45, 5.1.2-15, and 5.1.2-17).

Test data show that the collapse of the superheated steam bubble in the upper portion of the reactor vessel downcomer annulus resulted in the downcomer fluid accelerating upward and impacting the bottom of the core barrel flange where the core bypass holes are located. The impact of the downcomer liquid on the solid surface of the core barrel flange produced the "bang" heard during the test. The low pressure created in the upper downcomer annulus by the collapse of the steam bubble also resulted in a rapid increase in steam flow from the core barrel, through the upper head, and into the downcomer. Refer to Subsection 7.1 for a more detailed treatment of condensation/depressurization events at the OSU test facility.

Pressurizer and surge line response during the ADS phase of the test was similar for Matrix Test SB18 and the reference test, with the exception of a slight offset in timing due to the earlier opening of the ADS-1 valve in Matrix Test SB18 (Figure 5.1.2-5).

IRWST injection started within []^{a,b,c} for the two tests at about []^{a,b,c} (Figure 5.1.2-37).

IRWST Injection Phase

During the performance of Matrix Test SB01, the pressurizer reflooded to about []^{a,b,c} from about []^{a,b,c}. This phenomenon was attributed to a negative pressure being formed in the pressurizer and ADS 1-3 separator when HL-2 filled with subcooled fluid to a level that started to fill the surge line while the ADS 1-3 sparger was still submerged in the IRWST. A vacuum breaker was installed on the ADS 1-3 sparger line inside the IRWST following the performance of Matrix Test SB01 to prevent a recurrence of a reflood caused by negative pressure. The vacuum breaker performed its function, and under similar conditions, a pressurizer reflood did not occur during Matrix Test SB18 (Figure 5.1.2-5).

Both CMTs reflooded during the second hour of Matrix Test SB18 as the CMTs did in Matrix Test SB01 (Figures 5.1.2-30 through 5.1.2-34). The reflood occurred about []^{a,b,c} earlier, and the draindown was completed about []^{a,b,c} earlier in Matrix Test SB18 than in the reference test. In Matrix Test SB18, the CMTs were completely empty about the time that sump injection started through the primary sump injection line check valves, but about []^{a,b,c} prior to the sump injection valves opening. In Matrix Test SB01, the CMTs were completely empty at

about the time that the primary sump injection valves opened. The drain rate for the CMTs was faster in Matrix Test SB18, even though the IRWST drain rate for both tests was consistent.

Condensation/depressurization events were observed during the CMT reflood during Matrix Test SB18 similar to those during Matrix Test SB01.

Primary sump injection started at about []^{a,b,c} earlier in Matrix Test SB18 than in Matrix Test SB01. DAS rack 1 failed and stopped acquiring data at []^{a,b,c} which eliminated all pressure, differential, and level transmitter data from that time to the end of the test. The test engineer recorded data in the Test Log from the local transmitters at 15-minute intervals for the remainder of the test for injection flows, IRWST level, and auctioneered reactor heater sheath temperature. The recorded data appears in Table 5.1.2-4.

Primary sump injection valves opened at []^{a,b,c} and the test was stopped 30 minutes later. The facility response during sump injection recirculation during Matrix Test SB18 appears to be consistent with the data obtained during Matrix Test SB01.

5.1.2.5 Comparison of Component Responses

Reactor

Reactor response during the performance of Matrix Test SB18 was similar to reactor response during Matrix Test SB01, with the exception of event times. The lowest collapsed level recorded in the LDP-127 test data was []^{a,b,c} at []^{a,b,c} which was about []^{a,b,c} higher and []^{a,b,c} later than Matrix Test SB01 (Figure 5.1.2-15). During a condensation/depressurization event that occurred at about []^{a,b,c} the collapsed level transitioned from []^{a,b,c} and back to []^{a,b,c} over a []^{a,b,c} period. Reactor heater rod cooling was maintained during both level excursions (Figure 5.1.2-44).

Core Makeup Tanks

CMT response during the performance of Matrix Test SB18 was similar to CMT response in Matrix Test SB01, with the exception of event times. In Matrix Test SB18, both CMTs emptied about []^{a,b,c} into the test, which was very consistent with CMT performance in the reference test (Figure 5.1.2-6). CMT reflood during the second hour of both matrix tests was consistent because CMT-2 was the first to reflood in each test (Figures 5.1.2-30 and 5.1.2-31). The levels attained in the CMTs during reflood were within []^{a,b,c} from one test to the other. Also in both tests, the rapid reflood of the CMTs was the result of a condensation/depressurization event occurring in the CMTs when subcooled fluid filled the balance lines and spilled into the tanks filled with superheated steam. In both tests, the final draindown of the CMTs was controlled by IRWST draindown due to interaction of the CMT and IRWST levels on the CMT discharge line check valves.

Accumulators

Accumulator response during the performance of Matrix Test SB18 was similar to accumulator response in Matrix Test SB01, with the exception of event timing.

Pressurizer

The pressurizer response during Matrix Test SB18 produced the only major differences between the tests. During the performance of Matrix Test SB01, the pressurizer exhibited a second reflood at about []^{a,b,c} but a similar event did not occur during Matrix Test SB18 (Figure 5.1.2-5). As was described in Subsection 5.1.1.4 in the Pressurizer Response, the reflood was caused by negative pressure developing in the pressurizer and ADS 1-3 separator with respect to the pressure in the reactor vessel. Negative pressure was precipitated by several occurrences: 1) the ADS 1-3 sparger located in the IRWST was submerged, 2) the hot legs had refilled with subcooled fluid into the surge line, and 3) the combination of 1 and 2 resulted in condensation of steam in the pressurizer and ADS 1-3 separator with subsequent cooling. The problem of negative pressure developing in the pressurizer and ADS 1-3 separator was corrected prior to the performance of Matrix Test SB18 by a facility modification that consisted of a vacuum breaker being installed on the ADS 1-3 sparger line inside the IRWST.

There was one operational difference between the two tests. During Matrix Test SB01, the pressurizer heater remained energized at about 1.5 kW. This was corrected prior to the performance of Matrix Test SB18 by a change in heater control logic. During Matrix Test SB01, the logic was supposed to drive the heater power demand to zero, resulting in zero power from the pressurizer heater SCRs to the heaters. According to the data for Matrix Test SB01, it can be postulated that the SCR control circuitry had not been properly tuned. The pressurizer heater control problem was corrected prior to the performance of Matrix Test SB18 by a change in the logic which opened the heater SCR contractor to de-energize the heaters at the start of the test (Figure 5.1.2-24).

All other pressurizer responses during Matrix Test SB18 were similar to the responses during Matrix Test SB01, with the exception of event timing.

Passive Residual Heat Removal Heat Exchanger

The PRHR HX response during Matrix Test SB18 was similar to Matrix Test SB01, with the exception of event timing and the response of the HX wide-range level data after about []^{a,b,c}. During Matrix Test SB01, the HX partially refilled when the RCS loops were filled with subcooled fluid. Following the refill, when small pressure and level oscillations began to occur, it is possible that the oscillations caused the PRHR HX inlet line to "burp," allowing a negative pressure in the HX to equalize with the RCS. Equalization of pressures allowed equalization of PRHR levels with those of the RCS. During Matrix Test SB01, once the levels equalized, the PRHR level remained essentially constant.

Data obtained during the performance of Matrix Test SB18 indicate that PRHR HX performance was consistent with the performance during Matrix Test SB01 until the final draindown of the HX. During Matrix Test SB18, the HX began to drain, but the data then indicated the drain stopped and the HX began a slow refill for as long as data were obtained (Figure 5.1.2-68). It is possible that the HX was refilling, but a more logical possibility is that wide-range level transmitter LDP-802 was slowly losing its reference leg due to a low saturated pressure in the HX tubes.

Steam Generators

SG response during the performance of Matrix Test SB18 was similar to SG response in Matrix Test SB01, with the exception of event timing.

Cold Legs and Hot Legs

The RCS cold-leg and hot-leg response during the performance of Matrix Test SB18 was similar to the response in Matrix Test SB01, with the exception of event timing.

In-Containment Refueling Water Storage Tank

IRWST response during the performance of Matrix Test SB18 was similar to IRWST response during the reference test, except that during Matrix Test SB18, it took about []^{a,b,c} longer to reach the low-low level setpoint, which opened the primary sump injection valves. The tank draindown rates were identical until about []^{a,b,c} when the available DAS data ended for Matrix Test SB18 (Figure 5.1.2-35). At about []^{a,b,c} in Matrix Test SB18 the time that primary sump injection began through the check valves in the sump injection lines in both tests, it is possible that sump injection flow caused a reduction in IRWST injection rate and, therefore, the extended draindown time (Table 5.1.2-4).

Break and ADS System Response

The BAMS response during the performance of Matrix Test SB18 was similar to the response in Matrix Test SB01, with the exception of event timing.

5.1.2.6 Mass Balance

The mass balance results for Matrix Test SB18 test data were calculated based on water inventory before and after the test and are provided in Appendix E. The mass at the end of the test was within []^{a,b,c} percent of the mass at the beginning of test as compared to []^{a,b,c} percent for Matrix Test SB01.

5.1.2.7 Conclusions

The test was performed with minimal problems and is considered acceptable. Although not all of the facility initial conditions met the specified acceptance criteria, the deviations did not impact the quality of the data. The instrumentation problems encountered were not critical to the performance of the facility mass and energy balances.

Facility response to the test was as anticipated for the conditions that were established. The data clearly demonstrate that cooling of the reactor heater rods was maintained throughout the duration of the test.

**TABLE 5.1.2-1
MATRIX TEST SB18 INITIAL CONDITIONS**

Parameter	Instrument No.	Specified Initial Condition	Actual Initial Condition	Comments
Pressurizer pressure ⁽¹⁾	PT-604	370 ± 2 psig	[] ^{a,b,c}	
HL-1 temperature ⁽¹⁾	SC-141	420 ± 2°F		
HL-2 temperature ⁽¹⁾	SC-140	420 ± 2°F		
SG-1 pressure ⁽¹⁾	PT-301	285 ± 5 psig		
SG-2 pressure ⁽¹⁾	PT-302	285 ± 5 psig		
Pressurizer level ⁽¹⁾	LDP-601	65 ± 5 in.		Level signal temperature-compensated by TF-605
SG-1 narrow-range level ⁽¹⁾	LDP-303	26 ± 3 in.		Level signal temperature-compensated by TF-301
SG-2 narrow-range level ⁽¹⁾	LDP-304	26 ± 3 in.		Level signal temperature-compensated by TF-310
IRWST temperature ⁽²⁾	TF-709	< 80°F		
CMT-1 temperature ⁽²⁾	TF-529	< 80°F		
CMT-2 temperature ⁽²⁾	TF-532	< 80°F		
ACC-1 temperature ⁽²⁾	TF-403	< 80°F		
ACC-2 temperature ⁽²⁾	TF-404	< 80°F		
IRWST level ⁽²⁾	LDP-701	Level established by fill-line elevation		
ACC-1 level ⁽²⁾	LDP-401	Level established by standpipe at 37 in.		
ACC-2 level ⁽²⁾	LDP-402	Level established by standpipe at 37 in.		
ACC-1 pressure ⁽²⁾	PT-401	232 ± 2 psig		[] ^{a,b,c} below required pressure
ACC-2 pressure ⁽²⁾	PT-402	232 ± 2 psig		[] ^{a,b,c} below required pressure

TABLE 5.1.2-1 (Continued)
MATRIX TEST SB18 INITIAL CONDITIONS

Parameter	Instrument No.	Specified Initial Condition	Actual Initial Condition	Comments
CMT-1 level ⁽²⁾	LDP-507	Full	<input type="checkbox"/> a,b,c	
CMT-2 level ⁽²⁾	LDP-502	Full	<input type="checkbox"/>	

Note:

- (1) Data for the indicated parameter were recorded in the test procedure as an initial condition for the test. The value was determined by the test engineer from the appropriate control board indicator.
- (2) Data were not recorded in the procedure, but the test engineer verified that the specified conditions were achieved while establishing initial conditions. The value of the parameter was determined post-test by calculating the average DAS indication for a time of about 2 minutes before the break valve opened.

TABLE 5.1.2-2
MA. RIX TEST SB18 INOPERABLE INSTRUMENTS/INVALID DATA CHANNELS

Instrument No.	Instrument Type	Description of Problem
DP-905	Differential pressure transmitter	Data questionable throughout test
FDP-605	Differential pressure transmitter flow	Over-ranged early in test
FMM-201* FMM-202* FMM-203* FMM-204*	Magnetic flow meter	Removed from system
FMM-501*	Magnetic flow meter	Data invalid between [] ^{a,b,c} and after [] ^{a,b,c} when the CMT is empty
FMM-502	Magnetic flow meter	Data invalid after [] ^{a,b,c} due to possible steam in balance line
FMM-503	Magnetic flow meter	Data invalid after [] ^{a,b,c} due to possible steam in balance line
FMM-504*	Magnetic flow meter	Data invalid between [] ^{a,b,c} and after [] ^{a,b,c} when the CMT is empty
FMM-802*	Magnetic flow meter	Data invalid after steam forms in PRHR HX inlet line, which appears to be at about [] ^{a,b,c}
FMM-804*	Magnetic flow meter	Data valid until PRHR HX initially drained at [] ^{a,b,c} after this time the possibility of steam in the outlet line invalidates the data
FMM-905*	Magnetic flow meter	Negative values after break separator level exceeds the break elevation at about [] ^{a,b,c} are invalid
HFM-103 HFM-105 HFM-111 HFM-201 HFM-505 HFM-510 HFM-703 HFM-801	Heat flux meter	Inoperable throughout test
HPS-509-1 through 3	Heated phase switch	

TABLE 5.1.2-2 (Continued)
MATRIX TEST SB18 INOPERABLE INSTRUMENTS/INVALID DATA CHANNELS

Instrument No.	Instrument Type	Description of Problem
LDP-201 LDP-202 LDP-203 LDP-204 LDP-205 LDP-206	Differential pressure transmitter – level	Data invalid due to effect of vertical portion of sense line attached to top of pipe; data can show level trends and when pipe empties or starts to drain, but absolute level indication cannot be used
LDP-215* LDP-216 LDP-217 LDP-218* LDP-219* LDP-220 LDP-221 LDP-222*	Differential pressure transmitter – level	Inoperable – when tube voids reference leg steams off (Subsection 2.4)
LDP-801	Differential pressure cell – level	Inoperable – indicates full when HX not full
TF-103*	Thermocouple fluid temperature	Replaced with thermal stratification thermocouples
TF-104*	Thermocouple fluid temperature	Replaced with thermal stratification thermocouples
TF-170	Thermocouple fluid temperature	Affected by leakage from reactor vessel downcomer
TF-501*	Thermocouple fluid temperature	Inoperable – indicates ambient throughout test
TF-504*	Thermocouple fluid temperature	Inoperable – indicates ambient throughout test
TF-702	Thermocouple fluid temperature	Inoperable – indicates ambient throughout test
TFM-103 TFM-105 TFM-111 TFM-705	Thermocouple wall temperature	Inoperable throughout test
TW-503	Thermocouple wall temperature	Inoperable throughout test

Note:

* Instruments marked with an asterisk are critical instruments. See Subsection 5.1.2.2 for discussion.

TABLE 5.1.2-3 (Continued)
MATRIX TEST SB18 SEQUENCE OF EVENTS

Event ⁽¹⁾	Data Source ⁽²⁾	SB18 Time After Break (sec.)	SB01 Time After Break (sec.)	Delta Time (sec.)

a,b,c

TABLE 5.1.2-3 (Continued)
MATRIX TEST SB18 SEQUENCE OF EVENTS

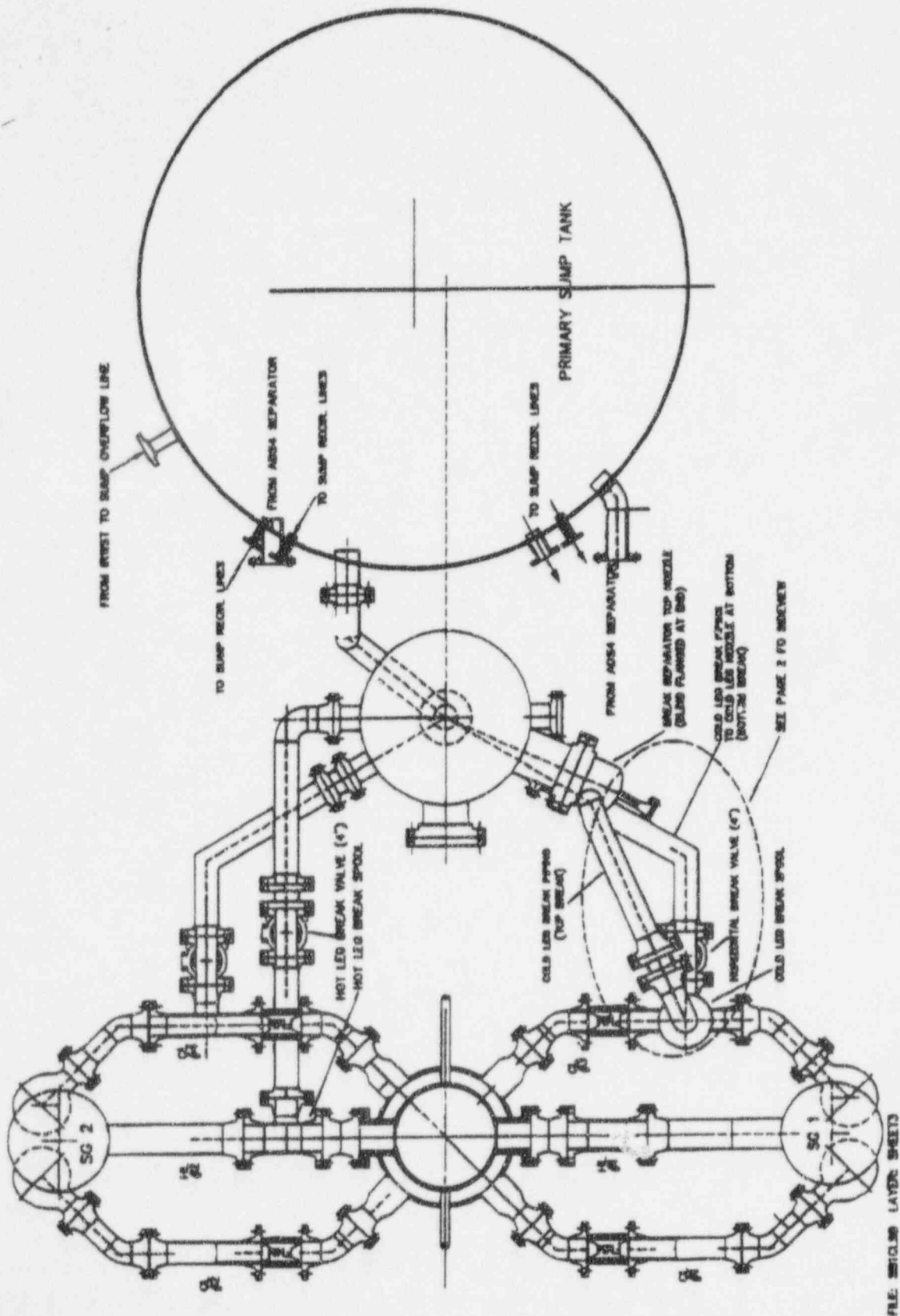
Event⁽¹⁾	Data Source⁽²⁾	SB18 Time After Break (sec.)	SB01 Time After Break (sec.)	Delta Time (sec.)

The bar charts for Table 5.1.2-3 on pages 5.1.2-19 through 5.1.2-24 are not included in this nonproprietary document.

a.b.c

**TABLE 5.1.2-4
DATA RECORDED IN SB18 TEST LOG**

Clock Time	LDP-701 IRWST Level (in. H ₂ O)	FMM-205 DVI-1 Flow (gpm)	FMM-701 IRWST-1 Flow (gpm)	FMM-901 Sump-1 Flow (gpm)	FMM-206 DVI-2 Flow (gpm)	FMM-702 IRWST-2 Flow (gpm)	FMM-902 Sump-1 Flow (gpm)	Reactor Heater Sheath Temperature (°F)



FILE: 5101.00 LAYER: SHEETS

Figure 5.1.2-1 Primary Loop and Break Piping Layout

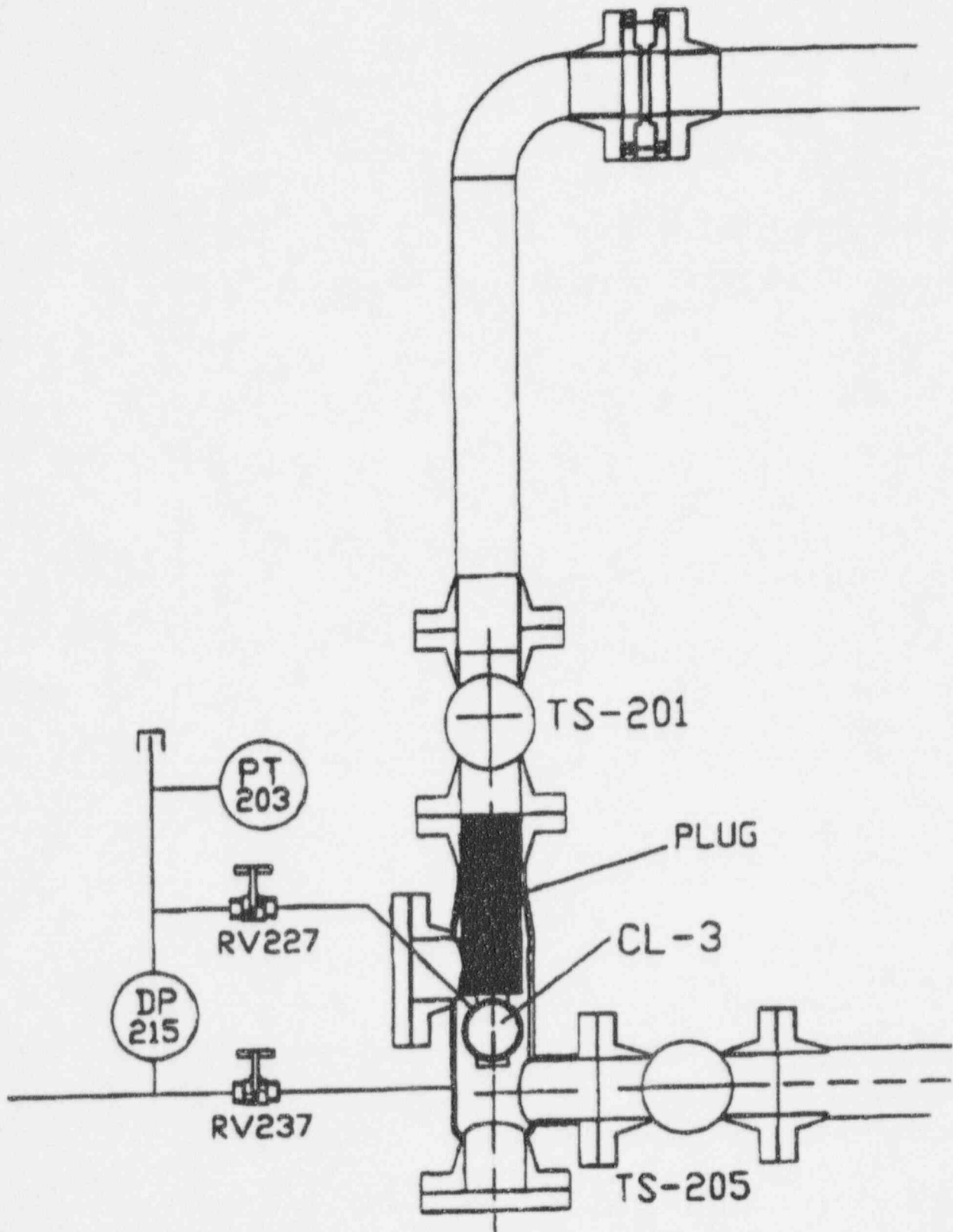


Figure 5.1.2-2 Primary Loop and Break Pipe Arrangement

Figures 5.1.2-3 through 5.1.2-80 are not included in this nonproprietary document.

5.1.3 Effect of Backpressure (Matrix Test SB19 Comparison with Matrix Test SB01)

This section identifies and describes the response of the facility based on a comparison between Matrix Test SB01 (OSU Test U0001) and Matrix Test SB19 (OSU Test U0019). The simulated break for Matrix Test SB19 was located on the bottom of CL-3 with a simulated failure of one of the ADS-4 lines. CL-3 is on the CMT side of the facility (Figures 5.1.3-1 and 5.1.3-2). Matrix Test SB19 was identical to Matrix Test SB01, except that in Matrix Test SB19, containment backpressure was simulated by automatic control of BAMS header pressure. The purpose of performing Matrix Test SB19 was to gain a comparison of how the facility responded to a small-break LOCA, with the same physical configuration, with and without containment backpressure simulation.

The transient began when break valve TS-205 opened and continued through ADS actuation; CMT, accumulator, and IRWST injection; and primary sump recirculation injection.

Matrix Test SB19 was performed on July 14, 1994. Test duration was about 6 hours. The performance of this test was considered successful because reactor vessel heater rod cooling was maintained.

Subsection 5.1.3.1 provides details related to facility configuration and initial conditions for the test. A description of inoperable instruments is provided in Subsection 5.1.3.2, and Subsection 5.1.3.3 references the sequence of events. A summary of the overall system response and any component responses that differed from the reference test SB01 are described in Subsections 5.1.3.4 and 5.1.3.5, respectively. A summary of the mass balance results is provided in Subsection 5.1.3.6. Conclusions, as they apply to Matrix Test SB19, are in Subsection 5.1.3.7.

Facility responses to the break are documented by the data-plot package at the end of this section. The numbering and content of the data plots for Matrix Test SB19 are identical to the data plots provided in Subsection 5.1.1 for Matrix Test SB01, with the exception that some ranges and time samples have been changed to allow for differences between the two tests. For example, the data plot of instrument channel LDP-601 for Matrix Test SB01 appears in Figure 5.1.1-5. The data plot for the same channel in Matrix Test SB19 appears in Figure 5.1.3-5. The discussion of Matrix Test SB19 does not refer to all of the figures in the data-plot package at the end of the section. Only figures required to explain a different response from that of Matrix Test SB01 are referred to in the text. A data plot with the suffix x indicates extended time.

5.1.3.1 System Configuration and Initial Conditions

The test was performed per an approved written procedure, met the specified initial conditions with three exceptions described in this subsection, and required no operator action.

Matrix Test SB19 simulated a 2-in. cold-leg break LOCA with long-term cooling and no nonsafety systems operating. The RNS and CVS pumps did not operate during this test. Containment

backpressure was simulated by automatic control of BAMS header pressure. A flow nozzle simulating one line of flow was installed in the ADS 4-1 line (HL-1 to the ADS 4-1 separator) to provide the single-failure simulation, and a flow nozzle simulating two lines of flow was installed in the ADS 4-2 line (HL-2 to the ADS 4-2 separator). Flow nozzles simulating two lines of flow each were installed in the ADS 1-3 inlet lines. The reactor heater control decay algorithm maintained the maximum reactor heater power output for 140 seconds. Reactor heater power then began to decay to simulate the total decay energy input of the AP600 nuclear fuel (Appendix F).

Differences between the facility configuration for the two tests were:

- After the performance of Matrix Test SB01, a vacuum breaker was installed on the ADS 1-3 sparger line inside the IRWST to eliminate negative pressures in the pressurizer and ADS 1-3 separator.
- Cold-leg flow instruments FMM-201, FMM-202, FMM-203, and FMM-204 were removed from the system and replaced with pipe spools due to continuous failures (RCP differential pressure instruments DP-203, DP-202, DP-205, and DP-206 were used to monitor for pump degradation).
- CMT balance line isolation valves RCS-529 and RCS-530 were in the AUTO and OPEN positions as initial conditions for Matrix Test SB01. For Matrix Test SB19, the valves were closed and opened by the operator 1 minute after pressing the TEST pushbutton to prevent heatup at the top of the CMTs prior to the break valve opening.
- A []^{a,b,c} vent line with an in-line check valve was installed from the top of the primary sump to the BAMS header downstream of valve CSS-906. The []^{a,b,c} vent line was in service for this test which allowed primary sump steam flow to be monitored by break separator []^{a,b,c} steam flow transmitter FVM-906.

The facility fill and vent, startup, and heatup were performed per the same approved operating procedures as were used for Matrix Test SB01. A zero check was performed for all differential pressure instruments. Initial conditions for the test were established. Refer to Subsection 2.7 for pre-test operations. The test engineer failed to record the control board indications prior to this test, but all controllers had been in the AUTO position and controlling within the specified band for about 20 minutes prior to test actuation. The initial conditions from DAS, averaged over about 2 minutes prior to the break valve opening, are presented in Table 5.1.3-1.

The following three initial condition parameters, none of which invalidate this test, were out of specification:

- HL-1 temperature (SC-141) was []^{a,b,c} percent below the required temperature band. This was within the instrumentation system accuracy requirements.

- ACC-1 pressure was []^{a,b,c} percent below the required pressure band. The accumulator was pressurized to the required pressure, as indicated on local pressure indicator PI-401, prior to test actuation. The loss of pressure between tank pressurization and test actuation was possibly due to cooling of the nitrogen gas in the accumulator. Test analysis starting with the recorded lower accumulator overpressure is still possible.
- ACC-2 pressure was []^{a,b,c} percent below the required pressure band. The accumulator was pressurized to the required pressure, as indicated on local pressure indicator PI-402, prior to test actuation. The loss of pressure between tank pressurization and test actuation was possibly due to cooling of the nitrogen gas in the accumulator. Test analysis starting with the recorded lower accumulator overpressure is still possible.

5.1.3.2 Inoperable Instruments

Table 5.1.3-2 is a list of instruments considered inoperable during all or portions of this test. Some of the instruments listed in the table are on the Critical Instrumentation List (Subsection 3.2, Table 3.2-2) and, therefore, are addressed here.

FMM-201, FMM-202, FMM-203, and FMM-204 measured flow (gpm) in each of the four cold legs. A decision was made to continue testing without the availability of these instruments. Replacement flow meters repeatedly failed; their continued use was precluded due to cracking of the ceramic liners from thermal stratification in the loop piping. The necessary boundary conditions for loop flow could be determined from cold-leg differential pressure transmitters DP-202, DP-203, DP-205, and DP-206.

CMT-1 and CMT-2 injection flow meters FMM-501 and FMM-504 and passive residual heat removal (PRHR) inlet and outlet flow meters FMM-802 and FMM-804 provided accurate data when sensing liquid, but became inaccurate when sensing two-phase or steam flow.

FMM-701 measured IRWST-1 injection flow. When the primary sump valves were opened, the flow meter indicated a negative flow as water flowed from the primary sump to the IRWST. The meter was not designed to measure reverse flow, so this measurement was invalid; however, total IRWST flow was measured by FMM-702.

FMM-905 measured break separator loop seal flow to the primary sump. As the transient proceeded, the primary sump and break separator levels exceeded the elevation of the break at the bottom of CL-3. When this occurred, break flow initially stopped and then reversed. Flow reversal through the break occurred at about []^{a,b,c} rendering subsequent data invalid.

SG tube level data (LDP-215, LDP-218, LDP-219, and LDP-222) were biased by vaporization of the water in the transmitter reference leg after the SG tubes started draining. However, the data provide accurate indication of the time when the tubes were empty.

PT-201 measured RCS pressure at the top of the SG-1 long tube. On August 15, 1994, it was discovered that the transmitter had an incorrect zero compensation which resulted in a negative error and negative data at low pressures. The transmitter zero was corrected at that time. PT-201 data obtained during Matrix Test SB19 had the zero correction performed on the transmitter, and the corrected data appears as PT_201. Negative data and corrected negative data can be used to determine trends but is considered inaccurate. PT_201 data is considered unreliable for values less than 1.1 psig, but a sufficient amount of other pressure data are available.

Data provided by ADS-4 separator instrumentation prior to the ADS 4-1 and ADS 4-2 valves opening at 1133 seconds were invalid due to the closed position of the ADS-4 valves and the ADS-4 separator loop seal valves. The instruments affected are: FMM-602, FMM-603, FVM-602, FVM-603, LDP-611, and LDP-612. Test analysis will not be affected, since ADS-4 flow did not begin until the valves opened.

TF-501 and TF-504 measured CMT fluid temperature from the long thermocouple rod location near the bottom of each CMT. The thermocouples appeared to have measured ambient conditions throughout the test, indicating a short in the thermocouple wiring. With these thermocouples inoperable, the required long thermocouple rod availability "seven out of ten and no more than one in succession failed" was met.

Considering these critical instrument failures, sufficient instrumentation was available to allow the performance of mass balances as demonstrated in Subsection 5.1.3.6 and Appendix E. An energy balance will be performed and reported in the *AP600 Low-Pressure Integral Systems Test at Oregon State University Test Analysis Report*, WCAP-14292.⁽²⁾

5.1.3.3 Sequence of Events

Table 5.1.3-3 provides the sequence of events for Matrix Tests SB01 and SB19. The first pages of the table provide the time of occurrence for selected events in both tests and the difference in time of event occurrence between the two tests. The subsequent pages of the table provide a visual representation of the time comparison by use of a bar chart. On both the numeric table and the bar chart, events are sorted in chronologic order for Matrix Test SB19.

The first pages of Table 5.1.3-3 indicate the source of the actual time data. A D in the Data Source column indicates that the recorded time was obtained from a software program that monitored digital events in the facility, including pump starts and stops, valve limit switch actuations, and alarms. An A in the Data Source column indicates that the time data were obtained by reviewing test data recorded by the DAS. Although test data from the DAS were in a digital format, the DAS monitored analog events such as pressure, flow, and temperature.

5.1.3.4 Test Results and Evaluation

This section will evaluate the overall system response to the LOCA event in Matrix Test SB19 and will be subdivided into three different phases. The different event phases, each of which are characterized by the system's behavior and thermal-hydraulic phenomena occurring in the systems are as follows:

- Initial Depressurization Phase: simulated break initiation to ADS-1 actuation
- ADS Phase: ADS-1 actuation to start of IRWST injection
- IRWST Injection Phase: start of IRWST injection to end of test

Initial Depressurization Phase

As with the reference test, Matrix Test SB19 began when the TEST pushbutton was pressed. Break valve TS-205 received an open signal from the programmable logic controller (PLC) 120 seconds later (time zero on the data plots). All time references in this section are with respect to time zero. At 0.5 second, an S signal was generated by the PLC.

PLC timing for various similar event initiations were within a second for Matrix Tests SB01 and SB19. CLDP-127 indicated that the reactor vessel began to lose inventory, i.e. steam formation began, at about []^{a,b,c} (Figure 5.1.3-3), about []^{a,b,c} later than when steam formation occurred in reference test SB01.

In Matrix Test SB19, the pressurizer and pressurizer surge line emptied at []^{a,b,c} respectively (Figure 5.1.3-5), about []^{a,b,c} earlier for the pressurizer and []^{a,b,c} earlier for the pressurizer surge line than in Matrix Test SB01. The difference in time can be attributed to higher break flow rates early in Matrix Test SB19 (Figure 5.1.3-62).

The early emptying of the pressurizer and pressurizer surge line in Matrix Test SB19 did not result in earlier CMT transition from recirculation to draindown (Figure 5.1.3-6). CMT-1 transition occurred at about []^{a,b,c} in Matrix Test SB19, compared with []^{a,b,c} in Matrix Test SB01. It appears CMT-2 started to transition at about 100 seconds in Matrix Test SB19 but the balance line refilled. CMT-2 transition actually occurred at about 270 seconds in Matrix Test SB19, compared with []^{a,b,c} in Matrix Test SB01.

The algorithm for core decay heat simulation of reactor power used during Matrix Test SB19 was the same algorithm used during reference test SB01. The core decay heat simulation of reactor heater power followed the programmed algorithm just as it did in Matrix Test SB01 (Appendix F).

During Matrix Test SB19, the SG U-tubes emptied from between []^{a,b,c} earlier than the U-tubes during Matrix Test SB01 (Figures 5.1.3-7 and 5.1.3-8). The SG channel heads and hot legs drained earlier during Matrix Test SB19 than during Matrix Test SB01, with the exception of

HL-2 which drained about []^{a,b,c} later during Matrix Test SB19 (Figures 5.1.3-9, 5.1.3-10, and 5.1.3-11). The difference in drain time for the SG U-tubes, channel heads, and hot legs can be attributed to the higher break flow rates early in Matrix Test SB19 (Figure 5.1.3-62).

There was essentially no difference in the PRHR HX response between Matrix Tests SB01 and SB19 during this phase of the test (Figures 5.1.3-41, 5.1.3-66, and 5.1.3-67).

During Matrix Test SB19, the fluid level inside the reactor vessel core barrel reached its minimum collapsed level of []^{a,b,c} at about []^{a,b,c} per CLDP-127 (Figure 5.1.3-15), about []^{a,b,c} later and about []^{a,b,c} lower than during Matrix Test SB01. A minimum core barrel level of 60 in. was reached during the depressurization phase. Also in Matrix Test SB19, during a condensation/depressurization event that occurred at about []^{a,b,c} the collapsed level transitioned from []^{a,b,c} then back to []^{a,b,c} period. Heater-rod cooling was maintained during both instances (Figure 5.1.3-44).

Initial RCS depressurization was similar for both tests from break valve opening until []^{a,b,c} when the ADS-1 valve opened in Matrix Test SB19 causing pressure to decrease at a greater rate than for Matrix Test SB01 where the ADS-1 valve did not open until []^{a,b,c}. The period of quasi-equilibrium pressure between the RCS and the secondary side of the SGs was about []^{a,b,c} (Figure 5.1.3-45) for both tests. In the first few seconds after the break valve opened the SGs were isolated on both the feedwater and steam sides to minimize RCS heat losses. The only cooling available to the SGs was heat losses to ambient conditions. With RCS pressure decreasing due to the break and SG pressure increasing due to heat absorption from the RCS, the pressures converged at about []^{a,b,c}. At about []^{a,b,c} when inventory losses through the break caused RCS pressure to drop below the pressure on the SG secondary side, the SGs became a heat source for the RCS.

ADS Phase

CMT-1 reached its low level setpoint at []^{a,b,c} triggering the ADS-1 valve opening at about []^{a,b,c} in Matrix Test SB19, as compared with []^{a,b,c} for the CMT-1 low level setpoint to be reached and []^{a,b,c} for the ADS-1 valve to open in reference test SB01 (Figure 5.1.3-6). The RCS pressure response following ADS-1 opening was similar for both tests (Figure 5.1.3-45); facility response to the opening of ADS-2, ADS-3, and ADS-4 valves was also similar.

CMT injection flow data appeared consistent between the two tests (Figure 5.1.3-16). In Matrix Test SB19, the CMT-2 low level setpoint was not reached until about []^{a,b,c} after CMT-1 reached its setpoint. In Matrix Test SB01, the two CMTs attained their low level setpoints within []^{a,b,c} of each other and prior to accumulator injection beginning. A possible explanation for the delay of setpoint achievement in CMT-2 during Matrix Test SB19 is the timing of initiation of accumulator injection which started for both accumulators about []^{a,b,c} before ADS-1 opened.

Accumulator injection created backpressure in the DVI header that partially or completely shut off CMT injection by closing CMT injection line check valves; the accumulators must necessarily have a higher overpressure than the RCS and the CMTs in order to inject.

Accumulator injection during Matrix Test SB19 began about []^{a,b,c} before the ADS-1 valve opened, about []^{a,b,c} earlier than in Matrix Test SB01 (Figure 5.1.3-16). The earlier accumulator injection in Matrix Test SB19 was attributed to the faster depressurization rate following the quasi-equilibrium pressure plateau between primary and secondary pressures (Figure 5.1.3-45). The faster depressurization rate in Matrix Test SB19 can be attributed to higher break flow rates over the first []^{a,b,c} (Figure 5.1.3-28). The accumulator flow profiles and interaction with the CMTs was consistent for both tests (Figure 5.1.3-16).

Early in Matrix Test SB19, condensation/depressurization events occurred at about 545 and 615 seconds, as compared with []^{a,b,c} during reference test SB01. DP-114 and DP-130 exhibited large negative spikes indicative of instantaneous high steam flow from the reactor vessel upper plenum through the upper head and into the downcomer area (Figure 5.1.3-19). At the same time, CLDP-127 showed a sharp-spike decrease in level indication, and CLDP-116 and CLDP-140 indicated sharp-spike increases (Figure 5.1.3-15). The parameters of RCS pressure, reactor vessel levels, and DVI rates were almost identical at the time of the event in both tests (Figures 5.1.3-45, 5.1.3-15, and 5.1.3-17). A loud "bang" was heard in the BAMS steam discharge header and recorded in the test log at []^{a,b,c} into the test. A condensation/depressurization event in the BAMS steam discharge header may have been the precursor for the event at []^{a,b,c}

Test data revealed that the collapse of the superheated steam bubble in the upper portion of the reactor vessel downcomer annulus resulted in the downcomer fluid accelerating upward and impacting the bottom of the core barrel flange where the core bypass holes are located. The low pressure created in the upper downcomer annulus by the collapse of the steam bubble also resulted in a rapid increase of steam flow from the core barrel, through the upper head, and into the downcomer. Subsection 7.1 provides a more detailed treatment of condensation/depressurization events.

The pressurizer and pressurizer surge line reflooded during blowdown through the ADS 1-3 valves (Figure 5.1.3-5) during both tests. During Matrix Test SB19, the pressurizer re-emptied about []^{a,b,c} earlier than during Matrix Test SB01, probably the result of faster RCS depressurization and the vacuum breaker installed on the ADS 1-3 sparger line inside the IRWST (Figure 5.1.3-45).

The PRHR HX inlet head level transmitter recorded HX level changes during Matrix Test SB19 but did not respond during Matrix Test SB01 (Figures 5.1.3-66 and 5.1.3-67). During Matrix Test SB01, the HX appeared to reach a minimum level of []^{a,b,c} at about []^{a,b,c} refill to []^{a,b,c} at about []^{a,b,c} and then return to a minimum again at []^{a,b,c}. In Matrix Test SB19, the HX level was predominantly greater than []^{a,b,c} during the ADS phase and appeared to maintain more flow. One possible cause for what appeared to be a more efficient PRHR HX response

during Matrix Test SB19 is that RCS levels remained higher than the levels during Matrix Test SB01 (Figure 5.1.3-15).

IRWST injection began at []^{a,b,c} about []^{a,b,c} earlier during Matrix Test SB19 than during Matrix Test SB01 (Figure 5.1.3-37). Since the start of IRWST injection is dependent on the differential pressure between the reactor vessel and the IRWST, and the force for injection is gravity, the early injection during Matrix Test SB19 was probably the result of the faster RCS depressurization and the increased pressure in the IRWST due to containment pressure simulation.

IRWST Injection Phase

The early start of IRWST injection at 1030 seconds during Matrix Test SB19 had two major effects on the facility's overall response. First, CMT injection was stopped by the IRWST injection head prior to the CMTs emptying completely, while in Matrix Test SB01 the CMTs emptied before IRWST injection started (Figures 5.1.3-6 and 5.1.3-16). Second, with no delay between CMT and IRWST injection, the cold legs refilled and subcooled about []^{a,b,c} earlier than during Matrix Test SB01 (Figures 5.1.3-42, 5.1.3-43, 5.1.3-53, and 5.1.3-54). Because the cold legs maintained some level in the early part of Matrix Test SB19, flow was maintained through the break; in Matrix Test SB01, when the cold legs emptied, break flow stopped between about []^{a,b,c} (Figure 5.1.3-28).

Both CMTs reflooded during both tests (Figures 5.1.3-6 and 5.1.3-30 through 5.1.3-34); however, the timing of CMT reflood and CMT response during reflood were different. CMT-1 reflood occurred at about []^{a,b,c} in Matrix Test SB19, []^{a,b,c} earlier than in Matrix Test SB01. CMT-2 reflood occurred at about []^{a,b,c} earlier than in Matrix Test SB01. The earlier reflood of the CMTs in Matrix Test SB19 was directly attributed to the earlier reflood of the cold legs. Reflood of the CMTs occurred for the same reasons described in reference test SB01 (Subsection 5.1.1).

In Matrix Test SB19, the CMT was at higher temperatures than in Matrix Test SB01 when the balance line refilled. When the cooler fluid in the balance line reached a long horizontal section of pipe at about []^{a,b,c} the fluid flashed causing a spike increase in CMT pressure. The pressure spike resulted in a rapid reduction of level in the balance line and a spike discharge from the CMT into the DVI. The CMT pressure then began to decrease again but from a higher pressure. The pressure spike phenomena occurred once in CMT-1 and four times in CMT-2. This increasing pressure spike phenomena did not occur in the reference test SB01 data.

Condensation/depressurization events were observed during the CMT reflood during SB19 like occurred during Matrix Test SB01.

During reference test SB01, the pressurizer reflooded to about []^{a,b,c} over the period of about []^{a,b,c}. This phenomena was attributed to negative pressure formed in the

pressurizer and ADS 1-3 separator when HL-2 filled to the surge-line level with subcooled fluid while the ADS 1-3 sparger was still submerged in the IRWST. A vacuum breaker was installed on the ADS 1-3 sparger line inside the IRWST following the performance of Matrix Test SB01 to prevent a recurrence of a reflood caused by negative pressure. A pressurizer reflood did not occur during Matrix Test SB19 (Figure 5.1.3-5).

Primary sump injection started at about []^{a,b,c} in Matrix Test SB19, about []^{a,b,c} later than in Matrix Test SB01 (Figure 5.1.3-37). During Matrix Test SB01, injection flow started through the primary sump injection line check valves when the fluid levels in the sump and the IRWST equalized, about []^{a,b,c} before the sump injection valves opened. During Matrix Test SB19, injection flow did not start until almost []^{a,b,c} after the primary sump injection valves opened. A possible explanation for the delay in sump injection during Matrix Test SB19 is that BAMS pressure increased from about []^{a,b,c} and caused a slight differential pressure between the IRWST and the primary sump (Figure 5.1.3-74x).

Sump injection recirculation continued for 2 hours. The facility response while in the sump injection recirculation mode during Matrix Test SB19 appeared consistent with the data obtained during Matrix Test SB01.

5.1.3.5 Comparison of Component Responses

Reactor

Reactor response was almost identical for Matrix Tests SB01 and SB19, with the exception of times. The lowest collapsed level recorded in the CLDP-127 test data for Matrix Test SB19 was []^{a,b,c} at []^{a,b,c} later than in Matrix Test SB01 (Figure 5.1.3-15). During a condensation/depressurization event that occurred at about []^{a,b,c} the indicated level transitioned from []^{a,b,c} Reactor heater rod cooling was maintained during both level excursions (Figure 5.1.3-44).

Core Makeup Tanks

The early emptying of the pressurizer and pressurizer surge line in Matrix Test did not result in earlier CMT transition from recirculation to draindown (Figure 5.1.3-6). CMT-1 transition occurred at about []^{a,b,c} in Matrix Test SB19, compared with []^{a,b,c} in Matrix Test SB01. CMT-2 transition occurred at about []^{a,b,c} in Matrix Test SB19, compared with []^{a,b,c} in Matrix Test SB01. To initiate the CMT transition from recirculation to draindown, the fluid coupling between the cold legs and the balance lines must be broken. In both tests, CL-1 and CL-3 fluid temperatures (measured []^{a,b,c} from the top inside diameter of the reactor nozzle flange) were subcooled when the CMTs transitioned from recirculation to draindown (Figures 5.1.3-53 and 5.1.3-54). One indication that the cold legs have partially drained is that their top thermocouples will indicate superheat. A possible explanation for the transition delay in Matrix Test SB19 is that

containment backpressure simulation delayed the start of cold leg draindown; i.e., the transition from single to two-phase flow. Due to the location of SC-105 and SC-101 in the cold-leg flow stream, the broken fluid coupling between the cold legs and the balance lines would occur before the thermocouples would sense cold-leg draindown.

Both CMTs reflooded during both tests (Figures 5.1.3-5 and 5.1.3-30 through 5.1.3-34); however, the timing of CMT reflood and CMT response during reflood were different. CMT-1 reflood occurred at about []^{a,b,c} in Matrix Test SB19, []^{a,b,c} earlier than in Matrix Test SB01. CMT-2 reflood occurred at about []^{a,b,c} earlier than in SB01. Reflood of the CMTs occurred for the same reasons described in reference test SB01 (Subsection 5.1.1). The reason for the earlier CMT reflood in Matrix Test SB19 was that the cold legs refilled with subcooled fluid earlier than in Matrix Test SB01. The balance lines refilled due to the condensation of steam in the CMT or the balance line and the subsequent reduction in CMT pressure with respect to RCS pressure.

In Matrix Test SB19, the CMT was at higher temperatures than in Matrix Test SB01 when the balance line refilled. When the cooler fluid in the balance line reached a long horizontal section of pipe at about []^{a,b,c} (representing a larger hot surface area than the vertical section of pipe), the fluid flashed causing a spike increase in CMT pressure. The pressure spike resulted in a rapid reduction of level in the balance line and a spike discharge from the CMT into the DVI. The CMT pressure would then begin to decrease again but from a higher pressure. The pressure spike phenomena occurred once in CMT-1 and four times in CMT-2. In CMT-2 the first two events occurred at the []^{a,b,c} level and the last two occurred at the next horizontal pipe run located at about the []^{a,b,c} level. This increasing pressure spike phenomena did not occur in the reference test SB01 data.

In addition, in Matrix Test SB19, CMT-1 was the first to reflood and the first to drain completely; in Matrix Test SB01, CMT-2 was the first to reflood and the first to drain completely.

Condensation/depressurization events were observed during the CMT reflood during Matrix Test SB19 like occurred during Matrix Test SB01.

CMT injection was sufficient to maintain reactor heater rod cooling until IRWST injection began.

Accumulators

Accumulator response was identical for Matrix Tests SB01 and SB19, with the exception of event timing.

The accumulators increased or stabilized reactor vessel indicated fluid levels.

Pressurizer

In Matrix Test SB19, the pressurizer and pressurizer surge line emptied at []^{a,b,c} respectively (Figure 5.1.3-5), about []^{a,b,c} earlier for the pressurizer and []^{a,b,c} earlier for the pressurizer surge line than in Matrix Test SB01. The difference in time can be attributed to higher break flow rates early in Matrix Test SB19 (Figure 5.1.3-62).

The pressurizer reflooded during Matrix Test SB01, but a similar event did not occur during Matrix Test SB19 (Figure 5.1.3-5). As described in Subsection 5.1.1.4, the reflood was caused by a negative pressure developing in the pressurizer and ADS 1-3 separator with respect to the pressure in the reactor vessel. The negative pressure was precipitated by several things: the ADS 1-3 sparger located in the IRWST was submerged; the hot legs had refilled with subcooled fluid into the surge line; and the combination of the previous items resulted in condensation of steam in the pressurizer and ADS 1-3 separator with subsequent cooling.

The problem of a negative pressure being developed in the pressurizer and ADS 1-3 separator had been corrected prior to the performance of Matrix Test SB19 by a facility modification that installed a vacuum breaker on the ADS 1-3 sparger line inside the IRWST.

The other difference between the two tests was that during Matrix Test SB01, the pressurizer heaters remained energized at about 1.5 kW. This was corrected prior to performance of Matrix Test SB19 by a procedural change that required the test crew to open the pressurizer heater breaker when the S signal was verified (Figure 5.1.3-24). During Matrix Test SB01 the logic was supposed to drive the heater power demand to zero resulting in zero power from the heater SCRs to the heaters. According to the data for Matrix Test SB01 it can be postulated that the SCR control circuitry had not been properly tuned.

All other pressurizer responses during Matrix Test SB19 were similar to the responses during Matrix Test SB01 with the exception of timing.

Passive Residual Heat Removal Heat Exchanger

There was a difference in the PRHR HX performance during the ADS phase of SB19 than during SB01 (Figures 5.1.3-66 and 5.1.3-67). The PRHR HX inlet head level transmitter recorded heat exchanger level changes during Matrix Test SB19 but did not record a level change during Matrix Test SB01. During Matrix Test SB01 the heat exchanger appeared to reach a minimum level of []^{a,b,c} at about []^{a,b,c} and refill to []^{a,b,c} at about []^{a,b,c} and return to a minimum again at []^{a,b,c}. In Matrix Test SB19 the heat exchanger level was predominantly greater than []^{a,b,c} during this phase of the test and appeared to maintain more flow. One possible cause for what appears to be more efficient PRHR HX response during Matrix Test SB19 is that RCS levels remained higher than the levels did during Matrix Test SB01 (Figure 5.1.3-15).

The PRHR HX response during Matrix Test SB19 was similar to reference test SB01 except for the timing of events and the response of the HX wide-range level data after about []^{a,b,c}. During Matrix Test SB01 the HX partially refilled during the period of time that the RCS loops were filled with subcooled fluid. Following the refill, when small pressure and level oscillations began to occur, it is possible that the oscillations caused the PRHR HX inlet line to "burp" allowing a negative pressure in the HX to equalize with the RCS. Equalization of pressures allowed equalization of PRHR levels with those of the RCS. During Matrix Test SB01, once the levels equalized the PRHR level remained essentially constant.

Data obtained during the performance of Matrix Test SB19 indicate that PRHR performance was consistent with the performance during Matrix Test SB01 until the final draindown of the HX. During Matrix Test SB19 the HX began to drain but, the data then suggests that the drain stopped and the HX began a slow refill for as long as data was obtained (Figure 5.1.3-68). It is possible that the HX was refilling, but another possibility is that the wide-range level instrument LDP-802 was slowly losing its reference leg due to vaporization from the lower saturated pressure in the HX.

Steam Generators

SG response during the performance of Matrix Test SB19 was similar to their response during Matrix Test SB01 with the exception of event timing.

Cold Legs and Hot Legs

The RCS cold-leg response during Matrix Test SB19 was different than during Matrix Test SB01 in that the cold legs refilled earlier in the test (based on reactor vessel downcomer levels Figure 5.1.3-15). During Matrix Test SB01 the cold legs began to empty at about []^{a,b,c} and did not refill until about []^{a,b,c}. During Matrix Test SB19 the cold legs began to empty about []^{a,b,c} earlier but refilled at about []^{a,b,c}. A possible explanation for the early refill during Matrix Test SB19 is that IRWST injection started earlier and DVI flow was greater than break flow (Figures 5.1.3-17 and 5.1.3-28).

The RCS hot legs response during the performance of Matrix Test SB19 was similar to their response during Matrix Test SB01 with the exception of event timing.

In-Containment Refueling Water Storage Tank

IRWST response during the performance of SB19 was similar to IRWST response during the reference test (SB01) except that during Matrix Test SB19 the low-low level setpoint and opening the primary sump injection valves occurred about []^{a,b,c} earlier. The earlier opening of the sump injection valves during Matrix Test SB19 may have been the result of sump injection not occurring through the sump injection line check valves allowing IRWST injection to remain at a higher rate for longer.

The IRWST injection was sufficient to recover reactor vessel levels and maintain the reactor heater rods cooled.

Break and ADS Measurement System

BAMS response during the performance of Matrix Test SB19 was significantly different from the response during Matrix Test SB01 due to the containment back-pressure simulation used during Matrix Test SB19 (Figures 5.1.3-73, 5.1.3-74, 5.1.3-74x, and 5.1.3-75). Following break valve opening, the BAMS header pressure tracked the projected algorithm curve for containment backpressure simulation and reached a maximum pressure of about []^{a,b,c}. The projected algorithm curve maximum pressure for the facility was about []^{a,b,c}. The BAMS header pressure stayed at []^{a,b,c} until []^{a,b,c} and then began to decrease. Actual pressure remained below projected pressure early in the test except for a brief period between []^{a,b,c}. The BAMS pressure control valve (CSS-901) was in the AUTO and CLOSED positions at the start of the test. The control valve closed when header pressure dropped below the programmed value, then re-opened to control pressure at about 16,000 seconds. BAMS header pressure attained the projected pressure again at about []^{a,b,c} and maintained projected pressure for the remainder of the test. A possible explanation as to why the actual pressure did not reach the projected pressure and maintain it throughout the test is that the BAMS heat losses were greater than anticipated.

5.1.3.6 Mass Balance

The mass balance results for Matrix Test SB19 test data were calculated based on water inventory before and after the test and are provided in Appendix E. The mass at the end of the test was within 0.5 percent of the mass at the beginning of the test as compared to 5.8 percent for Matrix Test SB01.

5.1.3.7 Conclusions

The test was performed with minimal problems and is considered acceptable. Although not all of the facility initial conditions met the specified acceptance criteria, the deviations did not impact the quality of the data. The instrumentation problems encountered were not critical to the performance of the facility mass and energy balances.

Facility response to the test was as anticipated for the conditions that were established. The data clearly demonstrate that cooling of the reactor heater rods was maintained throughout the duration of the test.

TABLE 5.1.3-1
MATRIX TEST SB19 INITIAL CONDITIONS

Parameter	Instrument No.	Specified Initial Condition	Actual Initial Condition	Comments
Pressurizer pressure ⁽¹⁾	PT-604	70 ± 2 psig		a,b,c
HL-1 temperature ⁽¹⁾	SC-141	$430 \pm$ °F		[] ^{a,b,c} below required temperature
HL-2 temperature ⁽¹⁾	SC-140	$420 \pm$ °F		
SG-1 pressure ⁽¹⁾	PT-301	285 ± 5 psig		
SG-2 pressure ⁽¹⁾	PT-302	285 ± 5 psig		
Pressurizer level ⁽¹⁾	LDP-601	65 ± 5 in.		Uncompensated level (corrected for specific volume change)
SG-1 narrow-range level ⁽¹⁾	LDP-303	26 ± 3 in.		Uncompensated level (corrected for specific volume change)
SG-2 narrow-range level ⁽¹⁾	LDP-304	26 ± 3 in.		Uncompensated level (corrected for specific volume change)
IRWST temperature ⁽²⁾	TF-709	< 80°F		
CMT-1 temperature ⁽²⁾	TF-529	< 80°F		
CMT-2 temperature ⁽²⁾	TF-532	< 80°F		
ACC-1 temperature ⁽²⁾	TF-403	< 80°F		
ACC-2 temperature ⁽²⁾	TF-404	< 80°F		
IRWST level ⁽²⁾	LDP-701	Level established by fill line elevation		
ACC-1 level ⁽²⁾	LDP-401	Level established by standpipe at 37 in.		
ACC-2 level ⁽²⁾	LDP-402	Level established by standpipe at 37 in.		

TABLE 5.1.3-1 (Continued)
MATRIX TEST SB19 INITIAL CONDITIONS

Parameter	Instrument No.	Specified Initial Condition	Actual Initial Condition	Comments
ACC-1 pressure ⁽²⁾	PT-401	232 ± 2 psig	[] ^{a,b,c}	[] ^{a,b,c} below required pressure
ACC-2 pressure ⁽²⁾	PT-402 PT-402	232 ± 2 psig	[]	[] ^{a,b,c} below required pressure
CMT-1 level ⁽²⁾	Full	LDF-507	[]	
CMT-2 level ⁽²⁾	Full	LDP-502	[]	

Note:

- (1) The test engineer failed to record the control board indications prior to this test, but all controllers had been in the AUTO position and controlling within the specified band for about 20 minutes prior to test actuation. The initial conditions from DAS, averaged over about 2 minutes prior to the break valve opening, are recorded here.
- (2) Data were not recorded in procedure, but the test engineer verified that specified conditions were achieved while establishing initial conditions. The value of the parameter was determined post-test by calculating the average DAS indication for a time of about 2 minutes before the break valve opened.

TABLE 5.1.3-2
MATRIX TEST SB19 INOPERABLE INSTRUMENTS/INVALID DATA CHANNELS

Instrument No.	Instrument Type	Description of Problem
FMM-201* FMM-202* FMM-203* FMM-204*	Magnetic flow meter	Removed from system (Subsection 5.1.3.2)
FMM-501*	Magnetic flow meter	Data invalid after 13,053 seconds when CMT was empty
FMM-502	Magnetic flow meter	Data invalid after 270 seconds due to possible steam in balance line
FMM-503	Magnetic flow meter	Data invalid after 246 seconds due to possible steam in balance line
FMM-504*	Magnetic flow meter	Data invalid after 13,249 seconds when CMT was empty
FMM-701*	Magnetic flow meter	Negative values after break separator level exceeded break elevation at about 12,450 seconds invalid
FMM-802*	Magnetic flow meter	Data invalid after steam formed in PRHR HX inlet line (about 130 seconds)
FMM-804*	Magnetic flow meter	Data valid until PRHR HX initially drained at 1750 seconds; after this time, the possibility of steam in the outlet line invalidated the data
FMM-905	Magnetic flow meter	Negative values invalid after break separator level exceeded the break elevation at about 13,400 seconds
HFM-103 HFM-105 HFM-505 HFM-510 HFM-703 HFM-801	Heat flux meter	Inoperable throughout test
HPS-203-1 through HPS-203-3 HPS-509-1 through HPS-509-3	Heated phase switch	Inoperable throughout test
LDP-201 LDP-202 LDP-203 LDP-204 LDP-205 LDP-206	Differential pressure transmitter - level	Data invalid due to effect of vertical portion of sense line attached to top of pipe; data can show level trends and when pipe empties or starts to drain, but absolute level indication can not be used
LDP-207 LDP-208 LDP-209	Differential pressure transmitter - level	Inoperable; ranged improperly; data can show level trends but absolute level indication can not be used
LDP-215* LDP-216 LDP-217 LDP-218* LDP-219* LDP-220 LDP-221 LDP-222*	Differential pressure transmitter - level	Inoperable; when tube voids, reference leg steams off; see Subsection 2.4

TABLE 5.1.3-2 (Continued)
MATRIX TEST SB19 INOPERABLE INSTRUMENTS/INVALID DATA CHANNELS

Instrument No.	Instrument Type	Description of Problem
LDP-801	Differential pressure cell - level	Inoperable; indicated full when HX not full
PT_101	Pressure transmitter	Data less than 6.1 psig invalid
PT_102	Pressure transmitter	Data less than 6.2 psig invalid
PT_103	Pressure transmitter	Data less than 6.2 psig invalid
PT_104	Pressure transmitter	Data less than 6.4 psig invalid
PT_108	Pressure transmitter	Data less than 8.4 psig invalid
PT_109	Pressure transmitter	Data less than 6.3 psig invalid
PT_111	Pressure transmitter	Data less than 6.0 psig invalid
PT_112	Pressure transmitter	Data less than 8.8 psig invalid
PT_113	Pressure transmitter	Data less than 6.4 psig invalid
PT_201*	Pressure transmitter	Data less than 1.1 psig invalid
PT_202	Pressure transmitter	Data less than 5.9 psig invalid
PT_203	Pressure transmitter	Data questionable throughout test
PT_205	Pressure transmitter	Data less than 6.1 psig invalid
PT-610*	Pressure transmitter	Over-ranged from 358 to 1330 seconds
PT-611*	Pressure transmitter	Over-ranged from 340 to 1466 seconds
PT-701	Pressure transmitter	Over-ranged from 344 to 1420 seconds
TF-170	Thermocouple fluid temperature	Affected by leakage from reactor downcomer
TF-203 TF-501* TF-504* TF-615 TF-619 TF-702	Thermocouple fluid temperature	Inoperable; indicated ambient throughout test
TFM-103 TFM-105 TFM-703	Thermocouple wall temperature	Inoperable throughout test
TH-317-1 TH-317-4	Thermocouple heater rod	Heater rod replaced with non-instrumented rod
TW-503	Thermocouple wall temperature	Inoperable throughout test
TW-534 TW-547 TW-552	Thermocouple wall temperature	Inoperable; indicated ambient throughout test

Note:

* Instruments marked with an asterisk are critical instruments. See Subsection 5.1.3.2 for discussion.

Table 5.1.3-3 on pages 5.1.3-18 through 5.1.3-25 are not included in this nonproprietary document.

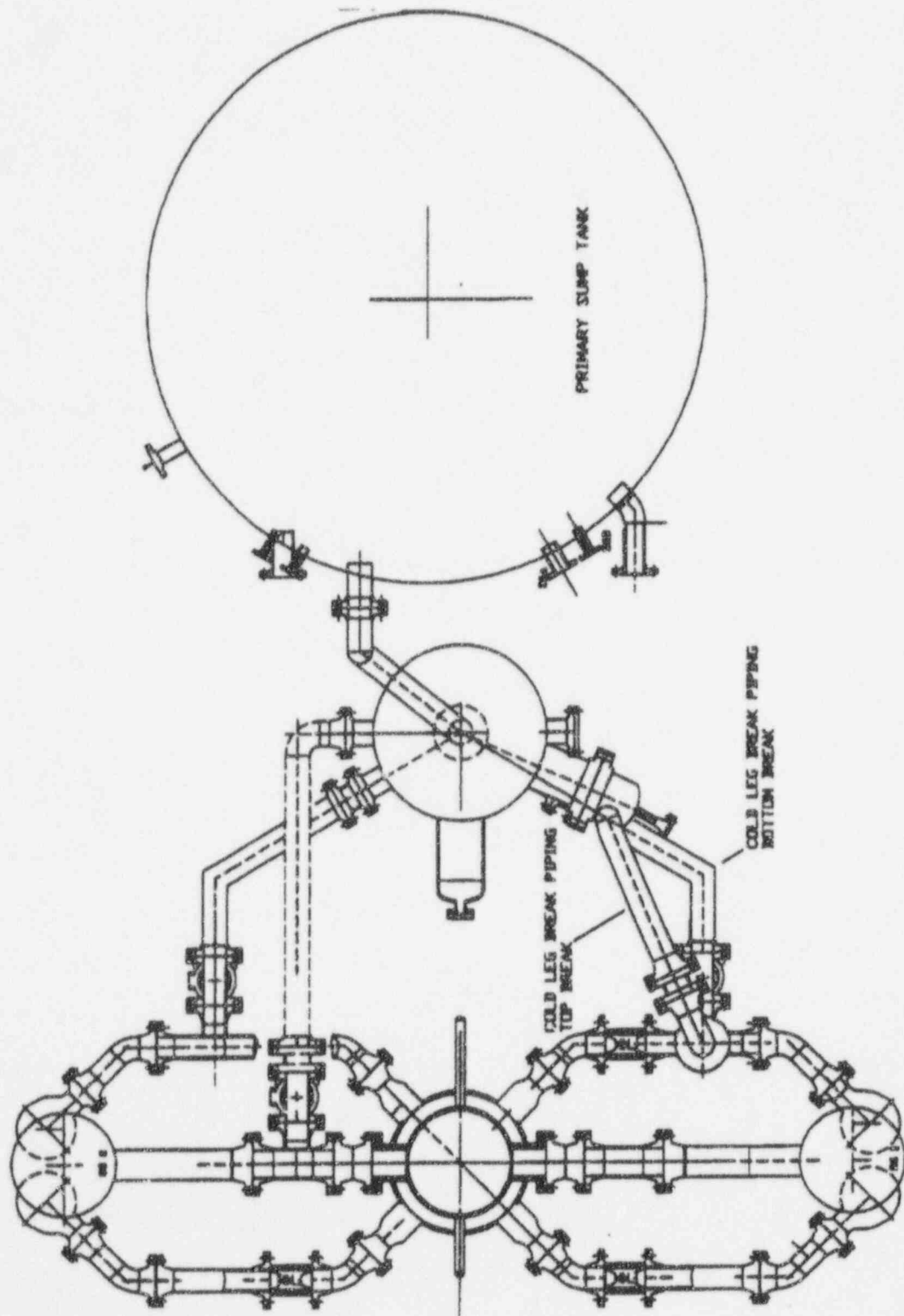


Figure 5.1.3-1 Primary Loop and Break Piping Layout

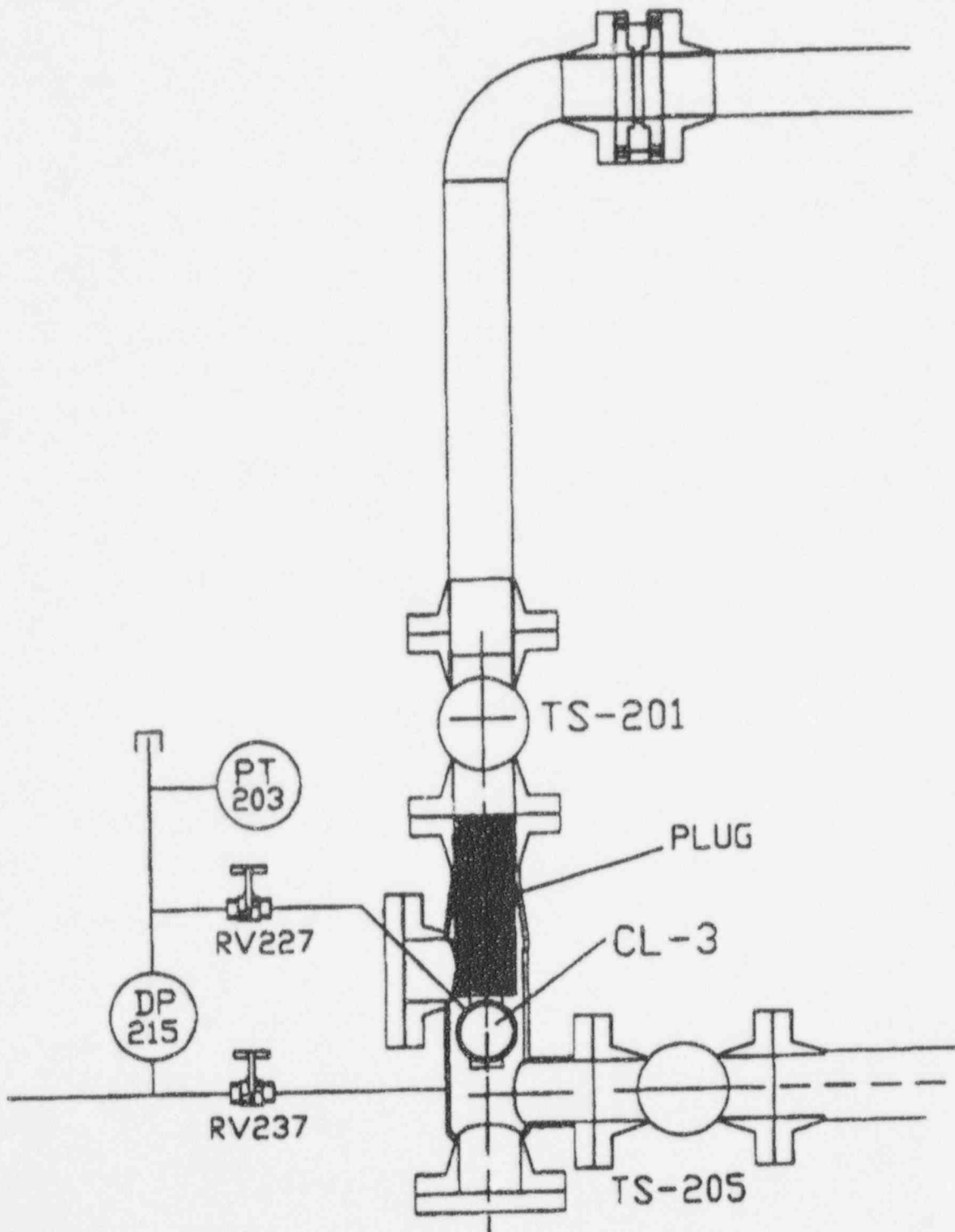


Figure 5.1.3-2 Primary Loop and Break Pipe Arrangement

Figures 5.1.3-3 through 5.1.3-80 are not included in this nonproprietary document.

5.1.4 Effect of a Larger Break Size (Matrix Test SB21 Comparison with Matrix Test SB01)

In this section, the test results from Matrix Test SB21 (OSU Test U0021) are compared with those of Matrix Test SB01 (OSU Test U0001). The simulated large-break LOCA (LBLOCA) was located on the top and the bottom of CL-3 with a simulated single failure being one of the ADS-4 lines. CL-3 is on the CMT side of the facility (Figures 5.1.4-1 and 5.1.4-2). The purpose of performing Matrix Test SB21 was to compare facility response to a LBLOCA, using the same physical configuration as Matrix Test SB01, with the exception of break size.

Matrix Test SB21 was performed on August 3, 1994. The transient began when break valves TS-201 and TS-205 opened and continued through ADS actuation; CMT/accumulator/IRWST injection; and primary sump recirculation injection. The performance of this test was considered successful because reactor heater rod cooling was maintained.

Subsection 5.1.4.1 provides details related to the systems' configuration and initial conditions for the test. A description of inoperable instruments is provided in Subsection 5.1.4.2, and Subsection 5.1.4.3 references the sequence of events. A summary of the overall system response and any component responses that differed from the reference test are described in Subsections 5.1.4.4 and 5.1.4.5, respectively. A summary of the mass balance results is provided in Subsection 5.1.4.6. Conclusions, as they apply to Matrix Test SB21, are in Subsection 5.1.4.7.

The facility responses to the break are documented by the data plots, referenced as figures in the text, at the end of this section. The numbering and content of the data plots for Matrix Test SB21 are identical to the data plots provided in Subsection 5.1.1 for Matrix Test SB01, with the exception that some ranges and time samples have been changed to allow for differences in the two tests. For example, the data plot for instrument channel LDP-601 for Matrix Test SB01 is shown in Figure 5.1.1-5; the data plot for the same channel in Matrix Test SB21 is shown in Figure 5.1.4-5. Not all of the figures in the data plot package at the end of the section are referenced. Only those figures required to explain a different response from that of Matrix Test SB01 are referred to in the text. The additional figures are provided for the benefit of readers who wish to compare additional Matrix Test SB21 parameters to the comparable parameters for Matrix Test SB01. A data plot with the suffix x indicates extended time.

5.1.4.1 System Configuration and Initial Conditions

The test was performed per an approved written procedure and met the specified initial conditions with three exceptions that are discussed in this subsection. All actions were automatic, with the exception that operator response was required for closing CSS-902 and CSS-906 in the BAMS header when total steam flow decreased to approximately []^{a,b,c}

Matrix Test SB21 simulated a double 4-in. cold-leg break LOCA with long-term cooling, without the operation of nonsafety systems. The normal residual heat removal system (RNS) and chemical and

volume control system (CVS) pumps did not operate during this test. Inserts simulating the 4-in. top and bottom cold-leg breaks were installed in the break spools located at the top and bottom of CL-3. The top 4-in. break flow was initially directed vertically (up) and then horizontally to the break separator upper nozzle. The bottom 4-in. break flow was initially directed vertically (down) and then horizontally to the break separator cold-leg nozzle.

A flow nozzle simulating one line of flow was installed in the ADS 4-1 line—HL-1 to ADS 4-1 separator—to provide the single failure simulation, and a flow nozzle simulating two lines of flow was installed in the ADS 4-2 line—HL-2 to the ADS 4-2 separator. Additionally, flow nozzles simulating two lines of flow each were installed in the ADS 1-3 inlet lines.

The differences in facility configuration for the two tests were:

- After the performance of Matrix Test SB01, a vacuum breaker was installed on the ADS 1-3 sparger line inside the IRWST to eliminate negative pressures in the pressurizer and ADS 1-3 separator.
- FMM-201, FMM-202, FMM-203, and FM-204, which measured cold-leg flow, were removed from the system and replaced with pipe spools because of continuous failures. RCP differential pressure instrument data (DP-202, DP-203, DP-205, and DP-206) could be used to monitor pump degradation.
- CMT balance line isolation valves RCS-529 and RCS-530 were in the AUTO and OPEN positions, as part of the initial conditions for Matrix Test SB01, but were closed and opened by the operator 1 minute after the TEST pushbutton was pressed in Matrix Test SB21 to prevent heatup at the top of the CMTs prior to break valve opening.
- A 6-in. vent line with an in-line check valve was installed from the top of the primary sump to the BAMS header downstream of CSS-906. The 6-in. vent line had a blank installed and was not in service for this test.
- TF-103 and TF-104 were removed from CL-3 and CL-4, respectively, and were replaced with thermocouple rods connected to an independent recording system to provide data for a cold-leg thermal stratification study.
- A new set of decay heat curve algorithms was programmed into the reactor controller to maintain reactor heater power at 600 kW for 300 seconds prior to initiating the power decay during Matrix Test SB21 (Appendix F). During Matrix Test SB01, power was held at 600 kW for 140 seconds prior to initiating the power decay.
- BAMS steam header valves CSS-901, CSS-902, CSS-905, and CSS-906 were all open at the beginning of Matrix Test SB21, and then CSS-902 and CSS-906 were closed by the operator

when steam flow was at []^{a,b,c} as measured by a combined indication from FVM-901 and FVM-902 (Appendix G, Dwg. OSU 600901). CSS-902 and CSS-906 were closed at the start of reference test SB01.

The facility fill and vent, startup, and heatup were performed per the same approved operating procedures used for Matrix Test SB01. A zero check was performed for all differential pressure instruments as was done for the reference test. Initial conditions for the test were established and recorded in the procedure. Refer to Subsection 2.7 for pre-test operation. The test ran for about 5-1/2 hours.

Table 5.1.4-1 shows the initial conditions recorded from the operator's panel and the average of other initial condition parameters for approximately 2 minutes prior to the break valves opening from the DAS.

There were three initial condition parameters out of specification, none of which should invalidate this test.

- CMT-2 temperature, indicated by TF-532, was []^{a,b,c} above the limiting maximum temperature of 80°F. TF-532 is located on the CMT-2 long thermocouple rod, about []^{a,b,c} down from the inside top of the CMT.

The next three thermocouples down on the long thermocouple rod, their dimensions from the inside top of the CMT, and their average temperature for about 2 minutes prior to break valve opening are listed in the following:

<u>Thermocouple</u>	<u>Dimension</u>	<u>Average temperature</u>
TF-548	[] ^{a,b,c}	[] ^{a,b,c}
TF-530	[] ^{a,b,c}	[] ^{a,b,c}
TF-526	[] ^{a,b,c}	[] ^{a,b,c}

These data suggest that a small percentage of CMT volume was at a temperature greater than []^{a,b,c}. Test analysis using the CMT recorded temperature data, taking into account the temperature variations at the top of the CMT, should still be possible.

- ACC-1 pressure, indicated by PT-401, was []^{a,b,c} or []^{a,b,c} below the required pressure band. The accumulator was pressurized to the required pressure, as indicated on local pressure indicator PI-401, prior to test actuation. The loss of pressure between tank pressurization and test actuation was possibly due to nitrogen gas cooling in the accumulator. Test analysis starting with the recorded lower accumulator overpressure should still be possible.

- ACC-2 pressure, indicated by PT-402, was []^{ab,c} or []^{ab,c} below the required pressure band. The accumulator was pressurized to the required pressure, as indicated on local pressure indicator PI-402, prior to test actuation. The loss of pressure between tank pressurization and test actuation was possibly due to nitrogen gas cooling in the accumulator. Test analysis starting with the recorded lower accumulator overpressure should still be possible.

5.1.4.2 Inoperable Instruments

Table 5.1.4-2 contains a list of instruments considered inoperable or invalid during all or portions of this test. Some of the instruments listed are on the Critical Instrument List (Subsection 3.2, Table 3.2-2) and, therefore, are addressed here.

FMM-201, FMM-202, FMM-203, and FMM-204 measured flow (gpm) in each of the four cold legs. A decision was made to continue testing without the availability of these instruments. Replacement flow meters repeatedly failed; their continued use was precluded due to cracking of the ceramic liners from thermal stratification in the loop piping. The necessary boundary conditions for loop flow could be determined from cold-leg differential pressure transmitters DP-202, DP-203, DP-205, and DP-206.

FMM-401 measured ACC-1 injection flow and provided accurate data when sensing liquid, but became erratic when filled with nitrogen following accumulator injection. ACC-1 level channel LDP-401 may be used as a backup for FMM-401.

CMT-1 and CMT-2 injection flow meters FMM-501 and FMM-504 and PRHR inlet and outlet flow meters FMM-802 and FMM-804 provided accurate data when sensing liquid, but became inaccurate when sensing two-phase or steam flow.

FMM-701 measured IRWST-1 injection flow when the primary sump valves were opened. The flow meter indicated a negative flow as water flowed from the primary sump to the IRWST. The meter was not designed to measure reverse flow, so this measurement was invalid. However, total IRWST flow was measured by FMM-702.

FMM-905 measured break separator loop seal flow to the primary sump. As the transient proceeded, the primary sump and break separator levels exceeded the elevation of the break at the bottom of CL-3. When this occurred, break flow initially stopped and then reversed. Flow reversal through the break occurred at about []^{ab,c} rendering subsequent data invalid.

SG tube level data (LDP-215, LDP-218, LDP-219, and LDP-222) were biased by vaporization of the water in the transmitter reference leg after the SG tubes started draining. However, the data provide accurate indication of the time when the tubes are empty.

PT-201 measured RCS pressure at the top of the SG-1 long tube. On August 15, 1994, it was discovered that the transmitter had an incorrect zero compensation, which resulted in a negative error and negative data at low pressures. The transmitter zero was corrected at that time. PT-201 data obtained during Matrix Test SB21 had the zero correction performed, and the corrected data appear as PT_201. Negative data and corrected negative data can be used to determine trends, but are considered inaccurate. PT_201 was not considered reliable for values less than 1.1 psig, but a sufficient amount of other pressure data are available.

TF-103 and TF-104 measured CL-3 and CL-4 bottom-of-pipe fluid temperatures entering the reactor vessel. Both thermocouples were removed to accommodate installation of thermal stratification measurement instrumentation. It was permissible for both thermocouples to be inoperable because TF-101 and TF-102, which measured the CL-3 reactor flange top and CL-4 reactor flange top, were operable during the performance of Matrix Test SB21.

TF-501 and TF-504 measured CMT fluid temperature from the long thermocouple rod location near the bottom of each CMT. The thermocouples appear to have measured ambient conditions throughout the test, which would indicate a short somewhere in the thermocouple wiring. With these thermocouples inoperable, the required long thermocouple rod thermocouple availability of "seven out of ten and no more than one in succession failed" was met.

Data provided by ADS-4 separator instrumentation prior to the ADS 4-1 and ADS 4-2 valves opening at []^{a,b,c} were invalid due to the closed position of the ADS-4 valves and the ADS-4 separator loop seal valves. The instruments affected are: FMM-602, FMM-603, FVM-602, FVM-603, LDP-611, and LDP-612. Test analysis will not be affected, since ADS-4 flow did not begin until the valves opened.

Considering the critical instrument failures listed, sufficient instrumentation was available to allow the performance of mass balances as demonstrated in Subsection 5.1.4.6 and Appendix E. An energy balance will be performed and reported in the *AP600 Low-Pressure Integral Systems Test at Oregon State University, Test Analysis Report, WCAP-14292*.⁽²⁾

5.1.4.3 Sequence of Events

Table 5.1.4-3 contains the sequence of events for Matrix Tests SB21 and SB01. The first pages provide selected event times from both tests and the difference between event times. The subsequent pages of the table provide a visual representation of the time comparison using bar charts. On both the numeric table and the bar charts, the events are sorted in the chronologic order in which they occurred in Matrix Test SB21.

The table defines the source of actual time values. A D in the Data Source column indicates the recorded time was obtained from a software program that monitored digital events in the facility. These included pump starts and stops, valve limit switch actuations, and alarms. The term *valve*

opening means the valve has actuated and the closed limit switch is being opened (valve coming off the seat). An A in the Data Source column indicates the time data were obtained by reviewing test data recorded by the DAS. Although the test data from the DAS were in digital format, the DAS monitored analog events such as pressure, flow, and temperature from the data.

5.1.4.4 Test Results and Evaluation

This section compares the results of Matrix Test SB21 with the results of reference test SB01. In doing so, the overall system response to the LBLOCA event in Matrix Test SB21 is evaluated. The section is divided into three different phases, each characterized by the systems' behavior and thermal-hydraulic phenomena occurring in the systems. The phases are as follows:

- Initial Depressurization Phase: simulated break initiation to ADS-1 actuation
- ADS Phase: ADS-1 actuation to start of IRWST injection
- IRWST Injection Phase: start of IRWST injection to end of test

Initial Depressurization Phase

As with Matrix Test SB01, this test began with the actuation of the TEST pushbutton. Break valves TS-201 and TS-205 received an open signal from the PLC []^{a,b,c} later (time zero). After an additional 0.5 second, an S signal was generated by the PLC, which time-sequences signals to initiate various events such as resetting controllers, stopping pumps, and repositioning valves.

The initial depressurization phase for Matrix Test SB21 began similarly to Matrix Test SB01. PLC timing for various event initiations was within 1 second of the same event for Matrix Test SB01, with the exception of the main feed pump and RCP trips. The main feed pump tripped []^{a,b,c} later and the RCPs tripped []^{a,b,c} earlier in Matrix Test SB21 than in Matrix Test SB01.

At about []^{a,b,c} steam percent, as calculated from LDP-127 data, indicated that the reactor vessel began to lose inventory, i.e., steam formation began (Figure 5.1.4-3). This was about []^{a,b,c} earlier than when steam formation occurred in Matrix Test SB01.

In Matrix Test SB21, the pressurizer and pressurizer surge line became empty at []^{a,b,c} respectively (Figure 5.1.4-5). This occurred about []^{a,b,c} earlier for the pressurizer and []^{a,b,c} earlier for the surge line than in Matrix Test SB01. The time difference can be attributed to the fact that the larger break resulted in break flow rates being about double early in Matrix Test SB21 compared with Matrix Test SB01 (Figure 5.1.4-62).

The early emptying of the pressurizer and surge line resulted in earlier CMT transition from recirculation mode to draindown, i.e., the time that the CMT balance line level began to decrease (Figure 5.1.4-6). CMT-1 transition occurred at about []^{a,b,c} in Matrix Test SB21, as

compared with []^{a,b,c} in Matrix Test SB01. CMT-2 transition occurred at about []^{a,b,c} in Matrix Test SB21, as compared with []^{a,b,c} in Matrix Test SB01.

The core decay heat simulation of reactor heater power followed the programmed algorithm just as it did in reference test SB01 (Appendix F).

The SG U-tubes were completely empty anywhere between []^{a,b,c} in Matrix Test SB21, which was about []^{a,b,c} earlier than the U-tubes emptied in Matrix Test SB01 (Figures 5.1.4-7 and 5.1.4-8). The SG cold-leg channel heads drained earlier in Matrix Test SB21 by as much as []^{a,b,c} for SG-1 and []^{a,b,c} for SG-2 than in Matrix Test SB01 (Figures 5.1.4-9 and 5.1.4-10). The CL-3 channel head was the first to empty at []^{a,b,c} and the CL-2 channel head the last at []^{a,b,c} in Matrix Test SB21. The difference in drain time for the SG U-tubes and channel heads can be attributed to the larger break, resulting in higher break flow rates early in Matrix Test SB21 (Figure 5.1.4-62).

Both accumulators began to inject into the DVI nozzles at []^{a,b,c} as compared with about []^{a,b,c} for Matrix Test SB01 (Figure 5.1.4-16). The combination of accumulator and CMT injection was sufficient to compensate for the loss of RCS inventory through the break and maintain reactor vessel levels essentially constant after about []^{a,b,c} (Figure 5.1.4-15). LDP-127 indicated a core barrel level of about []^{a,b,c} and the downcomer level transmitters, LDP-116 and LDP-140, indicated a level of about []^{a,b,c}.

There was a marked increase in both steam and liquid flows from the break separator at about []^{a,b,c} during Matrix Test SB21 (Figure 5.1.4-62). The flow increase coincided with the operator's closing CSS-902 and CSS-906 when total steam flow leaving the BAMS header decreased to approximately []^{a,b,c}. The reason for the steam flow increase recorded by FVM-905 is that closing CSS-906 isolated the 8-in. vent line from the break separator, allowing flow only through the 6-in. vent line. Closing CSS-902 and CSS-906 also caused about a []^{a,b,c} increase in the break separator pressure, with essentially no change in primary sump pressure, resulting in a pressure differential that increased liquid flow from the break separator (Figure 5.1.4-74).

The PRHR HX response during this phase was similar for both tests (Figures 5.1.4-41, 5.1.4-66, and 5.1.4-67).

For Matrix Test SB21, fluid level inside the reactor vessel core barrel reached its minimum collapsed level of []^{a,b,c} at about []^{a,b,c} as indicated by LDP-127 data (Figure 5.1.4-15). The minimum level occurred about []^{a,b,c} earlier and about []^{a,b,c} lower than during Matrix Test SB01. Reactor vessel heater rod cooling was maintained at that level (Figure 5.1.4-44).

Due to the break size and resultant rapid loss of RCS fluid inventory during Matrix Test SB21, the initial depressurization, when compared with Matrix Test SB01, was very different (Figure 5.1.4-45). A period of quasi-equilibrium pressure existed between the RCS and the secondary side of the SGs for

about []^{a,b,c} in Matrix Test SB01. In Matrix Test SB21, RCS pressure decreased below that of the SG secondary side at about []^{a,b,c} after being at a quasi-equilibrium pressure for only about []^{a,b,c}. In the first few seconds after break valve opening, the SGs were isolated on both the feedwater and steam sides in order to minimize RCS heat losses. The only cooling available to the SGs was heat losses to ambient. With RCS pressure decreasing due to the break and SG pressure increasing due to heat absorption from the RCS, the pressures converged at about []^{a,b,c}. At about []^{a,b,c} inventory losses through the break caused RCS pressure to drop below the pressure on the SG secondary side, and the SGs became a heat source for the RCS.

The rapid RCS depressurization and early start of CMT draindown in Matrix Test SB21 resulted in CMT-2 reaching its low level setpoint at []^{a,b,c} and the ADS-1 valve opening []^{a,b,c} later at []^{a,b,c}. This was []^{a,b,c} earlier than the ADS-1 valve was observed to open during Matrix Test SB01.

ADS Phase

When the ADS-1 valve opened, injection flow from each accumulator increased by about []^{a,b,c} and injection flow from each CMT decreased by about []^{a,b,c} (Figure 5.1.4-16). The reduction in CMT flow was possibly due to induced backpressure from the accumulator flow increase reacting against the CMT injection line check valves. When the ADS-2 valve opened at []^{a,b,c} injection flow from each accumulator increased to about []^{a,b,c} and the CMT injection flows decreased to zero. Similar injection results were seen in reference test SB01, but about []^{a,b,c} later in the test and with lower flow rates. The ADS-3 valve opening had little effect on any other parameters.

The initial flow from ADS 1-3 during Matrix Test SB21 were about double the flow during Matrix Test SB01, but the flow durations were shorter due to the rapid depressurization from the larger break (Figure 5.1.4-61). Pressurizer reflood began within []^{a,b,c} of the ADS-2 valve opening (Figure 5.1.4-5). Pressurizer reflood during Matrix Test SB21 was possibly due in part to the divergence of pressurizer and reactor vessel upper head pressures, with reactor vessel pressure being the higher of the two, as it was in Matrix Test SB01 (Figure 5.1.4-63).

Also, about the same time that the ADS-1 valve opened in Matrix Test SB21, irregular oscillations in temperatures, pressures, and flow began (Figures 5.1.4-15, 5.1.4-47, and 5.1.4-63). The oscillations were not observed in Matrix Test SB01. The oscillations were possibly produced by another phenomenon that was not observed in the reference test, detectable flow through the SGs. Flow through the primary side of the SGs, from the hot legs to the cold legs, was sufficient to cause differential pressure indications on DP-211 and DP-212 (Figure 5.1.4-81). Detectable flow through the SGs and the oscillations stopped about the time the CMT-1 balance line was filling, around []^{a,b,c}.

Accumulator injection flow began to decrease as the accumulators were nearly empty, allowing CMT injection flow to recommence (Figures 5.1.4-16 and 5.1.4-64). When the accumulators were empty, CMT injection flow stabilized at about []^{a,b,c} per tank. ACC-1 and ACC-2 were empty at []^{a,b,c} respectively. These times were []^{a,b,c} earlier than for the respective accumulator in Matrix Test SB01.

PRHR HX cooling in Matrix Test SB21 appears to have decreased to 1 to 2 gpm at about []^{a,b,c} versus about []^{a,b,c} in Matrix Test SB01 (Figures 5.1.4-40, 5.1.4-41, and 5.1.4-66). Matrix Test SB21 data then indicate an increase of flow through the PRHR HX short tubes at about []^{a,b,c} which would continue until about []^{a,b,c}

When RCS pressure decreased to []^{a,b,c} at approximately []^{a,b,c} (about []^{a,b,c} earlier than in Matrix Test SB01), the two IRWST injection valves were automatically opened by a signal from the PLC. IRWST injection could not occur until RCS pressure decreased to near atmospheric, since the IRWST is a static system depending on gravity flow and operating at BAMS steam header pressure (Figure 5.1.4-45).

At []^{a,b,c} CMT-2 reached its low-low setpoint, causing the ADS 4-1 and ADS 4-2 valves to open. These two additional RCS vent paths decreased RCS pressure sufficiently so that IRWST injection to the DVI nozzles was initiated at about []^{a,b,c} earlier than during Matrix Test SB01 (Figure 5.1.4-48). The actuation of IRWST injection is dependent on the differential pressure between the reactor vessel and the IRWST, and the force for injection is gravity. Therefore, the early injection during Matrix Test SB21 was probably the result of the faster RCS depressurization.

IRWST Injection Phase

The early start of IRWST injection during Matrix Test SB21 had two major effects on the facility overall response. First, CMT injection was stopped by the IRWST injection head prior to the CMTs being completely empty as in Matrix Test SB01 (Figure 5.1.4-6). Secondly, the cold legs refilled and subcooled at about []^{a,b,c} earlier than in Matrix Test SB01 (Figures 5.1.4-42, 5.1.4-43, 5.1.4-53, and 5.1.4-54). An effect of the cold legs maintaining some level in the early part of the test was that flow was maintained through the break in Matrix Test SB21, whereas in Matrix Test SB01, when the cold legs emptied, break flow stopped between about []^{a,b,c} (Figure 5.1.4-28).

Both CMTs reflooded during Matrix Test SB21 as they did during Matrix Test SB01 (Figures 5.1.4-6, 5.1.4-30, and 5.1.4-31). Major differences between Matrix Tests SB21 and SB01 were the timing of the CMT reflood and CMT response during the reflood. CMT-1 reflood occurred at about []^{a,b,c} in Matrix Test SB21, or []^{a,b,c} earlier than in Matrix Test SB01. CMT-2 reflood occurred at about []^{a,b,c} earlier than in Matrix Test SB01. The reflood of the CMTs occurred for the same reasons as described for reference test SB01 in Subsection

5.1.1. The reason for the earlier CMT reflood in Matrix Test SB21 is that the cold legs refilled with subcooled fluid earlier than in Matrix Test SB01. The balance lines refilled due to the condensation of steam from the CMT on the cooler fluid in the balance line and the subsequent reduction in CMT pressure.

Condensation/depressurization events were observed during the CMT reflood during Matrix Test SB21 like those that occurred during Matrix Test SB01.

In Matrix Test SB01, the pressurizer reflooded to about []^{a,b,c} over the period of about []^{a,b,c}. This phenomenon was attributed to a lower pressure being formed in the pressurizer and ADS 1-3 separator when HL-2 filled with subcooled fluid to a level that started to fill the surge line while the ADS 1-3 sparger was still submerged in the IRWST. A vacuum breaker was installed on the ADS 1-3 sparger line inside the IRWST following the performance of Matrix Test SB01 to prevent a recurrence of a reflood caused by negative pressure. The vacuum breaker performed its function and, under similar conditions, a pressurizer reflood did not occur during Matrix Test SB21 (Figure 5.1.4-5).

Primary sump injection started at about []^{a,b,c} earlier in Matrix Test SB21 than in Matrix Test SB01 (Figure 5.1.4-37). The start of primary sump injection in Matrix Test SB21 was somewhat different than in Matrix Test SB01. In Matrix Test SB01, injection flow started through the primary sump injection line check valves when the fluid levels in the sump and the IRWST equalized, about []^{a,b,c} before the sump injection valves opened. In Matrix Test SB21, injection flow did not start until about []^{a,b,c} after the primary sump injection valves opened. A possible explanation for the delay in sump injection during Matrix Test SB21 is that the IRWST and primary sump levels were not yet equalized; the IRWST was at the higher level, shutting off flow from the primary sump (Figures 5.1.4-35 and 5.1.4-37).

The test continued in the sump injection recirculation mode for 2 hours. For Matrix Test SB21, the facility response while in this mode appears to be consistent with the data obtained in Matrix Test SB01.

5.1.4.5 Comparison of Component Responses

Reactor

The algorithm for core decay heat simulation of reactor power used during Matrix Test SB21 was a different algorithm than the one used during reference test SB01. A new set of decay heat curve algorithms was programmed into the reactor controller to maintain reactor heater power at 600 kW for 300 seconds prior to initiating the power decay in Matrix Test SB21. During Matrix Test SB01, the power was held at 600 kW for 140 seconds prior to initiating the power decay. The core decay heat simulation of reactor heater power followed the programmed algorithm just as it did in Matrix Test SB01 (Appendix F).

Reactor response during the performance of Matrix Test SB21 was consistent with reactor response during Matrix Test SB01, with the exception of event timing.

Core Makeup Tanks

The early emptying of the pressurizer and surge line resulted in earlier CMT transition from recirculation mode to draindown, i.e., the time that the CMT balance line level began to decrease (Figure 5.1.4-6). The CMT-1 transition occurred at about []^{a,b,c} in Matrix Test SB21 compared with []^{a,b,c} in Matrix Test SB01. The CMT-2 transition occurred at about []^{a,b,c} in Matrix Test SB21 compared with []^{a,b,c} in Matrix Test SB01. To initiate the CMT transition from recirculation mode to draindown, the fluid coupling between the cold legs and the balance lines must be broken. In both tests, CL-1 and CL-3 fluid temperatures, measured []^{a,b,c} from the top inside diameter of the reactor nozzle flange (as indicated by SC-105 and SC-101), were subcooled at the time the CMTs transitioned from recirculation mode to draindown (Figures 5.1.4-53 and 5.1.4-54). One method of determining that the cold legs have partially drained is that their top thermocouples indicate superheat. Due to the location of SC-105 and SC-101 in the cold-leg flow stream, the fluid uncoupling between the cold legs and the balance lines would occur before the thermocouples could sense cold-leg draindown.

Both CMTs reflooded in Matrix Test SB21 as they did in Matrix Test SB01 (Figures 5.1.4-30 and 5.1.4-31). In Matrix Test SB21, the CMT draindown was terminated prior to the tanks injecting their full volume due to the early initiation of IRWST injection. Another major difference between Matrix Tests SB21 and SB01 was the timing of the CMT reflood. CMT-1 reflood occurred at about []^{a,b,c} in Matrix Test SB21, or []^{a,b,c} earlier than in Matrix Test SB01. CMT-2 reflood occurred at about []^{a,b,c} earlier than in Matrix Test SB01. The reflood of the CMTs occurred for the same reasons as described for reference test SB01 in Subsection 5.1.1. The reason for the earlier CMT reflood in Matrix Test SB21 is that the cold legs refilled with subcooled fluid earlier than in Matrix Test SB01. The balance lines refilled due to the condensation of steam from the CMT on the cooler fluid in the balance line and the subsequent reduction in CMT pressure with respect to RCS pressure.

Condensation/depressurization events were observed during the CMT reflood in Matrix Test SB21 like those that occurred in Matrix Test SB01.

Accumulators

Accumulator response during the performance of Matrix Test SB21 was similar to the response of Matrix Test SB01, with the exception of event timing.

Pressurizer

In Matrix Test SB21, the pressurizer and pressurizer surge line were empty at []^{a,b,c} respectively (Figure 5.1.4-5). This occurred earlier by about []^{a,b,c} for the pressurizer and []^{a,b,c} for the surge line than in reference test SB01. The time difference can be attributed to higher break flow rates early in Matrix Test SB21 (Figure 5.1.4-62).

During the performance of Matrix Test SB01, the pressurizer exhibited a second reflood at about []^{a,b,c} but a common event did not occur during Matrix Test SB21 (Figure 5.1.4-5). As was described in Subsection 5.1.1.4 in the Pressurizer Response, the reflood was caused by a lower pressure developing in the pressurizer and ADS 1-3 separator with respect to pressure in the reactor vessel. The negative pressure was precipitated by several things: 1) the ADS 1-3 sparger located in the IRWST was submerged, 2) the hot legs had refilled with subcooled fluid into the surge line, and 3) the combination of 1 and 2 resulted in condensation of steam in the pressurizer and ADS 1-3 separator with subsequent cooling.

The problem of a lower pressure being developed in the pressurizer and ADS 1-3 separator than in the RCS had been corrected prior to the performance of Matrix Test SB21 by a facility modification, the installation of a vacuum breaker on the ADS 1-3 sparger line inside the IRWST.

Another difference between the two tests was that during Matrix Test SB01, the pressurizer heaters remained energized at about []^{a,b,c}. This was corrected prior to the performance of Matrix Test SB21 by a procedural change that required the operators to open the pressurizer heater breaker when the S signal was verified (Figure 5.1.4-24). During Matrix Test SB01, the logic was supposed to drive the heater power demand to zero, resulting in zero power from the pressurizer heater SCRs to the heaters. The data for Matrix Test SB01 suggest that the SCR control circuitry had not been properly tuned at that time.

All other pressurizer responses during Matrix Test SB21 were similar to the responses during Matrix Test SB01, with the exception of event timing.

Passive Residual Heat Removal Heat Exchanger

There was a difference in PRHR HX performance during the ADS phase of Matrix Test SB21 (Figures 5.1.4-66 and 5.1.4-67). The PRHR HX inlet head level transmitter recorded HX level changes during Matrix Test SB21 but did not record a level change during Matrix Test SB01. In Matrix Test SB01, the HX appeared to reach a minimum level of []^{a,b,c} at about []^{a,b,c} refill to []^{a,b,c} at about []^{a,b,c} and return to a minimum again at []^{a,b,c}. In Matrix Test SB21, the HX level was predominantly higher than []^{a,b,c} during the first []^{a,b,c} and higher than []^{a,b,c} until about []^{a,b,c}. It also appeared to maintain more flow. A possible cause for what appears to be more efficient PRHR HX response during Matrix Test SB21 is that RCS levels remained higher than Matrix Test SB01 levels (Figure 5.1.4-15).

The PRHR HX response during Matrix Test SB21 was similar to reference test SB01, except for event timing and the response of the HX wide-range level data after about []^{a,b,c}. In Matrix Test SB01, the HX partially refilled when the RCS loops were filled with subcooled fluid. Following the refill, when small pressure and level oscillations began to occur, it is possible that the oscillations caused the PRHR HX inlet line to "burp," allowing negative pressure in the HX to equalize with the RCS. Equalization of pressures allowed equalization of PRHR levels with those of the RCS. In Matrix Test SB01, once the levels equalized, the PRHR level remained essentially constant.

Data obtained during the performance of Matrix Test SB21 indicate that PRHR performance was consistent with the performance during Matrix Test SB01 until the final draindown of the HX. In Matrix Test SB21, the HX drained to []^{a,b,c} at about []^{a,b,c} but then appeared to begin a slow refill for as long as data were obtained (Figure 5.1.4-68). It is possible that the HX was refilling, but a more logical possibility is that LDP-802 was slowly losing its reference leg due to vaporization at a lower saturation pressure.

Steam Generators

At about the same time that the ADS-1 valve opened in Matrix Test SB21 ([]^{a,b,c}), irregular oscillations in temperatures, pressures, and flow began (Figures 5.1.4-15, 5.1.4-47, and 5.1.4-63). The oscillations were not observed in Matrix Test SB01. The oscillations were probably produced by another phenomenon not observed in Matrix Test SB01, detectable flow through the SGs. Flow through the primary side of the SGs, from the hot legs to the cold legs, was sufficient to cause differential pressure indications on DP-211 and DP-212 (Figure 5.1.4-81). A possible cause for the oscillations is fluid at saturation temperature in the hot legs being superheated in the SGs and then condensing in the cold legs, resulting in multiple depressurization events in localized areas. Detectable flow through the SGs and the oscillations stopped about the time that the CMT-1 balance line was filling, around []^{a,b,c}. For the balance line to fill, the cold legs had to be full.

During the period of flow through the primary side of the SGs, there were oscillations of about a []^{a,b,c} magnitude in the SG wide-range level (Figure 5.1.4-82). The flow also subcooled much of the fluid in the secondary side of the SGs. The SG fluid temperatures leveled off when primary-side flow stopped. Then as saturation temperature dropped, the temperatures followed saturation (Figures 5.1.4-83 and 5.1.4-84). SG downcomer fluid temperatures, located []^{a,b,c} above the tube sheet, subcooled almost immediately during Matrix Test SB21 and were still subcooled at the end of the test (Figures 5.1.4-85 and 5.1.4-86).

Cold Legs and Hot Legs

The RCS cold-leg response during Matrix Test SB21 was different than during Matrix Test SB01 in that the cold legs refilled earlier in the test (based on reactor vessel downcomer levels; Figure 5.1.4-15). A possible explanation for the early refill in Matrix Test SB21 is that IRWST injection started earlier and DVI flow was greater than break flow (Figures 5.1.4-17 and 5.1.4-28).

There was a difference in detectable flow through the SG primary sides in Matrix Tests SB21 and SB01. The primary side flow is discussed in the Steam Generator Response. Another difference was that the cold legs never superheated during Matrix Test SB21 (Figures 5.1.4-81, 5.1.4-42, 5.1.4-43, 5.1.4-53, and 5.1.4-54). The cold legs probably did not superheat because of their early refill.

In-Containment Refueling Water Storage Tank

The IRWST response during the performance of Matrix Test SB21 was similar to the IRWST response during reference test SB01, except that during Matrix Test SB21, the low-low level setpoint and the primary sump injection valves opened about 4800 seconds earlier. The earlier opening of the sump injection valves during Matrix Test SB21 may have been the result of sump injection not occurring through the sump injection line check valves, allowing IRWST injection to remain at a higher rate for longer.

Break and ADS Measurement System

The BAMS response during the performance of Matrix Test SB21 was different from the response during Matrix Test SB01 because of the initial header valve alignment and the larger break (Figures 5.1.4-73, 5.1.4-74, and 5.1.4-75). Following break valve opening, BAMS header pressure was about []^{a,b,c} higher than in Matrix Test SB01. Peak BAMS header steam flows were about a factor of []^{a,b,c} greater than the steam flows in Matrix Test SB01, but with the more rapid depressurization rate in Matrix Test SB21, the steam flow duration was shorter.

There was a marked increase in both steam and liquid flows from the break separator at about []^{a,b,c} during Matrix Test SB21 (Figure 5.1.4-62). The flow increase coincided with the operator's closing CSS-902 and CSS-906 when total steam flow leaving the BAMS header decreased to approximately []^{a,b,c}. The reason for the steam flow increase, as recorded by FVM-905, is that closing CSS-906 isolated the []^{a,b,c} vent line from the break separator, allowing flow only through the []^{a,b,c} vent line. Closing CSS-902 and CSS-906 also caused about a []^{a,b,c} increase in the break separator pressure, with essentially no change in primary sump pressure, and causing a pressure differential that resulted in the increased liquid flow from the break separator (Figure 5.1.4-74).

5.1.4.6 Mass Balance

The mass balance results for Matrix Test SB21 were calculated based on water inventory before and after the test and are provided in Appendix E. The mass at the end of the test was within []^{a,b,c} percent of the mass at the beginning of the test as compared to []^{a,b,c} percent for reference test SB01.

5.1.4.7 Conclusions

The test was performed with minimal problems and is considered acceptable. Although not all of the facility initial conditions met the specified acceptance criteria, the deviations did not impact the quality of the data. The instrumentation problems encountered were not critical to the performance of the facility mass and energy balances.

Facility response to the test was as anticipated for the conditions that were established. The data clearly demonstrate that cooling of the reactor heater rods was maintained throughout the duration of the test.

TABLE 5.1.4-1
MATRIX TEST SB21 INITIAL CONDITIONS

Parameter	Instrument No.	Specified Initial Condition	Actual Initial Condition	Comments
Pressurizer pressure ⁽¹⁾	PT-604	370 ± 2 psig	[] a,b,c	
HL-1 temperature ⁽¹⁾	SC-141	420 ± 2°F		
HL-2 temperature ⁽¹⁾	SC-140	420 ± 2°F		
SG-1 pressure ⁽¹⁾	PT-301	285 ± 5 psig		
SG-2 pressure ⁽¹⁾	PT-302	285 ± 5 psig		
Pressurizer level ⁽¹⁾	LDP-601	65 ± 5 in.		Level signal temperature-compensated by TF-605
SG-1 narrow-range level ⁽¹⁾	LDP-303	26 ± 3 in.		Level signal temperature-compensated by TF-301
SG-2 narrow-range level ⁽¹⁾	LDP-304	26 ± 3 in.		Level signal temperature-compensated by TF-310
IRWST temperature ⁽²⁾	TF-709	< 80°F		
CMT-1 temperature ⁽²⁾	TF-529	< 80°F		
CMT-2 temperature ⁽²⁾	TF-532	< 80°F		[] ^{a,b,c} above required temperature
ACC-1 temperature ⁽²⁾	TF-403	< 80°F		
ACC-2 temperature ⁽²⁾	TF-404	< 80°F		
IRWST level ⁽²⁾	LDP-701	Level established by fill line elevation		
ACC-1 level ⁽²⁾	LDP-401	Level established by standpipe at 37 in.		
ACC-2 level ⁽²⁾	LDP-402	Level established by standpipe at 37 in.		
ACC-1 pressure ⁽²⁾	PT-401	232 ± 2 psig		[] ^{a,b,c} below required pressure
ACC-2 pressure ⁽²⁾	PT-402	232 ± 2 psig	[]	[] ^{a,b,c} below required pressure

TABLE 5.1.4-1 (Continued)
MATRIX TEST SB21 INITIAL CONDITIONS

Parameter	Instrument No.	Specified Initial Condition	Actual Initial Condition	Comments
CMT-1 level ⁽²⁾	LDP-507	Full	<input type="checkbox"/> a,b,c	
CMT-2 level ⁽²⁾	LDP-502	Full	<input type="checkbox"/>	

Note:

- (1) Data for the indicated parameter were recorded in the test procedure as an initial condition for the test. The value was determined by the test engineer from the appropriate control board indicator.
- (2) Data were not recorded in the procedure, but the test engineer verified that specified conditions were achieved while establishing initial conditions. The value of the parameter was determined post-test by calculating the average DAS indication for a time of about 2 minutes before the break valve opened.

**TABLE 5.1.4-2
MATRIX TEST SB21 INOPERABLE INSTRUMENTS/INVALID DATA CHANNELS**

Instrument No.	Instrument Type	Description of Problem
DP-216	Differential pressure transmitter	Inoperable throughout test
FMM-201* FMM-202* FMM-203* FMM-204*	Magnetic flow meter	Removed from system (Subsection 5.1.4.2)
FMM-401*	Magnetic flow meter	Inoperable after ACC-1 emptied at [] ^{a,b,c} when it appeared to have filled with nitrogen
FMM-501*	Magnetic flow meter	Data invalid after [] ^{a,b,c} seconds when the CMT was empty
FMM-502	Magnetic flow meter	Data invalid after [] ^{a,b,c} due to possible steam in balance line
FMM-503	Magnetic flow meter	Data invalid after [] ^{a,b,c} due to possible steam in balance line
FMM-504*	Magnetic flow meter	Data invalid after [] ^{a,b,c} when the CMT was empty
FMM-701*	Magnetic flow meter	Negative values after primary sump valves opened at [] ^{a,b,c} invalid (Subsection 5.1.3.2)
FMM-703	Magnetic flow meter	Inoperable throughout test
FMM-802*	Magnetic flow meter	Data invalid after steam formed in PRHR HX inlet line at about [] ^{a,b,c}
FMM-804*	Magnetic flow meter	Data valid until PRHR HX initially drained at [] ^{a,b,c} after this time, the possibility of steam in the outlet line invalidated the data
FMM-905*	Magnetic flow meter	Negative values after break separator level exceeded the break elevation at about [] ^{a,b,c} invalid
HFM-103 HFM-105 HFM-505 HFM-703	Heat flux meter	Inoperable throughout test
HPS-203-1 through -3 and HPS-509-1 through -3	Heated phase switch	Inoperable throughout test
LDP-139 LDP-113	Differential pressure transmitter - level	Inoperable throughout test

TABLE 5.1.4-2 (Continued)
MATRIX TEST SB21 INOPERABLE INSTRUMENTS/INVALID DATA CHANNEL

Instrument No.	Instrument Type	Description of Problem
LDP-201 LDP-202 LDP-203 LDP-204 LDP-205 LDP-206	Differential pressure transmitter - level	Data invalid due to effect of vertical portion of sense line attached to top of pipe; data can show level trends and when pipe empties or starts to drain, but absolute level indication can not be used
LDP-215* LDP-216 LDP-217 LDP-218* LDP-219* LDP-220 LDP-221 LDP-222*	Differential pressure transmitter - level	Inoperable - when tube voided, reference leg steamed off (Subsection 2.4)
LDP-611	Differential pressure transmitter - level	Data prior to ADS 4-1 opening at [] ^{a,b,c} should be ignored
LDP-612	Differential pressure transmitter - level	Data prior to ADS 4-2 opening at [] ^{a,b,c} should be ignored
LDP-801	Differential pressure cell - level	Inoperable - indicated full when HX not full
PT_101	Pressure transmitter	Data less than 6.1 psig invalid
PT_102	Pressure transmitter	Data less than 6.2 psig invalid
PT_103	Pressure transmitter	Data less than 6.2 psig invalid
PT_104	Pressure transmitter	Data less than 6.4 psig invalid
PT_108	Pressure transmitter	Data less than 8.4 psig invalid
PT_109	Pressure transmitter	Data less than 6.3 psig invalid
PT_111	Pressure transmitter	Data less than 6.0 psig invalid
PT_112	Pressure transmitter	Data less than 8.8 psig invalid
PT_113	Pressure transmitter	Data less than 6.4 psig invalid
PT_201*	Pressure transmitter	Data less than 1.1 psig invalid
PT_202	Pressure transmitter	Data less than 5.9 psig invalid
PT_205	Pressure transmitter	Data less than 6.1 psig invalid
PT-801	Pressure transmitter	Not used for this test
PT-802	Pressure transmitter	Not used for this test
TF-103*	Thermocouple fluid temperature	Replaced with thermal stratification thermocouples

TABLE 5.1.4-2 (Continued)
MATRIX TEST SB21 INOPERABLE INSTRUMENTS/INVALID DATA CHANNEL

Instrument No.	Instrument Type	Description of Problem
TF-104*	Thermocouple fluid temperature	Replaced with thermal stratification thermocouples
TF-170	Thermocouple fluid temperature	Inoperable due to leaking O-ring in core barrel
TF-203 TF-501* TF-504* TF-615 TF-619	Thermocouple fluid temperature	Inoperable - indicated ambient throughout test
TFM-103 TFM-105 TFM-703	Thermocouple wall temperature	Inoperable throughout test
TH-317-1 through TH-317-4	Thermocouple heater rod	Heater rod replaced with non-instrumented rod
TW-503	Thermocouple wall temperature	Inoperable throughout test
TW-534 TW-547 TW-552	Thermocouple wall temperature	Inoperable - indicated ambient throughout test

Note:

*Instruments marked with an asterisk are critical instruments. See Subsection 5.1.4.2 for discussion.

Table 5.1.4-3 on pages 5.1.4-21 through 5.1.4-29 is not included in this nonproprietary document.

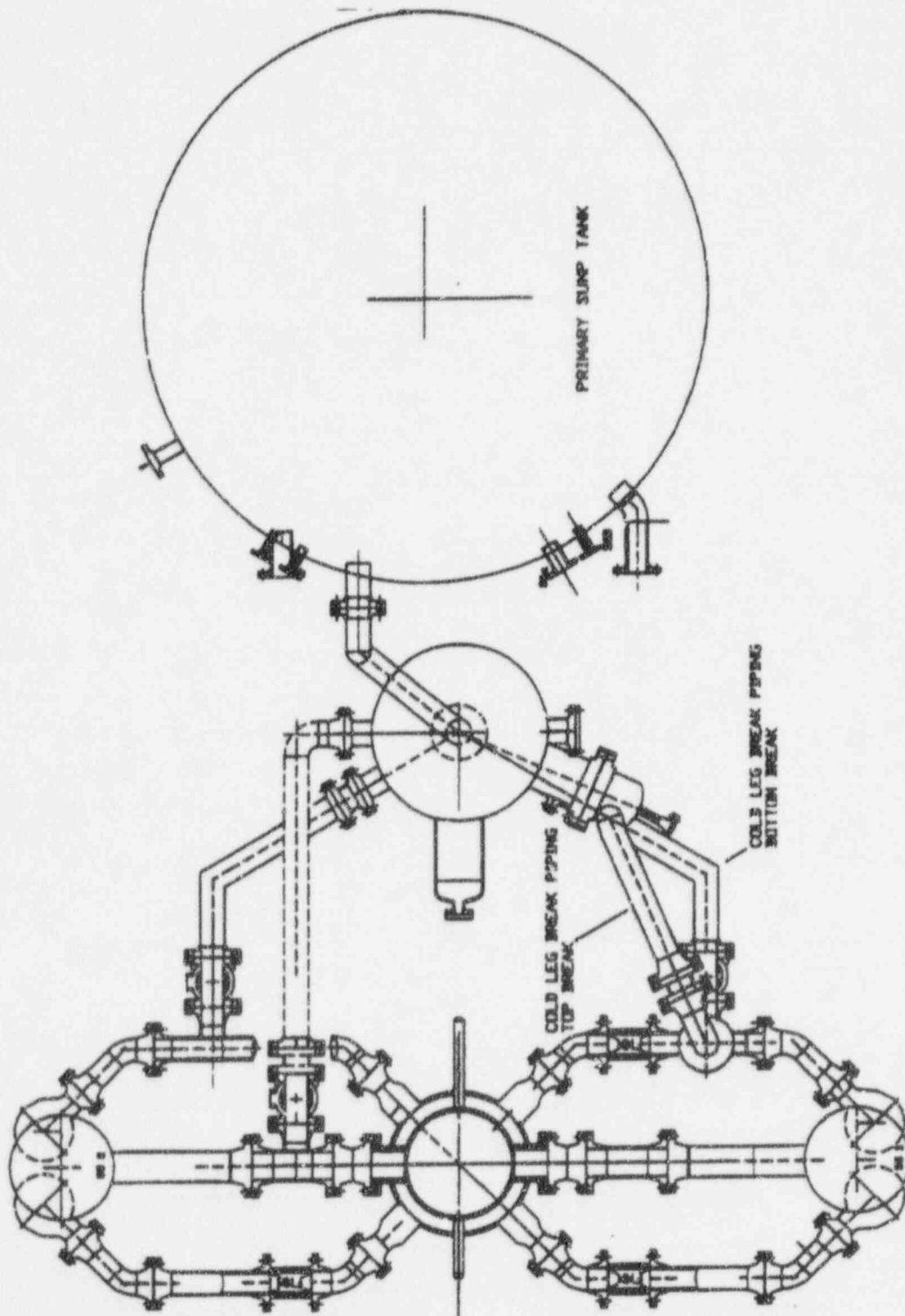


Figure 5.1.4-1 Primary Loop and Break Piping Layout

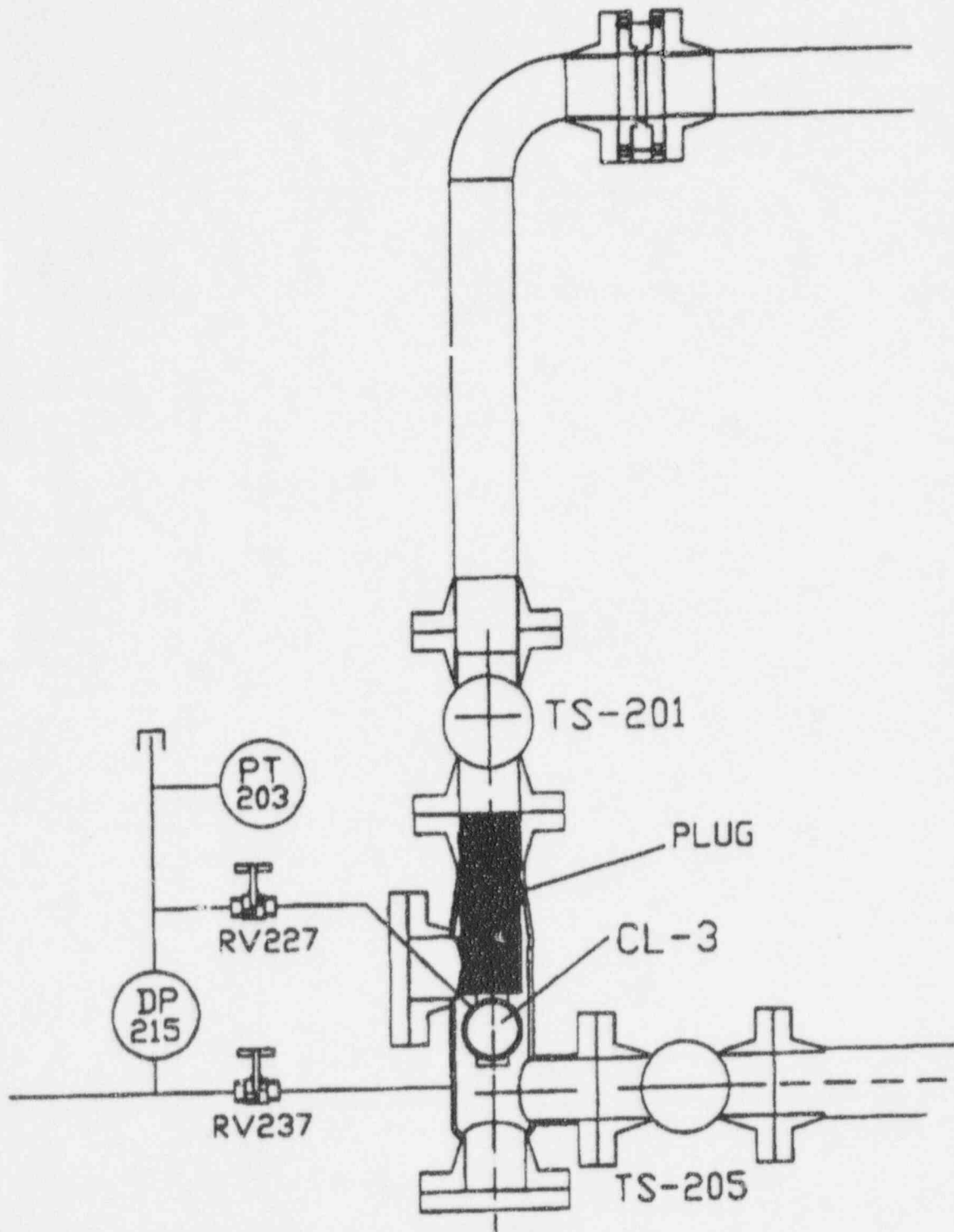


Figure 5.1.4-2 Primary Loop and Break Pipe Arrangement

Figures 5.1.4-3 through 5.1.4-86 are not included in this nonproprietary document.

5.1.5 Effect of a Smaller Break Size (Matrix Test SB23 Comparison with Matrix Test SB01)

In this section, the results of Matrix Test SB23 (OSU Test U0023) are compared with the results of Matrix Test SB01 (OSU Test U0001). These two tests were identical, except that Matrix Test SB23 simulated a 1/2-in. pipe break and reference test SB01 simulated a 2-in. pipe break. Both simulated breaks were located at the bottom of CL-3. In both tests, failure of one leg of one ADS-4 line was simulated by orificing one ADS-4 line for 50-percent design flow area and the other for 100-percent design flow area.

Matrix Test SB23 was performed on August 9, 1994, with a test duration of about 7.8 hours. During the transient, the CMTs and accumulators injected their water inventories, the IRWST injected water, and circulation through the primary sump was established. The test was terminated at 28,000 seconds after long-term cooling had been demonstrated. The core remained cooled throughout the test, and excessive temperature increases were not observed; therefore, this test was considered successful.

Subsection 5.1.5.1 provides details related to the system configuration and initial conditions. Subsection 5.1.5.2 provides the description of inoperable instruments, and Subsection 5.1.5.3 lists the sequence of events. A discussion of the test results and evaluation can be found in Subsection 5.1.5.4, and Subsection 5.1.5.5 provides a comparison of component responses. A summary of the mass balance results appears in Subsection 5.1.5.6. The conclusions, as they apply to the comparison of results of Matrix Tests SB23 and SB01, can be found in Subsection 5.1.5.7.

System responses to the break are documented by data plots, referenced as figures in text, at the end of this section. The numbering and content of the data plots for Matrix Test SB23 are identical to the data plots provided in Section 5.1.1 for Matrix Test SB01, with the exception that some ranges and time samples have been changed to allow for differences in the two tests. For example, the data plot for instrument channel LDP-601 for Matrix Test SB01 is shown in Figure 5.1.1-5; the data plot for the same channel for Matrix Test SB23 is shown in Figure 5.1.5-5. Not all figures in the data plot package are referenced; only those figures required to explain a different response from that of Matrix Test SB01 are referred to in text.

5.1.5.1 System Configuration and Initial Conditions

Matrix Test SB23 was performed in accordance with an approved written procedure. The test facility was configured in the normal arrangement described in Section 2. The configuration was identical to Matrix Test SB01, except for the size of the simulated break. All actions were automatic after the test started with no operator response required. The appropriate prerequisites were completed, and the initial conditions were satisfied.

The required break simulation piping and break instrumentation were installed per Dwg. OSU 600904 and break piping layouts (Figures 5.1.5-1a and 5.1.5-1b). A break hole ([]^{a,b,c}),

simulating a 1/2-in. cold-leg break in the AP600, was installed in the bottom of the pipe break spool in CL-3.

A flow nozzle simulating one line of flow was installed in the ADS 4-1 line (HL-1 to the ADS 4-1 separator) to provide the single failure simulation, and a flow nozzle simulating two lines of flow was installed in the ADS 4-2 line (HL-2 to the ADS 4-2 separator). Additionally, flow nozzles simulating two lines of flow each were installed in the ADS 1-3 inlet lines.

The nonsafety systems were not in operation for Matrix Tests SB23 or SB01.

Pretest operations such as fill and vent processes were performed and are defined in greater detail in Subsection 2.7. Instruments were checked for required calibrations.

Table 5.1.5-1 is a comparison of the specified and actual pre-test conditions for Matrix Test SB23. There was one initial condition parameter which did not meet the specification. Pressure in ACC-1 and ACC-2 (PT-401 and PT-402) was []^{a,b,c} respectively, lower than the specification. The loss of pressure between tank pressurization and test actuation was possibly caused by nitrogen gas cooling in the accumulator. Test analysis with the recorded lower accumulator overpressure should still be possible.

The heater rod bundle power was adjusted prior to break initiation to achieve the required hot-leg temperatures. At the initiation of the break, rod bundle power was set at 600 kW. The actual power decay curves are provided in Appendix F. The differences between the actual and specified power decay are acceptable. Pressurizer power was terminated at initiation of the break.

5.1.5.2 Inoperable Instruments

Table 5.1.5-2 contains a listing of instruments considered inoperable or invalid during all or portions of this test. Some of the instruments listed are on the Critical Instrument List (Subsection 3.2, Table 3.2-2) and, therefore, are addressed here.

FMM-201, FMM-202, FMM-203, and FMM-204 measured flow (gpm) in each of the four cold legs. A decision was made to continue testing without the availability of these instruments. Replacement flow meters repeatedly failed; their continued use was precluded due to cracking of the ceramic liners from thermal stratification in the loop piping. The necessary boundary conditions for loop flow could be determined from DP-202, DP-203, DP-205, and DP-206.

FMM-501, FMM-504, FMM-802, and FMM-804 provided accurate data when filled with water, but became inaccurate when sensing a two-phase mixture or steam.

FMM-701 measured IRWST-1 injection flow when the primary sump valves were opened, the flow meter indicated a negative flow as water flowed from the primary sump to the IRWST. The meter

was not designed to measure reverse flow, so this measurement was invalid after about []^{a,b,c} However, total IRWST flow was measured by FMM-702.

FMM-905 measured break separator loop seal flow to the primary sump. As the transient proceeded, the primary sump and break separator levels exceeded the elevation of the break at the bottom of CL-3. When this occurred, break flow initially stopped and then reversed. Flow reversal through the break occurred between about []^{a,b,c}

SG tube level data (LDP-215, LDP-218, LDP-219, and LDP-222) were biased by vaporization of the water in the transmitter reference leg after the SG tubes started draining. However, the data provide accurate indication of the time when the tubes are empty.

PT-201 measured RCS pressure at the top of the SG-1 long tube. On August 15, 1994, it was discovered that the transmitter had an incorrect zero compensation, which resulted in a negative error and negative data at low pressure. The transmitter zero was corrected at that time. PT-201 data obtained during Matrix Test SB23 had the zero correction performed, and the corrected data appear as PT_201. Negative data and corrected negative data can be used to determine trends, but are considered inaccurate. PT_201 is not considered reliable, but a sufficient amount of other pressure data is available.

Data provided by ADS-4 separator instrumentation prior to the ADS 4-1 and ADS 4-2 valves opening at 2575 seconds were invalid due to the closed position of the ADS-4 valves and the ADS-4 separator loop seal valves. The instruments affected are: FMM-602, FMM-603, FVM-602, FVM-603, LDP-611, and LDP-612. Test analysis will not be affected, since ADS-4 flow did not begin until the valves opened.

Considering these critical instrument failures, sufficient instrumentation was available to allow the performance of mass balances as demonstrated in Subsection 5.1.5.6 and Appendix E. An energy balance will be performed and reported in the *AP600 Low-Pressure Integral Systems Test at Oregon State University Test Analysis Report, WCAP-14292*.⁽²⁾

5.1.5.3 Sequence of Events

The sequence of events for Matrix Test SB23 is compared with those of Matrix Test SB01 in Table 5.1.5-3 and the associated bar graphs. The table and bar graphs are arranged in chronologic order based on Matrix Test SB23. Because the simulated break area in Matrix Test SB23 is about []^{a,b,c} of the area of the simulated break in Matrix Test SB01, the resultant lower primary coolant loss rates caused delays of []^{a,b,c} in most of the events that occurred after the break. Exceptions to this were the smaller delays in reflooding of CMT-1 ([]^{a,b,c}), primary sump overflow ([]^{a,b,c}), and primary sump injection ([]^{a,b,c}). Because of the low rate of flow through the simulated break, the primary sump injection valves opened about []^{a,b,c} later in Matrix Test SB23 than in Matrix Test SB01. Because of limited flow

through the smaller break, the time for the IRWST to drain to the low level trip signal, which initiated the opening of the primary sump injection valves, was delayed.

The test proceeded through CMT, accumulator, IRWST, and primary sump injection. Matrix Test SB23 was terminated at about []^{a,b,c} after recirculation from the primary sump maintained steady-state operation for more than 2 hours.

5.1.5.4 Tests Results and Evaluation

Facility responses for Matrix Test SB23 are reviewed in the same three phases employed in reference test SB01:

- Initial Depressurization Phase: simulated break initiation to ADS-1 Actuation
- ADS Phase: ADS-1 actuation to start of IRWST injection
- IRWST Injection Phase: start of IRWST injection to end of test

Initial Depressurization Phase

Equipment responses to the S signal after actuation of the TEST pushbutton for Matrix Test SB23 were within 1 second of those for reference test SB01. The slight difference probably resulted from interpolation errors introduced by the data acquisition scanning rates.

After the break valve opened, liquid flowed from the break at an average rate of about []^{a,b,c} (Figure 5.1.5-28). Because the break was so small, steam produced by flashing of the break flow was below the detection limit for the BAMS steam flow meters (Figure 5.1.5-75).

Reactor pressure increased initially, since the small break flow was insufficient to remove the energy being added to the primary system from the core heater bundle. At about []^{a,b,c} the pressure relief valves opened for about []^{a,b,c}. After the relief valves closed, reactor pressure fell slowly to about []^{a,b,c} (Figure 5.1.5-2) at about []^{a,b,c} and then dropped about []^{a,b,c} when the SG primary and secondary pressures reached quasi-equilibrium (Figure 5.1.5-45). Reactor pressure continued to decrease slowly for the remainder of the initial depressurization phase, reaching []^{a,b,c}.

The pressurizer emptied more slowly, requiring []^{a,b,c} in Matrix Test SB23 compared with []^{a,b,c} in Matrix Test SB01. The pressurizer surge line emptied at []^{a,b,c} which also reflected the effect of the smaller break flow on inventory loss in the RCS (Figure 5.1.5-5).

The SG-1 tubes and channel heads in Matrix Test SB23 drained between []^{a,b,c} about []^{a,b,c} later than in reference test SB01. The SG-1 tubes drained earlier than the SG-2 tubes by []^{a,b,c} possibly because of the lower backpressure in SG-1 caused by the simulated break in the cold leg connected to this SG (Figures 5.1.5-7 and 5.1.5-9).

Once the SG tubes started to drain, their level measurements were erroneous because of water vaporization in the reference legs. As a result, refilling of the SG tubes, if it occurs, must be determined from temperature measurements. In this test, the SG did not refill; steam in the SGs remained superheated after draining (Figures 5.1.5-83 and 5.1.5-84).

The ADS-1 valve opened at []^{a,b,c} later in Matrix Test SB01 than in Matrix Test SB23, terminating the initial depressurization phase. Since opening of this valve was initiated by the low level signal from CMT-1, the difference in timing was a result of the delay in CMT drainage because of the smaller break flow.

ADS Phase

Both accumulators started to inject their water inventories just after the ADS-1 valve opened when direct vessel injection (DVI) pressure reached the accumulator pressures (Figure 5.1.5-16). When the ADS-1 valve opened and the pressurizer was vented, the pressurizer refilled, partially drained, refilled again, then drained, emptying at about 3600 seconds (Figure 5.1.5-5). The combined effect of cold water injection from the accumulators and the opening of the ADS valves resulted in a rapid decrease in reactor pressure from about 170 psig to atmospheric pressure between 2260 and 2650 seconds (Figure 5.1.5-45). Core heater temperatures near the top of the core decreased simultaneously from about 420°F to about 270°F (Figure 5.1.5-44).

Injection of water from the IRWST to the DVI lines started at []^{a,b,c} respectively, when pressure in the IRWST exceeded pressure in the two DVI lines (Figure 5.1.5-48).

IRWST Injection Phase

After IRWST flow began, the core remained cooled (Figure 5.1.5-44x). IRWST flow reached a maximum of []^{a,b,c} in each line at about []^{a,b,c} and then fell steadily to about []^{a,b,c} just before primary sump injection began at about []^{a,b,c} (Figure 5.1.5-48). IRWST flow increased sharply by []^{a,b,c} at about []^{a,b,c} probably as a result of condensation events in the CMTs that caused sudden low pressures in the downcomer and DVI lines. After IRWST flow decreased at []^{a,b,c} the flow rate fluctuated by several gpm in both lines until about []^{a,b,c}. After this time, IRWST flow steadied, then fell when primary sump injection began.

Flow from the primary sump was initially established through CSS-921, CSS-922, CSS-923, and CSS-924 in the lines bypassing the primary sump injection valves when the level in the IRWST was reduced sufficiently to permit these check valves to open. When the IRWST low-low level setpoint was reached at []^{a,b,c} the primary sump injection valves were opened by the PLC. The test was terminated about []^{a,b,c} later. Steady-state flows and temperatures were achieved in the reactor during this period. Core coolant reached saturation in the upper portion, indicating that this part of the core the core was being cooled by boiling (Figure 5.1.5-81).

5.1.5.5 Component Responses

The component responses in Matrix Test SB23 were similar to those in Matrix Test SB01, except that they were delayed up to several thousand seconds because of the smaller break.

5.1.5.6 Mass Balance

Mass balance results for Matrix Test SB23 were calculated from water inventories in the facility components at the start and conclusion of the test. The final water inventory agreed with the initial inventory within []^{a,b,c} percent. Details of the mass balance calculations are provided in Appendix E.

5.1.5.7 Conclusions

The test was performed with minimal problems and is considered acceptable. Although not all of the facility initial conditions met the specified acceptance criteria, the deviations did not impact the quality of the data. The instrumentation problems encountered were not critical to the performance of the facility mass and energy balances.

Facility response to the test was as anticipated for the conditions that were established. The data clearly demonstrate that cooling of the reactor heater rods was maintained throughout the duration of the test.

TABLE 5.1.5-1
MATRIX TEST SB23 INITIAL CONDITIONS

Parameter	Instrument No.	Specified Initial Condition	Actual Initial Condition	Comments
Pressurizer pressure ⁽¹⁾	PT-604	370 ± 2 psig		a,b,c
HL-1 temperature ⁽¹⁾	SC-141	420 ± 2°F		
HL-2 Temperature ⁽¹⁾	SC-140	420 ± 2°F		
SG-1 pressure ⁽¹⁾	PT-301	285 ± 5 psig		
SG-2 pressure ⁽¹⁾	PT-302	285 ± 5 psig		
Pressurizer level ⁽¹⁾	LDP-601	65 ± 5 in.		Level signal was temperature-compensated by TF-605
SG-1 narrow range level ⁽¹⁾	LDP-303	26 ± 3 in.		Level signal was temperature-compensated by TF-301
S-2 narrow range level ⁽¹⁾	LDP-304	26 ± 3 in.		Level signal was temperature-compensated by TF-310
IRWST temperature ⁽²⁾	TF-709	< 80°F		
CMT-1 temperature ⁽²⁾	TF-529	< 80°F		
CMT-2 temperature ⁽²⁾	TF-532	< 80°F		
ACC-1 temperature ⁽²⁾	TF-403	< 80°F		
ACC-2 temperature ⁽²⁾	TF-404	< 80°F		
IRWST level ⁽²⁾	LDP-701	Level established by fill-line elevation		

TABLE 5.1.5-1 (Continued)
MATRIX TEST SB23 INITIAL CONDITIONS

Parameter	Instrument No.	Specified Initial Condition	Actual Initial Condition	Comments
ACC-1 level ^(2,3)	LDP-401	Level established by standpipe at 37 in.	[] a,b,c	
ACC-2 level ^(2,3)	LDP-402	Level established by standpipe at 37 in.	[]	
ACC-1 pressure ⁽²⁾	PT-401	232 ± 2 psig	[]	Pressure was [] ^{a,b,c} low; condition acceptable
ACC-2 ⁽²⁾ Pressure	PT-402	232 ± 2 psig	[]	Pressure was [] ^{a,b,c} low; condition acceptable
CMT-1 level ⁽²⁾	Full	LDP-507	[]	
CMT-2 level ⁽²⁾	Full	LDP-502	[]	

Note:

- (1) Data for the indicated parameter were recorded in the test procedure as an initial condition for the test. The value was determined by the test engineer from the appropriate control board indicator.
- (2) Data were not recorded in procedure, but the test engineer verified that specified conditions were achieved while establishing initial conditions. The value of the parameter was determined post-test by calculating the average DAS indication for a time of about 2 minutes before the break valve opened.
- (3) The bourdon pressure tube local indicator (PI-401 or PI-402) was tubed to the lower portion of the reference leg of the accumulator level transmitter (LDP-401 or LDP-402). As pressure in the accumulator was increased, air inside the bourdon tube was compressed, thereby lowering the reference leg liquid level, resulting in a false indication of measured level.

TABLE 5.1.5-2
MATRIX TEST SB23 INOPERABLE INSTRUMENTS/INVALID DATA CHANNELS

Instrument No.	Instrument Type	Description of Problem
FMM-201*	Magnetic flow meter	Removed from system
FMM-202*	Magnetic flow meter	Removed from system
FMM-203*	Magnetic flow meter	Removed from system
FMM-204*	Magnetic flow meter	Removed from system
FMM-401	Magnetic flow meter	Failed
FMM-502*	Magnetic flow meter	Data invalid after 2310 seconds because of steam in balance line
FMM-503*	Magnetic flow meter	Failed
FMM-703	Magnetic flow meter	Over-ranged from about 2450 to 2610 seconds
FMM-802*	Magnetic flow meter	Data invalid after steam forms in PRHR HX inlet line at about 2325 seconds
FMM-804*	Magnetic flow meter	Data valid until PRHR HX initially drained at 2325 seconds after which the possibility of steam in the outlet line invalidated the data
HFM-103	Heat flux meter	Failed
HFM-105	Heat flux meter	Failed
HFM-505	Heat flux meter	Failed
HFM-510	Heat flux meter	Failed
HPS-203-1 through HPS-203-3	Heated phase switch	Inoperable throughout test
HPS-509-1 through HPS-509-3	Heated phase switch	Removed
LDP-102	Differential pressure transmitter - level	Failed
LDP-201 LDP-202 LDP-203 LDP-204 LDP-205 LDP-206	Differential pressure transmitter - level	Data invalid due to effect of vertical portion of sense line attached to top of pipe; data can show level trends, when the pipe is empty or starts to drain, but absolute level indication can not be used

TABLE 5.1.5-2 (Continued)
MATRIX TEST SB23 INOPERABLE INSTRUMENTS/INVALID DATA CHANNELS

Instrument No.	Instrument Type	Description of Problem
LDP-207 through LDP-209	Differential pressure transmitter - level	Inoperable; ranged improperly; data can show trends, but absolute level indication can not be used
LDP-215* LDP-215 LDP-216 LDP-217 LDP-218* LDP-219* LDP-220 LDP-221 LDP-222*	Differential pressure transmitter - level	Data invalid when tube drained and reference leg started to vaporize
LDP-802* LDP-804	Differential pressure transmitter - level	Data valid until PRHR HX initially drained at 2325 seconds; data suspect because of possible vaporization of their common reference line
PT_101	Pressure transmitter	Data less than 6.1 psig invalid
PT_102	Pressure transmitter	Data less than 6.2 psig invalid
PT_103	Pressure transmitter	Data less than 6.2 psig invalid
PT_104	Pressure transmitter	Data less than 6.4 psig invalid
PT_108	Pressure transmitter	Data less than 8.4 psig invalid
PT_109	Pressure transmitter	Data less than 6.3 psig invalid
PT_111	Pressure transmitter	Data less than 6.0 psig invalid
PT_112	Pressure transmitter	Data less than 8.8 psig invalid
PT_113	Pressure transmitter	Data less than 6.4 psig invalid
PT_201*	Pressure transmitter	Data less than 1.1 psig invalid
PT_202	Pressure transmitter	Data less than 5.9 psig invalid
PT_205	Pressure transmitter	Data less than 6.1 psig invalid
TF-103*	Thermocouple fluid temperature	Removed and replaced with thermocouple for thermal stratification test
TF-104*	Thermocouple fluid temperature	Removed and replaced with thermocouple for thermal stratification test
TF-170	Thermocouple fluid temperature	Read low throughout test
TFM-103 TFM-105	Thermocouple for HFM-703	Inoperable; indicated ambient temperature throughout test

TABLE 5.1.5-2 (Continued)
MATRIX TEST SB23 INOPERABLE INSTRUMENTS/INVALID DATA CHANNELS

Instrument No.	Instrument Type	Description of Problem
TH-317-1 through TH-317-4	Thermocouple heater rod	Inoperable; heater rod removed prior to test
TW-503	Thermocouple wail temperature	Inoperable throughout test

Note:

* Instruments marked with an asterisk are critical instruments. See Subsection 5.1.5.2 for discussion.

Table 5.1.5-3 on pages 5.1.5-12 through 5.1.5-19 is not included in this nonproprietary document.

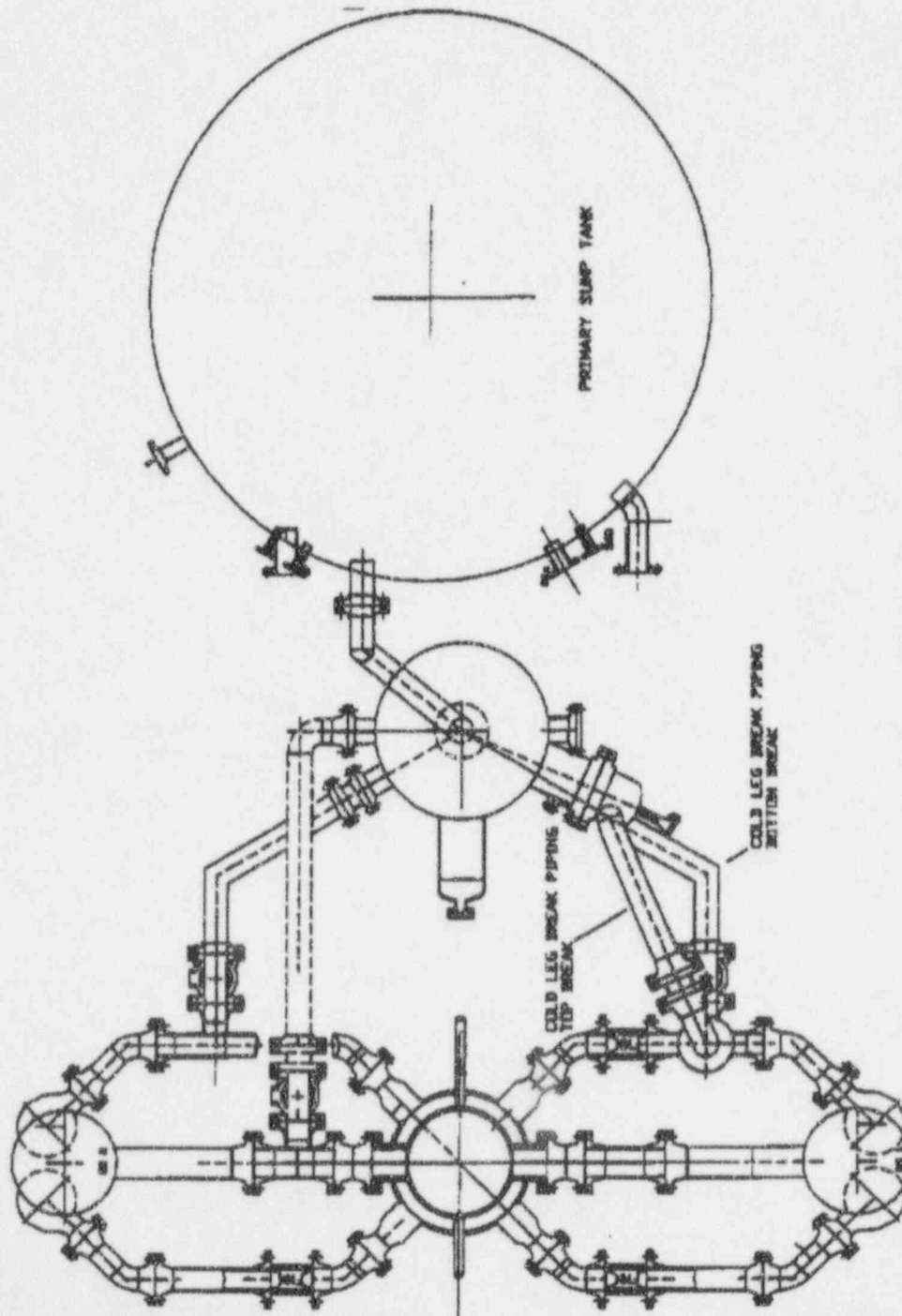


Figure 5.1.5-1a Primary Loop and Break Pipe Arrangement (Sh. 1 of 2)

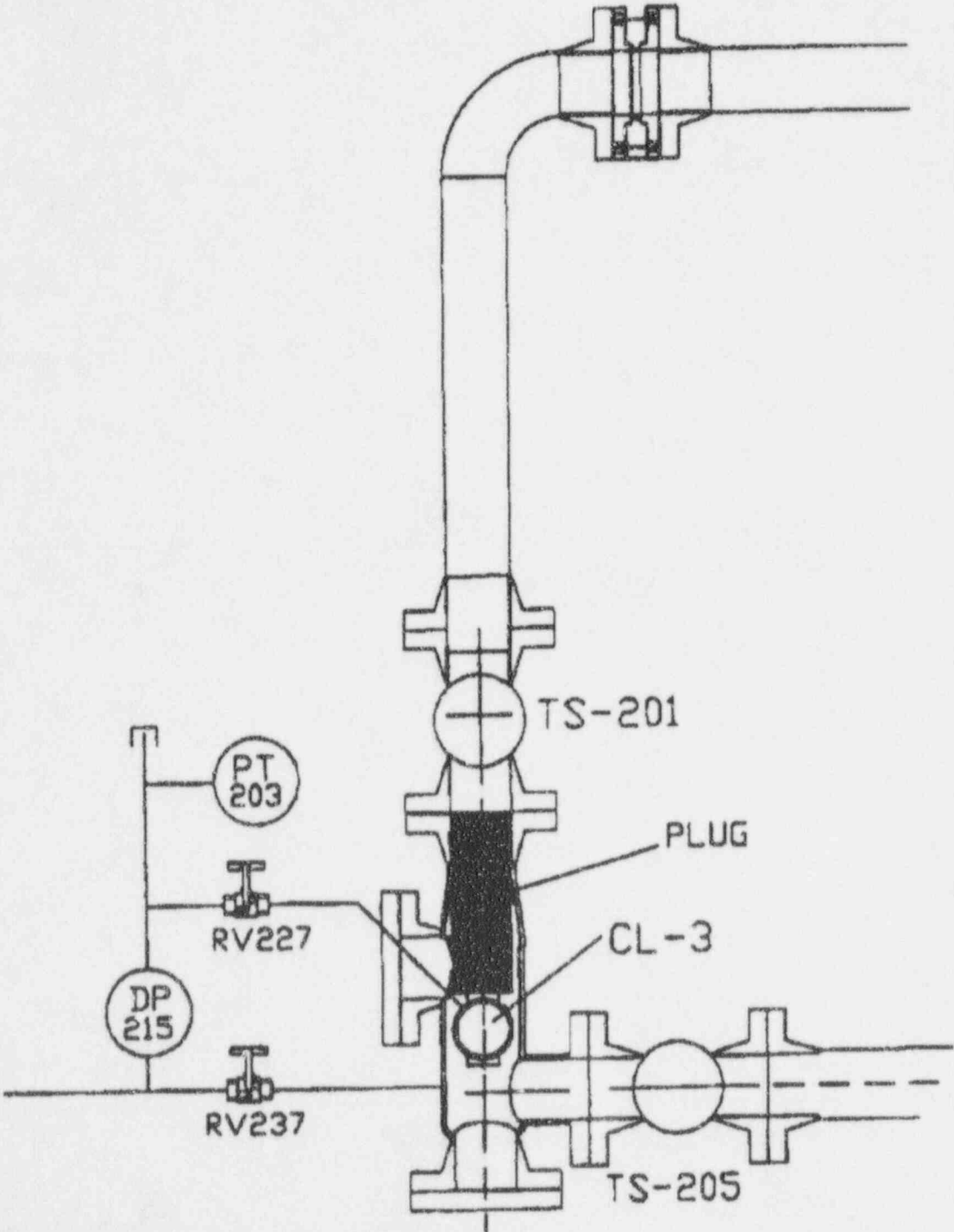


Figure 5.1.5-1b Primary Loop and Break Pipe Arrangement (Sh. 2 of 2)

Figures 5.1.5-2 through 5.1.5-106 are not included in this nonproprietary document.

5.1.6 Effect of an Intermediate Break Size (Matrix Test SB05 Comparison with Matrix Test SB01)

In this section, the results of Matrix Test SB05 (OSU Test U0005) are compared with those of Matrix Test SB01 (OSU Test U0001). These two tests were identical, except that Matrix Test SB05 simulated a 1-in. pipe break and reference test SB01 simulated a 2-in. pipe break. Both simulated breaks were located at the bottom of CL-3. In both tests, failure of one leg of one ADS-4 line was simulated by orificing one ADS-4 line for 50-percent design flow area and the other for 100-percent design flow area.

Matrix Test SB05 was performed on June 21, 1994. During the transient, the CMTs and accumulators injected their water inventories, the IRWST injected water, and circulation through the primary sump was established. The test was terminated at 23,000 seconds after long-term cooling had been demonstrated. The core remained cooled throughout the test, and excessive temperature increases were not observed; therefore, the test was successful.

Subsection 5.1.6.1 provides details related to the system configuration and initial conditions. Subsection 5.1.6.2 provides the description of inoperable instruments, and Subsection 5.1.6.3 lists the sequence of events. A discussion of the test results and evaluation can be found in Subsection 5.1.6.4, and Subsection 5.1.6.5 is a comparison of component responses. A summary of the mass balance results appears in Subsection 5.1.6.6. The conclusions, as they apply to the comparison of the tests, can be found in Subsection 5.1.6.7.

System responses to the break are documented by data plots, referenced as figures in text, at the end of this section. The numbering and content of the data plots for Matrix Test SB05 are identical to the data plots provided in Section 5.1.1 for Matrix Test SB01, with the exception that some ranges and time samples have been changed to allow for differences in the two tests. For example, the data plot for instrument channel LDP-601 for Matrix Test SB01 is shown in Figure 5.1.1-5; the data plot for the same channel for Matrix Test SB05 is shown in Figure 5.1.6-5. Not all of the figures in the data plot package are referenced; only those figures required to explain a different response from that of Matrix Test SB01 are referred to in text. An x suffix in a data plot figure number indicates extended time.

5.1.6.1 System Configuration and Initial Conditions

Matrix Test SB05 was performed in accordance with an approved written procedure. The test facility was configured in the normal arrangement described in Section 2. The configuration was identical to Matrix Test SB01, except for the size of the simulated break. All actions were automatic after the test started with no operator response required.

The required break simulation piping and its instrumentation were installed per Dwg. OSU 600904 (Appendix G) and the break piping layouts in Figures 5.1.6-1a and 5.1.6-1b. A break hole

[]^{a,b,c} simulating a 1-in. cold-leg break in the AP600, was installed in the bottom of the pipe break spool in CL-3.

A flow nozzle simulating one line of flow was installed in the ADS 4-1 line (HL-1 to the ADS 4-1 separator) to provide the single failure simulation, and a flow nozzle simulating two lines of flow was installed in the ADS 4-2 line (HL-2 to the ADS 4-2 separator). Additionally, flow nozzles simulating two lines of flow each were installed in the ADS 1-3 inlet lines.

The nonsafety systems were not in operation for Matrix Tests SB05 and SB01.

Pre-test operations such as fill and vent processes were performed and are defined in greater detail in Subsection 2.7. Instruments were checked for required calibrations.

Table 5.1.6-1 is a comparison of the specified and actual pre-test conditions for Matrix Test SB05. There was one initial condition parameter which did not meet the specification. Pressure in ACC-2, indicated by PT-402, was []^{a,b,c} lower than the specification. The loss of pressure between tank pressurization and test actuation was possibly caused by nitrogen gas cooling in the accumulator. Test analysis with the recorded lower accumulator overpressure should still be possible.

The heater rod bundle power was adjusted prior to break initiation to achieve the required hot-leg temperatures. At the initiation of the break, the rod bundle power was set at 600 kW. The actual power decay curves are provided in Appendix F. The differences between the actual and specified power decay are acceptable. Pressurizer power was terminated at initiation of the break.

5.1.6.2 Inoperable Instruments

Table 5.1.6-2 is a list of instruments considered inoperable or invalid during all or portions of this test. Some of the instruments listed are on the Critical Instrument List (Subsection 3.2, Table 3.2-2) and, therefore, are addressed here.

FMM-201, FMM-202, FMM-203, and FMM-204 measured flow (gpm) in each of the four cold legs. A decision was made to continue testing without the availability of these instruments. Replacement flow meters repeatedly failed; their continued use was precluded due to cracking of the ceramic liners from thermal stratification in the loop piping. The necessary boundary conditions for loop flow could be determined from DP-202, DP-203, DP-205, and DP-206.

FMM-501, FMM-504, FMM-802, and FMM-804 provided accurate data when sensing liquid, but became inaccurate when sensing two-phase or steam flow.

FMM-701 measured IRWST-1 injection flow. When the primary sump valves were opened, the flow meter indicated a negative flow as water flowed from the primary sump to the IRWST. The meter

was not designed to measure reverse flow, so this measurement was invalid. However, total IRWST flow was measured by FMM-702.

FMM-905 measured break separator loop seal flow to the primary sump. As the transient proceeded, the primary sump and break separator levels exceeded the elevation of the break at the bottom of CL-3. When this occurred, break flow initially stopped and then reversed. Flow reversal through the break occurred at about []^{a,b,c} rendering subsequent data invalid.

SG tube level data (LDP-215, LDP-218, LDP-219, and LDP-222) were biased by vaporization of the water in the transmitter reference leg after the SG tubes started draining; however, data provide accurate indication of the time when the tubes are empty.

LDP-401 and LDP-402 measured ACC-1 and ACC-2 levels, respectively. Due to air trapped in the sense lines for the transmitters, data from these transmitters were invalid. However, the initial level of the tank was established by a standpipe, so it was constant from test to test. The drain rate can be calculated using FMM-401 and FMM-402. Alternately, a pressure correction may be applied directly to the level indications of LDP-401 and LDP-402.

PT-201 measured RCS pressure at the top of the SG-1 long tube. On August 15, 1994, it was discovered that the transmitter had an incorrect zero compensation, which resulted in a negative error and negative data at low pressures. The transmitter zero was corrected at that time. PT-201 data obtained during Matrix Test SB05 had the zero correction performed, and the corrected data appear as PT_201. Negative data and corrected negative data can be used to determine trends, but are considered inaccurate. PT_201 was not considered reliable for values less than 1.1 psig, but a sufficient amount of other pressure data is available.

TF-501 and TF-504 measured CMT fluid temperature from the long thermocouple rod location near the bottom of each CMT. The thermocouples appear to have measured ambient conditions throughout the test, which would indicate a short somewhere in the thermocouple wiring. With these thermocouples inoperable, the required long thermocouple rod thermocouple availability of "seven out of ten and no more than one in succession failed" was met.

Data provided by ADS-4 separator instrumentation prior to the ADS 4-1 and ADS 4-2 valves opening at 978 seconds were invalid due to the closed position of the ADS-4 valves and the ADS-4 separator loop seal valves. The instruments affected are: FMM-602, FMM-603, FVM-602, FVM-603, LDP-611, and LDP-612. Test analysis will not be affected, since ADS-4 flow did not begin until the valves opened.

Considering these critical instrument failures, sufficient instrumentation was available to allow the performance of mass balances as demonstrated in Subsection 5.1.6.6 and Appendix E. An energy balance will be performed and reported in the *AP600 Low-Pressure Integral Systems Test at Oregon State University Test Analysis Report, WCAP-14292*.⁽²⁾

5.1.6.3 Sequence of Events

The sequence of events for Matrix Test SB05 is compared with those of Matrix Test SB01 in Table 5.1.6-3 and its associated bar graphs. The table and bar graphs are arranged in chronologic order based on Matrix Test SB05. The first page of Table 5.1.6-3 indicates the source of the actual time data. A D in the Data Source column indicates the recorded time was obtained from a software program that monitored digital events in the facility, including pump starts and stops, valve limit switch actuations, and alarms. The term *valve opening* means the valve has actuated and the closed limit switch is being opened (valve coming off the seat). An A in the Data Source column indicates the time data were obtained by reviewing test data obtained from the data acquisition system (DAS). Although the test DAS were in digital format, the DAS monitored analog events of pressure, flow, and temperature. Because the simulated break area in Matrix Test SB05 is about 1/4 the area of the simulated break in Matrix Test SB01, the rates of depressurization and water inventory loss from the RCS were lower, resulting in delays of []^{a,b,c} in most of the events that occurred after the break. The CMTs reflooded earlier in Matrix Test SB05. The CMTs reflooded earlier because the RCS refilled more rapidly when IRWST injection started because the rate of water loss through the simulated break was smaller than the reference test SB01 loss rate. The pressurizer in Matrix Test SB05 reflooded earlier than in Matrix Test SB01 because the net water volume in the RCS increased faster when the accumulators injected and the break flow was smaller.

The test proceeded through CMT, accumulator, IRWST, and primary sump injection. Matrix Test SB05 was terminated at about 23,000 seconds, after recirculation from the primary sump maintained steady-state operation for several hours.

5.1.6.4 Test Results and Evaluation

Facility responses for Matrix Test SB05 will be reviewed in the same three phases employed in reference test SB01:

- Initial Depressurization Phase: simulated break initiation to ADS-1 actuation
- ADS Phase: ADS-1 actuation to start of IRWST injection
- IRWST Injection Phase: start of IRWST injection to end of test

Initial Depressurization Phase

For Matrix Test SB05, equipment responses to the S signal after the TEST pushbutton was pressed were within 1 second of those of Matrix Test SB01. The slight time difference was probably the result of interpolation errors introduced by the data recording scanning rates.

When the break valve opened, liquid flow reached a maximum of []^{a,b,c} (Figure 5.1.6-62), compared with []^{a,b,c} in Matrix Test SB01. The Matrix Test SB05 maximum steam flow was

[]^{a,b,c} compared with about []^{a,b,c} for Matrix Test SB01. These lower flows are expected because of the smaller break diameter in Matrix Test SB05 (Figure 5.1.6-75).

For the first []^{a,b,c} (Figure 5.1.6-45), RCS pressure decreased because of water loss through the break, cooling provided by the PRHR, and cold water circulation from the CMTs. From about []^{a,b,c} pressure remained nearly constant at about []^{a,b,c}. This period coincided with the period during which primary and secondary pressure in the SG was in quasi-equilibrium (Figure 5.1.6-45). There were small RCS pressure rises of about []^{a,b,c} that occurred at []^{a,b,c} and were accompanied by CMT flow increases. These pressure rises may have been caused by the cold-leg side of the SG tubes draining, since the levels in these tubes were fluctuating at this time (Figures 5.1.6-7 and 5.1.6-8), or the pressurizer surge line draining (Figure 5.1.6-5). These fluids were the only source of transient energy input that could have caused this pressure increase at this time.

The SG-2 tubes in Matrix Test SB05 drained []^{a,b,c} after the same tubes drained in reference test SB01. Draining of the SG-1 tubes in Matrix Test SB05 was delayed []^{a,b,c} compared with the same tubes in Matrix Test SB01 (Figures 5.1.6-7 and 5.1.6-8). Once the SG tubes started to drain, their level measurements were erroneous because of water evaporation in the common reference legs of the SG tube level transmitters; however, level data can be used to indicate trends.

The measured level in the upper plenum of the reactor (LDP-139) decreased from an initial level of []^{a,b,c} (Figure 5.1.6-12). Based on these data, the maximum steam content in the upper plenum was about []^{a,b,c} percent at about []^{a,b,c} (Figure 5.1.6-4). This level was higher than the equivalent level in Matrix Test SB01 and occurred several hundred seconds later. This is consistent with the expected results from the smaller break.

Note: This steam content is an average and is comprised of a two-phase mixture with a steam volume above the mixture. The distribution of steam between the two-phase mixture and the steam above the mixture cannot be determined from the data.

As indicated by the lack of large temperature increases in the core heater wall temperatures during the entire test, the core remained cooled (Figure 5.1.6-44). The short-term temperature rises (duration of about []^{a,b,c}) were probably spurious signals, as indicated by their short duration. A temperature increase of about []^{a,b,c} at about []^{a,b,c} was probably real and coincided with the pressure rise discussed previously.

The pressurizer emptied at []^{a,b,c} in Matrix Test SB05 compared with []^{a,b,c} in Matrix Test SB01. Similarly, the Matrix Test SB05 pressurizer surge line emptied at []^{a,b,c} compared with []^{a,b,c} for reference test SB01 (Figure 5.1.6-5). These results are consistent with the relationship of break size in these tests.

In Matrix Test SB05, the pressurizer started to reflood at []^{a,b,c} as a result of steam being vented when the ADS-1 valve opened (Figure 5.1.6-5). A peak level was attained while the accumulators were injecting. A second peak was reached when CMT flow increased after the accumulators emptied. The decrease in pressurizer level between these peaks may have been the result of the compressibility of nitrogen from the accumulators, which would inject into the system when the accumulator water inventory was exhausted. The level fell as the CMT flows decreased, and the ADS-4 valves opened until the pressurizer emptied again at []^{a,b,c}

CMT-1 transitioned from recirculation to draindown at []^{a,b,c} later than in Matrix Test SB01 (Figure 5.1.6-6). CMT-2 reached this transition at []^{a,b,c} later than in Matrix Test SB01. When the transition occurred, flow rates from each CMT approximately doubled (Figure 5.1.6-16). At []^{a,b,c} the CMT-1 low level setpoint was reached, and the signal to open the ADS-1 valve was initiated []^{a,b,c} later. This CMT-1 low level was reached []^{a,b,c} earlier in Matrix Test SB01.

Before the ADS-1 valve opened, however, system pressure fell below the accumulator pressure, and both accumulators started injection of their water inventories at []^{a,b,c} after the accumulators began to inject in Matrix Test SB01. In Matrix Test SB01, the accumulators injected []^{a,b,c} before the ADS-1 valve opened. Accumulator flow rates are provided in Figure 5.1.6-16.

ADS Phase

Per facility logic, the ADS-1 valve opened []^{a,b,c} after the CMT-1 low level setpoint was reached at []^{a,b,c} about []^{a,b,c} later than in Matrix Test SB01. The rate of RCS depressurization increased when the ADS-1 valve opened; however, ADS-2 and ADS-3 valves opening did not affect the rate of pressure reduction (Figure 5.1.6-45). The ADS-2 and ADS-3 valves opened about []^{a,b,c} later than the valves in Matrix Test SB01. This difference is consistent with the delayed opening of the ADS-1 valve, since they were triggered by the same signal, which had a longer delay in Matrix Test SB05.

The CMT-2 transition from recirculation to draindown was delayed relative to CMT-1 because the pressure in CL-3 was slightly lower than in the other cold legs. The same effect delayed the achievement of CMT-2's low level setpoint. Therefore, CMT-1 transitioned from recirculation earlier and drained slightly earlier.

There was only one downcomer condensation event in Matrix Test SB05, whereas several such events occurred in Matrix Test SB01. The sudden condensation of steam in the downcomer at about []^{a,b,c} caused a sharp, short rise in downcomer levels (Figure 5.1.6-15), and a negative differential pressure spike across the upper support plate and through the upper core support plate bypass holes (Figure 5.1.6-19). The latter negative differential pressure indicated a high flow rate of

steam through the bypass holes from the upper head to the downcomer, correspondent to a similar event in Matrix Test SB01 at about []^{a,b,c}

Injection in IRWST-1 and IRWST-2 started at []^{a,b,c} compared with []^{a,b,c} respectively, in Matrix Test SB01 (Figure 5.1.6-48). This difference is consistent with the effect of the smaller flow in Matrix Test SB05.

IRWST Injection Phase

Both CMTs in Matrix Test SB05 started to reflood at about []^{a,b,c} (Figure 5.1.6-6x), about []^{a,b,c} earlier than the respective CMTs in Matrix Test SB01. However, CMT-2 stopped refilling for about []^{a,b,c} then refilled completely. The CMTs in Matrix Test SB01 reflooded at widely different times, i.e., []^{a,b,c} for CMT-1 and []^{a,b,c} for CMT-2. The difference between CMT behavior in Matrix Test SB05 versus Matrix Test SB01 is consistent with the lower break flow rate in Matrix Test SB05, which led to earlier refilling of the cold-leg/CMT balance line. When these balance lines filled and spilled over into the top of the CMT, the cold liquid caused a sudden condensation of steam in the CMT. The resulting pressure decrease caused rapid filling of the tank with liquid from the RCS through the DVI and CMT injection lines. This phenomenon is discussed more completely in Subsection 5.1.1.4.

The CMTs reflooded within about []^{a,b,c} of each other in Matrix Test SB05, whereas reflooding in Matrix Test SB01 occurred over a much wider time range (about []^{a,b,c}). This difference in timing probably resulted from the effect of the larger break on the CL-1 backpressure in Matrix Test SB01.

Primary sump injection in line 1 and line 2 started at about []^{a,b,c} respectively, more than []^{a,b,c} later than in Matrix Test SB01. Flow from the primary sump was initiated through CCS-922 and CCS-924 when pressure in the primary sump equaled pressure at the break (Figure 5.1.6-37). The primary sump injection valves opened at []^{a,b,c} when the low-low level setpoint was reached in the IRWST. Test operation continued for almost 2 more hours with cooling provided by recirculation through the primary sump.

5.1.6.5 Comparison of Component Responses

Other than differences in timing and some rates of change because of the smaller break in Matrix Test SB05, the responses of the components in Matrix Tests SB01 and SB05 were comparable, except for the pressurizer.

Pressurizer

The pressurizer in Matrix Test SB05 only reflooded once (at []^{a,b,c}), whereas the pressurizer in Matrix Test SB01 reflooded a second time, late in the transient, at about []^{a,b,c}. This

different response was caused by the modifications made to the system to eliminate negative pressures in the pressurizer (described in Subsections 5.1.1.5 and 5.1.2.5). In Matrix Test SB05, pressurizer power was de-energized at the start of the test by the PLC, whereas power to the pressurizer heaters was maintained at about 1.5 kW in Matrix Test SB01.

5.1.6.6 Mass Balance

Mass balance results for Matrix Test SB05 were calculated from water inventories in the facility components at the start and conclusion of the test. The final water inventory agreed with the initial inventory within []^{a,b,c} Details of the mass balance analysis are provided in Appendix E.

5.1.6.7 Conclusions

Facility response to Matrix Test SB05 was as anticipated for the established conditions. Although not all of the facility initial conditions met the specified acceptance criteria, the deviations did not impact the quality of the data. The instrumentation problems encountered were not critical to the performance of the facility mass and energy balances.

The lower break flow rates in the simulated 1-in. break (Matrix Test SB05) produced similar system responses (including CMT recirculation, draining, and reflooding; accumulator injection; IRWST injection; and primary sump injection) compared with the simulated 2-in. break in reference test SB01. Actuation of these components was delayed from []^{a,b,c} compared with Matrix Test SB01 because of the lower break flow and resultant slower rates of depressurization and level changes in the CMTs, accumulators, and IRWST.

**TABLE 5.1.6-1
MATRIX TEST SB05 INITIAL CONDITIONS**

Parameter	Instrument No.	Specified Initial Condition	Actual Initial Condition	Comments
Pressurizer pressure ⁽¹⁾	PT-604	370 ± 2 psig	<input type="checkbox"/> a,b,c	
HL-1 temperature ⁽¹⁾	SC-141	420 ± 2°F	<input type="checkbox"/>	
HL-2 temperature ⁽¹⁾	SC-140	420 ± 2°F	<input type="checkbox"/>	
SG-1 pressure ⁽¹⁾	PT-301	285 ± 5 psig	<input type="checkbox"/>	
SG-2 pressure ⁽¹⁾	PT-302	285 ± 5 psig	<input type="checkbox"/>	
Pressurizer level ⁽¹⁾	LDP-601	65 ± 5 in.	<input type="checkbox"/>	Level signal was temperature-compensated by SC-605
SG-1 narrow-range level ⁽¹⁾	LDP-303	26 ± 3 in.	<input type="checkbox"/>	Level signal was temperature-compensated by TF-305 and TF-307
SG-2 narrow-range level ⁽¹⁾	LDP-304	26 ± 3 in.	<input type="checkbox"/>	Level signal was temperature-compensated by TF-306 and TF-308
IRWST temperature ⁽²⁾	TF-709	< 80°F	<input type="checkbox"/>	
CMT-1 temperature ⁽²⁾	TF-529	< 80°F	<input type="checkbox"/>	
CMT-2 temperature ⁽²⁾	TF-532	< 80°F	<input type="checkbox"/>	
ACC-1 temperature ⁽²⁾	TF-403	< 80°F	<input type="checkbox"/>	
ACC-2 temperature ⁽²⁾	TF-404	< 80°F	<input type="checkbox"/>	
IRWST level ⁽²⁾	LDP-701	Level established by fill-line elevation	<input type="checkbox"/>	
ACC-1 level ^(2,3)	LDP-401	Level established by standpipe at 37 in.	<input type="checkbox"/>	
ACC-2 level ^(2,3)	LDP-402	Level established by standpipe at 37 in.	<input type="checkbox"/>	
ACC-1 pressure ⁽²⁾	PT-401	232 ± 2 psig	<input type="checkbox"/>	
ACC-2 pressure ⁽²⁾	PT-402	232 ± 2 psig	<input type="checkbox"/>	Pressure was [<input type="checkbox"/>] ^{a,b,c} low; condition acceptable

TABLE 5.1.6-1 (Continued)
MATRIX TEST SB05 INITIAL CONDITIONS

Parameter	Instrument No.	Specified Initial Condition	Actual Initial Condition	Comments
CMT-1 level ⁽²⁾	LDP-507	Full	a,b,c	
CMT-2 level ⁽²⁾	LDP-502	Full		

Note:

- (1) Data for the indicated parameter were recorded in the test procedure as an initial condition for the test. The value was determined by the test engineer from the appropriate control board indicator.
- (2) Data were not recorded in procedure, but the test engineer verified that the specified conditions were achieved while establishing initial conditions. The value of the parameter was determined post-test by calculating the average DAS indication for a time of about 2 minutes before the break valve opened.
- (3) The bourdon pressure tube local indicator (PI-401 or PI-402) was tubed to the lower portion of the reference leg of the accumulator level transmitter (LDP-401 or LDP-402). As pressure in the accumulator increased, air inside the bourdon tube was compressed, thereby lowering the reference leg liquid level, resulting in a false indication of measured level.

**TABLE 5.1.6-2
MATRIX TEST SB05 INOPERABLE INSTRUMENTS/INVALID DATA CHANNELS**

Instrument No.	Instrument Type	Description of Problem
FMM-201*	Magnetic flow meter	Removed from system
FMM-202*	Magnetic flow meter	Removed from system
FMM-203*	Magnetic flow meter	Removed from system
FMM-204*	Magnetic flow meter	Removed from system
FMM-502*	Magnetic flow meter	Data invalid after 544 seconds because of steam in balance line
FMM-503*	Magnetic flow meter	Data invalid after 456 seconds because of steam in balance line
FMM-701*	Magnetic flow meter	Data invalid after 16,700 seconds because of reverse flow from primary sump to IRWST
FMM-802*	Magnetic flow meter	Data invalid after steam formed in PRHR HX inlet line at about 300 seconds
FMM-804*	Magnetic flow meter	Data valid until PRHR HX initially drained at 580 seconds after which the possibility of steam in the outlet line invalidated data
FMM-902 FMM-905*	Magnetic flow meter	Negative values indicated because of reverse flow from primary sump/break separator until levels in IRWST/primary sump/break separator were equal
HFM-103	Heat flux meter	Failed
HFM-105	Heat flux meter	Failed
HFM-201	Heat flux meter	Failed
HFM-601	Heat flux meter	Failed
HPS-203-1 through HPS-203-3	Heated phase switch	Inoperable throughout test
HPS-509-1 through HPS-509-3	Heated phase switch	Inoperable throughout test
LDP-127	Differential pressure transmitter - level	Data invalid before 8640 seconds; isolation valve inadvertently closed until this time
LDP-201 LDP-202 LDP-203 LDP-204 LDP-205 LDP-206	Differential pressure transmitter - level	Data invalid due to effect of vertical portion of sense line attached to top of pipe; data can show level trends, when pipe is empty or starts to drain, but absolute level indication can not be used
LDP-207 through LDP-209	Differential pressure transmitter - level	Inoperable; ranged improperly; data can show trends, but absolute level indication can not be used

TABLE 5.1.6-2 (Continued)
MATRIX TEST SB05 INOPERABLE INSTRUMENTS/INVALID DATA CHANNELS

Instrument No.	Instrument Type	Description of Problem
LDP-215* LDP-215 LDP-216 LDP-217 LDP-218* LDP-219* LDP-220 LDP-221 LDP-222*	Differential pressure transmitter - level	Data invalid when tube drains and reference leg starts to vaporize
LDP-401* LDP-402*	Differential pressure transmitter - level	Data invalid; see note 3 of Table 5.1.6-2
LDP-802* LDP-804	Differential pressure transmitter - level	Data valid until PRHR HX initially drained at 1000 seconds after which data suspect because of possible vaporization of the common reference line
PT_101	Pressure transmitter	Data less than 6.1 psig invalid
PT_102	Pressure transmitter	Data less than 6.2 psig invalid
PT_103	Pressure transmitter	Data less than 6.2 psig invalid
PT_104	Pressure transmitter	Data less than 6.4 psig invalid
PT_108	Pressure transmitter	Data less than 8.4 psig invalid
PT_109	Pressure transmitter	Data less than 6.3 psig invalid
PT_111	Pressure transmitter	Data less than 6.0 psig invalid
PT_112	Pressure transmitter	Data less than 8.8 psig invalid
PT_113	Pressure transmitter	Data less than 6.4 psig invalid
PT_201*	Pressure transmitter	Data less than 1.1 psig invalid
PT_202	Pressure transmitter	Data less than 5.9 psig invalid
PT_205	Pressure transmitter	Data less than 6.1 psig invalid
PT-801	Pressure transmitter	Not reliable after 1000 seconds
TF-170	Thermocouple fluid temperature	Read low throughout test
TF-501	Thermocouple fluid temperature	Read low throughout test
TF-504	Thermocouple fluid temperature	Read low throughout test
TFM-103 TFM-105 TFM-201 TFM-601	Thermocouple for HFM-703	Inoperable; indicated ambient temperature throughout test
TH-317-1 through TH-317-4	Thermocouple heater rod	Inoperable; heater rod removed prior to test
TW-503	Thermocouple wall temperature	Inoperable throughout test
TW-534	Thermocouple wall temperature	Inoperable; indicated ambient throughout test
TW-552	Thermocouple wall temperature	Inoperable; indicates ambient throughout test

Note:

* Instruments marked with an asterisk are critical instruments. See Subsection 5.1.6.2 for discussion.

**TABLE 5.1.6-3
MATRIX TEST SB05 SEQUENCE OF EVENTS**

Event ⁽¹⁾	Data Source ⁽²⁾	SB05 Time After Break (sec.)	SB01 Time After Break (sec.)	Delta Time (sec.)
TEST Pushbutton Depressed				
Break Valve Open Signal				
Break Valve Starts to Open				
Feed Pump Trips				
CMT-1 Outlet Valve Starts to Open				
CMT-2 Outlet Valve Starts to Open				
PRHR HX Outlet Valve Starts to Open				
Reactor Coolant Pumps Trip				
Pressurizer Empty (LDP-601)				
SG-1 Cold-Leg Short Tube Empty (LDP-221)				
SG-1 Hot-Leg Short Tube Empty (LDP-217)				
CL-3 Channel Head Empty (LDP-213)				
CMT-1 Recirculation Flow Stops (LDP-509)				
SG-2 Cold-Leg Long Tube Empty (LDP-222)				
SG-2 Cold-Leg Short Tube Empty (LDP-220)				
SG-2 Hot-Leg Long Tube Empty (LDP-218)				
SG-2 Hot-Leg Short Tube Empty (LDP-216)				
CMT-2 Recirculation Flow Stops (LDP-510)				
Time of Minimum Reactor Level Observed During Test (LDP-127)				
HL-1 Pipe Starts to Drain (LDP-205)				
HL-2 Pipe Starts to Drain (LDP-206)				
CL-1 Channel Head Empty (LDP-211)				
CMT-1 Low Level Signal				
Pressurizer Surge Line Empty (LDP-602)				
ACC-2 Injection Starts (FMM-402)				
ACC-1 Injection Starts (FMM-401)				
ADS-1 Valve Starts to Open				
SG-2 Hot-Leg Elbow Starts Draining (LDP-208)				
SG-1 Hot-Leg Long Tube Empty (LDP-215)				
SG-1 Cold-Leg Long Tube Empty (LDP-219)				
Pressurizer Refloods (LDP-601)				
CL-4 Channel Head Empty (LDP-212)				
CL-2 Channel Head Empty (LDP-210)				
SG-2 Hot-Leg Channel Head Empty (LDP-214)				

TABLE 5.1.6-3 (Continued)
MATRIX TEST SB05 SEQUENCE OF EVENTS

Event ⁽¹⁾	Data Source ⁽²⁾	SB05 Time After Break (sec.)	SB01 Time After Break (sec.)	Delta Time (sec.)
ADS-2 Valve Starts to Open				
CMT-2 Low Level Signal				
SG-2 Hot-Leg Elbow Minimum (LDP-208)				
HL-2 Pipe Empty (LDP-206)				
HL-1 Pipe Empty (LDP-205)				
ADS-3 Valve Starts to Open				
IRWST-2 Injection Valve Starts to Open				
Reactor Pressure Low				
IRWST-1 Injection Valve Starts to Open				
ACC-2 Empty (LDP-402)				
ACC-1 Empty (LDP-401)				
CMT-2 Level Low-Low				
ADS 4-1 Valve Starts to Open				
ADS 4-2 Valve Starts to Open				
CMT-1 Level Low-Low				
CMT-2 Empty (LDP-502)				
IRWST-1 Injection Starts (FMM-701)				
IRWST-2 Injection Starts (FMM-702)				
CMT-1 Empty (LDP-507)				
CMT-2 Starts to Reflood (LDP-502)				
CMT-1 Starts to Reflood (LDP-507)				
Primary Sump Starts to Overflow to Secondary Sump (LDP-901)				
Primary Sump-2 Injection Starts (FMM-902)				
Primary Sump-1 Injection Starts (FMM-901)				
Primary Sump-1 Injection Valve Starts to Open				
Primary Sump-2 Injection Valve Starts to Open				
SG-1 Hot-Leg Channel Head Empty (LDP-209)				
SG-1 Hot-Leg Elbow Starts Draining (LDP-207)				
SG-1 Hot-Leg Elbow Minimum (LDP-207)				

Note:

- (1) Data from the instrument channel in parenthesis were used to determine level, flow, or pressure conditions.
 (2) D = time data obtained from a software program that monitored the input and output of the facility's PLC.
 A = time data obtained by reviewing data from the instrument channel listed in the Event Description column.
 (3) O.O.S. = out of service

The Bar Charts for Table 5.1.6-3 on pages 5.1.6-15 through 5.1.6-19 are not included in this nonproprietary document.

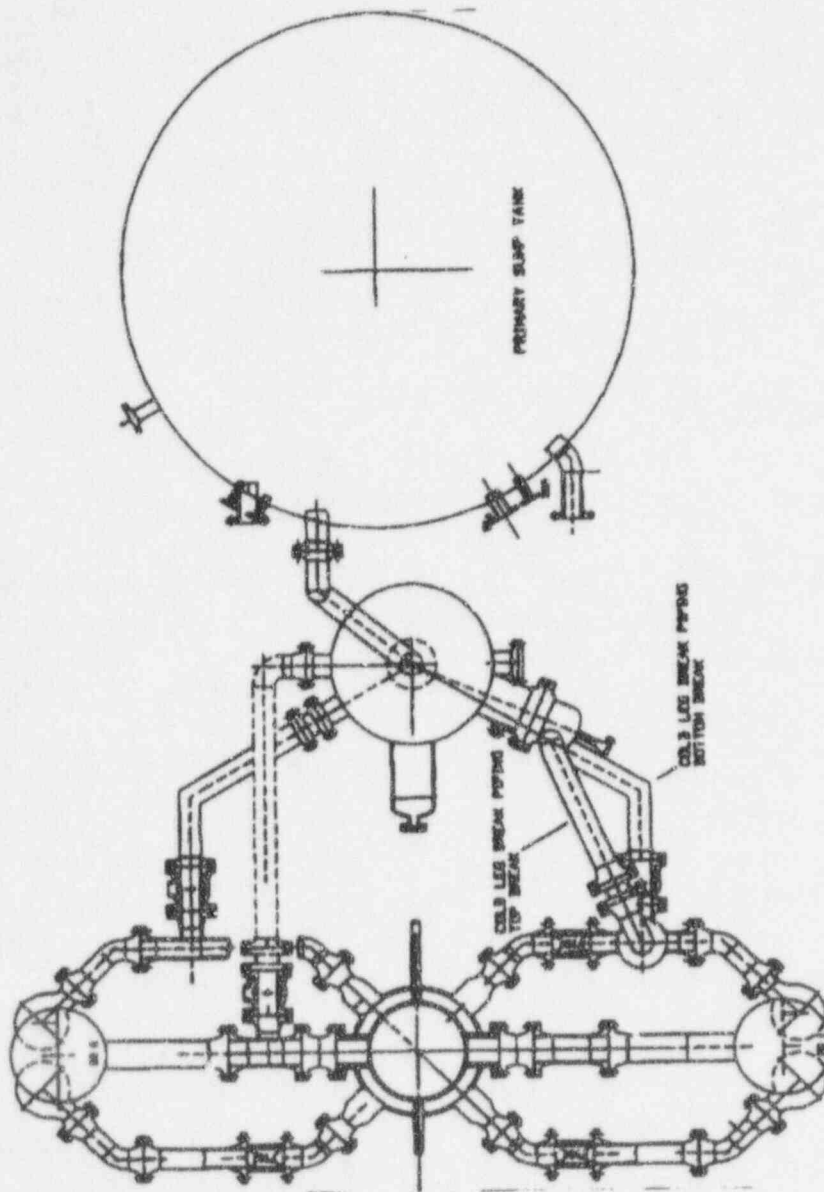


Figure 5.1.6-1a Primary Loop and Break Pipe Arrangement (Sh. 1 of 2)



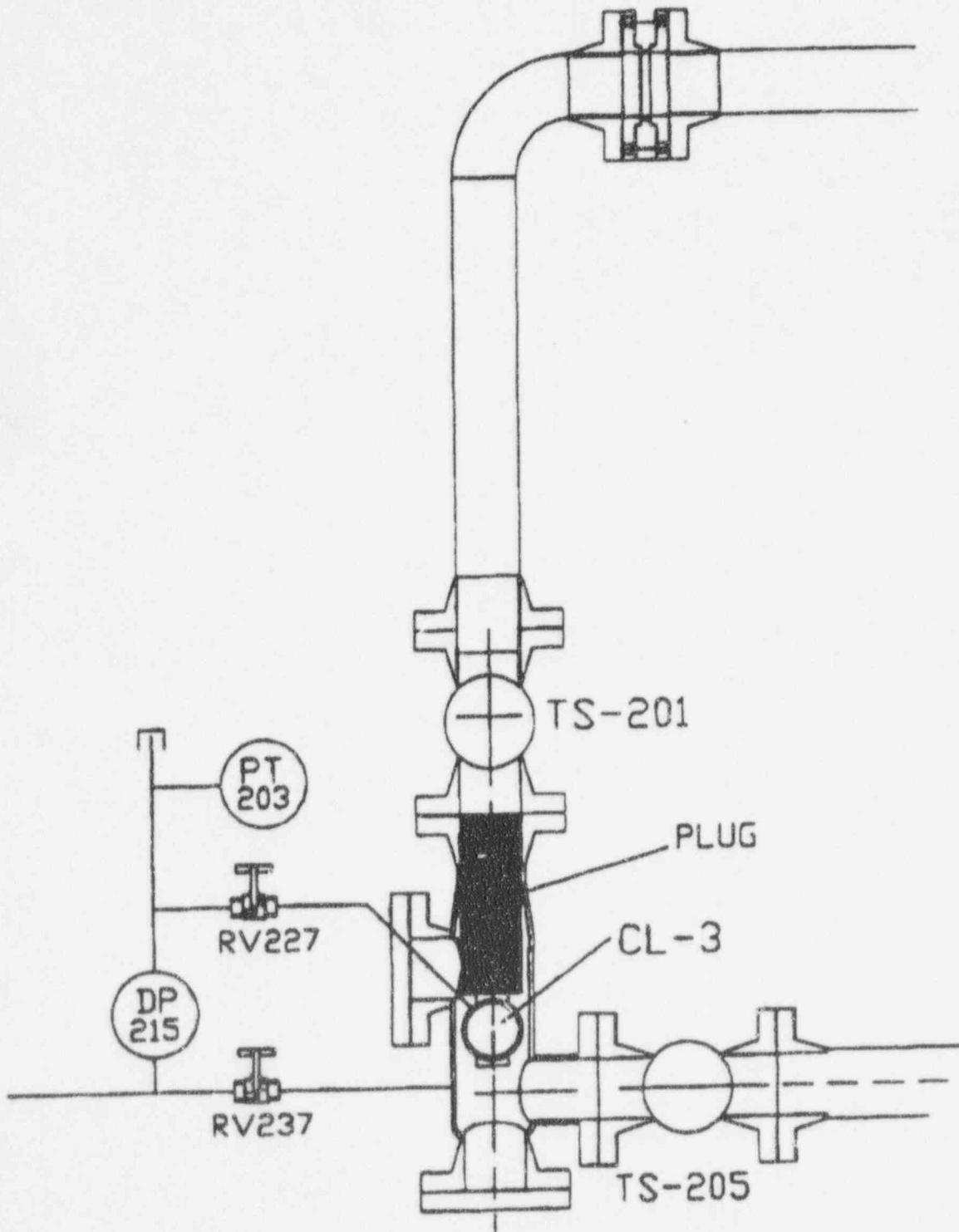


Figure 5.1.6-1b Primary Loop and Break Pipe Arrangement (Sh. 2 of 2)

Figures 5.1.6-2 through 5.1.6-80 are not included in this nonproprietary document.

5.2 Cold-Leg Breaks with Operation of Nonsafety Systems

Matrix Tests SB04 (OSU Test U0204) and SB24 (OSU Test U0024) were performed with the nonsafety-related systems, chemical and volume control system (CVS) and normal residual heat removal system (RNS), operating. Both systems functioned as planned during the simulated break transients. In this section, the results of Matrix Test SB04 (2-in. cold-leg break with operation of nonsafety systems) are discussed in detail, and the results of Matrix Test SB24 (1/2-in. cold-leg break with operation of nonsafety systems) are compared with the data from this large simulated break.

5.2.1 Reference 2-in. Cold-Leg Break (Matrix Test SB04)

This section provides the test results for Matrix Test SB04, including the initial conditions, data plots, evaluation of overall results, and detailed discussions of test facility components performance. The simulated 2-in. break was located at the bottom of cold leg-3 (CL-3), which returns primary coolant from steam generator-1 (SG-1) to the reactor.

To simulate failure of one of the ADS-4 lines, a flow nozzle with a 50-percent design flow area was installed in ADS 4-1, and a flow nozzle with the full design flow area was installed in ADS 4-2. During this test, the RNS and CVS pumps remained in operation to provide system response data for a 2-in. cold-leg break with these conditions. Facility responses to the break are documented by data plots, referenced as figures in the text.

The test was terminated at about 3400 seconds after the core makeup tanks (CMTs) refilled. The CMTs refilled with water supplied by the RNS pump to the reactor coolant system (RCS). During the entire test, heater rods in the reactor vessel simulating core fuel rods remained cooled by water or a two-phase water/steam mixture. Performance of this test was successful.

Subsection 5.2.1.1 provides details related to the test procedure, system configuration, and initial conditions. A description of inoperable instruments appears in Subsection 5.2.1.2, and Subsection 5.2.1.3 references the sequence of events. Subsection 5.2.1.4 describes the test results and evaluation. Component responses appear in Subsection 5.2.1.5, and a summary of mass balance results appear in Subsection 5.2.1.6. The conclusions, as they apply to Matrix Test SB04, appear in Subsection 5.2.1.7.

5.2.1.1 System Configuration and Initial Conditions

Matrix Test SB04 was performed on June 27, 1994, in accordance with an approved written test procedure.

The test facility was configured in the normal arrangement described in Section 2, with the exception of the following specific modifications:

- 2-in. simulated break located at the bottom of CL-3
- Simulated failure of one leg of one of the ADS-4 lines
- Nonsafety-related systems (CVS and RNS pumps) operated as programmed throughout the test
- Valves to the RNS suction line were aligned to connect the in-containment refueling water storage tank (IRWST) instead of the feedwater storage tank

The 2-in. break was simulated by a []^{a,b,c} diameter orifice in the downward branch line from a spoolpiece installed in CL-3. A normally closed, pneumatically actuated ball valve isolated the orifice from the system prior to break initiation. The required break simulation piping and break

instrumentation were installed per Drawing OSU 600904 (Appendix G) and the break piping layouts in Figures 5.2.1-1a and 5.2.1-1b. Here, the liquid and vapor fractions of the leakage flow were separated and individually measured. Liquid flowed to the primary sump tank, and vapor was discharged from the facility.

Prior to initiation of the test, steady-state operating data were recorded for about 120 seconds to record pre-test conditions. Table 5.2.1-1 provides a comparison of the pre-test conditions averaged over the 120-second period with the conditions required by the test specifications. All pre-test operating conditions were achieved prior to the test, with the exception of several hot-leg temperatures that were 1° to 2°F above the limit. Decay heat from the reactor fuel was simulated by electrically powered heater rods installed in the core barrel of the reactor vessel. Comparison of the actual power in this test with the specified decay heat power is provided in Appendix F.

Prior to initiation of the test, a check list of required prerequisites was completed. Key prerequisites in this check list included:

- Installation of simulated break piping and instrumentation
- Installation of proper flow nozzles in the ADS
- Valve line-up in accordance with an approved operating procedure
- Fill-and-vent system in accordance with an approved operating procedure
- Data acquisition system (DAS) instrumentation verification
- Water conductivity in specification
- Verification of relief valve setpoints
- Temporary break valve control lines and instrumentation lines correctly connected

Following satisfaction of these prerequisites, the facility was brought to full power using approved operating procedures. Control valves, pump switches, fan switches, and controllers were set in accordance with the instructions in the written test procedure, and their positions were verified by a written check list. After initializing the DAS, the software program used to monitor digital events in the plant was made operational and synchronized with the DAS. When the initial conditions were satisfied, the test was initiated by pressing the TEST pushbutton.

5.2.1.2 Inoperable Instruments

Table 5.2.1-2 is a list of instruments considered inoperable or invalid during all or portions of this test. Some of the instruments listed are on the Critical Instrument List (Subsection 3.2, Table 3.2-2) and, therefore, are addressed here.

FMM-201, FMM-202, FMM-203, and FMM-204 measured flow (gpm) in each of the four cold legs. A decision was made to continue testing without the availability of these instruments. Replacement flow meters repeatedly failed; their continued use was precluded due to cracking of the ceramic liners

from thermal stratification in the loop piping. The necessary boundary conditions for loop flow could be determined from DP-202, DP-203, DP-205, and DP-206.

FMM-501, FMM-504, FMM-802, and FMM-804 provided accurate data when sensing liquid, but became inaccurate when sensing two-phase or steam flow.

Steam generator (SG) tube level data (LDP-215, LDP-218, LDP-219, and LDP-222) were biased by vaporization of the water in the transmitter reference leg after the SG tubes started draining. However, the data provide accurate indication of the time when the tubes are empty.

LDP-401 and LDP-402 measured ACC-1 and ACC-2 levels, respectively. Due to air trapped in the sense lines for the transmitters, data from these transmitters were invalid. However, the initial level of the tank was established by a standpipe, so it was constant from test to test. The drain rate can be calculated using FMM-401 and FMM-402, respectively. Alternately, a pressure correction may be applied directly to the level indications of LDP-401 and LDP-402.

PT-201 measured reactor coolant system (RCS) pressure at the top of the SG-1 long tube. On August 15, 1994, it was discovered that the transmitter had an incorrect zero compensation, which resulted in a negative error and negative data at low pressures. The transmitter zero was corrected at that time. PT-201 data obtained during Matrix Test SB04 had the zero correction performed, and the corrected data appear as PT_201. Negative data and corrected negative data can be used to determine trends, but are considered inaccurate. PT_201 is not reliable, but a sufficient amount of other pressure data are available.

TF-501 and TF-504 measured CMT fluid temperature from the long thermocouple rod location near the bottom of each CMT. The thermocouples appear to have measured ambient conditions throughout the test, which would indicate a short somewhere in the thermocouple wiring. With these thermocouples inoperable, the required long thermocouple rod thermocouple availability of "seven out of ten and no more than one in succession failed" was met.

Data provided by ADS-4 separator instrumentation were invalid because the ADS-4 valves and the ADS-4 separator loop seal valves did not open during this test. The instruments affected are: FMM-602, FMM-603, FVM-602, FVM-603, LDP-611, and LDP-612.

Considering these critical instrument failures, sufficient instrumentation was available to allow the performance of mass balances as demonstrated in Subsection 5.2.1.6 and Appendix E. An energy balance will be performed and reported in the *AP600 Low-Pressure Integral Systems Test at Oregon State University Test Analysis Report*, WCAP-14292.⁽²⁾

5.2.1.3 Sequence of Events

The response of the test facility to the simulated break is summarized both in tabular and bar-chart form in Table 5.2.1-3. This test configuration resulted in ADS 1-3 actuation and CMT, accumulator, CVS, and RNS injections. The RNS pump injected cold water from the IRWST into the SG-2 channel head. The test was terminated about 13 minutes after the CMT refilled. Total test time was about 3400 seconds (i.e., less than 1 hour).

After the TEST pushbutton was pressed, steady-state data were recorded for about 120 seconds. At time zero, the break valve opening signal was generated, and the indication that the break valve had opened (lower limit switch) was recorded at []^{a,b,c}. The pressurizer heater was manually tripped several seconds prior to the S signal. At []^{a,b,c} the safety system's actuation signal S initiated the following actions:

- Feedwater to secondary side of SGs shut off ([]^{a,b,c})
- Passive residual heat removal (PRHR) outlet isolation valve opened ([]^{a,b,c})
- Valves on CMT injection lines opened ([]^{a,b,c})
- Reactor coolant pumps (RCPs) tripped at []^{a,b,c} and coasted to zero flow at []^{a,b,c}

As primary coolant flowed through the break, pressure in the primary system decreased rapidly, and the indicated level in the reactor dropped. At []^{a,b,c} the indicated level in the upper head had fallen, resulting in the formation of steam. CVS pump injection started at []^{a,b,c}. The level in the reactor continued to decrease. The SG tube began to drain at about []^{a,b,c} then emptied completely by []^{a,b,c}.

Eight to ten seconds after the CMT balance lines started to drain, the associated CMT started to drain ([]^{a,b,c} for CMT-1 and []^{a,b,c} for CMT-2). Both accumulators injected water at []^{a,b,c} when direct vessel injection (DVI) pressure fell below the total accumulator pressure (nitrogen pressure, plus static head). At []^{a,b,c} RNS flow started. At []^{a,b,c} the ADS-1 valve opened ([]^{a,b,c} after the CMT low level was reached), causing the pressurizer to refill at []^{a,b,c} since water flow into the system was greater than flow out of the simulated break. Pressure continued to drop as the system was cooled by the injected water. The ADS-2 valve opened at []^{a,b,c} ([]^{a,b,c} after the CMT low level was reached), and the ADS-3 valve opened at []^{a,b,c} ([]^{a,b,c} after the CMT low level was reached). When reactor pressure fell to less than []^{a,b,c} both IRWST isolation valves opened. Since the RNS pump was operating, water from the IRWST was pumped into the system when DVI pressure fell below the discharge pressure of the pump. At []^{a,b,c} CMT-1 refilled; CMT-2 refilled at []^{a,b,c}. Although the refilling of either CMT had been specified as the end of the test, an additional 13 minutes (780 seconds) of operation were recorded to ensure that stable conditions had been achieved.

5.2.1.4 Test Results and Evaluation

Complex interactions among the subsystems that compose the plant model were observed during Matrix Test SB04; therefore, events during this test were divided into the following three phases to facilitate discussion of overall system and subsystem performance:

- Initial Depressurization Phase: simulated break initiation to ADS-1 actuation
- ADS Phase: ADS-1 actuation to start of IRWST injection
- IRWST Injection Phase: start of IRWST injection to end of test

Initial Depressurization Phase

As high-pressure, high-temperature water flowed through the simulated break nozzle, it flashed into a two-phase mixture of steam and water because of the sudden pressure reduction. The liquid and steam flow components were separated in the break separator of the break and ADS measurement system (BAMS), and their flows were individually measured. The liquid flow rate (break separator loop seal flow) from the break reached a maximum of about []^{a,b,c} then fell to about []^{a,b,c} (Figure 5.2.1-2). At []^{a,b,c} liquid flow decreased to about []^{a,b,c} then rose slowly to about []^{a,b,c} and then decreased slowly to about []^{a,b,c} during the remainder of the test. The region of nearly constant flow (between []^{a,b,c}) occurred during the period of quasi-equilibrium between the primary- and secondary-system pressure/temperature (Figure 5.2.1-45). The decrease in break flow at []^{a,b,c} resulted from the effects of pressure reduction and cold water from the CMTs, which injected at []^{a,b,c}. Steam flow from the break (Figure 5.2.1-3) reached a maximum of []^{a,b,c} and fell to about []^{a,b,c} (the SG transitioned from recirculation to draindown and the pressurizer drained). Steam flow appeared to decrease sharply at []^{a,b,c} as a result of RCS pressure reduction and CMT injection. After the ADS-1 valve opened at about []^{a,b,c} steam flow through the simulated break became negligible for the remainder of the test.

After the simulated break valve opened, the measured level in the reactor decreased (Figure 5.2.1-4), and its pressure fell (Figure 5.2.1-5). At about []^{a,b,c} the CMT isolation valves opened, and cold water flowed from the CMTs through the DVI line into the reactor downcomer. At this time, the CMT balance lines remained full, and water flowed into the DVI from the CMTs by natural circulation, driven by the density difference between hot water in the balance line and cold water in the CMTs. During this period, the indicated reactor level continued to decline, since flow through the simulated break was greater than the makeup flows.

In this period, makeup water flowed into the reactor vessel from the CMTs, pressurizer, and CVS. Pressurizer water was driven into HL-2 by the higher pressure in the pressurizer until it emptied at about []^{a,b,c} (Figures 5.2.1-6 and 5.2.1-7). When the pressurizer reached the low-low level

setpoint at about []^{a,b,c} the CVS pump injected cold water from the feed storage tank to the SG-2 cold-leg channel head. Figure 5.2.1-8 is a graph correlating CVS and RNS flows with time.

Boiling occurred in the upper section of the core heaters at about []^{a,b,c} as indicated by slightly higher than saturation temperatures of the heater surface thermocouples (Figure 5.2.1-10). As the system depressurized, water in the core flashed from the decrease in pressure and vaporized because of heat input from the core. The maximum steam percent in the upper core occurred between []^{a,b,c} and was estimated to be []^{a,b,c} percent. The steam percent was estimated using the upper core level data (LDP-110) provided in Figure 5.2.1-9. Steam percent was estimated from the equation below:

$$\text{Steam percent} = \frac{\text{level}(100\% \text{ water}) - \text{level}(\text{with steam})}{\text{level}(100\% \text{ water})} \times 100$$

During this period, the lower core remained filled with liquid water (LDP-109).

Core heater temperatures (Figure 5.2.1-10) were []^{a,b,c} higher than the saturation temperature during the earlier stages of the transient, suggesting that boiling occurred at all locations measured (at core heights of []^{a,b,c}). At about []^{a,b,c} the temperature at the []^{a,b,c} level fell below saturation, inferring subcooled heat transfer below the level. The remainder of the heater temperatures remained substantially above the saturation temperature, indicating that boiling heat transfer occurred in the upper portion of the core (reflected by thermocouples at []^{a,b,c}).

The heaters remained cooled during the entire transient—by two-phase steam/water for the first []^{a,b,c} and then by nucleate boiling. Short temperature excursions of about []^{a,b,c} occurred during condensation events at []^{a,b,c}. These excursions resulted from flow reversals in the core barrel as a result of low pressures in the downcomer caused by condensation events. Core coolant temperatures increased by about []^{a,b,c} between []^{a,b,c} (Figure 5.2.1-10). This temperature rise followed the effect of the pressure transient on the saturation temperature. The cause of this pressure transient is not certain, but it appears to coincide with the transition from recirculation to tube drainage in the SG which provided a flow path to equalize hot-leg and cold-leg pressures.

Level data for the []^{a,b,c} volume above the upper-core plate (LDP-112; Figure 5.2.1-9) indicated that it remained full of water during the entire transient. However, since the volume below the upper-core plate contained about []^{a,b,c} percent steam and the volume above the upper-core plate was nearly []^{a,b,c} percent steam during its minimum, the volume just above the upper-core plate could not have remained liquid. One possible explanation for this apparent anomaly is an instrumentation failure; however, all other similar instrumentation in the reactor behaved normally. Therefore, it is unlikely that there was an instrumentation error. A more probable explanation is that the instrumentation measured an annular layer of liquid water along the wall (these pressure taps are flush

with the core barrel wall). Since the two-phase steam/water mixture was flowing at a high velocity through the holes in the upper core plate, an annular layer of water could be maintained at the outer diameter of the core barrel. It is this continuous layer of water at the wall that may have been measured by LDP-112.

The indicated level in the reactor vessel (LDP-127) reached a minimum of about []^{a,b,c} between []^{a,b,c} (Figure 5.2.1-4). This level was slightly above to the upper core plate. When DVI pressure (Figure 5.2.1-5) reached accumulator pressure []^{a,b,c} both accumulators injected water into the reactor annulus through the respective DVI lines (Figure 5.2.1-19). The measured level in the reactor started to rise when the accumulators began injecting water. Water injected from the RNS ([]^{a,b,c}), resulted in a continued increase in reactor level, even after the accumulators emptied at []^{a,b,c}. The RNS pumps started at about []^{a,b,c} when system pressure reached []^{a,b,c} however, the full flow did not develop until the CVS pump was shut off (Figure 5.2.1-8).

As the system depressurized due to continued flow through the simulated break and cold-water injection, liquid in the hot legs reached saturation temperature at about []^{a,b,c} and began to flash (Figures 5.2.1-13 and 5.2.1-14). This steam caused apparent level fluctuations in the SG tubes as the steam bubbles passed through the tubes (Figures 5.2.1-15 and 5.2.1-16). Water in the SG tubes also flashed as pressure decreased. The SG tubes started to drain between []^{a,b,c} and the SG tubes emptied between []^{a,b,c}. The SG-1 channel head emptied by []^{a,b,c} and the SG-2 channel head emptied by []^{a,b,c} (Figures 5.2.1-17 and 5.2.1-18).

CMT-1 reached the low-level setpoint at []^{a,b,c} which caused the ADS-1 valve to open at []^{a,b,c}. Opening of the ADS-1 valve concluded this phase of the test.

ADS Phase

The ADS-1 valve opened at about []^{a,b,c} about []^{a,b,c} after CMT-1 reached its low level setpoint, resulting in the following system effects:

- The pressurizer refilled, reaching its maximum level at about []^{a,b,c} (Figure 5.2.1-7).
- Flow rates from the accumulators rose from about []^{a,b,c} to a maximum of []^{a,b,c} (Figure 5.2.1-19).
- RNS flow increased from []^{a,b,c} (Figure 5.2.1-8).
- The rate of depressurization of the entire system (including reactor vessel, pressurizer, hot legs, cold legs, and CMTs) increased (Figures 5.2.1-5, 5.2.1-6, 5.2.1-20, and 5.2.1-21).

ADS-2 actuated at []^{a,b,c} after the CMT-1 low level setpoint was reached). System pressures continued to decrease at about the same rate measured after the ADS-1 valve opened, and then asymptotically approached atmospheric pressure at about []^{a,b,c}. The reactor vessel continued to refill with negligible effects on the refilling rate from the ADS-2 valve opening (Figure 5.2.1-4).

Liquid flow through ADS 1-3 ranged from about []^{a,b,c} with a short peak (about a []^{a,b,c} duration) at []^{a,b,c} when ADS-2 actuated (Figure 5.2.1-2). From []^{a,b,c} to test termination, liquid flow averaged about []^{a,b,c}. This flow was probably a two-phase mixture of steam and water that had refilled the pressurizer at []^{a,b,c}. During this period, steam vaporized from the liquid in the pressurizer (which had refilled at about []^{a,b,c}). Steam flow from the ADS 1-3 separator ranged from []^{a,b,c} with the maximum occurring when ADS-2 actuated. Separator steam flow was []^{a,b,c} seconds to the end of the test (Figure 5.2.1-53).

At []^{a,b,c} the CVS pump shut down (Figure 5.2.1-8). This shutdown was initiated when the liquid level in the pressurizer reached its normal level.

IRWST-1 and IRWST-2 isolation valves opened at []^{a,b,c} respectively, when the reactor fell below the low-low pressure setpoint ([]^{a,b,c}); however, flow from this tank was blocked by higher pressure from the RNS pump, which is connected to the same piping that leads to the DVI lines. Check valves in the IRWST lines prevented RNS flow from entering the IRWST.

IRWST Injection Phase

Both accumulators emptied by about []^{a,b,c} (Figure 5.2.1-22). By this time, system pressure had reached atmospheric pressure. The system water level slowly rose as the RNS injected water at a higher rate than the loss rate through the simulated break. During this period, system temperatures continued to drop.

At []^{a,b,c} respectively, CMT-1 and CMT-2 began to refill as indicated by the rise in level indication (Figure 5.2.1-23x). The CMTs refilled as a result of condensation events. This phenomenon is discussed in detail in Subsection 7.1. Although refilling of the CMTs satisfied the test completion objective, the test was continued for about 13 minutes to provide steady-state data.

5.2.1.5 Component Responses

Responses of the major test facility components are discussed in detail in this section. The components included in this review are:

- Reactor
- CMTs

- Accumulators
- Pressurizer
- PRHR HX
- SGs
- Cold legs and hot legs
- IRWST
- BAMS
- Nonsafety-related systems

Reactor

As soon as the break valve opened, the indicated level in the upper plenum of the reactor fell sharply while the level in the downcomer region remained nearly constant just below the upper bypass holes in the upper head. The upper-plenum levels are shown in Figures 5.2.1-9 and 5.2.1-9x, for the first []^{a,b,c} and from []^{a,b,c} to test termination, respectively. Downcomer and wide-range reactor levels are shown in Figures 5.2.1-4 and 5.2.1-4x. Indicated levels in the upper plenum and core barrel fell because water flowing out of the break was greater than the water flowing into the reactor from the pressurizer. The CVS pump started at []^{a,b,c}

The indicated level in the core barrel increased several inches for short periods of time as the CVS injected and the SG tubes drained, allowing water to drain into the channel heads, and from there, into the hot and cold legs. The overall level in the core barrel, however, decreased steadily and reached a minimum of about []^{a,b,c}. The level started to rise at this time because both accumulators injected water into the DVI line. The rate of the rising level increased further at []^{a,b,c} when RNS injection began. Several condensation events that caused very short-lived, but sharp, level drops occurred at about []^{a,b,c}. Sudden condensation of steam at the top of the downcomer caused low pressure in this volume, producing reverse flow from the lower plenum into the downcomer. Sudden drops in core barrel level and sudden increases in downcomer level resulted from these short, but intense, flow reversals during the condensation events. Subsection 7.1 provides a detailed discussion of these condensation events. ADS-2 actuation at []^{a,b,c} also caused an apparent decrease in level. Since these indications were very rapid (less than []^{a,b,c}), it is probable that they were dynamic pressure pulses rather than actual level changes.

After []^{a,b,c} the core barrel level became slightly greater than the downcomer level, and both levels remained relatively constant until the test was terminated.

Pressures in the reactor, DVI, and downcomer are shown during the initial []^{a,b,c} period in Figure 5.2.1-5. These pressures follow each other very closely throughout the test. After []^{a,b,c} these pressures had decreased to near atmospheric pressure. Actual data records revealed that the downcomer pressure was about []^{a,b,c} higher than the reactor upper-plenum region while the RCPs were operating. During the pump coastdown period, this pressure difference decreased

until the upper plenum pressure became greater than the downcomer pressure at about []^{a,b,c}. This difference, which was []^{a,b,c} continued during the depressurization period until both pressures approached atmospheric pressure. This pressure differential resulted in the level difference between the downcomer and the upper-plenum/core-barrel region discussed previously.

Reactor and DVI line pressures followed each other closely during the entire test. The pressures dropped sharply for the first []^{a,b,c} until the RCPs shut off. The pumps maintained a high flow rate through the simulated break, resulting in a high rate of depressurization (Figure 5.2.1-5).

At about []^{a,b,c} the pressures rose about []^{a,b,c} because hot water from the SGs partially drained into the hot and cold legs. From []^{a,b,c} the pressures remained nearly constant at about []^{a,b,c}. This pressure plateau was caused by a quasi-equilibrium in between the primary-system temperature and the secondary-system temperature in the SGs (Figure 5.2.1-45). As the SG tubes drained completely at about []^{a,b,c} RCS pressure began to fall again. At []^{a,b,c} the ADS-1 valve opened, increasing the rate of depressurization. Small inflections in pressures of several pounds per square inch occurred from the condensation events at about []^{a,b,c}. The pressures reached atmospheric pressure at about []^{a,b,c} (Figure 5.2.1-5).

Differential pressures across the upper support plate and the upper head are illustrated in Figures 5.2.1-24 and 5.2.1-24x for the first []^{a,b,c} and from []^{a,b,c} to test termination, respectively. Initially, differential pressure across the upper-support plate was about []^{a,b,c} of water, indicative of the dynamic pressure drop from forced flow. Differential pressure across the upper-support plate fell to 0 at about []^{a,b,c} which coincided with the end of RCP coastdown. This differential pressure remained at 0, except for short-term negative spikes that coincided with condensation events. The negative pressure differential spikes that coincided with the condensation events indicated increased pressure differences across the upper head and higher steam flows through the bypass holes.

Large negative differential pressures (less than negative 22 in. of water) indicated significant flow through the bypass holes in the upper head from the upper plenum to the downcomer. Short, intense, negative differential pressure spikes that occurred coincident with condensation events confirmed high rates of steam flow from the upper plenum to the downcomer during these events. After []^{a,b,c} differential pressure across the upper head remained at about []^{a,b,c} of water, with the exception of an excursion at about []^{a,b,c} as a result of a condensation event. This negative differential pressure was caused by evaporation of water in the lines connecting the pressure transmitter and actually represents no or very little flow. Subsection 2.4 discusses this instrumentation effect in detail.

The following temperatures are graphically presented in the identified figures and are discussed in this section:

- Figures 5.2.1-25 and 5.2.1-25x: Reactor fluid temperatures at the top of the reactor, reactor upper vessel at 90 degrees, upper reactor vessel at 270 degrees, and 1/2-in. above the upper support plate; and saturation temperature based on PT-107
- Figures 5.2.1-26 and 5.2.1-26x: Downcomer fluid temperatures at the hot-leg centerline, hot-leg bottom, below DVI line, upper flange, and bottom flange; and saturation temperatures based on PT-107
- Figures 5.2.1-27 through 5.2.1-30x: Fluid temperatures in the reactor core at various elevations from 10.5 to 51.86 in., saturation temperatures based on PT-113
- Figures 5.2.1-10 and 5.2.1-10x: Heater rod temperatures, and saturation temperatures based on PT-113

Fluid temperatures at the top of the reactor (TF-120; Figure 5.2.1-25) and the top of the downcomer (TF-168; Figure 5.2.1-26) are compared with saturation temperatures based on pressure at the reactor top. These temperatures were slightly subcooled prior to break initiation. As pressure fell, the top of the reactor reached saturation temperature in about []^{a,b,c} and the downcomer steam volume at its top reached saturation temperature at about []^{a,b,c}. Both temperatures followed the saturation temperature to about []^{a,b,c} as the reactor depressurized. The downcomer temperature superheated relative to reactor pressure beyond this time because the SGs stopped draining and furnishing saturated liquid to the cold leg. As the level in the downcomer dropped, steam in the top portion remained hot (i.e., superheated relative to reactor pressure), and pressure continued to decrease. Steam at the reactor vessel top also became superheated relative to the local pressure as pressure declined, and heat was supplied to the vapor by the reactor vessel. Condensation events (at about []^{a,b,c}) resulted in temperature decreases from superheat to well below saturation in the downcomer top, indicating that subcooled water from the bottom of the reactor was drawn into this region as steam condensed.

During the first two condensation events in the downcomer, superheated steam in the top of the reactor (TF-120) fell to saturation. This probably was caused by cool water ejected into the top of the reactor through the holes in the downcomer top by the level surge in the downcomer caused by the sudden pressure reduction during these condensation events. For the third condensation event ([]^{a,b,c}), the steam temperature at the reactor top was only slightly reduced and remained above the saturation temperature. In this case, the downcomer pressure surge may have been smaller and did not eject cold liquid into the reactor top. The small temperature decrease probably resulted from the expansion of the steam as the core barrel level decreased during this condensation event.

Downcomer temperatures at lower elevations are shown in Figures 5.2.1-26 and 5.2.1-26x. These downcomer temperatures remained subcooled for the entire test because of the continuous injection of cold water from the CVS and RNS, in addition to injections of cold water from the CMTs and accumulators. The highest temperatures in the downcomer occurred adjacent to HL-2, which reached

the saturation temperature between []^{a,b,c} Hot-leg fluid temperatures were near saturation during this period because saturated water was draining from the SG into the hot leg and flowing into the downcomer. Fluid temperatures in the downcomer and hot leg varied between []^{a,b,c} and then became nearly steady at about []^{a,b,c} for the remainder of the test. The apparent discrepancy in temperatures measured by TF-169 and TF-170 was probably caused by leakage of cooler water from the downcomer contacting TF-170. Therefore, temperatures recorded by this thermocouple should be disregarded.

Fluid temperatures in the core at elevations from []^{a,b,c} are compared with the saturation temperature at midcore in Figures 5.2.1-27 through 5.2.1-30x. These plots have been divided into four sets for clarity, each with several core temperatures and the saturation temperature. Temperatures increase as elevation through the core increases. However, during the test, the saturation temperature was never exceeded, demonstrating that dryout did not occur in the core during this test. Fluid temperatures rose briefly for all locations at about []^{a,b,c} because of flow reversals caused by condensation events in the downcomer.

Core heater rod temperatures measured by thermocouples installed near the surface of the heater rod sheaths were compared with the saturation temperature at the upper core spacer grid (Figures 5.2.1-10 and 5.2.1-10x). Core heater rod temperatures were never significantly higher than the saturation temperature, demonstrating that the heaters remained cooled by liquid or a two-phase mixture during the entire test. Short-term temperature rises recorded during the test may have been caused either by brief periods of lack of coolant contact with the heater surface or an electric field effect from the heaters on the instrumentation.

Core Makeup Tanks

Since both CMTs behaved similarly in this test, their responses are discussed collectively in this section.

Natural recirculation flow of []^{a,b,c} from the CMTs began about []^{a,b,c} after break initiation (Figure 5.2.1-31), coincident with coastdown of the RCP pump. Differential pressure for this flow arose from the higher density of cold water in the CMT.

Flow from the CMTs continued until the transition from recirculation to draindown when the CMT balance lines drained between []^{a,b,c} as indicated by the sudden drop in balance-line levels (Figure 5.2.1-32).

Once the balance lines drained, flow from the CMT, which was now driven by the liquid head in the tank, increased to []^{a,b,c} Flow declined slowly as the liquid head in the CMTs dropped. Flow from the CMTs stopped between []^{a,b,c} because backpressure created by the RNS pump, which started at 405 seconds, was sufficient to balance the driving pressure for the CMTs. There was no further flow from the CMTs for the remainder of the test.

Liquid levels in the CMTs (Figure 5.2.1-23) remained constant as long as the balance line remained full (Figure 5.2.1-32). Hot water flowed into the CMTs, leading to a small increase in temperature during the natural convection phase.

CMT-1 drained at []^{a,b,c} CMT-2 drained at []^{a,b,c} Drainage from the CMTs stopped at about []^{a,b,c} after startup of the RNS pump. CMT-1 reflooded at []^{a,b,c} CMT-2 reflooded at []^{a,b,c} (Figure 5.2.1-23x). Only about []^{a,b,c} percent of the CMTs' water inventory had been injected before the RNS pump halted their flow.

Pressures in the CMTs (PT-501 and PT-502) are compared with reactor upper-head pressure (PT-107) in Figure 5.2.1-21. Since the CMT tops are connected to cold legs through the balance lines, the pressures closely follow the reactor top pressure for the entire test. Events that influence the behavior of the reactor top pressure are discussed in the reactor response discussion of Subsection 5.2.1.5.

When the CMT-1 and CMT-2 started to drain at about []^{a,b,c} respectively, saturated steam accumulated at the top of each tank (Figures 5.2.1-33 and 5.2.1-35). As pressure in the CMTs continued to drop, the local saturation temperature decreased and the steam became superheated relative to the pressure. As depressurization continued, the saturation temperature became lower than the tank wall temperature, and the CMT metal became a heat source. This phenomenon was observed in CMT-1 at about []^{a,b,c} for CMT-2), at which time steam at the top of the tank superheated.

The metal wall continued to transfer heat to the steam until the CMTs reflooded. Cold water in the lower portion of the CMT then rose to the top of the tank (Figures 5.2.1-33 and 5.2.1-35). Reflooding occurred at about []^{a,b,c} for CMT-1 and []^{a,b,c} for CMT-2, as shown by the sudden decrease in temperatures (Figures 5.2.1-34 and 5.2.1-36). These refills resulted from condensation events in the CMTs initiated by cooler water flowing into the CMTs from the balance lines. These events are described in greater detail in Subsection 7.1.

When the CMTs were partially empty, a hot water layer existed in each CMT, separating superheated steam at the top of the tank and subcooled water at the bottom. Thickness of the saturated hot water layer varied. For CMT-1, by the time thermocouple TF-509, the thermocouple []^{a,b,c} below TF-513, reached saturation temperature, all thermocouples above it had already superheated and all thermocouples below it were subcooled (Figure 5.2.1-33), suggesting that the saturated hot water layer in CMT-1 was located between []^{a,b,c} (distance to the next lower thermocouple). Similar results were observed for CMT-2.

Accumulators

Each accumulator was filled with []^{a,b,c} of ambient temperature water and was pressurized to about []^{a,b,c} with nitrogen. Both accumulators injected water at about []^{a,b,c} when RCS pressure decreased to about []^{a,b,c} Flow initiation, as indicated by flow (Figure 5.2.1-19)

and level (Figure 5.2.1-22) changes at []^{a,b,c} coincided with the time that DVI pressures reached []^{a,b,c} (Figure 5.2.1-5). Initial flow for both accumulators varied between []^{a,b,c} until the ADS-1 valve opened. Flow rose over the next []^{a,b,c} to a maximum of about []^{a,b,c} fell to []^{a,b,c} between []^{a,b,c} rose to []^{a,b,c} and then declined as the tanks emptied at []^{a,b,c}. The cause of the reduction in flow from []^{a,b,c} cannot be explained.

CMT flow influenced flow injection from the accumulators, since the CMT and accumulator for each DVI line were connected to a common line. As pressure in the CMT line varied, backpressure in the accumulator injection line affected accumulator injection flow. Although the RNS pump was operating during accumulator injection, it did not have a significant effect on accumulator flow because its discharge pressure was reduced by an orifice upstream of the junctions with the lines from the accumulators.

Pressurizer

During normal operation, the pressurizer maintains RCS pressure by control of the electric power to a heater submerged in water. The pressurizer also provides a surge volume to accommodate primary coolant volumetric changes resulting from temperature variations. Initial power to the pressurizer required to maintain system pressure was several kilowatts during the steady-state period prior to test initiation. Six seconds after the simulated break initiation, power to the heaters was shut off.

Liquid levels in the pressurizer and the surge line are shown in Figures 5.2.1-7 and 5.2.1-7x. As primary coolant flowed through the simulated break in the cold leg, the level in the pressurizer fell immediately because of differential pressure between the pressurizer and the break. The pressurizer emptied completely at about []^{a,b,c}. The surge line level indication oscillated initially and then decreased before the pressurizer emptied. Since it is impossible to drain the surge line before the pressurizer is empty, this effect was caused by steam flashing in the surge line. Hot water draining from the pressurizer flashed into a steam-water mixture in the surge line, since pressure was decreasing rapidly, resulting in a lower mean density for two-phase flow and an apparent level decrease. At about []^{a,b,c} when the pressurizer emptied, steam volume in the pressurizer surge line was estimated at []^{a,b,c} percent. The surge line drained completely at []^{a,b,c}. Surge line refill began at about []^{a,b,c} when the ADS-1 valve opened and vented the pressurizer. The pressurizer level increased a few seconds later, after the time delay required to fill the surge line. The pressurizer filled completely. Level surges in the surge line and pressurizer during refill were caused by pressure surges resulting from the ADS-2 and ADS-3 valves opening and condensation events.

Passive Residual Heat Removal Heat Exchanger

Inlet and outlet flow rates from the PRHR HX for the initial 1000 seconds and from 1000 seconds to test termination are provided in Figures 5.2.1-37 and 5.2.1-37x, respectively. Prior to break initiation,

both flow rates were 0, since the PRHR isolation valve was closed. When the valve opened at []^{a,b,c} natural circulation flow was established in the PRHR HX because of the higher density of the cooled water in the HX. For about []^{a,b,c} liquid flowed through the PRHR HX since inlet and outlet flows were about the same during this period (discounting sharp rises due to pressure surges). Liquid flowed from HL-2 through the PRHR HX and returned to the SG-2 cold-leg channel head because of the pressure difference between HL-2 and the SG-2 channel head. When the short tubes of SG-2 drained at about []^{a,b,c} pressures in the SG-2 channel head and HL-2 equalized, eliminating the pressure necessary to lift the liquid to the high point in the PRHR inlet piping, which was over []^{a,b,c} above the PRHR HX inlet. When this occurred, water in the inlet line of the PRHR HX drained.

Steam from HL-2 continued to flow into the PRHR HX because of the differential pressure between the HL-2 water and the saturation pressure in the PRHR HX. However, this steam rate was insufficient to keep the inlet head of the PRHR HX full of water. Since the upstream pressure at the top of the PRHR HX was determined by the saturation pressure of water at the local temperature, the pressure differential was insufficient to maintain flow through the PRHR HX (i.e., the PRHR HX became vapor locked).

Between []^{a,b,c} flow into the PRHR HX was mostly steam since inlet flow measured by the magnetic flow meters was much higher than outlet flow. Between []^{a,b,c} the indicated flow rates oscillated at an average of zero flow; then both increased from []^{a,b,c} returned to oscillating about []^{a,b,c} and showed positive intermittent flow rates between []^{a,b,c}. During the periods of flow, outlet flow varied between 5 and 10 gpm (discounting short, high flows).

The liquid levels in the PRHR HX inlet header and the entire HX for the initial 1000 seconds and from 1000 to 2000 seconds are shown in Figures 5.2.1-38 and 5.2.1-38x, respectively. Both the inlet head and overall HX levels remained nearly full during the first []^{a,b,c} after the PRHR valve opened, confirming that liquid was flowing through the PRHR HX as indicated by the flow meters. The level the inlet head fell to 0 in. by about []^{a,b,c} and remained at 0 in. until starting to increase slowly at []^{a,b,c} to a height of about []^{a,b,c}. During this period, the PRHR HX fell to a minimum of about []^{a,b,c} then increased slowly until it was []^{a,b,c}. The levels indicated that the PRHR HX was receiving steam that condensed in the HX at a rate less than the steam outflow rate during the early part of the test ([]^{a,b,c}), then steam flow increased, resulting in a level increase. The increase in steam flow at []^{a,b,c} was caused by SG-2 cold-leg channel heads refill, which occurred at about []^{a,b,c}. As the SG channel head and tube level increased, differential pressure from the PRHR HX to the SG channel head decreased, reducing the outflow from the PRHR HX and increasing its fluid level.

Fluid temperature at the inlet of the PRHR HX followed the saturation temperature based on pressure at the top of the reactor (Figures 5.2.1-39 and 5.2.1-39x) for the first []^{a,b,c} fell below

saturation temperature until []^{a,b,c} rose to near saturation temperature between []^{a,b,c} and then decreased again to reach a temperature nearly []^{a,b,c} below saturation from []^{a,b,c} to test termination. This temperature profile indicated that saturated water or steam entered the PRHR HX during the initial []^{a,b,c} and the period between []^{a,b,c}. Condensate entered the PRHR HX between []^{a,b,c} because the inlet temperature ranged between []^{a,b,c}. If there had been no condensate flow, the PRHR HX inlet would have reached equilibrium with the IRWST (i.e., below []^{a,b,c}).

Midpoint temperatures of the instrumented short and long tubes indicated warm condensate (up to []^{a,b,c}) in both tubes for about []^{a,b,c}. Then, the warmer temperature alternated between the short and long instrumented tubes, indicating unstable flow through the HX during the period between []^{a,b,c}. At []^{a,b,c} midpoint temperatures converged at []^{a,b,c} indicating very low or no flow. After a slow increase, short-tube midpoint temperatures rose sharply by []^{a,b,c}, fell back, rose by []^{a,b,c}, then fell back. The pulses coincided with the reflooding of CMT-1 and CMT-2. When each CMT reflooded, water was drawn into the CMT by the collapse of the trapped steam bubble.

The PRHR HX remained above []^{a,b,c} until []^{a,b,c}. At []^{a,b,c} the outlet temperature increased to []^{a,b,c} and remained at this level until the end of the test. Temperature patterns confirmed flow measurements; i.e., the flow meter oscillated about []^{a,b,c} and then indicated high flows for several []^{a,b,c}.

In summary, the PRHR HX functioned in natural circulation liquid flow for the initial []^{a,b,c} until the transition from recirculation to draindown in the SG. Steam from HL-2 was then condensed, either in the PRHR HX (up to []^{a,b,c}) or in the piping. Because of small (or negative) pressure differences, the HX remained partially filled without draining after the transition from recirculation to draindown. Flow through the HX was unstable with steam alternately flowing through the short and long PRHR HX tubes. Steam flowed preferentially through the short tubes during the latter part of the test. Since flow rates through the PRHR HX were small, the effect of this system on the overall test facility response was minimal.

Steam Generators

Feedwater to both SGs was shut off []^{a,b,c} after break initiation. Secondary steam flow decreased to []^{a,b,c} (Figure 5.2.1-40) as the secondary-side was isolated. The brief indication of steam flow in SG-1 between []^{a,b,c} appeared to be an instrumentation anomaly, since the steam header flow meter did not measure any steam flow during this time.

Levels in representative short and long tubes of the SGs (Figures 5.2.1-15, 5.2.1-15x, 5.2.1-16, and 5.2.1-16x) were measured by pressure differentials. As the levels in the SG channel heads decreased,

the tubes of the SG drained. The times shown in the Sequence of Events, Table 5.2.1-3 were derived from these figures.

Level measurements were inaccurate after the tubes emptied, because water in the reference high-pressure legs of the differential level transmitters was vaporized by heat from the secondary side of the SGs. This generic problem is discussed in detail in Subsection 2.4. The level data incorrectly indicated that the SGs refilled with water shortly after the tubes emptied. This did not occur because temperature measurements (Figures 5.2.1-41, 5.2.1-41x, 5.2.1-42, and 5.2.1-42x) indicated that the SG tubes filled with superheated steam.

Liquid level in the cold-leg plenum of each SG fell abruptly at about []^{a,b,c} for SG-1 and []^{a,b,c} for SG-2 (Figures 5.2.1-17, 5.2.1-17x, 5.2.1-18, and 5.2.1-18x). Later in the test, the SG-2 cold leg started to refill at []^{a,b,c} because the RNS pump (which started at []^{a,b,c}) was pumping about []^{a,b,c} of water from the IRWST into the RCS. The cold-leg level in SG-1 remained empty, because water from the downcomer tended to flow out the simulated break in CL-3 rather than accumulate in the SG-1 cold-leg plenum.

The SG-2 hot-leg plenum level behaved similarly to the cold-leg plenum; however, it emptied about []^{a,b,c} later than the cold-leg plenum. This difference was probably caused by the more rapid loss of coolant from the simulated break in CL-3. The SG-1 hot-leg plenum levels were inaccurate because the range for this instrument was incorrectly calibrated, as discussed in Subsection 2.4.

Fluid temperatures in the tubes (primary side) of the SGs remained at saturation until shortly after drainage (Figures 5.2.1-41 and 5.2.1-42). Steam filled the tubes after drainage and superheated as the RCS continued to depressurize and heat was transferred from the SG secondary coolant structure (Figures 5.2.1-43 and 5.2.1-44). Pressures in the primary and secondary sides of the SGs were equal from about []^{a,b,c} (Figure 5.2.1-45). This steam reached thermal equilibrium with the SG secondary coolant, which were significantly higher in pressure (and temperature) than the primary. Steam in the tubes remained superheated for the remainder of the test (Figures 5.2.1-41x and 5.2.1-42x), as the SG secondary sides cooled very gradually, reaching a minimum of about []^{a,b,c} at test termination. Fluid temperatures in the short tubes of SG-2 decreased sharply to the saturation temperature at times ([]^{a,b,c}) that correspond to condensation events in the reactor-vessel downcomer. These events caused the liquid level in the downcomer to rise, resulting in an increase in the cold-leg levels. The level surges were sufficiently large to fill the SG-1 short tubes briefly during the condensation events at []^{a,b,c}. Level surges consistent with these are indicated in the channel head level data, with the exception of the transient in SG-1 at []^{a,b,c}. Although the temperature decreased, indicating inflow of saturated liquid, there was no concomitant effect in the cold-leg plenum. This apparent anomaly possibly resulted from a surge of saturated steam rather than liquid for this case, since the plenum was empty. The level surge could have been sufficient to displace the superheated steam with saturated vapor from the cold-leg piping and, thus, would not produce a level indication for the SG cold-leg plenum.

Cold Legs and Hot Legs

When the RCPs stopped and coasted to no measurable flow in the first []^{a,b,c} some cold-leg levels indicated an increase and some a decrease (Figures 5.2.1-46 and 5.2.1-46x). The apparent level changes were not real, but were caused by dynamic pressure differentials resulting from flow effects on the pressure measurements because of tap location and/or installation. Therefore, the level indications after the pumps stopped are used as full levels for the purposes of this discussion.

The cold legs remained full for the initial []^{a,b,c} because water supplied by the pressurizer, CVS, and SGs was about equal to break flow. When the pressurizer emptied, however, the levels in all of the cold legs fell sharply. As the SGs continued to drain, cold-leg levels rose []^{a,b,c}. Injections from the CMTs and accumulators did not provide sufficient flow to significantly affect the levels. When the ADS-1 valve opened at []^{a,b,c} the levels in the cold legs decreased rapidly, and pressurizer refilled (because it was now vented) and depleted the water inventory in the RCS. In addition, the CVS pump shut off at []^{a,b,c} reducing the water supply to the cold legs.

Level indications became erratic, oscillating at short frequencies from below 0 to over-range. These were most likely dynamic pressure effects caused by steam or two-phase flow, and it is probable that the cold-legs were empty from []^{a,b,c}. These differential pressure oscillations were the greatest in CL-3, which contained the simulated break. After []^{a,b,c} (Figure 5.2.1-46x), cold-leg levels rose slowly to several inches, with the exception of CL-2.

Fluid temperature at the reactor flange top and bottom (at the inlet to the RCP) and the saturation temperature based on reactor pressure are compared for CL-1 through CL-4 in Figures 5.2.1-47 through 5.2.1-50x. Temperature patterns for CL-2 through CL-4 are similar and confirm the level indications. From about []^{a,b,c} thermocouples in the top of the reactor flanges for these three cold legs were at the saturation temperature, indicating the presence of steam at this level (i.e., 1 1/2 in. from the top of the pipe). The lower thermocouple remained below the saturation temperature demonstrating that these thermocouples (located 1/2 in. from the flange bottom) were covered with water.

Temperatures in CL-2 through CL-4 from []^{a,b,c} to test termination (Figures 5.2.1-48, 5.2.1-48x, 5.2.1-49, 5.2.1-49x, 5.2.1-50, and 5.2.1-50x) were below the saturation temperature during this entire period. Temperatures show that these cold legs were filled with subcooled water to a minimum of the height of the upper thermocouples.

Temperatures for CL-1 (Figures 5.2.1-47 and 5.2.1-47x) differ from the other cold legs. The thermocouple at RCP-1 was superheated from about []^{a,b,c} which could only occur if the vertical leg from the SG to the pump were filled with steam. The superheat decreased at times that coincide with condensation events (i.e., []^{a,b,c}), as a result of level fluctuations from the pressure imbalances initiated by this event. The period of low level in CL-1

lasted longer (from about []^{a,b,c}) than in the other cold legs. The anomalous behavior of CL-1 may be related to its connection to the same SG channel head as CL-3, the leg with the simulated break. Rapid depressurization resulted in earlier drainage of SG-1 tubes and, therefore, lower liquid inventories after about []^{a,b,c} (when the tubes of SG-1 emptied).

CL-1 and CL-4 pressures (Figures 5.2.1-20) agreed very closely with reactor pressure during the entire test.

Level data for the SG-2 HL-2 elbow (Figures 5.2.1-12 and 5.2.1-12x) indicated that this level fell several inches during the test, but refilled completely at about []^{a,b,c}. Wide oscillations from []^{a,b,c} were probably caused either by pressure variations or steam bubbles rising through the liquid.

HL-1 and HL-2 liquid levels both decreased after about []^{a,b,c} similarly to the level behavior in the cold legs. The levels in both hot legs decreased, and the pipes emptied at about []^{a,b,c}. The hot legs refilled partially between []^{a,b,c} although the level indications oscillated widely as a result of dynamic pressure variations. The hot-leg levels rose slowly at about []^{a,b,c} and reached full level at about []^{a,b,c} (Figures 5.2.1-12 and 5.2.1-12x).

HL-1 and HL-2 temperatures at []^{a,b,c} from the reactor vessel flange top and []^{a,b,c} from the reactor vessel flange bottom (Figures 5.2.1-13, 5.2.1-13x, 5.2.1-14, and 5.2.1-14x) followed the saturation temperature based on the reactor vessel for about []^{a,b,c} indicating the presence of saturated liquid or steam. Between []^{a,b,c} these temperatures for both hot legs (SC-140, SC-141, TF-142, and TF-143) became subcooled, indicating that the hot legs refilled with water. These temperatures agreed with the level measurements that showed refilling of the hot legs during this period. Hot-leg temperatures then followed the saturation temperature until about []^{a,b,c} when the temperatures subcooled slightly, indicating that the pipes were filled with water.

The hot legs refilled initially at []^{a,b,c} because the reactor vessel had been refilled to the level of the hot legs. The level decreased at about []^{a,b,c} (as indicated by an increase in temperature and a decrease in level indication) because the level in the reactor started to decrease after the accumulators completed injection at []^{a,b,c}.

In-Containment Refueling Water Storage Tank

The IRWST injection system was not actuated during this test. Water was supplied to the suction of the RNS pump from this tank. Water in the IRWST also acted as a heat sink for steam vented through ADS 1-3 and heat rejected from the PRHR HX. Figures 5.2.1-51 and 5.2.1-51x show the temperature of the water in the IRWST during this test.

Break and ADS Measurement System

When the break valve opened, pressure upstream of the break orifice and differential pressure across the break orifice were equal and closely followed reactor vessel pressure (Figure 5.2.1-52). CL-3 fluid discharged from the break hole flashed because of reduced pressure. Two-phase mixture exiting the break hole was piped to the break separator. Liquid flow rose steadily for the first []^{a,b,c} then fell by about one-third from []^{a,b,c} (Figure 5.2.1-2). This constant flow occurred during the period when RCS pressure had become constant; therefore, the driving force at the break orifice was constant. Steam flow decreased slowly without significant oscillations. Steam flow then declined, mirroring the decrease in pressure upstream of the break. It became so small that it was unmeasurable at []^{a,b,c} (Figure 5.2.1-3).

Liquid flow decreased sharply at about []^{a,b,c} and then rose slowly from []^{a,b,c}. The increase in liquid flow during this period resulted from water injections from the CMTs and accumulators. Liquid flow became constant at about []^{a,b,c} at about []^{a,b,c} until test termination. Since the RNS pump supplied []^{a,b,c} of water into the DVI lines, about half the water flowed out of the system through the simulated break and half refilled the system.

Since the ADS-4 valves were not actuated during this test, the ADS-4 separators were not used.

Nonsafety-Related Systems

The nonsafety-related systems (CVS and RNS) functioned in this test as programmed in the control logic (Figures 5.2.1-8 and 5.2.1-8x). CVS injection started at []^{a,b,c} and continued at a flow rate of []^{a,b,c} at []^{a,b,c}. The CVS pump was shut off when the pressurizer low-level level reset.

Flow was initiated from the RNS when DVI pressures decreased below RNS pump discharge pressure. This flow started at about []^{a,b,c} and rose to a total of []^{a,b,c} through each DVI). RNS flow remained constant at these rates until test termination.

5.2.1.6 Mass Balance

Mass balance for this test was calculated from water inventories in the components before and after the test. Water mass at the completion of the test agreed with pre-test water mass within []^{a,b,c} percent. Details of this mass balance are provided in Appendix E.

5.2.1.7 Conclusions

The test was performed with minimal problems and is considered acceptable. Although not all of the facility initial conditions met the specified acceptance criteria, the deviations did not impact the quality

of the data. The instrumentation problems encountered were not critical to the performance of the facility mass and energy balances.

Facility response to the test was as anticipated for the conditions that were established. The data clearly demonstrated that cooling of the reactor heater rods was maintained throughout the duration of the test.

This test was successfully concluded when the CMTs started to refill. Adequate cooling of the core heaters was achieved during the entire test. The capacity of the RNS was sufficiently large to start refilling the system even with a simulated 2-in. break.

TABLE 5.2.1-1
MATRIX TEST SB04 INITIAL CONDITIONS

Parameter	Instrument No.	Specified Initial Condition	Actual Initial Condition	Comments
Pressurizer pressure ⁽¹⁾	PT-604	370 ± 2 psig	[] ^{a,b,c}	
HL-1 temperature ⁽¹⁾	SC-141	420 ± 2°F		
HL-2 temperature ⁽¹⁾	SC-140	420 ± 2°F		
SG-1 pressure ⁽¹⁾	PT-301	285 ± 5 psig		
SG-2 pressure ⁽¹⁾	PT-302	285 ± 5 psig		
Pressurizer level ⁽¹⁾	LDP-601	65 ± 5 in.		Level signal was temperature-compensated by TF-605
SG-1 narrow-range level ⁽¹⁾	LDP-303	26 ± 3 in.		Level signal was temperature-compensated by TF-301
SG-2 narrow-range level ⁽¹⁾	LDP-304	26 ± 3 in.		Level signal was temperature-compensated by TF-310
IRWST temperature ⁽²⁾	TF-709	< 80°F		
CMT-1 temperature ⁽²⁾	TF-529	< 80°F		
CMT-2 temperature ⁽²⁾	TF-532	< 80°F		
ACC-1 temperature ⁽²⁾	TF-403	< 80°F		
ACC-2 temperature ⁽²⁾	TF-404	< 80°F		
IRWST level ⁽²⁾	LDP-701	Level established by fill-line elevation		
ACC-1 level ^(2,3)	LDP-401	Level established by standpipe at 37 in.		
ACC-2 level ^(2,3)	LDP-402	Level established by standpipe at 37 in.		
ACC-1 pressure ⁽²⁾	PT-401	232 ± 2 psig		
ACC-2 pressure ⁽²⁾	PT-402	232 ± 2 psig	[]	

TABLE 5.2.1-1 (Continued)
MATRIX TEST SB04 INITIAL CONDITIONS

Parameter	Instrument No.	Specified Initial Condition	Actual Initial Condition	Comments
CMT-1 level ⁽²⁾	LDP-507	Full	[] a.b.c	
CMT-2 level ⁽²⁾	LDP-502	Full	[]	

Note:

- (1) Data for the indicated parameter were recorded in the test procedure as an initial condition for the test. The value was determined by the test engineer from the appropriate control board indicator.
- (2) Data were not recorded in procedure, but the test engineer verified that specified conditions were achieved while establishing initial conditions. The value of the parameter was determined post-test by calculating the average DAS indication for a time of about 2 minutes before the break valve opened.
- (3) The bourdon pressure tube local indicator (PI-401 or PI-402) was tubed to the lower portion of the reference leg of the accumulator level transmitter (LDP-401 or LDP-402). As pressure in the accumulator was increased, air inside the bourdon tube was compressed, thereby lowering the reference leg liquid level, resulting in a false indication of measured level.

TABLE 5.2.1-2
MATRIX TEST SB04 INOPERABLE INSTRUMENTS/INVALID DATA CHANNELS

Instrument No.	Instrument Type	Description of Problem
FMM-201*	Magnetic flow meter	Removed from system
FMM-202*	Magnetic flow Meter	Removed from system
FMM-203*	Magnetic flow meter	Removed from system
FMM-204*	Magnetic flow meter	Removed from system
FMM-502*	Magnetic flow meter	Data invalid after 800 seconds because of steam in balance line
FMM-503*	Magnetic flow meter	Data invalid after 800 seconds because of steam in balance line
FMM-802*	Magnetic flow meter	Data invalid after steam formed in PRHR HX inlet line at about 120 seconds
FMM-804*	Magnetic flow meter	Data valid until PRHR HX initially drained at 580 seconds; after which the possibility of steam in the outlet line invalidated the data
FVM-602	Vortex flow meter	Ignore data since ADS-4 did not actuate
FVM-603	Vortex flow meter	Ignore data since ADS-4 did not actuate
HFM-103	Heat flux meter	Failed
HFM-105	Heat flux meter	Failed
HFM-112	Heat flux meter	Failed
HFM-201	Heat flux meter	Failed
HFM-505	Heat flux meter	Data appear erratic
HFM-601	Heat flux meter	Failed
HFM-902	Heat flux meter	Data appear erratic
HPS-203-1 through HPS 203-3	Heated phase switch	Inoperable throughout test
HPS-509-1 through HPS-509-3	Heated phase switch	Inoperable throughout test
LDP-201 LDP-202 LDP-203 LDP-204 LDP-205 LDP-206	Differential pressure transmitter - level	Data invalid due to effect of vertical portion of sense line attached to top of pipe; data can show level trends when the pipe is empty or starts to drain, but absolute level indication can not be used

TABLE 5.2.1-2 (Continued)
MATRIX TEST SB04 INOPERABLE INSTRUMENTS/INVALID DATA CHANNELS

Instrument No.	Instrument Type	Description of Problem
LDP-207 through LDP-209	Differential pressure transmitter - level	Inoperable; ranged improperly; data can show trends, but absolute level indication can not be used
LDP-215* LDP-216 LDP-217 LDP-218* LDP-219* LDP-220 LDP-221 LDP-222*	Differential pressure transmitter - level	Data invalid when tube drained and reference leg started to vaporize
LDP-401* LDP-402*	Differential pressure transmitter - level	Data invalid; see note 3 of Table 5.2.1-2
LDP-608	Differential pressure transmitter - level	Over-ranged at 625 to 800 seconds
LDP-804	Differential pressure transmitter - level	Data valid until PRHR HX initially drained at 580 seconds; after which data are suspect because of possible vaporization of the common reference line
PT-101	Pressure transmitter	Data less than 6.1 psig invalid
PT-102	Pressure transmitter	Data less than 6.2 psig invalid
PT-103	Pressure transmitter	Data less than 6.2 psig invalid
PT-104	Pressure transmitter	Data less than 6.4 psig invalid
PT-108	Pressure transmitter	Data less than 8.4 psig invalid
PT-109	Pressure transmitter	Data less than 6.3 psig invalid
PT-111	Pressure transmitter	Data less than 6.0 psig invalid
PT-112	Pressure transmitter	Data less than 8.8 psig invalid
PT-113	Pressure transmitter	Data less than 6.4 psig invalid
PT-201*	Pressure transmitter	Data less than 1.1 psig invalid
PT-202	Pressure transmitter	Data less than 5.9 psig invalid
PT-205	Pressure transmitter	Data less than 6.1 psig invalid
PT-801	Pressure transmitter	Not reliable after 475 seconds
TF-170	Thermocouple fluid temperature	Read low throughout test

TABLE 5.2.1-2 (Continued)
MATRIX TEST SB04 INOPERABLE INSTRUMENTS/INVALID DATA CHANNELS

Instrument No.	Instrument Type	Description of Problem
TF-203	Thermocouple fluid temperature	Read low throughout test
TF-501*	Thermocouple fluid temperature	Read low throughout test
TF-504*	Thermocouple fluid temperature	Inoperable; indicated ambient temperature throughout test
TFM-703	Thermocouple for HFM-703	Inoperable; indicated ambient temperature throughout test
TH-317-1 through TH-317-4	Thermocouple heater rod	Inoperable; heater rod removed prior to test
TW-503	Thermocouple wall temperature	Inoperable throughout test
TW-534	Thermocouple wall temperature	Inoperable; indicated ambient throughout test
TW-552	Thermocouple wall temperature	Inoperable; indicated ambient throughout test

Note:

* Instruments marked with an asterisk are critical instruments. See Subsection 5.2.1.2 for discussion.

**TABLE 5.2.1-3
MATRIX TEST SB04 SEQUENCE OF EVENTS**

Event ⁽¹⁾	Data Source ⁽²⁾	Time After Break (sec.)	
TEST Pushbutton Depressed	D		a,b,c
Break Valve Open Signal	D		
Break Valve Starts To Open	D		
Feed Pump Trips	D		
CMT-1 Outlet Valve Starts To Open	D		
CMT-2 Outlet Valve Starts To Open	D		
PRHR HX Outlet Valve Starts To Open	D		
Reactor Coolant Pumps Trip	D		
CVS Pump Injection Starts (FMM-801)	A		
Pressurizer Empty (LDP-601)	A		
HL-1 Pipe Starts To Drain (LDP-205)	A		
SG-1 Hot-Leg Elbow Starts Draining (LDP-207)	A		
Pressurizer Surge Line Empty (LDP-602)	A		
SG-1 Cold-Leg Short Tube Empty (LDP-221)	A		
SG-1 Cold-Leg Long Tube Empty (LDP-219)	A		
SG-2 Cold-Leg Short Tube Empty (LDP-220)	A		
SG-1 Hot-Leg Short Tube Empty (LDP-217)	A		
SG-1 Hot-Leg Long Tube Empty (LDP-215)	A		
CL-3 Channel Head Empty (LDP-213)	A		
SG-2 Cold-Leg Long Tube Empty (LDP-222)	A		
CL-1 Channel Head Empty (LDP-211)	A		
CMT-1 Recirculation Flow Stops (LDP-509)	A		
CMT-2 Recirculation Flow Stops (LDP-510)	A		
SG-2 Hot-Leg Short Tube Empty (LDP-216)	A		
SG-2 Hot-Leg Long Tube Empty (LDP-218)	A		

TABLE 5.2.1-3 (Continued)
MATRIX TEST SB04 SEQUENCE OF EVENTS

Event ⁽¹⁾	Data Source ⁽²⁾	Time After Break (sec.)
HL-2 Pipe Starts To Drain (LDP-206T)	A	_____ a,b,c
CL-2 Channel Head Empty (LDP-210)	A	_____
CL-4 Channel Head Empty (LDP-22)	A	_____
Time Of Minimum Reactor Level Observed During Test (LDP-127)	A	_____
ACC-1 Injection Starts (FMM-401)	A	_____
ACC-2 Injection Starts (FMM-402)	A	_____
RNS Pump Injection Starts (FMM-803)	A	_____
CMT-1 Low Level Signal	D	_____
ADS-1 Valve Starts To Open	D	_____
Pressurizer Refloods (LDP-601)	A	_____
HL-2 Pipe Empty (LDP-206)	A	_____
SG-1 Hot-Leg Elbow Minimum (LDP-207)	A	_____
ADS-2 Valve Starts To Open	D	_____
SG-2 Hot-Leg Channel Head Empty (LDP-214)	A	_____
SG-1 Hot-Leg Elbow Minimum (LDP-208)	A	_____
ADS-3 Valve Starts To Open	D	_____
Reactor Pressure Low	D	_____
IRWST-2 Injection Valve Starts To Open	D	_____
IRWST-1 Injection Valve Starts To Open	D	_____
ACC-1 Empty (LDP-401)	A	_____
ACC-2 Empty (LDP-402)	A	_____
CMT-1 Starts To Reflood (LDP-507)	A	_____
CMT-2 Starts To Reflood (LDP-502)	A	_____

Note:

- (1) Data from the instrument channel in parenthesis were used to determine level, flow, or pressure conditions.
- (2) D = time data obtained from a software program that monitored the input and output of the facility's PLC.
A = time data obtained by reviewing data from the instrument channel listed in the Event Description column.

The Bar Charts for Table 5.2.1-3 on pages 5.2.1-29 through 5.2.1-32 are not included in this nonproprietary document.

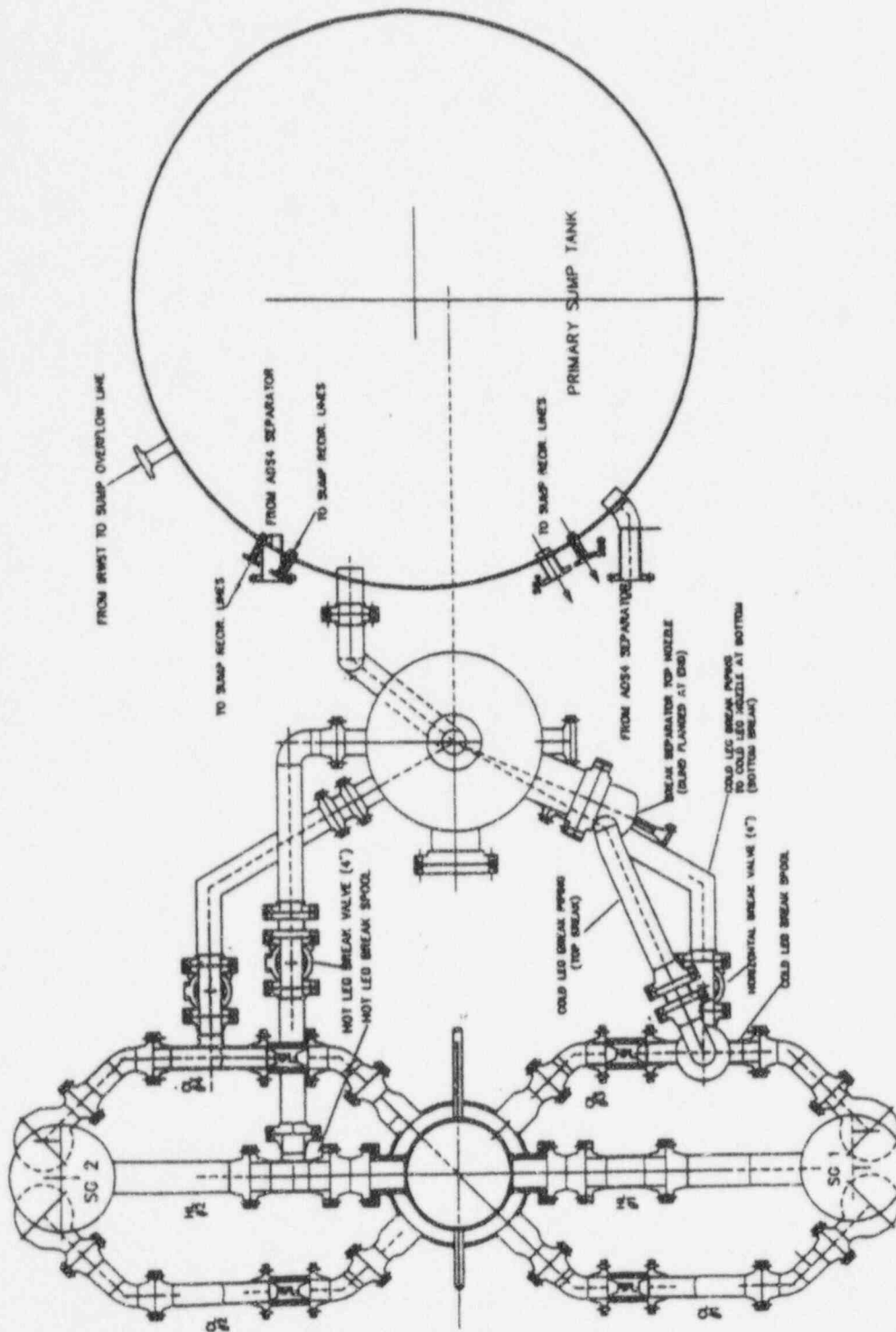


Figure 5.2.1-1a Primary Loop and Break Piping Layout (Sh. 1 of 2)

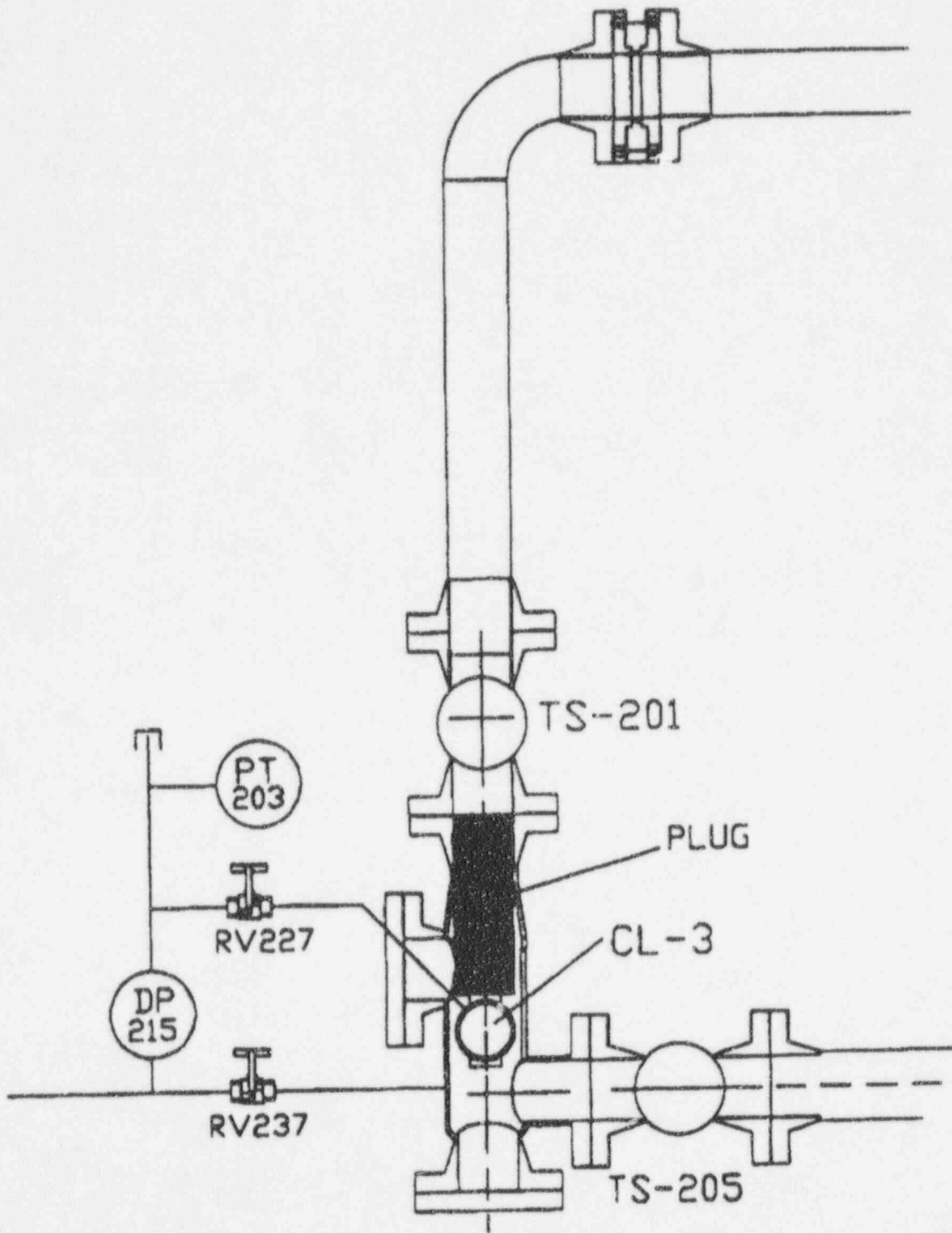


Figure 5.2.1-1b Primary Loop and Break Pipe Arrangement (Sh. 2 of 2)

Figures 5.2.1-2 through 5.2.2-53x are not included in this nonproprietary document.

5.2.2 Effect of a Smaller Break Size (Matrix Test SB24 Comparison with Matrix Test SB04)

In this section, the results of Matrix Test SB24 (OSU Test U0024) are compared with those of Matrix Test SB04 (OSU Test U0204). These two tests were identical, except that the break simulated in SB24 was a 1/2-in. pipe break and the break simulated in SB04 was a 2-in. pipe break. Both simulated breaks were located at the bottom of CL-3, and the nonsafety-related systems were operating in accordance with the preprogrammed control logic for the AP600. In both tests, failure of one leg of one ADS-4 line was simulated.

The transient began with the opening of the valve isolating the simulated break and continued through refilling of the system through the RNS. The accumulators injected when DVI pressure decreased below the nitrogen pressure in the accumulators. The ADS was not actuated in this test because pressure did not reach the setpoints for actuation. The test was terminated at about 9500 seconds (about 2-1/2 hours) after refilling, and a constant rate of temperature/pressure decline had been demonstrated. Performance of this test was successful because the core heater rods remained covered with water, and their temperatures remained below or close to the water saturation temperature.

Subsection 5.2.2.1 provides details related to system configuration and initial conditions. A description of inoperable instruments appears in Subsection 5.2.2.2, and Subsection 5.2.2.3 references the sequence of events. Subsection 5.2.2.4 describes the test results and evaluation. A comparison of component responses appears in Subsection 5.2.2.5, and a summary of mass balance results appear in Subsection 5.2.2.6. The conclusions, as they apply to Matrix Tests SB24 and SB04, appear in Subsection 5.2.2.7. Data plots, (referenced in text as figures), for this section have the same numbers after the section identification numbers as Matrix Test SB04 to facilitate the comparison of data for these two tests.

5.2.2.1 System Configuration and Initial Conditions

The test was performed in accordance with an approved written test procedure. There were no special or unique requirements for the test other than those specified in the initial conditions in Table 5.2.2-1. The specified conditions were checked on the control board prior to test implementation.

The test facility was configured in the normal arrangement (described in Section 2) and was identical to that of Matrix Test SB04, except for the size of the simulated break.

The appropriate prerequisites were completed, and the initial conditions were satisfied. The required break simulation piping and break instrumentation were installed per Dwg. OSU 600904 and the break piping layouts in Figures 5.2.2-1a and 5.2.2-1b. A break hole ([]^{ab,c}) simulating a 1/2-in. cold-leg break was installed in the bottom of the pipe break spool in CL-3. A 50-percent flow nozzle was installed in the ADS 4-1 line (on HL-1) and a 100-percent flow nozzle was installed in the ADS 4-2 line (on HL-2) to provide the assumed single failure. Flow nozzles that simulate two lines were installed in the ADS 1-3 piping.

The heater rod power was adjusted prior to break initiation in order to achieve the required hot-leg temperatures. At initiation of the break, the bundle power was set at 600 kW. Power to the heater rod bundle was maintained at 600 kW for 140 seconds after the start of the test. After 140 seconds, rod bundle power followed an exponential decay curve. The actual power decay curves are provided in data plots in Appendix F. The differences between the actual and specified power decay are considered acceptable. Pressurizer power was terminated at break initiation.

Testing was initiated when test facility conditions, as read from the test facility control board, agreed with the specified initial conditions within acceptable tolerances. All actions were automatic and required no operator action.

Table 5.2.2-1 provides a comparison of the specified and actual initial conditions for Matrix Test SB24. The values in this table were averaged over approximately 2 minutes preceding the test. Test initial conditions were achieved for SG pressure, pressurizer pressure, pressurizer level, SG-1 narrow-range level, and SG-2 narrow-range level. Test initial conditions for the hot-leg temperature were found to be acceptable, with the test results not adversely affected. These measurements outside the tolerance band were accepted, since the deviations were insignificant.

5.2.2.2 Inoperable Instruments

Table 5.2.2-2 is a list of the instruments considered inoperable or invalid during all or portions of this test. Some of the instruments listed are on the Critical Instrument list (Subsection 3.2, Table 3.2-2) and, therefore, are addressed here.

FMM-201, FMM-202, FMM-203, and FMM-204 measured flow (gpm) in each of the four cold legs. A decision was made to continue testing without the availability of these instruments. Replacement flow meters repeatedly failed; their continued use was precluded due to cracking of the ceramic liners from thermal stratification in the loop piping. The necessary boundary conditions for loop flow could be determined from DP-202, DP-203, DP-205, and DP-206.

TF-103 and TF-104 measured CL-3 and CL-4 bottom-of-pipe fluid temperatures entering the reactor downcomer. Both thermocouples were removed to accommodate installation of thermal stratification measurement instrumentation. Both the mocouples were allowed to be inoperable as long as TF-101 and TF-102 were operable. TF-101 and TF-102 were operable during the performance of Matrix Test SB24.

PT-201 measured RCS pressure at the top of the SG-1 long tube. On August 15, 1994, it was discovered that the transmitter had an incorrect zero compensation, which resulted in a negative error and negative data at low pressures. The transmitter zero was corrected at that time. PT-201 data obtained during Matrix Test SB24 had the zero correction performed, and the corrected data appear as PT_201. Since the pressure remained positive during this test, corrected pressure data for PT_201 are valid.

TF-504 measured CMT fluid temperature from the long thermocouple rod location near the bottom of each CMT. This thermocouple appears to have measured ambient conditions throughout the test, which would indicate a short somewhere in the thermocouple wiring. With this thermocouple inoperable, the required long thermocouple rod thermocouple availability of "seven out of ten and no more than one in succession failed" was met.

Data provided by ADS-4 separator instrumentation were invalid because of the closed position of the ADS-4 valves and the ADS-4 separator loop seal valves during this entire test. The instruments affected are: FMM-602, FMM-603, FVM-602, FVM-603, LDP-611, and LDP-612. Test analysis will not be affected, since ADS-4 flow did not begin until the valves opened.

Considering these critical instrument failures, sufficient instrumentation was available to allow the performance of mass balances as demonstrated in Subsection 5.1.1.6 and Appendix E. An energy balance will be performed and reported in the *AP600 Low-Pressure Integral Systems Test at Oregon State University Test Analysis Report, WCAP-14292*.⁽²⁾

5.2.2.3 Sequence of Events

The sequence of events for Matrix Tests SB24 and SB04 are compared in Table 5.2.2-3 and associated bar graphs based on the chronologic order of event occurrence in Matrix Test SB24. Since the Matrix Test SB24 break area was about []^{a,b,c} of the area of the Matrix Test SB04 break, the rate of flow through the Matrix Test SB24 simulated break was much lower, and, hence, the rate of depressurization was significantly slower.

The CVS pump started to inject water at []^{a,b,c} compared with []^{a,b,c} for Matrix Test SB04. The accumulators injected water into the DVI lines at []^{a,b,c} when DVI pressure fell below the nitrogen pressure. Since the reactor vessel level did not fall sufficiently to uncover the hot legs or cold legs, those lines and the SG tubes remained filled with water. The pressurizer emptied at []^{a,b,c} for Matrix Test SB04, and reflooded at []^{a,b,c}. ADS 1-3 and ADS-4 never actuated because the setpoints for these components were never reached. Cold water circulated from the CMTs by natural circulation. Because the transition from recirculation to draindown did not occur, they continued to provide natural circulation flow. The RNS pump injected water at about []^{a,b,c} when the pressure in the SG-2 channel head reached RNS pump discharge pressure. The test was terminated at []^{a,b,c} when steady temperature and pressure decreases had been demonstrated.

5.2.2.4 Test Results and Evaluation

Since the ADS was not actuated during this test, the discussion of the test results will not be separated into phases, as was the case for Matrix Test SB04. In general, the slow rate of coolant loss and, therefore, slow depressurization permitted the CVS and RNS to maintain the system at a nearly full condition during the entire transient. The accumulators injected when their pressures became equal to

system pressure and the pressurizer emptied and refilled; however, because the rate of depressurization was so much lower, the time scale for these events was thousands of seconds compared with hundreds of seconds in Matrix Test SB04. Specific comparisons of the key events for Matrix Tests SB24 and SB04 are discussed in this section.

Liquid flow (Figure 5.2.2-2) from the break separator increased to a peak of slightly less than []^{a,b,c} and then remained between []^{a,b,c} until the RNS pump was shut off at []^{a,b,c}. Comparable break separator liquid flow rates for Matrix Test SB04 ranged up to a maximum of []^{a,b,c} and down to a minimum of []^{a,b,c} with a steady-state rate of []^{a,b,c}. Also, significant steam flows ([]^{a,b,c}) were measured for Matrix Test SB04. Steam flow was so low that it could not be measured in Matrix Test SB24 (Figure 5.2.2-3). Steam flow was negligible in Matrix Test SB24 except for the initial 10 seconds after break initiation.

Reactor and DVI pressure (Figure 5.2.2-5) fell much more slowly in Matrix Test SB24 compared with Matrix Test SB04 because of the lower break flow in Matrix Test SB24. In Matrix Test SB04, the RCS reached atmospheric pressure at about []^{a,b,c}. The pressure was still about []^{a,b,c} when Matrix Test SB24 was terminated at []^{a,b,c}.

The level indications for the upper plenum and upper head (Figure 5.2.2-9) showed that steam formed only in the upper head of Matrix Test SB24. The water level gradually decreased in the upper head until the accumulators injected (about []^{a,b,c}) and the RNS pump started (about []^{a,b,c}), then the level increased slowly to near the top of the reactor vessel.

The maximum estimated percent steam in the upper part of the core (LDP-110; Figure 5.2.2-9) of []^{a,b,c} percent was reached []^{a,b,c} after break initiation. The steam content gradually decreased as cold water was injected into the downcomer until it became negligible at about []^{a,b,c}. This steam content compares with []^{a,b,c} percent in Matrix Test SB04, as would be expected due to the smaller simulated break.

Steam percent was estimated from the equation below:

$$\text{Steam percent} = \frac{\text{level}(100\% \text{ water}) - \text{level}(\text{with steam})}{\text{level}(100\% \text{ water})} \times 100$$

Coolant in the core remained subcooled in Matrix Test SB24, except for the initial []^{a,b,c} when the coolant was at saturation (Figure 5.2.2-11). In Matrix Test SB04, coolant in the upper core remained at saturation until the RNS actuated at []^{a,b,c} then returned to saturation at about []^{a,b,c} and remained saturated until the end of the test. Therefore, Matrix Test SB24, the core was cooled after the initial []^{a,b,c} by single-phase water. This differed from Matrix Test SB04, in which steam was produced in the upper portion of the core for most of the test.

As flow continued through the simulated break, cold water flowed by natural circulation from the CMTs. Water injected from the pressurizer until it emptied (at about []^{a,b,c}) into HL-2 (Figure 5.2.2-7). The pressurizer in Matrix Test SB04 emptied in about []^{a,b,c} because of the higher differential pressure between the pressurizer and the large break in CL-3. The accumulators injected at about []^{a,b,c} in Matrix Test SB24 (Figure 5.2.2-19), again, much later than the accumulators in Matrix Test SB04 because of the slow depressurization.

The CVS pump in Matrix Test SB24 started at []^{a,b,c} when pressurizer instrumentation reached the low-low level setpoint, and it shut off at about []^{a,b,c} when the pressurizer reached normal level (Figure 5.2.2-8). The comparable Matrix Test SB04 starting time was []^{a,b,c} its termination time was []^{a,b,c}. Similarly, RNS injection began at about []^{a,b,c} for Matrix Test SB24, compared with []^{a,b,c} for Matrix Test SB04. The longer times for both CVS and RNS actuation resulted from the slower depressurization rate of Matrix Test SB24.

The system continued to refill, since RNS flow was greater than the inventory loss through the simulated break. At about []^{a,b,c} the pressurizer reflooded (Figure 5.2.2-7). Since the system had refilled and reached a rate of steady decline in temperature and pressure, the test was terminated at []^{a,b,c}.

5.2.2.5 Comparison of Component Responses

Component responses of Matrix Tests SB24 and SB04 are compared in this section. Those components with similar behaviors are not discussed; however, Matrix Test SB24 data for all of the components are provided in the figures. Components with dissimilar behaviors, discussed below, were:

- Reactor
- CMTs
- Pressurizer
- Cold legs and hot legs
- SGs
- PRHR HX

Reactor

In Matrix Test SB24, the level in the upper head (LDP-115) reached a minimum of []^{a,b,c} below its full level at about []^{a,b,c} (Figure 5.2.2-9). The level began to rise when the accumulators injected at []^{a,b,c} and continued to increase when the RNS pump started at []^{a,b,c}. The level in the upper head during Matrix Test SB04 fell to the upper support plate before the level started to refill at []^{a,b,c} when its accumulators injected and refilled completely after the RNS started at []^{a,b,c}.

The downcomer (Figure 5.2.2-4) remained full during Matrix Test SB24; therefore, there was no steam flow from the upper head through the holes in the top downcomer plate as shown by the upper head pressure difference (DP-130) (Figure 5.2.2-24). Since there was no steam in the downcomer, there were no condensation events in Matrix Test SB24. Steam formation in the reactor vessel, and core fluid and heater temperatures were discussed in detail in Subsection 5.2.2.4 and, therefore, are not repeated here.

In summary, the reactor level remained close to the top of the upper head during the entire transient and refilled to the top of the reactor vessel after the RNS pump started. A small quantity of steam was produced in the core in the first []^{a,b,c} then, the core was cooled by subcooled water injected initially by the accumulators and CVS and later by the RNS.

Core Makeup Tanks

The CMTs in Matrix Test SB24 did not transition to draindown because their balance lines remained filled with liquid as a result of low flow through the simulated break. The CMTs remained filled with liquid during the entire test (Figure 5.2.2-23). Natural circulation flow (Figure 5.2.2-31) was driven by the density difference between the colder water in the CMTs and the water in the system. As hot water from the cold leg entered the CMT, water temperature in the tanks rose, decreasing the density and, hence, the flow rate. At about []^{a,b,c} flow through CMT-1 halted because the density driving force became inadequate to provide the necessary driving head. Flow from CMT-1 stopped at about []^{a,b,c} because of this density effect combined with flow from the RNS pump.

Cold Legs and Hot Legs

The hot and cold legs in Matrix Test SB24 remained filled (Figures 5.2.2-12 and 5.2.2-46) with subcooled water (Figures 5.2.2-47 through 5.2.2-50) compared with Matrix Test SB04 in which these legs drained and filled with superheated steam. CL-2 and CL-1 coolant temperatures were cooler than those in CL-3 and CL-4. CL-2 was cooler because cold water from the CVS was injected in the SG-2 channel head; the cooler temperatures in CL-1 may have been the result of heat losses to the environment by the stagnant coolant in this line.

Steam Generators

The response of the SGs in Matrix Test SB24 differed significantly from that in Matrix Test SB04. Since the loss of inventory through the simulated break was low enough that coolant makeup from the CVS and accumulators kept the hot and cold legs full, water in the SGs did not drain from either the channel heads (Figures 5.2.2-17 and 5.2.2-18) or the tubes (Figures 5.2.2-15 and 5.2.2-16). Pressure in the primary side of the SGs remained higher than secondary pressure throughout the test (Figure 5.2.2-45).

The temperature of the water in the tubes was about []^{a,b,c} below the saturation temperature based on reactor pressure during the initial []^{a,b,c} (Figures 5.2.2-43 and 5.2.2-44). Later, water in the tubes became even more subcooled relative to the reactor pressure. This confirmed that RCS pressure was being maintained by the saturation pressure in the reactor vessel.

The temperatures of the water in the tubes and the water in the shell of each SG were nearly identical, indicating that thermal equilibrium was reached, and each SG was slowly cooling through heat losses to the environment. Only one thermocouple, TF-218, located at the top of the long tube in SG-2, deviated. This thermocouple indicated a higher temperature than either the shell-side fluid temperatures or the other water temperatures in the tubes. One possible explanation would be that the level in the shell side had decreased sufficiently so that the top of the tube was uncovered and its cooling was delayed relative to the rest of the tubes.

Passive Residual Heat Removal Heat Exchanger

PRHR provided natural circulation cooling throughout Matrix Test SB24, as shown by continuous flow (Figure 5.2.2-37), full level in the inlet header and PRHR HX (Figure 5.2.2-38), and temperature distribution in the PRHR HX (Figure 5.2.2-39). Flow decreased from the initial rate of about []^{a,b,c} at the end of the test because the inlet temperature decreased as RCS temperature declined. This reduced the density difference across the PRHR HX and, hence, the pressure differential for natural circulation flow. Although the IRWST temperature rose, the outlet temperature of the PRHR HX was not significantly affected.

The PRHR HX provided natural circulation cooling during the entire Matrix Test SB24 because inventory loss through the simulated break was slow enough that the accumulator and nonsafety-related system injections were sufficient to keep the system full so that natural circulation through the PRHR HX was maintained.

5.2.2.6 Mass Balance

The mass balance for Matrix Test SB24 was calculated from the water inventory at the start and conclusion of the test. The final water inventory agreed with the initial inventory within []^{a,b,c} percent. Details of the individual component inventories and their mass balance analysis are provided in Appendix E.

5.2.2.7 Conclusions

The test was performed with minimal problems and is considered acceptable. Although not all of the facility initial conditions met the specified acceptance criteria, the deviations did not impact the quality of the data. The instrumentation problems encountered were not critical to the performance of the facility mass and energy balances.

Facility response to the test was as anticipated for the conditions that were established. The data clearly demonstrated that cooling of the reactor heater rods was maintained throughout the duration of the test.

Matrix Test SB24 was significantly less stressful to the plant because the 1/2-in. simulated break limited inventory loss. With this slow rate of loss, the CVS and RNS were able to keep the hot legs, cold legs, and SGs full of water. The level decreased in the reactor about []^{a,b,c} and then refilled when the accumulators injected and the RNS actuated. The CMTs did not inject in this test because the balance line remained full. However, natural circulation continued through the CMTs through the test.

The core remained covered with water, and the core heater rods were cooled by subcooled water during almost the entire test. Some steam was produced in the core during the initial 60 to 70 seconds; however, beyond this initial period, core heat was removed by single-phase subcooled water. Core heat was removed by the nonsafety-related systems' cold water injection, natural circulation through the CMTs, and natural circulation in the CMTs.

There were no condensation events during Matrix Test SB24. Since the downcomer remained full of water, there was no steam volume to subcool and suddenly condense as in tests with larger simulated breaks.

TABLE 5.2.2-1
MATRIX TEST SB24 INITIAL CONDITIONS

Parameter	Instrument No.	Specified Initial Condition	Actual Initial Condition	Comments
Pressurizer pressure ⁽¹⁾	PT-604	370 ± 2 psig		
HL-1 temperature ⁽¹⁾	SC-141	420 ± 2°F		
HL-2 temperature ⁽¹⁾	SC-140	420 ± 2°F		
SG-1 pressure ⁽¹⁾	PT-301	285 ± 5 psig		
SG-2 pressure ⁽¹⁾	PT-302	285 ± 5 psig		
Pressurizer level ⁽¹⁾	LDP-601	65 ± 5 in.		Level signal was temperature-compensated by TF-605
SG-1 narrow-range level ⁽¹⁾	LDP-303	26 ± 3 in.		Level signal was temperature-compensated by TF-301
SG-2 narrow-range level ⁽¹⁾	LDP-304	26 ± 3 in.		Level signal was temperature-compensated by TF-310
IRWST temperature ⁽²⁾	TF-709	< 80°F		
CMT-1 temperature ⁽²⁾	TF-529	< 80°F		
CMT-2 temperature ⁽²⁾	TF-532	< 80°F		Accepted
ACC-1 temperature ⁽²⁾	TF-403	< 80°F		
ACC-2 temperature ⁽²⁾	TF-404	< 80°F		
IRWST level ⁽²⁾	LDP-701	Level established by fill-line elevation		

TABLE 5.2.2-1 (Continued)
MATRIX TEST SB24 INITIAL CONDITIONS

Parameter	Instrument No.	Specified Initial Condition	Actual Initial Condition	Comments
ACC-1 level ^(2,3)	LDP-401	Level established by standpipe at 37 in.	<input type="checkbox"/>	a,b,c
ACC-2 level ^(2,3)	LDP-402	Level established by standpipe at 37 in.	<input type="checkbox"/>	
ACC-1 pressure ⁽²⁾	PT-401	232 ± 2 psig	<input type="checkbox"/>	Pressure was [<input type="checkbox"/>] ^{a,b,c} low; condition acceptable
ACC-2 pressure ⁽²⁾	PT-402	232 ± 2 psig	<input type="checkbox"/>	Pressure was [<input type="checkbox"/>] ^{a,b,c} low; condition acceptable
CMT-1 level ⁽²⁾	Full	LDP-507	<input type="checkbox"/>	
CMT-2 level ⁽²⁾	Full	LDP-502	<input type="checkbox"/>	

Note:

- (1) Data for the indicated parameter were recorded in the test procedure as an initial condition for the test. The value was determined by the test engineer from the appropriate control board indicator.
- (2) Data were not recorded in procedure, but the test engineer verified that specified conditions were achieved while establishing initial conditions. The value of the parameter was determined post-test by calculating the average DAS indication for a time of about 2 minutes before the break valve opened.
- (3) The bourdon pressure tube local indicator (PI-401 or PI-402) was tubed to the lower portion of the reference leg of the accumulator level transmitter (LDP-401 or LDP-402). As pressure in the accumulator was increased, air inside the bourdon tube was compressed, thereby lowering the reference leg liquid level, resulting in a false indication of measured level.

**TABLE 5.2.2-2
MATRIX TEST SB24 INOPERABLE INSTRUMENTS/INVALID DATA CHANNELS**

Instrument No.	Instrument Type	Description of Problem
FMM-201*	Magnetic flow meter	Removed from system
FMM-202*	Magnetic flow meter	Removed from system
FMM-203*	Magnetic flow meter	Removed from system
FMM-204*	Magnetic flow meter	Removed from system
FVM-602	Vortex flow meter	Ignore data since ADS-4 did not actuate
FVM-603	Vortex flow meter	Ignore data since ADS-4 did not actuate
HFM-103	Heat flux meter	Failed
HFM-105	Heat flux meter	Failed
HFM-112	Heat flux meter	Failed
HFM-113	Heat flux meter	Failed
HFM-201	Heat flux meter	Failed
HFM-505	Heat flux meter	Data appear erratic
HFM-510	Heat flux meter	Failed
HFM-601	Heat flux meter	Failed
HFM-703	Heat flux meter	Failed
HPS-203-1 through HPS-203-3	Heated phase switch	Inoperable throughout test
HPS-509-1 through HPS-509-3	Heated phase switch	Inoperable throughout test
PT_101	Pressure transmitter	Data less than 6.1 psig invalid
PT_102	Pressure transmitter	Data less than 6.2 psig invalid
PT_103	Pressure transmitter	Data less than 6.2 psig invalid
PT_104	Pressure transmitter	Data less than 6.4 psig invalid
PT_108	Pressure transmitter	Data less than 8.4 psig invalid
PT_109	Pressure transmitter	Data less than 6.3 psig invalid
PT_111	Pressure transmitter	Data less than 6.0 psig invalid
PT_112	Pressure transmitter	Data less than 8.8 psig invalid
PT_113	Pressure transmitter	Data less than 6.4 psig invalid

TABLE 5.2.2-2 (Continued)
MATRIX TEST SB24 INOPERABLE INSTRUMENTS/INVALID DATA CHANNELS

Instrument No.	Instrument Type	Description of Problem
PT_101	Pressure transmitter	Data less than 6.1 psig invalid
PT_201*	Pressure transmitter	Data less than 1.1 psig invalid
PT_202	Pressure transmitter	Data less than 5.9 psig invalid
PT_205	Pressure transmitter	Data less than 6.1 psig invalid
PT_108	Pressure Transmitter	Data less than 8.4 psig invalid
TF-103	Thermocouple fluid temperature	Removed from system
TF_105	Thermocouple fluid temperature	Removed from system
TF-170	Thermocouple fluid temperature	Read low throughout test
TF-203	Thermocouple fluid temperature	Read low throughout test
TF-504	Thermocouple fluid temperature	Inoperable; indicated ambient throughout test
TFM-103 TFM-105 TFM-113 TFM-201 TFM-703	Thermocouple for HFMs	Inoperable throughout test
TH-317-1 through TH-317-4	Thermocouple heater rod	Inoperable; heater rod removed prior to test
TW-503	Thermocouple wall temperature	Inoperable throughout test

Note:

* Instruments marked with an asterisk are critical instruments. See Subsection 5.2.2.2 for discussion.

Table 5.2.2-3 on pages 5.2.2-13 through 5.2.2-15 are not included in this nonproprietary document.

PRIMARY LOOP & BREAK PIPE ARRANGEMENT

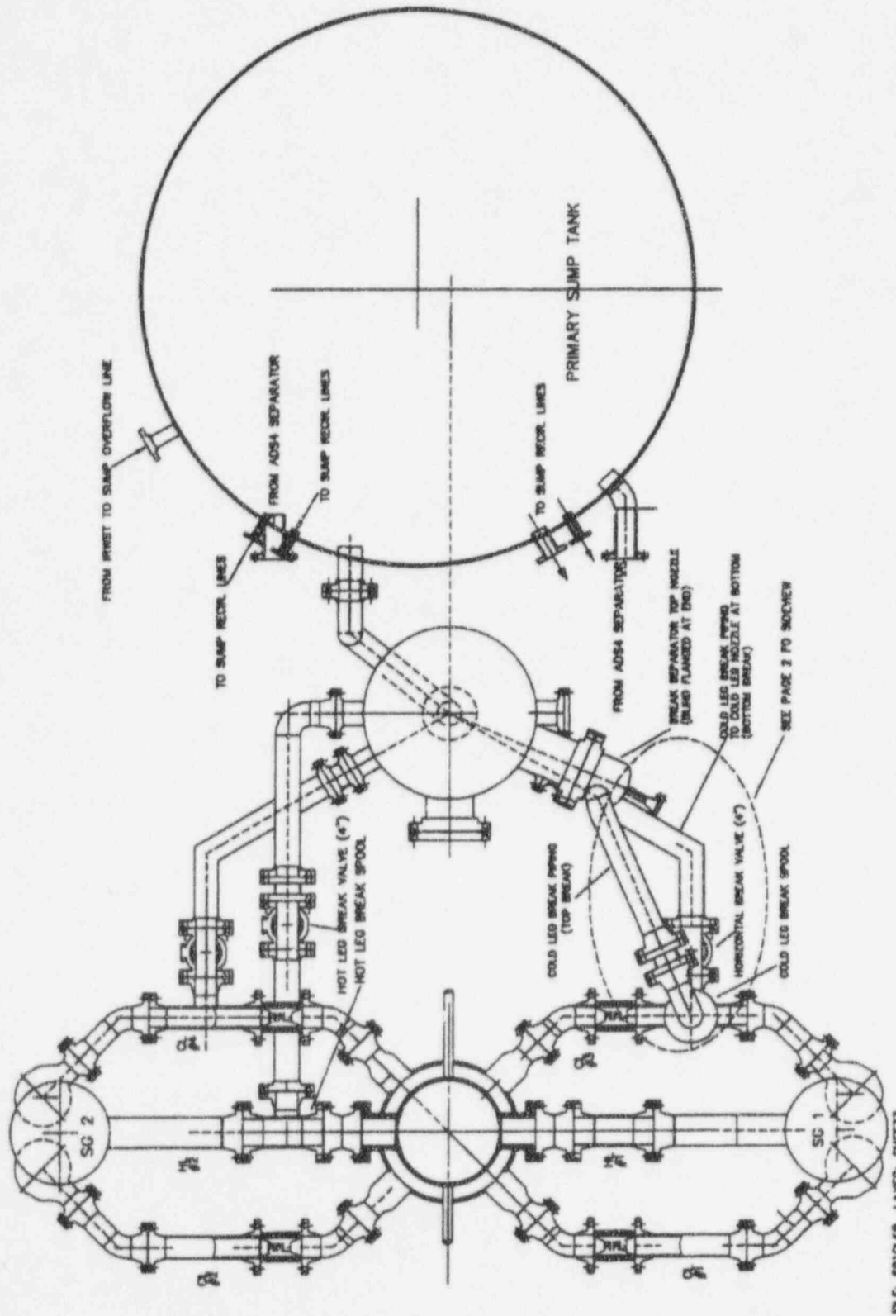


Figure 5.2.2-1a Primary Loop and Break Pipe Arrangement (Sh. 1 of 2)

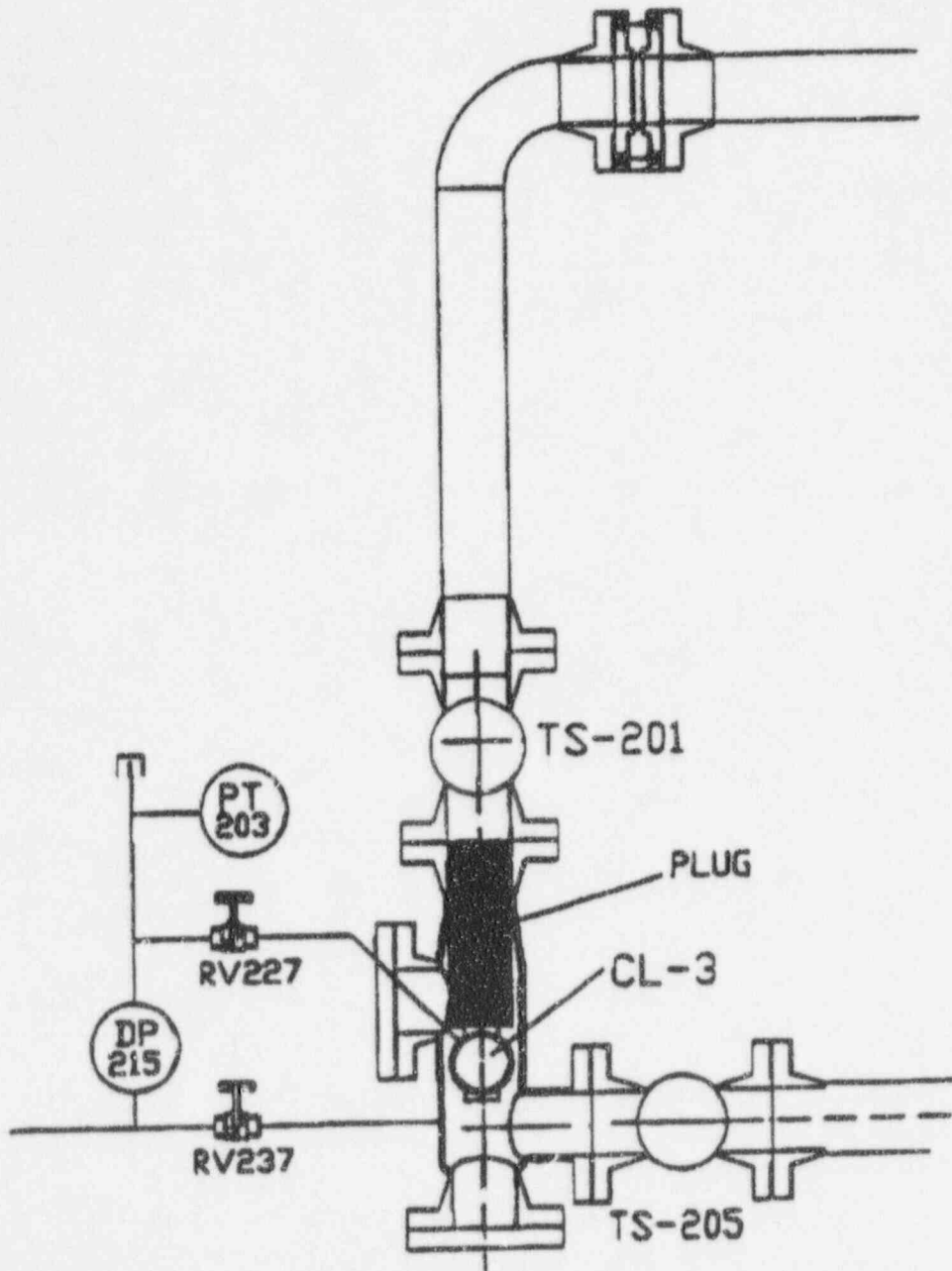


Figure 5.2.2-1b Primary Loop and Break Pipe Arrangement (Sh. 2 of 2)

Figures 5.2.2-2 through 5.2.2-53 are not included in this nonproprietary document.

5.3 Core Makeup Tank/Cold-Leg Balance Line Breaks

Matrix Tests SB10 (OSU Test U0110) and SB09 (OSU Test U0009) characterized the thermal-hydraulic phenomena and system response to a break in the horizontal portion of the core makeup tank-1 (CMT-1) balance line. Both tests were performed using the same break location. Matrix Test SB10 simulated a double-ended guillotine (DEG) break; Matrix Test SB09 simulated a single-ended 2-in. break. Tests covered the entire transient from the initial break through long-term cooling, roughly spanning 22,000 to 29,000 seconds. In both tests, the equipment was configured to simulate failure of one of the two automatic depressurization system (ADS)-4 lines. Results of Matrix Tests SB10 and SB09 appear in Subsections 5.3.1 and 5.3.2, respectively.

5.3.1 Reference Double-Ended Guillotine Line Break (Matrix Test SB10)

This section provides the thermal-hydraulic test results from Matrix Test SB10 for a DEG CMT-1 balance line break. The simulated break was located between cold leg-3 (CL-3) and the vertical portion of the CMT-1 balance line, and was configured to simulate the failure of one of the two ADS-4 lines. Facility responses to the break are documented by data plots, referenced as figures in text. Matrix Test SB10 is the reference test for CMT-1 balance line breaks.

The test performed met the specified initial conditions. Any exceptions to the initial conditions are discussed in Subsection 5.3.1.1. Matrix Test SB10 is considered successful. Cooling of the heater bundle was maintained throughout this event. The transient began from the break and continued through ADS actuation and CMT, accumulator, in-containment refueling water storage tank (IRWST), and primary sump injection.

Matrix Test SB10 was performed on June 24 and 25, 1994. Test duration was about 8.5 hours.

Subsection 5.3.1.1 provides details related to system configuration and initial conditions.

Subsection 5.3.1.2 provides the test sequence of events. Subsections 5.3.1.4 and 5.3.1.5 provide an overall summary of the system response and component-specific responses for Matrix Test SB10, respectively. A description of types and effects of inoperable instruments appears in Subsection 5.3.1.3. A summary of the mass balance results appears in Subsection 5.3.1.6. The conclusions, as they apply to Matrix Test SB10, appear in Subsection 5.3.1.7.

5.3.1.1 System Configuration and Initial Conditions

Test performance followed an approved written test procedure. Initial conditions for Matrix Test SB10 are specified in Table 5.3.1-1. A select set of initial instruments (identified in Table 5.3.1-1) were checked on the control board prior to test implementation. The control board contained provisions to display compensated level indications to confirm initial conditions. Prior to pressurization, the accumulator levels were established by filling the tanks until a visual check showed water overflowing from the standpipe. This method ensured that accumulator levels were the same for all tests, independent of instrument indication. Additional details relative to the filling of tanks and lines are provided in Subsection 2.7.

The required break simulation piping and break instrumentation were installed according to the piping and instrumentation diagram (P&ID) (Appendix G Dwg. OSU 600904) and the break piping layouts in Figures 5.3.1-1 and 5.3.1-2. The ADS 4-1 and ADS 4-2 lines were connected and piped to the 8-in. ADS 4-1 separator. The break spool and insert that simulated a DEG break in the AP600 were installed in the balance line connecting CL-3 and CMT-1. Balance-line flow from CL-3 was directed into the break separator; the remainder of the balance line up to the CMT was connected to the 5-in. ADS 4-2 separator. A 50-percent flow nozzle was installed in ADS 4-1 on hot leg 1 (HL-1), and a 100-percent flow nozzle was installed in ADS 4-2 on HL-2 to provide the assumed single failure.

Flow nozzles that simulate two lines were installed in the ADS 1-3 nozzles. Break valve TS-202 isolated the CMT-1 side of the break. Break valve TS-203 isolated the CL-3 side of the break (Appendix G, Dwg. OSU 600904).

Liquid break flow from the cold-leg side of the break was measured by break separator liquid flow meter FMM-905. Break steam flow from the cold-leg side of the break was measured by break separator steam flow meter FVM-905 installed in the []^{a,b,c} steam line of the break separator. The []^{a,b,c} steam line from the break separator was isolated throughout the test (Dwg. OSU 600901).

Fill and vent was performed according to the approved operating procedure. Instruments were checked for required calibration.

With TS-202 and TS-203 closed, RCS-901 and RCS-902 were opened to pressurize the CMT-1 balance line. After the appropriate prerequisites were completed and the test facility reached specified initial conditions, RCS-901 and RCS-902 were closed to maintain the < 80°F initial condition at the top of CMT-1. As final valve alignments were established, the CMT discharge valves were placed in the AUTO and CLOSED position, limiting CMT-1 pressure to that obtained while the vessel was arriving at full pressure and temperature. RCS-529 and RCS-530 were placed in the OPEN and AUTO positions 1 minute after the TEST pushbutton was pressed. The CMT-1 balance line portion up to the isolation valves then came to reactor coolant system (RCS) pressure.

Testing was initiated when test facility conditions, as read from the test facility control board and local indication, agreed with specified initial conditions within acceptable tolerances. The transient continued through ADS actuation and CMT, accumulator, IRWST, and sump injection. All actions were automatic and required no operator action, except isolation of two valves: CSS-902 and CSS-906. These were simultaneously closed when total steam flow through CSS-901 was less than []^{a,b,c}. The steam flow was read on FVM-901 and FVM-902. These valves were isolated to provide more accurate discharge flow values.

Heater rod bundle power was adjusted prior to break initiation to achieve the required hot-leg temperatures. Pressurizer power was terminated 6 seconds after initiation of the break.

Table 5.3.1-1 provides a comparison of the specified and actual conditions for Matrix Test SB10. Initial conditions for the test were established and recorded in the procedure. Refer to Subsection 2.7 for pretest operations. Table 5.3.1-1 shows the initial conditions recorded from the operator's panel and the average of the same parameters for about 2 minutes prior to the break valve opening from DAS.

There were three condition parameters out of specification in Table 5.3.1-1, none of which should invalidate this test, that will be discussed here.

- HL-1 temperature (SC-141) was []^{a,b,c} percent above the required temperature band. HL-2 temperatures (SC-140) was []^{a,b,c} percent above the required temperature band. This was within the accuracy requirements of the instrumentation system.
- Accumulator levels (LDP-401 and LDP-402) exceeded the planned levels. The explanation for this situation is defined in note 3 of Table 5.3.1-1. The condition was considered acceptable because the level was set by a standpipe at 37 in.
- Accumulator-1 (ACC-1) pressure (PT-401) was []^{a,b,c} percent below the required pressure band. ACC-2 pressure (PT-402) was []^{a,b,c} percent below the required pressure band. The accumulators were pressurized to the required pressure, as indicated on PI-401 and PI-402 prior to test actuation. The loss of pressure between tank pressurization and test actuation was possibly due to cooling of the nitrogen gas in accumulator. Test analysis starting with the recorded lower accumulator and overpressure should still be possible.

The reactor heater power controller was programmed using the algorithm defined in Subsection 2.3.2 to obtain the scaled decay power heat input rate.

5.3.1.2 Inoperable Instruments

Table 5.3.1-2 is a list of instruments considered inoperable or invalid during all or portions of this test. Some of the instruments listed are on the Critical Instrument List (Subsection 3.2, Table 3.2-2) and, therefore, are addressed here.

FMM-201, FMM-202, FMM-203, and FMM-204 measured flow (gpm) in each of the four cold legs. A decision was made to continue testing without the availability of these instruments. Replacement flow meters repeatedly failed; their continued use was precluded due to cracking of the ceramic liners from thermal stratification in the loop piping. The necessary boundary conditions for loop flow could be determined from DP-202, DP-203, DP-205, and DP-206.

FMM-401 measured ACC-1 injection flow into direct vessel injection line 1 (DVI-1). After injection, the meter exhibited erroneous results due to nitrogen in line; therefore, any results after 490 seconds are invalid.

FMM-501, FMM-504, FMM-802, and FMM-804 provided accurate data when sensing liquid, but became inaccurate when sensing two-phase or steam flow.

FMM-701 measured IRWST-1 injection flow. When the primary sump valves opened, the flow meter indicated a negative flow as water flowed from the primary sump to the IRWST. The meter was not designed to measure reverse flow, so this measurement was invalid; however, total IRWST flow was measured by FMM-702.

FMM-905 measured break separator flow from the separator to the primary sump. When the primary sump level was equal to or higher than the break separator pipe connection, FMM-905 indicated a negative flow as water flowed from the primary sump to the break separator. The meter was not designed to measure reverse flow, so this measurement was invalid.

Steam generator (SG) tube level data (LDP-215, LDP-218, LDP-219, and LDP-222) were biased by vaporization of the water in the transmitter reference leg after the SG tubes started draining. However, data provide accurate indication of the time when the tubes were empty.

LDP-401 and LDP-402 measured ACC-1 and ACC-2 levels, respectively. Due to air trapped in the transmitters sense lines, data from these transmitters were invalid. The initial level of the tank, however, was established by a standpipe, so it was constant test to test. The drain rate can be calculated using FMM-401 and FMM-402, respectively. Alternately, a pressure correction may be applied directly to the level indication of LDP-401 and LDP-402.

PT-201 measured RCS pressure at the top of the SG-1 long tube. On August 15, 1994, it was discovered that the transmitter had an incorrect zero compensation which resulted in a negative error and negative data at low pressures. The transmitter zero was corrected at that time. PT-201 data obtained during Matrix Test SB19 had the zero correction performed on it; the corrected data appear as PT_201. Negative data and corrected negative data can be used to determine trends by are considered inaccurate. PT_201 data are considered unreliable for values less than []^{a,b,c} but a sufficient amount of other pressure data are available.

TF-501 and TF-504, located on the long thermocouple rod location near the bottom of each CMT, appeared to have measured ambient conditions throughout the test, which would indicate a short somewhere in the thermocouple wiring. With these thermocouples inoperable, the required long thermocouple rod thermocouple availability of seven out of ten and no more than one in succession failed was met.

LDP-802 measured PRHR HX wide-range level. The PRHR HX may have been refilling, but a more logical reason is that LDP-802 was slowly losing its reference leg due to a low saturated pressure in the HX tubes.

Data provided by ADS-4 separator instrumentation prior to the ADS 4-1 and ADS 4-2 valves opening at 745 seconds were invalid due to the closed position of the ADS-4 valves and the ADS-4 separator loop seal valves. The instruments affected were: FMM-602, FMM-603, FVM-602, FVM-603, LDP-611, AND LDP-612. Test analysis will not be affected, since ADS-4 flow did not begin until the valves opened.

Considering these critical instrument failures, sufficient instrumentation was available to allow the performance of mass balances as demonstrated in Subsection 5.3.1.6 and Appendix E. An energy

balance will be performed and reported in the *AP600 Low-Pressure Integral Systems Test at Oregon State University Test Analysis Report WCAP-14292*.⁽²⁾

5.3.1.3 Sequence of Events

The chronologic sequence of events is shown in Table 5.3.1-3. The actual time of event occurrence is listed along with the planned time of event occurrence. The table also provides the source of the actual time values. A D in the Data Source column indicates the recorded time was obtained from a software program that monitored digital events in the plant, including pump starts and stops, valve limit switch actuations, and alarms. An A in the Data Source column indicates the time was obtained by reviewing data from the data acquisition system (DAS). Although data from the DAS are digital, analog events such as pressure, flow, and temperature were monitored.

Tables 5.3.1-3 also depicts a bar graph representation of the sequence of events for Matrix Test SB10 sorted in chronologic order to provide a quick visual reference of the timing of events. The results of this timing will be described in more detail in the following sections.

5.3.1.4 Test Results and Evaluation

This section contains an overall description of the events that occurred during Matrix Test SB10, including references to specific instrumentation channels cross-plotted and used in the test results evaluation.

The simulated loss-of-coolant accident (LOCA) event resulted in interactions between different systems and simulated components in the facility. For this reason, the event was subdivided into the following three phases to characterize the system's thermal-hydraulic phenomena and component effects.

- Initial Depressurization Phase: simulated break initiation to ADS-1 actuation
- ADS Phase: ADS-1 actuation to start of IRWST injection
- IRWST Injection Phase: start of IRWST injection to end of test

The behavior of specific components is discussed in Subsection 5.3.1.5.

Initial Depressurization Phase

Prior to initiation of the event, all applicable systems achieved normal operating conditions and initial boundary conditions, as described in Subsection 5.3.1.1. Time zero represents when the signal to open was sent to break valves TS-202 and TS-203.

The DEG break flow arrangement was initially monitored by two sets of instruments. Set one was composed of DP-215 and PT-203. Set two was composed of DP-216 and PT-206. Immediately following the opening of the break valve, subcooled liquid flowed from the cold leg to the break

separator, and, as a result, RCS pressure decreased (Figures 5.3.1-3 and 5.3.1-4). Differential pressure indicated (DP-216) a lower pressure than the full reactor pressure due to a delay in opening the warming lines, as described in Subsection 5.3.1.1. The reactor and downcomer levels reflected the drop in core water inventory through the break (Figures 5.3.1-5 and 5.3.1-6). The reactor level (LDP-127) dropped immediately following the break opening, whereas the level in the downcomer (LDP-116 and LDP-140) remained constant from []^{a,b,c} (Figure 5.3.1-5). The reactor level fell to its minimum level at []^{a,b,c} (LDP-113; Figure 5.3.1-6), whereas the downcomer level dropped about []^{a,b,c} from a full condition (LDP-116; Figure 5.3.1-5).

The upper head and upper portion of the upper plenum started to void immediately after the reactor coolant pumps (RCPs) tripped. The plenum voided more rapidly than the upper head because the upper head fluid was separated from the upper plenum by the upper support plate. Fluid could only exit the upper head to the downcomer via []^{a,b,c} bypass holes in the upper flange of the core barrel or by gravity-drain to the upper plenum via eight holes in the upper support plate.

One-half second after the signal to open the break valves, an S signal was generated, causing the following planned events to occur during the first []^{a,b,c} after the break signal: the pressurizer heater breaker was manually opened at []^{a,b,c} the feedwater pumps tripped at []^{a,b,c} the CMT-1 and CMT-2 outlet valves opened at []^{a,b,c} the passive residual heat removal heat exchanger (PRHR HX) outlet valve opened at []^{a,b,c} and the RCPs tripped at []^{a,b,c}. Liquid from the pressurizer (LDP-601) and CMT-2, injected into the reactor as the reactor depressurized (Figures 5.3.1-7 and 5.3.1-8). Depressurization in the reactor vessel and pressurizer occurred at the same rate (Figures 5.3.1-9 and 5.3.1-10) as a result of the decrease in liquid inventory and the flashing that occurred during the break.

Core heater groups 1 and 2 provided a total initial input of 600 kW up to []^{a,b,c} KW-102 and KW-104 (group 2) indicated a sharp drop for 8 seconds immediately preceding the break initiation point, however, this momentary drop in indicated power did not show any adverse effects on the overall decay heat profile. At []^{a,b,c} the heater controller continued to follow the scaled power decay rate for the remainder of the transient. The decay power curves appear in Appendix F. The total power comparison results indicated excellent agreement between planned decay rates and measured values. The pressurizer heater breakers were manually opened by the operators after verifying the S signal, the break valves opened, and pressurizer heater power (KW-601) changed from 1.5 to 0.0 kW.

In []^{a,b,c} the pressurizer level had dropped to a zero level, and the core and downcomer levels continued to drop due to the large inventory loss from the DEG break and slower rate of injection (Figure 5.3.1-7). CMT-2 responded rapidly by injecting its inventory into the DVI line upon opening its isolation valve at []^{a,b,c} after break initiation (Figure 5.3.1-8). As the CMT-2 began discharging, natural circulation started to replace inventory in CMT-2 from CL-1. A CMT-2 injection flow rate of []^{a,b,c} continued until about []^{a,b,c} when the level in the balance line fell, allowing CMT-2 flow to increase to []^{a,b,c} (Figure 5.3.1-11). At about

[]^{a,b,c} when the reactor pressure dropped to []^{a,b,c} ACC-1 and ACC-2 injected to the downcomer through the DVI lines because pressure in the accumulators exceeded reactor pressure. Reactor depressurization occurred at such a high rate that the accumulators injected prior to ADS-1 actuation. The ADS-1 actuation sequence was controlled by the CMT low-level indication ([]^{a,b,c} for OSU) plus a []^{a,b,c} delay. Injection by the accumulators slowed the injection flow rate from CMT-2 (Figure 5.3.1-11) due to the higher localized pressure at the junction of the CMT-2 and DVI lines. The higher localized pressure effect actually slowed and suspended CMT flow, as flow from CMT-2 dropped from []^{a,b,c} and remained at []^{a,b,c} until accumulator injection decreased from peak flow. This suspension of CMT flow was coincident to the combined ACC-1 and ACC-2 injection approach of peak injection rates. CMT-1 showed no change in level because the break occurred on the horizontal section of the balance line before the top of CMT-1, leaving the top of CMT-1 at atmospheric pressure. CMT-1 injection flow was precluded because pressure in the DVI line was higher than the head of water in CMT-1.

Subcooled liquid flow through the PRHR HX began []^{a,b,c} after the break valves opened and a natural circulation mode was established. The flow rates appear in Figure 5.3.1-12. The initial flow spikes, (FMM-804) were due to the opening of valve RCS-804. FMM-802 continued to show high flow-rate spikes (over-range values) from []^{a,b,c} because two-phase flow entered the PRHR HX at about []^{a,b,c} as the hot legs began to drain. Magnetic flow meters used at OSU did not provide accurate indications during two-phase or reverse flow conditions; therefore, indicated flow-rate values from FMM-802 during these periods are not accurate. However, the PRHR HX outlet flow rate, though erratic at times, is correct, since steam entering the PRHR HX was condensed and TF-804 reflected subcooled water ([]^{a,b,c}) being returned to the cold-leg channel head of SG-2 (Figure 5.3.1-68).

As the reactor vessel and pressurizer continued to depressurize and their levels dropped, pressure and liquid levels in the RCS legs dropped. Due to rapid depressurization in the core and upper plenum, fluid in the upper plenum flashed while the fluid level in the upper plenum dropped to the hot-leg elevation. The cold-leg levels dropped to zero (LDP-201 through LDP-204) just before the hot legs started to drain (LDP-205 and LDP-206; Figures 5.3.1-13 and 5.3.1-14). Both the cold-leg and hot-leg levels began to drop at about []^{a,b,c} and reached []^{a,b,c}. The level in the HL-1 elbow (LDP-207) was incorrectly ranged, did not provide accurate values, was inconsistent with other data (e.g., LDP-206), and was subject to high flow due to draining of SG-2 and the pressurizer (Figure 5.3.1-14). As the hot legs drained, this volume was replaced with two-phase fluid, and the HL-1 fluid had a void fraction very close to that shown in the upper plenum (Figure 5.3.1-64). The void fraction in HL-2 was only slightly lower due to the selective removal of vapor from the hot leg by the PRHR HX inlet line.

Using data from the level channels and the calibrated range of the instruments, a core steam percent for each channel was calculated. The equation used to calculate steam percent was:

$$\text{Steam percent} = \left(1 - \frac{\text{compensated level}}{\text{instrument range}}\right) 100$$

In []^{a,b,c} of the break opening, the primary side of SG-1 showed a rapid drop in level (Figure 5.3.1-16). The SG-1 level decrease continued until []^{a,b,c} when LDP-211 and LDP-213 indicated a drop to zero level (Figure 5.3.1-17). The level in the SG-1 hot-leg channel head (LDP-209) was incorrectly ranged and did not provide accurate values. LDP-207 and LDP-209 were considered inoperable for this test. As the primary-side pressure dropped, any remaining SG water was transformed into superheated steam (Figure 5.3.1-19), indicated by thermocouples in the tubes remaining well above the saturation temperature. A parameter identified as TSAT was included in this report to represent the saturation temperature as a function of reactor pressure (PT-107). Figure 5.3.1-16 presents the indication of a rapid drop in U-tube levels (from []^{a,b,c}) followed by an indication of a rapid increase in level (suggesting a refill of the SG U-tubes from []^{a,b,c}). This indicated that refill did not occur, because both the cold and hot legs were drained before []^{a,b,c} and the SG U-tube levels were drained at []^{a,b,c} when DP-211 and DP-212 dropped to 0 after a positive differential pressure (flow) indication (Figure 5.3.1-18). Once the SG U-tubes drained, they did not refill during the remainder of the test. This false indication was due to the arrangement of LDP reference legs, as described in Subsection 2.4.1. The response described previously for SG-1 is consistent for SG-2.

Voiding in the hot legs resulted in draining in the SG U-tubes and subsequent draining of the SG channel heads (LDP-211 and LDP-213; Figure 5.3.1-17). The connection from hot-leg to cold-leg sides was broken in SG-1 about []^{a,b,c} after the break. About []^{a,b,c} later, the recirculation mode ended and draindown of the U-tubes started in SG-2 (DP-211 and DP-212; Figure 5.3.1-18). From []^{a,b,c} DP-211 and DP-212 indicated a differential pressure of about []^{a,b,c} of water. After RCP trip, DP-211 and DP-212 showed 0 differential pressure, as expected, and a very short duration of natural circulation occurred from []^{a,b,c}. As the SGs drained, the levels dropped, and a positive differential pressure existed from []^{a,b,c} reflecting drainage of the cold-leg sides of the SGs. The cold-leg sides drained about []^{a,b,c} ahead of the hot legs. When DP-211 indicated []^{a,b,c} drain flow ended, and the U-tubes were drained for SG-1. SG-2 drained at about []^{a,b,c} based on indications from DP-212 (Figure 5.3.1-18).

During initial depressurization of the primary loop, secondary-side pressures increased, but primary pressure decreased (Figure 5.3.1-20). The initial differential pressure (primary pressure > secondary pressure) reflected heat transfer from the primary to the secondary side. The primary and secondary pressures approached a common pressure of []^{a,b,c}. This common-pressure period lasted []^{a,b,c}. At about []^{a,b,c} the primary and secondary pressures

diverged (primary pressure < secondary pressure), allowing the secondary side to transfer heat into the primary side via the SG U-tubes. Heat transfer to the primary side combined with drainage of the SGs caused superheating in the SG U-tubes. The U-tubes remained at superheated conditions for the rest of the test (Figure 5.3.1-19) due to the slow decay of SG pressure and energy in the secondary side.

A comparison of fluid temperatures from the primary side of the U-tubes to the bulk fluid temperatures on the secondary side of the SGs is provided in Figure 5.3.1-21. Both primary-side (SG-1 and SG-2 short and long tube thermocouples) and secondary-side (SG-1 and SG-2 downcomer thermocouples) temperatures reached a common value of []^{a,b,c}. During this same time, primary- and secondary-side pressures reached a common pressure of about []^{a,b,c} defined as the pressure plateau. As the reactor continued to depressurize, primary temperatures diverged from saturated conditions, as indicated by the TSAT parameter (Figure 5.3.1-21). The temperature difference between the primary-side and to secondary-side thermocouples indicated that the secondary side was transferring heat to the primary-side and keeping the primary-side U-tubes superheated.

From break initiation to about []^{a,b,c} a natural circulation flow developed from CL-1 to CMT-2 (FMM-502). The CMT-2 level remained stable (LDP-502; Figure 5.3.1-8). At about []^{a,b,c} the natural circulation mode ended and the draindown mode started in the CMT-2 balance line, as indicated when flow through FMM-502 dropped to zero and the CL-1/CMT-2 balance line level suddenly dropped. When the transition from recirculation to draindown mode occurred in the CMT-2 balance line, the following resulted. First, the level in the CMT decreased because the liquid draining into the core was no longer being replaced by water from CL-1 (Figure 5.3.1-8). Second, the CMT-2 balance line level decreased as the region in the upper portion of the balance leg voided. The CMT-2 balance line emptied at about []^{a,b,c} (Figure 5.3.1-8). Third, CMT-2 injection flow to the vessel increased from []^{a,b,c} (Figure 5.3.1-11).

As the system continued to depressurize beyond []^{a,b,c} CMT-2 continued to drain to the reactor vessel at a slower rate due to the injection of ACC-1 and ACC-2. LDP-502 in Figure 5.3.1-8 and FMM-504 in Figure 5.3.1-11 indicate that, as accumulator injection increased localized pressure at the DVI line junction, the CMT-2 flow rate was reduced, and CMT-2 injection was suspended from []^{a,b,c}. Once accumulator injection was completed, as indicated by ACC-2 injection flow rate, flow from CMT-2 returned at a rate of about []^{a,b,c}.

At []^{a,b,c} CMT-2 had drained to the low level setpoint, and a 15-second delay timer automatically actuated before the ADS-1 valve opened. At this time, reactor pressure was []^{a,b,c} and the vessel level had already reached its lowest point of []^{a,b,c} (Figure 5.3.1-5). The vessel level increased due to accumulator injection but both the hot legs and cold legs were drained. Both the upper head and the upper portion of the downcomer were superheated (Figure 5.3.1-22). Figures 5.3.1-23 and 5.3.1-24 indicate that saturated steam was occupying the hot legs even though they began draining after []^{a,b,c}. Superheated steam continued to exist in the SG tubes, since the SGs acted as heat sources; secondary pressure and temperatures remained high with little heat loss (Figures 5.3.1-20 and 5.3.1-21).

ADS Phase

The purpose of the ADS is to depressurize the RCS to allow injection of the accumulators at intermediate pressure and to allow injection of the IRWST at low pressure for long-term cooling.

Depressurization is first accomplished by an inventory loss through three parallel valves: ADS-1, ADS-2, and ADS-3. These valves open in sequence after one of the CMTs reaches a low level setpoint, providing a flow path from the top of the pressurizer, through the ADS 1-3 separator, to the ADS 1-3 sparger located in the IRWST. (Dwg. OSU 600203). Opening of the ADS 4-1 and ADS 4-2 valves occurs when either CMT reaches its low-low level setpoint. The ADS-4 valves provide the final depressurization of the RCS by supplying a flow path from the hot legs to the primary sump via the ADS 4-1 and 4-2 separators.

The ADS period was initiated []^{a,b,c} after the break with the opening of the ADS-1 valve. ADS-1 flow was indicated by a transmitter measuring differential pressure due to flow (FDP-605). FDPs were located upstream of each of the ADS valves to measure flow through the valves. The opening of ADS-2 and ADS-3 valves occurred in the next []^{a,b,c} (FDP-604 and FDP-606; Figure 5.3.1-25). The ADS-1 valve opening resulted in a peak differential pressure of []^{a,b,c} after []^{a,b,c}. Superheated steam remaining in the pressurizer (TF-602 and TF-605; Figure 5.3.1-63) was released to the ADS 1-3 separator where the steam was allowed to separate and was measured by a vortex flow meter (FVM-601). Water was measured by a magnetic flow meter (FMM 601) prior to injection/discharge into the IRWST via the sparger dispersion tube (Figures 5.3.1-26 and 5.3.1-27). Once these ADS valves opened, they remained open throughout the remainder of the transient. The ADS-2 valve opened at []^{a,b,c} with a differential peak pressure of []^{a,b,c} occurring []^{a,b,c} after opening. The peak differential pressure decreased rapidly to about []^{a,b,c}. The ADS-1 and ADS-2 valve openings reduced RCS pressure from []^{a,b,c} over a []^{a,b,c} period. ADS actuation increased the rate of primary system depressurization, as measured by reactor upper head pressure (Figure 5.3.1-9), and resulted in a higher injection flow ([]^{a,b,c} to about []^{a,b,c} peak) from the accumulators (FMM-401 and FMM-402; Figure 5.3.1-11). ADS actuation forced flow from the bottom of the pressurizer to the top and out through a single line to the ADS valves, through the ADS 1-3 separator, and into the IRWST via the sparger. Steam flow through the pressurizer caused the pressurizer wide-range level and the pressurizer surge-line level (Figure 5.3.1-7) to indicate a false-high signal due to momentum effects.

When the ADS-1 valve opened (Table 5.3.1-3), the pressurizer surge line and the pressurizer initially became filled with a two-phase mixture. This sudden surge of flow through the pressurizer was reflected in the rapid increase in surge line and pressurizer wide-range level indications. LDPs indicate accurate level values in steady-state or nonflowing conditions; LDP-601 and LDP-602 measurements during ADS-1 actuation include the differential pressure due to flow. The increased injection flow of the accumulators and CMT-2 caused a high influx of liquid flow through the reactor. From []^{a,b,c} the surge line and pressurizer became partially filled with steam and

liquid consistent with the accumulator injection period, to the extent that liquid flow was measured from the ADS 1-3 separator (Figure 5.3.1-27). As steam flow ended at []^{a,b,c} (end of accumulator injection), liquid flow through the ADS 1-3 separator decreased from []^{a,b,c} over []^{a,b,c}. During this period, the pressurizer was filled with []^{a,b,c} percent steam and []^{a,b,c} percent liquid supported by an []^{a,b,c} percent steam vapor in the surge line (Figure 5.3.1-65). At about []^{a,b,c} the ADS-4 valves opened, causing a rapid decrease in vessel pressure and, subsequently, permitting slow draindown of the pressurizer into the hot legs. At about []^{a,b,c} the pressurizer emptied and the surge line was filled to a []^{a,b,c} level. A more detailed explanation of flow conditions in the pressurizer is provided in the pressurizer components description of Subsection 5.3.1.3.

Rapid injection of cold water from the accumulators (at []^{a,b,c} into the event) subcooled the upper region of the downcomer annulus (which contained some superheated fluid, measured by TF-168, until the accumulators injected) and continued the temporary refill of the core region to the top of the DVI line (Figures 5.3.1-22 and 5.3.1-5). The combined opening of the ADS-1 and ADS-2 valves and the accumulators' injection caused the collapse of the steam bubble at the top of the downcomer []^{a,b,c} after the break. Collapse of the steam bubble caused a differential pressure across the bypass plate, superheated steam in the upper head, and saturated steam or subcooled liquid in the downcomer. To compensate for this sudden imbalance, a backflow occurred, as reflected in the sharp temperature decrease from []^{a,b,c} at []^{a,b,c} (TF-120; Figure 5.3.1-22). This condensation event is also reflected in rapid changes in thermocouple TF-168 (Figure 5.3.1-22) and differential pressure transmitters DP-114 and DP-130 (Figure 5.3.1-28).

Figures 5.3.1-28 and 5.3.1-29 provide comparison plots of the differential pressure values across the upper support plate (DP-114), and between the upper head and downcomer (DP-130). These differential pressure changes reflected rapid steam condensation events in which the subcooled water entered the downcomer region from the DVI, and immediately condensed the superheated steam in the downcomer, causing a large decrease in pressure and differential pressure, causing a flow reversal in the downcomer region. Fluid from the core and downcomer regions reversed and rapidly filled the downcomer to the upper head bypass plate. TF-168 was located in the downcomer above the cold-leg elevation and aligned at 270°az in line above HL-2 (Appendix H). Thermocouple TF-168 was used to help confirm such condensation events. Shortly after the event took place, the top of the reactor returned to superheated conditions. This generic condensation event was studied and is explained in more detail in Subsection 7.1.

The rapid decrease in reactor pressure due to ADS-2 actuation resulted in a sharp increase in the accumulator injection rate over the period of []^{a,b,c} (Figure 5.3.1-11). During the ADS-2 actuation period, the peak total injection flow occurred based on the combined sources of the CMT-2, ACC-1, and ACC-2, as measured at the DVI lines. DVI flows were monitored by flow meters FMM-205 and FMM-206 for DVI-1 and DVI-2 lines, respectively (Figure 5.3.1-30). The peak injection flow rate of []^{a,b,c} per side occurred at []^{a,b,c} after ADS-2 valve opening. The fluid inventory in the reactor core region recovered to a level slightly above the bottom of the hot

legs, superheated steam occupied the upper head, and saturated steam filled the hot legs and cold legs. Stored energy of the SG continued to provide heat into the primary system via the SG U-tubes and maintained the superheated steam in the U-tubes of both SGs.

When reactor pressure decreased to []^{a,b,c} at []^{a,b,c} the signal to open RCS-711 and RCS-712 was automatically initiated. The two parallel IRWST injection lines contained a set of check valves to preclude backflow from the RCS to the IRWST. These check valves (RCS-713 and RCS-715 in line with FMM-701, and RCS-714 and RCS-716 in line with FMM-702) permitted injection into the DVI line when reactor pressure decreased to the equivalent of the IRWST liquid head. Based on the design configuration described previously, IRWST injection can occur without operator or automatic actuation once valves RCS-711 and RCS-712 open.

At []^{a,b,c} when RCS pressure was []^{a,b,c} the opening of the ADS-3 valve caused the continued decrease in RCS pressure. The primary portion of the accumulators' injection continued through []^{a,b,c}. As the accumulator-injection surge was completed, CMT-2 injection flow resumed at a peak flow rate of []^{a,b,c} however, the core and downcomer liquid levels decreased due to the decreased flow (Figures 5.3.1-11 and 5.3.1-5). At []^{a,b,c} the CMT-2 level was about []^{a,b,c}. ADS-4 valves opened when the level in at least one of the CMTs dropped to the CMT low-low limit ([]^{a,b,c}) and at least []^{a,b,c} had passed since one of the CMT levels dropped to the low level setpoint of []^{a,b,c}. This criteria was achieved at []^{a,b,c} when the liquid level in CMT-2 decreased to []^{a,b,c}.

At []^{a,b,c} both ADS-4 valves were open, directing flow to the ADS 4-1 separator to be separated and measured by FVM-603 and FMM-603 (Figures 5.3.1-26 and 5.3.1-27). Saturated liquid from the ADS-4 lines was then discharged into the primary sump. Also at []^{a,b,c} the pressurizer liquid level indicated a significant decrease, and discharge through the ADS 1-3 valves ended (Figures 5.3.1-7 and 5.3.1-27). FMM-603 indicated that, as the ADS-4 valves opened, flow through the ADS 4-1 separator was initiated and gradually increased to a peak flow rate of about []^{a,b,c} at about []^{a,b,c} (Figure 5.3.1-27).

IRWST Injection Phase

The IRWST injection phase began when RCS pressure decreased to the pressure corresponding to the water elevation of the IRWST. IRWST flow entered the DVI lines through DVI-1 and DVI-2 beginning at []^{a,b,c} respectively (FMM-701 and FMM-702; Figure 5.3.1-31). IRWST injection flow steadily increased from an average flow rate of []^{a,b,c} to a peak IRWST flow rate of []^{a,b,c} per side at []^{a,b,c}.

At []^{a,b,c} the CMT-2 level was about []^{a,b,c} and CMT-2 injection flow was []^{a,b,c}. All injection flow from the accumulators had terminated; the accumulators had injected their water inventory. CMT-1 was full with subcooled water (< 80°F) at atmospheric pressure. Because the balance line was broken, CMT-1 was unable to inject until the pressure at the junction of the CMT-1

outlet and DVI-1 lines was below the liquid head level of CMT-1. CMT-1 flow through DVI-1 began at []^{a,b,c} (FMM-501; Figure 5.3.1-11). CMT-1 liquid injection flow was confirmed when the CMT-1 level decreased (LDP-507; Figure 5.3.1-8). The CMT-1 balance line level (LDP-509) was over-ranged and does not accurately indicate the level; the break was in this line and the LDP was measuring the differential pressure between the RCS and the atmosphere (open side of the break). Therefore, this level can not be used as an indication of level in the CMT balance line. After peak IRWST injection flow was achieved at []^{a,b,c} flow continued to decrease slowly based on the IRWST head.

As IRWST and CMT-1 injection continued, both the downcomer liquid level and the core liquid level increased (Figure 5.3.1-5). At []^{a,b,c} vessel and downcomer collapsed liquid levels appeared to be equal. Figure 5.3.1-22 shows that, at []^{a,b,c} based on the sharp temperature excursions, a third localized steam bubble collapse occurred. The upper head remained filled with superheated steam (TF-120 and TF-171; Figure 5.3.1-32). The outlet plenum contained saturated steam and liquid, as measured by TF-169 (upper reactor fluid temperature at 90 degrees orientation) and TF-170 (upper reactor fluid temperature at 270 degrees orientation) (Figure 5.3.1-32). Bulk fluid temperature in the core region remained at the saturated temperature or subcooled throughout the transient (TR-001; Figure 5.3.1-33). During early depressurization, little temperature variation occurred across the rod bundle. Injection from the CMT-2, accumulators, and IRWST had not only cooled the core but contributed to a temperature gradient in the core. At []^{a,b,c} a []^{a,b,c} temperature gradient across the heater rod bundle was created and maintained until about []^{a,b,c}

Also during this period, the pressurizer remained filled with both saturated steam and liquid, with no indicated flow through the pressurizer or flow out of the ADS 1-3 valves. The SG U-tubes remained filled with superheated steam that decreased in temperature from about []^{a,b,c}. The PRHR HX continued to condense saturated steam from HL-2 and returned an indicated flow of []^{a,b,c} of []^{a,b,c} water to the bottom of the cold-leg plenum of SG-2 (Figure 5.3.1-12).

The ADS-4 valves' opening caused the continued decrease in RCS pressure and allowed the IRWST to inject. Liquid levels in both the downcomer and core regions increased to the point where both the hot and cold legs refilled with liquid inventory due to IRWST injection. At about []^{a,b,c} the downcomer level was []^{a,b,c} (LDP-116 and LDP-140; Figure 5.3.1-5); however, the core collapsed liquid level was []^{a,b,c} (LDP-127; Figure 5.3.1-5). As IRWST and CMT-1 injection continued, the downcomer level became stable at about []^{a,b,c} and, at about []^{a,b,c} the core collapsed liquid level (LDP-127) reached a level to refill the hot legs.

The hot legs filled at about []^{a,b,c} when a drop in HL-1 and HL-2 temperatures was indicated (Figures 5.3.1-23 and 5.3.1-24).

Temperatures in the cold legs confirmed that the cold legs were beginning to refill. Beginning at about []^{a,b,c} cold-leg bottom temperatures (measured by CL-1, CL-2, CL-3, and CL-4 at

the reactor flange bottom) dropped from superheated to saturated conditions (Figures 5.3.1-34 to 5.3.1-37). Once the cold legs reached a full condition (about []^{a,b,c}), the cold-leg top temperatures (SC-105, SC-106, SC-101, and SC-102) exhibited a constant temperature. A temperature gradient existed from the top to the bottom of the cold-leg pipes (Figures 5.3.1-34 to 5.3.1-37). The hot-leg temperature became subcooled at about []^{a,b,c} suggesting a full condition (Figures 5.3.1-23 and 5.3.1-24).

Refilling the cold legs with liquid covered the CMT-2 balance line opening. As the CMT-2 balance line partially filled, the level in the balance line increased (LDP-510; Figure 5.3.1-8). Refill of CMT-2 continued until a level of []^{a,b,c} was reached at []^{a,b,c}. As CMT-2 refilled, no flow was discharged. Figure 5.3.1-8 shows the liquid level of CMT-1 to the break (LDP-507 and LDP-509). The CMT-1 balance line level (LDP-509) was not responding as an LDP due to high flow through the break. Pressure in the variable leg was higher than the reference leg and was not providing a true level indication; therefore, data from this channel (LDP-509) should not be used.

IRWST and CMT-1 injection continued at a slowly decreasing rate with a total combined flow of []^{a,b,c} at []^{a,b,c} (FMM-205 and FMM-206) with the majority of this flow coming from the IRWST (Figure 5.3.1-30). At []^{a,b,c} CMT-2 refilled to a level of []^{a,b,c} and remained full until about []^{a,b,c}. At []^{a,b,c} after the break event, flow from CMT-2 entered the DVI line (FMM-504; Figure 5.3.1-38). The effect of draindown on the CMT-2 liquid level, as measured by LDP-502, is shown in Figure 5.3.1-39. Figure 5.3.1-39 also shows the continued draindown of CMT-1 (LDP-507) until about []^{a,b,c} when CMT-1 emptied. CMT-2 emptied at []^{a,b,c}.

During the period from []^{a,b,c} the downcomer region reached a maximum over-ranged liquid level of []^{a,b,c} and the core reached a maximum liquid level of []^{a,b,c} which is about at the []^{a,b,c} (Figure 5.3.1-40). Both levels decreased after []^{a,b,c} as flow exiting through the ADS-4 valves (FMM-603; Figure 5.3.1-45), to the primary sump slightly exceeded combined injection flow from the IRWST and CMTs, as measured by the sum of FMM-205 and FMM-206 (Figure 5.3.1-41).

With the core heaters still generating heat and with little flow out of the vessel, the bulk core liquid temperature increased from subcooled (average temperature of []^{a,b,c}) so that the top layers of the core became saturated at []^{a,b,c} (TR-001-8; Figure 5.3.1-46).

Superheated steam continued to exist in the upper head; however, the temperature decreased from []^{a,b,c} (Figure 5.3.1-42). Beginning at about []^{a,b,c} temperatures in both the cold and hot legs increased from subcooled ([]^{a,b,c}) and approached a steady-state saturated temperature of []^{a,b,c} (Figures 5.3.1-82 and 5.3.1-84). It should be noted that the saturated temperature at local pressure TSAT value was calculated based on PT-107. For Matrix Test SB10, the PT-107 value had a slight zero offset causing a minimum value indication of []^{a,b,c} where the saturated temperature should not be lower than 212°F. It is not clear when the

zero affect occurred in the transient; therefore, a correction was not applied to the PT-107 data. Also during this period, the liquid level in the upper head drained to a level just below the upper support plate. This draindown was indicated by a sharp increase in temperature measured by thermocouple TF-171. Thermocouple TF-171, located directly above the upper support plate, indicated a superheated temperature of []^{a,b,c} (Figure 5.3.1-42). The top of the downcomer annulus also voided and filled with superheated steam, as indicated by the temperature increase to []^{a,b,c} (TF-168; Figure 5.3.1-44). An oscillation was seen beginning at []^{a,b,c} (FMM-603; Figure 5.3.1-45 and FMM-701 and FMM-702; Figure 5.3.1-43). These oscillations may be due to repeated momentary relief of steam buildup in the upper head or SG through the hot legs and ADS-4 valves since all other vent paths were filled with saturated liquid (e.g., cold legs). The U-tube thermocouples in the SGs continued to indicate []^{a,b,c} superheated steam at []^{a,b,c}. These tubes were superheated for the remainder of the test ([]^{a,b,c}).

At []^{a,b,c} pressure in the DVI lines was less than pressure corresponding to the water elevation of the primary sump. Flow from the primary sump (FMM-901 and FMM-902) entered the DVI line (Figure 5.3.1-43). Flow was initially limited through the double-check valve arrangement (see valves CSS-921 through CSS-924, Dwg. OSU 600206). At []^{a,b,c} when the IRWST reached the low-low setpoint, the programmable logic controller (PLC) automatically opened CSS-909 and CSS-910, which allowed the flow rate to increase to a total combined peak flow rate of []^{a,b,c} (FMM-901 and FMM-902; Figure 5.3.1-43). However, FMM-702 indicated a continuing flow of []^{a,b,c} and FMM-701 indicated a negative or zero flow at the same time (Figure 5.3.1-43). A comparison of flows measured by FMM-205 and FMM-206, which represent total flow in the DVI lines, indicated a total combined flow of []^{a,b,c} from each line (Figure 5.3.1-41). Therefore, the indicated negative value for FMM-701 represented a reverse-flow condition in which flow from the primary sump entered the IRWST. As previously discussed, magnetic flow meters used at OSU cannot measure reverse flow and will read negative if the flow is in the reverse direction of the normal flow path. This accounts for the negative flow value for FMM-701; however, the negative value does not reflect an accurate measure of reverse flow.

Liquid levels in both the downcomer and the core fell until about []^{a,b,c}. The downcomer levels (LDP-116 and LDP-140) stabilized with the cold leg at an elevation of []^{a,b,c} (cold-leg centerline), and the hot legs drained (LDP-127) with an elevation of []^{a,b,c}. The level in the hot legs cannot be directly confirmed by the temperatures in the hot legs, cold legs, upper head, and downcomer (Figures 5.3.1-44, 5.3.1-82, and 5.3.1-84) because all of the temperatures were just above the saturation temperature.

At about []^{a,b,c} the system reached an equilibrium condition with the fluid temperature in the core, downcomer, upper head, cold legs, and hot legs at between []^{a,b,c} and the primary sump injection mode in progress. The primary sump injection mode occurred when an equal volume of liquid was discharged through the ADS-4 valves, then returned to the vessel through the DVI lines (Figures 5.3.1-43 and 5.3.1-45). At this time, []^{a,b,c} of flow exited through the ADS-4

valves to the primary sump (FMM-603; Figure 5.3.1-45). An equivalent combined flow of []^{a,b,c} was returned by the primary sump drain valves to the DVI line (FMM-901 and FMM-902; Figures 5.3.1-41 and 5.3.1-43). The test was terminated after at least 2 hours of stable sump injection was achieved.

5.3.1.3 Component Responses

Reactor

Discussion of reactor response includes the regions: reactor core, upper plenum, upper head, and downcomer annulus. The regions will be discussed in this order. Level response of the downcomer annulus was measured by two wide-range and several narrow-range level transmitters (Figure H-2). Wide-range channels were positioned 90 degrees from one another. Data from these two channels were in excellent agreement. Both channels were also in agreement with their associated narrow-range channels.

When the TEST pushbutton was pressed, the reactor controller was in auto-local, controlling hot-leg average temperature at 420°F (the reactor controller automatically controls that temperature by varying the demand signal to the heaters). At time zero, the programmable logic controller (PLC) sent a signal to open the break valve and then 0.5 second later signaled the reactor controller to shift control to auto-remote with total power demand initially at 600 kW (the setpoint is generated by an algorithm programmed into the controller, and the controller automatically controls the demand to the heaters to control the setpoint kW). The power algorithm programs full power (600 kW) for the first 140 seconds and then lets power decay at an exponential rate that simulates the decay heat input of the AP600 nuclear reactor following a trip from full power (Appendix F).

When the signal to open the break occurred, the S signal was initiated and system pressure dropped; however, since the coolant everywhere in the reactor vessel was at or below the saturation temperature for system pressure, no boiling or flashing occurred. []^{a,b,c} after break initiation, the RCPs tripped, and the upper head reached saturation temperature of []^{a,b,c}. As the core level and pressure dropped due to loss of inventory out the break, the entire upper head, upper plenum, and upper annulus regions reached saturation temperature (TF-120, TF-171, TF-169, and TF-168; Figures 5.3.1-22 and 5.3.1-32). At 140 seconds, heater input power was shifted from 600 kW and then let power decay at an exponential rate that simulated the decay heat input of the AP600 reactor following a trip from full power. Actual power decay curves are provided in Appendix F.

Figures 5.3.1-5 and 5.3.1-22 show the collapsed liquid levels in the core/downcomer region and the temperatures in the upper head/downcomer region, respectively, during the Matrix Test SB10 event. At []^{a,b,c} the indicated level in the core reached a minimum level, even though 100 percent of the inventory from the pressurizer, and primary sides of the SGs, and 28 percent of CMT-2 had been added. Reactor core response was evaluated using temperature data from thermocouples located in the core. Data from thermocouples mounted on a thermocouple rod at the center of the core were

used to assess axial temperature distribution. These thermocouples were given a TR designator. Data from the top thermocouple of six heater rods were used to assess radial temperature distribution at the top of the core. These thermocouples were given a TH designator (Dwg. OSU 600007 and 600008). The overall core collapsed liquid level showed that the core was covered throughout the whole event. Thermocouple rod temperatures/core-center thermocouple and heater rod temperatures showed no long-duration temperature spikes indicative of a core uncover (TR-001; Figures 5.3.1-33 and 5.3.1-46) (TH-101-4 through TH-505-4; Figures 5.3.1-47 and 5.3.1-48).

The break created a depressurization in the RCS. Temperatures at the center of the core became saturated within []^{a,b,c} of the break. As the test progressed, RCS pressure decreased as the result of the break and actuation of ADS 1-3, and ADS-4. The core cooled and maintained saturation temperature as the RCS depressurized (Figures 5.3.1-33 and 5.3.1-46). Subcooled temperatures at the bottom of the core first appeared at about []^{a,b,c} shortly after ADS-1 actuated. Up to this time, core temperatures were equal to or slightly below the saturation temperature as indicated by TSAT. At about the time of ADS-2 actuation, the rate of RCS depressurization increased significantly, resulting in a more rapid saturation temperature decrease. Core cooling continued with DVI, so the bottom of the core started to subcool.

Elevation in the core at which subcooling existed increased as the test progressed. From []^{a,b,c} TR-001-7 and TR-001-8 remained at saturated conditions (elevation []^{a,b,c} and []^{a,b,c} respectively). The remainder of the thermocouples were subcooled (Figure 5.3.1-33). Heating elements in the heater rods simulated the active fuel of the AP600. The top of the heating elements in the heater rods was located at 47 in. from the bottom of the reactor vessel. Thus, by the end of the test, fluid in the center of the core was subcooled []^{a,b,c} percent of the length of the active core (TR-001-1 through TR-001-8; Figure 5.3.1-46).

Data from the thermocouples installed in the tops of six heaters staggered radially across the core indicated that the design for a "flat" heat-flux profile was achieved in the core (Figures 5.3.1-47 and 5.3.1-48). The center heaters were generally at a temperature only []^{a,b,c} lower than the midcenter and outer heaters. The lower-center temperatures were probably due to a slightly higher flow rate through the center of the core. There were no notable temperature excursions, although spikes did occur as in the unheated thermocouple rod temperatures.

Core steam percent may be calculated by using data from three level transmitters that measure core level: LDP-109, LDP-110, and LDP-138 (Appendix H). LDP-138 is a wide-range transmitter that spanned the entire core area, from the top of the lower core plate to the bottom of the upper core plate. LDP-109 and LDP-110 are narrow-range transmitters whose summed span equals that of the wide-range transmitter. The narrow-range transmitters are mounted in the same position as LDP-138 (0°az) and share the same taps.

There is close agreement between core steam percent calculations using core level data from the wide-range (LDP-138) and narrow-range level transmitters (LDP-109 and LDP-110). LDP-108 and LDP-109

have equal spans, which together cover the same span as wide-range level transmitter LDP-138. Therefore, the sum of their calculated core steam percent should equal the calculated steam percent of wide-range channel LDP-138 (Figure 5.3.1-87).

The maximum steam percent in the core occurred at about []^{a,b,c} the same time as the minimum core level. A secondary peak steam percent occurred at the minimum downcomer level at []^{a,b,c}. From this time on, the core steam percent was constant or decreased, but never increased. In other words, core levels measured by the wide-range transmitter or either of the narrow-range transmitters never decreased after []^{a,b,c} but remained constant or increased (Figure 5.3.1-87).

In summary, the core showed indications of an increasing core steam percent immediately after the break valve opened. Temperatures in the core quickly reached saturation. Core cooling maintained temperatures at saturation as the RCS depressurized and lowered saturation temperature. Maximum core steam percentage are occurred after ADS-1 actuation and at the same time as minimum core level. At maximum core steam percentage and throughout the test, there were no excursions of temperature from either the heated or unheated rod thermocouples. The bottom of the core started cooling at the time of ADS-2 actuation and remained subcooled.

The upper head and the upper plenum are separated by the upper support plate. Both the upper plenum and upper head began to drain immediately after the break. The upper plenum reached its minimum level at []^{a,b,c} about the same time as the maximum core steam percent (Figure 5.3.1-87). The upper head took longer to void (about []^{a,b,c}) because of its restrictive flow. In order to empty, the upper head had to gravity-drain either through holes in the upper support plate to the upper plenum and/or through bypass holes in the core barrel flange to the downcomer. The flow paths were sufficiently restrictive to delay the upper head void well past the time that the upper plenum reached its minimum level.

Differential pressure across the upper support plate and the flow bypass holes was monitored by DP-114 and DP-130, respectively (Dwg. OSU 600101). A positive value of differential pressure indicates that flow is moving in the direction of flow during normal operation before the RCPs trip. When the pumps were running, flow was from the downcomer, through the bypass holes into the upper head, continuing from the upper head into the upper plenum via holes in the upper support plate. A negative value for differential pressure indicates that flow is reversed from this description.

The direction of flow into and out of the upper head was indicated by data from DP-114 and DP-130 (Figures 5.3.1-28 and 5.3.1-29). At the time of the break, differential pressure across the bypass holes was []^{a,b,c} and differential pressure across the upper support plate was []^{a,b,c}. Thus, the flow was per design, from the downcomer to the upper plenum. At []^{a,b,c} flow reversed, and both differential pressures were negative. This flow reversal was due to the pressurization of the reactor core barrel above the downcomer pressure.

Differential pressure across the bypass holes remained negative for the remainder of the test. After []^{a,b,c} flow was always from the upper head into the downcomer annulus (Figures 5.3.1-28 and 5.3.1-29). By the time the upper head emptied at about []^{a,b,c} differential pressures across the bypass holes and upper support plate were at their first maximum negative value. A second maximum negative differential pressure occurred following ADS-4 opening. Both differential pressures steadily decreased in magnitude as the steam-flow rate to the downcomer decayed.

Note: Data for differential pressure across the bypass holes given by DP-130 must be reduced by a value between []^{a,b,c}. The magnitude of the correction factor is a function of water level in the upper head above the reference leg tap for DP-130. The variable leg tap for DP-130 is located in the downcomer. When this tap is uncovered, the correction factor for DP-130 is []^{a,b,c}. This unusual correction factor is a result of mounting a differential pressure transmitter in a vertical position while measuring differential pressure in a column that does not stay full of water. A similar correction applies to DP-114; however, the correction factor is []^{a,b,c} of water. The full explanation for this correction factor is given in Subsection 2.4.

Note: Data from DP-114 and DP-130 provide a method to check the validity of data from LDP-116, LDP-140, and LDP-127. The method to use DP-130 and DP-114 as data verifiers can be found in Subsection 2.4.

Both accumulators injected subcooled water that started core liquid level recovery (LDP-127; Figure 5.3.1-5). At []^{a,b,c} with the vessel drained below the cold-legs and hot-legs levels, the upper head (TF-120 and TF-171) became superheated; however, the upper plenum became saturated (Figures 5.3.1-22 and 5.3.1-32). Even though the downcomer bulk fluid temperature remained subcooled, the upper []^{a,b,c} of the downcomer region filled with superheated steam (TF-168; Figure 5.3.1-22). The combination of voiding in the upper portion of the downcomer and the direct connection to the superheated upper head through the bypass holes caused the downcomer to fill with superheated steam.

Eight downcomer fluid thermocouples (TF-147 to TF-150 and TF-164 to TF-167), mounted []^{a,b,c} above the top of the DVI nozzles, allowed monitoring of the temperature in the downcomer. TF-147 to TF-150 were mounted at 180°az above the DVI-2 penetration; TF-164 to TF-167 were mounted at 0°az above the DVI-1 penetration (Dwg. OSU 600101). The thermocouples were mounted at one of two elevations. TF-147, TF-148, TF-164, and TF-167 were located about []^{a,b,c} above the top of the DVI line penetration to the downcomer. TF-149, TF-150, TF-166, and TF-167 were located about []^{a,b,c} above the top of the DVI line penetration to the downcomer.

From []^{a,b,c} data from the eight thermocouples revealed temperatures in the downcomer were below saturated conditions (Figure 5.3.1-80). The thermocouples uncovered after the accumulators completed injection. The downcomer level at the time was just at the DVI nozzles, the minimum downcomer level. The thermocouples were not covered again until about []^{a,b,c}

Some temperature fluctuations may be due to mixture of saturated steam generated from fluid in the downcomer and superheated steam flowing from the SGs, through the cold legs, and to the break at the cold-leg balance line.

The upper head remained superheated throughout most of the transient, except when condensation events caused a sudden drop in temperature; details of these events are described in Subsection 7.1. As ADS actuation occurred, core liquid levels continued to recover to a level of []^{a,b,c} at []^{a,b,c}. A second drop in the core level occurred just prior to the ADS-4 valves opening, even after the emptying of the accumulators and the single-injection feed from CMT-2. A recovery of the core liquid level began when IRWST injection started in the []^{a,b,c} period. Recovery of the core and downcomer liquid levels peaked at []^{a,b,c} when both the downcomer became full and the hot legs and cold legs filled to an elevation equivalent of []^{a,b,c} (LDP-127; Figure 5.3.1-40).

As IRWST draindown slowed, and the level in the primary sump increased, sump injection was initiated (at about []^{a,b,c}). As sump injection progressed, the upper head, core region, and upper downcomer cooled to a steady-state saturated temperature condition of []^{a,b,c} (Figures 5.3.1-44 and 5.3.1-46).

Break and ADS Measurement System

The BAMS provided a means to collect, measure, and redirect flow to the primary and secondary sumps for subsequent return to the reactor vessel via the DVI lines. Elevation of the separators (break separator, ADS 1-3, ADS 4-1, and ADS 4-2) and their cross-connecting pipe were modeled to simulate the physical conditions in the reactor cavity and containment areas.

Prior to initiation of the break, all loop seals were filled in accordance with test procedures. Only the ADS 1-3 loop seal was heat traced. On the break opening, break flow from the cold-leg balance line was directed to the break separator, and flow from the pipe attached to CMT-1 was directed to the ADS 4-2 separator (Figure 5.3.1-27). Levels in the break separator and primary sump (LDP-905 and LDP-901) increased immediately following the break (Figures 5.3.1-49 and 5.3.1-50). Steam separated in the break separator was directed through in-line vortex flow meters where the steam flow was measured before being discharged from the building. Figures 5.3.1-51, 5.3.1-52, and 5.3.1-26 illustrate steam flows at various locations and times during the transient.

FVM-901 and FVM-902 indicated a combined steam flow discharge rate of []^{a,b,c} about []^{a,b,c} after the break (Figure 5.3.1-51). Since these two parallel vortex flow meters were the last flow meters before the steam was released, all released flow from the BAMS system was measured. For Matrix Test SB10, the operator closed valves CSS-902 and CSS-906 (Appendix G, Dwg. OSU 600901) when the combined peak flow through FVM-901 and FVM-902 was less than []^{a,b,c}. At about []^{a,b,c} this occurred, and, from that point on, flow exiting the building was directed through FVM-901. The majority of steam flow occurred from []

]^{a,b,c} with the largest portion flowing out of the break and to the break separator (FVM-905 and FVM-906; Figure 5.3.1-51). After initial release through the break, the only additional steam flow occurred from the ADS 1-3 separator during ADS valve openings and went into the IRWST through the sparger (FVM-601; Figure 5.3.1-26). Steam flow of []^{a,b,c} occurred over a []^{a,b,c} interval through FVM-701 following ADS-2 valve opening to the IRWST (Figure 5.3.1-52). This is probably due to air being pushed out of the IRWST as the level increased. Some measurable steam flow occurred from the transfer of hot liquid to the primary sump (FVM-903). These values were small compared with steam produced through the break. A total of []^{a,b,c} of steam exited the primary system and building through the break and ADS measurement system (BAMS) as a result of this transient.

Figure 5.3.1-49 shows the liquid level changes in the IRWST due to ADS 1-3 valve opening (LDP-701), in the break separator due to break flow (LDP-905), and in the primary sump fed by separators (LDP-901). The secondary sump level (LDP-902) was unaffected until about []^{a,b,c} when overflow from the primary sump occurred (Figure 5.3.1-50). The break separator level changed rapidly (LDP-905; Figure 5.3.1-49), when the break opened, which compares well with measured flow from the break separator to the primary sump (FMM-905; Figure 5.3.1-27). The initial peak level in the break separator occurred from []^{a,b,c} with a level of []^{a,b,c}. The primary sump level increased immediately following the break, initially due to flow from the break separator. No flow to the primary sump occurred from the ADS 4-1 separator (FMM-603) and ADS 4-2 separator (FMM-602) early in the transient. Flow from the ADS 1-3 separator to the IRWST caused the IRWST level to increase from []^{a,b,c} at []^{a,b,c} when IRWST injection started (Figures 5.3.1-27 and 5.3.1-49).

When the primary sump level reached about []^{a,b,c} (about []^{a,b,c}), sump liquid covered the loop seal pipe from the break separator (Figures 5.3.1-49 and 5.3.1-50). Once this occurred, any liquid added to either the primary sump or the break separator was reflected in the liquid levels (LDP-901 and LDP-905). In effect, both levels increased together until the primary sump reached the overflow level of []^{a,b,c} above the centerline of the DVI line. The secondary sump received overflow from the primary sump. Overflow to the secondary sump first occurred at about []^{a,b,c} as the primary sump level reached []^{a,b,c}. As primary sump injection was initiated at []^{a,b,c} the level in the sump decreased slightly. The primary sump inventory was replaced with a []^{a,b,c} flow from the ADS 4-1 separator (FMM-603; Figure 5.3.1-45).

Core Makeup Tanks

Thermal-hydraulic behavior in the CMTs was quite asymmetrical throughout Matrix Test SB10 due to the break location; therefore, data from each CMT will be described separately.

CMT-2 Related Response

The system was filled with subcooled liquid at []^{a,b,c} prior to break initiation. Isolation valves in the discharge lines were opened []^{a,b,c} after the break, and natural circulation flow started in the loop formed by CMT-2, CMT-2 discharge, DVI line, pressure vessel, CL-1, and cold-leg balance line. CMT-2 injection flow (FMM-504) and the axial temperature profile (TF-504 to TF-532) are illustrated in Figures 5.3.1-11, 5.3.1-53, and 5.3.1-54.

With the onset of natural circulation flow through the CMT, subcooled water started to flow through the cold-leg balance line into CMT-2, as shown by a rapid temperature increase (TF-532) and a discharge flow rate of []^{a,b,c} (FMM-504). Within []^{a,b,c} after break initiation, the top []^{a,b,c} percent of CMT volume was at temperature of []^{a,b,c}. The CMT transitioned from recirculation to draindown at []^{a,b,c} as indicated by sharp decrease in the balance line level (LDP-510; Figure 5.3.1-8). During this transition from recirculation to draindown, the CMT-2 injection flow rate increased to []^{a,b,c} (Figure 5.3.1-11). As cold-leg levels dropped, saturated steam filled the cold-leg balance line and, at about []^{a,b,c} became slightly superheated, as shown by TF-536 and the thermocouple at the top of CMT-2 (TF-546; Figures 5.3.1-55 and 5.3.1-56).

During accumulator injection and ADS 1-3 actuation ([]^{a,b,c}), the CMT-2 level remained constant but the space above the []^{a,b,c} water level became superheated ([]^{a,b,c} increase over saturation temperature). Figures 5.3.1-55 and 5.3.1-56 show the interaction between the water layer and the upper head of the CMT. The upper portion of the CMT-2 dome was exposed to []^{a,b,c} liquid (TF-546), and the inside wall surface temperature quickly changed from []^{a,b,c} (TW-556; Figure 5.3.1-55). The outside wall temperatures also increased but at a slower rate, beginning at []^{a,b,c} and increasing to a peak of []^{a,b,c} over []^{a,b,c} (TW-554). The outside wall temperature on the CMT-2 dome at a corresponding radial direction (TW-548) showed excellent agreement with TW-554 (Dwg. OSU 600502). Quickly heating the metal mass at the top of the CMT allowed storage of thermal energy that was returned to the system by heating up the saturated steam entering the dome of the CMT, beginning at []^{a,b,c} (TF-556 and TF-558; Figure 5.3.1-55) and continuing until about []^{a,b,c} when they became subcooled (Figure 5.3.1-53).

The upper layers of saturated steam in the CMT were superheated ([]^{a,b,c}) due to exposure to higher wall temperatures and rapid depressurization during ADS-1 and ADS-2 valve actuation. Characterization of the early stages of the CMT-2 superheating effect was performed by review of the thermocouples along the axial length of the CMT, upper CMT dome inside-wall temperatures, and a combination of fluid and wall temperatures at the top layers (Figures 5.3.1-57, 5.3.1-58, and 5.3.1-59, respectively). All fluid thermocouples above the []^{a,b,c} percent volume layer indicated temperatures above the saturation temperature from []^{a,b,c} however, most of these thermocouples (TF-516, TF-518, TF-522, TF-526, and TF-530) reflected superheated conditions at []^{a,b,c} about []^{a,b,c} after the ADS-2 valve opened and rapid

depressurization of the system occurred. Thermocouples TF-556 and TF-564, which are located very close to the same elevation as TF-516 (except closer to the walls), exhibited an earlier departure from saturation at []^{a,b,c} with a temperature of []^{a,b,c} (Figure 5.3.1-57). Upper-dome inside-wall temperatures indicated a peak wall temperature of []^{a,b,c} (Figure 5.3.1-57) and slowly decreased to about []^{a,b,c}. Both the upper-dome and upper-inside-wall temperatures reached peak temperature values of []^{a,b,c} between []^{a,b,c} (Figure 5.3.1-59). Therefore, a []^{a,b,c} difference (fluid temperatures > wall temperatures) existed between the wall and the saturated steam volume above the water surface at the []^{a,b,c} point. This common effect of CMT steam heating is described in detail in Subsection 7.2.

As accumulator injection was completed and prior to ADS-4 actuation, the upper portion of the cold legs superheated to a temperature of []^{a,b,c} (Figures 5.3.1-34 to 5.3.1-37). On ADS-4 actuation at []^{a,b,c} the cold legs dropped to saturation conditions but the upper CMT-2 temperatures remained []^{a,b,c} above saturation temperature due to early dome metal heating. The effect of upper dome heating and subsequent superheating of saturated steam in the upper portion of the CMT had less effect on the lower portion of the CMT. As the CMT continued to drain, the lower inside surface reached saturation temperature late in the transient due to increased surface area to be heated and lack of cold-leg flow entering the CMT during the transition from recirculation to draindown. At about []^{a,b,c} the upper layers of the CMT dropped to slightly above saturation temperature and remained at these conditions until the CL-1 balance line began to refill (Figure 5.3.1-8). Temperatures in the top of CMT-2 (TF-532; Figure 5.3.1-53) indicated superheated steam had re-entered CL-1 (SC-105; Figure 5.3.1-34) from the reactor vessel via the bypass holes (TF-168; Figure 5.3.1-22) from []^{a,b,c} or from the SGs. Because the cold leg refilled with superheated steam, steam also filled the CMT-2 balance line.

During this same period, the hot and cold legs refilled with water due to injection from the IRWST and CMT-1. At about []^{a,b,c} CL-1 refilled and sealed off the entrance of the CMT balance line with saturated liquid and continued to fill the balance line. This isolated the superheated steam in CMT-2 by the liquid seal and the check valve located in the discharge line of CMT-2 (Dwg. OSU 600206). As IRWST and CMT-1 injection continued and the core/hot-leg levels increased, liquid continued to fill the balance line. The trapped steam contained in CMT-2 decreased in temperature due to heat loss through the CMT walls. This decrease in steam temperature lowered the pressure which caused more liquid to fill the balance line. At about []^{a,b,c} the balance line became filled and some liquid flowed into the top of CMT-2 (LDP-510; Figure 5.3.1-8). As more of the liquid entered the top of CMT-2, the slightly superheated steam continued to condense, reducing the local pressure and increasing flow into the CMT. At []^{a,b,c} the CMT level was about []^{a,b,c} and all CMT temperatures sharply decreased from saturated conditions to []^{a,b,c} (Figure 5.3.1-53). This sudden temperature decrease combined with the sharp increase in CMT-2 level (from []^{a,b,c}) suggested that the steam bubble existing in CMT-2 collapsed. Balance line flow showed a small flow of about []^{a,b,c}. As a possible condensation event occurred, a localized low pressure was created due to the collapsed bubble causing a []^{a,b,c} increase of flow at []^{a,b,c} through FMM-502. This possible condensation

event was also evident at other locations in the system. Sudden refill due to the condensation event subcooled the CMT (Figure 5.3.1-53). As pressure in CMT-2 and the RCS achieved equilibrium, refill ended.

After the termination of refill, CMT-2 remained stable with subcooled water with only a []^{a,b,c} difference from bottom to top of the liquid layer (Figure 5.3.1-53). There was no flow to the reactor vessel due to the higher localized line pressure in the vessel caused by IRWST injection flow. From []^{a,b,c} the cold-leg balance line slowly filled with saturated steam that entered and condensed in CMT-2 at about []^{a,b,c} (Figure 5.3.1-54). This additional flow into CMT-2 caused a []^{a,b,c} increase in the top layers of the CMT and only a slight increase in the CMT level.

CMT-2 injection began at []^{a,b,c} as IRWST injection decreased to the low-low level. CMT-2 emptied at []^{a,b,c} and the remaining liquid and vapor stratified (Figure 5.3.1-54).

CMT-1 Related Response

The system was filled with subcooled liquid (69°F) prior to break initiation. On break initiation, balance-line flow was directed to the break separator, and any liquid in the horizontal portion of the balance line drained into either the ADS 4-1 separator or CMT-1. The break isolated CMT-1 with the top open to atmospheric pressure, but the initiation of injection flow was controlled by reactor pressure. Due to high pressure in the reactor vessel/DVI line, no flow occurred even after the isolation valves in the discharge lines opened at the []^{a,b,c} mark. CMT-1 remained isolated and the liquid in the tank remained isothermal at 69°F (Figures 5.3.1-60 and 5.3.1-61). About []^{a,b,c} after ADS-4 actuation ([]^{a,b,c}), pressure in the reactor vessel and DVI line was less than CMT-1 head elevation. A discharge flow ([]^{a,b,c} peak at []^{a,b,c}) from CMT-1 occurred (Figures 5.3.1-8 and 5.3.1-11). CMT-1 flow was limited by DVI line pressure due to parallel injection of the IRWST. CMT-1 draindown continued until []^{a,b,c} when the tank emptied. The tank remained empty for the remainder of the transient.

Accumulators

The accumulators were located below the CMTs in the system and provided water injection into the DVI lines by an expansion of nitrogen gas volume stored in the accumulator at an average pressure of []^{a,b,c} set at initial conditions. Water from the accumulators was expelled into the injection line when primary system pressure dropped below []^{a,b,c}. Accumulator injection started before ADS-1 actuation with a low flow rate of []^{a,b,c} per accumulator; however, when ADS-1 actuated, the injection rate sharply increased (Figure 5.3.1-11). The accumulator injection rate reached a peak injection flow rate of []^{a,b,c} immediately following ADS-2 valve opening. Accumulator injection lasted about []^{a,b,c} the tanks emptied at []^{a,b,c} (Figure 5.3.1-62).

Pressurizer

The pressurizer immediately drained to the reactor vessel after the break occurred and was completely drained in about []^{a,b,c} (LDP-601 and LDP-602; Figure 5.3.1-7). Water in the pressurizer flashed due to loss of system pressure, and the temperature of the water (TF-602) dropped from a value of []^{a,b,c} before the break to []^{a,b,c} (Figure 3.5.1-63). The pressurizer was superheated until about []^{a,b,c} then remained at saturation temperature.

When ADS-1 actuated at []^{a,b,c} temperatures in the upper portion of the pressurizer decreased as the steam flow from the reactor vessel entered and exited the top of the pressurizer. Just prior to ADS actuation, the hot legs (LDP-206) and the upper plenum (LDP-113) were filled with []^{a,b,c} percent steam (Figure 5.3.1-64). The hot-leg elbow/SG-2 channel heads were partially filled with two-phase fluid (LDP-208 and LDP-214). When the ADS-1 valve opened at []^{a,b,c} the pressurizer surge line and the pressurizer initially filled with a two-phase mixture. The combination of the ADS valve actuation with the injection of the accumulators and CMT-2 caused a high influx of liquid flow through the reactor, which discharged two-phase flow through the pressurizer and exited through the ADS valves. A steam percentage versus time plot of the pressurizer and surge line confirmed the filling of the pressurizer with liquid from []^{a,b,c} (Figure 5.3.1-65). Just prior to []^{a,b,c} steam percentage in the pressurizer and surge line was []^{a,b,c} percent, reflecting an empty condition (Figure 5.3.1-7). The surge line and pressurizer refilled with two-phase flow, decreasing the steam percentage to about []^{a,b,c} percent at []^{a,b,c} ADS-1 valve actuation caused a small increase in liquid and steam flow through and into the ADS 1-3 separator (Figure 5.3.1-66). Figure 5.3.1-66 shows a comparison of the liquid and steam flow exiting through the ADS valves and ADS 1-3 separator downstream from the ADS 1-3 valves.

At []^{a,b,c} when the larger ADS-2 valve opened, system pressure decreased and ACC-1 and ACC-2 injection flow increased rapidly from []^{a,b,c} which caused a continued decrease in the pressurizer steam percentage. This decrease in steam percentage indicated that the pressurizer was being filled with an increasing amount of liquid supported by a two-phase steam environment in the smaller-diameter surge line. The measured flow of liquid into the ADS 1-3 separator from the pressurizer during this period also supports this conclusion. Steam flow peaks were consistent with ADS-1 opening ([]^{a,b,c}), ADS-2 opening ([]^{a,b,c}), and ADS-3 opening ([]^{a,b,c}). The liquid flow rate for flow exiting the separator showed a peak flow rate of []^{a,b,c} at about []^{a,b,c} that tapered off to 0 at []^{a,b,c} (ADS-4 valve opening). The drop in the steam flow rate (FVM-601; Figure 5.3.1-66) at []^{a,b,c} suggested that two-phase flow through the pressurizer ended, and only liquid was collected in the pressurizer.

At []^{a,b,c} steam percentage in the pressurizer reached a minimum value of []^{a,b,c} percent, supported by a surge line with a steam percentage of []^{a,b,c} percent (Figure 5.3.1-65). From []^{a,b,c} accumulator injection decreased rapidly but still provided adequate driving force to transfer liquid from the pressurizer to the ADS 1-3 separator for a period of time. As flow

from CMT-2 continued into the reactor, the partially filled pressurizer retained the liquid, and the two-phase environment in the surge line maintained this level.

At []^{a,b,c} ADS-4 valves opened and caused a further decrease in reactor pressure and diverted steam filling the hot legs to the ADS 4-1 separator. As system pressure decreased and IRWST injection flow started, the steam bubble in the surge line became unstable, and liquid from the pressurizer began to drain slowly into the hot legs through the surge line. System depressurization due to ADS-4 actuation ended both steam and liquid flow to the ADS 1-3 separator (Figure 5.3.1-66), and the steam percentage in the pressurizer increased as the liquid volume decreased (Figure 5.3.1-65). Draining of the pressurizer from []^{a,b,c} was reflected by an increase in liquid content in the HL-2 elbow (Figure 5.3.1-64) and surge line (Figure 5.3.1-65).

At []^{a,b,c} the pressurizer was completely voided, and the surge line was filled with []^{a,b,c} percent water and []^{a,b,c} percent steam (Figure 5.3.1-65) with an indicated liquid level of about []^{a,b,c} (Figure 5.3.1-7). This condition remained stable from []^{a,b,c} when primary sump injection caused a drop in surge line level from []^{a,b,c}. From []^{a,b,c} through the end of the transient, the pressurizer remained voided (Figure 5.3.1-67).

Passive Residual Heat Removal Heat Exchanger

At the initiation of the event, the PRHR HX was filled with subcooled liquid. After []^{a,b,c} RCS-804 (Figure 5.3.1-12) opened, and quickly became over-ranged with a high flow rate of []^{a,b,c} after about []^{a,b,c} Figures 5.3.1-68 and 5.3.1-69 show the temperature profile for the PRHR HX throughout the transient. Within []^{a,b,c} the PRHR HX inlet temperature had increased from []^{a,b,c} while the outlet temperature line was about []^{a,b,c}. As the primary system began to drain (at about 120 seconds), the hot legs filled with two-phase fluid and a portion of this fluid flowed from HL-2 to the PRHR HX (Figure 5.3.1-12). PRHR HX inlet and outlet lines contained FMM-802 and FMM-804, respectively, which can produce erratic or inaccurate data for two-phase flow conditions. Therefore, the PRHR HX inlet flow rates appeared erratic and sometimes over-ranged after the line became filled with steam after ([]^{a,b,c}).

Since flow out of the PRHR HX remained subcooled for the entire test (Figures 5.3.1-68 and 5.3.1-69), data from FMM-804 (Figure 5.3.1-12) were not affected by fluid phase. However, the measured flow rate through the HX outlet line was small and oscillating. By []^{a,b,c} flow oscillated rapidly between negative []^{a,b,c} and positive []^{a,b,c} making it difficult to determine how much mass was passing through the HX.

FMM-802 (Figure 5.3.1-12) measured flow from HL-2 to the PRHR HX. As HL-2 became voided, PRHR HX inlet flow data will become invalid. It cannot be determined precisely when the hot leg voided sufficiently to affect the inlet flow measurement. Although the PRHR HX inlet temperature reached saturation temperature at []^{a,b,c} (Figure 5.3.1-68), the state of the fluid was

uncertain. The saturated temperature of the fluid allowed it to be liquid, steam, or two-phase. However, steam percentage calculations using the SG-2 hot-leg elbow indicated that voiding of the hot legs was well established when ADS-2 actuated at []^{a,b,c} at which time the rate of voiding in the hot leg increased (Figure 5.3.1-14). As FMM-802 was exposed to two-phase and/or steam flow, the output was no longer valid; therefore, flow values are not valid after []^{a,b,c}

The two-phase mixture was condensed and subcooled in the PRHR HX and returned at a flow of about []^{a,b,c} of []^{a,b,c} liquid to the bottom of the cold-leg channel head in SG-2. During the initial depressurization and prior to ADS-1 actuation, a significant variation in the inlet flow was observed, which was caused by the variation in the void fraction in the fluid in HL-2. When the ADS actuated, the reactor and the hot leg became subcooled by cold flow from the accumulators. The driving head for flow in the PRHR HX decreased and almost stopped at about []^{a,b,c}. Subcooled fluid in the hot leg never filled the PRHR HX supply line as system pressure decreased (Figure 5.3.1-70).

The PRHR HX levels (LDP-801 and LDP-802) showed that the inlet header was drained from []^{a,b,c} and the HX tubes drained to about []^{a,b,c} (Figure 5.3.1-70). This time span is coincident with draindown of the cold legs and hot legs. Spikes were also observed in the PRHR HX outlet flow at []^{a,b,c} which are coincident with condensation events that occurred at various locations in the system (Figure 5.3.1-12). TF-808 (on the short tube at mid-length) showed a sharp increase from []^{a,b,c} beginning at []^{a,b,c} and remained at this temperature until []^{a,b,c} (Figure 5.3.1-68), shortly after ADS-4 actuation ([]^{a,b,c}).

The level measured by LDP-802 (Figure 5.3.1-70) was about []^{a,b,c} which suggested that TF-808 was uncovered. TF-809 remained subcooled at []^{a,b,c} (Figure 5.3.1-68), possibly because TF-809 was in the long leg of the PRHR HX and the length of cooling path was longer compared with the short leg (TF-808). At about []^{a,b,c} the inlet temperature of the short tube increased and the inlet temperature of the long tube decreased (response of the two tubes reversed). The short tube was the one with the significant temperature difference between inlet and outlet; long-tube temperatures correlated to IRWST temperatures at their thermocouple location. Long-tube temperatures indicated no significant temperature across the tube for the rest of the test, except to reflect IRWST temperature at the long tube thermocouple location.

From []^{a,b,c} the PRHR HX refilled to about []^{a,b,c} of the total liquid level; however, the upper head level partially filled before the main body of the HX, which reached a level of []^{a,b,c} (Figure 5.3.1-70). The level increase in the PRHR HX at []^{a,b,c} is not clearly understood, however, one explanation may be a condensation event. Because the inlet channel head completed filling at the same time that the tube level started increasing (Figure 5.3.1-70), flow reversal through the HX was a possible explanation for both level events. This would have required pressure in the SG-2 cold-leg channel head to be greater than the pressure in HL-2; however, the pressure in SG-2 was never greater than HL-2. Backward flow through the HX

would have resulted in the outlet temperature of the HX (from the SG-2 cold-leg channel head) being greater than the inlet temperature (from HL-2). This was never the case because the outlet temperature was always subcooled; the inlet temperature reached saturation temperature at []^{ab,c} (Figure 5.3.1-68).

Data from the fluid thermocouples in the HX provided no further evidence that there was any flow reversal through the HX and no insight into the reflooding of the tubes at []^{ab,c}. A condensation event that occurred at []^{ab,c} caused the level to drop to []^{ab,c} (Figure 5.3.1-70), and FMM-804 reflected a discharge flow of []^{ab,c} over []^{ab,c} (Figure 5.3.1-12).

After this event, the levels in both the inlet head and HX body refilled slowly from []^{ab,c} as the hot legs and cold legs refilled.

At []^{ab,c} when reactor pressure had decreased and flow injection from the IRWST had slowed, the PRHR HX began to inject condensed water back into the vessel via the SG-2 channel head (LDP-802; Figure 5.3.1-71), (TF-803; Figure 5.3.1-69), and (FMM-804; Figure 5.3.1-72).

As IRWST flow ended and primary sump injection initiated, the PRHR HX continued to condense steam generated in the core, but at a slower rate since the HX was transferring heat to the air instead of to the IRWST water.

In summary, data indicated that the PRHR HX provided a cooling flow to the RCS that continued through the entire test. Outlet flow and level of the HX oscillated, probably from a chugging effect as steam from HL-2 condensed in the HX. The low flow rates suggest that the HX was more effective early in the transient.

Steam Generators

One long tube and one short tube in the SG were instrumented for level and temperature measurement (Dwg. OSU 600301). Transmitters measured the level in the hot-leg and cold-leg sides of the tubes; thermocouples in the tubes measured temperature at the top of the tubes and at mid-elevation of both the hot-leg and cold-leg sides.

Seventy seconds after the break valve opened, the SG tubes started to drain in both SGs (Figures 5.3.1-16 and 5.3.1-17 contain data for SG-1). Both SGs, including the hot-leg and cold-leg channel heads, were essentially drained before ADS-1 actuation at []^{ab,c}. The sequence of tube and channel-head draining is provided in Table 5.3.1-3.

Before the break occurred, steam production in the secondary side of the SG acted as a heat sink to the primary side. Feedwater and steam isolation occurred automatically after the break was initiated (Table 5.3.1-3). The isolation of steam and feedwater "bottled up" the SGs. Until the RCS

depressurized below the pressure of the SG's secondary side, the only energy loss from the SGs was ambient heat loss through the insulation. When RCS pressure decreased below secondary steam pressure, the SG secondary side became a heat source to the RCS.

The SGs acted as a heat sink until pressures in both the SG and primary side reached a common pressure. After the break, pressure of the secondary side increased toward the primary-side hot-leg pressure (Figure 5.3.1-20) which, at the same time, was dropping. Temperature on the primary side was higher than the secondary side, indicating that heat transfer occurred from the primary to the secondary side. After []^{a,b,c} pressure on the SG secondary side and the U-tube primary side reached a common value of []^{a,b,c} and the temperatures reached a common value of []^{a,b,c} (Figure 5.3.1-21). During the first []^{a,b,c} the SG U-tubes partially emptied and broke the flow through the SG. Transition from recirculation to draindown of the SG and the large heat source of the SG caused the U-tubes to become superheated, and they remained in this condition throughout the transient. With both the hot-leg and cold-leg channel heads empty, superheated steam filled the entire primary side of the SG, which caused fluid temperatures in the region of the RCP inlets to superheat (Figures 5.3.1-34, 5.3.1-35, 5.3.1-36, and 5.3.1-37). As described in the cold-leg response subsection, the SGs supplied superheated steam to the cold legs via the differential pressure between the hot legs and the cold legs. Temperature in both the primary and secondary side continued to decrease at a rate of about []^{a,b,c} for the first []^{a,b,c}

The SG U-tubes liquid level instruments (Figure 5.3.1-14) were not providing a true indication of level due to loss of fluid in the reference and variable legs; therefore, the SG U-tube level values are not applicable beyond []^{a,b,c} (This generic instrument measurement effect is described in Section 2.4.) In summary, the SGs completely drained by ADS-1 actuation. Steam in the tubes superheated when RCS pressure decreased below secondary-side steam pressure. Superheating of all tubes was completed at []^{a,b,c} before ADS-1 actuation, and the tubes remained superheated for the rest of the test. The SGs supplied superheated steam to the cold legs, with the differential pressure between the hot legs and cold legs supplying the head for flow.

Cold Legs and Hot Legs

The upper head became saturated at about []^{a,b,c} following the break. In []^{a,b,c} the upper head drained, and the cold legs (initially full of single-phase liquid) showed an initial drop in levels (Figure 5.3.1-13). HL-1 and HL-2 indicated a similar draining at []^{a,b,c} (Figure 5.3.1-14). The pressurizer drained about []^{a,b,c} after the break; the SG U-tubes and channel head drained by []^{a,b,c}. As the levels in the cold legs dropped below the top of the pipe, flow through the balance line to CMT-2 stopped due to the transition from recirculation to draindown. As the SG drained, pressure in both the reactor vessel and the secondary side of the SG reached a common pressure and temperature ([]^{a,b,c}); little or no heat transfer occurred. After about 140 seconds, saturated steam in the SG U-tubes superheated. As the SG continued to respond as a heat source, superheated steam filled the primary side of the SG just above

the top layer of the partially drained cold legs (TF-201, TF-202, and TF-204; Figures 5.3.1-34, 5.3.1-35, 5.3.1-36, and 5.3.1-37).

Based on temperatures in the upper portion of the downcomer, superheated steam entered and occupied the top layers of the cold legs beginning at []^{a,b,c} (Figure 5.3.1-22). Superheated steam conditions were maintained in the cold legs due to either metal temperatures in the reactor vessel upper head via the bypass holes or superheated steam flow from the SGs. Both sources were superheated at that time. The instability of the cold-leg temperatures, beginning as early as []^{a,b,c} indicated some voiding was occurring in the cold legs. The liquid level in the cold legs was initially replaced with two-phase saturated fluid with some of the upper layer approaching superheat conditions.

In addition, from []^{a,b,c} the top layer of the cold legs exhibited peak temperatures of []^{a,b,c} the same as the downcomer temperature (TF-168; Figure 5.3.1-22). This suggested that, during this period, superheated steam was filling the very top layer of the cold legs. With the open connection between the upper head and the SG through the voided cold legs, DP-130 (Figure 5.3.1-28) indicated steam entered the cold leg from the upper head. Over the period from []^{a,b,c} however, DP-201, DP-204, DP-207 and DP-208 all indicated a positive differential pressure equal to []^{a,b,c} of water, suggesting that some steam flow may have entered the cold legs from the SGs.

The formation of superheated steam in the cold legs can be explained by the rapid depressurization of the RCS; however, the cold legs remained superheated for the duration of the test (Figures 5.3.1-34 to 5.3.1-37). This could have occurred only if a source of thermal energy was available to the cold legs.

The only possible sources of thermal energy to the cold legs were:

- Heating of steam in the cold legs by cold-leg piping
- Addition of superheated steam from the SGs
- Addition of superheated steam from the upper head via the bypass holes in the core barrel flange

Superheating of the cold legs from the upper head is not likely. The temperature of the upper head is lower than the fluid temperatures of the cold legs at the reactor vessel flange (Figures 5.3.1-34 to 5.3.1-37).

If the steam in the cold legs was maintained at a superheated condition by the walls of the cold legs, the temperature on the inside wall of the pipe would have been greater than the cold-leg fluid temperature. There were no inside-wall thermocouples in the cold-leg piping to measure temperature on the inside wall of the cold leg. The only cold-leg wall thermocouples were part of the heat flux meters (HFM) mounted on the outside wall of the piping. These thermocouples were given a TFM designation. A thermocouple was mounted on each cold leg at the top of its flanged connection to the reactor vessel (Dwg. OSU 600101, Sh. 2). The recorded temperature of the thermocouples mounted at

the top of the reactor vessel flange was greater than the recorded temperature of the thermocouples mounted on the side of the pipe, so, the hotter flange thermocouples were used for evaluation.

Figures 5.3.1-73, 5.3.1-74, and 5.3.1-75 show the effects of vessel/piping metal on the cold-leg temperatures and support the previous discussion. Early in the transient, with the reactor temperatures in the vessel and cold legs at [

] ^{a,b,c} (TF-171 and TFM-111; Figures 5.3.1-73 to 5.3.1-75). TF-171 was located [] ^{a,b,c} above the upper support plate and measured localized fluid temperatures but was significantly influenced by the metal plate temperature based on the distance from the plate. TFM-111 was located on the exterior of the CL-1 piping flange, roughly [] ^{a,b,c} from the downcomer/cold-leg interface. TFM-111 indicated a lower external temperature than the interior wall temperature, based on through-wall heat conduction.

As the upper head and plenum drained in [] ^{a,b,c} the upper support plate and cold-leg piping metal temperatures dropped slightly to [] ^{a,b,c} respectively (Figure 5.3.1-73). The reactor vessel continued to depressurize via ADS 1-3 valve opening, allowing saturated steam in the upper head to reach superheated conditions. This superheated steam filled the top of the downcomer via the bypass holes until it reached the top of the cold leg. The hotter metal temperatures in the cold legs maintained the upper layer of the cold legs at superheated conditions. The ADS-4 valve openings continued to reduce reactor pressure and permitted the initiation of IRWST injection flow, which started refill of the loops and cooling of the superheated steam in the cold legs at [] ^{a,b,c} (SC-105; Figure 5.3.1-74). Cold-leg temperatures remained slightly above saturated conditions until the cold legs refilled with subcooled water beginning at [] ^{a,b,c}. The cold-leg fluid temperature (SC-105) and piping metal temperatures (TFM-111) subcooled at [] ^{a,b,c} after the hot legs and cold legs completely refilled (Figure 5.3.1-75).

Both the cold and hot legs drained at about [] ^{a,b,c}. The hot legs were filled with saturated steam from the reactor vessel or possibly the SGs (SC-140, SC-141, SC-205, SC-206; Figure 5.3.1-76). The loops voided until after accumulator injection, ADS actuation, and IRWST injection provided adequate inventory for refill (LDP-201, LDP-202, LDP-203, LDP-204, LDP-205, LDP-206; Figures 5.3.1-13 and 5.3.1-14). The effect of hot-leg piping metal temperatures (TFM-109 and TFM-113) also had a significant effect on the temperature profiles in the hot legs (Figure 5.3.1-76).

Figure 5.1.3-76 shows that, early in the transient, externally mounted thermocouples on the hot legs (TFM-113 and TFM-109 located on the top of the HL-1 and HL-2 flanges, respectively) indicated temperatures of [] ^{a,b,c}. These temperatures remained essentially unchanged even though fluid temperatures in the hot legs were slightly superheated and decreased along the saturation line. Because the metal temperatures remained in the mid-[] ^{a,b,c} levels, hot-leg temperatures remained saturated (from [] ^{a,b,c}) while the hot legs were voided (Figures 5.3.1-77, 5.3.1-78, and 5.3.1-79). The response of TF-171 (which measures the fluid temperature locally above the upper support plate) showed an early temperature increase above the saturation temperature line,

suggesting that the upper support plate, having been exposed to the higher fluid temperature, helped to superheat any saturated steam passing through and into the upper head.

Figure 5.3.1-80 provides a plot comparing the output of several thermocouples in the downcomer annulus at an elevation equal to the hot-leg centerline (TF-147, TF-148, TF-166, and TF-167), some 3 in. below the hot-leg centerline (TF-149, TF-150, TF-164, and TF-165), and two located about []^{a,b,c} below the DVI line (TF-134 and TF-152). All temperatures except those below the DVI line exhibited similar subcooled temperatures until about []^{a,b,c} when the thermocouples approached saturated temperatures. At []^{a,b,c} when the downcomer annulus reached its minimum level (LDP-140 and LDP-116; Figure 5.3.1-5), the annulus thermocouples reached superheated temperatures, which existed in the upper downcomer region and cold legs (TF-168; Figure 5.3.1-22). Immediately following ADS-4 actuation at []^{a,b,c} the downcomer started to refill, and the thermocouples were quenched and returned to subcooled conditions. This confirms that the cold legs were voided, and the minimum downcomer annulus liquid level was below the bottom of the DVI line.

Thermocouples in the core region exhibited relative uniform temperature, except TF-170, which was at the same vertical elevation as TF-169. These thermocouples penetrated the vessel and the core barrel before entering the fluid. A seal was designed and installed around thermocouple TF-170 as it penetrated the core barrel; however, the 40°F difference between TF-169 and TF-170 suggested that the seal may not be as effective as intended (Figure 5.3.1-76). TF-155 indicated the downcomer temperature in the general proximity of the TF-170 thermocouple penetration (Figure 5.3.1-76). The temperature profile and the significant temperature difference in the downcomer indicated that some cooler downcomer fluid was bypassing the seal and affecting the output of TF-170. Therefore, the results of TF-170 should not be directly used for comparison with TF-169.

The hot legs showed initial voiding at about []^{a,b,c} and appeared to be empty at []^{a,b,c}. Up to []^{a,b,c} the average fluid temperatures were about []^{a,b,c} higher than the saturation temperature as indicated by TSAT (Figure 5.3.1-77). It should be noted that TSAT (PT-107) may have a small offset. With the hot legs empty and the hot-leg piping exhibiting temperatures in excess of []^{a,b,c} the slightly superheated steam continued to follow the saturation curve (Figure 5.3.1-78).

Between []^{a,b,c} the hot legs and cold legs began refilling and reached the filled condition at about []^{a,b,c}. Figure 5.3.1-78 shows the transition of both the top and bottom of the hot legs from superheated to saturated to subcooled from []^{a,b,c}. This figure also indicates that heating of the upper support plate and superheating of the upper head had little direct effect on the temperature profiles of the hot legs during this period.

This was not the case for the cold legs, as described earlier in this section. At []^{a,b,c} sharp changes in temperature occurred due to a condensation event in CMT-2. Condensation events

such as in CMT-2 were reflected throughout many subsystems. The hot legs remained subcooled until about []^{a,b,c} (Figure 5.3.1-79).

Levels in both the hot and cold legs remained stable until about []^{a,b,c} when flow from the IRWST and CMT-1 decreased, and CMT-2 flow (from refill) initiated, caused a slight drop in the vessel level (LDP-127, LDP-116, and LDP-140; Figure 5.3.1-40). As primary sump injection started at []^{a,b,c} cold-leg levels dropped slightly to just above the bottom of the pipe ([]^{a,b,c} relative to LDP-127), resulting in a partially filled cold leg (LDP-201, LDP-202, LDP-203, and LDP-204; Figure 5.3.1-81). Cold-leg temperatures remained subcooled from about []^{a,b,c} (Figure 5.3.1-82). As the sump recirculation mode occurred, saturated water at about []^{a,b,c} injected, causing the cold leg to reach saturated temperature conditions.

Similarly, hot-leg levels remained partially filled ([68.0 in.] relative to LDP-127) (LDP-205 and LDP-206; Figure 5.3.1-83). Levels in the hot leg supported liquid flow to the primary sump via the ADS-4 valves and primary sump injection from []^{a,b,c} (end of the test). Hot-leg temperatures remained subcooled from []^{a,b,c} as the core heating with reduced injection flow caused the hot-leg temperatures to increase (Figure 5.3.1-84). The hot legs remained at a uniform temperature of about []^{a,b,c} for the remainder of the test.

In-Containment Refueling Water Storage Tank

Thermal response of the IRWST was influenced by the addition of heat from the PRHR HX and the direct injection of hot liquid from the ADS 1-3 separator. Initially, a []^{a,b,c} axial temperature gradient existed from the top to the bottom of the IRWST, with the bottom at []^{a,b,c} (Figure 5.3.1-85). Opening of the PRHR HX outlet valve caused a slight localized temperature increase in the upper one-third of the tank. As ADS-1-3 valves opened, the upper layers of the tank increased from []^{a,b,c} locally. This localized temperature increase created a stable temperature difference of []^{a,b,c} from the middle to the top layers, after the conclusion of the ADS phase. With continued heating from the PRHR HX, the upper half of the IRWST increased to an average temperature of []^{a,b,c} (TF-710, TF-709, and TF-707; Figure 5.3.1-85).

After []^{a,b,c} the IRWST drained below the PRHR HX tubes, and about []^{a,b,c} of []^{a,b,c} water remained in the tank (Figure 5.3.1-86). Thermocouples TF-705, TF-707, TF-709 and TF-710 were exposed to tank ambient air temperatures (Figure 5.3.1-86). From []^{a,b,c} through the end of test, these thermocouples increased to an average temperature of about []^{a,b,c} (Figure 5.3.1-86). As primary sump injection occurred at about []^{a,b,c} backflow of hot water from the primary sump entered the IRWST (FMM-701; Figure 5.3.1-43).

5.3.1.6 Mass Balance

Mass balance results for Matrix Test SB10 were calculated based on water inventory before and after the test event and are provided in Appendix E. Inventory at the end of the test was within []^{a,b,c} percent of the inventory at the beginning of the test.

5.3.1.7 Conclusions

The test was performed with minimal problems and is considered acceptable. Although not all of the facility initial conditions met the specified acceptance criteria, the deviations did not impact the quality of the data. The instrumentation problems encountered were not critical to the performance of the facility mass and energy balances.

Facility response to the test was as anticipated for the conditions that were established. The data clearly demonstrate that cooling of the reactor heater rods was maintained throughout the duration of the test.

TABLE 5.3.1-1
MATRIX TEST SB10 INITIAL CONDITIONS

Parameter	Instrument No.	Specified Initial Condition	Actual Initial Condition	Comments
Pressurizer pressure ⁽¹⁾	PT-604	370 ± 2 psig	<input type="checkbox"/> a,b,c	
HL-1 temperature ⁽¹⁾	SC-141	420 ± 2°F	<input type="checkbox"/>	Accepted
HL-2 temperature ⁽¹⁾	SC-140	420 ± 2°F	<input type="checkbox"/>	Accepted
SG-1 pressure ⁽¹⁾	PT-301	285 ± 5 psig	<input type="checkbox"/>	
SG-2 pressure ⁽¹⁾	PT-302	285 ± 5 psig	<input type="checkbox"/>	
Pressurizer level ⁽¹⁾	LDP-601	65 ± 5 in.	<input type="checkbox"/>	Level signal was temperature-compensated by TF-605
SG-1 narrow-range level ⁽¹⁾	LDP-303	26 ± 3 in.	<input type="checkbox"/>	Level signal was temperature-compensated by TF-301
SG-2 narrow-range level ⁽¹⁾	LDP-304	26 ± 3 in.	<input type="checkbox"/>	Level signal was temperature-compensated by TF-310
IRWST temperature ⁽²⁾	TF-709	< 80°F	<input type="checkbox"/>	
IRWST level ⁽²⁾	LDP-701	Level established by fill-line elevation	<input type="checkbox"/>	
CMT-1 temperature ⁽²⁾	TF-529	< 80°F	<input type="checkbox"/>	
CMT-2 temperature ⁽²⁾	TF-532	< 80°F	<input type="checkbox"/>	
ACC-1 temperature ⁽²⁾	TF-403	< 80°F	<input type="checkbox"/>	
ACC-2 temperature ⁽²⁾	TF-404	< 80°F	<input type="checkbox"/>	
ACC-1 level ⁽²⁾	LDP-401	Level established by standpipe at 37 in.	<input type="checkbox"/>	Accepted; accumulator level was fixed by a standpipe ⁽³⁾
ACC-2 level ⁽²⁾	LDP-402	Level established by standpipe at 37 in.	<input type="checkbox"/>	

TABLE 5.3.1-1 (Continued)
MATRIX TEST SB10 INITIAL CONDITIONS

Parameter	Instrument No.	Specified Initial Condition	Actual Initial Condition	Comments
ACC-1 pressure ⁽²⁾	PT-401	232 ± 2 psig	[] ^{a,b,c}	Accepted; pressure was [] ^{a,b,c} low
ACC-2 pressure ⁽²⁾	PT-402	232 ± 2 psig	[]	Accepted; pressure was [] ^{a,b,c} low
CMT-1 level ⁽²⁾	LDP-507	Full	[]	
CMT-2 level ⁽²⁾	LDP-502	Full	[]	

Note:

- (1) Data for the indicated parameter were recorded in the test procedure as an initial condition for the test. The value was determined by the test engineer from the appropriate control board indicator.
- (2) Data were not recorded in procedure, but the test engineer verified that specified conditions were achieved while establishing initial conditions. The value of the parameter was determined post-test by calculating the average DAS indication for a time of about 2 minutes before the break valve opened.
- (3) The bourdon pressure tube indicator (PI-401 or PI-402) was tubed to the lower portion of the reference leg of the accumulator level transmitter (LDP-401 or LDP-402). As pressure in the accumulator increased, air inside the bourdon tube was compressed, thereby lowering the reference leg liquid, resulting in a false-high indication of measured level.

**TABLE 5.3.1-2
MATRIX TEST SB10 INOPERABLE INSTRUMENTS/INVALID DATA CHANNELS**

Instrument No.	Instrument Type	Description of Problem
FMM-201* FMM-203* FMM-202* FMM-204*	Magnetic flow meter	Removed due to mechanical failure
FMM-502	Magnetic flow meter	Data invalid after 109 seconds due to possible steam in balance line
FMM-503	Magnetic flow meter	Data invalid after 0 second due to possible steam in balance line
FMM-501*	Magnetic flow meter	Data invalid after 12,243 seconds when CMT was empty
FMM-504*	Magnetic flow meter	Data invalid between 1486 and 2200 seconds and after 13,000 seconds when CMT was empty
FMM-601	Magnetic flow meter	Out of range from 300 to 320 seconds
FMM-701*	Magnetic flow meter	Data for negative flow invalid; negative flow existed after sump valves opened; meter not designed to measure negative flow
FMM-905	Magnetic flow meter	Data for negative flow invalid; negative flow existed after primary sump level equaled break separator connecting pipe level; meter not designed to measure negative flow
FMM-802*	Magnetic flow meter	Data invalid after steam formed in PRHR HX inlet line; uncertain when this occurs, but likely about 120 seconds after break
FMM-804*	Magnetic flow meter	Data valid until PRHR HX initially drained at 500 seconds; after which the possibility of steam in outlet line invalidated data
FMM-902	Magnetic flow meter	Negative flow indication invalid; data valid until flow occurred after 14,019 seconds
HFM-112 HFM-103 HFM-105 HFM-505	Heat flux meter	Unavailable

TABLE 5.3.1-2 (Continued)
MATRIX TEST SB10 INOPERABLE INSTRUMENTS/INVALID DATA CHANNELS

Instrument No.	Instrument Type	Description of Problem
HFM-201 HFM-601	Heat flux meter	Out of range temporarily
HPS-203-1 through HPS-203-3	Heated thermocouple measuring fluid phase	Failed
HPS-509-1 through HPS-509-3	Heated thermocouple sensing fluid phase	Failed
LCT-901	Primary sump load cell	Failed; erratic results during test
LDP-201 through LDP-206	Differential pressure transmitter - level	Data invalid due to effect of vertical portion of sense line attached to top of pipe; data can show level trends when pipe is empty or starts to drain, but absolute level indication can not be used
LDP-207 LDP-208 LDP-209	Differential pressure transmitter - level	Inoperable; ranged improperly; data can show level trends but absolute level indication can not be used
LDP-215* LDP-216 LDP-217 LDP-218* LDP-219* LDP-220 LDP-221 LDP-222*	Differential pressure transmitter - level	Data invalid; when SG tube drained, reference leg started to vaporize (see Subsection 2.4)
LDP-401* LDP-402*	Differential pressure transmitter - level	Data invalid; see Subsection 5.3.1.2
LDP-509	Differential pressure transmitter - level	Level values invalid due to break location
LDP-802* LDP-801	Differential pressure transmitter - level	Data valid until PRHR initially drained at 500 seconds; after which data suspect due to possible boiling of common reference line of LDP-802 and LDP-804
LDP-801	Differential pressure transmitter - level	Inoperable; level over-ranged for significant portion of transient
PT-611	Pressure transmitter	Failed
PT_101	Pressure transmitter	Data less than 6.1 psig invalid
PT_102 PT_103	Pressure transmitter	Data less than 6.2 psig invalid
PT_104	Pressure transmitter	Data less than 6.4 psig invalid

TABLE 5.3.1-2 (Continued)
MATRIX TEST SB10 INOPERABLE INSTRUMENTS/INVALID DATA CHANNELS

Instrument No.	Instrument Type	Description of Problem
PT_108	Pressure transmitter	Data less than 8.4 psig invalid
PT_109	Pressure transmitter	Data less than 6.3 psig invalid
PT_111	Pressure transmitter	Data less than 6.0 psig invalid
PT_112	Pressure transmitter	Data less than 8.8 psig invalid
PT_113	Pressure transmitter	Data less than 6.4 psig invalid
PT_201*	Pressure transmitter	Data less than 1.1 psig invalid
PT_202	Pressure transmitter	Data less than 5.9 psig invalid
PT_205	Pressure transmitter	Data less than 6.1 psig invalid
TF-170	Thermocouple	Inoperable throughout test
TFM-103 TFM-105 TFM-201	Thermocouple for heat flux meter	Unavailable
TH-317-1 through TH-317-4	Thermocouple measuring heater temperature	Removed with heater rod C2-317
TW-210	Thermocouple	Erratic reading
TF-504 TW-552 TW-534	Thermocouple	Failed by false indication of temperature

Note:

* Instruments marked with an asterisk are critical instruments. See Subsection 5.3.1.2 for discussion.

TABLE 5.3.1-3
MATRIX TEST SB10 SEQUENCE OF EVENTS

Event ⁽¹⁾	Data Source ⁽²⁾	Time After Break (sec.)
TEST Pushbutton Pressed	D	 a.b.c
Break Valve Open Signal	D	
CMT-1 Circulation Flow Stops (LDP-509)	A	
Break Valve Starts to Open	D	
Feed Pump Trips	D	
CMT-1 Outlet Valve Starts to Open	D	
CMT-2 Outlet Valve Starts to Open	D	
PRHR HX Outlet Valve Starts to Open	D	
Reactor Coolant Pumps Trip	D	
Pressurizer Empty (LDP-601)	A	
SG-1 Cold-Leg Short Tube Empty (LDP-221)	A	
SG-2 Cold-Leg Short Tube Empty (LDP-220)	A	
SG-1 Cold-Leg Long Tube Empty (LDP-219)	A	
SG-2 Cold-Leg Long Tube Empty (LDP-222)	A	
CL-3 Channel Head Empty (LDP-213)	A	
SG-1 Hot-Leg Short Tube Empty (LDP-217)	A	
SG-2 Hot-Leg Short Tube Empty (LDP-216)	A	
SG-2 Hot-Leg Long Tube Empty (LDP-218)	A	
CL-1 Channel Head Empty (LDP-211)	A	
CMT-2 Circulation Flow Stops (LDP-510)	A	
CL-4 Channel Head Empty (LDP-212)	A	
CL-2 Channel Head Empty (LDP-210)	A	
HL-1 Pipe Starts to Drain (LDP-205)	A	
HL-2 Pipe Starts to Drain (LDP-206)	A	
Pressurizer Surge Line Empty (LDP-602)	A	
ACC-1 Injection Starts(FMM-401)	A	
ACC-2 Injection Starts(FMM-402)	A	

TABLE 5.3.1-3 (Continued)
MATRIX TEST SB10 SEQUENCE OF EVENTS



Event ⁽¹⁾	Data Source ⁽²⁾	Time After Break (sec.)
Time of Minimum Reactor Level Observed During Test (LDP-127)	A	
SG-1 Hot-Leg Long Tube Empty (LDP-215)	A	
SG-2 Hot-Leg Elbow Starts Draining (LDP-208)	A	
CMT-2 Low Level Signal	D	
HL-2 Pipe Empty (LDP-206)	A	
ADS-1 Valve Starts to Open	D	
HL-1 Pipe Empty (LDP-205)	A	
ADS-2 Valve Starts to Open	D	
SG-2 Hot-Leg Channel Head Empty (LDP-214)	A	
Reactor Pressure Low	D	
IRWST-2 Injection Valve Starts to Open	D	
IRWST-1 Injection Valve Starts to Open	D	
ADS-3 Valve Starts to Open	D	
ACC-2 Empty (LDP-402)	A	
Pressurizer Refloods (LDP-601)	A	
ACC-1 Empty (LDP-401)	A	
CMT-2 Level Low-Low	D	
ADS 4-1 Valve Starts to Open	D	
ADS 4-2 Valve Starts to Open	D	
IRWST-1 Injection Starts(FMM-701)	A	
IRWST-2 Injection Starts(FMM-702)	A	
CMT-2 Empty (LDP-502)	A	
CMT-1 Low Level Signal	D	
CMT-2 Starts to Reflood (LDP-502)	A	
CMT-1 Level Low-Low	D	
CMT-1 Empty (LDP-507)	A	
Primary Sump Starts to Overflow to Secondary Sump (LDP-901)	A	

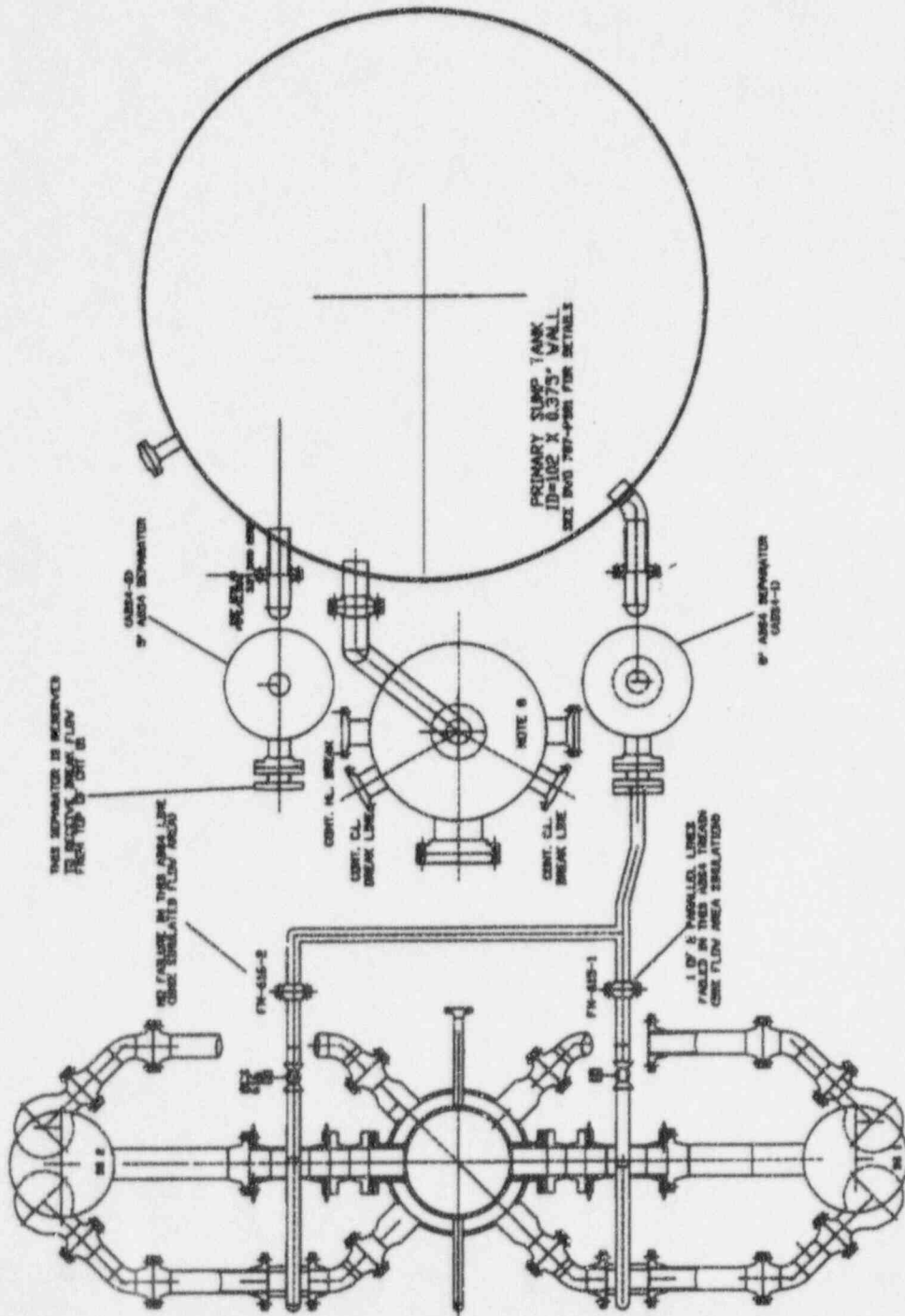
TABLE 5.3.1-3 (Continued)
MATRIX TEST SB10 SEQUENCE OF EVENTS

Event(1)	Data Source ⁽²⁾	Time After Break (sec.)	
			a.b.c
Primary Sump-1 Injection Starts (FMM-901)	A		
Primary Sump-1 Injection Valve Starts to Open	D		
Primary Sump-2 Injection Valve Starts to Open	D		
CMT-1 Starts to Reflood (LDP-507)	A		
SG-1 Hot-Leg Channel Head Empty (LDP-209)	A		
SG-1 Hot-Leg Elbow Starts Draining (LDP-207)	A		
SG-1 Hot-Leg Elbow Minimum (LDP-207)	A		
SG-1 Hot-Leg Elbow Minimum (LDP-207)	A		

Note:

- (1) Data from the instrument channel in parenthesis were used to determine level, flow, or pressure conditions
- (2) D = time data obtained from a software program that monitored the input and output of the facility's PLC. A = time data obtained by reviewing data from the instrument channel listed in the Event Description column
- (3) O.O.S. = out of service

The Bar Charts for Table 5.3.1-3 on pages 5.3.1-43 through 5.3.1-47 are not included in this nonproprietary documents.



FILE: D:\COMPAS\ADS-4 LAYER 2200

Figure 5.3.1-1 ADS-4 to Separator Pipe Arrangement for Matrix Test SB10

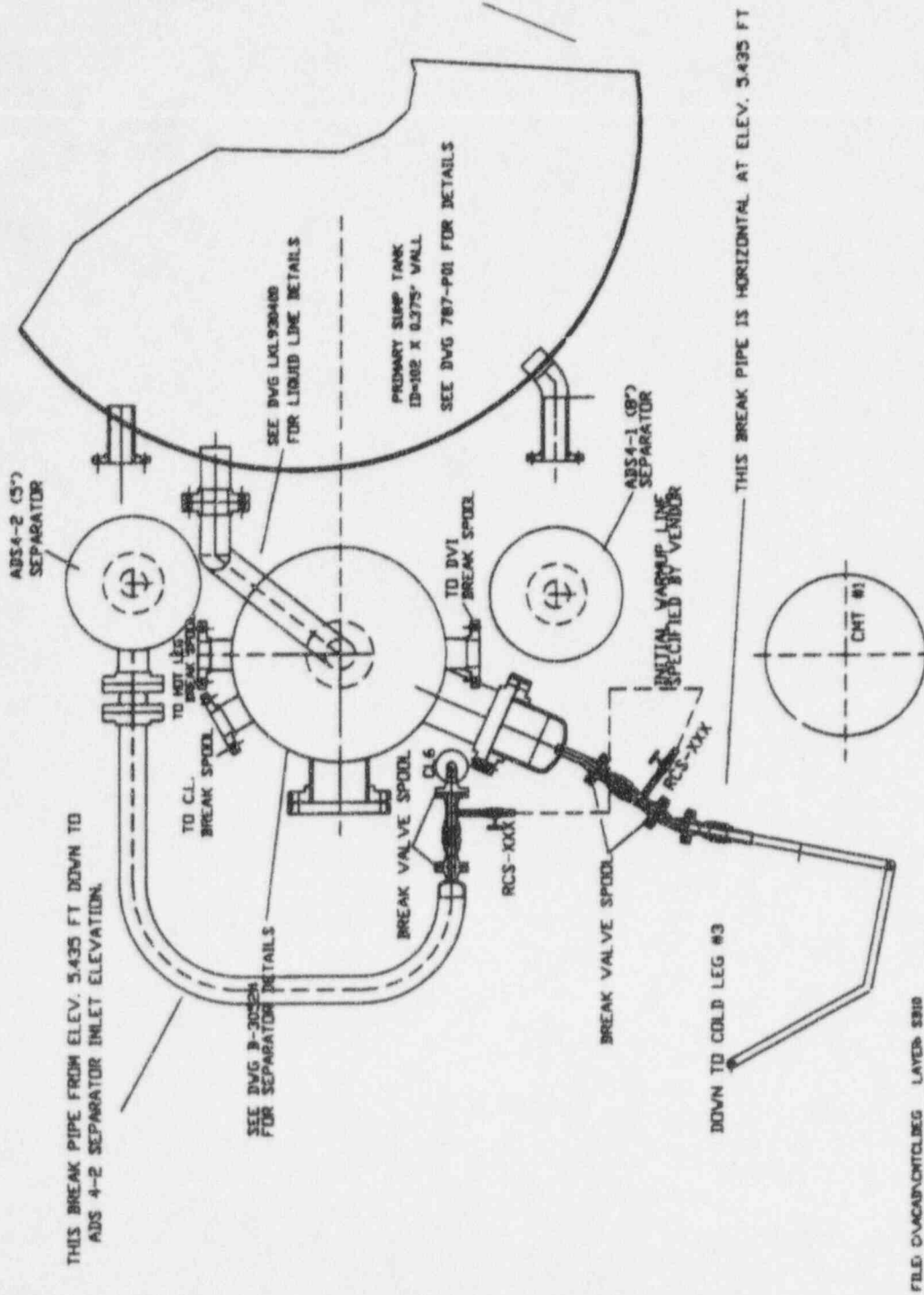


Figure 5.3.1-2 CMT-1 Balance Line DEG Break Pipe Arrangement

Figures 5.3.1-3 through 5.3.1-87 are not included in this nonproprietary document.

5.3.2 Effect of a Smaller Break Size (Matrix Test SB09 Comparison with Matrix Test SB10)

This section provides the test results of Matrix Test SB09 (OSU Test U0009) for a simulated 2-in. break on the CMT-1 balance line. The simulated break was located between CL-3 and the vertical portion of the CMT-1 balance line, with an assumed failure of one of the two parallel ADS-4 lines. Matrix Test SB09 is directly related to Matrix Test SB10 (OSU Test U0110), a double-ended CMT-1 balance-line break. Both breaks existed at the same location but differ by the size of the break. Therefore, this section identifies and describes the response of the system based on a comparison between Matrix Test SB10 (the reference test, described in detail in Subsection 5.3.1) and Matrix Test SB09. Facility responses to the break are documented by data plots, referenced as figures in text.

Matrix Test SB09 was performed on June 29 and 30, 1994. Test duration was about 6.0 hours. The test performed met the specified initial conditions. Any exceptions to the initial conditions are discussed in Subsection 5.3.2.1. The transient began from the break and continued through ADS actuation, and CMT, accumulator, IRWST, and sump recirculation injection. An increased water inventory beyond that exhibited in Matrix Test SB10 occurred during the critical portion of the test. The top of the heater bundle was always cooled during this event; therefore, the Matrix Test SB09 was considered successful.

Subsection 5.3.2.1 provides details related to the test configuration and initial conditions. Subsection 5.3.2.2 defines the inoperable instruments or time ranges for which data may not be valid. Subsection 5.3.2.3 provides the sequence of events. Subsections 5.3.2.4 and 5.3.2.5 describe the overall summary of the system response and any component-specific differences from the reference test, respectively. A summary of the mass balance results is provided in Subsection 5.3.2.6. Conclusions, as they apply to Matrix Test SB09, are provided in Subsection 5.3.2.7.

5.3.2.1 System Configuration and Initial Conditions

Matrix Test SB09 was performed according to an approved written procedure and simulated a single-ended 2-in. break of the CMT-1 balance line. The required break simulation piping and break instrumentation were installed per piping and instrumentation diagrams (Dwg. OSU 600904) and break piping layouts (Figures 5.3.2-1 and 5.3.2-2). Break discharge was piped to the break separator. All other connections to the break separator were isolated using blind inserts in the piping source.

Before break initiation, the break separator was isolated from the break sources by two break valves. Break valve TS-202 isolated the CL-3 side of the break; break valve TS-203 isolated the CMT side of the break.

Liquid break flow was measured by flow meter FMM-905. Break steam flow was measured by flow meter FVM-905, installed in the []^{a,b,c} steam line of the break separator. The []^{a,b,c} steam line from the break separator was isolated throughout the test (Dwg. OSU 600901).

The ADS 4-1 line was connected and piped into the []^{a,b,c} ADS 4-1 separator. The ADS 4-2 line was connected to the []^{a,b,c} ADS 4-2 separator. A 50-percent flow nozzle was installed on hot leg-1 (HL-1) of ADS 4-1 to provide the assumed single failure, and a 100-percent flow nozzle was installed on HL-2 of ADS 4-2. The chemical and volume control system (CVS) and residual heat removal system (RNS) were not used in this test. The CVS and RNS pumps did not run. Flow nozzles that simulate two lines of flow each were installed in the ADS 1-3 nozzles. Fill and vent was performed per facility operating procedures. Instruments were checked for required calibration.

The initial conditions for Matrix Test SB09 are specified in Table 5.3.2-1. A select set of initial instruments (identified in Table 5.3.2-1) were checked on the control board prior to test implementation. The control board contained provisions to display compensated level indications to confirm initial conditions, except for some tank levels. Tank levels were established by filling the tanks until a visual check showed water overflowing from the standpipe. Pre-test operations, such as fill and vent processes, are defined in detail in Subsection 2.7.

The appropriate prerequisites were completed, and initial conditions were satisfied. The two sides of the break were connected by a warmup line and two series isolation valves (RCS-901 and RCS-902). With the break valves closed, the isolation valves were opened for a period of time before break initiation to pressurize the CMT-1 injection line to simulate normal plant operation. After the appropriate prerequisites were completed, and the test facility reached specified initial conditions, RCS-901 and RCS-902 were closed to maintain the < 80°F initial condition at the top of CMT-1. As final valve alignments were established, CMT discharge valves were placed in the AUTO and CLOSED positions, limiting CMT-1 pressure to that obtained while the vessel was at full pressure and temperature. One minute after the TEST pushbutton was actuated, RCS-529 and RCS-530 were placed in the OPEN and AUTO position. The CMT-1 balance line portion up to the isolation valves reached reactor coolant system (RCS) pressure.

Testing was initiated when test facility conditions, as read from the test facility control board and local indications, agreed with specified initial conditions within acceptable tolerances. The transient continued through ADS actuation, and CMT, accumulator, IRWST, and sump injection. All actions were automatic and required no operator action.

Heater rod bundle power was adjusted prior to break initiation to achieve the required hot-leg temperatures. Pressurizer heater power was terminated at break initiation.

Table 5.3.2-1 provides a comparison of the specified and actual conditions for Matrix Test SB09. Initial conditions for the test were established and recorded in the procedure. Table 5.3.2-1 shows the initial conditions recorded from the operator's panel and the average of the same parameters for about 2 minutes prior to the break valve opening.

There were 2 initial condition parameters out of specification in Table 5.3.2-1, none of which should invalidate this test, that will be discussed here.

- Accumulator levels (LDP-401 and LDP-402) exceeded the planned levels. The explanation for this situation is defined in note 3 of Table 5.3.2-1. The condition was considered acceptable because the level was set by a standpipe at 37 in.
- ACC-1 pressure (PT-401) was []^{a,b,c} percent below the required pressure band.
ACC-2 pressure (PT-402) is []^{a,b,c} percent below the required pressure band.
The accumulators were pressurized to the required pressure prior to test actuation. The loss of pressure between tank pressurization and test actuation was possibly due to cooling of the nitrogen gas in the accumulator. Test analysis, starting with the recorded lower accumulator overpressure, should still be possible.

Each of the two reactor heater power controllers were programmed using the same algorithm as in Matrix Test SB10 (defined in Subsection 2.3.2) to obtain the scaled decay power heat input rate. The core heater groups produced power input consistent with Matrix Test SB10, and the comparison plots of the decay heat power curves are reflected in Appendix F.

5.3.2.2 Inoperable Instruments

Table 5.3.1-2 is a list of instruments considered inoperable or invalid during all or portions of this test. Some of the instruments listed are on the Critical Instrument List (Subsection 3.2, Table 3.2-2) and, therefore, are addressed here.

FMM-201, FMM-202, FMM-203, and FMM-204 measured flow (gpm) in each of the four cold legs. A decision was made to continue testing without the availability of these instruments. Replacement flow meters repeatedly failed; their continued use was precluded due to cracking of the ceramic liners from thermal stratification in the loop piping. The necessary boundary conditions for loop flow could be determined from DP-202, DP-203, DP-205, and DP-206.

FMM-401 provided comparable results and response until injection dropped to []^{a,b,c}. Subsequent data indicated flow of []^{a,b,c} after the indicated accumulator-1 (ACC-1) level equalled 0, which is not correct. Flow injection data after []^{a,b,c} were not accurate and, therefore, should not be used or assumed to be []^{a,b,c}.

FMM-701 measured IRWST-1 injection flow. When the primary sump valves opened, the flow meter indicated a negative flow as water flowed from the primary sump to the IRWST. The meter was not designed to measure reverse flow, so this measurement was invalid; however, total IRWST flow was measured by FMM-702.

FMM-905 measured break separator flow from the separator to the primary sump. When the primary sump level was equal to or higher than the break separator pipe connection, FMM-905 indicated a negative flow as water flowed from the primary sump to the break separator. The meter was not designed to measure reverse flow, so this measurement was invalid.

FMM-501, FMM-504, FMM-802, and FMM-804 provided accurate data when sensing liquid, but became inaccurate when sensing two-phase or steam flow.

LDP-207, LDP-208, and LDP-209 were calibrated incorrectly for specific tap location (range > physical dimension). No correction was performed at this time.

SG-tube level data (LDP-215, LDP-218, LDP-219, and LDP-222) were biased by vaporization of the water in the transmitter reference leg after the SG tubes started draining. However, data provide accurate indication of the time when the tubes were empty.

LDP-401 and LDP-402 measured ACC-1 and ACC-2 levels, respectively. Due to air trapped in the transmitter sense lines, data from these transmitters were invalid. The initial level of the tank, however, was established by a standpipe, so it was constant test to test. The drain rate can be calculated using FMM-401 and FMM-402, respectively. Alternately, a pressure correction may be applied directly to the level indication of LDP-401 and LDP-402.

LDP-802 measured PRHR HX wide-range level. The PRHR HX may have been refilling, but a more likely reason is that LDP-802 was slowly losing its reference leg due to a low saturated pressure in the HX tubes.

Considering these critical instrument failures, sufficient instrumentation was available to allow the performance of mass balances as demonstrated in Subsection 5.3.2.6 and Appendix E. An energy balance will be performed and reported in the *AP600 Low-Pressure Integral Systems Test at Oregon State University Test Analysis Report, WCAP-14292*.⁽²⁾

5.3.2.3 Sequence of Events

The chronologic sequence of events appears in Table 5.3.2-3. Actual time the event occurred is listed along with the planned time of event occurrence. The table also provides the source of the actual time values. A D in the Data Source column indicates the recorded time was obtained from a software program that monitored digital events in the plant such as pump starts and stops, valve limit switch actuations, and alarms. An A in the Data Source column indicates the time was obtained by reviewing data from the data acquisition system (DAS). Although data from the DAS are digital, analog events such as pressure, flow, and temperature were monitored.

Table 5.3.2-3 contains Matrix Test SB10 sequence of events data for comparison with Matrix Test SB09. The time differential was calculated based on Matrix Test SB09 timing, where positive

time values indicate that Matrix Test SB09 events occurred later than the reference test events. Table 5.3.2-3 also contains a bar-graph representation of the sequence of events for both Matrix Tests SB09 and SB10 sorted in chronologic order to provide a quick visual reference of the timing of events. As expected, most of the Matrix Test SB09 events occurred later than the equivalent Matrix Test SB10 events due to the larger break in Matrix Test SB10. The results of this timing will be described in more detail in the following section.

5.3.2.4 Test Results and Evaluation

This section contains an overall description of the events that occurred during Matrix Test SB09 compared with Matrix Test SB10. The description contains references to specific instrumentation channels cross-plotted and used in the test-result evaluation. A matched set of data plots, like those described in detail and presented for Matrix Test SB10, are included at the end of this section. As data comparisons are presented, Matrix Test SB10 data plots will be referenced but will not be repeated in this section. The same figures and figure numbers appear at the end of Subsection 5.3.1. In certain cases, special cross plots of instruments and/or combined instruments have been prepared and included at the end of the standard figures. The data-plot figures list the instrument number and description. The behavior of specific components is discussed in Subsection 5.3.2.5.

Initial Conditions

The initial conditions for both tests were generally within 1 percent of the required initial condition values, with the following exceptions: CMT-2 initial temperature was []^{a,b,c} higher in Matrix Test SB09 than in Matrix Test SB10 ([]^{a,b,c}); and both accumulator temperatures were 6.1 percent higher in Matrix Test SB09 than in Matrix Test SB10 ([]^{a,b,c}). These minor differences were not considered critical to the performance of Matrix Test SB09.

Sequence of Events

A detailed review of the sequence of events comparison between Matrix Tests SB09 and SB10 indicated that subsystem actuations (i.e., accumulator injection) occurred as planned with respect to each individual test. When comparing subsystem actuations, the results of Matrix Test SB09 followed Matrix Test SB10 results, except for the following:

- For Matrix Test SB09, the feed pump and reactor coolant pumps (RCPs) tripped 2 seconds later than in the reference test. The feed pump and RCPs are actuated by the plant controller. These late trips of the feed pump and RCPs did not significantly effect the overall system response; however, this delay in trip should be considered when modeling the Matrix Test SB09 transient.

- Actuation of injection flow from CMT-2, the accumulators, and the IRWST occurred from between []^{a,b,c} later in Matrix Test SB09 than in Matrix Test SB10. The majority of the time difference was in the range of []^{a,b,c}

Note: The term *time difference* or *delay* means the time that an actuation occurred in Matrix Test SB09 relative to the same time an actuation occurred in Matrix Test SB10, using the Matrix Test SB10 time as the reference time.

- CMT-1 actuation initiated earlier by about []^{a,b,c} and completely emptied at []^{a,b,c} after the break for Matrix Test SB09, []^{a,b,c} ahead of when CMT-1 emptied in Matrix Test SB10.

Delayed actuation of the injection flows in Matrix Test SB09 was expected since the break size was considerably smaller than the break in Matrix Test SB10. Loss of inventory was less and rate of depressurization was slower for the smaller break. Both effects allowed more time before required actuation of injection flow occurred.

Reactor Pressure and Core Level

The reactor vessel and core region collapsed liquid levels represented indications of the overall system response to the break transient. Figures 5.3.2-87 to 5.3.2-89 present the pressure and core levels for comparison of Matrix Test SB10 with Matrix Test SB09. Reactor vessel pressure for Matrix Test SB09 (PT-107) showed a marked delay ([]^{a,b,c}) in depressurization from []^{a,b,c} when the accumulators could inject. The slower depressurization rate of Matrix Test SB09 caused the delay in actuation of RCS-711 and RCS-712 by []^{a,b,c}. After the ADS-4 valves actuated, reactor pressure decayed and remained at 0 psig for the remainder of the test.

LDP-127 reflected the core liquid inventory for both tests as the transient progressed from initial break to the end of the test (Figures 5.3.2-87 to 5.3.2-89). LDP-127 indicated a minimum collapsed reactor wide-range level of []^{a,b,c} for Matrix Test SB10, compared with a minimum value of []^{a,b,c} for Matrix Test SB09. For both tests, the core level recovered during accumulator injection, and then fell to a second minimum value.

The second minimum level for Matrix Test SB10 occurred at []^{a,b,c} compared with []^{a,b,c} for Matrix Test SB09. As IRWST injection continued, core levels in both tests recovered to a uniform level of []^{a,b,c} at about []^{a,b,c} (Figure 5.3.2-87). From []^{a,b,c} core liquid levels showed a peak variation of []^{a,b,c} (Figure 5.3.2-88). Core levels for both tests returned to a common level of []^{a,b,c} which was above the top of the cold legs, at about []^{a,b,c}. Matrix Tests SB10 and SB09 core levels responded in a similar manner for the remainder of the transient. From this comparison, it can be seen that, as the transient progressed into long-term cooling, the overall response of the system was essentially identical for both tests.

Reactor Downcomer Level

When used in conjunction with the reactor core level, the reactor downcomer level provided supporting evidence of draindown of the reactor vessel, hot legs, and cold legs. LDP-116 and LDP-140 measured the liquid level from the bottom of the downcomer to just below the upper head bypass holes. Based on Matrix Test SB10, the effect of steam filling the upper portion of the downcomer represents a key parameter for comparison purposes. Figures 5.3.2-90 to 5.3.2-92 show the response of these channels over the entire range of the transient. Even though LDP-140 was at 180°az and LDP-116 was at 270°az (90 degrees apart), their response was essentially the same. This agreement suggests that, in the downcomer region, level was uniform around the vessel for tests.

In both Matrix Tests, the overall response was similar; however, the magnitude and time of each occurrence was different. The downcomer level increased when RCP flow ended at []^{a,b,c} after the break occurred giving the first true level response. This level continued for about 100 seconds when the reactor vessel began to drain. The initial drop in downcomer level (LDP-116 and LDP-140) occurred at about []^{a,b,c} and began to recover due to the injection of CMT-2 (Figure 5.3.2-90). The downcomer collapsed level recovered to about []^{a,b,c} for Matrix Test SB10; the Matrix Test SB09 downcomer level remained at []^{a,b,c}. Both tests exhibited a second drop in downcomer level: []^{a,b,c} (just before ADS-4 actuation) for Matrix Test SB10 and []^{a,b,c} (just after ADS-2 actuation) for Matrix Test SB09 (Figure 5.3.2-90). In both tests, the downcomer level increased to a peak (over-ranged) level value of []^{a,b,c} from []^{a,b,c} during IRWST injection (Figure 5.3.2-91). During this same period, the Matrix Test SB10 downcomer level increased to []^{a,b,c} more quickly than the Matrix Test SB09 downcomer. Beginning at []^{a,b,c} the downcomer level for both tests remained at a constant level of []^{a,b,c} until about []^{a,b,c} just prior to sump injection (Figure 5.3.2-92).

During the transition from IRWST injection to sump injection, the downcomer level indicated a difference in level of about []^{a,b,c} between Matrix Test SB10 ([]^{a,b,c}) and Matrix Test SB09 ([]^{a,b,c}). LDP-116 and LDP-140 indicated that the cold legs were empty (the bottom of the cold leg is a level equal to []^{a,b,c} instruments indicate a level of []^{a,b,c} during Matrix Test SB09 (Figure 5.3.2-92). This level did not increase for the remainder of the test. The difference is attributed to excess liquid spilled through the overflow line to the secondary sump []^{a,b,c} earlier for Matrix Test SB09 during the period from []^{a,b,c}. Since the downcomer levels were comparable and the differences are understood, test data for Matrix Test SB09 appear to support the anticipated system responses.

Overall Netflow

Netflow, as a comparison parameter, provides a direct comparison of the overall system performance between similar types of tests. Netflow is the difference between spill flow (flow spilled to the break separator or sump) minus total direct vessel injection (DVI) flow. Total injection flow is the sum of

flow through DVI-1 and DVI-2 (FMM-205 and FMM-206, respectively). Total discharge or spill flow is the sum of flow exiting the primary system through FMM-905, FMM-603, FMM-602, and FMM-601.

These three variables are plotted from []^{a,b,c} for Matrix Tests SB09 and SB10 (Figures 5.3.2-93 and 5.3.2-94). The netflow summation is demonstrated by these two figures. It should be noted that even though flow was discharged through ADS actuation, part of this liquid may be returned by IRWST injection. Netflow and the core region wide-range level comparison between Matrix Tests SB10 and SB09 are shown in Figures 5.3.2-95 and 5.3.2-96. Negative netflow values indicate that more injection than discharge flow occurred.

From the initial break to []^{a,b,c} netflow between tests tracked very well with an initial positive netflow rate of about []^{a,b,c} followed by a near-zero netflow rate from []^{a,b,c}. This near-zero netflow rate was due to early injection from the CMTs for both tests. Earlier injection flow from the accumulators and ADS 1-3 actuation caused a significant negative netflow rate of []^{a,b,c} which in turn caused the core level to increase (LDP-127). The Matrix Test SB10 netflow rate transitioned from a negative to a positive flow rate as injection flow from the accumulators reached 0 and CMT-2 injection flow resumed. As CMT-2 flow increased, netflow returned to 0 at about []^{a,b,c} just prior to ADS-4 actuation in Matrix Test SB10. After ADS-4 actuation and IRWST injection, netflow stabilized with an average []^{a,b,c} (Figure 5.3.2-95).

During the period from []^{a,b,c} Matrix Test SB09 indicated differences based on early injection from CMT-1 along with CMT-2 injection. From []^{a,b,c} a positive netflow of []^{a,b,c} occurred due to the small injection flow from both CMT-1 and CMT-2. As CMT-2 draindown continued (at []^{a,b,c}), injection flow increased and resulted in a negative netflow that continued when the accumulators injected ([]^{a,b,c}). This negative netflow trend ended at about []^{a,b,c} as peak accumulator flow ([]^{a,b,c} per accumulator) ended, and reduced flow from the CMTs returned. CMT flow peaked at about []^{a,b,c} with a flow of []^{a,b,c} per CMT and decreased slowly until about []^{a,b,c}. Netflow approached a negative value of []^{a,b,c} (Figure 5.3.2-95).

From []^{a,b,c} to the end of the test, netflow for both Matrix Tests SB10 and SB09 was slightly negative ([]^{a,b,c}) and remained at this same value except for two condensation events that occurred in Matrix Test SB09 []^{a,b,c} (Figures 5.3.2-96 and 5.3.2-97). Condensation events occurred in Matrix Test SB10 at the following times: []^{a,b,c} (Figures 5.3.2-96 and 5.3.2-97). The plot of core collapsed liquid level and netflow demonstrated a close comparison between Matrix Tests SB10 and SB09, even though, early in the transient, actuation of various injection sources occurred at different times.

CMT and Accumulator Injection Flow

The break size effect was also reflected in the response of the CMTs and accumulators. CMT-1 and ACC-1 responses are reflected in Figure 5.3.2-98. CMT-2 and ACC-2 responses are reflected in Figure 5.3.2-99. For Matrix Test SB09, draindown of CMT-1 began at about []^{a,b,c} with a small flow but increased to []^{a,b,c} (Figure 5.3.2-98). CMT-1 injection occurred about []^{a,b,c} ahead of CMT-1 injection during Matrix Test SB10. In Matrix Test SB09, the early injection of CMT-1, when combined with the injection of CMT-2, maintained the core liquid inventory at a higher level than in Matrix Test SB10. ACC-1 injection occurred as the reactor pressure dropped below the nitrogen gas pressure set prior to the start of the test ([]^{a,b,c}). ACC-1 injection also suppressed CMT-1 injection flow until accumulator injection fell to []^{a,b,c} for Matrix Test SB09. CMT-1 emptied at []^{a,b,c} in Matrix Test SB09, []^{a,b,c} before CMT-1 emptied in Matrix Test SB10. In both tests, CMT-1 did not refill due to the broken balance line; however, during Matrix Test SB09, thermocouple rod temperatures in CMT-1 indicated that steam was condensed in CMT-1 late in the transient (Figure 5.3.2-61). The extent of this condensation was not significant, and no measurable level was recorded in the tank.

For both tests, CMT-2 exhibited similar responses, beginning with an injection flow rate of []^{a,b,c} during the first []^{a,b,c} after break initiation (Figure 5.3.2-99). CMT-2 was in a recirculation mode during the early part of the transient []^{a,b,c} for Matrix Test SB10; []^{a,b,c} for Matrix Test SB09). During this recirculation mode, saturated water flowed through the CMT-2 balance line into CMT-2. During the transition from recirculation to draindown, CMT-2 flow increased, and two-phase flow filled the CMT-1 balance line. The peak injection flow rate of []^{a,b,c} for both tests occurred shortly before accumulator injection initiated. In both tests, the effect of accumulator injection on CMT-2 injection was the same: during the accumulator injection flow period, CMT-2 injection flow was suppressed and sometimes suspended. This effect was indicated by a sharp decrease in the CMT-2 flow rate as accumulator injection flow occurred (Figure 5.3.2-99). After ACC-2 injection ended, CMT-2 injection flow returned to a second peak flow rate of []^{a,b,c}. CMT-2 flow continued at a decreasing rate until the tank emptied at []^{a,b,c} for Matrix Test SB10 and []^{a,b,c} for Matrix Test SB09. The longer duration of injection flow during Matrix Test SB10 may be attributed to the complete suspension of CMT-2 flow during accumulator injection; CMT-2 flow during Matrix Test SB09 was not suspended ([]^{a,b,c}).

CMT-2 refilled to []^{a,b,c} for Matrix Test SB10 and []^{a,b,c} for Matrix Test SB09 shortly after the tank was drained initially (Figure 5.3.2-100). In both tests, refill of CMT-2 occurred over about an []^{a,b,c} period following draindown. In both tests, the end of CMT-2 tank refill can be correlated with steam condensation events that occurred at []^{a,b,c} (Matrix Test SB10) and []^{a,b,c} (Matrix Test SB09). These condensation events were reflected by sharp inflection points on LDP-127 (Figures 5.3.2-87 and 5.3.2-88). In both tests, the condensation event occurred in CMT-2, not in the upper-head/downcomer area; Subsection 5.3.1.5 provides the explanation for the possible cause in the CMT component discussion. CMT-2 tanks remained filled at their applicable

levels until about []^{a,b,c} when CMT-2 began to drain. Draindown was complete by about []^{a,b,c} just prior to sump injection.

5.3.2.5 Comparison of Component Responses

The following component responses have been reviewed and determined to be essentially the same or similar enough to represent the same response; therefore, any minor differences are not described.

- Break and ADS flow measurement system (BAMS)
- Accumulators
- Pressurizer
- PRHR HX
- SGs
- Cold legs and hot legs
- IRWST
- Core temperatures

Components that contain significant differences between Matrix Tests SB10 and SB09 are presented in the following subsections.

Reactor

The overall response of the core and reactor vessel was similar for both tests, except in the areas of overall timing (addressed earlier in Subsection 5.3.2.4) and higher superheated temperatures in the upper head and upper portion of the downcomer. For Matrix Test SB09, the downcomer temperature (TF-168) became superheated at about []^{a,b,c} as the upper head drained down to the upper support plate level, and steam from the upper head entered the downcomer via the bypass holes (Figure 5.3.2-101). []^{a,b,c} after ADS-1 actuated (see Table 5.3.2-3), the upper head superheated (TF-120).

Both upper-head and downcomer temperatures generally followed the decrease in reactor temperature until ADS-3 actuation (see Table 5.3.2-3). A sharp increase in upper-head temperature may be due to the superheating effect from the heat transfer of energy stored in the upper support plate to the saturated steam flowing through it (TF-171). The upper support plate was exposed to higher fluid temperatures earlier in the transient (Figure 5.3.2-101). The upper head and upper support plate reached a common peak temperature of []^{a,b,c} then slowly decreased in temperature. The downcomer temperature (TF-168) remained superheated and relatively close to the upper-head temperature from []^{a,b,c} (Figure 5.3.2-102). It is not clear why higher superheated downcomer temperatures in Matrix Test SB09 were sustained from []^{a,b,c} while downcomer temperatures in Matrix Test SB10 were only []^{a,b,c} above reactor saturated temperature (Figure 5.3.1-22).

Similarly, for Matrix Test SB10, both upper-head and downcomer temperatures reached superheated conditions earlier due to the larger break and quicker drainage of the upper head and downcomer. Two condensation events occurred (at []^{a,b,c}) in Matrix Test SB10 and caused large decreases in both the upper-head and downcomer thermocouple temperatures (TF-120 and TF-168, respectively); otherwise, these temperatures would have been significantly higher (Figures 5.3-22 and 5.3-44). In both tests, the upper head decreased in temperature until the hot legs and cold legs began to refill, then upper-head temperatures increased sharply at about []^{a,b,c} for Matrix Test SB09 and []^{a,b,c} for Matrix Test SB10 (Figures 5.3.2-102 and 5.3.1-22). In Matrix Test SB09, the upper region of the downcomer (TF-168) showed no increase in temperature, and the thermocouple located immediately above the upper support plate (TF-171) showed only a []^{a,b,c} increase (Figure 5.3.2-102). A review of cold-leg and hot-leg temperatures during this period indicated no significant increase in temperature. A comparison of differential pressure across the upper support plate and differential pressure across the bypass holes indicated that there was no flow across the upper support plate or through the bypass holes (DP-114 and DP-130; Figures 5.3.2-101 and 5.3.2-102). When DP-130 indicates negative []^{a,b,c} of water, the value is []^{a,b,c} when DP-114 indicates positive []^{a,b,c} of water, the value is []^{a,b,c}. One possible explanation is that, since the flow was stagnate, steam trapped in the head was superheated by the surrounding metal. However, upper head metal temperature (TFM-105) was not available for Matrix Test SB09 to sustain this assumption. Superheated steam in the head caused a slight increase in the downcomer annulus (TF-168) and a significant and sustained temperature increase in the upper head (TF-120; Figures 5.3.2-101 and 5.3.2-102). Since both the hot legs and cold legs were partially or completely filled, superheated steam had no vent path, so heat slowly dissipated into the head structure (Figure 5.3.2-101). Further evaluation and analysis is required to characterize this phenomena.

Core Makeup Tanks

CMT-1 response for Matrix Test SB09 was considerably different than CMT-1 response for Matrix Test SB10. In Matrix Test SB10, pressure at the top of CMT-1 dropped to atmospheric pressure because of the break. The break and reduced pressure precluded recirculation mode and only allowed draindown, adding cold (about 80°F) water to the reactor vessel late in the transient.

As draindown occurred for Matrix Test SB09, hot water entered the top of CMT-1 with a peak temperature of []^{a,b,c} (Figure 5.3.2-60). As draindown continued, the upper layers of the CMT increased to the core-saturated temperature condition. Slow draindown and no replacement of liquid or steam from []^{a,b,c} allowed liquid temperatures in CMT-1 to dissipate heat to the tank walls and lower bulk fluid temperatures to about []^{a,b,c}. CMT-1 remained empty for the remainder of the test. Some steam did enter CMT-1 at about []^{a,b,c} as CSS-909 and CSS-910 opened (Figure 5.3.2-61). No measurable liquid level occurred as a result of this steam entering and condensing in CMT-1.

For Matrix Tests SB09 and SB10, CMT-2 response was similar overall; however, the resulting CMT-2 temperature profiles were considerably different. When the CMT-2 injection valves opened

[]^{a,b,c} after the break, the recirculation mode was established to permit a low injection flow of cold water into the reactor as saturated water from CL-1 entered the top of CMT-2 (Figures 5.3.2-53 and 5.3.2-54). This recirculation mode raised the temperatures in the top layers of the CMT to the saturation temperature based on reactor pressure. As ADS-1 occurred at []^{a,b,c} and the reactor quickly depressurized, the top layers of CMT-2 superheated ([]^{a,b,c}) with a temperature of about []^{a,b,c}. This same response occurred for Matrix Test SB10; however, the temperatures at which the top layers of the CMT superheated were in the range of []^{a,b,c} almost []^{a,b,c} less than Matrix Test SB09 values (Figures 5.3.1-53 and 5.3.1-54).

During this same period in both tests, the cold legs were beginning to drain, allowing steam from either the upper head or the SGs to fill the void at the top of the cold legs. As more of the cold legs in Matrix Test SB09 voided of liquid, steam filled the pipe, allowing steam from the cold legs to enter the top layers of CMT-2 from []^{a,b,c} (TF-532; Figure 5.3.2-53). Draindown of CMT-2 continued until the tank emptied at []^{a,b,c} and the temperatures in the CMT cooled down to []^{a,b,c} and approached saturated conditions (Figure 5.3.2-54).

In both tests, CMT-2 started to refill shortly after draindown completed. Refill was initiated by a condensation event at []^{a,b,c} for Matrix Test SB10 and []^{a,b,c} for Matrix Test SB09 (Figures 5.3.1-53 and 5.3.2-54, respectively). Once refilled, CMT-2 temperatures indicated a subcooled condition until the second draindown occurred (see Table 5.3.2-3).

As the second draindown progressed, steam again entered the top of the CMT and quickly raised the top of the CMT-2 from subcooled at []^{a,b,c}. On completion of draindown, the upper layers of the CMT remained at a saturated temperature of []^{a,b,c} while the discharge thermocouples remained subcooled (Figures 5.3.2-54). CMT-2 remained empty for the remainder of the test.

5.3.2.6 Mass Balance

Mass balance results for Matrix Test SB09 were calculated based on water inventory before and after the Matrix Test SB09 event and are provided in Appendix E. Table E.5.3.2-1 provides a detailed listing of the inventories of water in the various components before the event. Table E.5.3.2-2 provides a detailed listing of the inventories of water in the various components at the end of test. The inventory at the end of test was within 1.1 percent of the inventory at the beginning of the test.

5.3.2.7 Conclusions

The test was performed with minimal problems and is considered acceptable. Although not all of the facility initial conditions met the specified acceptance criteria, the deviations did not impact the quality of the data. The instrumentation problems encountered were not critical to the performance of the facility mass and energy balance.

Facility response to the test was as anticipated for the conditions that were established. The data clearly demonstrate that cooling of the reactor heater rods was maintained throughout the duration of the test.

**TABLE 5.3.2-1
MATRIX TEST SB09 INITIAL CONDITIONS**

Parameter	Instrument No.	Specified Initial Condition	Actual Initial Condition	Comments
Pressurizer pressure ⁽¹⁾	PT-604	370 ± 2 psig	<input type="checkbox"/> a,b,c	
HL-1 temperature ⁽¹⁾	SC-141	420 ± 2°F	<input type="checkbox"/>	
HL-2 temperature ⁽¹⁾	SC-140	420 ± 2°F	<input type="checkbox"/>	
SG-1 pressure ⁽¹⁾	PT-301	285 ± 5 psig	<input type="checkbox"/>	
SG-2 pressure ⁽¹⁾	PT-302	285 ± 5 psig	<input type="checkbox"/>	
Pressurizer level ⁽¹⁾	LDP-601	65 ± 5 in.	<input type="checkbox"/>	Level signal was temperature-compensated by TF-605
SG-1 narrow-range level ⁽¹⁾	LDP-303	26 ± 3 in.	<input type="checkbox"/>	Level signal was temperature-compensated by TF-301
SG-2 narrow-range level ⁽¹⁾	LDP-304		<input type="checkbox"/>	Level signal was temperature-compensated by TF-301
IRWST temperature ⁽²⁾	TF-709	< 80°F	<input type="checkbox"/>	
IRWST level ⁽²⁾	LDP-701	Level established by fill-line elevation	<input type="checkbox"/>	
CMT-1 temperature ⁽²⁾	TF-529	< 80°F	<input type="checkbox"/>	
CMT-2 temperature ⁽²⁾	TF-532	< 80°F	<input type="checkbox"/>	
ACC-1 temperature ⁽²⁾	TF-403	< 80°F	<input type="checkbox"/>	
ACC-2 temperature ⁽²⁾	TF-404		<input type="checkbox"/>	

TABLE 5.3.2-1 (Continued)
MATRIX TEST SB09 INITIAL CONDITIONS

Parameter	Instrument No.	Specified Initial Condition	Actual Initial Condition	Comments
ACC-1 level ^(2,3)	LDP-401	Level set by standpipe at 37 in.	[] ^{a,b,c}	Accepted; accumulator level was fixed by a standpipe
ACC-2 level ^(2,3)	LDP-402		[]	
ACC-1 pressure ⁽²⁾	PT-401	232 ± 2 psig	[]	Accepted; pressure was [] ^{a,b,c} low
ACC-2 pressure ⁽²⁾	PT-402		[]	
CMT-1 level ⁽²⁾	LDP-507	Full	[]	
CMT-2 level ⁽²⁾	LDP-502		[]	

Note:

- (1) Data for the indicated parameter were recorded in the test procedure as an initial condition for the test. The value was determined by the test engineer from the appropriate control board indicator.
- (2) Data were not recorded in procedure, but the test engineer verified that specified conditions were achieved while establishing initial conditions. The value of the parameter was determined post-test by calculating the average DAS indication for a time of about 2 minutes before the break valve opened.
- (3) The bourdon pressure tube indicator (PI-401 or PI-402) was tubed to the lower portion of the reference leg of the accumulator level transmitter (LDP-401 or LDP-402). As pressure in the accumulator increased, air inside the bourdon tube was compressed, thereby lowering the reference leg liquid level, resulting in a false-high indication of measured level.

TABLE 5.3.2-2
MATRIX TEST SB09 INOPERABLE INSTRUMENTS/INVALID DATA CHANNELS

Instrument No.	Instrument Type	Description of Problem
FMM-201* FMM-203* FMM-202* FMM-204*	Magnetic flow meter	Removed due to mechanical failure
FMM-401*	Magnetic flow meter	Positive value after 1500 seconds was invalid because tank was empty
FMM-502	Magnetic flow meter	Data invalid after 138 seconds due to possible steam in balance line
FMM-503	Magnetic flow meter	Data invalid after 0 second due to possible steam in balance line
FMM-501*	Magnetic flow meter	Data invalid after 1664 seconds when CMT was empty
FMM-504*	Magnetic flow meter	Data invalid between 1222 and 3400 seconds and after 13,200 seconds when CMT was empty
FMM-701*	Magnetic flow meter	Data for negative flow invalid; negative flow existed after sump valves opened; meter not designed to measure negative flow
FMM-905*	Magnetic flow meter	Data for negative flow invalid; negative flow existed after primary sump level equaled break separator connecting pipe level; meter not designed to measure negative flow
FMM-802*	Magnetic flow meter	Data invalid after steam formed in PRHR HX inlet line; uncertain when this occurred, but likely 50 seconds after break
FMM-804*	Magnetic flow meter	Data valid until PRHR HX initially drained at 500 seconds; after which the possibility of steam in outlet line invalidated data
HFM-112 HFM-103 HFM-105	Heat flux meter	Unavailable
HFM-201 HFM-601 HFM-703	Heat flux meter	Out of range temporarily
HPS-203-1 through HPS-203-3	Heated thermocouple measuring fluid phase	Failed

TABLE 5.3.2-2 (Continued)
MATRIX TEST SB09 INOPERABLE INSTRUMENTS/INVALID DATA CHANNELS

Instrument No.	Instrument Type	Description of Problem
HPS-509-1 through HPS-509-3	Heated thermocouple sensing fluid phase	Failed
LCT-901	Primary sump load cell	Failed; erratic results during test
LDP-201 through LDP-206	Differential pressure transmitter - level	Data invalid due to effect of vertical portion of sense line attached to top of pipe; data can show level trends when pipe is empty or starts to drain, but absolute level indication cannot be used
LDP-207 LDP-208 LDP-209	Differential pressure transmitter - level	Inoperable; ranged improperly; data can show level trends but absolute level indication cannot be used
LDP-215* LDP-216 LDP-217 LDP-218* LDP-219* LDP-220 LDP-221 LDP-222*	Differential pressure transmitter - level	Data invalid; when SG tube drained, reference leg started to vaporize (see Subsection 2.4)
LDP-401* LDP-402*	Differential pressure transmitter - level	Data invalid; see Subsection 5.3.1.2
LDP-509	Differential pressure transmitter - level	Level values invalid due to break location
LDP-801	Differential pressure transmitter - level	Inoperable; level over-ranged for significant portion of transient
LDP-802* LDP-804	Differential pressure transmitter - level	Data valid until PRHR initially drained at 500 seconds; after which data suspect due to possible boiling of common reference line of LDP-802 and LDP-804
PT_101	Pressure transmitter	Data less than 6.1 psig invalid
PT_102 PT_103	Pressure transmitter	Data less than 6.2 psig invalid
PT_104	Pressure transmitter	Data less than 6.4 psig invalid
PT_108	Pressure transmitter	Data less than 8.4 psig invalid
PT_109	Pressure transmitter	Data less than 6.3 psig invalid
PT_111	Pressure transmitter	Data less than 6.0 psig invalid
PT_112	Pressure transmitter	Data less than 8.8 psig invalid
PT_113	Pressure transmitter	Data less than 6.4 psig invalid

TABLE 5.3.2-2 (Continued)
MATRIX TEST SB09 INOPERABLE INSTRUMENTS/INVALID DATA CHANNELS

Instrument No.	Instrument Type	Description of Problem
PT_201	Pressure transmitter	Data less than 1.1 psig invalid
PT_202	Pressure transmitter	Data less than 5.9 psig invalid
PT_205	Pressure transmitter	Data less than 6.1 psig invalid
TF-170	Thermocouple	Invalid temperature for entire test due to leakage past seal; data influenced by downcomer temperatures
TF-203	Thermocouple	Failed
TF-615	Thermocouple	Failed; invalid data
TFM-105 TFM-703	Thermocouple for heat flux meter	Unavailable
TH-317-1 through TH-317-4	Thermocouple measuring heater temperature	Removed with heater rod C2-317
TW-552 TW-534 TW-547	Thermocouple	Failed by false indication of temperature

Note:

* Instruments marked with an asterisk are critical instruments. See Subsection 5.3.2.2 for discussion.

Table 5.3.2-3 on pages 5.3.2-19 through 5.3.2-22 is not included in this nonproprietary document.

The Bar Charts for Table 5.3.2-3 on pages 5.3.2-23 through 5.3.2-27 are not included in this nonproprietary document.

FIGURE 1 CMT #1 - CL #3 SBLOCA BREAK PIPE ARRANGEMENT
(TOP VIEW)

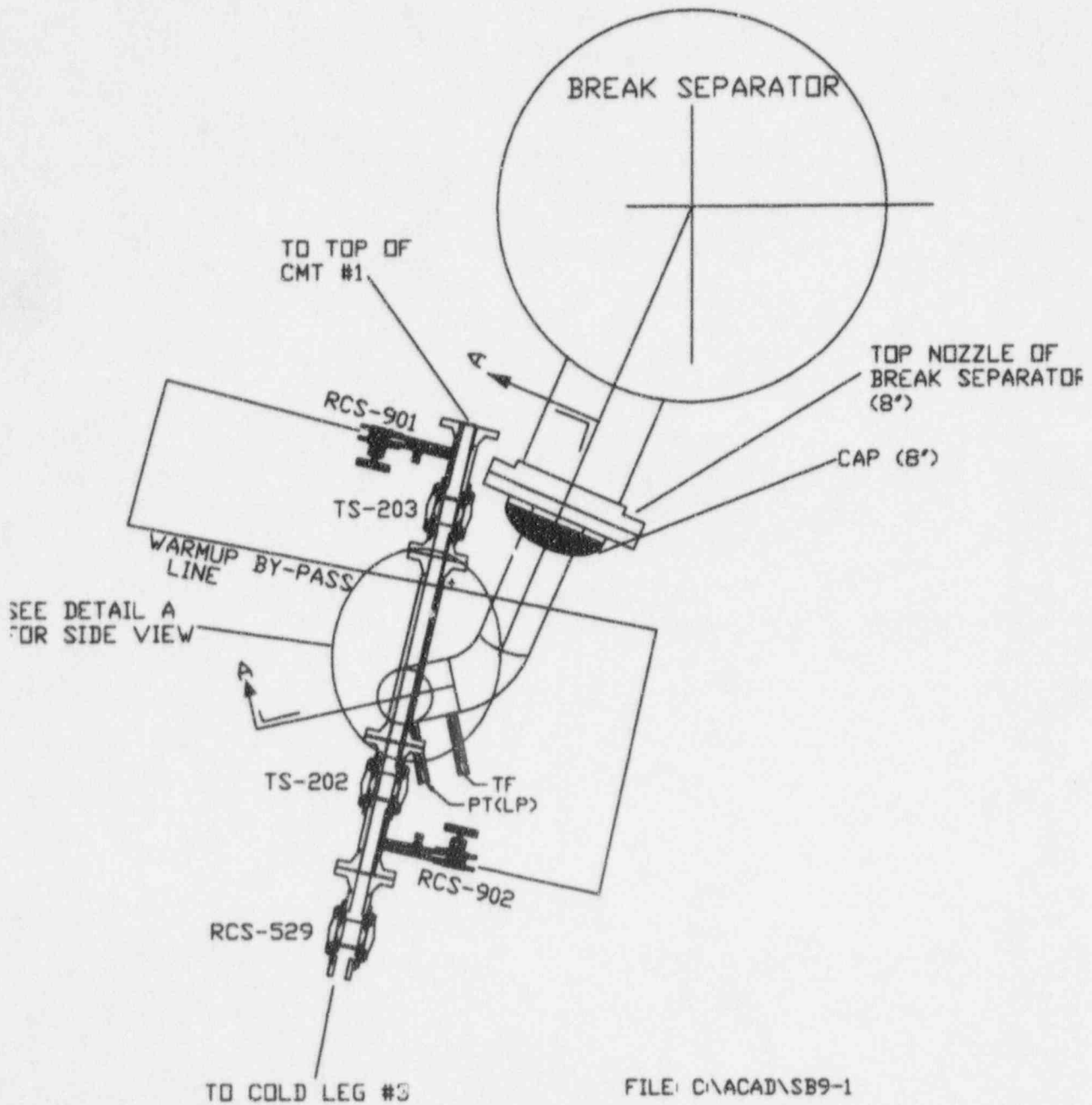
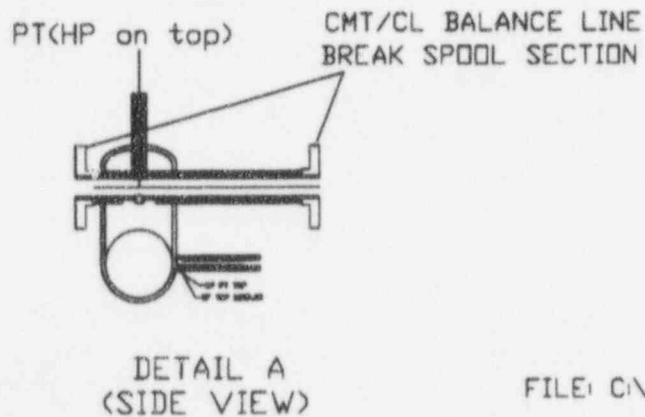
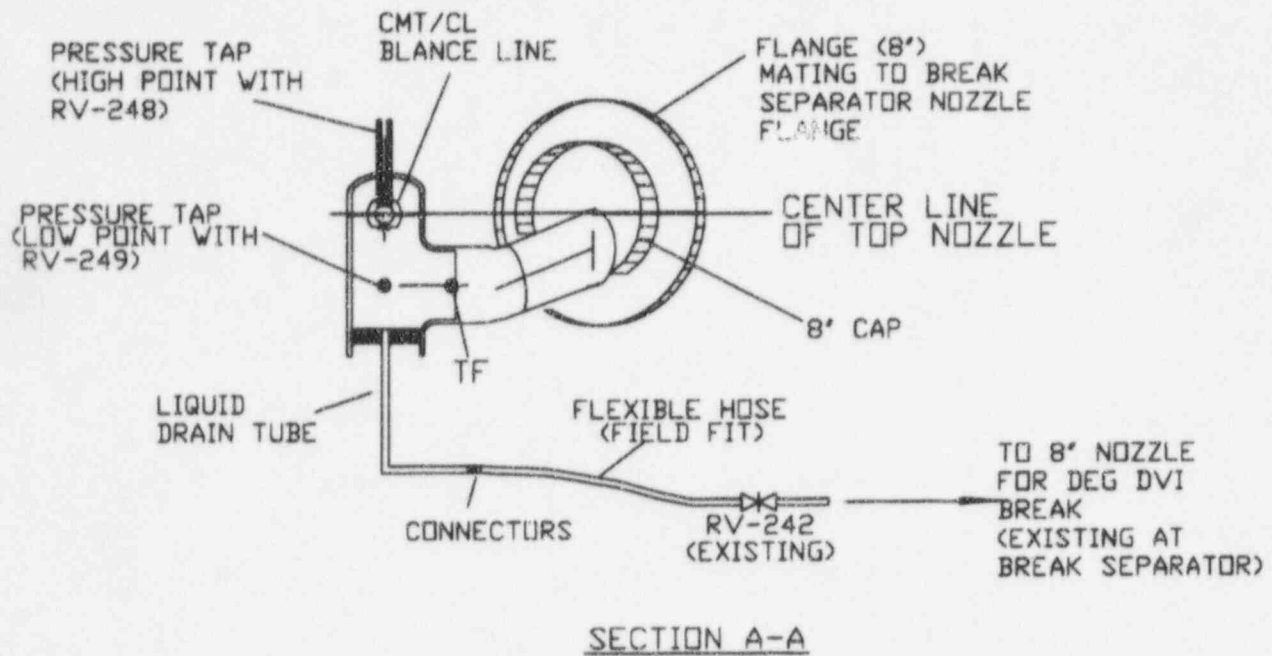


Figure 5.3.2-1 CMT-1 Balance-Line Break Pipe Arrangement for Matrix Test SB09

FIGURE 2 CMT#1 - CL#3 SBLOCA BREAK PIPE ARRANGEMENT
(SIDE VIEW AND DETAILS)



FILE: C:\ACAD\SB9-2

Figure 5.3.2-2 CMT-1 2-In. Balance-Line Break Pipe Arrangement

Figures 5.3.2-3 through 5.3.2-102 are not included in this nonproprietary document.

5.4 Direct Vessel Injection Line Breaks

Matrix Tests SB12 (OSU Test U0112), SB13 (OSU Test U0113), and SB28 (OSU Test U0028) characterized the thermal-hydraulic phenomena and system response to a break in the direct vessel injection (DVI) line. Two of the tests, Matrix Tests SB12 and SB28, were double-ended guillotine (DEG) breaks; Matrix Test SB13 was a 2-in. break of DVI-1. Matrix Test SB12 was used as a reference test for comparison with the other two. The comparison of Matrix Test SB13 with Matrix Test SB12 allowed the evaluation of the effect of a smaller break. The comparison of Matrix Test SB28 with Matrix Test SB12 allowed the evaluation of the results of multiple failures. Results of reference test SB12 appear in Subsection 5.4.1. Results of comparison tests SB13 and SB28 appear in Subsections 5.4.2 and 5.4.3, respectively.

5.4.1 Reference Double-Ended Guillotine Line Break (Matrix Test SB12)

This section of the report discusses the test results of Matrix Test SB12, a simulated DEG break of DVI-1. The test was successfully conducted on July 21, 1994, and took about 3 hours.

The first part of this section describes the system configuration and initial conditions of Matrix Test SB12, followed by a table of inoperable instruments. Next, a sequence of events is provided. The sequence of events table provides time events in a tabular and a bar-chart format. Following the sequence of events subsection is a description of the overall system interactions in the test. Finally, a discussion of component responses is provided. This section provides a more detailed discussion of the test by reviewing it from the component level.

The text references data from instrumentation channels which are plotted and included as figures to this report. The data plots contain the instrument numbers and their descriptions. Numerous multi-channel plots are used to describe the thermal-hydraulic behavior observed in the test.

5.4.1.1 System Configuration and Initial Conditions

Matrix Test SB12, a simulated DEG break of DVI-1, was conducted using an approved written procedure. Reactor-side break flow was piped to the break separator. All other connections to the break separator were isolated by using blind inserts in the piping source. The core makeup tank (CMT) and accumulator-side break flow was not aligned to a separator, but was aligned directly to the sump. Piping connected the primary sump to DVI-1 downstream of the CMT-1 and accumulator-1 (ACC-1) junction tee (Figure 5.4.1-1).

Before break initiation, the break separator and primary sump were isolated from the break sources by two break valves (Figure 5.4.1-1). TS-203 isolated the reactor side of the break; TS-202 isolated the CMT side of the break.

Liquid break flow from the reactor side of the break was measured by FMM-905. The break steam flow from the reactor side of the break was measured by FVM-905, installed in the []^{a,b,c} steam line of the break separator. The []^{a,b,c} steam line from the break separator was isolated throughout the test (Appendix G, Dwg. OSU 600901).

Liquid break flow from the CMT-1 and ACC-1 side of the break was measured by FMM-501 and FMM-401, respectively (Appendix G, Dwg. OSU 600206). Steam break flow from the CMT side of the break was measured after it passed through the primary sump. The []^{a,b,c} primary sump exhaust line was connected to the []^{a,b,c} steam line of the break separator. Steam flow from the

primary sump was measured by FVM-906. Both FVM-903 and FVM-906 measured any steam injected into the primary sump from CMT-1.

Break instrumentation measured the pressure upstream of the break and differential pressure across the break. The following summarizes this pressure instrumentation. Flow indication and break valve numbers are also summarized for each of the two sides of the break.

	Break Valve	Liquid Flow Meter	Steam Flow Meter	Differential Pressure Across Break	Pressure Upstream of Break
Reactor side of the break	TS-203	FMM-905	FVM-905	DP-215	PT-203
CMT/Accumulator side of the break	TS-202	FMM-401 and FMM-501	FVM-906	DP-216	PT-206

The two sides of the break were connected by a warmup line and two series isolation valves (RCS-901 and RCS-902; Figure 5.4.1-1). With the break valves closed, the isolation valves were opened for a period of time before break initiation to pressurize the CMT-1 injection line to simulate normal plant operation.

Seven temporary thermocouples were installed in the primary sump or lines connected to the primary sump. The purpose of the thermocouples was to obtain additional data on break steam and liquid temperatures. To accommodate these additional thermocouples, seven thermocouples, located in the two short thermocouple rods in CMT-1, were disconnected from the data acquisition system (DAS). The wiring that connected the CMT-1 thermocouples to the DAS was used to connect the seven temporary thermocouples to the DAS. Table 5.4.1-4 provides the DAS channel assignment of the temporary thermocouples. All temporary thermocouples were given a 900-series channel number. The channel numbers of the seven disconnected CMT-1 thermocouples were not recorded in the Matrix Test SB12 data files; instead, the seven temporary channels were recorded.

Nozzles were installed in the automatic depressurization system (ADS) 1 and 3 lines to simulate one-line operation. A nozzle was installed in the ADS-2 line to simulate two-line operation. Nozzles were installed in the ADS 4-1 and 4-2 lines to simulate 100-percent flow, or two-line operation.

The nonsafety systems, chemical and volume control system (CVS) and normal residual heat removal system (RNS), were not used in this test. The CVS and RNS pumps did not run.

Before the test was initiated by pressing the TEST pushbutton, a standard facility heatup and checkout was performed. The details of the heatup and checkout can be found in Section 2.7.

Table 5.4.1-1 contains the initial system conditions for Matrix Test SB12. The data recorded for control board indications of pressurizer pressure and level, steam generator (SG) pressures and levels, and hot-leg (HL) temperatures were obtained from the values recorded in the procedure. All other values for initial conditions were obtained from averaging the DAS data for about 2 minutes. This was the time interval between when the DAS started to record data and when the signal to open the break valves occurred.

Table 5.4.1-1 indicates the initial conditions of ACC-1 and ACC-2 were out of specification. ACC-1 pressure (PT-401) was 3.4 psig or 1.5 percent below the required pressure band. ACC-2 pressure (PT-402) was 1.6 psig or 0.7 percent below the required pressure band. The loss of pressure between tank pressurization and test actuation was possibly due to the nitrogen gas cooling in the accumulator. Test analysis starting with the recorded lower accumulator pressure is still possible.

The transient was initiated by simultaneously opening the two break valves and continued through CMT and accumulator injection, ADS actuation, in-containment refueling water storage tank (IRWST) injection, and primary sump injection. All actions were automatic and required no operator action. The total test time was about 3 hours.

5.4.1.2 Inoperable Instruments

Table 5.4.1-2 contains the listing of invalid data and instruments that were inoperable or invalid for all or portions of this test. Some of the instruments listed in the table are on the Critical Instrument List (Subsection 3.2, Table 3.2-2) and, therefore, are listed here.

FDP-605 measured the differential pressure (psid) across the ADS-1 flow nozzle. The transmitter over-ranged momentarily when the ADS-1 valve opened. Total flow through the ADS 1-3 valve complex can be determined by measuring ADS 1-3 separator liquid and steam flow from FMM-601 and FVM-601.

FMM-201, FMM-202, FMM-203, and FMM-204 measured flow (gpm) in each of the four cold legs. A decision was made to continue testing without the availability of these instruments. Replacement flow meters repeatedly failed; their continued use was precluded due to cracking of the ceramic liners from thermal stratification in the loop piping. The necessary boundary conditions for loop flow could be determined from DP-202, DP-203, DP-205, and DP-206.

CMT-1 and CMT-2 injection flow meters FMM-501 and FMM-504 and passive residual heat removal (PRHR) inlet and outlet flow meters FMM-802 and FMM-804 provided accurate data when sensing liquid, but became inaccurate when sensing two-phase or steam flow.

SG tube level data (LDP-215, LDP-218, LDP-219, and LDP-222) were biased by vaporization of the water in the transmitter reference leg after the SG tubes started to drain; however, data provided accurate indication of the time when the tubes were empty.

LDP-401 and LDP-402 measured ACC-1 and ACC-2 levels. Due to air trapped in the sense lines for the transmitters, data for these transmitters were invalid. However, the initial level of the tank was established by a standpipe, so the level was constant test to test. The drain rates can be calculated using ACC-1 and ACC-2 flow meters FMM-401 and FMM-402. Alternately, a pressure correction may be applied directly to the level indications of LDP-401 and LDP-402.

LDP-802 measured the level of the PRHR HX. Data from this transmitter were valid until the HX drained at 600 seconds. After this time, data are suspect due to possible boiling of common reference line of LDP-802 and LDP-804.

PT-201 measured reactor coolant system (RCS) pressure at the top of SG-1 long tube. On August 15, 1994, it was discovered that the transmitter had an incorrect zero compensation, which resulted in a negative error and negative data at low pressures. The transmitter zero was corrected at that time. PT_201 data obtained during Matrix Test SB12 had the zero correction performed, and the corrected data appear as PT_201. Negative data and corrected negative data can be used to determine trends, but are considered inaccurate. There is sufficient other pressure data during the period when PT_201 data were invalid.

LDP-611 and LDP-612 measured the level of ADS 4-1 and ADS 4-2 separators. The transmitters sense line pressures were affected by primary sump pressure before ADS-4 actuation occurred. Although the transmitters were operable, data from these transmitters should be ignored before ADS-4 actuation. After ADS actuation, the data were valid.

FVM-603 and FVM-602 measured steam flow exiting the ADS 4-1 and ADS 4-2 separators to the break and ADS measurement system (BAMS) header. Flow indications prior to the ADS 4-1 and ADS 4-2 valves opening were false indications that were probably due to reverse flow from the BAMS header to the separators.

Rack 1 data acquisition stopped about 16 minutes before rack 2 and rack 3. Data recorded by rack 1 were sufficient for a successful test.

Considering these critical instrument failures, sufficient instrumentation was available to allow the performance of mass balances as demonstrated in Subsection 5.4.1.6 and Appendix E. An energy balance will be performed and reported in the *AP600 Low-Pressure Integral Systems Test at Oregon State University Test Analysis Report WCAP-14292*.⁽²⁾

5.4.1.3 Sequence of Events

Table 5.4.1-3 contains the sequence of events of Matrix Test SB12. The first two pages of the table provide the event times of selected events in the test. The ensuing pages of the table use bar charts of the data to provide a visual representation of the sequence of events. Both the numeric table and the bar charts sort the events in chronologic order.

The first two pages of Table 5.4.1-3 indicate the source of the actual time data. A D in the Data Source column indicates the recorded time was obtained from a software program that monitored digital events in the facility, including pump starts and stops, valve limit switch actuations, and alarms. An A in the Data Source column indicates the time data was obtained by reviewing test data obtained from the DAS. Although test data from the DAS were a digital format, the DAS monitored analog events such as pressure, flow, and temperature.

5.4.1.4 Test Results and Evaluation

This section contains an overall description of the events that occurred during Matrix Test SB12. The description is divided into three phases:

- Initial Depressurization Phase: simulated break initiation to ADS-1 actuation
- ADS Phase: ADS-1 actuation to start of IRWST injection
- IRWST Injection Phase: start of IRWST injection to end of test

Initial Depressurization Phase

Prior to initiation of the break, all applicable systems achieved normal operating conditions and initial boundary conditions as described in Table 5.4.1-1. The transient was then initiated at time 0 by opening the break valves, TS-202 and TS-203.

One-half second after the break valves opened, the steam controller setpoint reset to control steam header pressure at []^{a,b,c}. This setpoint closed the steam header control valve, stopping steam flow from the SGs. The steam controller's output signal kept the steam header valve closed for the entire test.

The reactor controller setpoint also changed 1/2 second after the break valves opened. Prior to the break, the reactor controller adjusted the reactor heaters' power to maintain an average hot-leg temperature of []^{a,b,c}. One-half second after break initiation, the reactor controller function changed. The controller output then controlled heater power to simulate decay heat after a reactor trip. The heater controller demand signal and actual heater power output are shown in Appendix F.

Table 5.4.1-3 indicates that, per design logic, the following events occurred in the first []^{a,b,c} pressurizer power was disabled; the main feed pump tripped; the passive residual heat removal heat exchanger (PRHR HX) outlet valve opened; the CMT-1 and CMT-2 injection valves opened; and the reactor coolant pumps (RCPs) tripped.

Break flow from the reactor side of the break started immediately (FMM-905; Figure 5.4.1-2 and FVM-905; Figure 5.4.1-3). The break system had been aligned so that steam from the break separator flowed through the []^{a,b,c} break separator steam header. The []^{a,b,c} break separator steam header was isolated from the break separator by closed valve CSS-906. Steam flow through the

[]^{a,b,c} header came from the primary sump []^{a,b,c} exhaust line (Appendix G, Dwg. OSU 600901).

Both the liquid and steam flow from the break separator increased from 0 at the time of break valve opening until about []^{a,b,c} FMM-905 indicated a flow of about []^{a,b,c} (Figure 5.4.1-2). The steam flow meter (FVM-905) indicated a flow of about []^{a,b,c} (Figure 5.4.1-3). At []^{a,b,c} both flows decreased dramatically. Before the ADS-1 valve opened at []^{a,b,c} liquid flow had decreased about []^{a,b,c} percent to a flow of []^{a,b,c}. Steam flow had decreased about []^{a,b,c} percent to a flow of []^{a,b,c}.

This decrease in break flow in a period of []^{a,b,c} was due to the uncovering of the DVI-1 penetration in the downcomer annulus. When compensated for density, LDP-116 and LDP-140 revealed a collapsed annulus level of about []^{a,b,c} (Figure 5.4.1-14). The top of the DVI penetration was []^{a,b,c}. Thus, after []^{a,b,c} the level in the downcomer dropped below the DVI line. DVI break flow coming from the reactor became two-phase flow when the level dropped below the DVI nozzle. Initiation of two-phase flow created a sharp drop in pressure at the inlet of TS-203, which was recorded by PT-203 (Figure 5.4.1-15).

Break flow from the CMT-1/ACC-1 side of the break started immediately when the break valves opened. After TS-202 opened, ACC-1 injected directly into the primary sump. Its injection (break) flow rate was recorded by FMM-401. []^{a,b,c} after the break valves opened, the CMT-1 injection isolation valve automatically opened. Break flow from CMT-1 was recorded by FMM-501 (Figure 5.4.1-4).

Driving head for ACC-1 flow was the pressure difference between the nitrogen gas pressure in the accumulator (initially 227 psig) and the atmospheric pressure of the primary sump. The driving head for CMT-1 flow was the pressure difference between cold leg-3 (CL-3) pressure sensed at the top of the CMT (via the CMT-1 balance line) and the atmospheric pressure of the sump.

The high differential heads for CMT-1 and ACC-1 flow created a rapid drain of these tanks. Without a DVI break, CMT flow is created by a relatively small thermal head between the CMT fluid temperature and the reactor fluid temperature. Also, the accumulator does not inject until reactor coolant system (RCS) pressure is less than the initial nitrogen gas pressure in the tank, usually after ADS-1 actuation. As a result of the tank discharging to atmospheric pressure, CMT-1 wide-range level indication was about []^{a,b,c} percent of initial tank level and ACC-1 wide-range level indication was about []^{a,b,c} percent of initial tank level when ADS-1 actuated at []^{a,b,c} (Figures 5.4.1-5 and 5.4.1-6).

A detailed discussion of the response of CMT-1 and ACC-1 to the break is given in Subsection 5.4.1.5. However, it is worth noting here that the injection flow of ACC-1 was terminated briefly before the tank was empty. Flow went to 0 for about []^{a,b,c} from about []^{a,b,c} (Figure 5.4.1-4). The cessation of flow may have been due to higher backpressure

created in the common injection line to the sump when injection water from CMT-1 reached []^{a,b,c} (Figure 5.4.2-70). Backpressure was created when the water flashed to steam in the primary sump, which was near atmospheric pressure.

The large break flow rate created a rapid depressurization and level decrease in the RCS. Table 5.4.1-3 shows that the pressurizer, pressurizer surge line, and SG tubes and channel heads were empty at ADS-1 actuation. LDP-116 and LDP-140 (compensated for density) revealed that the cold legs were empty when ADS-1 actuated. In fact, by this time, the downcomer annulus liquid level was at the bottom of the DVI line, or about []^{a,b,c} (Figure 5.4.1-14).

When ADS-1 actuated, RCS pressure measured at the top of the SG-1 and SG-2 tubes was only []^{a,b,c} below the secondary steam pressure of []^{a,b,c} (Figure 5.4.1-66). This shows that the secondary side of the SGs had become a heat source to the RCS before ADS-1 actuation.

In all breaks, there is a period when the primary and secondary plant pressures arrive at a quasi-equilibrium condition for a period of time. For Matrix Test SB12, this period was very short, about []^{a,b,c} from []^{a,b,c} after the break (Figure 5.4.1-66). After this time, the secondary side, or steam side, of the SGs became a heat source to the fluid in the RCS.

The large size of the break very quickly produced steam in the reactor upper head, reactor upper plenum, and hot legs. The description of the steam formation in these regions used data from the following level channels:

Channel Number	Channel Monitors	Void Fraction Data on Figure
LDP-112	Lower portion of upper reactor plenum	5.4.1-16
LDP-113	Upper portion of upper reactor plenum	5.4.1-16
LDP-115	Upper reactor head	5.4.1-16
LDP-207	SG-1 hot-leg elbow	5.4.1-17
LDP-208	SG-2 hot-leg elbow	5.4.1-17
LDP-209	SG-1 hot-leg channel head	5.4.1-17
LDP-214	SG-2 hot-leg channel head	5.4.1-17

Using data from the level channels and the calibrated range of instruments, a core steam percent for each channel was calculated. The equation used to calculate steam percent was:

$$\text{Steam percent} = \left(1 - \frac{\text{compensated level}}{\text{instrument range}} \right) 100$$

Data plots of the calculation results were plotted in the figures referenced in the previous table. Until the RCPs tripped at []^{a,b,c} level measurements in the RCS responded to differential pressures created by RCS flow. This, in turn, affected the steam percent calculations and provided incorrect data for the first []^{a,b,c} of the test.

The plotted core steam percent data indicated steam started to form in the upper head and upper portion of the upper plenum immediately after the RCPs tripped. The plenum voided more rapidly than the upper head because the upper head fluid was separated from the upper plenum by the upper support plate. The only way for the fluid to exit the upper head was to flow to the downcomer annulus via ten small bypass holes in the upper flange of the core barrel, or to gravity-drain to the upper plenum via eight small holes in the upper support plate.

At []^{a,b,c} the upper portion of the upper plenum was over []^{a,b,c} percent voided; the upper head was only []^{a,b,c} percent voided. At ADS-1 actuation, however, the difference in void was only []^{a,b,c} percent, with the upper plenum at []^{a,b,c} percent and the upper head at []^{a,b,c} percent (Figure 5.4.1-16).

The level instrumentation in the hot-leg channel heads and hot-leg elbows of the SGs provided oscillating data, generally 20 percent of full range. The data are a result of the draining of the SGs. This observation is supported by a comparison of the level channels between the two SGs. The void fraction data of the two SGs are essentially the same when allowances are made for the []^{a,b,c}-percent oscillations in level data (Figure 5.4.1-17).

Data plots for the steam percent in the SG-1 and SG-2 channel heads show a sharp increase in void fraction at about []^{a,b,c} that coincides with the completion of the draining of the SG tubes, hot-leg side (Table 5.4.1-3). The hot-leg channel heads reached their maximum void fraction []^{a,b,c} later, at []^{a,b,c} or when the draining of the SG hot-leg channel head was completed.

While the SG hot-leg channel heads drained, the steam percent in the hot-leg elbows increased. By the time the channel heads emptied, the steam percent in both SG elbows was about []^{a,b,c}-percent. The steam percent was about at this value at the time of ADS-1 actuation.

Before ADS-1 actuation, CMT-2 was the only source of makeup inventory available to the RCS. The DVI-1 break made CMT-1 and ACC-1 unavailable for injection into the core. IRWST injection did not start before ADS-1 actuation because RCS pressure was greater than the static head created by the

water level in the IRWST; ACC-2 injection did not start for the same reason. The initial nitrogen gas pressure of []^{a,b,c} in ACC-2 was not a sufficient head to overcome RCS pressure before ADS-1 actuated. RCS pressure was about []^{a,b,c} at ADS-1 actuation (Figure 5.4.1-7).

CMT-2 injection started immediately after the isolation valve in its injection line automatically opened at []^{a,b,c}. Flow to the core was recorded by FMM-504 (Figure 5.4.1-8). Flow was relatively constant at []^{a,b,c} until CMT-2 transitioned from recirculation to draindown flow. The most apparent indication of the transition in the CMT was the rapid decrease in water level in its balance line. The level channel that monitored the CMT-2 balance line level was LDP-510 (Figure 5.4.1-9). The flow transitioned in CMT-1 at about []^{a,b,c} although its oscillating balance line level provided an indication it attempted to do so earlier at []^{a,b,c}.

When the flow transitioned in CMT-2, several actions occurred. First, the level in the CMT began to decrease because the liquid draining into the core was no longer being replaced by hotter water from CL-1 (Figure 5.4.1-5). Second, the balance line level for CMT-2/CL-1 started to decrease as the region in the upper portion of the balance line started to void. The balance line for CMT-2 started to empty at about []^{a,b,c} (Figure 5.4.1-9). Third, CMT-2 injection flow to the vessel increased (Figure 5.4.1-8). The increase in CMT-2 injection flow will be discussed in more detail in Subsection 5.4.1.5 in the component response for CMTs. Injection flow of CMT-2 over-ranged flow instrument FMM-504 from []^{a,b,c} until the time of ADS-1 actuation at []^{a,b,c} (FMM-504 was ranged for []^{a,b,c} for Matrix Test SB12).

The suction for the PRHR HX was HL-2. It discharged to the cold-leg plenum of SG-2. When the PRHR HX outlet valve automatically opened at []^{a,b,c} natural circulation flow was established immediately, as recorded by the HX inlet and outlet flow meters (Figure 5.4.1-10). Within []^{a,b,c} the inlet temperature of the HX was at saturation temperature. The outlet temperature increased from an initial temperature of []^{a,b,c} to a temperature of []^{a,b,c} when ADS-1 actuated (Figure 5.4.1-11).

Both inlet and outlet PRHR HX flow meters are magnetic meters, which are inaccurate when partially or fully voided with steam. Thus, the inlet flow measurements must be used with caution, for it is unknown how soon after reaching saturation temperature at []^{a,b,c} that two-phase flow developed. Magnetic flow meters do, however, provide accurate indication of flow when the liquid is subcooled. The outlet temperature of the HX was subcooled up to ADS-1 actuation (and during the entire test), so the outlet flow meter was used to determine the outlet flow rate (Figure 5.4.1-11). At the time of ADS-1 actuation, the outlet flow meter recorded a flow rate of []^{a,b,c} returning to CL-2 and CL-4. The flow rate did not vary much from this value for the duration of the test.

As stated earlier, the primary side of both SGs was completely drained at the time of ADS actuation. In fact, Table 5.4.1-3 shows that the tubes of both SGs were empty by []^{a,b,c}. For the first []^{a,b,c} the indicated temperatures in the tubes stayed subcooled or saturated. As the SG tubes drained, steam temperatures in the tubes followed the saturation temperature of the RCS

(Figures 5.4.1-12 and 5.4.1-13). At ADS-1 actuation, the tube temperatures were at RCS saturation temperatures. The indicated SG tube temperatures increased to a superheated condition after ADS-1 actuation.

Actuation of the ADS occurred relatively quickly. The short interval between the initial break and actuation of ADS-1 was a result of the rapid drainage of CMT-1 to the primary sump. The facility control logic opened ADS-1 []^{a,b,c} after the level in either CMT reached a low level setpoint. The faster either CMT drained, the quicker ADS-1 actuated. In Matrix Test SB12, the drain rate of CMT-1 was the highest experienced in any break. When the CMT-1 outlet valve automatically opened at []^{a,b,c} it was aligned directly to the primary sump. The CMT was at initial RCS pressure, and the primary sump was at atmospheric pressure. This driving head for CMT flow was the largest experienced by the CMTs during testing.

The injection (break) flow of CMT-1 was sufficiently large to over-range FMM-501 for the entire period of CMT-1 liquid injection (Figure 5.4.1-4). CMT-1 injection was complete and the tank was empty at 148 seconds. FMM-501 data were invalid after this time because the magnetic flow meter's indication was not accurate when measured in a steam environment. The calibrated range of FMM-501 was []^{a,b,c} for this test. Thus, CMT-1 quickly reached its low level setpoint at []^{a,b,c}. Per design logic, the ADS-1 valve started opening at []^{a,b,c} after CMT-1 reached its low level setpoint.

When TS-202 opened, ACC-1 injected immediately to the primary sump. The initial injection (break) flow of ACC-1 was sufficiently large to over-range flow meter FMM-401 from []^{a,b,c} (Figure 5.4.1-4). The calibrated range of FMM-401 for Matrix Test SB12 was []^{a,b,c}. The injection flow of ACC-1 was abruptly interrupted at about []^{a,b,c}. This cessation of flow was due to the backpressure created by CMT-1 injection in the common discharge line of CMT-1 and ACC-1. The injection flow of ACC-1 did not start again until after ADS-1 actuation.

ADS Phase

When CMT-1 reached a low level setpoint at []^{a,b,c} (Table 5.4.1-3), it provided an input to the facility's programmable logic controller (PLC). Per design, the PLC supplied a signal to open the ADS-1 valve []^{a,b,c} later. At []^{a,b,c} the ADS-1 valve opened and actuated its lower limit switch. The control logic of the PLC also provided time-delayed signals to open the ADS-2 and ADS-3 valves. Also per design, the lower limit switch of ADS-2 was actuated at []^{a,b,c} and the lower limit switch of ADS-2 was actuated at []^{a,b,c}.

When ADS-1 actuated at []^{a,b,c} RCS pressure was []^{a,b,c} (Figure 5.4.1-19). ADS liquid flow through the ADS 1-3 sparger was monitored by FMM-601; ADS steam flow to the ADS 1-3 sparger was monitored by FVM-601 (Figure 5.4.1-18). Liquid flow through the ADS-1 valve lasted a very short time. Liquid flow lasted only []^{a,b,c} after the ADS-1 valve opened and peaked at []^{a,b,c} (Figure 5.4.1-18). Before the ADS-2 valve opened, flow through ADS-1 had

stopped. Until ADS-2 actuation, steam flow from the ADS was negligible (about []^{a,b,c}) when compared with break flows (Figure 5.4.1-3). These data imply that depressurization of the RCS between ADS-1 and ADS-2 was governed by the large break flows and was not a result of ADS-1 actuation.

The liquid flow rate from the reactor side of the DVI break was largely unaffected by ADS-1 actuation. About []^{a,b,c} before ADS-1 actuation (at []^{a,b,c}), the collapsed liquid level in the downcomer annulus had reached the elevation of the DVI penetration, resulting in a sharp drop in reactor-side liquid break flow from []^{a,b,c} (Figure 5.4.1-2). When ADS-1 actuated, flow increased very slightly to []^{a,b,c} and decayed back to []^{a,b,c} by the time the ADS-2 valve opened.

Steam flow from the reactor side of the break was similarly unaffected by ADS-1 actuation. In fact, ADS-2 and ADS-3 actuation also had little effect. From the time the DVI nozzle became uncovered, steam flow from the break at the reactor smoothly decayed from []^{a,b,c} at []^{a,b,c} (before ADS-1 actuation) to 0 cfm at []^{a,b,c} after ADS-3 actuation; (Figure 5.4.1-3).

ADS-1 actuation also had little effect on break flow from the CMT/accumulator side of the break. When the ADS-1 valve opened, CMT-1 was injecting to the primary sump. As described earlier, ACC-1 flow had stopped before ADS-1 actuation due to the interaction with CMT-1 flow. ACC-1 did not inject again until after CMT-1 was empty, shortly after ADS-2 actuation. Thus, the only effect ADS-1 had on the CMT/accumulator side of the break was to decrease the pressure on the top of CMT-1, which tended to decrease the break flow rate of CMT-1 to the primary sump. The injection flow meter was over-ranged during this test, so a direct measurement of CMT-1 flow was not available (Figure 5.4.1-4). The wide-range level plot of CMT-1, however, reveals a relatively constant rate of level decrease from []^{a,b,c} (before ADS-1 actuation) until the tank was empty at about []^{a,b,c} (after ADS-2 actuation; Figure 5.4.1-5). Decreasing RCS pressure had the effect of slowing CMT-1 injection (break) flow slightly.

When ADS-1 actuation occurred, CMT-2 was injecting into the reactor vessel via DVI-2. At the time, the CMT-2 injection flow rate was greater than the []^{a,b,c} range of its injection flow meter (Figure 5.4.1-8). ACC-2 did not inject into the reactor before ADS-1 actuation because RCS pressure was greater than the initial nitrogen gas pressure in ACC-2 (Figure 5.4.1-8).

ADS-1 actuation had the opposite effect on ACC-2 and CMT-2 injection flows. As mentioned, the rate of RCS pressure decline increased slightly when the ADS-1 valve opened. RCS pressure decreased sufficiently at []^{a,b,c} (after the ADS-1 valve opened) for ACC-2 to begin injection. The plot of ACC-2 injection flow shows that the flow increased quickly to about []^{a,b,c} and, from there, slowly increased to about []^{a,b,c} when ADS-2 actuated (Figure 5.4.1-8). As ACC-2 flow increased, CMT-2 flow decreased.

These combined facts revealed that ADS-1 actuation had a small effect on the rate of depressurization of the RCS. The loss of inventory through the ADS-1 valve was small when compared with DVI break flows.

ADS-2 actuation had a greater effect on the RCS depressurization rate than ADS-1 actuation (Figure 5.4.1-19). The effect was a direct result of inventory loss through the ADS and an indirect effect through its influence on break flow from the reactor side of the DVI break.

When the ADS-2 valve opened at []^{a,b,c} RCS pressure was []^{a,b,c}. Liquid flow to the ADS 1-3 sparger was short-lived, just as it was after ADS-1 actuation. The duration of liquid flow was shorter than after ADS-1 actuation, lasting only about []^{a,b,c} (Figure 5.4.1-18). Liquid flow to the sparger oscillated for the remainder of the test. ADS-3 and ADS-4 actuation had no discernable effect on liquid flow.

After ADS-2 actuation, ADS steam flow to the IRWST was large when compared with steam flow to the primary sump from the break (Figures 5.4.1-3 and 5.4.1-20). When ADS-2 liquid flow from the separator terminated, steam flow immediately increased to about []^{a,b,c}. From this time, steam flow from the ADS decayed smoothly to 0 cfm at []^{a,b,c} (after ADS-4). This indicated that the actuation of ADS-3 and ADS-4 apparently had little effect on the rate of ADS 1-3 steam flow.

The indirect influence of ADS-2 actuation on reactor-side DVI break flow is seen in the plot of break separator liquid flow (Figure 5.4.1-2). The liquid flow varied very little between ADS-1 and ADS-2 actuation. After ADS-2 actuation, flow increased immediately from []^{a,b,c}. This effect was not seen when ADS-3 actuated at []^{a,b,c} but was seen again when ADS-4 actuated at []^{a,b,c}.

Break flow from CMT-1 and ACC-1 was not significantly affected by ADS-2 actuation. CMT-1 had drained []^{a,b,c} after the ADS-2 valve opened at []^{a,b,c} (Figure 5.4.1-5). Draining of CMT-1 created a direct path for steam flow from CL-3 to the primary sump via the balance and injection lines of CMT-1. ADS-2 actuation had little effect on CMT-1 pressure; therefore, it had little effect on CMT-1 flow. Break flow from ACC-1 was unaffected by ADS-2 actuation because the ACC-1 break flow rate was only a function of ACC-1 and primary sump pressures. When ADS-2 actuated, it did not affect these parameters.

ADS-3 and ADS-4 actuation had little effect on the CMT-1/ACC-1 break flow rate for the same reasons stated for ADS-2.

ADS-2 had a measurable impact on the injection flow of CMT-2 and ACC-2 (on the "unbroken" side of the test facility). This effect is best demonstrated by the plot of three sets of data: ACC-2 injection flow (FMM-402), CMT-2 injection flow (FMM-504), and the difference in tank pressures between ACC-2 and CMT-2 (PT-502 minus PT-402; Figure 5.4.1-21). When ADS-2 actuated at

[]^{a,b,c} pressure in the RCS and, therefore, pressure in CMT-2, decreased faster than pressure in the accumulator as it lost inventory. This is seen on the plot as an increase in delta pressure between ACC-2 and CMT-2, from []^{a,b,c} later. The result was an increased ACC-2 injection flow rate of about []^{a,b,c} that lasted until it was empty at about []^{a,b,c} (after ADS-4). Decreasing flow from CMT-2 during this time was a result of both the fluid in the CMT heating and decreasing level in the tank, thereby decreasing the thermal driving head for CMT-2 flow.

The net result of ADS-1 through ADS-3 actuation was to increase the rate of RCS depressurization. RCS pressure decreased from []^{a,b,c} when ADS-1 actuated to a pressure of []^{a,b,c} when ADS-4 actuated. The description of RCS inventory change from ADS-1 actuation to ADS-4 actuation is more complicated, but can be simplified by reviewing the data of the downcomer annulus.

The plot of the downcomer annulus level shows that the collapsed level had decreased to about []^{a,b,c} before ADS-1 actuated at []^{a,b,c} (Figure 5.4.1-14). This collapsed level was lower than the DVI penetration, which means flow from the reactor vessel side of the break was two-phase flow. The level continued to decrease until ACC-2 started injecting at []^{a,b,c}. The level then stabilized at []^{a,b,c} until ADS-2 actuation. When the ADS-2 valve opened, ACC-2 injection flow increased, but was offset by ADS flow to the IRWST and break flow to the primary sump. The result was a downcomer-level decrease to a minimum level of []^{a,b,c} after ADS-2 actuated (or []^{a,b,c}). The level reached its minimum and quickly returned to a level of []^{a,b,c} when ADS-4 actuated at []^{a,b,c}. When ADS-4 actuated, the level stabilized at []^{a,b,c} until IRWST injection started.

The level in the downcomer reached its minimum elevation between ADS-2 and ADS-3 actuation. At the same time, core wide-range level channel LDP-127 recorded its minimum collapsed level (Figure 5.4.1-23). No temperature excursions were recorded as a result of the core reaching its minimum level. This statement is supported by review of the heater rod temperatures at the top of the core, where the temperature would be expected to be the maximum (Figure 5.4.1-22). Heater rod temperatures were well-behaved, with no temperature excursions, even at the lowest recorded downcomer annulus and core levels.

ADS-4 actuation was designed to occur when either of the CMTs reached its low-low level setpoint, with at least []^{a,b,c} having elapsed since ADS-3 actuation. The "broken" CMT-1 obtained its low-low level setpoint before ADS-3 actuation (Table 5.4.1-3). Therefore, the ADS-4 valves opened at []^{a,b,c} after the ADS-3 valve opened. The small difference of []^{a,b,c} is a result of recording ADS-3 and ADS-4 actuation by limit-switch operation of the valve, rather than timing of valve solenoid de-energization.

When ADS-4 actuated at []^{a,b,c}, RCS pressure was []^{a,b,c} (Figure 5.4.1-19). The ADS 4-1 and ADS 4-2 valves opened, initiating flow from the hot legs to the primary sump via the

ADS-4 separators (Appendix G, Dwg. OSU 600203). Liquid flow from the ADS 4-1 and ADS 4-2 separators was measured by FMM-603 and FMM-602, respectively (Figure 5.4.1-24). Steam flow from the ADS-4 separators was measured by FVM-603 and FVM-602 (Figure 5.4.1-20).

Steam flows from both separators were barely measurable, lasting only about []^{a,b,c} with peak flows of only about []^{a,b,c}. Liquid flow rates from the ADS-4 separators were identical, but lasted []^{a,b,c} with peak flows of []^{a,b,c}. The rate of RCS depressurization changed very little as a result of ADS-4 actuation; the large break dominated the pressure decline.

IRWST Injection Phase

IRWST injection valves were closed when the break valves opened. Control logic opened these valves when pressure in the RCS was less than []^{a,b,c} (PT-107). This valve logic prevented backflow through the IRWST check valves before the IRWST started to inject flow. The valves opened at about []^{a,b,c} more than []^{a,b,c} before either IRWST injection flow started (Table 5.4.1-3).

Normal IRWST injection to the reactor vessel occurred when static pressure from the water in the IRWST was larger than RCS pressure. Matrix Test SB12 introduced a variation to this process due to the configuration of the DVI-1. The IRWST, CMT-1, and ACC-1 were connected to a common discharge or break header that attached directly to the primary sump. When backpressure in the common discharge line was less than IRWST static pressure, the IRWST began to discharge to the primary sump. Backpressure in the common discharge line was provided by ACC-1 tank pressure.

Flow from ACC-1 stopped at about []^{a,b,c} as the tank emptied (Figure 5.4.1-4). IRWST-1 flow to the primary sump started about []^{a,b,c} later, at []^{a,b,c} (Figure 5.4.1-25). IRWST flow started when the remaining nitrogen in ACC-1 created a backpressure for IRWST injection flow of about []^{a,b,c}. Because of the break, IRWST-1 injected to the primary sump instead of the RCS. As a result, IRWST-1 injection flow had no effect on the RCS inventory.

IRWST-2 injection did not commence until after pressure in the RCS was below the static head of the IRWST. Flow from IRWST-2 started at []^{a,b,c} after the ADS-4 valves opened (Figure 5.4.1-25). Two other closely related events took place at the same time: ACC-2 emptied and stopped injection flow at []^{a,b,c} and CMT-2 injection flow went from []^{a,b,c} to its final maximum value of about []^{a,b,c} (Figure 5.4.1-8).

Until the onset of sump injection, only IRWST-2 and CMT-2 were available to cool the RCS and replace inventory. The CMT-2 injection flow rate continually decreased until the tank drained at []^{a,b,c}. IRWST-2 injection flow continued for the remainder of the test (Figure 5.4.1-25).

The simultaneous commencement of IRWST injection and the increase in CMT-2 flow (after ADS-4 actuation) had an apparent effect on RCS inventory. The result is seen on the data plot of downcomer

annulus level (Figure 5.4.1-14). The level in the downcomer was essentially constant from the time of ADS-4 actuation at []^{a,b,c} until CMT-2 flow increased at []^{a,b,c} (Figure 5.4.1-21). From this time until about []^{a,b,c} either the collapsed level of the downcomer annulus or the collapsed level of the reactor continually increased (Figure 5.4.1-26). This means that the combined IRWST-2 and CMT-2 injection flow from the "unbroken" side of the facility was greater than the combined flow from the break and ADS-4, thereby increasing the inventory in the RCS.

The level in the primary sump continually increased from the time of the break until the primary sump overflowed into the secondary sump at []^{a,b,c} (Figure 5.4.1-27). When the water level in the primary sump increased above the level of the break separator penetration into the sump, the flow rate from the reactor side of the break started to decrease. At about []^{a,b,c} the level in the primary sump increased sufficiently to create a flow from the primary sump, backward through the break separator, and into the reactor vessel via the DVI break (Figure 5.4.1-28). The driving head for backflow was at its maximum when the primary sump overflowed because the water level in the primary sump could not increase above this level. As the primary sump level increased and break flow decreased, flow from the ADS 4-1 and ADS 4-2 separators increased.

The primary sump injection valves were designed to open when the level in the IRWST was less than []^{a,b,c}. A signal was generated at []^{a,b,c} to open both primary sump valves (Table 5.4.1-3). FMM-902 recorded positive primary sump-2 injection flow to the reactor about []^{a,b,c} after the sump valves opened; however, FMM-901 recorded primary sump-1 negative injection flow as soon as the sump valves opened. The primary sump-1 injection line sustained backflow from the IRWST to the primary sump for the remainder of the test as the level in the tanks equalized (Figure 5.4.1-25).

5.4.1.5 Component Responses

CMT-1

CMT-1 was located on the "broken" side of the plant, i.e., its injection line was routed to the primary sump (Figure 5.4.1-1). Injection flow to the primary sump started immediately when the CMT-1 discharge valve automatically opened at []^{a,b,c}. Flow over-ranged FMM-501, so data from this channel are invalid. Flow values may be obtained by determining the rate of change of the wide-range tank level from LDP-507 (Figure 5.4.1-29).

The CMT-1 level did not decrease until the CMT transitioned between recirculation and draindown flow. Until then, liquid leaving the tank was replaced by hotter liquid from CL-3, thereby keeping the tank full of water. Two instrument channels provided indications of the cessation of recirculation flow: CMT-1 balance line level (LDP-509; Figure 5.4.1-29) and CMT-1 tank pressure (PT-501; Figure 5.4.1-30).

When CMT-1 transitioned from recirculation to draindown flow, single-phase balance-line flow ceased as steam formed at the highest point in the balance line. The formation of steam was measured as a decreasing level in the balance line. The balance line level began to decrease from its full range at []^{a,b,c} indicating that recirculation flow had stopped (Figure 5.4.1-29). At the same time, CMT-1 pressure measured at the top of the tank increased to essentially the pressure of the cold legs (Figure 5.4.1-30). Head loss in the balance line was small due to a low steam flow created as CMT-1 drained. Thus, the differential pressure between CL-3 and CMT-1 became small.

Note: The pressure of CMT-1 is plotted with the pressures of CL-1 and CL-4 only. CL-2 and CL-3 pressure data were not plotted because the narrow-range pressure transmitters in CL-2 and CL-3 were over-ranged at []^{a,b,c}.

CMT-1 began to drain at []^{a,b,c} when it transitioned from recirculation to draindown flow injection and it continued to drain until it was empty at []^{a,b,c} between ADS-1 and ADS-2 actuation (Figure 5.4.1-29). After CMT-1 emptied, a direct path for steam flow was created between CL-3 and the primary sump, via the balance line and CMT-1 injection line. The balance line steam flow rate created a relatively large pressure drop between CL-3 and the top of CMT-1. LDP-509 over-ranged because it responded to the pressure difference between CL-3 and CMT-1 (Figure 5.4.1-29). As the balance line pressure drop increased, CMT-1 pressure decreased and diverged from the cold-leg pressures (Figure 5.4.1-30).

Data from LDP-509 were invalid after []^{a,b,c} after which its level indication was altered by the flow pressure drop in the CMT-1 balance line. Although the pressure drop was small while CMT-1 contained water, it became large when the CMT emptied and steam flowed directly to the primary sump.

FMM-503 also provided accurate indication only until the CMT transitioned to draindown flow. When this occurred at []^{a,b,c} the meter recorded a step decrease in flow (Figure 5.4.1-29). FMM-503 is a magnetic flow meter that does not provide accurate flow indications in a steam environment. When the CMT-1 balance line level decreased, it placed the balance line flow meter in a steam environment. This invalidated any data from FMM-503 any time after []^{a,b,c} because the meter remained in a steam environment for the remainder of the test.

The temperature response of CMT-1 is best described using multichannel plots of three different parameters: tank wall temperatures, fluid temperatures next to the tank wall, and a vertical profile of fluid temperatures using a thermocouple rake in the tank that runs from top to bottom. A representative sample of these temperatures is plotted on three graphs, using temperatures from the top to the bottom of the tank. Reference Appendix G, Dwg. OSU 600501 for specific thermocouple locations.

Data from thermocouples mounted on the CMT-1 long thermocouple rake are plotted with data from the CMT-1 inlet temperature (TF-531) and the saturated temperature of the tank (Figure 5.4.1-69).

The saturated temperature is derived from the reactor pressure data from PT-107. As the CMT drained, the temperature at a given elevation increased as the hot water level in the tank decreased. The temperature continued to increase until the thermocouple temperature became equal to the saturation temperature in the tank.

At about []^{a,b,c} the rake thermocouple data of CMT-1 indicated the onset of a superheated steam environment in the CMT (Figure 5.4.1-69). CMT-1 emptied at this time, after it completed its injection to the primary sump. Thus, data from the rake thermocouples suggest that superheated steam did not exist in CMT-1 until the tank emptied. This statement is contradicted by the data from fluid thermocouples mounted 1 in. from the inside wall of the CMT, spanning the height of the CMT (Figure 5.4.1-70). As the tank drained, these thermocouples were exposed to the steam environment of the CMT, just as the rake and wall thermocouples were. As they became uncovered, data from these thermocouples provided evidence of superheating of the steam at their elevation, even before CMT-1 drained. Further analysis of the temperature indications provided by thermocouples on the long and short rakes, or rods, in both CMTs is provided in Subsection 7.2.

Wall temperature thermocouples provided reasonable temperature data (Figure 5.4.1-71). The wall thermocouples heated to a maximum temperature equal to less than the steam temperature as the thermocouples uncovered and started cooling. When the tank drained, wall temperatures were in the range of []^{a,b,c}

CMT-1 did not reflood during the test. By []^{a,b,c} the CMT wall temperatures and fluid temperatures had reached equilibrium.

CMT-2

The injection line of CMT-2 was not "broken" during this test, so it performed its normal function. The response of CMT-2 was different than the response of CMT-1 simply because CMT-1 drained to the atmospheric pressure of the primary sump and CMT-2 injected into the reactor vessel. There are more similarities between the responses of CMT-1 and CMT-2, however, than differences.

Injection flow to the reactor vessel started immediately when the CMT-2 discharge valve automatically opened at 6 seconds. Flow did not over-range FMM-504 until CMT-2 transitioned from recirculation to draindown flow (Figure 5.4.1-8). When recirculation flow ceased at []^{a,b,c} the pressure difference between the top of CMT-2 and the cold-legs decreased (Figure 5.4.1-67). This interaction between CMT pressure and recirculation flow was discussed in the CMT-1 response subsection. The decreased pressure difference between the cold legs and CMT-2 produced a CMT-2 injection flow rate that exceeded the []^{a,b,c} span of FMM-504.

The transition from recirculation flow decreased the CMT-2 balance line level LDP-510; (Figure 5.4.1-9). The balance line level went to 12 in. within []^{a,b,c} of cessation of

recirculation flow at []^{a,b,c} The level in the CMT-2 balance line was at []^{a,b,c} and remained at []^{a,b,c} for the rest of the test.

FMM-502 recorded a steady balance line flow during the period between the opening of the CMT-2 discharge valve and []^{a,b,c} (Figure 5.4.1-68). Flow data from FMM-502 are invalid after []^{a,b,c} because, after this time, the balance line was not full, placing the flow meter in a steam environment. The magnetic flow meter was only accurate for liquid flow measurement.

As with CMT-1, the level in CMT-2 did not change until the CMT transitioned from recirculation to draindown flow. The level started to decrease at about []^{a,b,c} The CMT emptied at about []^{a,b,c} Unlike the interaction between CMT-1 and ACC-1, when CMT-2 emptied, it had no effect on the ACC-2 flow rate because ACC-2 emptied before CMT-2 (Figures 5.4.1-6 and 5.4.1-68).

The actuation of ADS had a noticeable effect on the injection flow rate of CMT-2 (Figure 5.4.1-68). When the ADS-1 valve opened at []^{a,b,c} the CMT-2 injection flow meter was already over-ranged; however, within about []^{a,b,c} of the ADS-1 valve opening, CMT-2 injection flow was back in the instrument range of []^{a,b,c} for FMM-504. Injection flow continued to decrease until ADS-2 actuated at []^{a,b,c} A sharp increase in flow resulted immediately, and CMT-2 injection flow over-ranged for the last time in the test. Within []^{a,b,c} of ADS-2 actuation, CMT-2 injection flow was in range and decreasing.

The oscillations in CMT-2 injection flow were attributable to ADS actuation. When the ADS-1 or ADS-2 valve opened, pressure in the RCS decreased quickly. The pressure decrease in CMT-2 was delayed slightly as the saturation condition in the CMT responded to the change in balance-line pressure. As a result, injection flow from CMT-2 increased quickly. At the same time, ACC-2 flow was increasing due to decreasing RCS pressure (Figure 5.4.1-8). The increasing flow rate from ACC-2 created backpressure in the injection line, which tended to decrease flow from CMT-2. Injection flow from CMT-2 was temporarily stopped at []^{a,b,c} from the backpressure of ACC-2 flow. Flow from CMT-2 restarted within []^{a,b,c} as ACC-2 drained and finished its injection flow. CMT-2 did not reflood during this test.

Pressurizer

The pressurizer and pressurizer surge line drained quickly after the break initiation, completely draining before ADS-1 actuated. The relatively large break drained the pressurizer by []^{a,b,c} and then drained the surge line by []^{a,b,c} The empty levels translate into a []^{a,b,c}-percent void when plotted as a steam percent (Figure 5.4.1-31).

When the ADS-1 valve opened at []^{a,b,c} it had a small effect on the pressurizer steam percent. The small ADS-1 liquid flow lasted about []^{a,b,c} Steam flow from the pressurizer through the ADS 1-3 separator was maintained until ADS-2 actuation, but it was only about []^{a,b,c} (Figure 5.4.1-18).

At ADS-1 actuation, the pressurizer steam percent decreased about []^{a,b,c} percent (from []^{a,b,c} percent) for several seconds. The surge line steam percent evidenced a somewhat larger effect from ADS-1 actuation. After ADS-1 actuation, the steam percent in the surge line decreased from about []^{a,b,c} percent to about []^{a,b,c} percent where it remained until ADS-2 actuation (Figure 5.4.1-31).

The opening of the ADS-2 valve created a very small liquid flow through the ADS 1-3 separator. ADS-2 liquid flow only lasted []^{a,b,c} just as it did when ADS-1 actuated. This time, however, there was high, sustained steam flow through the ADS 1-3 separator (Figure 5.4.1-18). There was a direct correlation between the steam flow rate of ADS-2 and the steam percent of the pressurizer. Before ADS-2 actuation, the pressurizer was []^{a,b,c}-percent steam (Figure 5.4.1-31). When ADS-2 actuated, the steam percent in the pressurizer started to decrease immediately and continued to decrease until ADS steam flow from the ADS 1-3 separator stopped at []^{a,b,c}. With the cessation of steam flow from the pressurizer, the pressurizer steam percent started to increase from its minimum value of about []^{a,b,c} percent.

When pressurizer steam flow ceased at []^{a,b,c} the steam percent of the pressurizer was actually less than that of the surge line, indication that the moisture content of the two-phase liquid in the pressurizer was greater than that of the surge line. At this time, the pressurizer started to gravity-drain to the hot leg via the surge line. The steam percent of both the surge line and the HL-2 elbow started to decrease at the same time that the pressurizer steam percent started to increase (Figures 5.4.1-31 and 5.4.1-17). Draining of the pressurizer continued until it emptied at []^{a,b,c}. The pressurizer did not refill in this test.

The actuation of ADS-3 at []^{a,b,c} had no measurable effect on the response of the pressurizer.

The response of the pressurizer can best be summarized by reviewing the differential pressure between the RCS and the pressurizer, and the differential pressure between the pressurizer and the ADS 1-3 separator (Figure 5.4.1-32).

Before the break occurred at time zero, the pressure difference between RCS pressure and pressurizer pressure was about []^{a,b,c}. The positive value of the pressure difference indicated that RCS pressure measured at the top of the reactor head was greater than pressurizer pressure measured in the vapor space at the top of the pressurizer before the break occurred. These two pressures would have been equal if corrected for instrument error and the static head between the top of the reactor and the top of the pressurizer; however, without these corrections, the initial pressure difference can be used as the zero datum point.

The initial difference in pressure between the pressurizer and the ADS 1-3 separator was []^{a,b,c}. This was expected because the pressurizer was at initial conditions for the test, and the separator was at atmospheric pressure. The ADS valves were initially closed to prevent flow.

When the break valve opened at 0 second, the RCS depressurized as inventory was lost to the break. The pressurizer started to drain, which increased its steam percent (Figure 5.4.1-31). When the ADS-1 valve opened at []^{a,b,c} the pressurizer and surge line were completely voided. Before the ADS-1 valve opened, the differential pressure between the RCS and the pressurizer had decreased to about []^{a,b,c}

When ADS-2 actuated at []^{a,b,c} the differential pressure response was different and distinct. The RCS/pressurizer pressure difference peaked at a positive []^{a,b,c} immediately after the ADS-2 valve opened, forcing fluid from the RCS through the pressurizer to the ADS 1-3 separator. Liquid flow lasted only []^{a,b,c} then oscillated to about []^{a,b,c} (Figure 5.4.1-18). Steam flow from the pressurizer, however, increased dramatically to over []^{a,b,c} when the ADS-2 valve opened, then decayed to []^{a,b,c}. The plots of differential pressure show that []^{a,b,c} is when the differential pressure between the RCS and the pressurizer became equal to its pre-break "zero value," which allowed the pressurizer to start to drain its liquid back into the hot leg.

The pressurizer steam percent content was at its minimum at []^{a,b,c} or, in other words, the pressurizer collapsed level was at its maximum (Figure 5.4.1-31). An interesting observation is that the moisture content of the pressurizer was greater than the moisture content in the surge line at []^{a,b,c} when ADS flow ceased (Figure 5.4.1-31). As a result, the steam percent of the pressurizer surge line decreased, and the steam percent of the pressurizer increased until the pressurizer was completely voided at about []^{a,b,c}

During the period between ADS-2 actuation and the minimum steam percent in the pressurizer, ADS-3 actuated at []^{a,b,c}. As with the case of ADS-1, the response of the pressurizer to ADS-3 actuation was minimal. Differential pressure between the reactor and the pressurizer increased slightly (Figure 5.4.1-32), but had little effect on the rate of steam percent decrease in the pressurizer (Figure 5.4.1-31).

Passive Residual Heat Removal Heat Exchanger

Flow to the PRHR HX was initiated when the outlet valve of the HX automatically opened at []^{a,b,c}. Both the PRHR HX inlet and outlet flow meters recorded a forward flow immediately after the outlet valve opened (Figure 5.4.1-10). In the first []^{a,b,c} of the test, the outlet flow rate of the HX peaked at []^{a,b,c}. The flow rate decreased quickly from this peak. When the ADS-1 valve opened at []^{a,b,c} outlet flow of the PRHR HX had already decayed to []^{a,b,c} then maintained a value of less than or equal to []^{a,b,c} for the remainder of the test.

FMM-804 is a magnetic flow meter and cannot measure steam or two-phase flow. Since the flow out of the PRHR HX remained subcooled for the entire test (Figure 5.4.1-33), data from this meter were not affected by fluid phase. The measured flow rate through the HX outlet line was small and

oscillating. By []^{a,b,c} the flow oscillated rapidly between negative []^{a,b,c} and positive []^{a,b,c} making it difficult to determine how much mass was passing through the HX.

Even though PRHR HX outlet flow was difficult to determine, temperature data from CL-2 and CL-4 provided verification that outlet flow existed. The effluent from the HX was provided to CL-2 and CL-4 via the SG-2 cold-leg channel head. The returning cold water flowed along the bottom of CL-2 and CL-4 to the reactor vessel. Data from thermocouples located in the top of the cold legs at the reactor vessel flanges reveal that all of the cold legs were superheated by []^{a,b,c} (Figure 5.4.1-39). The cold legs remained superheated for the remainder of the test. Temperatures recorded by thermocouples mounted at the bottom of CL-2 and CL-4 were either saturated or subcooled for the entire test (Figure 5.4.1-40). The PRHR HX effluent provided the cold water to cool the bottom of CL-2 and CL-4. Data from the bottom-of-pipe thermocouples in CL-1 and CL-3 indicate that the bottom of these pipes became superheated by []^{a,b,c}

FMM-802 is a magnetic flow meter that measured flow from HL-2 to the HX. After HL-2 started to void, the inlet flow data became invalid. It cannot be determined precisely when the hot leg voided sufficiently to affect the inlet-flow measurement. Although the PRHR HX inlet temperature reached saturation temperature at []^{a,b,c} (Figure 5.4.1-33), the state of the fluid was uncertain. The saturated temperature of the fluid allowed it to be liquid, steam, or two-phase. Steam percent calculations using the SG-2 hot-leg elbow indicated that the voiding of the hot legs was well established when ADS-1 actuated at []^{a,b,c} at which time the rate of voiding in the hot leg increased (Figure 5.4.1-17). Thus, it is certain the data from FMM-802 are invalid sometime before []^{a,b,c}

The PRHR HX wide-range level data indicate that the HX started draining when the break valve opened (Figure 5.4.1-35). The level in the HX reached a minimum level of about []^{a,b,c}. At []^{a,b,c} the level decrease terminated, then increased to about []^{a,b,c} at []^{a,b,c} when data acquisition stopped.

Because the inlet channel head completed filling at the same time that the tube level started increasing (Figure 5.4.1-35), flow reversal through the HX could be a possible explanation for both level events. This would have required pressure in the SG-2 cold-leg channel head to be greater than pressure in HL-2. Pressure in SG-2, however, was never greater than pressure in HL-2 (Figure 5.4.1-36). If backward flow through the HX had occurred, it would have resulted in the outlet temperature of the HX (from the SG-2 cold-leg channel head) being greater than the inlet temperature (from HL-2). This was never the case; the outlet temperature was always subcooled; the inlet temperature reached saturation temperature at []^{a,b,c} (Figure 5.4.1-11). Data from the fluid thermocouples in the HX provide further evidence that there was no flow reversal through the HX, but provide no insight into the reflooding of the tubes at []^{a,b,c}

There is another possible explanation for the apparent increase in wide-range level and inlet channel head level of the PRHR HX. The transmitters that measure these levels share a common reference

leg. It is possible the transmitters' reference leg vaporized and decreased in level, creating a false indication of increasing level for both the inlet channel head and tubes of the HX.

Two of the tubes in the PRHR HX have instruments: one long and one short. Each tube has three fluid thermocouples. One is mounted at the top (inlet side) of the tube in the horizontal section, one is mounted in the center of the vertical section, and one is mounted at the bottom (outlet side) of the tube in the horizontal section (Appendix G, Dwg. OSU 600701).

There are four distinctive temperature responses in the tubes in the first []^{a,b,c} after the break. For the first []^{a,b,c} the long tubes showed a hot inlet temperature with a significant temperature difference between inlet and outlet (Figure 5.4.1-37). During this same time, the short-tube inlet temperature was small, and there was very little temperature difference between the inlet and outlet of the tube. These temperatures implied that the major portion of the HX cooling was done by the long tubes. A direct measurement of flow through each tube was unavailable, but the temperatures also implied that the major flow was through the long tubes.

At about []^{a,b,c} the second phase started with the inlet temperature of the short tube increasing and the inlet temperature of the long tube decreasing. The response of the two tubes reversed. The short tube was the one with the significant temperature difference between inlet and outlet; the long-tube temperatures correlated to the IRWST temperatures at their thermocouple location. The long-tube temperatures indicated no significant temperature across the tube for the rest of the test, except to reflect IRWST temperature at the long-tube thermocouple location.

The change in response between the long- and short-tube temperatures at []^{a,b,c} as the inlet channel drained was expected. As the channel head drained, it would have uncovered the long tubes at the top of the channel head, forcing more flow through the lower, or shorter, tubes. This response, however, was not reflected in channel head level. The channel head was completely drained at []^{a,b,c} (Figure 5.4.1-35).

At about []^{a,b,c} the PRHR HX tubes entered a third distinct phase. From []^{a,b,c}, both the long and short tubes indicated that there was no flow through the tubes, since their temperatures were at the temperature of the IRWST. This condition was not reflected in the data for PRHR HX outlet flow (Figure 5.4.1-10).

The fourth and final stage of PRHR HX response occurred at []^{a,b,c} when all three short-tube temperatures increased sharply (Figure 5.4.1-37). The short-tube inlet temperature increased about []^{a,b,c} was established between the short-tube inlet and the short-tube outlet. The long tube was unaffected.

From []^{a,b,c} until the end of the test, all thermocouples in the long and short tubes increased in temperature (approaching the HX inlet temperature or HL-2 temperature) (Figure 5.4.1-38). The

temperatures probably increased because temperature of the cooling medium of the IRWST was increasing.

In summary, data indicate that the PRHR HX provided a cooling flow to the RCS that continued through the entire test. The outlet temperature of the HX remained less than []^{a,b,c} and was about []^{a,b,c} for a major portion of the test. PRHR HX flow to CL-2 and CL-4 was detected by thermocouples mounted at the bottom of CL-2 and CL-4. These thermocouples measured saturated temperatures at the bottom of the pipe while the upper portion of the pipe was superheated. Outlet flow and level of the HX oscillated, probably from a chugging effect as steam from HL-2 condensed in the HX. Flow data reveal that after []^{a,b,c} outlet flow generally oscillated between 0 and []^{a,b,c}.

Cold Legs

The cold legs drained quickly after the break valve opened. The span of LDP-104 was from the top of the cold legs to the centerline of the DVI lines in the downcomer annulus (Figure 5.4.1-41). Data from this transmitter reveal that the cold legs started to drain at about []^{a,b,c} and the downcomer annulus drained to the centerline of the DVI lines by []^{a,b,c}. Thus, the level in the downcomer annulus was at the DVI elevation by the time ADS-1 actuated at []^{a,b,c}.

The cold legs refilled about []^{a,b,c} into the test. Data from the thermocouples mounted at the bottom of CL-1 and CL-3 show a rapid decrease in temperature at about []^{a,b,c} (Figure 5.4.1-40). The temperatures dropped from a superheated condition to a saturated condition just as the level in the downcomer increased above the bottom of the cold legs. The temperatures at the bottom of CL-2 and CL-4 were already at saturation due to the cooling effect of PRHR HX effluent returning to CL-2 and CL-4.

After the cold legs drained, there was no liquid to act as a cooling medium. The only method for the cold legs to cool was conduction through the insulated pipe wall. Pressure in the cold legs was continually dropping due to the inventory loss through the break and ADS lines after each stage of the ADS actuated. The depressurization created a rapidly decreasing saturation temperature in the cold legs. Steam in the cold legs did not cool as quickly as saturation temperature decreased. The result was formation of superheated steam in the cold legs measured by upper and lower pipe thermocouples (Figures 5.4.1-39 and 5.4.1-40).

The formation of superheated steam in the cold legs can be explained by the rapid depressurization of the RCS; however, the cold legs remained at superheated temperature for the duration of the test (Figure 5.4.1-39). This could have occurred only if a source of thermal energy was available to the cold legs.

The only possible sources of thermal energy to the cold legs were:

- Heating of the steam in the cold legs by the cold-leg piping
- Addition of superheated steam from the SGs
- Addition of superheated steam from the upper head via the bypass holes in the core barrel flange

The superheating of the cold legs from the upper head was not likely. The temperature of the upper head was lower than the fluid temperatures of the cold legs at the reactor vessel flange (Figure 5.4.1-39).

If steam in the cold legs was maintained at a superheated condition by the walls of the cold legs, the pipe temperature on the inside wall of the pipe would have been greater than the cold-leg fluid temperature. There were no inside-wall thermocouples in the cold-leg piping to measure temperature on the inside wall of the cold leg. The only cold-leg wall thermocouples were part of the heat flux meters (HFM) mounted on the outside wall of the piping. The thermocouple portion of the HFM was given a TFM designation. A thermocouple was mounted on the side of each cold leg near the discharge of the RCPs (Appendix G, Dwg. OSU 600203). Another thermocouple was mounted on each cold leg at the top of its flanged connection to the reactor vessel (Appendix G, Dwg. OSU 600102, Sh. 2). The recorded temperature of the thermocouples mounted at the top of the reactor vessel flange was greater than the recorded temperature of the thermocouples mounted on the side of the pipe, so the hotter flange thermocouples were used for evaluation.

A temperature difference was calculated for CL-1, CL-2, and CL-3 between the wall temperature at the reactor vessel flange and the fluid temperature at the flange (Figure 5.4.1-42). It was not possible to calculate this temperature difference for CL-4 because the TFM at this location was out of service. Data provide mixed results. After the initial transient, fluid temperatures in CL-1 and CL-2 were always higher than their wall temperatures. The fact that this condition was maintained for 3 hours, it implied that the walls of CL-1 and CL-2 did not provide a heat source for superheating. However, the wall temperature of CL-3 was always hotter than the fluid temperature, until about []^{a,b,c} implying that the walls of CL-3 could have been a source of superheating to the other cold legs. This seems improbable for two reasons. First, no response was seen from CL-1 and CL-2 after the fluid temperature of CL-3 exceeded the wall temperature ([]^{a,b,c}). Second, it is unlikely that CL-3 steam could have communicated with fluid from the other cold legs, because a portion of the break flow was from CL-3 to CMT-1. Backflow from CL-3 to the other cold legs was unlikely.

The most likely source of superheating to the cold legs was the SGs. A few seconds after the break, the secondary side of the SGs was "bottled up." The steam isolation valves closed, and feedwater was isolated (Table 5.4.1-3). Without cooling, steam in the SG tubes stayed at a high superheated temperature equal to the secondary-side steam temperature (Figures 5.4.1-43 and 5.4.1-44). All that was required for superheated steam to reach the cold legs from either SG was a sufficient differential pressure to drive the steam from the hot legs to the cold legs via the SG U-tubes. This differential

pressure was measured across the upper core plate (DP-114) and bypass holes (DP-130; Figure 5.4.1-45). The sum of these two differential pressures represented the pressure difference between the upper plenum and the downcomer annulus, which is equivalent to the differential pressure between the hot legs and the cold legs. After []^{a,b,c} the magnitude of the differential pressures was small but steady. The resultant steam flow rate through the SGs would have been small, but sufficient to maintain the cold-leg superheat.

Note: A more detailed discussion of upper core plate and bypass hole differential pressures is given in the reactor response portion of this subsection.

In summary, the cold legs emptied very quickly after the break. They were completely empty by ADS-1 actuation and stayed empty until about []^{a,b,c} into the test. When the cold legs did start to fill at about []^{a,b,c} they did not fill completely. Steam in the cold legs stayed superheated for the duration of the test. The source of superheating was probably the SGs.

In-Containment Refueling Water Storage Tank

The response of the IRWST was well behaved. Two long thermocouple rods extended the height of the IRWST (Appendix G, Dwg. 600701). Data from eight thermocouples on one of these rods are plotted as a representative temperature profile in the IRWST (Figure 5.4.1-46). The first thermocouples started heating with PRHR HX actuation and continued heating as ADS flow supplied the sparger in the IRWST with hot fluid. Heating of the thermocouples took place from the top down, as the less dense hot water rose to the top of the tank. The hottest temperatures sensed by any thermocouple was []^{a,b,c}

A steam flow meter was mounted in the exhaust line from the IRWST exhaust to the BAMS header. This flow meter recorded sharp peaks of steam flow during the first []^{a,b,c} of the test (Figure 5.4.1-47). The magnitude of the peaks was less than []^{a,b,c}. These indications were invalid, for the temperature at the top of the tank did not reach saturation until about []^{a,b,c}. The flow meter did not record any further flow for the remainder of the test.

IRWST injection flow to DVI-1 and DVI-2 started at two different times (Figure 5.4.1-25). The reason for the time shift was that IRWST injection to DVI-1 supplied the "broken" side of the facility and injected into the primary sump; IRWST injection to DVI-2 supplied flow to the reactor through the "unbroken" DVI line.

IRWST-1 flow started at []^{a,b,c} when backpressure in its injection line decreased below the static head of the IRWST. This was coincident with the cessation of flow from ACC-1 as the accumulator tank emptied (Figure 5.4.1-4). IRWST-2 flow started at []^{a,b,c} when pressure in the reactor became low enough for the static head of the IRWST to overcome it. IRWST-2

injection did not commence until after ADS-4 actuated and decreased the pressure in the RCS (Table 5.4.1-3).

Reactor

The discussion of the reactor response entails several different distinct regions: downcomer annulus, reactor core, and upper plenum and upper head. The regions will be discussed in this order.

The level response of the downcomer annulus is measured by two wide-range and several narrow-range level transmitters (Appendix G, Dwg. OSU 600101). The wide-range channels are positioned 90 degrees from one another. Data from these two channels are in excellent agreement. Both channels are also in agreement with their associated narrow-range channels.

The level in the downcomer annulus dropped rapidly as a result of the break. LDP-116 and LDP-140 indicated that the downcomer water level dropped to the elevation of the DVI line penetration about []^{a,b,c} before ADS-1 actuated (Figure 5.4.1-48). DVI-1 penetration at the reactor vessel was the location of one of two parts of the DVI DEG break. The reactor vessel side of the break was no longer covered by water when the level in the downcomer annulus decreased to the elevation of the DVI penetration. Break flow data indicate a sharp decrease in break flow at []^{a,b,c} as flow from the break became two-phase (Figure 5.4.1-2). ADS-1 actuated about []^{a,b,c} after the break uncovered. During these []^{a,b,c} break flow decreased from []^{a,b,c}. Break flow actually reached a "steady-state" value in the []^{a,b,c} before ADS-1 actuation.

When ADS-1 actuated at []^{a,b,c} the collapsed level in the downcomer was at about []^{a,b,c} below the bottom of the DVI penetration. The break flow rate from the vessel was largely unaffected by ADS-1 actuation and remained essentially constant until ADS-2 actuated. ACC-2 started to inject into the core at []^{a,b,c} after ADS-1 actuated (Figure 5.4.1-8). ACC-2 injection stopped the level decrease in the downcomer (Figure 5.4.1-48). The downcomer level remained relatively constant until the actuation of ADS-2.

Automatic opening of the ADS 1-3 valve at []^{a,b,c} decreased the collapsed level in the downcomer annulus quickly. Within []^{a,b,c} after the ADS-2 valve opened, the level in the downcomer dropped about []^{a,b,c}. This level is most significant because it was the lowest level obtained in the downcomer during the test (about []^{a,b,c}). Although ADS-2 actuation produced the minimum level in the core, it was not directly a result of ADS-2 flow. Rather, it was the predominance of reactor vessel break flow that created the low level.

When the ADS-2 valve opened, ADS-2 liquid flow increased for only []^{a,b,c} (Figure 5.4.1-2) with no appreciable effect on the RCS inventory and, therefore, no effect on the downcomer level. Immediately after the ADS-2 valve opened, however, liquid break flow from the vessel increased almost []^{a,b,c} (Figure 5.4.1-2). An increased RCS

depressurization rate from ADS-2 accounted for some of the increased break flow as water in the downcomer flashed to steam; an increased flow rate from ACC-2 accounted for the rest. Because the level in the downcomer was below the level of the DVI nozzle, ACC-2 injected directly into the steam space in the downcomer where a portion of the flow may have flashed. This increased steam inventory could have been available to the broken DVI nozzle as break flow.

At about []^{a,b,c} after ADS-2 actuation, the increasing ACC-2 flow balanced the increase in break flow, and the level decrease in the downcomer terminated. At []^{a,b,c} the level was a minimum for the test at []^{a,b,c}. From this time on, the level in the downcomer was either increasing or steady, but never decreasing (Figure 5.4.1-48).

Eight downcomer fluid thermocouples, mounted []^{a,b,c} above the top of the DVI nozzles, monitored the temperature in the downcomer. The eight thermocouples were TF-147 through TF-150, and TF-164 through TF-167. Their orientation and relative elevation are shown in Appendix G (Dwg. OSU 600101, Sh. 2). TF-147 through TF-150 were mounted at []^{a,b,c} above the "unbroken" DVI-2 penetration. TF-164 through TF-167 were mounted at 0°az above the "broken" DVI-1 penetration. The thermocouples were mounted at one of two elevations. TF-147, TF-148, TF-164, and TF-167 were located about []^{a,b,c} above the top of the DVI line penetration to the downcomer. TF-149, TF-150, TF-166, and TF-167 were located about []^{a,b,c} above the top of the DVI line penetration to the downcomer.

From []^{a,b,c} (between ADS-2 and ADS-3 actuation) until []^{a,b,c} data from the eight thermocouples revealed temperatures in the downcomer fluctuated between superheated and saturated conditions (Figure 5.4.1-49). The thermocouples were already uncovered at the time of ADS-1 actuation ([]^{a,b,c}). The downcomer level at the time was below the DVI nozzles. The thermocouples were not covered again until about []^{a,b,c}. Thus, the temperature fluctuations were not a function of downcomer level. It is more likely that the fluctuations in temperature were due to mixing of saturated steam generated from the fluid in the downcomer and superheated steam flowing from the SGs, through the cold legs, and to the break at the DVI-1 reactor vessel penetration.

The supposition that two steam temperatures mix in the downcomer is borne out by data from other thermocouples in the downcomer. A series of thermocouples at 0° and 180°az provided a temperature profile in the downcomer (Appendix G, Dwg. OSU 600101, Sh. 2). Plots of the data from a representative sample of these thermocouples describe the temperature behavior during the first []^{a,b,c} of the test (Figures 5.4.1-50 and 5.4.1-51). The level in the downcomer decreased to a minimum of []^{a,b,c}. All the thermocouples plotted in Figures 5.4.1-50 and 5.4.1-51 were uncovered at []^{a,b,c} except TF-128 and TF-158. The only thermocouples that ever indicated superheated steam were those thermocouples installed at an elevation above the DVI penetrations. This means thermocouples below the DVI penetration were always in a saturated steam environment when uncovered, whereas thermocouples above the DVI elevation experienced varying periods of saturated and superheated steam.

Data from the thermocouples are plotted for the entire test duration (Figures 5.4.1-52 and 5.4.1-53). These plots show little temperature stratification in the downcomer for the region below the DVI elevations. In fact, after []^{a,b,c} the stratification is only []^{a,b,c}. The small temperature stratification is a result of good mixing from the DVI.

Temperatures of TF-147, TF-149, TF-164, and TF-166 decreased below saturation temperature when the level in the downcomer increased enough to cover the thermocouples. The first of the thermocouples was covered at about []^{a,b,c}.

In summary, the downcomer level dropped rapidly after break initiation. It reached a minimum level of []^{a,b,c}. After this time, the level was either steady or increasing for the remainder of the test. Downcomer temperature was dependent on elevation. Fluid thermocouples below the DVI nozzle remained at or below saturation temperature. Thermocouples above the DVI nozzle measured superheated steam temperatures. The possible sources of this superheated steam are described in the cold-leg response subsection. Very small stratification existed in the downcomer water temperature due to mixing from the DVI.

Reactor core response was evaluated using temperature data from thermocouples located in the core. Data from thermocouples mounted on a thermocouple rod at the center of the core were used to assess axial temperature distribution. These thermocouples were given a TR designator. Data from the top thermocouple of eight heaters were used to assess radial temperature distribution at the top of the core. These thermocouples were given a TH designator (Appendix G, OSU Dwg. 600007 and 60008).

The break created a depressurization in the RCS. Temperatures at the center of the core became saturated within []^{a,b,c} of break initiation. As the test progressed, RCS pressure decreased as the result of the break and actuation of ADS-1 through ADS-4. The core cooled, maintaining saturation temperature as the RCS depressurized (Figure 5.4.1-54). Subcooling temperatures at the bottom of the core first appeared at about []^{a,b,c} shortly after ADS-4 actuation. Up until this time, the rate of core cooling was equal to the rate of saturation temperature decrease. At about the time of ADS-4 actuation, the rate of RCS depressurization decreased significantly, slowing the saturation temperature decrease. Core cooling continued with DVI, so the bottom of the core started to subcool.

Elevation in the core at which subcooling existed increased as the test progressed. By the end of the test, TR-001-5, located []^{a,b,c} from the bottom of the reactor vessel, recorded a subcooled temperature. Heating elements in the heater rods simulated the active fuel of the AP600. The top of the heating elements in the heater rods was located []^{a,b,c} from the bottom of the reactor vessel. Thus, by the end of the test, fluid in the center of the core was subcooled []^{a,b,c} percent of the length of the active core.

Temperature spikes were recorded for some of the thermocouples in the center thermocouple rod. In the first []^{a,b,c} of the test, the spikes were as large as []^{a,b,c}. After []^{a,b,c} the spikes were only about []^{a,b,c}.

Data from the thermocouples installed in the top of six heaters staggered radially across the core indicate that the design for a "flat" heat flux profile was achieved in the core (Figure 5.4.1-55). The center heaters were generally at a temperature of only []^{a,b,c} lower than the midcenter and outer heaters. The lower center temperatures were probably due to a slightly higher flow rate through the center of the core. There were no notable temperature excursions, although small-magnitude spikes did occur as in the unheated thermocouple rod temperatures.

Steam percent in the core may be calculated by using data from three level transmitters that measure core level: LDP-109, LDP-110, and LDP-138 (Appendix G, Dwg. OSU 60010, Sh. 1). One of these level transmitters, LDP-138, is a wide-range transmitter that spanned the entire core area, from the top of the lower core plate to the bottom of the upper core plate. The other two transmitters are narrow-range transmitters whose summed span equal that of the wide-range transmitter. The narrow-range transmitters are mounted like LDP-138 at 0°az and share the same taps.

There is close agreement between core steam percent calculations using core level data from the wide-range and narrow-range level transmitters. LDP-109 and LDP-110 have equal spans, which together cover the same span as wide-range level transmitter LDP-138; therefore, the mean of their calculated core steam percent should equal the calculated core steam percent of LDP-138. A plot of these results indicates that essentially identical core steam percent results are achieved using either the data from LDP-138 or the average core steam percent calculation from LDP-109 and LDP-110 (Figure 5.4.1-58).

The maximum steam in the core occurred at about []^{a,b,c} the same time as the minimum downcomer level. Core levels measured by the wide-range transmitter or either of the narrow-range transmitters never decreased after []^{a,b,c} but were nearly constant or increasing (Figures 5.4.1-58 and 5.4.1-59).

The same system effects that created the minimum downcomer level also provided the maximum core steam percent. Refer to the previous discussion of downcomer response for this explanation.

In summary, the core showed indications of increasing core steam percent immediately after the break valve opened. Temperatures in the core quickly reached saturation. Core cooling maintained temperatures at saturation as the RCS depressurized and lowered saturation temperature. Maximum core steam percent occurred after ADS-2 actuation, at the same time as the minimum downcomer level. At maximum core steam percent and throughout the test, there were no excursions of temperature from either the heated or unheated rod thermocouples. The bottom of the core started cooling at the time of ADS-4 actuation. By the end of the test, about []^{a,b,c} percent of the core was subcooled.

The upper head and the upper plenum are separated by the upper support plate. Both the upper plenum and upper head began to void immediately after the break. The upper plenum was completely empty at []^{a,b,c} the upper head took longer to void (about []^{a,b,c}) because of its restrictive flow. For it to empty, it had to gravity-drain to the upper plenum through holes in the upper support plate, and/or it had to flow through bypass holes in the core barrel flange to the downcomer. The flow paths were sufficiently restrictive to delay the voiding of the upper head well past the time that the upper plenum voided.

Differential pressure across the upper support plate and the flow bypass holes were monitored by DP-114 and DP-130, respectively (Appendix G, Dwg. OSU 600101, Sh. 1). A positive value of differential pressure indicated that flow was in the direction of flow during normal operation, before the RCPs tripped. When the pumps were running, flow was from the downcomer, through the bypass holes into the upper head, continuing from the upper head into the upper plenum via the holes in the upper support plate. A negative value for differential pressure indicated that flow was reversed from this description.

The direction of flow into and out of the upper head was indicated by data from DP-114 and DP-130 (Figure 5.4.1-60). At the time of the break, differential pressure across the bypass holes was positive []^{a,b,c} and DP-114 was slightly positive. Thus, flow was per system design, from the downcomer to the upper plenum. At []^{a,b,c} flow reversed and both differential pressures were negative. This flow reversal was due to the pressurization of the reactor core barrel above the downcomer pressure.

Differential pressure across the bypass holes remained negative for the rest of the test. After []^{a,b,c} flow was always from the upper head into the downcomer annulus (Figure 5.4.1-60). By the time the upper head emptied at []^{a,b,c} differential pressures across the bypass holes and the upper support plate were at their maximum negative value. Both differential pressures steadily decreased in magnitude in time as the steam flow rate to the downcomer decayed. When the test terminated, there was a very small steam flow to the downcomer from the upper plenum via the upper head.

Note: Data for differential pressure across the bypass holes given by DP-130 must be reduced by a value between []^{a,b,c}. The magnitude of the correction factor is a function of water level in the upper head above the reference leg tap for DP-130. The variable leg tap for DP-130 is located in the downcomer. When this tap is uncovered, the correction factor for DP-130 is []^{a,b,c}. This unusual correction factor is a result of mounting a differential pressure transmitter in a vertical position while measuring differential pressure in a column that does not stay full of water.

The temperature in the upper head was monitored by two thermocouples, TF-171 and TF-120 (Figure 5.4.1-61). Both thermocouples indicated superheated conditions by []^{a,b,c} when steam from the upper plenum was flowing into the upper head and out through the bypass holes into

the downcomer. Since the temperature of steam in the upper plenum was saturated, heating of the steam had to come from the energy released from the walls of the upper head and/or the energy released from the upper support plate as steam from the upper plenum passed through it. Since the upper head had drained by []^{a,b,c} and there was no cooling flow to it, the upper head acted as a source of superheated steam for the downcomer for the entire test. The flow rate was small, however, so the superheated steam had little effect on the cold-leg temperatures, although it did affect the temperature in the upper portion of the downcomer. The temperature in the upper downcomer tracked the temperature in the upper head.

Note: The upper-plenum temperature was monitored by two thermocouples, TF-169 and TF-170. Data from TF-170 indicating subcooled conditions in the upper plenum []^{a,b,c} and continuing through the test are invalid. TF-169 indicates the correct saturated temperature conditions (Figure 5.4.1-61). It is possible that TF-170 was affected by downcomer fluid leaking through the O-ring seals of TF-170 at the core barrel wall.

In summary, the upper plenum collapsed level decreased quickly. It voided at []^{a,b,c} followed by the upper head emptying at []^{a,b,c}. The upper head voided more slowly, for it had to void through the bypass holes or the holes in the upper support plate. The normal flow of liquid is from the downcomer through the upper head into the upper plenum. When the break occurred, this flow direction reversed. The upper plenum supplied saturated steam to the upper head. Saturated steam from the upper plenum was superheated as it passed through the holes in the upper support plate and by the walls of the upper head. The supply of superheated steam from the upper head maintained a superheated temperature in the upper portion of the downcomer. The flow rate from the upper head was small, so it had little effect on the temperatures in the cold legs.

Steam Generators

One long tube and one short tube in each SG was instrumented for level and temperature measurement (Appendix G, Dwg. OSU 600301). The level transmitters measured level in the hot-leg and cold-leg side of the tubes. Thermocouples in the tubes measured temperature at the top of the tubes and at mid-elevation of both the hot-leg and cold-leg sides.

Within []^{a,b,c} of the break valve opening, the SG tubes started to drain in both SGs (Figures 5.4.1-62 and 5.4.1-63). Both SGs were essentially drained before ADS-1 actuation at []^{a,b,c} including the hot-leg and cold-leg channel heads (Figures 5.4.1-64 and 5.4.1-65). The sequence of tube and channel head draining is provided in Table 5.4.1-3.

Before the break occurred, steam production in the secondary side of the SG acted as a heat sink to the primary side. Feedwater and steam isolation occurred automatically after the break was initiated (Table 5.4.1-3). The isolation of steam and feedwater "bottled up" the SGs. Until the RCS depressurized below the pressure of the SGs' secondary side, the only energy loss from the SGs was

ambient heat loss through the insulation. When RCS pressure decreased below secondary steam pressure, the SG secondary side became a heat source to the RCS.

Secondary steam pressure and primary steam pressure were in quasi-equilibrium for []^{a,b,c} (Figure 5.4.1-66). On a smaller break, the depressurization rate of the RCS would have been smaller and the equilibrium period would have been longer. The SG tube temperatures followed the saturation temperature of the RCS until the secondary side of the SGs became a heat source to the primary side. Shortly before ADS-1 actuation, steam temperatures in the tubes started to superheat from heat transferred from the secondary to the primary side of the SGs (which were drained by this time). About []^{a,b,c} after ADS-1 actuation, all tube thermocouples reported superheated conditions in the tubes (Figures 5.4.1-43 and 5.4.1-44). The tube temperatures stayed superheated for the duration of the test and decreased in temperature with the secondary steam temperature.

SG tube level data show the SGs refilling (Figures 5.4.1-62 and 5.4.1-63). These data are invalid. The reference leg of the level transmitters is located internally to each SG. As the SGs started to drain, the reference leg taps for the tube level transmitters uncovered. The reference leg was then exposed to a steam environment. The reference leg started to boil and decrease in level. The decreasing level in the reference leg gave a false-high reading for tube level. When the SG tubes were fully drained, the level data erroneously recorded the tubes partially filled. As the reference leg continued to boil, decreasing reference leg level, the tube level data incorrectly showed the tubes refilling. When the reference leg voided, the differential pressure between reference and variable legs was equal, just as if the tubes were full. SG tube temperature data, however, verified that the tubes remained drained because the tube temperature remained superheated after the SGs drained.

In summary, the SGs completely drained by the time ADS-1 actuated. Steam in the tubes superheated when RCS pressure decreased below the secondary steam pressure. Superheating of all tubes was completed []^{a,b,c} after ADS-1 actuation, and the tubes remained superheated for the rest of the test. The SGs supplied superheated steam to the cold legs, with the differential pressure between the hot legs and cold legs supplying the head for flow.

5.4.1.6 Mass Balance

The mass balance results for Matrix Test SB12 were calculated based on water inventory before and after the test and are provided in Appendix E. Mass at the end of the test was within 2 percent of the mass at the beginning of the test.

5.4.1.7 Conclusions

The test was performed with minimal problems and is considered acceptable. Although not all of the facility initial conditions met the specified acceptance criteria, the deviations did not impact the quality of the data. The instrumentation problems encountered were not critical to the performance of the facility mass and energy balances.

Facility response to the test was as anticipated for the conditions that were established. The data clearly demonstrate that cooling of the reactor heater rods was maintained throughout the duration of the test.

**TABLE 5.4.1-1
MATRIX TEST SB12 INITIAL CONDITIONS**

Parameter	Instrument No.	Specified Initial Condition	Actual Initial Condition	Comments
Pressurizer pressure ⁽¹⁾	PT-604	370 ± 2 psig	<input type="checkbox"/> a,b,c	
HL-1 temperature ⁽¹⁾	SC-141	420 ± 2°F	<input type="checkbox"/>	
HL-2 temperature ⁽¹⁾	SC-140	420 ± 2°F	<input type="checkbox"/>	
SG-1 pressure ⁽¹⁾	PT-301	285 ± 5 psig	<input type="checkbox"/>	
SG-2 pressure ⁽¹⁾	PT-302	285 ± 5 psig	<input type="checkbox"/>	
Pressurizer level ⁽¹⁾	LDP-601	65 ± 5 in.	<input type="checkbox"/>	Level signal was temperature-compensated by TF-605
SG-1 narrow-range level ⁽¹⁾	LDP-303	26 ± 3 in.	<input type="checkbox"/>	Level signal was temperature-compensated by TF-301
SG-2 narrow-range level ⁽¹⁾	LDP-304	26 ± 3 in.	<input type="checkbox"/>	Level signal was temperature-compensated by TF-310
IRWST temperature ⁽²⁾	TF-710	< 80°F	<input type="checkbox"/>	
CMT-1 temperature ⁽²⁾	TF-529	< 80°F	<input type="checkbox"/>	
CMT-2 temperature ⁽²⁾	TF-532	< 80°F	<input type="checkbox"/>	
ACC-1 temperature ⁽²⁾	TF-403	< 80°F	<input type="checkbox"/>	
ACC-2 temperature ⁽²⁾	TF-404	< 80°F	<input type="checkbox"/>	
IRWST level ⁽²⁾	LDP-402	Level established by overflow elevation	<input type="checkbox"/>	
ACC-1 level ^(2,3)	LDP-401	Level established by standpipe at 37 in.	<input type="checkbox"/>	Accepted; accumulator level was fixed by a standpipe
ACC-2 level ^(2,3)	LDP-402	Level established by standpipe at 37 in.	<input type="checkbox"/>	Accepted; accumulator level was fixed by a standpipe

TABLE 5.4.1-1 (Continued)
MATRIX TEST SB12 INITIAL CONDITIONS

Parameter	Instrument No.	Specified Initial Condition	Actual Initial Condition	Comments
ACC-1 pressure ⁽²⁾	PT-401	232 ± 2 psig	[] ^{a,b,c}	Pressure was [] ^{a,b,c} low; condition acceptable
ACC-2 pressure ⁽²⁾	PT-402	232 ± 2 psig	[]	Pressure was [] ^{a,b,c} low; condition acceptable
CMT-1 level ⁽²⁾	Full	LDP-507	[]	
CMT-2 level ⁽³⁾	Full	LDP-502	[]	

Note:

- (1) Data for the indicated parameter were recorded in the test procedure as an initial condition for the test. The value was determined by the test engineer from the appropriate control board indicator.
- (2) Data were not recorded in procedure, but the test engineer verified that specified conditions were achieved while establishing initial conditions. The value of the parameter was determined post-test by calculating the average DAS indication for a time of about 2 minutes before the break valve opened.
- (3) The bourdon pressure tube local indicator (PI-401 and PI-402) was tubed to the lower portion of the reference leg of the accumulator level transmitter (LDP-401 and LDP-402). As pressure in the accumulator increased, air inside the bourdon tube was compressed, thereby lowering the reference leg liquid level, resulting in a false indication of measured level.

**TABLE 5.4.1-2
MATRIX TEST SB12 INOPERABLE INSTRUMENTS/INVALID DATA CHANNELS**

Instrument No.	Instrument Type	Inoperable Description
FDP-605*	Differential pressure transmitter - flow	Over-ranged with initial flow
FMM-201 through FMM-204*	Magnetic flow meter	Removed due to mechanical failure
FMM-501*	Magnetic flow meter	Over-ranged when CMT-1 outlet valve opened at 6 seconds; stayed over-ranged while tank was draining; data invalid after tank drained because FMM could not measure steam flow
FMM-502	Magnetic flow meter	Data invalid after 126 seconds due to possible steam in balance line; meter can not measure steam or two-phase flow
FMM-503	Magnetic flow meter	Data invalid after 100 seconds due to possible steam in balance line; meter cannot measure steam or two-phase flow
FMM-504*	Magnetic flow meter	Over-ranged between about 70 and 110 seconds, and 140 and 160 seconds; data invalid after tank drained because FMM can not measure steam flow
FMM-701*	Magnetic flow meter	Data for negative flow invalid; negative flow existed after sump valves opened, but meter is not designed to measure negative flow
FMM-802*	Magnetic flow meter	Data invalid after steam formed in PRHR HX inlet line; uncertain when this occurred, but likely at about 25 seconds after break
FMM-804*	Magnetic flow meter	Data valid until PRHR HX indicated a minimum level at about 5000 seconds; after this time, the possibility of steam in outlet line invalidated data
HFM-103	Heat flux meter	Failed
HFM-105	Heat flux meter	Failed
HFM-108	Heat flux meter	Failed
HFM-505	Heat flux meter	Failed
HFM-703	Heat flux meter	Failed
HPS-203-1 through HPS-203-3	Heated phase switch	Failed
HPS-509-1 through HPS-509-3	Heated phase switch	Failed

TABLE 5.4.1-2 (Continued)
MATRIX TEST SB12 INOPERABLE INSTRUMENTS/INVALID DATA CHANNELS

Instrument No.	Instrument Type	Inoperable Description
LDP-201 through LDP-206	Differential pressure transmitter - level	Data invalid due to effect of vertical portion of sense line attached to top of pipe; data can show level trends and when pipe empties or starts to drain, but absolute level indication can not be used
LDP-215* LDP-216 LDP-217 LDP-218* LDP-219* LDP-220 LDP-221 LDP-222*	Differential pressure transmitter - level	Data invalid; when SG tube drained, reference leg started to vaporize (see Subsection 2.4)
LDP-207 LDP-208 LDP-209	Differential pressure transmitter - level	Inoperable; transmitters ranged improperly; data can show level trends, but absolute level indication can not be used
LDP-401* LDP-402*	Differential pressure transmitter - level	Data invalid; see note 3 in Table 5.4.1-1, and Subsection 5.4.1.2.
LDP-802* LDP-804	Differential pressure transmitter - level	Data valid until PRHR initially drained at 600 seconds; after this time, data suspect due to possible boiling of common reference line of LDP-802 and LDP-804
LDP-509	Differential pressure transmitter - level	Data invalid after 70 seconds due to steam flow in balance line creating a flow differential pressure measured by LDP-509
LDP-802 LDP-804	Differential pressure transmitter - level	Data of both instruments suspect after LDP-802 started increasing in level at about 1200 seconds; after this time, possible boiling of common reference line of LDP-802 and LDP-804 may invalidate data
PT_101	Pressure transmitter	Data less than 6.1 psig invalid
PT_102	Pressure transmitter	Data less than 6.2 psig invalid
PT_103	Pressure transmitter	Data less than 6.2 psig invalid
PT_104	Pressure transmitter	Data less than 6.4 psig invalid
PT_108	Pressure transmitter	Data less than 8.4 psig invalid
PT_109	Pressure transmitter	Data less than 6.3 psig invalid
PT_111	Pressure transmitter	Data less than 6.0 psig invalid
PT_112	Pressure transmitter	Data less than 8.8 psig invalid

TABLE 5.4.1-2 (Continued)
MATRIX TEST SB12 INOPERABLE INSTRUMENTS/INVALID DATA CHANNELS

Instrument No.	Instrument Type	Inoperable Description
PT_113	Pressure transmitter	Data less than 6.4 psig invalid
PT_201*	Pressure transmitter	Data less than 1.1 psig invalid
PT_202	Pressure transmitter	Data less than 5.9 psig invalid
PT_205	Pressure transmitter	Data less than 6.1 psig invalid
TF-170	Thermocouple	Unavailable due to leaking O-ring in core barrel
TF-615	Thermocouple	Failed
TF-619	Thermocouple	Failed
TFM-103	Thermocouple for heat flux meter	Failed
TFM-105	Thermocouple for heat flux meter	Failed
TFM-108	Thermocouple for heat flux meter	Failed
TFM-703	Thermocouple for heat flux meter	Failed
TH-102-1	Thermocouple	Failed
TH-317-1 through TH-317-4	Thermocouple	Removed with heater rod C2-317
TW-503	Thermocouple	Failed
TW-534	Thermocouple	Failed
TW-552	Thermocouple	Failed; read ambient temperature throughout test

Note:

* Instruments marked with an asterisk are critical instruments. See subsection 5.4.1.2 for discussion.

**TABLE 5.4.1-3
MATRIX TEST SB12 SEQUENCE OF EVENTS**

Event ⁽¹⁾	Data Source ⁽²⁾	Time After Break (sec.)
TEST Pushbutton Depressed	D	[] a,b,c
Break Valve Open Signal	D	
Break Valve Starts to Open	D	
Feed Pump Trips	D	
CMT-1 Outlet Valve Starts to Open	D	
CMT-2 Outlet Valve Starts to Open	D	
PRHR HX Outlet Valve Starts to Open	D	
ACC-1 Injection Starts (FMM-401)	A	
Reactor Coolant Pumps Trip	D	
SG-1 Hot-Leg Elbow Starts to Drain (LDP-207)	A	
SG-1 Cold-Leg Short Tube Empty (LDP-221)	A	
Pressurizer Empty (LDP-601)	A	
SG-2 Cold-Leg Short Tube Empty (LDP-220)	A	
SG-1 Cold-Leg Long Tube Empty (LDP-219)	A	
SG-2 Cold-Leg Long Tube Empty (LDP-222)	A	
Pressurizer Surge Line Empty (LDP-602)	A	
SG-1 Hot-Leg Short Tube Empty (LDP-217)	A	
SG-1 Hot-Leg Long Tube Empty (LDP-215)	A	
CL-1 Channel Head Empty (LDP-211)	A	
CL-3 Channel Head Empty (LDP-213)	A	
CMT-2 Recirculation Flow Stops (LDP-510)	A	
SG-2 Hot-Leg Short Tube Empty (LDP-216)	A	
SG-2 Hot-Leg Long Tube Empty (LDP-218)	A	
CL-2 Channel Head Empty (LDP-210)	A	
CL-4 Channel Head Empty (LDP-212)	A	
CMT-1 Recirculation Flow Stops (LDP-509)	A	
CMT-1 Low Level Signal	D	[]

TABLE 5.4.1-3 (Continued)
MATRIX TEST SB12 SEQUENCE OF EVENTS

Event ⁽¹⁾	Data Source ⁽²⁾	Time After Break (sec.)
SG-1 Hot-Leg Channel Head Empty (LDP-209)	A	a,b,c
SG-2 Hot-Leg Elbow Starts to Drain (LDP-208)	A	
HL-1 Pipe Starts to Drain (LDP-205)	A	
HL-2 Pipe Starts to Drain (LDP-206)	A	
SG-2 Hot-Leg Channel Head Empty (LDP-214)	A	
ADS-1 Valve Starts to Open	D	
ACC-2 Injection Starts (FMM-402)	A	
CMT-1 Level Low-Low	D	
CMT-2 Low Level Signal	D	
ADS-2 Valve Starts to Open	D	
CMT-1 Empty (LDP-507)	A	
SG-1 Hot-Leg Elbow Minimum (LDP-207)	A	
HL-2 Pipe Empty (LDP-206)	A	
SG-2 Hot-Leg Elbow Minimum (LDP-208)	A	
Time of Minimum Reactor Level Observed During Test (LDP-127)	A	
HL-1 Pipe Empty (LDP-205)	A	
ADS-3 Valve Starts to Open	D	
Reactor Pressure Low	D	
IRWST-2 Injection Valve Starts to Open	D	
IRWST -1 Injection Valve Starts to Open	D	
ACC-1 Empty (LDP-401)	A	
IRWST-1 Injection Starts (FMM-701)	A	
ADS 4-1 Valve Starts to Open	D	
ADS 4-2 Valve Starts to Open	D	
ACC-2 Empty (LDP-402)	A	
IRWST-2 Injection Starts (FMM-702)	A	
CMT-2 Level Low-Low	D	

TABLE 5.4.1-3 (Continued)
MATRIX TEST SB12 SEQUENCE OF EVENTS

Event ⁽¹⁾	Data Source ⁽²⁾	Time After Break (sec.)
CMT-2 Empty (LDP-502)	A	a,b,c
Primary Sump Starts to Overflow to Secondary Sump (LDP-901)	A	
Primary Sump-1 Injection Valve Starts to Open	D	
Primary Sump-2 Injection Valve Starts to Open	D	
Primary Sump-2 Injection Starts (FMM-902)	A	
Primary Sump-1 Injection Starts (FMM-901)	A	
CMT-2 Starts to Reflood (LDP-502)	A	
CMT-1 Starts to Reflood (LDP-507)	A	
Pressurizer Refloods (LDP-601)	A	

Note:

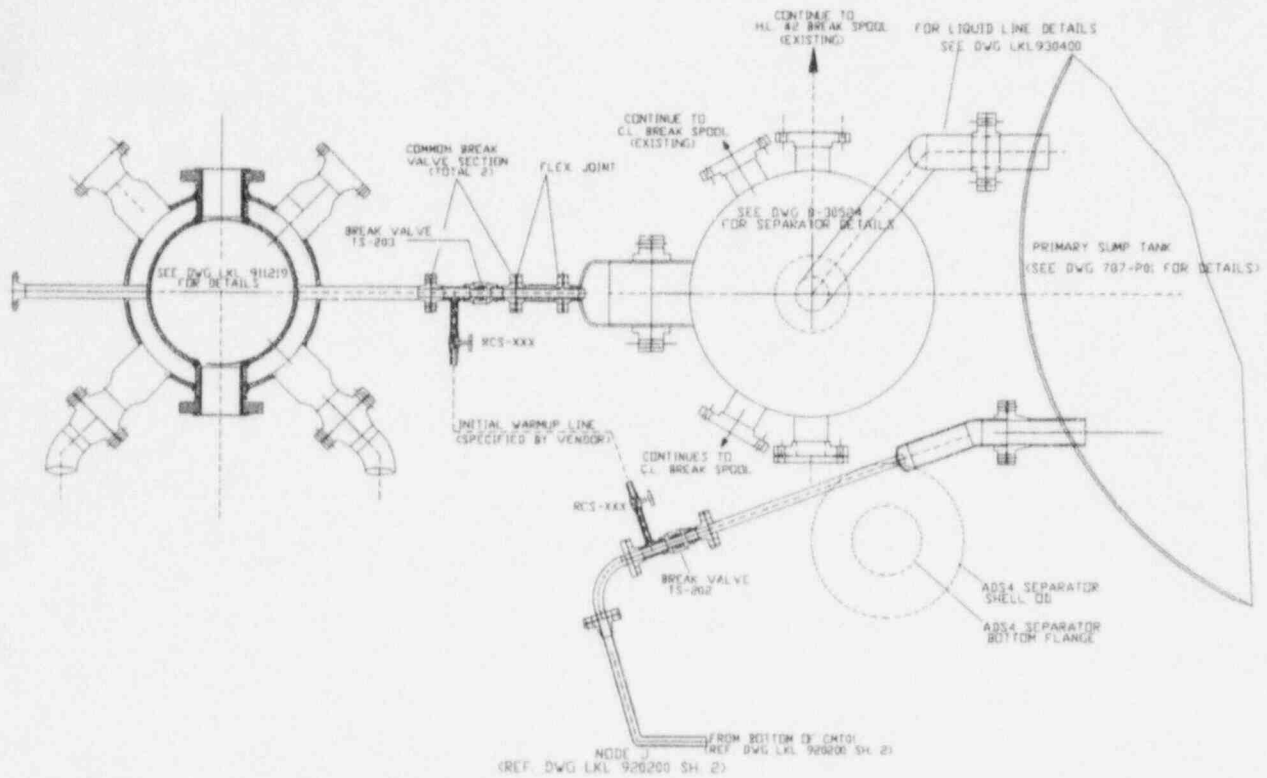
- (1) Data from the instrument channel in parenthesis were used to determine level, flow, or pressure conditions.
- (2) D = time data obtained from a software program that monitored the input and output of the facility's PLC.
A = time data obtained by reviewing data from the instrument channel listed in the Event Description column.

The Bar Charts for Table 5.4.1-3 on pages 5.4.1-42 through 5.4.1-46 are not included in this nonproprietary document.

TABLE 5.4.1-4
TEMPORARY TEST THERMOCOUPLES

Temporary Thermocouple No.	Temporary Thermocouple Location	CMT-1 Thermocouple Replaced
TW-901	Side wall of primary sump	TF-551
TW-902	Side wall of secondary sump	TF-553
TW-903	Top of primary sump	TF-555
TW-904	Top of secondary sump	TF-557
TF-919	Break line to primary sump (CMT side)	TF-559
TF-921	6-in. vent line from primary sump	TF-561
TF-923	Bottom of primary sump	TF-563

NOTE: BOTH BREAK LINES ARE HORIZONTAL AT DVI LEVEL.



FILE: C:\ACAD\SB12 LAYER: DVI DEGR

Figure 5.4.1-1 Primary Loop and Break Pipe Arrangement

Figures 5.4.1-2 through 5.4.1-71 are not included in this nonproprietary document.

5.4.2 Effect of a Smaller Break Size (Matrix Test SB13 Comparison with Matrix Test SB12)

This section of the report will compare the test results of Matrix Test SB13 with reference test SB12. Matrix Test SB13 simulated a 2-in. break of the DVI-1 line. Matrix Test SB12, described in Subsection 5.4.1, simulated a DEG break of the DVI-1 line.

The first part of the comparison describes the system configuration and initial conditions of Matrix Test SB13, followed by a table of inoperable instruments. A sequence of events table provides a comparison of event times in Matrix Tests SB12 and SB13. The comparison is made in tabular and bar-chart format. Following the sequence of events is a description of the overall system interactions in Matrix Test SB13. The test description is divided into three phases, as was done in the section for Matrix Test SB12 results. The description emphasizes the differences between the test results of Matrix Tests SB12 and SB13. Finally, a discussion of component responses provides a more detailed discussion of the test by reviewing it from the component level. Again, the emphasis is on differences between the results of Matrix Tests SB12 and SB13.

Data plots are provided as figures at the end of the section. The numbering and content of the data plots for Matrix Test SB13 in Subsection 5.4.2 are identical to the data plots provided in Matrix Test SB12. For example, the data plot of instrument channel FMM-905 for Matrix Test SB12 is contained in Figure 5.4.1-2. Matrix Test SB13 data for the same channel are contained in Figure 5.4.2-2. The text of the Matrix Test SB13 report contained in this section does not discuss all data plots contained in Subsection 5.4.2.

Matrix Test SB13 was started on June 7, 1994 and successfully completed on June 8, 1994. Test duration was about 7 hours.

5.4.2.1 System Configuration and Initial Conditions

Matrix Test SB13 was performed using an approved written procedure.

To simulate a 2-in. break of DVI-1, piping was installed from DVI-1 to the break separator (Figure 5.4.2-1). The temporary piping from the break separator was connected to the DVI line via two break valves. One break valve isolated the break nozzle and the separator inlet from the common injection line of CMT-1 and ACC-1. The other break valve isolated the common break nozzle and the inlet to the break separator from the portion of the DVI line connected to the reactor.

When the test was started, the injection piping of CMT-1 and ACC-1 was aligned to the break separator via break valve TS-203 and the common break nozzle. At the same time, break valve TS-202 opened allowing backflow from the reactor vessel to the common break nozzle and the same inlet connection to the break separator. The break nozzle simulated a 2-in. break on DVI-1.

The break configuration of Matrix Test SB13 was different than the break configuration of reference test Matrix Test SB12. The DEG break of Matrix Test SB12 aligned the injection piping of ACC-1 and CMT-1 directly to the primary sump rather than to the break separator. Break flow from the reactor was directed to the break separator.

Pressure upstream of the break and break differential pressure on the reactor side of the break was measured by PT-203 and DP-215, respectively. Pressure upstream of break and break differential pressure on the CMT/accumulator side of the break was measured by PT-206 and DP-216, respectively.

Nozzles were installed in ADS 1-3 to simulate operation with two of two lines. A nozzle was installed in the ADS 4-1 line to simulate operation with one of two lines. A nozzle was installed in the ADS 4-2 line to simulate operation with two of two lines.

The nonsafety systems, CVS and RNS, were not used in this test. The CVS and RNS pumps did not run.

Before the test was initiated by pressing the TEST pushbutton, a standard facility heatup and checkout were performed. Details of the startup and checkout can be found in Subsection 2.7.

Table 5.4.2-1 contains the initial system conditions for Matrix Test SB13. Data recorded for control board indication of pressurizer pressure and level, SG pressures and levels, and hot-leg temperatures were obtained from the values recorded in the procedure. All other values for initial conditions were obtained by averaging the DAS data for about 2 minutes before test initiation. This was the time interval between the time DAS started to record data and the signal to open the break valve.

Initial conditions of ACC-1 and ACC-2 pressure were out of specification, as recorded in Table 5.4.2-1. Neither condition invalidated the results of the test.

ACC-1 pressure was []^{a,b,c} or []^{a,b,c} percent low, and ACC-2 pressure was []^{a,b,c} or []^{a,b,c} percent low at test initiation. The proper tank pressures were verified by local calibrated gauges PI-401 and PI-402 as the tanks were pressurized with nitrogen. The loss of pressure between tank pressurization and test start was possibly due to cooling of nitrogen gas in the accumulators. Test analysis starting with the lower accumulator pressure is still possible.

The transient was initiated by simultaneously opening the two break valves and continued through CMT and accumulator injection, ADS actuation, IRWST injection, and primary sump injection. All actions were automatic and required no operator action.

5.4.2.2 Inoperable Instruments

Table 5.4.2-2 is a list of instruments considered inoperable or invalid during all or portions of this test. Some of the instruments listed are on the Critical Instruments List (Subsection 3.2, Table 3.2-2) and therefore, are listed here.

FDP-604, FDP-605, and FDP-606 measured the differential pressure (psid) across the ADS 1-3 flow nozzles. The transmitters over-ranged momentarily when their respective ADS valves opened. Total flow through the ADS 1-3 valve complex can be determined by measuring ADS 1-3 separator liquid and steam flows from FMM-601 and FVM-601.

FMM-201, FMM-202, FMM-203, and FMM-204 measured flow (gpm) in each of the four cold legs. A decision was made to continue testing without the availability of these instruments. Replacement flow meters repeatedly failed; their continued use was precluded due to cracking of the ceramic liners from thermal stratification in the loop piping. The necessary boundary conditions for loop flow was determined from DP-202, DP-203, DP-205, and DP-206.

FMM-501, FMM-504, FMM-802, and FMM-804 provided accurate data when sensing liquid, but became inaccurate when sensing two-phase or steam flow.

FMM-701 measured IRWST-1 injection flow. When the primary sump valves opened, the flow meter indicated a negative flow as water flowed from the primary sump to the IRWST. The meter was not designed to measure reverse flow, so this measurement was invalid. Total IRWST flow, however, was measured by FMM-702.

SG tube level data (LDP-215, LDP-218, LDP-219, and LDP-222) are biased by vaporization of water in the transmitter reference leg after the SG tubes started to drain; however, the data provide accurate indication of the time when the tubes were empty.

LDP-401 and LDP-402 measured ACC-1 and ACC-2 levels. Due to air trapped in the sense lines for the transmitters, data for these transmitters are invalid. The initial level of the tank, however, was established by a standpipe, so it was constant test to test. The drain rates can be calculated using FMM-401 and FMM-402. Alternately, a pressure correction may be applied directly to the level indications of LDP-401 and LDP-402.

LDP-802 measured the level of the PRHR HX. Data from this transmitter are valid until the HX drained at 600 seconds. After this time, data are suspect due to possible boiling of common reference line of LDP-802 and LDP-804.

PT-201 measured RCS pressure at the top of SG-1 long tube. On August 15, 1994, it was discovered that the transmitter had an incorrect zero compensation, which resulted in a negative error and negative data at low pressures. The transmitter zero was corrected at that time. PT-201 data obtained during

Matrix Test SB13 had the zero correction performed, and the corrected data appear as PT_201. Negative data and corrected negative data can be used to determine trends, but are considered inaccurate. There is sufficient other pressure data during the period when PT_201 data are invalid.

LDP-611 and LDP-612 measured the level of ADS 4-1 and ADS 4-2 separators. Transmitter sense line pressures were affected by primary sump pressure before ADS-4 actuation occurred. Although the transmitters were operable, data from these transmitters should be ignored before ADS-4 actuation. After ADS actuation, the data are valid.

FVM-603 and FVM-602 measured steam flow exiting the ADS 4-1 and ADS 4-2 separators to the BAMS header. Flow indications prior to the opening of the ADS 4-1 and ADS 4-2 valves were false indications that were probably due to reverse flow from the BAMS header to the separators.

5.4.2.3 Sequence of Events

Table 5.4.2-3 contains the sequence of events of Matrix Tests SB12 and SB13. The first two pages of the table provide the event times of selected events in both tests and the difference in time between the events in the two tests. The ensuing pages of the table provide a visual representation of the time comparison by using bar charts. Both the numeric table and the bar charts sort the events in chronologic order as they occurred in Matrix Test SB13.

The first page of Table 5.4.2-3 indicates the source of the actual time data. A D in the Data Source column indicates the recorded time was obtained from a software program that monitored digital events in the facility, including pump starts and stops, valve limit switch actuations, and alarms. An A in the Data Source column indicates the time data was obtained by reviewing test data obtained from the DAS. Although the test data from the DAS was a digital format, the DAS monitored analog events such as pressure, flow, and temperature.

5.4.2.4 Test Results and Evaluation

This section contains an overall description of the events that occurred during Matrix Test SB13. The emphasis in the section is a comparison of Matrix Test SB13 results to reference test Matrix Test SB12 results.

The description is divided into three phases:

- Initial Depressurization Phase: simulated break initiation to ADS-1 actuation
- ADS Phase: ADS-1 actuation to start of IRWST injection
- IRWST Injection Phase: start of IRWST injection to end of test

Note: Some of the following discussion compares the differences in the facility response time between Matrix Tests SB12 and SB13. Unless otherwise stated, the reference for comparing the event timing between the two tests is the data contained in Table 5.4.2-3.

Initial Depressurization Phase

The DEG DVI-1 break configuration of Matrix Test SB12 provided two independent break flow paths to the primary sump. The first path directed flow from the reactor, through the broken DVI-1, and into the primary sump via the break separator. The second break flow path directed flow from CMT-1 and ACC-1 directly into the primary sump. Therefore, data for the break separator liquid flow rate and the steam flow rate were attributable to flow from the reactor side of the break only.

In Matrix Test SB13, break flow to the break separator included all flow inputs to DVI-1. This consisted of the break flow from the reactor and injection flow paths from CMT-1, ACC-1, and IRWST-1 injection lines (Figure 5.4.2-1).

The 2-in. DVI break of Matrix Test SB13 was a smaller break than the DEG break of Matrix Test SB12. The lower rate of inventory loss in Matrix Test SB13 is obvious when comparing Matrix Tests SB12 and SB13 data for pressurizer surge line, SG tubes, and SG channel heads drain times. In both tests, these components drained before ADS-1 actuated; however, in Matrix Test SB13, all of these components drained more slowly than in Matrix Test SB12. In general, it took [

] ^{a,b,c} longer to drain these components in Matrix Test SB13 than it did in Matrix Test SB12. ADS-1 actuation was [] ^{a,b,c} slower in Matrix Test SB13 than in Matrix Test SB12.

The difference between the break configurations in Matrix Tests SB12 and SB13 produced different drain rates for CMT-1. In Matrix Test SB12, break flow from CMT-1 was not affected by reactor break flow. CMT-1 had a flow path directly to the primary sump, which meant CMT-1 break flow experienced a backpressure essentially equal to atmospheric pressure. In Matrix Test SB13, however, the 2-in. break configuration created a common flow path for all break flow sources. Reactor break flow created a backpressure in DVI-1 as it flowed backward to the break separator. Backpressure in the DVI-1 slowed the drain rate of CMT-1. As a result, CMT-1 reached its low level setpoint [] ^{a,b,c} later in Matrix Test SB13 than in Matrix Test SB12.

The drain rate of CMT-1 was important because it directly affected the timing of ADS-1 actuation. The control logic of the facility actuated ADS-1 [] ^{a,b,c} after either CMT reached its low level setpoint. In both tests, CMT-1 reached its low level setpoint before CMT-2. Since CMT-1 reached its low level setpoint [] ^{a,b,c} later in Matrix Test SB13 than in Matrix Test SB12, ADS-1 actuated [] ^{a,b,c} later in Matrix Test SB13 than in Matrix Test SB12. ADS-2 and ADS-3 actuation were timed from ADS-1 actuation, so they, too, had similar delay times.

The effect of the break configuration on ACC-1 response was seen in the timing of ACC-1 flow in Matrix Tests SB12 and SB13. In Matrix Test SB12, backpressure for ACC-1 break flow was the

primary sump, which was essentially at atmospheric pressure. Thus, break flow from ACC-1 started immediately after the break. In contrast, Matrix Test SB13 data show ACC-1 did not start to inject to the break until after ADS-1 actuation (Figure 5.4.2-4). Before ADS-1 actuated to decrease RCS pressure, DVI-1 pressure was greater than the ACC-1 initial gas pressure of []^{a,b,c}. Therefore, the ACC-1 did not start to inject to the break until after RCS pressure was decreased by ADS-1 actuation.

ACC-2 was on the "unbroken" side of the facility in both Matrix Tests SB12 and SB13. In both tests, ACC-2 did not inject during the initial depressurization phase (Figure 5.4.2-8). Until ADS-1 actuated, RCS pressure was greater than the initial pressure of the nitrogen gas in the accumulators .

CMT-2 was also on the "unbroken" side of the facility in both Matrix Tests SB12 and SB13. In both tests, CMT-2 injected immediately when the break valve opened (Figure 5.4.2-8). CMT-2 transitioned from recirculation to draindown flow in the initial depressurization phase of both tests. The transition occurred later in Matrix Test SB13 than in Matrix Test SB12 (Table 5.4.2-3). CMT-2 injection flow during Matrix Test SB13 was less than one-third of that in Matrix Test SB12 (Figure 5.4.2-8) for the recirculation phase and after the transition to draindown flow.

It is worth noting the behavior of CMT parameters in both tests when the tank transitioned from recirculation to draindown flow. The time of this transition (recorded in Table 5.4.2-3) can be determined by reviewing plotted data from either the CMT balance line level or its injection flow rate. When the balance line level indication decreased below its full-range indication, steam had started to form in the top of the line (Figure 5.4.2-9), indicating that the tank was no longer in recirculation mode. At the same time, injection flow started a small oscillation (Figures 5.4.2-4 and 5.4.2-8).

In Matrix Tests SB12 and SB13, the CMTs transitioned from recirculation to draindown flow early in the initial depressurization phase. For Matrix Test SB13, the transition was complete in both tanks by []^{a,b,c}. The transition in reference test Matrix Test SB12 was complete by []^{a,b,c}. The transition occurred earlier in Matrix Test SB12 due to the faster RCS drain caused by the larger break.

Matrix Tests SB12 and SB13 data for liquid and steam break separator flows can not be directly compared. As previously described, the break separator had different flow sources in each test. In both tests, the break separator liquid flow rate was measured by FMM-905, and the break separator steam flow rate was measured by FVM-905 (Appendix G, OSU Dwg. 600901).

In Matrix Test SB12, break separator flows were a result of break flow from the reactor only. Thus, FMM-905 and FVM-905 provided direct measurements of break flow from the reactor. Before ADS-1 actuated in Matrix Test SB13, however, break separator flows had two sources: CMT-1 break flow and reactor break flow. To compare Matrix Tests SB12 and SB13 reactor break flows, it is necessary to calculate the reactor break flow in Matrix Test SB13. This is accomplished by subtracting the sum of the liquid flow rate of CMT-1 (FMM-501) and ACC-1 (FMM-401) from the liquid flow rate of the

break separator (FMM-905). ACC-1 flow was []^{a,b,c} during the initial depressurization phase before ADS-1 actuation (Figure 5.4.2-72).

After the CMT-1 outlet isolation valve opened at []^{a,b,c} CMT-1 liquid break flow increased to about []^{a,b,c} (Figure 5.4.2-4). Flow from CMT-1 stayed relatively constant until ADS-1 actuated, at []^{a,b,c}. The calculation for liquid break flow from the reactor indicated a transient flow for the first []^{a,b,c} (Figure 5.4.2-72). Liquid break flow from the reactor was roughly equal to liquid break flow from CMT-1 until ADS-1 actuated.

The CMT-1 outlet temperature was less than []^{a,b,c} for the initial depressurization phase, so steam was not produced at the break (Figure 5.4.2-70). Break separator steam flow was produced by flow from the reactor. This is verified by break separator steam flow data for the first []^{a,b,c} after break initiation. When the break valve opened at 0 second, steam flow was immediately measured by FVM-905 (Figure 5.4.2-3). Steam flow went to []^{a,b,c} for about []^{a,b,c} after the CMT-1 outlet valve opened at []^{a,b,c}. When the CMT outlet valve opened, cold water from CMT-1 mixed with hot water from the reactor vessel. For a short period, the temperature of the mixture at the break was low enough to prevent steam formation at the break.

After the initial transient of []^{a,b,c} steam flow from the break separator varied between []^{a,b,c} (Figure 5.4.2-3). The effect of mixing cold break flow from CMT-1 with hot break flow from the reactor can be seen when a comparison is made with break separator steam flow from Matrix Test SB12. In Matrix Test SB12, break separator steam flow peaked at about []^{a,b,c} before ADS-1 actuation.

There are few similarities between the liquid break flow behaviors of Matrix Tests SB12 and SB13 during the initial depressurization phase. Because Matrix Test SB12 was a simulated DEG break, and Matrix Test SB12 was a simulated 2-in. break, the smaller break of Matrix Test SB13 produced smaller break flow rates. During the initial depressurization phase, CMT-1 break flow was about []^{a,b,c} (Figure 5.4.2-4), whereas, in Matrix Test SB12, CMT-1 flow overranged the outlet flow meter, which was calibrated to []^{a,b,c}. Similarly, liquid break flow from the reactor in Matrix Test SB13 ranged between []^{a,b,c} (Figure 5.4.1-72), while the same flow in Matrix Test SB12 increased to a peak of []^{a,b,c} before ADS-1 actuation (Figure 5.4.1-2).

The smaller 2-in. break flow rate of Matrix Test SB13 was reflected in the response of the cold legs. In reference test Matrix Test SB12, the cold legs completely drained before ADS-1 actuation. In fact, the reactor vessel downcomer level reached the level of the DVI nozzle. This is in contrast to Matrix Test SB13 where the downcomer level was maintained at between []^{a,b,c} before ADS-1 actuation (Figure 5.4.2-14). The bottom of the cold-leg pipe was at about []^{a,b,c} which implies that the cold legs never drained in Matrix Test SB13 during the initial depressurization phase. The downcomer level of []^{a,b,c} was maintained for a majority of the time in the initial depressurization phase (Figure 5.4.2-14).

The slower rate of depressurization in Matrix Test SB13 provided a longer period of quasi-equilibrium between the RCS and the secondary side of the SG. At the initiation of the break, SG steam flow and feedwater flow were isolated. The only cooling available to the SGs was through ambient heat loss. As a result, SG steam pressure started to increase as heat was transferred from the primary side of the SGs, across the SG tubes, and into the SG secondary side (Figure 5.4.2-7). At the same time, reactor pressure was decreasing due to inventory loss through the break. Steam and reactor pressure converged quickly. From about []^{a,b,c} until ADS-1 actuation, the pressure difference between primary and secondary pressures was less than []^{a,b,c}. For about []^{a,b,c} before ADS-1 actuation, RCS pressure varied less than []^{a,b,c}. Immediately before ADS-1 actuation, pressures equalized.

As reported in Subsection 5.4.1, the same quasi-equilibrium period in Matrix Test SB12 lasted only about []^{a,b,c}. In addition, the SG secondary side became a heat source to the RCS before ADS-1 actuation; the large break rapidly depressurized the RCS to a pressure less than the SG secondary-side pressure.

For Matrix Test SB12 results, a steam percent was calculated for various regions in the reactor vessel and the hot legs. The calculated steam percent in the upper head and upper plenum showed similar results in Matrix Tests SB12 and SB13 (Figure 5.4.2-16). The upper-head steam percent calculation was based on LDP-115. The steam percent calculation for the upper portion of the upper plenum was based on LDP-113, and the lower portion of the upper plenum was based on LDP-112.

In both tests, the steam measurement in the upper head initially lagged behind the steam measurement in the upper portion of the upper plenum. As proposed in Matrix Test SB12, a possible explanation for the delay is that the only way for the upper head to drain liquid is to gravity-drain the downcomer via ten small bypass holes in the upper flange of the core barrel, or to gravity-drain to the upper plenum via eight small holes in the upper support plate (Appendix H, Dwg. LKL 911218, Sh. 2).

The PRHR HX response in Matrix Test SB13 was similar to the response in reference test Matrix Test SB12. In both tests, outlet temperatures of the HX were subcooled during the initial depressurization phase and for the entire test (Figure 5.4.2-11). Outlet flow data indicated an oscillating flow rate during the initial depressurization phase, just as it had in Matrix Test SB12 (Figure 5.4.2-10). In Matrix Test SB13, these oscillations dampened as time progressed. Outlet flow from the HX had decreased to less than []^{a,b,c} by the time ADS-1 actuated, with essentially no oscillation in the flow. This flow rate is comparable to the PRHR HX outlet flow of []^{a,b,c} in Matrix Test SB12 at the time of ADS actuation.

Inlet flow to the PRHR HX is measured by a magnetic flow meter that does not provide accurate results for steam flow. The inlet temperature to the PRHR HX reached saturation temperature about []^{a,b,c} after the break valves opened in Matrix Test SB13, compared with []^{a,b,c} in Matrix Test SB12 (Figure 4.5.2-11). It is not known when flow to the HX changed to two-phase

flow, so data from inlet flow meter must be used with caution. Based on the response of the meter, data from FMM-802 can not be used after []^{a,b,c} (Figure 4.5.2-10).

ADS Phase

In Matrix Test Matrix Test SB13, the ADS-1 valve opened at []^{a,b,c} a delay of []^{a,b,c} compared with reference test Matrix Test SB12. As previously discussed, the time delay in Matrix Test SB13 was due to the slower RCS inventory loss, which created a slower CMT-1 drain rate. The ADS-1 valve opened []^{a,b,c} after the level in CMT-1 reached its low level setpoint. CMT-1 reached its low level setpoint []^{a,b,c} later in Matrix Test SB13 than in Matrix Test SB12. Thus, ADS-1 actuation was delayed in Matrix Test SB13.

In Matrix Test SB13, the RCS had reached an essentially steady-state pressure of []^{a,b,c} before ADS-1 actuated, compared with a lower pressure of []^{a,b,c} in Matrix Test SB12 (Figure 5.4.2-19). When the ADS-1 valve opened, RCS pressure began to decrease from its essentially steady-state pressure. Before the ADS-2 valve opened []^{a,b,c} later, the inventory loss through the ADS and the break created a RCS pressure drop of about []^{a,b,c}. This pressure decrease was about the same as the pressure drop of []^{a,b,c} in Matrix Test SB12.

The RCS pressure drop between the ADS-2 and the ADS-3 valve opening was also comparable in Matrix Tests SB12 and SB13. In Matrix Test SB13, pressure decreased []^{a,b,c} between ADS-2 and ADS-3 actuation. In Matrix Test SB12, this pressure decrease was []^{a,b,c} or within []^{a,b,c} percent of one another.

ADS-1 liquid flow to the IRWST sparger was short-lived in both tests (Figure 5.4.2-2); however, the near-zero oscillatory behavior of the liquid sparger flow was not observed in Matrix Test SB13 after ADS-2 and ADS-3 actuation as it was in Matrix Test SB12. Instead, sustained liquid flow to the IRWST sparger was observed until about []^{a,b,c}.

Steam flow from the ADS to the IRWST sparger was sustained for a longer period in Matrix Test SB13 than in reference test SB12. Steam flowed from the pressurizer to the IRWST for about []^{a,b,c} in Matrix Test SB13, but for only about []^{a,b,c} in reference test SB12. Although flow was maintained for a longer period in Matrix Test SB13, the peak value of the steam flow rate after ADS-2 and ADS-3 actuation was less in Matrix Test SB13 than in Matrix Test SB12 (Figure 5.4.2-20).

As discussed in Subsection 5.4.1, liquid and steam break flow in reference test SB12 was generally unaffected by ADS actuation. This was not the case for break flow in Matrix Test SB13.

About []^{a,b,c} after ADS-1 actuated, pressure in the RCS decreased sufficiently for ACC-1 to overcome the backpressure in DVI-1 and start to inject to the break (Figure 5.4.2-4). Flow from ACC-1 mixed with flow from CMT-1 and the reactor. The resultant mixture's lowered temperature

created a single-phase flow from the break, as observed by the cessation of steam flow from the break separator (Figure 5.4.2-3).

Backpressure created by flow from ACC-1 stopped flow from both the CMT-1 and the reactor for a time after ADS-3 actuated (Figures 5.4.2-4 and 5.4.2-72). As ACC-1 flow decreased from its peak value, break flow from CMT-1 and the reactor increased from []^{a,b,c}. Break flow from the reactor started again at about []^{a,b,c} while break flow from CMT-1 started at about []^{a,b,c}.

In Matrix Test SB12, break flow from ACC-1 had no effect on break flow from the reactor. ACC-1 injected directly into the primary sump and, therefore, did not interact with break flow from the reactor.

ACC-2 was located on the "unbroken" side of the facility in both tests, and its general behavior was similar. In both instances, ACC-2 did not inject until after ADS-1 had actuated and, thereby decreased RCS pressure below the initial nitrogen cover gas pressure of the accumulator (Figure 5.4.2-4). Also in both tests, flow from the accumulator increased immediately after ADS-2 actuated, however, there was a notable difference in ACC-2 flow at the time of ADS-3 actuation. In Matrix Test SB13, ACC-2 injection flow increased about []^{a,b,c} percent to []^{a,b,c} after the actuation of ADS-3. In Matrix Test SB12, ACC-2 injection flow was already at its maximum of []^{a,b,c} before ADS-3 actuated and did not change following the actuation of ADS-3.

As ACC-2 flow increased in Matrix Test SB13, CMT-2 injection flow decreased due to backpressure created by ACC-2 flow (Figure 5.4.2-8). When ACC-2 reached its maximum injection flow after ADS-3 actuation, backpressure in DVI-2 was sufficient to momentarily stop CMT-2 injection flow at about []^{a,b,c}. As ACC-2 decreased from its maximum injection flow rate, CMT-2 flow increased from []^{a,b,c}. The same interaction between CMT-2 and ACC-2 was observed in reference test Matrix Test SB12.

The minimum downcomer level in Matrix Test SB13, obtained after ADS-3 actuation at about [460 seconds,] was []^{a,b,c} (Figure 5.4.2-14). In Matrix Test SB12, the minimum level obtained between ADS-2 and ADS-3 actuation, was about []^{a,b,c}. This difference was expected due to the larger break size in reference test SB12.

When the minimum downcomer level of []^{a,b,c} was recorded for Matrix Test SB13, the same minimum collapsed level of []^{a,b,c} was obtained for the reactor wide-range level (Figure 5.4.2-23).

Just as in reference test Matrix Test SB12, there were two competing effects on the RCS inventory when the ADS-1 and ADS-3 opened. Immediately after each ADS valve opened, ADS flow to the IRWST increased, resulting in a decrease in RCS inventory. To balance this effect, ACC-2 flow increased due to the lower RCS pressure. The net result on inventory was recorded by the downcomer wide-range level channels (Figure 5.4.2-14). After each valve actuation, the level in the downcomer

decreased until the additional inventory loss from the increased ADS flow was balanced by the increasing flow from ACC-2.

Of particular note is the rate of downcomer level decrease immediately after ADS-1 and ADS-2 actuation (Figure 5.4.2-14). Before the ADS-1 valve opened, the level in the downcomer was about []^{a,b,c} which was a level within the cold leg. After the valve opened, the downcomer level decreased []^{a,b,c} in about []^{a,b,c}. Increased injection from ACC-2 stopped the level decrease at a level below the DVI nozzles. The scenario was repeated with ADS-2 actuation. This time, the level dropped []^{a,b,c} in about []^{a,b,c} to a level about []^{a,b,c} below the DVI nozzle elevation.

No temperature excursions were observed when the core reached its minimum level. Heater-rod temperatures at the top of the core, where temperatures were expected to be highest, were well-behaved with no temperature excursions (Figure 5.4.2-22). The same result was obtained in reference test SB12 where the collapsed level in the core was even lower than in Matrix Test SB13.

When the ADS-4 valves opened at []^{a,b,c} RCS pressure was only about []^{a,b,c} (Figure 5.4.2-19). RCS pressure in Matrix Test SB12 was about []^{a,b,c} when ADS-4 actuated. Although the break in Matrix Test SB12 was larger than in Matrix Test SB13, and the RCS depressurized faster in Matrix Test SB12, the delay in ADS-4 actuation in Matrix Test SB13 allowed RCS pressure to decrease to a lower value before ADS-4 actuated. The time delay in ADS-4 actuation in Matrix Test SB13 was due to the slower rate of CMT-1 drain. In both tests, ADS-4 actuated on the low-low level setpoint in CMT-1.

Steam flow from ADS 4-1 and 4-2 were barely measurable and lasted less than []^{a,b,c} after the valves opened in both tests. The sustained steam flows of ADS 4-1 and ADS 4-2 peaked at about []^{a,b,c} (Figure 5.4.2-20).

Liquid flow from ADS 4-1 and ADS 4-2 were not identical in Matrix Test SB13 as they were in reference test SB12. In the reference test, the resistance of the ADS-4 lines were the same. Matrix Test SB13 conditions modeled ADS 4-1 with one of two lines operational, while ADS 4-2 was modeled with two of two lines operational. The configuration for ADS-4 implied that the liquid flow through ADS 4-1 should have been less than flow through ADS 4-2; however, flow through ADS 4-1 was at first greater when the ADS-4 valves opened, and then became less than ADS 4-2 flow at about []^{a,b,c} (Figure 5.4.2-24 and 5.4.2-24x). There is no evidence to indicate that the ADS-4 flow data are invalid, but there is currently no explanation for the relationship between the liquid flow rate of ADS 4-1 and ADS 4-2.

IRWST Injection Phase

The normal IRWST injection flow path to the reactor vessel downcomer is via the DVI penetration at the reactor vessel. The IRWST injected to the vessel when pressure in the RCS became smaller than

the static head of water in the IRWST. For the RCS to decrease to a pressure lower than the IRWST static head, the RCS had to depressurize after the opening of the ADS-4 valves. ADS 4-1 and 4-2 valves opened at []^{a,b,c}

A variation on the normal mode of IRWST injection was introduced in Matrix Test SB13 as a result of the break configuration. In Matrix Test SB13, IRWST-1 injection did not flow to the vessel, but to the break separator via the DVI-1 break flow path. The backpressure to flow experienced by IRWST-1 injection flow was the pressure in the "broken" DVI-1. IRWST-1 injection flow to the break started at []^{a,b,c} sooner than IRWST-2 injection flow to the vessel (Figure 5.4.2-25). Similar results were observed in Matrix Test SB12 where IRWST-1 started to inject to the break about []^{a,b,c} before IRWST-2 started to inject to the reactor vessel.

IRWST-2 injection flow started at []^{a,b,c} (Figure 5.4.2-25). CMT-2 and IRWST-2 injected together for only []^{a,b,c} before CMT-2 emptied. Between []^{a,b,c} the only cooling available to the core was IRWST-2 injection. At [7600 seconds,] the reflooded CMT-2 started injecting again and continued to inject until []^{a,b,c} (Figure 5.4.2-8x).

The response of DVI-2 flow to the core during the IRWST injection phase was different in Matrix Test SB13 than in reference test SB12. Where IRWST-2 and CMT-2 simultaneously injected to the core for only []^{a,b,c} in Matrix Test SB13, they injected together for almost []^{a,b,c} in Matrix Test SB12. In addition, the CMTs never reflooded in Matrix Test SB12.

Because the CMTs never refilled or reflooded in the reference test, the event will be examined here. The reflooding of the CMTs is treated in detail in the component responses subsection of this report.

The minimum level in the reactor downcomer occurred at about []^{a,b,c} during the ADS phase (Figure 5.4.2-26). From this time forward, the level increased in the downcomer until the cold legs filled at about []^{a,b,c}. The downcomer level was slightly greater than []^{a,b,c} when the cold legs filled.

At []^{a,b,c} the CMT-1 balance-line level started to increase, followed by a CMT-2 balance-line level increase at []^{a,b,c} (Figure 5.4.2-9x). Coincident with the balance-line increase was a decrease in internal tank pressure of each CMT (Figure 5.4.2-30x). It is possible that the two events are related. The possible scenario can be explained by describing the behavior of CMT-2 only because both CMTs responded in the same way.

When the colds leg filled, CMT-2 was isolated from the steam atmosphere of CL-1. The subcooled liquid from CL-1, which entered the balance line of CMT-2, may have started to condense steam in the balance line, thereby decreasing pressure in the balance line and CMT. The pressure decrease in the balance line created an imbalance between RCS and balance line pressure which resulted in the liquid level increase. The level increase in the balance line was relatively slow. It took almost []^{a,b,c} to completely fill the small volume of the balance line, a response that suggests the liquid

level increase came from condensation. This assumption is supported further by the pressure response of CMT-2; the tank pressure of CMT-2 started to decrease at precisely the time the level in the CMT-2 balance line increased. As the liquid level in the CMT-2 balance line increased, pressure in CMT-2 decreased.

The level and pressure response of CMT-2 when the balance line filled and overflowed into the tank provided additional evidence of the effect the subcooled liquid in the balance line had on the steam environment of CMT-2. The CMT-2 level started to increase rapidly when the balance line became full and overflowed into the tank. The tank filled to a level of []^{a,b,c} over two-thirds full, in about []^{a,b,c}. This rate of fill was not possible when utilizing the facility's CVS or RNS pumps. Concurrent with the rapid fill of CMT-2 was a depressurization in CMT-2. Tank pressure decreased rapidly, over-ranging the CMT-2 pressure transmitter in the negative direction. The rapid fill of CMT-2 and the negative pressure spike when the tank started to fill are representative of the rapid condensation and depressurization event that took place in CMT-2 when subcooled water from the balance line flowed into the steam environment of the tank.

The response to the possible condensation event in CMT-2 was not limited to the CMT. For example, as water rushed to fill CMT-2 during the condensation event, the injection rate of IRWST-2 spiked higher, and the collapsed level of the reactor spiked lower (Figures 5.4.2-25 and 5.4.2-26).

The events that occurred as the CMT-2 balance line filled and overflowed into CMT-2 were repeated for CMT-1. The only difference was the time delay between the CMT-2 and CMT-1 balance lines filling completely and overflowing to their respective tanks.

After reflooding, the level of both CMTs stayed essentially constant for several []^{a,b,c}. As the level in the IRWST decreased, backpressure in each DVI line decreased. Backpressure was low enough at about []^{a,b,c} for CMT-1 to start injecting to the break (Figure 5.4.2-4x). Backpressure was low enough at about []^{a,b,c} for CMT-2 to start injecting to the vessel (Figure 5.4.2-8x). Injection flow from CMT-1 and CMT-2 was not steady. Instead, backpressure from the IRWST would alternately back seat and unseat the CMT injection check valves, which started and stopped flow from the tanks.

5.4.2.3 Comparison of Component Responses

Core Makeup Tanks

The difference in break configuration between Matrix Tests SB12 and SB13 had a direct influence on the response of CMT-1 in both tests. The simulated DEG break of SB12 had CMT-1 and ACC-1 piped directly to the primary sump via a common injection line. The primary sump provided backpressure essentially equal to atmospheric pressure. In contrast, the single-ended guillotine break of Matrix Test SB13 had CMT-1, ACC-1, and the reactor injecting to the break separator via the common DVI-1 line. Break flow from the RCS created pressure in DVI-1 that provided a higher

resistance to CMT-1 flow than the atmospheric pressure in Matrix Test SB12. The higher resistance to CMT-1 flow in Matrix Test SB13 resulted in a smaller rate of injection flow and a slower drain of the tank.

The slower drain rate of CMT-1 in Matrix Test SB13 delayed the actuation of ADS-1 (Table 5.4.2-3). When the level in either CMT reached a low level setpoint, ADS-1 actuated after a []^{a,b,c} delay. In both tests, the location of the break resulted in CMT-1 draining before CMT-2. The CMT-1 low level setpoint was obtained at []^{a,b,c} in Matrix Test SB13, []^{a,b,c} later than in Matrix Test SB12. Since the delay between the CMT-1 low level setpoint and ADS-1 actuation was the same in both tests, the actuation of ADS-1 occurred []^{a,b,c} later in Matrix Test SB13 than in Matrix Test SB12.

The slower drain rate of CMT-1 in Matrix Test SB13 also delayed the actuation of ADS 4-2. Similar to the operation of ADS-1, the ADS-4 valves opened after a time delay when CMT-1 reached its low-low level setpoint. CMT-1 reached its low-low level setpoint at []^{a,b,c} over 400 seconds later than in Matrix Test SB12.

Immediately after the CMT-1 outlet valve opened in SB-12, CMT-1 injection flow exceeded the []^{a,b,c} range of FMM-501. This was not true for Matrix Test SB13 where the injection flow rate was always less than []^{a,b,c} except about []^{a,b,c} immediately after ADS-1 opened (Figure 5.4.2-4). During this short time, the recorded injection flow peaked at []^{a,b,c}. This value was above the calibrated range of the instrument but within its range capability. Thus, FMM-501 data are considered valid for the duration of the test.

CMT-1 transitioned from recirculation to draindown flow at []^{a,b,c} later than in Matrix Test SB12. The balance line flow indication of FMM-503 is not valid after this time because the magnetic flow meter does not provide accurate indication in a steam environment.

CMT-1 did not empty in Matrix Test SB13 until after the start of IRWST injection, whereas, in Matrix Test SB12, the tank was empty and injection flow stopped before ADS-3 actuated (Figure 5.4.2-4). There was a short period of []^{a,b,c} in Matrix Test SB13 when CMT-1 flow was []^{a,b,c} before the tank emptied. Backpressure from the ACC-1 flow created this stoppage of flow from CMT-1 about []^{a,b,c} after ADS-3 actuated. CMT-1 flow returned, however, as ACC-1 drained, and then continued until CMT-1 emptied at []^{a,b,c} about []^{a,b,c} after IRWST-1 injection started.

Another notable difference between the response of CMT-1 in Matrix Test SB12 and Matrix Test SB13 was the refilling or reflooding of the CMTs. CMT-1 reflooded at []^{a,b,c} after CMT-2 had reflooded at []^{a,b,c}. Since CMT reflooding did not take place in Matrix Test SB12, the event will be examined here. A detailed description of the process will be given for CMT-1 only because the mechanism of reflooding is similar in CMT-2.

The reflood of CMT-1 began with the refilling of the CMT-1 balance leg which started to increase in level at []^{a,b,c} (Figure 5.4.2-9x). This was the same time the level in the downcomer annulus reached the top of the cold legs, or []^{a,b,c} (Figure 5.4.2-26). The level in the downcomer did not increase above the top of the cold legs, so it can be surmised that the increasing level in the cold-leg balance line was not the result of a static head. It is possible that steam in the balance line started to condense when the cold-leg water elevation rose to the top of the pipe and created an interface between the steam in the balance line and the cold water. Condensation of the steam did two things: slowly increased the water level in the balance line and slowly decreased the pressure in CMT-1.

The slow increase in level in the CMT-1 balance line is seen clearly in Figure 5.4.2-9x. It took almost (1000 seconds) for the balance line to completely fill. The plot of PT-501 shows the pressure decreasing in the tank as the balance line fills (Figure 5.4.2-30x). It should be noted that the calibrated range of PT-501 was []^{a,b,c}. The vacuum reading of the transmitter during this period can only be used for trend indication, not an absolute pressure measurement. The pressure transmitter over-ranged in the negative direction as the balance line filled. During the time PT-501 was over-ranged in the negative direction, its data can not be used for trend indication, either.

Even with the limitations imposed by the pressure indication of PT-501, the CMT-1 reflooding process can be examined. A downward spike in balance-line level occurred immediately after the balance line filled. At the same time, pressure in the CMT-1 spiked above the maximum negative indication of PT-501. These data, taken with the slight increase in CMT-1 level of []^{a,b,c} suggest cold water from the balance line overflowed into the CMT, created a pressure spike, and forced a lower level in the balance line. The balance line once again started to increase in level. The balance line did not completely refill until []^{a,b,c} after its sharp level decrease.

When the balance line filled the second time at []^{a,b,c} it initiated a refill of CMT-1. The tank refilled to a level of about []^{a,b,c}. This fill rate of CMT-1 could not be achieved using either the RNS or CVS pumps. The rapid decrease in CMT-1 fluid temperatures when the tank started to reflood indicated a depressurization had occurred when cold water from the balance line flowed into the steam environment of the CMT. PT-501 provided no information because it was over-ranged in the negative direction before the reflood occurred. Nonetheless, there are additional data that reflect the result of the possible depressurization in the CMT. IRWST injection flow showed a marked increase when CMT-1 and CMT-2 began to reflood (Figure 5.4.2-25). At the same time IRWST injection flow increased, the reactor wide-range level decreased (Figure 5.4.26). The depressurization that occurred in the CMT when cold water entered the CMT from the balance line may have diverted some cooling flow from the reactor to the lower-pressure CMT, creating a decreased wide-range level in the core.

After its reflood at []^{a,b,c} CMT-1 periodically injected to the break (Figure 5.4.2-4x) until the tank emptied again at about []^{a,b,c} (Figure 5.4.2-5x). The CMT did not reflood for the remainder of the test.

Superheated fluid temperature conditions existed in CMT-1, just as in Matrix Test SB12. The superheated conditions had the same source, namely the upper wall of the CMT. A more detailed discussion of the temperature response of the CMT is provided in Subsection 7.2.

CMT-1 transitioned from recirculation to draindown flow at []^{a,b,c} later than in Matrix Test SB12. The balance-line flow indication of FMM-503 is not valid after this time because the magnetic flow meter does not provide an accurate indication in a steam environment.

In reference test SB12, CMT-2 injection flow was greater than in Matrix Test SB13 (Figure 5.4.2-8) although the general flow behavior was similar. The flow was greater in Matrix Test SB12 than in Matrix Test SB13 because the level in the downcomer decreased faster in Matrix Test SB12 due to the larger break size (Figure 5.4.2-14). A lower downcomer level resulted in smaller backpressure for CMT-2 injection flow and faster drain of the tank. As a result, CMT-2 emptied about []^{a,b,c} later in Matrix Test SB13, at []^{a,b,c}

Flow transitioned in CMT-2 from recirculation to draindown flow at []^{a,b,c} later than in Matrix Test SB12. Data from FMM-502 are invalid after CMT-2 recirculation flow stops at []^{a,b,c} because for the magnetic flow meter does not provide an accurate indication in a steam environment.

The interaction of CMT-2 and ACC-2 injection flow was similar in the two tests; in both tests, CMT-2 flow decreased as ACC-2 flow increased, and CMT-2 flow was momentarily stopped as ACC-2 reached its maximum injection rate.

Reflooding or refilling of CMT-2 did not occur in the reference test. The mechanism for reflooding a CMT was described in the CMT-1 response subsection and is the same process for the reflood of CMT-2. Refill of both balance lines started at the same time, but CMT-2 filled first at []^{a,b,c} because there was no pressure spike in CMT-2 to decrease the level in the balance line as the pressure spike in CMT-1 did (Figure 5.4.2-9x and 5.4.2-30x). There was an increase in CMT-2 pressure as the refill terminated at a level of about []^{a,b,c}. It took only []^{a,b,c} to fill CMT-1 to its final reflooded level, a result identical to CMT-2. Oscillatory injection flow from the reflooded CMT-2 started at about []^{a,b,c} and stopped when the tank emptied at about []^{a,b,c} (Figure 5.4.2-8x). CMT-2 did not reflood during the remainder of the test.

Pressurizer

The effects of the smaller break in Matrix Test SB13 were seen clearly in the drain time of the pressurizer and the pressurizer surge line. In Matrix Test SB12, the surge line was empty within []^{a,b,c} but it took []^{a,b,c} for the surge line to drain in Matrix Test SB13 (Figure 5.4.2 31). In both tests, the surge line was empty shortly before ADS-1 actuation.

The peak liquid flow rate from the pressurizer after ADS-1 actuation was more than twice as great in Matrix Test SB13 as in Matrix Test SB12 (Figure 5.4.2-2). ADS-2 and ADS-3 flow rates had similar disparities. When ADS-2 actuated in Matrix Test SB12, liquid flow from the pressurizer was lasted only about []^{a,b,c} and then oscillated about 0 when the ADS-3 valve opened. In contrast, the Matrix Test SB13 response to ADS-2 actuation was a sustained flow of []^{a,b,c} that increased to []^{a,b,c} when ADS-3 actuated. ADS-1 through ADS-3 flow data from these two tests suggest that the break flow of Matrix Test SB13 did not dominate the depressurization of the RCS as did the larger break flow of Matrix Test SB12.

During ADS actuation in Matrix Test SB13, the liquid content of the pressurizer increased, just as it did in Matrix Test SB12 (Figure 5.4.2-31). The pressurizer started to drain after ADS liquid and steam flow ceased, but it took twice as long for the pressurizer to drain as in reference test SB12. Table 5.4.2-3 indicates that the pressurizer reflooded at about []^{a,b,c} in Matrix Test SB13. In fact, data from LDP-601 indicate that the pressurizer level increased to less than []^{a,b,c} when it reflooded, while LDP-602 data indicate that the surge-line level was less than []^{a,b,c} percent full. The surge line level data make the data of the pressurizer reflood suspect.

Control logic for the facility tripped the pressurizer heaters at []^{a,b,c}. Data from KW-601 indicate a continuing power output of about []^{a,b,c} after the pressurizer heaters were to trip.

Passive Residual Heat Removal Heat Exchanger

Data from Matrix Test SB12 established that subcooled liquid from the PRHR HX outlet was returned to CL-2 and CL-4 via the SG-2 cold-leg plenum. The effluent cooled the bottom of CL-2 and CL-4 while the pipes were drained and the upper portion of the piping was superheated.

The PRHR HX did not provide the same effect on CL-2 and CL-4 during Matrix Test SB13. The effluent temperature was subcooled for the duration of the test (Figures 5.4.2-33 and 5.4.2-34), but there were periods when the cold legs were empty and the bottoms of CL-2 and CL-4 were not subcooled. At about []^{a,b,c} the collapsed level indication of the downcomer revealed that the level was below the bottom of the cold legs and remained there until about []^{a,b,c} (Figure 5.4.2-14). Bottom-of-pipe temperatures for CL-2 and CL-4 were not subcooled during this condition as they were in Matrix Test SB12, but instead, became superheated during this time (Figure 5.4.2-40). Cold-leg temperature is discussed later in this subsection.

The cold legs drained between []^{a,b,c} and data from the HX wide-range level transmitter indicate the HX drained and started to refill (Figure 5.4.2-35). The HX initially emptied at about []^{a,b,c} then partially refilled between []^{a,b,c}. After []^{a,b,c} the HX was essentially empty with an indicated level of about []^{a,b,c} until []^{a,b,c}. From []^{a,b,c} the indicated level slowly increased in the HX until it was about []^{a,b,c} percent full at the end of the test. The response of the HX level was similar in

Matrix Test SB12 where the HX level decreased to a minimum at []^{a,b,c} and then slowly increased in level until the end of the test.

Data from the HX level demonstrate that there was inventory available in the PRHR HX to provide cooling water to the cold legs while they were empty between []^{a,b,c} but only after the HX had initially drained at []^{a,b,c} and then started to refill. It is not clear what caused the refill of the HX, or why the available inventory would not cool the cold legs.

There is no direct evidence to prove it, but it is possible that data from LDP-802 are not valid for the time after the HX initially drained. The supposition has to do with the sense line of LDP-802, rather than the transmitter itself. The indicated level increase in the HX may have been a result of the reference leg of the transmitter boiling and decreasing the level. The resultant differential pressure decrease across the transmitter would have had the same effect as the level in the HX increasing. The sense line may have started to boil when pressure in the HX decreased below the saturated pressure for the temperature of the liquid in the sense line.

As stated, there is no direct evidence that the sense line of LDP-802 decreased in level due to boiling because pressure of the HX was not measured. There is indirect evidence, however, because LDP-801 displayed the same response (Figure 5.4.2-35). Data from LDP-801 indicate that the level was increasing in the inlet plenum at the same time that data from LDP-802 indicate the HX was starting to refill. The inlet head of the HX could not fill before the HX was nearly full. The two transmitters did share a common reference leg, so both increasing levels may have been due to boiling of the reference leg.

The response from FMM-804 provided a high level of confidence that there was outlet flow from the HX until the HX initially drained at about []^{a,b,c} (Figure 5.4.2-10). After this time and for the remainder of the test, flow was identical to Matrix Test SB12 results where flow oscillated about 0 with spikes of about []^{a,b,c}. Because temperature data from the bottom of CL-2 and CL-4 did not indicate the presence of cooling water from the HX while the pipe was drained, it is not possible to determine if the outlet flow was a small, chugging type of flow or if steam in the flow meter provided an invalid oscillatory flow indication.

FMM-802 is a magnetic flow meter that could not accurately measure steam or two-phase flow. The temperature of the inlet flow to the HX was saturated by []^{a,b,c}. After this time, data from this meter are suspect because it is not known whether the fluid was a saturated liquid, saturated vapor, or a two-phase mixture.

Cold Leg

Within []^{a,b,c} the break in Matrix Test SB13 decreased the level in the downcomer to about the top of the cold legs, or []^{a,b,c} (Figure 5.4.2-14). The level remained essentially constant until ADS-1 actuation. ADS-1 actuation at []^{a,b,c} created a level decrease that drained the cold

legs within []^{a,b,c} The level did not increase above the bottom of the cold-leg pipes again until about []^{a,b,c} At about []^{a,b,c} the level decreased below the bottom of the cold legs once more, and did not refill the cold legs for the remainder of the test.

The cold-leg level response was quite different in Matrix Test SB12 due to the larger break size. The cold legs drained before ADS-1 actuated and did not refill above the bottom of the cold legs until about []^{a,b,c} The level remained above the cold legs for the remainder of the test. Acquisition of test data terminated in Matrix Test SB12 at about []^{a,b,c}

The temperature response in CL-1 and CL-3 was similar in Matrix Test SB12 and Matrix Test SB13 in that, while the cold legs were empty, the temperatures at the top and bottom of the legs were saturated or superheated (Figures 5.4.2-39 and 5.4.2-40). The bottom-of-pipe temperature response in CL-2 and CL-4 was different in the two tests.

The cooling effect from the PRHR HX was apparent in Matrix Test SB12; the bottom-of-pipe temperatures in CL-2 and CL-4 never superheated while the pipes were empty. This was not the case in Matrix Test SB13. Between the time the cold legs drained immediately after ADS-1 actuation and the time they refilled at []^{a,b,c} the bottom temperatures of both CL-2 and CL-4 indicated superheated conditions (Figure 5.4.2-40). The bottom of CL-4 superheated first at about []^{a,b,c} and CL-2 superheated last at []^{a,b,c} As discussed in the PRHR HX subsection, it is not clear when, or if, flow from the PRHR HX terminated. Nonetheless, the superheated conditions of the bottom of CL-2 and CL-4 suggest that flow from the HX may have stopped when the wide-range level of the HX indicated it first drained at about []^{a,b,c}

In-Containment Refueling Water Storage Tank

The drain rate of the IRWST was slower in Matrix Test SB13 than in Matrix Test SB12 because IRWST-1 injection started sooner in Matrix Test SB12, and the rate of injection was higher (Figures 5.4.2-27 and 5.4.2-25). Both the delay and the slower rate of IRWST injection can be attributed to the faster depressurization of the RCS during the larger break of Matrix Test SB12. The initiation of IRWST-1 and IRWST-2 injection were delayed about []^{a,b,c} in Matrix Test SB13 compared with Matrix Test SB12.

The IRWST thermocouple temperatures did not obtain saturation temperature before they were uncovered (Figure 5.4.2-46). The temperature of the water in the tank was never greater than []^{a,b,c} until the tank stopped draining at about []^{a,b,c} After the thermocouples were uncovered, the gas temperature at their elevation started to increase. By the end of the test, gas at the []^{a,b,c} level in the tank had reached saturation temperature.

These results were similar to Matrix Test SB12 in that thermocouples in the IRWST never reached saturation before they were uncovered. The maximum liquid temperature in the tank during its drain

was about []^{a,b,c} The thermocouples heated to saturation temperature as they uncovered, just as in Matrix Test SB13.

When the primary sump injection valves opened at []^{a,b,c} backflow started in the IRWST-1 injection line. Flow was recorded as a negative reading by FMM-701 (Figure 5.4.2-25x). Although a negative flow existed in the IRWST-1 injection line after []^{a,b,c} the magnitude of the recorded flow is not valid because the magnetic flow meter was not designed to record negative flow.

The negative flow in the IRWST-1 injection line was due to the relatively small line resistance in the IRWST-1 injection line from the IRWST to the connection tee with the primary sump. When the primary sump valves opened, there was a smaller resistance to flow from the primary sump backward through the IRWST-1 line than there was to the direct injection flow path from the primary sump to the reactor.

Reactor

The reactor response discussion will be divided into discussions of the downcomer annulus, core, upper plenum, and upper head, just as was done in Matrix Test SB12.

When the break valve opened in Matrix Test SB12, the level in the downcomer decreased to the level at the top of the cold legs and stayed there until ADS-1 actuated. The larger break of Matrix Test SB12 completely drained the cold legs before ADS-1 actuated, even though ADS-1 actuation occurred at []^{a,b,c} in Matrix Test SB12 and did not occur until []^{a,b,c} in Matrix Test SB13 (Figure 5.4.2-14). The minimum water level in the downcomer was also directly affected by the break size; the collapsed level in the downcomer decreased to only []^{a,b,c} in Matrix Test SB13 as opposed to []^{a,b,c} in Matrix Test SB12. Both minimum levels were below the DVI elevation. The minimum collapsed level in the downcomer occurred later in Matrix Test SB13 than in Matrix Test SB12; []^{a,b,c}

In both tests, only CMT-2 and ACC-2 injection flows were available to stop the level decrease in the reactor. CMT-1, ACC-1, and IRWST-1 injections flowed to the DVI-1 break and IRWST-2 injection did not start until downcomer level had recovered in each test.

The phenomenon of temperature stratification in the downcomer was repeated in Matrix Test SB13. Data from eight downcomer thermocouples best describe the occurrence. Four thermocouples were located above the DVI nozzle (TF-147, TF-149, TF-164, and TF-166) and four thermocouples were located below the DVI nozzles (TF-132, TF-134, TF-152, and TF-154). From []^{a,b,c} all eight thermocouples were uncovered; the lowest of them was at a level of []^{a,b,c} (Figure 5.4.2-14). Temperature data from the thermocouples reveal superheated steam conditions for thermocouples above the DVI nozzle and subcooled conditions for thermocouples below the DVI nozzle (Figures 5.4.2-50 and 5.4.2-51). Since the collapsed level in the downcomer annulus was

below all eight thermocouples, the subcooled temperature of the bottom four thermocouples could not have been due to them being underwater between []^{a,b,c}

The orientation of the thermocouples may explain the inconsistency. All of the thermocouples are located at 0° or 180°az. This placed the four lower thermocouples directly beneath the DVI nozzles which were installed at the same azimuth. In addition, the downward-turned elbows of the DVI nozzles would have directed cold injection flow water directly onto the thermocouples below it. The cold water impinging directly on the thermocouples may have resulted in a subcooled temperature reading in the steam space of the downcomer.

This assumption has supporting evidence in additional data from []^{a,b,c} when all the downcomer thermocouples were covered with water (Figures 5.4.2-52 and 5.4.2-53). Data show the temperatures of the downcomer thermocouples below the DVI nozzle to be in close agreement, while temperatures for the thermocouples above the DVI nozzle are variable and show no correlation to the lower thermocouple temperatures. This result may be due to the mixing of water below the DVI nozzles as DVI flow was directed downward by the DVI turning elbows.

A similar effect is apparent in Matrix Test SB12 from []^{a,b,c} to the end of the test when the downcomer level was above all eight thermocouples. The four lower thermocouple temperatures were in close agreement while the four upper thermocouples ranged from []^{a,b,c} hotter.

Although the core experienced no temperature excursions during either test, the reactor response in Matrix Test SB13 had many differences from that in Matrix Test SB12. The first difference was a direct result of the size of the break. Axial temperatures at the center of the core were measured by a series of thermocouples mounted on a vertical rod. Data from the thermocouples indicate the core was saturated about []^{a,b,c} after the break valve opened, compared with []^{a,b,c} in Matrix Test SB12 (Figure 5.4.2-54).

Subcooling in the core progressed from the bottom to the top of the core, as expected. Subcooling occurred earlier in Matrix Test SB13 than in the reference test. By []^{a,b,c} subcooling was measured by thermocouple TR-001-5 located at []^{a,b,c} percent of core height. The same thermocouple did not measure subcooling in Matrix Test SB12 until after []^{a,b,c}

Two temperature transients in the core were measured by the axial thermocouples located at the center of the core. During the transients, temperatures in the core increased. Timing of the transients coincide with, and were a result of, the reflood of the CMTs. The first transient started at about []^{a,b,c} the second at about []^{a,b,c}. These times coincided with the reflood of CMT-2 and CMT-1, respectively. The fill of the CMTs created a decrease in flow to the core because a portion of the injection flow was diverted to the CMTs. As a result of the flow decrease to the core, temperatures in the core increased. The temperature transient had no effect on heater-rod temperatures at the top of the heater rods (Figure 5.4.2-55).

Heater-rod temperatures at the top of the core were essentially identical in the two tests. Temperature data from Matrix Test SB13 reveal the same "flat" radial heat flux experienced in Matrix Test SB12.

The minimum collapsed level in the core, or maximum steam percent, occurred at about the same time as the minimum collapsed level in the downcomer, or []^{a,b,c} (Figure 5.4.2-56). The relationship between the times of minimum levels in the downcomer and the core was the same in Matrix Test SB12, although the actual minimum level in the core was higher in Matrix Test SB13.

Superheated steam conditions appeared in the upper head shortly after ADS-1 actuation at []^{a,b,c} (Figure 5.4.2-61). Saturated steam from the upper plenum was superheated by the wall of the upper head. Saturated steam flowed into the upper head via the upper support plate, was heated by the walls of the upper head, and flowed to the lower pressure of the downcomer via the bypass holes in the flange of the core barrel. All of this was consistent with the behavior in Matrix Test SB12, except steam flow from the upper head to the downcomer ceased for a time. Flow cessation was recorded by DP-130. Its indication went from less than []^{a,b,c} (Figure 5.4.2-60). When the water level was below the bottom tap of DP-130, a []^{a,b,c} offset in the reading was created, so an indication of []^{a,b,c} of water implied no flow through the bypass holes existed.

During the period of steam flow cessation, the temperature in the upper head increased because the only cooling effect in the upper head during this time was ambient heat loss (Figure 5.4.2-61). Between []^{a,b,c} there were two brief intervals of flow from the upper head to the downcomer. When CMT-2 and CMT-1 reflooded at []^{a,b,c} respectively, DP-130 recorded a differential pressure greater than []^{a,b,c} which denoted flow through the bypass holes. Flow from the upper head to the downcomer was created when the CMTs started to refill and created a local depressurization in the CMTs.

Both TF-169 and TF-170 monitor the temperature in the upper plenum. Data from both thermocouples indicate a subcooled temperature condition in the upper plenum by []^{a,b,c}. It is likely that data from both thermocouples are invalid because subcooled conditions could not have been possible in the upper plenum by []^{a,b,c}. The thermocouple may have been affected by the downcomer leaking through the O-ring seals of the thermocouples at the core barrel wall.

Steam Generators

Both SG tubes emptied before ADS-1 actuated, just as in SB12 (Figures 5.4.2-62 and 5.4.2-63). The SGs were drained when the minimum indicated level of []^{a,b,c} was obtained. Like Matrix Test SB12, the tube-level indication erroneously indicated that the SGs refilled—once they drained, both SGs stayed empty. The errors in level indication were a result of the boiling in each SG level transmitters' common reference leg and the level decrease as the SGs drained.

The slower rate of depressurization in Matrix Test SB13 provided a longer period of quasi-equilibrium between the RCS and the secondary side of the SGs. At break initiation, SG steam and feedwater flow were isolated. The only cooling available to the SGs was through ambient heat loss. As a result, SG steam pressure started to increase as heat was transferred from the primary side of the SG, across the SG tubes, and into the secondary side (Figure 5.4.2-7). At the same time, reactor pressure was decreasing due to inventory loss through the break. Steam and reactor pressure converged quickly. From about []^{a,b,c} until ADS-1 actuation, the difference between primary and secondary pressures was less than []^{a,b,c}. For about []^{a,b,c} before ADS-1 actuation, RCS pressure varied less than []^{a,b,c}. Immediately before ADS-1 actuation, the pressures equalized.

As reported in Subsection 5.4.1, the same quasi-equilibrium period in Matrix Test SB12 lasted only about []^{a,b,c}. In addition, the SG secondary side became a heat source to the RCS before ADS-1 actuation because the large break rapidly depressurized the RCS to a pressure less than the SG secondary pressure. In Matrix Test SB13, the SG secondary side did not become a heat source to the RCS until after ADS-1 actuation.

5.4.1.6 Mass Balance

The mass balance results for Matrix Test SB13 were calculated based on water inventory before and after the test and are provided in Appendix E. Mass at the end of the test was within []^{a,b,c} percent of mass at the beginning of the test.

5.4.1.7 Conclusions

The test was performed with minimal problems, and is considered acceptable. Although not all facility initial conditions met the specified acceptance criteria, deviations did not impact the quality of the data. The instrumentation problems encountered were not critical to the performance of the facility mass and energy balances.

Facility response to the test was as anticipated for the conditions that were established. The data demonstrated that cooling of the reactor heater rods was maintained throughout the test.

TABLE 5.4.2-1
MATRIX TEST SB13 INITIAL CONDITIONS

Parameter	Instrument No.	Specified Initial Condition	Actual Initial Condition	Comments
Pressurizer pressure ⁽¹⁾	PT-604	370 ± 2 psig	<input type="checkbox"/> a,b,c	
HL-1 temperature ⁽¹⁾	SC-141	420 ± 2°F	<input type="checkbox"/>	
HL-2 temperature ⁽¹⁾	SC-140	420 ± 2°F	<input type="checkbox"/>	
SG-1 pressure ⁽¹⁾	PT-301	285 ± 5 psig	<input type="checkbox"/>	
SG-2 pressure ⁽¹⁾	PT-302	285 ± 5 psig	<input type="checkbox"/>	
Pressurizer level ⁽¹⁾	LDP-601	65 ± 3 in.	<input type="checkbox"/>	Level signal was temperature-compensated by TF-605
SG-1 narrow-range level ⁽¹⁾	LDP-303	26 ± 3 in.	<input type="checkbox"/>	Level signal was temperature-compensated by TF-301
SG-2 narrow-range level ⁽¹⁾	LDP-304	26 ± 3 in.	<input type="checkbox"/>	Level signal was temperature-compensated by TF-310
IRWST temperature ⁽²⁾	TF-709	< 80°F	<input type="checkbox"/>	
CMT-1 temperature ⁽²⁾	TF-529	< 80°F	<input type="checkbox"/>	
CMT-2 temperature ⁽²⁾	TF-532	< 80°F	<input type="checkbox"/>	
ACC-1 temperature ⁽²⁾	TF-403	< 80°F	<input type="checkbox"/>	
ACC-2 temperature ⁽²⁾	TF-404	< 80°F	<input type="checkbox"/>	
IRWST level ⁽²⁾	LDP-701	Level established by fill-line elevation	<input type="checkbox"/>	
ACC-1 level ^(2,3)	LDP-401	Level established by standpipe at 37 in.	<input type="checkbox"/>	Accepted; accumulator level was fixed by a standpipe
ACC-2 level ^(2,3)	LDP-402	Level established by standpipe at 37 in.	<input type="checkbox"/>	Accepted; accumulator level was fixed by a standpipe

TABLE 5.4.2-1 (Continued)
MATRIX TEST SB13 INITIAL CONDITIONS

Parameter	Instrument No.	Specified Initial Condition	Actual Initial Condition	Comments
ACC-1 pressure ⁽²⁾	PT-401	232 ± 2 psig	<input type="checkbox"/> ^{a,b,c}	Pressure was [] ^{a,b,c} low; condition acceptable
ACC-2 pressure ⁽²⁾	PT-402	232 ± 2 psig	<input type="checkbox"/>	Pressure was [] ^{a,b,c} low; condition acceptable
CMT-1 level ⁽²⁾	LDP-507	Full	<input type="checkbox"/>	
CMT-2 level ⁽²⁾	LDP-502	Full	<input type="checkbox"/>	

Note:

- (1) Data for the indicated parameter were recorded in the test procedure as an initial condition for the test. The value was determined by the test engineer from the appropriate control board indicator.
- (2) Data were not recorded in procedure, but the test engineer verified that specified conditions were achieved while establishing initial conditions. The value of the parameter was determined post-test by calculating the average DAS indication for a time of about 2 minutes before the break valve opened.
- (3) The bourdon pressure tube local indicator (PI-401 or PI-402) was tubed to the lower portion of the reference leg of the accumulator level transmitter (LDP-401 or LDP-402). As pressure in the accumulator was increased, air inside the bourdon tube was compressed, thereby lowering the reference leg liquid level, resulting in a false indication of measured level.

**TABLE 5.4.2-2
MATRIX TEST SB13 INOPERABLE INSTRUMENTS/INVALID DATA CHANNELS**

Instrument No.	Instrument Type	Description of Problem
FDP-604*	Differential pressure transmitter - flow	Over-ranged with initial flow
FDP-605*	Differential pressure transmitter - flow	Over-ranged with initial flow
FDP-606*	Differential pressure transmitter - flow	Over-ranged with initial flow
FMM-201 through 204*	Magnetic flow meter	Removed due to mechanical failure
FMM-501*	Magnetic flow meter	Data invalid after tank drained; could not measure steam flow
FMM-502	Magnetic flow meter	Data invalid after 126 seconds due to possible steam in balance line; meter cannot measure steam or two-phase flow
FMM-503	Magnetic flow meter	Data invalid after 100 seconds due to possible steam in balance line; meter cannot measure steam or two-phase flow
FMM-504*	Magnetic flow meter	Data invalid after tank drained; could not measure steam flow
FMM-701*	Magnetic flow meter	Data for negative flow invalid; negative flow exists after sump valves open, but meter not designed to measure negative flow
FMM-802*	Magnetic flow meter	Data invalid after steam forms in PRHR HX inlet line; uncertain when this occurs, but likely 50 seconds after break
FMM-804*	Magnetic flow meter	Data valid until PRHR HX initially drained at 600 seconds; after this time, possibility of steam in outlet line invalidated data
HFM-112	Heat flux meter	Failed
HFM-201	Heat flux meter	Failed
HFM-505	Heat flux meter	Erratic
HFM-703	Heat flux meter	Failed
HPS-203-1 through HPS-203-3	Heated phase switch	Failed
HPS-509-1 through HPS-509-3	Heated phase switch	Removed

TABLE 5.4.2-2 (Continued)
MATRIX TEST SB13 INOPERABLE INSTRUMENTS/INVALID DATA CHANNELS

Instrument No.	Instrument Type	Description of Problem
LDP-201 through LDP-206	Differential pressure transmitter - level	Data invalid due to effect of vertical portion of sense line attached to top of pipe; data can show level trends when pipe is empty or starts to drain, but absolute level indication cannot be used
LDP-215* LDP-216 LDP-217 LDP-218* LDP-219* LDP-220 LDP-221 LDP-222*	Differential pressure transmitter - level	Data invalid; when SG tube drained, reference leg started to vaporize (see Subsection 2.4)
LDP-207 LDP-208 LDP-209	Differential pressure transmitter - level	Inoperable; transmitters ranged improperly; data can show level trends, but absolute level indication cannot be used
LDP-401* LDP-402*	Differential pressure transmitter - level	Data invalid; see note 3 in Table 5.4.2-1 and Subsection 5.4.2.2
LDP-802* LDP-804	Differential pressure transmitter - level	Data valid until PRHR initially drained at 600 seconds; after this time, data suspect due to possible boiling of common reference line of LDP-802 and LDP-804
PT_101	Pressure transmitter	Data less than 6.1 psig invalid
PT_102	Pressure transmitter	Data less than 6.2 psig invalid
PT_103	Pressure transmitter	Data less than 6.2 psig invalid
PT_104	Pressure transmitter	Data less than 6.4 psig invalid
PT_108	Pressure transmitter	Data less than 8.4 psig invalid
PT_109	Pressure transmitter	Data less than 6.3 psig invalid
PT_111	Pressure transmitter	Data less than 6.0 psig invalid
PT_112	Pressure transmitter	Data less than 8.8 psig invalid
PT_113	Pressure transmitter	Data less than 6.4 psig invalid
PT_201*	Pressure transmitter	Data less than 1.1 psig invalid
PT_202	Pressure transmitter	Data less than 5.9 psig invalid
PT_205	Pressure transmitter	Data less than 6.1 psig invalid
TF-169	Thermocouple	Unavailable due to leaking O-ring in core barrel
TFM-112	Thermocouple for heat flux meter	Failed

TABLE 5.4.2-2 (Continued)
MATRIX TEST SB13 INOPERABLE INSTRUMENTS/INVALID DATA CHANNELS

Instrument No.	Instrument Type	Description of Problem
TFM-201	Thermocouple for heat flux meter	Failed
TFM-703	Thermocouple for heat flux meter	Failed
TR-318-1	Thermocouple	Failed
TW-210	Thermocouple	Erratic reading
TW-534	Thermocouple	Failed
TW-552	Thermocouple	Failed

Note:

* Instruments marked with an asterisk are critical instruments. See Subsection 5.4.2.2 for discussion.

Table 5.4.2-3 on pages 5.4.2-29 through 5.4.2-31 is not included in this nonproprietary document.

The Bar Charts for Table 5.4.2-3 on pages 5.4.2-32 through 5.4.2-36 are not included in this nonproprietary document.

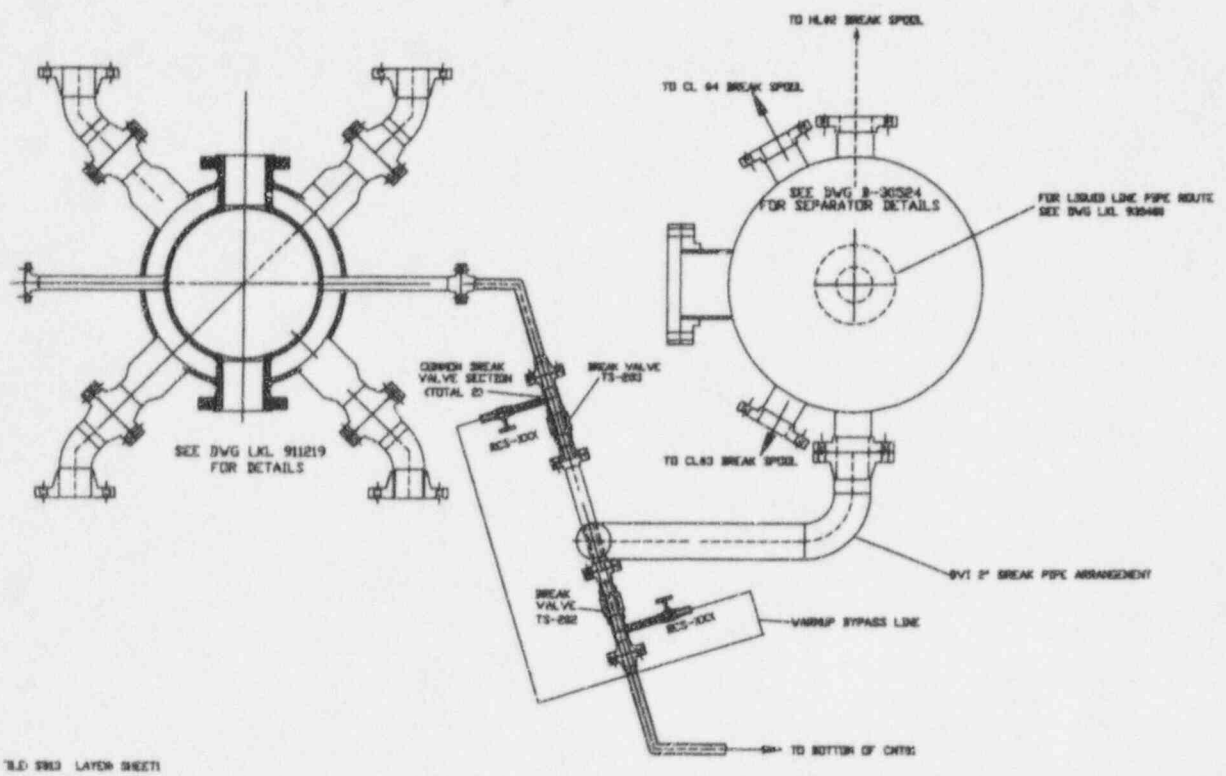


Figure 5.4.2-1 Primary Loop and Break Piping Layout

Figures 5.4.2-2 through 5.4.2-72 are not included in this nonproprietary document.

5.4.3 Effect of Additional Failures (Matrix Test SB28 Comparison with Matrix Test SB12)

This section of the report will compare the test results of Matrix Test SB28 to the reference test SB12 test results described in Subsection 5.4.1. Both tests simulated a DEG break of DVI-1. The configurations of the two tests were identical except for four items. In Matrix Test SB28, ACC-1, the PRHR HX, and ADS 4-1 and 4-2 separators were isolated, and the nozzle installation of the ADS was different than that used in Matrix Test SB12. The ADS nozzle installation is described in Subsection 5.4.3.1.

Matrix Test SB28 was successfully performed on July 21, 1994. The test duration was about 5 hours.

Included in this comparison is a description of the system configuration and initial conditions of Matrix Test SB28, followed by a table listing the inoperable instruments. Next, a sequence of events table provides a comparison of event times in Matrix Tests SB12 and SB28. The comparison is made in both tabular and bar-chart format. Following the sequence of events is a description of the overall system interactions observed during Matrix Test SB28. The test description is divided into three phases, just as was done in the description of Matrix Test SB12 results. The description emphasizes the differences between the test results of Matrix Tests SB12 and SB28. Finally, a discussion of component responses is provided. This section provides a more detailed discussion of the test by reviewing it from the component level. Again, the emphasis is on differences between the test results of Matrix Tests SB12 and SB28.

Data plots are provided as figures at the end of the section. The numbering and content of the data plots for Matrix Test SB28 in Subsection 5.4.3 are identical to the data plots provided in Matrix Test SB12. For example, the data plot of instrument channel FMM-905 for Matrix Test SB12 is contained in Figure 5.4.1-2. The Matrix Test SB28 test data for the same channel are contained in Figure 5.4.3-2. A data plot with the suffix x indicates extended time.

Not all of the figures in the data plot package at the end of this section are referenced. Only those figures required to explain a different response from that of Matrix Test SB12 are referred to in the text.

5.4.3.1 System Configuration and Initial Conditions

Matrix Test SB28 was performed using an approved written procedure.

The break configuration was identical to the break configuration of Matrix Test SB12, described in Subsection 5.4.1.1. Figure 5.4.3-1 provides a drawing of the configuration piping. Reactor-side break flow was piped to the break separator. All other connections to the break separator were isolated using blind inserts in the piping source. The CMT-1 side of the break was not aligned to a separator, but was aligned directly to the primary sump. Piping connected the primary sump to DVI-1 downstream of the CMT-1 and ACC-1 junction tee.

Before break initiation, the primary sump and the break separator were isolated from the break sources by two break valves (Figure 5.4.3-1). Break valve TS-203 isolated the reactor side of the break. Break valve TS-202 isolated the CMT side of the break.

Liquid break flow from the reactor side of the break was measured by FMM-905. Break steam flow from the reactor side of the break was measured by FVM-905, installed in the 6-in. steam line of the break separator. The 8-in. steam line from the break separator was isolated throughout the test.

Liquid break flow from CMT-1 was measured by FMM-501. Steam break flow from the CMT side of the break was measured after it passed through the primary sump. The 6-in. primary sump exhaust line contained FVM-906, which measured any steam injected into the primary sump from CMT-1.

Break instrumentation measured pressure upstream of the break and differential pressure across the break. The following summarizes this pressure instrumentation as well as flow indication and break valve numbers for each of the two sides of the break.

Reactor Side of the Break:

- TS-203 -- Break valve
- FMM-905 -- Liquid flow meter
- FVM-906 -- Steam flow meter
- DP-215 -- Differential pressure across break
- PT-203 -- Pressure upstream of break

CMT Side of the Break:

- TS-202 -- Break valve
- FMM-501 -- Liquid flow meter
- FVM-906 -- Steam flow meter
- DP-216 -- Differential pressure across break
- PT-206 -- Pressure upstream of break

The two sides of the break were connected by a warm-up line and two series isolation valves (RCS-901 and RCS-902; Figure 5.4.3-1). With the break valves closed, the isolation valves were opened for a period of time before break initiation to pressurize the CMT-1 injection line to simulate normal plant operation.

Seven temporary thermocouples were installed in the primary sump or lines connected to the primary sump. The purpose of the thermocouples was to obtain additional data on break steam and liquid temperatures. To accommodate these additional thermocouples, seven thermocouples located in the two short thermocouple rods in CMT-1 were disconnected from the DAS. The wiring that connected the CMT-1 thermocouples to the DAS was used to connect the seven temporary thermocouples to the

DAS. Table 5.4.3-4 provides the DAS channel assignment of the temporary thermocouples. All temporary thermocouples were given a 900-series channel number. The channel numbers of the seven disconnected CMT-1 thermocouples were not recorded in the Matrix Test SB28 data files; instead, the seven temporary channels were recorded.

Nozzles were installed in ADS 1-3 lines to simulate operation with two of two lines. This is different than Matrix Test SB12 where ADS-1 and ADS-3 nozzles simulated operation with one of two lines, and the ADS-2 nozzle simulated operation with two of two lines.

The CVS and RNS were not used in this test. The CVS and RNS pumps did not run.

Before the test was initiated by pressing the TEST pushbutton, a standard facility heatup and checkout was performed. The details of the heatup and checkout can be found in Subsection 2.7.

Table 5.4.3-1 contains the initial system conditions for Matrix Test SB28. The data recorded for control board indications of pressurizer pressure and level, SG pressures and levels, and hot-leg temperatures were obtained from the values recorded in the procedure. All other values for initial conditions were obtained from averaging the DAS data for about 2 minutes before test initiation. This was the time interval between the DAS starting to record data and the signal to open the break valve.

ACC-2 pressure was []^{a,b,c} low at test initiation. The proper tank pressures were verified by local calibrated gauge PI-402 as the tanks were pressurized with nitrogen. The loss of pressure between tank pressurization and test start was possibly due to cooling of nitrogen gas in the accumulators. Test analysis starting with the lower accumulator pressures is still possible.

CMT-1 and CMT-2 temperatures at the top of the tank were []^{a,b,c} respectively, above specification at test initiation. Test analysis with this small deviation for initial conditions is still possible.

The transient was initiated by simultaneously opening the two break valves and continued through CMT and accumulator injection, ADS actuation, IRWST injection, and primary sump injection. All actions were automatic and required no operator action. Total test time was about 5 hours.

5.4.3.2 Inoperable Instruments

Table 5.4.3-2 is a list of instruments considered inoperable or invalid for all or portions of this test. Some of the instruments listed are on the Critical Instrument List (Subsection 3.2, Table 3.2-2) and, therefore, are listed here.

FDP-604 and FDP-605 measured the differential pressure (psid) across the ADS 1-3 flow nozzles. The transmitters over-ranged momentarily when their respective ADS valves opened. Total flow through the ADS 1-3 valve complex can be determined by measuring ADS 1-3 separator liquid and steam flow from FMM-601 and FVM-601.

FMM-201, FMM-202, FMM-203, and FMM-204 measured flow (gpm) in each of the four cold legs. A decision was made to continue testing without the availability of these instruments. Replacement flow meters repeatedly failed; their continued use was precluded due to cracking of the ceramic liners from thermal stratification in the loop piping. The necessary boundary conditions for loop flow could be determined from DP-202, DP-203, DP-205, and DP-206.

FMM-501 and FMM-504 provided accurate data when sensing liquid, but became inaccurate when sensing two-phase or steam flow. FMM-504 over-ranged momentarily, however, flow from CMT-2 can be determined using CMT-2 level data from LDP-502.

SG tube level data (LDP-215, LDP-218, LDP-219, and LDP-222) was biased by vaporization of the water in the transmitter reference leg after the SG tubes started to drain; however, the data provide accurate indication of the time when the tubes were empty.

TF-103 and TF-104 measured CL-3 and CL-4 bottom-of-pipe fluid temperatures entering the reactor. Both thermocouples were removed to accommodate installation of thermal stratification measurement instrumentation. Both thermocouples were allowed to be inoperable as long as TF-101 and TF-102 were operable. TF-101 and TF-102 were operable during the performance of Matrix Test SB28.

The ADS 4-1 separator, the ADS 4-2 separator, and the PRHR HX were all isolated in this test. Any changes in their respective parameters (temperature, flow, or level) were not due to liquid or steam flow through these components. For example, the temperature changes in the PRHR HX tubes was due to the heating effect of the IRWST, not to flow through the HX.

5.4.3.3 Sequence of Events

Table 5.4.3-3 contains the sequence of events of Matrix Tests SB12 and SB28. The first pages of the table provide the event times of selected events in both tests and the differences in time between the events in the two tests. The ensuing pages of the table use a bar chart of the data to provide a visual representation of the sequence of events. Both the numeric table and the bar charts sort the events in chronologic order as they occurred in Matrix Test SB28.

The first pages of Tables 5.4.3-3 indicate the source of the actual time data. A D in the Data Source column indicates the recorded time was obtained from a software program that monitored digital events in the facility, including pump starts and stops, valve limit switch actuations, and alarms. An A in the Data Source column indicates the time data were obtained by reviewing test data obtained from the DAS. Although the test data from the DAS were in a digital format, the DAS monitored analog events such as pressure, flow, and temperature.

5.4.3.4 Test Results and Evaluation

This section contains an overall description of the events that occurred during Matrix Test SB28. The emphasis in the section is a comparison of Matrix Test SB28 results to reference test SB12 results.

The description is divided into three phases:

- Initial Depressurization Phase: simulated break initiation to ADS-1 actuation
- ADS Phase: ADS-1 actuation to start of IRWST injection
- IRWST Injection Phase: start of IRWST injection to end of test

Note: Some of the following discussion compares the differences in the facility response time between Matrix Tests SB12 and SB28. Unless otherwise stated, the reference for comparing the event timing between the two tests is the data contained Table 5.4.3-3.

Initial Depressurization Phase

Until ADS-1 actuated in Matrix Test SB28, there were two configuration differences between Matrix Tests SB28 and SB12 that had the potential to affect the facility response to the break: the isolation of ACC-1 and the PRHR HX in Matrix Test SB28.

In Matrix Test SB12, CMT-1 and ACC-1 shared a common break flow path to the primary sump, which provided an interaction between the flows from the two tanks. The isolation of ACC-1 in Matrix Test SB28 had no significant effect on the drain rate of CMT-1, because the tank reached its low level setpoint at the same time in both tests. This response is important because facility logic actuated ADS-1 []^{a,b,c} after either of the CMTs reached the low level setpoint. Thus, the actuation time of ADS-1 was []^{a,b,c} in both tests, because, in both tests, CMT-1 reached a low level setpoint at []^{a,b,c}

The isolation of the PRHR HX in Matrix Test SB28 eliminated the possibility of cooling by the HX. The effluent from the PRHR HX was piped to the SG-2 cold-leg channel head where CL-2 and CL-4 were attached. Before ADS-1 actuation, the effect of this cooling loss is not obvious from temperature data, because, in both tests, temperatures at the bottom and top of the cold-leg pipes maintained saturation conditions until ADS-1 actuation.

The isolation of the HX may have created a difference in the RCS depressurization rate during the initial depressurization phase. In all breaks, there is a period when the primary and secondary plant pressures arrive at a quasi-equilibrium condition. In Matrix Test SB28, RCS pressure decreased and SG pressure increased to within []^{a,b,c} of one another by []^{a,b,c} (Figure 5.4.3-66). From []^{a,b,c} until ADS-1 actuated at []^{a,b,c} RCS pressure stayed essentially constant, varying only []^{a,b,c}. By the time ADS-1 actuated, RCS and SG pressure had equalized at about []^{a,b,c}. A similar period of quasi-equilibrium between RCS and SG pressures occurred

in reference test SB12, but RCS pressure decreased []^{a,b,c} over the same 60-second period. When ADS-1 actuated, RCS pressure was about []^{a,b,c} less than SG pressure. The operation of the PRHR HX in Matrix Test SB12 may have created the faster RCS depressurization rate by removing heat from the RCS.

During the initial depressurization phase of the two tests, both liquid and steam break flows were essentially the same. Liquid break flow was measured by FMM-501 and FMM-905 (Figures 5.4.3-2 and 5.4.3-4), and the steam break flow was measured by FVM-905 and FVM-906 (Figure 5.4.3-3).

The comparison of the sequence of events between tests (Table 5.4.3-3) provides evidence that the system timing response was essentially the same for each test before ADS-1 actuation. Small variations in the recorded event timing between the two tests can largely be attributed to analog test data interpretation.

The end of the depressurization period occurred at []^{a,b,c} in Matrix Test SB28. By this time, the pressurizer, pressurizer surge line, SG tubes, SG channel heads, and cold legs were drained. The collapsed level in the downcomer was about []^{a,b,c} below the elevation of the DVI nozzles (Figure 5.4.3-14). The same system conditions were found in Matrix Test SB12 when ADS-1 actuated at []^{a,b,c}

In summary, the system configuration differences between Matrix Tests SB12 and SB28 had little or no impact on the observed facility response during the initial depressurization period, except for the isolation of the PRHR HX. The isolation of the PRHR HX in Matrix Test SB28 may have decreased the RCS depressurization rate when compared with reference test SB12.

ADS Phase

The end of the ADS phase is defined as the time when IRWST injection commences. This definition is somewhat blurred in Matrix Test SB28, because IRWST-1 injection started at []^{a,b,c} and IRWST-2 injection started at []^{a,b,c}. For clarity of presentation of the Matrix Test SB28 test results, the ADS phase will be considered to end when IRWST-2 injection flow started. This organization of the test results is reasonable, because IRWST-1 injection did not flow to the reactor, but to the primary sump via the "broken" DVI-1 line. This section includes references to the effect of the delay of IRWST-2 injection with respect to reference test SB12, but the general discussion of events following the onset of IRWST-2 injection will be covered in the next section.

In the ADS phase, three of the four system configuration differences between Matrix Tests SB28 and SB12 impacted the facility response to the break. The isolation of ACC-1 did not appear to have an impact, but PRHR HX isolation, ADS 4-1 and 4-2 isolation, and changes in ADS-1 and ADS-3 nozzle sizes did make a measurable difference in the test results.

ACC-1 and CMT-1 were connected directly to the primary sump via a common discharge line. The only potential influence the isolation of ACC-1 had in Matrix Test SB28 was to affect the drain rate of CMT-1. As already mentioned, CMT-1 reached its low level setpoint in both tests at the same time. In addition, the CMT reached its low level setpoint and emptied at the same time (Table 5.4.3-3). Thus, the isolation of ACC-1 had no measurable effect on the facility response during the ADS phase.

The effect of PRHR HX isolation can be observed by the review of cold-leg temperature data. When the PRHR HX was not isolated during testing, its effluent was directed to the SG-2 cold-leg channel head. CL-2 and CL-4 were connected to the SG-2 cold-leg channel head. If any subcooled liquid flowed from the outlet of the PRHR HX, it was directed to the reactor downcomer via the SG-2 cold-leg channel head and the two cold legs. In Matrix Test SB12, TF-108 and TF-104 measured temperatures in CL-2 and CL-4, respectively. As discussed in section 5.4.1.5, these thermocouples measured saturated or subcooled temperatures when the pipe was empty. During the same period, TF-107 and TF-103 measured superheated temperatures at the bottom of CL-1 and CL-3, respectively. These effects are attributed to cold water from the PRHR HX flowing from SG-2 to the reactor along the bottom of CL-2 and CL-4 pipes. In Matrix Test SB28, TF-104 was unavailable for data collection due to a modification in the facility; however, TF-108 measured a superheated condition at the bottom of the CL-2 when the pipe was empty (Figure 5.4.3-40). The absence of a saturated or subcooled fluid temperature at the bottom of CL-2 is a direct result of the isolation of the PRHR HX in Matrix Test SB28.

In Matrix Test SB28, the ADS-1 and ADS-3 nozzles simulated operation with two of two lines instead of the simulation of operation with one of two lines as in reference test SB12. The ADS-2 nozzle simulated operation with two of two lines in both tests. As a result of using the less restrictive nozzles in the ADS-1 line, measured liquid and steam flow rates through the ADS 1-3 separator were greater in Matrix Test SB28 than in Matrix Test SB12 (Figure 5.4.3-18). When ADS-2 actuated in Matrix Test SB28, the loop seal of ADS 1-3 separator was blown out. As a result, ADS 1-3 separator liquid flow data are not valid from about []^{a,b,c} because the magnetic meter monitoring the flow did not accurately measure steam flow. The data for ADS 1-3 separator steam flow are also affected by the loss of the loop seal on the separator. Some of the steam flow that would normally have been measured by FVM-601 bypassed the meter by flowing through the loop seal. Thus, the indicated steam flow rate from []^{a,b,c} is less than the actual steam flow rate.

When ADS-1 actuated in Matrix Test SB28, RCS pressure was about []^{a,b,c} higher than it was when ADS-1 actuated in the reference test (Figure 5.4.3-19). In the discussion of the depressurization phase, it was suggested that this pressure difference was due to the cooling effect of the PRHR HX in the reference test. Between ADS-1 and ADS-3 actuation, the RCS depressurization rate was higher in Matrix Test SB28 than in Matrix Test SB12. As a result, RCS pressure was the same in both tests when ADS-3 actuated. Since the PRHR HX was isolated in Matrix Test SB28, it did not contribute to the higher RCS depressurization rate. The larger ADS flows may have increased RCS depressurization rate in Matrix Test SB28 sufficiently to overcome the lack of depressurization from the isolated PRHR HX.

The response of ACC-2 on the "unbroken" side of the facility was essentially the same in both tests, except for slight timing shifts for the start of ACC-2 injection (a difference of []^{a,b,c}) and ACC-2 drain time (a difference of []^{a,b,c}) (Table 5.4.3-3).

Similar results were obtained for CMT-2 on the "unbroken" side of the facility, until ACC-2 drained at about []^{a,b,c}. Until this time, the CMT-2 flow rate was nearly identical in the two tests (Figure 5.4.3-8). In Matrix Test SB28, the CMT-2 flow rate increased to []^{a,b,c} immediately after ACC-2 drained, about twice the flow rate experienced in the reference test. Data from Matrix Test SB28 reveal the relatively higher flow rate was maintained until CMT-2 drained at []^{a,b,c}. CMT-2 did not drain in Matrix Test SB12 until []^{a,b,c} due to the lower injection flow rate after ACC-2 drained (Figure 5.4.3-5).

The absolute time when CMT-2 emptied is not as important as the relationship between the cessation of CMT-2 injection and the start of IRWST-2 injection. Since DVI-1 was "broken," DVI-2 injection was the only source of core cooling. DVI-1 injection consisted of injection flows from ACC-2, CMT-2, and IRWST-2. ACC-2 drained first, leaving CMT-2 and IRWST-2 to cool the core. In the reference test, the injection flow from IRWST-2 started []^{a,b,c} before CMT-2 completed draining. In Matrix Test SB28, IRWST-2 injection did not start until []^{a,b,c} after CMT-2 emptied. No cooling was available to the core between the time CMT-2 completed draining at []^{a,b,c} and IRWST-2 injection flow started at []^{a,b,c}.

The delay of IRWST-2 injection in Matrix Test SB28 was caused by ADS-4 isolation. With a loss of ADS-4, final depressurization of the RCS to ambient conditions was not assisted by an inventory loss through ADS-4 as it was in the reference test. After ADS-4 actuated at []^{a,b,c} in Matrix Test SB12, the RCS pressure decrease allowed IRWST-2 injection to start about []^{a,b,c} later. In contrast, RCS depressurization in Matrix Test SB28 was caused by relatively small inventory losses through the break and ADS 1-3. RCS pressure did not decrease sufficiently in Matrix Test SB28 to allow IRWST-2 injection flow until []^{a,b,c}.

The delay of IRWST-2 injection caused by ADS-4 isolation impacted core levels and temperatures in Matrix Test SB28. The downcomer level started to decrease after CMT-2 emptied at []^{a,b,c} and continued to decrease to a minimum level of about []^{a,b,c} (Figure 5.4.3-14). The onset of IRWST-2 injection at []^{a,b,c} started to increase the downcomer level from this minimum. The downcomer level would only increase or remain constant for the remainder of the test. The reactor wide-range level channel recorded a minimum collapsed level of 32 in. at the same time as the downcomer level channel reached its minimum level of 31 in. (Figure 5.4.3-23).

The delay of IRWST-2 injection resulted in an increase in downcomer temperatures. In Matrix Test SB28, downcomer temperatures were saturated by []^{a,b,c} in contrast to the subcooled conditions found in the downcomer in Matrix Test SB12 after: []^{a,b,c} (Figures 5.4.3-50 through 5.4.3-53). Similarly, core temperatures remained hotter in Matrix Test SB28 (Figure 5.4.3-54). Centerline core temperatures remained at or near saturation for the test duration, whereas, in the

reference test, centerline temperatures started to subcool at the bottom of the core by []^{a,b,c}. By the end of Matrix Test SB12, over 75 percent of the core centerline temperatures indicated a subcooled condition.

As previously mentioned, liquid and steam break flow in Matrix Tests SB28 and SB12 were essentially the same during the initial depressurization phase, or until ADS-1 actuation. This remained true after ADS-1 actuation until about []^{a,b,c} with one exception. After ADS-2 actuation, liquid break flow did not increase in Matrix Test SB28 as it had in Matrix Test SB12. From ADS-2 actuation at []^{a,b,c} until []^{a,b,c} after ADS-3 actuation at []^{a,b,c} test results show a divergence in liquid break flow data between the two tests (Figure 5.4.3-2). This may be due to the downcomer level obtained in the two tests. In Matrix Test SB12, the downcomer level increased above the bottom of the DVI line, or about []^{a,b,c} which increased the liquid flow rate from the break. The downcomer level in Matrix Test SB28 never increased above the bottom of the DVI line during the ADS phase (Figure 5.4.3-14).

IRWST Injection Phase

As previously stated, the effect of ADS-4 isolation was observed by the lack of DVI cooling flow to the core between []^{a,b,c}. The lack of cooling flow during the ADS phase resulted in pronounced temperature increases in the heater rods for about []^{a,b,c} starting about the time of IRWST-2 injection flow (Figure 5.4.3-55). The maximum temperature was recorded by heater thermocouple TH-101-4 at the top and center of the core. The maximum recorded heater temperature was []^{a,b,c}.

IRWST-1 and IRWST-2 injection flows were not balanced in Matrix Test SB28 as they were in the reference test due to different backpressures at the point of injection (Figure 5.4.3-25). IRWST-1 flowed to the primary sump at atmospheric pressure; IRWST-2 flowed to the RCS at a slightly elevated pressure due to the isolation of ADS-4.

The total IRWST injection flow rate was smaller in Matrix Test SB28 than in the reference test. This difference resulted in a slower drain rate of the IRWST and a slower fill rate of the primary sump in Matrix Test SB28 (Figure 5.4.3-27). The slower fill rate of the primary sump, in turn, delayed overflow to the secondary sump by over []^{a,b,c}.

Only IRWST-2 injection was delivered to the core. IRWST-1 injection flow was directed to the primary sump via the "broken" DVI-1 line. IRWST-2 injection flow started at []^{a,b,c} decreased in rate as the IRWST drained, and stopped at about []^{a,b,c} when the static head of the water level in the IRWST was insufficient to overcome the RCS backpressure. When IRWST-2 injection flow stopped, the downcomer and reactor levels started to decrease (Figures 5.4.3-25 and 5.4.3-26).

IRWST-2 injection did not flow to the reactor for the remainder of the test; however, when the primary sump injection valves opened at []^{a,b,c} data show a sharp increase in IRWST-1 and IRWST-2 injection flow as the IRWST started to drain to the primary sump (Figure 5.4.3-25). At the same time, the primary sump injection flow meters reported negative flow. The primary sump magnetic flow meters were not designed to measure negative flow, so negative-value data are invalid. The data did accurately reflect the correct direction of flow from the IRWST to the primary sump as the sump filled. The indicated flow rate for IRWST-1 was larger than IRWST-2 while filling the primary sump. The larger flow rate was a result of the smaller piping resistance of the larger-diameter IRWST-1 piping from the IRWST to the primary sump injection tee.

When the IRWST and primary sump equalized levels at about []^{a,b,c} there was still no injection flow to the reactor. Pressure in the reactor remained higher than the static pressure of the water in the primary sump and the IRWST. Thus, the level in the downcomer and the core decreased from about []^{a,b,c} when IRWST-2 injection stopped at []^{a,b,c} to a minimum level of about []^{a,b,c} (Figure 5.4.3-26). The low core level and lack of cooling to the core heater rods resulted in heating of the rods. The temperature of the heaters in the top middle of the core increased to over []^{a,b,c}. At []^{a,b,c} HTR-C1-102 shorted to ground causing SCR-1 load-side phase A and phase C 600-amp fuses to blow. No damage was done to the silicon-controlled rectifier (SCR) or its controller. Subsequent investigation revealed that HTR-A1-310 also had a low resistance reading to ground.

Shortly after SCR-1 tripped, the operator tripped the other heaters from the control panel. The facility immediately depressurized due to lack of energy addition in the core.

Test data after []^{a,b,c} are invalid because system conditions after heater failure are represented.

5.4.3.5 Comparison of Component Responses

CMT-1 Response

CMT-1 alignment in Matrix Test SB28 was identical to reference test SB12. CMT outlet piping was directed to the primary sump instead of the normal connection to the reactor. The two tests were different with respect to ACC-1. In the reference test, ACC-1 injection shared a common flow path to the primary sump with flow from CMT-1. In Matrix Test SB28, ACC-1 was isolated.

The CMT-1 drain rate was the same in both tests, indicating there was little effect on CMT-1 flow from ACC-1 flow in Matrix Test SB12. The time data of Table 5.4.3-3 show that the CMT-1 low level, low-low level, and tank empty occurred at essentially the same time for Matrix Test SB28 as for Matrix Test SB12. The transition from recirculation to draindown flow did occur slightly earlier in the reference test, but the difference was only []^{a,b,c}

The range of FMM-501 was increased from []^{a,b,c} in the reference test to allow better flow data. After the tank drained at 141 seconds the data from FMM-501 are invalid because the magnetic flow meter does not accurately measure steam flow. A sharp increase in indicated CMT-1 injection flow at about []^{a,b,c} was probably the meter's response to steam flow (Figure 5.4.3-4).

Data from FMM-503 and LDP-509 are invalid after flow transition at []^{a,b,c}. The magnetic flow meter data are invalid because the balance line was in a steam environment after transition from recirculation to draindown flow. The level transmitter data are invalid because a pressure drop created by flow in the balance line altered the results. Although the effect was small when CMT-1 contained water, it became large when the CMT emptied and steam flowed directly to the primary sump.

CMT-1 did not reflood during either test.

CMT-2

In Matrix Test SB28, CMT-2 was aligned to the reactor via its normal injection flow path, just as it was in the reference test. CMT-2 response was the same until ACC-2 emptied and stopped injection at about []^{a,b,c} when CMT-2 transitioned from recirculation to draindown flow and reached its low level setpoint. After ACC-2 completed its injection, however, the injection flow rate obtained by CMT-2 was different in the two tests. In Matrix Test SB28, flow increased to about []^{a,b,c} but it was only []^{a,b,c} in the reference test (Figure 5.4.3-8). As a result of the higher flow rate, CMT-2 emptied []^{a,b,c} sooner in Matrix Test SB28 than it did in Matrix Test SB12.

FMM-504 was over-ranged during the same periods in Matrix Tests SB28 and SB12 (Figure 5.4.3-8). FMM-504 first over-ranged at []^{a,b,c} when the CMT transitioned from recirculation to draindown flow. After flow decreased to within the meter's range at []^{a,b,c} it over-ranged again at []^{a,b,c} when ADS-2 actuated. This over-range condition lasted about []^{a,b,c}.

Data for CMT-2 balance line flow are invalid after the CMT transitioned from recirculation to draindown flow at []^{a,b,c} because of the possibility of steam in the balance line creating erroneous flow indication.

CMT-2 did not reflood during Matrix Tests SB28 or SB12.

Pressurizer

The isolation of ADS-4 in Matrix Test SB28 created a pressurizer level response that was not observed in the reference test. Unlike in the reference test, the pressurizer never drained after partially refilling during ADS-1 actuation. This level was maintained for the duration of the test, even when the surge line indicated it was empty.

Note: Figures 5.4.3-31 and 5.4.3-31x are plots of the steam percent of the pressurizer and pressurizer surge lines. A value of []^{a,b,c} percent steam indicates that the pressurizer or pressurizer surge line contains no liquid, or is empty, and a value of []^{a,b,c} percent steam indicates that the pressurizer or pressurizer surge line is full of liquid.

The pressurizer drained during the initial depressurization phase and then started to fill with liquid again when ADS-1 actuated (Figure 5.4.3-31). At []^{a,b,c} the pressurizer had reached its minimum steam percent (maximum liquid level) of about []^{a,b,c} percent steam. Until []^{a,b,c} the pressurizer level response was the same as its response in the reference test, but thereafter there were no similarities.

In the reference test, the pressurizer started to drain at []^{a,b,c} and completed draining by []^{a,b,c}. In Matrix Test SB28, the pressurizer never completely drained. In fact, when the heater rod failed at []^{a,b,c} the pressurizer steam percent was about []^{a,b,c} percent, indicating the liquid level was about []^{a,b,c} percent (Figure 5.4.3-31x). When the test was stopped by turning off the remaining heater bank at about []^{a,b,c} the pressurizer finished draining within []^{a,b,c}.

The difference in pressurizer level response may be due to the isolation of ADS-4 in Matrix Test SB28. When ADS-4 actuated at []^{a,b,c} in the reference test, RCS pressure was about []^{a,b,c}. The inventory loss through ADS-4 accelerated the depressurization of the RCS. RCS pressure decreased to about []^{a,b,c} by the time the pressurizer finished draining at []^{a,b,c}. In Matrix Test SB28 RCS pressure was []^{a,b,c} essentially the same as it was in Matrix Test SB12 (Figure 5.4.3-19). However, since ADS-4 did not actuate, the rate of RCS depressurization was relatively small. RCS pressure drifted slowly downward from []^{a,b,c} until it reached a pressure of about []^{a,b,c} when the heaters failed at []^{a,b,c}. The level in the pressurizer drifted downward at the same rate, indicating that RCS pressure may have maintained the level in the pressurizer, even with the pressurizer surge line empty (Figure 5.4.3-31).

This data suggest that the early drain of the pressurizer after ADS-1 through ADS-3 actuation may be dependent on ADS-4 operation decreasing RCS pressure sufficiently to allow the drain.

Passive Residual Heat Removal Heat Exchanger

The PRHR HX was isolated in Matrix Test SB28. The increase in PRHR HX temperatures was due to heating of the static fluid in the PRHR HX by the IRWST fluid (Figures 5.4.3-37 and 5.4.3-38). IRWST temperatures increased due to ADS 1-3 actuation. As the IRWST drained, its vapor space may have also been heated by the steam environment of the BAMS header.

Cold Legs

The cold legs drained before ADS-1 actuation, just as they did in the reference test; however, unlike the reference test, they never refilled. The level in the downcomer never obtained a level greater than []^{a,b,c} in Matrix Test SB28 (Figure 5.4.3-26). The bottom of the cold legs was at a downcomer level of about []^{a,b,c}

In both tests, superheated temperatures were observed in the cold legs while they drained (Figures 5.4.3-39 and 5.4.3-40). Since the PRHR HX was isolated in Matrix Test SB28, it did not provide subcooled liquid to the bottom of CL-2 and CL-4 as it did in the reference test. Thus, no subcooled temperatures were observed at the bottom of these pipes as they were in Matrix Test SB12.

Note: Before this test was performed, TF-103 and TF-104 were removed from CL-3 and CL-4, respectively. It was necessary to remove them so a thermocouple rake could be inserted in their location for a stratification study. The test data for TF-103 and TF-104 are invalid.

In-Containment Refueling Water Storage Tank

The total IRWST injection flow rate was smaller in Matrix Test SB28 than in the reference test. As a result, the IRWST drained more slowly in Matrix Test SB28. A measure of this slower drain rate was the opening time of the primary sump injection valves. The valves opened when the IRWST level reached a low-low level setpoint of []^{a,b,c}. In Matrix Test SB28, the primary sump injection valves opened at []^{a,b,c} almost []^{a,b,c} later than Matrix Test SB12.

The IRWST thermocouple temperatures did not reach saturation temperature before they were uncovered (Figure 5.4.3-46). These results were similar to Matrix Test SB12 results in that the thermocouples in the IRWST never reached saturation before they were uncovered. In both tests, the thermocouples heated to saturation temperature as they uncovered.

Reactor

The reactor response was very different between Matrix Tests SB12 and SB28 due to the simulated failure of all lines of ADS-4, thereby affecting injection flow from the IRWST. The best indication of this difference is provided by the plots of the steam percent in the upper and lower portions of the core (Figures 5.4.3-58 and 5.4.3-59).

For the first []^{a,b,c} the core steam percent in Matrix Test SB28 was very similar to the core steam percent in Matrix Test SB12; however, timing of CMT-2 injection flow and IRWST-2 injection flow in the two tests initiated a very different response in the core. In Matrix Test SB12, IRWST-2 injection flow started before CMT-2 was empty, so both tanks simultaneously provided cooling flow between []^{a,b,c} when IRWST-2 injection started, and []^{a,b,c} when CMT-2 emptied. In contrast, IRWST-2 injection flow was delayed in Matrix Test SB28 due to the isolation of

all of ADS-4. Without ADS-4 actuation to decrease RCS pressure, IRWST-2 injection flow was delayed until []^{a,b,c}. Since CMT-2 emptied at []^{a,b,c} this meant there was no core cooling between []^{a,b,c}.

As a result of CMT/IRWST injection timing, the core steam percent increased after []^{a,b,c} in Matrix Test SB28. In Matrix Test SB12, the core steam percent continually decreased from its early maximum until the end of the test when about []^{a,b,c} percent of the core was subcooled. In Matrix Test 28, the entire core was at saturation temperature after []^{a,b,c} (Figure 5.4.3-54), and never subcooled for the remainder of the test. From about []^{a,b,c} the upper core steam percent ranged between []^{a,b,c} and []^{a,b,c} percent, while the lower core contained no steam.

Another increase in the core steam percent during Matrix Test SB28 occurred when the IRWST level reached its low level setpoint at []^{a,b,c}. The IRWST low level initiated the opening of the primary sump valves, which created a drain flow path from the IRWST to the primary sump. The loss of cooling flow resulted in the upper core steam percent reaching about []^{a,b,c} percent before a heater rod failed.

Steam Generator

The SG level and temperature responses in Matrix Tests SB12 and SB28 were essentially the same.

Both SGs were empty before ADS-1 actuated, just as in Matrix Test SB12 (Figures 5.4.3-62 and 5.4.3-63). The SGs were drained when the minimum indicated level of []^{a,b,c} was obtained. Like Matrix Test SB12, the tube level indication erroneously indicated that the SGs refilled; once the SGs drained, both stayed empty. The errors in level indication were a result of the SG level transmitters common reference leg in each generator boiling and decreasing in level as the SGs drained.

The slower rate of RCS depressurization in Matrix Test SB28 provided a longer period of quasi-equilibrium between the RCS and the secondary side of the SGs. At the initiation of the break, SG steam flow and feedwater flow were isolated. The only cooling available to the SGs was through ambient heat loss. As a result, SG steam pressure started to increase as heat was transferred from the primary side, across the tubes, and into the secondary side (Figure 5.4.3-7). At the same time, reactor pressure was decreasing due to inventory loss through the break. Steam pressure and reactor pressure converged quickly. From about []^{a,b,c} until ADS-1 actuation, the difference between primary and secondary pressures was less than []^{a,b,c} (Figure 5.4.3-66). Immediately before ADS-1 actuation, the pressures equalized.

As reported in Subsection 5.4.1, the same quasi-equilibrium period in Matrix Test SB12 lasted only about []^{a,b,c}. In addition, the SG secondary side became a heat source to the RCS before ADS-1 actuation. In Matrix Test SB28, the SG secondary side did not become a heat source to the

RCS until after ADS-1 actuation. The operation of the PRHR HX in Matrix Test SB12 may have created the faster depressurization rate by removing heat from the RCS.

5.4.1.6 Mass Balance

The mass balance results for Matrix Test SB28 were calculated based on water inventory before and after the test, and are provided in Appendix E. Mass at the end of the test was within 6.8 percent of the mass at the beginning of the test.

5.4.1.7 Conclusions

At []^{a,b,c} the low level in the core caused reactor heater rod HTR-C1-102 to short to ground, thereby tripping SCR-1. Until this time, the test was performed with minimal problems. Data obtained during this test are considered valid until the time that the heater rod failed. Although not all of the facility initial conditions met the specified acceptance criteria, the deviations did not impact the quality of the data.

TABLE 5.4.4-1
MATRIX TEST SB28 INITIAL CONDITIONS

Parameter	Instrument No.	Specified Initial Condition	Actual Initial Condition	Comments
Pressurizer pressure ⁽¹⁾	PT-604	370 ± 2 psig	[] ^{a,b,c}	
HL-1 temperature ⁽¹⁾	SC-141	420 ± 2°F		
HL-2 temperature ⁽¹⁾	SC-140	420 ± 2°F		
SG-1 pressure ⁽¹⁾	PT-301	285 ± 5 psig		
SG-2 pressure ⁽¹⁾	PT-302	285 ± 5 psig		
Pressurizer level ⁽¹⁾	LDP-601	65 ± 5 in.		Level signal was temperature-compensated by TF-605
SG-1 narrow-range level ⁽¹⁾	LDP-303	26 ± 3 in.		Level signal was temperature-compensated by TF-301
SG-2 narrow-range level ⁽¹⁾	LDP-304	26 ± 3 in.		Level signal was temperature-compensated by TF-310
IRWST temperature ⁽²⁾	TF-709	< 80°F		
CMT-1 temperature ⁽²⁾	TF-529	< 80°F		Temperature was 2.5°F high; condition acceptable
CMT-2 temperature ⁽²⁾	TF-532	< 80°F		Temperature was 3.8°F high; condition acceptable
ACC-1 temperature ⁽²⁾	TF-403	Isolated for test; no acceptance criteria	[]	

TABLE 5.4.4-1 (Continued)
MATRIX TEST SB28 INITIAL CONDITIONS

Parameter	Instrument No.	Specified Initial Condition	Actual Initial Condition	Comments
ACC-2 temperature ⁽²⁾	TF-404	< 80°F	[] ^{a,b,c}	
IRWST level ⁽²⁾	LDP-701	Level established by fill-line elevation		
ACC-1 level ⁽²⁾	LDP-401	Isolated for test; no acceptance criteria		
ACC-2 level ⁽²⁾	LDP-402	Level established by standpipe at 37 in.		
ACC-1 pressure ⁽²⁾	PT-401	Isolated for test; no acceptance criteria		
ACC-2 pressure ⁽²⁾	PT-402	232 ± 2 psig		Pressure was [] ^{a,b,c} low; condition acceptable
CMT-1 level ⁽²⁾	LDP-507	Full		
CMT-2 level ⁽²⁾	LDP-502	Full		

Note:

- (1) Data for the indicated parameter were recorded in the test procedure as an initial condition for the test. The value was determined by the test engineer from the appropriate control board indicator.
- (2) Data were not recorded in procedure, but the test engineer verified that specified conditions were achieved while establishing initial conditions. The value of the parameter was determined post-test by calculating the average DAS indication for a time of about 2 minutes before the break valve opened.

TABLE 5.4.3-2
MATRIX TEST SB28 INOPERABLE INSTRUMENTS/INVALID DATA CHANNELS

Instrument No.	Instrument Type	Description of Problem
FDP-604*	Differential pressure transmitter - flow	Over-ranged with initial flow
FDP-605*	Differential pressure transmitter - flow	Over-ranged with initial flow
FMM-201 through FMM-204*	Magnetic flow meter	Removed due to mechanical failure
FMM-501*	Magnetic flow meter	Data invalid after tank drained; meter can not measure steam flow
FMM-502	Magnetic flow meter	Data invalid after 66 seconds due to possible steam in balance line; meter can not measure steam or two-phase flow
FMM-503	Magnetic flow meter	Data invalid after 77 seconds due to possible steam in balance line; meter can not measure steam or two-phase flow
FMM-504*	Magnetic flow meter	Over-ranged between about 70 and 115 seconds, and 140 and 165 seconds; data invalid after tank drained because meter can not measure steam flow
FMM-601	Magnetic flow meter	Data invalid between 145 and 280 seconds because loop seal of ADS 1-3 separator was blown out during this time
HFM-103	Heat flux meter	Failed
HFM-105	Heat flux meter	Failed
HFM-112	Heat flux meter	Failed
HFM-505	Heat flux meter	Failed
HFM-703	Heat flux meter	Failed
HPS-509-1 through HPS-509-3	Heated phase switch	Removed
LDP-201 through LDP-206	Differential pressure transmitter - level	Data invalid due to effect of vertical portion of sense line attached to top of pipe; data can show level trends when pipe is empty or starts to drain, but absolute level indication can not be used

TABLE 5.4.3-2 (Continued)
MATRIX TEST SB28 INOPERABLE INSTRUMENTS/INVALID DATA CHANNELS

Instrument No.	Instrument Type	Description of Problem
LDP-215* LDP-216 LDP-217 LDP-218* LDP-219* LDP-220 LDP-221 LDP-222*	Differential pressure transmitter - level	Data invalid; when SG tube drains, reference leg starts to vaporize (see Subsection 2.4)
SC-TH-102-4	Thermocouple	Failed at end of test when HTR-C1-102 failed
TF-103*	Thermocouple	Thermocouple was removed and replaced with thermocouple rod for thermal stratification measurements
TF-104*	Thermocouple	Thermocouple was removed and replaced with thermocouple rod for thermal stratification measurements
TF-169	Thermocouple	Unavailable due to leaking O-ring in core barrel
TF-702	Thermocouple	Failed
TFM-103	Thermocouple for heat flux meter	Failed
TFM-105	Thermocouple for heat flux meter	Failed
TFM-703	Thermocouple for heat flux meter	Failed
TH-102-1 through TH-102-3	Thermocouple	Failed at end of test when HTR-C1-102 failed
TH-317-1 through TH-317-4	Thermocouple	Removed with heater rod C2-317
TW-503	Thermocouple	Errated

Note:

*Instruments marked with an asterisk are critical instruments. See Subsection 5.4.3.2 for discussion.

Table 5.4.3-3 on pages 5.4.3-20 through 5.4.3-22 is not included in this nonproprietary document.

The Bar Charts for Table 5.4.3-3 on pages 5.4.3-23 through 5.4.3-27 are not included in this nonproprietary document.

Table 5.4.1-4 is not included in this nonproprietary document.



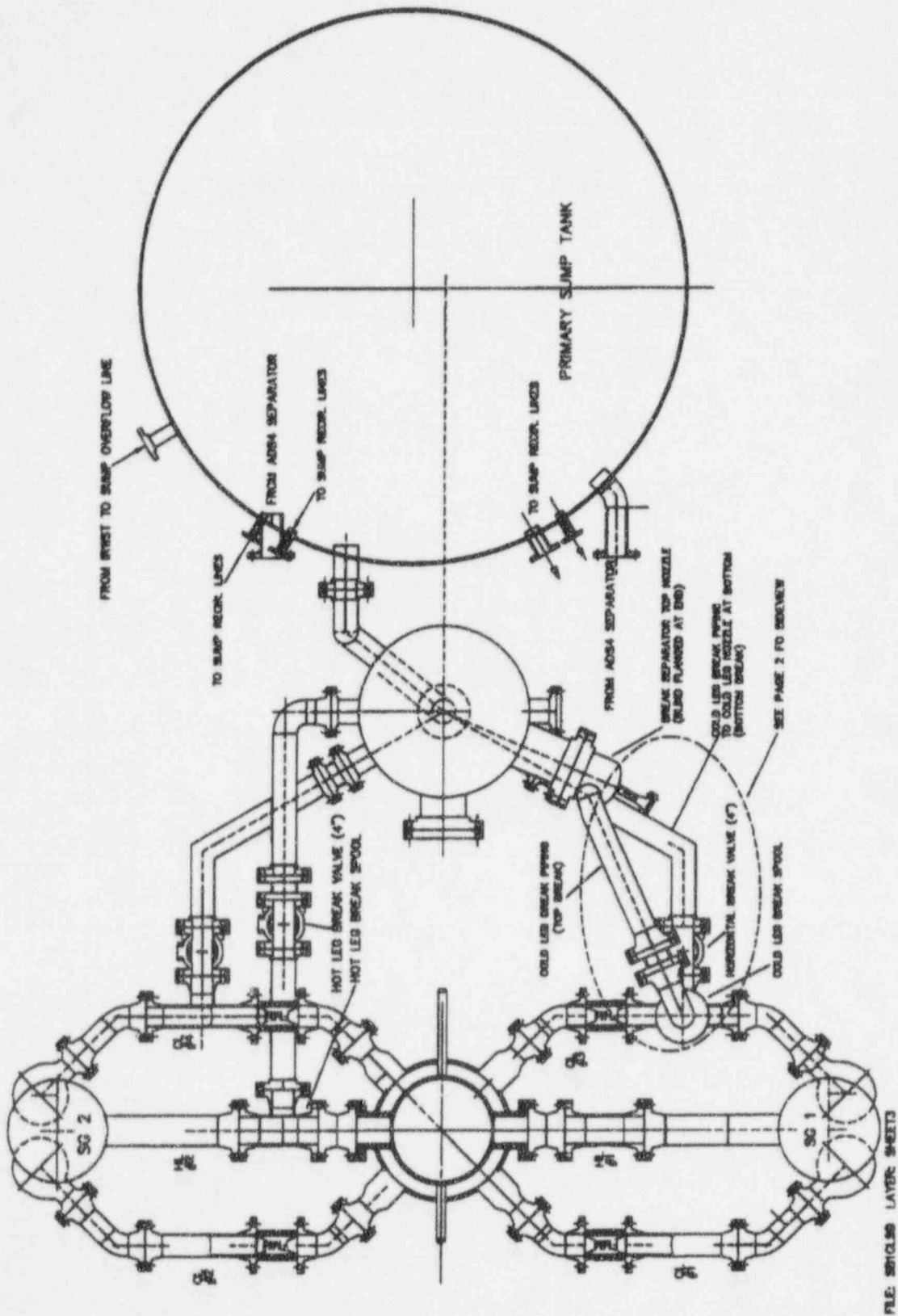


Figure 5.4.3-1 Primary Loop and Break Pipe Arrangement

Figures 5.4.3-2 through 5.4.3-71 are not included in this nonproprietary document.

5.5 Automatic Depressurization System Impact

Matrix Tests SB14 and SB26 characterized the thermal-hydraulic phenomena and system response to inadvertent actuation of the automatic depressurization system (ADS) without a break at any other lines. Both tests were performed using the same simulated break location. Matrix Test SB14 simulated inadvertent actuation of the ADS-1 valve with an assumed failure of one of the two ADS-4 lines. Matrix Test SB26 also simulated inadvertent actuation of the ADS-1 valve with multiple failures of the ADS-4 system and no passive residual heat removal heat exchanger (PRHR HX) available. The tests covered the transient from initial break through long-term cooling, about [

] ^{a,b,c} Based on single failure testing, Matrix Test SB14 was identified as the reference test for this simulated break location. Results of Matrix Tests SB14 and SB26 appear in Subsections 5.5.1 and 5.5.2, respectively.

5.5.1 Inadvertent ADS Actuation (Matrix Test SB14)

This section provides the thermal-hydraulic test results from Matrix Test SB14 (OSU Test U0014) for inadvertent actuation of the ADS with no other break. The simulated loss-of-coolant (LOCA) accident was through the ADS-1 valve located at the top of the pressurizer. The ADS-4 was configured to simulate 50 percent failure of one of the two ADS-1 lines.

The test met the specified initial conditions. Any exceptions to the initial conditions are discussed in Subsection 5.5.1.1. Matrix Test SB14 was performed on July 7, 1994 with a test duration of about 5.5 hours. The transient began when the ADS-1 valve opened and continued through ADS actuation and core makeup tank (CMT), accumulator, in-containment refueling water storage tank (IRWST), and primary sump injection. Cooling of the heater bundle was maintained throughout this event; therefore, the test was considered successful.

Subsection 5.5.1.1 provides details related to the system configuration and initial conditions. A description of inoperable instruments is provided in Subsection 5.5.1.2, and Subsection 5.5.1.3 references the sequence of events. Subsection 5.5.1.4 describes the test results and evaluation. Component responses are given in Subsection 5.5.1.5, and a summary of mass balance results is provided in Subsection 5.5.1.6. The conclusions as they apply to Matrix Test SB14 are given in Subsection 5.5.1.7. The facility responses are documented by the data plots, referenced as figures in text, at the end of this section.

5.5.1.1 System Configuration and Initial Conditions

Test performance followed an approved written procedure. Prior to pressurization, accumulator levels were established by filling the tanks until a visual check showed water overflowing from the standpipe. This method ensured that accumulator levels were the same for all tests, independent of instrument indication. All actions were automatic and required no operator action.

The facility was configured and blind inserts installed in all other breaks in accordance with Dwg. OSU 600904 (Appendix G). The ADS 4-1 line was connected and piped into the ADS 4-1 separator. The ADS 4-2 line was connected to the ADS 4-2 separator. A 50 percent flow nozzle was installed in the ADS 4-1 line from hot leg-1 (HL-1) to provide the assumed single failure, and a 100 percent flow nozzle was installed in the ADS 4-2 line from HL-2. Additionally, flow nozzles simulating two lines were installed in the ADS 1-3 nozzles.

The inadvertent ADS-1 actuation LOCA did not require special break spool piping arrangements. The break separator was aligned so that no direct flow entered the break separator during the inadvertent ADS actuation transient. Liquid flow that occurred due to the inadvertent ADS-1 actuation was measured by FMM-601. Steam flow that occurred due to the simulated break was measured by FVM-601. These instruments also recorded discharges due to ADS-2 and ADS-3 actuation. The

resulting discharge flow was directed to the IRWST via the sparger. Overflow from the IRWST was directed to the primary sump via the overflow line and was measured by FMM-703.

CSS-902 and CSS-906 were closed throughout the transient. Closing these valves isolated FVM-902 and FVM-906 and allowed more accurate measurement of steam flows by FVM-901.

The nonsafety-related systems, chemical and volume control system (CVS) and normal residual heat removal system (RNS), were isolated and not used for Matrix Test SB14.

Fill and vent was performed according to an approved operating procedure. Refer to Subsection 2.7 for pre-test operations.

As final valve alignments were established, the CMT discharge valves were placed in AUTO and closed, limiting CMT-1 pressure to that obtained while the vessel was arriving at full pressure and temperature. With CMT balance line valves RCS-529 and RCS-530 placed in the OPEN and AUTO positions (1 minute after the TEST pushbutton was pressed), both CMTs reached reactor coolant system (RCS) pressure.

Testing was initiated when test facility conditions, as read from the test facility control board and local indication, agreed with specified initial conditions within acceptable tolerances. The transient continued through ADS actuation and CMT, accumulator, IRWST, and sump injection.

Note: ADS actuation occurs when either CMT reaches the low level setpoint. To achieve ADS actuation a Rosemount 268 communicator was attached to LDP-502 to permit the operator to induce a CMT low level signal. A 13.5-mA signal simulates a 35-in. level in CMT-2. This is below the low level setpoint but above the low-low level setpoint. On initiation of the CMT low level signal, a delay of 15 seconds occurs before the signal is sent to open RCS-601.

The heater rod bundle power was adjusted prior to break initiation to achieve the required hot-leg temperatures. Pressurizer power was terminated 6 seconds after initiation of the break.

The reactor heater power controller was programmed using the algorithm defined in Subsection 2.3.2 to obtain the scaled decay power heat input rate.

Core heater groups 1 and 2 provided a total initial input of 600 kW up to 140 seconds. At 140 seconds, the heater controller continued to follow the scaled power decay rate for the remainder of the transient. The decay power curves appear in Appendix F. The total power comparison results indicated excellent agreement between planned decay rates and measured values. The pressurizer heater breakers were manually opened by the operators after verifying the S signal.

Table 5.5.1-1 provides a comparison of the specified and actual conditions for Matrix Test SB14. The initial conditions were recorded from the operator's panel. A select set of instruments on the control

board was checked prior to the test. The control board had provisions to display compensated level indications.

There was one initial condition parameter out of specification. Accumulator-2 (ACC-2) pressure, indicated by PT-402, was []^{a,b,c} or []^{a,b,c} percent below the required pressure band. The accumulator was pressurized to the required pressure, as indicated on local pressure indicator PI-402, prior to test actuation. The loss of pressure between tank pressurization and test actuation was possibly due to nitrogen gas cooling in the accumulator. Test analysis starting with the recorded lower accumulator overpressure should still be possible.

5.5.1.2 Inoperable Instruments

Table 5.5.1-2 provides a listing of the instrumentation channels considered inoperable or invalid during all or portions of this test. Some of the instruments listed are on the Critical Instruments List (Subsection 3.2, Table 3.2-2) and, therefore, are addressed here.

FDP-604 and FDP-605 measured the differential pressure (in. H₂O) across the ADS-2 and ADS-1 flow nozzles, respectively. The transmitters over-ranged momentarily when their respective ADS valve opened. Total flow through the ADS 1-3 valve complex can be determined by measuring ADS 1-3 separator liquid (FMM-601), and steam flows from FVM-601, and any water held up in the ADS 1-3 separator.

FMM-201, FMM-202, FMM-203, and FMM-204 measured flow (gpm) in each of the four cold legs. A decision was made to continue testing without the availability of these instruments. Replacement flow meters repeatedly failed; their continued use was precluded because of cracking of the ceramic liners from thermal stratification in the loop piping. The necessary boundary conditions for loop flow could be determined from DP-202, DP-203, DP-205, and DP-206.

FMM-401 measured ACC-1 injection flow into DVI-1, and FMM-402 measured ACC-2 injection flow into DVI-2. After accumulator injection, the meter exhibited erroneous results due to nitrogen in the line; therefore, any results after []^{a,b,c} are invalid.

FMM-501, FMM-504, FMM-802, and FMM-804 provided accurate data when liquid solid, but were inaccurate when sensing two-phase or steam flow.

FMM-701 measured IRWST-1 injection flow. When the primary sump valves were opened, the flow meter indicated a negative flow as water flowed from the primary sump to the IRWST. The meter was not designed to measure reverse flow, so this measurement was invalid. However, total IRWST flow was measured by FMM-702.

FMM-905 measured break separator flow to the primary sump. When the primary sump became filled to or above the connecting pipe level the flow meter indicated negative flow as water flowed from the

primary sump to the break separator. The meter was not designed to measure reverse flow so this measurement was invalid.

LDP-401 and LDP-402 measured ACC-1 and ACC-2 levels, respectively. Due to air trapped in the sense lines for the transmitters, the data from these transmitters were invalid. However, the initial level of the tank was established by a standpipe, so it was constant from test to test. The drain rate can be calculated using FMM-401 and FMM-402, respectively. Alternatively, a pressure correction may be applied directly to the level indicators of LDP-401 and LDP-402.

SG tube level data (LDP-215, LPP-218, LDP-219, and LDP-222) was biased by vaporization of the water in the transmitter reference leg after the SG tubes started draining. However, the data provide accurate indication of the time when the tubes are empty.

LDP-502 measured the wide range CMT-2 level. This channel was used to actuate the inadvertent ADS transient as described in the note in Subsection 5.5.1.1. Therefore a constant []^{a,b,c} output signal was indicated throughout the transient. The sum of LDP-504, LDP-506, and LDP-508 provide the true CMT-2 level.

LDP-802 measured passive residual heat removal heat exchanger (PRHR HX) wide-range level. The PRHR HX may have been refilling, but a more logical reason is that the wide-range transmitter LDP-802 was slowly losing its reference leg due to a low saturation pressure in the HX tubes.

PT-201 measured RCS pressure at the top of the SG-1 long tube. On August 15, 1994, it was discovered that the transmitter had an incorrect zero compensation, which resulted in a negative error and negative data at low pressures. The transmitter zero was corrected at that time. PT-201 data obtained during Matrix Test SB14 had the zero correction performed, and the corrected data appear as PT_201. Negative data and corrected negative data can be used to determine trends, but are considered inaccurate. PT_201 data are not considered reliable for values less than []^{a,b,c} but a sufficient amount of other pressure data are available.

Data provided by ADS-4 separator instrumentation prior to the ADS 4-1 and ADS 4-2 valves opening at []^{a,b,c} were invalid due to the closed position of the ADS-4 valves and the ADS-4 separator loop seal valves. The instruments affected are: FMM-602, FMM-603, FVM-602, FVM-603, LDP-611, and LDP-612. Test analysis will not be affected, since ADS-4 flow did not begin until the valves opened.

Considering these critical instrument failures, sufficient instrumentation was available to allow the performance of mass balances as demonstrated in Subsection 5.5.1.6 and Appendix E. An energy balance will be performed and reported in the *AP600 Low-Pressure Integral Systems Test at Oregon State University Test Analysis Report, WCAP-14292.*⁽²⁾

5.5.1.3 Sequence of Events

The chronologic sequence of events is shown in Table 5.5.1-3. The first pages of the table provide the actual times of selected events in the test. Table 5.5.1-3 also depicts a bar-graph representation of the sequence of events sorted in chronologic order to provide a quick visual reference of the timing of events. D in the Data Source column indicates the recorded time was obtained from a software program that monitored digital events in the plant. These events included pump starts and stops, valve limit switch actuations, and alarms. The term *valve opening* means the valve has actuated and the closed limit switch is being opened (valve coming off the seat). A in the Data Source column indicates the time was obtained by reviewing data from the DAS. Although the data are in digital format, the DAS monitored analog events such as pressure, flow, and temperature.

5.5.1.4 Test Results and Evaluation

This section contains an overall description of the events that occurred during Matrix Test SB14, including references to specific instrumentation channels cross-plotted and used in the test result evaluation. The data plots list instrument number and description. The simulated LOCA resulted in interactions between different systems and simulated components in the facility. For this reason, the event was subdivided into the following two phases to characterize the systems' thermal-hydraulic phenomena and component effects:

- Initial Depressurization Phase: simulated ADS-1 actuation to start of IRWST injection
- IRWST Injection Phase: start of IRWST injection to end of test

Initial Depressurization Phase

The transient was initiated at time zero by the opening of the ADS-1 valve, RCS-601. One-half second after the ADS-1 valve opened, the steam controller setpoint reset to control steam header pressure at []^{a,b,c}. This setpoint closed the steam header control valve, stopping steam flow from the steam generators (SGs). The steam controller's output signal kept the steam header valve closed for the entire test.

The reactor controller setpoint also changed 1/2 second after the ADS-1 valve opened (break equivalent). Prior to the break, the reactor controller adjusted the reactor heaters' power to maintain an average hot-leg temperature of []^{a,b,c}. One-half second after break initiation, the reactor controller function changed. The controller output then controlled heater power to simulate decay heat after a reactor trip (Appendix F).

The inadvertent ADS actuation flow arrangement was initially indicated by three instruments. The opening of the ADS-1 valve was indicated by differential pressure flow indicator FDP-605 (Figure 5.5.1-1). Both liquid flow and steam flow exited the RCS through the ADS-1 valve. Liquid flow of about []^{a,b,c} was measured by FMM-601 (Figure 5.5.1-2); steam flow of about

[]^{a,b,c} from []^{a,b,c} was measured by FVM-601 (Figure 5.5.1-3). Immediately following the opening of the ADS-1 valve, saturated liquid flowed from the pressurizer to the ADS 1-3 separator, and RCS pressure decreased. The sharp increase from []^{a,b,c} differential pressure, indicated by FDP-605, confirmed that the ADS-1 valve opened (Figure 5.5.1-1).

When the ADS-1 valve opened (break initiation), both reactor pressure and pressurizer pressure decreased from []^{a,b,c} within []^{a,b,c} (Figures 5.5.1-4 and 5.5.1-5). Pressurizer pressure and reactor pressure remained at []^{a,b,c} until about []^{a,b,c} when ADS-2 valve actuation occurred.

[]^{a,b,c} after the TEST pushbutton was pressed, an S signal was initiated. The following events occurred during the next []^{a,b,c} pressurizer heater power was disabled at []^{a,b,c} the feedwater pumps tripped at []^{a,b,c} the CMT-1 and CMT-2 outlet valves opened at []^{a,b,c} the PRHR HX outlet valve opened at []^{a,b,c} and the RCPs tripped at []^{a,b,c}

The reactor and downcomer levels reflected the drop in vessel inventory through the ADS-1 valve (Figure 5.5.1-6). Vessel level (LDP-127) started dropping at []^{a,b,c} whereas the level in the downcomer (LDP-116 and LDP-140) remained constant from []^{a,b,c} (Figure 5.5.1-6). Vessel level fell to its minimum within []^{a,b,c} whereas downcomer level dropped about []^{a,b,c} from full condition. LDP-113, which spans from the direct vessel injection (DVI) bottom to the upper support plate, also confirmed that the vessel level appeared to drop somewhere below bottom of the DVI line (Figure 5.5.1-7).

The upper head and upper portion of the upper plenum started to void immediately after the reactor coolant pumps (RCPs) tripped. The plenum voided more rapidly than the upper head because the upper head fluid was separated from the upper plenum by the upper support plate. Fluid could only exit the upper head to the downcomer via the small bypass holes in the upper flange of the core barrel or by gravity-draining to the upper plenum via eight holes in the upper support plate (Appendix H, Dwg. LKL911218).

By control design, the PRHR HX outlet valve was planned to open []^{a,b,c} after the ADS-1 valve opened; however, RCS-804 unexpectedly opened at time zero. This allowed forced flow through the PRHR HX while the RCPs were running (FMM-804; Figures 5.5.1-8 and 5.5.1-9). FMM-802 showed high flow-rate spikes (over-range values) from []^{a,b,c} seconds because two-phase flow entered the PRHR HX at about []^{a,b,c}. Magnetic flow meters do not provide accurate indications during two-phase or reverse-flow conditions; therefore, indicated flow-rate values from FMM-802 during these periods may not be absolutely accurate.

From []^{a,b,c} the PRHR HX outlet flow varied from []^{a,b,c} (Figure 5.5.1-9). From []^{a,b,c} the outlet flow became stable at a rate of about []^{a,b,c}. After []^{a,b,c} the PRHR HX was empty (Figure 5.5.2-69). Any steam that reached the PRHR HX

slowly condensed and began to refill the HX tubes. FMM-804 exhibited over-ranged flow values that were not representative of the actual operation. A more detailed discussion of the PRHR HX operation is described in Subsection 5.5.1.5.

Initially, two-phase liquid from the pressurizer flowed out through the ADS 1-3 valves (Figure 5.5.1-10), as indicated by the liquid level increase in LDP-601 and the over-range of LDP-602 (Figure 5.5.1-2). Most of the liquid flow out of the pressurizer occurred from []^{a,b,c} with a peak flow rate of []^{a,b,c} occurring after ADS-2 valve actuation. Two-phase pressurizer flow was separated in the ADS 1-3 separator into water and steam and measured by FMM-601 and FVM-601, respectively (Figures 5.5.1-2 and 5.5.1-3). The steam flow lasted from []^{a,b,c} with a peak flow of []^{a,b,c} which occurred at []^{a,b,c}

In []^{a,b,c} pressurizer level peaked at a []^{a,b,c} and the core and downcomer levels dropped due to the large inventory loss from the ADS-1 valve and slow rate of injection from the CMTs (Figure 5.5.1-6). As both CMTs began discharging, a natural circulation mode started to replace inventory in the CMTs from the cold legs. A CMT-2 injection flow rate of []^{a,b,c} continued until about []^{a,b,c} when the transition from recirculation to draindown occurred, allowing CMT-2 flow to increase to []^{a,b,c} (Figure 5.5.1-11). At []^{a,b,c} reactor pressure dropped to []^{a,b,c} and ACC-1 and ACC-2 began injecting to the downcomer through the DVI lines. Reactor depressurization rate increased immediately following ADS-3 actuation. Accumulator injection slowed the injection flow rate from CMT-2 (Figure 5.5.1-11) due to the higher localized pressure at the junction of the CMT-2 and DVI lines. The higher localized pressure slowed and suspended CMT flow, as the flow from CMT-2 dropped from []^{a,b,c} at []^{a,b,c} and remained at []^{a,b,c} until accumulator injection decreased from peak flow.

As the reactor vessel and pressurizer continued to depressurize and their levels dropped, the pressure and liquid levels in the RCS cold and hot legs dropped. Due to rapid depressurization in the core and upper plenum, the liquid in the upper plenum flashed while the fluid level in the upper plenum dropped to the elevation of the hot legs. The cold-leg levels dropped to 0 (LDP-201 through LDP-204) just before the hot legs started to drain (LDP-205 and LDP-206; Figures 5.5.1-13 and 5.5.1-14). It should be noted that level indications are based on differential pressure indications subject to variation because of high liquid flow and two-phase flow conditions. Level indications were used to determine general level trends and approximate timing of events.

Both the cold-leg and hot-leg levels began to drop at about []^{a,b,c} and reached 0 between []^{a,b,c}. The level in the HL-1 elbow (LDP-207) was incorrectly ranged and did not provide accurate values. The level indicated by LDP-208 was inconsistent with other data (from LDP-206) and was subject to sudden flow changes because of SG-2 draining and the initial discharge through the pressurizer. As the hot legs drained, the HL-2 fluid had a steam percentage very close to that shown in the upper plenum (Figures 5.5.1-25 and 5.5.1-26). The steam percentage in HL-2 may have been lower due to the removal of vapor from the hot leg by the PRHR HX inlet line.

Using data from the level channels and calibrated range of the instruments, a steam percent for each channel was calculated. The equation used to calculate steam percent was:

$$\text{Steam percent} = \left[1 - \frac{\text{compensated level}}{\text{instrument range}} \right] \times 100$$

Within []^{a,b,c} of the ADS-1 valve opening, the primary side of both SGs showed a rapid drop in level (Figure 5.5.1-15 for SG-1). The SG-1 level decrease continued about []^{a,b,c} when the levels in LDP-211 and LDP-213 indicated a drop to []^{a,b,c} (Figure 5.5.1-16). The level in the SG-1 channel head (LDP-209) was incorrectly ranged and did not provide accurate values. LDP-207 and LDP-209 were considered inoperable for this test. As the primary-side pressure dropped (Figure 5.5.1-17 for SG-1), the thermocouples in the SG tubes remained well above the saturation temperature. A parameter identified as TSAT was included in this report to represent the saturation temperature as a function of reactor pressure, as measured by upper head pressure PT-107. Figure 5.5.1-15 shows a rapid drop in U-tube levels (from []^{a,b,c}), followed by a rapid increase in level (suggesting a refill of the SG U-tubes from []^{a,b,c}). This indicated refill does not occur. The cold and hot legs were drained before []^{a,b,c} and the SG channel head levels were drained at []^{a,b,c} as DP-211 and DP-212 reached []^{a,b,c} (Figure 5.5.1-18). Once the SG U-tubes were drained, they did not refill during the remainder of the test. This false indication was due to the arrangement of LDP reference legs, as described in Subsection 2.4.1. The response described previously for SG-1 is consistent for SG-2.

Draining of the SG U-tubes and subsequent draining of the SG channel heads are indicated by the drop in levels of LDP-211 and LDP-213 (Figure 5.5.1-16). The top of the U-tubes in SG-1 began to drain about []^{a,b,c} after the break. About []^{a,b,c} later, the recirculation mode ended and the draindown of the U-tubes started in both SG-1 and SG-2 (DP-211 and DP-212; Figure 5.5.1-18). As the SGs began to drain, the U-tube levels dropped and a positive differential pressure (DP-211 and DP-212) existed from []^{a,b,c} reflecting draining of the cold-leg sides of the SGs. The cold-leg sides drained about []^{a,b,c} ahead of the hot legs. Shortly after DP-211 and DP-212 reached []^{a,b,c} the drain flow was ended and the U-tubes drained. It is believed that LDP-211, LDP-213, LDP-212, and LDP-210 provide closer approximation as to when the U-tubes drained because of the reference top for the DPs maybe affected late in the draindown process when the lower tap becomes uncovered.

During initial depressurization of the primary loop, secondary-side pressures increased slightly and primary pressure decreased (Figure 5.5.1-19). The initial differential pressure (primary pressure greater than secondary pressure) reflected heat transfer from the primary to the secondary side. Primary pressure dropped immediately from []^{a,b,c} due to the opening of the ADS-1 valve, and the pressure remained at []^{a,b,c} from []^{a,b,c}. When the ADS-2 valve opened at []^{a,b,c} the pressure quickly decreased to []^{a,b,c}. Primary and secondary pressures approached a common pressure of []^{a,b,c} at []^{a,b,c}. This common-pressure period lasted about []^{a,b,c}. At about []^{a,b,c} the primary and secondary pressures

diverged (primary pressure less than secondary pressure), allowing the secondary side to transfer heat to the primary side via the SG U-tubes. The heat transfer to the primary side, combined with draining of the SGs, caused superheating in the SG U-tubes. The U-tubes remained at superheated conditions for the remainder of the test (Figure 5.5.1-20).

A comparison of fluid temperatures from the primary side of the U-tubes to the bulk fluid temperatures on the secondary side of the SGs is shown in Figure 5.5.1-20. Both primary side (SG-1 and SG-2 short-tube and long-tube thermocouples) and secondary side (SG-1 and SG-2 downcomer thermocouples) temperatures reached a common value of 420°F. During this same time, the primary-side and secondary-side pressures reached a common pressure of about []^{a,b,c} defined as the *pressure plateau*. As the reactor continued to depressurize, the primary temperatures diverged from saturated conditions, as indicated by the TSAT parameter.

From ADS-1 valve opening (break initiation) to about []^{a,b,c} a natural circulation flow developed from the cold legs to the CMTs (CL-1 to CMT-2 and CL-3 to CMT-1), based on the flow to CMT-1 and CMT-2 measured by FMM-503 and FMM-502, respectively. Both CMT-1 and the equivalent CMT-2 level (sum of CMT-2 narrow-range levels) remained stable (SUM-502 and LDP-507; Figure 5.5.1-12). At about []^{a,b,c} the natural recirculation mode ended and draindown started in the CMT-2 balance line. This was indicated by flow through FMM-502 dropping to []^{a,b,c} and a sudden drop in level (LDP-510; Figure 5.5.1-12). The transition from natural recirculation to draindown occurred at []^{a,b,c} for CMT-1. When the transition from the recirculation to draindown occurred in the balance lines for both CMTs, the following resulted. First, the level in the CMT began to decrease because the liquid draining into the core was no longer being replaced by water from the cold legs (Figure 5.5.1-12). Second, both balance line levels started to decrease as the region in the upper portion of the balance line started to void. Both CMT balance lines were empty at about []^{a,b,c} (Figure 5.5.1-12). Third, both CMT injection flows to the vessel increased from []^{a,b,c} (Figure 5.5.1-11).

The ADS-2 and ADS-3 valve opening signal occurred at []^{a,b,c} respectively (FDP-604 and FDP-606; Figure 5.5.1-1). Eleven seconds after the ADS-2 valve opened, differential pressure reached a peak of []^{a,b,c}. Peak differential pressure remained steady until the ADS-3 valve opened, which caused differential pressure to slowly decrease to about []^{a,b,c} at []^{a,b,c}. The ADS-1 and ADS-2 valve openings reduced RCS pressure from []^{a,b,c} over a []^{a,b,c} period. ADS actuation increased the rate of primary system depressurization, as measured by reactor upper head pressure (Figure 5.5.1-4).

ADS-2 and ADS-3 actuation caused both steam and liquid flow through the ADS 1-3 separator to increase sharply. Liquid flow through the ADS 1-3 separator increased from []^{a,b,c} from []^{a,b,c} (Figure 5.5.1-2). Steam flow increased from about []^{a,b,c} during the same time period (Figure 5.5.1-3).

Following ADS-3 valve actuation at []^{a,b,c} the pressurizer steam percentage reached an initial peak value of []^{a,b,c} percent steam, the surge line approached []^{a,b,c} percent steam, and liquid flow through the ADS 1-3 separator started to decrease from []^{a,b,c} (Figure 5.5.1-63). The reactor continued to depressurize, and the pressure dropped from []^{a,b,c} in []^{a,b,c} (PT-107; Figure 5.5.1-19).

Rapid injection of cold water from the accumulators (at []^{a,b,c} into the event) maintained the downcomer annulus saturated and ended the initial vessel and downcomer level decrease (Figure 5.5.1-6). At []^{a,b,c} the minimum vessel level occurred at a compensated collapsed liquid level of []^{a,b,c} based on reactor wide-range level indicator LDP-127. Downcomer level reached a minimum value also at []^{a,b,c} with a compensated collapsed liquid level of []^{a,b,c} based on wide-range downcomer level indicators LDP-116 and LDP-140.

The rapid decrease in reactor pressure because of ADS-3 actuation resulted in a sharp increase in the accumulator injection rate over the period of []^{a,b,c} (Figure 5.5.1-11). During the ADS-2 actuation period, the peak total injection flow occurred based on the combined sources of CMT-1 and CMT-2, as measured at the DVI lines. Flow was indicated by FMM-205 and FMM-206 for DVI-1 and DVI-2, respectively. The peak injection flow rate of []^{a,b,c} occurred at about []^{a,b,c} after ADS-3 valve opening and during ACC injection (Figure 5.5.1-24). The reactor vessel began to reflect a recovery in the vessel level at []^{a,b,c} but did not reach the peak level of []^{a,b,c} until []^{a,b,c} (Figure 5.5.1-6).

The inadvertent ADS actuation (break) resulted in steam in the reactor upper head, upper plenum, and hot legs. The description of the steam formation in these regions uses data from the following level channels:

- LDP-112 -- Lower portion of upper reactor plenum
- LDP-113 -- Upper portion of upper reactor plenum
- LDP-115 -- Upper reactor head
- LDP-206 -- HL-2
- LDP-208 -- SG-2 hot-leg elbow
- LDP-214 -- SG-2 hot-leg channel head

The plotted steam percent data indicated steam in the upper head and upper portion of the upper plenum immediately after the RCPs tripped. The upper plenum voided more rapidly than the upper head because the upper head fluid was separated from the upper plenum by the upper support plate.

At []^{a,b,c} the upper portion of the upper plenum was over []^{a,b,c} percent voided (LDP-113); the upper head was only []^{a,b,c} percent voided. After ADS-2 actuation, the steam percentage was []^{a,b,c} percent in the upper plenum and []^{a,b,c} percent in the upper head (Figure 5.5.1-25).

The data plots for the steam percentage in the SG-2 channel heads show a sharp increase in steam percentage at about []^{a,b,c} (Figure 5.5.1-26). This occurs shortly after the completion of the draining of the SG tubes, hot-leg side. The hot-leg channel heads reached their maximum void fraction []^{a,b,c} later, at []^{a,b,c} or when the SG hot-leg channel head was completely drained (Figure 5.5.1-26). While the hot-leg SG channel heads were draining, the steam percentage in the hot-leg elbows was increasing. By the time the channel heads were drained, the steam percentage in both SG-2 elbow was about []^{a,b,c} percent (Figure 5.5.1-26).

After ADS-3 actuation, the upper portion of the upper plenum reached []^{a,b,c} percent steam from []^{a,b,c} (Figure 5.5.1-25). At []^{a,b,c} injection flow from the accumulators increased the core inventory and quenched the core. This injection flow from the accumulators caused the steam percentage in the upper portion of the upper plenum to decrease to []^{a,b,c} percent at []^{a,b,c}.

From []^{a,b,c} as the upper head and upper plenum were draining, steam filled the head and remained at a saturation condition (Figure 5.5.1-21). With the rapid depressurization after ADS-3 actuation and decreased injection from the accumulators, the upper head and downcomer temperatures went from saturation to a superheated condition. The downcomer superheated conditions were caused by the steam flow from the upper head to pass into the upper region of the downcomer (Figure 5.5.1-27). The steam flow was the result of differential pressure across the bypass holes (DP-130). Superheating of the saturated steam in the upper head was probably due to the heat transfer from the upper head and the upper support plate to the steam passing through the upper support plate. This heat transfer occurs as the upper support plate becomes uncovered due to the draining of the upper head. Evidence to this effect comes from the fact that TF-171, located 1/2 in. above the upper support plate, remains at saturated conditions until the upper head becomes drained at []^{a,b,c} (Figure 5.5.1-29). Subsequently, this thermocouple indicates an increased temperature from []^{a,b,c} to a peak of []^{a,b,c} at []^{a,b,c}. The upper support plate, exposed earlier to []^{a,b,c} transferred this stored heat energy to the saturated steam to produce superheated steam as the reactor pressure rapidly decreased.

It should be noted that TF-170, which is located above the upper core plate (Figure 5.5.1-29), provided erroneous results (considerably lower temperatures than expected). One explanation for the low temperature indication is a seal leakage from the downcomer to the core. Therefore, TF-170 should not be used for analysis purposes; TF-169 should be used instead.

When reactor pressure decreased to []^{a,b,c} (about []^{a,b,c} per Table 5.5.1-3), the signal to open RCS-711 and RCS-712 was automatically initiated. The two parallel IRWST injection lines contained a set of check valves to preclude backflow from the RCS to the IRWST. These check valves (RCS-713 and RCS-715 in line with FMM-701, and RCS-714 and RCS-716 in line with FMM-702) permitted injection into the DVI line when reactor pressure decreased to the equivalent of the IRWST liquid head. Based on this design configuration, IRWST injection can occur without

operator or automatic actuation once RCS-711 and RCS-712 open. However, due to the higher reactor pressure, injection flow from the IRWST did not take place until about []^{a,b,c}

At about []^{a,b,c} RCS pressure was []^{a,b,c} and both accumulator flows were decreasing to []^{a,b,c} which permitted the CMTs to resume injection into the reactor vessel. As the accumulator injection was completed, injection flows from both CMTs resumed at a peak flow rate of []^{a,b,c} per side (Figure 5.1.1-11); however, the reduced total DVI injection resulted in a decrease in core and downcomer liquid levels. At []^{a,b,c} the CMT-2 and CMT-1 levels were approximately []^{a,b,c} respectively, which is equivalent to the []^{a,b,c} percent volume level in the CMT (Figure 5.5.1-12). This []^{a,b,c} percent volume level is the level at which ADS-1 actuation would typically occur.

With both the hot legs and cold legs empty and injection flow only from the CMTs, the core and downcomer levels started to decrease for a second time. The downcomer reached a minimum level of about []^{a,b,c} at []^{a,b,c} whereas the vessel wide-range level reached a minimum level of []^{a,b,c} at about []^{a,b,c} (Figure 5.5.1-6). During this period, the upper portion of the upper plenum (LDP-113) indicated an increasing steam percentage from []^{a,b,c} percent, confirming the reduction in vessel liquid inventory (Figure 5.5.1-25).

The ADS-4 valves were actuated when the level in one of the CMTs dropped to the CMT low-low level ([]^{a,b,c}) and at least []^{a,b,c} had passed since one of the CMT levels dropped to the low level setpoint of []^{a,b,c}. This criterion was achieved at []^{a,b,c} when the liquid level in CMT-1 decreased to []^{a,b,c}.

At []^{a,b,c} both ADS-4 valves were opened and directed flow to the ADS 4-1 and ADS 4-2 separators (FVM-603, FVM-602, FMM-603, and FMM-602; Figures 5.5.1-3 and 5.5.1-2). Saturated liquid from the ADS-4 lines was discharged into the primary sump. Also at []^{a,b,c} the pressurizer liquid level indicated a significant decrease, and discharge through the ADS-1, ADS-2, and ADS-3 valves ended (Figures 5.5.1-10 and 5.5.1-2). Liquid flow indicated that as the ADS-4 valves were opened, flow through the ADS 4-1 and ADS 4-2 separators was initiated and gradually increased to a peak combined flow rate of []^{a,b,c} at about []^{a,b,c}.

IRWST Injection Phase

The IRWST injection phase began when RCS pressure decreased to the pressure corresponding to the water elevation of the IRWST. IRWST flow through DVI-1 began at []^{a,b,c} and through DVI-2 at []^{a,b,c} (FMM-701 and FMM-702, respectively; Figure 5.5.1-30). IRWST injection flow steadily increased from an average flow rate of []^{a,b,c} per IRWST line to a peak IRWST flow rate per IRWST line of []^{a,b,c} at []^{a,b,c}.

At []^{a,b,c} CMT-2 was empty (based on the sum of the narrow-range level indications of LDP-504 and LDP-506) and CMT-1, which was still draining, contained []^{a,b,c} of water

(Figure 5.5.1-12). All injection flow from the accumulators had terminated; the accumulators had injected their water inventory. At []^{a,b,c} CMT-1 emptied, limiting the overall injection flow to only that from the IRWST lines. After peak IRWST injection flow was achieved at []^{a,b,c} flow continued to decrease slowly based on the IRWST head.

As IRWST injection continued, both the downcomer liquid level and the core liquid level increased (Figure 5.5.1-6). At []^{a,b,c} the vessel and downcomer collapsed liquid levels appeared to be equal at about []^{a,b,c}. The upper head remained filled with superheated steam (temperatures exceeded TSAT), as measured at the upper head and directly above the upper support plate by TF-120 and TF-171. The upper plenum contained saturated steam and liquid, as measured by TF-169 (upper reactor fluid temperature) (Figure 5.5.1-29). The bulk fluid temperature in the core region remained at saturated temperature or subcooled throughout the transient, as measured by thermocouple rod TR-001 in which the thermocouples are located axially ([]^{a,b,c}) across the heater rod bundle (Figure 5.5.1-31). During early depressurization, little temperature variation occurred across the heater rod bundle. Injection from the CMTs, accumulators, and the IRWST had not only cooled the heater rod bundle but contributed to a temperature gradient in the heater rod bundle. At []^{a,b,c} a []^{a,b,c} temperature gradient across the heater rod bundle was created and maintained until about []^{a,b,c}.

Also during this period ([]^{a,b,c}), the pressurizer was drained of liquid with no indicated flow through the pressurizer or flow out of the ADS 1-3 valves (Figures 5.5.1-10 and 5.5.1-2). The SG U-tubes remained filled with superheated steam that decreased in temperature from about []^{a,b,c}. The PRHR HX continued to condense any steam that reached the HX tubes, but the indicated outlet flow measured by FMM-804 was over-ranged and not representative of the actual small outlet flow (Figure 5.5.1-9).

The liquid levels in both the downcomer and core regions increased to the point where both the hot and cold legs refilled with liquid inventory due to IRWST injection. As the IRWST injection continued beyond []^{a,b,c} both the downcomer and core levels slowly increased.

At about []^{a,b,c} steam bubble collapses occurred, as indicated by spikes in the core/downcomer liquid levels (Figure 5.5.1-6), upper head/downcomer temperatures (TF-120 and TF-168; Figure 5.5.1-21) and cold-leg temperatures (Figures 5.5.1-32 through 5.5.1-35). Most of the thermocouple rod temperatures, located in the core area (TR-001-1 through TR-001-8) indicated a short term (about []^{a,b,c}) temperature increase in response to the steam bubble collapse (Figure 5.5.1-31). The thermocouple rod temperatures increased as the flow that normally goes up in the core region reversed back toward the downcomer region.

Temperatures in the cold legs indicated that the cold legs began to refill at about []^{a,b,c}. The cold-leg bottom temperatures (TF-107, TF-108, TF-103, and TF-104; Figures 5.5.1-32 through 5.5.1-35) reflected a drop in temperature from a superheated to saturated/subcooled condition. Once the cold legs reached full level (about []^{a,b,c}), cold-leg top temperatures measured by

TF-105, TF-106, SC-101, and SC-102 exhibited a constant temperature, and some stratification existed from the top to the bottom of the pipe (Figures 5.5.1-32 through 5.5.1-35). Similar temperature effects were achieved in the hot legs at about []^{a,b,c} (Figures 5.5.1-22 and 5.5.1-23).

The refilling of the cold legs with liquid covered the CMT balance lines. As the CMT balance lines became partially filled by condensation, a flow was created from CL-1 to CMT-2 and from CL-3 to CMT-1 (Figure 5.5.1-36). This was measured by a level change indicated by LDP-510 and LDP-509. The refilling of both CMT-1 and CMT-2 continued until a level of []^{a,b,c} respectively, was reached at []^{a,b,c}. As both CMTs were refilling, no flow was discharged into the DVI line from the CMTs.

Level remained in both CMTs until the pressure in the DVI lines was less than the pressure corresponding to the water elevation of CMT-1 or CMT-2. At []^{a,b,c} after inadvertent ADS-1 actuation, flow from CMT-1 entered the DVI line (FMM-501; Figure 5.5.1-37). At []^{a,b,c} after the break event, flow from CMT-2 entered the DVI line (FMM-504; Figure 5.5.1-37). The effect on CMT-2 liquid level due to the draindown is shown in Figure 5.5.1-36. Instrument tag SUM-502 is the sum of LDP-504, LDP-506, and LDP-508 narrow-range levels for CMT-2. This figure also shows the continued draindown of CMT-1 (LDP-507) until about []^{a,b,c} when CMT-1 became empty. CMT-2 emptied at []^{a,b,c}.

From []^{a,b,c} the downcomer region reached a peak refill liquid level of []^{a,b,c} and the vessel reached a peak refill liquid level of []^{a,b,c} (Figure 5.5.1-38). Reactor vessel level began to decrease after []^{a,b,c} as the flow exiting through the ADS-4 valves (FMM-602 and FMM-603; Figure 5.5.1-39), to the primary sump slightly exceeded the combined injection flow from the IRWST and CMTs (FMM-205 and FMM-206; Figure 5.5.1-40).

At []^{a,b,c} the top layers of the heater bundle became saturated at []^{a,b,c} (TR-001-8; Figure 5.5.1-41).

Superheated steam continued to exit the upper head from about []^{a,b,c} and DP-130 did not indicate flow. However, the temperature decreased from []^{a,b,c} at []^{a,b,c} to []^{a,b,c} at []^{a,b,c} (Figure 5.5.1-42). Temperatures in the cold and hot legs began to increase from subcooled and approached a steady-state saturated temperature of []^{a,b,c} at about []^{a,b,c} (Figure 5.5.1-81). Also during this period, the liquid level in the upper head remained at a level just below the upper support plate. TF-171, located directly above this plate, indicated a superheated temperature of []^{a,b,c} at []^{a,b,c} (Figure 5.5.1-42). The top of the downcomer annulus indicated a slowly decreasing temperature, reaching []^{a,b,c} at []^{a,b,c} (TF-168; Figure 5.5.1-43).

At approximately []^{a,b,c} with the upper head superheated, an increase in IRWST injection flow began to occur (Figure 5.5.1-44). A sharp increase in flow was also seen on FMM-602 and

FMM-603 (Figure 5.5.1-39) beginning at []^{a,b,c} This sudden increase in injection flow was due to a lower reactor pressure.

During this same time period, a sudden drop in the downcomer level also occurred (from []^{a,b,c}) over a []^{a,b,c} time frame (Figure 5.5.1-38). It is not clear as to what caused this drop in downcomer level. The downcomer and vessel levels continued to decrease at comparable rates, but the vessel level remained higher than the downcomer level until primary sump injection occurred. As flow from the primary sump began, the downcomer level increased from []^{a,b,c} in a []^{a,b,c} period.

Flow from the primary sump entered DVI-1 (FMM-901) at []^{a,b,c} and DVI-2 (FMM-902) at []^{a,b,c} (Figure 5.5.1-44). Flow was initially limited through the double-check valve arrangement (CSS-921 through CSS-924, Dwg. OSU 600206, Appendix G). A small flow of []^{a,b,c} per injection line entered the DVI lines based on the driving head of the primary sump.

At []^{a,b,c} when the IRWST reached the low-low level setpoint, the programmable logic controller (PLC) automatically opened CSS-909 and CSS-910, and the flow rate increased to a total combined peak flow rate of []^{a,b,c} (FMM-901 and FMM-902; Figure 5.5.1-44). FMM-702 indicated a continuing flow of []^{a,b,c} at []^{a,b,c} and FMM-701 indicated a negative or zero flow at the same time (Figure 5.5.1-44). A flow comparison with FMM-205 and FMM-206, which measure the total flows in the DVI lines, indicated a total combined flow of []^{a,b,c} ([]^{a,b,c} from each line) (Figure 5.5.1-40). Therefore, the indicated negative value for FMM-701 represents a reverse-flow condition in which flow from the primary sump enters the IRWST. As previously discussed, magnetic flow meters used at OSU cannot measure reverse flow and will read negative if the flow is in the reverse direction of the normal flow path. However, the negative value does not reflect an accurate measure of reverse flow.

Liquid levels in both the downcomer and the vessel continued to fall until about []^{a,b,c}. The downcomer levels (LDP-116 and LDP-140) stabilized at an indicated level of []^{a,b,c} (below the cold leg), and the vessel level (LDP-127) indicated a collapsed level of []^{a,b,c}.

At about []^{a,b,c} the system reached an equilibrium condition with the fluid temperature in the core, downcomer, upper head, cold legs, and hot legs at about []^{a,b,c} (Figures 5.5.1-41 through 5.5.1-43). At this time, []^{a,b,c} of flow exited through the ADS-4 valves to the primary sump (FMM-602 and FMM-603; Figure 5.5.1-39). A combined flow of []^{a,b,c} was returned by the primary sump drain valves to the DVI line (FMM-901 and FMM-902; Figures 5.5.1-40 and 5.5.1-44). The test was terminated after at least 2 hours of stable sump injection was achieved.

5.5.1.5 Component Responses

Reactor

The discussion of reactor response entails several different regions: reactor core, upper plenum, upper head, and downcomer annulus. The regions are discussed in this order.

Level response of the downcomer annulus is measured by two wide-range and several narrow-range level transmitters (Appendix H, OSU Dwg. 600101). The wide-range channels are positioned 90 degrees from one another. The data from these two channels are in excellent agreement. Both channels are also in agreement with their associated narrow-range channels.

When the TEST pushbutton was pressed, the reactor controller was in auto-local, controlling hot-leg average temperature at []^{a,b,c} (the reactor controller automatically controls that temperature by varying the demand signal to the heaters). At time zero, the PLC sent a signal to open the break valve and then 0.5 second later signaled the reactor controller to shift control to auto-remote with total power demand initially at 600 kW (the setpoint is generated by an algorithm programmed into the controller, and the controller automatically controls the demand to the heaters to control the setpoint kW). The power algorithm programs full power (600 kW) for the first []^{a,b,c} and then lets power decay at an exponential rate that simulates the decay heat input of the AP600 nuclear reactor following a trip from full power (Appendix F).

When the ADS-1 valve inadvertently actuated (break occurred), the S signal was initiated and system pressure began to drop. []^{a,b,c} after break initiation, the RCPs tripped and the upper head reached the saturation temperature of []^{a,b,c}. As core level and pressure dropped due to loss of inventory out of the ADS-1 valve, the entire upper head, upper plenum, and upper annulus regions reached saturation temperature (TF-120, TF-171, TF-169, and TF-168; Figures 5.5.1-21 and 5.5.1-29).

Figures 5.5.1-6 and 5.5.1-21 show the collapsed liquid levels in the core/downcomer region and the temperatures in the upper head/downcomer region, respectively. At []^{a,b,c} the level in the core reached a minimum level, even though []^{a,b,c} percent of the inventory from the primary sides of the SGs and []^{a,b,c} percent of CMT-1 and CMT-2 inventory had been added. Reactor core response was evaluated using temperature data from thermocouples located in the core. Data from thermocouples mounted on a thermocouple rod at the center of the core were used to assess axial fluid temperature distribution. These thermocouples were given a TR designator. Data from the top thermocouple of six heater rods were used to assess heater rod radial temperature distribution at the top of the core. These thermocouples were given a TH designator (Appendix G, Dwg. OSU 600007 and OSU 600008). Thermocouple rods (TR-001-1 through TR-001-8) and heater rods (TH-101-4 through TH-505-4) showed no long-duration temperature spikes indicative of a core uncover (Figures 5.5.1-31, 5.5.1-41, 5.5.1-45, and 5.5.1-46). Some temperature spikes were evident.

The inadvertent ADS-1 actuation (break) created a depressurization in the RCS. Temperatures at the center of the core became saturated within []^{a,b,c} of the break. As the test progressed, RCS pressure decreased as the result of the break and actuation of ADS-2, ADS-3, and ADS-4. The core cooled and maintained at saturation temperature as the RCS depressurized (Figures 5.5.1-31 and 5.5.1-41). Subcooled temperatures at the bottom of the core first appeared at about []^{a,b,c}. Up to this time, the core temperatures were equal to or slightly below the saturation temperature as indicated by TSAT. At about the time of ADS-3 actuation, the rate of RCS depressurization decreased significantly, slowing the saturation temperature decrease. Core cooling continued with DVI, so the bottom of the core started to subcool.

From []^{a,b,c} TR-001-6, TR-001-7, and TR-001-8 remained at saturated conditions (elevation 43.13 through 51.86 in., respectively). The remainder of the thermocouples were subcooled. Heating elements in the heater rods simulated the active fuel of the AP600. The top of the heating elements in the heater rods was located []^{a,b,c} from the bottom of the reactor vessel. Thus, by the end of the test, fluid in the center of the core (TR-001) was subcooled only []^{a,b,c} percent (TR-001-1 and TR-001-2) of the length of the active core (Figure 5.5.1-41).

Data from the thermocouples, installed in the top of six heaters staggered radially across the core, indicated that the design for a "flat" heat flux profile was achieved in the core (Figures 5.5.1-45 and 5.5.1-46). The center heaters were generally at a temperature only []^{a,b,c} lower than the midcenter and outer heaters. The lower center temperatures were probably due to a slightly higher flow rate through the center of the core.

Steam percentage in the core may be calculated by using data from three level transmitters that measure core level: LDP-109, LDP-110, and LDP-138 (Appendix H, Dwg. LKL 911218). LDP-138 is a wide-range transmitter that spanned the entire core area, from the top of the lower core plate to the bottom of the upper core plate. LDP-109 and LDP-110 are narrow-range transmitters whose summed span equal that of the wide-range transmitter. The narrow-range transmitters are mounted in the same azimuth as LDP-138 (0 degree) and share the same taps.

There is close agreement between core steam percentage calculations using core level data from the wide-range (LDP-138) and narrow-range level transmitters (LDP-109 and LDP-110; Figures 5.5.1-47 and 5.5.1-48). Transmitters LDP-109 and LDP-110 have equal spans, which together cover the same span as wide-range level transmitter LDP-138.

The maximum steam percentage in the core occurred at about []^{a,b,c} close to the same time as the minimum core level. From this time on, the core steam percentage was constant or decreased, but never increased. In other words, core levels measured by the wide-range transmitter or either of the narrow-range transmitters never decreased after []^{a,b,c} but remained constant or increased.

In summary, the core showed indications of increasing core steam percentage immediately after the inadvertent ADS-1 actuation. Temperatures in the core quickly reached saturation. Core cooling maintained temperatures at saturation as the RCS depressurized and lowered saturation temperature. Maximum core steam percentage occurred after ADS-3 actuation and at the same time as minimum core level. Throughout the test, there were no excursions of temperature indicated by the heater rod thermocouples or unheated rod thermocouples. The bottom of the core started cooling at the time of ADS-3 actuation and remained subcooled.

The upper head and upper plenum are separated by the upper support plate. Both the upper plenum and upper head began to drain immediately after the break. The upper plenum reached its minimum level at []^{a,b,c} the same time as the maximum steam percentage in the core (Figures 5.5.1-7 and 5.5.1-25). The upper head took longer to void, about []^{a,b,c} because of its restrictive flow. In order to empty, the upper head had to gravity-drain either through holes in the upper support plate to the upper plenum and/or through bypass holes in the core barrel flange to the downcomer. The flow paths were sufficiently restrictive to delay the upper head void well past the time that the upper plenum reached its minimum level.

Differential pressure across the upper support plate and the flow bypass holes was monitored by DP-114 and DP-130, respectively (Appendix G, Dwg. OSU 600101). A positive value of differential pressure indicated that flow was in the direction of flow during normal operation, before the RCPs tripped. When the pumps were running, flow was from the downcomer, through the bypass holes into the upper head, continuing from the upper head into the upper plenum via the holes in the upper support plate. A negative value for differential pressure indicated that flow was reversed or that there was no liquid.

The direction of flow into and out of the upper head was indicated by data from DP-114 and DP-130 (Figures 5.5.1-27 and 5.5.1-28). At the time of the break, differential pressure across the bypass holes was a positive []^{a,b,c} and DP-114 was a positive []^{a,b,c}. Thus, the flow was per design, from the downcomer to the upper plenum. At []^{a,b,c} flow reversed and both differential pressures were negative. This flow reversal was due to the draining of the downcomer.

Differential pressure across the bypass holes remained negative for the remainder of the test. After []^{a,b,c} flow was always from the upper head into the downcomer annulus (Figures 5.5.1-27 and 5.5.1-28). By the time the upper head emptied at []^{a,b,c} differential pressures across the bypass holes and upper support plate were at their first maximum negative value. A second maximum negative differential pressure across the bypass holes and upper support plate occurred following ADS-4 opening. Both differential pressures steadily decreased in magnitude in time as the steam-flow rate to the downcomer decayed.

Note: Data for differential pressure across the bypass holes given by DP-130 must be reduced by a value between []^{a,b,c}. The magnitude of the correction factor is a function of water level in the upper head above the variable leg tap for DP-130. The variable leg tap for

DP-130 is located in the downcomer. When this tap is uncovered, the correction factor for DP-130 is []^{a,b,c}. This unusual correction factor is a result of mounting a differential pressure transmitter in a vertical position while measuring differential pressure in a column that does not stay full of water. A similar correction applies to DP-114; however, the correction factor is []^{a,b,c}. The full explanation for this correction factor is given in Subsection 2.4.

Note: Data from DP-114 and DP-130 provide a method to check the validity of data from LDP-127, LDP-116, and LDP-140. The method to use DP-130 and DP-114 as a data verification can be found in Subsection 2.4.

Both accumulators began injecting subcooled water at about []^{a,b,c} which started core liquid level recovery at about []^{a,b,c} (LDP-127; Figure 5.5.1-6). At []^{a,b,c} with the vessel drained below the cold-leg and hot-legs levels, the upper head, as measured by TF-120 and TF-171, became superheated; however, the upper plenum became saturated (Figures 5.5.1-21 and 5.5.1-29). Even though the downcomer bulk fluid temperature remained subcooled, TF-168 indicated that the upper []^{a,b,c} of the downcomer region was superheated (Figure 5.5.1-21).

Eight downcomer fluid thermocouples (TF-147 through TF-150 and TF-164 through TF-167), mounted []^{a,b,c} above the top of the DVI nozzles, monitored the temperature in the downcomer. TF-147 through TF-150 were mounted []^{a,b,c} above the DVI-2 penetration; TF-164 through TF-167 were mounted []^{a,b,c} above the DVI-1 penetration (Appendix H, Dwg. OSU 600101). The thermocouples were mounted at one of two elevations. TF-147, TF-148, TF-166, and TF-167 were located about []^{a,b,c} above the top of the DVI line penetration to the downcomer. TF-149, TF-150, TF-164, and TF-165 were located about []^{a,b,c} above the top of the DVI line penetration to the downcomer.

During three distinct periods, these thermocouples became superheated by a steam layer in the upper downcomer region. The three periods — []^{a,b,c} — where the hot-leg centerline thermocouples reached superheated conditions occurred close to the following events:

- Period 1 occurred shortly after ADS-3 actuation and during early accumulator actuation with the core and downcomer at minimum levels (Figure 5.5.1-6).
- Period 2 occurred at ADS-4 actuation when the core was at its second minimum level but the downcomer was close to the hot-leg centerline level (Figure 5.5.1-6).
- Period 3 occurred as both core and downcomer levels were rising and shortly after CMT injection from both CMT-1 and CMT-2 ended and only IRWST injection was available (Figures 5.5.1-6 and 5.5.1-11).

Throughout the early part of the transient, TF-134 and TF-152 (below the DVI line), exhibited subcooled conditions. All other thermocouples (TF-149, TF-150, TF-164, and TF-165), located []^{a,b,c} below the hot-leg centerline exhibited subcooled-to-saturated conditions with a significant variation. This is probably due to mixing at the interface between superheated steam, saturated steam and subcooled liquid. Shortly after the hot legs started to refill (about []^{a,b,c}), the thermocouples were quenched and returned to subcooled conditions.

From []^{a,b,c} the top four thermocouples (TF-147, TF-148, TF-166, and TF-167) indicated superheated temperatures in the downcomer (Figure 5.5.1-79). Subsequently, all of the thermocouples became subcooled during accumulator injection. From []^{a,b,c} six of the eight thermocouples increased in temperature (superheated) just prior to ADS-4 actuation due to the limited amount of injection flow from CMT-1 and CMT-2. The downcomer level at the time was just at the DVI nozzles, the minimum downcomer level. The thermocouples became covered with water immediately following ADS-4 actuation and remained subcooled until about []^{a,b,c}. The thermocouples became uncovered again from []^{a,b,c} as IRWST injection started. As the injection flow and overall core and downcomer levels increased, the thermocouples became covered and subcooled. Some temperature fluctuations may be due to mixture of saturated steam generated from fluid in the downcomer and superheated steam flowing from the SGs, through the cold legs, and to the break at the cold-leg balance line.

The upper head remained superheated throughout most of the transient, except when condensation events caused a sudden drop in temperature; details of these events are described in Subsection 7.1. As ADS actuation occurred, core liquid levels continued to recover to a level of []^{a,b,c} at []^{a,b,c}. A second drop in core level occurred just prior to the ADS-4 valves opening, even after the emptying of the accumulators and injection from both CMT-1 and CMT-2. A recovery of the core liquid level began as IRWST injection started in the []^{a,b,c} period. Recovery of the core and downcomer liquid levels peaked at []^{a,b,c} when both the downcomer became full and the hot legs and cold legs filled to an elevation equivalent of []^{a,b,c} (Figure 5.5.1-38).

As IRWST draindown slowed and the level in the primary sump increased, sump injection was initiated (at about []^{a,b,c}). As this sump injection progressed, the upper head, core region, and downcomer cooled to a steady-state temperature condition of []^{a,b,c} slightly above the saturation temperature.

Break and ADS Measurement System

The BAMS provided a means to collect, measure, and redirect flow to the primary and secondary sumps for subsequent return to the reactor vessel via the DVI lines. Elevation of the separators (break separator, ADS 1-3, ADS 4-1, and ADS 4-2) and their cross-connecting pipe were modeled to simulate the physical conditions in the reactor cavity and containment areas.

Prior to initiation of the break, all loop seals were filled and in accordance with test procedures. Only the ADS 1-3 loop seal was heat-traced. On inadvertent ADS-1 actuation (break), flow from the pressurizer through the ADS-1 valve was directed to the ADS 1-3 separator (Figure 5.5.1-2). Levels in the break separator (LDP-905) did not increase until sump level reached the loop seal. The primary sump liquid level instrument, LDP-901, increased immediately following the break (Figures 5.5.1-49 and 5.5.1-50).

FVM-901 indicated a steam flow discharge rate of []^{a,b,c} which occurred about []^{a,b,c} after the break (Figure 5.5.1-51). Most steam flow occurred from []^{a,b,c} (Figures 5.5.1-3, 5.5.1-51, and 5.5.1-52), with the largest portion associated with steam flow out of the ADS 1-3 separator (FVM-601). A total of []^{a,b,c} of steam exited the primary system and building through the BAMS as a result of this transient.

Figure 5.5.1-49 shows the liquid level changes measured by LDP-701 in the IRWST and in the primary sump (LDP-901). At about []^{a,b,c} after the ADS-1 valve opened, the IRWST overflowed to the primary sump (FMM-703; Figure 5.5.1-2).

Break separator level (LDP-905) remained unchanged (Figure 5.5.1-49) until the primary sump backflowed into the break separator via the break separator loop seal at []^{a,b,c} (FMM-905; Figure 5.5.1-2). Once this occurred, any liquid added to either the primary sump or the break separator was reflected in the liquid levels (LDP-901 and LDP-905). In effect, both levels increased together until the primary sump reached the overflow level of []^{a,b,c} above the centerline of the DVI line. The peak level in the break separator occurred at []^{a,b,c} with a level of []^{a,b,c}.

The secondary sump level (LDP-902), was unaffected until about []^{a,b,c} when overflow from the primary sump occurred (Figures 5.5.1-49 and 5.5.1-50). As primary sump injection initiated at []^{a,b,c} the level in the sump decreased slightly. The sump level was replaced with a []^{a,b,c} flow from the ADS 4-1 and ADS 4-2 separators (Figure 5.5.1-39).

Core Makeup Tanks

Thermal-hydraulic behavior in the CMTs was quite symmetrical throughout Matrix Test SB14 due to the break location (inadvertent ADS-1 actuation); therefore, data from CMT-2 are described initially in detail followed by a summary of differences relative to CMT-1 separately.

The CMTs are filled with subcooled liquid at []^{a,b,c} prior to break initiation. The isolation valves in the discharge lines were opened []^{a,b,c} after the inadvertent ADS-1 actuation, and natural circulation flow started in the loop formed by CMT-2, the CMT-2 discharge, the DVI line, the pressure vessel, CL-1, and the cold-leg balance line. CMT-2 injection flow (FMM-504) and the axial temperature profile (TF-504 through TF-532) are illustrated in Figures 5.5.1-11, 5.5.1-53, and 5.5.1-54.

With the onset of natural circulation flow through the CMT, subcooled water started to flow through the balance line into CMT-2, as shown by a rapid temperature increase measured by TF-532 at the top of CMT-2 and a discharge flow rate of []^{a,b,c} measured by FMM-504 (Figure 5.5.1-11). Within []^{a,b,c} after initiation of the transient, the top []^{a,b,c} percent of CMT volume was []^{a,b,c}. The CMT transitioned from recirculation to draindown at []^{a,b,c} indicated by a drop to 0 (FMM-502) and a complementary sharp decrease in the level measured by LDP-510 (Figure 5.5.1-12). During this transition from recirculation to draindown, the CMT-2 injection flow rate increased to []^{a,b,c} (Figure 5.5.1-11). As cold-leg levels dropped, saturated steam filled the CL-1 balance line and at about []^{a,b,c} became slightly superheated (TF-536 and TF-546; Figures 5.5.1-55 and 5.5.1-56).

During accumulator injection and ADS-2 and ADS-3 opening ([]^{a,b,c}), the CMT-2 level remained constant, but the space above the []^{a,b,c} water level became slightly superheated ([]^{a,b,c} increase over saturation temperature). Figures 5.5.1-55 and 5.5.1-56 show the interaction between the water layer and the upper head of the CMT. The recirculation mode occurred from []^{a,b,c}. The upper portion of the CMT-2 dome was exposed to []^{a,b,c} liquid, indicated by TF-546, and the inside wall surface temperature changed from []^{a,b,c} (TW-556; Figure 5.5.1-55). The outside wall temperatures also increased, but at a slower rate, beginning at []^{a,b,c} and increasing to a peak of []^{a,b,c} (over []^{a,b,c}), as indicated by TW-554. The outside wall temperature on the CMT-2 dome at a corresponding radial direction (TW-548) showed excellent agreement with TW-554 (Appendix G, Dwg. OSU 600502). The recirculation mode quickly heated the metal mass at the very top of the CMT and allowed storage of some thermal energy that was returned to the system by heating up the saturated steam entering the dome of the CMT, beginning at []^{a,b,c} and continuing until about []^{a,b,c} (Figures 5.5.1-55 and 5.5.1-56).

The upper layers of saturated steam in the CMT were superheated ([]^{a,b,c}) due to exposure to higher wall temperatures and the rapid depressurization during ADS-2 and ADS-3 valve actuation. Characterization of the early stages of the CMT-2 superheating effect was indicated by the thermocouples along the axial length of the CMT, upper CMT dome inside-wall temperatures, and a combination of fluid and wall temperatures at the top layers (Figures 5.5.1-57, 5.5.1-58, and 5.5.1-59, respectively). Fluid thermocouples above the []^{a,b,c} percent volume layer (TF-530 and TF-548) indicated temperatures above the saturation temperature about []^{a,b,c}. However, two of these thermocouples (TF-526 and TF-532) reflected superheated conditions at []^{a,b,c} after the ADS-3 valve opened and rapid depressurization of the system occurred. TF-556 and TF-564, which are located very close to the same elevation as TF-518 (except closer to the walls), exhibited a later increase only up to the saturation condition temperature at []^{a,b,c} with a temperature of []^{a,b,c} (Figure 5.5.1-57).

Upper-dome inside-wall temperatures indicated a peak wall temperature of []^{a,b,c} at []^{a,b,c} (Figure 5.5.1-58) and slowly decreased to about []^{a,b,c} at []^{a,b,c}. Both the upper-dome temperatures and upper-inside-wall temperatures reached peak temperature values of []^{a,b,c}.

between []^{a,b,c} (Figure 5.5.1-59). Therefore, a []^{a,b,c} temperature difference (fluid temperatures greater than wall temperatures) existed between the wall and the saturated steam volume above the water surface at the []^{a,b,c} point. This common heating of the upper steam in the CMT is explained in more detail in Subsection 7.2.

As accumulator injection was completed and prior to ADS-4 actuation, the upper portion of the cold legs superheated to a temperature of []^{a,b,c} (Figures 5.5.1-32 through 5.5.1-35). On ADS-4 actuation at []^{a,b,c} the cold legs remained superheated while the upper CMT-2 temperatures continued to decrease in temperature, approaching saturation temperature due to limited early dome metal heating. The effect of upper dome heating and some superheating of saturated steam in the upper portion of the CMT had less effect on the lower portion of the CMT. As the CMT continued to drain, the lower inside surface reached saturation temperature late in the transient due to increased surface area to be heated and lack of cold-leg flow entering the CMT during the transition from recirculation mode to draindown. At about []^{a,b,c} the upper layers of the CMT had dropped to slightly above saturation temperature and remained at these conditions until the CL-1 balance line started to refill at about []^{a,b,c} (Figures 5.5.1-36 and 5.5.1-60). The balance line levels increased from a minimum to a maximum from []^{a,b,c} refilling due to level increase (IRWST injection) and slowly condensing any saturated steam. Temperatures in the top of CMT-2 (TF-532; Figure 5.5.1-54) indicated that subcooled liquid had re-entered CL-1 (SC-105; Figure 5.5.1-74). Because the cold leg refilled with subcooled liquid, two-phase liquid also filled the CL-1 balance line.

During this same period, the hot legs and cold legs refilled with water due to injection from the IRWST. At about []^{a,b,c} CL-1 refilled and sealed off the entrance of the CMT balance line with subcooled liquid, and continued to fill the balance line. This isolated the subcooled vapor in CMT-2 by the liquid seal and the check valve located in the discharge line of CMT-2 (Appendix G, Dwg. OSU 600206). As IRWST injection continued and the core/hot-leg levels increased, liquid continued to fill the balance line. The trapped vapor contained in CMT-2 decreased in temperature due to heat loss through the CMT walls. This decrease in temperature lowered the pressure in the CMT, which caused more liquid to fill the balance line. At about []^{a,b,c} the balance line became filled and some liquid flowed into the top of CMT-2 (LDP-510; Figure 5.5.1-36). As more of the liquid entered the top of CMT-2, the slightly subcooled vapor continued to condense, reducing the local pressure and increasing flow into the CMT. At []^{a,b,c} the CMT level was about []^{a,b,c} and all CMT temperatures sharply increased from subcooled, []^{a,b,c} to saturated conditions (Figure 5.5.1-54). This temperature increase, combined with the slow increase in CMT-2 level from []^{a,b,c} over []^{a,b,c} suggests that there was no steam bubble collapsed. Because the pressure in CMT-2 and cold legs were in equilibrium the refill ended.

After refilling stopped, CMT-2 was only partially filled with subcooled water with a []^{a,b,c} temperature difference from the bottom to the top of the liquid layer. There was no flow to the reactor vessel because IRWST injection flow caused higher localized line pressure in the vessel. CMT-2 injection began at []^{a,b,c} as IRWST injection decreased toward the low-low level.

CMT-2 drained empty at []^{a,b,c} and the remaining liquid and vapor stratified (Figure 5.5.1-54).

CMT-1 was filled with subcooled liquid at []^{a,b,c} prior to the inadvertent ADS-1 actuation (break). On break initiation, CMT-1 responded in the same manner as described in the CMT-2 response (Figures 5.5.1-60 and 5.5.1-61). A comparison between the CMT-1 response and the CMT-2 response indicates the following (Figures 5.5.1-53 and 5.5.1-54):

- Both reached upper-dome temperatures of []^{a,b,c} at about []^{a,b,c}
- Both exhibited the transition from recirculation mode to draindown within []^{a,b,c} of each other.
- Both reflected a decrease in injection flow due to accumulator injection.
- Both reflected some upper layer superheating beginning at about []^{a,b,c}
- Both approached saturated temperature conditions about []^{a,b,c} and slowly decreased in temperature to subcooled conditions about []^{a,b,c}
- Both refilled and discharged within []^{a,b,c}. However, CMT-1 refilled with only []^{a,b,c} of water as compared with 11 in. for CMT-2.
- Both reflected stratified temperature profiles after final draindown, but CMT-1 reflected a wider stratified temperature range of []^{a,b,c}

Based on this assessment, the response of CMT-1 is essentially the same as that of CMT-2 as described earlier.

Accumulators

The accumulators were located below the CMTs in the system and provided water injection into the DVI lines by an expansion of nitrogen gas volume stored in the accumulator at an average pressure of []^{a,b,c} set at initial conditions. Water from the accumulators was expelled into the injection line when primary system pressure dropped below []^{a,b,c} for ACC-1 and []^{a,b,c} for ACC-2. Accumulator injection started after ADS-3 actuation with an immediate sharp increase from []^{a,b,c} per accumulator at []^{a,b,c}. This was about []^{a,b,c} following ADS-3 actuation (Figure 5.5.1-11). An average accumulator injection rate of []^{a,b,c} was sustained from []^{a,b,c}. Accumulator injection lasted until about []^{a,b,c} (Figure 5.5.1-62).

Pressurizer

The pressurizer was initially filled with water at a level of about []^{a,b,c} and a temperature of []^{a,b,c}. On inadvertent ADS-1 actuation, liquid inventory was discharged from the top of the pressurizer to the ADS 1-3 separator and reactor vessel level began to decrease (Figure 5.5.1-6). Flow to the ADS 1-3 separator was reflected in a sharp increase in FMM-601 liquid flow from []^{a,b,c} and FVM-601 steam flow (Figure 5.5.1-65). The rapid discharge of flow from the pressurizer caused an initial drop in pressurizer pressure (Figure 5.5.1-5) and RCS pressure, and some initial voiding in the pressurizer (Figure 5.5.1-63). A sharp decrease in ADS 1-3 loop seal flow, from []^{a,b,c} occurred following the trip of the RCPs.

On ADS-2 actuation at []^{a,b,c} an increase in steam percentage from []^{a,b,c} percent occurred in both the pressurizer and surge line (Figure 5.5.1-63). ADS-2 actuation allowed more liquid and steam flow to exit the pressurizer and deplete RCS inventory, as reflected by a sharp increase in ADS 1-3 loop seal flow — from []^{a,b,c} (over-ranged) (Figure 5.5.1-65).

Water in the pressurizer flashed due to the loss of system pressure, and the temperature of the water based on TF-602 (top of pressurizer) dropped from an initial value of []^{a,b,c} before the break to []^{a,b,c} at []^{a,b,c} (Figure 5.5.1-64). The pressurizer was superheated until about []^{a,b,c} and then remained at saturation temperature.

When ADS-3 actuated at []^{a,b,c} temperatures in the upper portion of the pressurizer decreased and the steam percentage increased from []^{a,b,c} percent at about []^{a,b,c} (Figure 5.5.1-63). Just prior to ADS-3 actuation, the hot legs (LDP-208) and the upper plenum (LDP-113) were filled with two-phase fluid with []^{a,b,c} percent steam (Figures 5.5.1-25 and 5.5.1-26). When the ADS-3 valve opened, the pressurizer surge line and the pressurizer already contained a two-phase mixture. The combination of the ADS valve actuation, followed shortly after by the injection of the accumulators and CMTs, caused a high influx in liquid flow through the reactor, which discharged two-phase flow through the pressurizer and exited through the ADS valves. ACC-1 and ACC-2 injection flow increased rapidly from []^{a,b,c} which caused a continued decrease in the pressurizer steam percentage. A steam percentage versus time plot (lower steam percent indicates more water) of the pressurizer and surge line indicates that the pressurizer filled with liquid from []^{a,b,c} (Figure 5.5.1-63). Just prior to []^{a,b,c} steam percentage in the pressurizer and surge line was []^{a,b,c} percent, reflecting a partially empty condition (Figure 5.5.1-63). Figure 5.5.1-65 shows comparison rates of the liquid and steam flow exiting through the ADS valves and ADS 1-3 separator downstream from the ADS 1-3 valves. The liquid flow rate for flow exiting the ADS 1-3 separator showed a peak flow rate of []^{a,b,c} (over-ranged) at about []^{a,b,c} that tapered off to []^{a,b,c} (ADS-4 valve opening).

At []^{a,b,c} (shortly after accumulator injection was completed), the steam percentage in the pressurizer started to increase. The pressurizer steam percentage increased to []^{a,b,c} percent at

[]^{a,b,c} supported by a surge line with a steam percentage of []^{a,b,c} percent (Figure 5.5.1-63).

At []^{a,b,c} the ADS-4 valves opened and caused a further decrease in reactor pressure. As system pressure decreased and IRWST injection flow started, the steam bubble in the surge line became unstable, and liquid from the pressurizer began to drain slowly into the hot legs through the surge line. System depressurization due to ADS-4 actuation ended both steam and liquid flow to the ADS 1-3 separator (Figure 5.5.1-65), and the steam percentage in the pressurizer increased as the liquid volume decreased (Figure 5.5.1-63). Draining of the pressurizer from []^{a,b,c} was reflected by an increase in pressurizer steam percentage.

At []^{a,b,c} the pressurizer and surge line were completely voided and filled with []^{a,b,c} percent steam (Figure 5.5.1-63) with an indicated liquid level of about []^{a,b,c} (Figure 5.5.1-10). The surge line level increased from []^{a,b,c} during the time period from []^{a,b,c} to []^{a,b,c}. Following primary sump injection, surge line level dropped from []^{a,b,c} (Figure 5.5.1-66).

From []^{a,b,c} the pressurizer reflected an increase in level from []^{a,b,c} and remained in this condition for the remainder of the test (Figure 5.5.1-66). It is not clear why the pressurizer refilled during this late part of the transient while the surge line level remained at []^{a,b,c}.

Passive Residual Heat Removal Heat Exchanger

Prior to the initiation of the event, the PRHR HX subsystem was filled with subcooled liquid. At the time the inadvertent ADS-1 valve was actuated, PRHR HX return line valve RCS-804 was opened. Immediately, a flow rate of []^{a,b,c} started through the system because the RCPs remained on until the []^{a,b,c} mark (Figure 5.5.1-9). Figures 5.5.1-67 and 5.5.1-68 show the temperature profile for the PRHR HX throughout the transient. The PRHR HX inlet temperature immediately increased from []^{a,b,c} (within []^{a,b,c}); the outlet temperature increased to about []^{a,b,c}.

PRHR HX inlet and outlet lines contain FMM-802 and FMM-804, respectively, which can produce erratic or inaccurate data for two-phase flow conditions. FMM-802 measured flow from HL-2 to the PRHR HX. As HL-2 emptied, the PRHR HX inlet flow became filled with two-phase liquid. It cannot be determined precisely when the hot leg voided sufficiently to affect the inlet flow measurement. Although the PRHR HX inlet temperature reached saturation temperature at []^{a,b,c} (Figure 5.4.1-67), the state of the fluid was uncertain. However, steam percentage values using the SG-2 hot-leg elbow indicated that voiding of the hot legs was well established when ADS-3 actuated at []^{a,b,c} at which time the rate of voiding in the hot leg increased (Figure 5.5.1-26). Thus, it is certain the data from FMM-802 are invalid after []^{a,b,c}. PRHR HX outlet flow (FMM-804) indicated a flow rate of []^{a,b,c} of []^{a,b,c} liquid occurred from []^{a,b,c}.

During draindown, two-phase mixture that entered the PRHR HX was condensed to a subcooled condition and returned to the bottom of the cold-leg channel head in SG-2. Shortly after ADS-3 actuated, the reactor and hot leg became saturated and followed the saturated curve (TSAT). Flow into the PRHR HX appeared to decrease and almost stop from []^{a,b,c}. During this period, PRHR HX outlet flow (FMM-804) was about []^{a,b,c} (Figure 5.5.1-9).

The PRHR HX levels (LDP-801 and LDP-802) showed that the upper inlet header was drained at about []^{a,b,c} and the HX tubes drained to about []^{a,b,c} by []^{a,b,c}. This time span coincided with draindown of the cold legs, hot legs (Figures 5.5.1-13 and 5.5.1-14), and SG-2 channel head. Over-range spikes were also observed in the PRHR HX outlet flow; inlet flows, though erratic, tended toward a zero flow condition (Figure 5.5.1-9).

At about []^{a,b,c} TF-808 and TF-809 (Figure 5.1.1-67) indicated temperature decreases to []^{a,b,c} (the same temperature as the PRHR HX outlet measured by TF-804). All three thermocouples (TF-808, TF-809, and TF-804) remained at roughly []^{a,b,c} from []^{a,b,c} when a sharp increase in TF-804 (PRHR HX outlet) occurred (Figure 5.1.1-67). Also at this point in time, the PRHR HX inlet temperature dropped from a saturated condition to subcooled, []^{a,b,c}. Since IRWST liquid level still covered the entire PRHR HX, these sharp temperature changes suggest that the entire PRHR HX was completely drained and a low pressure occurred in the HX. This low pressure (vacuum) caused steam from the SG-2 channel head to enter the bottom of the HX, or the liquid level from SG-2 reached the outlet plenum. This was reflected in a sharp increase in TF-804 (Figure 5.1.5-67). From []^{a,b,c} both the wide-range and narrow-range level indicators (LDP-802 and LDP-801) showed a slowly increasing level (Figure 5.5.1-69). It is possible that the HX was refilling, but a more logical possibility is that LDP-802 was slowly losing its reference leg due to a low saturated pressure in the HX tubes.

Shortly after ADS-4, LDP-802 indicated an increase in level. Since the hot-leg levels indicated an empty condition, this suggests that two-phase mixture existed in the hot legs and PRHR HX inlet, allowing steam to be condensed in the HX. However, because of this steam environment and voided tube conditions, the inlet and outlet flow meters and level indicators are considered to exhibit suspect data, and the data only provide a general insight as to the near-term functions occurring in the PRHR HX.

From []^{a,b,c} the PRHR HX appeared to refill to about two-thirds of the total liquid level. However, the upper-head level appeared to partially fill before the main body of the HX, which reached a level of []^{a,b,c} at []^{a,b,c} (Figure 5.5.1-69). The sharp drop in the wide-range PRHR HX level (LDP-802) may be attributed to a condensation event that occurred in the downcomer region and was reflected in several plant instruments. This condensation event also occurred about the time the hot legs reached full condition and the cold legs were beginning to refill due to IRWST injection.

After the condensation event, the levels in both the inlet channel head and HX body indicated a slow refill from []^{a,b,c} as the hot legs and cold legs refilled.

As IRWST flow ended about []^{a,b,c} and primary sump injection initiated, the PRHR HX continued to condense steam generated in the core, but at a slower rate, since the HX was transferring heat to the air in the IRWST instead of to the IRWST water.

In summary, the data indicate that the PRHR HX provided some initial cooling flow to the RCS.

Steam Generators

One long tube and one short tube in each SG were instrumented for level and temperature measurement (Appendix G, Dwg. OSU 600301). The level transmitters measured level in the hot-leg and cold-leg sides of the tubes. Thermocouples in the tubes measured temperature at the top of the tubes and at mid-elevation of both the hot-leg and cold-leg sides.

Within []^{a,b,c} of the inadvertent ADS-1 actuation (break valve opening), the SG tubes started to drain in both SGs (Figure 5.5.1-15). Both SGs U-tubes were essentially drained shortly after ADS-3 actuation at []^{a,b,c} including the hot-leg elbows and cold-leg channel heads (Figures 5.5.1-16). The sequence of tube and channel-head draining is provided in Table 5.5.1-3.

Before the break occurred, steam production in the secondary side of the SG acted as a heat sink to the primary side. Feedwater and steam isolation occurred automatically after the break was initiated (Table 5.5.1-3). The isolation of steam and feedwater "bottled up" the SGs. The SGs acted as a heat sink until pressures in both the SG and primary side reached a common pressure. Initially after the break, pressure of the secondary side increased slightly toward the primary side hot-leg pressure (Figure 5.5.1-19), which at the same time was dropping. Temperature on the primary side was higher than the secondary side, indicating that heat transfer occurred from the primary to the secondary side. After []^{a,b,c} pressure on the SG secondary side and the U-tube primary side reached a common value of []^{a,b,c} and the temperatures reached a common value of []^{a,b,c} (Figure 5.5.1-20). During the first []^{a,b,c} the SG U-tubes were partially emptied and ended the flow through the SG. Transition from recirculation to draindown of the SG and the large heat source of the SG caused the U-tubes to become superheated, and they remained in this condition throughout the transient. With both the hot-leg and cold-leg channel heads empty, superheated steam filled the entire primary side of the SG, which caused fluid temperatures in the region of the RCP inlets to superheat (Figures 5.5.1-32, 5.5.1-33, and 5.5.1-35). As described in the Cold Leg Response, the SGs supplied superheated steam to the cold legs via the differential pressure between the hot legs and the cold legs. Temperature in both the primary and secondary side continued to decrease slowly at a rate of about []^{a,b,c} for the first []^{a,b,c} (Figure 5.5.1-17).

The SG U-tube liquid level instruments (Figure 5.5.1-15) were not providing a true indication of level after the draindown occurred at []^{a,b,c} due to the loss of fluid in the reference and variable

legs (this generic instrument measurement effect was described in Subsection 2.4). Therefore, the SG U-tube level values are not applicable after tube draindown starts. In summary, the SGs completely drained shortly after ADS-3 actuation. The steam in the tubes superheated when RCS pressure decreased below secondary steam pressure. Superheating of all tubes was completed at []^{a,b,c} after ADS-3 actuation, and the tubes remained superheated for the rest of the test. The SGs supplied superheated steam to the cold legs, with the differential pressure between the hot legs and cold legs supplying the head for flow.

Cold Legs and Hot Legs

The inadvertent actuation of the ADS-1 valve caused immediate draining of the upper head and upper plenum as liquid exited the RCS through the pressurizer and saturated steam began forming in the upper head. In []^{a,b,c} the upper head was about []^{a,b,c} percent drained, and the upper plenum was also partially drained. The draining of the upper head and upper plenum are indicated by drops in liquid levels (LDP-115 and LDP-113) and increases in steam percentage of these same instruments (Figures 5.5.1-7 and 5.5.1-25).

By about []^{a,b,c} the cold legs (initially full of single-phase liquid) showed an initial drop in levels (Figure 5.5.1-13). HL-1 and HL-2 also indicated a similar draining at []^{a,b,c} (Figure 5.5.1-14). This was consistent since the SG U-tubes and channel head became drained by []^{a,b,c}. As the levels in the cold legs began to drop below the top of the pipe, flow to CMT-2 through the balance line stopped. As the SG drained, pressures in both the reactor vessel and the secondary side of the SG were coming to a common pressure and temperature. As the SG continued to provide a heat source, superheated steam filled the primary side of the SG just above the top layer of the partially drained cold legs, as evidenced by the superheated temperatures of thermocouples TF-201, TF-202, and TF-204 at the top of the RCP casing, about []^{a,b,c} above the top surface of the cold legs (Figures 5.5.1-32, 5.5.1-33, and 5.5.1-35). Based on temperatures in the upper portion of the downcomer, superheated steam occupied the top layers of the cold legs beginning at []^{a,b,c} (Figure 5.5.1-21).

From []^{a,b,c} the top layers of the cold legs exhibited peak temperatures of about []^{a,b,c} initially the same as the downcomer temperature (TF-168). Superheated steam was filling the very top layer of the cold legs with the exception of times when condensation events occurred (about []^{a,b,c}). A negative value of DP-130 (less than approximately []^{a,b,c}) indicates steam entered the cold leg from the upper head (Figure 5.5.1-27).

The formation of superheated steam in the cold legs can be explained by the rapid depressurization of the RCS. However, the cold legs remained at superheated temperatures for a significant duration of the test (Figures 5.5.1-32 through 5.5.1-35). This could have occurred only if a source of thermal energy was available to the cold legs.

The only possible sources of thermal energy to the cold legs were:

- Heating of steam in the cold legs by cold-leg piping
- Addition of superheated steam from the SGs
- Addition of superheated steam from the upper head via the bypass holes in the core barrel flange
- Combination of heat from the SGs and/or upper head at different times

Superheating of the cold legs from the upper head is not likely. The temperature of the upper head is close to the fluid temperatures of the cold legs at the reactor vessel flange, but the upper head temperature decays faster than the cold-leg fluid temperatures (Figure 5.5.1-29).

If the steam in the cold legs was maintained at a superheated condition by the walls of the cold legs, the pipe temperature on the inside wall of the pipe would have been greater than the cold-leg fluid temperature. There were no inside-wall thermocouples in the cold-leg piping to measure temperature on the inside wall of the cold leg. The only cold-leg wall thermocouples were part of the heat flux meters (HFM) mounted on the outside wall of the piping. These thermocouples were given a TFM designation. A thermocouple was mounted on each cold leg at the top of its flanged connection to the reactor vessel (Appendix G, Dwg. OSU 600101, Sh. 2). The recorded temperature of the thermocouples mounted at the top of the reactor vessel flange was greater than the recorded temperature of the thermocouples mounted on the side of the pipe, so the hotter flange thermocouples were used for evaluation.

Figures 5.5.1-72, 5.5.1-73, and 5.5.1-74 show the vessel/piping metal effects on the cold-leg temperatures and supports the previous discussion. Early in the transient, with the reactor temperatures in the vessel and cold legs at []^{a,b,c} the piping and upper support plate were exposed to temperatures between []^{a,b,c} respectively (TFM-111 and TF-171). TF-171 was located []^{a,b,c} above the upper support plate and measured localized fluid temperatures, but was significantly influenced by the metal plate temperature based on the distance from the plate. TFM-111 was located on the exterior of the CL-1 piping flange, roughly []^{a,b,c} from the downcomer/cold-leg interface. TFM-111 indicated a lower external temperature than the interior wall temperature, based on through-wall heat conduction.

As the upper head and plenum rapidly drained in []^{a,b,c} these metal temperatures (upper support plate and cold-leg piping) only dropped slightly to []^{a,b,c} respectively (Figure 5.5.1-72). The reactor vessel continued to depressurize via ADS-2 and ADS-3 valve opening, allowing the saturated steam in the upper head to reach superheated conditions based on the combined depressurization and hotter metal temperature of the upper support plate. This superheated steam filled the top of the downcomer via the bypass holes until it reached the top of the cold leg. The hotter

metal temperatures in the cold legs and the possible steam feed from the SG (higher superheated conditions shown by TF-201) maintained the upper layer of the cold legs at superheated conditions. The ADS-4 valve opening continued to reduce reactor pressure and permitted the initiation of IRWST injection flow, which started a refilling of the loops and cooling of the superheated steam in the cold legs at []^{a,b,c} (Figure 5.5.1-74). The piping metal temperatures showed little effect on the fluid temperatures, beginning at []^{a,b,c}. The cold-leg temperatures (SC-101, SC-102, SC-105, and SC-106) remained significantly above saturated conditions until the cold legs became refilled with subcooled water, beginning at []^{a,b,c}. All the cold-leg fluid and piping metal temperatures became subcooled at []^{a,b,c} after the hot legs and cold legs were completely refilled (Figure 5.5.1-74).

It should be noted that during Matrix Test SB14 from about []^{a,b,c} the temperatures of the bottom thermocouples in the cold legs reached superheated conditions over long durations of time (Figures 5.5.1-32 through 5.5.1-35). In addition, CL-2 and CL-4 temperatures at the RCP inlet flange (TF-202 and TF204, respectively) reached superheated conditions shortly after ADS-4 actuation.

Both the cold legs and hot legs became drained of liquid at approximately []^{a,b,c} respectively, and the hot legs were filled with saturated steam. The loops became void of liquid (Figures 5.5.1-13 and 5.5.1-14) until after accumulator, CMT, and IRWST injection provided adequate inventory for the loops to become refilled. The hot-leg piping metal temperatures had no significant effect on the temperature profiles in the hot legs (Figure 5.5.1-75).

Figure 5.5.1-75 shows that early in the transient, externally mounted thermocouples on the hot legs (TFM-113 and TFM-114 located on the top of HL-1 and HL-2 flanges, respectively) indicated temperatures of []^{a,b,c}. These temperatures slowly decayed even though the fluid temperatures in the hot legs remained saturated and decreased along the saturation line (Figures 5.5.1-76, 5.5.1-77, and 5.5.1-78). The hot-leg temperatures became subcooled beginning about []^{a,b,c} as indicated by the drop in temperature of the HL-2 and HL-1 thermocouples at the reactor vessel flange (SC-140 and SC-141). The response of TF-171, which measures the fluid temperature locally above the upper support plate, showed an early temperature increase above the saturation temperature (TSAT) line, suggesting that this plate, once exposed to the higher fluid temperature, was helping to superheat any saturated steam passing through the plate to the upper head.

The levels in both the cold legs and hot legs remained stable until about []^{a,b,c} (Figures 5.5.1-80 and 5.5.1-82, respectively) when the flow from the IRWST decreased and the CMT-1 and CMT-2 flows (from refill) ended, causing a drop in the vessel, downcomer, hot-leg, and cold-leg levels (LDP-127, LDP-116, and LDP-140; Figure 5.5.1-38). Based on the cold-leg levels, all four of the cold-leg levels dropped by []^{a,b,c} (Figure 5.5.1-80).

As primary sump injection started at []^{a,b,c} the cold-leg levels remained empty (LDP-201 through LDP-204; Figure 5.5.1-80). The downcomer wide-range levels (LDP-116 and LDP-140)

confirmed that the downcomer level was at []^{a,b,c} relative to LDP-140. The cold-leg temperatures remained subcooled from about []^{a,b,c} (Figure 5.5.1-81). As the primary sump injection occurred, saturated water at about []^{a,b,c} started injecting, which caused the cold leg to reach the saturated temperature conditions.

The hot-leg levels appeared to indicate a full condition at about []^{a,b,c} based on LDP-205 and LDP-206 (Figure 5.5.1-82). The reactor wide-range level indicated a level of []^{a,b,c} relative to LDP-127, which suggests the core and hot-leg levels would be at or slightly above the bottom of the hot-leg pipe. The hot-leg temperatures were subcooled from []^{a,b,c} (Figure 5.5.1-83). These hot-leg temperatures then increased to about []^{a,b,c} and remained there for the duration of the test.

In-Containment Refueling Water Storage Tank

The thermal response of the IRWST was influenced by the heat addition of the PRHR HX and the direct injection of hot liquid from the ADS 1-3 separator. Initially, a []^{a,b,c} temperature difference existed from the top to the bottom, with the bottom at []^{a,b,c} (Figure 5.5.1-84). For Matrix Test SB14, the inadvertent actuation of the ADS-1 valve and the opening of the PRHR HX outlet valve caused a sharp overall temperature increase of []^{a,b,c} throughout the tank from []^{a,b,c}. This overall temperature increase was primarily due to the large injection of RCS water at []^{a,b,c} to the IRWST. From []^{a,b,c} approximately []^{a,b,c} of water entered the IRWST and was subsequently diverted by the overflow line to the primary sump.

As the ADS-2, ADS-3, and ADS-4 valves were opened ([]^{a,b,c}), the upper layers of the tank increased from []^{a,b,c} locally. After the opening of ADS-4 valves, the flow to the IRWST via the ADS 1-3 separator decreased significantly. The temperature gradient remained with a stable temperature difference of []^{a,b,c}. With the continued heating due to the PRHR HX, the upper half of the IRWST increased to a []^{a,b,c} average temperature (TF-710, TF-709, and TF-707).

From []^{a,b,c} the level in the IRWST continued to drop, uncovering the bottom of the PRHR HX. The hot-leg level dropped so that a steam vent path occurred from the core to the pressurizer via the surge line (Figures 5.5.1-82 and 5.5.1-66). As steam entered the surge line and pressurizer, the pressurizer acted as a separator where steam entered the ADS 1-3 separator and water was collected in the surge line and pressurizer. Saturated steam that exited the pressurizer through the ADS valves was separated and a small quantity of saturated water entered the IRWST via the sparger (Figure 5.5.1-86) in a fluctuating flow. This saturated water raised air temperature, as measured by TF-705, TF-707, and TF-710, from about []^{a,b,c}. FMM-601 showed a fluctuating ADS 1-3 separator flow with a discharge temperature of []^{a,b,c} (TF-719) at []^{a,b,c}.

At []^{a,b,c} the IRWST was drained below the PRHR HX tubes with about []^{a,b,c} of []^{a,b,c} water (Figure 5.5.1-85). The upper IRWST temperatures were based on thermocouples exposed to the tank ambient temperature during draindown, which increased due to saturated liquid

flow from the ADS 1-3 separator to the sparger. At this time, the primary sump isolation valves opened and some primary sump water backflowed through IRWST-1, indicated by negative flow (FMM-701; Figure 5.5.1-86). Flow from the IRWST continued through IRWST-2 line at a rate of about []^{a,b,c} from []^{a,b,c} to the end of the test (Figure 5.5.1-44). The backflow of water from the primary sump to the IRWST and some flow from the ADS 1-3 separator caused a slight increase in water temperature (TF-701).

5.5.1.6 Mass Balance

The mass balance results for Matrix Test SB10 were calculated based on water inventory before and after Matrix Test SB14 and are provided in Appendix E. The inventory at the end of test is within []^{a,b,c} percent of the inventory at the beginning of the test. It should be noted that following adjustments were made to the calculation:

- LDP-208 value was used instead of LDP-207.
- LDP-214 value was used instead of LDP-209.
- LDP-219 was set to 0 to reflect the empty SG U-tubes.

5.5.1.7 Conclusions

The test was performed with minimal problems and is considered acceptable. Although not all of the instruments met the specified acceptance criteria, the deviations did not impact the quality of the data. The instrumentation problems encountered were not critical to the performance of an overall mass and energy balance.

Facility response to the test was as anticipated for the conditions that were established. The data clearly demonstrate that cooling of the reactor heater rods was maintained throughout the duration of test.

**TABLE 5.5.1-1
MATRIX TEST SB14 INITIAL CONDITIONS**

Parameter	Instrument No.	Specified Initial Condition	Actual Initial Condition	Comments
Pressurizer pressure ⁽¹⁾	PT-604	370 ± 2 psig	— a,b,c	
HL-1 temperature ⁽¹⁾	SC-141	420 ± 2°F		
HL-2 temperature ⁽¹⁾	SC-140	420 ± 2°F		
SG-1 pressure ⁽¹⁾	PT-301	285 ± 5 psig		
SG-2 pressure ⁽¹⁾	PT-302	285 ± 5 psig		
Pressurizer level ⁽¹⁾	LDP-601	65 ± 5 in.		Level signal temperature-compensated by TF-605
SG-1 narrow-range level ⁽¹⁾	LDP-303	26 ± 3 in.		Level signal temperature-compensated by TF-301
SG-2 narrow-range level ⁽¹⁾	LDP-304	26 ± 3 in.		Level signal temperature-compensated by TF-310
IRWST temperature ⁽²⁾	TF-709	< 80°F		
CMT-1 temperature ⁽²⁾	TF-529	< 80°F		
CMT-2 temperature ⁽²⁾	TF-532	< 80°F		
ACC-1 temperature ⁽²⁾	TF-403	< 80°F		
ACC-2 temperature ⁽²⁾	TF-404	< 80°F		
IRWST level ⁽²⁾	LDP-701	Level established by fill line elevation		
ACC-1 level ^(2,3)	LDP-401	Level established by standpipe at 37 in.		Accepted; accumulator level was fixed by a standpipe
ACC-2 level ^(2,3)	LDP-402	Level established by standpipe at 37 in.		Accepted; accumulator level was fixed by a standpipe
ACC-1 pressure ⁽²⁾	PT-401	232 ± 2 psig		
ACC-2 pressure ⁽²⁾	PT-402	232 ± 2 psig	—	Pressure was [] ^{a,b,c} or [] ^{a,b,c} low; condition acceptable

TABLE 5.5.1-1 (Continued)
MATRIX TEST SB15 INITIAL CONDITIONS

Parameter	Instrument No.	Specified Initial Condition	Actual Initial Condition	Comments
CMT-1 level ⁽²⁾	LDP-507	Full	<input type="checkbox"/> a,b,c	
CMT-2 level ⁽²⁾	LDP-502	Full	<input type="checkbox"/>	

Note:

- (1) Data for the indicated parameter were recorded in the test procedure as an initial condition for the test. The value was determined by the test engineer from the appropriate control board indicator.
- (2) Data were not recorded in the procedure, but the test engineer verified specified conditions were achieved while establishing initial conditions. The value of the parameter was determined post-test by calculating the average DAS indication for a time of about 2 minutes before the break valve opened.
- (3) The bourdon pressure tube local indicator (PI-401 or PI-402) was tubed to the lower portion of the reference leg of the accumulator level transmitter (LDP-401 or LDP-402). As pressure in the accumulator was increased, air inside the bourdon tube was compressed, thereby lowering the reference leg liquid level, resulting in a false indication of measured level.

TABLE 5.5.1-2
MATRIX TEST SB14 INOPERABLE INSTRUMENTS/INVALID DATA CHANNELS

Instrument No.	Instrument Type	Inoperable Description
FDP-604* FDP-605*	Flow differential pressure transmitter	Over-ranged with initial flow
FMM-201* FMM-202* FMM-203* FMM-204*	Magnetic flow meter	Removed from system due to mechanical failure
FMM-401* FMM-402*	Magnetic flow meter	Data invalid after 400 seconds due to nitrogen in line; meter can not measure steam, vapor, or two-phase flow
FMM-501*	Magnetic flow meter	Data invalid between 1044 and 4700 seconds and after 8000 seconds when CMT was empty
FMM-504*	Magnetic flow meter	Data invalid between 982 and 5100 seconds and after 8300 seconds when CMT was empty
FMM-502	Magnetic flow meter	Data invalid after 86 seconds due to possible steam in balance line; meter can not measure steam or two-phase flow
FMM-503	Magnetic flow meter	Data invalid after 70 seconds due to possible steam in balance line; meter can not measure steam or two-phase flow
FMM-601*	Magnetic flow meter	Momentarily over-ranged with initial flow
FMM-701*	Magnetic flow meter	Data for negative flow invalid; negative flow existed after sump valves open, but meter not designed to measure negative flow
FMM-703	Magnetic flow meter	Momentarily over-ranged with initial flow
FMM-802*	Magnetic flow meter	Data invalid after steam formed in PRHR HX inlet line; uncertain when this occurred, but likely 28 seconds after break
FMM-804*	Magnetic flow meter	Data valid until PRHR HX initially drained at 200 seconds; after this time; possibility of steam in outlet line invalidated data
FMM-902*	Magnetic flow meter	Data invalid from 0 to 12,000 seconds due to zero shift before flow occurred; may be due to air in line
FMM-905*	Magnetic flow meter	Data for negative flow invalid; negative flow existed after primary sump level \geq break separator level, but meter not designed to measure negative flow

TABLE 5.5.1-2 (Continued)
MATRIX TEST SB14 INOPERABLE INSTRUMENTS/INVALID DATA CHANNELS

Instrument No.	Instrument Type	Inoperable Description
HFM-103 HFM-105 HFM-112 HFM-505 HFM-703 HFM-902 HFM-201 HFM-601	Heat flux meter	Failed
HPS-203-1 through HPS-203-3 HPS-509-1 through HPS-509-3	Heated phase switch	Failed
LDP-201 LDP-202 LDP-203 LDP-204 LDP-205 LDP-206	Differential pressure transmitter - level	Data invalid due to effect of vertical portion of sense line attached to top of pipe; data can show level trends, when pipe is empty or starts to drain, but absolute level indication can not be used
LDP-207 LDP-208 LDP-209	Differential pressure transmitter - level	Level values invalid due to incorrect calibration range for specific tap location
LDP-215* LDP-216 LDP-217 LDP-218* LDP-219* LDP-220 LDP-221 LDP-222*	Differential pressure transmitter - level	Data can not be used directly, but must be interpreted because reference legs boil as SGs drain (Subsection 2.4)
LDP-401* LDP-402*	Differential pressure transmitter - level	Data invalid (note 3 in Table 5.5.1-2)
LDP-502*	Differential pressure transmitter - level	Data unavailable because this channel used to initiate transient
LDP-802* LDP-804	Differential pressure transmitter - level	Data valid until PRHR initially drained at 600 seconds; after this time, data suspect due to possible boiling of common reference line of LDP-802 and LDP-804
PT_101	Pressure transmitter	Data less than 6.1 psig invalid
PT_102 PT_103	Pressure transmitter	Data less than 6.2 psig invalid

TABLE 5.5.1-2 (Continued)
MATRIX TEST SB14 INOPERABLE INSTRUMENTS/INVALID DATA CHANNELS

Instrument No.	Instrument Type	Inoperable Description
PT_104	Pressure transmitter	Data less than 6.4 psig invalid
PT_108	Pressure transmitter	Data less than 8.4 psig invalid
PT_109	Pressure transmitter	Data less than 6.3 psig invalid
PT_111	Pressure transmitter	Data less than 6.0 psig invalid
PT_112	Pressure transmitter	Data less than 8.8 psig invalid
PT_113	Pressure transmitter	Data less than 6.4 psig invalid
PT_201*	Pressure transmitter	Data less than 1.1 psig invalid
PT_202	Pressure transmitter	Data less than 5.9 psig invalid
PT_205	Pressure transmitter	Data less than 6.1 psig invalid
TF-170	Thermocouple	Unavailable due to leaking O-ring in core barrel
TF-203 TF-615 TF-619	Thermocouple	Failed because of invalid data
TFM-103 TFM-105	Thermocouple for heat flux meter	Failed
TH-317-1 through TH-317-4	Thermocouple	Removed with heater rod C2-317
TW-210 TW-503 TW-552 TW-534	Thermocouple	Failed

Note:

*Instruments marked with an asterisk are critical instruments. See Subsection 5.5.1.2 for discussion.

**TABLE 5.5.1-3
MATRIX TEST SB14 SEQUENCE OF EVENTS**

Event⁽¹⁾	Description in Bar Chart⁽²⁾	Data Source⁽³⁾	Time After Break (sec.)
TEST Pushbutton Pressed	TEST PB Pressed	D	
Break Valve Open Signal (CMT-2 Low-Level)	Break Vlv Open Sig	D	
PRHR HX Outlet Valve Starts to Open	PRHR HX Vlv Open	D	
ADS-1 Valve Starts to Open (Break)	ADS-1 Vlv Open (Break)	D	
Feed Pump Trips	Feed Pump Trips	D	
CMT-1 Outlet Valve Starts to Open	CMT-1 Inj Vlv Open	D	
CMT-2 Outlet Valve Starts to Open	CMT-2 Inj Vlv Open	D	
Reactor Coolant Pumps Trip	RCPs Trip	D	
ADS-2 Valve Starts to Open	ADS-2 Vlv Open	D	
CMT-2 Circulation Flow Stops (LDP-510)	CMT-2 Recirc Flow Stops	A	
SG-1 Cold-Leg Short Tube Empty (LDP-221)	SG-1 CL Sht Tube Empty	A	
SG-1 Cold-Leg Long Tube Empty (LDP-219)	SG-1 CL Lng Tube Empty	A	
SG-2 Cold-Leg Long Tube Empty (LDP-222)	SG-2 CL Lng Tube Empty	A	
CMT-1 Circulation Flow Stops (LDP-509)	CMT-1 Recirc Flow Stops	A	
SG-2 Cold-Leg Short Tube Empty (LDP-220)	SG-2 CL Sht Tube Empty	A	
SG-2 Hot-Leg Short Tube Empty (LDP-216)	SG-2 HL Sht Tube Empty	A	
SG-2 Hot-Leg Long Tube Empty (LDP-218)	SG-2 HL Lng Tube Empty	A	
HL-2 Pipe Starts to Drain (LDP-206)	HL-2 Pipe Starts Drain	A	
CL-3 Channel Head Empty (LDP-213)	CL-3 Chan Head Empty	A	
HL-1 Pipe Starts to Drain (LDP-205)	HL-1 Pipe Starts Drain	A	
CL-1 Channel Head Empty (LDP-211)	CL-1 Chan Head Empty	A	
ADS-3 Valve Starts to Open	ADS-3 Vlv Open	D	
SG-2 Hot-Leg Channel Head Empty (LDP-214)	SG-2 HL Chan Head Empty	A	
ACC-1 Injection Starts (FMM-401)	ACC-1 Inj Starts	A	
CL-4 Channel Head Empty (LDP-212)	CL-4 Chan Head Empty	A	

TABLE 5.5.1-3 (Continued)
MATRIX TEST SB14 SEQUENCE OF EVENTS

Event ⁽¹⁾	Description in Bar Chart ⁽²⁾	Data Source ⁽³⁾	Time After Break (sec.)
ACC-2 Injection Starts (FMM-402)	ACC-2 Inj Starts	A	
SG-1 Hot-Leg Long Tube Empty (LDP-215)	SG-1 HL Lng Tube Empty	A	
CL-2 Channel Head Empty (LDP-210)	CL-2 Chan Head Empty	A	
SG-2 Hot-Leg Elbow Starts Draining (LDP-208)	HL-2 Elbow Starts to Drain	A	
SG-1 Hot-Leg Short Tube Empty (LDP-217)	SG-1 HL Sht Tube Empty	A	
HL-2 Pipe Empty (LDP-206)	HL-2 Pipe Empty	A	
Time of Minimum Reactor Level Observed During Test (LDP-127)	Time of Min Reactor Level	A	
HL-1 Pipe Empty (LDP-205)	HL-1 Pipe Empty	A	
Reactor Pressure Low	Reactor Pressure Lo	D	
IRWST-2 Injection Valve Starts to Open	IRWST-2 Inj Vlv Open	D	
IRWST-1 Injection Valve Starts to Open	IRWST-1 Inj Vlv Open	D	
CMT-2 Low Level Signal*	CMT-2 Level Lo	D	
ACC-2 Empty (LDP-402)	ACC-2 Empty	A	
ACC-1 Empty (LDP-401)	ACC-1 Empty	A	
CMT-1 Low Level Signal	CMT-1 Level Lo	D	
CMT-2 Level Low-Low*	CMT-2 Level Lo-Lo	D	
ADS 4-1 Valve Starts to Open	ADS 4-1 Vlv Open	D	
ADS 4-2 Valve Starts to Open	ADS 4-2 Vlv Open	D	
CMT-1 Level Low-Low	CMT-1 Level Lo-Lo	D	
CMT-2 Empty (LDP-502)*	CMT-2 Empty	A	
IRWST-2 Injection Starts (FMM-702)	IRWST-2 Inj Starts	A	
IRWST-1 Injection Starts (FMM-701)	IRWST-1 Inj Starts	A	
CMT-1 Empty (LDP-507)	CMT-1 Empty	A	
Pressurizer Empty (LDP-601)	Pressurizer Empty	A	
Pressurizer Surge Line Empty (LDP-602)	Surge Line Empty	A	
CMT-1 Starts to Reflood (LDP-507)	CMT-1 Refloods	A	
CMT-2 Starts to Reflood (LDP-502)*	CMT-2 Refloods	A	

TABLE 5.5.1-3 (Continued)
MATRIX TEST SB14 SEQUENCE OF EVENTS

Event ⁽¹⁾	Description in Bar Chart ⁽²⁾	Data Source ⁽³⁾	Time After Break (sec.)
Primary Sump-2 Injection Starts (FMM-902)	Pri Sump-2 Inj Starts	A	a,b,c
Primary Sump Starts to Overflow to Secondary Sump (LDP-901)	Pri Sump Overflows	A	
Primary Sump-1 Injection Starts (FMM-901)	Pri Sump-1 Inj. Starts	A	
Pressurizer Refloods (LDP-601)	Pressurizer Refloods	A	
Primary Sump-1 Injection Valve Starts to Open	Pri Sump-1 Inj Vlv Open	D	
Primary Sump-2 Injection Valve Starts to Open	Pri Sump-2 Inj Vlv Open	D	
SG-1 Hot-Leg Channel head Empty (LDP-209)	SG-1 HL Chan Head Emp	A	
SG-1 Hot-Leg Elbow Starts Draining (LDP-207)	HL-1 Elbow Starts to Drain	A	
SG-1 Hot-Leg Elbow Minimum (LDP-207)	HL-1 Elbow Level Min	A	
SG-1 Hot-Leg Elbow Minimum (LDP-207)	HL-2 Elbow Level Min	A	

Note:

- (1) Data from the instrument channel in parenthesis were used to determine level, flow, or pressure conditions.
- (2) The attached bar chart provides a graphic representation of the timing of events.
- (3) D = time data obtained from a software program that monitored the input and output of the facility's PLC.
A = time data obtained by reviewing data from the instrument channel listed in the Event Description.
- (4) O.O.S. = out of service
- (*) Data obtained from alternate instruments LDP-506 and LDP-504 for this test.

The Bar Charts for Table 5.5.1-3 on pages 5.5.1-42 through 5.5.1-46 are not included in this nonproprietary document.

Figures 5.5.1-1 through 5.5.1-88 are not included in this nonproprietary document.

5.5.2 Multiple ADS Failures (Matrix Test SB26)

This section identifies and describes the response of the system based on a comparison between Matrix Test SB14 (OSU Test U0014), simulated inadvertent ADS-1 actuation, and Matrix Test SB26 (OSU Test U0126), simulated inadvertent ADS actuation with multiple ADS failures. Matrix Test SB26 was configured to simulate complete failure of the ADS-1 valve; therefore, the opening of the ADS-2 valve initiated break flow. Matrix Test SB26 also simulated failure of both ADS-4 lines. The PRHR HX was not operable. Both tests were performed using the same simulated break location, but differed by the size of the ADS valve opening (break) and the number of assumed failures.

Matrix Test SB26 was performed on August 29, 1994 with a test duration of about 3.0 hours. The test performed met the specified initial conditions. Any exceptions to the initial conditions are discussed in Subsection 5.5.2.1. The transient began with inadvertent ADS actuation (break) and continued through ADS actuation, and CMT, accumulator, and some IRWST injection. The test ended prematurely before primary sump injection. Matrix Test SB26 exhibited a response consistent with Matrix Test SB14 up to the point of ADS-4 actuation. Due to the lack of depressurization from ADS-4 actuation (planned simulation of ADS-4 failure), IRWST injection was limited to periodic short-term injection that did not adequately reduce reactor pressure or supply water inventory to maintain cooling of the heater bundle throughout the event. The core water inventory level exhibited in Matrix Test SB26 was significantly less than that in reference test SB14.

Subsection 5.5.2.1 provides details related to test configuration and initial conditions.

Subsection 5.5.2.2 defines inoperable instruments or time ranges for which data may not be valid.

Subsection 5.5.2.3 lists the sequence of events. Subsections 5.5.2.4 and 5.5.2.5 describe the overall summary of the system response and any component-specific differences from the reference test, respectively. A summary of the mass balance results is provided in Subsection 5.5.2.6. Conclusions, as they apply to Matrix Test SB26, are provided in Subsection 5.5.2.7.

5.5.2.1 System Configuration and Initial Conditions

Matrix Test SB26 was performed according to an approved written procedure. It simulated inadvertent ADS actuation with multiple ADS failures and the PRHR HX inoperable. Break simulation piping and break instrumentation were not required for this test, and blank inserts were installed in the break piping based on the piping and instrumentation diagrams (Appendix G, Dwg. OSU 600904). Inadvertent ADS actuation (break) discharge flow was piped to the ADS 1-3 separator and, subsequently, to the IRWST.

An inadvertent ADS actuation LOCA does not require special break spool piping arrangements. Liquid flow was measured by FMM-601; steam flow was measured by FVM-601 (Appendix G, OSU Dwgs. 600203 and 600206). Discharge flow from the ADS 1-3 separator was directed to the IRWST via the sparger. Any overflow from the IRWST due to rapid increase in liquid volume passed

to the primary sump via the overflow line. Flow through the overflow line was measured by FMM-703.

The ADS-1 valve was isolated by closing valve RCS-601 and disconnecting the air supply. The flow nozzles used in the ADS-2 and ADS-3 valves were configured to represent two lines of flow. The ADS 4-1 and ADS 4-2 lines were isolated by manually closing valves RCS-615 and RCS-616 and preventing any flow through the ADS-4 valves. The PRHR HX was also isolated by manually closing valve RCS-804. The valve alignment for measuring steam discharge from the BAMS was the same for Matrix Tests SB26 and SB14 (Appendix G, OSU Dwg. 600901).

The nonsafety systems were not in operation for this test. The CVS and RNS pumps did not run.

Prior to Matrix Test SB26, thermocouples TF-103 and TF-104 were removed from CL-3 and CL-4, respectively, and replaced with two thermocouple rods that contained six thermocouples per rod to characterize thermal stratification in the cold legs. The new thermocouple rods were connected to two Fluke HYDRA data buckets capable of monitoring 20 channels each. The output was not included in the DAS; however, thermocouples TF-103 and TF-104 still provided an indication of ambient conditions. This indication was invalid and should not be used for code evaluation.

Water hammer detection equipment (i.e., additional pressure transmitters) was installed before Matrix Test SB26 was initiated. The instrumentation was installed and calibrated in accordance with facility operating procedures. Installation of the water hammer detection instrumentation had no effect on any other installed instrumentation.

Pre-test operations such as fill and vent processes were performed. They are defined in greater detail in Subsection 2.7.

As final valve alignments were established, CMT discharge valves were placed in the AUTO and CLOSED positions. One minute after the test pushbutton was actuated, RCS-529 and RCS-530 were opened. The balance line and CMT-1 reached RCS pressure.

Testing was initiated when test facility conditions, as read from the test facility control board and local indication, agreed with specified initial conditions within acceptable tolerances. The transient continued through ADS actuation, and CMT, accumulator, and IRWST injection. All actions were automatic and required no operator action.

Note: ADS actuation occurs on CMT low level. To achieve ADS actuation, a Rosemount 268 communicator was attached to LDP-502 so that the operator could induce a CMT low level signal. An inducement of a 13.50-mA signal simulated a 35-in. level in CMT-2. This is below the low level setpoint but above the low-low level setpoint. On initiation of the CMT low level signal, a delay of 15 seconds occurs before a signal is sent to RCS-601 to open.

Heater rod bundle power was adjusted prior to break initiation in order to achieve the required hot-leg temperatures. Pressurizer power was terminated at break initiation.

Table 5.5.2-1 provides a comparison of the specified and actual conditions for Matrix Test SB26. A zero check was performed for all differential pressure instruments. Initial conditions for the test were established and recorded in the procedure. The control board contained provisions to display compensated level indications to confirm initial conditions. Table 5.5.2-1 shows the initial conditions recorded from the operator's panel and the average of some parameters for about 2 minutes prior to the break valve opening from the DAS.

There were two initial condition parameters out of specification. Neither should invalidate the test.

- Accumulator levels, indicated by LDP-401 and LDP-402, exceeded the planned levels. The explanation for this is defined in Note 3 of Table 5.5.2-1. The condition was considered acceptable because the level was set by a standpipe at 37 in.
- ACC-1 pressure, indicated by PT-401, was 4.3 psig or 1.8 percent below the required pressure band. ACC-2 pressure, indicated by PT-402, was 10.3 psig or 4.6 percent below the required pressure band. The accumulator was pressurized to the required pressure prior to test actuation. The loss of pressure between tank pressurization and test actuation was possibly due to nitrogen gas cooling in the accumulator. Test analysis starting with the recorded lower accumulator overpressure should still be possible.

Each of the two reactor heater power controllers were programmed using the same algorithm (Subsection 2.3.2) as in Matrix Test SB14 to obtain the scaled decay power heat input rate. The heater rod groups produced power input consistent with Matrix Test SB14, and the comparison plots of the decay heat power curves are reflected in Appendix F.

5.5.2.2 Inoperable Instruments

Table 5.5.2-2 provides a listing of the instrumentation channels considered inoperable and/or possessing limited applicability for Matrix Test SB26. Some of the instruments listed are on the Critical Instrument List (Subsection 3.2, Table 3.2-2) and, therefore, are addressed here.

FDP-604 measured the differential pressure (in. H₂O) across the ADS-2 flow nozzle. The transmitter over-ranged momentarily when the ADS valve opened. Total flow through the ADS 1-3 valve complex can be determined by measuring ADS 1-3 separator liquid (FMM-601) and steam flows (FVM-601) and any water held up in the ADS 1-3 separator.

FMM-201, FMM-202, FMM-203, and FMM-204 measured flow (gpm) in each of the four cold legs. A decision was made to continue testing without the availability of these instruments. Replacement flow meters repeatedly failed; their continued use was precluded due to cracking of the ceramic liners

from thermal stratification in the loop piping. The necessary boundary conditions for loop flow could be determined from cold-leg differential pressure transmitters DP-202, DP-203, DP-205, and DP-206.

FMM-401 measured ACC-1 injection flow into DVI-1. After injection, the meter exhibited erroneous results due to nitrogen in the line; therefore, any results after 500 seconds are invalid.

FMM-501 and FMM-504 provided accurate data when measuring liquid solid, but became inaccurate when sensing two-phase or steam flow.

FMM-902 measured primary sump injection flow. Data provided by FMM-902 were invalid due to the closed position of the valve. The valve never opened due to the premature test termination.

SG-tube level data (LDP-215, LDP-218, LDP-219, and LDP-222) were biased by vaporization of the water in the transmitter reference leg after the SG tubes started draining. However, the data provide accurate indication of the time when the tubes are empty.

LDP-502 measured wide-range CMT-2 level. This channel was used to actuate the inadvertent ADS transient as described in the Note in Subsection 5.5.2.1. Therefore, a constant 35-in. output signal was indicated throughout the transient. The sum of LDP-504, LDP-506, and LDP-508 provide the true CMT-2 level.

TF-501 and TF-504 measured CMT fluid temperature from the long thermocouple rod location near the bottom of each CMT. The thermocouples appear to have measured ambient conditions throughout the test, which would indicate a short somewhere in the thermocouple wiring. With these thermocouples inoperable, the required long thermocouple rod thermocouple availability of "seven out of ten and no more than one in succession failed" was met.

An energy balance will be performed and reported in the *AP600 Low-Pressure Integral Systems Test at Oregon State University Test Analysis Report, WCAP-14292*.⁽²⁾

5.5.2.3 Sequence of Events

Table 5.5.2-3 contains the sequence of events data for comparison of event occurrence between Matrix Tests SB26 and SB14. There is also a bar-graph representation of the sequence of events for both tests, sorted in chronologic order, for a quick visual reference.

The actual time the event occurred is listed. The table also provides the source of the actual time values. D in the Data Source column indicates the recorded time was obtained from a software program that monitored digital events in the plant, including pump starts and stops, valve limit switch actuations, and alarms. An A in the Data Source column indicates the time was obtained by reviewing data from the DAS. Although data from the DAS are digital, analog events such as pressure, flow, and temperature were monitored.

The time differential was calculated based on Matrix Test SB26 timing; positive time values indicated that Matrix Test SB26 events occurred later than the reference test events. Most of the Matrix Test SB26 events occurred slightly later than the equivalent Matrix Test SB14 events due to the fact that the ADS-1 valve was not opened to support initial depressurization as in Matrix Test SB14. In addition, Matrix Test SB26 was terminated at about []^{a,b,c} compared with []^{a,b,c} for reference test SB14.

5.5.2.4 Test Results and Evaluation

This section contains an overall description of the events that occurred during Matrix Test SB26 compared with reference test SB14. The description contains references to specific instrumentation channels cross-plotted and used in the test result evaluation.

A matched set of data plots, like those described in detail and presented for Matrix Test SB14, are included at the end of this section. As data comparisons are presented, Matrix Test SB14 data plots will be referenced but will not be repeated in this section. The same figures and figure numbers appear at the end of Subsection 5.5.1. In certain cases, special cross plots of instruments and/or combined instruments have been prepared and included at the end of the standard figures. The data plot figures list the instrument number and description.

Initial Conditions Comparison

The initial conditions for both tests were generally within 1 percent of the required initial conditions values with the following exceptions: IRWST temperature was []^{a,b,c} percent higher in Matrix Test SB26 than in Matrix Test SB14, and both accumulator pressures were []^{a,b,c} percent higher in Matrix Test SB14 than in Matrix Test SB26 ([]^{a,b,c}). These minor differences were not considered critical to the performance of Matrix Test SB26.

Sequence of Events Comparison

A detailed review of the sequence of events comparison between Matrix Tests SB26 and SB14 indicated that subsystem actuations (i.e., accumulator injection) occurred as planned with respect to each individual test. Generally, Matrix Test SB26 events occurred very close to the events for Matrix Test SB14 — up to the point when ADS-4 actuation was to take place. The lack of ADS-4 actuation in Matrix Test SB26 limited depressurization to a low pressure at or below the IRWST head. However, when comparing subsystem actuations, the results of Matrix Test SB26 followed Matrix Test SB14 results, except for the following:

- For Matrix Test SB26, the PRHR HX was not used; in Matrix Test SB14, the PRHR HX started at time zero. For Matrix Test SB26, the RCPs tripped 1 second earlier than in the reference test. The early trip of the RCPs did not significantly affect the overall system

response; however, this time difference in trip should be considered when modeling the Matrix Test SB26 transient.

- Power-operated relief valve RCS-610 opened for about []^{a,b,c} in Matrix Test SB26, but did not open in Matrix Test SB14. It opened between the time the RCPs tripped and the ADS-2 valve opened as primary pressure increased to the relief valve setting. This actuation of the relief valve should be considered when modeling the Matrix Test SB26 transient. Since relief valves discharge was not collected (through the main discharge header) or measured, steam flow lost through the relief valve was not recoverable and was not included in steam flow calculations.
- CMT, accumulator, and IRWST injection flow began []^{a,b,c} later in Matrix Test SB26 than in Matrix Test SB14. Most of the time difference was in the range of []^{a,b,c} up to the point that ADS-4 actuation was to take place.

Note: The term *time difference* or *delay* means the time that an actuation occurred in Matrix Test SB26 relative to the same time an actuation occurred in reference test SB14, using reference test SB14 time as the reference time.

- The CMTs did not reflood later in the transient due to the considerably lower core and downcomer inventory. Therefore, the timing of these events was not comparable.
- The pressurizer did not empty; therefore, the timing of the pressurizer reflood was not comparable.
- The primary sump did not fill up to the normal overflow level due to the lack of depressurization of the RCS (ADS-4 valves were not used for Matrix Test SB26) and, therefore, primary sump injection was never actuated. Therefore, the timing of these events was not comparable.

Loss of inventory (in the form of steam) and the rate of depressurization were about the same until the time of ADS-4 actuation []^{a,b,c} should have occurred between Matrix Tests SB26 and SB14. The lack of depressurization via the ADS-4 valves caused a significant delay in IRWST valve actuation and caused an intermittent actuation of IRWST injection flow.

Reactor Pressure and Core Level Comparison

The reactor vessel and core region collapsed liquid levels represented indications of the overall system response to the loss-of-coolant transient. Figures 5.5.2-87 through 5.5.2-89 present the pressure and vessel levels for comparison of Matrix Test SB26 with reference test SB14. Reactor vessel pressure for Matrix Test SB26, indicated by reactor upper head pressure indicator PT-107, showed a marked increase in pressure from []^{a,b,c} beginning after the RCPs tripped (Figure 5.5.2-87). The

pressure was limited to []^{a,b,c} (setpoint) by RCS-610, which opened at about []^{a,b,c} located on the top of the pressurizer (Appendix G, OSU Dwg. 600203). This pressure surge was probably due to the change in the power/flow ratio as the RCPs tripped, coupled with the lack of PRHR HX flow to support initial cooling and depressurization. The relief valve reseated after []^{a,b,c} as pressure decreased to []^{a,b,c}. The amount of steam loss through the relief valve was not known because no instrumentation was installed to measure such releases.

After ADS-2 valve actuation, RCS pressure quickly dropped to []^{a,b,c} as primary-side and secondary-side pressures came into equilibrium (Figure 5.5.2-19). Even though the ADS-2 and ADS-3 valves opened within []^{a,b,c} for each test (i.e., []^{a,b,c} respectively), the depressurization curve reflects a shift of about []^{a,b,c}. The slower depressurization rate of Matrix Test SB26 caused the delay in actuation of the accumulators []^{a,b,c} and RCS-711 and RCS-712 []^{a,b,c}. At []^{a,b,c} the pressures of both tests reached about []^{a,b,c} (Figure 5.5.2-87). With ADS-4 actuation in Matrix Test SB14, reactor pressure initially dropped to []^{a,b,c} and continued to slowly decay until about []^{a,b,c} at []^{a,b,c} (Figure 5.5.2-88). Without ADS-4 actuation in Matrix Test SB26, reactor pressure slowly decayed to about []^{a,b,c} and stayed at []^{a,b,c} for the remainder of the test (Figures 5.5.2-88 and 5.5.2-89).

In both tests, LDP-127 reflected core liquid inventory as the transient progressed from initial depressurization to the end of the test (Figures 5.5.2-87 through 5.5.2-89). LDP-127 indicated a minimum collapsed reactor wide-range level of []^{a,b,c} in []^{a,b,c} for Matrix Test SB14, as compared with a minimum value of []^{a,b,c} in []^{a,b,c} for Matrix Test SB26. LDP-113, which spans from the cold legs down to the DVI line, confirmed that for both tests the core levels did drop below the DVI line at about []^{a,b,c} (Figures 5.5.2-87 through 5.5.2-89). LDP-113 also confirmed that during accumulator injection, the levels in the core did recover consistent with the wide-range level indications. For both tests, core level recovered during accumulator injection and then began to fall to a second minimum value.

The second minimum level for Matrix Test SB14 occurred at about []^{a,b,c} (with a level of about []^{a,b,c}), as compared with []^{a,b,c} (with a level of about []^{a,b,c}) for Matrix Test SB26. The significant difference in level and time is attributed to the lack of ADS-4 valve actuation in Matrix Test SB26. The depressurization and venting due to ADS-4 actuation caused reactor pressure to drop from []^{a,b,c}. As the reactor pressure fell below about []^{a,b,c} IRWST injection occurred (IRWST head was about []^{a,b,c} equivalent). As IRWST injection occurred, core levels in Matrix Test SB14 recovered to a uniform level of []^{a,b,c} at about []^{a,b,c} (Figure 5.5.2-88).

In comparison, IRWST injection did not occur in Matrix Test SB26 until reactor pressure decreased below []^{a,b,c} (at []^{a,b,c} per Figure 5.5.2-105). IRWST injection was not continuous and was of a short duration (about []^{a,b,c}). These short-duration IRWST injections produced slight increases in core levels. Longer duration injections ([]^{a,b,c}), beginning at

[]^{a,b,c}, caused the first of a series of core level increases from []^{a,b,c} (Figures 5.5.2-88 and 5.5.2-89). The short-duration IRWST injections continued from []^{a,b,c} when Matrix Test SB26 was terminated (Figures 5.5.2-88 and 5.5.2-89).

From []^{a,b,c} vessel liquid levels for Matrix Test SB14 remained stable at about []^{a,b,c} until vessel level slowly decreased as the CMTs refilled and subsequently injected a second time (Figure 5.5.1-87). At []^{a,b,c} Matrix Test SB26 was terminated; therefore, comparisons with Matrix Test SB14 beyond that time are no longer valid. Matrix Tests SB14 and SB26 vessel levels responded in a similar manner up to the point when ADS-4 actuation should have occurred. Since the Matrix Test SB26 transient never progressed into long-term cooling and was terminated early, the overall response of the system was significantly different after ADS-4 should have occurred (about []^{a,b,c}).

Reactor Downcomer Level Comparison

When used in conjunction with reactor core level, reactor downcomer level provided supporting evidence of draindown of the reactor vessel, hot legs, and cold legs. LDP-116 and LDP-140 measured the liquid level from the bottom of the downcomer to just below the upper head bypass holes. Based on Matrix Test SB14, the effect of steam filling the upper portion of the downcomer represents a key parameter for comparison purposes. Figures 5.5.2-90 through 5.5.2-92 show the response of these channels over the entire range of the transient. Even though LDP-140 was at 180°az and LDP-116 was at 270°az (90 degrees apart), their responses were essentially the same. This agreement suggests that in the downcomer region downcomer level was uniform around the vessel for tests.

In both matrix tests, the overall response was similar up until the point when ADS-4 actuation would have occurred; however, the magnitude and time of each occurrence was different. The downcomer level indication was influenced by RCP flow until []^{a,b,c} after the inadvertent ADS actuation signal occurred. When the pumps tripped, indicated level increased to []^{a,b,c}. This level continued for about []^{a,b,c} for Matrix Test SB14 and about []^{a,b,c} for Matrix Test SB26, when the reactor vessel began to drain. The initial drop in downcomer level occurred at about []^{a,b,c} and began to recover due to the injection of the accumulators and CMTs (Figure 5.5.2-90). The downcomer collapsed level recovered to about []^{a,b,c} at []^{a,b,c} for Matrix Test SB14; the Matrix Test SB26 downcomer level recovered to a peak level of []^{a,b,c} from []^{a,b,c}.

Both tests exhibited a second drop in downcomer level: []^{a,b,c} at []^{a,b,c} (just before ADS-4 actuation) for Matrix Test SB14 and []^{a,b,c} at []^{a,b,c} (just after ADS-2 actuation) for Matrix Test SB26 (Figure 5.5.2-90). At about []^{a,b,c} when ADS-4 actuation occurred in Matrix Test SB14 and CMT-2 reached the low-low setpoint for Matrix Test SB26, the downcomer levels started to diverge. In Matrix Test SB14, the downcomer level increased to a peak level value of []^{a,b,c} from []^{a,b,c} during IRWST injection (Figure 5.5.2-91). The downcomer level for Matrix Test SB14 remained at []^{a,b,c} from []^{a,b,c}.

From []^{a,b,c} the downcomer level in Matrix Test SB26 exhibited a continued level decrease below the top of the core (Figure 5.5.2-90). A minimum collapsed liquid downcomer level of []^{a,b,c} occurred at []^{a,b,c} (Figure 5.5.2-91). This significant downcomer level decrease is due to sustained reactor pressure exceeding IRWST water head pressure. Without the ADS-4 valves opening (in Matrix Test SB26), the only vent path was through the ADS-2 and ADS-3 valves. The limited venting capability resulted in a higher reactor pressure (by about []^{a,b,c}) precluding the injection of IRWST water.

As reactor pressure dropped below []^{a,b,c} IRWST injection flow occurred in short durations as described in the previous section. The downcomer levels cycled four times from []^{a,b,c} from []^{a,b,c} (Figures 5.5.2-91 and 5.5.2-92). This peak downcomer level of []^{a,b,c} was equivalent to an elevation below the DVI line level.

From []^{a,b,c} the downcomer level for Matrix Test SB14 started to decrease from []^{a,b,c} until just prior to primary sump injection (Figure 5.5.2-92). During IRWST injection, a direct comparison between Matrix Tests SB14 and SB26 is not possible due to the significant difference between the system response (ADS-4 actuation) in Matrix Test SB26.

Overall Net Flow Comparison

Net flow provides a direct comparison of the overall system performance between similar types of tests. Net flow is spill flow (flow spilled to the break separator or sump), minus total DVI flow. Total injection flow is the sum of flow through DVI-1 and DVI-2 (FMM-205 and FMM-206, respectively). Total discharge or spill flow is the sum of flow exiting the primary system through FMM-905 (not applicable for Matrix Test SB14/SB26 comparison), FMM-603 (not applicable for Matrix Test SB26), FMM-602 (not applicable for Matrix Test SB26 comparison), and FMM-601. It must be noted that this comparison does not consider differences in temperatures between inflows and outflows, nor does it consider separator holdup. It should also be noted that some time delay could occur to due separator holdup.

These three variables are plotted over the []^{a,b,c} time period for the tests in Figures 5.5.2-93 and 5.5.2-94. The net flow summation is demonstrated by these two figures. The net flow and the core region wide-range level comparison between Matrix Tests SB14 and SB26 is shown in Figures 5.5.2-95 through 5.5.2-97. Negative net flow values indicate that more injection flow than discharge flow occurred.

From the initial inadvertent opening of the ADS valve (break) to []^{a,b,c} net flow between tests indicated an initial positive net flow rate of about []^{a,b,c} as liquid exited the ADS valves (Figure 5.5.2-95). It should be noted that in Matrix Test SB26, no flow passed through the ADS-1 valve by test design configuration. The sharp net flow increase was followed by a small drop to []^{a,b,c} due to increased CMT-1 and CMT-2 injection flow as the CMT transitioned from

recirculation to draindown. There was a second sharp increase in net flow as ADS-3 actuation occurred at []^{a,b,c} for Matrix Test SB26 (Figure 5.5.2-95).

The net flow rate change from []^{a,b,c} to a []^{a,b,c} as the combined CMT and accumulator injection flows was exhibited in both tests. This []^{a,b,c} net flow continued from []^{a,b,c} as ACC-1 and ACC-2 quickly injected their entire inventories to retain vessel liquid level. LDP-127 reflected the vessel level decrease following ADS valve openings and the vessel level recovery following CMT and accumulator injection flows.

For both tests, a near-zero net-flow rate occurred from []^{a,b,c} as core liquid inventory became stabilized by CMT-1 and CMT-2 flows (Figure 5.5.2-95). At about []^{a,b,c} a []^{a,b,c} net-flow rate was indicated for Matrix Test SB26, as injection flow from the CMTs ended and the reactor vessel was not depressurized via the ADS-4 valves. This positive net-flow rate occurred due to continued discharge of two-phase flow through the ADS-2 and ADS-3 valves without any additional IRWST injection. For Matrix Test SB14, ADS-4 valves opened at []^{a,b,c} which reduced the pressure from []^{a,b,c} by []^{a,b,c}. As reactor pressure decreased below []^{a,b,c} IRWST injection flow started and provided []^{a,b,c} flow immediately to maintain the net-flow at []^{a,b,c} (Figure 5.5.2-95). The IRWST injection flow rate balanced or exceeded the discharge flow through the ADS-4 valves for Matrix Test SB14 from []^{a,b,c} when primary sump injection flow occurred (Figure 5.5.2-97).

At about []^{a,b,c} the reactor vessel pressure for Matrix Test SB26 became stable at []^{a,b,c} which was slightly higher than the liquid head of the IRWST, and precluded IRWST injection flow. As the water inventory continued to decrease, more of the heater bundle became exposed, which caused more steam to be produced and the thermocouple rods to reflect a sharp temperature increase of the entire core to saturated conditions (Figures 5.5.2-31 and 5.5.2-25).

The first of several short-term IRWST injection flows occurred when reactor pressure dropped below []^{a,b,c}. As these IRWST injection flows occurred, small short-duration negative net flow indications were produced, as shown in Figure 5.5.2-96. In all cases, the net flow became []^{a,b,c} after the IRWST injections ended. The limited amount of IRWST injection flow was not adequate to cool the core sufficiently to reduce core pressure below []^{a,b,c} to permit continuous IRWST injection flow. The test was terminated at about []^{a,b,c} after it appeared to the test crew that continued operation would not reduce the RCS pressure.

CMT and Accumulator Injection Flow Comparison

The effect of the ADS-1 valve not opening in Matrix Test SB26 was reflected in the response of the CMTs and accumulators. CMT-1 and ACC-1 responses are shown in Figure 5.5.2-98. CMT-2 and ACC-2 responses are shown in Figure 5.5.2-99. The general response of both the accumulators and CMTs between Matrix Tests SB14 and SB26 was essentially the same, except for the slight time shift (later for Matrix Test SB26 than SB14). Both tests exhibited the four general CMT flow regimes:

initial recirculation mode, initial draindown, draindown as influenced by accumulator flow, and post-accumulator draindown. In both tests, accumulator injection flows occurred in a similar manner; however, the amplitude of injection flow was less and the duration was slightly longer during Matrix Test SB26 than SB14.

For both Matrix Tests, the recirculation mode started when RCS-535 and RCS-536 opened, with an initial flow rate of []^{a,b,c}. During this recirculation mode, saturated water flowed through the cold-leg balance lines into the CMTs. During the transition from recirculation to draindown at about []^{a,b,c} CMT-1 and CMT-2 flow increased to []^{a,b,c} at about []^{a,b,c} and two-phase flow filled the cold-leg balance lines. The peak injection flow rate of []^{a,b,c} for both tests occurred shortly before accumulator injection was initiated. In both tests, the effect of accumulator injection on both CMT-1 and CMT-2 injection was the same: during the accumulator injection flow period, CMT injection flow was suppressed and sometimes suspended. This effect was indicated by a sharp decrease in CMT-1 and CMT-2 flow rates as accumulator injection flow occurred (Figures 5.5.2-98 and 5.5.2-99). For both CMTs in Matrix Test SB26, the CMT response was later by []^{a,b,c}.

ACC-1 and ACC-2 injection occurred as reactor pressure dropped below the nitrogen gas pressure set prior to the beginning of the test (see Table 5.2-1). ACC-1 and ACC-2 injection flow suppressed CMT-1 and CMT-2 injection flow until accumulator injection fell to []^{a,b,c} at []^{a,b,c} for Matrix Test SB26. In Matrix Test SB14, peak accumulator flow rates of []^{a,b,c} were achieved at about []^{a,b,c}. In Matrix Test SB26, peak accumulator flow rates of only []^{a,b,c} were achieved at about []^{a,b,c} but the duration of flow was about []^{a,b,c} longer.

After ACC-1 and ACC-2 injection ended (post-accumulator draindown), both CMT-1 and CMT-2 injection flows returned to a second peak flow rate of []^{a,b,c}. Both CMT-1 and CMT-2 flow continued at a decreasing rate until the tanks became emptied. For Matrix Test SB14, CMT-1 and CMT-2 became empty at []^{a,b,c} respectively. For Matrix Test SB26, CMT-1 and CMT-2 became empty at []^{a,b,c} respectively (Figures 5.5.2-98 and 5.5.2-99).

In Matrix Test SB26, CMT-1 and CMT-2 did not refill (Figures 5.5.2-36 and 5.5.2-37) due to the low water inventory in the core (no IRWST injection flow). However, during Matrix Test SB26, thermocouple rod temperatures in CMT-1 and CMT-2 indicated that steam was condensed in the CMTs late in the transient, but no measurable level or injection flow was indicated.

For Matrix Test SB14, both CMT-1 and CMT-2 refilled to []^{a,b,c} respectively (Figure 5.5.1-36). Both CMTs refilled over a []^{a,b,c} period following initial draindown. The detailed description of the refill process is presented in Subsection 5.5.1-5 for Matrix Test SB14. Both CMT-1 and CMT-2 remained filled until about []^{a,b,c} when CMT-1 and CMT-2, respectively began to drain (Figure 5.5.1-36). Draindown was complete by about []^{a,b,c} just prior to primary sump injection. The effect of the refill in Matrix Test SB14

can not be quantitatively compared, since the lack of ADS-4 valve actuation and core cooling by the IRWST had a more significant effect in Matrix Test SB26.

5.5.2.5 Comparison of Component Responses

The following component responses have been reviewed and determined to be essentially the same, similar enough to represent the same response, or the component was not used. Therefore, any minor differences are not described.

- CMTs
- Accumulators
- SGs

Components that contain significant differences between Matrix Tests SB14 and SB26 are presented in the following subsections.

Reactor

Until the time that ADS-4 valve actuation occurred, the overall responses of the core and reactor vessel were similar for both tests, except in the following areas: overall timing (addressed in Subsection 5.5.2.4), higher superheated temperatures in the upper head and upper portion of the downcomer, and heater rod temperatures for Matrix Test SB26. ADS-4 valve actuation occurred at []^{a,b,c} in Matrix Test SB14, but never occurred in Matrix Test SB26 due to test design. After this time, the response comparison between tests, though similar, was considerably different in the ability to inject liquid into the RCS to maintain the core in a coolable environment.

For Matrix Test SB26, the downcomer temperature (TF-168) superheated at about []^{a,b,c} as the upper head drained down to the upper-support plate level and steam from the upper head entered the downcomer via the bypass holes (Figure 5.5.2-100). During this same time ([]^{a,b,c}), the upper head superheated (TF-120; Figures 5.5.2-21 and 5.5.2-100).

For Matrix Test SB26, both upper-head and downcomer temperatures generally followed the decrease in reactor temperature following ADS-3 actuation (Figure 5.5.2-21 and Table 5.5.2-3). A sharp increase in upper-head temperature may have been due to the superheating effect from the heat transfer of energy stored in the upper-support plate to the saturated steam flowing through it (TF-171). The upper-support plate was exposed to higher fluid temperatures earlier in the transient (Figure 5.5.2-100). The upper head and upper-support plate reached a common peak temperature of []^{a,b,c} at about []^{a,b,c} and then slowly decreased in temperature. The downcomer temperature (TF-168) remained superheated and relatively close to the upper-head temperature from []^{a,b,c} (Figure 5.5.2-101). The upper-head and downcomer temperatures exhibited in Matrix Test SB26 were higher than in Matrix Test SB14 over the range of []^{a,b,c}

Similarly, for Matrix Test SB14, both upper-head and downcomer temperatures reached superheated conditions, quickly following drainage of the upper head and downcomer. A single small condensation event occurred at []^{a,b,c} in Matrix Test SB14 and caused a decrease in the downcomer thermocouple (TF-168) indication, without a significant effect on the upper-head temperature (Figures 5.5.1-21 and 5.5.1-43). In Matrix Test SB14, the upper head temperature decreased until the hot legs and cold legs began to refill. As the hot legs and cold legs began to refill, upper-head temperatures increased sharply at about []^{a,b,c} for Matrix Test SB14 (Figures 5.5.1-21 and 5.5.1-88). A similar increase in upper-head temperatures also occurred at []^{a,b,c} in Matrix Test SB26, but was not coincident with any refill of the hot legs or cold legs (Figure 5.5.2-101).

Injection flow for both the accumulators and CMTs during the early portion of the transient ([]^{a,b,c}) had similar effects on the core for both Matrix Tests SB14 and SB26. As the inadvertent ADS actuation occurred, the vessel liquid levels dropped and steam developed in the upper head. In addition, core temperatures, as measured by TR-001-1 through TR-001-8, indicated a temperature profile that matched the saturated liquid profile (Figure 5.5.2-31). As accumulator injection flow occurred, most of the core subcooled, and at the end of accumulator injection (about []^{a,b,c} for both tests), a []^{a,b,c} stratification became evident (Figure 5.5.2-31). Heater rods across the core reflected a very small variation in temperature, and the overall temperature profile followed the liquid saturation profiles shown by variable TSAT (Figure 5.5.2-45).

As ADS-4 actuation occurred at []^{a,b,c} for Matrix Test SB14 and IRWST injection flow started at []^{a,b,c} a []^{a,b,c} gradient, measured by thermocouple rods, continued. Some small thermal spikes of []^{a,b,c} were indicated over very short periods.

In contrast to the more uniform cooling in Matrix Test SB14, the lack of IRWST injection flow affected the core temperatures significantly from about []^{a,b,c} to the end of Matrix Test SB26. Beginning at about []^{a,b,c} stratified temperatures exhibited by TR-001-1 through TR-001-8 temperatures ended and approached a saturated temperature of about []^{a,b,c} (Figure 5.5.2-31). This sudden shift in the temperature profile indicated that the lower portions of the core were heating up to saturated temperature conditions. At this time ([]^{a,b,c}) CMT-1 and CMT-2 injection flow had just ended and accumulator flow was completed (Figure 5.5.2-11). Because of the lack of ADS-4 actuation and the subsequent depressurization of the reactor pressure below the pressure equivalent of the IRWST liquid head, IRWST injection flow was not available. The effects of the lack of IRWST injection flow was evidenced by long duration temperature excursions of the reactor heater thermocouples that ranged from []^{a,b,c} above the saturated temperature which occurred at about []^{a,b,c} (Figures 5.5.2-45 and 5.5.2-46). Temperature spikes of []^{a,b,c} were also measured by the reactor thermocouple rods over the range of []^{a,b,c} (Figures 5.5.2-31 and 5.5.2-41). As indicated earlier, some IRWST injection did occur once reactor pressure dropped below about []^{a,b,c} and these occurrences were reflected in temporary temperature decreases of the lowest

thermocouple rod temperature (TR-001-1) at elevation []^{a,b,c} however, these short IRWST injection flows did not significantly affect the other thermocouple rod temperatures.

Break and ADS Measurement System

The BAMS response for both tests was quite similar up until about []^{a,b,c} when the effect of ADS-4 valve actuation was reflected in the IRWST, primary sump, break separator, and secondary sump levels (Figures 5.5.1-49 and 5.5.2-49). Before []^{a,b,c} IRWST level increased to peak levels of []^{a,b,c} at about []^{a,b,c} for Matrix Tests SB14 and SB26, respectively (Figures 5.5.2-49 and 5.5.2-50). The Matrix Test SB26 IRWST level was higher due to higher ADS 1-3 loop seal flow rate (FMM-601) and a delayed discharge of overflow from the IRWST to the primary sump (Figure 5.5.2-2).

The IRWST overflow loop seal meter (FMM-703) measured the overflow to the primary sump (Figures 5.5.2-102 and 5.5.2-103). The IRWST overflow for Matrix Test SB14 reflected an earlier start but flat lined (over-ranged) beginning at []^{a,b,c} with a flow of []^{a,b,c} based on the maximum calibrated range (Figure 5.5.2-102). It can be assumed, therefore, that the flow exceeded the calibrated values. For Matrix Test SB26, the IRWST overflow reached a peak flow of about []^{a,b,c} at []^{a,b,c} (Figure 5.5.2-102). In both tests after []^{a,b,c} the overflow rates decreased to about []^{a,b,c} (Figure 5.5.2-103); however, the overflow rate in Matrix Test SB26 continued at a rate of []^{a,b,c} until []^{a,b,c}. In Matrix Test SB14, the overflow rate decreased to []^{a,b,c} after IRWST injection started at about []^{a,b,c} (Figure 5.5.2-103).

For Matrix Test SB14, IRWST injection flow caused the IRWST level to slowly decrease beginning at about []^{a,b,c} (Figures 5.5.1-49 and 5.5.1-50), but in Matrix Test SB26, IRWST level remained at []^{a,b,c} until at least []^{a,b,c} (Figures 5.5.2-49 and 5.5.2-50). After []^{a,b,c} short-duration IRWST injection flows only reduced the level by about []^{a,b,c} for Matrix Test SB26 (Figures 5.5.2-106 and 5.5.2-50). Matrix Test SB14 was configured to allow ADS-4 flow to exit the RCS and enter the primary sump via the ADS 4-1 and ADS 4-2 separators and be measured by FMM-603 and FMM-602, respectively. In Matrix Test SB26, no ADS-4 flow occurred; thus, the primary sump level in Matrix Test SB14 increased more rapidly than in Matrix Test SB26 (Figures 5.5.1-49 and 5.5.1-50). As IRWST water entered the RCS via the DVI lines and subsequently exited through ADS-4 valves to the primary sump, the primary sump level increased and the IRWST level decreased. The lack of ADS-4 valve actuation in Matrix Test SB26 held up water in the IRWST and limited primary sump filling via the only available discharge mechanism (IRWST overflow). Therefore, IRWST remained filled and the primary sump was being filled by only the IRWST overflow (from the ADS-2 and ADS-3 valves). The break separator never changed in level because the primary sump never became filled with an adequate supply to back flow into the break separator through the loop seal (Figure 5.5.2-50).

In-Containment Refueling Water Storage Tank

Figures 5.5.2-104 through 5.5.2-106 show the relationship between upper-head pressure (PT-107) and IRWST injection flow (FMM-701) for both Matrix Tests SB14 and SB26. IRWST injection flow (FMM-701) was the same (FMM-702) but is not reported here. As explained earlier, ADS-4 actuation occurred at about []^{a,b,c} and IRWST injection flow started at about []^{a,b,c} in Matrix Test SB14, but ADS-4 never actuated in Matrix Test SB26.

In Matrix Test SB14, the upper-head pressure dropped from []^{a,b,c} at which time IRWST injection flow was initiated through IRWST-1 (FMM-701; Figure 5.5.2-104). For Matrix Test SB26, the upper-head pressure remained at around []^{a,b,c} until about []^{a,b,c} well past the time when ADS-4 actuation would have occurred. The upper-head pressure during Matrix Test SB26 decreased slowly from []^{a,b,c} from []^{a,b,c} and remained at or slightly above []^{a,b,c} until about []^{a,b,c} (Figure 5.5.2-105). At []^{a,b,c} when the upper-head pressure dropped to about []^{a,b,c} IRWST flow of only []^{a,b,c} started. The flow ended at []^{a,b,c} only []^{a,b,c} after being initiated. This started the cyclic injection from the IRWST that was repeated five times from []^{a,b,c} (Figure 5.5.2-106). During each of these cyclic IRWST injection periods, IRWST flow was never adequate enough to reduce RCS pressure to permit full, continuous IRWST injection flow.

Throughout this same period ([]^{a,b,c}), the upper-head pressure in Matrix Test SB14 remained below []^{a,b,c} and, generally, at a value of []^{a,b,c}. This lower RCS pressure allowed full IRWST injection flow, and the ADS-4 valves provided the necessary vent path for steam to exit the vessel without building up RCS pressure (Figures 5.5.2.104 through 5.5.2-106).

The effects of the lack of IRWST injection in Matrix Test SB26 were also evident by the temperature increases measured by the thermocouple rod located in the IRWST (Figures 5.5.2-84 and 5.5.2-85). From the inadvertent ADS actuation at time 0 to []^{a,b,c} the temperature profiles for Matrix Tests SB14 and SB26 were nearly identical. However, as liquid inventory in the reactor vessel was being steamed off without replacement by IRWST injection flow, the average temperature of the upper half of the IRWST increased from []^{a,b,c} from []^{a,b,c} (Figures 5.5.2-84 and 5.5.2-85). This temperature increase was significant in comparison to only a []^{a,b,c} increase over the same time frame for Matrix Test SB14 (Figures 5.5.1-84 and 5.5.1-85). For Matrix Test SB26, the average temperature of the upper half of the IRWST continued to increase from []^{a,b,c} achieving a peak temperature of []^{a,b,c} at []^{a,b,c}. The average temperature of the upper half of the IRWST in Matrix Test SB14 was only []^{a,b,c} at []^{a,b,c} comparatively.

Passive Residual Heat Removal Heat Exchanger

For Matrix Test SB26, the PRHR HX was not used, by design, in order to help characterize and compound the effects of multiple failures of the ADS on overall system response. Also for Matrix

Test SB26, even though the inadvertent ADS actuation signal started the transient, no liquid or steam flow passed through the ADS-1 valve (RCS-605). However, for Matrix Test SB14, the PRHR HX was used and liquid/steam was allowed to flow through the ADS-1 valve. Figure 5.5.2-107 reflects a comparison of reactor pressure (PT-107) and PRHR HX outlet flow (FMM-804) for both matrix tests during the first []^{a,b,c} when the PRHR HX had the most significant effects on the transient.

In Matrix Test SB14 (described in detail in Subsection 5.5.1.5), the PRHR HX outlet valve was opened early at time zero instead of 6 seconds after inadvertent ADS-1 actuation. The simultaneous opening of the ADS-1 valve and the PRHR HX outlet valves depressurized the overall system from []^{a,b,c} within []^{a,b,c} and provided some cooling of RCS liquid via the PRHR HX over the first []^{a,b,c}. In Matrix Test SB26, with the ADS-1 valve closed and the PRHR HX unavailable, RCS pressure increased to the pressure relief setpoint of []^{a,b,c} after the RCPs were tripped. It is not clear whether the pressure relief valve would have lifted if the PRHR HX were active. Therefore, characterization of the effect of not using the PRHR HX during the inadvertent ADS actuation tests was complicated by changing two parameters at the same time and will require additional analysis beyond this report.

Cold Legs and Hot Legs

The responses of both the hot-leg and cold-leg levels were generally in full agreement from the start of the test through about []^{a,b,c} for both Matrix Tests SB14 and SB26 (Figures 5.5.1-6, 5.5.1-14, 5.5.1-13, 5.5.2-6, 5.5.2-14, and 5.5.2-13). The same is true for the response of the hot-leg and cold-leg temperatures over the same time period (Figures 5.5.1-22, 5.5.1-23, 5.5.1-32 to 5.5.1-35, 5.5.2-22, 5.5.2-23, and 5.5.2-32 to 5.5.2-35).

After []^{a,b,c} both the hot-legs and cold-legs in Matrix Test SB26 never refilled for the remainder of the transient, which ended at []^{a,b,c}. The hot legs and cold legs never refilled due to the lack of adequate IRWST injection flow to re-establish core water inventory. Hot-leg temperatures throughout the remainder of the transient followed the saturation conditions line as indicated by TSAT in Figures 5.5.2-22, 5.5.2-23, and 5.5.2-83. Cold-leg temperatures in Matrix Test SB26 reached superheated conditions beginning about []^{a,b,c} with a temperature of about []^{a,b,c} (Figures 5.5.2-32 through 5.5.2-35). Cold-leg temperatures were superheated for the remainder of the transient with slowly decreasing profile (Figures 5.5.2-32 to 5.5.2-35, and 5.5.2-81). Cold-leg temperatures eventually decreased to about []^{a,b,c} at []^{a,b,c}.

In Matrix Test SB14, cold-leg levels increased. The cold legs began to refill about []^{a,b,c} and were full at about []^{a,b,c} as indicated by wide-range downcomer levels (LDP-116 and LDP-140) and cold-leg levels (LDP-201 through LDP-204) and the drop in cold-leg temperatures from superheated to saturated or subcooled conditions (Figures 5.5.1-32 through 5.5.1-35). The hot-legs also refilled beginning about []^{a,b,c} and were full about []^{a,b,c}. The refilling of the cold legs allowed steam to slowly collect in the balance lines and allow eventual refill of the

CMTs. The response of both the hot legs and cold legs for Matrix Test SB14 are described in more in Subsection 5.5.1.4.

In summary, the lack of adequate IRWST injection flow due to the unavailability of the ADS-4 valves precluded the transition into primary sump injection. The lack of adequate IRWST injection limited the heater rod bundle water inventory, and the hot legs and cold legs never refilled.

5.5.2.6 Mass Balance

The mass balance results for Matrix Test SB26 were calculated based on water inventory before and after the Matrix Test SB26 event and are provided in Appendix E. Table E.5.5.2-1 provides a detailed listing of the inventories of water in the various components before the event. Table E.5.5.2-2 provides a detailed listing of the inventories of water in the various components at the end of test. The inventory at the end of test was within []^{a,b,c} percent of the inventory at the beginning of the test.

5.5.2.7 Conclusions

The test was performed with minimal problems, as discussed previously. Although not all instruments met the specified acceptance criteria, the deviations were considered small, and the test is considered acceptable and successful because valuable thermal-hydraulic data were obtained relative to the impact of the unavailability of the ADS-4 valves.

Several of the top heater rods exhibited temperature spikes beyond the calibrated limits due to the lack of IRWST injection flow as a result of the unavailability of the ADS-4 valves. Matrix Test SB26 as compared with Matrix Test SB14 was only slightly slower over the first []^{a,b,c} and discharged about the same amount of steam from the simulated break. The results of Matrix Test SB26 compared very well with the system response of Matrix Test SB14, up until the time when ADS-4 would have been actuated. Matrix Test SB26 did demonstrate that complete failure to open the ADS-4 valves with the PRHR HX out of service can have significant detrimental effects on the heater rod bundle.

TABLE 5.5.2-1
MATRIX TEST SB26 INITIAL CONDITIONS

Parameter	Instrument No.	Specified Initial Condition	Actual Initial Condition	Comments
Pressurizer pressure ⁽¹⁾	PT-604	370 ± 2 psig		a,b,c
HL-1 temperature ⁽¹⁾	SC-141	420 ± 2°F		
HL-2 temperature ⁽¹⁾	SC-140	420 ± 2°F		
SG-1 pressure ⁽¹⁾	PT-301	285 ± 5 psig		
SG-2 pressure ⁽¹⁾	PT-302	285 ± 5 psig		
Pressurizer level ⁽¹⁾	LDP-601	65 ± 5 in.		Level signal was temperature-compensated by TF-605
SG-1 narrow-range level ⁽¹⁾	LDP-303	26 ± 3 in.		Level signal was temperature-compensated by TF-301
SG-2 narrow-range level ⁽¹⁾	LDP-304	26 ± 3 in.		Level signal was temperature-compensated by TF-310
IRWST temperature ⁽²⁾	TF-709	< 80°F		
CMT-1 temperature ⁽²⁾	TF-529	< 80°F		
CMT-2 temperature ⁽²⁾	TF-532	< 80°F		
ACC-1 temperature ⁽²⁾	TF-403	< 80°F		
ACC-2 temperature ⁽²⁾	TF-404	< 80°F		
IRWST level ⁽²⁾	LDP-701	Level established by fill line elevation		
ACC-1 level ⁽²⁾	LDP-401	Level established by standpipe at 37 in.		Accepted; accumulator level was fixed by a standpipe
ACC-2 level ⁽²⁾	LDP-402	Level established by standpipe at 37 in.		Accepted; accumulator level was fixed by a standpipe
ACC-1 pressure ⁽²⁾	PT-401	232 ± psig		Pressure was [] ^{a,b,c} low condition acceptable

TABLE 5.5.2-1 (Continued)
MATRIX TEST SB26 INITIAL CONDITIONS

Parameter	Instrument No.	Specified Initial Condition	Actual Initial Condition	Comments
ACC-2 pressure ⁽²⁾	PT-402	232 ± psig		Pressure was [] ^{a,b,c} low; condition acceptable
CMT-1 level ⁽²⁾	LDP-507	Full		
CMT-2 level ⁽²⁾	LCP-502	Full		

Note:

- (1) Data for the indicated parameter were recorded in the test procedure as an initial condition for the test. The value was determined by the test engineer from the appropriate control board indicator.
- (2) Data were not recorded in the procedure, but the test engineer verified that specified conditions were achieved while establishing initial conditions. The value of the parameter was determined post-test by calculating the average DAS indication for a time of about 2 minutes before the break valve opened.

TABLE 5.5.2-2
MATRIX TEST SB26 INOPERABLE INSTRUMENTS/ INVALID DATA CHANNELS

Instrument No.	Instrument Type	Description of Problem
FDP-604*	Differential pressure transmitter - flow	Over-ranged with initial flow
FMM-201* FMM-202* FMM-203* FMM-204*	Magnetic flow meter	Removed from system due to mechanical failure
FMM-401*	Magnetic flow meter	Negative value due to nitrogen in line
FMM-501*	Magnetic flow meter	Data invalid after 1068 seconds when CMT was empty
FMM-502 FMM-503	Magnetic flow meter	Data invalid after 96 seconds due to possible steam in balance line; meter can not measure steam or two-phase flow
FMM-504*	Magnetic flow meter	Data invalid after 1114 seconds when CMT was empty
FMM-902*	Magnetic flow meter	Negative flow indication invalid; data valid when primary sump valve opened; sump valve never opened
HFM-103 HFM-105 HFM-113 HFM-510 HFM-505 HFM-703	Heat flux meter	Unavailable
HPS-509-1 through HPS-509-3	Heated thermocouple sensing fluid phase	Unavailable
LDP-201 through LDP-206	Differential pressure transmitter - level	Data invalid due to effect of vertical portion of sense line attached to top of pipe; data can show level trends, when pipe is empty or starts to drain, but absolute level indication cannot be used
LDP-215* LDP-216 LDP-217 LDP-218* LDP-219* LDP-220 LDP-221 LDP-222	Differential pressure transmitter - level	Data can not be used directly, but must be interpreted because reference legs boil as SGs drain (Subsection 2.4)
LDP-502*	Differential pressure transmitter - level	Data unavailable because this channel used to initiate transient

TABLE 5.5.2-2 (Continued)
MATRIX TEST SB26 INOPERABLE INSTRUMENTS/INVALID DATA CHANNELS

Instrument No.	Instrument Type	Description of Problem
TF-103* TF-104*	Thermocouple	These thermocouples were removed and replaced with thermocouple rods for thermal stratification measurements; data indicated not valid
TF-142*	Thermocouple	Invalid for test; at higher temperatures proper response was not provided; TF-140 can be used in its place
TF-170	Thermocouple	Invalid temperature for entire test due to leakage past seal; data influenced by downcomer temperatures
TF-501* TF-504*	Thermocouple	Data invalid since thermocouples read close to ambient conditions throughout test; thermocouple must have shorted out
TFM-113 TFM-708	Thermocouple on heat flux meter	Unavailable
TH-317-1 through TH-317-4	Thermocouple measuring heater temperature	Removed with heater and C2-317
TW-503	Thermocouple	Failed by false indication of temperature

Note:

* Instruments marked with an asterisk are critical instruments. See Subsection 5.5.2.2 for discussion.

Table 5.5.2-3 on pages 5.5.2-22 through 5.5.2-24 is not included in this nonproprietary document.

The Bar Charts for Table 5.5.2-3 on pages 5.5.2-25 through 5.5.2-28 are not included in this nonproprietary document.

Figures 5.5.2-1 through 5.5.2-107 are not included in this nonproprietary document.

5.6 Inadvertent S Signal (Matrix Test SB31)

Matrix Test SB31 (OSU Test U0031), was performed to determine the response of the test facility to an inadvertent S signal. For this test, there was no simulated break, and nonsafety-related systems did not operate. The test results for Matrix Test SB31 are described in this section, including test procedure and initial conditions, data plots, and evaluation of overall results. Since none of the injection systems were activated during this test, discussion of component responses is not required.

The test was terminated after about 5500 seconds, when a continuous decline in reactor coolant system (RCS) pressurizer pressure had been observed for more than 1 hour. During this test, the reactor core remained covered with water, the core makeup tanks (CMTs) remained in natural circulation, and the accumulators did not inject, and the automatic depressurization system (ADS) did not activate. After an initial pressure/temperature rise of RCS coolant which resulted in opening the RCS pressure relief valve, the passive residual heat removal heat exchanger (PRHR HX) removed more heat than the core heaters supplied. Therefore, RCS pressure decreased steadily.

Since the ADS did not activate, and RCS pressure did not decrease sufficiently to initiate in-containment refueling water storage tank (IRWST) injection, the discussion of this test is limited to the initial depressurization phase, which encompasses initiation of the S signal to test termination. The test was considered successful.

5.6.1 System Configuration and Initial Conditions

In this section, the system configuration, initial conditions, and test procedure for Matrix Test SB31 are described. Matrix Test SB31 was performed on August 31, 1994, in accordance with an approved written test procedure.

The test facility was configured in the normal arrangement, as described in Section 2.0. Specifically, this test incorporated the following features:

- No simulated break
- Nonsafety-related systems off for test duration
- Single failure in ADS-4

To simulate the failure of one of the ADS-4 lines, a flow nozzle with 50 percent of the design flow area was installed in the ADS 4-1 line. A flow nozzle with the full design flow area was installed in the ADS 4-2 line.

Prior to test initiation, steady-state operating data were recorded for about 120 seconds to establish pre-test conditions. Table 5.6-1 provides a comparison of the pre-test conditions with the conditions required by test specifications. All pre-test operating conditions were achieved prior to test initiation except accumulator-1 (ACC-1) and ACC-2 pressures which were 2.3 and 3.5 percent lower,

respectively, than specified. The loss of pressure between tank pressurization and test actuation was possibly caused by nitrogen cooling in the accumulator. Test analysis with the lower accumulator overpressure should still be possible.

Decay heat from the reactor fuel was simulated by electrically powered heater rods installed in the core region of the reactor vessel. A comparison of the actual power with the specific decay heat power for Matrix Test SB31 is provided in Appendix F.

5.6.2 Inoperable Instruments

Table 5.6-2 is a list of instruments considered inoperable or invalid during all or portions of this test. Some of the instruments listed are on the Critical Instrument List (Subsection 3.2, Table 3.2-2) and, therefore, are addressed here.

FMM-201, FMM-202, FMM-203, and FMM-204 measured flow (gpm) in each of the four cold legs. A decision was made to continue testing without the availability of these instruments. Replacement flow meters repeatedly failed; their continued use was precluded due to cracking of the ceramic liners from thermal stratification in the loop piping. The necessary boundary conditions for loop flow could be determined from DP-202, DP-203, DP-205, and DP-206.

TF-103 and TF-104 measured CL-3 and CL-4 bottom-of-pipe fluid temperatures entering the reactor downcomer. Both thermocouples were removed to accommodate installation of thermal stratification measurement instrumentation. Both thermocouples were allowed to be inoperable as long as TF-101 and TF-102 were operable. TF-101 and TF-102 were operable during the performance of Matrix Test SB24.

Data provided by ADS-4 separator instrumentation were invalid because the ADS-4 valves and the ADS-4 loop seal valves did not open in this test. The instruments affected were FMM-602, FMM-603, FVM-602, FVM-603, LDP-611, and LDP-612.

Considering these critical instrument failures, sufficient instrumentation was available to allow the performance of mass balances as demonstrated in Subsection 5.6.5 and Appendix E. An energy balance will be performed and reported in the *AP600 Low-Pressure Integral Systems Test at Oregon State University Test Analysis Report WCAP-14292*.⁽²⁾

5.6.3 Sequence of Events

Table 5.6-3 contains the sequence of events for Matrix Test SB31. This table provides the event times of selected events in the test arranged in chronological order.

The first pages of Table 5.6-3 indicate the source of the actual time data. A D in the Data Source column indicates the recorded time was obtained from a software program that monitored digital

events in the facility. These events included pump starts and stops, valve limit switch actuations, and alarms. The term *valve opening* means the valve has actuated and the closed limit switch is being opened (valve coming off the seat). An A in the Data Source column indicates the time data were obtained by reviewing test data obtained from the data acquisition system (DAS). Although the test data from the DAS were in digital format, the DAS monitored analog events such as pressure, flow, and temperature from the data.

The test sequence was initiated by actuating the TEST pushbutton, which triggered the DAS to begin acquiring data. Approximately the first 2 minutes of data were used to establish the initial conditions for the test. Two minutes after TEST pushbutton actuation, the steam generator (SG) pressure setpoint was raised, the reactor shifted to power (kW) control mode with a programmed power demand, the main feedwater pump tripped and feedwater was isolated, the PRHR HX outlet valve and CMT discharge valves opened, and the reactor coolant pumps (RCPs) tripped. Forced flow was initiated through the PRHR HX and the CMTs until the RCPs stopped, at which time the flow changed to natural circulation flow.

At []^{a,b,c} the RCS pressure relief valve opened for about []^{a,b,c} to reduce RCS pressure. The RCS and SGs remained full of water, and neither the CMTs nor the accumulators emptied their inventories into the system. The test was terminated at []^{a,b,c}

5.6.4 Test Results and Evaluation

The results of Matrix Test SB31 are discussed in this section. This test consisted of only one phase, since neither ADS actuation nor IRWST injection was achieved for the duration of the test operation. When flow from the RCPs stopped about []^{a,b,c} after the S signal, coolant temperatures in the reactor core (Figure 5.6-1) increased about []^{a,b,c} and pressure increased about []^{a,b,c} (Figure 5.6-2). After the pressure relief valve opened at []^{a,b,c} pressure and temperature decreased steadily for the remainder of the test.

Cooling was provided by cold water injection by natural circulation through the CMTs (Figure 5.6-3) and the PRHR HX (Figure 5.6-6). Hot water flowing from the cold-leg balance lines into the tanks, increased the CMTs water temperature. As the mean density of water in the CMTs was reduced, the driving head for natural circulation declined (Figures 5.6-4 and 5.6-5). Thus, flow from the CMTs fell linearly from its initial rate of []^{a,b,c} at the end of the test (Figure 5.6-3).

Flow through the PRHR HX (Figure 5.6-6), at []^{a,b,c} provided most of the heat rejection from the RCS in Matrix Test SB31. Coolant from HL-2 was cooled from hot-leg temperature ([]^{a,b,c} in the PRHR HX by natural circulation (Figure 5.6-7). Water stored in the IRWST stratified with the higher temperature water accumulating at the top of the tank (Figure 5.6-8).

Boiling briefly occurred in the core, from about []^{a,b,c} with a maximum steam percent of []^{a,b,c} estimated from the compensated core level data (LDP-110; Figure 5.6-9). Level data for the reactor (Figure 5.6-10) show that the reactor remained full of water during the remainder of the test.

The core was cooled by the steam-water mixture during the initial []^{a,b,c} and by subcooled water thereafter (Figure 5.6-11). Short duration ([]^{a,b,c}) temperature spikes (both positive and negative), with magnitudes up to []^{a,b,c} occurred in the core heaters (Figures 5.6-11 and 5.6-12). These temperature spikes can be seen more clearly in Figure 5.6-12, which is an expanded scale plot of selected core heater temperatures at the top of the core. The smaller temperature rises (< 40°F) may have been caused by local bubbles of steam blanketing the immediate area adjacent to the affected thermocouples. Temperature decreases may have been caused by slugs of colder, unmixed flow from the PRHR HX or CMT that periodically contacted the heaters. Large temperature rises were inconsistent with the maximum heating rate of the core heater rods and, therefore, may be an electrical effect resulting from the power input to the core heater rods.

The reactor downcomer, hot legs, cold legs, CMTs, and SGs (both channel heads and tubes) remained filled with water during the entire test, as shown by their level measurements (Figures 5.6-13 through 5.6-20). The slight variations in CMT levels (Figure 5.6-20) were due to the temperature compensation of raw level data. CMT balance line levels remained full, indicating that the CMTs did not drain.

Since RCS pressure never fell below the accumulator pressures, the accumulators did not inject their water inventories into the system; however, RCS pressure had decreased to within 5 psi of the accumulator pressures when the test was terminated (Figure 5.6-21). The level in ACC-2 increased linearly during the test (Figure 5.6-22). This rise in level may have been caused by a small leak in the check valve in the ACC-2 injection line, which permitted higher pressure water from the DVI to flow back into the tank.

Temperatures throughout the RCS remained below saturation, except for the first []^{a,b,c}. Figures 5.6-24 through 5.6-33 provide the temperature data for Matrix Test SB31. The pressure (and, hence, the temperature) in the primary side of the SG remained above that of the secondary side (Figure 5.6-34); therefore, the secondary side of the SG did not supply energy to the primary side in this test.

5.6.5 Mass Balance

Mass balance was calculated from the water inventories in the components before and after the test. Water mass at the completion of the test agreed with the pre-test water mass within []^{a,b,c} percent. Details of this mass balance are provided in Appendix E.

5.6.6 Conclusions

The test was performed with minimal problems and is considered acceptable. Although not all of the facility initial conditions met the specified acceptance criteria, the deviations did not impact the quality of the data. The instrumentation problems encountered were not critical to the performance of the facility mass and energy balances.

Facility response to the test was as anticipated for the conditions that were established. The data clearly demonstrated that cooling of the reactor heater rods was maintained throughout the duration of the test.

The inadvertent S signal resulted in a short-term high pressure that caused the RCS pressure relief valve to open for about []^{a,b,c} Natural circulation through the CMTs and the PRHR HX reduced system pressure and temperature steadily after the initial pressure relief. Since system pressure did not decrease below the accumulator pressures, these devices did not inject. The CMTs remained in natural circulation operation during the test because the RCS remained full of water.

TABLE 5.6-1
MATRIX TEST SB31 INITIAL CONDITIONS

Parameter	Instrument No.	Specified Initial Condition	Actual Initial Condition	Comments
Pressurizer pressure ⁽¹⁾	PT-604	370 ± 2 psig		a,b,c
HL-1 temperature ⁽¹⁾	SC-141	420 ± 2°F		
HL-2 temperature ⁽¹⁾	SC-140	420 ± 2°F		
SG-1 pressure ⁽¹⁾	PT-301	285 ± 5 psig		
SG-2 pressure ⁽¹⁾	PT-302			
Pressurizer level ⁽¹⁾	LDP-601	65 ± 5 in.		Level signal was temperature-compensated by SC-608
SG-1 narrow-range level ⁽¹⁾	LDP-303	25 ± 3 in.		Level signal was temperature-compensated by TF-305 and TF-307
SG-2 narrow-range level ⁽¹⁾	LDP-304	26 ± 3 in.		Level signal was temperature-compensated by TF-316 and TF-308
IRWST temperature ⁽²⁾	TF-709	< 80°F		
CMT-1 temperature ⁽²⁾	TF-529	< 80°F		
CMT-2 temperature ⁽²⁾	TF-532	< 80°F		
ACC-1 temperature ⁽²⁾	TF-403	< 80°F		
ACC-2 temperature ⁽²⁾	TF-404	< 80°F		
IRWST level ⁽²⁾	LDP-701	Level established by full-line elevation		
ACC-1 level ^(2,3)	LDP-401	Level established by standpipe at 37 in.		
ACC-2 level ^(2,3)	LDP-402	Level established by standpipe at 37 in.		

TABLE 5.6-1 (Continued)
MATRIX TEST SB31 INITIAL CONDITIONS

Parameter	Instrument No.	Specified Initial Condition	Actual Initial Condition	Comments
ACC-1 pressure ⁽²⁾	PT-401	232 ± 2 psig	[] ^{a,b,c}	Pressure was [] ^{a,b,c} low; condition acceptable
ACC-2 pressure ⁽²⁾	PT-402			Pressure was [] ^{a,b,c} low; condition acceptable
CMT-1 level ⁽²⁾	LDP-507	Full	[]	
CMT-2 level ⁽²⁾	LDP-502			

Note:

- (1) Data for the indicated parameter were recorded in the test procedure as an initial condition for the test. The value was determined by the test engineer from the appropriate control board indicator.
- (2) Data were not recorded in procedure, but the test engineer verified that specified conditions were achieved while establishing initial conditions. The value of the parameter was determined post-test by calculating the average DAS indication for a time of about 2 minutes before the break valve opened.
- (3) The bourdon pressure tube local indicator (PI-401 or PI-402) was tubed to the lower portion of the reference leg of the accumulator level transmitter (LDP-401 or LDP-402). As pressure in the accumulator was increased, air inside the bourdon tube was compressed, thereby lowering the reference leg liquid level, resulting in a false indication of measured level.

TABLE 5.6-2
MATRIX TEST SB31 INOPERABLE INSTRUMENTS/INVALID DATA CHANNELS

Instrument No.	Instrument Type	Description of Problem
FMM-201*	Magnetic flow meter	Removed from system
FMM-202*	Magnetic flow meter	Removed from system
FMM-203*	Magnetic flow meter	Removed from system
FMM-204*	Magnetic flow meter	Removed from system
FVM-602	Vortex flow meter	Ignore data since ADS-4 did not actuate
FVM-603	Vortex flow meter	Ignore data since ADS-4 did not actuate
HFM-103	Heat flux meter	Failed
HFM-105	Heat flux meter	Failed
HFM-112	Heat flux meter	Failed
HFM-113	Heat flux meter	Failed
HFM-201	Heat flux meter	Failed
HFM-505	Heat flux meter	Data appear erratic
HFM-510	Heat flux meter	Failed
HFM-601	Heat flux meter	Failed
HFM-703	Heat flux meter	Failed
HPS-203-1 through HPS-203-3	Heated phase switch	Inoperable throughout test
HPS-509-1 through HPS-509-3	Heated phase switch	Inoperable throughout test
TF-103*	Thermocouple fluid temperature	Removed from system
TF-104*	Thermocouple fluid temperature	Removed from system
TF-142	Thermocouple fluid temperature	
TF-170	Thermocouple fluid temperature	Read low throughout test
TF-601	Thermocouple fluid temperature	Read low throughout test

Instrument No.	Instrument Type	Description of Problem
TFM-103 TFM-105 TFM-113 TFM-703	Thermocouple for HFMs	Inoperable throughout test
TH-317-1 through TH-317-4	Thermocouple heater rod	Inoperable; heat rod removed prior to test
TW-503	Thermocouple wall temperature	Inoperable throughout test

Note:

* Instruments marked with an asterisk are critical instruments. See Subsection 5.6.2 for discussion.

TABLE 5.6-3
MATRIX TEST SB31 SEQUENCE OF EVENTS

Event ⁽¹⁾	Data Source ⁽²⁾	Time After Break (sec.)
TEST Pushbutton Depressed	D	[] a,b,c
Feed Pump Trips		
CMT-1 Outlet Valve Starts to Open	D	
CMT-2 Outlet Valve Starts to Open	D	
PRHR HX Outlet Valve Starts to Open	D	
Reactor Coolant Pumps Trip	D	
Relief Valve (RCS 610) Open	D	
Relief Valve (RCS 610) Closed	D	
End of Test	A	

Note:

- (1) Data from the instrument channel in parentheses were used to determine level, flow, or pressure conditions.
- (2) D = time data obtained from a software program that monitored the input and output of the facility's PLC. A = Time data obtained by reviewing data from the instrument channel listed in the Event Description column.

The Bar Charts for Table 5.6-3 on pages 5.6-11 through 5.6-16 are not included in this nonproprietary document.

Figures 5.6-1 through 5.6-34 are not included in this nonproprietary document.

5.7 Hot-Leg Break (Matrix Test SB15)

This section provides the test results for Matrix Test SB15 (OSU Test U0015). Matrix Test SB15 simulated a 2-in. hot-leg (HL) break loss-of-coolant accident (LOCA) with long-term cooling and without operation of nonsafety systems. The break was located at the bottom of HL-2 with a simulated failure of one of the automatic depressurization system-4 (ADS-4) lines. HL-2 is on the in-containment refueling water storage tank (IRWST) side of the facility (Figures 5.7-1a and 5.7-1b).

Subsection 5.7.1 provides details related to the test procedure, system configuration, and initial conditions. A description of inoperable instruments is provided in Subsection 5.7.2, and Subsection 5.7.3 references the sequence of events. Subsection 5.7.4 describes the test results and evaluation. Component responses are given in Subsection 5.7.5, and a summary of mass balance results is provided in Subsection 5.7.6. The conclusions as they apply to Matrix Test SB15 are given in Subsection 5.7.7. The facility responses to the break are documented by the data plots, referenced as figures in the text, at the end of this section. A data plot with the suffix x indicates extended time.

Matrix Test SB15 was performed on July 2, 1994. The performance of this test was successful because the reactor heater rod cooling was maintained.

5.7.1 System Configuration and Initial Conditions

The test was conducted per an approved written procedure. All actions were automatic after the test started, with no operator response required.

A flow nozzle simulating one line of flow was installed in the ADS 4-1 line—HL-1 to the ADS 4-1 separator—to provide the single failure simulation, and a flow nozzle simulating two lines of flow was installed in the ADS 4-2 line—HL-2 to the ADS 4-2 separator. Additionally, flow nozzles simulating two lines of flow each were installed in the ADS 1-3 inlet lines.

The reactor heater control decay algorithm maintained maximum reactor heater power output for 140 seconds, and then power began to decay to simulate the total post-trip energy input of the AP600 nuclear fuel (Appendix F). This test was performed with reactor heater rod HTR-C2-317 removed and replaced with a dummy rod. Refer to Subsection 2.7 for pre-test operations.

Table 5.7-1 shows initial facility conditions for Matrix Test SB15. There was one initial condition parameter out of specification.

- Accumulator-1 (ACC-1) and ACC-2 pressures, indicated by PT-401 and PT-402, were []^{a,b,c} respectively, below the required pressure band.

The accumulators were pressurized to the required pressure prior to test actuation. The loss of pressure between tank pressurization and test actuation was possibly due to the nitrogen gas

cooling in the accumulator. Test analysis starting with the recorded lower accumulator overpressure should still be possible.

Test duration was about 3.9 hours.

5.7.2 Inoperable Instruments

Table 5.7-2 is a list of instruments considered inoperable or invalid during all or portions of this test. Some of the instruments listed are on the Critical Instrument List (Subsection 3.2, Table 3.2-2) and, therefore, are addressed here.

FDP-605 measured the differential pressure (in. H₂O) across the ADS-1 flow nozzle. This transmitter over-ranged momentarily when the ADS-1 valve opened. Total flow through the ADS 1-3 valve complex can be determined by measuring ADS 1-3 separator liquid and steam flows from FMM-601 and FVM-601.

FMM-201, FMM-202, FMM-203, and FMM-204 measured flow (gpm) in each of the four cold legs. A decision was made to continue testing without the availability of these instruments. Replacement flow meters repeatedly failed; their continued use was precluded due to cracking of the ceramic liners from thermal stresses. The necessary boundary conditions for loop flow could be determined from DP-202, DP-203, DP-205, and DP-206.

FMM-501, FMM-504, FMM-802, and FMM-804 provided accurate data when sensing liquid, but became inaccurate when sensing two-phase or steam flow.

FMM-905 measured break separator loop seal flow to the primary sump. As the transient proceeded, the primary sump and break separator levels exceeded the elevation of the break at the bottom of HL-2. When this occurred, break flow initially stopped and then reversed. Flow reversal through the break occurred at about []^{a,b,c} rendering subsequent data invalid.

Steam generator (SG) tube level data (LDP-215, LDP-218, LDP-219, and LDP-222) were biased by vaporization of the water in the transmitter reference leg after the SG tubes started draining. However, the data provide accurate indication of the time when the tubes are empty.

LDP-401 and LDP-402 measured ACC-1 and ACC-2 levels, respectively. Due to air trapped in the sense lines for the transmitters, the data from these transmitters were invalid. However, the initial level of the tank was established by a standpipe, so it was constant from test to test. The drain rate can be calculated using the ACC-1 and ACC-2 flow meters (FMM-401 and FMM-402, respectively). Alternately, a pressure correction may be applied directly to the level indications of LDP-401 and LDP-402.

PT-201 measured reactor coolant system (RCS) pressure at the top of the SG-1 long tube. On August 15, 1994, it was discovered that the transmitter had an incorrect zero compensation, which resulted in a negative error and negative data at low pressures. The transmitter zero was corrected at that time. PT-201 data obtained during Matrix Test SB15 had the zero correction performed, and the corrected data appear as PT_201. Negative data and corrected negative data can be used to determine trends, but are considered inaccurate. PT_201 was not considered reliable for values less than 1.1 psig, but a sufficient amount of other pressure data are available.

TF-501 and TF-504 measured CMT fluid temperature from the long thermocouple rod location near the bottom of each CMT. The thermocouples appear to have measured ambient conditions throughout the test, which would indicate a short somewhere in the thermocouple wiring. With these thermocouples inoperable, the required long thermocouple rod thermocouple availability of "seven out of ten and no more than one in succession failed" was met.

Data provided by ADS-4 separator instrumentation prior to the ADS 4-1 and ADS 4-2 valves opening at 944 seconds were invalid due to the closed position of the ADS-4 valves and the ADS-4 separator loop seal valves. The instruments affected are: FMM-602, FMM-603, FVM-602, FVM-603, LDP-611, and LDP-612. Test analysis will not be affected, since ADS-4 flow did not begin until the valves opened.

Considering these critical instrument failures, sufficient instrumentation was available to allow the performance of mass balances as demonstrated in Subsection 5.7.6 and Appendix E. An energy balance will be performed and reported in the *AP600 Low-Pressure Integral Systems Test at Oregon State University Test Analysis Report, WCAP-14292*.⁽²⁾

5.7.3 Sequence of Events

Table 5.7-3 contains the sequence of events for Matrix Test SB15. The first pages of the table provide the event times of selected events in the test. The subsequent pages of the table contain bar charts of the data to provide a visual representation of the sequence of events. Both the numeric table and bar chart sort the events in chronologic order.

The first pages of Table 5.7-3 indicate the source of the actual time data. In the Data Source column, D indicates the recorded time was obtained from a software program that monitored digital events in the facility. These events included pump starts and stops, valve limit switch actuations, and alarms. The term *valve opening* means the valve has actuated and the closed limit switch is being opened (valve coming off the seat). An A in the Data Source column indicates the time data were obtained by reviewing test data obtained from the data acquisition system (DAS). Although the test data from the DAS were in digital format, the DAS monitored analog events such as pressure, flow, and temperature.

The test sequence was initiated by actuating the TEST pushbutton, which triggered the DAS to begin acquiring data. Approximately the first 2 minutes of data were used to establish the initial conditions for the test. Two minutes after TEST pushbutton actuation, a signal was sent to open the break valve located at the bottom of the spool piece in HL-2. In the first []^{a,b,c} following the signal to the break valve, the SG pressure setpoint was raised, the reactor shifted to power (kW) control mode with a programmed power demand, the main feedwater pump tripped and feedwater was isolated, the passive residual heat removal heat exchanger (PRHR HX) outlet valve and core makeup tank (CMT) discharge valves opened, and the reactor coolant pumps (RCPs) tripped. Forced flow was initiated through the PRHR HX and the CMTs until the RCPs stopped at 10 seconds, at which time the flow changed to natural circulation flow.

As the RCS depressurized and lost inventory through the break, pressurizer level decreased rapidly and steam formation began in the reactor vessel upper head. At about []^{a,b,c} the CMTs began to drain. The pressurizer and pressurizer surge line became completely empty of liquid, at []^{a,b,c} respectively. Steam formed in the SG tubes and pushed the remaining water out of the bottom of the tubes. Shortly thereafter, the SG channel heads began to empty. When CMT level decreased to the low level setpoint at []^{a,b,c} the ADS valve sequence was initiated per the control system design.

The ADS-1 valve opened, causing an increase in the rate of RCS depressurization. The ADS-2 and ADS-3 valves then sequenced open, further increasing the rate of depressurization. When RCS pressure decreased to below that of the accumulators, the accumulators began to inject into the direct vessel injection (DVI) lines, which stopped CMT injection by closing the CMT discharge line check valves.

The reactor pressure low-low setpoint was reached, sending an automatic opening signal to the IRWST injection valves. IRWST injection did not start at this time because RCS pressure was still too high to be overcome by the IRWST static head.

The accumulators emptied and depressurized, and CMT injection began again. When the CMT low-low level was reached, an automatic opening signal was sent to the ADS 4-1 and ADS 4-2 valves. These additional vent paths for the RCS helped decrease RCS pressure low enough to initiate IRWST injection. Depressurization also caused reflooding of the pressurizer surge line and pressurizer.

Both CMTs initially emptied at []^{a,b,c} CMT-2 started to reflood at []^{a,b,c} and CMT-1 started to reflood at []^{a,b,c} The primary sump started to overflow into the secondary sump at about []^{a,b,c} The test was terminated at about []^{a,b,c} after primary sump injection flow was initiated.

5.7.4 Test Results and Evaluation

The LOCA event simulated in the OSU test facility resulted in interactions between the systems and components in the facility. For this reason, it is convenient to subdivide the event into different phases, each characterized by the systems' behavior and thermal-hydraulic phenomena occurring within the systems. The different event phases selected for the purpose of detailed evaluation of the LOCA event are as follows:

- Initial Depressurization Phase: simulated break initiation to ADS-1 actuation
- ADS Phase: ADS-1 actuation to start of IRWST injection
- IRWST Injection Phase: start of IRWST injection to end of test

Initial Depressurization Phase

The test began with the actuation of the TEST pushbutton. After a 120-second delay, break valve TS-204, located at the bottom of HL-2, received an open signal (time zero). After an additional 0.5 second, an S signal was generated by the programmable logic controller (PLC), which time-sequences signals to initiate various events such as resetting controllers, stopping pumps, and repositioning valves.

The SG steam pressure controller reset to control pressure at []^{a,b,c} to minimize heat removal by the SGs. The value of []^{a,b,c} was high enough that the valve would not re-open, yet low enough not to challenge the SG safety valves. Simultaneously, the reactor controller transferred from the temperature (hot-leg average temperature in °F) control mode to the power (kW) control mode, with demand programmed for 600-kW total power. The main feedwater pump tripped, and the SG feedwater control valves closed at 4 seconds, isolating feedwater to the SG.

At []^{a,b,c} with the RCPs still running, the PRHR HX outlet valve opened, allowing forced flow through the PRHR HX to begin and, therefore, cooled fluid to enter the system at the SG-2 outlet channel head from the HX. At []^{a,b,c} the RCPs tripped and the flow through the PRHR HX shifted from forced to natural circulation flow.

When the break valve opened, flow through the simulated break flashed into steam and water and then passed into the break separator, where the liquid and steam components were separated and measured. Liquid flow reached a maximum rate of []^{a,b,c} about []^{a,b,c} after the simulated break was initiated (Figure 5.7-5). Liquid break flow then decreased gradually to a fluctuating range of 10 to 18 gpm until the ADS-1 valve opened at []^{a,b,c}. When the ADS-1 valve opened, the liquid break flow decreased to about []^{a,b,c}. Steam flow from the simulated break peaked at []^{a,b,c} []^{a,b,c} after break initiation (Figure 5.7-10). Steam flow decreased slowly to about []^{a,b,c} at []^{a,b,c}. Nearly steady flow of []^{a,b,c} continued during the quasi-equilibrium (Figure 5.7-53) between the SG primary and secondary pressures (from about []^{a,b,c}). Steam flow through the simulated break fell rapidly to []^{a,b,c} at about

[]^{a,b,c} as the pressure rapidly decreased because of cold water injections from the CMTs and accumulators, and the opening of the ADS-1 and ADS-2 valves.

The CMT outlet valves opened at []^{a,b,c} and recirculation flow of about []^{a,b,c} was established through the CMTs (Figure 5.7-2). This flow was driven by the pressure difference created by the lower temperature, higher density fluid in the CMTs compared with the higher temperature water in the balance lines and reactor. At approximately []^{a,b,c} the CMT balance lines drained (Figure 5.7-25) and flow from the CMTs transitioned from recirculation to draindown. The drainage flow fluctuated but averaged about []^{a,b,c}. This drainage flow increased the RCS liquid inventory, resulting in the slow level rise in the reactor.

The pressurizer drained rapidly and became empty at []^{a,b,c}. The pressurizer surge line became empty shortly afterwards at []^{a,b,c} (Figure 5.7-26). Drainage of the pressurizer and its surge line was very rapid because they were connected directly to the hot leg with the simulated break.

As soon as the pumps coasted to []^{a,b,c} flow, the indicated liquid level in the reactor began to drop sharply (Figure 5.7-16). The minimum collapsed reactor level of []^{a,b,c} occurred at about []^{a,b,c}. The estimated maximum steam percentage in the upper half of the core based on the minimum level measurement, indicated by LDP-110 (Figure 5.7-7), at []^{a,b,c} was []^{a,b,c}.

$$\text{Steam percent} = \frac{\text{level (100\% water)} - \text{level (with steam)}}{\text{level (100\% water)}} \times 100$$

When available, temperature-compensated levels were used.

Coolant temperatures in the core remained below saturation in the lower two-thirds of the core (up to []^{a,b,c}), and the coolant was saturated (and presumably two-phase) in the upper one-third of the core ([]^{a,b,c}), as shown by the core coolant temperatures (Figure 5.7-50). Heater rod cooling was provided by subcooled liquid or by a two-phase mixture of steam and water, which prevented excessive heater temperatures (Figure 5.7-55). Short-term ([]^{a,b,c}) temperature peaks of []^{a,b,c} occurred, possibly as a result of short-term insufficient liquid contact with the heater rod in the vicinity of the thermocouple.

Primary system pressure decreased at almost a constant rate until the primary and secondary system pressures reached quasi-equilibrium between []^{a,b,c} (Figure 5.7-53). After []^{a,b,c} the RCS pressures decreased at a constant rate until the ADS-1 valve opened. The primary system (hot legs, cold legs, reactor, and pressurizer) pressures rose about 10 psi for about 15 seconds at about 156 and 188 seconds (Figures 5.7-30 and 5.7-31). These peaks occurred during the drainage of the SG-1 and SG-2 tubes (Figures 5.7-20 and 5.7-22). The SG tubes refilled briefly after their initial partial drainage, possibly as a result of the transition from recirculation mode to

draindown in the CMTs. The SG tubes began their final drainage at about []^{a,b,c} and became empty between []^{a,b,c}. The pressures in the primary and secondary sides of the SGs both reached quasi-equilibrium between []^{a,b,c} (Figure 5.7.1-53).

At []^{a,b,c} CMT-1 low level was reached and the ADS-1 opening signal was initiated. Per design, the ADS-1 valve opened at []^{a,b,c} ([]^{a,b,c} after CMT-1 reached its low/low level), ending the initial depressurization phase.

ADS Phase

When the ADS-1 valve opened at []^{a,b,c} the pressurizer started to refill (Figure 5.7-26). The pressurizer reached its full level at about []^{a,b,c} and remained nearly full during this phase, except for a brief drop in level between []^{a,b,c}.

Both accumulators started to inject water into the DVI lines at []^{a,b,c} (Figure 5.7-2) when DVI pressure fell to accumulator pressure. With the rapid depressurization of the RCS (Figure 5.7-31) because of venting through the ADS-1 and ADS-2 valves, flow from both accumulators reached a maximum []^{a,b,c} at []^{a,b,c}. Accumulator injection continued at []^{a,b,c} until the accumulators became empty at about []^{a,b,c} (Figure 5.7-2).

Flow from the CMTs decreased when accumulator flow began. CMT-1 flow fell to []^{a,b,c} when accumulator flow reached its maximum ([]^{a,b,c}); CMT-2 flow decreased to []^{a,b,c} (Figure 5.7-2). Flow from both CMTs increased to about []^{a,b,c} when accumulator water inventories were exhausted. Reactor collapsed wide-range level increased to about []^{a,b,c} and remained at this level until []^{a,b,c} shortly after the accumulator injections halted (Figure 5.7-16).

The reactor and downcomer levels converged at about []^{a,b,c} and fell to a constant, common level of about []^{a,b,c}. When the ADS-4 valves located in the hot legs opened at []^{a,b,c} the reactor level started to drop slowly; downcomer level remained constant (Figure 5.7-16).

During this phase, the coolant temperature in the core followed the pressure in a downward trend. The temperatures near the top of the core were at saturation, indicating boiling. Temperatures lower in the core were subcooled (Figure 5.7-50). The core heater rod temperatures also followed the trend of the pressure/saturation temperatures (Figure 5.7-55). Short-term thermal rises of up to []^{a,b,c} were indicated in the heater rods. Short-term temperature drops of up to []^{a,b,c} were indicated. The temperature rises may have been caused by temporary steam blanketing near the thermocouple. The temperature decrease was possibly caused by the heaters contacting unmixed, colder injection flow.

The IRWST isolation valves opened at about []^{a,b,c} when the reactor pressure fell below []^{a,b,c}. However, IRWST flow did not start until about []^{a,b,c} when the CMT flows stopped (Figure 5.7-54). The initiation of flow from the IRWST concluded this phase of the test.

IRWST Injection Phase

Although the IRWST injection valves opened at about []^{a,b,c} flow from the IRWST started after []^{a,b,c} in the two IRWST injection lines. Flow from the IRWST was hydraulically blocked by the fluid head in the CMTs. When the level in the CMTs decreased below the level in the IRWST, the IRWST injected into the DVI lines. The CMTs became empty at []^{a,b,c} and CMT-1 and CMT-2 started to reflood at []^{a,b,c} respectively. The CMTs reflooded when the balance lines filled and spilled into the CMTs, condensing the superheated steam (Figures 5.7-25x, 5.7-46x, and 5.7-47x). These condensations caused short-term level and pressure transients in the RCS. Condensation events are discussed in more detail in Subsection 7.1.

CMT-1 started to drain again at []^{a,b,c} and became empty at about []^{a,b,c} CMT-2 started to drain at []^{a,b,c} and became empty at about []^{a,b,c} (Figure 5.7-25x). Primary sump injection flow began at []^{a,b,c} when primary sump level became sufficient to open the primary sump injection check valves, which had been backseated by the head of water in the IRWST (Figure 5.7-54). The test was terminated at []^{a,b,c} since the test objectives of operating until primary sump flow was initiated had been achieved.

5.7.5 Component Responses

Reactor

Level in the reactor core barrel, as measured by LDP-127, indicated a decrease immediately after the simulated break valve opened (Figure 5.7-16). The level became constant between about []^{a,b,c} probably because the pressurizer and SGs were emptying at a rate sufficiently high to make up the liquid loss through the simulated break. After the pressurizer became empty (LDP-602; Figure 5.7-26), the indicated level in the core barrel decreased again, reaching a minimum of about []^{a,b,c} at []^{a,b,c}. Two perturbations in level, which occurred at []^{a,b,c} were related to pressure pulses (PT-107, PT-108, and PT-109; Figure 5.7-31). These pressure increases, which may have been the result of higher temperature water draining from the SG tubes, caused an increase in water level in the CMTs (LDP-502 and LDP-507; Figure 5.7-25) and, therefore, an accompanying decrease in water level in the reactor core barrel (Figure 5.7-16).

CMT drainage flows and accumulator injection slowly increased the level in the core barrel until it reached a maximum indicated level of about []^{a,b,c}. After the accumulators emptied, the levels in the core barrel and downcomer equalized and decreased to an indicated minimum of about []^{a,b,c}. This value corresponded to a collapsed level about []^{a,b,c} above the upper core support plate location (Figure 5.7-16).

Three negative level excursions occurred at about []^{a,b,c}. These level perturbations were caused by condensation events, the first in the PRHR HX (LDP-802; Figure 5.7-29x), and the latter two in the CMTs, as indicated by LDP-509 and LDP-510

(Figure 5.7-25x). The sudden condensation in these components caused rapid pressure loss and caused the components to fill with primary coolant. This coolant inventory loss from RCS piping and the reactor, as well as the pressure pulse, was indicated by the reactor level instrumentation.

Both the reactor core barrel and the downcomer levels increased slowly to a maximum of about []^{a,b,c} (core barrel) as the IRWST injected coolant into the DVIs. Since the core barrel was vented to the atmosphere through HL-2 and the simulated break, its pressure was lower than the downcomer, which lagged the core barrel level by about []^{a,b,c} during IRWST injection.

At about []^{a,b,c} very slight level oscillations began. As the core barrel level decreased below the downcomer level, these oscillations increased in amplitude. The oscillations decreased at about []^{a,b,c} at which time the levels decreased several inches and the core barrel level again exceeded the downcomer level. A detailed discussion of the cause of these level (and flow) oscillations will be provided in the *AP600 Low-Pressure Integral Systems Test at Oregon State University Test Analysis Report, WCAP-14292*.⁽²⁾

Steam flow from the downcomer to the upper plenum occurred from about []^{a,b,c}. This effect was unique to this test because the hot-leg break reduced the upper plenum pressure. During the initial IRWST injection phase, from about []^{a,b,c} steam flowed from the upper plenum to the downcomer, as shown by differential pressure across the downcomer top plate. From []^{a,b,c} there was no steam flow across the downcomer top plate. Then, a small steam flow began as the level oscillations began. This flow ended when the level oscillations became dampened at about []^{a,b,c} (DP-130; Figure 5.7-11x).

Temperatures in the upper head (TF-120) and downcomer top (TF-168) became superheated between []^{a,b,c} (Figure 5.7-35), confirming that the levels had decreased below these thermocouples during this period. The upper head remained superheated for the remainder of the test, except for a brief period at []^{a,b,c} when this temperature decreased to saturation as a result of the condensation event in the CMT. The temperature at the top of the downcomer declined briefly to about []^{a,b,c} at []^{a,b,c} as a result of the same condensation event. This temperature was below saturation between about []^{a,b,c} indicating that the liquid level was above this thermocouple (TF-168) for this period. TF-152, located lower in the downcomer, ([]^{a,b,c} above the upper core support plate) remained below the saturation temperature for the entire test, confirming that the liquid level remained above this thermocouple. TF-147, located []^{a,b,c} above the upper core support plate, became superheated for about []^{a,b,c} and from []^{a,b,c}. Therefore, the minimum level in the downcomer was at least []^{a,b,c} above the upper core support plate. Except for several short periods, []^{a,b,c} and []^{a,b,c} the downcomer liquid level was greater than []^{a,b,c} above the upper core support plate (Figures 5.7-42 and 5.7-42x).

Core coolant temperatures at the center of the core (TR-001-1 through TR-001-6) which range from []^{a,b,c} from the bottom of the heater rods, remained below the saturation temperature for

the initial []^{a,b,c} (Figures 5.7-50 and 5.7-50x). Core coolant temperatures at the top []^{a,b,c} of the heater rods (TR-001-7 and TR-001-8) were at saturation temperature for the entire test, indicating that boiling occurred in this part of the core throughout the test. After []^{a,b,c} boiling was taking place as far as the []^{a,b,c} heater rod location. Temperature excursions of []^{a,b,c} were indicated at several axial lengths during the initial []^{a,b,c} and several temperature excursions of up to []^{a,b,c} were indicated at the top heater rod location between []^{a,b,c}.

Core heater temperatures at the top of the heater rods ([]^{a,b,c} from the reactor bottom) generally followed the core saturation temperatures as the reactor depressurized, but were []^{a,b,c} higher than coolant temperature. Both positive and negative short-term temperature excursions up to about []^{a,b,c} were indicated in several rods up to about []^{a,b,c}. Beyond this time, the temperature excursion were smaller in magnitude, []^{a,b,c} (Figures 5.7-55 and 5.7-55x).

The diminished temperature excursions occurred after the condensation events in the CMTs. These short-term temperature rises may have been caused by momentary dry-out of the heater surface. Temperature decreases were caused by colder injection water, which had not mixed thoroughly with the hot fluid, contacting the heater rods in the region. The earlier, large temperature indications may have been spurious electrical signals.

In summary, the two-phase mixture in the reactor remained well above the simulated core. Boiling occurred in the upper part of the simulated core. This boiling was limited to the upper several inches of the core heaters during the initial phases of the test and to the upper []^{a,b,c} during the later phase (beyond []^{a,b,c}). Although short-duration thermal excursions in core heaters and core coolant occurred, the simulated core cooling was maintained during the test. There were no condensation events in the reactor, since the core barrel was vented through the hot leg break and the downcomer remained nearly filled with water.

Core Makeup Tanks

Natural circulation through the CMTs began as soon as the CMT outlet valves opened (Figure 5.7-2). Flow from both CMTs, which reached constant rates of []^{a,b,c} were driven by the pressure differences resulting from the density differences between the cold water in the tanks and the hot water in the downcomer and cold legs. When the balance legs started to drain at about []^{a,b,c} (LDP-509 and LDP-510; Figure 5.7-25), flow from both CMTs transitioned from recirculation to draindown. The flow rates increased to an average of about []^{a,b,c} although the flow rates fluctuated over a wide range (from []^{a,b,c}). The CMT flow rates increased to about []^{a,b,c} between []^{a,b,c}. Flow from the CMTs decreased during the period of accumulator injection, from about []^{a,b,c}. The CMT flow rates increased to []^{a,b,c} after the accumulators became empty at []^{a,b,c} and then decreased rapidly after []^{a,b,c} as their levels decreased. The CMTs became empty at []^{a,b,c}.

Fluid temperatures in the CMTs increased stepwise with time during the recirculation phase as hot water from the cold-leg balance line replaced the initial cold water in the tanks (Figures 5.7-46 and 5.7-47). As water level dropped in the tank during draindown, the steam that replaced the liquid became superheated relative to RCS pressure, which continued to decrease (Figures 5.7-25 and 5.7-25x). As the level decreased, steam at lower positions in the tanks became superheated. When the condensation events in the CMTs occurred at []^{a,b,c} the steam temperatures decreased sharply to about []^{a,b,c}. Also, when the condensation occurred, cold water from the downcomer flowed through the CMT balance lines to refill the CMTs. The CMTs refilled only about halfway, possibly because nitrogen from the accumulators collected in the CMTs. As water from the downcomer flowed out the cold leg, this lost volume was made up by liquid from the core barrel, which reversed and flowed back into the downcomer. This phenomenon, which occurred in most of the tests, is discussed in detail in Subsection 7.1.

CMT-1 started to drain again at []^{a,b,c} and CMT-2 began to drain at about []^{a,b,c} when their respective balance line started to drain. The CMT flow rates fluctuated between []^{a,b,c} until CMT-1 became empty again at about []^{a,b,c} and CMT-2 became empty at []^{a,b,c}. The CMTs remained empty for the remainder of the test.

Accumulators

Both accumulators responded identically throughout the test. Flow from both accumulators was initiated at []^{a,b,c} just after the ADS-1 valve started to open, when DVI pressure fell below the total pressure (liquid head and nitrogen pressure) in the accumulators (Figure 5.7-2). The accumulator flow rates increased at []^{a,b,c} when the ADS-2 valve opened and reached a maximum of about []^{a,b,c}. Flow from the accumulators decreased slightly to []^{a,b,c} until the ADS-3 valve opened at []^{a,b,c} causing an increase of several gpm for each accumulator flow rate. The accumulators became empty at about []^{a,b,c} and remained empty for the remainder of the test (Figure 5.7-24). Spurious flow indications from FMM-401 (Figures 5.7-2 and 5.7-2x) after ACC-1 became empty at []^{a,b,c} should be disregarded.

Pressurizer

Electric power to the pressurizer heaters was turned off by manually opening the circuit breaker immediately after the S signal was verified. As the primary coolant discharged through the simulated break, the pressure (Figure 5.7-34) and the level (Figure 5.7-26) in the pressurizer decreased. The pressurizer became empty at []^{a,b,c} and the pressurizer surge line became empty at []^{a,b,c}.

When the ADS-1 valve opened at []^{a,b,c} and vented the pressurizer, the surge line and pressurizer refilled. Although the surge line level data (Figure 5.7-26) showed that the surge line was not completely filled, the two-phase mixture in the surge line or possibly liquid with a trapped steam bubble supported the liquid in the pressurizer. This support resulted from the higher pressure in the

hot leg to which the pressurizer surge line was connected. When the ADS-4 valves opened at []^{a,b,c} the pressure in the hot leg was vented and the pressurizer drained. The pressurizer became empty at []^{a,b,c} and remained empty for the remainder of the test.

The liquid level in the surge line rose to about []^{a,b,c} as IRWST injection pressure supported this liquid column. CMT condensation events caused steep drops in the surge line levels at []^{a,b,c}. As IRWST level and, hence, its pressure decreased, the level in the surge line declined slowly until the end of the test.

Passive Residual Heat Removal Heat Exchanger

The PRHR HX did not contribute significant heat rejection in this test. Since the PRHR HX received its inlet flow from HL-2 (where the simulated break had been installed), the PRHR HX only functioned during the initial []^{a,b,c}. Outlet flow during the initial []^{a,b,c} fluctuated from []^{a,b,c} but averaged about []^{a,b,c} (Figure 5.7-4). When HL-2 started to drain at about []^{a,b,c} PRHR flow decreased sharply. Outlet flow fluctuated between []^{a,b,c} until the SG-2 hot-leg elbow reached a minimum at []^{a,b,c}. For the remainder of the test, outlet flow fluctuated around []^{a,b,c} indicating that the flow meter was not filled with liquid. Large inlet flow fluctuations indicate that this flow meter was not completely filled.

Temperatures in the PRHR HX tubes showed that hot inlet flow was being cooled from saturation temperature to about []^{a,b,c} for about []^{a,b,c} (Figure 5.7-49). At this time, the temperatures in the PRHR HX converged at []^{a,b,c} indicating that inlet flow had become negligible and the HX tubes were being cooled to the IRWST water temperature. These temperature measurements confirm the flow measurements discussed in the previous paragraph.

At about []^{a,b,c} both the HX inlet temperature, as measured by TF-803, and HX outlet temperature, as measured by TF-804, were higher than the temperatures at the midpoints of the instrumented HX tubes, as measured by TF-808 and TF-809 (Figure 5.7-49x). These temperatures indicated that steam was flowing to the HX from both the inlet and outlet lines, and the flow was sufficient to heat the headers, but insufficient to heat the tube bundle. At []^{a,b,c} the outlet temperature increased to saturation temperature, []^{a,b,c} and then abruptly fell to about []^{a,b,c}. This sudden decrease in temperature was probably a condensation event in the outlet header of the PRHR HX that resulted in level perturbations in the downcomer and core barrel exactly at this time.

The temperatures in the PRHR HX headers declined then until they reached the same temperature as the tubes (about []^{a,b,c}). This behavior indicates lack of flow, resulting in cooling of the entire HX to IRWST temperature. At about []^{a,b,c} the inlet header suddenly increased to saturation temperature, []^{a,b,c} and the remainder of the HX remained near []^{a,b,c}. The increasing temperature in the inlet header at this time may have been caused by the drop in IRWST water level that decreased cooling or the restart of saturated fluid through the inlet line.

Steam Generators

Both SGs responded similarly to the transient, except that the break location affected the timing of primary-side draindowns. The secondary-side pressure of both SGs rose initially by about []^{a,b,c} and the primary pressure of both SGs decreased as the RCS lost mass through the simulated break (Figure 5.7-53). The SG-1 and SG-2 primary-side and secondary-side pressures reached quasi-equilibrium between []^{a,b,c}. The primary-side pressure for both SGs decreased rapidly after this time, which corresponded to the SG channel heads draining. Secondary-side pressure decreased at a slow rate during the remainder of the test as its energy was reduced by heat losses to the environment.

Both SG-1 and SG-2 long and short tubes partially drained at []^{a,b,c} which coincided with RCS pressure rising about []^{a,b,c}. After each partial draining, the level recovered and then decreased again. After the second cycle, the SG-1 tubes emptied between []^{a,b,c} (Figure 5.7-20). SG-2 tubes emptied between []^{a,b,c} (Figure 5.7-22). Similarly, the SG-1 channel heads (both hot leg and cold leg) became empty at []^{a,b,c} and the SG-2 channel heads drained at []^{a,b,c} (Figure 5.7-23). SG-2 would be expected to drain before SG-1, since the simulated break was in HL-2, the hot leg connected to SG-2. This was not the case because the flow from the pressurizer into HL-2 delayed drainage of the SG-2 hot-leg side of the tubes and flow from the PRHR HX into the SG-2 cold-leg channel head delayed drainage of the cold-leg side of the tubes. Level measurements in the SG tubes after the initial draindown were erroneous because of vaporization of the water in the reference leg and should be disregarded.

Thermal behavior of both SGs was similar (Figures 5.7-44, 5.7-44x, 5.7-45, and 5.7-45x). Initially, the fluid in the tubes was subcooled and became saturated liquid during the quasi-equilibrium the primary/secondary pressures. When the tubes drained, steam in the tubes became superheated relative to the decreasing pressure in the RCS. The temperatures in the short tubes in both SGs fell sharply to saturation and then returned to their initial superheat conditions at []^{a,b,c} in response to the condensation event. The other two condensation events apparently did not produce sufficiently large pressure transients to result in level increases large enough for the saturated water in the hot or cold legs to rise to the thermocouple levels in the SG tubes.

Cold Legs and Hot Legs

The four cold legs responded similarly in this test since the simulated break was in HL-2. Although the differential pressure instrumentation used to measure levels in the horizontal hot-leg and cold-leg piping could not be used for exact level data, these instruments did provide information to identify initiation of draining, time when the pipes became empty, and level trends. These instruments are discussed in more detail in Subsection 2.4. Data from these instruments (Figures 5.7-18, 5.7-18x, 5.7-19, and 5.7-19x), together with the temperature measurements, were used for the basis of the discussion of the cold legs and hot legs in this section.

The cold legs (Figure 5.7-18) began to drain at about []^{a,b,c} when the downcomer water level decreased to the top of the cold legs (Figure 5.7-16) and became empty between []^{a,b,c}. Confirmation that the cold legs were empty at these times was indicated by the superheated temperatures at the bottoms of the cold leg reactor flanges—TF-107 (CL-1), TF-103 (CL-3), and TF-104 (CL-4) (Figures 5.7-36, 5.7-38, and 5.7-39). CL-2 apparently did not drain completely since the bottom reactor flange temperature, TF-108, remained below saturation temperature (Figure 5.7-37). The cold legs partially refilled at about []^{a,b,c} as a result of the condensation event in the PRHR HX. The conclusion is supported by the subcooled temperatures indicated after []^{a,b,c} at the bottom of the reactor flanges. The cold legs remained partially full of water until they filled completely when the second condensation event occurred at []^{a,b,c}. They remained filled until about []^{a,b,c} when the top flange temperatures approached the saturation temperature. Since the downcomer level was above the cold-leg nozzles at this time, it is unlikely that the cold legs had drained.

The hot legs started to drain at about []^{a,b,c} (Figure 5.7-19). LDP-208 should be disregarded for this test because it was misranged. Level measurements (Figure 5.7-19x) indicate that the hot legs started to refill at about []^{a,b,c} when the condensation event in the PRHR HX occurred. Complete refilling of both hot legs was confirmed by the decrease of the temperature at the hot-leg reactor flanges to less than saturation (Figures 5.7-40 and 5.7-41). Both hot legs remained below saturation temperature until about []^{a,b,c} except for several hundred seconds after each condensation event at []^{a,b,c} (Figures 5.7-40x and 5.7-41x). At about []^{a,b,c} the flange temperatures again approached saturation, indicating that the hot legs had been filled with saturated fluid since the core barrel level was above the hot leg nozzles in the reactor at []^{a,b,c} (Figure 5.7-16x).

The behavior of the fluid levels and temperature in the two hot legs was similar, even though the 2-in. simulated break was installed in HL-2. It is possible that the water inventory and injection flows in the core barrel were sufficient to maintain the level in both hot legs irrespective of the flow through the break in HL-2.

In-Containment Refueling Water Storage Tank

Steam and liquid from the ADS 1-3 separator discharged through a sparger in the IRWST, where the steam was condensed by contact with the cold water. Liquid level in the IRWST rose about []^{a,b,c} (Figure 5.7-28). At about []^{a,b,c} the liquid in the IRWST reached the overflow line to the primary sump (Figure 5.7-6). The overflow line maintained the level constant until injection of water from the IRWST into the DVI lines. As the steam condensed, its heat content raised the temperature of the IRWST water. The upper []^{a,b,c} increased from []^{a,b,c} by the time injection began. The water stratified; that is, the higher temperature water remained at the top and colder water remained at the bottom. For example, the lower []^{a,b,c} of water inventory remained at []^{a,b,c} until injection started; this lower volume was discharged first (Figure 5.7-48).

Injection of water from the IRWST began at about []^{a,b,c} when DVI pressures fell below IRWST pressure (Figure 5.7-56). Flow started in both lines within about []^{a,b,c} of each other, indicating that the pressures in the DVI lines were equivalent. The IRWST flows peaked at about []^{a,b,c} in each line when the CMTs reflooded and then declined approximately linearly with time to about []^{a,b,c} as the IRWST water level declined. IRWST flow became unstable, fluctuating by []^{a,b,c} as the flow further declined (on average) to []^{a,b,c}. The flow rates decreased because the reflooded CMTs were injecting water into the common line with the IRWST. At about []^{a,b,c} the fluctuations reduced, the flow temporarily increased to []^{a,b,c} at []^{a,b,c} and then it declined as the primary sump flow started just before test termination.

Break and ADS Measurement System

Break flow flashed into steam and liquid as it was discharged from the break hole simulating the []^{a,b,c} hot-leg piping break. This two-phase mixture was separated into single-phase liquid and steam streams by the break separator. Liquid flow (FMM-905; Figure 5.7-5) peaked at about []^{a,b,c} immediately after the break and gradually declined as the pressure decreased to several gpm at about []^{a,b,c}. The flow then decreased very slowly as the IRWST injection flow declined. At about []^{a,b,c} water from the break separator began to flow into the break (Figure 5.7-5x) as its level became higher than the break elevation.

Steam flow from the break separator peaked at about []^{a,b,c} immediately after the break and declined gradually to about []^{a,b,c} at []^{a,b,c} (Figure 5.7-10). Steam flow then fell rapidly to []^{a,b,c} at about []^{a,b,c} which was shortly after the ADS-1 and ADS-2 valves had opened and depressurized the RCS.

The ADS-4 discharges were separated into single-phase streams of liquid and steam by the ADS separators when the two ADS-4 valves opened. The initial liquid flows from ADS 4-1 and ADS 4-2 peaked at []^{a,b,c} respectively (Figure 5.7-5). Steam flows from the ADS-4 separators indicated very low flows (about []^{a,b,c}) briefly when the ADS-4 valves were opened and then became immeasurably small for the remainder of the test (Figures 5.7-8 and 5.7-8x). When the ADS-4 valves opened at []^{a,b,c} the hot legs had been depressurized to atmospheric pressure and saturation temperature, precluding flashing into two-phase flow. Liquid flows from the ADS 4-1 and ADS 4-2 separator both decreased approximately linearly to about []^{a,b,c} respectively, at []^{a,b,c}. At []^{a,b,c} both flows started to fluctuate with an average increase of []^{a,b,c}. These flows decreased slightly when the oscillation became dampened at []^{a,b,c} and then started to fluctuate again near the end of the test when reverse flow occurred through the break (Figure 5.7-5x).

5.7.6 Mass Balance

A mass balance for this test was calculated from water inventories in the components before and after the test. Water mass at the completion of the test agreed with pre-test mass within []^{a,b,c}. Details of this mass balance are provided in Appendix E.

5.7.7 Conclusions

This test was successfully concluded when flow from the primary sump was initiated. Adequate cooling of the heaters simulating the core was achieved during the entire test. There were no condensation events in this test because the core barrel was vented through the hot leg break and the downcomer water level remained higher than in previous tests. There were, however, condensation events in the CMTs, resulting in their refilling. The collapsed level in the core barrel remained well above the core during the entire test, reaching a minimum of []^{a,b,c} above the upper core support plate.

The test was performed with minimal problems and is considered acceptable. Although not all of the facility initial conditions met the specified acceptance criteria, the deviations did not impact the quality of the data. The instrumentation problems encountered were not critical to the performance of the facility mass and energy balances.

Facility response to the test was as anticipated for the conditions that were established. The data clearly demonstrate that cooling of the reactor heater rods was maintained throughout the duration of the test.

TABLE 5.7-1
MATRIX TEST SB15 INITIAL CONDITIONS

Parameter	Instrument No.	Specified Initial Condition	Actual Initial Condition	Comments
Pressurizer pressure ⁽¹⁾	PT-604	370 ± 2 psig	— a,b,c	
HL-1 temperature ⁽¹⁾	SC-141	420 ± 2°F		
HL-2 temperature ⁽¹⁾	SC-140	420 ± 2°F		
SG-1 pressure ⁽¹⁾	PT-301	285 ± 5 psig		
SG-2 pressure ⁽¹⁾	PT-302	285 ± 5 psig		
Pressurizer level ⁽¹⁾	LDP-601	65 ± 5 in.		Level signal temperature-compensated by SC-608
SG-1 narrow-range level ⁽¹⁾	LDP-303	26 ± 3 in.		Level signal temperature-compensated by TF-301
SG-2 narrow-range level ⁽¹⁾	LDP-304	26 ± 3 in.		Level signal temperature-compensated by TF-310
IRWST temperature ⁽²⁾	TF-709	< 80°F		
CMT-1 temperature ⁽²⁾	TF-529	< 80°F		
CMT-2 temperature ⁽²⁾	TF-532	< 80°F		
ACC-1 temperature ⁽²⁾	TF-403	< 80°F		
ACC-2 temperature ⁽²⁾	TF-404	< 80°F		
IRWST level ⁽²⁾	LDP-701	Level established by fill-line elevation		
ACC-1 level ^(2,3)	LDP-401	Level established by standpipe at 37 in.		
ACC-2 level ^(2,3)	LDP-402	Level established by standpipe at 37 in.		

TABLE 5.7-1 (Continued)
MATRIX TEST SB15 INITIAL CONDITIONS

Parameter	Instrument No.	Specified Initial Condition	Actual Initial Condition	Comments
ACC-1 pressure ⁽²⁾	PT-401	232 ± 2 psig	[] ^{a,b,c}	Pressure was [] ^{a,b,c} or [] ^{a,b,c} low; condition acceptable
ACC-2 pressure ⁽²⁾	PT-402	232 ± 2 psig	[]	Pressure was [] ^{a,b,c} or [] ^{a,b,c} low; condition acceptable
CMT-1 level ⁽²⁾	LDP-507	Full	[]	
CMT-2 level ⁽²⁾	LDP-502	Full	[]	

Note:

- (1) Data for the indicated parameter were recorded in the test procedure as an initial condition for the test. The value was determined by the test engineer from the appropriate control board indicator.
- (2) Data were not recorded in the procedure, but the test engineer verified that specific conditions were achieved while establishing initial conditions. The value of the parameter was determined post-test by calculating the average DAS indication for a time of about 2 minutes before the break valve opened.
- (3) The bourdon pressure tube local indicator (PI-401 or PI-402) was tubed to the lower portion of the reference leg of the accumulator level transmitter (LDP-401 or LDP-402). As pressure in the accumulator was increased, air inside the bourdon tube was compressed, thereby lowering the reference leg liquid level, resulting in a false indication of measured level.

TABLE 5.7-2
MATRIX TEST SB15 INOPERABLE INSTRUMENTS/INVALID DATA CHANNELS

Instrument No.	Instrument Type	Description of Problem
FDP-605	Differential pressure transmitter - flow	Over-ranged when ADS-1 valve opened
FMM-201* FMM-202* FMM-203* FMM-204*	Magnetic flow meter	Removed from system
FMM-502*	Magnetic flow meter	Data invalid after [] ^{a,b,c} because of steam in the balance line
FMM-503*	Magnetic flow meter	Data invalid after [] ^{a,b,c} because of steam in the balance line
FMM-802*	Magnetic flow meter	Data invalid after steam forms in PRHR HX inlet line, which appears to be at about [] ^{a,b,c}
FMM-804*	Magnetic flow meter	Data valid until PRHR HX initially drained at 420 seconds; after this time the possibility of steam in the outlet line invalidated the data
HFM-103 HFM-105 HFM-505 HFM-510 HFM-601	Heat flux meter	Failed
HPS-203-1 through 3	Heated phase switch	Inoperable throughout test
HPS-509-1 through 3	Heated phase switch	Removed
LDI ³ 102	Differential pressure transmitter -- level	Failed
LDP-113	Differential pressure transmitter -- level	Data invalid during entire test because of dynamic flow effects from hot-leg break

TABLE 5.7-2 (Continued)
MATRIX TEST SB15 INOPERABLE INSTRUMENTS/INVALID DATA CHANNELS

Instrument No.	Instrument Type	Description of Problem
LDP-139	Differential pressure transmitter – level	Data invalid during entire test because of dynamic flow effects from hot-leg break
LDP-201 LDP-202 LDP-203 LDP-204 LDP-205 LDP-206	Differential pressure transmitter – level	Data invalid due to effect of vertical portion of sense line attached to top of pipe; data can show level trends, when the pipe is empty or starts to drain, but absolute level indication cannot be used
LDP-207 LDP-208 LDP-209	Differential pressure transmitter – level	Inoperable – ranged improperly; data can show trends, but absolute level indication cannot be used
LDP-215* LDP-216 LDP-217 LDP-218* LDP-219* LDP-220 LDP-221 LDP-222*	Differential pressure transmitter – level	Data invalid when tube drained and the reference leg started to vaporize
LDP-802* LDP-804	Differential pressure transmitter – level	Data valid until PRHR HX initially drained at 420 seconds; data suspect after this time because of possible vaporization in common reference line
PT_101	Pressure transmitter	Data less than 6.1 psig invalid
PT_102	Pressure transmitter	Data less than 6.2 psig invalid
PT_103	Pressure transmitter	Data less than 6.2 psig invalid
PT_104	Pressure transmitter	Data less than 6.4 psig invalid
PT_108	Pressure transmitter	Data less than 8.4 psig invalid
PT_109	Pressure transmitter	Data less than 6.3 psig invalid
PT_111	Pressure transmitter	Data less than 6.0 psig invalid
PT_112	Pressure transmitter	Data less than 8.8 psig invalid
PT_113	Pressure transmitter	Data less than 6.4 psig invalid
PT_201*	Pressure transmitter	Data less than 1.1 psig invalid

TABLE 5.7-2 (Continued)
MATRIX TEST SB15 INOPERABLE INSTRUMENTS/INVALID DATA CHANNELS

Instrument No.	Instrument Type	Description of Problem
PT_202	Pressure transmitter	Data less than 5.9 psig invalid
PT_205	Pressure transmitter	Data less than 6.1 psig invalid
TF-103*	Thermocouple fluid temperature	Removed and replaced with thermocouple for thermal stratification test
TF-104*	Thermocouple fluid temperature	Removed and replaced with thermocouple for thermal stratification test
TF-170 TF-501* TF-504*	Thermocouple fluid temperature	Read low throughout test
TFM-103 TFM-105	Thermocouple for HFM-703	Inoperable; indicated ambient temperature throughout test
TH-317-1 through 4	Thermocouple heater rod	Inoperable; heater rod removed prior to test
TW-503	Thermocouple wall temperature	Inoperable throughout test

Note:

* Instruments marked with an asterisk are critical instruments. See Subsection 5.7.2 for discussion.

**TABLE 5.7-3
MATRIX TEST SB15 SEQUENCE OF EVENTS**

Event ⁽¹⁾	Description in B&E Chart ⁽²⁾	Data Source ⁽³⁾	Time after Break (sec.)
TEST Pushbutton Depressed	TEST PB Pressed	D	— ^{a,b,c}
Break Valve Open Signal	Break Vlv Open Sig	D	
Break Valve Starts to Open	Break Vlv Open	D	
Feed Pump Trips	Feed Pump Trips	D	
CMT-1 Outlet Valve Starts to Open	CMT-1 Inj Vlv Open	D	
CMT-2 Outlet Valve Starts to Open	CMT-2 Inj Vlv Open	D	
PRHR HX Outlet Valve Starts to Open	PRHR HX Vlv Open	D	
Reactor Coolant Pumps Trip	RCPs Trip	D	
Pressurizer Empty (LDP-601)	Pressurizer Empty	A	
CMT-1 Recirculation Flow Stops (LDP-509)	CMT-1 Recirc Flow Stops	A	
CMT-2 Recirculation Flow Stops (LDP-510)	CMT-2 Recirc Flow Stops	A	
Time of Minimum Reactor Level Observed During Test (LDP-127)	Time of Min Rx Level	A	
Pressurizer Surge Line Empty (LDP-602)	Surge Line Empty	A	
SG-1 Cold-Leg Short Tube Empty (LDP-221)	SG-1 CL Shrt Tube Empty	A	
SG-1 Cold-Leg Long Tube Empty (LDP-219)	SG-1 CL Lng Tube Empty	A	
SG-1 Hot-Leg Long Tube Empty (LDP-215)	SG-1 HL Lng Tube Empty	A	
SG-1 Hot-Leg Short Tube Empty (LDP-217)	SG-1 HL Shrt Tube Empty	A	
SG-2 Cold-Leg Long Tube Empty (LDP-222)	SG-2 CL Lng Tube Empty	A	
SG-2 Hot-Leg Long Tube Empty (LDP-218)	SG-2 HL Lng Tube empty	A	
SG-2 Cold-Leg Short Tube Empty (LDP-220)	SG-2 CL Shrt Tube Empty	A	
SG-2 Hot-Leg Short Tube Empty (LDP-216)	SG-2 HL Shrt Tube Empty	A	
SG-1 Hot-Leg Channel head Empty (LDP-209)	HL-1 Chan Head Empty	A	
CL-3 Channel Head Empty (LDP-213)	CL-3 Chan Head Empty	A	
CL-1 Channel Head Empty (LDP-211)	CL-1 Chan Head Empty	A	

TABLE 5.7-3 (Continued)
MATRIX TEST SB15 SEQUENCE OF EVENTS

Event ⁽¹⁾	Description in Bar Chart ⁽²⁾	Data Source ⁽³⁾	Time After Break (sec.)
SG-1 Hot-Leg Elbow Starts Draining (LDP-207)	HL-1 Elbow Starts to Drain	A	a,b,c
HL-1 Pipe Starts to Drain (LDP-205)	HL-1 Pipe Starts to Drain	A	
SG-1 Hot-Leg Elbow Minimum (LDP-207)	HL-1 Elbow Level Min	A	
HL-2 Pipe Starts to Drain (LDP-206)	HL-2 Pipe Starts to Drain	A	
SG-2 Hot-Leg Elbow Starts Draining (LDP-208)	HL-2 Elbow Starts to Drain	A	
CL-4 Channel Head Empty (LDP-212)	CL-4 Chan Head Empty	A	
CL-2 Channel Head Empty (LDP-210)	CL-2 Chan Head Empty	A	
SG-2 Hot Leg Channel Head Empty (LDP-214)	HL-2 Chan Head Empty	A	
CMT-1 Low Level Signal	CMT-1 Level Lo Empty	D	
ADS-1 Valve Starts to Open	ADS-1 Vlv Open	D	
ACC-2 Injection Starts (FMM-402)	ACC-2 Inj Starts	A	
ACC-1 Injection Starts (FMM-401)	ACC-1 Inj Starts	A	
CMT-2 Low Level Signal	CMT-2 Level Lo	D	
ADS-2 Valve Starts to Open	ADS-2 Vlv Open	D	
HL-2 Pipe Empty (LDP-206)	HL-2 Pipe Empty	A	
HL-1 Pipe empty (LDP-205)	HL-1 Pipe Empty	A	
ADS-3 Valve Starts to Open	ADS-3 VLV Open	D	
Pressurizer Refloods (LDP-601)	Pressurizer Refloods	A	
IRWST-2 Injection Valve Starts to Open	IRWST-2 Inj Vlv Open	D	
Reactor Pressure Low	Reactor Pressure Lo	D	
IRWST-1 Injection Valve Starts to Open	IRWST-1 Inj Vlv Open	D	
ACC-1 Empty (LDP-401)	ACC-1 Empty	A	
ACC-2 Empty (LDP-402)	ACC-2 Empty	A	
SG-2 Hot-Leg Elbow Minimum (LDP-208)	HL-2 Elbow Level Min	A	

TABLE 5.7-3 (Continued)
MATRIX TEST SB15 SEQUENCE OF EVENTS

Event ⁽¹⁾	Description in Bar Chart ⁽²⁾	Data Source ⁽³⁾	Time After Break (sec.)
CMT-2 Level Low-Low	CMT-2 Level Lo-Lo	D	a,b,c
ADS 4-1 Valve Starts to Open	ADS 4-1 Vlv Open	D	
ADS 4-2 Valve Starts to Open	ADS 4-2 Vlv Open	D	
CMT-1 Level Low-Low	CMT-1 Level Lo-Lo	D	
IRWST-2 Injection Starts (FMM-702)	IRWST-2 Inj Starts	A	
IRWST-1 Injection Starts (FMM-701)	IRWST-1 Inj Starts	A	
CMT-2 Empty (LDP-502)	CMT-2 Empty	A	
CMT-1 Empty (LDP-507)	CMT-1 Empty	A	
CMT-2 Starts to Reflood (LDP-502)	CMT-2 Refloods	A	
CMT-1 Starts to Reflood (LDP-507)	CMT-1 Refloods	A	
Primary Sump Starts to Overflow to Secondary Sump (LDF-901)	Pri Sump Overflows	A	

Note:

- (1) Data from the instrument channel in parenthesis were used to determine level, flow, or pressure conditions.
- (2) The attached bar chart provides a graphic representation of the timing of events.
- (3) D = time data obtained from a software program that monitored the input and output of the facility's PLC.
A = time data obtained by reviewing data from the instrument channel listed in the Event Description column.

The Bar charts for Table 5.7-3 on pages 5.7-25 through 5.7-30 are not included in this nonproprietary document.

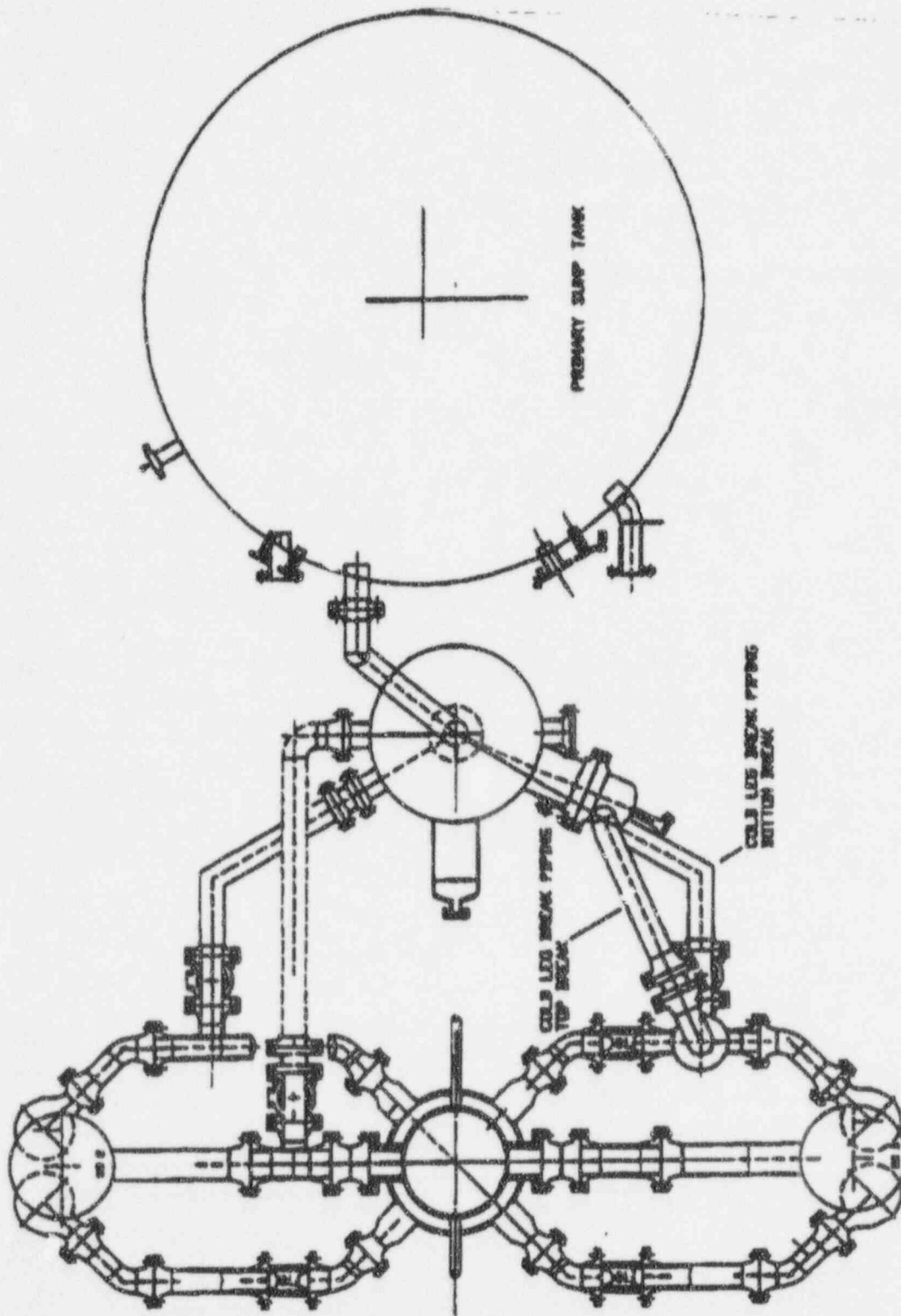


Figure 5.7-1a Primary Loop and Break Pipe Arrangement (Sh. 1 of 2)

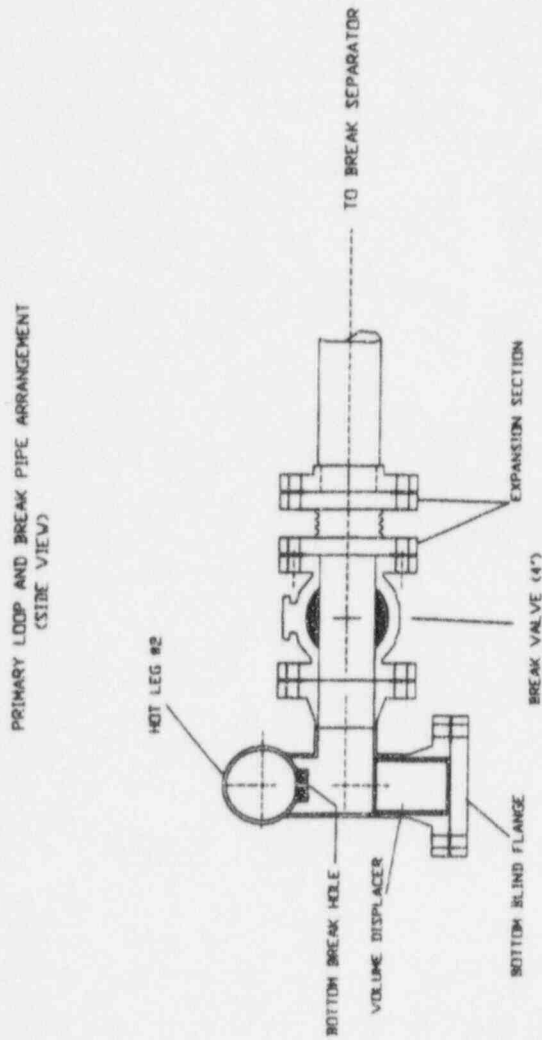


Figure 5.7-1b Primary Loop and Break Pipe Arrangement, Side View (Sh. 2 of 2)

Figures 5.7-2 through 5.7-56 are not included in this nonproprietary document.

6.0 MATRIX TEST GROUP COMPARISONS

The matrix tests in this section were previously evaluated in Section 5 as a reference or comparison test. This section uses the results from the tests to evaluate the system response to two other variables not evaluated in Section 5.

Section 6.1 evaluates the effect of break location on system response. All of the tests reviewed were 2-in. breaks. Matrix Test SB01 had a break of cold-leg 3 (CL-3); Matrix Test SB09 had a break of core makeup tank-1 (CMT-1) balance line; Matrix Test SB13 had a break of direct vessel injection line 1 (DVI-1), and Matrix Test SB15 had a break of hot leg-2 (HL-2).

Section 6.2 evaluates the effects of nonsafety system operation on system response. The two tests compared, Matrix Test SB01 and Matrix Test SB04, had identical test configurations except that the nonsafety residual heat removal pump and nonsafety-related chemical and volume control pump were allowed to operate in Matrix Test SB04.

6.1 Effect of 2-In. Break Location (Matrix Tests SB13 and SB15 Comparison with Matrix Test SB01)

This section compares facility response to the same size break at different locations. The four matrix tests below simulated a 2-in. break at the specified location. The tests are listed in order of their break location elevation, with the test at the lowest break elevation listed first.

- Matrix Test SB13 Direct vessel injection line 1 (DVI-1) break
- Matrix Test SB15 Bottom of hot leg-2 (HL-2) break
- Matrix Test SB01 Bottom of cold leg-3 (CL-3) break
- Matrix Test SB09 Core makeup tank-1 (CMT-1)/CL-3 balance line break

The only difference in system configuration between these tests was the location of the break. In all tests, both CMTs, both accumulators, both in-containment refueling water storage tank (IRWST) injection lines, and the passive residual heat removal heat exchanger (PRHR HX) were in service. In addition, the configuration of the automatic depressurization system (ADS) 1 - 3, and ADS-4 nozzles was identical, and the nonsafety systems were isolated. Differences in facility response in the four tests were due to the influence of the location of the break.

The sequence or timing of important events in the four tests is summarized in Table 6.1-1. Data are presented in tabular and bar-chart format. The bar charts provide a visual comparison of the events between tests. Both the table and the bar charts are ordered according to Matrix Test SB01 event times. Unless otherwise stated, Table 6.1-1 is the reference for any times used in this section.

6.1.1 Influence of Break Location on Break Flow Rates

The influence of break location can be evaluated using the break flow rate data of FMM-905 or the primary sump mass data of LCT-901.

The break flow rate measured by FMM-905 was different in each of the four tests (Figures 6.1-1 and 6.1-2). The flow rate from the DVI break did not appear to be a function of elevation. In the first []^{a,b,c} the break from the lowest elevation (DVI-1) had the smallest break flow rate, but then had the largest flow rate from []^{a,b,c}. Likewise, the break flow rate from the highest elevation (CMT-1/CL-3 balance line) had flow rates approximating that of the hot-leg and cold-leg breaks during the first []^{a,b,c} but was then alternately smaller then larger than these two break flow rates until []^{a,b,c}. The results do not take into consideration any break mass retention or holdup in the break separator during the transient.

Another method of evaluating the possible influence of break elevation on break flow is to use the data from LCT-901, which measured the liquid mass contained in the primary sump. Before ADS-4 actuation, the only source of liquid to the primary sump was break flow. ADS-4 actuated at []^{a,b,c} in Matrix Test SB13; all other ADS-4 actuations were between []

^{a,b,c} Again, the discussion does not take into consideration any break mass retention or holdup during the transient.

Two plots of primary sump mass with respect to time are used with two different time scales. Figure 6.1-3 has a time scale of []^{a,b,c} a period before any ADS-4 actuations. Figure 6.1-4 spans the period from []^{a,b,c} Data for Matrix Test SB09 are invalid after []^{a,b,c} because of problems with instrument channel LCT-901.

Review of the data for primary sump mass provides the same result as the break flow data: there was no direct correlation between break elevation and break flow or inventory loss from the reactor coolant system (RCS). Test data for the first []^{a,b,c} (prior to ADS-4 actuation) of Matrix Test SB13 provide an example (Figure 6.1-3). After this time the primary sump mass was affected by both break and ADS-4 flow. In the first []^{a,b,c} the changing break flow rate in Matrix Test SB13 created an RCS inventory loss that went from the third highest in magnitude between []^{a,b,c} to equaling the largest RCS inventory loss at []^{a,b,c}. By the time ADS-4 actuated in Matrix Test SB13, the RCS inventory loss was 57 percent greater than in any of the other tests.

Another example is provided by the first []^{a,b,c} of primary sump data for Matrix Test SB15 (HL-2). In the first []^{a,b,c} mass in the primary sump was smallest for Matrix Test SB15. By []^{a,b,c} primary sump mass was over 16 percent greater than in either Matrix Test SB01 or SB09 (Figure 6.1-4).

6.1.2 Influence of Break Location on ADS Actuation

One of the most significant parameters affected by the location of the simulated 2-in. break was the actuation of ADS-1. Table 6.1-1 indicates that the earliest ADS-1 actuation was at []^{a,b,c} in Matrix Test SB13, and the latest actuation was at []^{a,b,c} in Matrix Test SB09.

The only variable between the four tests was the location of the break. Since ADS-1 actuated at different times in the four tests, it follows that the break location must have created this difference by influencing the CMT flow rates. Since facility logic actuated ADS-1 []^{a,b,c} after either CMT reached the low level setpoint, times of ADS-1 actuation provided a relative measure of the CMT draindown rates between tests.

CMT-1 and CMT-2 injection flow rates varied significantly between tests, both before and after ADS-1 actuated (Figures 6.1-5 through 6.1-8). CMT-1 and CMT-2 flow also differed in the same test. The differences were small in Matrix Tests SB01 and SB15, but were pronounced in Matrix Tests SB09 and SB13 (Figures 6.1-9 through 6.1-12). All of the differences are explainable by analyzing the location of the break with respect to the CMTs.

The earliest ADS-1 actuation occurred in Matrix Test SB13. In this test, the DVI-1 line was broken, creating a direct flow path from CMT-1 to the primary sump. The CMT-1 flow rate in Matrix Test SB13 was the highest in any of the tests for either of the CMTs due to this low-resistance flow path to the primary sump (Figure 6.1-1). The resultant high CMT draindown rate encouraged the relatively early actuation of ADS-1. A measure of the early ADS-1 actuation was that it occurred before the pressurizer surge line emptied. This did not occur in the other tests. CMT-1 injection flow was significantly greater than flow from CMT-2 in Matrix Test SB13 because the location of the break created a higher resistance to break flow from CMT-2 to the break than it did for CMT-1 (Figure 6.1-11).

The break location in Matrix Test SB09 created the opposite effect on CMT-1 injection flow. CMT-1 experienced a high injection flow rate in Matrix Test SB13 due to the low resistance between CMT-1 and the DVI-1 break; the break in the CMT-1/CL-3 balance line in Matrix Test SB09 decreased pressure at the top of CMT-1. This decrease in pressure was sufficient to limit CMT-1 injection flow to the smallest magnitude in any of the tests (Figure 6.1-5). As in Matrix Test SB13, a significant flow difference existed between CMT-1 and CMT-2 injection, but, in this case, the CMT-2 injection flow rate was higher (Figure 6.1-10). ADS-1 actuation in Matrix Test SB09 was a result of a low level in CMT-2 — the only case in the four tests where ADS-1 was actuated by CMT-2.

The break in Matrix Tests SB01 and SB15 produced results similar to one another. CMT-1 and CMT-2 injection flow rates were closely matched (Figures 6.1-9 and 6.1-12). These data were expected for Matrix Test SB15 because each CMT had a similar resistance to flow from the CMT to the hot-leg break. In Matrix Test SB01, the slightly larger CMT-1 flow between about []^{a,b,c} was possibly due to the CL-3 break being closer to the CMT-1 injection point at the reactor vessel. The total variance between the times when CMT-1 and CMT-2 reached their low level setpoints was only []^{a,b,c}. In fact, the CMT-2 low level setpoint was obtained at the same time in Matrix Tests SB01 and SB15.

CMT injection flow and ADS-1 actuation times did not appear to be a function of RCS inventory loss. The plots of CMT level versus primary sump fluid weight reveal the wide variance between CMT levels and primary sump mass when ADS-1 actuated (Figures 6.1-13 through 6.1-16). Just as the CMT flow injection data implied that the break elevation was not a factor in CMT draindown rates, the primary sump weight data imply that the CMT draindown rates were not strongly affected by the rate of RCS inventory loss through the break. Instead, the data again suggest that the largest influence in CMT draindown rate and ADS-1 actuation is the physical location of the break with respect to the CMT.

6.1.3 Influence of Break Location on Downcomer Levels

Downcomer levels varied widely between the four tests for the first []^{a,b,c} (Figures 6.1-17 through 6.1-20). Although the downcomer levels were obviously dependent on break location, how the levels were dependent is not obvious. In Matrix Test SB13, the minimum downcomer level

obtained after ADS-1 actuation was significantly lower compared with the other tests (Figure 6.1-17). The lower inventory in the downcomer was probably due to unavailability of accumulator-1 (ACC-1) inventory when it started injecting to the break after ADS-1 actuation at []^{a,b,c}. Between []^{a,b,c} when ACC-1 started to inject to the break, and []^{a,b,c} when ACC-1 emptied, the break flow rate in Matrix Test SB13 was higher than the other tests (Figure 6.1-21). The higher break flow rate may have been a direct result of ACC-1 injection to the primary sump via the break in the DVI-1 line. The loss of ACC-1 inventory to the sump in Matrix Test SB13 may account for the lower level in the downcomer for the remainder of the test (Figure 6.1-22).

6.1.4 Influence of Break Location on Core Levels

There were no temperature excursions in any of the four tests as a result of the 2-in. break.

The core had two narrow-range level transmitters with equal []^{a,b,c} spans. The lower transmitter was LDP-109 and the upper transmitter was LDP-110. Data from these transmitters were used to review the influence of break location on the core. Any reference to level when discussing the data of LDP-109 and LDP-110 implies a collapsed level. A level indication less than []^{a,b,c} indicates the existence of a steam percent greater than 0 in the measured regions.

Except for Matrix Test SB13, the lower core level was largely unaffected by the breaks (Figures 6.1-23 and 6.1-24). Matrix Test SB13 was the exception due to the effect of ACC-1 injection. ACC-1 and CMT-1 injected into the break of the DVI-1 line. When ADS-1 actuated at []^{a,b,c} the injection from ACC-1 and ACC-2 was not sufficient to immediately counteract the inventory loss through ADS-1, due to the portion of ACC-1 inventory that was lost directly to the primary sump. However, by []^{a,b,c} the level in the lower portion of the core had been effectively restored.

Different break locations initiated different responses in the upper core (Figure 6.1-25 and 6.1-26). It is possible to select different time frames in different tests, and discuss the possible influences of the break on upper-core level. However, a simple explanation of break location effects is not obvious because the relative levels in the four different tests change over the duration of the test. One condition is obvious: the low level in the upper core in Matrix Test SB13. Again, a possible explanation is the loss of inventory from ACC-1 and CMT-1 due to the break in DVI-1.

Table 6.1-1 on pages 6.1-5 through 6.1-7 is not included in this nonproprietary document.

The Bar Charts for Table 6.1-1 on pages 6.1-9 through 6.1-14 are not included in this nonproprietary document.

Figures 6.1-1 through 6.1-25 are not included in this nonproprietary document.

6.2 Effects of Nonsafety Systems (Matrix Test SB04 Comparison with Matrix Test SB01)

The effects of the operation of nonsafety systems on passive safety system response and overall facility response can be assessed by comparing the baseline test, Matrix Test SB01 (OSU Test U0001), with Matrix Test SB04 (OSU Test U0004). Both Matrix Tests SB01 and SB04 were 2-in. breaks located at the bottom of CL-3. Matrix Test SB04 was performed with forced injection from the chemical and volume control system (CVS) and normal residual heat removal system (RNS) pumps, and Matrix Test SB01 was performed without the operation of nonsafety systems.

Table 6.2.1-1 contains the sequence of events for Matrix Tests SB01 and SB04. The first pages of the table provide selected event times from both tests and the difference between event times. The subsequent pages of the table provide a visual representation of the time comparison using bar charts. For both the numeric table and the bar charts, the events are sorted in the chronologic order in which they occurred in Matrix Test SB01.

The table defines the source of actual time values. A D in the Data Source column indicates the recorded time was obtained from a software program that monitored digital events in the facility. These events included pump starts and stops, valve limit switch actuations, and alarms. An A in the Data Source column indicates the time data were obtained by reviewing test data recorded by the data acquisition system (DAS). Although the test data from the DAS were in digital format, the DAS monitored analog events such as pressure, flow, and temperature from the data.

The CVS pump started when pressurizer level dropped to the low-low level setpoint of []^{a,b,c} and stopped when pressurizer level rose to the low-low level reset of []^{a,b,c}. The CVS pump started at []^{a,b,c} and immediately began injecting cold water from the feedwater storage tank into the steam generator-2 (SG-2) cold-leg channel head at []^{a,b,c}. CVS injection continued at that rate until the pump was automatically stopped by the programmable logic controller (PLC) at []^{a,b,c}.

The RNS pump started, with the S signal present, when pressurizer pressure decreased to []^{a,b,c} and continued operating throughout the test. RNS injection did not start until about []^{a,b,c} when the pump discharge head finally exceeded RCS pressure. The RNS injection rate slowly increased as RCS pressure decreased and reached full flow of about []^{a,b,c} at []^{a,b,c}.

The depressurization rates for the two tests were similar until about []^{a,b,c} when the Matrix Test SB04 depressurization rate increased significantly as compared with the rate in Matrix Test SB01. Also, break flow during Matrix Test SB04 was predominantly greater than Matrix Test SB01 break flow. A possible explanation for the disparity between these parameters is that additional cold fluid injection from the CVS pump in Matrix Test SB04 maintained bulk fluid in the loops subcooled early in the test, whereas loop bulk fluid temperatures were at saturation in Matrix Test SB01.

Fluid addition from the CVS pump also impacted the transition of the CMTs from the recirculation mode to draindown, which was delayed by about []^{a,b,c} as compared with Matrix Test SB01. Even with the transition delay, CMT-1 reached the low level setpoint about []^{a,b,c} earlier in Matrix Test SB04, which resulted in the ADS-1 valve opening about []^{a,b,c} earlier. It is possible that a condensation/depressurization event in CMT-1 at about []^{a,b,c} during Matrix Test SB01, with a subsequent CMT reflood, may have contributed to the transition delay. In Matrix Test SB04, CMT draindown was stopped at about []^{a,b,c} when the backpressure caused by RNS pump flow to the DVI nozzles was sufficient to close the CMT discharge line check valves. A result of CMT draindown being stopped was that ADS-4 never occurred in Matrix Test SB04.

The calculated steam percent in the heater rod volume of the reactor vessel was similar for both tests until CMT injection began to decrease in Matrix Test SB01, at which time RNS injection was still cooling the heaters in Matrix Test SB04. The calculated steam percent for Matrix Test SB01 increased from about []^{a,b,c} at which time IRWST injection began to restore RCS fluid inventory and, therefore, established better cooling.

Although the IRWST injection valves opened in both tests, IRWST injection never occurred in Matrix Test SB04 because the backpressure caused by RNS pump flow to the DVI nozzles closed the IRWST injection line check valves.

In summary, the nonsafety systems had a significant effect on the small-break loss-of-coolant accident (SBLOCA) event. The additional fluid injection from the CVS pump cooled the bulk fluid in the RCS and caused a subsequent faster depressurization prior to ADS-1 valve opening. The calculated steam percent in the heater rod volume was not affected until RNS pump injection. The RNS injection was sufficient to refill the RCS and maintain subcooled or saturated conditions throughout the RCS.

**TABLE 6.2.1-1
SEQUENCE OF EVENTS FOR EFFECTS OF NONSAFETY SYSTEMS ON 2-IN. BREAKS**

Event ⁽¹⁾	Data Source ⁽²⁾	SB01 Time After Break (sec.)	SB04 Time After Break (sec.)	Delta Time (sec.)
TEST Pushbutton Depressed				
Break Valve Open Signal				
Break Valve Starts to Open				
Feed Pump Trips				
CMT-1 Outlet Valve Starts to Open				
CMT-2 Outlet Valve Starts to Open				
PRHR HX Outlet Valve Starts to Open				
Reactor Coolant Pumps Trip				
CMT-1 Recirculation Flow Stops (LDP-509)				
CMT-2 Recirculation Flow Stops (LDP-510)				
Pressurizer Empty (LDP-601)				
Pressurizer Surge Line Empty (LDP-602)				
SG-1 Hot-Leg Short Tube Empty (LDP-217)				
SG-1 Hot-Leg Long Tube Empty (LDP-215)				
CL-1 Channel Head Empty (LDP-211)				
CL-3 Channel Head Empty (LDP-213)				
SG-1 Cold-Leg Short Tube Empty (LDP-221)				
SG-1 Cold-Leg Long Tube Empty (LDP-219)				
SG-2 Cold-Leg Short Tube Empty (LDP-220)				
SG-2 Cold-Leg Long Tube Empty (LDP-222)				
SG-2 Hot-Leg Short Tube Empty (LDP-216)				
Time of Minimum Reactor Level Observed During Test (LDP-127)				
SG-2 Hot Leg Long Tube Empty (LDP-218)				
HL-1 Pipe Starts to Drain (LDP-205)				
CL-4 Channel Head Empty (LDP-212)				
CL-2 Channel Head Empty (LDP-210)				

TABLE 6.2.1-1 (Continued)
SEQUENCE OF EVENTS FOR EFFECTS OF NONSAFETY SYSTEMS ON 2-IN. BREAKS

Event ⁽¹⁾	Data Source ⁽²⁾	SB01 Time After Break (sec.)	SB04 Time After Break (sec.)	Delta Time (sec.)
CMT-1 Low Level Signal				
ACC-2 Injection Starts (FMM-402)				
ACC-1 Injection Starts (FMM-401)				
ADS-1 Valve Starts to Open				
CMT-2 Low Level Signal				
SG-2 Hot-Leg Elbow Starts Draining (LDP-208)				
SG-2 Hot-Leg Channel Head Empty (LDP-214)				
HL-2 Pipe Starts to Drain (LDP-206)				
HL-2 Pipe Empty (LDP-206)				
ADS-2 Valve Starts to Open				
HL-1 Pipe Empty (LDP-205)				
ADS-3 Valve Starts to Open				
Reactor Pressure Low				
IRWST-2 Injection Valve Starts to Open				
SG-2 Hot-Leg Elbow Minimum (LDP-208)				
IRWST-1 Injection Valve Starts to Open				
Pressurizer Refloods (LDP-601)				
ACC-1 Empty (LDP-401)				
ACC-2 Empty (LDP-402)				
CMT-1 Level Low-Low				
ADS 4-1 Valve Starts to Open				
ADS 4-2 Valve Starts to Open				
CMT-2 Level Low-Low				
CMT-2 Empty (LDP-502)				
IRWST-2 Injection Starts (FMM-702)				
IRWST-1 Injection Starts (FMM-701)				
CMT-1 Empty (LDP-507)				
CMT-2 Starts to Reflood (LDP-502)				
CMT-1 Starts to Reflood (LDP-507)				
Primary Sump Starts to Overflow to Secondary Sump (LDP-901)				

a,b,c

TABLE 6.2.1-1 (Continued)
SEQUENCE OF EVENTS FOR EFFECTS OF NONSAFETY SYSTEMS ON 2-IN. BREAKS

Event ⁽¹⁾	Data Source ⁽²⁾	SB01 Time After Break (sec.)	SB04 Time After Break (sec.)	Delta Time (sec.)
Primary Sump-2 Injection Starts (FMM-902)				
Primary Sump-1 Injection Starts (FMM-901)				
Primary Sump-1 Injection Valve Starts to Open				
Primary Sump-2 Injection Valve Starts to Open				
SG-1 Hot-Leg Channel Head Empty (LDP-209)				
SG-1 Hot-Leg Elbow Starts Draining (LDP-207)				
SG-1 Hot-Leg Elbow Minimum (LDP-207)				

Note:

- (1) Data from the instrument channel in parenthesis were used to determine level, flow, or pressure conditions.
- (2) D = time data obtained from a software program that monitored the input and output of the facility's PLC. A = time data obtained by reviewing data from the instrument channel listed in the Event Description column.
- (3) O.O.S. = out of service

The Bar Charts for Table 6.2.1-1 on pages 6.2-6 through 6.2-11 are not included in this nonproprietary document.

7.0 OTHER TEST OBSERVATIONS

This section contains discussions about two unanticipated thermal-hydraulic phenomena, associated with the facility response to transients, that were observed in several of the tests. The facility response to condensation events that produced bangs during testing is examined.

The appearance of superheated steam in the core makeup tank (CMT) is also discussed. The CMTs are unheated and uninsulated vessels; consequently, the appearance of superheat during matrix testing is investigated. The superheat was traced to temperature stratification of the CMT's walls and fluids. At some point in the transient, the upper walls of the CMT provided heat to the saturated steam.

7.1 Condensation Events

Condensation events were observed during the performance of the matrix tests at the Oregon State University (OSU) test facility. The effects of the condensation events were recorded by the data acquisition system (DAS) and were directly observed by test personnel during the performance of the test. Condensation events produced noises ranging from very loud noises, described as *sharp knocks*, to barely audible noises, described as *pings*. The presence of condensation events was not surprising considering the water/steam interfaces produced in the test facility after the simulated break. Even the most severe condensation event, however, did not result in damage to the test facility.

Condensation events occur when saturated or subcooled liquid partially or fully collapses a steam bubble. The steam bubble collapse produces a local low-pressure region, which accelerates the surrounding fluid toward the low-pressure region. If the accelerated liquid impacts a solid object, the momentum transfer from the liquid to the solid object can produce vibration and noise. Test experience, review of data from the 17 tests contained in this report, and video records of a select number of tests have produced evidence of test conditions that produce the most significant condensation events.

Several level, flow, and temperature instrument channels recorded abrupt changes in the process during a condensation event. However, a study of the test data has revealed a combination of five instrument channels that provided good evidence that a condensation event had occurred. The instruments are:

- LDP-116 -- Downcomer annulus wide-range level at 270°az
- LDP-140 -- Downcomer annulus wide-range level at 180°az
- LDP-127 -- Reactor wide-range water level
- DP-114 -- Differential pressure across the upper support plate
- DP-130 -- Differential pressure across the core bypass holes

The three wide-range level channels usually measured collapsed level. However, during periods of high flow, such as during the accelerated flow from a condensation event, the level transmitters responded to flow-induced differential pressure and recorded it as a changing level. Differential pressure transmitters DP-114 and DP-130 measured steam flow during a condensation event as it flowed from the upper plenum, into the upper head via the holes in the upper support plate, and on to the upper portion of the downcomer annulus via the bypass holes in the core barrel flange (Appendix H, Dwg. LKL 911218, Sh. 2). The data from these transmitters may be used to determine the time of a condensation event. All five transmitters would record a change during the most significant condensation events; however, small local depressurizations would influence only a few of the transmitters.

The most significant and frequent condensation events appeared to occur during accumulator injection and during the reflood of the CMTs. When a condensation event occurred during accumulator injection, the steam bubble in the downcomer collapsed. The liquid in the downcomer accelerated

upward and impacted the bottom of the core barrel where the core bypass holes were located. The impact of the accelerated liquid on the core barrel flange produced noise and vibration.

LDP-116 and LDP-140 recorded the upward flow of the liquid in the downcomer as an increasing level. During the transient, the low pressure created in the downcomer resulted in a rapid increase in steam flow from the upper plenum, through the upper head, and to the downcomer via the core bypass holes. The increase in steam flow was recorded by DP-114 and DP-130 as a more-negative differential pressure indication. The negative sense of the data indicated the direction of flow was opposite to the flow direction before the simulated break occurred and the reactor coolant pumps (RCPs) were running. A sharp spike in data was also observed for the core wide-range water level transmitter, LDP-127.

Using the level of noise produced by a condensation event as a measurement, the observation of the test personnel revealed the most significant condensation event occurred during the accumulator injection of Matrix Test SB01. The event was duplicated during the performance of Matrix Test SB18, which was the validating, repeat test of reference test SB01.

The other significant and frequent type of condensation event occurred during the refill, or reflood, of the CMTs. When the cold legs refilled and water entered a CMT balance line, the relatively cold water started to slowly condense the steam in the balance line. As the condensation continued, the pressure in the vapor space of the balance line and of the CMT started to decrease. In fact, the pressure decreased to less than atmospheric pressure. The pressure imbalance between the cold leg and the CMT vapor space increased the liquid level in the balance line. When the balance line level was sufficiently high, the liquid from the balance line spilled into the CMT, collapsing the superheated steam bubble in the CMT. The in-rush of water to the low-pressure region of the CMT resulted in an increase in in-containment refueling water storage tank (IRWST) injection flow and a decreasing level in the core as some of the cooling water was diverted to the CMT fill. Core cooling was still maintained, however, as evidenced by the core temperatures.

7.2 CMT Temperature Measurement

The thermal-hydraulic phenomena of superheated saturated steam in the CMTs, usually during the early portion ([]^{a,b,c}) of the transient, was observed in many of the matrix tests. The cause of superheating in the CMTs is not obvious since the CMTs were at ambient temperatures prior to the initiation of the loss-of-coolant break. This section describes the effect of the superheated temperatures in the CMTs.

The location of thermocouples used in this section is provided in Appendix G, OSU Dwg. 600501 and 600502 for CMT-1 and CMT-2, respectively. One correction should be noted relative to the azimuthal orientation of the long thermocouple rod or rake in the CMTs. The drawings show the rake installed at 135°az, but its correct orientation is 315°az.

Temperature plots of thermocouples included in this section are based on the following radial locations:

- Centerline thermocouple from a radially mounted rod (indicated by the term *Center*)
- Thermocouples located 1 in. from the CMT wall (indicated by the term *Height*)
- Thermocouples located near center on a vertically oriented long thermocouple rod (indicated by the term *Long T/C Rod*)
- Thermocouples located on inside wall of CMT (indicated by the term *Vol Hgt-In*)
- Thermocouples located on outside wall of CMT (indicated by the term *Vol Hgt-Ou*)

The phenomena described for Matrix Test SB13 is applicable to many other matrix tests. Test results for Matrix Test SB13 are compared with test results from Matrix Tests SB01, SB10, and SB12 to confirm the observations of Matrix Test SB13.

CMT temperature data were plotted as a function of CMT level instead of time, as in the matrix test descriptions in Section 5. Temperature data were plotted against CMT level instead of time because the response in the CMT was a strong function of level in the tank, not elapsed time.

7.2.1 Matrix Test SB13 (U0113) Observation and Evaluation

Matrix Test SB13, a simulated a 2-in. break of DVI-1, reflected a relatively quick injection of the CMTs. As explained in Subsection 5.4 ?, the duration for CMT recirculation flow was limited (about []^{a,b,c}) before draindown of the CMTs. From []^{a,b,c} saturated water at about []^{a,b,c} entered both CMTs, causing localized heating of the water and the inside wall of the upper portion of the CMTs.

As the CMTs drained, the wall temperatures in the upper portion of the tank (50- and 75-percent volume levels) initially increased to saturation temperature, then followed the saturation temperature (Figures 7.2-3 through 7.2-6), until the temperature decrease stopped abruptly. This same behavior was observed for the 20-percent volume level in CMT-1 but not in CMT-2 (Figures 7.2-2 and 7.2-1).

As the tank drained, the upper walls of CMT-2 appeared to become a heat source to the steam in the tank, and the lower portion of the CMT walls acted as a heat sink. This observation is based on the relative temperatures of the CMT-2 wall and fluid temperatures at the same elevation. At the 20- and 50- percent volume levels, the steam temperature was always greater than the wall temperatures after the wall and fluid temperatures started to increase (Figures 7.2-1 and 7.2-3), implying that the wall at the 20- and 50-percent volume levels remained a heat sink during the tank-drain period.

At the 75-percent volume level, the temperatures of the fluid (TF-516, TF-524, and TF-544) and wall (TW-532) became equal when the CMT-2 level reached 38 in. (Figure 7.2-5). Before the tank drained another inch, the inside and outside wall temperatures (TW-538 and TW-532) became equal and relatively constant, but the fluid temperatures (TF-516, TF-524, and TF-544) continued to decrease with saturation temperature. As the tank continued to drain, the temperature of the walls at the 75-percent volume level decreased very little, and so became superheated as the saturation temperature continued to decrease. The wall temperatures (TW-538 and TW-532) remained superheated after the tank drained below []^{a,b,c}. When CMT-2 emptied, the temperature of the steam at the 75-percent volume level (Figure 7.2-5) was about []^{a,b,c} above the temperature of the wall (TW-532 and TW-538) at that same elevation. Thus, the superheated wall at the level of 75-percent volume and above appeared to act as a heat source to the fluid at the 75-percent volume level.

When the level in CMT-2 was about []^{a,b,c} the temperature at the 50-percent volume level 1 in. from the wall (TF-514; Figure 7.2-3) started to increase above the inside wall temperature (TW-522). The temperature increase indicated heating from the wall above the 50-percent volume level.

Comparison of Matrix Test SB13 CMT-1 and CMT-2 data revealed similar temperature effects for CMT-1 at the 20- and 75-percent volume level elevations (Figures 7.2-2 and 7.2-6). That is, the walls at the 20-percent volume elevation acted as a heat sink, and the walls at the 75-percent elevation acted as a heat source before the tank completed draining. The 50-percent volume level response was different, in that the walls acted as a heat source in CMT-1 (Figure 7.2-4). This is probably due to the faster draindown of CMT-1, which left the walls at the 50-percent volume level []^{a,b,c} hotter in CMT-1 than in CMT-2.

To further investigate the effect of superheating in the CMTs, thermocouples at four vertical elevations (41, 37, 29, and 14 in.) were plotted with two to three thermocouples per level for CMT-1 and CMT-2 in Matrix Test SB13 (Figures 7.2-7 and 7.2-8). As CMT-2 drained, a significant temperature gradient was created with superheated steam at the top of the CMT and saturated steam at the bottom of the CMT. Thermal stratification is clearly demonstrated from the data when CMT-2 emptied. A temperature gradient of []^{a,b,c} existed between the bottom of the CMT-2 and the

75-percent volume elevation (Figure 7.2-7). Table 7.2-1 summarizes the levels at which the thermocouples reached both saturated and superheated conditions. Note that the fluid thermocouples at the 75-percent volume level reached superheated conditions when the tank level was []^{a,b,c} lower than the elevation of the thermocouple. However, the thermocouple at the 50-percent volume level did not reach superheated temperature until the level in the CMT was []^{a,b,c} below the thermocouple. The thermocouples at the 20-percent volume level never reached superheated conditions because the walls at the bottom of the CMT were acting as heat sinks, and the metal heating effects from the upper portion of the CMT had less heating effect due to the larger vertical distance.

The same response of thermal stratification described for CMT-2 was observed in CMT-1 (Figure 7.2-8). The summary results for the various levels are presented in Table 7.2-2. Note the significant difference in temperature (about []^{a,b,c}) between the thermocouples at the 50-percent volume level and those at the 68-percent volume level when the tank emptied. Four thermocouples (two in each CMT) were located at an elevation midway between the 75- and 60-percent volume levels and designated as the 68-percent volume levels (TF-517 and TF-509 in CMT-1; TF-520 and TF-512 in CMT-2).

Although steam entering the CMTs from the balance line was superheated, heating from the walls of the CMT increased the temperature of the steam even more. The CMT-1 balance line inlet temperature data in Matrix Test SB13 (Figure 7.2-10) shows that the inlet temperature to CMT-1 was less than the fluid temperatures at the 75-percent volume level by the time the tank level decreased to []^{a,b,c}. This would not have been possible if the upper walls of the CMT did not act as a heat source to the steam in the tank.

The CMT-2 balance line inlet temperature influenced the CMT-2 response differently from that described for CMT-1. The 75-percent volume level temperatures remained slightly below the balance-line temperature at the CMT inlet (TF-546; Figure 7.2-9) during most of the CMT-2 draindown. As CMT-2 emptied, the 75-percent volume level temperatures superheated and came within []^{a,b,c} of the CMT-2 balance-line inlet temperature (TF-546).

A comparison of temperature responses for fluid thermocouples located on the vertical thermocouple rod (T/C Rod), centerline thermocouple (Center), and thermocouples 1 in. from the CMT-1 and CMT-2 walls is provided Figures 7.2-12 and 7.2-11. Three vertical elevations (75-, 50-, and 20-percent volume levels) were used to evaluate whether superheating at various elevations occurred in a consistent sequence. Figure 7.2-11 indicates that, for the 75-percent volume level, the thermocouple rod thermocouple became superheated first (TF-516 at []^{a,b,c}); followed by the centerline thermocouple (TF-544 at []^{a,b,c}), then the thermocouple located 1 in. from the wall (TF-524 at []^{a,b,c}). The CMT-1 response (Figure 7.2-12) indicated a different superheating sequence: T/C rod thermocouple (TF-513 at []^{a,b,c}), the thermocouple located 1 in. from the wall (TF-521 at []^{a,b,c}), and the centerline thermocouple (TF-543 at []^{a,b,c}). This superheating sequence evaluation was performed for CMT-2 and CMT-1 using test data from Matrix Tests SB12, SB01, and SB10 using Figures 7.2-25, 7.2-26, 7.2-39, 7.2-40, 7.2-53, and 7.2-54, respectively. The results

indicated that a clear or consistent pattern of superheating sequence was not evident for any of the CMT levels (20-, 50- or 75-percent volume level fluid thermocouples).

Superheating in the CMTs during draindown was primarily affected by draindown, RCS depressurization, and recirculation flow from the cold legs. CMT pressure versus CMT level data were plotted for CMT-2 and CMT-1 for Matrix Test SB13 (Figures 7.2-13 and 7.2-14). CMT-2 data indicated that the CMT pressure of []^{a,b,c} was maintained as the CMT-2 level decreased from []^{a,b,c}. Subsequently, the CMTs drained at a rate of []^{a,b,c} (obtained from applicable CMT level-versus-time data), while pressure decayed at a rate of []^{a,b,c} of CMT elevation.

In comparison, CMT-1 pressure of []^{a,b,c} was maintained as the level decreased from []^{a,b,c} (Figure 7.2-14). The draindown rate of []^{a,b,c} and a depressurization rate of []^{a,b,c} of level occurred, suggesting that slower pressure decreases and longer exposure to constant higher pressure would create higher superheated temperatures in the CMTs. The CMT-1 level decreased further during a period of relatively constant pressure. In addition, the pressure was higher than for any other CMT level, resulting in higher superheated temperatures. Table 7.2-3 provides draindown rates and RCS depressurization data for each CMT in Matrix Tests SB12, SB01, and SB10 (Figures 7.2-27, 7.2-28, 7.2-41, 7.2-42, 7.2-55, and 7.2-56, respectively). CMT draindown rates were obtained from CMT level data presented in each of the applicable test description sections (See Section 5). Table 7.2-3 also contains the time at recirculation mode, average temperatures of various levels at the time the CMT emptied, and steam condition of the upper layers at the time the CMT emptied. Data from Table 7.2-3 confirm that CMTs with slower pressure decreases and longer exposure to a constant pressure result in higher superheated temperatures (see CMT-1 data for Matrix Test SB12).

7.2.2 Matrix Test SB12 (U0112) Observation and Evaluation

Matrix Test SB12, a simulated double-ended guillotine (DEG) break of DVI-1, reflected a quick injection of CMT-1. CMT-2 response was slower and comparable with that of the CMT-2 response in Matrix Test SB13. The general response (superheating) of CMT-1 in Matrix Test SB12 was similar to that in Matrix Test SB13, but the temperatures in the CMT were considerably higher.

Draindown of CMT-1 was 10 to 15 times faster than the tests listed in Table 7.2-3 while the pressure in the CMT slowly decayed (Figures 7.2-27 and 7.2-28). This high draindown rate and slower pressure decay caused higher RCS water and steam flow rates through the CMT and maintained high temperatures from the top to the bottom of CMT-1 (Figure 7.2-24). Average CMT-1 fluid temperatures when CMT-1 emptied were superheated and about []^{a,b,c} higher than in all other tests.

A comparison of wall and fluid temperatures at 20-, 50-, and 75-percent volume levels (Figures 7.2-15 through 7.2-20) indicated that, for both CMT-1 and CMT-2, the fluid temperatures were always higher than the wall temperatures.

Superheating of the CMT-2 fluid temperatures as a result of tank-wall heating rather than superheated steam coming in from the balance line was confirmed because most of the 75-percent volume level temperatures exceeded the balance line at the CMT inlet temperature (TF-546; Figure 7.2-23).

Figure 7.2-28 reflects the slow pressure decay as CMT-1 pressure decreased from []^{a,b,c} during CMT-1 draindown. Draindown- and pressure-related data for Matrix Test SB12 are shown in Table 7.2-3. These data suggest that CMT temperatures will reach superheated conditions at a faster rate when faster draindown occurs and the CMTs are at higher constant pressure for a longer period.

7.2.3 Matrix Test SB01 (U0001) Observation and Evaluation

Matrix Test SB01, a simulated 2-in. cold-leg (CL) break at the bottom of CL-3, reflected a slower injection of both of the CMTs. The response of both CMT-1 and CMT-2 in Matrix Test SB01 was comparable with that of CMT-2 in Matrix Test SB13. The results of Matrix Test SB01 are presented in Figures 7.2-29 through 7.2-42 for the same type of plots described for Matrix Test SB13.

The general superheating response (CMT upper walls became a heat source to the steam in the tank, and the lower portion of the CMT walls acted as a heat sink) was evident for both CMT-1 and CMT-2 of Matrix Test SB01. Figures 7.2-33 and 7.2-34 demonstrate the upper wall heating effect, and Figures 7.2-29 through 7.2-32 show that, for the 20- and 50-percent volume levels, the walls acted as heat sinks.

The fluid thermocouples (i.e., T/C rod, 1 in. from wall, and centerline) became superheated as the CMTs drained and became exposed to the steam environment heated from the upper head and walls (Figure 7.2-35). As the thermocouples became superheated, thermocouple temperatures increased above the saturation conditions reflected by TSAT. As the CMTs drained, each lower level thermocouple reflected superheated conditions with a variation of almost []^{a,b,c} between the top and bottom of CMT-2.

Even though balance-line and CL-1 thermocouples were superheated during CMT draindown, they did not directly provide the energy to create and maintain the superheated conditions in CMT-1 (Figure 7.2-38). The upper-head walls acted as heat sources after being exposed initially to recirculated water at high temperatures. Thermocouples (TF-536, TW-526, and TW-530) were considered inoperable for Matrix Test SB01 (Table 5.1.1-2).

7.2.4 Matrix Test SB10 (U0110) Observation and Evaluation

Matrix Test SB10, a simulated DEG break of the CMT-1 cold-leg balance line, reflected a delay in CMT-1 injection and slow injection of CMT-2 inventory. The results of Matrix Test SB10 are reflected in Figures 7.2-43 through 7.2-56.

The response of CMT-1 was different from other CMT-1 responses because the break location removed the flow path from CL-3 to CMT-1 and caused the pressure at the top of CMT-1 to drop to atmospheric pressure immediately. Therefore, CMT-1 remained at initial temperature (about []^{a,b,c}) and increased only about []^{a,b,c} as CMT-1 drained late in the transient.

The CMT-2 pressure decay rate reflected a similarity to the CMT-2 response in Matrix Test SB13 (Figure 7.2-55). Pressure in CMT-2 decreased from []^{a,b,c} as the CMT-2 drained []^{a,b,c} of tank level). CMT-2 pressure remained at []^{a,b,c} over a draindown duration of []^{a,b,c} the shortest duration of any test evaluated. A comparison of data from Table 7.2-3 indicated that Matrix Test SB10 had the lowest superheated fluid temperatures of all tests evaluated. These data also confirm that CMT temperatures will reach superheated conditions at a faster rate when a faster draindown occurs and the CMTs are at a higher pressure for a longer period of time.

7.2.5 Summary

In conclusion, data from Matrix Tests SB13, SB12, SB01, and SB10 indicate the existence of temperature stratification of the walls and fluid in the CMTs. The temperature of the steam when the tanks emptied varied from about []^{a,b,c} (saturated conditions at the bottom of the tank) to fluid temperatures of []^{a,b,c} at the top of the tank. Fluid superheating in the tanks was between []^{a,b,c}

Generally, the source of superheating for steam in the tank was the upper walls of the CMTs at the 75-percent volume level or above. The upper portions of the CMTs acted as a heat source to the steam while the lower walls acted as a heat sink.

Pressure and draindown rate results suggest that CMTs with slower pressure decreases and longer exposure to higher temperatures at a given elevation in the tank created higher superheated temperatures in the CMT.

a,b,c

TABLE 7.2-1 MATRIX TEST SB13 CMT-2 FLUID TEMPERATURE CONDITION CHANGES SUMMARY			
Level Description (%)	Elevation (in.)	Level when Reached Saturation	Level when Reached Superheated Conditions

TABLE 7.2-2 MATRIX TEST SB13 CMT-1 FLUID TEMPERATURE CONDITION CHANGES SUMMARY			
Level Description (%)	Elevation (in.)	Level when Reached Saturation	Level when Reached Superheated Conditions

TABLE 7.2-3
CMT SUPERHEATING PARAMETERS SUMMARY

Test.	CMT No.	Time at Recirculation Mode (sec.)	Draindown Rate (Average Level change/sec.)	Level Decrease at Constant High Pressure (in. @ psig)	Pressure Decay Rate (psig/in. of height)	Average of 20-, 50- and 75-Percent Level Temperatures at CMT Empty Condition	Average Fluid Temperature Status at CMT Empty Condition

Note:

- (1) Pressure decay rates do not include the initial depressurization from 375 psig to the initial pressure plateau (e.g., for Matrix Test SB13 the initial depressurization from 375 to 318 psig was not included in the decay rate).
- (2) Pressure immediately dropped from 375 psig to atmospheric pressure on break initiation.

a,b,c

Figures 7.2-1 through 7.2-56 are not included in this nonproprietary document.

8.0 References

1. Zuber, N., "Appendix D: A Hierarchical, Two-Tiered Scaling Analysis," *An Integral Structure and Scaling Methodology for Severe Accident Technical Issue Resolution*, U.S. Nuclear Regulatory Commission, Washington, DC 20555, NUREG/CR-5809, November 1991.
2. WCAP-14292, *AP600 Low-Pressure Integral Systems Test at Oregon State University Test Analysis Report*.
3. WCAP-14141, *AP600 Test and Analysis Plan for Design Certification*.
4. WCAP-13234, *Long-Term Cooling Test Specification*, Rev. 2, August 1994.
5. "Rules for Construction of Unfired Pressure Vessels," *ASME Boiler and Pressure Vessel Code*, Section VIII, 1992.
6. WCAP-14270, *AP600 Low-Pressure Integral Systems Test at Oregon State University Facility Scaling Report*, January 1995.
7. WCAP-14124, *AP600 Low-Pressure Integral Systems Test at Oregon State University Facility Description Report*, July 1994.

APPENDIX A
DATA REDUCTION METHODS AND VALIDATION PROCESS

A.1 Introduction

The overall data reduction and data validation process is described in Section 3. This appendix describes the specific details of how the data were reduced and validated. It also provides examples of some data reduction and validation steps.

A.2 Day-of-Test Report

The first step in the data validation process, writing the Day-of-Test Report, was performed by the test site personnel immediately following the test. (A sample of the format is shown in Figure A-1.) The Day-of-Test Report was issued with the electronic data files to the Westinghouse Energy Center a few days after the test. Typically, the Day-of-Test Report was reviewed in parallel with processing the data files at Westinghouse.

Communications between the test site and the Westinghouse Energy Center were not limited to the Day-of-Test Report. Frequent telecommunications were held between the two sites.

A.3 Data Reduction Steps

A.3.1 Zero-Time Correction

The data acquisition system (DAS) at the Oregon State University (OSU) test site assigned an incorrect zero time to the data files. This zero time was corrected at the Westinghouse Energy Center after all tests were completed. This was done by reviewing various channels from each of the three instrumentation racks to find the precise time that the test was initiated. After determining the precise zero time, the correction was added to all time records for all data files.

For most tests, the zero time needed to be corrected by about []^{a,b,c}

A.3.2 Burst Scan and Continuous Scan Data

The continuous scan data were reviewed and issued as part of the Quick Look Report process. The burst scan data were not reviewed for the Quick Look Report because of the schedule involved. However, the burst scan data were needed to replace the continuous scan data for this report due to the faster scan rate. The burst scan data were recorded every []^{a,b,c} for the first []^{a,b,c} of the test; the continuous scan data were recorded every []^{a,b,c} for the entire test.

The burst scan and continuous scan data were compared to determine if there were any differences between the two sets of data. The most effective way to make this comparison was to plot the two types of data. Examples are shown in Figures A-2 through A-5. As can be seen from these graphs,

the two data plots fall on top of each other. With the faster scan rate, more spikes are recorded for the burst scan data.

For this report, the continuous scan data were appended to the burst scan data for the period after []^{a,b,c} (depending on the test) to create a hybrid data file. Thus, the hybrid file contains data that have a scan rate of []^{a,b,c} for the first []^{a,b,c} and a scan rate of []^{a,b,c} for all data thereafter. For most data plots in this report, the transition from burst scan to continuous scan is quite visible, since the density of the data changes by at least a factor of []^{a,b,c}

A.3.3 Pressure Transmitter Corrections

After most of the tests were completed at the OSU test site on August 10, 1994, it was discovered that the zero point for several pressure transmitters was incorrectly set. The pressure transmitters were reset on August 15, 1994. The respective data for tests conducted prior to August 15 were corrected for this report. However, the data for these channels in the Quick Look Reports were incorrect. The affected pressure transmitters and the respective correction are shown in Table A-1.

A.3.4 Calibration File Corrections

After the tests were completed at the OSU test site, it was discovered on September 28, 1994, that nine channels had an error in the calibration file. The respective data for tests conducted after Matrix Test SB12 (July 21) were corrected for this report. However, the data for these channels in the Quick Look Reports were incorrect. The affected channels and the tests are shown in Table A-2.

A.3.5 Noninteger Characters in Data Fields

The DAS at the OSU test site assigned noninteger characters to values that exceeded the range of the instrument. These noninteger characters were changed at Westinghouse in order to plot and review the data. These noninteger characters were called *rawhuge*, *huge+*, or *huge-*. Generally, these characters were replaced with a value of []^{a,b,c}. However, if a heated pressure switch (HPS) had either *rawhuge* or *huge+* in the data field, it was replaced with []^{a,b,c} if it had *huge-*, it was replaced with []^{a,b,c} percent. For channel KW-601, the noninteger characters were replaced with a value of []^{a,b,c}

A.4 Initial Condition Calculations

The average of the initial conditions for the following parameters was calculated using Microsoft Excel™ software and reported in the Quick Look Report. The average was based on the time prior to test initiation, typically about []^{a,b,c}. The measured pressurizer and steam generator (SG) levels were compensated by the density difference between the cold differential pressurizer reference

leg temperature and the hot temperature of the fluid in the facility. Deviations from the allowable tolerances were generally very small and acceptable.

- Pressurizer pressure (PT-604)
- Hot leg-1 (HL-1) temperature (SC-141, SC-205, TF-143)
- HL-2 temperature (SC-140, SC-206, TF-142)
- SG-1 pressure (PT-301)
- SG-2 pressure (PT-302)
- Pressurizer level (LDP-601) (compensated by SC-608)
- SG-1 level (LDP-303) (compensated by TF-305/TF-307)
- SG-2 level (LDP-304) (compensated by TF-306/TF-308)
- IRWST temperature (TF-701)
- CMT-1 temperature (TF-529)
- CMT-2 temperature (TF-532)
- ACC-1 temperature (TF-403)
- ACC-2 temperature (TF-404)
- IRWST level (LDP-701)
- ACC-1 level (LDP-401)
- ACC-2 level (LDP-402)
- ACC-1 pressure (PT-401)
- ACC-2 pressure (PT-402)
- PRHR inlet line temperature (TF-803)
- CMT-1 level (LDP-507)
- CMT-2 level (LDP-502)
- CMT-1 pressure (PT-501)
- CMT-2 pressure (PT-502)

See Appendix B for the compilation of the specified and actual initial conditions.

In addition to the calculation of the initial test conditions, the actual and specified heater rod power decay curves were also generated and plotted on the same graph. These curves were reviewed and included in the Quick Look Report and in this report for both power supplies (KW-101 and KW-102). The redundant power supply measurements (KW-103 and KW-104) were also plotted against the specified power decay curves. The specified power decay curve is shown in Section 2. For most tests, the deviation from the specified power decay curves was very small. See Appendix B for compilation of power decay comparisons.

**TABLE A-1
PRESSURE TRANSMITTER CORRECTIONS**

Transmitter ⁽¹⁾	Correction (psi)	Affected Tests
PT-101	+6.1	SB01, SB10, SB12, SB14, SB04, SB05, SB09, SB13, SB19, SB21, SB23, SB24, SB02, ⁽²⁾ SB03, ⁽²⁾ SB06, ⁽²⁾ SB07, ⁽²⁾ SB11, ⁽²⁾ SB15 ⁽²⁾
PT-102	+6.21	
PT-103	+6.2	
PT-104	+6.4	
PT-108	+8.4	
PT-109	+6.3	
PT-111	+6.0	
PT-112	+8.75	
PT-113	+6.4	
PT-201	+1.1	
PT-202	+5.9	
PT-205	+6.13	
PT-301	-3.4	
PT-302	-3.0	

Note:

- (1) PT-110 is not included in list.
- (2) Not included in this report.

**TABLE A-2
CALIBRATION FILE CORRECTIONS**

Channels Affected	Affected Tests
DP-401	SB11, SB02, SB21, SB23, SB24, SB25, SB27, SB26, SB31, SB28, SB29, SB18
DP-503	
FMM-205	
FMM-206	
FMM-502	
FMM-503	
FMM-701	
FMM-702	
FMM-905	

DAY-OF-TEST REPORT

Test Facility: _____

Test No. _____ Date _____ Time _____

Initial Conditions:

SpecifiedActual

Facility Configuration:

SpecifiedActual

Any Observations, Unexpected Events During Test?

Any Failed Instruments Observed Prior to or During Test?

Any Deviation from Test Procedures?

Are Critical Instruments Functional? Plot Critical Instruments

Any Facility Maintenance Performed Since Last Test?

Data Tape File Name (s):

Facility Engineer: _____

Facility Manager: _____

Figure A-1 Day-of-Test Report

The Figures for Appendix A on pages A-8 through A-11 are not included in this nonproprietary document.

APPENDIX B

Test No.	Date Performed	DAS Test No.	Test Accepted	Procedure Description	Long-Term Cooling	PRHR
SB01	6/1/94	U0001	Yes	2-in. Cold-leg break, bottom of CL-3	Yes	No
SB02	8/1/94	U0002	Yes	2-in. Cold-leg break, bottom of CL-4	No	Yes
SB03	6/16/94	U0003	Yes	2-in. Cold-leg break, bottom of CL-4	Yes	No
SB04	6/3/94	U0004	No	2-in. Cold-leg break, top of CL-3	No	Yes
SB04	6/27/94	U0104	No	2-in. Cold-leg break, top of CL-3	No	Yes
SB04	6/28/94	U0204	Yes	2-in. Cold leg break, top of CL-3	No	Yes
SB05	6/21/94	U0005	Yes	1-in. Cold-leg break, bottom of CL-3	Yes	Yes
SB06	7/19/94	U0006	Yes	4-in. Cold-leg break, bottom of CL-3	No	Yes
SB07	6/23/94	U0007	Yes	2-in. Cold-leg break, bottom of CL-3	No	Yes
SB09	6/29/94	U0009	Yes	2-in. CMT-1/CL-3 balance-line break	No	Yes
SB10	6/14/94	U0010	No	CMT-1/CL-3 balance-line DEG break	Yes	Yes
SB10	6/25/94	U0110	Yes	CMT-1/CL-3 balance-line DEG break	Yes	Yes
SB11	7/28/94	U0011	Yes	DEG DVI Line break	Yes	Yes
SB12	6/10/94	U0012	No	DEG DVI Line break	Yes	Yes
SB12	7/21/94	U0112	Yes	DEG DVI Line break	Yes	Yes
SP13	6/7/94	U0013	No	2-in. DVI Line break	Yes	Yes
SB13	6/8/94	U0113	Yes	2-in. DVI Line break	Yes	Yes

ANSTEC APERTURE CARD

Also Available on
Aperture Card

VS	RNS	Nozzle Configuration				Separator Assignment			Break Source
		ADS-1 (RCS-601)	ADS-2 (RCS-602)	ADS-3 (RCS-603)	ADS-4-1 (RCS-615) (%)	ADS-4-2 (RCS-616) (%)	5-in. ADS 4-2	8-in. ADS 4-1	
Off	Off	2S	2S	2S	50	100	HL-2	HL-1	CL-3
Off	Off	2S	2S	2S	50	100	HL-2	HL-1	CL-4
Off	Off	2S	2S	2S	50	100	HL-2	HL-1	CL-3
TO	AUTO	2S	2S	2S	50	100	HL-2	HL-1	CL-3
TO	AUTO	2S	2S	2S	50	100	HL-2	HL-1	CL-3
TO	AUTO	2S	2S	2S	50	100	HL-2	HL-1	CL-3
Off	Off	2S	2S	2S	50	100	HL-2	HL-1	CL-3
Off	Off	2S	2S	2S	50	100	HL-2	HL-1	CL-3
Off	Off	1S	1S	1S	Isolated	100	Isolated	HL-1	CL-3
Off	Off	2S	2S	2S	50	100	HL-2	HL-2	CL-3
Off	Off	2S	2S	2S	50	100	CMT-1	HL-1, HL-2	CL-3
Off	Off	2S	2S	2S	50	100	CMT-1	HL-1, HL-2	CL-3
Off	Off	2S	2S	2S	50	100	HL-2	HL-1	Reactor side
Off	Off	1S	2S	1S	100	100	HL-2	HL-1	Reactor side
Off	Off	1S	2S	1S	100	100	HL-2	HL-1	Reactor side
Off	Off	2S	2S	2S	50	100	HL-2	HL-1	Break source
Off	Off	2S	2S	2S	50	100	HL-2	HL-1	Break source

Test No.	Date Performed	DAS Test No.	Test Accepted	Procedure Description	Long-Term Cooling	PRHR	C
SB14	7/7/94	U0014	Yes	Inadvertent ADS-1 with no break	Yes	Yes	O
SB15	7/12/94	U0015	Yes	2-in. Hot-leg break, bottom of HL-2	No	Yes	O
SB18	9/15/94	U0018	Yes	2-in. CL-3 break	Yes	Yes	O
SB19	7/14/94	U0019	Yes	2-in. Cold-leg break, bottom of CL-3	Yes	Yes	O
SB21	8/3/94	U0021	Yes	Simulated long-term cooling	Yes	On	O
SB23	8/9/94	U0023	Yes	1/2-in. Cold-leg break, bottom of CL-3	Yes	On	O
SB24	8/10/94	U0024	Yes	1/2-in. Cold-leg break, bottom of CL-3	Yes	On	O
SB25	8/16/94	U0025	Yes	Mid-loop operation	Yes	Off	O
SB26	8/27/94	U0026	No	Probabilistic Risk Assessment multiple failures without PRHR	Yes	Off	O
SB26	8/29/94	U0126	Yes	Probabilistic Risk Assessment multiple failures without PRHR	Yes	Off	O
SB27	8/17/94	U0027	Yes	Inadvertent ADS-1	Yes	Off	O
SB28	9/7/94	U0028	Yes	Probabilistic Risk Assessment case DEG DVI line break	Yes	Off	O
SB29	9/12/94	U0029	Yes	2-in. Cold-leg break, bottom of CL-3	Yes	On	O
SB31	8/31/94	U0031	Yes	Spurious S signal without ADS	Yes	On	O

RNS	Nozzle Configuration				Separator Assignment			Break Source
	ADS-1 (RCS-601)	ADS-2 (RCS-602)	ADS-3 (RCS-603)	ADS-4-1 (RCS-615) (%)	ADS-4-2 (RCS-616) (%)	5-in. ADS 4-2	8-in. ADS 4-1	
Off	2S	2S	2S	50	100	HL-2	HL-1	Isolated
Off	2S	2S	2S	50	100	HL-2	HL-1	HL-2
Off	2S	2S	2S	50	100	HL-2	HL-1	CL-3
Off	2S	2S	2S	50	100	HL-2	HL-1	CL-3
Off	2S	2S	2S	50	100	HL-2	HL-1	CL-3
Off	2S	2S	2S	50	100	HL-2	HL-1	CL-3
On	2S	2S	2S	50	100	HL-2	HL-1	CL-3
Off	2S	2S	2S	N/A	N/A	N/A	N/A	N/A
Off	2S	2S	2S	N/A	N/A	N/A	N/A	N/A
Off	2S	2S	2S	N/A	N/A	N/A	N/A	N/A
Off	2S	2S	2S	50	100	HL-2	HL-1	N/A
Off	N/A	1S	2S	N/A	N/A	N/A	N/A	Reactor
Off	2S	2S	2S	50	100	HL-2	HL-1	CL-3
Off	2S	2S	2S	50	100	HL-2	HL-1	N/A

ANSTEC
APERTURE
CARD

Also Available on
Aperture Card

APPENDIX C
INSTRUMENTATION DATA BASE

APPENDIX C
INSTRUMENTATION DATA BASE

Tag No.	Name	Location	Thermocouple Diameter	Thermocouple Depth	Thermocouple Type	DAS Rack	DAS Row	DAS Channel	Drawing No.	Sheet No.	Grid
BAMSC	Break and ADS Measurement Controller	OP	-	-	-	-	-	N/A	TIC 787-E200	1	-
BGI-01	IRWST Level Indicator	OP	-	-	-	-	-	N/A	TIC 787-E200	1	-
BGI-02	PST Level Indicator	OP	-	-	-	-	-	N/A	TIC 787-E200	1	-
BGI-03	Secondary Sump Level Indicator	OP	-	-	-	-	-	N/A	TIC 787-E200	1	-
BGI-04	Primary Sump Level Indicator	OP	-	-	-	-	-	N/A	TIC 787-E200	1	-
BGI-05	ACC01 Level Indicator	OP	-	-	-	-	-	N/A	TIC 787-E200	1	-
BGI-06	PZR level Indicator	OP	-	-	-	-	-	N/A	TIC 787-E200	1	-
BGI-07	ACC02 level Indicator	OP	-	-	-	-	-	N/A	TIC 787-E200	1	-
BGI-08	CMT02 level Indicator	OP	-	-	-	-	-	N/A	TIC 787-E200	1	-
BGI-09	CMT01 Level Indicator	OP	-	-	-	-	-	N/A	TIC 787-E200	1	-
BGI-10	ADS1-3 Separator Level Indicator	OP	-	-	-	-	-	N/A	TIC 787-E200	1	-
BGI-11	ADS4-1 Separator Level Indicator	OP	-	-	-	-	-	N/A	TIC 787-E200	1	-
BGI-12	ADS4-2 Separator Level Indicator	OP	-	-	-	-	-	N/A	TIC 787-E200	1	-
BGI-13	Break Separator Level Indicator	OP	-	-	-	-	-	N/A	TIC 787-E200	1	-
BGI-14	CRP M/U Tank Level Indicator	OP	-	-	-	-	-	N/A	TIC 787-E200	1	-
CT-103A	KW-103 Pb-A Current XFMR	RX-HTR	-	-	-	-	-	N/A	OSU 600007	1	-
CT-103B	KW-103 Pb-B Current XFMR	RX-HTR	-	-	-	-	-	N/A	OSU 600007	1	-
CT-103C	KW-103 Pb-C Current XFMR	RX-HTR	-	-	-	-	-	N/A	OSU 600007	1	-
CT-104A	KW-104 Pb-A Current XFMR	RX-HTR	-	-	-	-	-	N/A	OSU 600007	1	-
CT-104B	KW-104 Pb-B Current XFMR	RX-HTR	-	-	-	-	-	N/A	OSU 600007	1	-
CT-104C	KW-104 Pb-C Current XFMR	RX-HTR	-	-	-	-	-	N/A	OSU 600007	1	-
DAS-CTD-1	DAS Trigger Rack 1	-	-	-	-	-	-	-	-	-	-
DAS-CTD-2	DAS Trigger Rack 2	-	-	-	-	-	-	-	-	-	-
DAS-CTD-3	DAS Trigger Rack 3	-	-	-	-	-	-	-	-	-	-
DP-111	DP across Upper Core Plate	RX-PE	-	-	-	1	1	L16	OSU 600101	1	B6
DP-114	DP across Upper Support Plate	RX-PE	-	-	-	1	1	H17	OSU 600101	1	D6
DP-121	DP between DVI-1 and CL-1	RX-PE	-	-	-	1	1	L17	OSU 600101	1	C6
DP-122	DP between DVI-2 and CL-1	RX-PE	-	-	-	1	2	H00	OSU 600101	1	C2
DP-123	DP between DVI-1 and CL-3	RX-PE	-	-	-	1	2	L00	OSU 600101	1	C6
DP-124	DP between DVI-2 and CL-4	RX-PE	-	-	-	1	2	H01	OSU 600101	1	D2
DP-125	HL-1 entrance losses	RX-PE	-	-	-	1	2	L01	OSU 600101	1	C2
DP-126	HL-2 entrance losses	RX-PE	-	-	-	1	2	H02	OSU 600101	1	C2
DP-128	DVI-1 entrance losses	RX-PE	-	-	-	1	2	L02	OSU 600101	1	B2
DP-129	DVI-2 entrance losses	RX-PE	-	-	-	1	2	H03	OSU 600101	1	B2
DP-130	Upper Head DP	RX-PE	-	-	-	1	2	L03	OSU 600101	1	D3
DP-201	CL-1 DP	CL1	-	-	-	1	3	H01	OSU 600203	1	A5
DP-202	RCP-2 DP	CL2	-	-	-	1	3	L01	OSU 600203	1	A3
DP-203	RCP-1 DP	CL1	-	-	-	1	3	H02	OSU 600203	1	A6
DP-204	CL-2 DP	CL2	-	-	-	1	3	L02	OSU 600203	1	A4
DP-205	RCP-3 DP	CL3	-	-	-	1	3	H03	OSU 600203	1	B6

APPENDIX C
INSTRUMENTATION DATA BASE (Continued)

Tag No.	Name	Location	Thermocouple Diameter	Thermocouple Depth	Thermocouple Type	DAS Rack	DAS Row	DAS Channel	Drawing No.	Sheet No.	Grid
DP-206	RCP-4 DP	CL4	-	-	-	1	3	L03	OSU 600203	1	B3
DP-207	CL-3 DP	CL3	-	-	-	-	3	H04	OSU 600203	1	B5
DP-208	CL-4 DP	CL4	-	-	-	1	3	L04	OSU 600203	1	B4
DP-209	HL-1 DP	HL1	-	-	-	1	3	H05	OSU 600203	1	B5
DP-210	HL-2 DP	HL2	-	-	-	1	3	L05	OSU 600203	1	A4
DP-211	SG-1 Short Tube Entrance Losses	SG01	-	-	-	1	3	H17	OSU600301	1	B4
DP-212	SG-2 Long Tube Exit Losses	SG02	-	-	-	1	3	L17	OSU600301	1	B3
DP-213	SG-1 Long Tube Exit Losses	SG01	-	-	-	1	3	H18	OSU600301	1	B6
DP-214	SG-2 Long Tube Entrance Losses	SG02	-	-	-	1	3	L18	OSU600301	1	B1
DP-215	HL Break DP	CL Break	-	-	-	1	3	H06	OSU 600904	1	C4
DP-216	HL Break DP	HL Break	-	-	-	1	3	L06	OSU 600904	1	-
DP-401	ACC-1 Injection DP	ACC01	-	-	-	1	5	L15	OSU 600206	1	C5
DP-402	ACC-2 Injection DP	ACC02	-	-	-	1	5	H16	OSU 600206	1	A6
DP-501	CMT-1 Injection DP	CMT01 DVI	-	-	-	1	4	L06	OSU 600206	1	C5
DP-502	CMT-2 Injection DP	CMT02 DVI	-	-	-	1	4	H07	OSU 600206	1	A5
DP-503	CMT-1 Balance Line DP	CMT01 CL Bal	-	-	-	1	3	H11	OSU 600206	1	D5
DP-504	CMT-2 Balance Line DP	CMT02 CL Bal	-	-	-	1	4	L08	OSU 600206	1	B5
DP-601	ADS4-1 Separator Entrance DP	ADS04	-	-	-	1	5	H00	OSU 600203	1	B5
DP-602	ADS4-2 Separator Entrance DP	ADS04	-	-	-	1	5	L00	OSU 600203	1	B4
DP-611	PZR Surge Line DP	PZR Surge Line	-	-	-	1	6	H00	OSU 600203	1	B3
DP-701	IRWST/DVI-1 Injection DP	IRWST DVI	-	-	-	1	5	L18	OSU 600206	1	A2
DP-702	IRWST/DVI-2 Injection DP	IRWST DVI	-	-	-	1	5	H19	OSU 600206	1	A1
DP-905	Break Separator Entrance DP	LGBR	-	-	-	1	4	H09	OSU 600904	1	C5
DPI-001	Filter Bank #1 DP Indicator	Demn	-	-	-	-	-	N/A	OSU 600002	2	A5
DPI-002	Filter Bank #2 DP Indicator	Demn	-	-	-	-	-	N/A	OSU 600002	2	B5
DPI-003	Filter Bank #3 DP Indicator	Demn	-	-	-	-	-	N/A	OSU 600002	2	C5
DPI-004	Filter Bank #4 DP Indicator	Demn	-	-	-	-	-	N/A	OSU 600002	2	C5
ESL-001	Low Voltage Switch -480V AC System	MCP	-	-	-	-	-	N/A	TIC 787-E204	1	-
FDP-604	ADS- Flow	ADS-2	-	-	-	1	6	L00	OSU 600203	1	C1
FDP-605	ADS- Flow	ADS-1	-	-	-	1	5	H01	OSU 600203	1	D1
FDP-606	ADS-3 Flow	ADS-3	-	-	-	1	5	L01	OSU 600203	1	D1
FI-001	RCP-1 Seal Water Flow Indicator	GSW	-	-	-	-	-	N/A	OSU 600903	1	B2
FI-002	RCP-2 Seal Water Flow Indicator	GSW	-	-	-	-	-	N/A	OSU 600903	1	B3
FI-003	RCP-3 Seal Water Flow Indicator	GSW	-	-	-	-	-	N/A	OSU 600903	1	B3
FI-004	RCP-5 Seal Water Flow Indicator	GSW	-	-	-	-	-	N/A	OSU 600903	1	B4
FI-805	RNSP Local Flow Indicator	RNS Fil	-	-	-	-	-	-	OSU 600002	1	B4
FMM-001	SG-01 Feed Flow	MF	-	-	-	1	1	H02	OSU 600002	1	C3
FMM-002	SG-02 Feed Flow	MF	-	-	-	1	1	L02	OSU 600002	1	C2
FMM-201	CL-1 Loop Flow	CL1	-	-	-	1	1	H00	OSU 600203	1	A5
FMM-202	CL-2 Loop Flow	CL2	-	-	-	1	1	L00	OSU 600203	1	A4
FMM-203	CL-3 Loop Flow	CL3	-	-	-	1	1	H01	OSU 600203	1	C5
FMM-204	CL-4 Loop Flow	CL4	-	-	-	1	1	L01	OSU 600203	1	C4
FMM-205	DVI-1 Flow	DVI	-	-	-	1	6	H02	OSU 600206	1	C4
FMM-206	DVI-2 Flow	DVI	-	-	-	1	6	L02	OSU 600206	1	A4
FMM-401	ACC-1 Injection Flow	ACC01	-	-	-	1	5	L16	OSU 600206	1	C6
FMM-402	ACC-2 Injection Flow	ACC02	-	-	-	1	5	H17	OSU 600206	1	A5
FMM-501	CMT-1 Injection Flow	CMT01 DVI	-	-	-	1	4	L09	OSU 600206	1	C5
FMM-502	CMT-2 CL Bal Line Flow	CMT02 CL Bal	-	-	-	1	4	H10	OSU 600206	1	A5
FMM-503	CMT-1 CL Bal Line Flow	CMT01 CL Bal	-	-	-	1	4	L10	OSU 600206	1	C4

APPENDIX C
INSTRUMENTATION DATA BASE (Continued)

Tag No.	Name	Location	Thermocouple Diameter	Thermocouple Depth	Thermocouple Type	DAS Rack	DAS Row	DAS Channel	Drawing No.	Sheet No.	Grid
FMM-504	CMT-2 Injection Flow	CMT02 DVI	-	-	-	1	4	H11	OSU 600206	1	A5
FMM-601	ADS1-3 Loop Seal Flow	ADS1-3	-	-	-	1	12	H00	OSU 600203	1	C1
FMM-602	ADS4-2 Loop Seal Flow	ADS04-2	-	-	-	1	12	L00	OSU 600901	1	A2
FMM-603	ADS4-1 Loop Seal Flow	ADS04-1	-	-	-	1	12	H01	OSU 600901	1	A5
FMM-701	IRWST/DVI-1 Injection Flow	IRWST DVI	-	-	-	1	6	H03	OSU 600206	1	B2
FMM-702	IRWST/DVI-2 Injection Flow	IRWST DVI	-	-	-	1	6	L03	OSU 600206	1	A1
FMM-703	IRWST Overflow	IRWST Overflow	-	-	-	1	5	L05	OSU 600206	1	C2
FMM-801	CVSP Discharge Flow	CVS Fill	-	-	-	1	1	H03	OSU 600002	1	A4
FMM-802	PRHR Inlet Flow	PRHR HX	-	-	-	1	6	H04	OSU 600206	1	C1
FMM-803	RNSP to DVI-2 Flow	RNS	-	-	-	1	3	L07	OSU 600206	1	A3
FMM-804	PRHR Outlet Flow	PRHR HX	-	-	-	1	6	L04	OSU 600206	1	B1
FMM-805	RNSP Discharge Flow	RNS Fill	-	-	-	1	1	L03	OSU 600002	1	B4
FMM-901	Pn Sump/DVI-1 Injection Flow	Sump DVI	-	-	-	1	6	H05	OSU 600206	1	C4
FMM-902	Pn Sump/DVI-2 Injection Flow	Sump DVI	-	-	-	1	6	L05	OSU 600206	1	A3
FMM-903	CR to Primary Sump	COND RTN	-	-	-	1	12	L01	OSU 600002	1	C4
FMM-904	CR to IRWST	COND RTN	-	-	-	1	12	H02	OSU 600002	1	D4
FMM-905	Break Separator Loop Seal Flow	BAMS	-	-	-	1	12	L02	OSU 600901	1	A4
FMT-001	FMM-001 Transmitter	MF	-	-	-	-	-	-	OSU 600002	1	C3
FMT-002	FMM-002 Transmitter	MF	-	-	-	-	-	-	OSU 600002	1	C2
FMT-201	FMM-201 Transmitter	CL1	-	-	-	-	-	-	OSU 600203	1	A5
FMT-202	FMM-202 Transmitter	CL2	-	-	-	-	-	-	OSU 600203	1	A4
FMT-203	FMM-203 Transmitter	CL3	-	-	-	-	-	-	OSU 600203	1	C5
FMT-204	FMM-204 Transmitter	CL4	-	-	-	-	-	-	OSU 600203	1	C4
FMT-205	FMM-205 Transmitter	DVI	-	-	-	-	-	-	OSU 600206	1	C4
FMT-206	FMM-206 Transmitter	DVI	-	-	-	-	-	-	OSU 600206	1	A4
FMT-401	FMM-401 Transmitter	ACC01	-	-	-	-	-	-	OSU 600206	1	C6
FMT-402	FMM-402 Transmitter	ACC02	-	-	-	-	-	-	OSU 600206	1	A5
FMT-501	FMM-501 Transmitter	CMT01 DVI	-	-	-	-	-	-	OSU 600206	1	C5
FMT-502	FMM-502 Transmitter	CMT02 CL Bal	-	-	-	-	-	-	OSU 600206	1	A5
FMT-503	FMM-503 Transmitter	CMT01 CL Bal	-	-	-	-	-	-	OSU 600206	1	C4
FMT-504	FMM-504 Transmitter	CMT02 DVI	-	-	-	-	-	-	OSU 600206	1	A5
FMT-601	FMM-601 Transmitter	ADS1-3	-	-	-	-	-	-	OSU 600203	1	C1
FMT-602	FMM-602 Transmitter	ADS04-2	-	-	-	-	-	-	OSU 600901	1	A2
FMT-603	FMM-603 Transmitter	ADS04-1	-	-	-	-	-	-	OSU 600901	1	A5
FMT-701	FMM-701 Transmitter	IRWST DVI	-	-	-	-	-	-	OSU 600206	1	B2
FMT-702	FMM-702 Transmitter	IRWST DVI	-	-	-	-	-	-	OSU 600206	1	A1
FMT-703	FMM-703 Transmitter	IRWST Overflow	-	-	-	-	-	-	OSU 600206	1	C2
FMT-801	FMM-801 Transmitter	CVS Fill	-	-	-	-	-	-	OSU 600002	1	A4
FMT-802	FMM-802 Transmitter	PRHR HX	-	-	-	-	-	-	OSU 600206	1	C1
FMT-803	FMM-803 Transmitter	RNS	-	-	-	-	-	-	OSU 600206	1	A3
FMT-804	FMM-804 Transmitter	PRHR HX	-	-	-	-	-	-	OSU 600206	1	B1
FMT-805	FMM-805 Transmitter	RNS Fill	-	-	-	-	-	-	OSU 600002	1	B4
FMT-901	FMM-901 Transmitter	Sump DVI	-	-	-	-	-	-	OSU 600206	1	C4
FMT-902	FMM-902 Transmitter	Sump DVI	-	-	-	-	-	L05	OSU 600206	1	A3
FMT-903	FMM-903 Transmitter	COND RTN	-	-	-	-	-	L01	OSU 600002	1	C4
FMT-904	FMM-904 Transmitter	COND RTN	-	-	-	-	-	H02	OSU 600002	1	D4
FMT-905	FMM-905 Transmitter	BAMS	-	-	-	-	-	L02	OSU 600901	1	A4
PNP-001	City Water Supply Flow Totalizer	Demn	-	-	-	-	-	N/A	OSU 600002	2	A6
PSL-001	RCP Seal Water Low Flow Switch	GSW	-	-	-	-	-	N/A	OSU 600903	1	C4
FVM-001	SG-1 Steam Flow	MS	-	-	-	1	1	H04	OSU 600002	1	C2
FVM-002	SG-2 Steam Flow	MS	-	-	-	1	1	L04	OSU 600002	1	D1

**APPENDIX C
INSTRUMENTATION DATA BASE (Continued)**

Tag No.	Name	Location	Thermocouple Diameter	Thermocouple Depth	Thermocouple Type	DAS Rack	DAS Row	DAS Channel	Drawing No.	Sheet No.	Grid
FVM-003	Steam Header Total Steam Flow	MS	-	-	-	1	1	H05	OSU 600002	1	D2
FVM-004	City Water to DI System Flow	Deman	-	-	-	-	-	-	OSU 600002	2	C6
FVM-601	ADS1-3 Separator Steam Flow	ADS1-3	-	-	-	1	12	H03	OSU 600203	1	C1
FVM-602	ADS4-2 Separator Steam Flow	ADS04-2	-	-	-	1	12	L03	OSU 600901	1	D2
FVM-603	ADS4-1 Separator Steam Flow	ADS04-1	-	-	-	1	12	H04	OSU 600901	1	C5
FVM-701	IRWST Steam Exhaust	IRWST Vent	-	-	-	1	6	L14	OSU 600206	1	C2
FVM-901	BAMS HDR 6" Steam Flow	BAMS	-	-	-	1	12	L04	OSU 600901	1	D3
FVM-902	BAMS HDR 10" Steam Flow	BAMS	-	-	-	1	12	H05	OSU 600901	1	D3
FVM-903	Primary Sump Steam Exhaust	BAMS	-	-	-	1	6	H15	OSU 600901	1	C3
FVM-905	Break Separator 6" Steam Flow	BAMS	-	-	-	1	12	L05	OSU 600901	1	D4
FVM-906	Break Separator 8" Steam Flow	BAMS	-	-	-	1	12	H06	OSU 600901	1	D4
HPM-101	Heat Losses from Upper RPV, Level I-I @ 67.5 degrees	RX-TE	-	Surface	-	3	1	H00 L00	OSU 600101	2	C1
HPM-102	Heat Losses from Upper RPV, Level P-P @ 22.5 degrees	RX-TE	-	Surface	-	3	1	H01 L01	OSU 600101	2	C3
HPM-103	Heat Losses from Lower RPV, Mid Spacer Grid @ 22.5 degrees	RX-TE	-	Surface	-	3	1	H02 L02	OSU 600101	2	B3
HPM-104	Heat Losses from Upper RPV, Level K-K @ 270 degrees	RX-TE	-	Surface	-	3	1	H03 L03	OSU 600101	2	C4
HPM-105	Heat Losses from top of RPV, @ 90 degrees	RX-TE	-	Surface	-	3	1	H04 L04	OSU 600101	2	D4
HPM-106	Heat Losses from bottom of RPV, @ 22.5 degrees	RX-TE	-	Surface	-	3	1	H05 L05	OSU 600101	2	A4
HPM-107	Heat Losses from CL-2 flange at RPV	RX-TE	-	Surface	-	3	1	H06 L06	OSU 600101	2	C3
HPM-108	Heat Losses from CL-4 flange at RPV	RX-TE	-	Surface	-	3	1	H07 L07	OSU 600101	2	C3
HPM-109	Heat Losses from HL-2 flange at RPV	RX-TE	-	Surface	-	3	1	H08 L08	OSU 600101	2	C3
HPM-110	Heat Losses from DVI-2 flange at RPV	RX-TE	-	Surface	-	3	1	H09 L09	OSU 600101	2	C3
HPM-111	Heat Losses from CL-1 flange at RPV	RX-TE	-	Surface	-	3	1	H10 L10	OSU 600101	2	C5
HPM-112	Heat Losses from CL-3 flange at RPV	RX-TE	-	Surface	-	3	1	H11 L11	OSU 600101	2	C5
HPM-113	Heat Losses from HL-1 flange at RPV	RX-TE	-	Surface	-	3	1	H12 L12	OSU 600101	2	C5
HPM-114	Heat Losses from DVI-1 flange at RPV	RX-TE	-	Surface	-	3	1	H13 L13	OSU 600101	2	C4
HPM-201	Heat Losses from CL-1, Upstream of FMM-201	CL1	-	Surface	-	3	1	H14 L14	OSU 600203	1	A5
HPM-202	Heat Losses from CL-2, Upstream of FMM-202	CL2	-	Surface	-	3	1	H15 L15	OSU 600203	1	A4
HPM-203	Heat Losses from CL-3, Upstream of FMM-203	CL3	-	Surface	-	3	1	H16 L16	OSU 600203	1	C6
HPM-204	Heat Losses from CL-4, Upstream of FMM-204	CL4	-	Surface	-	3	1	H17 L17	OSU 600203	1	C4
HPM-205	Heat Losses from HL-1	HL1	-	Surface	-	3	1	H18 L18	OSU 600203	1	B5
HPM-206	Heat Losses from HL-2	HL1	-	Surface	-	3	1	H19 L19	OSU 600203	1	B3
HPM-301	Heat Losses form SG-01, bottom, HL Side	SG01	-	Surface	-	3	2	H00 L00	OSU 600301	1	A5
HPM-302	Heat Losses form SG-02, bottom, HL Side	SG02	-	Surface	-	3	2	H01 L01	OSU 600301	1	A2
HPM-303	Heat Losses form SG-01, Lower Downcomer Region	SG01	-	Surface	-	3	2	H02 L02	OSU 600301	1	C5
HPM-304	Heat Losses form SG-02, Lower Downcomer Region	SG02	-	Surface	-	3	2	H03 L03	OSU 600301	1	C1
HPM-305	Heat Losses form SG-01, Upper Downcomer Region	SG01	-	Surface	-	3	2	H04 L04	OSU 600301	1	C5

APPENDIX C
INSTRUMENTATION DATA BASE (Continued)

Tag No.	Name	Location	Thermocouple Diameter	Thermocouple Depth	Thermocouple Type	DAS Rack	DAS Row	DAS Channel	Drawing No.	Sheet No.	Grid
HPM-306	Heat Losses from SG-02, Upper Downcomer Region	SG02	-	Surface	-	3	2	H05 L05	OSU 600301	1	C1
HPM-401	Heat Losses from ACC-01	ACC01	-	Surface	-	3	2	H06 L06	OSU 600206	1	C6
HPM-402	Heat Losses from ACC-02	ACC02	-	Surface	-	3	2	H07 L07	OSU 600206	1	A6
HPM-501	Heat Losses from CMT-01, bottom	CMT01	-	Surface	-	3	2	H08 L08	OSU 600501	1	A2
HPM-502	Heat Losses from CMT-02, bottom	CMT02	-	Surface	-	3	2	H09 L09	OSU 600502	1	A2
HPM-503	Heat Losses from CMT-01, 50% Volume-Level	CMT01	-	Surface	-	3	2	H10 L10	OSU 600501	1	C2
HPM-504	Heat Losses from CMT-02, 50% Volume-Level	CMT02	-	Surface	-	3	2	H11 L11	OSU 600502	1	C2
HPM-505	Heat Losses from CMT-01, top	CMT01	-	Surface	-	3	2	H12 L12	OSU 600501	1	D5
HPM-506	Heat Losses from CMT-02, top	CMT02	-	Surface	-	3	2	H13 L13	OSU 600502	1	D3
HPM-507	Heat Losses from CMT-01/CL-3 Balance Line	CMT01 CL Bal	-	Surface	-	3	2	H14 L14	OSU 600206	1	C4
HPM-510	Heat Losses from CMT-02/CL-1 Balance Line	CMT02 CL Bal	-	Surface	-	3	2	H17 L17	OSU 600206	1	A5
HPM-601	Heat Losses from ADS4-1 line, upstream of RCS-615	ADS04	-	Surface	-	3	2	H18 L18	OSU 600203	1	B5
HPM-602	Heat Losses from lower PZR, Heater Region	PZR	-	Surface	-	3	2	H19 L19	OSU 600203	1	D2
HPM-603	Heat Losses from PZR Surge Line	PZR Surge Line	-	Surface	-	3	3	H00 L00	OSU 600203	1	C3
HPM-604	Heat Losses from PZR bottom	PZR	-	Surface	-	3	3	H01 L01	OSU 600203	1	C2
HPM-605	Heat Losses from upper PZR	PZR	-	Surface	-	3	3	H02 L02	OSU 600203	1	D2
HPM-606	Heat Losses from ADS1-3 common line into separator	ADS1-3	-	Surface	-	3	3	H03 L03	OSU 600203	1	D1
HPM-607	Heat Losses from PZR top	PZR	-	Surface	-	3	3	H04 L04	OSU 600203	1	D2
HPM-608	Heat Losses from ADS4-2 line, upstream of RCS-616	ADS04	-	Surface	-	3	3	H05 L05	OSU 600203	1	B4
HPM-701	Heat Losses from lower IRWST	IRWST	-	Surface	-	3	3	H06 L06	OSU 600701	1	C3
HPM-702	Heat Losses from upper IRWST	IRWST	-	Surface	-	3	3	H07 L07	OSU 600701	1	D3
HPM-703	Heat Losses from top of IRWST	IRWST	-	Surface	-	3	3	H08 L08	OSU 600701	1	D2
HPM-801	Heat Losses from PRHR HX inlet	PRHR HX	-	Surface	-	3	3	H09 L09	OSU 600206	1	B1
HPM-802	Heat Losses from PRHR HX outlet	PRHR HX	-	Surface	-	3	3	H10 L10	OSU 600206	1	B1
HPM-901	Heat Losses from Primary Sump	Primary Sump	-	Surface	-	3	3	H11 L11	OSU 600901	1	A3
HPM-902	Heat Losses from Secondary Sump	Secondary Sump	-	Surface	-	3	3	H12 L12	OSU 600901	1	A3
HPM-903	Heat Losses from Primary Sump/DVI-01 Injection Line	Sump DVI	-	Surface	-	3	3	H13 L13	OSU 600206	1	C4
HPM-904	Heat Losses from Primary Sump/DVI-02 Injection Line	Sump DVI	-	Surface	-	3	3	H14 L14	OSU 600206	1	A3
HPS-201-1	CL-1 Heat Transfer Coefficient	CL1	-	1.00 in	-	3	12	H00	OSU 600203	1	A5
HPS-201-2	CL-1 Heater dT above fluid temperature	CL1	-	1.00 in	-	3	12	L00	OSU 600203	1	A5
HPS-201-3	CL-1 Fluid temperature	CL1	-	1.00 in	-	3	12	H01	OSU 600203	1	A5
HPS-202-1	CL-2 Heat Transfer Coefficient	CL2	-	1.00 in	-	3	12	L01	OSU 600203	1	A4
HPS-202-2	CL-2 Heater dT above fluid temperature	CL2	-	1.00 in	-	3	12	H02	OSU 600203	1	A4
HPS-202-3	CL-2 Fluid temperature	CL2	-	1.00 in	-	3	12	L02	OSU 600203	1	A4
HPS-203-1	CL-3 Heat Transfer Coefficient	CL3	-	1.00 in	-	3	12	H03	OSU 600203	1	C5

APPENDIX C
INSTRUMENTATION DATA BASE (Continued)

Tag No.	Name	Location	Thermocouple Diameter	Thermocouple Depth	Thermocouple Type	DAS Rack	DAS Row	DAS Channel	Drawing No.	Sheet No.	Grid
HPS-203-2	CL-3 Heater dT above fluid temperature	CL3	-	1.00 in	-	3	12	L03	OSU 600203	1	C5
HPS-203-3	CL-3 Fluid temperature	CL3	-	1.00 in	-	3	12	H04	OSU 600203	1	C5
HPS-204-1	CL-4 Heat Transfer Coefficient	CL4	-	1.00 in	-	3	12	L04	OSU 600203	1	C4
HPS-204-2	CL-4 Heater dT above fluid temperature	CL4	-	1.00 in	-	3	12	H05	OSU 600203	1	C4
HPS-204-3	CL-4 Fluid temperature	CL4	-	1.00 in	-	3	12	L05	OSU 600203	1	C4
HPS-205-1	HL-1 Heat Transfer Coefficient	HL1	-	1.00 in	-	3	12	H06	OSU 600203	1	B5
HPS-205-2	HL-1 Heater dT above fluid temperature	HL1	-	1.00 in	-	3	12	L06	OSU 600203	1	B5
HPS-205-3	HL-1 Fluid temperature	HL1	-	1.00 in	-	3	12	H07	OSU 600203	1	B5
HPS-206-1	HL-2 Heat Transfer Coefficient	HL2	-	1.00 in	-	3	12	L07	OSU 600203	1	B3
HPS-206-2	HL-2 Heater dT above fluid temperature	HL2	-	1.00 in	-	3	12	H08	OSU 600203	1	B3
HPS-206-3	HL-2 Fluid temperature	HL2	-	1.00 in	-	3	12	L08	OSU 600203	1	B3
HPS-509-1	CMT-01 CL Balance Line Heat Transfer Coefficient	CMT01 CL Bal	-	1.00 in	-	3	12	H09	OSU 600206	1	D4
HPS-509-2	CMT-01 CL Balance Line Heater dT above fluid temperature	CMT01 CL Bal	-	1.00 in	-	3	12	L09	OSU 600206	1	D4
HPS-509-3	CMT-01 CL Balance Line Fluid temperature	CMT01 CL Bal	-	1.00 in	-	3	12	H10	OSU 600206	1	D4
HPS-512-1	CMT-02 CL Balance Line Heat Transfer Coefficient	CMT02 CL Bal	-	1.00 in	-	3	12	L10	OSU 600206	1	B5
HPS-512-2	CMT-02 CL Balance Line Heater dT above fluid temperature	CMT02 CL Bal	-	1.00 in	-	3	12	H11	OSU 600206	1	B5
HPS-512-3	CMT-02 CL Balance Line Fluid temperature	CMT02 CL Bal	-	1.00 in	-	3	12	L11	OSU 600206	1	B5
HPS-604-1	Lower PZR Surge Line Heat Transfer Coefficient	PZR Surge Line	-	1.00 in	-	3	12	H12	OSU 600203	1	C3
HPS-604-2	Lower PZR Surge Line Heater dT above fluid temperature	PZR Surge Line	-	1.00 in	-	3	12	L12	OSU 600203	1	C3
HPS-604-3	Lower PZR Surge Line Fluid temperature	PZR Surge Line	-	1.00 in	-	3	12	H13	OSU 600203	1	C3
HPS-606-1	ADS1-3 Common Inlet Heat Transfer Coefficient	ADS1-3	-	1.00 in	-	3	12	L13	OSU 600203	1	D2
HPS-606-2	ADS1-3 Common Inlet Heater dT above fluid temperature	ADS1-3	-	1.00 in	-	3	12	H14	OSU 600203	1	D2
HPS-606-3	ADS1-3 Common Inlet Fluid temperature	ADS1-3	-	1.00 in	-	3	12	L14	OSU 600203	1	D2
HPS-607-1	Upper PZR Surge Line Heat Transfer Coefficient	PZR Surge Line	-	1.00 in	-	3	12	H15	OSU 600203	1	C2
HPS-607-2	Upper PZR Surge Line Heater dT above fluid temperature	PZR Surge Line	-	1.00 in	-	3	12	L15	OSU 600203	1	C2
HPS-607-3	Upper PZR Surge Line Fluid temperature	PZR Surge Line	-	1.00 in	-	3	12	H16	OSU 600203	1	C2
HPS-801-1	PRHR HX Inlet Heat Transfer Coefficient	PRHR HX	-	1.00 in	-	3	12	L16	OSU 600206	1	B1
HPS-801-2	PRHR HX Inlet Heater dT above fluid temperature	PRHR HX	-	1.00 in	-	3	12	H17	OSU 600206	1	B1
HPS-801-3	PRHR HX Inlet Fluid temperature	PRHR HX	-	1.00 in	-	3	12	L17	OSU 600206	1	B1
HTC-001	Heat TRACE Controller # 1	OP	-	-	-	-	-	N/A	TIC 787-E200	1	-
HTC-002	Heat TRACE Controller # 2	OP	-	-	-	-	-	N/A	TIC 787-E200	1	-
IND-001	MFP Discharge Pressure	OP	-	-	-	-	-	N/A	TIC 787-E200	1	-
IND-101	CL-3 Temperature	OP	-	-	-	-	-	N/A	TIC 787-E200	1	-
IND-102	CL-4 Temperature	OP	-	-	-	-	-	N/A	TIC 787-E200	1	-
IND-103	Autoneered Reactor Sheath Temperature	OP	-	-	-	-	-	N/A	TIC 787-E200	1	-

APPENDIX C
INSTRUMENTATION DATA BASE (Continued)

Tag No.	Name	Location	Thermocouple Diameter	Thermocouple Depth	Thermocouple Type	DAS Rack	DAS Row	DAS Channel	Drawing No.	Sheet No.	Grid
IND-105	CL-1 Temperature	OP	-	-	-	-	-	N/A	TIC 787-E200	1	-
IND-106	CL-2 Temperature	OP	-	-	-	-	-	N/A	TIC 787-E200	1	-
IND-107	Rx Pressure	OP	-	-	-	-	-	N/A	TIC 787-E200	1	-
IND-201	CL-1 Headloss/Flow	OP	-	-	-	-	-	N/A	TIC 787-E200	1	-
IND-202	CL-2 Headloss/Flow	OP	-	-	-	-	-	N/A	TIC 787-E200	1	-
IND-203	CL-3 Headloss/Flow	OP	-	-	-	-	-	N/A	TIC 787-E200	1	-
IND-204	CL-4 Headloss/Flow	OP	-	-	-	-	-	N/A	TIC 787-E200	1	-
IND-205	HL-1 Temperature	OP	-	-	-	-	-	N/A	TIC 787-E200	1	-
IND-206	HL-2 Temperature	OP	-	-	-	-	-	N/A	TIC 787-E200	1	-
IND-301	SG-01 Pressure	OP	-	-	-	-	-	N/A	TIC 787-E200	1	-
IND-302	SG-02 Pressure	OP	-	-	-	-	-	N/A	TIC 787-E200	1	-
IND-601M	ADS1-3 Separator Loop Seal Flow	OP	-	-	-	-	-	N/A	TIC 787-E200	1	-
IND-601V	ADS1-3 Separator Steam Flow	OP	-	-	-	-	-	N/A	TIC 787-E200	1	-
IND-602M	ADS04-2 Separator Loop Seal Flow	OP	-	-	-	-	-	N/A	TIC 787-E200	1	-
IND-602V	ADS04-2 Separator Steam Flow	OP	-	-	-	-	-	N/A	TIC 787-E200	1	-
IND-603M	ADS04-1 Separator Loop Seal Flow	OP	-	-	-	-	-	N/A	TIC 787-E200	1	-
IND-603V	ADS04-1 Separator Steam Flow	OP	-	-	-	-	-	N/A	TIC 787-E200	1	-
IND-608	PZR Temperature	OP	-	-	-	-	-	N/A	TIC 787-E200	1	-
IND-701	IRWST Temperature	OP	-	-	-	-	-	N/A	TIC 787-E200	1	-
IND-715	IRWST Temperature	OP	-	-	-	-	-	N/A	TIC 787-E200	1	-
IND-902	Secondary Sump Temperature	OP	-	-	-	-	-	N/A	TIC 787-E200	1	-
IND-903	Primary Sump Temperature	OP	-	-	-	-	-	N/A	TIC 787-E200	1	-
IND-905M	Break Separator Loop Seal Flow	OP	-	-	-	-	-	N/A	TIC 787-E200	1	-
IND-905P	Break Separator Pressure	OP	-	-	-	-	-	N/A	TIC 787-E200	1	-
IND-905V	Break Separator Steam Flow	OP	-	-	-	-	-	N/A	TIC 787-E200	1	-
IND-914	Cond Return Tank Outlet Temperature	OP	-	-	-	-	-	N/A	TIC 787-E200	1	-
IND-917	BAMS Header 6" Line Temperature	OP	-	-	-	-	-	N/A	TIC 787-E200	1	-
KW-101	Group 1 Power Transmitter	RX-HTR	-	-	-	2	12	H00	OSU 600007	1	-
KW-102	Group 2 Power Transmitter	RX-HTR	-	-	-	2	12	H01	OSU 600007	1	-
KW-103	Group 1 Power Transmitter	RX-HTR	-	-	-	2	12	H02	OSU 600007	1	-
KW-104	Group 2 Power Transmitter	RX-HTR	-	-	-	2	12	H03	OSU 600007	1	-
KW-601	PZR Power Transmitter	RX-HTR	-	-	-	2	12	H04	OSU 600203	1	A1
LC-701	IRWST Weight Transducer	IRWST	-	-	-	-	-	N/A	OSU 600701	1	A2
LC-702	IRWST Weight Transducer	IRWST	-	-	-	-	-	N/A	OSU 600701	1	A2
LC-703	IRWST Weight Transducer	IRWST	-	-	-	-	-	N/A	OSU 600701	1	A2
LC-704	IRWST Weight Transducer	IRWST	-	-	-	-	-	N/A	OSU 600701	1	A2
LC-901	Primary Sump Weight Transducer	Primary Sump	-	-	-	-	-	N/A	OSU 600901	1	A4
LC-902	Secondary Sump Weight Transducer	Secondary Sump	-	-	-	-	-	N/A	OSU 600901	1	A2
LC-903	Primary Sump Weight Transducer	Primary Sump	-	-	-	-	-	N/A	OSU 600901	1	A4
LC-904	Secondary Sump Weight Transducer	Secondary Sump	-	-	-	-	-	N/A	OSU 600901	1	A2
LC-905	Primary Sump Weight Transducer	Primary Sump	-	-	-	-	-	N/A	OSU 600901	1	A4
LC-906	Secondary Sump Weight Transducer	Secondary Sump	-	-	-	-	-	N/A	OSU 600901	1	A2
LC-907	Primary Sump Weight Transducer	Primary Sump	-	-	-	-	-	N/A	OSU 600901	1	A4
LC-908	Secondary Sump Weight Transducer	Secondary Sump	-	-	-	-	-	N/A	OSU 600901	1	A2

APPENDIX C
INSTRUMENTATION DATA BASE (Continued)

Tag No.	Name	Location	Thermocouple Diameter	Thermocouple Depth	Thermocouple Type	DAS Rack	DAS Row	DAS Channel	Drawing No.	Sheet No.	Grid
LCS-701	IRWST Load Cell Summing Box	IRWST	-	-	-	-	-	N/A	OSU 600701	1	A1
LCS-901	Primary Sump Load Cell Summing Box	Primary Sump	-	-	-	-	-	N/A	OSU 600901	1	A4
LCS-902	Secondary Sump Load Cell Summing Box	Secondary Sump	-	-	-	-	-	N/A	OSU 600901	1	A2
LCT-701	IRWST Load Cell Transmitter	IRWST	-	-	-	2	12	H05	OSU 600701	1	A1
LCT-901	Primary Sump Load Cell Transmitter	Primary Sump	-	-	-	2	12	H06	OSU 600901	1	A4
LCT-902	Secondary Sump Load Cell Transmitter	Secondary Sump	-	-	-	2	12	H07	OSU 600901	1	A2
LDP-001	PST Level	PST	-	-	-	1	1	L05	OSU 600002	1	D6
LDP-101	CL to Bypass Nozzle Water Level (270)	RX-PE	-	-	-	1	2	H06	OSU 600101	1	C2
LDP-102	CL to Bypass Nozzle Water Level (180)	RX-PE	-	-	-	1	2	L06	OSU 600101	1	C2
LDP-103	DVI to CL Water Level (270)	RX-PE	-	-	-	1	2	H07	OSU 600101	1	C2
LDP-104	DVI to CL Water Level (180)	RX-PE	-	-	-	1	2	L07	OSU 600101	1	C2
LDP-105	Upper Core Plate to DVI Water Level (270)	RX-PE	-	-	-	1	2	H08	OSU 600101	1	B2
LDP-106	Bottom of Core to Lower Core Plate Water Level (180)	RX-PE	-	-	-	1	2	L08	OSU 600101	1	B2
LDP-107	Bottom of Core to Lower Core Plate Water Level (270)	RX-PE	-	-	-	1	2	H09	OSU 600101	1	A2
LDP-108	Bottom of Core to Lower Core Plate Water Level (0)	RX-PE	-	-	-	1	2	L09	OSU 600101	1	A6
LDP-109	Lower Core Plate to Mid-Core Spacer Grid (0)	RX-PE	-	-	-	1	2	H10	OSU 600101	1	B6
LDP-110	Mid-Core Spacer Grid to Upper-Core Spacer Grid (0)	RX-PE	-	-	-	1	2	L10	OSU 600101	1	B6
LDP-112	Upper Core Plate to DVI Water Level (0)	RX-PE	-	-	-	1	2	H11	OSU 600101	1	C6
LDP-113	DVI to Bottom of Upper Support Plate (0)	RX-PE	-	-	-	1	2	L11	OSU 600101	1	C6
LDP-115	Top of Upper Support Plate to Top of Reactor (0)	RX-PE	-	-	-	1	2	H12	OSU 600101	1	D6
LDP-116	Bottom of Reactor to Bottom of Bypass Holes (270)	RX-PE	-	-	-	1	2	L12	OSU 600101	1	C2
LDP-117	Upper Core Spacer Grid to DVI Water Level (180)	RX-PE	-	-	-	1	2	H13	OSU 600101	1	B2
LDP-118	Lower Core Plate to Upper Core Plate (270)	RX-PE	-	-	-	1	2	L13	OSU 600101	1	B2
LDP-119	Lower Core Plate to Upper Core Support Grid (180)	RX-PE	-	-	-	1	2	H14	OSU 600101	1	B2
LDP-127	Reactor Wide Range Water Level (0)	RX-PE	-	-	-	1	1	H06	OSU 600101	1	C6
LDP-138	Upper Core Spacer Grid to Bottom of Upper Support Plate (180)	RX-PE	-	-	-	1	2	L14	OSU 600101	1	B6
LDP-139	Top of Lower Core Plate to Upper Core Spacer Grid (0)	RX-PE	-	-	-	1	2	H15	OSU 600101	1	B6
LDP-140	Bottom of Reactor to Bottom of Flow Holes (180)	RX-PE	-	-	-	1	2	L15	OSU 600101	1	D3
LDP-201	CL-1 Water Level	CL1	-	-	-	1	3	L11	OSU 600203	1	A5
LDP-202	CL-2 Water Level	CL2	-	-	-	1	3	H12	OSU 600203	1	A4
LDP-203	CL-3 Water Level	CL3	-	-	-	1	3	L12	OSU 600203	1	C5
LDP-204	CL-4 Water Level	CL4	-	-	-	1	3	H13	OSU 600203	1	C4
LDP-205	HL-1 Water Level	HL1	-	-	-	1	3	L13	OSU 600203	1	B5
LDP-206	HL-2 Water Level	HL2	-	-	-	1	3	H14	OSU 600203	1	B3
LDP-207	SG-01 to HL#1 Elbow Plenum Water Level	HL1	-	-	-	1	3	L14	OSU 600203	1	B6
LDP-208	SG-02 to HL#2 Elbow Plenum Water Level	HL2	-	-	-	1	3	H15	OSU 600203	1	B3

APPENDIX C
INSTRUMENTATION DATA BASE (Continued)

Tag No.	Name	Location	Thermocouple Diameter	Thermocouple Depth	Thermocouple Type	DAS Rack	DAS Row	DAS Channel	Drawing No.	Sheet No.	Grid
LDP-209	SG-01 HL Plenum Water Level	SG01	-	-	-	1	3	H19	OSU 600301	1	A4
LDP-210	SG-02 CL#4 Plenum Water Level	SG02	-	-	-	1	3	L19	OSU 600301	1	B1
LDP-211	SG-01 CL#3 Plenum Water Level	SG01	-	-	-	1	4	H00	OSU 600301	1	A6
LDP-212	SG-02 CL#2 Plenum Water Level	SG02	-	-	-	1	4	L00	OSU 600301	1	B1
LDP-213	SG-01 CL#1 Plenum Water Level	SG01	-	-	-	1	4	H01	OSU 600301	1	A6
LDP-214	SG-02 HL Plenum Water Level	SG02	-	-	-	1	4	L01	OSU 600301	1	A3
LDP-215	SG-01 Long Tube HL Water Level	SG01	-	-	-	1	4	H02	OSU 600301	1	C6
LDP-216	SG-02 Short Tube HL Water Level	SG02	-	-	-	1	4	L02	OSU 600301	1	C1
LDP-217	SG-01 Short Tube HL Water Level	SG01	-	-	-	1	4	H03	OSU 600301	1	C6
LDP-218	SG-02 Long Tube HL Water Level	SG02	-	-	-	1	4	L03	OSU 600301	1	C1
LDP-219	SG-01 Long Tube CL Water Level	SG01	-	-	-	1	4	H04	OSU 600301	1	C6
LDP-220	SG-02 Short Tube CL Water Level	SG02	-	-	-	1	4	L04	OSU 600301	1	C1
LDP-221	SG-01 Short Tube CL Water Level	SG01	-	-	-	1	4	H05	OSU 600301	1	C6
LDP-222	SG-02 Long Tube CL Water Level	SG02	-	-	-	1	4	L05	OSU 600301	1	C1
LDP-301	SG-01 WR Level	SG01	-	-	-	1	1	L06	OSU 600301	1	C4
LDP-302	SG-02 WR Level	SG02	-	-	-	1	1	H07	OSU 600301	1	C3
LDP-303	SG-01 NR Level	SG01	-	-	-	1	1	L07	OSU 600301	1	C4
LDP-304	SG-02 NR Level	SG02	-	-	-	1	1	H08	OSU 600301	1	C3
LDP-401	ACC-01 Level	ACC01	-	-	-	1	1	L08	OSU 600206	1	C6
LDP-402	ACC-02 Level	ACC02	-	-	-	1	1	H09	OSU 600206	1	A6
LDP-501	CMT-01 NR Level (Bottom)	CMT01	-	-	-	1	4	L17	OSU 600501	1	B1
LDP-502	CMT-02 WR Level	CMT02	-	-	-	1	1	L09	OSU 600502	1	C1
LDP-503	CMT-01 NR Level (Middle)	CMT01	-	-	-	1	4	H18	OSU 600501	1	C1
LDP-504	CMT-02 NR Level (Bottom)	CMT02	-	-	-	1	4	L18	OSU 600502	1	B1
LDP-505	CMT-01 NR Level (Top)	CMT01	-	-	-	1	4	H19	OSU 600501	1	D1
LDP-506	CMT-02 NR Level (Middle)	CMT02	-	-	-	1	4	L19	OSU 600502	1	C1
LDP-507	CMT-01 WR Level	CMT01	-	-	-	1	1	H10	OSU 600501	1	C1
LDP-508	CMT-02 NR Level (Top)	CMT02	-	-	-	1	5	H13	OSU 600502	1	D1
LDP-509	CL-3 to CMT-01 Balance Line Water Level	CMT01 CL Bal	-	-	-	1	5	L13	OSU 600206	1	C4
LDP-510	CL-1 to CMT-02 Balance Line Water Level	CMT02 CL Bal	-	-	-	1	5	H14	OSU 600206	1	A5
LDP-601	PZR WR Level	PZR	-	-	-	1	1	L10	OSU 600203	1	D2
LDP-602	PZR Surge Line Level	PZR Surge Line	-	-	-	1	6	H10	OSU 600203	1	B3
LDP-605	PZR Upper Surge Line Pipe Level	PZR Surge Line	-	-	-	1	6	L10	OSU 600203	1	C2
LDP-606	PZR Surge Line Pipe Level @ PZR Inlet	PZR Surge Line	-	-	-	1	6	H11	OSU 600203	1	C2
LDP-607	PZR Middle Surge Line Pipe Level	PZR Surge Line	-	-	-	1	6	L11	OSU 600203	1	C3
LDP-608	PZR Lower Surge Line Pipe Level	PZR Surge Line	-	-	-	1	6	H12	OSU 600203	1	C3
LDP-609	PZR Surge Line Pipe Level @ HL-2	PZR Surge Line	-	-	-	1	6	L12	OSU 600203	1	B3
LDP-610	ADS1-3 Separator Level	ADS1-3	-	-	-	1	12	L06	OSU 600203	1	C2
LDP-611	ADS4-1 Separator Level	ADS04-1	-	-	-	1	12	H07	OSU 600901	1	B6

APPENDIX C
INSTRUMENTATION DATA BASE (Continued)

Tag No.	Name	Location	Thermocouple Diameter	Thermocouple Depth	Thermocouple Type	DAS Rack	DAS Row	DAS Channel	Drawing No.	Sheet No.	Grid
LDP-612	ADS4-2 Separator Level	ADS04-2	-	-	-	1	12	L07	OSU 600901	1	B1
LDP-701	IRWST Level	IRWST	-	-	-	1	1	H11	OSU 600701	1	C3
LDP-801	PRHR HX Inlet Head Level	PRHR HX	-	-	-	1	6	H13	OSU 600206	1	B1
LDP-802	PRHR HX WR Level	PRHR HX	-	-	-	1	5	L08	OSU 600206	1	B1
LDP-901	Primary Sump Level	Primary Sump	-	-	-	1	1	L11	OSU 600901	1	B4
LDP-902	Secondary Sump Level	Secondary Sump	-	-	-	1	1	H12	OSU 600901	1	B2
LDP-903	CRT Level	COND RTN	-	-	-	1	12	H08	OSU 600002	1	D5
LDP-905	Break Separator Level	BAMS	-	-	-	1	12	L08	OSU 600901	1	B5
LSL-001	RCP Seal Water Tank Level Switch	GSW	-	-	-	-	-	N/A	OSU 600903	1	D3
PI-001	MCP Discharge Local Pressure Gage	MF	-	-	-	-	-	N/A	OSU 600002	1	B4
PI-201	Reactor Coolant System Local Pressure Gage	HL1	-	-	-	-	-	N/A	OSU 600203	1	B5
PI-401	ACC-01 Local Pressure Gage	ACC01	-	-	-	-	-	N/A	OSU 600206	1	D6
PI-402	ACC-02 Local Pressure Gage	ACC02	-	-	-	-	-	N/A	OSU 600206	1	B6
PI-801	CVSP Discharge Local Pressure Gage	CVS Fill	-	-	-	-	-	N/A	OSU 600002	1	A4
PI-802	RNSP Discharge Local Pressure Gage	RNS Fill	-	-	-	-	-	N/A	OSU 600002	1	B4
PI-901	Primary Sump Pressure	Primary Sump	-	-	-	-	-	N/A	OSU 600901	1	B4
PI-902	CRP Dsch. Press	COND RTN	-	-	-	-	-	N/A	OSU 600002	1	C4
PSL-001	Air Receiver Pressure Switch	Air System	-	-	-	-	-	N/A	OSU 600003	-	-
PSL-002	PMP Suction HDR Press Sw	Demun	-	-	-	-	-	N/A	OSU 600002	1	C5
PSL-003	RNS Pump Suct. Hdr Press. Sw	RNS Fill	-	-	-	-	-	N/A	OSU 600002	1	B4
PT-001	MFP Discharge Pressure	MF	-	-	-	1	1	L12	OSU 600002	1	B4
PT-002	MS Header Pressure	MS	-	-	-	1	6	L13	OSU 600002	1	D2
PT-003	Lab Room Barometer	Lab	-	-	-	1	6	H14	TBD	-	-
PT-101	CL-1 Pressure @ Reactor Flange	RX-PE	-	-	-	1	2	H16	OSU 600101	1	D6
PT-102	CL-2 Pressure @ Reactor Flange	RX-PE	-	-	-	1	2	L16	OSU 600101	1	D2
PT-103	CL-3 Pressure @ Reactor Flange	RX-PE	-	-	-	1	2	H17	OSU 600101	1	C6
PT-104	CL-4 Pressure @ Reactor Flange	RX-PE	-	-	-	1	2	L17	OSU 600101	1	D2
PT-107	Reactor Upper Head Pressure	RX-PE	-	-	-	1	1	H13	OSU 600101	1	D5
PT-108	Bottom of Reactor Pressure	RX-PE	-	-	-	1	2	H18	OSU 600101	1	A6
PT-109	DVI-1 Pressure @ Reactor Flange	RX-PE	-	-	-	1	2	L18	OSU 600101	1	B6
PT-110	DVI-2 Pressure @ Reactor Flange	RX-PE	-	-	-	1	2	H19	OSU 600101	1	B2
PT-111	Reactor Annular Pressure @ Flow Bypass Holes	RX-PE	-	-	-	1	2	L19	OSU 600101	1	D2
PT-112	Reactor Annular Pressure @ Bottom of Reactor	RX-PE	-	-	-	1	3	H00	OSU 600101	1	B3
PT-113	Reactor Pressure Below Mid-Core Spacer Grid	RX-PE	-	-	-	1	3	L00	OSU 600101	1	B6
PT-201	SG-01 Long Tube Pressure (Top)	SG01	-	-	-	1	3	H07	OSU 600301	1	D6
PT-202	HL-2 Pressure @ SG-02 Flange	HL2	-	-	-	1	3	L15	OSU 600203	1	B3
PT-203	CL Break Pressure @ Break Valve	CL Break	-	-	-	1	3	H16	OSU 600904	1	C4
PT-204	SG-02 Long Tube Pressure (Top)	SG02	-	-	-	1	4	H06	OSU 600301	1	D1
PT-205	HL-1 Pressure @ SG-01 Flange	HL1	-	-	-	1	5	H08	OSU 600203	1	B5

APPENDIX C
INSTRUMENTATION DATA BASE (Continued)

Tag No.	Name	Location	Thermocouple Diameter	Thermocouple Depth	Thermocouple Type	DAS Rack	DAS Row	DAS Channel	Drawing No.	Sheet No.	Grid
PT-206	HL Break Pressure @ Break Valve	HL Break	-	-	-	1	3	L16	OSU 600904	1	-
PT-301	SG-01 Pressure	SG01 MS	-	-	-	1	1	L13	OSU 600002	1	C2
PT-302	SG-02 Pressure	SG02 MS	-	-	-	1	1	H14	OSU 600002	1	C1
PT-401	ACC-01 Pressure	ACC01	-	-	-	1	5	L17	OSU 600206	1	D6
PT-402	ACC-02 Pressure	ACC02	-	-	-	1	5	H18	OSU 600206	1	B6
PT-501	CMT-01 Pressure	CMT01	-	-	-	1	5	L14	OSU 600501	1	D1
PT-502	CMT-02 Pressure	CMT02	-	-	-	1	5	H15	OSU 600502	1	D1
PT-602	PZR NR Pressure	PZR	-	-	-	1	1	H18	OSU 600203	1	D2
PT-603	PZR WR Pressure	PZR	-	-	-	1	5	H09	OSU 600203	1	D2
PT-604	PZR WR Pressure	PZR Balance Line	-	-	-	1	1	L14	OSU 600203	1	D2
PT-605	ADS1-3 Separator Pressure	ADS1-3	-	-	-	1	5	L09	OSU 600203	1	C1
PT-606	IRWST Sparger Line Pressure	ADS1-3	-	-	-	1	6	L15	OSU 600206	1	C1
PT-610	ADS4-2 Separator Pressure	ADS04-2	-	-	-	1	5	H12	OSU 600901	1	B1
PT-611	ADS4-1 Separator Pressure	ADS04-1	-	-	-	1	5	L12	OSU 600901	1	B6
PT-701	IRWST Pressure	IRWST	-	-	-	1	1	H15	OSU 600701	1	D3
PT-801	CVSP Discharge Pressure	CVS Fill	-	-	-	1	1	L15	OSU 600002	1	A4
PT-802	RNSP Discharge Pressure	RNS Fill	-	-	-	1	1	H16	OSU 600002	1	B4
PT-901	Primary Sump Pressure	Primary Sump	-	-	-	1	6	H16	OSU 600901	1	B4
PT-902	BAMS Header Pressure	BAMS	-	-	-	1	12	H09	OSU 600901	1	D3
PT-905	Break Separator Pressure	LGBR	-	-	-	1	12	L09	OSU 600904	1	C5
PUMPC	Pump Controller	OP	-	-	-	-	-	N/A	TIC 787-E200	1	-
PX-103A	Group 1/KW-103 Power (Voltage) Transformer	RX-HTR	-	-	-	-	-	N/A	OSU 600007	1	-
PX-103B	Group 1/KW-103 Power (Voltage) Transformer	RX-HTR	-	-	-	-	-	N/A	OSU 600007	1	-
PX-104A	Group 2/KW-104 Power (Voltage) Transformer	RX-HTR	-	-	-	-	-	N/A	OSU 600007	1	-
PX-104B	Group 2/KW-104 Power (Voltage) Transformer	RX-HTR	-	-	-	-	-	N/A	OSU 600007	1	-
PZRC	Pressurizer Controller	OP	-	-	-	-	-	N/A	TIC 787-E200	1	-
RXC	Reactor Controller	OP	-	-	-	-	-	N/A	TIC 787-E200	1	-
SC-101	TF-101/CL-3 Signal Conditioner	DASG1	-	-	-	3	11	H00	TIC 787-E500G1	1	-
SC-102	TF-102/CL-4 Signal Conditioner	DASG1	-	-	-	3	11	L00	TIC 787-E500G1	1	-
SC-105	TF-105/CL-1 Signal Conditioner	DASG1	-	-	-	3	11	H01	TIC 787-E500G1	1	-
SC-106	TF-106/CL-2 Signal Conditioner	DASG1	-	-	-	3	11	L01	TIC 787-E500G1	1	-
SC-140	TF-140/HL-2 Signal Conditioner	DASG1	-	-	-	3	11	H06	TIC 787-E500G1	1	-
SC-141	TF-141/HL-1 Signal Conditioner	DASG1	-	-	-	3	11	L06	TIC 787-E500G1	1	-
SC-205	TF-205/HL-1 Signal Conditioner	DASG1	-	-	-	3	11	H02	TIC 787-E500G1	1	-
SC-206	TF-206/HL-2 Signal Conditioner	DASG1	-	-	-	3	11	L02	TIC 787-E500G1	1	-
SC-301	TF-301/SG-01 Signal Conditioner	DASG1	-	-	-	3	11	H05	TIC 787-E500G1	1	-
SC-310	TF-310/SG-02 Signal Conditioner	DASG1	-	-	-	3	11	L05	TIC 787-E500G1	1	-
SC-608	TF-608/PZR Signal Conditioner	DASG1	-	-	-	3	11	H03	TIC 787-E500G1	1	-
SC-715	TF-715/IRWST Signal Controller	DASG1	-	-	-	3	11	L03	TIC 787-E500G1	1	-
SC-902	TF-902/Secondary Sump Signal Conditioner	DASG1	-	-	-	3	11	H04	TIC 787-E500G1	1	-
SC-903	TF-903/Primary Sump Signal Conditioner	DASG1	-	-	-	3	11	L04	TIC 787-E500G1	1	-

APPENDIX C
INSTRUMENTATION DATA BASE (Continued)

Tag No.	Name	Location	Thermocouple Diameter	Thermocouple Depth	Thermocouple Type	DAS Rack	DAS Row	DAS Channel	Drawing No.	Sheet No.	Grid
SC-914	TF-914/CRT Signal Conditioner	DASG1	-	-	-	3	11	H07	TIC 787-E500G1	1	-
SC-917	TF-917/BAMS Header Signal Conditioner	DASG1	-	-	-	3	11	L07	TIC 787-E500G1	1	-
SC-TH-101-3	TH-101-3/Group1 Heater Rod Signal Conditioner	DASG1	-	-	-	3	11	H08	TIC 787-E500G1		
SC-TH-102-4	TH-102-4/Group1 Heater Rod Signal Conditioner	DASG1	-	-	-	3	11	L08	TIC 787-E500G1	1	-
SC-TH-103-3	TH-103-3/Group 1 Heater Rod Signal Conditioner	DASG1	-	-	-	3	11	H09	TIC 787-E500G1	1	-
SC-TH-104-4	TH-104-4/Group 1 Heater Rod Signal Conditioner	DASG1	-	-	-	3	11	L09	TIC 787-E500G1	1	-
SC-TH-304-3	TH-304-3/Group2 Heater Rod Signal Conditioner	DASG1	-	-	-	3	11	H10	TIC 787-E500G1	1	-
SC-TH-314-3	TH-314-3/Group2 Heater Rod Signal Conditioner	DASG1	-	-	-	3	11	L10	TIC 787-E500G1	1	-
SG-001	PST Lower Sight Glass	PST	-	-	-	-	-	N/A	OSU 60002	1	C6
SG-002	PST Upper Sight Glass	PST	-	-	-	-	-	N/A	OSU 60002	1	D6
SG1C	Steam Generator #1 Controller	OP	-	-	-	-	-	N/A	TIC 787-E200	1	-
SG2C	Steam Generator #2 Controller	OP	-	-	-	-	-	N/A	TIC 787-E200	1	-
SOC	Steam Out Controller	OP	-	-	-	-	-	N/A	TIC 787-E200	1	-
TCHT-001	CRT Heater Bundle Temperature	COND RTN	-	N/A	J	-	-	N/A	OSU 60002	1	D4
TCHT-002	CRT Fluid Temperature	COND RTN	-	N/A	J	-	-	N/A	OSU 60002	1	D4
TF-001	RCP-01 Seal Water Temperature	GSW	0.125 in	3.00 in	K	-	-	N/A	OSU 60903	1	B2
TF-002	RCP-02 Seal Water Temperature	GSW	0.125 in	3.00 in	K	-	-	N/A	OSU 60903	1	B3
TF-003	RCP-03 Seal Water Temperature	GSW	0.125 in	3.00 in	K	-	-	N/A	OSU 60903	1	B3
TF-004	RCP-04 Seal Water Temperature	GSW	0.125 in	3.00 in	K	-	-	N/A	OSU 60903	1	B4
TF-005	Lab Ambient Temperature, Low	Lab	0.125 in	N/A	K	1	11	H16 L16	TBD	-	-
TF-006	Lab Ambient Temperature, Middle	Lab	0.125 in	N/A	K	1	11	H17 L17	TBD	-	-
TF-007	Lab Ambient Temperature, High	Lab	0.125 in	N/A	K	1	11	H18 L18	TBD	-	-
TF-101	CL-1/Reactor Flange, Top	RX-TE	0.25 in	1.25 in	K	-	-	N/A	OSU 600101	2	C5
TF-102	CL-2/Reactor Flange, Top	RX-TE	0.25 in	1.25 in	K	-	-	N/A	OSU 600101	2	C5
TF-103	CL-3/Reactor Flange, Bottom	RX-TE	0.25 in	0.50 in	K	1	7	H00 L00	OSU 600101	2	C5
TF-104	CL-4/Reactor Flange, Bottom	RX-TE	0.25 in	0.50 in	K	1	7	H01 L01	OSU 600101	2	C5
TF-105	CL-1/Reactor Flange, Top	RX-TE	0.25 in	1.25 in	K	-	-	N/A	OSU 600101	2	C5
TF-106	CL-2/Reactor Flange, Top	RX-TE	0.25 in	1.25 in	K	-	-	N/A	OSU 600101	2	C5
TF-107	CL-1/Reactor Flange, Bottom	RX-TE	0.25 in	0.50 in	K	1	7	H02 L02	OSU 600101	2	C5
TF-108	CL-2/Reactor Flange, Bottom	RX-TE	0.25 in	0.50 in	K	1	7	H03 L03	OSU 600101	2	C5
TF-113	DVI-1/Reactor Flange, Top	RX-TE	0.125 in	0.40 in	K	1	7	H04 L04	OSU 600101	2	C4
TF-114	DVI-2/Reactor Flange, Bottom	RX-TE	0.125 in	0.40 in	K	1	7	H05 L05	OSU 600101	2	C3
TF-115	DVI-1/Reactor Flange, Bottom	RX-TE	0.125 in	0.125 in	K	1	7	H06 L06	OSU 600101	2	C4
TF-116	DVI-2/Reactor Flange, Top	RX-TE	0.125 in	0.125 in	K	1	7	H07 L07	OSU 600101	2	C3
TF-118	Lower Rx Vessel Layer Y-Y @ 30 degrees	RX-TE	0.25 in	2.125 in	K	2	1	H00 L00	OSU 600101	2	A3
TF-120	Top of Reactor @ 8.5° and 350 degrees of Center	RX-TE	0.25 in	1.00 in	K	2	1	H01 L01	OSU 600101	2	D4
TF-126	Lower Rx Vessel Layer A-A @ 225 degrees	RX-TE	0.25 in	1.25 in	K	1	7	H08 L08	OSU 600101	2	A3
TF-127	Lower Rx Vessel Layer A-A @ 315 degrees	RX-TE	0.25 in	1.25 in	K	1	7	H09 L09	OSU 600101	2	A3
TF-128	Lower Rx Vessel Layer C-C @ 0 degrees	RX-TE	0.25 in	1.25 in	K	2	1	H02 L02	OSU 600101	2	A4

**APPENDIX C
INSTRUMENTATION DATA BASE (Continued)**

Tag No.	Name	Location	Thermocouple Diameter	Thermocouple Depth	Thermocouple Type	DAS Rack	DAS Row	DAS Channel	Drawing No.	Sheet No.	Grid
TF-129	Lower Rx Vessel Layer C-C @ 32 degrees	RX-TE	0.25 in	1.25 in	K	2	1	H03 L03	OSU 600101	2	A4
TF-130	Lower Rx Vessel Layer G-G @ 0 degrees	RX-TE	0.25 in	1.25 in	K	2	1	H04 L04	OSU 600101	2	B4
TF-131	Lower Rx Vessel Layer G-G @ 11.3 degrees	RX-TE	0.25 in	1.25 in	K	2	1	H05 L05	OSU 600101	2	B4
TF-132	Upper Rx Vessel Layer F-F @ 0 degrees	RX-TE	0.25 in	1.25 in	K	2	1	H06 L06	OSU 600101	2	B4
TF-133	Upper Rx Vessel Layer F-F @ 8 degrees	RX-TE	0.25 in	1.25 in	K	2	1	H07 L07	OSU 600101	2	B4
TF-134	Upper Rx Vessel Layer E-E @ 0 degrees	RX-TE	0.25 in	1.25 in	K	2	1	H08 L08	OSU 600101	2	C4
TF-135	Upper Rx Vessel Layer E-E @ 6.2 degrees	RX-TE	0.25 in	1.25 in	K	2	1	H09 L09	OSU 600101	2	C4
TF-140	HL-2/Reactor Flange, Top	RX-TE	0.25 in	1.70 in	K	-	-	N/A	OSU 600101	2	C3
TF-141	HL-1/Reactor Flange, Top	RX-TE	0.25 in	1.70 in	K	-	-	N/A	OSU 600101	2	C5
TF-142	HL-2/Reactor Flange, Bottom	RX-TE	0.25 in	0.50 in	K	1	7	H10 L10	OSU 600101	2	C3
TF-143	HL-1/Reactor Flange, Bottom	RX-TE	0.25 in	0.50 in	K	1	7	H11 L11	OSU 600101	2	C5
TF-147	Upper Rx Vessel Layer I-I @ 180 degrees	RX-TE	0.25 in	1.25 in	K	2	1	H10 L10	OSU 600101	2	C2
TF-148	Upper Rx Vessel Layer I-I @ 188 degrees	RX-TE	0.25 in	1.25 in	K	2	1	H11 L11	OSU 600101	2	C2
TF-149	Upper Rx Vessel Layer H-H @ 180 degrees	RX-TE	0.25 in	1.25 in	K	2	1	H12 L12	OSU 600101	2	B2
TF-150	Upper Rx Vessel Layer H-H @ 186.2 degrees	RX-TE	0.25 in	1.25 in	K	2	1	H13 L13	OSU 600101	2	B2
TF-151	Upper Rx Vessel Layer E-E @ 186.2 degrees	RX-TE	0.25 in	1.25 in	K	2	1	H14 L14	OSU 600101	2	C3
TF-152	Upper Rx Vessel Layer E-E @ 180 degrees	RX-TE	0.25 in	1.25 in	K	2	1	H15 L15	OSU 600101	2	C3
TF-153	Upper Rx Vessel Layer F-F @ 180 degrees	RX-TE	0.25 in	1.25 in	K	2	1	H16 L16	OSU 600101	2	B3
TF-154	Upper Rx Vessel Layer F-F @ 188 degrees	RX-TE	0.25 in	1.25 in	K	2	1	H17 L17	OSU 600101	2	B3
TF-155	Lower Rx Vessel Layer G-G @ 180 degrees	RX-TE	0.25 in	1.25 in	K	2	1	H18 L18	OSU 600101	2	B3
TF-156	Lower Rx Vessel Layer G-G @ 191.3 degrees	RX-TE	0.25 in	1.25 in	K	2	1	H19 L19	OSU 600101	2	B3
TF-157	Lower Rx Vessel Layer C-C @ 212 degrees	RX-TE	0.25 in	1.25 in	K	2	2	H00 L00	OSU 600101	2	A3
TF-158	Lower Rx Vessel Layer C-C @ 180 degrees	RX-TE	0.25 in	1.25 in	K	2	2	H01 L01	OSU 600101	2	A3
TF-162	Lower Rx Vessel Layer A-A @ 45 degrees	RX-TE	0.25 in	1.25 in	K	1	7	H12 L12	OSU 600101	2	A4
TF-163	Lower Rx Vessel Layer A-A @ 135 degrees	RX-TE	0.25 in	1.25 in	K	1	7	H13 L13	OSU 600101	2	A4
TF-164	Upper Rx Vessel Layer H-H @ 0 degrees	RX-TE	0.25 in	1.25 in	K	2	2	H02 L02	OSU 600101	2	C2
TF-165	Upper Rx Vessel Layer H-H @ 6.2 degrees	RX-TE	0.25 in	1.25 in	K	2	2	H03 L03	OSU 600101	2	C2
TF-166	Upper Rx Vessel Layer I-I @ 0 degrees	RX-TE	0.25 in	1.25 in	K	2	2	H04 L04	OSU 600101	2	D2
TF-167	Upper Rx Vessel Layer I-I @ 8 degrees	RX-TE	0.25 in	1.25 in	K	2	2	H05 L05	OSU 600101	2	D2
TF-168	Upper Rx Vessel Layer K-K @ 270 degrees	RX-TE	0.25 in	1.25 in	K	2	2	H06 L06	OSU 600101	2	C4
TF-169	Upper Rx Vessel Layer M-M @ 90 degrees	RX-TE	0.063 in	in fully- 5"	K	2	2	H07 L07	OSU 600101	2	B3
TF-170	Upper Rx Vessel Layer M-M @ 270 degrees	RX-TE	-	in fully- 5"	K	3	7	H00 L00	OSU 600101	2	B3
TF-171	Top of Reactor Down to within 0.50" of Upper Support Plate	RX-TE	0.25 in	w/in 0.5" USP*	K	3	7	H01 L01	OSU 600101	2	C4

APPENDIX C
INSTRUMENTATION DATA BASE (Continued)

Tag No.	Name	Location	Thermocouple Diameter	Thermocouple Depth	Thermocouple Type	DAS Rack	DAS Row	DAS Channel	Drawing No.	Sheet No.	Grid
TF-172	Lower Rx Vessel Layer AA-AA @ 0 degrees	RX-TE	0.25 in	D/2	K	3	7	H02 L02	OSU 600101	2	A4
TF-173	Lower Rx Vessel Layer AA-AA @ 270 degrees	RX-TE	0.25 in	D/2-1.58	K	3	7	H03 L03	OSU 600101	2	A4
TF-201	CL-1 @ RCP-1 Inlet	CL1	0.25 in	D/3	K	1	7	H14 L14	OSU 600203	1	A6
TF-202	CL-2 @ RCP-2 Inlet	CL2	0.25 in	D/3	K	1	7	H15 L15	OSU 600203	1	A3
TF-203	CL-3 @ RCP-3 Inlet	CL3	0.25 in	D/3	K	1	7	H16 L16	OSU 600203	1	C6
TF-204	CL-4 @ RCP-4 Inlet	CL4	0.25 in	D/3	K	1	7	H17 L17	OSU 600203	1	C3
TF-205	HL-1 @ SG-1 Outlet	HL1	0.25 in	1.68 in	K	-	-	N/A	OSU 600203	1	B6
TF-206	HL-2 @ SG-2 Outlet	HL2	0.25 in	1.68 in	K	-	-	N/A	OSU 600203	1	B3
TF-207	SG-01 Short Tube Middle Outlet Side	SG01	0.0625 in	N/A	K	2	2	H08 L08	OSU 600301	1	C5
TF-208	SG-02 Short Tube Middle Outlet Side	SG02	0.0625 in	N/A	K	2	2	H09 L09	OSU 600301	1	C2
TF-209	SG-01 Short Tube Middle Inlet Side	SG01	0.0625 in	N/A	K	2	2	H10 L10	OSU 600301	1	C5
TF-210	SG-02 Short Tube Middle Inlet Side	SG02	0.0625 in	N/A	K	2	2	H11 L11	OSU 600301	1	C2
TF-211	SG-01 Long Tube Middle Outlet	SG01	0.0625 in	N/A	K	2	2	H12 L12	OSU 600301	1	C4
TF-212	SG-02 Long Tube Middle Outlet	SG02	0.0625 in	N/A	K	2	2	H13 L13	OSU 600301	1	C2
TF-213	SG-01 Long Tube Middle Inlet	SG01	0.0625 in	N/A	K	2	2	H14 L14	OSU 600301	1	C5
TF-214	SG-02 Long Tube Middle Inlet	SG02	0.0625 in	N/A	K	2	2	H15 L15	OSU 600301	1	C2
TF-215	SG-01 Short Tube Top	SG01	0.0625 in	N/A	K	2	2	H16 L16	OSU 600301	1	D5
TF-216	SG-02 Short Tube Top	SG02	0.0625 in	N/A	K	2	2	H17 L17	OSU 600301	1	D2
TF-217	SG-01 Long Tube Top	SG01	0.0625 in	N/A	K	2	2	H18 L18	OSU 600301	1	D5
TF-218	SG-02 Long Tube Top	SG02	0.0625 in	N/A	K	2	2	H19 L19	OSU 600301	1	D2
TF-301	SG-01 Steam Header	SG01 MS	0.125 in	D/3	K	-	-	N/A	OSU 600002	1	C2
TF-305	SG-01 Downcomer HL Side	SG01	0.125 in	0.50 in	K	3	7	H04 L04	OSU 600301	1	B4
TF-306	SG-02 Downcomer HL Side	SG02	0.125 in	0.50 in	K	3	7	H05 L05	OSU 600301	1	B2
TF-307	SG-01 Downcomer cL Side	SG01	0.125 in	0.50 in	K	3	7	H06 L06	OSU 600301	1	B5
TF-308	SG-02 Downcomer cL Side	SG02	0.125 in	0.50 in	K	3	7	H07 L07	OSU 600301	1	B1
TF-310	SG-02 Steam Header	SG02 MS	0.125 in	D/3	K	-	-	N/A	OSU 600002	1	C1
TF-311	SG-01 Feed Header	MF	0.125 in	D/2	K	1	7	H18 L18	OSU 600002	1	C2
TF-312	SG-02 Feed Header	MF	0.125 in	D/2	K	1	7	H19 L19	OSU 600002	1	C1
TF-401	ACC-01 Outlet	ACC01	0.125 in	D/2	K	1	8	H00 L00	OSU 600206	1	C6
TF-402	ACC-02 Outlet	ACC02	0.125 in	D/2	K	1	8	H01 L01	OSU 600206	1	A6
TF-403	ACC-01 Tank Temperature @ Top	ACC01	0.25 in	D/3	K	1	8	H02 L02	OSU 600206	1	C6
TF-404	ACC-02 Tank Temperature @ Top	ACC02	0.25 in	D/3	K	1	8	H03 L03	OSU 600206	1	A6
TF-405	ACC-01 Injection Line	ACC01	0.25 in	D/2	K	1	8	H04 L04	OSU 600206	1	C5
TF-406	ACC-02 Injection Line	ACC02	0.125 in	D/2	K	1	8	H05 L05	OSU 600206	1	A5
TF-501	CMT-01 Long T/C Rod @ 0.30°	CMT01	0.040 in	N/A	K	1	8	H06 L06	OSU 600501	1	B5
TF-502	CMT-02 Injection Line	CMT02 DVI	0.125 in	D/2	K	1	8	H07 L07	OSU 600206	1	A5
TF-503	CMT-01 @ 1/2 Lower Head Height, 135 degrees	CMT01	0.25 in	1.00 in	K	2	3	H00 L00	OSU 600501	1	B3
TF-504	CMT-02 Long T/C Rod @ 0.30°	CMT02	0.040 in	N/A	K	2	3	H01 L01	OSU 600502	1	B5
TF-505	CMT-01 @ 20% Volume-Height, 135 degrees	CMT01	0.25 in	1.00 in	K	2	3	H02 L02	OSU 600501	1	B3
TF-506	CMT-02 @ 1/2 Lower Head Height, 135 degrees	CMT02	0.25 in	1.00 in	K	2	3	H03 L03	OSU 600502	1	B3
TF-507	CMT-01 Long T/C Rod @ 20.87°	CMT01	0.040 in	N/A	K	2	3	H04 L04	OSU 600501	1	B5
TF-508	CMT-02 @ 20% Volume-Height, 135 degrees	CMT02	0.25 in	1.00 in	K	2	3	H05 L05	OSU 600502	1	B3

APPENDIX C
INSTRUMENTATION DATA BASE (Continued)

Tag No.	Name	Location	Thermocouple Diameter	Thermocouple Depth	Thermocouple Type	DAS Rack	DAS Row	DAS Channel	Drawing No.	Sheet No.	Grid
TF-509	CMT-01 Long T/C Rod @ 36.891"	CMT01	0.040 in	N/A	K	2	3	H06 L06	OSU 600501	1	C5
TF-510	CMT-02 Long T/C Rod @ 20.87"	CMT02	0.040 in	N/A	K	1	8	H08 L08	OSU 600502	1	B5
TF-511	CMT-01 @ 50% Volume-Height, 135 degrees	CMT01	0.25 in	1.00 in	K	2	3	H07 L07	OSU 600501	1	C3
TF-512	CMT-02 Long T/C Rod @ 36.891"	CMT02	0.040 in	N/A	K	2	3	H08 L08	OSU 600502	1	C5
TF-513	CMT-01 Long T/C Rod @ 40.591"	CMT01	0.040 in	N/A	K	2	3	H09 L09	OSU 600501	1	C5
TF-514	CMT-02 @ 50% Volume-Height, 135 degrees	CMT02	0.25 in	1.00 in	K	2	3	H10 L10	OSU 600502	1	C3
TF-515	CMT-01 Long T/C Rod @ 43.411"	CMT01	0.040 in	N/A	K	2	3	H11 L11	OSU 600501	1	C5
TF-516	CMT-02 Long T/C Rod @ 40.591"	CMT02	0.040 in	N/A	K	2	3	H12 L12	OSU 600502	1	C5
TF-517	CMT-01 @ 75% Volume-Height minus 3.7", 135 degrees	CMT01	0.25 in	1.00 in	K	2	8	H19 L19	OSU 600501	1	C3
TF-518	CMT-02 Long T/C Rod @ 43.411"	CMT02	0.040 in	N/A	K	2	3	H13 L13	OSU 600502	1	C5
TF-519	CMT-01 Long T/C Rod @ 46.231"	CMT01	0.040 in	N/A	K	2	3	H14 L14	OSU 600501	1	C5
TF-520	CMT-02 @ 75% Volume-Height minus 3.7", 135 degrees	CMT02	0.25 in	1.00 in	K	2	3	H15 L15	OSU 600502	1	C3
TF-521	CMT-01 @ 75% Volume-Height, 135 degrees	CMT01	0.25 in	1.00 in	K	3	7	H08 L08	OSU 600501	1	C3
TF-522	CMT-02 Long T/C Rod @ 46.231"	CMT02	0.040 in	N/A	K	2	3	H16 L16	OSU 600502	1	C5
TF-523	CMT-01 Long T/C Rod @ 49.051"	CMT01	0.040 in	N/A	K	2	3	H17 L17	OSU 600501	1	D5
TF-524	CMT-02 @ 75% Volume-Height, 135 degrees	CMT02	0.25 in	1.00 in	K	3	7	H09 L09	OSU 600502	1	C3
TF-525	CMT-01 @ 1/2 Upper-Head Height, 135 degrees	CMT01	0.25 in	1.00 in	K	3	7	H10 L10	OSU 600501	1	D3
TF-526	CMT-02 Long T/C Rod @ 49.051"	CMT02	0.040 in	N/A	K	2	3	H18 L18	OSU 600502	1	D5
TF-527	CMT-01 Long T/C Rod @ 51.871"	CMT02	0.040 in	N/A	K	2	3	H19 L19	OSU 600502	1	D5
TF-528	CMT-02 @ 1/2 Upper-Head Height, 135 degrees	CMT02	0.25 in	1.00 in	K	3	7	H11 L11	OSU 600502	1	D3
TF-529	CMT-01 Long T/C Rod @ 56.611"	CMT01	0.040 in	N/A	K	2	4	H00 L00	OSU 600501	1	D5
TF-530	CMT-02 Long T/C Rod @ 51.871"	CMT02	0.040 in	N/A	K	2	4	H01 L01	OSU 600502	1	D5
TF-531	CMT-01 Balance Line @ CMT inlet	CMT01 CL Bal	0.125 in	D/3	K	1	8	H09 L09	OSU 600206	1	D5
TF-532	CMT-02 Long T/C Rod @ 56.611"	CMT02	0.040 in	N/A	K	2	4	H02 L02	OSU 600502	1	D5
TF-533	CMT-01/CL Balance Line @ CL-3	CMT01 CL Bal	0.125 in	D/2	K	2	4	H03 L03	OSU 600206	1	B4
TF-535	CMT-01 Injection Line	CMT01 DV1	0.125 in	L/2	K	1	8	H10 L10	OSU 600206	1	C5
TF-536	CMT-02/CL Balance Line @ CL-1	CMT02 CL Bal	0.125 in	D/2	K	1	8	H11 L11	OSU 600206	1	A4
TF-537	CMT-01 @ 20% Volume-Height, 135 degrees	CMT01	0.375 in	D/2	K	3	7	H12 L12	OSU 600501	1	B3
TF-538	CMT-02 @ 20% Volume-Height, 135 degrees	CMT02	0.375 in	D/2	K	3	7	H13 L13	OSU 600502	1	B3
TF-539	CMT-01 @ 50% Volume-Height, 135 degrees	CMT01	0.375 in	D/2	K	3	7	H14 L14	OSU 600501	1	C3
TF-540	CMT-02 @ 50% Volume-Height, 135 degrees	CMT02	0.375 in	D/2	K	3	7	H15 L15	OSU 600502	1	C3

APPENDIX C
INSTRUMENTATION DATA BASE (Continued)

Tag No.	Name	Location	Thermocouple Diameter	Thermocouple Depth	Thermocouple Type	DAS Rack	DAS Row	DAS Channel	Drawing No.	Sheet No.	Grid
TF-541	CMT-01 @ 60% Volume-Height, 135 degrees	CMT01	0.375 in	D/2	K	3	7	H16 L16	OSU 600501	1	C3
TF-542	CMT-02 @ 60% Volume-Height, 135 degrees	CMT02	0.375 in	D/2	K	3	7	H17 L17	OSU 600502	1	C3
TF-543	CMT-01 @ 75% Volume-Height, 135 degrees	CMT01	0.375 in	D/2	K	3	7	H18 L18	OSU 600501	1	C3
TF-544	CMT-02 @ 75% Volume-Height, 135 degrees	CMT02	0.375 in	D/2	K	3	7	H19 L19	OSU 600502	1	C3
TF-546	CMT-02 Balance Line @ CMT Inlet	CMT02 CL Bal	0.125 in	D/3	K	3	8	H01 L01	OSU 600206	1	B5
TF-547	CMT-01 Long T/C Rod @ 54.241"	CMT01	0.040 in	N/A	K	3	8	H02 L02	OSU 600501	1	D5
TF-548	CMT-02 Long T/C Rod @ 54.241"	CMT02	0.040 in	N/A	K	3	8	H03 L03	OSU 600502	1	D5
TF-549	CMT-01 Discharge Line	CMT01 DVI	0.125 in	D/3	K	3	8	H04 L04	OSU 600206	1	C5
TF-550	CMT-02 Discharge Line	CMT02 DVI	0.125 in	D/3	K	3	8	H05 L05	OSU 600206	1	A5
TF-551	CMT-01 Short T/C Rod (225 degrees) 5.5" from top	CMT01	0.040 in	N/A	K	3	10	H00 L00	OSU 600501	1	D5
TF-552	CMT-02 Short T/C Rod (225 degrees) 5.5" from top	CMT02	0.040 in	N/A	K	3	10	H01 L01	OSU 600502	1	D5
TF-553	CMT-01 Short T/C Rod (225 degrees) 8.69" from top	CMT01	0.040 in	N/A	K	3	10	H02 L02	OSU 600501	1	C5
TF-554	CMT-02 Short T/C Rod (225 degrees) 8.69" from top	CMT02	0.040 in	N/A	K	3	10	H03 L03	OSU 600502	1	C5
TF-555	CMT-01 Short T/C Rod (225 degrees) 14.19" from top	CMT01	0.040 in	N/A	K	3	10	H04 L04	OSU 600501	1	C5
TF-556	CMT-02 Short T/C Rod (225 degrees) 14.19" from top	CMT02	0.040 in	N/A	K	3	10	H05 L05	OSU 600502	1	C5
TF-557	CMT-01 Short T/C Rod (315 degrees) 5.9" from top	CMT01	0.040 in	N/A	K	3	10	H06 L06	OSU 600501	1	D4
TF-558	CMT-02 Short T/C Rod (315 degrees) 5.9" from top	CMT02	0.040 in	N/A	K	3	10	H07 L07	OSU 600502	1	D4
TF-559	CMT-01 Short T/C Rod (315 degrees) 8.69" from top	CMT01	0.040 in	N/A	K	3	10	H08 L08	OSU 600501	1	C4
TF-560	CMT-02 Short T/C Rod (315 degrees) 8.69" from top	CMT02	0.040 in	N/A	K	3	10	H09 L09	OSU 600502	1	C4
TF-561	CMT-01 Short T/C Rod (315 degrees) 11.44" from top	CMT01	0.040 in	N/A	K	3	10	H10 L10	OSU 600501	1	C4
TF-562	CMT-02 Short T/C Rod (315 degrees) 11.44" from top	CMT02	0.040 in	N/A	K	3	10	H11 L11	OSU 600502	1	C4
TF-563	CMT-01 Short T/C Rod (315 degrees) 14.19" from top	CMT01	0.040 in	N/A	K	3	10	H12 L12	OSU 600501	1	C4
TF-564	CMT-02 Short T/C Rod (315 degrees) 14.19" from top	CMT02	0.040 in	N/A	K	3	10	H13 L13	OSU 600502	1	C4
TF-601	PZR Surge Line @ PZR Inlet	PZR Surge Line	0.25 in	1.18 in	K	1	8	H12 L12	OSU 600203	1	C2
TF-602	ADS1-3 Common Line @ Top PZR	PZR	0.25 in	D/2	K	1	8	H13 L13	OSU 600203	1	D2
TF-603	PZR Surge Line @ HL-2	PZR Surge Line	0.25 in	1.18 in	K	1	8	H14 L14	OSU 600203	1	B3
TF-605	PZR Water Space	PZR	0.25 in	1.00 in	K	1	8	H15 L15	OSU 600203	1	D2
TF-608	PZR Water Space @ Center of Heater Bundle	PZR	0.25 in	D/2	K	-	-	N/A	OSU 600203	1	D2
TF-609	ADS4-1 Line Temperature Upstream of RCS-615	ADS04	0.125 in	D/3	K	1	8	H17 L17	OSU 600203	1	B5
TF-610	ADS4-2 Line Temperature Upstream of RCS-616	ADS04	0.125 in	D/3	K	1	8	H18 L18	OSU 600203	1	B4
TF-614	PZR Steam Vent Line, Upstream of RCS-610	PZR Spray Line	0.125 in	D/2	K	1	8	H19 L19	OSU 600203	1	D3
TF-615	ADS1-3 Common Line From PZR	ADS1-3	0.25 in	D/3	K	1	9	H00 L00	OSU 600203	1	D2
TF-616	ADS1-3 Separator Loop Seal Temperature	ADS1-3	0.25 in	D/3	K	1	9	H01 L01	OSU 600203	1	C1
TF-617	ADS1-3 Separator Steam Outlet Temperature	ADS1-3	0.25 in	D/3	K	1	9	H02 L02	OSU 600203	1	C1

APPENDIX C
INSTRUMENTATION DATA BASE (Continued)

Tag No.	Name	Location	Thermocouple Diameter	Thermocouple Depth	Thermocouple Type	DAS Rack	DAS Row	DAS Channel	Drawing No.	Sheet No.	Grid
TF-618	ADS4-2 Loop Seal Temperature	ADS04-2	0.25 in	D/3	K	1	9	H03 L03	OSU 600901	1	A1
TF-619	ADS4-1 Loop Seal Temperature	ADS04-1	0.25 in	D/3	K	1	9	H04 L04	OSU 600901	1	A6
TF-620	ADS4-2 Inlet From HL-2	ADS04-2	0.25 in	D/2	K	1	9	H05 L05	OSU 600901	1	B2
TF-621	ADS4-1 Inlet From HL-1	ADS04-1	0.25 in	D/2	K	1	9	H06 L06	OSU 600901	1	B6
TF-622	ADS4-2 Separator Steam Outlet Temperature	ADS04-2	0.25 in	D/3	K	1	9	H07 L07	OSU 600901	1	D2
TF-623	ADS4-1 Separator Steam Outlet Temperature	ADS04-1	0.25 in	D/3	K	1	9	H08 L08	OSU 600901	1	D5
TF-701	IRWST/PRHR T/C Rod @ Bottom	IRWST	0.040 in	N/A	K	1	9	H09 L09	OSU 600701	1	B2
TF-702	IRWST/PRHR T/C Rod @ 7.987"	IRWST	0.040 in	N/A	K	3	8	H06 L06	OSU 600701	1	B2
TF-703	IRWST/PRHR T/C Rod @ 15.974"	IRWST	0.040 in	N/A	K	3	8	H07 L07	OSU 600701	1	C2
TF-704	IRWST/PRHR T/C Rod @ 25.852"	IRWST	0.040 in	N/A	K	2	4	H05 L05	OSU 600701	1	C2
TF-705	IRWST/PRHR T/C Rod @ 35.73"	IRWST	0.040 in	N/A	K	2	4	H06 L06	OSU 600701	1	C2
TF-706	IRWST/PRHR T/C Rod @ 45.608"	IRWST	0.040 in	N/A	K	2	4	H07 L07	OSU 600701	1	C2
TF-707	IRWST/PRHR T/C Rod @ 55.486"	IRWST	0.040 in	N/A	K	2	4	H08 L08	OSU 600701	1	C2
TF-708	IRWST/PRHR T/C Rod @ 65.364"	IRWST	0.040 in	N/A	K	2	4	H09 L09	OSU 600701	1	C2
TF-709	IRWST/PRHR T/C Rod @ 75.242"	IRWST	0.040 in	N/A	K	2	4	H10 L10	OSU 600701	1	D2
TF-710	IRWST/PRHR T/C Rod @ 86.358"	IRWST	0.040 in	N/A	K	2	4	H11 L11	OSU 600701	1	D2
TF-711	IRWST/PRHR T/C Rod @ 97.474"	IRWST	0.040 in	N/A	K	2	4	H12 L12	OSU 600701	1	D2
TF-712	IRWST/PRHR T/C Rod @ 108.59"	IRWST	0.040 in	N/A	K	1	9	H10 L10	OSU 600701	1	D2
TF-713	IRWST Discharge to DVI-01 @ IRWST	IRWST	0.25 in	N/A	K	1	9	H11 L11	OSU 600701	1	B3
TF-714	IRWST Discharge to DVI-02 @ IRWST	IRWST	0.25 in	N/A	K	1	9	H12 L12	OSU 600701	1	B2
TF-715	IRWST Sparger T/C Rod @ 8.965"	IRWST	0.040 in	N/A	K	-	-	N/A	OSU 600701	1	B2
TF-716	IRWST Sparger T/C Rod @ 36.708"	IRWST	0.040 in	N/A	K	2	4	H13 L13	OSU 600701	1	C2
TF-717	IRWST Sparger T/C Rod @ 66.342"	IRWST	0.040 in	N/A	K	2	4	H14 L14	OSU 600701	1	C2
TF-718	IRWST Sparger T/C Rod @ 98.452"	IRWST	0.040 in	N/A	K	1	9	H13 L13	OSU 600701	1	D2
TF-719	IRWST Sparger Outlet	SPARGER	0.0625 in	N/A	K	3	8	H08 L08	OSU 600701	1	C2
TF-720	IRWST/DVI-2 Injection Line	IRWST DVI	0.125 in	N/A	K	3	8	H09 L09	OSU 600206	1	A3
TF-721	IRWST/DVI-1 Injection Line	IRWST DVI	0.125 in	N/A	K	3	8	H10 L10	OSU 600206	1	C3
TF-722	IRWST Steam Exhaust Line, Downstream of FVM-701	IRWST DVI	0.25 in	N/A	K	3	10	H14 L14	OSU 600206	1	C2
TF-723	IRWST/Primary Sump Overflow, Downstream of PMM-703	IRWST DVI	0.25 in	N/A	K	3	10	H15 L15	OSU 600206	1	C2
TF-801	CVSP Discharge Header Temperature	CVS Full	0.125 in	D/2	K	1	9	H14 L14	OSU 600002	1	A4
TF-802	RNSP Discharge Header Temperature	RNS Full	0.125 in	D/2	K	1	9	H15 L15	OSU 600002	1	B4
TF-803	PRHR HX Inlet	PRHR HX	0.125 in	D/2	K	1	9	H16 L16	OSU 600206	1	B1
TF-804	PRHR HX Outlet	PRHR HX	0.125 in	D/2	K	1	9	H17 L17	OSU 600206	1	B1
TF-805	PRHR HX Long Tube Outlet Bend	PRHR	0.0625 in	N/A	K	2	4	H15 L15	OSU 600701	1	A6

APPENDIX C
INSTRUMENTATION DATA BASE (Continued)

Tag No.	Name	Location	Thermocouple Diameter	Thermocouple Depth	Thermocouple Type	DAS Rack	DAS Row	DAS Channel	Drawing No.	Sheet No.	Grid
TF-806	PHRH HX Short Tube Outlet Bend	PRHR	0.0625 in	N/A	K	2	4	H16 L16	OSU 600701	1	B5
TF-808	PHRH HX Short Tube Center	PRHR	0.0625 in	N/A	K	2	4	H17 L17	OSU 600701	1	C5
TF-809	PHRH HX Long Tube Center	PRHR	0.0625 in	N/A	K	2	4	H18 L18	OSU 600701	1	C6
TF-810	PHRH HX Short Tube Inlet Bend	PRHR	0.0625 in	N/A	K	2	4	H19 L19	OSU 600701	1	D5
TF-811	PHRH HX Long Tube Inlet Bend	PRHR	0.0625 in	N/A	K	2	5	H00 L00	OSU 600701	1	D6
TF-812	PRHR HX Outlet Head Temperature	PRHR	0.125 in	D/2	K	3	8	H11 L11	OSU 600701	1	B4
TF-813	RNSP Discharge to DVI-1	RNS	0.125 in	D/3	K	3	8	H12 L12	OSU 600206	1	C4
TF-814	RNSP Discharge to DVI-2	RNS	0.125 in	D/3	K	3	8	H13 L13	OSU 600206	1	A3
TF-901	Primary Sump Inlet from Fill Line	Primary Sump	0.25 in	1.00 in	K	1	9	H18 L18	OSU 600901	1	A3
TF-902	Secondary Sump Inlet from Fill Line	Secondary Sump	0.25 in	1.00 in	K	-	-	N/A	OSU 600901	1	A3
TF-903	Primary Sump Temperature @ Sump Injection Line	Primary Sump	0.25 in	1.00 in	K	-	-	N/A	OSU 600901	1	A4
TF-904	Pr. Sump/DVI-2 Injection Line	Secondary Sump	0.125 in	D/2	K	1	9	H19 L19	OSU 600206	1	A3
TF-905	Primary Sump Temperature @ Sump Crossover Level	Primary Sump	0.25 in	1.00 in	K	1	10	H00 L00	OSU 600901	1	B3
TF-906	Primary Sump Exhaust to BAMS Header	Primary Sump	0.25 in	D/2	K	3	10	H16 L16	OSU 600901	1	C3
TF-907	Primary Sump Temperature @ Top (manway)	Primary Sump	0.25 in	1.00 in	K	1	10	H01 L01	OSU 600901	1	B3
TF-908	Break Separator Inlet Temperature	BAMS	0.25 in	D/3	K	3	9	H10 L10	OSU 600901	1	B4
TF-909	Pr. Sump/DVI-1 Injection Line	Sump DVI	0.125 in	D/2	K	1	10	H02 L02	OSU 600206	1	C4
TF-910	CRP Discharge to Primary Sump	COND RTN	0.125 in	D/2	K	3	8	H14 L14	OSU 600002	1	C4
TF-911	CRP Discharge to IRWST	COND RTN	0.125 in	D/2	K	3	8	H15 L15	OSU 600002	1	D4
TF-912	Break Separator Loop Seal Temperature	BAMS	0.25 in	D/3	K	1	8	H16 L16	OSU 600901	1	A4
TF-913	Break Separator Steam Outlet Temperature	BAMS	0.25 in	D/3	K	1	11	H15 L15	OSU 600901	1	C5
TF-914	CRP Suction Header	COND RTN	0.25 in	D/2	K	-	-	N/A	OSU 600002	1	C5
TF-915	Break Separator 6" Line, Downstream, of FVM-905	BAMS	0.25 in	D/3	K	3	9	H11 L11	OSU 600901	1	D4
TF-916	BAMS Header 10" Line, Upstream of CSS-902	BAMS	0.25 in	D/3	K	3	9	H12 L12	OSU 600901	1	D3
TF-917	BAMS Header 6" Line, Upstream of CSS-901	BAMS	0.25 in	D/3	K	-	-	N/A	OSU 600901	1	D3
TF-918	Break Separator 8" Line, Downstream of FVM-906	BAMS	0.25 in	D/3	K	3	9	H13 L13	OSU 600901	1	D4
TFM-101	Thermocouple, Type-T, for HPM-101	RX-TE	N/A	N/A	T	3	4	H00 L00	OSU 600101	2	C1
TFM-102	Thermocouple, Type-T, for HPM-102	RX-TE	N/A	N/A	T	3	4	H01 L01	OSU 600101	2	C3
TFM-103	Thermocouple, Type-T, for HPM-103	RX-TE	N/A	N/A	T	3	4	H02 L02	OSU 600101	2	B3
TFM-104	Thermocouple, Type-T, for HPM-104	RX-TE	N/A	N/A	T	3	4	H03 L03	OSU 600101	2	C4
TFM-105	Thermocouple, Type-T, for HPM-105	RX-TE	N/A	N/A	T	3	4	H04 L04	OSU 600101	2	D4
TFM-106	Thermocouple, Type-T, for HPM-106	RX-TE	N/A	N/A	T	3	4	H05 L05	OSU 600101	2	A4
TFM-107	Thermocouple, Type-T, for HPM-107	RX-TE	N/A	N/A	T	3	4	H06 L06	OSU 600101	2	C3
TFM-108	Thermocouple, Type-T, for HPM-108	RX-TE	N/A	N/A	T	3	4	H07 L07	OSU 600101	2	C3

**APPENDIX C
INSTRUMENTATION DATA BASE (Continued)**

Tag No.	Name	Location	Thermocouple Diameter	Thermocouple Depth	Thermocouple Type	DAS Rack	DAS Row	DAS Channel	Drawing No.	Sheet No.	Grid
TFM-109	Thermocouple, Type-T, for HFM-109	RX-TE	N/A	N/A	T	3	4	H08 L08	OSU 600101	2	C3
TFM-110	Thermocouple, Type-T, for HFM-110	RX-TE	N/A	N/A	T	3	4	H09 L09	OSU 600101	2	C3
TFM-111	Thermocouple, Type-T, for HFM-111	RX-TE	N/A	N/A	T	3	4	H10 L10	OSU 600101	2	C5
TFM-112	Thermocouple, Type-T, for HFM-112	RX-TE	N/A	N/A	T	3	4	H11 L11	OSU 600101	2	C5
TFM-113	Thermocouple, Type-T, for HFM-113	RX-TE	N/A	N/A	T	3	4	H12 L12	OSU 600101	2	C5
TFM-114	Thermocouple, Type-T, for HFM-114	RX-TE	N/A	N/A	T	3	4	H13 L13	OSU 600101	2	C4
TFM-201	Thermocouple, Type-T, for HFM-201	CL1	N/A	N/A	T	3	4	H14 L14	OSU 600203	1	A5
TFM-202	Thermocouple, Type-T, for HFM-202	CL2	N/A	N/A	T	3	4	H15 L15	OSU 600203	1	A4
TFM-203	Thermocouple, Type-T, for HFM-203	CL3	N/A	N/A	T	3	4	H16 L16	OSU 600203	1	C6
TFM-204	Thermocouple, Type-T, for HFM-204	CL4	N/A	N/A	T	3	4	H17 L17	OSU 600203	1	C4
TFM-205	Thermocouple, Type-T, for HFM-205	HL1	N/A	N/A	T	3	4	H18 L18	OSU 600203	1	B5
TFM-206	Thermocouple, Type-T, for HFM-206	HL2	N/A	N/A	T	3	4	H19 L19	OSU 600203	1	B3
TFM-301	Thermocouple, Type-T, for HFM-301	SG01	N/A	N/A	T	3	5	H00 L00	OSU 600301	1	A5
TFM-302	Thermocouple, Type-T, for HFM-302	SG02	N/A	N/A	T	3	5	H01 L01	OSU 600301	1	A2
TFM-303	Thermocouple, Type-T, for HFM-303	SG01	N/A	N/A	T	3	5	H02 L02	OSU 600301	1	C5
TFM-304	Thermocouple, Type-T, for HFM-304	SG02	N/A	N/A	T	3	5	H03 L03	OSU 600301	1	C1
TFM-305	Thermocouple, Type-T, for HFM-305	SG01	N/A	N/A	T	3	5	H04 L04	OSU 600301	1	C5
TFM-306	Thermocouple, Type-T, for HFM-306	SG02	N/A	N/A	T	3	5	H05 L05	OSU 600301	1	C1
TFM-401	Thermocouple, Type-T, for HFM-401	ACC01	N/A	N/A	T	3	5	H06 L06	OSU 600206	1	C6
TFM-402	Thermocouple, Type-T, for HFM-402	ACC02	N/A	N/A	T	3	5	H07 L07	OSU 600206	1	A6
TFM-501	Thermocouple, Type-T, for HFM-501	CMT01	N/A	N/A	T	3	5	H08 L08	OSU 600501	1	A2
TFM-502	Thermocouple, Type-T, for HFM-502	CMT02	N/A	N/A	T	3	5	H09 L09	OSU 600502	1	A2
TFM-503	Thermocouple, Type-T, for HFM-503	CMT01	N/A	N/A	T	3	5	H10 L10	OSU 600501	1	C2
TFM-504	Thermocouple, Type-T, for HFM-504	CMT02	N/A	N/A	T	3	5	H11 L11	OSU 600502	1	C2
TFM-505	Thermocouple, Type-T, for HFM-505	CMT01	N/A	N/A	T	3	5	H12 L12	OSU 600501	1	D3
TFM-506	Thermocouple, Type-T, for HFM-506	CMT02	N/A	N/A	T	3	5	H13 L13	OSU 600502	1	D3
TFM-507	Thermocouple, Type-T, for HFM-507	CMT01 CL Bal	N/A	N/A	T	3	5	H14 L14	OSU 600206	1	C4
TFM-510	Thermocouple, Type-T, for HFM-510	CMT02 CL Bal	N/A	N/A	T	3	5	H17 L17	OSU 600206	1	A5
TFM-601	Thermocouple, Type-T, for HFM-601	ADS04	N/A	N/A	T	3	5	H18 L18	OSU 600203	1	B5
TFM-602	Thermocouple, Type-T, for HFM-602	PZR	N/A	N/A	T	3	5	H19 L19	OSU 600203	1	D2
TFM-603	Thermocouple, Type-T, for HFM-603	PZR Surge Line	N/A	N/A	T	3	6	H00 L00	OSU 600203	1	C3
TFM-604	Thermocouple, Type-T, for HFM-604	PZR	N/A	N/A	T	3	6	H01 L01	OSU 600203	1	C2

APPENDIX C
INSTRUMENTATION DATA BASE (Continued)

Tag No.	Name	Location	Thermocouple Diameter	Thermocouple Depth	Thermocouple Type	DAS Rack	DAS Row	DAS Channel	Drawing No.	Sheet No.	Grid
TFM-605	Thermocouple, Type-T, for HFM-605	PZR	N/A	N/A	T	3	6	H02 L02	OSU 600203	1	D2
TFM-606	Thermocouple, Type-T, for HFM-606	ADS1-3	N/A	N/A	T	3	6	H03 L03	OSU 600203	1	D1
TFM-607	Thermocouple, Type-T, for HFM-607	PZR	N/A	N/A	T	3	6	H04 L04	OSU 600203	1	D2
TFM-608	Thermocouple, Type-T, for HFM-608	ADS04	N/A	N/A	T	3	6	H05 L05	OSU 600203	1	B4
TFM-701	Thermocouple, Type-T, for HFM-701	IRWST	N/A	N/A	T	3	6	H06 L06	OSU 600701	1	C3
TFM-702	Thermocouple, Type-T, for HFM-702	IRWST	N/A	N/A	T	3	6	H07 L07	OSU 600701	1	D3
TFM-703	Thermocouple, Type-T, for HFM-703	IRWST	N/A	N/A	T	3	6	H08 L08	OSU 600701	1	D2
TFM-801	Thermocouple, Type-T, for HFM-801	PRHR HX	N/A	N/A	T	3	6	H09 L09	OSU 600206	1	B1
TFM-802	Thermocouple, Type-T, for HFM-802	PRHR HX	N/A	N/A	T	3	6	H10 L10	OSU 600206	1	B1
TFM-901	Thermocouple, Type-T, for HFM-901	Primary Sump	N/A	N/A	T	3	6	H11 L11	OSU 600901	1	A3
TFM-902	Thermocouple, Type-T, for HFM-902	Secondary Sump	N/A	N/A	T	3	6	H12 L12	OSU 600901	1	A3
TFM-903	Thermocouple, Type-T, for HFM-903	Sump DV1	N/A	N/A	T	3	6	H13 L13	OSU 600206	1	C4
TFM-904	Thermocouple, Type-T, for HFM-904	Sump DV1	N/A	N/A	T	3	6	H14 L14	OSU 600206	1	A3
TH-101-1	Heater Rod B1-101 @ 28.13"	RX-HTR	0.032 in	N/A	K	2	5	H05 L05	OSU 600007	1	-
TH-101-2	Heater Rod B1-101 @ 34.13"	RX-HTR	0.032 in	N/A	K	2	5	H06 L06	OSU 600007	1	-
TH-101-3	Heater Rod B1-101 @ 40.13"	RX-HTR	0.032 in	N/A	K	-	-	N/A	OSU 600007	1	-
TH-101-4	Heater Rod B1-101 @ 46.13"	RX-HTR	0.032 in	N/A	K	2	5	H08 L08	OSU 600007	1	-
TH-102-1	Heater Rod C1-102 @ 16.13"	RX-HTR	0.032 in	N/A	K	2	5	H09 L09	OSU 600007	1	-
TH-102-2	Heater Rod C1-102 @ 22.13"	RX-HTR	0.032 in	N/A	K	2	5	H10 L10	OSU 600007	1	-
TH-102-3	Heater Rod C1-102 @ 34.13"	RX-HTR	0.032 in	N/A	K	2	5	H11 L11	OSU 600007	1	-
TH-102-4	Heater Rod C1-102 @ 40.13"	RX-HTR	0.032 in	N/A	K	-	-	N/A	OSU 600007	1	-
TH-103-1	Heater Rod B1-103 @ 28.13"	RX-HTR	0.032 in	N/A	K	2	5	H13 L13	OSU 600007	1	-
TH-103-2	Heater Rod B1-103 @ 34.13"	RX-HTR	0.032 in	N/A	K	2	5	H14 L14	OSU 600007	1	-
TH-103-3	Heater Rod B1-103 @ 40.13"	RX-HTR	0.032 in	N/A	K	-	-	N/A	OSU 600007	1	-
TH-103-4	Heater Rod B1-103 @ 46.13"	RX-HTR	0.032 in	N/A	K	2	5	H16 L16	OSU 600007	1	-
TH-104-1	Heater Rod C1-104 @ 16.13"	RX-HTR	0.032 in	N/A	K	2	5	H17 L17	OSU 600007	1	-
TH-104-2	Heater Rod C1-104 @ 22.13"	RX-HTR	0.032 in	N/A	K	2	5	H18 L18	OSU 600007	1	-
TH-104-3	Heater Rod C1-104 @ 34.13"	RX-HTR	0.032 in	N/A	K	2	5	H19 L19	OSU 600007	1	-
TH-104-4	Heater Rod C1-104 @ 40.13"	RX-HTR	0.032 in	N/A	K	-	-	N/A	OSU 600007	1	-
TH-302-1	Heater Rod C2-302 @ 16.13"	RX-HTR	0.032 in	N/A	K	2	6	H01 L01	OSU 600007	1	-
TH-302-2	Heater Rod C2-302 @ 22.13"	RX-HTR	0.032 in	N/A	K	2	6	H02 L02	OSU 600007	1	-
TH-302-3	Heater Rod C2-302 @ 34.13"	RX-HTR	0.032 in	N/A	K	2	6	H03 L03	OSU 600007	1	-
TH-302-4	Heater Rod C2-302 @ 40.13"	RX-HTR	0.032 in	N/A	K	2	6	H04 L04	OSU 600007	1	-
TH-304-1	Heater Rod B2-304 @ 28.13"	RX-HTR	0.032 in	N/A	K	2	6	H05 L05	OSU 600007	1	-
TH-304-2	Heater Rod B2-304 @ 34.13"	RX-HTR	0.032 in	N/A	K	2	6	H06 L06	OSU 600007	1	-
TH-304-3	Heater Rod B2-304 @ 40.13"	RX-HTR	0.032 in	N/A	K	-	-	N/A	OSU 600007	1	-
TH-304-4	Heater Rod B2-304 @ 46.13"	RX-HTR	0.032 in	N/A	K	2	6	H08 L08	OSU 600007	1	-
TH-307-1	Heater Rod C2-304 @ 16.13"	RX-HTR	0.032 in	N/A	K	2	6	H09 L09	OSU 600007	1	-
TH-307-2	Heater Rod C2-304 @ 22.13"	RX-HTR	0.032 in	N/A	K	2	6	H10 L10	OSU 600007	1	-
TH-307-3	Heater Rod C2-304 @ 34.13"	RX-HTR	0.032 in	N/A	K	2	6	H11 L11	OSU 600007	1	-
TH-307-4	Heater Rod C2-304 @ 40.13"	RX-HTR	0.032 in	N/A	K	2	6	H12 L12	OSU 600007	1	-
TH-309-1	Heater Rod B2-309 @ 28.13"	RX-HTR	0.032 in	N/A	K	2	6	H13 L13	OSU 600007	1	-
TH-309-2	Heater Rod B2-309 @ 34.13"	RX-HTR	0.032 in	N/A	K	2	6	H14 L14	OSU 600007	1	-
TH-309-3	Heater Rod B2-309 @ 40.13"	RX-HTR	0.032 in	N/A	K	2	6	H15 L15	OSU 600007	1	-
TH-309-4	Heater Rod B2-309 @ 46.13"	RX-HTR	0.032 in	N/A	K	2	6	H16 L16	OSU 600007	1	-
TH-312-1	Heater Rod C2-312 @ 16.13"	RX-HTR	0.032 in	N/A	K	2	6	H17 L17	OSU 600007	1	-

**APPENDIX C
INSTRUMENTATION DATA BASE (Continued)**

Tag No.	Name	Location	Thermocouple Diameter	Thermocouple Depth	Thermocouple Type	DAS Rack	DAS Row	DAS Channel	Drawing No.	Sheet No.	Grid
TH-312-2	Heater Rod C2-312 @ 22.13'	RX-HTR	.032 in	N/A	K	2	6	H18 L18	OSU 600007	1	-
TH-312-3	Heater Rod C2-312 @ 34.13'	RX-HTR	.032 in	N/A	K	2	6	H19 L19	OSU 600007	1	-
TH-312-4	Heater Rod C2-312 @ 40.13'	RX-HTR	.032 in	N/A	K	2	7	H00 L00	OSU 600007	1	-
TH-314-1	Heater Rod B2-314 @ 28.13'	RX-HTR	.032 in	N/A	K	2	7	H01 L01	OSU 600007	1	-
TH-314-2	Heater Rod B2-314 @ 34.13'	RX-HTR	.032 in	N/A	K	2	7	H02 L02	OSU 600007	1	-
TH-314-3	Heater Rod B2-314 @ 40.13'	RX-HTR	.032 in	N/A	K	-	-	N/A	OSU 600007	1	-
TH-317-1	Heater Rod C2-317 @ 16.13'	RX-HTR	.032 in	N/A	K	2	7	H05 L05	OSU 600007	1	-
TH-317-2	Heater Rod C2-317 @ 22.13'	RX-HTR	.032 in	N/A	K	2	7	H06 L06	OSU 600007	1	-
TH-317-3	Heater Rod C2-317 @ 34.13'	RX-HTR	.032 in	N/A	K	2	7	H07 L07	OSU 600007	1	-
TH-317-4	Heater Rod C2-317 @ 40.13'	RX-HTR	.032 in	N/A	K	2	7	H08 L08	OSU 600007	1	-
TH-319-1	Heater Rod B2-319 @ 28.13'	RX-HTR	.032 in	N/A	K	2	7	H09 L09	OSU 600007	1	-
TH-319-2	Heater Rod B2-319 @ 34.13'	RX-HTR	.032 in	N/A	K	2	7	H10 L10	OSU 600007	1	-
TH-319-3	Heater Rod B2-319 @ 40.13'	RX-HTR	.032 in	N/A	K	2	7	H11 L11	OSU 600007	1	-
TH-319-4	Heater Rod B2-319 @ 46.13'	RX-HTR	.032 in	N/A	K	2	7	H12 L12	OSU 600007	1	-
TH-501-1	Heater Rod B2-501 @ 28.13'	RX-HTR	.032 in	N/A	K	2	7	H13 L13	OSU 600007	1	-
TH-501-2	Heater Rod B2-501 @ 34.13'	RX-HTR	.032 in	N/A	K	2	7	H14 L14	OSU 600007	1	-
TH-501-3	Heater Rod B2-501 @ 40.13'	RX-HTR	.032 in	N/A	K	2	7	H15 L15	OSU 600007	1	-
TH-501-4	Heater Rod B2-501 @ 46.13'	RX-HTR	.032 in	N/A	K	2	7	H16 L16	OSU 600007	1	-
TH-503-1	Heater Rod B2-503 @ 28.13'	RX-HTR	.032 in	N/A	K	2	7	H17 L17	OSU 600007	1	-
TH-503-2	Heater Rod B2-503 @ 34.13'	RX-HTR	.032 in	N/A	K	2	7	H18 L18	OSU 600007	1	-
TH-503-3	Heater Rod B2-503 @ 40.13'	RX-HTR	.032 in	N/A	K	2	7	H19 L19	OSU 600007	1	-
TH-503-4	Heater Rod B2-503 @ 46.13'	RX-HTR	.032 in	N/A	K	2	8	H00 L00	OSU 600007	1	-
TH-505-1	Heater Rod B2-505 @ 28.13'	RX-HTR	.032 in	N/A	K	2	8	H01 L01	OSU 600007	1	-
TH-505-2	Heater Rod B2-505 @ 34.13'	RX-HTR	.032 in	N/A	K	2	8	H02 L02	OSU 600007	1	-
TH-505-3	Heater Rod B2-505 @ 40.13'	RX-HTR	.032 in	N/A	K	2	8	H03 L03	OSU 600007	1	-
TH-505-4	Heater Rod B2-505 @ 46.13'	RX-HTR	.032 in	N/A	K	2	8	H04 L04	OSU 600007	1	-
TH-507-1	Heater Rod B2-507 @ 28.13'	RX-HTR	.032 in	N/A	K	2	8	H05 L05	OSU 600007	1	-
TH-507-2	Heater Rod B2-507 @ 34.13'	RX-HTR	.032 in	N/A	K	2	8	H06 L06	OSU 600007	1	-
TH-507-3	Heater Rod B2-507 @ 40.13'	RX-HTR	.032 in	N/A	K	2	8	H07 L07	OSU 600007	1	-
TH-507-4	Heater Rod B2-507 @ 46.13'	RX-HTR	.032 in	N/A	K	2	8	H08 L08	OSU 600007	1	-
TH-601	PZR Heater Rod #1	PZR	.032 in	N/A	K	2	5	H01 L01	OSU 600203	1	A1
TH-602	PZR Heater Rod #2	PZR	.032 in	N/A	K	2	5	H02 L02	OSU 600203	1	A1
TH-603	PZR Heater Rod #3	PZR	.032 in	N/A	K	2	5	H03 L03	OSU 600203	1	A1
TI-001	PST Local Thermometer	PST	-	-	-	-	-	N/A	OSU 600002	1	C6
TI-002	RCP Seal Water Supply Temperature to Mixer	GSW	-	-	-	-	-	N/A	OSU 600903	1	C4
TI-003	RCP Seal Water Pump Suction Thermometer	GSW	-	-	-	-	-	N/A	OSU 600903	1	C4
TI-004	RCP Seal Water Return Temperature	GSW	-	-	-	-	-	N/A	OSU 600903	1	C4
TI-201	RCS Main Temperature Gage	HL1	-	1.00 in	-	-	-	N/A	OSU 600903	1	B5
TI-501	CMT-01 Warmup Line Local Thermometer	CMT01 CL Bal	-	-	-	-	-	N/A	OSU 600206	1	C4
TI-502	CMT-02 Warmup Line Local Thermometer	CMT02 CL Bal	-	-	-	-	-	N/A	OSU 600206	1	A5
TI-701	IRWST Local Thermometer	IRWST	-	-	-	-	-	N/A	OSU 600701	1	B3
TI-802	PRHR Warmup Line Local Thermometer	PRHR HX	-	-	-	-	-	N/A	OSU 600206	1	A1
TI-901	Primary Sump Local Thermometer	Primary Sump	-	-	-	-	-	N/A	OSU 600901	1	A3
TI-902	Secondary Sump Local Thermometer	Secondary Sump	-	-	-	-	-	N/A	OSU 600901	1	A3
TR-001-1	Core Thermocouple Rod D-001 @ 10.50'	RX-HTR	.0625 in	N/A	K	1	10	H03 L03	OSU 600007	1	-
TR-001-2	Core Thermocouple Rod D-001 @ 19.13'	RX-HTR	.0625 in	N/A	K	1	10	H04 L04	OSU 600007	1	-
TR-001-3	Core Thermocouple Rod D-001 @ 25.13'	RX-HTR	.0625 in	N/A	K	1	10	H05 L05	OSU 600007	1	-

APPENDIX C
INSTRUMENTATION DATA BASE (Continued)

Tag No.	Name	Location	Thermocouple Diameter	Thermocouple Depth	Thermocouple Type	DAS Rack	DAS Row	DAS Channel	Drawing No.	Sheet No.	Grid
TR-001-4	Core Thermocouple Rod D-001 @ 31.13"	RX-HTR	.0625 in	N/A	K	1	10	H06 L06	OSU 600007	1	-
TR-001-5	Core Thermocouple Rod D-001 @ 37.13"	RX-HTR	.0625 in	N/A	K	1	10	H07 L07	OSU 600007	1	-
TR-001-6	Core Thermocouple Rod D-001 @ 43.13"	RX-HTR	.0625 in	N/A	K	1	10	H08 L08	OSU 600007	1	-
TR-001-7	Core Thermocouple Rod D-001 @ 49.13"	RX-HTR	.0625 in	N/A	K	1	10	H09 L09	OSU 600007	1	-
TR-001-8	Core Thermocouple Rod D-001 @ 51.13"	RX-HTR	.0625 in	N/A	K	1	10	H10 L10	OSU 600007	1	-
TR-303-1	Core Thermocouple Rod D-303 @ 10.51"	RX-HTR	.0625 in	N/A	K	1	10	H11 L11	OSU 600007	1	-
TR-303-2	Core Thermocouple Rod D-303 @ 19.13"	RX-HTR	.0625 in	N/A	K	1	10	H12 L12	OSU 600007	1	-
TR-303-3	Core Thermocouple Rod D-303 @ 25.13"	RX-HTR	.0625 in	N/A	K	1	10	H13 L13	OSU 600007	1	-
TR-303-4	Core Thermocouple Rod D-303 @ 31.13"	RX-HTR	.0625 in	N/A	K	1	10	H14 L14	OSU 600007	1	-
TR-303-5	Core Thermocouple Rod D-303 @ 37.13"	RX-HTR	.0625 in	N/A	K	1	10	H15 L15	OSU 600007	1	-
TR-303-6	Core Thermocouple Rod D-303 @ 43.13"	RX-HTR	.0625 in	N/A	K	1	10	H16 L16	OSU 600007	1	-
TR-303-7	Core Thermocouple Rod D-303 @ 49.13"	RX-HTR	.0625 in	N/A	K	1	10	H17 L17	OSU 600007	1	-
TR-303-8	Core Thermocouple Rod D-303 @ 51.13"	RX-HTR	.0625 in	N/A	K	1	10	H18 L18	OSU 600007	1	-
TR-308-1	Core Thermocouple Rod E-308 @ 22.13"	RX-HTR	.0625 in	N/A	K	1	10	H19 L19	OSU 600007	1	-
TR-308-2	Core Thermocouple Rod E-308 @ 34.13"	RX-HTR	.0625 in	N/A	K	1	11	H00 L00	OSU 600007	1	-
TR-308-3	Core Thermocouple Rod E-308 @ 46.13"	RX-HTR	.0625 in	N/A	K	1	11	H01 L01	OSU 600007	1	-
TR-313-1	Core Thermocouple Rod D-313 @ 10.50"	RX-HTR	.0625 in	N/A	K	1	11	H02 L02	OSU 600007	1	-
TR-313-2	Core Thermocouple Rod D-313 @ 19.13"	RX-HTR	.0625 in	N/A	K	1	11	H03 L03	OSU 600007	1	-
TR-313-3	Core Thermocouple Rod D-313 @ 25.13"	RX-HTR	.0625 in	N/A	K	1	11	H04 L04	OSU 600007	1	-
TR-313-4	Core Thermocouple Rod D-313 @ 31.13"	RX-HTR	.0625 in	N/A	K	1	11	H05 L05	OSU 600007	1	-
TR-313-5	Core Thermocouple Rod D-313 @ 37.13"	RX-HTR	.0625 in	N/A	K	1	11	H06 L06	OSU 600007	1	-
TR-313-6	Core Thermocouple Rod D-313 @ 43.13"	RX-HTR	.0625 in	N/A	K	1	11	H07 L07	OSU 600007	1	-
TR-313-7	Core Thermocouple Rod D-313 @ 49.13"	RX-HTR	.0625 in	N/A	K	1	11	H08 L08	OSU 600007	1	-
TR-313-8	Core Thermocouple Rod D-313 @ 51.13"	RX-HTR	.0625 in	N/A	K	1	11	H09 L09	OSU 600007	1	-
TR-318-1	Core Thermocouple Rod F-318 @ 28.13"	RX-HTR	.0625 in	N/A	K	1	11	H10 L10	OSU 600007	1	-
TR-318-2	Core Thermocouple Rod F-318 @ 40.13"	RX-HTR	.0625 in	N/A	K	1	11	H11 L11	OSU 600007	1	-
TR-318-3	Core Thermocouple Rod F-318 @ 51.86"	RX-HTR	.0625 in	N/A	K	1	11	H12 L12	OSU 600007	1	-
TS-001	RCP Seal Water System High Temperature Switch	OP	-	-	-	-	-	N/A	TIC 787-E200	1	-
TSH-001	SCR Cabinet High Temperature Switch	SCR	-	-	-	-	-	N/A	TIC 787-E204	1	-
TW-201	SG-01 Short Tube Bottom Outlet	SG01	0.020 in	N/A	K	2	8	H09 L09	OSU 600301	1	B5
TW-202	SG-02 Short Tube Bottom Outlet	SG02	0.020 in	N/A	K	2	8	H10 L10	OSU 600301	1	B2
TW-203	SG-01 Short Tube Bottom Inlet	SG01	0.020 in	N/A	K	2	8	H11 L11	OSU 600301	1	B5

APPENDIX C
INSTRUMENTATION DATA BASE (Continued)

Tag No.	Name	Location	Thermocouple Diameter	Thermocouple Depth	Thermocouple Type	DAS Rack	DAS Row	DAS Channel	Drawing No.	Sheet No.	Grid
TW-204	SG-02 Short Tube Bottom Inlet	SG02	0.020 in	N/A	K	2	8	H12 L12	OSU 600301	1	B2
TW-205	SG-01 Long Tube Bottom Outlet	SG01	0.020 in	N/A	K	2	8	H13 L13	OSU 600301	1	B4
TW-206	SG-02 Long Tube Bottom Outlet	SG02	0.020 in	N/A	K	2	8	H14 L14	OSU 600301	1	B2
TW-208	SG-02 Long Tube Bottom Inlet	SG02	0.020 in	N/A	K	2	8	H15 L15	OSU 600301	1	B2
TW-209	SG-01 Short Tube Top Outlet	SG01	0.020 in	N/A	K	2	8	H16 L16	OSU 600301	1	C5
TW-210	SG-02 Short Tube Top Outlet	SG02	0.020 in	N/A	K	2	8	H17 L17	OSU 600301	1	C2
TW-216	SG-02 Long Tube Top Inlet	SG02	0.020 in	N/A	K	2	9	H04 L04	OSU 600301	1	C2
TW-501	CMT-01 @ 2/3 Lower Head Height, 270 degrees	CMT01	0.040 in	N/A	K	2	9	H05 L05	OSU 600501	1	B2
TW-502	CMT-02 @ 2/3 Lower Head Height, 270 degrees	CMT02	0.040 in	N/A	K	2	9	H06 L06	OSU 600502	1	B2
TW-503	CMT-01 @ 2/3 Lower Total-Head Height, 270 degrees	CMT01	0.040 in	N/A	K	2	9	H07 L07	OSU 600501	1	B2
TW-504	CMT-02 @ 2/3 Lower Total-Head Height, 270 degrees	CMT02	0.040 in	N/A	K	2	9	H08 L08	OSU 600502	1	B2
TW-505	CMT-01 @ 20% Volume-Height, 90 degrees	CMT01	0.040 in	N/A	K	2	9	H09 L09	OSU 600501	1	B3
TW-506	CMT-02 @ 20% Volume-Height, 90 degrees	CMT02	0.040 in	N/A	K	2	9	H10 L10	OSU 600502	1	B3
TW-507	CMT-01 @ 20% Volume-Height, 90 degrees	CMT01	0.040 in	N/A	K	2	9	H11 L11	OSU 600501	1	B3
TW-508	CMT-02 @ 20% Volume-Height, 90 degrees	CMT02	0.040 in	N/A	K	2	9	H12 L12	OSU 600502	1	B3
TW-509	CMT-01 @ 20% Volume-Height, 270 degrees	CMT01	0.040 in	N/A	K	2	9	H13 L13	OSU 600501	1	B2
TW-510	CMT-02 @ 20% Volume-Height, 270 degrees	CMT02	0.040 in	N/A	K	2	9	H14 L14	OSU 600502	1	B2
TW-511	CMT-01 @ 20% Volume-Height, 270 degrees	CMT01	0.040 in	N/A	K	2	9	H15 L15	OSU 600501	1	B2
TW-512	CMT-02 @ 20% Volume-Height, 270 degrees	CMT02	0.040 in	N/A	K	2	9	H16 L16	OSU 600502	1	B2
TW-513	CMT-01 @ 50% Volume-Height minus 7.387", 270 degrees	CMT01	0.040 in	N/A	K	2	9	H17 L17	OSU 600501	1	B2
TW-514	CMT-02 @ 50% Volume-Height minus 7.387", 270 degrees	CMT02	0.040 in	N/A	K	2	9	H18 L18	OSU 600502	1	B2
TW-515	CMT-01 @ 50% Volume-Height minus 7.387", 270 degrees	CMT01	0.040 in	N/A	K	2	9	H19 L19	OSU 600501	1	B2
TW-516	CMT-02 @ 50% Volume-Height minus 7.387", 270 degrees	CMT02	0.040 in	N/A	K	2	10	H00 L00	OSU 600502	1	B2
TW-517	CMT-01 @ 50% Volume-Height, 90 degrees	CMT01	0.040 in	N/A	K	2	10	H01 L01	OSU 600501	1	C3
TW-518	CMT-02 @ 50% Volume-Height, 90 degrees	CMT02	0.040 in	N/A	K	2	10	H02 L02	OSU 600502	1	C3
TW-519	CMT-01 @ 50% Volume-Height, 90 degrees	CMT01	0.040 in	N/A	K	2	10	H03 L03	OSU 600501	1	C3
TW-520	CMT-02 @ 50% Volume-Height, 90 degrees	CMT02	0.040 in	N/A	K	2	10	H04 L04	OSU 600502	1	C3
TW-521	CMT-01 @ 50% Volume-Height, 90 degrees	CMT01	0.040 in	N/A	K	2	10	H05 L05	OSU 600501	1	C3
TW-522	CMT-02 @ 50% Volume-Height, 90 degrees	CMT02	0.040 in	N/A	K	2	10	H06 L06	OSU 600502	1	C3
TW-523	CMT-01 @ 50% Volume-Height, 270 degrees	CMT01	0.040 in	N/A	K	2	10	H07 L07	OSU 600501	1	C2

APPENDIX C
INSTRUMENTATION DATA BASE (Continued)

Tag No.	Name	Location	Thermocouple Diameter	Thermocouple Depth	Thermocouple Type	DAS Rack	DAS Row	DAS Channel	Drawing No.	Sheet No.	Grid
TW-524	CMT-02 @ 50% Volume-Height, 270 degrees	CMT02	0.040 in	N/A	K	2	10	H08 L08	OSU 600502	1	C2
TW-525	CMT-01 @ 50% Volume-Height, 270 degrees	CMT01	0.040 in	N/A	K	2	10	H09 L09	OSU 600501	1	C2
TW-526	CMT-02 @ 50% Volume-Height, 270 degrees	CMT02	0.040 in	N/A	K	2	10	H10 L10	OSU 600502	1	C2
TW-527	CMT-01 @ 60% Volume-Height, 270 degrees	CMT01	0.040 in	N/A	K	2	10	H11 L11	OSU 600501	1	C2
TW-528	CMT-02 @ 60% Volume-Height, 270 degrees	CMT02	0.040 in	N/A	K	2	10	H12 L12	OSU 600502	1	C2
TW-529	CMT-01 @ 60% Volume-Height, 270 degrees	CMT01	0.040 in	N/A	K	2	10	H13 L13	OSU 600501	1	C2
TW-530	CMT-02 @ 60% Volume-Height, 270 degrees	CMT02	0.040 in	N/A	K	2	10	H14 L14	OSU 600502	1	C2
TW-531	CMT-01 @ 75% Volume-Height, 90 degrees	CMT01	0.040 in	N/A	K	2	10	H15 L15	OSU 600501	1	C3
TW-532	CMT-02 @ 75% Volume-Height, 90 degrees	CMT02	0.040 in	N/A	K	2	10	H16 L16	OSU 600502	1	C3
TW-533	CMT-01 @ 75% Volume-Height, 90 degrees	CMT01	0.040 in	N/A	K	2	10	H17 L17	OSU 600501	1	C3
TW-534	CMT-02 @ 75% Volume-Height, 90 degrees	CMT02	0.040 in	N/A	K	2	10	H18 L18	OSU 600502	1	C3
TW-535	CMT-01 @ 75% Volume-Height, 270 degrees	CMT01	0.040 in	N/A	K	2	10	H19 L19	OSU 600501	1	C2
TW-536	CMT-02 @ 75% Volume-Height, 270 degrees	CMT02	0.040 in	N/A	K	2	11	H00 L00	OSU 600502	1	C2
TW-537	CMT-01 @ 75% Volume-Height, 270 degrees	CMT01	0.040 in	N/A	K	2	11	H01 L01	OSU 600501	1	C2
TW-538	CMT-02 @ 75% Volume-Height, 270 degrees	CMT02	0.040 in	N/A	K	2	11	H02 L02	OSU 600502	1	C2
TW-539	CMT-01 @ Upper Total-Head Height minus 2", 270 degrees	CMT01	0.040 in	N/A	K	2	11	H03 L03	OSU 600501	1	C2
TW-540	CMT-02 @ Upper Total-Head Height minus 2", 270 degrees	CMT02	0.040 in	N/A	K	2	11	H04 L04	OSU 600502	1	C2
TW-541	CMT-01 @ Upper Total-Head Height minus 2", 270 degrees	CMT01	0.040 in	N/A	K	2	11	H05 L05	OSU 600501	1	C2
TW-542	CMT-02 @ Upper Total-Head Height minus 2", 270 degrees	CMT02	0.040 in	N/A	K	2	11	H06 L06	OSU 600502	1	C2
TW-543	CMT-01 @ 2/3 Upper Head Height, 270 degrees	CMT01	0.040 in	N/A	K	2	11	H07 L07	OSU 600501	1	D2
TW-544	CMT-02 @ 2/3 Upper Head Height, 270 degrees	CMT02	0.040 in	N/A	K	2	11	H08 L08	OSU 600502	1	D2
TW-545	CMT-01 @ 2/3 Upper Head Height, 270 degrees	CMT01	0.040 in	N/A	K	2	11	H09 L09	OSU 600501	1	D2
TW-546	CMT-02 @ 2/3 Upper Head Height, 270 degrees	CMT02	0.040 in	N/A	K	2	11	H10 L10	OSU 600502	1	D2
TW-547	CMT-01 @ 1/3 Upper Head Height, 90 degrees	CMT01	0.040 in	N/A	K	2	11	H11 L11	OSU 600501	1	D3
TW-548	CMT-02 @ 1/3 Upper Head Height, 90 degrees	CMT02	0.040 in	N/A	K	2	11	H12 L12	OSU 600502	1	D3
TW-549	CMT-01 @ 1/3 Upper Head Height, 90 degrees	CMT01	0.040 in	N/A	K	2	11	H13 L13	OSU 600501	1	D3
TW-550	CMT-02 @ 1/3 Upper Head Height, 90 degrees	CMT02	0.040 in	N/A	K	2	11	H14 L14	OSU 600502	1	D3
TW-551	CMT-01 @ 1/3 Upper Head Height, 90 degrees	CMT01	0.040 in	N/A	K	2	11	H15 L15	OSU 600501	1	D3
TW-552	CMT-02 @ 1/3 Upper Head Height, 90 degrees	CMT02	0.040 in	N/A	K	2	11	H16 L16	OSU 600502	1	D3
TW-553	CMT-01 @ 1/3 Upper Head Height, 270 degrees	CMT01	0.040 in	N/A	K	2	11	H17 L17	OSU 600501	1	D2
TW-554	CMT-02 @ 1/3 Upper Head Height, 270 degrees	CMT02	0.040 in	N/A	K	2	11	H18 L18	OSU 600502	1	D2
TW-555	CMT-01 @ 1/3 Upper Head Height, 270 degrees	CMT01	0.040 in	N/A	K	2	11	H19 L19	OSU 600501	1	D2

APPENDIX C
INSTRUMENTATION DATA BASE (Continued)

Tag No.	Name	Location	Thermocouple Diameter	Thermocouple Depth	Thermocouple Type	DAS Rack	DAS Row	DAS Channel	Drawing No.	Sheet No.	Grid
TW-556	CMT-02 @ 1/3 Upper Head Height, 270 degrees	CMT02	0.040 in	N/A	K	3	8	H17 L17	OSU 600502	1	D2
TW-601	ADS1-3 Separator Wall Temperature	ADS1-3	#30 Wire	N/A	K	3	8	H18 L18	OSU 600203	1	C1
TW-602	ADS4-2 Separator Wall Temperature	ADS04-2	#30 Wire	N/A	K	3	8	H19 L19	OSU 600901	1	B1
TW-603	ADS4-1 Separator Wall Temperature	ADS04-1	#30 Wire	N/A	K	3	9	H00 L00	OSU 600901	1	B6
TW-801	PRHR HX Long Tube Outlet	PRHR	0.020 in	N/A	K	3	9	H01 L01	OSU 600701	1	B5
TW-802	PRHR HX Short Tube Outlet	PRHR	0.020 in	N/A	K	3	9	H02 L02	OSU 600701	1	B5
TW-803	PRHR HX Long Tube Lower Mid-piece	PRHR	0.020 in	N/A	K	3	9	H03 L03	OSU 600701	1	B6
TW-804	PRHR HX Short Tube Lower Mid-piece	PRHR	0.020 in	N/A	K	3	9	H04 L04	OSU 600701	1	B5
TW-805	PRHR HX Short Tube Upper Mid-piece	PRHR	0.020 in	N/A	K	3	9	H05 L05	OSU 600701	1	C5
TW-806	PRHR HX Long Tube Upper Mid-piece	PRHR	0.020 in	N/A	K	3	9	H06 L06	OSU 600701	1	C6
TW-807	PRHR HX Short Tube Inlet	PRHR	0.020 in	N/A	K	3	9	H07 L07	OSU 600701	1	D5
TW-808	PRHR HX Long Tube Inlet	PRHR	0.020 in	N/A	K	3	9	H08 L08	OSU 600701	1	D5
TW-905	Break Separator Wall Temperature	BAMS	#30 Wire	N/A	K	3	9	H09 L09	OSU 600901	1	B5
TWHT-01	Zone 1 (ADS 4-2 Separator) Heat Trace	ADS04-2	-	N/A	J	-	-	N/A	OSU 600901	1	B1
TWHT-02	Zone 2 (Break Separator) Heat Trace	BAMS	-	N/A	J	-	-	N/A	OSU 600901	1	B5
TWHT-03	Zone 3 (ADS 4-1 Separator) Heat Trace	ADS04-1	-	N/A	J	-	-	N/A	OSU 600901	1	B6
TWHT-04	Zone 4 (ADS 1-3 Separator) Heat Trace	ADS-1	-	N/A	J	-	-	N/A	OSU 600203	1	C1
TWHT-05	Zone 5 (ADS 1-3 Separator Loop Seal) Heat Trace	ADS-1	-	N/A	J	-	-	N/A	OSU 600203	1	C1
TWHT-06	Zone 6 (ADS 1-3 Separator Steam Outlet) Heat Trace	ADS-1	-	N/A	J	-	-	N/A	OSU 600203	1	C1
TWHT-07	Zone 7 (ADS 1-3 Separator Inlet) Heat Trace	ADS-1	-	N/A	J	-	-	N/A	OSU 600203	1	D1
TWHT-08	Zone 8 (Break Separator Inlet and 6" Line) Heat Trace	BAMS	-	N/A	J	-	-	N/A	OSU 600901	1	D5
TWHT-09	Zone 9 (Break Separator 8" Line) Heat Trace	BAMS	-	N/A	J	-	-	N/A	OSU 600901	1	D5
TWHT-10	Zone 10 (BAMS 6" Line and Common Inlet Header) Heat Trace	BAMS	-	N/A	J	-	-	N/A	OSU 600901	1	D3
TWHT-11	Zone 11 (BAMS 10" Line) Heat Trace	BAMS	-	N/A	J	-	-	N/A	OSU 600901	1	D3
TWHT-12	Zone 12 (ADS4-2 Separator Steam Outlet) Heat Trace	ADS04-2	-	N/A	J	-	-	N/A	OSU 600901	1	D1
TWHT-13	Zone 13 (ADS4-1 Separator Steam Outlet) Heat Trace	ADS04-1	-	N/A	J	-	-	N/A	OSU 600901	1	D6
TWHT-14	Zone 14 (IRWST Steam Exhaust) Heat Trace	BAMS	-	N/A	J	-	-	N/A	OSU 600901	1	C3
XC-001	MS-001 Close Solenoid	MS	-	-	-	-	-	N/A	OSU 600002	1	C2
XC-002	MS-002 Close Solenoid	MS	-	-	-	-	-	N/A	OSU 600002	1	C1
XC-503	RCS-503 Close Solenoid	CMT01 CL Bal	-	-	-	-	-	N/A	OSU 600206	1	D5
XC-504	RCS-504 Close Solenoid	CMT02 CL Bal	-	-	-	-	-	N/A	OSU 600206	1	B4
XC-529	RCS-529 Close Solenoid	CMT01 CL Bal	-	-	-	-	-	N/A	OSU 600206	1	D4
XC-530	RCS-530 Close Solenoid	CMT02 CL Bal	-	-	-	-	-	N/A	OSU 600206	1	B5
XC-535	RCS-535 Close Solenoid	CMT01 DV1	-	-	-	-	-	N/A	OSU 600206	1	C5
XC-536	RCS-536 Close Solenoid	CMT02 DV1	-	-	-	-	-	N/A	OSU 600206	1	A5
XC-601	RCS-601 Close Solenoid	ADS-1	-	-	-	-	-	N/A	OSU 600203	1	D1
XC-602	RCS-602 Close Solenoid	ADS-2	-	-	-	-	-	N/A	OSU 600203	1	D1
XC-603	RCS-603 Close Solenoid	ADS-3	-	-	-	-	-	N/A	OSU 600203	1	D1

APPENDIX C
INSTRUMENTATION DATA BASE (Continued)

Tag No.	Name	Location	Thermocouple Diameter	Thermocouple Depth	Thermocouple Type	DAS Rack	DAS Row	DAS Channel	Drawing No.	Sheet No.	Grid
XC-615	RCS-615 Close Solenoid	ADS01	-	-	-	-	-	N/A	OSU 600203	1	B5
XC-616	RCS-616 Close Solenoid	ADS04	-	-	-	-	-	N/A	OSU 600203	1	B4
XC-625	RCS-625 Close Solenoid	ADS04-1	-	-	-	-	-	N/A	OSU 600901	1	A6
XC-626	RCS-626 Close Solenoid	ADS04-2	-	-	-	-	-	N/A	OSU 600901	1	A1
XC-711	RCS-711 Close Solenoid	IRWST DVI	-	-	-	-	-	N/A	OSU 600206	1	C3
XC-712	RCS-712 Close Solenoid	IRWST DVI	-	-	-	-	-	N/A	OSU 600206	1	A3
XC-804	RCS-804 Close Solenoid	PRHR HDX	-	-	-	-	-	N/A	OSU 600206	1	B1
XC-902	CSS-902 Close Solenoid	BAMS	-	-	-	-	-	N/A	OSU 600901	1	D2
XC-905	CSS-905 Close Solenoid	BAMS	-	-	-	-	-	N/A	OSU 600901	1	C4
XC-906	CSS-906 Close Solenoid	BAMS	-	-	-	-	-	N/A	OSU 600901	1	D4
XC-909	CSS-909 Close Solenoid	Sump DVI	-	-	-	-	-	N/A	OSU 600206	1	D4
XC-910	CSS-910 Close Solenoid	Sump DVI	-	-	-	-	-	N/A	OSU 600206	1	C3
XC-BRK-1	Break Valve Close Solenoid	CL Break	-	-	-	-	-	N/A	OSU 600904	1	-
XC-BRK-2	Break Valve Close Solenoid	CL Break	-	-	-	-	-	N/A	OSU 600904	1	-
XO-001	MS-001 Open Solenoid	MS	-	-	-	-	-	N/A	OSU 600002	1	C2
XO-002	MS-002 Open Solenoid	MS	-	-	-	-	-	N/A	OSU 600002	1	C1
XO-503	RCS-503 Open Solenoid	CMT01 CL Bal	-	-	-	-	-	N/A	OSU 600206	1	D5
XO-504	RCS-504 Open Solenoid	CMT02 CL Bal	-	-	-	-	-	N/A	OSU 600206	1	B4
XO-529	RCS-529 Open Solenoid	CMT01 CL Bal	-	-	-	-	-	N/A	OSU 600206	1	D4
XO-530	RCS-530 Open Solenoid	CMT02 CL Bal	-	-	-	-	-	N/A	OSU 600206	1	B5
XO-535	RCS-535 Open Solenoid	CMT01 DVI	-	-	-	-	-	N/A	OSU 600206	1	C5
XO-536	RCS-536 Open Solenoid	CMT02 DVI	-	-	-	-	-	N/A	OSU 600206	1	A5
XO-601	RCS-601 Open Solenoid	ADS-1	-	-	-	-	-	N/A	OSU 600203	1	D1
XO-602	RCS-602 Open Solenoid	ADS-2	-	-	-	-	-	N/A	OSU 600203	1	D1
XO-603	RCS-603 Open Solenoid	ADS-3	-	-	-	-	-	N/A	OSU 600203	1	D1
XO-610	RCS-610 Open Solenoid	PZR Spray Line	-	-	-	-	-	N/A	OSU 600203	1	D3
XO-615	RCS-615 Open Solenoid	ADS04	-	-	-	-	-	N/A	OSU 600203	1	B5
XO-616	RCS-616 Open Solenoid	ADS04	-	-	-	-	-	N/A	OSU 600203	1	B4
XO-625	RCS-625 Open Solenoid	ADS04-1	-	-	-	-	-	N/A	OSU 600901	1	A6
XO-626	RCS-626 Open Solenoid	ADS04-2	-	-	-	-	-	N/A	OSU 600901	1	A1
XO-711	RCS-711 Open Solenoid	IRWST DVI	-	-	-	-	-	N/A	OSU 600206	1	C3
XO-712	RCS-712 Open Solenoid	IRWST DVI	-	-	-	-	-	N/A	OSU 600206	1	A3
XO-804	RCS-804 Open Solenoid	PRHR HDX	-	-	-	-	-	N/A	OSU 600206	1	B1
XO-902	CSS-902 Open Solenoid	BAMS	-	-	-	-	-	N/A	OSU 600901	1	D2
XO-905	CSS-905 Open Solenoid	BAMS	-	-	-	-	-	N/A	OSU 600901	1	C4
XO-906	CSS-906 Open Solenoid	BAMS	-	-	-	-	-	N/A	OSU 600901	1	D4
XO-909	CSS-909 Open Solenoid	Sump DVI	-	-	-	-	-	N/A	OSU 600206	1	D4
XO-910	CSS-910 Open Solenoid	Sump DVI	-	-	-	-	-	N/A	OSU 600206	1	C3
XO-BRK-1	Break Valve Open Solenoid	CL Break	-	-	-	-	-	N/A	OSU 600904	1	-
XO-BRK-2	Break Valve Open Solenoid	CL Break	-	-	-	-	-	N/A	OSU 600904	1	-
ZSC-001	MS-001 Close Limit Switch	MS	-	-	-	-	-	N/A	OSU 600002	1	C2
ZSC-002	MS-002 Close Limit Switch	MS	-	-	-	-	-	N/A	OSU 600002	1	C1
ZSC-503	RCS-503 Close Limit Switch	CMT01 CL Bal	-	-	-	-	-	N/A	OSU 600206	1	D5
ZSC-504	RCS-504 Close Limit Switch	CMT02 CL Bal	-	-	-	-	-	N/A	OSU 600206	1	B4
ZSC-529	RCS-529 Close Limit Switch	CMT01 CL Bal	-	-	-	-	-	N/A	OSU 600206	1	D4
ZSC-530	RCS-530 Close Limit Switch	CMT02 CL Bal	-	-	-	-	-	N/A	OSU 600206	1	B5
ZSC-535	RCS-535 Close Limit Switch	CMT01 DVI	-	-	-	-	-	N/A	OSU 600206	1	C5
ZSC-536	RCS-536 Close Limit Switch	CMT02 DVI	-	-	-	-	-	N/A	OSU 600206	1	A5
ZSC-601	RCS-601 Close Limit Switch	ADS-1	-	-	-	-	-	N/A	OSU 600203	1	D1
ZSC-602	RCS-602 Close Limit Switch	ADS-2	-	-	-	-	-	N/A	OSU 600203	1	D1
ZSC-603	RCS-603 Close Limit Switch	ADS-3	-	-	-	-	-	N/A	OSU 600203	1	D1
ZSC-610	RCS-610 Close Limit Switch	PZR Spray Line	-	-	-	-	-	N/A	OSU 600203	1	D3
ZSC-615	RCS-615 Close Limit Switch	ADS04	-	-	-	-	-	N/A	OSU 600203	1	B5
ZSC-616	RCS-616 Close Limit Switch	ADS04	-	-	-	-	-	N/A	OSU 600203	1	B4
ZSC-625	RCS-625 Close Limit Switch	ADS04-1	-	-	-	-	-	N/A	OSU 600901	1	A6
ZSC-626	RCS-626 Close Limit Switch	ADS04-2	-	-	-	-	-	N/A	OSU 600901	1	A1

APPENDIX C
INSTRUMENTATION DATA BASE (Continued)

Tag No.	Name	Location	Thermocouple Diameter	Thermocouple Depth	Thermocouple Type	DAS Rack	DAS Row	DAS Channel	Drawing No.	Sheet No.	Grid
ZSC-711	RCS-711 Close Limit Switch	IRWST DVI	-	-	-	-	-	N/A	OSU 600206	1	C3
ZSC-712	RCS-712 Close Limit Switch	IRWST DVI	-	-	-	-	-	N/A	OSU 600206	1	A3
ZSC-804	RCS-804 Close Limit Switch	PRHR HX	-	-	-	-	-	N/A	OSU 600206	1	B1
ZSC-902	CSS-902 Close Limit Switch	BAMS	-	-	-	-	-	N/A	OSU 600901	1	D2
ZSC-905	CSS-905 Close Limit Switch	BAMS	-	-	-	-	-	N/A	OSU 600901	1	C4
ZSC-906	CSS-906 Close Limit Switch	BAMS	-	-	-	-	-	N/A	OSU 600901	1	D4
ZSC-909	CSS-909 Close Limit Switch	Sump DVI	-	-	-	-	-	N/A	OSU 600206	1	D4
ZSC-910	CSS-910 Close Limit Switch	Sump DVI	-	-	-	-	-	N/A	OSU 600206	1	B3
ZSC-BRK-1	Break Valve Close Limit Switch	CL Break	-	-	-	-	-	N/A	OSU 600904	1	-
ZSC-BRK-2	Break Valve Close Limit Switch	CL Break	-	-	-	-	-	N/A	OSU 600904	1	-
ZSO-001	MS-001 Open Limit Switch	MS	-	-	-	-	-	N/A	OSU 600002	1	C2
ZSO-002	MS-002 Open Limit Switch	MS	-	-	-	-	-	N/A	OSU 600002	1	C1
ZSO-503	RCS-503 Open Limit Switch	CMT01 CL Bal	-	-	-	-	-	N/A	OSU 600206	1	D5
ZSO-504	RCS-504 Open Limit Switch	CMT02 CL Bal	-	-	-	-	-	N/A	OSU 600206	1	B4
ZSO-529	RCS-529 Open Limit Switch	CMT01 CL Bal	-	-	-	-	-	N/A	OSU 600206	1	D4
ZSO-530	RCS-530 Open Limit Switch	CMT02 CL Bal	-	-	-	-	-	N/A	OSU 600206	1	B5
ZSO-535	RCS-535 Open Limit Switch	CMT01 DVI	-	-	-	-	-	N/A	OSU 600206	1	C5
ZSO-536	RCS-536 Open Limit Switch	CMT02 DVI	-	-	-	-	-	N/A	OSU 600206	1	A5
ZSO-601	RCS-601 Open Limit Switch	ADS-1	-	-	-	-	-	N/A	OSU 600203	1	D1
ZSO-602	RCS-602 Open Limit Switch	ADS-2	-	-	-	-	-	N/A	OSU 600203	1	D1
ZSO-603	RCS-603 Open Limit Switch	ADS-3	-	-	-	-	-	N/A	OSU 600203	1	D1
ZSO-610	RCS-610 Open Limit Switch	PZR Spray Line	-	-	-	-	-	N/A	OSU 600203	1	D3
ZSO-615	RCS-615 Open Limit Switch	ADS04	-	-	-	-	-	N/A	OSU 600203	1	B5
ZSO-616	RCS-616 Open Limit Switch	ADS04	-	-	-	-	-	N/A	OSU 600203	1	B4
ZSO-625	RCS-625 Open Limit Switch	ADS04-1	-	-	-	-	-	N/A	OSU 600901	1	A6
ZSO-626	RCS-626 Open Limit Switch	ADS04-2	-	-	-	-	-	N/A	OSU 600901	1	A1
ZSO-711	RCS-711 Open Limit Switch	IRWST DVI	-	-	-	-	-	N/A	OSU 600206	1	C3
ZSO-712	RCS-712 Open Limit Switch	IRWST DVI	-	-	-	-	-	N/A	OSU 600206	1	A3
ZSO-804	RCS-804 Open Limit Switch	PRHR HX	-	-	-	-	-	N/A	OSU 600206	1	B1
ZSO-902	CSS-902 Open Limit Switch	BAMS	-	-	-	-	-	N/A	OSU 600901	1	D2
ZSO-905	CSS-905 Open Limit Switch	BAMS	-	-	-	-	-	N/A	OSU 600901	1	C4
ZSO-906	CSS-906 Open Limit Switch	BAMS	-	-	-	-	-	N/A	OSU 600901	1	D4
ZSO-909	CSS-909 Open Limit Switch	Sump DVI	-	-	-	-	-	N/A	OSU 600206	1	D4
ZSO-910	CSS-910 Open Limit Switch	Sump DVI	-	-	-	-	-	N/A	OSU 600206	1	B3
ZSO-BRK-1	Break Valve Open Limit Switch	CL Break	-	-	-	-	-	N/A	OSU 600904	1	-
ZSO-BRK-2	Break Valve Open Limit Switch	CL Break	-	-	-	-	-	N/A	OSU 600904	1	-



**APPENDIX D
DATA ERROR ANALYSIS**

Appendix D contains tables of the accuracies for the total instrumentation loop, including sensor/transmitters, signal conditioners, and the DAS. These tables are divided by the type of sensor and summarized in the following:

LIST OF TABLES		
Table No.	Header	Page No.
D-1	Errors for DPs	D-4, D-5
D-2	Errors for LDPs	D-6, D-7, D-8
D-3	Errors for PTs	D-9
D-4	Errors for FMMs	D-10
D-5	Errors for FVMs	D-11
D-6	Errors for Thermocouples	D-12, D-13, D-14, D-15, D-16, D-17, D-18, D-19, D-20, D-21
D-7	Errors for HFMs, HPs, and LCs	D-22, D-23, D-24, D-25
D-8	Errors for FDPs	D-26
D-9	kW Errors	D-27

The column headings in the tables are explained as follows:

Tag No.	Identification of the instrument.
Model No.	Manufacturer model number by which the instrument is identified.
Serial No.	Serial number of the instrument assigned by the manufacturer.
Cal Null	Lower value of the range of the instrument; calibrated to give [] ^{a,b,c} output in a loop of [] ^{a,b,c}
Cal High	Higher value of the range of the instrument; calibrated to give [] ^{a,b,c} output in a loop of [] ^{a,b,c}
Span	Calibrated span of the input sensor to give [] ^{a,b,c} output.
Eng. Units (EEU)	Engineering units of the physical variable being measured.
Linearity	Error contribution due to nonlinearity of the sensor.
Stability	Error contribution due to instability of the sensor during a specified time period. Usually the time period is 1 year, and the sensor is calibrated once a year.

Ambient Temperature	Error contribution due to the ambient temperature difference at which it was calibrated and the temperature at which it is being operated.
Calibration Instrument + Loop Check	Error contribution due to the inaccuracies in the instruments used for calibration and loop check.
DAS	Accuracy of DAS.
Signal Conditioner	Error due to a signal conditioner placed in between the thermocouple and DAS.
Total Probable Error	Square root of the sums of square of the errors described previously; namely, linearity, stability, ambient temperature, calibration instrument, and DAS.

TABLE D-8
ERRORS FOR FDPs

Tag No.	Model No.	Serial No.	Cal Null	Cal High	Span	Eng. Units	Linearity	Stability	Ambient Temperature	Calibration Instrument +Loop Check	DAS	Total Probable Error	Maximum Error
						(EEU)	(EEU)	(EEU)	(EEU)	(EEU)	(EEU)	(EEU)	(EEU)

a,b,c

TABLE D-9
KW ERRORS

Tag No.	Model No.	Serial No.	Cal Null	Cal High	Span	Eng. Units	CT	PT	Meter/Sig'nal Conditioner	Calibration Instrument +/- Loop Check	DAS	Total Probable Error
						(EEU)	(EEU)	(EEU)	(EEU)	(EEU)	(EEU)	(EEU)

a.b.c

**APPENDIX E
MASS BALANCE**

Tables E5.1.1-1 through E5.7-2 on pages E-4 through E-37 are not included in this nonproprietary document.

APPENDIX F
DECAY HEAT COMPARISONS

Appendix F contains the decay heat comparisons between planned decay heat input and actual measured decay heat input as measured by power meters KW-101, KW-102, KW-103, and KW-104. KW-103 is a redundant meter for KW-101. KW-104 is a redundant meter for KW-102. Three comparison plots are provided for each test described in Section 5. The first two comparison plots compare the averages of KW-101 and KW-103, and KW-102 and KW-104 with the planned decay heat power input algorithm. The third comparison plot compares the average sum of the KW meters with twice the planned algorithm. This comparison was performed to confirm that any variation from any set of heater rods bundles did not affect the overall decay heat input power. The planned decay heat input algorithm (described in Subsection 2.3.2) was compared with the data from the KW power meters.

Decay heat comparison results for each matrix test are presented in graphic form and ordered consistently with the applicable subsection of this report. For example, the decay heat comparisons for Matrix Test SB01 (average of KW-101 and KW-103, average of KW-102 and KW-104, and total decay heat input) described in Subsection 5.1.1 are presented on pages F-4, F-5, and F-6.

The Figures for Appendix F on pages F-4 through F-54 are not included in this nonproprietary document.

APPENDIX G
PIPING AND INSTRUMENTATION DIAGRAMS

The diagrams for Appendix G on pages G-3 through G-39 are not included in this nonproprietary document.

APPENDIX H

The contents of Appendix H are considered proprietary information and are not included in this nonproprietary document.

APPENDIX I
DATA FILES

The contents of Appendix I are considered proprietary information and are not included in this nonproprietary document.